Advanced Physicochemical Treatment Technologies

Edited by

Lawrence K. Wang, PhD, PE, DEE

Yung-Tse Hung, PhD, PE, DEE

Nazih K. Shammas, PhD

Advanced Physicochemical Treatment Technologies

Advanced Physicochemical Treatment Technologies

Edited by

Lawrence K. Wang, PhD, PE, DEE

Lenox Institute of Water Technology, Lenox, MA
Krofta Engineering Corporation, Lenox, MA
Zorex Corporation, Newtonville, NY

Yung-Tse Hung, PhD, PE, DEE

Department of Civil and Environmental Engineering
Cleveland State University, Cleveland, OH

Nazih K. Shammas, PhD

Lenox Institute of Water Technology, Lenox, MA
Krofta Engineering Corporation, Lenox, MA

Dedication

The Editors of the *Handbook of Environmental Engineering* series dedicate this volume and all subsequent volumes to Thomas L. Lanigan (1938–2006), the founder and president of Humana Press.

Preface

The past thirty years have seen the emergence of a growing desire worldwide that positive actions be taken to restore and protect the environment from the degrading effects of all forms of pollution — air, water, soil, and noise. Since pollution is a direct or indirect consequence of waste, the seemingly idealistic demand for "zero discharge" can be construed as an unrealistic demand for zero waste. However, as long as waste continues to exist, we can only attempt to abate the subsequent pollution by converting it to a less noxious form. Three major questions usually arise when a particular type of pollution has been identified: (1) How serious is the pollution? (2) Is the technology to abate it available? and (3) Do the costs of abatement justify the degree of abatement achieved? This book is one of the volumes of the *Handbook of Environmental Engineering* series. The principal intention of this series is to help readers formulate answers to the last two questions above.

The traditional approach of applying tried-and-true solutions to specific pollution problems has been a major contributing factor to the success of environmental engineering, and has accounted in large measure for the establishment of a "methodology of pollution control." However, the realization of the ever-increasing complexity and interrelated nature of current environmental problems renders it imperative that intelligent planning of pollution abatement systems be undertaken. Prerequisite to such planning is an understanding of the performance, potential, and limitations of the various methods of pollution abatement available for environmental scientists and engineers. In this series of handbooks, we will review at a tutorial level a broad spectrum of engineering systems (processes, operations, and methods) currently being utilized, or of potential utility, for pollution abatement. We believe that the unified interdisciplinary approach presented in these handbooks is a logical step in the evolution of environmental engineering.

Treatment of the various engineering systems presented will show how an engineering formulation of the subject flows naturally from the fundamental principles and theories of chemistry, microbiology, physics, and mathematics. This emphasis on fundamental science recognizes that engineering practice has in recent years become more firmly based on scientific principles rather than on its earlier dependency on empirical accumulation of facts. It is not intended, though, to neglect empiricism where such data lead quickly to the most economic design; certain engineering systems are not readily amenable to fundamental scientific analysis, and in these instances we have resorted to less science in favor of more art and empiricism.

Since an environmental engineer must understand science within the context of application, we first present the development of the scientific basis of a particular subject, followed by exposition of the pertinent design concepts and

operations, and detailed explanations of their applications to environmental quality control or remediation. Throughout the series, methods of practical design and calculation are illustrated by numerical examples. These examples clearly demonstrate how organized, analytical reasoning leads to the most direct and clear solutions. Wherever possible, pertinent cost data have been provided.

Our treatment of pollution-abatement engineering is offered in the belief that the trained engineer should more firmly understand fundamental principles, be more aware of the similarities and/or differences among many of the engineering systems, and exhibit greater flexibility and originality in the definition and innovative solution of environmental pollution problems. In short, the environmental engineer should by conviction and practice be more readily adaptable to change and progress.

Coverage of the unusually broad field of environmental engineering has demanded an expertise that could only be provided through multiple authorships. Each author (or group of authors) was permitted to employ, within reasonable limits, the customary personal style in organizing and presenting a particular subject area; consequently, it has been difficult to treat all subject material in a homogeneous manner. Moreover, owing to limitations of space, some of the authors' favored topics could not be treated in great detail, and many less important topics had to be merely mentioned or commented on briefly. All authors have provided an excellent list of references at the end of each chapter for the benefit of interested readers. As each chapter is meant to be self-contained, some mild repetition among the various texts was unavoidable. In each case, all omissions or repetitions are the responsibility of the editors and not the individual authors. With the current trend toward metrication, the question of using a consistent system of units has been a problem. Wherever possible, the authors have used the British system (fps) along with the metric equivalent (mks, cgs, or SIU) or vice versa. The editors sincerely hope that this duplicity of units' usage will prove to be useful rather than being disruptive to the readers.

The goals of the *Handbook of Environmental Engineering* series are: (1) to cover entire environmental fields, including air and noise pollution control, solid waste processing and resource recovery, physicochemical treatment processes, biological treatment processes, biosolids management, water resources, natural control processes, radioactive waste disposal and thermal pollution control; and (2) to employ a multimedia approach to environmental pollution control since air, water, soil and energy are all interrelated.

As can be seen from the above handbook coverage, the organization of the handbook series has been based on the three basic forms in which pollutants and waste are manifested: gas, solid, and liquid. In addition, noise pollution control is included in the handbook series.

This particular book Volume 5 *Advanced Physicochemical Treatment Technologies* is a sister book to Volume 3 *Physicochemical Treatment Processes* and Volume 4 *Advanced Physicochemical Treatment Processes*. Volumes 3 and 4 have already included the subjects of screening, comminution, equalization, neu-

tralization, mixing, coagulation, flocculation, chemical precipitation, recarbon-ation, softening, oxidation, halogenation, chlorination, disinfection, ozonation, electrolysis, sedimentation, dissolved air flotation, filtration, polymeric adsorption, granular activated carbon adsorption, membrane processes, sludge treatment processes, potable water aeration, air stripping, dispersed air flotation, powdered activated carbon adsorption, diatomaceous earth precoat filtration, microscreening, membrane filtration, ion exchange, fluoridation, defluoridation, ultraviolet radiation disinfection, chloramination, dechlorination, advanced oxidation processes, chemical reduction/oxidation, oil water separation, evaporation and solvent extraction. This book, Volume 5, includes the subjects of pressurized ozonation, electrochemical processes, irradiation, nonthermal plasma, thermal distillation, electrodialysis, reverse osmosis, biosorption, emerging adsorption, emerging ion exchange, emerging flotation, fine pore aeration, endocrine disruptors, small filtration systems, chemical feeding systems, wet air oxidation, and lime calcination. All three books have been designed to serve as comprehensive physicochemical treatment textbooks as well as wide-ranging reference books. We hope and expect that the books will prove of equal high value to advanced undergraduate and graduate students, to designers of water and wastewater treatment systems, and to scientists and researchers. The editors welcome comments from readers in all of these categories.

The editors are pleased to acknowledge the encouragement and support received from their colleagues and the publisher during the conceptual stages of this endeavor. We wish to thank the contributing authors for their time and effort, and for having patiently borne our reviews and numerous queries and comments. We are very grateful to our respective families for their patience and understanding during some rather trying times.

Lawrence K. Wang, Lenox, MA
Yung-Tse Hung, Cleveland, OH
Nazih K. Shammas, Lenox, MA

Contents

13 Wet Air Oxidation for Waste Treatment
Linda Y. Zou, Yuncang Li, and Yung-Tse Hung *575*

14 Lime Calcination
Gupta Sudhir Kumar, Anushuya Ramakrishnan, and Yung-Tse Hung *611*

Contributors

JIRAPAT ANANPATTARACHAI, PhD CANDIDATE • *Research Assistant, Department of Environmental Engineering, King Mongkut's University of Technology Thonburi, Bangkok, Thailand*

GUAHUA CHEN, PhD • *Associate Professor, Department of Chemical Engineering, Hong Kong University of Science & Technology, Hong Kong, China*

J. PAUL CHEN, PhD • *Associate Professor, Division of Environmental Science and Engineering, National University of Singapore, Singapore*

EDWARD S.K. CHAIN, PhD • *Retired Professor, School of Civil and Environmental Engineering, Georgia Institute of Technology, Atlanta, GA*

YUNG-TSE HUNG, PhD, PE, DEE • *Professor, Department of Civil and Environmental Engineering, Cleveland State University, Cleveland, OH*

PUANGRAT KAJITVICHYANUKUL, PhD • *Assistant Professor, Department of Environmental Engineering, King Mongkut's University of Technology, Thonburi, Bangkok, Thailand*

GUPTA SUDHIR KUMAR, PhD • *Professor, Centre for Environmental Science and Engineering, Indian Institute of Technology, Bombay, Powai, Mumbai, Maharashtra, India*

YUNCANG LI, PhD • *Research Fellow, School of Engineering and Technology, Faculty of Science and Technology, Deakin University, Geelong, Victoria, Australia*

SOH-FONG LIM, MEng • *Research Scholar, Department of Chemical and Environmental Engineering, National University of Singapore, Singapore*

MASAAKI OKUBO, PhD • *Associate Professor, Department of Mechanical Engineering, Osaka Prefecture University, Osaka, Japan*

ANUSHUYA RAMAKRISHNAN, MSc • *Research Scholar, Centre for Environmental Science and Engineering, Indian Institute of Technology, Bombay, Powai, Mumbai, Maharashtra, India*

NAZIH K. SHAMMAS, PhD • *Professor and Environmental Engineering Consultant, Ex-Dean and Director, Lenox Institute of Water Technology, Lenox, MA, Krofta Engineering Corporation, Lenox, MA*

PING-XIN SHENG, PhD • *Research Fellow, Division of Environmental Science and Engineering, National University of Singapore, Singapore*

YEN-PENG TING, PhD • *Associate Professor, Department of Chemical and Biomolecular Engineering, National University of Singapore, Singapore*

LAWRENCE K. WANG, PhD, PE, DEE • *Dean & Director (Retired), Lenox Institute of Water Technology, Lenox, MA; Assistant to the President, Krofta Engineering Corporation, Lenox, MA; Vice President, Zorex Corporation, Newtonville, NY*

TOSHIAKI YAMAMOTO, PhD • *Professor, Department of Mechanical Engineering, Osaka Prefecture University, Osaka, Japan*

LEI YANG, PhD • *Research Fellow, Department of Chemical and Biomolecular Engineering, National University of Singapore, Singapore*

RUTH YU-LI YEH, PhD • *Professor, Department of Chemical Engineering, Ming Hsin University of Science and Technology, Hsin-Chu, Taiwan*

ROBERT C. ZIEGLER, PhD • *Section Head (Retired),Environmental Systems Section, Arvin-Calspan, Inc., Buffalo, NY*

LINDA ZOU, PhD • *Associate Professor, Institute of Sustainability and Innovation, Werribe Campus, Victoria University, Melbourne, Australia*

1
Pressurized Ozonation

Lawrence K. Wang and Nazih K. Shammas

1. INTRODUCTION

Increasing population and improving standards of living are placing increasing burdens on water resources. The preservation of the limited natural water supplies and, in the near future, the necessity for direct recycling of water in some parts of the world will require improved technologies for the removal of contaminants from wastewater.

There are many contaminants in wastewater, which vary from time to time, and they are not well characterized with respect to chemical species. Commonly, the level of organic contamination is expressed by biochemical oxygen demand (BOD), chemical oxygen demand (COD), or total organic carbon (TOC). Ozone and oxygen are powerful oxidants, which can oxidize many contaminants in wastewater and sludge biosolids. Ozone is more powerful than oxygen, but it must be generated at the point of use because it is an unstable material.

For many years in European countries, ozone has been used for disinfecting drinking water. It has also been used for treating some special industrial wastes, notably for removing cyanides and phenols. Since 1980, ozone has been used for wastewater, industrial wastes, and sludge treatment on a large scale (1–6). Oxidative purification and

disinfection with ozone as a tertiary wastewater treatment or sludge treatment has a number of inherent advantages:

  a. Reduction in BOD and COD.
  b. Reduction of odor, color, turbidity, and surfactants.
  c. Pathogenic organisms are destroyed.
  d. The treatment products are beneficial.
  e. The effluent water has a high dissolved oxygen (DO) concentration.

The relatively high cost of ozone generation requires a high ozone-utilization efficiency if ozone treatment is to be economically competitive. A principal disadvantage to the use of ozone in waste treatment is its cost. However, recent advances in ozone generation have rendered the ozonation process more competitive.

This chapter deals with two newly developed oxygenation–ozonation (Oxyozosynthesis®) systems for wastewater and sludge treatment. Each treatment scheme consists of a wet well for flow equalization and pH adjustment, a hyperbaric reactor for oxygenation and ozonation, a flotation clarifier for degasification and solid–water separation, and a filter belt press for final sludge dewatering. Special emphasis is placed on theory, kinetics, and disinfection effect of ozonation and oxygenation (7–12).

1.1. Oxyozosynthesis Sludge Management System

As shown in Figs. 1 and 2, the new sludge management system consists of the following unit operations and processes: sludge production from clarifiers, flow equalization and pH adjustment in a wet well, oxygenation–ozonation in a hyperbaric reactor vessel (Fig. 3), flotation, dewatering in a belt press, and resource recovery of final product as fuel or for land application.

A full-scale Oxyozosynthesis sludge management system was installed at the West New York Sewage Treatment Plant (WNYSTP), West New York, NJ. The plant treats domestic wastewater flow of 10 MGD and produces 22,000 gpd of primary sludge. Primary raw sludge is pumped from sumps located at the bottom of the primary sedimentation clarifiers by means of two positive-displacement pumps to a sludge grinder, then to the wet well. As the wet well is being filled with ground sludge, a chemical metering pump is used to add a 10% sulfuric acid solution to adjust the pH value to between 3.5 and 4.0. A mechanical mixer and a pH meter are mounted in the wet well for proper mixing and pH monitoring, respectively. Following acidification, the sludge is pumped by a progressive cavity pump to one of the two batch-operated hyperbaric reactor vessels, each capable of treating 1500 gal of sludge in 90 min by oxygenation and ozonation. To start each reactor vessel, the pressure in the reactor is increased to 40 psig with liquid oxygen first and then up to 60 psig with ozone. There are two operational modes:

  a. **Continuous oxygenation–ozonation.** After the startup with oxygen and ozone, ozone is continuously fed into the reactor for a total of 90 min. The pressure is maintained at 60 psig by bleeding off (or recycling) the excess gas.
  b. **Noncontinuous oxygenation–ozonation.** After the startup with oxygen and ozone, ozone is then shut off, to isolate the reactor and maintain the conditions for 90 min.

During the first 90 min contact time in the oxygenation–ozonation reactor, pathogenic bacteria, viruses, total suspended solids, and volatile suspended solids in the

1.
CLARIFIER (part of city treatment) accepts city sewage and separates sludge, which goes to wet well.

2.
SULFURIC ACID pumped from tank to sludge wet well.

SLUDGE

OZONE GENERATOR

OXYGEN

4.
HYPERBARIC VESSEL
Sludge is pressurized to 60 psi with oxygen and ozone, creating bacteria free water and solids. Ozone dissipates in process.

3.
WET WELL
Sludge is combined with sulfuric acid to alter pH.

5.
FLOTATION CHAMBER
Solids float to surface and are skimmed from water.

6.
CLEAN WATER
Bacteria free, available for any use, or may be pumped into rivers or streams without harm.

7. BELT PRESS dries mud-like solids which emerge as a dry, paper type fuel called "croal" (compressed residual oxyozosynthesis altered litter).

8. CROAL is a dry, inert fuel which burns like wood or soft coal at over 7500 BTU.

Fig. 1. General view of oxygenation–ozonation (Oxyozosynthesis™) system.

sludge are all significantly reduced. The reactor effluent is then released (at a flow rate of about 1500 gal/90 min) into an open flotation unit where DO, ozone, and carbon dioxide gases are released out of the solution to form tiny bubbles, which adhere to the residual suspended solids causing them to float and thickened at the top of the unit. The flotation unit is equipped with revolving paddles (or scoops) that transport these floating solids onto a filter belt press for sludge dewatering. The subnatant liquor is recycled

WASTEWATER SLUDGE DISPOSAL SYSTEM

Master control Panel

The layout shown is an oxyozonation sludge treatment facility currently operating at the West New York, New Jersey, Sewage Treat-ment Plant.

This particular plant treats nearly 17,000 gallons of raw sludge daily, while occupying 600 square feet.

Ultimate Disposal

Continuous screen belt press

Ash flotation chambers

Hyperbaric reactor vessels

Unit #1

Unit #2

Wet sludge well

Existing clarifiers

"Supernatant" return to clarifier influent
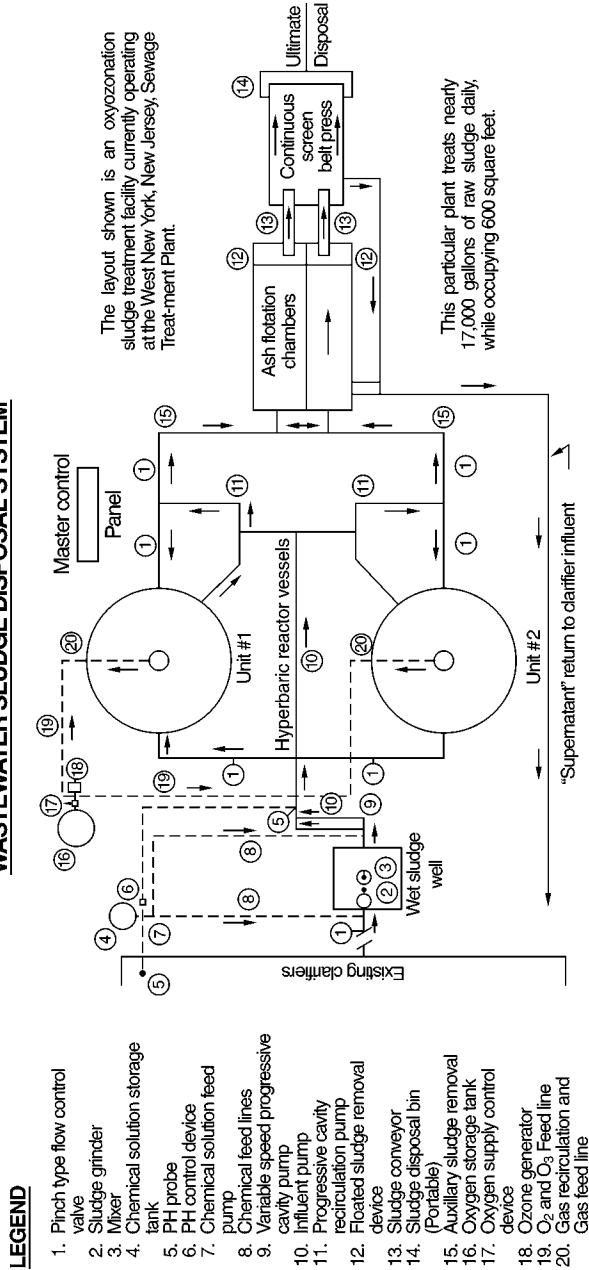
LEGEND

1. Pinch type flow control valve
2. Sludge grinder
3. Mixer
4. Chemical solution storage tank
5. PH probe
6. PH control device
7. Chemical solution feed pump
8. Chemical feed lines
9. Variable speed progressive cavity pump
10. Influent pump
11. Progressive cavity recirculation pump
12. Floated sludge removal device
13. Sludge conveyor
14. Sludge disposal bin (Portable)
15. Auxiliary sludge removal
16. Oxygen storage tank
17. Oxygen supply control device
18. Ozone generator
19. O_2 and O_3 Feed line
20. Gas recirculation and Gas feed line

Fig. 2. Flow diagram of Oxyozosynthesis sludge management system.
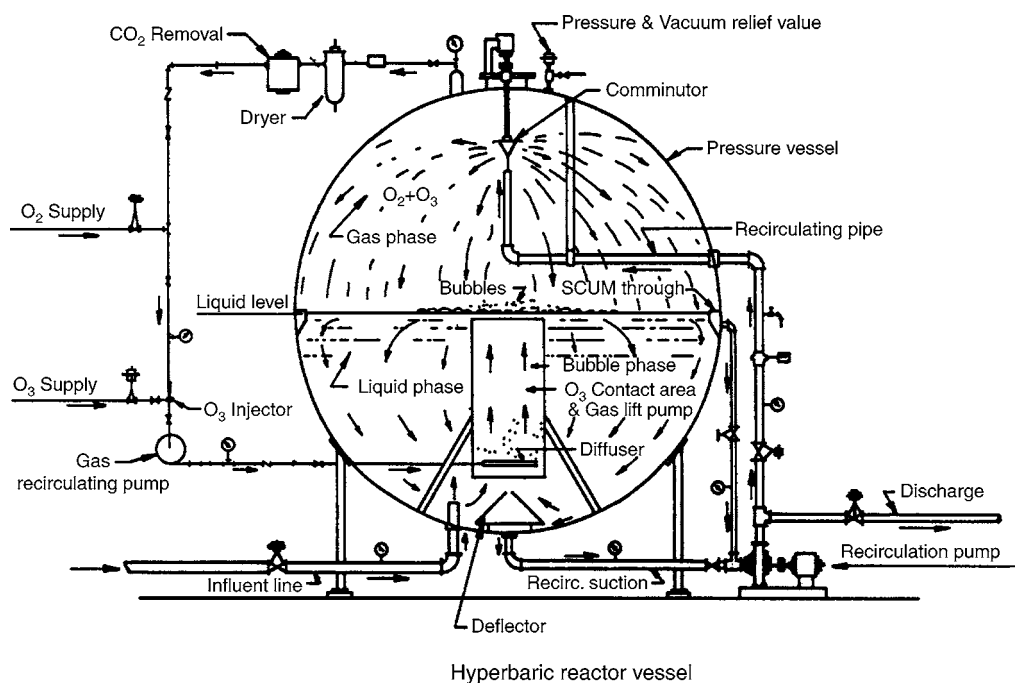
Fig. 3. The hyperbaric reactor vessel.

to the head of the sewage treatment plant for further treatment with the incoming wastewater flow.

The filter belt press produces a dry high-nutrient sludge cake with low metal content and high BTU value. The sludge cake can be recycled by spreading on agricultural land, reused as a fuel source, or disposed off in a landfill. The dry sludge can also be reused as secondary fiber in paper manufacturing or as raw material for building blocks.

1.2. Oxyozosynthesis Wastewater Reclamation System

As shown in Fig. 4, the new wastewater reclamation system consists of the following unit operations and processes: wastewater collection and preliminary treatment (bar screens and grit chambers), flow equalization and pH adjustment in a wet well, oxygenation–ozonation in a hyperbaric reactor vessel, dissolved gas flotation (DGF), and filtration.

A pilot-scale Oxyozosynthesis wastewater reclamation system was installed at the Lenox Institute of Water Technology, Lenox, MA. The pilot plant treats a wastewater flow of 6 gpm and produces small amount of sludge. Raw wastewater is pumped from sumps located at the bottom of the grit chambers by means of positive-displacement pumps to a wet well. As the wet well is being filled with the raw wastewater, a chemical metering pump is used to add a 10% sulfuric acid solution to adjust the pH value to between 3.5 and 4.0 by a chemical metering pump. A mechanical mixer and a pH meter are mounted in the wet well for proper mixing and pH monitoring, respectively.

From the wet well, a progressive cavity pump delivers the acidified wastewater to a batch-operated hyperbaric reactor vessel capable of treating 100 gal of wastewater in

WASTEWATER RECLAMATION SYSTEM

Master control Panel

The layout shown is an oxyozonation wastewater reclamation facility currently operating at the Lenox Institute

Unit #1

Unit #2

Hyperbaric reactor vessels

Existing grit chambers

Wet well

Equalization and flocculation

Continuous flotation and filtration

Recycled Water

Sludge Disposal
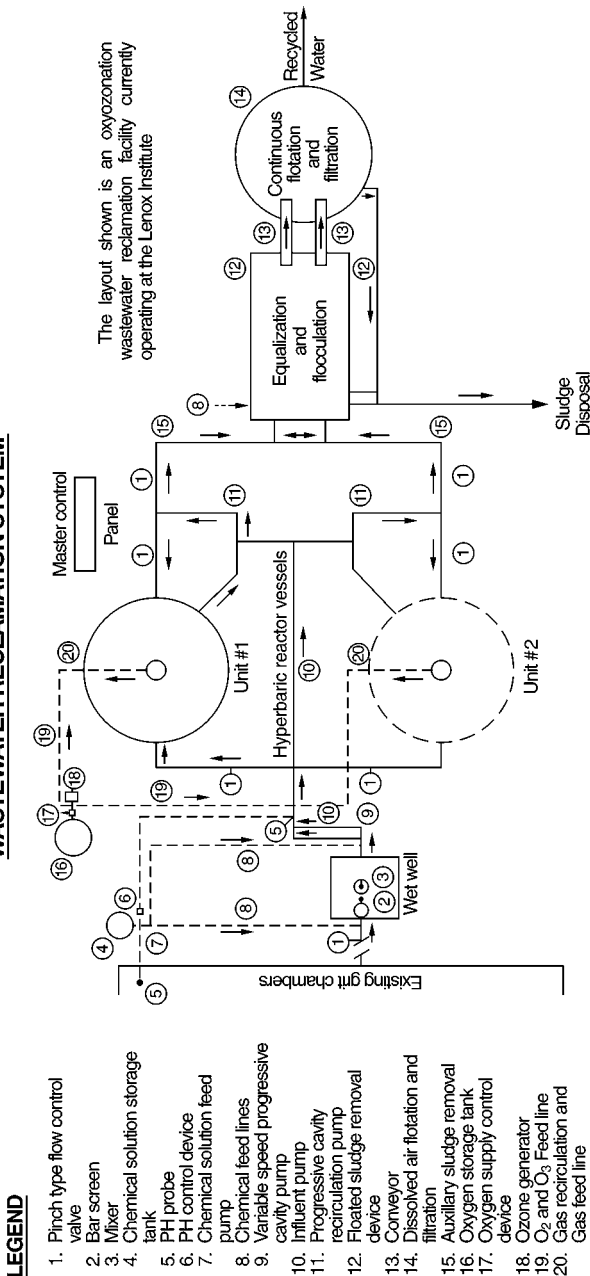
Fig. 4. Flow diagram of Oxyozosynthesis wastewater reclamation system.

6

30–60 min depending on the characteristics of the wastewater. To start the reactor vessel, the pressure in the reactor is increased to 40 psig with liquid oxygen first, and then to 60 psig with ozone. There are two operational modes:

   a. **Continuous oxygenation–ozonation.** After the startup with oxygen and ozone, ozone is continuously fed into the reactor for a total of 30–60 min. The pressure is maintained at 60 psig by bleeding off (or recycling) the excess gas.
   b. **Noncontinuous oxygenation–ozonation.** After the startup with oxygen and ozone, ozone is then shut off, to isolate the reactor and maintain the conditions for 30–60 min.

During the first 30–60 min contact time in the oxygenation–ozonation reactor, pathogenic bacteria, viruses, total suspended and volatile suspended solids, phenols, cyanides, manganese, and so on, in wastewater are all significantly reduced. The reactor effluent is released into a DGF unit, where flocculant(s) can be added and the dissolved gases come out of aqueous phase forming tiny bubbles, which adhere to the flocs and residual suspended solids causing them to float to the top of the unit. Heavy metals, iron, phosphate, humic acids, hardness, toxic volatile organics, and so on, will all react with the flocculant(s) to form insoluble flocs that are floated. The flotation unit is equipped with revolving paddles (or scoops) that transport these floating solids onto a subsequent filter belt press for final sludge dewatering. A dual-media filter further polishes the subnatant clarified water.

The filter effluent quality is close to that of potable water, having extremely low color, turbidity, suspended solids, hardness, iron, manganese, trihalomethane precursor (humic acid), heavy metal, volatile organics, phenol, cyanide, and so on. The product water is suitable for reuse for industrial and agricultural purposes. Further treatment of the final filter effluent by adsorption on activated carbon is optional.

2. DESCRIPTION OF PROCESSES

2.1. Ozonation and Oxygenation Process

Ozone gas is sparingly soluble in water. The solubility of ozone in water increases with its increasing partial pressure, decreasing water pH, and decreasing temperature. However, oxidation rate increases with increasing temperature. For economic operation of the hyperbaric oxygenation–ozonation reactor, it is operated at room temperature and a pressure in the range of 40–60 psig, the influent liquid sludge pH is reduced with sulfuric acid to a value in the 3.5–4.0 range.

The addition of oxygen at 40 psig and ozone at 60 psig ensure proper partial pressures for solubilizing both oxygen and ozone gases in the sludge. Both DO and ozone act to oxidize chemically the reducing pollutants found in the liquid sludge, thus decreasing BOD and COD, which results in the formation of oxygenated organic intermediates and end products. Ozonation–oxygenation treatment also reduces color and odor in waste sludge.

Because there is a wide range of ozone reactivity with the diverse organic content of wastewater, both the required ozone dose and reaction time are dependent on the quality of the influent to the ozonation process. Generally, higher doses and longer contact times are required for ozone oxidation reactions than are required for wastewater disinfection using ozone. Ozone tertiary treatment may eliminate the need for a final disinfection

Table 1
Effectiveness of Ozone as an Oxidant

Ozone dosage (mg/L)	COD (mg/L)		BOD$_5$ (mg/L)		TOC (mg/L)	
	Influent	Effluent	Influent	Effluent	Influent	Effluent
50	318	262	142	110	93	80
100	318	245	142	100	93	77
200	318	200	142	95	93	80
325	318	159	142	60	93	50
50	45	27	13	7	20.5	15.5
100	45	11	13	3	20.5	9
200	45	5.5	13	1.5	20.5	5

Source: US EPA.

step. Ozone breaks down to elemental oxygen in a relatively short period of time (its half-life is about 20 min). Consequently, it must be generated on-site using either air or oxygen as the feed gas. Ozone generation utilizes a silent electric arc or corona through which air or oxygen passes, and yields ozone in the air/oxygen mixture, the percentage of ozone being a function of voltage, frequency, gas flow rate, and moisture. Automatic devices are commonly applied to control and adjust the ozone generation rate.

For sludge treatment or wastewater reclamation, it is a developing technology. Recent developments and cost reduction in ozone generation and ozone dissolution technology make the process very competitive. A full-scale application is currently in the demonstration stage at the WNYSTP, West New York, NJ. If oxygen-activated sludge is employed in the system, ozone treatment may be even more economically attractive, because a source of pure oxygen is available facilitating ozone production.

For poor-quality wastewater or sludge with extremely high COD, BOD, and/or TOC contents (>300 mg/L), ozone treatment can be economical only if there is adequate pre-treatment. The process will not produce any halogenated hydrocarbons. Table 1 shows the reduction of overall COD, BOD, and TOC, achieved in the US Environmental Protection Agency (EPA) controlled tests after a 90 min contact time with ozone oxidation. Beyond the 70% COD removal level, the oxidation rate is significantly slowed. In laboratory tests, COD removal never reaches 100% even at a high ozone dose of 300 mg/L.

As a disinfectant with common dosages of 3–10 mg/L, ozone is an effective agent for deactivating common forms of bacteria, bacterial spores, and vegetative microorganisms found in wastewater, as well as eliminating harmful viruses. Additionally, ozone acts to chemically oxidize materials found in the wastewater and sludge, forming oxygenated organic intermediates and end products. Furthermore, ozone treatment reduces wastewater color and odor. Ozone disinfection is applicable in cases, where chlorine (Cl$_2$) disinfection might produce potentially harmful chlorinated organic compounds. If oxygen-activated sludge is employed in the system, ozone disinfection is economically attractive, because a source of pure oxygen is available for facilitating ozone production. However, ozone disinfection does not form a residual that will persist and can be easily measured to ensure adequate dosage. Ozonation may not be economically competitive with chlorination under nonrestrictive local conditions.

Table 2
Effectiveness of Ozone as a Disinfectant

Source	Influent	Dose (mg/L)	Contact time (min)	Effluent residual
US EPA	Secondary effluent	5.5–6	≤1	<2 fecal coliforms/100 mL
US EPA	Secondary effluent	10	3	99% inactivation of fecal coliform
US EPA	Secondary effluent	1.75–3.5	13.5	<200 fecal coliforms/ 100 mL
US EPA	Drinking water	4	8	Sterilization of virus
WNYSTP	Primary sludge	NA	60	>99% inactivation of fecal coliform
SIT/LI	Secondary sludge	NA	60	>99% inactivation of fecal coliform

Source: US EPA.

Easily oxidizable wastewater organic materials consume ozone at a faster rate than disinfection, therefore, the effectiveness of disinfection is inversely correlated with effluent quality but directly proportional to ozone dosage. When sufficient concentration is introduced, ozone is a more complete disinfectant than chlorine. Results of disinfection by ozonation have been reported by various sources, which are summarized in Table 2.

2.2. Flotation Process

DGF is mainly used to remove suspended and colloidal solids by flotation resulting from the decrease in their apparent density. The influent feed liquid can be raw water, wastewater, or liquid sludge. The flotation system consists of four major components: gas supply, pressurizing pump, retention tank, and flotation chamber. According to Henry's Law, the solubility of gas in aqueous solution increases with increasing pressure. A pressurizing pump is used to saturate the feed stream with gas at pressures several times the atmospheric pressure (25–70 psig). The pressurized feed stream is held at this high pressure for about 0.5–3 min in a retention tank (hyperbaric vessel) designed to provide the required time for dissolution of gas into the treatment stream. Following the retention vessel, the stream is released back to atmospheric pressure in the flotation chamber. Most of the pressure drop occurs downstream from a pressure-reducing valve and in the transfer line between the retention vessel and the flotation chamber, so that the turbulent effect of depressurization is minimized. The sudden reduction in pressure in the flotation chamber results in the release of microscopic gas bubbles (average diameter 80 µm or smaller) that attach themselves to the suspended and colloidal particles present in water. This results in an agglomeration, due to entrained gas giving a net combined specific gravity less than that of water thereby resulting in flotation. The vertical rising rate of gas bubbles ranges between 0.5 and 2 ft/min. The floated materials rise to the surface of the flotation chamber, where they are continuously scooped by specially designed flight scrapers or other skimming devices. The surface sludge layer or float can in certain cases attain a thickness
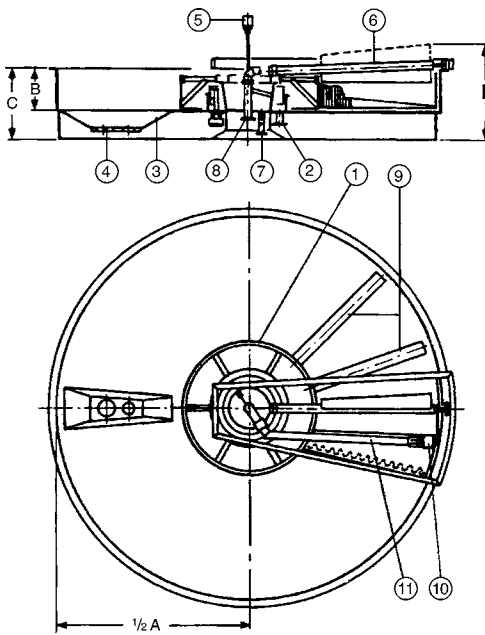
1 ROTATING CENTER SECTION
2 CLARIFIED WATER OUTLET
3 SETTLED SLUDGE SUMP
4 SETTLED SLUDGE OUTLET
5 ROTARY CONTACT
6 SPIRAL SCOOP
7 FLOATED SLUDGE OUTLET
8 UNCLARIFIED WATER INLET
9 CLARIFIED WATER EXTRACTION PIPES
10 GEAR MOTOR
11 DISTRIBUTION DUCT

TYPE		DIMENSIONS						FLOW		
A ft	A mm	B in	B mm	C in	C mm	D in	D mm	m³/min	US GPM	m³/h
8	2400	23.5	600	33	850	45	1150	0,56	148	34
10	3200	23.5	600	33	850	49	1250	1,00	263	60
12	3900	25.5	650	35	900	51	1300	1,50	394	90
15	4500	25.5	650	37	950	57	1450	2,00	525	120
18	5500	25.5	650	37	950	58	1480	3,00	789	180
20	6100	25.5	650	37	950	61	1560	3,65	961	219
22	6700	25.5	650	37	950	62	1580	4,40	1160	264
24	7200	25.5	650	37	950	63	1600	5,08	1340	305
27	8100	25.5	650	37	950	67	1700	6,44	1695	386
30	9000	25.5	650	37	950	71	1820	7,95	2090	477
33	10000	25.5	650	37	950	72	1840	9,80	2580	588
36	11000	25.5	650	37	950	73	1860	11,87	3125	712
40	12200	26	660	38	960	76	1920	14,60	3840	876
44	13400	27	685	39	985	78	1980	17,60	4630	1056
49	14800	27	685	39	985	82	2070	21,50	5650	1290
55	16800	27	685	39	985	87	2200	27,70	7290	1662

A DIAMETER of SUPRACELL
B DEPTH of SUPRACELL TANK
C DEPTH of SUPRACELL TANK WITH BOTTOM SUPPORT
D MINIMUM OVERALL HEIGHT of SUPRACELL

Fig. 5. A single-cell high rate DAF system (Supracell).

of several inches and be relatively stable. The layer thickens with time, but undue long delays in removal will cause release of particulates back to the liquid. The clarified effluent is usually drawn off from the bottom of the flotation chamber, which can be recovered for reuse or for final disposal. Figures 5 and 6 illustrate up-to-date DGF systems using single cell and double cell, respectively. The flotation system is known as dissolved air flotation (DAF) only when air is used. In the Oxyozosynthesis system, the dissolved gases include oxygen, ozone, carbon dioxide, and air.

The retention time in the flotation chamber is usually short, about 3–5 min depending on the characteristics of process water and the performance of the flotation unit. DGF units with such short retention times can treat water, wastewater, or sludge at an overflow rate of 3.5 gpm/ft² for a single unit, and up to 10.5 gpm/ft² for triple stacked units. A comparison between a DGF clarifier and a sedimentation tank shows that (13):

a. DGF floor space requirement is only 15% of the sedimentation tank.
b. DGF volume requirement is only 5% of the sedimentation clarifier.
c. The degrees of clarification of a DGF are similar to that of a sedimentation tank using the same flocculating chemicals.
d. The operational cost of the DGF clarifier is slightly higher than that for the sedimentation unit, which is offset by the considerably lower cost for financing the installation.

1. Raw water collection tank
2. Supracell feed pump
3. Supracell inlet pipe (inbedded in ground)
4. Inlet compartment
5. Settled sludge sump
6. Settled sludge discharge
7. Clarified water outlet
8. Clarified water return for level control (1)
9. Level control in supracell with pneumatic sensor and clarified water discharge regulating valve
10. Pressure pump for recycling of clarified water to the air dissolving tubes
11. Air dissolving tubes
12. Supracell main tank
13. Spiral scoop for collection of the floated sludge
14. Floated sludge
15. Steel legs
16. Second elevated supracell in steel construction

Fig. 6. A double-cell high rate DAF system (Supracell).

e. DGF clarifiers are usually prefabricated using stainless steel. This results in lower erection cost, better flexibility in construction, and ease of possible future upgrade compared with the *in situ* constructed heavy concrete sedimentation tanks.

Currently used DGF units are more reliable, have excellent performance for sludge thickening, and require less land area than gravity thickeners. However, the gas released to the atmosphere may strip volatile organic material from the sludge. The volume of sludge requiring ultimate disposal or reuse may be reduced, although its composition will be altered if chemical flotation aids are used. US EPA data from various air flotation units indicate that solids recovery ranges from 83 to 99% at solids loading rates of 7–48 lb/ft²/d. A summary of US EPA data that illustrate the excellent performance of DAF for thickening various types of sludges is shown in Table 3.

DAF is also an excellent process for solids separation in water treatment and wastewater reclamation (14–17). DAF is an integral part of the Oxyozosynthesis wastewater reclamation system. A bird's eye view of the advanced DAF unit with built-in chemical flocculation and filtration (Sandfloat) is shown in Fig. 7. The influent raw water or wastewater enters the inlet at the center near the bottom, and flows through a hydraulic

Table 3
Sludge Thickening by Dissolved Air Flotation

	Feed solids conc. (%)	Loading rate w/o polymer (lb/ft^2/d)	Loading rate w/polymer (lb/ft^2/d)	Float solids conc. (%)
Primary + WAS	2	20	60	5.5
Primary + (WAS + FeCl$_3$)	1.5	15	45	3.5
(Primary + FeCl$_3$) + WAS	1.8	15	45	4
WAS	1	10	30	3
WAS + FeCl$_3$	1	10	30	2.5
Digested primary + WAS	4	20	60	10
Digested primary + (WAS + FeCl$_3$)	4	15	45	8
Tertiary (alum)	1	8	24	2

Source: US EPA.
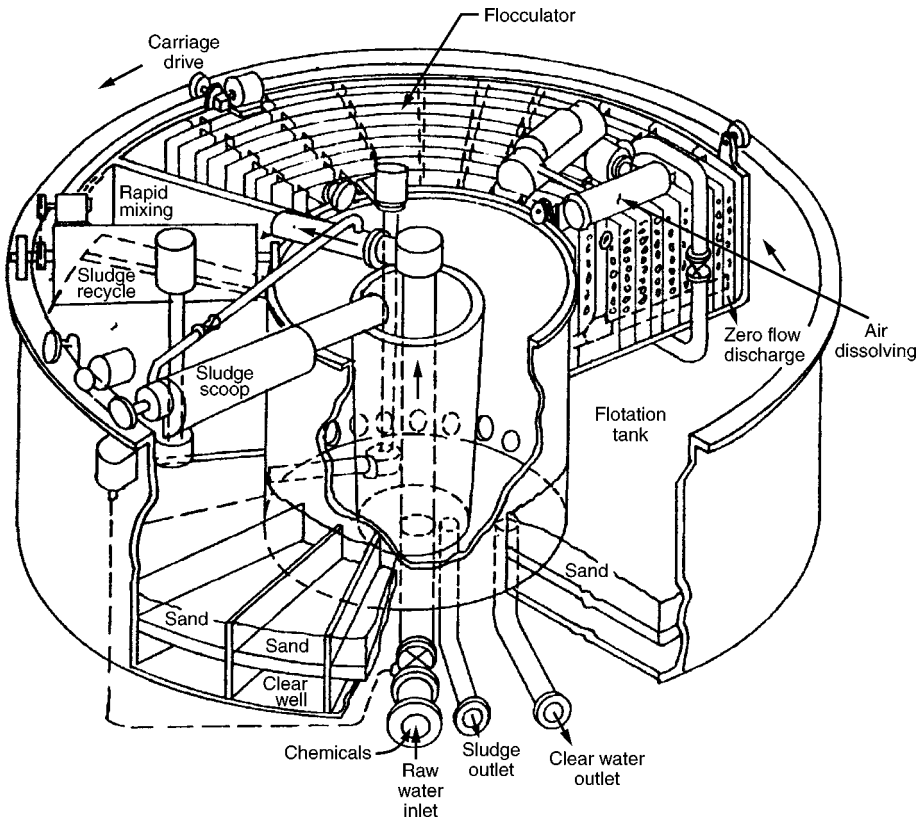
Fig. 7. Bird's eye view of a flocculation/flotation/filtration package unit (Sandfloat).

rotary joint and an inlet distributor into the rapid mixing section of the slowly moving carriage. The entire moving carriage consists of rapid mixer, flocculator, air dissolving tube, backwash pump, sludge discharge scoop, and sludge recycle scoop. From the rapid mixing

section, the water enters the hydraulic flocculator where flocs are gradually built up by gentle mixing. The flocculated water moves from the flocculator into the flotation tank clockwise with the same velocity as the entire carriage including the flocculator, which is moving counterclockwise simultaneously. The flocculator effluent velocity is compensated by the opposite velocity of the moving carriage, resulting in a "zero" horizontal velocity of the flotation tank influent. The flocculated water thus stands still in the flotation tank for optimum clarification. At the outlet of the flocculator, clarified or recycled water stream with microscopic air bubbles is added to the flotation tank, in order to float the insoluble flocs and suspended matter to the water surface. The float (scum/sludge) accumulated at the top of the unit is scooped off by a sludge discharge scoop and discharged into the center sludge collector, where there is a sludge outlet to an appropriate sludge treatment facility. The bottom of the Sandfloat is made up of multiple sections or wedges of sand filter and clear well. The clarified flotation effluent passes through the sand filter downward and enters the clear well. Through the circular hole underneath each sand filter section, the filter effluent enters the center portion of the clear well, where there is an outlet for the Sandfloat effluent. The filter sections are backwashed sequentially.

For the wastewater reclamation plant, DAF is an important process unit. Filtration is used for final polishing of the plant effluent. Table 4 represents the US EPA data on removal of various classical pollutants, toxic heavy metals, and toxic organics by flotation. For more information on the DAF process the reader is referred to refs. 18 and 19.

2.3. Filter Belt Press

The filter belt press or simply the belt press is used for sludge dewatering. Resembling a conveyor belt, the filter belt press consists of an endless filter belt that runs over a drive and guide rollers at each end. Several rollers support the filter belt along its length. Above the filter belt is a press belt that runs in the same direction and at the same speed; its drive roller is coupled with the drive roller of the filter belt. The press belt can be pressed on the filter belt by means of a pressure roller system whose rollers can be individually adjusted either horizontally or vertically. The sludge to be dewatered is fed onto the upper face of the filter belt and is continuously dewatered between the filter and press belts. After having passed the static pressure zone, further dewatering is achieved by the superimposition of shear forces to expedite the dewatering process. The supporting rollers of the filter belt and the pressure rollers of the pressure belt are adjusted in such a way that the belts and the sludge between them describe a S-shaped curve. Thus, there is a parallel displacement of the belts relative to each other owing to the differences in the radii. After further dewatering in the shear zone, the sludge is removed by a scraper.

Some units consist of two stages, where the initial draining zone is on the top level followed by an additional lower section wherein pressing and shearing occur. A significant feature of the filter belt press is that it employs a coarse mesh, relatively open weave, and metal medium fabric. This is feasible because of the rapid and complete cake formation obtainable when proper flocculation is achieved. Belt filters do not need vacuum systems and do not have the sludge pickup problem that is occasionally experienced with rotary vacuum filters. The belt press can handle the hard-to-dewater sludges more readily. The low moisture cake produced permits incineration of primary/secondary sludge combinations without auxiliary fuel. A large filtration area can be installed in a minimum of floor

Table 4
Removal of Various Pollutants, Toxic Heavy Metals, and Organics by Flotation

Pollutant	Data points Full scale	Effluent concentration Range	Median	Removal efficiency (%) Range	Median
Classical pollutants (mg/L)					
BOD$_5$	9	140–1000	250	4–87	68
COD	12	18–3200	1200	8–96	66
TSS	12	18–740	82	6–98	88
Total phosphorus	6	<0.05–12	0.66	50 to >99	98
Total phenols	10	<0.001–23	0.66	3 to >94	12
Oil and grease	11	16–220	84	57–97	79
Toxic pollutants (µg/L)					
Antimony	9	ND to 2300	20	4–95[a]	76
Arsenic	7	ND to 18	<10	8 to >99	45
Xylene	3	ND to 1000	200	95 to >99	97
Cadmium	9	BDL to <72	3	0 to >99	98[a]
Chromium	12	2–620	200	20–99	52
Copper	12	5–960	180	9–98	75
Cyanide	7	<10–2300	54	0 to <62	10
Lead	13	ND to 1000	70	9 to >99	98
Mercury	8	BDL to 2	BDL	33–88	75
Nickel	12	ND to 270	41	29 to >99	73
Selenium	3	BDL to 8.5	2		NM
Silver	5	BDL to 66	19		45
Thallium	3	BDL to 50	14		NM
Zinc	11	ND to 53,000	200	12 to >99	89
Bis(2-ethylhexyl) phthalate	8	30–1100	100	10–98	72
Butyl benzyl phthalate	5	ND to 42	ND	97 to >99	>99
Carbon tetrachloride	3	BDL to 210	36		75
Chloroform	6	ND to 24	9	20 to >99	58
Dichlorobromomethane	1		ND		>99
2,4-Dichlorophenol	1		6		NM
Di-*N*-butyl phthalate	6	ND to 300	20	0 to >99	97
Diethyl phthalate	1		ND		>99
Di-*N*-octyl phthalate	6	ND to 33	11	61 to >99	78
N-Nitrosodiphenylamine	1		620		66
N-Nitroso-di-*N*-propylamine	1		84		NM
2-Chlorophenol	1		2		NM
2,4-Dimethylphenol	2	ND to 28	14		>99
Pentachlorophenol	5	5–30	13		19
Phenol	8	9–2400	71	0–80	57
2,4,6-Trichlorophenol	1		3		NM
Benzene	3	5–200	120		NM
Chlorobenzene	1		57		NM

(Continued)

Table 4 *(Continued)*

Pollutant	Data points Full scale	Effluent concentration Range	Median	Removal efficiency (%) Range	Median
Dichlorobenzene	2	18–260	140		76
Ethylbenzene	7	ND to 970	44	3 to >99	65
Toluene	6	ND to 2100	580	10 to >99	39
Fluoranthene	2	0.5 to <10	5.2		NM
Fluorene	1		14		NM
Naphthalene	9	ND to 840	96	33 to >99	77
Pyrene	2	0.3–18	9.2		0
Anthracene/phenanthrene	5	0.2–600	10	45 to >98	81
2-Chloronaphthelene	1		17		0

Source: US EPA.
Blanks indicate data not available.
Abbreviations: BDL, below detection limit; ND, not detected; NM, not meaningful.
[a]Approximate value.

Table 5
Belt Press Performance

Feed solids (%)	Secondary: primary ratio	Polymer dosage[a]	Pressure Ib/in.^{2} g[b]	Cake solids (%)	Solids recovery (%)	Capacity[c]
9.5	100% primary	1.6	100	41	97–99	2706
8.5	1:5	2.4	100	38	97–99	2706
7.5	1:2	2.7	25–100	33–38	95–97	1485
6.8	1:1	2.9	25	31	95	898
6.5	2:1	3.1	25	31	95	858
6.1	3:1	4.1	25	28	90–95	605
5.5	100% secondary	5.5	25	25	95	546
5.6	100% primary	None	NA	39–43	>97	NA
3.8	100% secondary	None	NA	25	>95	NA

Source: US EPA.
[a]Pounds per ton dry solids.
[b]Pounds per sq. in. (gauge).
[c]Pound dry solids per hour per meter.

area. It is usually necessary to coagulate the sludge, generally with synthetic and high polymeric flocculants, to avoid the penetration of the filter belt by sludge. The sludge treated by ozonation, however, does not need any flocculants for sludge conditioning.

The process reliability is considered to be excellent. A period of more than 1 yr trouble-free operation has been achieved at the WNYSTP. Table 5 shows performance data collected at the WNYSTP. The last two entries in Table 5 represent the primary sludge at the WNYSTP and the secondary sludge that was collected from a nearby secondary treatment plant, which were oxidized before entering the belt press by oxygenation–ozonation for dewatering.

Table 6
Heavy Metal Contents of Dewatered Filter-Belt-Press Cake[a]

Heavy metals (mg/kg dry sludge)	West NY sludge cake	NJ DEP limits for land application	US EPA ceiling limits[b] for land application	US EPA high-quality limits[c] for land application
Cadmium	3	25	85	39
Chromium	14	1000	3000	1200
Copper	447	1000	4300	1500
Nickel	9	200	420	420
Lead	126	1000	840	300
Zinc	192	2500	7500	2800

Source: US EPA.
[a]The Oxyozosynthesis system hyperbaric unit was operated at pH 4.0 and contact time at 90 min.
[b]Absolute value of any single concentration (40 CFR part 503 regulations, US EPA, 1994).
[c]Monthly average values (40 CFR part 503 regulations, US EPA) (23).

Table 7
Toxic Organic Compounds in Dewatered Filter-Belt-Press Cake

Toxic organics (mg/kg dry sludge)	US EPA limitations	WNY dewatered sludge cake
Aldrin	0.10	<0.001
Chlordane	0.10	<0.001
Dieldrin	0.10	<0.001
Endrin	0.10	<0.001
Heptachlor	0.10	<0.001
Heptachlor epoxide	0.10	<0.001
Lindane	0.10	<0.001
Methoxychlor	0.25	<0.001
Mirex	0.25	<0.001
p, p'-DDT	0.25	<0.001
p, p'-DDE	0.25	<0.001
p, p'-TDE (DDD)	0.25	<0.001
Toxaphene	1	<0.001
PCB	0.50	<0.001

Source: US EPA.
[a]West NewYork sewage treatment plant; US EPA.
[b]Oxyozosynthesis process' Hyperbaric unit was operated at pH 4.0 and detention time at 90 min.
[c]1 mg/kg dry sludge = 1 ppm on dry weight basis.

2.4. Performance of Oxyozosynthesis Sludge Management System

The sludge management system consists of a pH adjustment unit, an innovative reactor for oxygenation–ozonation under moderate pressure (40–60 psi), DGF for sludge thickening, and an advanced filter belt press for sludge dewatering. The system's overall mechanical reliability is excellent. Tables 6 and 7 document the operational data at the

WNYSTP (20). It is shown that the resulting cake is low in heavy metals and toxic organics, and meets the requirements of the US EPA (40 CFR part 503 regulations) (21) and the NJ Department of Environmental Protection for sludge disposal. The ozone-treated sludge cake has low volatile solids content, high-suspended solids consistency, high fuel value (>7500 BTU/lb dry sludge), and is nonoffensive, odor free, and almost coliform free. In addition, the ozone-treated sludge can be thickened easily by flotation and dewatered by the filter belt press without any additional chemicals. The product sludge cake can be disposed of safely in a sanitary landfill site, spread on land for crop production, or reused as an ideal refuse-derived fuel (RDF).

The flotation unit uses the pressurized gases in the hyperbaric reactor vessel for water sludge separation. The pressurized gases include oxygen, ozone, and carbon dioxide. Under optimum operation, all gaseous ozone should disappear and the flotation process should release mainly oxygen and carbon dioxide. Because supplemental air is not needed in sludge flotation, a significant cost-savings in sludge thickening is achieved.

The side streams from the flotation unit and belt press are recycled to the top of the treatment plant for reprocessing; these streams contain low concentrations of suspended solids and no harmful microorganisms. The suspended solids, BOD, COD, and total Kjedahl nitrogen (TKN) of the recycle liquors are significantly lower than that produced from aerobic digestion, anaerobic digestion, and thermal treatment processes. Therefore, if the side streams are recycled, there will be no adverse effect on the biological wastewater treatment system. pH adjustment might be needed if the ratio of low pH recycle liquor flow to the plant influent flow is high.

The heavy metal content in the recycle liquors will not be high if the wastewater treatment plant treats only municipal sewage. In industrial areas, heavy metals could settle with the sludge by chemical precipitation or biological assimilation. Many of these heavy metals will become soluble and will be present in the recycle liquor if the pH of the influent sludge is lowered to 3.0–4.0 before entering the hyperbaric reactor for oxidation. In this case, two remedies are possible:

a. Operating the hyperbaric reactor without acidification. This implies a lower ozonation efficiency; or
b. Operating the flotation unit with chemical additions for both pH adjustment and heavy metals flotation. This is the perfect solution for removing the heavy metals and maintaining high ozonation efficiency in the hyperbaric reactor.

In summation, the Oxyozosynthesis sludge management system is a very promising and sound engineering development (22). It will be extremely competitive under the following conditions:

a. In the case of the United States, ocean dumping is not allowed.
b. Federal and state regulations for disposal of sludge on land are very stringent, whereby the treated sludge must be stabilized and rendered safe for cropland disposal.
c. Incineration is not allowed in urban areas with many high-rise buildings, because it creates air pollution.
d. Wet air oxidation is not allowed in urban areas or cannot be afforded in rural areas, because it creates odor problems.
e. Distance is too far to transport sludge to another plant or site for disposal.
f. There are engineering demonstration grants available to encourage testing and/or using innovative sludge management technology.

Table 8
Water Quality Criteria for Reclaimed Water Use in Apartment Complexes

Item	Unit	Criteria
Odor	–	Nonexistence
Color	Unit	<10
Turbidity	Unit	<5
TDS	mg/L	<1000
SS	mg/L	<5
pH	Unit	5.8–8.6
COD	mg/L	<20
BOD_5	mg/L	<10
PO_4^{3-}	mg/L	<1
MBAS	mg/L	<1
Coliform	Count/mL	Nonexistence
General bacteria	Count/mL	<100
Residual chlorine	mg/L	>0.2
TOC	mg/L	<15

2.5. Performance of Oxyozosynthesis Wastewater Reclamation System

The major components of the Oxyozosynthesis wastewater reclamation system (*see* Fig. 4) are two hyperbaric oxygenation–ozonation reactors (*see* Fig. 3) and a Sandfloat flotation–filtration package unit (*see* Fig. 7). The full-scale hyperbaric reactors have a capacity of 22,000 gpd (20,23). The package unit consists of chemical flocculation, DGF, and rapid sand filtration with a full-scale plant capacity of l MGD that was installed in the Town of Lenox, MA for potable water treatment (24).

The aim of this combined system is to convert municipal wastewater to a reusable water meeting the water quality criteria as indicated in Table 8, for reclaimed water reuse in apartment complexes (25). The ultimate goal is to renovate wastewater for reuse as a potable water supply that meets the US EPA drinking water standards (26).

3. FORMATION AND GENERATION OF OZONE

3.1. Formation of Ozone

The conversion of oxygen (O_2) into ozone (O_3) requires the rupture of the very stable O_2 molecules. Because the breaking of the oxygen–oxygen bond requires a great deal of energy, very energetic processes are required. In an electric discharge through an oxygen stream, collisions occur between electrons and oxygen molecules. A certain fraction of these collisions occur when the electrons have sufficient kinetic energy to dissociate the oxygen molecule:

$$O_2 + e^- \rightarrow 2[O] + e^- \tag{1}$$

Each of the oxygen atoms may subsequently form a molecule of ozone:

$$[O] + 2O_2 \rightarrow O_3 + O_2 \tag{2}$$

Collisions capable of dissociating oxygen molecules also occur when oxygen is bombarded with a high-speed α- or β-particles coming from radioactive processes or with the cathode rays brought out through the thin metal foil window of a Coolidge X-ray tube. The dissociation of oxygen, with subsequent formation of ozone, may also be brought about by the absorption of ultraviolet (UV; 150–190 nm) or γ-radiation, or even thermal dissociation. For instance, if oxygen that has just been heated to a very high temperature (>3000°C) is suddenly quenched with liquid oxygen, a certain amount of ozone is found.

The energetic processes necessary for producing ozone molecules are also capable of destroying them. Ozone can be dissociated according to Eq. (3):

$$O_3 \rightarrow O_2 + [O] \tag{3}$$

This would not matter, of course, if this reaction is always formed as in Eq. (2). Unfortunately there is another reaction:

$$[O] + O_3 \rightarrow 2O_2 \tag{4}$$

The higher the ozone concentration, the higher the rate for ozone destruction. Therefore, whatever may be the method that is used for producing ozone, the concentration cannot be increased beyond the limiting value, at which the rates of formation and destruction are equal.

Ozone can also be made from water by electrolysis. Under special conditions (high current density, low temperature, adding the correct amount of sulfuric or perchloric acid to the water, and so on) the anode gases might consist of a mixture of oxygen and ozone. The reaction, which is shown in Eq. (5), is more endothermic (207.5 kcal) than the reaction shown in Eq. (6) (34.1 kcal), therefore, it is difficult to carry out and poor ozone yields are usually obtained:

$$3H_2O \rightarrow O_3 + 3H_2 \tag{5}$$

$$3O_2 \rightarrow 2O_3 \tag{6}$$
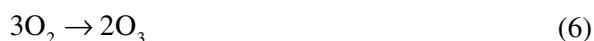
The yields and maximum concentrations attainable by these different processes vary considerably, as seen in Table 9. It should be noted that maximum energy yields could only be obtained by operating ozone generation at much less than the maximum ozone concentrations.

3.2. Generation of Ozone

The two technologies for generating ozone that have found practical application are the silent electric discharge and the photochemical methods. The latter is only used where small quantities of ozone and very low concentrations are desired. Practically, the electric discharge method is used for all other laboratory and industrial applications.

The instability of ozone with respect to decomposition back to oxygen dictates the need for an on-site production facility. This in turn dictates the need for a cost efficient, space efficient, low maintenance installation, if ozone is to be applied in wastewater and/or sludge treatment applications. In recent years, great strides have been taken in providing equipment and technology for such installations (27–30).

Table 9
Energy Yield and Maximum Ozone Concentration Attainable
by Various Generation Methods

Methods	Energy yield (g/kWh)	Ozone concentration
Electric discharge in oxygen	Up to 150	Up to 6 vol %
Electrolysis of water	Up to 12	Up to 20%
Photochemical		
1850–2537 Å	Up to 25	Up to 0.25%
1400–1700 Å		Up to 3.5%
Radiochemical		
Using O_2 gas	220	60 ppm
Using liquid O_2	108	5 mole %
Thermal	56	0.33 mole %
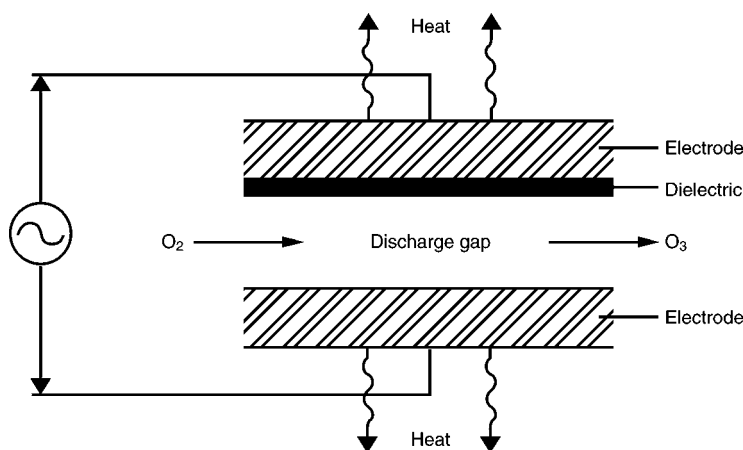
Fig. 8. Cross-section view of principal elements of a corona discharge ozone generator (*Source:* US EPA).

Figure 8 shows the principal elements of a corona discharge ozone generator (31,32). A pair of large-area electrodes is separated by a dielectric about 1–3 mm in thickness and an air discharge gap approx 3-mm wide. When an alternating current (AC) is applied across the discharge gap with voltages between 5 and 25 kV in the presence of an oxygen-containing gas, a portion of the oxygen is converted to ozone.

The excitation and acceleration of stray electrons within the high-voltage AC field cause the electrons to be attracted first to one electrode and then to the other. At sufficient velocity, these electrons split some oxygen molecules into free-radical oxygen atoms, as shown in Eq. (1). The free radical oxygen atoms then combine with other oxygen molecules to form ozone according to Eq. (2).

The decomposition of ozone back to oxygen as shown in Eq. (3) is accelerated with increasing temperature and moisture so that all generators must have a cooling device for heat removal and a drying device for moisture removal from the feed gas. For

Otto Plate Type Generator Unit

Glass dielectrics

Air Air

Discharge gap

Water cooled aluminum
block ground electrode

O_3

Air Air

Stainless steel high
voltage electrode

Tube Type Generator Unit

Water cooled stainless
steel ground electrode

A

High voltage
electrode

Discharge
gap

A

O_2 O_3

Glass tube
dielectric

O_2 O_3

Section "A-A"

Lowther Plate Generator Unit

High voltage
steel electrode

Ground steel
electrode

A

Glass separator

Aluminum heat
dissipator

O_3

Discharge gap

Ceramic dielectric
coated steel
electrode

O_2

Ceramic Dielectric

Glass separator

A

Section "A-A"

Fig. 9. Types of ozone generators.

optimization of ozone generation, the following practical engineering requirements should be met:

a. For prevention of ozone decomposition, heat removal should be as efficient as possible.
b. For dielectric material and electrode protection, the gap should be constructed so that the voltage can be kept relatively low, while maintaining reasonable operating pressures.

Table 10
Comparison of Conventional Ozone Generators (Ozonators)

Typical ozonator operating characteristics	Type of ozonator		
	Otto	Tube	Lowther
Feed	Air	Air, oxygen	Air, oxygen
Dew point of feed (°F)	−60	−60	−40
Cooling	Water	Water	Air
Pressure	0	3–15	1–12
Discharge gap (in.)	0.125	0.10	0.05
Voltage (kV peak)	7.5–20	15–19	8–10
Frequency (Hz)	50–500	60	2000
Dielectric thickness (in.)	0.12–0.19	0.10	0.02
Power requirements[a]			
Air feed	10.2	7.5–10	6.3–8.8
Oxygen feed	–	3.75–5	2.5–3.5

[a]kWh/lb of ozone at 1% conc.

c. For high-yield efficiency, a thin dielectric material with a high dielectric constant, such as glass, should be used.
d. For prolonged generator life and reduced maintenance problems, high frequency AC should be used. High frequency is less damaging to the dielectric surfaces than high voltage.

There are three basic types of commercial ozone generators (*see* Fig. 9). The characteristics and power requirements for the generators are given in Table 10. In addition to the generator's ozone yield per unit area of electrode surface, the concentration of ozone from the generator is regulated by:

a. Adjusting the flow rate of feed gas,
b. Adjusting the voltage across the electrodes, and/or
c. Selecting a suitable feed gas.

For economic reasons, it is advisable to feed oxygen or oxygen-enriched air (instead of ordinary air) to the ozone generators. However, for an electronic ozone generator using the latest semiconductors for power generation and titanium oxide ceramic electrodes for ozone generation, feeding ordinary air is common. This type of generator can deliver an ozone concentration of 2% by weight from predried air at 4.5 kWh per pound of ozone. This new ozone generation technology renders the cost of ozonation competitive with the cost of chlorine oxidation. Table 11 represents some comparative data in ozone technology. It is important to recognize that the low operating voltage (6.5 kV) of the titanium oxide ceramic electrode ensures longer life and minimum maintenance.

4. REQUIREMENTS FOR OZONATION EQUIPMENT

Basically, an ozonation system consists of (33):

a. Feed gas equipment.
b. Ozone generators.
c. Ozone contactors.

Table 11
Comparative Data in Ozone Technology

Electronic ozone generators	Conventional ozone generators
I. Air preparation: Oilless compressor and heatless air dryer Dryness of air: −60°F dew point Ozone production in relation to dryness of air: 98%	I. Air preparation: Refrigerated Dryness of air: −60 to −40°F dew point Ozone production in relation to dryness of air: 70–85%
II. Air requirements per lb of ozone: 10.69 scfm at 80 psi	II. Air requirements per lb of ozone: 20 scfm
III. Power requirements per lb of ozone: 4.035 kWh	III. Power requirements per lb of ozone: 10–12 kWh
IV. Energy saving per lb of ozone: Air: 2.13 kWh Power: 6.965 kWh Total: 9.095 kWh	IV.
V. Ozone concentration from predried air: 1.6–2% by weight, which represents two to three times higher sterilizing and oxidative power as compared with 1%	V. Ozone concentration from predried air: Maximum of 1% on the average
VI. Ozone producing electrodes: Material: titanium oxide ceramic Dielectric strength: $e = 85$ Dielectric constant: >15 kV/mm	VI. Ozone producing electrodes: Material: glass Dielectric strength: $e = 25$ Dielectric constant: <10 kV/mm
VII. Operating voltage: 6500 V	VII. Operating voltage: 12–16,000 V on the average
VIII. Probable failure in relationship to high voltage: 0.35%	VIII. Probable failure in relationship to high voltage: 8%
IX. Physical size of ozone generator: 19 lbs/d 30 ft³ Weight: 330 lbs	IX. Physical size of ozone generator: 19 lbs/d 60 ft³ Weight: 2000 lbs

Source: US Ozonair Corp.

4.1. Feed Gas Equipment

Conventional ozone generators are fed either with predried air or pure oxygen. The reason for the use of pure oxygen is primarily to increase the ozone concentration from 1 to 2% by weight. This factor represents a 2–3 times higher sterilizing and oxidative power. Because new electronic generators do not have any appreciable gain when fed with pure oxygen, it is therefore recommended that only predried air should be used.

For air preparation, equipments are required for air compression, air filtration, and air-drying:

a. **Air compression.** Oil-free compressor should be specified. More than 15 hp screw-type compressors are recommended owing to their extended life. The compressor rating should be up to 100 psi.

b. **Air filtration.** Prefilter, after-filter, and after-cooler are integral parts to be supplied and mounted on the compressor. Smaller size compressors up to 5 hp are mounted on air receiver tanks of appropriate size.

c. **Air drying.** Predried air at −60°F dew point is required in order to deliver 98% of the rated ozone capacity. Refrigerated or heated air dryers are capable of delivering a maximum of −50°F dew point and they are subject to failure. Only heatless air dryers should be specified. A pressure regulator is required to control an appropriate pressure for the ozone generator in 10–20 psi range. A moisture indicator (colometric) should be mounted after the air dryer. The required amount of air is usually based on a maximum flow rate of 10.7 ft^3/min/lb of produced ozone.

4.2. Ozone Generators

Previously, the specifications called for conventional ozone generators to have glass electrodes with transformers rated at 16,000 V. Many design engineers have specified two identical ozone generators (one as standby) especially for larger installations. New ozone generators are being designed for a constant ozone production and constant ozone concentration. Independently wired modules control the ozone output. The specifications are currently written along the following lines (34–36):

a. **Ozone generator.** The capacity is specified as weight of ozone per unit time such as lb/h or lb/d (kg/h or kg/d).
b. **Ozone concentration from predried air.** Minimum 1.6% by weight.
c. **Air requirements at –60°F dew point.** Maximum 10.7 ft^3/min/lb of ozone. Air pressure supplied to generator is 15 psi.
d. **Overall design.** Modular. Each module wired and controlled from the front panel or by remote control.
e. **Power consumption.** Not more than 4.5 kWh/pound of ozone produced.
f. **Power requirements.** 220 V AC, 50 or 60 cycles.
g. **Operating voltage.** Maximum 7 kV.
h. **Control.** Front panel pushbuttons (Start/Stop), power indicating light, airflow meter, DC ammeter, and AC voltmeter.
i. **Ozone resistant materials.** All parts, components, tubing, and piping that are in direct contact with ozone should be ozone resistant materials.

4.3. Ozone Contactors

It is essential to have efficient mass transfer of ozone into the liquid. The widely used diffuser system can transfer a maximum of 65–70% of the ozone into solution. The balance ozone (30–35%) is collected as an exhaust gas and burned. Several recently developed ozone contactors are being marketed with ozone transfer efficiency of more than 95% (37,38).

a. **In-line contactor for water treatment (Fig. 10).** The in-line contactor consists of Venturi-type ejector and two or more built-in static mixers. It is mounted directly in the water supply line. One or several contactors may be used and grouped into a single manifold. The maximum diameter of the contactor is 3 in. with a minimum of 40 ft of pipe run after the contactor. A minimum water pressure of 30 psi is required upstream of the contactor in order to balance the 40% pressure loss within the contactor. Depending on the degree of contamination, it is possible in some instances that only part of the flow can be supersaturated with dissolved ozone and then it is mixed with the untreated water flow.
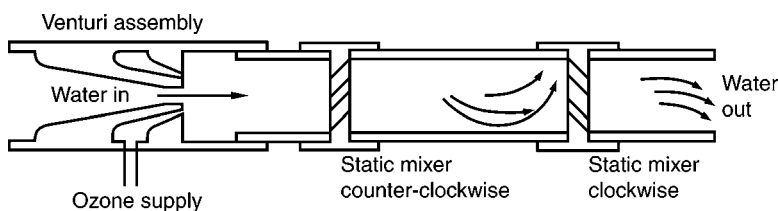
Fig. 10. In-line ozone contactor.
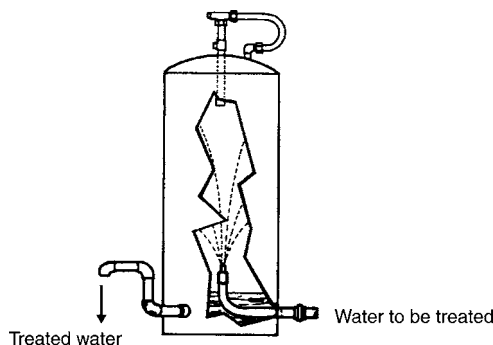
Fig. 11. FLPC ozone contactor.
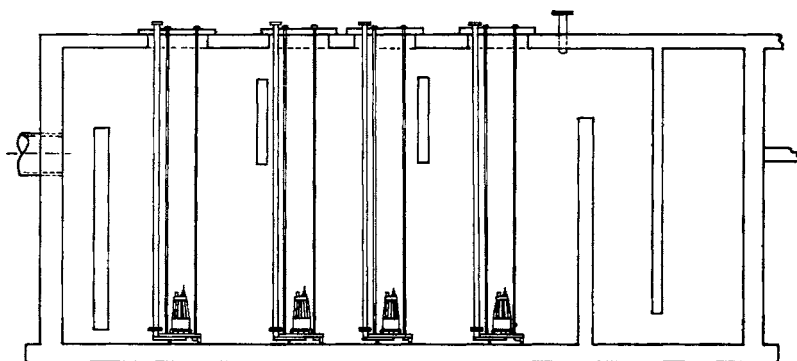
Fig. 12. Multicompartment turbine ozone contactor.

b. **Film layer purifying chamber (FLPC) contactor for water treatment (Fig. 11).** The basic principle is the reverse of bubbling. Contaminated water is emulsified (sprayed) into a powerful ozone concentration. The net result indicates that about 1.5 mg/L of ozone is dissolved instantly in the water (compared with 0.5 mg/L concentration in ozone bubbling). Under an influent water pressure of 30 psi, FLPC-treated water is discharged under gravity with a subsequent retention period of 2–4 min in the tank.

c. **Turbine contactor for wastewater treatment (Fig. 12).** The turbine contactor is used for wastewater treatment, where the ozone contact time has to be extended. Mass transfer of 10–12 lb of oxygen per horsepower as compared with 2–3 lb with an average aerator. At this stage ozone transfer of 99–100% can be achieved. For efficient wastewater treatment depending on the effluent contamination and the flow, one to four turbines may be used in
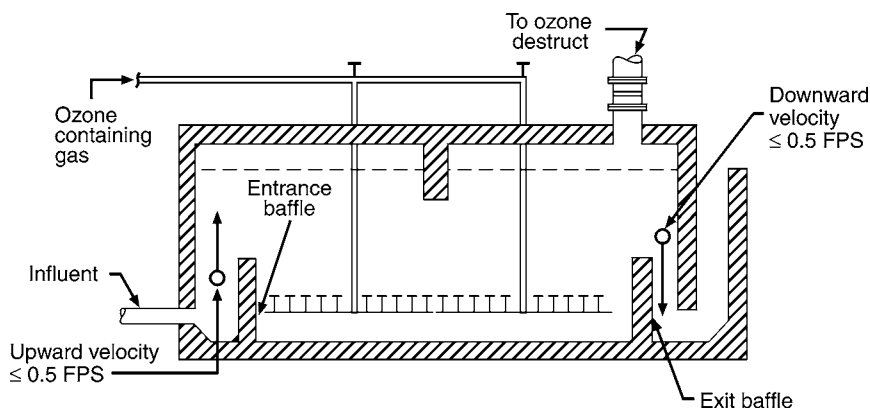
Fig. 13. Diffuser ozone contactor.

an oxidation ditch. Approximately more than 20% treatment effect will be obtained in a multicompartment contactor, where the effluent is introduced into fresh ozone residual, compared with treating the effluent in single compartment.

d. **Diffuser contactor for water and wastewater treatment (Fig. 13).** Disinfection and some chemical oxidation processes are mass-transfer-rate limited, whereas others are chemical-reaction-rate limited. Diffuser contactors are designed as a part of an overall system to optimize the tradeoffs between ozone transfer and the contact time required for achieving a specific treatment objective. Systems are designed for a minimum ozone transfer of 90% and a typical disinfection contact time of 15 min. Both the influent upward velocity and the effluent downward velocity should be ≤0.5 ft/s. Extensive pilot plant and modeling studies, considering such factors as diffuser type, size and porosity, and arrangement in relation to mass transfer, mixing, baffling, wall effects, and materials of construction, have led to the currently recommended designs.

e. **Hyperbaric vessel for both wastewater and sludge treatment (Fig. 14).** This innovative ozone–oxygen contactor is a combination of conventional diffuser contactor, FPLC contactor, and turbine contactor. It is an advanced contactor, which is suitable for wastewater effluent and sludge treatment. Oxygen is first pumped into the hyperbaric vessel until a pressure of 40 psig is reached. Ozone is then pumped into a small compartment in the reactor through a gas diffuser, eventually making its way into the second main compartment of the reactor. Part of the wastewater or sludge is recycled by a recirculation pump and emulsified (sprayed) into the powerful ozone–oxygen concentration zone near the top of the reactor with the aid of a comminutor. A film layer is thus created for efficient gas transfer.

5. PROPERTIES OF OZONE

Ozone is an unstable, colorless gas, and condenses as a dark blue liquid. It has a characteristic odor and the name is derived from the Greek word "ozein," which means to smell. The odor of ozone in the vicinity of an electrical machine is well known. It is generally encountered as a mixture of air or oxygen in a dilute form. Ozone is formed photochemically in the earth's stratosphere but, at ground levels, it exists only at large dilution. It is commercially produced in the form of electric discharge from air or oxygen. It is a potent germicide and powerful oxidant in both inorganic and organic reactions. With unsaturated organic compounds ozone adds the carbon–carbon double bond, forming ozonides. Decomposition of these ozonides always results in cleavage at the
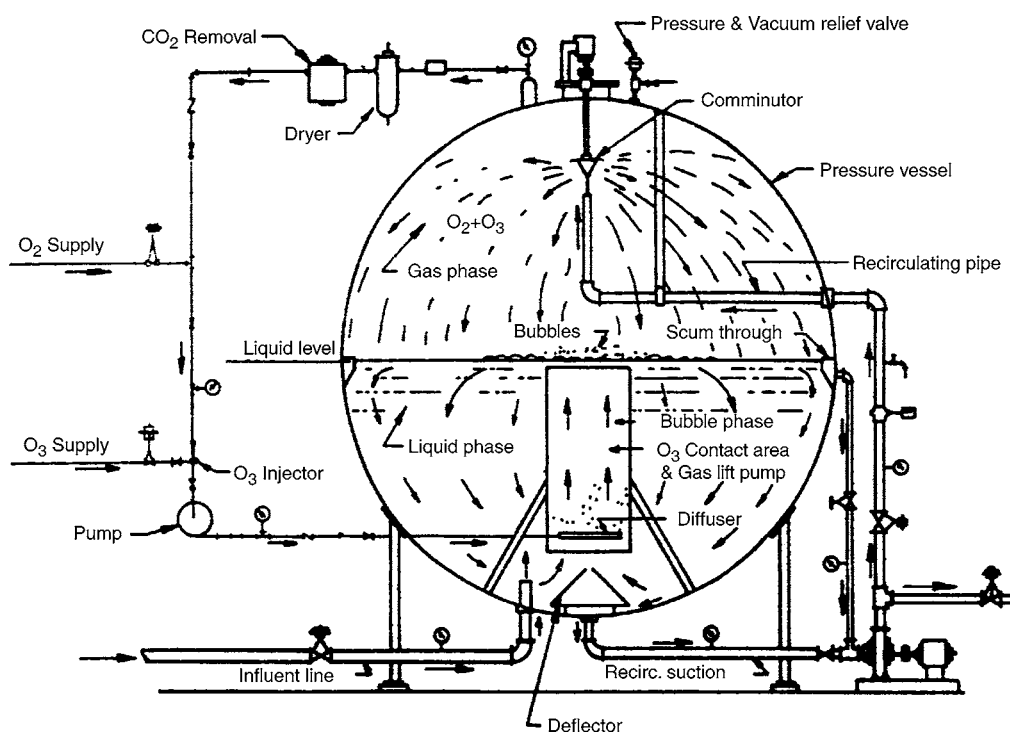
Fig. 14. Pressurized oxygen–ozone contactor (hyperbaric reactor vessel).

double bond, a property that has been used for structural analysis and in the commercial preparation of chemicals.

Ozone is normally produced at ordinary temperatures and concentrations. The color is not noticeable unless the gas is viewed through considerable depth. Ozone condenses as a dark blue liquid at −112°C. When the concentrations of ozone–oxygen mixtures are more than 20%, liquid ozone is easily exploded in either the liquid or vapor state. Explosions may be initiated by minute amounts of catalysts or organic matter, shocks, electric sparks, sudden changes in temperature or pressure, and so on.

Ozone has strong absorption bands in the infrared, the visible, and the UV. The maximum absorption is at 253.7 nm and it is particularly strong and affords a convenient means of measuring ozone concentrations in the stratosphere, in the laboratory, and in industrial situations. Other properties of ozone are given in Table 12.

Liquid ozone is reported to be miscible in all proportions with the following liquids: $CClF_3$, CCl_2F_2, CH_4, CO, F_2, NF_2, and OF_2. It forms two-layer systems with the following liquids: CF_4, N_2, and O_2; and ozone solutions in $CClF_3$ (approx 105 g/L) has been prepared commercially in small cylinders. It is necessary to refrigerate these cylinders (−75°C) to minimize the decomposition of ozone at higher temperatures.

The limited miscibility of ozone in oxygen is of practical importance because of the dense, oxygen-rich layer, which settles at the bottom and easily explodes. The mutual solubility of the two liquids decreases when the temperature is reduced. Thus, liquid ozone and oxygen are completely miscible at more than 93.2 K (at which temperature, the total

Table 12
Properties of Pure Ozone

Parameters		Data
Melting point (°C)		-192.5 ± 0.4
Boiling point (°C)		-111.9 ± 0.3
Critical temperature (°C)		-12.1
Critical pressure (atm)		54.6
Critical volume (cm³/mole)		111
Density and vapor pressure of liquid		
Temperature (°C)	*Density (g/cm³)*	*Vapor pressure (Torr)*
-183	1.574	0.11
-180	1.566	0.21
-170	1.535	1.41
-160	1.504	6.73
-150	1.473	24.8
-140	1.442	74.2
-130	1.410	190
-120	1.378	427
-110	1.347	865
-100	1.316	1605
Density of solid ozone (g/cm³) at 77.4 K		1.728
Viscosity of liquid (cP) at 77.6 K		4.17
at 90.2 K		1.56
Surface tension (dyn-cm) at 77.2 K		43.8
at 90.2 K		38.4
Parachor[a] at 90.2 K		75.7
Dielectric constant (liquid) at 90.2 K		4.79
Dipole moment, debye		0.55
Magnetic susceptibility (cgs units) gas		0.002×10^{-8}
Liquid		0.150
Heat capacity of liquid from 90 to 150 K		$C_p = 0.425 +$
		$0.0014(T-90)$
Heat of vaporization, (kcal/mole),		
at -111.9°C		3410
at -183°C		3650
Heat and free energy of formation	ΔH_f *(kcal/mole)*	ΔG_f *(kcal/mole)*
Gas at 298.15 K	34.15	38.89
Liquid at 90.15 K	30	–
Hypothetical gas at 0 K	34.74	–

[a]$M\gamma^{1/4}(D–d)$, where M, molecular weight; γ, surface tension; D, liquid density; d, vapor density.

pressure is 1.25 atm) but at 90.2 K (the atmospheric-pressure boiling point of liquid O_2), there is a separation into two layers, containing 17.6 and 67.2 mole percent ozone, respectively. At still lower temperatures the separation becomes even more pronounced.

Ozone gas is sparingly soluble in water and, especially at low temperatures, more sparingly soluble in other liquids. The solubility of ozone in water is given in Table 13.

Table 13
Solubility of Ozone in Water

Temperature (°C)	Bunsen coefficient	Henry's law coefficient (H × 10⁻⁴)
0	0.49	3.95
5	0.44	3.55
10	0.375	3
20	0.285	2.29
30	0.20	1.61
40	0.145	1.17
50	0.105	0.85
60	0.08	0.64

$$B = \frac{\text{Ozone concentration in liquid}}{\text{Ozone concentration in gas, reduced to STP}} \tag{7}$$

where B = Bunsen coefficient of solubility; H = Henry's constant, mole/atm (mole fraction of ozone in solution/partial pressure of ozone in gas, in atm).

The preparation of saturated ozone solutions is difficult to achieve because of the great tendency of ozone to react or to undergo decomposition. The thermal decomposition of ozone has been extensively studied in the temperature range 80–500°C. The mechanism is as shown in Eqs. (8)–(10).

$$O_2 + [O] + M \rightleftharpoons O_3 + M \tag{8,9}$$

$$[O] + O_3 \rightarrow 2O_2 \tag{10}$$

where M is a third element, O_2, O_3, N_2, He, or whatever is present. This leads to the rate expression as shown in Eq. (11).

$$-d(O_3)/dt = 2k_1k_3(O_3)^2/k_2O_2 \tag{11}$$

where k_1, k_2, and k_3 are the rate constants. Because the thermal decomposition of ozone is not a first-order process, the half-life of the ozone varies inversely with its initial concentration and directly with the oxygen concentration. Typical values are given in Table 14 (39).

Numerous substances can catalyze the decomposition of ozone. The reaction with N_2O_5 proceeds according to the mechanism as shown in Eqs. (12)–(15).

$$N_2O_5 \rightarrow NO_2 + NO_3 \tag{12}$$

$$NO_2 + NO_3 \rightarrow N_2O_5 \tag{13}$$

$$NO_2 + O_3 \rightarrow NO_3 + O_2 \tag{14}$$

$$NO_3 + NO_2 \rightarrow 2NO_2 + 0.5O_2 \tag{15}$$
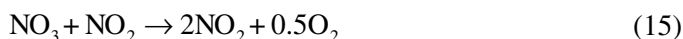
Table 14
Uncatalyzed Thermal Decomposition of Ozone in Ozone–Oxygen Mixtures[a]

Temp (°C)	$\dfrac{k_2}{2k_1 k_3}$	Half-life for indicated initial conc.[b]			
		Wt%: 5	2	1	0.5
		Vol%: 3.333	1.333	0.667	0.333
120	22.4	11.2[c]	28[c]	56[c]	112[c]
150	1.40	41.8	104.5	209	418
200	0.030	0.9	2.2	4.5	9
250	0.00133	0.04	0.10	0.20	0.40

[a]*See* ref. 39.
[b]Half-life = $(k_2/2k_1 k_3)$ $(100/\text{vol\% } O_3)$ in seconds.
[c]In minutes.

N_2O_5 is regenerated as long as any ozone remains, so that the net effect is the decomposition of ozone. This process was studied at 20°C and 400°C, because air always contains traces of N_2O_5 and may be of some importance in the case of ozone generated from air.

At room temperature, the decomposition of ozone apparently depends on surface reactions. A half-life of 20–100 h might be expected in clean vessels of glass, stainless steel, or other inert materials. Many solids catalyze the decomposition of ozone. The activity of such catalysts depends on subdivision, crystal structure, presence or absence of moisture, and so on. Preparations of iron oxide have been made that are extremely active in decomposing ozone.

In aqueous solutions, the decomposition of ozone is much more rapid than in the gaseous state. It is catalyzed by the hydroxyl ion. The initial reaction is shown in Eq. (16):

$$O_3 + OH^- \rightarrow O_2 + [HO_2] \tag{16}$$

followed by the reactions shown in Eqs. (17)–(20).

$$O_3 + [HO_2] \rightarrow 2O_2 + OH^- \tag{17}$$

$$O_3 + OH^- \rightarrow O_2 + [HO_2] \tag{18}$$

$$2[HO_2] \rightarrow O_3 + H_2O \tag{19}$$

$$[HO_2] + [HO] \rightarrow O_2 + H_2O \tag{20}$$

Ozone is more soluble in water than is oxygen, but because of a much lower available partial pressure, it is difficult to obtain a concentration of more than a few milligrams per liter under normal conditions of temperature and pressure. A comparison of the solubilities of ozone, chlorine, and oxygen by water temperature and gas concentration are represented in Table 15. A mathematical model describing DO concentration can be found elsewhere (40). The DO concentration is a function of water temperature, pressure, and chloride concentration.

In 1981, Hill et al. (41) performed ozone absorption in a pressurized bubble column (7.7 m tall and 5.25 cm inside diameter), which was operated in a semibatch mode with

Table 15
Comparison of the Solubilities of Ozone, Chlorine, and Oxygen

Gas	Solubility by water temperature (mg/L)			
	0°C	10°C	20°C	30°C
Oxygen				
At 100%	70.5	54.9	44.9	38.2
At 21%	14.8	11.5	9.4	8
Ozone				
At 100%	1374.3	1114.9	789	499.6
At 4%	55	44.6	31.6	20
Chlorine				
At 100%	14,816.5	9963.4	7263.6	5688.8
At 99.8%	14,789.4	9943.5	7249.1	5677.4

gas pressures up to 791 kPa (100 psig) and water temperatures ranging from 20 to 40°C. Also in 1981, Roth and Sullivan (42) reviewed and investigated the solubility of ozone in water under various pH values and water temperatures. Their reviewed data are presented in Table 16 and Eq. (21) is a mathematical model fitting their experimental data:

$$H = 3.84 \times 10^7 [OH^-]^{0.035} \exp(-2428/T) \tag{21}$$

where H is the Henry's Law constant (atm/mole fraction of ozone); $[OH^-]$ is the hydroxide concentration (g mole/L); T is the temperature (K).

Ozone apparently decomposes in water, but this is probably as a result of its strong oxidizing ability rather than simple decomposition. Ozone is much more soluble in acetic acid, acetic anhydride, dichloroacetic acid, chloroform, and carbon tetrachloride than in water. More technical information on ozonation can be found elsewhere (43–62).

It should be noted that HO_2 and HO in Eqs. (16)–(20) are free radicals, which are formed when ozone decomposes in aqueous solutions. The two free radicals have great oxidizing power, and in addition to disappearing rapidly as shown in Eq. (20), might react with impurities or pollutions present in solution, such as metal salts, organic substance, hydrogen, hydroxide ions, and so on. It is believed that the free radicals formed by the decomposition of ozone in water are the principal reacting species (58).

6. DISINFECTION BY OZONE

Smith and Bodkin (43) compared the bactericidal action of ozone and chlorine at varying values of pH. Ozone was much more as effective as chlorine over a wide pH range. At a temperature of 27.5°C and pH 5.0 and 6.0, ozone affected the sterility of a 1-L sample containing 8×10^5 bacteria/mL in 5 min. At pH 7.0, 8.0, and 9.0 the sterilization time was 7.5 min. The ozone concentration varied from 0.13 to 0.20 mg/L. In contrast, the concentration of chlorine required to sterilize as rapidly as ozone varied from 2.7 mg/L at pH 5.0 to 7.9 mg/L at pH 8.0.

Leiguarda et al. (44) presented a detailed account of the bactericidal action of ozone in both pure and river waters. Varying amounts of ozone were added to pure water free from ozone demand, and the water was inoculated with dilute suspensions of *Escherichia coli* or *Clostridium perfringens*. Samples were taken at various time intervals to determine the

Table 16
Ozone Solubility in Water[a]

Investigator	Temperature (°C)	H (atm/mole fraction)
Kawamura (1932)	5	2880
	10	3400
	20	4610
	30	6910
	40	9520
	50	13,390
	60	18,980
Kawamura (1932)		
7.57 N H_2SO_4	20	7420
2.02 N H_2SO_4	20	5810
1.01 N H_2SO_4	20	5350
0.18 N H_2SO_4	20	4770
0.11 N H_2SO_4	20	4770
Kirk-Othmer (1967)	0	2530
	5	2820
	10	3330
	20	4370
	30	6210
	40	8550
	50	11,770
Li (1977)		
pH 2.2	25	7840
pH 4.1	25	7600
pH 6.15	25	9000
pH 7.1	25	9400

[a]*See* ref. 42.
See refs. 108–111.

concentration of ozone and the number of bacteria present. The effects of temperature and pH on bactericidal action were also investigated. The results indicated that initially 10^4 *E. coli*/mL and 0.12 mg/L ozone were contained in water at pH 6.0 and maintained at a temperature of 10°C. No viable bacteria were found after 5 min and the ozone content had reduced to 0.09 mg/L. At pH 8.0 and higher temperatures, the efficiency was not significantly affected by temperature but was slightly more at pH 6.0 than at pH 8.0. In addition, tests were made on the effects of ozone on the naturally occurring bacterial flora of river water. The demand of ozone in this water was high and tests were made using 1–6 mg/L of ozone. There were sizable reductions in the number of bacteria even when the amount of ozone added was insufficient to satisfy the ozone demand of the water. All organisms were destroyed in the presence of 0.08 mg/L residual ozone after a contact period of 5 min. Similar results were obtained in experiments with river water samples that were coagulated, settled, and subsequently inoculated with *E. coli*. A total reduction of vegetative forms of *C. perfringens* occurred within 5 min when 0.12 mg/L ozone was initially added to water containing 1.4×10^4 bacteria/mL. In water containing *C. perfringens* in concentrations of 2×10^3 spores/mL, at a pH of 6.0 and maintained at a temperature of

24°C, no viable spores were found after a contact period of 15 min with 0.25 mg/L of ozone, or after 2 min with 5 mg/L. At pH 8.0, bactericidal efficiency was reduced. Spores were not affected by 0.25 mg/L of ozone even after 120 min.

In a symposium on the sterilization of water, Whitson (45) reported that ozonation affected the removal of microorganism and improved water filterability, color, taste, and odor. Bernier (46), while comparing the bactericidal efficiencies of chlorine and ozone, asserted that ozone was far superior disinfectant, being considerably faster than chlorine and not as notably affected by external factors such as pH and temperature.

Bringman (47) observed that 0.1 mg/L of active chlorine required 4 h to destroy 6×10^4 *E. coli* cells in water, whereas 0.1 mg/L of ozone required only 5 s. When the temperature was raised from 22 to 37°C, the ozone inactivation time decreased from 5 to 0.5 s. Wuhrmann and Meyrath (48) carried an investigation on the kinetics of ozone disinfection. During each experiment, the ozone concentration was kept constant by continuously bubbling air–ozone through the test solution. The results indicated that ozone disinfection was mainly a function of contact time, ozone concentration, and water temperature. These investigations revealed that the contact time with ozone was necessary for 99% destruction of *E. coli*, which was only one-seventh when observed with the same concentration of hypochlorous acid. The death rate for spores of *Bacillus* spp. was about 300 times more with ozone than with chlorine.

Hann (49) presented a detailed review of the differences between chlorination and ozonation as determined by other workers. It is reported that ozone disinfection was found to be more expensive. Turbidity interfered with its use and organic demand had to be satisfied before germicidal action was effective.

Based on experimental data Scott and Lesher (50) postulated a mode of action of ozone on *E. coli*. The primary attack of ozone was thought to be on the cell wall or the membrane of bacteria. The reaction is probably with the double bonds of lipids and that cell lysis depended on the extent of that reaction. Bringman (47) reported that the mode of action of ozone differed from that of chlorine. It was concluded that chlorine selectively attacked and destroyed certain enzymes, whereas ozone acted as a general protoplasmic oxidant. Christensen and Giese (51) suggested that the primary locus of activity of ozone was the bacterial cell surface. Barron (52) hypothesized that the primary bactericidal activity of ozone was the oxidation of sulfhydryl groups on enzymes. Murray and co-workers (53) at the University of Western Ontario recognized that the outermost layer of Gram-negative organisms is a lipoprotein followed by a lipopolysaccharide layer. It was surmised that these layers would be the first subject to be attacked by ozone. They also concluded that the attack by ozone on the cell wall results in a change in cell permeability eventually leading to lysis.

Smith (54) stated that under experimental conditions, where there were <1% survivors of *E. coli* and *Streptococcus faecalis* after 60-s exposure to 0.8 mg/L ozone, the unsaturated fatty acids (mainly C_{16} and C_{18} monoenoic acids) of the cell lipids were oxidized in the same time interval. The lipids present in bacteria are largely confined to the cytoplasmic membrane. Thus, the mechanism of disinfection of ozone is still open to question.

At the Eastern Sewage Works in the London Borough of Redbridge, Boucher and his associates (55,56) conducted experiments on microstraining and ozonation of wastewater effluents. Using an ozone dose of 10–20 mg/L most organisms were killed, although a

sterile effluent was never obtained. Chlorine followed by ozone produced better results. In his conclusion, Boucher commented: "Chlorination as an additional treatment to ozonation has not produced any advantage except to destroy most of the few organisms that sometimes survive ozonation. This is not considered a sufficient advantage in view of its many known disadvantages for effluent treatment, namely, the production of chloro-derivatives, which may be toxic to fish and other aquatic life or, which may produce persistent tastes, difficult to remove by subsequent waterworks treatment, and the possibility of rapid after growth of microorganisms in a receiving river and all its attendant problems."

Huibers et al. (57) determined that ozone treatment of effluents from secondary wastewater treatment plants could provide product water, which is within the United States requirements for chemical and bacteriological quality of potable water. Virtually all color, odor, and turbidity were removed. Oxygen-consuming organic materials, measured as COD, were reduced to <15 mg/L. Bacteriological tests revealed that there were no more living organisms.

In Los Angeles County, CA, a well-oxidized secondary effluent was treated with ozone for disinfection (62). It was found that 50 mg/L of ozone was required to meet the California requirement of 2.2 total coliforms per 100 mL. To achieve the 200 counts of fecal coliform per 100 mL, the ozone requirement was 10 mg/L. It was also found that the removal of suspended solids to 1 mg/L greatly improved the efficiency of ozone treatment. This study further revealed that to achieve excellent disinfection, the COD should be <12 mg/L and the nitrite should be <0.15 mg/L. The minimum required ozonation contact time was reported to be 10 min.

The kinetics of disinfection has been investigated by Morris (63). His concept of the lethality coefficient for a given disinfectant is presented next:

$$L = \ln (l00)/CT = 4.61/CT \tag{22}$$

where L is the lethality coefficient, $(mg/L)^{-1}$ min^{-1}; C is the residual concentration of disinfectant (mg/L); T is the time in minutes for 99% microorganism destruction (2-log destruction).

Table 17 indicates the effectiveness of ozone for disinfection of various bacteria and viruses at pH 7.0 and temperature of 10–15°C. Table 18 further illustrates that in comparison with various forms of chlorine, ozone is a much more powerful disinfectant against enteric bacteria, amebic cysts, viruses, and spores by factors of 10–100. The disinfection efficiency of ozone does not seem to be affected significantly within the normal pH range of 6.0–8.5. Table 19 further presents the oxidation potentials of nine strong chemical disinfectants among which ozone has the highest oxidation potential. This makes ozone the strongest disinfectant as well as the strongest oxidizing agent. The exact effect of temperature on ozone disinfection is still unknown. However, it is known that higher the water temperature, lower the efficiency of ozone mass transfer, which might translate to lower disinfection efficiency.

In summation, the advantages of using ozone for disinfection include, but are not limited to:

a. Ozone is a better virucide than chlorine.
b. Ozone removes color, odor, and taste (such as phenolic compounds).
c. Ozone oxidizes iron, manganese sulfides, and so on.

Table 17
Relative Efficiency of Ozone Disinfection

Organism	L	C
Escherichia coli	500	0.001
Streptococcus faecalis	300	0.0015
Polio virus	50	0.01
Entamoeba histolytica	5	0.1
Bacillus megatherium (spores)	15	0.03
Mycobacterium tuberculosis	100	0.005

pH, 7.0; temperature, 10–15°C; *L*, lethality coefficient/ (mg/L)/min; *C*, residual concentration of disinfectant (mg/L).

Table 18
Comparison of Lethality Coefficients for Ozone and Chlorine

Agent	Enteric bacteria	Amoebic cysts	Viruses	Spores
O_3	500	0.5	5	2
HOC1 as Cl_2	20	0.05	1 up	0.05
OC1$^-$ as Cl_2	0.2	0.0005	0.02	0.0005
NH_2Cl as $C1_2$	0.1	0.02	0.005	0.001

Table 19
Oxidation Potential of Chemical Disinfectants

Disinfectants	Chemical reactions	Oxidation potentials (EV)
Ozone	$O_3 + 2H^+ + 2e^- \rightarrow O_2 + H_2O$	2.07
Permanganate	$MnO_4^- + 4H^+ + 3e^- \rightarrow MnO_2 + 2H_2O$	1.67
Hypobromous acid	$HOBr + H^+ + e^- \rightarrow 0.5Br_2 + H_2O$	1.59
Chlorine dioxide	$ClO_2 + e^- \rightarrow ClO_2^-$	1.50
Hypochlorous acid	$HOC1 + H^+ + 2e^- \rightarrow Cl^- + H_2O$	1.49
Hypoiodous acid	$HOI + H^+ + e^- \rightarrow 0.5I_2 + H_2O$	1.45
Chlorine gas	$Cl_2 + 2e^- \rightarrow 2Cl^-$	1.36
Bromine	$Br_2 + 2e^- \rightarrow 2Br^-$	1.09
Iodine	$I_2 + 2e^- \rightarrow 2I^-$	0.54

d. Ozone oxidizes organic impurities or pollutants in water.
e. Ozone increases the DO content in water or wastewater.

7. OXIDATION BY OZONE

7.1. Ozone Reaction with Inorganics

Potassium ozonide (KO_3), can be prepared at low temperatures by ozone treatment of dry KOH, the superoxide KO_2, or the metal itself dissolved in liquid ammonia as shown in Eqs. (23)–(25).

$$3O_3 + 3KOH \rightarrow KOH \cdot H_2O + 2O_2 + 2KO_3 \qquad (23)$$

$$O_3 + KO_2 \rightarrow O_2 + KO_3 \qquad (24)$$

$$O_3 + K \rightarrow KO_3 \qquad (25)$$
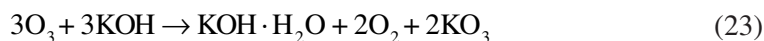
This reaction will not occur in an aqueous medium because KO_3 immediately decomposes in the presence of water, probably by the reactions shown in Eqs. (26a)–(26c):

$$KO_3 + H_2O \rightarrow K^+ + HO_3 + OH^- \qquad (26a)$$

$$HO_3 \rightarrow O_2 + [OH] \qquad (26b)$$

$$4[OH] \rightarrow 2H_2O + O_2 \qquad (26c)$$

The ozonides NaO_3 and $(CH_4)_4NO_3$ have also been prepared from ozone. However, they also would not be produced in an aqueous medium because of their decomposition in water, similar to that shown for KO_3. These ozonides are ionic crystals containing the O_3 ion.

The reaction of ozone with ammonia has been studied in the dry gaseous state, in liquid ammonia, in carbon tetrachloride solution, and in aqueous solution. The reaction is extremely fast and the end product is always ammonium nitrate. The reaction is shown in Eq. (27):

$$2NH_3 + 4O_3 \rightarrow NH_4NO_3 + 4O_2 + H_2O \qquad (27)$$
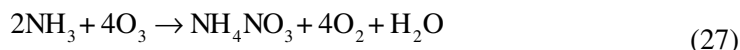
By carrying out the reaction at very low temperatures, the formation of the red ammonium ozonide, NH_4O_3, has been demonstrated. This compound decomposes rapidly to ammonium nitrate, oxygen, and water as shown in Eq. (28):

$$4NH_4O_3 \rightarrow 2NH_4NO_3 + O_2 + 4H_2O \qquad (28)$$
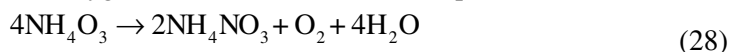
Ammonium salts do not react again with ozone.

The reaction of ozone with the lower oxides of nitrogen NO, NO_2, N_2O_3, and N_2O_4, is extremely rapid leading to the formation of nitrogen pentoxide, (N_2O_5), as shown in Eqs. (29)–(32):

$$2NO + O_3 \rightarrow N_2O_5 \qquad (29)$$

$$6NO_2 + O_3 \rightarrow 3N_2O_5 \qquad (30)$$

$$3N_2O_3 + 2O_3 \rightarrow 3N_2O_5 \qquad (31)$$

$$3N_2O_4 + O_3 \rightarrow 3N_2O_5 \qquad (32)$$

By the combined action of O_3, NO_2, and ClO_2 gases nitronium perchlorate (NO_2ClO_4) can be formed as shown in Eq. (33). This is a white solid with low vapor pressure and strong oxidizing properties:

$$3NO_2 + 3ClO_2 + 2O_3 \rightarrow 3NO_2ClO_4 \qquad (33)$$
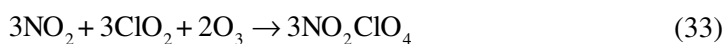
In aqueous solutions, nitrites are oxidized to nitrates as shown in Eq. (34):

$$O_3 + NO_2^- \rightarrow NO_3^- + O_2 \qquad (34)$$

This reaction has been used for the quantitative determination of ozone.

Ozone reacts rapidly with hydrogen sulfide (H_2S). In dry gas mixtures the only reaction product appears to be sulfur dioxide (SO_2), but the amount of ozone consumed per mole of H_2S has not yet been established with certainity. The reaction in water solution has not been adequately studied but there are reports that colloidal sulfur is among the products.

In the gas phase, ozone and SO_2 react slowly. In aqueous solutions, sulfates are produced. The reaction is pH dependent and complicated by induced oxidation of sulfites by oxygen, which is generally present along with the ozone. Thus, in sodium bisulfite solutions, ozone catalyzes the reaction between bisulfite and oxygen. As the dilution of ozone increases, this effect becomes more pronounced. In sufficiently diluted ozone, as many as 60 atoms of oxygen are consumed per molecule of ozone supplied. Similar observations have been made in the oxidation of aqueous SO_2 solutions.

Ozone liberates iodine (I_2) from iodide (I^-) solutions. The amount of iodine liberated per mole of ozone depends on the pH, concentration, temperature, and perhaps other factors. One mole of ozone liberates 1 mole of iodine, or its equivalent, in alkaline solutions; 1.1–1.3 moles of iodine at pH 7.0 and 2.5–3 moles of iodine in concentrated HI solutions. Ozone also oxidizes bromides to bromine (Br_2) as shown in Eq. (35):

$$O_3 + 2Br^- + H_2O \rightarrow Br_2 + 2OH^- + O_2 \tag{35}$$
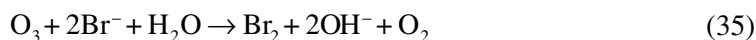
Chlorides are only oxidized in acid solutions and the reaction is quite slow.

Ozone oxidizes the cyanide ion (CN^-) to cyanate (CNO^-) as shown in Eq. (36). In the first stage of the reaction cyanate is oxidized further by ozone and converted to bicarbonate, nitrogen, and oxygen as shown in Eq. (37):

$$CN^- + O_3 \rightarrow CNO^- + O_2 \tag{36}$$

$$2CNO^- + 3O_3 + H_2O \rightarrow 2HCO^- + N_2 + 5O_2 \tag{37}$$
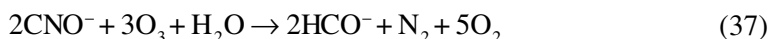
Thiocyanates (CNS^-) are oxidized to cyanide as indicated in Eq. (38):

$$CNS^- + 2O_3 + 2OH^- \rightarrow CN^- + SO_3^{2-} + 2O_2 + H_2O \tag{38}$$
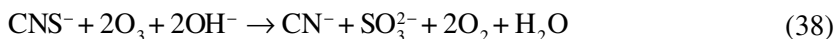
If the addition of ozone is continued, then the cyanide ion is oxidized to cyanate and the sulfite ion is oxidized to sulfate as shown in Eq. (39):

$$CN^- + SO_3^{2-} + 2O_3 \rightarrow CNO^- + SO_4^{2-} + 2O_2 \tag{39}$$
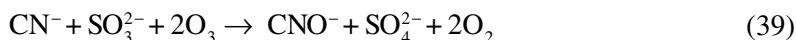
Finally the cyanate ion (CNO^-) can be oxidized to harmless bicarbonate, nitrogen, and oxygen according to Eq. (37):

Argentic (Ag^{2+}) salts can be produced by treating $AgNO_3$ solutions with ozone as shown in Eq. (40):

$$Ag^+ + 2O_3 \rightarrow Ag^{2+} + 3O_2 \tag{40}$$

Ferrous (Fe^{2+}) salts are oxidized to ferric (Fe^{3+}) salts. In dilute H_2SO_4 solution the reaction is as shown in Eq. (41):

$$2Fe^{2+} + O_3 + 2H^+ \rightarrow 2Fe^{3+} + O_2 + H_2O \tag{41}$$
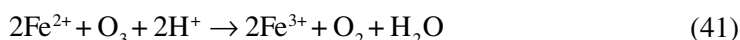
The reaction for the oxidation of ferrocyanide $Fe(CN)_6^{4-}$ to ferricyanide $Fe(CN)_6^{3-}$ proceeds according to Eq. (42). The engineering significance of this reaction is for its usefulness in the treatment of wastewater produced by the photoprocessing industry (32):

$$2Na_4Fe(CN)_6 \cdot 10H_2O + O_3 \rightarrow 2Na_3Fe(CN)_6 + O_2 + 9H_2O + 2NaOH \qquad (42)$$

This review of the reactions of ozone with inorganic pollutants in water and wastewater has failed to demonstrate that stable inorganic ozonides can be produced in aqueous solution. It is concluded that inorganic ozonides would not be a problem if ozone were used as the disinfectant for water or wastewater.

For practical water or wastewater treatment, ozone oxidizes inorganic impurities by straight chemical oxidation reaction. The examples are as follows:

a. Ozone reacts rapidly to oxidize ferrous ion (Fe^{2+}) into ferric ion (Fe^{3+}). Ferric ion can then be removed as insoluble ferric hydroxide at high pH or can coprecipitate with phosphate ion for both iron and phosphorus removals.
b. Ozone rapidly oxidizes manganous (Mn^{2+}) into insoluble manganese dioxide or soluble permangante (MnO_4^-). The permanganate is also an oxidizing agent. Stoichiometrically, 0.94 mg/L of potassium permanganate will further oxidize 1 mg/L of ferrous ion, or 1.92 mg/L of potassium permanganate will further oxidize 1 mg/L of manganous ion. Eventually, permanganate ion also converts into insoluble manganese dioxide in the aforementioned oxidation–reduction reaction.
c. Ozone can break down organometallic complexes of both iron and manganese, which usually defy the conventional oxidation processes for iron and manganese removal from potable water.
d. Ozone readily oxidizes sulfides and sulfites to stable sulfates and nitrites to stable nitrates.
e. Bromides and chlorides can be oxidized by ozone to bromine and chlorine, respectively, although these reactions are slow and dependent on the concentration of reactants.
d. The oxidation of iodides to iodine is the basis for the standard method used in the determination of ozone concentration (64).
e. The ammonium ion (NH_4^+) is apparently not attacked under normal pH values in wastewater treatment. So there is no wastage of ozone-oxidizing capacity with ammonia nitrogen, if present in a waste stream. However, ammonia is oxidized completely to nitrate by ozone if the wastewater pH is alkaline and remains as such. The molar ratio of ozone consumed per ammonia oxidized is about 12:1 (65).
f. In the process of treating photoprocessing water, silver is recovered electrolytically, and then the spent bleach baths of iron ferrocyanide complexes are ozonated. Ferrocyanide in the spent liquor is oxidized to ferricyanide, which is its original form. Thus the bleach is regenerated for reuse by the photoprocessor [*see* Eq. (42)].
g. Ozone may replace chlorine in the treatment of industrial wastewaters containing cyanide. Ozone oxidation takes place in multistages according to Eqs. (36–39). Ozonation of cyanide ions and dyes in aqueous solutions is documented in refs. 66,67.

7.2. *Ozone Reaction with Organic Material*

The exact mechanism for the chemical processes taking place when water or wastewater is subjected to treatment by ozone and oxygen is still under investigation. In general, part of ozone in the reactor oxidizes carbonaceous substances in water or wastewater, thus producing carbon dioxide and oxygen, as shown in Eq. (43):

$$2O_3 + C \text{ (organic)} \rightarrow CO_2 + 2O_2 \qquad (43)$$
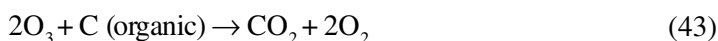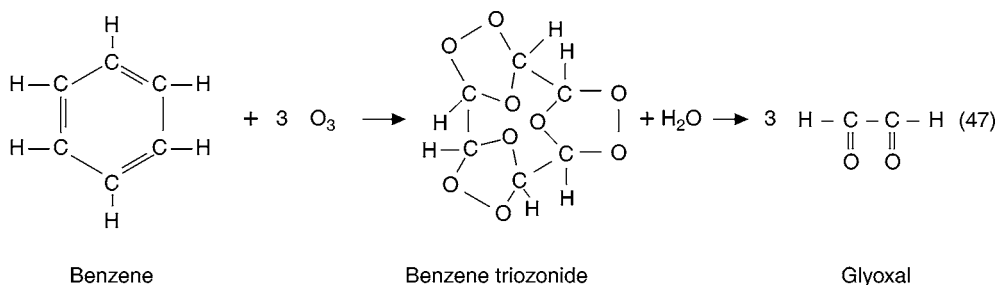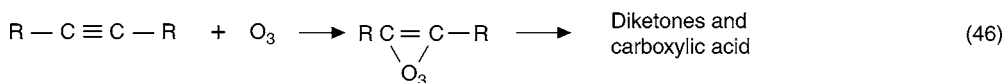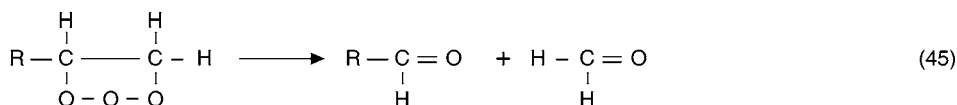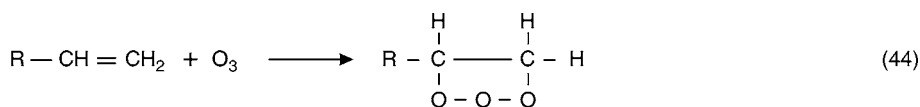
Fig. 15. Ozone reactions with organics Eqs. (44)–(47) (68).

The previous reaction is an oxidation reaction, and the carbon dioxide and oxygen are oxidation products. The remaining amount of available ozone reacts with organic substances yielding various intermediate and end products. The reaction is termed ozonolysis reaction and the end products are termed ozonolysis products.

In ozonolysis reactions, ozone reacts readily with unsaturated organic compounds, adding all its three oxygen atoms at a double bond or a triple bond. The resulting compounds are termed ozonides. Decomposition of ozonides generally results in a rupture at the position of the unsaturated bond, causing the formation of simpler organic substances, such as ketones, aldehydes, acids, and so on.

A typical reaction of ozone is its addition to the carbon–carbon bond of an ethylenic compound (68). This is illustrated by Eq. (44) in Fig. 15.

As previously discussed, the resulting ozone–olefin compound is known as an ozonide. Decomposition of the ozonide gives a mixture of oxygenated products containing carbonyl compounds. This is shown in Eq. (45) in Fig. 15. Ozonides are not isolated as such, because of their unstable and explosive nature, but are employed for the production of other chemical compounds. Useful products in good yields are obtained when the ozonides are reduced to produce carbonyl compounds or oxidized to produce carboxylic acids.

Ozone also adds to the carbon–carbon triple bond of acetylenic compounds, as shown in Eq. (46) of Fig. 15. Very few detailed studies of the reaction have been made. The usual products isolated are diketones and carboxylic acids. Ozone adds very slowly to benzene. Each benzene molecule can add three molecules of ozone and yields three moles of glyoxal as shown in Eq. (47) in Fig. 15. Methyl-substituted benzenes react

Eq. (48)

O-Xylene triozonides

Glyoxal

Diacetyl

2 - Methylglyoxal

Eq. (49)

I – Butene   Propionaldehyde   Formaldehyde
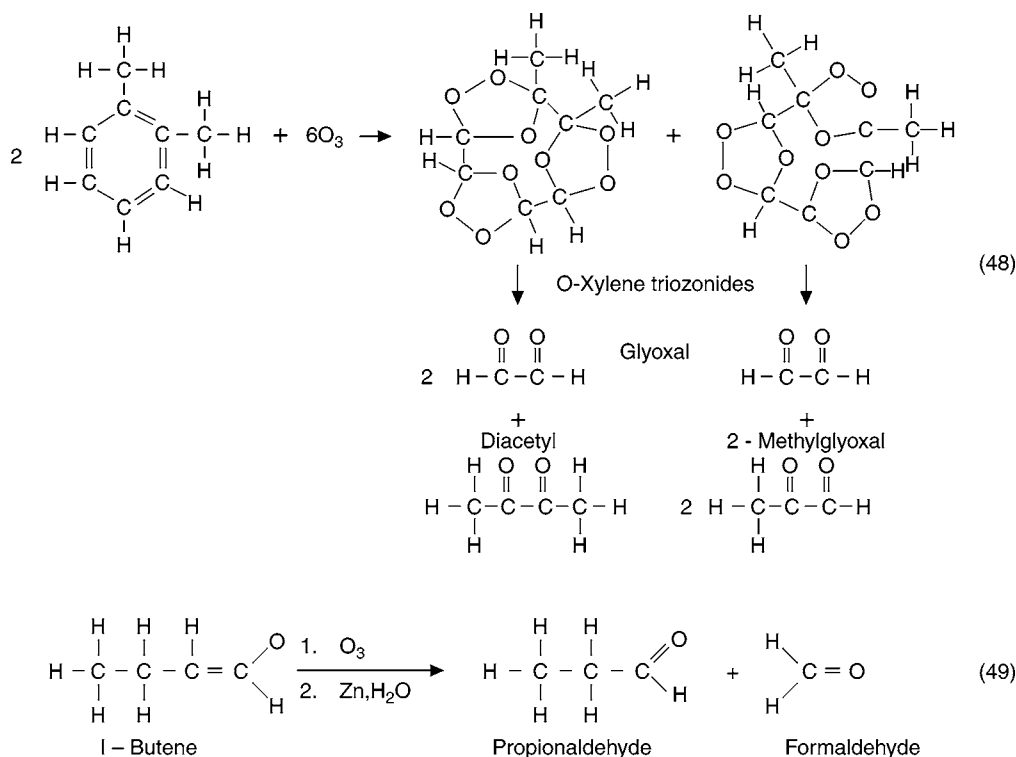
Fig. 16. Ozone reactions with organics Eqs. (48)–(49) (31,68).

more rapidly. Hexamethyl benzene reacts several thousand times more rapidly than benzene. Hydrolysis of the ozonide products produce the carbonyl compounds usually obtained in ozonolysis reactions. Equation (48) in Fig. 16 illustrates how two moles of methyl-substituted benzene react with six moles of ozone yielding three moles of glyoxal, one mole of diacetyl, and two moles of 2-methylglyoxal (31,68).

In polynuclear aromatic compounds, the various carbon bonds and atoms have different reactivities. The reaction with ozone is more complex and the composition of the products is difficult to predict. Oxidation at a carbon atom may, at times, predominate over ozone addition to a carbon–carbon double bond. While some aromatic compounds may add ozone rapidly and form ozonides, others may be oxidized to give quinones. Frequently, aromatic compounds react in both ways and the reaction mixture contains both oxidation and ozonolysis products.

Saturated hydrocarbons react very slowly with ozone at room temperature. However, at elevated temperatures, the reaction proceeds quite rapidly. Peroxides, ketones or aldehydes, alcohols, and acids are formed as the reaction products. Ethers are oxidized by ozone at the carbon next to the ether oxygen. Therefore, esters are found among the oxidation products. Lactones are produced by the reaction of ozone and cyclic ethers. Ozonation of cyclic formals produce carbonates.

Organic sulfides are oxidized by ozone through sulfoxides, RSOR′, to sulfones, $RSO_2R′$. The intermediate sulfoxide may be isolated. Primary and secondary amines are
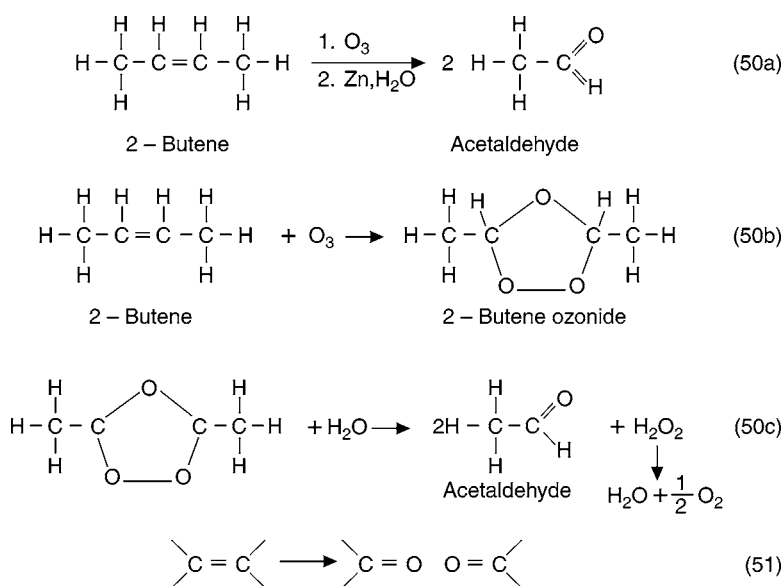
Fig. 17. Ozone reactions with organics Eqs. (50) and (51) (31).

only degraded by ozone but tertiary amines form tertiary amine oxides. Organic phosphates may be prepared by ozone oxidation of phosphites and phosphine oxides are formed from phosphines.

In addition to the ozonolysis and oxidation reactions where stoichiometric amounts of ozone are reacted, there are catalytic reactions where experimental conditions determine the amount of ozone used. The preparation of peroxyacids from aldehydes is one of these reactions. Ozone is only a catalyst or initiator of the oxidation. Intermittent ozonation of cumene is done in the production of cumene hydroperoxide.

Ozonolysis followed by hydrolysis is reliable, although at times dangerous as a result of the unstable and explosive nature of ozonides, which search for the double bond in organic compounds. This ozonolysis/hydrolysis reaction sequence can be illustrated by the difference in reaction products obtained by the reaction of ozone with 1-butene and 2-butene, as shown in Eq. (49) in Fig. 16 and Eq. (50a) in Fig. 17. Usually ozonized oxygen, containing up to 15% ozone, is passed at room temperature into a solution of the unsaturated compound. The ozonide formed is hydrolyzed either in the presence of a reducing agent to obtain aldehydes and ketones, or with hydrogen peroxide in acetic acid solution to get carboxylic acids (31).

The decomposition of an ozonide can also be affected by catalytic hydrogenation. The overall reaction is a breaking of the double bond with two carbonyl groups appearing in its place as represented by Eq. (51) in Fig. 17.

Ozonides, like most substances with the peroxide (O–O) bonds, are very unstable and may explode violently and unpredictably. Ozonation must therefore be carried out with due care and caution. The ozonides are usually not isolated but are destroyed by hydrolysis with water to yield carbonyl compounds that are generally quite easy to isolate and identify. The ozonation of 2-butene followed by hydrolysis to form acetaldehyde is an example of this, as shown in Eqs. (50b) and (50c) in Fig. 17.

Very few detailed studies have been made about the chemical pathways involved in ozonation of organic substances in water. In most studies in aqueous media, a cosolvent, a water emulsion, or a suspension has been employed.

Pryde (69) has ozonized methyl oleate and methyl lineoleate in water media and decomposed the peroxidic ozonolyses products to aldehydes and/or carboxylic acids under various conditions. Criegee and Lohaus (70) have synthesized peroxide from ozonolysis of cyclic sulfone in the presence of water.

Sturrock (71) has ozonized the aliphatic 9,10 bond of phenanthrene in an aqueous *t*-butyl alcohol medium and obtained a dialdehyde. Ozonolysis of acetylenic compounds (C≡C) in aqueous media have not been studied but presumably peroxides would be produced that readily decompose to carboxylic acids.

Ozonation of aromatic compounds appears to involve both 1,3-dipolar cyclo addition at a carbon–carbon bond to give ozonolysis products, and electrophilic ozone attack at individual carbon atoms (68). Regarding the ease of the ozone attack, the unsubstituted benzene ring is much less reactive than the olefinic double bond (68). Polycyclic aromatics such as phenanthrene, anthracene, and naphthalene reactivities fall in between (68). Alkyl and other substituents, which activate during electrophilic attack, facilitate ozone attack, while those which deactivate during electrophilic attack drastically reduce the rate of ozone attack on the aromatic nucleus (68). Benzene (72) and its homologs (68), however, react to give the ozonolysis products as shown in Eq. (47) in Fig. 15 and Eq. (48) in Fig. 16.

Considerable study has been done for the removal of phenolic wastes from water (73). Phenols are more reactive with ozone than most aromatics and phenol itself has been oxidized to carbon dioxide, formic acid, glyoxal, and oxalic acid (74). Eisenhauer (73,75) has carried out a detailed study on the reaction of ozone with phenol in water solutions and has identified catechol and *O*-quinone as intermediary products. However, the reaction went solely through these intermediates, which were not established. Muconic acid was assumed to be the next intermediate, followed by further ozonolysis of this unsaturated substance (73). Ozonation of other phenols and naphthols have also been shown to occur readily (76–79).

The ozonation of polycyclic hydrocarbons has been studied extensively (68,80,81), although most of the work has been done in nonaqueous media. Most aromatic and aliphatic unsaturated heterocyclics readily react with ozone (68). An exception is the pyridine ring, which reacts very slowly. Various organic substances with a nucleophilic atom in their structure are readily oxidized by ozone (68).

Various amino acids and proteins have been ozonized in water solution, but the ozone attack appears to have occurred at sulfur (cystine), aromatic, or heterocyclic unsaturated carbon–carbon bonds rather than nitrogen (82). When reactive groupings are not present in organic molecules, ozone attack on carbon hydrogen bonds becomes possible. Such reaction occurs readily with aldehydes (83–85), ethers (86,87), alcohols (88), and hydrocarbons (89,90) or hydrocarbon groupings (91) having secondary or tertiary carbon–hydrogen bonds. Through these reactions, aldhydes are converted to carboxylic acids, primary and secondary alcohols to carborylic acids, aldehydes or ketones, ethers to alcohols and esters, and hydrocarbons to alcohols and ketones. There appears to be general agreement that these ozonation reactions involve a hydrotrioxide intermediate.

However, the exact mode of formation of the intermediate and how it is converted to products is not clear.

The ozonation of ethers has recently been carried over to acetals, including sugar glycosides, to yield esters (92). Evidence is also available about the ozonation of sugar alcohols and of polysaccharides in aqueous medium (93), including the degradation of wood pulp (94–96). A simple carbon–hydrogen bond ozonation, which has been performed in water solution is that of malonic acid (97). The methylene group (CH_2) was converted to an alcohol and a ketone function. Oxalic acid and carbon dioxide were also produced. Because ozonides are active oxygen compounds, they could be used as oxidizing agents, polymerization catalysts, bleaching agents, and germicides. But their instability makes it difficult to prepare them with good yields and to use them safely in reactions. Ozonides or ozonolysis products have at times exploded on standing.

Commercially, ozonides are not handled as such, but serve only as intermediates to more stable products. The reduction of some organic ozonides will produce aldehydes in good yields and oxidation will produce carboxylic acids. Thermal composition of an ozonide will produce a mixture of aldehydes, acids, peroxy compounds, and some other byproducts. The nature of solvents determines what ozonolysis products will be obtained. In nonpolar hydrocarbon solvents, ozonides will be formed. In more polar solvents, a mixture of ozonides, peroxides, aldehydes, and acids will be produced.

Ozonolysis products are thermally unstable. The reaction must be maintained within a specific temperature range in order to prepare these compounds. Because the ozone addition reaction is highly exothermic, reaction vessels must be cooled in order to maintain the desired reaction temperature.

Amines and amino acids may be prepared by reductive amination of oxonides or ozonolysis products. Ozone adds three oxygen atoms to the double bond. Therefore, further oxidation of the ozonide is required to give two moles of acid. In most cases, oxidation with air or oxygen will give satisfactory results. However, some ozonides may be more difficult to oxidize, and in these cases, oxidation with peroxyacids is required.

Humic acid is a major precursor for trihalomethane (THM) formation. Glaze et al. (98) have reported on the ability of ozone to destroy humic acid. Guirguis et al. (99) confirmed that ozone makes organic compounds adsorbed better by activated carbon.

Prengle et al. (100) reported that ozone plus UV light could reduce an organic pesticide, malathion, to carbon dioxide and water and simultaneously could reduce the TOC in water. Likewise, Richard (101) found that ozone could degrade two other pesticides, parathion and marathion, to simple phosphoric acid.

8. OXYGENATION AND OZONATION SYSTEMS

8.1. Oxygenation Systems

The use of pure oxygen or oxygen-enriched air instead of air alone can improve upon many conventional water and waste treatment technologies. Some of the developments in this regard include the following:

a. Oxygenated-activated sludge process for wastewater treatment and/or nitrification.
b. Autothermal thermophilic oxygen digestion process for sludge treatment.
c. DO flotation process for iron and manganese removal from water.

  e. Oxygenation–ozonation process for sludge management and wastewater reclamation.
  f. Improved ozone generation technology using pure oxygen or oxygen-enriched air.

Potential sources of supply for oxygen include on-site oxygen generation plants, transport of liquid oxygen to the site, and use of an oxygen gaseous pipeline supply. On-site oxygen generation systems are the most economical and desirable form of oxygen supply for the aforementioned five applications, provided the plant is large enough (i.e., at least 1 MGD) to economically handle the capital cost for such installation.

A liquid oxygen supply system is useful for a small plant's operation, or as back-up oxygen supply and peak load equalization for plants of any size. Although the unit oxygen cost is generally high, the small plants could find this to be a good option because of the cost saving for capital investment. A pipeline oxygen supply system is practical if the treatment plant is in the vicinity of an oxygen generation facility.

There are two basic oxygen generation systems:

  a. The traditional cryogenic air separation (CAS) process for the large size plants.
  b. The pressure-swing adsorption (PSA) process for the somewhat smaller and more common plant sizes.

The standard CAS process (Fig. 18) involves the liquefaction of air followed by fractional distillation to separate it into its components (mainly nitrogen and oxygen). The entering air is first filtered and then compressed. It is then fed to the reversing heat exchangers, which perform the dual function of cooling and removing the water vapor and carbon dioxide by freezing these mixtures out onto the exchanger surfaces. This process is accomplished by periodically switching or "reversing" the feed air and the waste nitrogen streams through identical passes of the exchangers to regenerate their water vapor and carbon dioxide removal capacity. The air is next processed through "cold end gel traps," which are adsorbent beds, which remove the final traces of carbon dioxide as well as most of the hydrocarbons from the feed air. It is then divided into two streams, one of which feeds directly to the "lower column" of the distillation unit and the other is returned to the reversing heat exchangers and partially warmed to provide the required temperature difference across the exchanger. This second stream is then passed through an expansion turbine and fed into the "upper column" of the distillation unit. An oxygen-rich liquid exits from the bottom of the "lower column" and the liquid nitrogen from the top. Both streams are then subcooled and transferred to the upper column. In this column the descending liquid phase becomes progressively richer in oxygen until oxygen is collected as a product in the condenser reboiler. This oxygen stream is continually recirculated through an adsorption trap to remove all possible residual traces of hydrocarbons. The nitrogen exits from the top portion of the "upper column" and its heat is exchanged with the oxygen product to recover all available refrigeration and to regenerate the reversing heat exchangers as discussed earlier.

The PSA system uses two (or more) adsorbent vessels to provide a continuous and constant flow of oxygen gas. Figure 19 shows a PSA system with three adsorbers. In operation, the feed air is compressed by a nonlubricated compressor. This compressed air is separated into oxygen and nitrogen-rich streams as it flows through one of the adsorbent vessels. The adsorbent is a granular material (molecular sieve), which attracts and traps (adsorbs) the carbon dioxide, water, and nitrogen gas producing a relatively
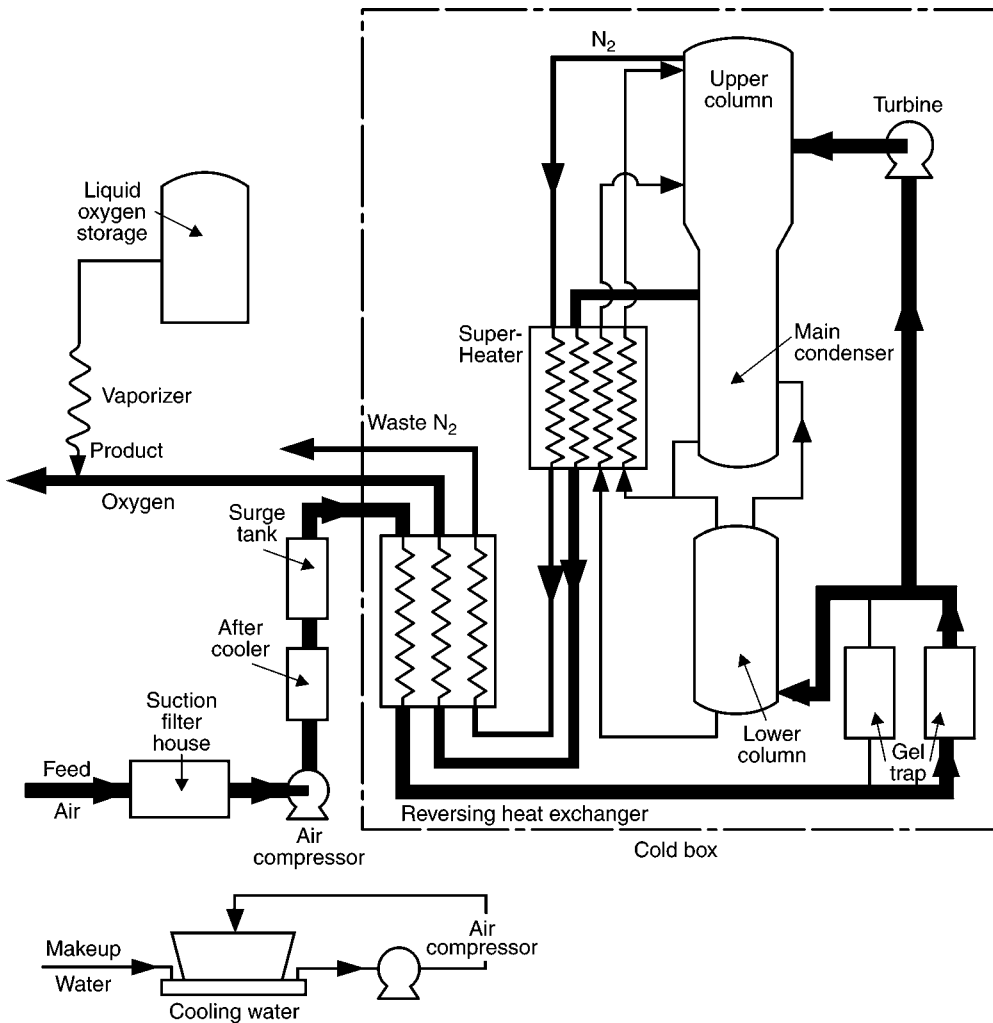
Fig. 18. CAS system for oxygen production (*Source:* Union Carbide Corp.).

high-purity oxygen product. While one bed is adsorbing, the other beds are in various stages of regeneration. The PSA oxygen generator operates on a pressure swing, an adsorption concept in which the oxygen is separated from the feed air by adsorption at high pressure and the adsorbent is regenerated by blow down to low pressure. The process operates on a repeated cycle that has two basic steps, adsorption and regeneration. During the adsorption step, feed airflow through one of the adsorbent vessels until the adsorbent is partially loaded with impurity. At that time the feed airflow is switched to another adsorber and the first adsorber is regenerated. During the regeneration step, the impurities (carbon dioxide, water, and nitrogen) are cleaned from the adsorbent so that the cycle (adsorption–generation) can be repeated.

Regeneration of the adsorber is carried out in three basic steps:

a. The adsorber is depressurized to atmospheric pressure to remove some impurities from the adsorbent and to make it easy to remove the remaining impurities.
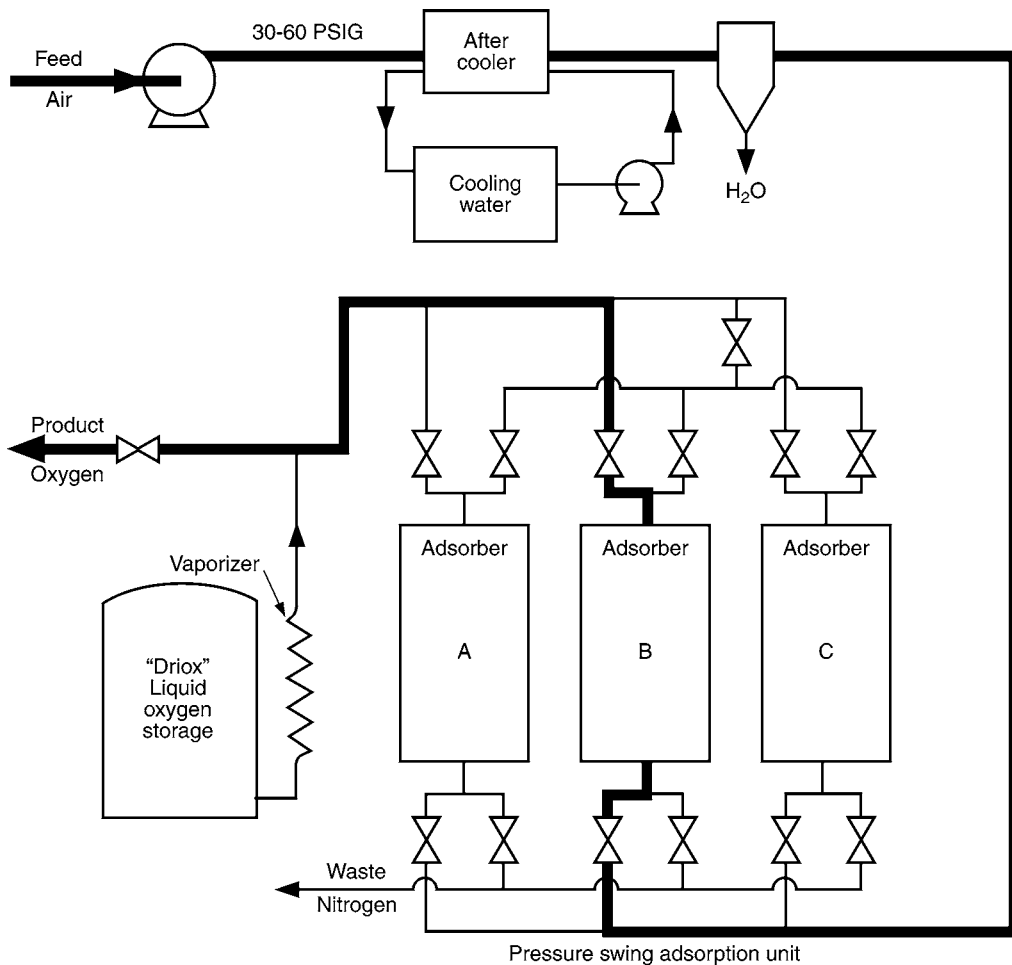
Fig. 19. PSA system for oxygen production (*Source:* Union Carbide Corp.).

b. The adsorber is purged with product oxygen to clean the remaining impurities.
c. The adsorber is repressurized to adsorption pressure and is again ready to separate the feed air.

8.2. Ozonation Systems

Generally there are four basic ozonation systems used in water and waste treatment. Figures 20–23 illustrate the four systems. Once the least cost basis system has been arrived then only the design of the contactor remains to be finalize for the ozone treatment system. For details and more information on ozonation technology, monitoring and control instrumentation, the reader is referred in refs. 102–106.

In the first system, compressed air is cooled to remove moisture and is fed to a dryer. The dry air is fed to the ozone generator and the ozone–air solution (1–3% ozone by weight) is mixed with the incoming water or waste in a contactor. The treated effluent and gases leave the contactor separately. Any excess ozone in the effluent soon decomposes to oxygen, while the ozone in the waste gas should be destroyed by heat or by chemical or catalytic decomposition. This system is applicable to very small installations.
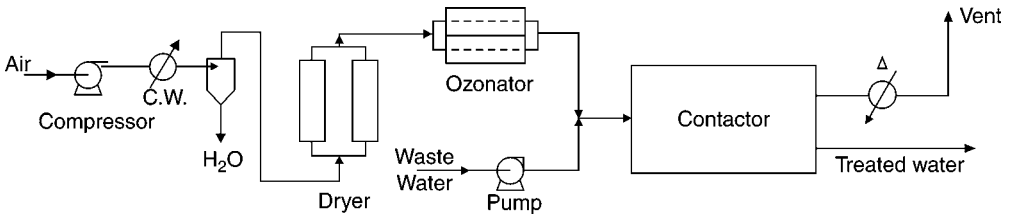
Fig. 20. Open-loop ozonation system using air (*Source:* W. R. Grace & Co.).
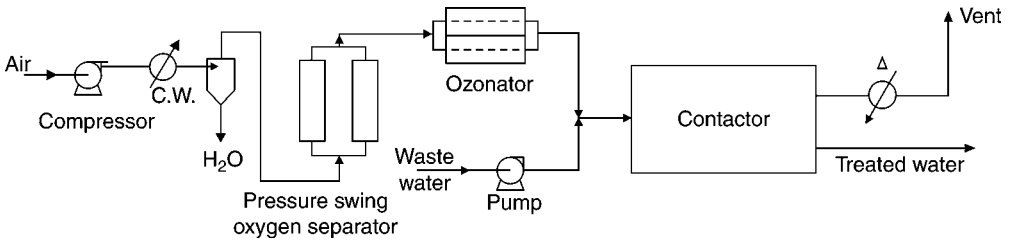
Fig. 21. Open-Loop ozonation system using oxygen-rich air (*Source:* W. R. Grace & Co.).
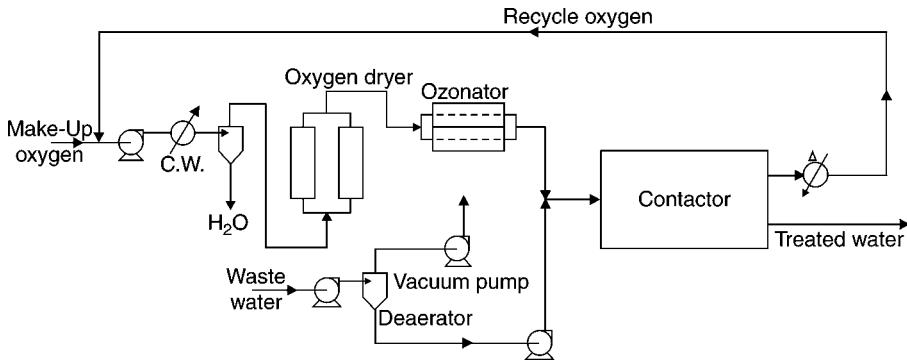
Fig. 22. Closed-loop ozonation system using oxygen (*Source:* W. R. Grace & Co.).
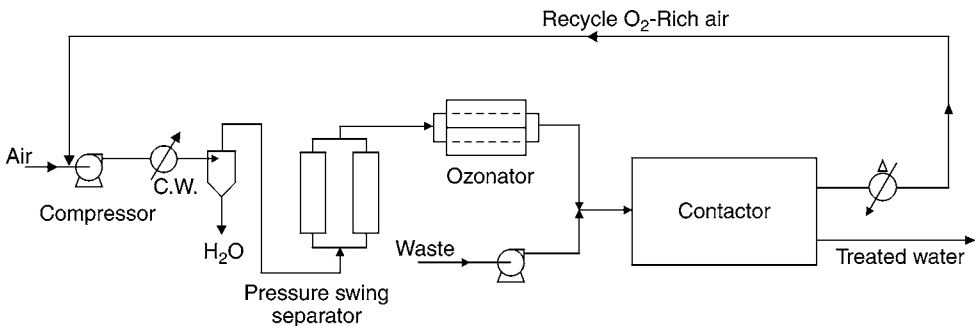
Fig. 23. Closed-loop ozonation system using oxygen-rich air (*Source:* W. R. Grace & Co.).

Table 20
Removal of Conventional Pollutants by Oxonation

Pollutant/parameter	Concentration		Removal (%)
	Influent	Effluent	
Classical pollutants (mg/L)			
BOD$_5$	5800	5200	10
COD	77,000	12,000	84
TSS	64	140	NM
Oil and grease	130	4	97
Total phenol	47	0.13	>99
Toxic pollutants (µg/L)			
Cyanide	560	1500	NM
Zinc	2200	90	96

Source: US EPA.
Sampling: Grab samples of equal volume collected throughout an 8-h/d; average of 2-d sampling.
Blanks indicate data not available.
NM, not meaningful.

The second system is similar to the first but is somewhat more cost efficient for larger installations, because air has been replaced by oxygen-enriched feed stream. The use of a PSA technique for producing oxygen-enriched air will reduce the capital and operating costs of the ozone generator.

The third system for ozone treatment is similar to the first but oxygen is fed to the generator and oxygen-rich off-gas is recycled to the front end of the loop. There is an additional deaeration step to remove nitrogen from the wastewater before its treatment so that it does not build up in the gas recycle.

In the fourth system, air is enriched to about 40% oxygen in the startup cycle. In each successive cycle, the recycled gas is cleaned, dried, enriched in oxygen, and any excess ozone is decomposed by the catalytic effect of the molecular sieves used in the pressure swing separator. The system can be programmed so that the economic point of ozone generation against oxygen generation (probably around 80% oxygen) is achieved. The other 20% will consist of nitrogen, carbon dioxide, and argon. By mixing adsorbents in the PSA separator, nitrogen, CO_2, and water will be removed in each cycle and oxygen increased. Air of course will be added for makeup. At <10% level, CO_2 and argon have little effect on ozone production efficiency and nitrogen has a positive effect. This system provides the following functions with a single PSA separator in a closed loop with the ozone generator and contact system.

  a. Oxygen enrichment.
  b. Removal of nitrogen and CO_2.
  c. Drying to −100°F dew point.
  d. Catalytic decomposition of excess ozone.

8.3. *Removal of Pollutants from Waste by Ozonation*

The removal data compiled by the US EPA are summarized in Tables 20–22. The tables clearly show that the ozonation process can efficiently remove not only the classical

Table 21
Removal of Toxic Pollutants by Ozonation

Pollutant	Removal (%)
Heavy metals	
Antimony	76
Arsenic	45
Xylene	97
Cadmium	98
Chromium	52
Copper	75
Lead	98
Mercury	75
Nickel	73
Silver	45
Organic chemicals	
Bis (2-ethylhexyl) phthalate	72
Butyl benzyl phthalate	99
Carbon tetrachloride	75
Chloroform	58
Dichlorobromomethane	99
Diethyl di-*N*-butyl phthalate	97
Diethyl phthalate	99
Di-*N*-octyl phthalate	78
N-nitrosodiphenylamine	66
2,4-Dimethylphenol	99
Pentachlorophenol	19
Phenol	57
Dichlorobenzene	76
Ethylbenzene	65
Toluene	39
Naphthalene	77
Anthracene/phenanthrene	81

Source: US EPA.

Table 22
Removal of Cyanide by Ozonation

		Cyanide		
		Concentration (μg/L)		
Flow rate (L/min)	Ozone feed rate (g/h)	Influent	Effluent	Removal (%)
3200		900	<20	>97
9.5	3	360	20	94
9.5	3	160	18	89
4.9	6	200	95	51

Source: US EPA.
Sampling: Grab.
Blanks indicate data not available.

pollutants such as BOD, COD, TSS, oil, grease, and phenol (Table 20), but also heavy metals and toxic organics (Tables 21 and 22). More information on ozonation and pressurized ozonation processes can be found elsewhere (107–111). Wang also reports that UV is an excellant deozonation process for removal of residual ozone from a treated waste stream (112).

NOMENCLATURE

B	Concentration of ozone in liquid/Concentration of ozone in gas, reduced to STP
	The Bunsen coefficient of solubility
C	Residual concentration of disinfectant (mg/L)
H	Henry's constant, mole/atm (mole fraction of ozone in solution/ partial pressure of ozone in gas, in atm)
k_1, k_2, and k_3	Rate constants
L	Lethality coefficient, $(\text{mg/L})^{-1} \, \text{min}^{-1}$
M	A chemical element
$[\text{OH}^-]$	Hydroxide concentration (g mole/L)
T	Temperature (K)
t	Time in minutes for 99% microorganism destruction (2-log destruction)

ACKNOWLEDGMENTS

REFERENCES

1. CEC, *Applications and Current Status of Ozone for Municipal and Industrial Wastewater Treatment*, California Energy Commission (CEC), www.energy.ca.gov (2001).
2. US Department of Energy, *Pressurized Ozone/Ultrafiltration Membrane System*, Office of Industrial Technologies, www.oit.doe.gov (2006).
3. Y. G. Park, Effect of ozonation for reducing membrane-fouling in the UF membrane, *Desalination* Vol. 147, pp. 43–48 (2002).
4. L. K. Wang, *Pretreatment and Ozonation of Cooling Tower Water*, *Part I*, US Dept. of Commerce, National Technical Information Service, Springfield, VA, Technical Report No. PB84-192053, April, 1983.
5. L. K. Wang, *Pretreatment and Ozonation of Cooling Tower Water*, *Part II*, US Dept. of Commerce, National Technical Information Service, Springfield, VA, Technical Report No. PB84-192046, August, 1983.

6. L. K. Wang, New dawn in flotation treatment of industrial water and wastes, *Proceeding of the 1990 Modern Engineering Technology Seminar*, Taipei, Taiwan, ROC., December, 1990.

7. J. N. Chen, *The Functional Increment of Ozonation Process and Application for Industrial Wastewater Treatment*, Institute of Environmental Engineering, NSC, NSC 87-2211-E-009-027 140.113.2.117/Backup/87-Eng/College_Of_Engineering/Environmental_Engineering.doc (1987).

8. L. K. Wang, M. H. S. Wang, G. G. Peery, and R. C. M. Cheugn, General theories of chemical disinfection and sterilization of sludge, Part 1, *Water and Sewage Works*, **125**(7), 30–32 (1978).

9. L. K. Wang, M. H. S. Wang, G. G. Peery, and R. C. M. Cheugn, General theories of chemical disinfection and sterilization of sludge, Part 2, *Water and Sewage Works*, **125**(8), 58–62 (1978).

10. L. K. Wang, M. H. S. Wang, G. G. Peery, and R. C. M. Cheugn, General theories of chemical disinfection and sterilization of sludge, Part 3, *Water and Sewage Works*, **125**(9), 99–104 (1978).

11. L. K. Wang, M. H. S. Wang, G. G. Peery, and R. C. M. Cheugn, General theories of chemical disinfection and sterilization of sludge, Part 4, *Water and Sewage Works*, **125**(10), 33–35 (1978).

12. L. K. Wang, *Principles and Kinetics of Oxygenation–Ozonation Waste Treatment System*, US Dept. of Commerce, National Technical Information Service, Springfield, VA, 1982, Technical Report No. PB83-127704.

13. N. Shammas and N. DeWitt, Flotation: a viable alternative to sedimentation in wastewater treatment, *Water Environment Federation*, *65th Annual Conference*, *Proceedings of Liquid Treatment Process Symposium*, New Orleans, LA, September 20–24, 1992, pp. 223–232.

14. N. Shammas, Physicochemically-enhanced pollutants separation in wastewater treatment, *Proc. International Conference: Rehabilitation and Development of Civil Engineering Infrastructure Systems—Upgrading of Water and Wastewater Treatment Facilities*, organized by The American University of Beirut and University of Michigan, Beirut, Lebanon, June 9–11, 1997.

15. N. Shammas and M. Krofta, A compact flotation—filtration tertiary treatment unit for wastewater reuse, *Water Reuse Symposium*, *AWWA*, Dallas, Texas, February 27–March 2, pp. 97–109 (1994).

16. M. Krofta, D. Miskovic, N. Shammas, D. Burgess, and L. Lampman, An innovative multiple stage flotation—filtration low cost municipal wastewater treatment system, *IAWQ 17th Biennial International Conference*, Budapest, Hungary, July 24–30, 1994.

17. M. Krofta, D. Miskovic, N. Shammas, and D. Burgess, Pilot—scale applications of a primary—secondary flotation system on three municipal wastewaters, *Specialist Conference on Flotation Processes in Water and Sludge Treatment*, Orlando, Florida, FL, April 26–28, 1994.

18. L. K. Wang, N. K. Shammas, W. A. Selke, and D. B. Aulenbach, Flotation thickening. In: *Advanced Physicochemical Treatment Processes*. L. K. Wang, Y. T. Hung and N. K. Shammas (eds.), Humana Press Inc., Totowa, NJ, 2005.

19. L. K. Wang, E. M. Fahey, and Z. Wu, Dissolved air flotation. In: *Physicochemical Treatment Processes*. L. K. Wang, Y. T. Hung, and N. K. Shammas (eds.), Humana Press Inc., Totowa, NJ, 2005.

20. S. A. Peterson, *Oxyozosynthesis Sludge Treatment Process-A Case Study of International Wastewater Reclamation Technologies Inc. New Process*, Internal Tech. Report, West New York Municipal Utility Authority, West New York, NJ, June, 1982.

21. US EPA, *A Plain English Guide to the EPA Part 503 Biosolids Rule*, EPA Office of Wastewater Management, Report No. EPA832/R-93/003, Washington, DC, September, 1994.

22. L. K. Wang, *Waste Treatment by Innovative Flotation-Filtration and Oxygenation-Ozonation Process*, US Dept. of Commerce, National Technical Information Service, Technical Report No. PB85-174738-A, 1984.

23. R. G. Zabady and R. N. Edwards, Oxyozonation process for treatment of municipal and industrial wastewaters and sludges: pilot studies, *52nd Annual Conference of the Water Pollution Control Association of Pennsylvania*, Pennsylvania State Univ., PA, August, 1980.

24. M. Krofta and L. K. Wang, *Development of Innovative Sandfloat System for Water Purification and Pollution Control*, US Dept. of Commerce, NTIS, Springfield, VA, Report No. PB83-l0796l, August, 1982.

25. T. Asano, On-site wastewater reclamation and reuse systems in commercial buildings and apartment complexes, *AWWA Water Resue Symposium II*, Washington, DC, August, 1981.

26. M. Krofta and L. K. Wang, *Treatment of Pittsfield Raw Water for Drinking Water Production by Innovative Process Systems*, US Dept. of Commerce, NTIS, Springfield, VA, Report No. PB82-l18795, February, 1981.

27. Ozonology Inc., *Innovation in Ozone Generating Technologies-Air Cooled Ozone Generators*, www.ozonology.com (2004).

28. O_3 Water Systems, *Commercial and Industrial Ozone Equipment*, www.o3water.com/Products/prozone.htm (2004).

29. S. G. Singer, *POU Ozonation Disinfection*, Semper Pure Systems, Inc., www.pure1.com/P1/NArticles2.htm (2004).

30. Editor, 2002 Buyer's guide: ozonators, *Environmental Protection*, **13**(3), 149 (2002).

31. T. E. Harr, Residual Chlorine in Wastewater Effluents Resulting from Disinfection, Technical Paper No. 38, NY State Dept. of Environ, Cons., March, 1975.

32. R. P. Ouellette, J. A. King, and P. N. Cheremisinoff, *Electrotechnology*, *Vol. 1*, *Wastewater Treatment and Separation Methods*, Ann Arbor Science Publishers Inc., Ann Arbor, MI, 1978.

33. Finnegan-Reztek, *How does an Ozone Generator Work?* www.fin-tek.com/ozone/howdoesanozonegeneratorwork.asp (2004).

34. R. Nathanson, Ozone: design parameters for using ozone on swimming pools, *Water Quality Products*, **8**, 4 (2003).

35. US EPA, *Technologies for Upgrading Existing or Designing New Drinking Water Treatment Facilities*, EPA/625-4-89/023, US Environmental Protection Agency, Washington, DC, 1989.

36. US Army, *Engineering and Design-Design of Wastewater Treatment Facilities Major Systems*, Engineering Manual No. 1110-2-501, US Army, Washington, DC, 1978.

37. GDT Corporation, *High Efficiency Ozone Contacting System*, GDT Water Process Corporation, Phoenix, Arizona, AZ, www.gdt-h2o.com (2003).

38. L. K. Wang, *Gas Dissolving System and Method*, US Patent No. 5049320, September, US Patent and Trademark Office, Washington, DC, 1991.

39. T. C. Manely and S. J. Niegawski, Ozone, *Encyclopedia of Chemical Technology*, 410.

40. L. K. Wang and D. C. Elmore, *Computer-Aided Modeling of Water Vapor Pressure*, *Gas Absorption Coefficient and Oxygen Solubility*, US Dept. of Commerce, NTIS, Springfield, VA, Tech. Report No. PB82-ll8787, October, 1981.

41. A. G. Hill, *Ozone Absorption in a Pressurized Bubble Colum*n, Tech. Paper presented at the AIChE National Meeting, Detroit, MI, August, 1981.

42. J. A. Roth and D. E. Sullivan, Solubility of ozone in water, *Eng. Chem. Fundam.*, **20**, 137–140 (1981).

43. W. W. Smith and R. E. Bodkin, The influence of hydrogen ion concentration on the bactericidal action of ozone and chlorine, *J. Bacteriol.* **47**, 445 (1944).

44. R. H. Leiguarda, Bactericidal action of ozone, *An. Asoc. Quim. Argent.*, **37**, 165 and *Wat. Poll. Abs.*, **22**, 268 (1949).

45. M. T. B. Whitson, Symposium on the Sterilization of Water (D) Other Processes with Special References to Ozone, *J. Inst. Water Engrs.*, **4**, 600 (1950).
46. H. Bernier, Ozone sterilization of the water supply of nice and coastal communities, *Tech. Sanit. Munic.*, **45**, 117 (1950) and *Wat. Poll. Abs.*, **24**, 243 (1951).
47. G. Bringman, Determination of the lethal activity of chlorine and ozone on *E. coli*, *Z. Hyg. Infektionskronkh.*, **139**, 130 (1954) and *Wat. Poll. Abs.*, **28**, 12 (1955).
48. K. Wuhrmann and J. Meyrath, The bactericidal action of ozone solution, *Schweiz, Z. Allgem. Pathol. Bakteriol.*, **18**, 1060 (1955) and *Wat. Poll. Abs.*, **29**, 223 (1956).
49. V. A. Hann, Disinfection of drinking water with ozone, *J. Am. Water Wks. Assoc.*, **48**, 1316 (1956).
50. D. B. M. Scott and E. C. Lesher, Effect of ozone on survival and permeability of *E. coli*, *J. Bacteriol.*, **85**, 567 (1963).
51. E. Christensen and A. C. Giese, Changes in absorption spectra of nucleic acids and their derivatives following exposure to ozone and ultraviolet radiation, *Arch. Biochem. Biophys.*, **51**, 208 (1954).
52. E. S. Barron, The role of free radicals of oxygen in reactions produced by ionizing radiations, *Radiation Res.*, **1**, 109 (1954).
53. R. G. E. Murray, Location of mucopeptide of selections of the cell wall of *E. coli* and other gram-negative bacteria, *Can. J. Microbiol.*, **11**, 547 (1965).
54. D. K. Smith, *Disinfection and Sterilization of Polluted Water with Ozone*, Report AM-6704, Ontario Research Foundation (1969).
55. P. L. Boucher, Microstraining and ozonation of water and wastewater, *Proceedings of the 22nd Industrial Waste Conference*, Purdue University *Engr. Ext. Series*, **129**, 771 (1967).
56. P. L. Boucher, Use of ozone in the reclamation of water from sewage effluent, *J. Inst. Pub. Health Engrs.*, **67**, 75 (1968).
57. D. T. Huibers, R. McNabney, and A. Halfon, *Ozone Treatment of Secondary Effluents from Wastewater Treatment Plants*, Robert A. Taft Water Res. Center, Report No. TWRC-4 (1969).
58. G. C. White, *Disinfection of Wastewater and Water for Reuse*, Van Nostrand Reinhold Co., NY, 1978.
59. R. S. Ramalho, *Introduction to Wastewater Treatment Processes*, Academic Press Inc., NY, 1977.
60. W. J. Weber, *Physicochemical Processes for Water Quality Control,* Wiley-Interscience, NY, 1972.
61. R. L. Sanks, *Water Treatment Plant Design*, Ann Arbor Science Publishers Inc., Ann Arbor, MI, 1979.
62. R. W. Legan, Alternative disinfection methods—a comparison of UV and ozone, *Indus. Water Eng.*, **19**(2), 12 (1982).
63. J. C. Morris, Aspects of the quantitative assessment of germicidal efficiency, in Chapter 1, *Disinfection, Water and Wastewater*, J. D. Johnson (ed.), Ann Arbor Science, Ann Arbor, MI, 1975.
64. APHA, AWWA, WEF, *Standard Methods for the Examination of Water and Wastewater*, American Public Health Association, Washington, DC, 2005.
65. P. C. Singer and W. B. Zilli, Ozonation of ammonia in wastewater, *Water Res.*, **9**, 127 (1975).
66. M. Teramota, Kinetics of the self-decomposition of ozone and the ozonation of cyanide ion and dyes in aqueous solutions, *J. Chem. Eng. Japan*, **14**, 383 (1981).
67. M. Teramota, Overall rate of ozone oxidation of cyanide in bubble column, *J. Chem. Eng. Japan,* **14**, 111 (1981).
68. P. S. Bailey, The reaction of ozone with organic compounds, *Chem. Rev.*, **58**, 925 (1958).
69. E. H. Pryde, D. J. Moore, and J. C. Cowan, Hydrolytic, reductive and pyrolytic decomposition of selected ozonolysis products water as an ozonization medium, *J. Am. Oil. Chem. Soc.*, **45**, 888 (1968).

70. R. Criegee and G. Lohaus, Die ozonide ungesättigter cyclischer sulfone, *Justus Liebig's Annalen der Chemie*, **583**, 1 (1953).

71. M. G. Sturrock, E. L. Cline, and K. J. Robinson, The Ozonation of phenanthrene with water as participating solvent, *J. Org. Chem.*, **28**, 2340 (1963).

72. W. P. Keaveney, R. V. Rush, and J. J. Pappas, Glyoxal from ozonolysis of benzene, *Indus. Eng. Chem. Product Res. Dev.*, **8**, 89 (1969).

73. H. R. Eisenhauer, The ozonation of phenolic wastes, *J. Water Poll. Con. Fed.*, **40**, 1887 (1968).

74. E. Bernatek and C. Frengen, Ozonolysis of phenols, I. Ozonolysis of phenol in ethyl acetate, *Acta Chem. Scandinavica*, **15**, 471 (1961).

75. H. R. Eisenhauer, Increased rate and efficiency of phenolic waste ozonation, *J. Water Poll. Con. Fed.*, **43**, 201 (1971).

76. C. H. Ni and J. N. Chen, Degradation of chlorophenols by a new high-pressurized ozonation system, *15th World Congress and Medical Therapy Conference*, IOA, London (2001).

77. L. B. Wingard, Jr. and R. K. Finn, Oxidation of catechol to *cis, cis*-muconic acid with ozone, *Indus. Eng. Chem. Product Res. Dev.*, **8**, 65 (1969).

78. E. Bernatek, J. Moskeland, and K. Valen, Ozonolysis of phenols, II. Catechol, resorcinol and quinol, *Acta Chem. Scandinavica*, **15**, 1454 (1961).

79. E. Bernatek and C. Frengen, Ozonolysis of phenols, III. 1-and 2-Naphthol, *Acta Chem. Scandinavica*, **15**, 2421 (1962).

80. P. S. Bailey, J. E. Batterbee, and A. G. Lane, Ozonation of benz (a) anthracene, *J. Am. Chem. Soc.*, **90**, 1027 (1968).

81. E. J. Moriconi and L. Salce, Ozonation of polycyclic aromatics, *Adv. Chem. Series*, No. 77, American Chemical Society, Washington, DC, 1968.

82. J. B. Mudd, R. Leavitt, A. Ongun, and T. T. McManus, Reaction of ozone with amino acids and proteins, *Atmos. Envir.*, **3**, 669 (1969).

83. H. M. White and P. S. Bailey, Ozonation of aromatic aldehydes, *J. Org. Chem.*, **30**, 3037 (1965).

84. R. E. Erickson, D. Bokalik, C. Richards, M. Scanlon, and G. Huddleston, Mechanism of ozonation reactions II. Aldehydes, *J. Org. Chem.*, **31**, 461 (1966).

85. A. A. Syrov and V. K. Tsyskovskii, Mechanisms of the action of ozone on aldehydes, *J. Org. Chem. USSR*, **6**, 1406 (1970).

86. C. C. Price and A. L. Tumolo, The course of ozonation of ethers, *J. Am. Chem. Soc.*, **86**, 4691 (1964).

87. R. E. Erickson, R. T. Hansen, and J. Harkins, Mechanism of ozonation reactions, III. Ethers, *J. A. Chem. Soc.*, **90**, 6777 (1968).

88. M. C. Whiting, A. J. N. Bolt, and J. H. Parish, The reaction between ozone and saturated compounds, *Advances in Chemistry Series*, No. 77, *Am. Chem. Soc.*, Washington, DC, 1968.

89. C. C. Schubert, S. J. Schubert, and R. N. Pease, The oxidation of lower paraffin hydrocarbons, II. Observations on the role of ozone in the slow combustion of isobutane, *J. Am. Chem. Soc.*, **78**, 2044 (1956).

90. G. A. Hamilton, B. S. Ribner, and T. M. Hellman, The mechanism of alkane oxidation by ozone, *Advances in Chemistry Series*, No. 77, *Am. Chem. Soc.*, Washington, DC, 1968.

91. J. E. Batterbee and P. S. Bailey, Ozonation of carbon-hydrogen bonds. Anthrone, *J. Org. Chem.*, **32**, 3899 (1967).

92. P. Deslongchamps and C. Moreau, Ozonolysis of acetals. (1) Ester syntheses, (2) THP ether cleavage, (3) Selective oxidation of B-glycoside, (4) Oxidative removal of benzylidene and ehtylidene protecting groups, *Can. J. Chem.*, **49**, 2465 (1971).

93. L. Mester, Role of formazan reaction in proving structure of ozone-oxidized carbohydrates, *Advances in Chemistry Series*, No. 21, *Am. Chem. Soc.*, Washington, DC, 1959.

94. NTNU, *Experimental Ozonation in a Pressurized Reactor*, The Pulp and Paper Group, Chemical Engineering Department, NTNU, Norway, www.chemeng.ntnu.no (1997).

95. S. T. Moe and A. K. Holen, High- and low-pressure ozonation of cellulose model compounds: a comparison of carbohydrate reaction specificity, *10th International Symposium on Wood and Pulping Chemistry* Vol. 2, pp. 354–357 (1999).

96. C. Schuerck, Ozonization of cellulose and wood, *J. Polymer Sci.*: *Part C*, *Polymer Symposia*, **2**, 79 (1963).

97. F. Dobinson, Ozonation of malonic acid in aqueous solution, *Chem. Indus.*, 853 (1959).

98. W. H. Glaze, R. Rawley, and S. Lin, *By-Products of Organic Compounds in the Presence of Ozone and UV Light*, Tech. Paper presented at the 101 Meeting, Cincinnati, OH, November, 1976.

99. W. A. Guirguis, P. Srivastava, T. Moister, R. Prober, and Y. Hanna, *Ozone Reactions with Organic Material in Sewage Non-Sorbuble by Activated Carbon,* Tech. Paper presented at the IOI Meeting, Cincinnati, OH, Nov., 1976.

100. H. W. Prengle, Jr., C. E. Mauk, and J. E. Payne, *Ozone–UV Oxidation of Pesticides in Aqueous Solution*, Tech. Paper presented at the IOI Meeting, Cincinnati, OH, November, 1976.

101. Y. Richard, *Organic Materials Produced Upon Ozonation of Water*, Tech. Paper presented at the IOI Meeting, Cincinnati, OH., November, 1976.

102. M. Everard, C. Seeley, and C. Bond, Biosolids and sustainability, *2020 Vision Seminar*, The Natural Step's www.naturalstep.org.uk (2002).

103. G. Ergler, *Ozone Pilot Plant Design*, O_3 Water Systems, Inc. www.o3water.com/Articles/PilotPlantDesign.htm (2003).

104. L. K. Wang, *A Modified Standard Method for the Determination of Ozone Residual Concentration by Spectrophotometer*, US Dept. of Commerce, National Technical Information Service, Springfield, VA, Technical Report No. PB84-204684, August, 1983.

105. L. K. Wang, *The State-of-the-art Technologies for Water Treatment and Management*, UNIDO Training Manual No. 8-8-95, United Nations Industrial Development Organization (UNIDO), Vienna, Austria, 1995.

106. IN USA Inc., *Ozone Monitoring and Control Instrumentation*, Needham, MA, www.inusacorp.com (2004).

107. N. K. Shammas and L. K. Wang, Ozonation, in *Physicochemical Treatment Processes*, L. K. Wang, Y. T. Hung, and N. K. Shammas (eds.), Humana Press Inc., Totowa, NJ, 2005, pp. 315–358.

108. L. K. Wang, Y. T. Hung, H. H. Lo, and C. Yapijakis. (eds.). *Handbook of Industrial and Hazardous Waste Treatment,* Marcel Dekker Inc./CRC Press, Boca Raton, FL, 2004.

109. L. K. Wang, Y. T. Hung, H. H. Lo, and C. Yapijakis (eds.). *Waste Treatment in the Process Industries.* CRC Press, Boca Raton, FL, 2006.

110. L. K. Wang, Y. T. Hung, H. H. Lo, and C. Yapijakis (eds.). *Hazardous Industrial Waste Treatment,* CRC Press, Boca Raton, FL, 2006.

111. US DOE. *Pressurized Ozone/Ultrafiltration Membrane System for Removing Total Dissolved Solids from Paper Mill Process Water*. US Dept. of Energy, Office of Industrial Technologies. Washington DC. www.recycle.com/linpac-nice3/documents/factsheet.pdf (2006).

112. L. K. Wang. *Innovative Ultraviolet, Ion Exchange, Membrane and Flotation Technologies,* National Association of Professional Engineers and Practicing Institute of Engineers, National Engineers Week Seminar, Feb. 12–17, 2006.

<div align="right">**2**</div>

Electrochemical Wastewater Treatment Processes

<div align="center">**Guohua Chen and Yung-Tse Hung**</div>

1. INTRODUCTION

Using electricity to treat water was first proposed in England in 1889 (1). The application of electrolysis in mineral beneficiation was patented by Elmore in 1904 (2). Electrocoagulation (EC) with aluminum and iron electrodes was patented in the United States in 1909. The EC of drinking water was first applied on a large scale in the United States in 1946 (3,4). Because of the relatively large capital investment and the expensive electricity supply, electrochemical water or wastewater technologies did not find wide application worldwide then. However, in the United States and the former USSR extensive research during the following half century has accumulated abundant amount of knowledge. With the ever increasing standard of drinking water supply and the stringent environmental regulations regarding the wastewater discharge, electrochemical technologies have regained their importance worldwide during the past two decades. There are companies supplying facilities for metal recoveries, for treating drinking water or process water, treating various wastewaters resulting from tannery, electroplating, diary, textile processing, oil and oil in water emulsion, and so on. Nowadays, electrochemical technologies have reached such a state that they are not only comparable with other technologies in terms of cost but also are more efficient and more compact. For some situations, electrochemical technologies may be the indispensable step in treating wastewaters containing refractory pollutants. In this chapter, the established technologies such as electrochemical reactors for metal recovery, EC, electroflotation (EF), and electro-oxidation (EO) will be examined. The emerging technologies such as electrophoto-oxidation, electro disinfection will not be discussed. Focus will be more

on the technologies rather than analyzing the sciences or mechanisms behind them. For books dealing with environmentally related electrochemistry, the readers are referred to other publications (5–8). Before introducing the specific technologies, are reviewed few terminologies that are concerned by electrochemical process engineers. The most frequently referred terminology besides potential and current may be the current density (*i*) the current per area of electrode. It determines the rate of a process. The next parameter is current efficiency (CE) the ratio of current consumed in producing a target product to that of total consumption. Current efficiency indicates both the specificity of a process and also the performance of the electrocatalysis involving surface reaction as well as mass transfer. The space-time yield, Y_{ST}, of a reactor is defined as the mass of product produced by the reactor volume in unit time with

$$Y_{ST} = \frac{iaM}{1000zF} CE \qquad (1)$$

The space–time yield gives an overall index of a reactor performance, especially the influence of the specific electrode area (*a*).

2. ELECTROCHEMICAL REACTORS FOR METAL RECOVERY

Since long time ago the electrochemical recovery of metals has been practiced in the form of electrometallurgy (9). The earliest reported application of electrochemical phenomena in chemical subjects was supposed to be carried out by Pliny in protecting iron with lead electroplating (10). The first recorded example of electrometallurgy was in mid-17th century in Europe (11). It involved the recovery of copper from cupriferous mine water electrochemically. During the past two and half-centuries, electrochemical technologies have grown into areas such as energy storage, chemical synthesis, metal production, surface treatment, and so on (12). The electrochemical mechanism for metal recovery is very simple. It basically is the cathodic deposition as:

$$M^{n+} + ne \rightarrow M \qquad (2)$$

The development of the process involves the improvement of CE as well as Y_{ST}.

2.1. Typical Reactors Applied

There are quite a few types of reactors found in applications of metal recovery from very basic reactors such as tank cells, plate and frame cells, rotating cells, to complicated three-dimensional reactor systems like fluidized bed, packed bed cell, or porous carbon packing cells. Tank cells, are one of the simplest and hence the most popular designs (Fig. 1). It can be easily scaled up or down depending on the load of a process. The electrode can be arranged in monopolar or bipolar mode (Fig. 2). The main application of this type of reactor system is the recovery of metals from high concentration process streams such as effluents from the electroplating baths, ethants, and eluates of an ion-exchange unit (11). The number of electrodes in a stack may vary from 10 to 100. The water flow is usually induced by gravity.

The plate and frame cell or sometimes called filter press, is one of the most popular electrochemical reactor designs (Fig. 3). It conveniently houses units with an anode, a cathode, and a membrane (if necessary) in one module. This module system makes the
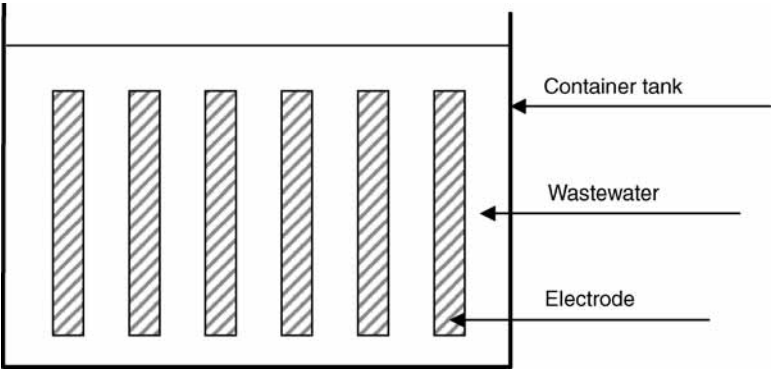
Fig. 1. Tank cell.
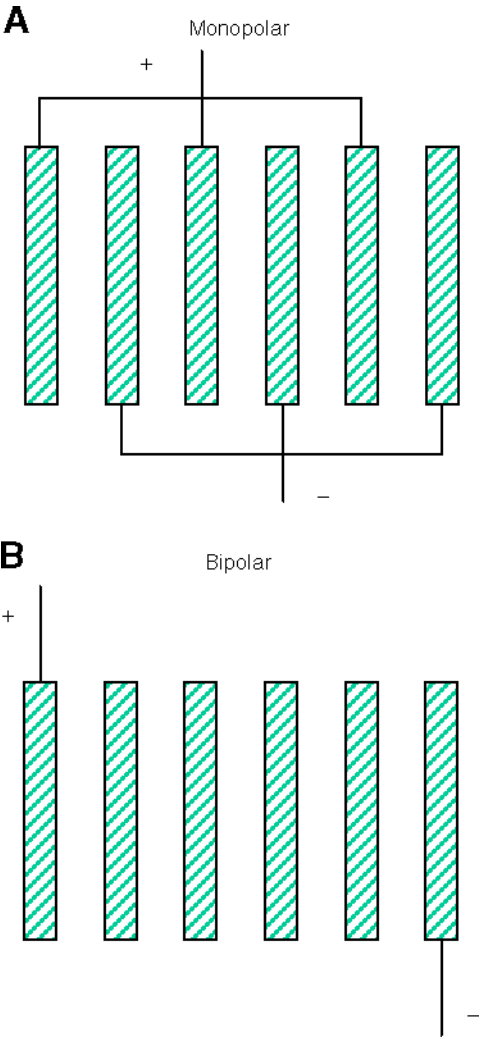
Fig. 2. Electrode arrangements.
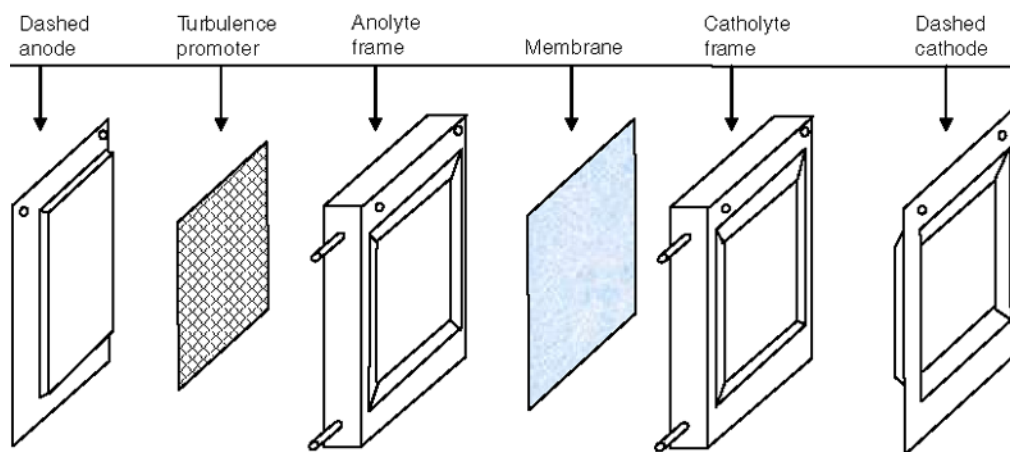
Fig. 3. Filter press reactor.

design, operation, and maintenance of the reactor relatively simple (13). In order to enhance mass transfer from the bulk to the electrode surface and also to remove the deposited metal powders from the cathode, the rotating cathode cell was designed and employed (Fig. 4; 14). It was found that this system can reduce copper content from 50 to 1.6 ppm by using the systems in a cascade version (15). The pump cell is another variant of rotating cathode cell (Fig. 5). By having a static anode and a rotating disk cathode, the narrow spacing between the electrodes allows the entrance of the effluent. The metals were electrically won and scraped as powders (16–18). Another design employs rotating rod cathodes in between inner and outer anodes. Besides metal recovery, if necessary, it is also possible to have the anodic destruction of cyanides (19).

Because the metal deposition happens at the surface of the cathode, it is necessary to increase the specific surface area in order to improve the space–time yield. Therefore, fluidized bed electrode was designed (Fig. 6; 20). The cathode was made of conductive particles in contact with a porous feeder electrode. The electrode can give a specific area of 200 m^2/m^3. Because of the fluidization of the particles by the water flow, the electrical contact is not always maintained, thus, the current distribution is not always uniform and the ohmic drop within the cell is high. In order to improve the contact between the electrode feeder and cathode particles, a large number of additional rod feeders were used (21). Inert particles were also employed in fluidized bed reactor to improve mass transfer rate in a ChemElec commercial design. Tumbling of bed electrodes are also available (Fig. 7).The packed bed cell sometimes overcomes noncontacting problem met in fluidized bed (Fig. 8; 22,23). Carbon granules were packed in a cell. The anode was separated by a diaphragm. The recently developed packed bed reactor by EA Technology Ltd (UK) and marking by Renovare International Inc. (US), RenoCell (Fig. 9) claims to excel in competition with many existing technologies. This three-dimensional porous, carbon cathode provides 500 times more plating area than conventional two-dimensional cells (24). In order to dilute metal pollutants to deposit properly on the cathode, it is suggested to seed metal powders by having concentrated metal solution at the beginning of the recovery process. Control of pH in the feed tank
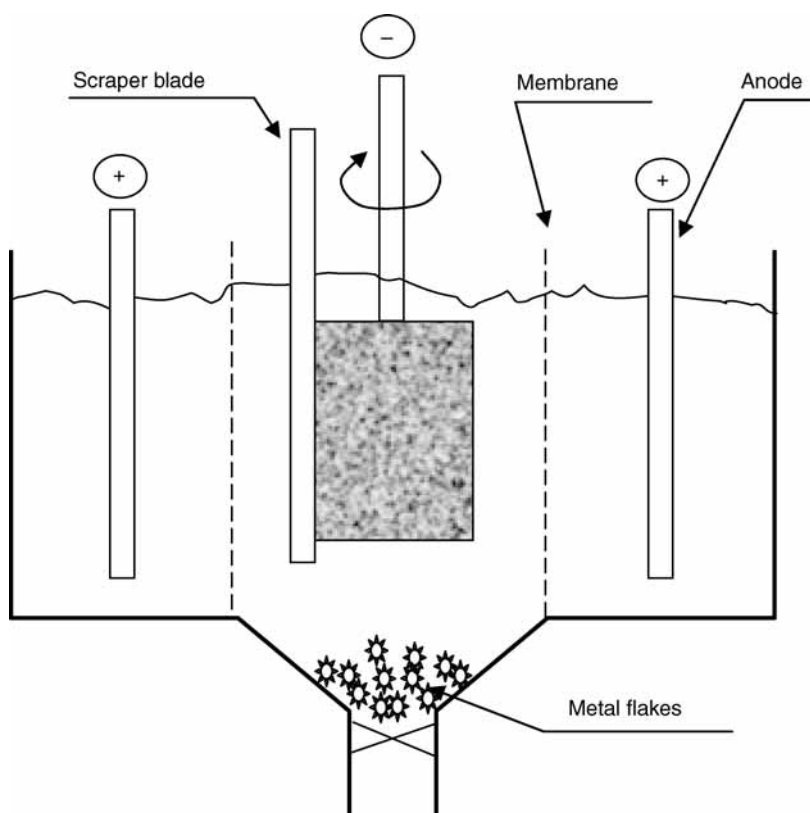
Fig. 4. Rotating cylinder electrode.
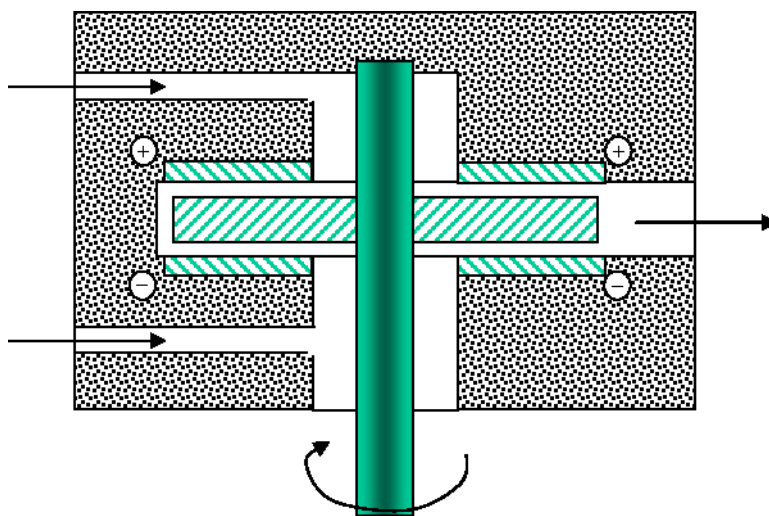
Fig. 5. Pump cell.
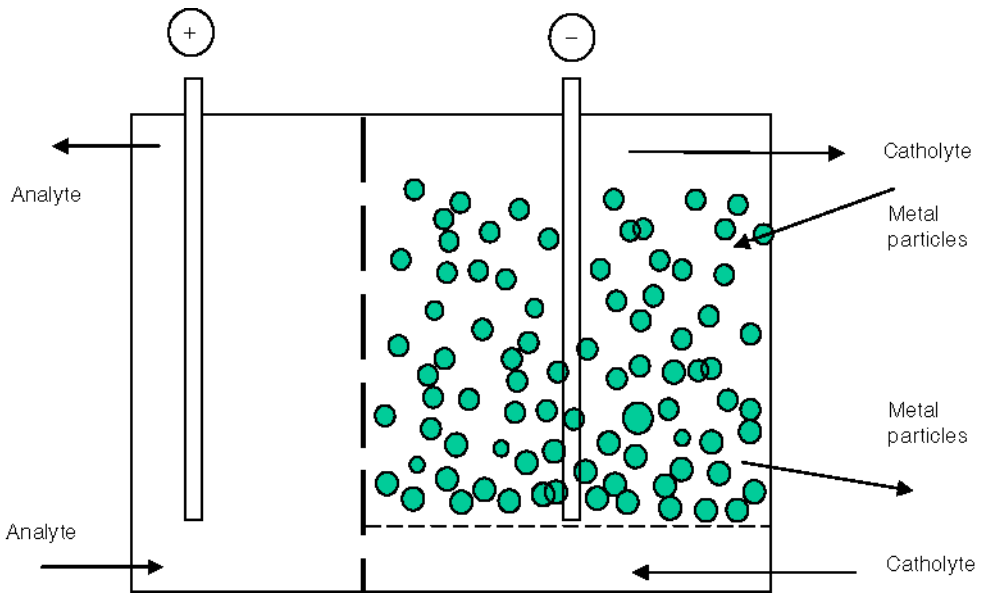
Fig. 6. Fluidized bed reactor.
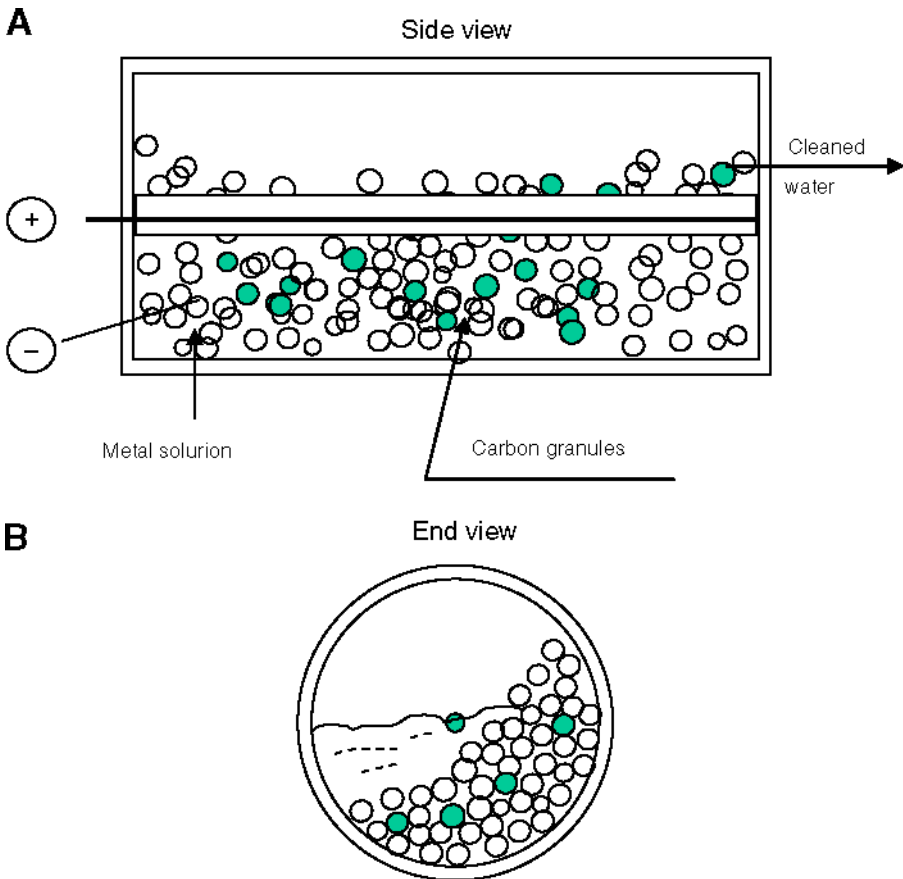
Fig. 7. Tumbling bed electrodes.
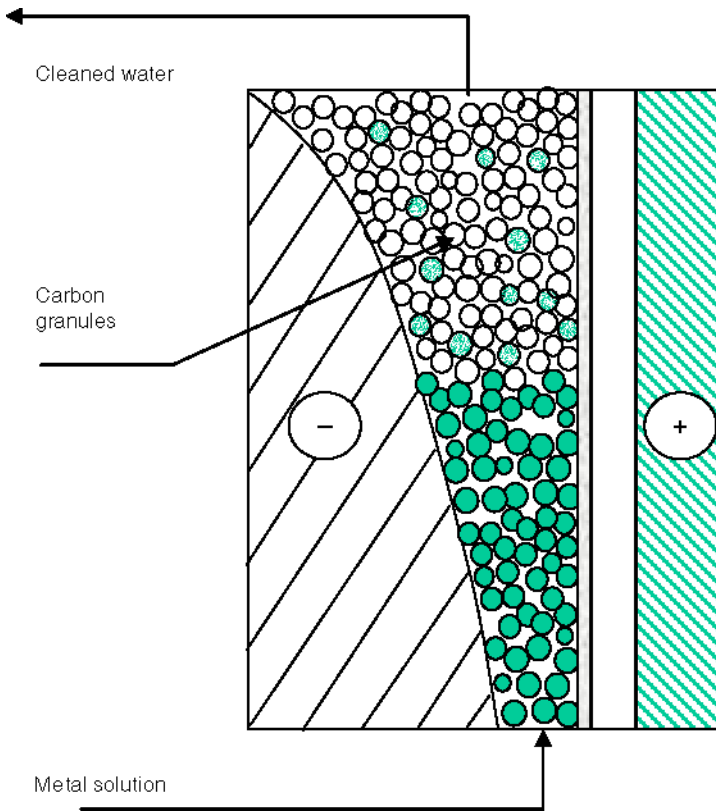
Fig. 8. Fixed bed reactor.
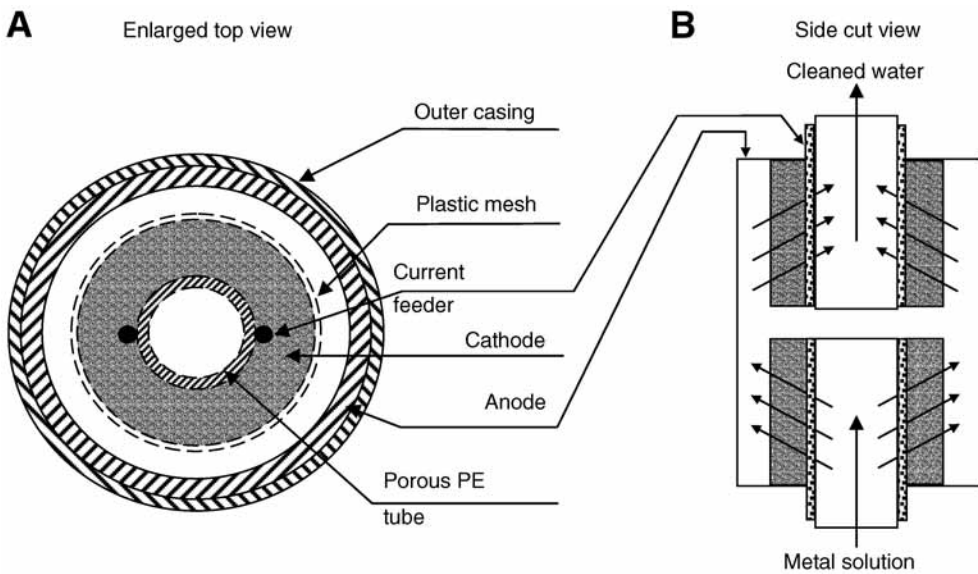
Fig. 9. Design of a renocell.

of a recirculating electrolyte is important to avoid precipitation of the metal. The following example might demonstrate the advantages of this invention.

"Hundred liters of a solution containing 19 ppm nickel in a 0.1 M Na_2SO_4 matrix were electrolyzed in the cell under conditions at 40°C and pH 4.0 and using a current density of 200 A/m² (based on geometric area). The nickel concentration was reduced from 19 ppm to 5 ppm in 120 min." The circulation flow rate was 20 L/min. Around 4 g/L of boric acid was added as buffer agent (24). The deposited metals can be removed from a felt cathode in a stripping cell using the carbon felt electrode as an anode. This system can work on single metal as well as metal mixtures. The circulating flow rate can vary between 15 L/min and 30 L/min. The current density is preferably between 100 and 300 A/m² based on geometric area. In exceptional cases in which very high acidity or alkalinity exists, a current density between 300 A/m² and 800 A/m² may be applied. The Reno Cell unit can be used alone, or in series or parallel depending on the quantity and quality of the effluent.

2.2. Electrode Materials

The anode electrode materials for metal recovery can be steel or dimensionally stable anodes (DSA). The latter was made of a thin layer of noble metal oxides on titanium substrate (25). It has been used extensively in electrochemical industry. More on this material will be discussed later on in Section 4. The cathode materials can be the metal to be recovered or graphite, carbon fibers, and so on. The cathode electrode feeder can be steel or titanium.

2.3. Application Areas

The electrochemical recovery of metals can be used in the metal surface finishing industry. It has to bear in mind that it is unable to provide a complete solution to the industry's waste management problems because it cannot treat all the metals either technically or economically. The electrolytic recovery of metals here involves two steps: collection of heavy metals and stripping of the collected metals. The collection step involves plating and the stripping can be accomplished chemically or electrochemically. Nowadays, metal powders can be formed on the surface of carbon cathodes. Therefore, physical separation is sufficient. The metals recovered can be of quite high purity.

Another application is in the printed circuit board manufacturing industry. Because of the well-defined process, the treatment can be accomplished relatively easier for this industry. For dilute effluent, an ion-exchange unit can be used to concentrate the metal concentration. For high concentration streams, they can be treated directly using a recovery system as in metal surface finishing industry. Application of metal recovery should be very much useful in metal winning in mining industry, especially in the production of precious metals such as gold (11).

3. ELECTROCOAGULATION

EC involves the generation of coagulants *in situ* by dissolving electrically either aluminum or iron ions from aluminum or iron electrodes, respectively. The metal ions generation takes place at the anode; hydrogen gas is released from the cathode. The hydrogen gas would also help to float the flocculated particles out of the water. This
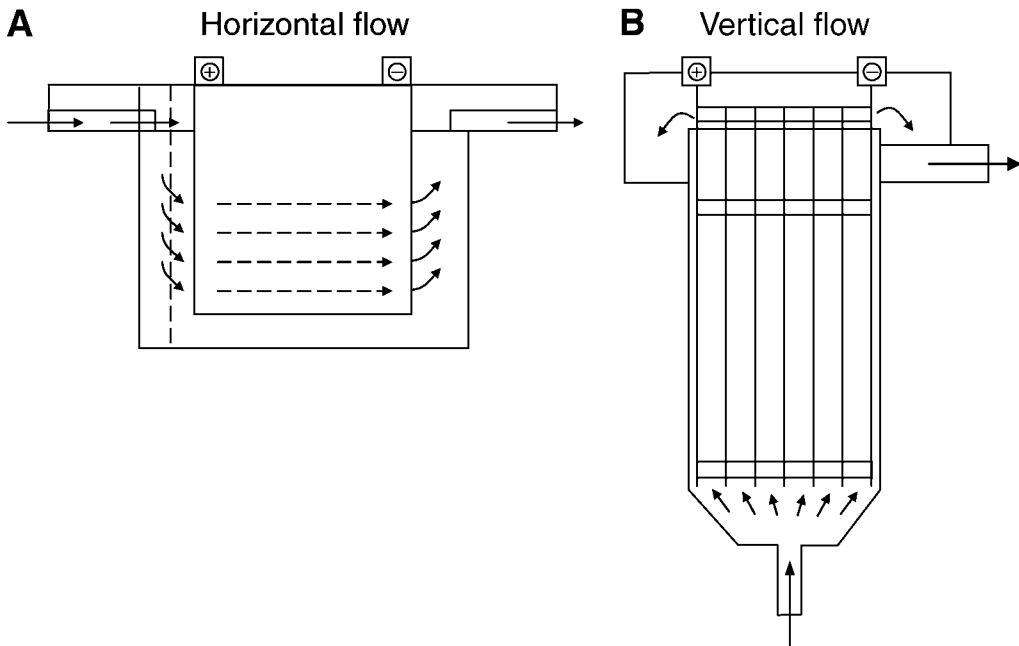
Fig. 10. Electrocoagulation units.

process sometimes is called electrofloculation. It is schematically shown in Fig. 10. The electrodes can be arranged in a monopolar or bipolar mode. The materials can be aluminum or iron in plate form or packed form of scraps such as steel turnings, millings, and so on.

The chemical reactions taking place at the anode are:

For aluminum anode:
$$Al - 3e \rightarrow Al^{3+}. \tag{3}$$

At alkaline conditions
$$Al^{3+} + 3OH^- \rightarrow Al(OH)_3. \tag{4}$$

At acidic conditions
$$Al^{3+} + 3H_2O \rightarrow Al(OH)_3 + 3H^+. \tag{5}$$

For iron anode:
$$Fe - 2e \rightarrow Fe^{2+}. \tag{6}$$

At alkaline conditions
$$Fe^{2+} + 2OH^- \rightarrow Fe(OH)_2. \tag{7}$$

At acidic conditions
$$4Fe^{2+} + O_2 + 2H_2O \rightarrow 4Fe^{3+} + 4OH^-. \tag{8}$$

In addition, there is oxygen evolution reaction:
$$2H_2O - 4e \rightarrow O_2 + 4H^+. \tag{9}$$

The reaction at the cathode is:
$$2H_2O + 2e \rightarrow H_2 + 2OH^-. \tag{10}$$
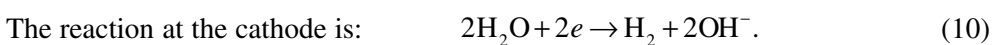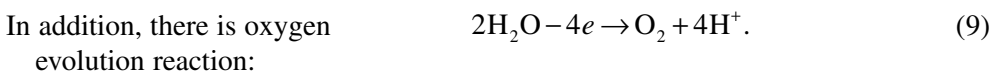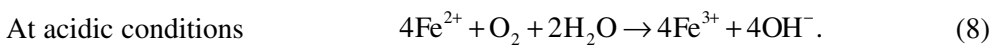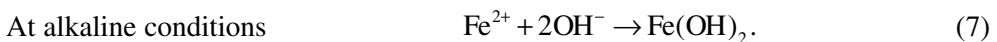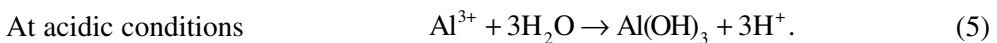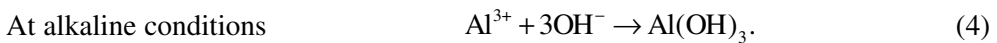
The nascent Al^{3+} or Fe^{2+} ions are very efficient coagulants for particulates flocculating. The hydrolyzed aluminum ions can form large networks of Al–O–Al–OH that can chemically adsorb pollutants such as F^- (26). Aluminum is usually used for water treatment and iron for wastewater treatment. The advantages of EC include high particulate removal efficiency, compact treatment facility, relatively low cost and possibility of complete automation.

3.1. Factors Affecting Electrocoagulation

3.1.1. Current Density or Charge Loading

The supply of current to the EC system determines the amount of Al^{3+} or Fe^{2+} ions released from the respective electrodes. For aluminum, the electrochemical equivalent mass is 335.6 mg/(A·h). For iron, the value is 1041 mg/(A·h). A large current means a small EC unit. However, when too large current is used, there is a high chance of wasting electrical energy in heating up the water. More importantly, a too large current density would result in a significant decrease in CE. In order for the EC system to operate for a long period of time without maintenance, its current density is suggested to be 20–25 A/m^2 unless there are measures taken for a periodical cleaning of the surface of electrodes. The current density selection should be made with other operating parameters such as pH, temperature as well as flow rate to ensure a high CE. The CE for aluminum electrode can be 120–140% whereas that for iron is around 100%. The over 100% CE for aluminum is attributed to the pitting corrosion effect especially when there are chlorine ions present. The CE depends on the current density as well as the types of the anions. Significantly enhanced CE, up to 160%, was obtained when low frequency sound was applied to iron electrodes (27).

The quality of the treated water depends on the amount of ions produced (mg) or charge loading, the product of current and time (A·h). Table 1 gives the values of the required Al^{3+} for treating some typical pollutants in water treatment (28). The operating current density or charge loading can be determined experimentally, if there are not any reported values available. It is our experience from treating restaurant wastewater that there is a critical charge loading required. Once the charge loading reaches the critical value, the effluent quality does not show significant improvement for further current increase (29).

3.1.2. Presence of NaCl

Table salt is usually employed to increase the conductivity of the water or wastewater to be treated. Besides its ionic contribution in carrying the electric charge, it was found that chloride ions could significantly reduce the adverse effect of other anions such as HCO_3^-, SO_4^{2-}. The existence of the carbonate or sulfate ions would lead to the precipitation of Ca^{2+} or Mg^{2+} ions that forms an insulating layer on the surface of the electrodes. This insulating layer would sharply increase the potential between electrodes and result in a significant decrease in the CE. Therefore, it is recommended that among the anions present, there should be 20% Cl^- to ensure a normal operation of EC in water treatment. The addition of NaCl would also lead to the decrease in power consumption because of the increase in conductivity. Moreover, the electrochemically-generated chlorine was found to be effective in water disinfections (30).

Table 1
The Aluminum Demand and Power Consumption
for Removing Pollutants From Water

Pollutant	Unit quantity	Preliminary purification		Purification	
		Al^{3+} (mg)	E (W·h/m^3)	Al^{3+} (mg)	E (W·h/m^3)
Turbidity	1 mg	0.04–0.06	5–10	0.15–0.2	20–40
Color	1 unit	0.04–0.1	10–40	0.1–0.2	40–80
Silicates	1 mg/SiO_2	0.2–0.3	20–60	1–2	100–200
Irons	1 mg Fe	0.3–0.4	30–80	1–1.5	100–200
Oxygen	1 mg O_2	0.5–1	40–200	2–5	80–800
Algae	1000	0.006–0.025	5–10	0.02–0.03	10–20
Bacteria	1000	0.01–0.04	5–20	0.15–0.2	40–80

3.1.3. pH Effect

The effects of pH of water or wastewater on EC are reflected by the CE as well as the solubility of metal hydroxides. When there are chloride ions present, the release of chlorine also would be affected. It is generally found that the aluminum current efficiencies are higher at either acidic or alkaline condition than at neutral. The performance of treatment depends on the nature of the pollutants with the best pollutant removal found near pH of 7.0. However, the power consumption is, higher at neutral pH because of the variation of conductivity. When conductivity is high, pH effect is not significant.

The effluent pH after electrocoagulation treatment would increase for acidic influent but decrease for alkaline influent. This is one of the advantages of this process. The increase of pH at acidic condition was attributed to hydrogen evolution at cathodes, reaction (10) by Vik and co-workers (31). In fact, besides hydrogen evolution, the formation of $Al(OH)_3$ near the anode would release H^+ leading to decrease of pH. In addition, there is also oxygen evolution reaction leading to pH decrease. When there are chlorine ions, there are following chemical reactions taking place:

$$2Cl^- - 2e \rightarrow Cl_2 \tag{11}$$

$$Cl_2 + H_2O \rightarrow HOCl + Cl^- + H^+ \tag{12}$$

$$HOCl \rightarrow OCl^- + H^+ \tag{13}$$

Hence, the increase of pH because of hydrogen evolution is more or less compensated by the H^+ release reactions earlier. For the increase in pH at acidic influent, the increase of pH is believed to be because of CO_2 release from hydrogen bubbling, because of the formation of precipitates of other anions with Al^{3+}, and because of the shift of equilibrium toward left for the H^+ release reactions. As far as the pH decrease at alkaline conditions, it can be the result of formation of hydroxide precipitates with other cations, the formation of $Al(OH)_4^-$ by (29).

$$Al(OH)_3 + OH^- \rightarrow Al(OH)_4^- \tag{14}$$
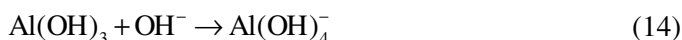
The pollutants removal efficiencies were found to be the best near neutral pH using aluminum electrode. When iron electrode was used in textile printing and dying wastewater treatment, alkaline influent was found to give better color as well as COD removal (32).

3.1.4. Temperature

Although EC has been around for more than 100 yr, the effect of temperature on this technology was not very much investigated. For water treatment, the literatures from former USSR (33) show that the CE of aluminum increases initially with temperature until about 60°C in which a maximum CE was found. Further increase in temperature results in a decrease in CE. The increase of CE with temperature was attributed to the increased activity of destruction of the aluminum oxide film on the electrode surface. When the temperature is too high, there is a shrink of the large pores of the $Al(OH)_3$ gel resulting in more compact flocs that are more likely to deposit on the surface of the electrode. Similar to the CE, the power consumption also gives a maximum at slightly lower value of temperature, 35°C, for treating oil-containing wastewater (34). This was explained by the opposite effects of temperature on CE and the conductivity of the wastewater. Higher temperature gives higher conductivity hence lower energy consumption.

3.1.5. Power Supply

When current passes through an electrochemical reactor, it must overcome the equilibrium potential difference, anode overpotential, cathode overpotential, and ohmic potential drop of the solution (7). The anode overpotential includes the activation overpotential and concentration overpotential, as well as the possible passive overpotential resulted from the passive film at the anode surface, whereas the cathode overpotential is principally composed of the activation overpotential and concentration overpotential. Therefore,

$$U_0 = E_{eq} + \eta_{a,a} + \eta_{a,c} + \eta_{a,p} + |\eta_{c,a}| + |\eta_{c,c}| + \frac{d}{\kappa}i \qquad (15)$$

It should be noted that the passive overpotential highly depends on the electrode surface state. For the new nonpassivated electrodes, the passive overpotential can be neglected and Eq. (15) simplifies to:

$$U_0 = E + \frac{d}{\kappa}i + K_l \ln i \qquad (16)$$

For old passivated electrodes

$$U_0 = E + \frac{d}{\kappa}i + K_l \ln i + \frac{K_2 i^n}{\kappa^m} \qquad (17)$$

On the right-hand side of Eq. (16) and Eq. (17), both K_1 and K_2 are constants. Although E is related to the transport number of Al^{3+} and OH^-, it approaches constant when κ is large, the case for EC. Equation (16) and Eq. (17) indicates that U_0 is independent on pH and it does not change significantly with flow rate. For new aluminum electrodes, $E = -0.76$, $K_1 = 0.20$. For passivated aluminum electrodes, $E = -0.43$, $K_1 = 0.20$, $K_2 = 0.016$ and $m = 0.47$, $n = 0.75$ (35).

With U_0 obtained, the total required electrolysis voltage U of an EC process can be calculated easily. For the monopolar mode, the total required electrolysis voltage is the same as the electrolysis voltage between electrodes, i.e.,

$$U = U_0 \qquad (18)$$

For the bipolar mode, the total required electrolysis voltage is U_0 times the number of total cell which is the number of electrodes minus one. Thus:

$$U = (N-1)U_0 \qquad (19)$$

N is usually less than 8 in order to maintain high CE for each electrode plate. Usually DC power supply is employed. In order to minimize the electrode surface oxidation or passivation, the direction of power supply is changed at a certain time interval. Fifteen minutes were found to be optimal for water treatment using aluminum electrodes. A three phase AC power supply was also used with six aluminum electrodes (three pairs) in treating colloidal wastewaters from petrochemical industries. Alternating current was also explored (36).

3.2. Electrode Materials

As stated earlier, the materials employed in EC are usually aluminum or iron. The electrodes can be made of Al or Fe plates or from scraps such as Fe or Al millings, cuttings, and so on. When the waste materials are used, supports for the electrode materials have to be made from insert materials. Care needs to be taken to make sure that there are no deposits of sludges in between the scraps. It is also necessary to rinse regularly the surface of the electrode plates or the scraps. Because there are a definite amount of metal ions required to remove a given amount of pollutants, it is usually to use iron for wastewater treatment and aluminum for water treatment because iron is relatively cheaper. The aluminum plates are also finding applications in wastewater treatment either alone or in combination with iron plates because of the high coagulation efficiency of Al^{3+} (26). When there are a significant amount of Ca^{2+} or Mg^{2+} ions in water, the cathode material is recommended to be stainless steel (28).

3.3. Typical Design

Depending on the orientation of the electrode plates, the EC cell can be horizontal or vertical (Fig. 10). To keep the EC system simple, the electrode plates are usually connected in bipolar mode. The water flowthrough the space between the plates can be multiple channels or a single channel, Fig. 11. Multiple channels are simple in the flow arrangement but the flow rate is also small. When the electrode surface passivation cannot be minimized otherwise, increasing the flow rate by using a single channel flow is recommended.

For water treatment, a cylindrical design can be used as shown in Fig. 12. It can efficiently separate the suspended solids (SS) from water. In order to prevent any blockings, scraper blades are installed inside the cylinder. The electrodes are so fitted that they are at the open space of the teeth of the comb. An alternative for cylindrical design is given in Fig. 13 in which a venturi is placed in the center of the cylinder with water and coagulants flowing inside it to give a good mixing. The EC reactor can be operated in continuous as well as in batch operation. For batch operation such as the cases for treating small amount of laundry wastewater or for the water supply of construction site, the automation is an important issue. The EC has to be followed by a sludge removal process. It is either a sedimentation unit or a flotation unit.
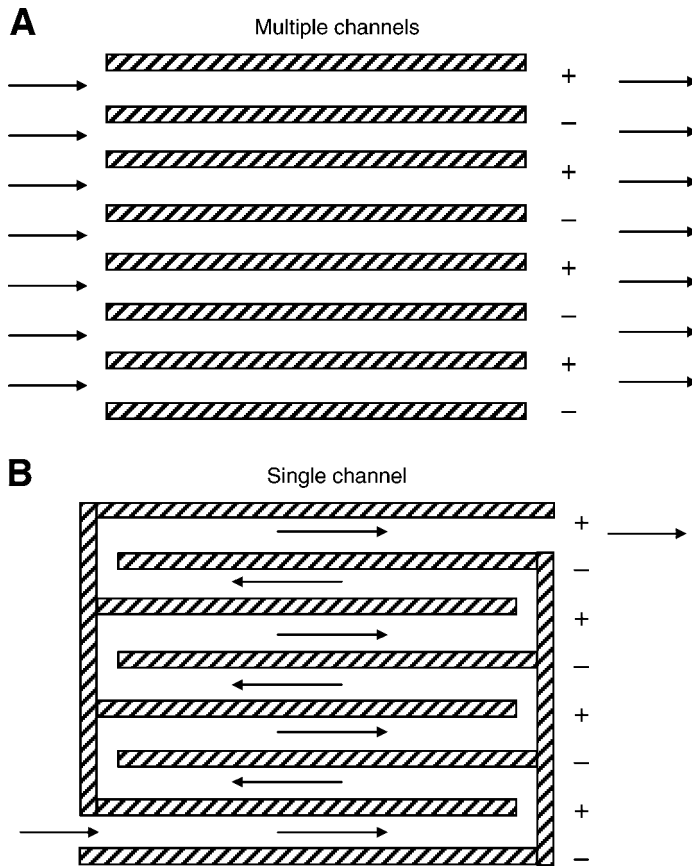
Fig. 11. Mode of water flow.

3.4. Effluents Treated by EC

Electrocogualtion is efficient in removing SS as well as oil and greases. It has been proven to be effective in water treatment such as drinking water supply for small or medium sized community, for marine operation and even for boiler water supply for industrial processes in which a large water treatment plant is not economical or necessary. It is very effective in coagulating the colloidal found in natural water so that it reduces the turbidity and color. It is also used in the removal or destruction of algae's or microorganisms. It can be used to remove irons, silicates, humus, dissolved oxygen, and so on. (28).

EC was found particularly useful in wastewater treatment (37). It has been employed in treating wastewaters from textile (38–41), catering (29,42), petroleum, tar sand and oil shale wastewater (43), carpet wastewater (44), municipal sewage (45), chemical fiber wastewater (46), oil–water emulsion (47,48), oily wastewater (34) clay suspension (49), nitrite (50), and dye stuff (51) from wastewater. Copper reduction, coagulation, and separation were also found effective (52).

4. ELECTROFLOTATION

EF is a simple process that floats pollutants to the surface of a water body by tiny bubbles of hydrogen and oxygen gases generated from water electrolysis (53).

A

End view

Scraper blade

B

Side view
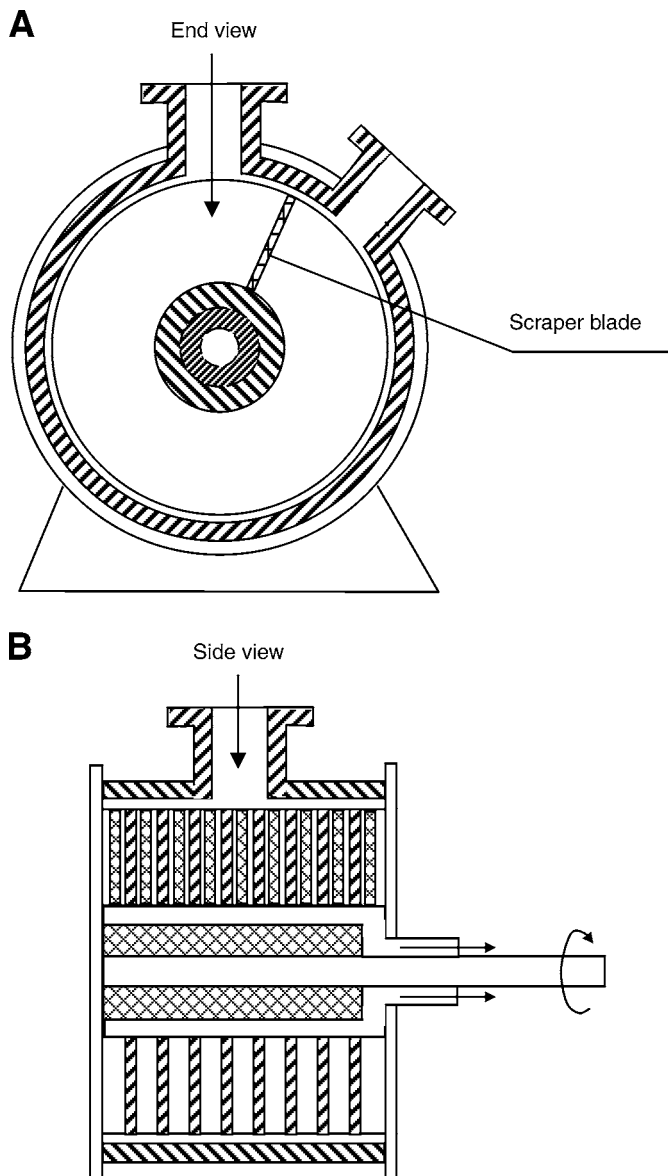
Fig. 12. Electrocoagulation unit with cylindrical electrodes.

Therefore, the electrochemical reactions at the cathode and anode are hydrogen and oxygen evolution reactions, respectively. EF was first proposed by Elmore in 1904 for flotation of valuable minerals from ores (2).

4.1. Factors Affecting EF

The performance of an EF system is reflected by the pollutant removal efficiency and the power and/or chemical consumptions. The pollutant removal efficiency is largely dependent on the size of the bubbles formed. For the power consumption, it relates to the cell design, electrode materials as well as the operating conditions such as current
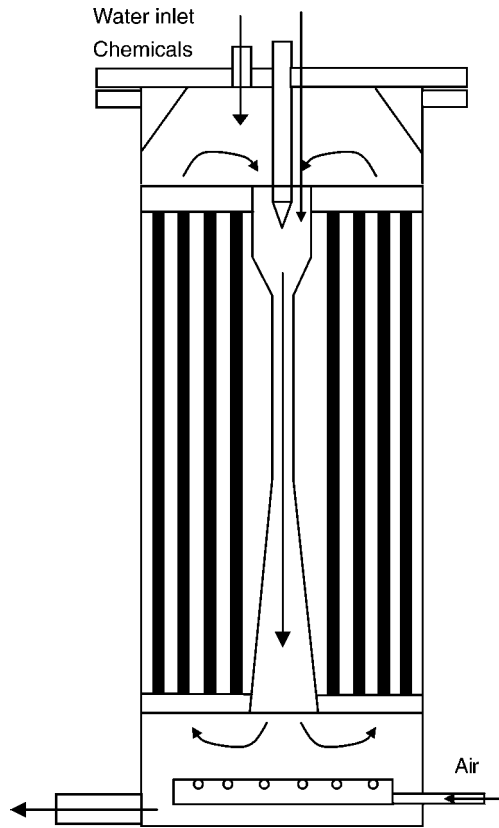
Fig. 13. Rod electrodes in a cylinder EC unit.

density, water conductivity, and so on. If the solid particles are charged, the opposite zeta-potential for the bubbles are recommended (54).

4.1.1. pH Effect

The size variation of the bubbles depends on water pH as well as the electrode material as shown in Table 2 (55). The hydrogen bubbles are smallest at neutral pH. For oxygen bubbles, their size increase with pH. It should be noted, however, the cathode materials affect the size of the hydrogen bubbles, so do the anode materials. The bubble sizes obey a log-normal distribution (54).

Using buffer solution, Llerena and co-workers (56) found that the recovery of sphalerite is optimal at pH between 3.0 and 4.0. They also documented that during this pH range, the hydrogen bubbles are the smallest, about 1 ± 2 μm. Decrease or increase of pH from 3.0 to 4.0 results in the increase of hydrogen bubbles. At pH of 6.0, the mean hydrogen bubble is 27 μm. At pH of 2.0, the hydrogen bubbles are about 23 μm when the current density was all fixed at 500 A/m^2 using a 304 SS wire. Oxygen and hydrogen were separated in their research and it was found that the increase of pH in the cathode chamber and pH decrease in the anode chamber are very quick when no buffer solutions were used. The recovery efficiency of oxygen is about half of that of hydrogen proportional to the amount of gas generated at a given current. This was also confirmed by O$_2$ and H$_2$ gas sparging.

Table 2
The Range of Gas Bubbles at Different pH
and Electrode Materials

	Hydrogen (μm)		Oxygen (μm)	
pH	Pt	Fe	C	Pt
2	45–90	20–80	18–60	15–30
7	5–30	5–45	5–80	17–50
12	17–45	17–60	17–60	30–70

Table 3
The Mean Gas Bubble Size at Different Current Density
and Electrode Materials (pH = 9.0)

	Current density (A/m^2)				
Electrode	125	200	250	300	375
Hydrogen gas bubbles diameter (μm)					
SS plate	34	32	29	26	22
200 mesh	39	35	32	31	28
100 mesh	45	40	38	30	32
60 mesh	49	45	42	40	37
Oxygen gas bubbles diameter (μm)					
Pt plate	48	–	46	–	42
200 mesh	50	–	45	–	38

4.1.2. Current Density

The gas bubbles depends also on the current density (57,58). The surface condition affects the particle size, too. The polished mirror surface of the stainless-steel plate gives the finest bubbles (Table 3). Besides size of bubble, the bubble flux, defined as the number of gas bubbles available per second per unit cross section area of the flotation cell, also plays a role in mineral flotation, recovery of different sized particles (58). A decrease of gas bubble sizes was found with the increase of current intensity (Table 3). Burns and co-workers (59) found that such a decrease in bubble size with increase in current density was true only at low end of current densities. When current density is higher than 200 A/m^2, no clear trend can be observed with gas bubbles ranging from 20 μm to 38 μm, Table 4.

4.1.3. Arrangement of the Electrodes

Usually, an anode is installed at the bottom, whereas a stainless steel screen cathode is fixed at 10–50 mm above the anode (56,60,61), Fig. 14. Such an electrode arrangement cannot ensure quick dispersion of the oxygen bubbles generated at the bottom anode into wastewater flow, affecting flotation efficiency. Moreover, if the conductivity of wastewater is low, energy consumption will be unacceptably high because of the large interelectrode spacing required for preventing the short-circuit between the upper flexible screen cathode and the bottom anode.

Chen and co-workers (62) proposed and tested the novel arrangement of electrodes with anode and cathode placed on the same plane as shown in Fig. 15. Effective

Table 4
The Mean Gas Bubble Size at Different Conditions

Ionic strength	Current density (A/m^2)	Gas	Mean size (µm)
0.1	52.3	O$_2$	18.6
	98.5		21.2
	129.2		23.3
	196.7		17.1
	212.3		37.9
	295.4		20
	393.8		20.7
	492.3		28.7
	590.8		26.2
	689.2		20.7
	787.7		25.3
	886.1		31.5
	55.4	H$_2$	29.7
	98.5		37.7
	196.9		19.3
0.01	33.8	O$_2$	27
	46.2		24.7
	58.5		22
	36.9	H$_2$	37.6
	43.1		37.3
	55.4		22

Polished graphite electrodes, DI water, Na$_2$SO$_4$.
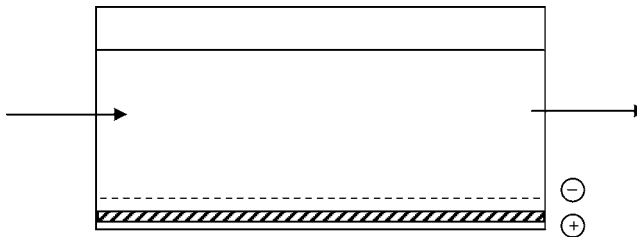
Fig. 14. Conventional electrodes arrangement for electroflotation.

flotation was obtained because of quick dispersion of the small bubbles generated into the wastewater flow. Quick bubble dispersion is essentially as important as the generation of tiny bubbles. For a conventional electrode system, only the upper screen cathode faces the wastewater flow, whereas the bottom anode does not interact with the flow directly. Therefore, the oxygen bubbles generated at the bottom anode cannot be dispersed immediately into the wastewater being treated. Consequently, some oxygen bubbles may coalesce to form useless large bubbles. This not only decreases the availability of the effective small bubbles, but also increases the possibility of breaking the flocs formed previously, affecting the flotation efficiency. When the anode and the cathode are leveled, such an open configuration allows both the cathode and the anode
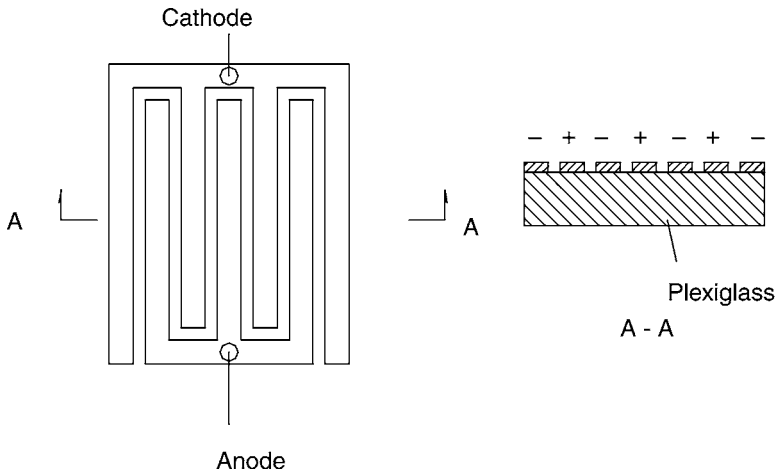
Fig. 15. Novel electrodes arrangement for electroflotation.
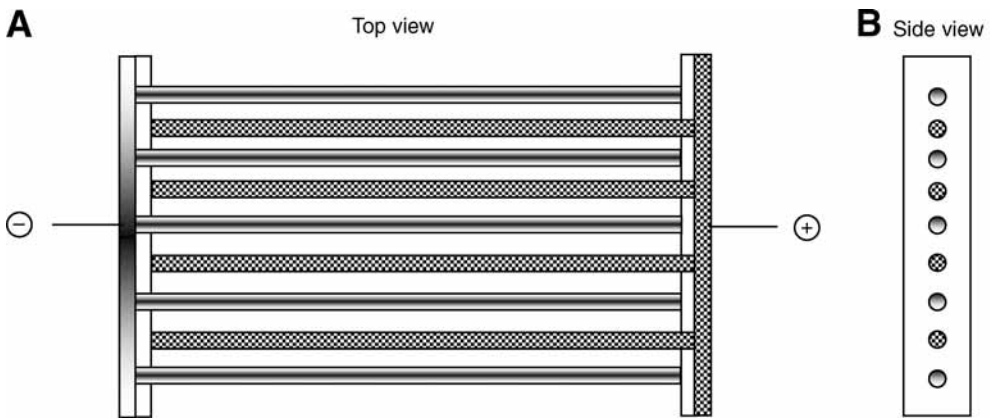
Fig. 16. Alternative electrode arrangement for electroflotation.

to contact the wastewater flow directly. Therefore, the bubbles generated at both electrodes can be dispersed into wastewater rapidly and attach onto the flocs effectively, ensuring high flotation efficiency. Another arrangement of the electrodes is shown in Fig. 16. It has the advantage of the uniform property of the surface of an electrode. It is also very much efficient (26).

Meanwhile, the open configuration has been proven quite effective in flotation of oil and SS. Significant electrolysis energy saving has also been obtained because of the small interelectrode gap used in the novel electrode system. It is useful to point out that the electrolysis voltage required in an EF process is mainly from the ohmic potential drop of the solution resistance, especially when the conductivity is low and the current density is high. Because the ohmic potential drop is proportional to the interelectrode distance, reducing this distance is of great importance for reducing the electrolysis

Table 5
Economic Parameters in Treating Oily Effluents

Treatment type	EF	DAF	IF	Settling
Bubble size (μm)	1–30	50–100	0.5–2	–
Specific electricity consumption, W/m^3	30–50	50–60	100–150	50–100
Air consumption, m^3/m^3 water	–	0.02–0.06	1	–
Chemical conditioning	IC	OC + F	OC	IC + F
Treatment time, minutes	10–20	30–40	30–40	100–120
Sludge volume as % of treated water	0.05–0.1	0.3–0.4	3–5	7–10
Oil removal efficiency (%)	99–99.5	85–95	60–80	50–70
Suspended solids removal efficiency (%)	99–99.5	90–95	85–90	90–95

energy consumption. For a conventional electrode system, because of the easy short-circuit between the upper flexible screen electrode and the bottom electrode, use of a very small spacing is technically difficult. But for the electrode system shown in Figs. 15 and 16, the interelectrode gap can be as small as 2 mm.

4.2. Comparison with Other Flotation Technologies

The effective EF obtained is primarily attributed to the generation of uniform and tiny bubbles. It is well known that the separation efficiency of a flotation process depends strongly on bubble sizes. This is because smaller bubbles provide larger surface area for particle attachment. The sizes of the bubbles generated by EF were found to be log-normally distributed with more than 90% of the bubbles in the range of 15–45 μm for titanium based DSA anode (62). In contrast, typical bubble sizes range from 50 to 70 μm for DAF (63). Burns et al. (59) reported that values of gas bubble size vary from 46.4 to 57.5 μm with the pressure decrease from 635 to 414 kPa for DAF. The electrostatic spraying of air (64) gives gas bubbles range from 10 to 180 μm with mean diameter being 33–41 μm (59). Impeller flotation (IF) produces much smaller gas bubbles but its pollutant removal efficiency is not good probably because of the quick coalesce of the tiny bubbles to form larger ones soon after they are generated. Table 5 summarizes the comparison of different flotation processes for treating oily wastewater (65). IC, OC, and F in the table denote inorganic coagulants, organic coagulants, and flocculants, respectively. EF clearly shows advantages over either DAF, settling or impeller flotation. When the conductivity is low, direct application of EF consumes large amount of electricity. For this case, addition of table salt (NaCl) is helpful (66).

4.3. Oxygen Evolution Electrodes

The electrode system is the most important part and thus considered as the heart of an EF unit. Although iron, aluminum, and stainless steel are cheap, readily available, and able to fulfill the simultaneous EC and EF, they are anodically soluble (29,56,59,67). To make matters worse, the bubbles generated at partially dissolved electrodes usually have large sizes because of the coarse electrodes surfaces (42). Graphite and lead oxide are among the most common insoluble anodes used in EF (59,68). They are also cheap and easily available, but both show high O_2 evolution overpotential and low durability. In addition, for the PbO_2 anodes, there exists a possibility to generate

highly toxic Pb^{2+}, leading to severe secondary pollution. A few researchers reported use of Pt or Pt-plated meshes as anodes (58,60). They are much more stable than graphite and lead oxide. However, the known high cost makes large-scale industrial applications impracticable.

The well known TiO_2–RuO_2 types of DSA® discovered by Beer (25) possess high quality for chlorine evolution but service lives are short for oxygen evolution (69). In the last decade, IrO_x-based DSA have received much attention. IrO_x presents a service life about 20 times longer than that of the equivalent RuO_2 (70). In general, Ta_2O_5, TiO_2, and ZrO_2 are used as stabilizing or dispersing agents to save cost and/or to improve the coating property (71–75). Occasionally, a third component such as CeO_2 is also added (70,75). It should be noted that although incorporation of Ta_2O_5, TiO_2, and ZrO_2 can save IrO_x loading, the requirement of molar percentage of the precious Ir component is still very high. The optimal IrO_x contents are 80 molar percent for IrO_x–ZrO_2, 70 molar percent for IrO_x–Ta_2O_5, and 40 molar percent for IrO_x–TiO_2, below which electrode service lives decrease sharply (73). The IrO_x–Ta_2O_5 coated titanium electrodes have been successfully used as anodes of EF (42,76). Nevertheless, because of the consumption of large amounts of the IrO_x, Ti/IrO_x–Ta_2O_5 electrodes are very expensive, limiting their wide application.

The recently discovered Ti/IrO_x–Sb_2O_5–SnO_2 anodes have extremely high electrochemical stability and good electrocatalytic activity for oxygen evolution (77,78). A Ti/IrO_x–Sb_2O_5–SnO_2 electrode containing only 10 molar percent of IrO_x nominally in the oxide coating could be used for 1600 h in an accelerated life test and was predicted to have a service life over 9 yr in strong acidic solution at a current density of 1000 A/m². Considering the much lower current density used and nearly neutral operating environments in EF, the IrO_x content in the coating layer can be reduced to 2.5 molar percent with sufficient electrochemical stability and good activity retained (62).

The electrode service life is strongly dependent on the current density used. A simple model relating the service life (SL) to the current density (i) has been obtained (35):

$$SL \propto \frac{1}{i^\alpha} \tag{20}$$

where α ranges from 1.4 to 2.

4.4. Typical Designs

The EF system consists of two electrodes, a power supply and a sludge handling unit. The electrodes are usually placed at the bottom or close to the bottom of the cell. Depending on the geometry of the EF cell, the electrodes can be placed vertically or horizontally. The horizontal placement is the most popular choice (60,79,80). EF is usually combined with EC or chemical flocculation (Fig. 17). In order for the chemical reagents to mix well with the pollutants before flotation, fluidized media have been used (Fig. 18; 81). This design allows an intensive contact of the solid phase in the mixing chamber with coagulants to form suspension particle agglomerates and at the same time not to break up the flocculates formed. The two stages of EF ensure the removal of finely dispersed particles. The installation of an ion-exchange membrane between the electrodes in the fine EF unit serves the purpose of controlling the pH of the treated
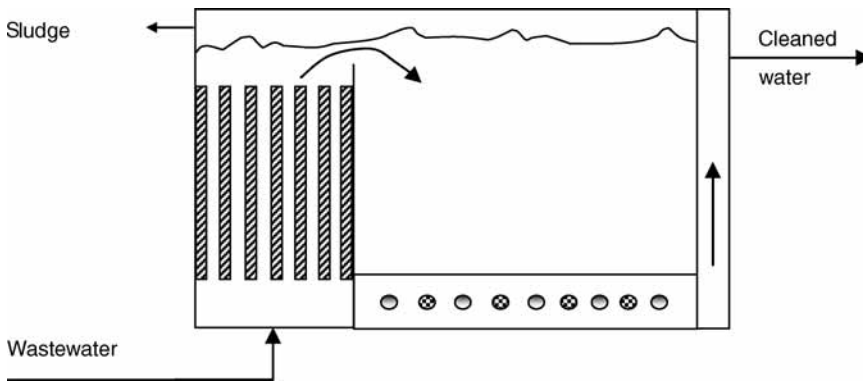
Fig. 17. Combined EC and electroflotation.
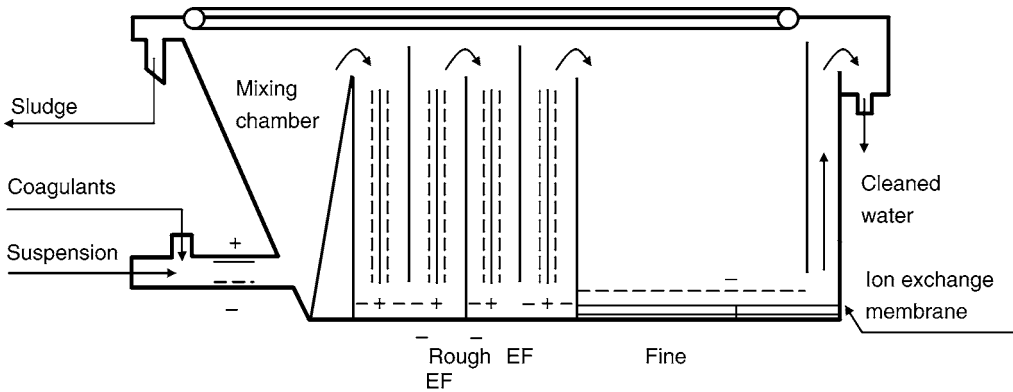
Fig. 18. Electroflotation with a fluidized media.

water. The addition of partitions in an EF unit helps better to utilize the gas generated and the flotation volume, if nonrectangular flotation unit is employed (Fig. 19; 82). Cocurrent and countercurrent EF systems were also investigated in industrial scale (Fig. 20; 83). Frequently, it may be necessary to separate the cathode and anode chambers in order to avoid the atomic hydrogen or oxygen to react with the solid particles in mining system, the automatic pH adjustment in each chamber has to be provided (84). Although there are equations available for the design of EF unit (85), the actual design of an industrial operation has to base on careful laboratory study.

The following example can provide some guidelines in the design of an EF system. This design was made and tested for highly concentrated industrial sewage from porcelain and faience industry (80). The schematic diagram is shown in Fig. 21. The system consists of a case, a sludge collector, and an electrode pile. The body is made of polypropylene and is of rectangular shape. The unit is divided by a partition to have two sections. Each section is further partitioned into two chambers. Electrode piles are placed vertically in each chamber. The body is equipped with inlet and outlet pipes with flanges connected with pipelines and sludge collectors consisting of a scrubbing devices and a geared motor.
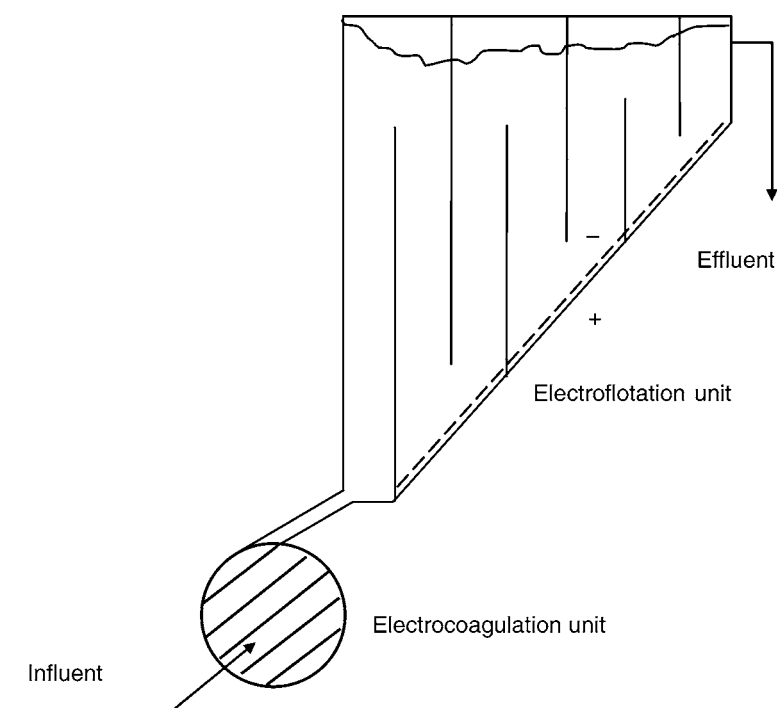
Fig. 19. Electroflotation with built-in partitions.

The electrode pile consists of a set of rectangular plates 1 mm thin. The cathodes are made of a stainless steel and the anodes are made of titanium based DSA type materials (Ti/Ru–TiO2). The spacing between the electrodes is 3 mm. To prevent the formation of sediment, crest shaped electrodes are used which are arranged within the same plane to avoid short circuit. DC power supply was employed. The overall dimensions are $2100 \times 1115 \times 1500$ mm^3 with the optimum height of the work zone being 0.8 m. The output of the system is up to 10 m^3/h. The specific power consumption is 0.2–0.4 kWh/m^3.

The equipments operation of the are as follows. The liquid is fed into the first two chambers and then spills over the partitions into the second two chambers before flowing into a water header through an opening in the bottom part. The scrubbing device shifts the sludge from the surface in a direction opposite to the liquid flow and into a collecting pocket with a conic bottom located at the end of the floater on the side of the liquid inlet. The sludge is removed from the system through a branch pipe. Chemical coagulants and flocculants may be injected into the feeding line to intensify the purification. For this type of wastewater, the established chemicals to use are aluminosilicon flocculant–coagulant (AKFK). Introduction of 15 mg/L aluminosilicon flocculant–coagulant into water containing 300 mg/L suspended particles removes 92–95% impurities whereas the same amount of aluminum sulfate removes only 15% impurities. Aluminosilicon flocculant–coagulant is made of SiO_2, Al_2O_3, and Fe_2O_3 with their respective concentrations being 25, 17, and 0.9 g/L. Table 6 lists the results of the EF process in comparison with sedimentation method.
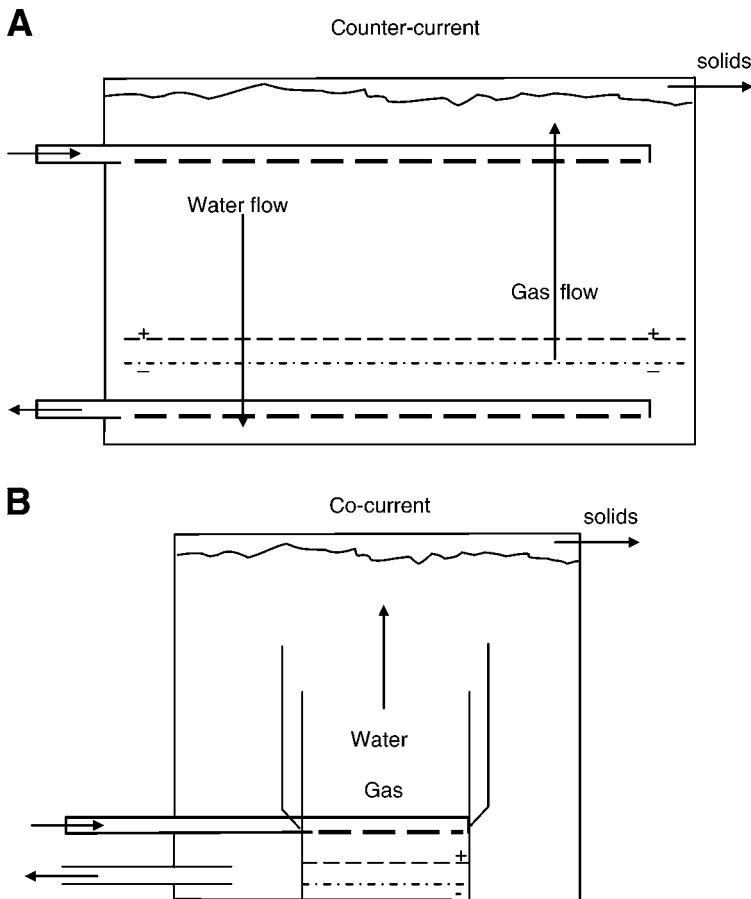
Fig. 20. Water–gas flow in an electroflotation unit.

4.5. Wastewaters Treated by EF

Mineral recovery remains the major user of EF (86). In water and wastewater treatment, flotation is the most effective process for the separation of oil and low-density SS (87–91). EF is found effective in treating palm oil mill effluent (68), oily wastewater or oil–water emulsion (61,65,66,92,93), spent cooling lubricant (94), wastewater from coke-production (95), mining wastewater (67), groundwater (60), food-processing wastewater (96), fat-containing solutions (97), restaurant wastewater (42) or food industry effluents (98), dairy wastewater (99), urban sewage (80), rural or single family water or sewage (100–102), pit waters (103), colloidal particles (54), heavy metal containing effluents (84,104–106), gold and silver recover from cyanide solution (107), and many other water and wastewaters (56,65,83).

5. ELECTRO-OXIDATION

Study on EO for wastewater treatment goes back to the 19th century, when electro-chemical decomposition of cyanide was investigated (108). Extensive investigation of
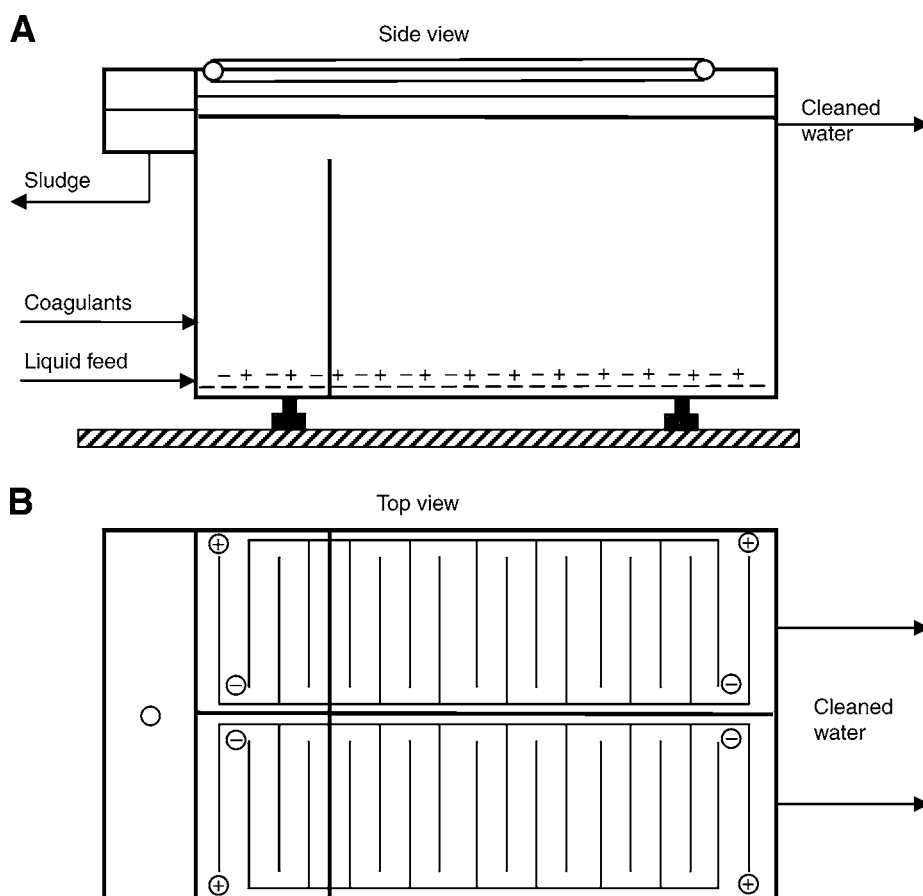
Fig. 21. A typical electroflotation unit design.

Table 6
Electroflotation of Industrial Sewage in Comparison With Sedimentation

Parameter	Purification method	
	Sedimentation	Electroflotation
Duration (h)	2–7	0.2–0.4
Coagulant consumption (g/L)	0.20–0.40	0.02–0.04
Efficiency (%)	70–80	95–99
Moisture of sediment (%)	98.5–99.8	92–95
Volume of sediment (%)	17–20	0.1–0.2

Initial conditions: pH, 7.0; BOD_5, 50–100 mg/L; SS, 1700–28,900 mg/L; milky color.

this technology commenced since the late 1970s. During the last two decades, research works have been focused on the efficiency in oxidizing various pollutants on different electrodes, improvement of the electrocatalytic activity and electrochemical stability of electrode materials, investigation of factors affecting the process performance,

and exploration of the mechanisms and kinetics of pollutant degradation. Experimental investigations focus mostly on the behaviors of anodic materials, the effect of cathodic materials was not investigated extensively, although, Azzam et al. (109) have found a considerable influence of the counter electrode material in the anodic destruction of 4-Cl phenol.

5.1. Indirect EO Processes

EO of pollutants can be fulfilled through different ways. Use of the chlorine and hypochlorite generated anodically to destroy pollutants is well known. This technique can effectively oxidize many inorganic and organic pollutants at high chloride concentration, typically more than 3 g/L (50,110–116). The possible formation of chlorinated organic compounds intermediates or final products hinders the wide application of this technique (112). Moreover, if the chloride content in the raw wastewater is low, a large amount of salt must be added to increase the process efficiency (116–119).

Pollutants can also be degraded by the electrochemically-generated hydrogen peroxide (120–125). This process is usually employed together with the *in situ* generated ferrous ion to have the Fenton reaction. In this system, the cathode is made of porous carbon-polytetrefluorethylene with oxygen feeding and the anode is either Pb/PbO_2, $Ti/Pt/PbO_2$, or Pt. Fe^{2+} salts can be added into the wastewater or formed *in situ* from a dissolving iron anode (123) to make an Electro-Fenton reaction. The degradation of aniline was found to be about 95% when Ultraviolet irradiation was also employed. Simply sparging oxygen into the solution also helps the removal of aniline when electricity is on (122). The electrically generated ozone is also reported for wastewater treatment (126,127).

Farmer and coworkers (128) proposed another kind of EO, mediated EO, in treating mixed, and hazardous wastes. In this process, metal ions, usually called mediators, are oxidized on an anode from a stable, low valence state to a reactive, high valence state, which in turn attack organic pollutants directly, and may also produce hydroxyl free radicals that promote destruction of the organic pollutants. Subsequently, the mediators are regenerated on the anode, forming a closed cycle. The typical mediators include Ag^{2+}, Co^{3+}, Fe^{3+}, Ce^{4+}, and Ni^{2+} (128–133). Mediated EO usually needs to operate in highly acidic media. In addition, there exists the secondary pollution from the heavy metals added. These disadvantages limit its application.

5.2. Direct Anodic Oxidation

EO of pollutants can also occur directly on anodes by generating physically adsorbed "active oxygen" (adsorbed hydroxyl radicals, $\cdot$ OH) or chemisorbed "active oxygen" (oxygen in the oxide lattice, MO_{x+1}) (134). This process is usually called anodic oxidation or direct oxidation. The physically adsorbed "active oxygen" causes the complete combustion of organic compounds (R), and the chemisorbed "active oxygen" (MO_{x+1}) participates in the formation of selective oxidation products:

$$R + (MO_x \cdot OH)_z = CO_2 + zH^+ + ze + MO_x \tag{21}$$

$$R + MO_{x+1} = RO + MO_x \tag{22}$$
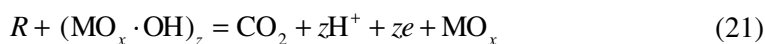
Table 7
Potential of Oxygen Evolution of Different Anodes (V vs NHE)

Anode	Value (V)	Conditions	Reference
Pt	1.3	0.5 M H_2SO_4	142
Pt	1.6	0.5 M H_2SO_4	219
IrO_2	1.6	0.5 M H_2SO_4	76,142
Graphite	1.7	0.5 M H_2SO_4	219
PbO_2	1.9	1 M $HClO_4$	155
SnO_2	1.9	0.5 M H_2SO_4	167
Pb–Sn (93:7)	2.5	0.5 M H_2SO_4	142
Ebonex (Titanium oxides)	2.2	1 M H_2SO_4	178
Si/BDD	2.3	0.5 M H_2SO_4	200,197
Ti/BDD	2.7	0.5 M H_2SO_4	203
DiaChem	2.8	0.5 M H_2SO_4	142

In general, OH is more effective for pollutant oxidation than O in MO_{x+1}. Because oxygen evolution, Reaction (9), can also take place at the anode, high overpotentials for O_2 evolution is required in order for reactions Eq. (21) and Eq. (22) to proceed with high CE. Otherwise, most of the current supplied will be wasted to split water.

The anodic oxidation does not need to add a large amount of chemicals to wastewater or to feed O_2 to cathodes, with no tendency of producing secondary pollution and fewer accessories required. These advantages make anodic oxidation more attractive than other EO processes. The important part of an anodic oxidation process is obviously the anode material. Anode materials investigated include glassy carbon (135), Ti/RuO_2, Ti/Pt–Ir (112,136), fiber carbon (110), MnO_2 (137,138), Pt-carbon black (139,140), porous carbon felt (141), stainless steel (50), and reticulated vitreous carbon (142,143). However, none of them have sufficient activity and at the same time stability. The anodes that were studied extensively are graphite, Pt, PbO_2, IrO_2, TiO_2, SnO_2, and diamond film. More details will be discussed subsequently.

5.2.1. Overpotential of Oxygen Evolution

As discussed previously, the anodic activity depends on the value of overpotential of oxygen evolution. Table 7 gives a comparison of most extensively investigated anode materials. For a better understanding of the performance of the anodes, the formation potentials of typical oxidants are listed in Table 8. It is clear that IrO_2, Pt, and graphite show much smaller values of overpotential of oxygen evolution. This indicates that effective oxidation of pollutants on these anodes occurs only at very low current densities or in the presence of high concentrations of chlorides or metallic mediators. When the current density is high, significant decrease of the CE is expected from the production of useless oxygen. The boron-doped diamond (BDD) film on titanium substrate (144) or other valve metals as in DiaChem electrodes (145) gives the highest value of oxygen evolution overpotential. Thus anodic oxidation can take place on its surface at significantly high current density with minimal amount of oxygen evolution side-reaction. This leads to an effective and efficient process. It is indeed the most active anode for oxidation of various pollutants as discussed in the following sections.

Table 8
Formation Potential of Typical Chemical Reactants

Oxidants	Formation potential
$H_2O/\cdot OH$ (Hydroxyl radical)	2.80
O_2/O_3 (Ozone)	2.07
$SO_4^{2-}/S_2O_8^{2-}$ (Peroxodisulfate)	2.01
MnO_2/MnO_4^{2-} (Permanganate ion)	1.77
H_2O/H_2O_2 (Hydrogen peroxide)	1.77
Cl^-/ClO_2^- (Chlorine dioxide)	1.57
Ag^+/Ag^{2+} (Silver [II] ion)	1.5
Cl^-/Cl_2 (Chlorine)	1.36
$Cr^{3+}/Cr_2O_7^{2-}$ (Dichromate)	1.23
H_2O/O_2 (Oxygen)	1.23

Source: Refs. 145,223.

5.2.2. *Performance of Anodic Oxidation*

Table 9 compares the performance of different anodes in the degradation of various pollutants under different conditions. Two parameters are of particular concern, one is the current density, and the other is the CE. Comninellis and Plattner (146) proposed to use electrochemical oxidability index (EOI) to differentiate the performances of different electrodes. EOI is the mean CE from the initial concentration of pollutant to the time when the pollutant is nearly zero, τ (143). To calculate EOI, one needs to know the instantaneous CE, ICE, defined as the CE at a given time of EO. Thus,

$$EOI = \frac{\int_0^\tau ICE\,dt}{\tau} \tag{23}$$

Because, so-defined EOI calculation significantly includes the contribution of ICE at long reaction time when the pollutant concentration is very low and mass transfer rather than electrochemical kinetics controls the process. Hence, the EOI so calculated is very low, ranging from less than 0.05–0.58 for electrochemically degrading various benzene derivatives on Pt anode (146). If EOI is to be used, we believe the value of τ should be so selected that it equals to the time when mass transfer control just starts. Because we do not have the values of ICE in which mass transfer control just begins, the average current efficiencies from initial to final values of a process are used for comparison instead.

For graphite electrodes the maximum CE obtained was as high as 70% at very low current densities ranging from 0.03 to 0.32 A/m² (147). When current densities increased to 10–100 A/m², the CE values were only 6–17% (148). Despite the satisfactory results obtained in oxidizing simple inorganic pollutants at very low current densities (149), Pt electrodes show poor efficiencies in anodic oxidation of organic compounds (150,151). The carbon black addition was found to enhance the performance of Ti/Pt anodic oxidation of aqueous phenol significantly (139). As mentioned before, IrO_2 has been widely investigated as an electrocatalyst for O_2 evolution. The low CE is expected (152,153). The low activity of this anode in oxidizing 1,4-benzoquinone may be related to the low current value that has to be employed (154).

Table 9
Comparison of the Performance of Different Anodes

Anode	Pollutant	Current density (A/m²)	CE (%)	Removal efficiency (%)	Comment	Reference
Granular graphite	Phenol	0.03–0.32	70	70, 50 mineralization	5 mo stable operation	147
Planar graphite	Phenol	10–100	24.6–63.5	6–17 (COD)	NaOH as electrolyte	148
Pt or Ti/Pt	Phenol	300	–	30 (TOC)	pH = 12, initial concentration 1000 mg/L, in 0.25 M Na_2SO_4	168
	Ammonia	8.5	53	95	pH = 8.2 using phosphate buffer, poor performance for organics	149
	Glucose	100–900	15–20	30	1 M H_2SO_4	224
	15 organics	–	5	–	–	151
PbO_2	Aniline	I = 2A	15–40	>90 in 1 h	Initial concentration 2.7 mM, pH = 2.0, packed bed of PbO_2	156

(Continued)

Table 9 (*Continued*)

Anode	Pollutant	Current density (A/m²)	CE (%)	Removal efficiency (%)	Comment	Reference
	Phenol	$I = 1, 2, 3A$	–	46–80	Anodic cell: initial concentration 14–56 mM, in 1 N sulfuric acid, packed bed of PbO_2	214
Ti/PbO_2	Phenol	300	–	40 (TOC)	pH = 12, initial concentration 1000 mg/L, in 0.25 M Na_2SO_4	168
	Landfill leachate	50–150	30 for COD / 10 for NH_4^+–N	90 for COD / 100 for NH_4^+–N	–	175
	Glucose	100–900	30–40	100	1 M H_2SO_4	224
	2-Chlorophenol	80–160	35–40	80–95 (COD)	Pb^{2+} formation, initial COD = 1000 mg/L, 25°C	160
IrO_2	Organic 1,4-benzoquinone	Low	17	–	–	152
		–	–	–	Rupture of rings only	154
	Chlorinated phenols	0.6	54	–	Na_2SO_4	153
	2-Chloro-phenol	50	1.8	–	–	
Ti/SnO_2-Sb_2O_5	2-Chloro-phenol	80–160	35–40	80–95, COD	Oxalic acid as intermediates	160

Glucose	100–900	<20	30	$1\,M$ H_2SO_4	224
Phenol	300	–	100	pH = 12.0, initial concentration 1000 mg/L, in 0.25 M Na_2SO_4	168
	500	58	–	70°C, 10 mM	152
	–	–	–	CV method, similar to PbO_2	174
Landfill leachate	–	–	–	Similar to PbO_2	175
Ebonex Trichloro-ethylene	Fixed potential 2.5–4.3 V	<32	10–70	Stable in aqueous media, Ti_4O_7 to TiO_2	182

PbO_2 is the most widely investigated anode material for EO. Usually, PbO_2 electrodes are prepared either by anodically polarizing metal lead in H_2SO_4 solutions (155,156) or by electrochemically coating PbO_2 films on Ti substrates (152). In order to increase the activity, PbO_2 is sometimes doped by Bi, Fe, Ag (157–159). For oxidation of organic pollutants like aniline PbO_2 anode is very efficient with reasonable value of CE (156). The operating current density is also of reasonable value, 80–160 A/m^2 (160). PbO_2 electrodes are relatively cheap and effective in oxidizing pollutants. The only concern for this electrode is the formation of Pb^{2+} ions from the electrochemical corrosion.

Pure SnO_2 is an *n*-type semiconductor with a band gap of about 3.5 eV. The valence band arises because of the overlap of filled oxygen 2p levels. The tin 5s states are at the bottom of the conduction band (161). This kind of oxide exhibits a very high resistivity at room temperature and thus cannot be used as an electrode material directly. However, its conductivity can be improved significantly by doping Ar, B, Bi, F, P, and Sb (162–168). In electrochemical application, Sb is the most common dopant of SnO_2. Doped SnO_2 films are usually used as transparent electrodes in high-efficiency solar cells, gas detectors, far IR detectors and transparent heating elements (161). The conductive SnO_2 films can be prepared by vapor deposition (163), sputtering (169), spray pyrolysis (168,170), sol–gel (171), and brush-dry-bake technique (172). The onset potential for O_2 evolution on Sb-doped SnO_2 is about 1.9 V vs NHE in 0.5 *M* H_2SO_4 solution (173), similar to that on PbO_2.

Kotz and coworkers (168) first reported anodic oxidation of pollutants on Sb-doped SnO_2 coated titanium electrodes (Ti/SnO_2–Sb_2O_5). The CE obtained on Ti/SnO_2–Sb_2O_5 was about 5 times higher than that on Pt (151). Comninellis (152) measured the CE of SnO_2–Sb_2O_5 to be 0.58 for 71% degradation of phenol, whereas the values for PbO_2, IrO_2, RuO_2 and Pt are 0.18, 0.17, 0.14, and 0.13 respectively at $i = 500$ A/m^2, pH = 12.5, initial concentration of 10 mM, reaction temperature of 70°C. Grimm et al. (174) investigated phenol oxidation on SnO_2–Sb_2O_5 and PbO_2 using a cyclic voltammetric method and also found that the former was more active. Nevertheless, Cossu et al. (175) reported that there was no substantial difference in activity between SnO_2–Sb_2O_5 and PbO_2 in treating landfill leachate. This might be associated with the presence of high concentrations of chlorides in this type of waste.

Despite the high efficiency for pollutant oxidation, Sb_2O_5–SnO_2 electrodes lack sufficient electrochemical stability just like PbO_2. Lipp and Pletcher (172) conducted a long term test of SnO_2–Sb_2O_5 in 0.1 *M* H_2SO_4 solution at a constant potential of 2.44 V vs NHE and found that the current dropped from initial 0.2 A to about 0.1 A within a few hours and to 0.06 A after 700 h. Correa-Lozano et al. (176) also investigated the stability of Sb_2O_5–SnO_2 electrodes and found that the service life of Ti/Sb_2O_5–SnO_2 was only 12 h under an accelerated life test performed at a current density of 1000 A/m^2 in 1 *M* H_2SO_4 solution. At 10,000 A/m^2 and 3 *M* H_2SO_4, this electrode can only last a few seconds (177). Although addition of IrO_2 into the SnO_2–Sb_2O_5 mixture increased the service life significantly (77,78), the resulting electrodes have an overpotential of O_2 evolution of 1.5 V vs NHE in 0.5 *M* H_2SO_4 electrolyte.

Pure TiO_2 has a band gap of 3.05 eV (178) and thus shows poor conductivity at a room temperature. TiO_2 is usually used as a photocatalyst in wastewater treatment. By doping with Nb and/or Ta, TiO_2 conductivity was successfully improved (179,180)

to be used as an electrocatalyst for pollutant oxidation. This type of electrodes is usually made by baking the Ti substrates coated with Nb and/or Ta-doped TiO_2 films at 450°C, followed by annealing the films at 650–800°C in the presence of H_2 and a small amount of water vapor to reduce the Nb(V) to Nb(IV). The preferred molar concentration of (Nb + Ta) in the oxide coating is 2–6% (179). TiO_2 electrodes are stable at low current densities (<30 A/m^2), but their lifetimes are significantly shortened when operated at high current densities (180). Another conductive titanium oxide is Ebonex® that is also able to serve as an anode material. Ebonex is a nonstoichiometric titanium oxide mixture comprised of Magneli phase titanium oxides Ti_4O_7 and Ti_5O_9, and made by heating TiO_2 to 1000°C in the presence of H_2 (181). Although Ebonex is stable in aqueous media throughout the practical pH range, anodic oxidation in 1 *M* sulfuric acid results in partial oxidation of Ti_4O_7 to TiO_2, and surface passivation under extreme conditions may be an issue (182).

5.2.3. BDD Electrode

Diamond is a fascinating material. Diamond is known for its high strength, extreme hardness, high resistance to thermal shock, and infrared transmissivity (183). It exhibits many unique technologically important properties, including high thermal conductivity, wide band gap, high electron and hole mobilities, high breakdown electric field, hardness, optical transparency, and chemical inertness (184). Structurally, diamond has a cubic lattice constructed from sp^3-hybridized tetrahedrally arranged carbon atoms with each carbon atom bonded to four neighbors (185). The stacking sequence is ABCABC with every third layer plane identical. This structure is fundamentally different from that of graphite which consists of layers of condensed polyaromatic sp^2-hybridized rings with each carbon atom bonded to three neighbors. Impurities in diamond can make it an insulator with a resistivity of $>10^6$ Ω·m and a band gap energy of 5.5 eV (181). A recent finding from Sweden shows that pure diamond can be a very good conductor of electrons (186). Diamond films are usually synthesized by chemical vapor deposition (CVD) (187). Early CVD of diamond was carried out by thermal decomposition of carbon-containing gases such as CH_4 and CO (188,189) at gas temperatures between 600°C and 1200°C. The gas temperatures were about the same as the surface temperature of the diamond seeds that were exclusively used as substrates. The diamond growth rates were only about 0.01 µm/h, too low to be of commercial significance. In addition, the material was often contaminated with nondiamond carbon and required frequent interruptions to remove the accumulated graphite by hydrogen etching at a temperature >1000°C and a pressure >50 atm, or by oxidizing in air at the atmospheric pressure (190). In the mid-1970s, Derjaguin and Fedoseev (191) recognized the crucial role of atomic hydrogen in etching graphite deposits preferentially and successfully synthesized diamond on nondiamond substrates at a commercially practical deposition rate (>1 µm/h). This was a historic milestone in the development of diamond CVD techniques. However, intensive interests in diamond CVD did not arise until the early 1980s when Matsumoto and coworkers (192,193) revealed the details of synthesizing high-quality diamond films on Si and Mo substrates using hot-filament CVD (HFCVD). The typical deposition conditions were: methane concentration 1% in hydrogen, substrate temperature 700–1000°C, filament temperature ~2000°C, total gas pressure 13–133 mbar,

and reaction time 3 h. Since then, new techniques such as microwave plasma-assisted CVD (194) and DC discharge CVD (195) were developed rapidly. The diamond growth rates are in the order of 0.1 to near 1000 μm/h (196), demonstrating the good prospect of diamond films for industrial applications.

The conductivity of diamond can be improved significantly by doping boron. Boron doping is usually achieved by adding B_2H_6 (197,198), or $B(OCH_3)_3$ (199,200) to the gas stream, or placing boron powder near the edges of the substrate prior to insertion into the CVD chamber (201). A general useful range of the boron/carbon weight ratio in the BDD is from approx 0.02 to 10^{-6} (202). The onset potential for O_2 evolution on BDD film on silicone substrate (Si/BDD) electrodes in 0.5 M H_2SO_4 solution is about 2.3 V vs NHE (200,203), 0.4 V higher than that on PbO_2 and SnO_2. This indicates that diamond electrodes have higher CE for pollutant oxidation. Besides the increase in oxygen overpotential, the increase in hydrogen overpotential was also found by doping nitrogen leading to the widest window for water split reaction (145). This conductive BDD film opened new frontiers of the diamond application in electrochemical synthesis and analysis, sensor development for in vitro or in vivo biomedical application, for long-term environmental studies. Particularly, BDD film was found to be the most active anodic material for degradation of refractory or priority pollutants such as ammonia, cyanide, phenol, chlorophenols, aniline, TCE, various dyes, surfactants, landfill leachate (144,204–207).

Unlike PbO_2, SnO_2, and TiO_2, the BDD thin films deposited on Si, Ta, Nb, and W by CVD have shown excellent electrochemical stability (200). The lifetime of Nb/BDD, for example, is over 850 h in the accelerated life test performed at 100,000 A/m^2 in 0.5 M H_2SO_4 solution. Even after several weeks of oxidation, the properties of these electrodes were not affected and poisoning of the surface was not detectable. However, Si/BDD electrodes are not suitable for industrial applications because Si substrates are very brittle and their conductivity is poor. Yet, large-scale usage of Nb/BDD, Ta/BDD, and W/BDD electrodes is impossible because of the unacceptably high costs of Nb, Ta, and W substrates.

Basically, the function of a substrate is to provide a facile pathway for the flow of current through the electrode assembly and a mechanical support for the thin diamond film. Probably the materials that can be used as substrates must simultaneously have three important attributes: good electrical conductivity, sufficient mechanical strength, and electrochemical inertness or easy formation of a protective film on its surface by passivation (202). In addition, the costs of the materials should be acceptable. Titanium possesses all these features and is therefore considered to be a good substrate material. Actually, this metal has been widely used in DSA® for over 30 yr. The deposition of stable BDD films on Ti substrates with CVD from the standard gas mixture of $H_2 + CH_4$ is very difficult up to date. Cracks may appear leading to the delamination of the diamond films under electrochemical attack at high loads (200). By adding $CH_2(OCH_3)_2$ in the precursor gas, Chen and coworkers (144,207) have managed to deposit a BDD film on Ti substrate with satisfactory stability. Nowadays, diamond films can be deposited on the substrates with various geometries up to 0.5 m^2 using hot-filament CVD method (208).

Carey et al. (202) patented the use of diamond films as anodes for organic pollutant oxidation. The Si/BDD electrodes they used were commercially obtained from Advanced Technology Materials, Inc. The boron concentrations in the diamond films were 1000–10,000 ppm. Different wastewaters and solutions were investigated. Some

Table 10
Treatment of Different Wastewaters and Solutions Using Si/BDD Electrodes

Wastewater/solution	Oxidation conditions	COD reduction (%)
Kodak E6 first developer	Initial COD 32,500 mg/L; solution volume 30 mL; current 0.31 A; current density 1000 A/m^2; electrolysis time 6.25h	73
Kodak E6 color developer	Initial COD 19,050 mg/L; solution volume 30 mL; current 0.31 A; current density 1000 A/m^2; electrolysis time 4.75 h	80
Phenol solution	Initial COD 3,570 mg/L; solution volume 60 mL; current 0.31 A; current density 1000 A/m^2; electrolysis time 18 h	94
Hydroquinone solution	Initial COD 23,530 mg/L; solution volume 60 mL; current 0.15 A; current density 500 A/m^2; electrolysis time 38 h	97

Source: Ref. 202.

Table 11
Oxidation of Various Organic Compounds on Si/BDD Electrodes

Compound	Oxidation conditions	CE (%)
Phenol	Initial concentration 0.002 M; current density 300 A/m^2; pH 2.0; charge loading 4.5 Ah/L; final phenol concentration <3 mg/L	33.4[a]
CN$^-$	Initial concentration 1 M; current density 360 A/m^2; 95% CN$^-$ elimination; 1 M KOH	41
Isopropanol	Initial concentration 0.17 M; current density 300 A/m^2; <90% conversion	>95
Acetic acid	Initial concentration 0.17 M; current density 300 A/m^2; 90% conversion; 1 M H$_2$SO$_4$	85

[a]Calculated value based on charge loading.
Source: Ref. 200,209,210.

results are summarized in Table 10. A Switzerland research group (200,209,210) also investigated anodic oxidation of various pollutants on Si/BDD electrodes. The results are summarized in Table 11. The CE obtained is very high, ranging from 33.4 to over 95%, depending on pollutant properties and oxidation conditions.

Beck et al. (211) compared Si/BDD with Ti/SnO$_2$, Ta/PbO$_2$, and Pt for oxidation of phenol. At a charge loading of 20 Ah/L, the total organic carbon (TOC) was reduced from

Table 12
Comparison of Ti/BDD With Ti/Sb$_2$O$_5$–SnO$_2$ for Pollutant Oxidation

				Ti/BDD		Ti/Sb$_2$O$_5$–SnO$_2$	
Pollutant	Current density (A/m^2)	Charge (Ah/L)	Initial COD (mg/L)	Final COD (mg/L)	CE (%)	Final COD (mg/L)	CE (%)
Acetic acid	200	5.53	1090	33	64	756	20.2
Maleic acid	200	6.43	1230	46	61.7	557	35
Phenol	100	4.85	1175	39	78.5	450	50.1
Orange II	200	6.25	1120	95	54.9	814	16.4
Reactive red HE-3B	200	6.25	920	45	46.9	714	11

Source: Ref. 206.
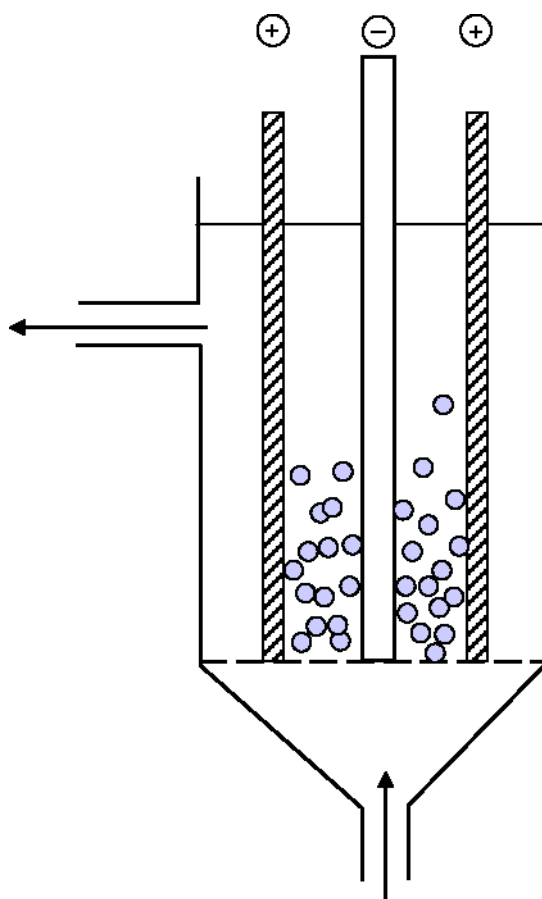
Fig. 22. Reactor with cylindrical electrodes.

initial 1500 mg/L to about 50 mg/L on Si/BDD, and to about 300, 650, and 950 mg/L on Ti/SnO$_2$, Ta/PbO$_2$, and Pt, respectively. Obviously, Si/BDD electrodes have much higher activity than other electrodes. The performance of Ti/BDD anode is given in Table 12 (206).
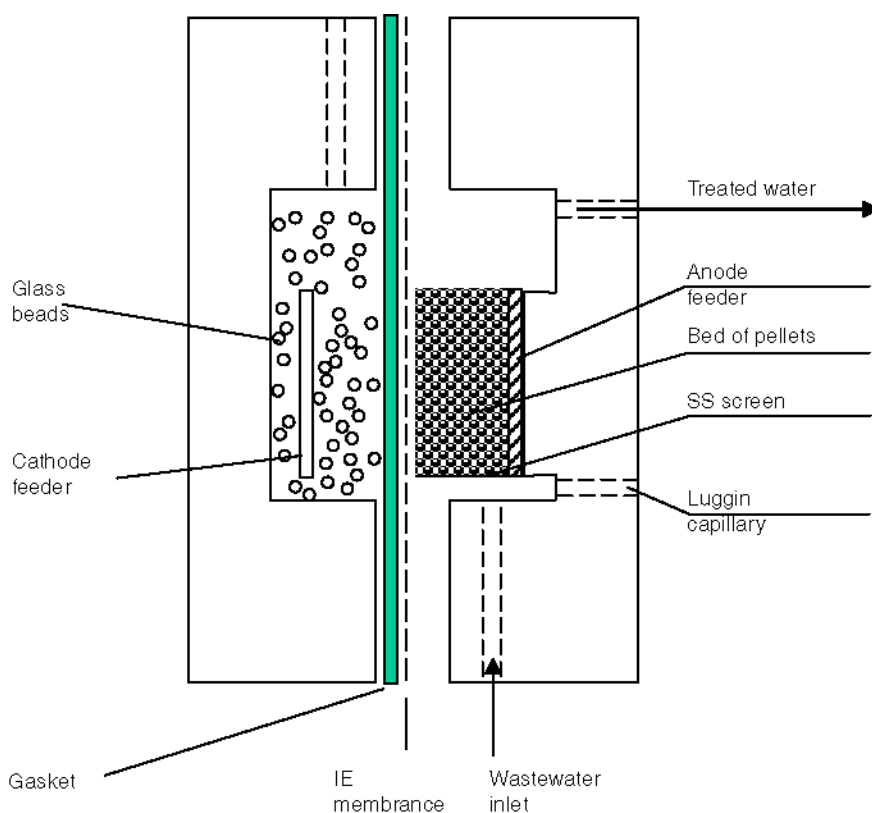
Fig. 23. Packed bed electrochemical reactor.

5.3. *Typical Designs*

The EO reactors are similar to those seen in Section 2.1. for metal recoveries. The concerns are also the *CE* and also the space–time yield. The simplest EO reactor design is the bipolar cell. Besides plane electrodes, the cylindrical electrodes can also be employed (140,212,213; Fig. 22). Inside the cylindrical anode, there are spherical particles with BDD coating serving as the bipolar electrodes. Packed bed of about 1 mm pellets of proper anode materials can also be used (214,215; Fig. 23). Figure 24 shows the bipolar trickle tower that can be employed with insulating net separating adjacent layers of bipolarized packing (216,217). Filter press reactor is another design (218). In order to improve mass transfer to the surface of the electrode, sonoelectrochemical process has been tested and proven enhancement was achieved (219,220). A thin layer of biofilm can be immobilized on the surface of electrodes to have a bioelectro reactor. It was found to be capable of oxidation and reduction simultaneous in nitrification and denitrification when respective microorganisms are immobilized on the anode (221–224).

6. SUMMARY

Electrochemical technologies have been investigated as the effluent treatment processes for over a century. Fundamental as well as engineering researches have established
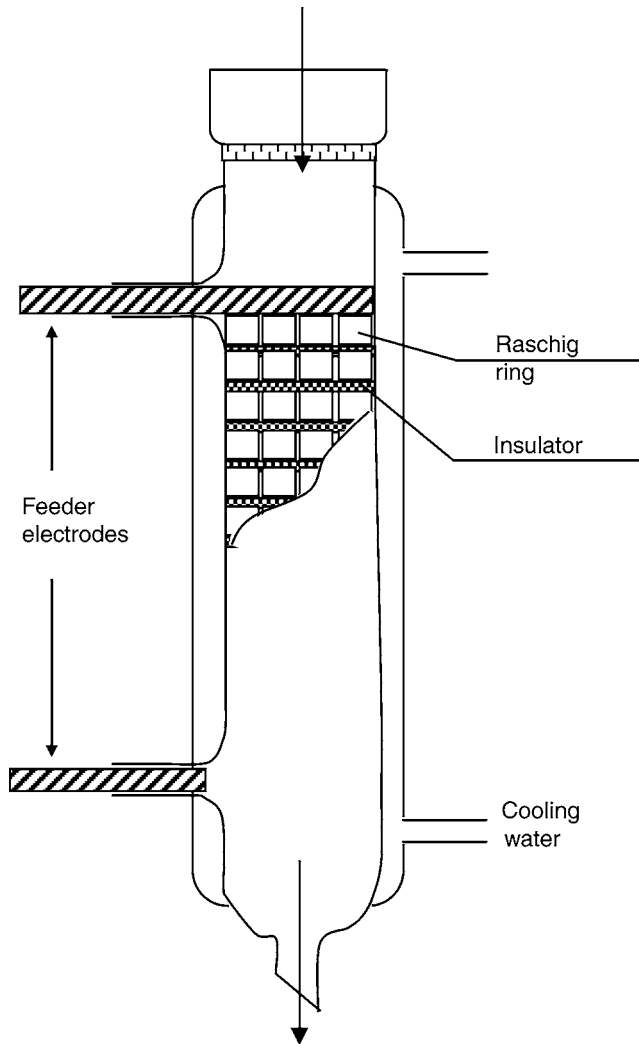
Fig. 24. Bipolar trickle tower electrochemical reactor.

the electrochemical deposition technology in metal recovery or heavy metal effluent treatment. EC has been used industrially and demonstrated its superior performances in treating effluents containing SS, oil and grease, and even organic or inorganic pollutants that can be flocculated. EF is widely used in the mining industries and is finding increasing applications in wastewater treatment. The uniform and tiny sized bubbles generated electrically give much better performance than dissolved air floatation, sedimentation or even impeller flotation. This process is compact and easy to facilitate with automatic control. With the invention of stable, active and cheap materials for oxygen evolution, this technology will gradually replace the conventional flotation techniques. Indirect oxidation is still a viable technology for treating toxic or biorefractory pollutants, although, there are concerns about the formation of chlorinated intermediates in the case of using chlorine ions or about the complicated facilities in the case of using electrically formed hydrogen

peroxide or ozone. Direct anodic oxidation represents one of the simplest technologies in the pollutant mineralization provided the anode materials are stable and have high overpotential of oxygen evolution. The investigation of various materials so far shows that titanium or other noble metal-based BDD film is the candidate for industrial application. It has the widest window for water split and is inert in tough situations. Further improvement in its stability in electrochemical application is required before its industrial acceptance (225–227).

NOMENCLATURE

a	Specific electrode area (m^2/m^3)
A	Area of electrode (m^2)
CE	Current efficiency
d	Net distance between electrodes (m)
E	Constant in Eq. (16) and Eq. (17) (V)
E_{eq}	Equilibrium potential difference between an anode and a cathode (V)
F	Faraday constant (C/mol)
i	Current density (A/m^2)
I	Current (A)
K_1	Constant in Eq. (16) and Eq. (17)
K_2	Constant in Eq. (17)
m	Constant in Eq. (17)
M	Molecular mass (g/mole)
n	Constant in Eq. (17)
N	Total electrode number of an EC unit
U	Total required electrolysis voltage of an EC process (V)
U_0	Electrolysis voltage between electrodes (V)
Y_{ST}	Space–time yield
z	Charge number
α	Constant in Eq. (20)
$\eta_{a,a}$	Anode activation overpotential (V)
$\eta_{a,c}$	Anode concentration overpotential (V)
$\eta_{a,p}$	Anode passive overpotential (V)
$\eta_{c,a}$	Cathode activation overpotential (V)
$\eta_{c,c}$	Cathode concentration overpotential (V)
κ	Conductivity of water/wastewater treated (S/m)

REFERENCES

1. P. P. Strokach, Electrochem. Ind. Process. Bio. 55, 375 (1975).
2. F. E. Elmore, A process for separating certain constituents of subdivided ores and like substances, and apparatus therefore, British patent 13,578 (1905).
3. F. E. Stuart, Electronic water purification; Progress report on the electronic coagulator—a new device which gives promise of unusually speedy and effective results, *Water and Sewage*, **84**, 24–26 (1946).
4. C. F. Bonilla, Possibilities of the electronic coagulator for water treatment, *Water and Sewage*, **85**, 21–22, 44–45 (1947).

5. T. R. Yu and G. L. Ji, *Electrochemical Methods in Soil and Water Research*, Pergamon Press, Oxford, 1993.
6. F. Goodridge and K. Scott, Electrochemical Process Engineering, A guide to the design of electrolytic plant, Plenum Press, NY, 1995.
7. K. Scott, *Electrochemical Processes for Clean Technology*, The Royal Society of Chemistry, London, 1995.
8. K. Rajeshwar and J. Ibanez, *Environmental Electrochemistry: Fundamentals and Applications in Pollution Abatement*, Academic Press, San Diago, 1997.
9. G. Dubpernel, In Selected Topics in the History of Electrochemistry; The Electrochemical Society: Princeton, p. 1, 1978.
10. K. C. Bailey, The Elder Pliny's Chapters on Chemical Subjects, Part II, Edward Arnold: London, p. 60, 1932.
11. B. Fleet, Evolution of Electrochemical Reactor Systems for Metal Recovery and Pollution Control, in Electrochemistry, Past and Present, J. T. Stock and M. V. Orna (eds.), Americal Chemical Society, Washington, DC, 1989.
12. J. J. Leddy, Industrial Electrochemistry, in Electrochemistry, Past and Present, J. T. Stock and M. V. Orna, (eds.), Americal Chemical Society, Washington, DC, p. 478, 1989.
13. S. Ehdaie, M. Fleischmann, R. E. W. Jansson, and A. E. Alghaoui, Application of the trickle tower to problems of pollution-control. I. the scavenging of metal-ions, *J. Appl. Electrochem.* **12**, 59–67 (1982).
14. D. R. Gabe and F. C. Walsh, The rotating cylinder electrode—a review of development, *J. Appl. Electrochem.* **13**(1), 3–22 (1983).
15. F. C. Walsh, D. R. Gabe, and N. A. Gardner, Development of the eco-cascade—cell reactor, *J. Appl. Electrochem.* **12**(3), 299–309 (1982).
16. R. E. W. Jasson and N. R. Tomov, *Chem. Eng.* 316, 867 (1977).
17. R. E. W. Jasson, R. J. Marshall, and J. E. Rizzo, The rotating electrolyser, I: The velocity field, *J. Appl. Electrochem.* **8**, 281–285 (1978).
18. R. E. W. Jasson, R. J. Marshall, and J. E. Rizzo, The rotating electrolyser, II: Transport properties and design equations, *J. Appl. Electrochem.* **8**, 287–291 (1978).
19. R. Kammel and E. Hasan Guenduez, Review and outlook on continuous metal electrowinning and recovery processes from aqueous solutions, *Metallurgical Soc. of AIME*, Warrendale, PA, USA. 647–657 (1982).
20. J. R. Backhurst, J. M. Coulson, F. Goodridge, R. E. Plimley, and M. Fleischmann, A preliminary investigation of fluidised bed electrodes, *J. Electrochem. Soc*. **116**, 1600–1607 (1969).
21. G. Van der Heiden, C. M. S. Raats, and H. F. Boon, *Chem and Ind. (London)*, **13**, 465 (1978).
22. G. Kreysa, *Chem. Ing. Tech.* **50**, 332 (1978).
23. G. Kreysa and C. Reynvaan, Optimal-design of packed-bed cells for high conversion, *J. Appl. Electrochem.* **12**(2), 241–251 (1982).
24. J. G. Sunderland and I. M. Dalrymple, Cell and method for the recovery of metal from dilute solutions, US Patent, 5, 690, 806 (1997).
25. H. B. Beer, Electrode and coating therefore, US patent 3, 632, 498 (1972).
26. F. Shen, P. Gao, X. Chen, and G. Chen, Electrochemical removal of fluoride ions from industrial wastewater, *Chem. Eng. Sci.* **58**, 987–993 (2003).
27. V. K. Kovatchva and M. D. Parlapanski, Sono-electrocoagulation of iron hydroxides, *Col. Surf.* **149**, 603–608 (1999).
28. L. A. Kul'skii, P. P. Strokach, V. A. Slipchenko, and E. I. Saigak, Water Purification by Electrocoagulation Kiev, Budivel'nik (1978).
29. X. Chen, G. H. Chen, and P. L. Yue, Separation of pollutants from restaurant wastewater by electrocoagulation. *Separ. Pur. Technol.* **19**, 65–76 (2000).

30. H. M. Wong, C. Shang, Y. K. Cheung, and G. Chen, Chloride Assisted Electrochemical Disinfection, The Eighth Mainland-Taiwan Environmental Protection Conference, Tsin Chu, Taiwan, 2002.

31. E. A. Vik, D. A. Carlson, A. S. Eikum, and E. T. Gjessing, Electrocoagulation of potable water. *Water Res.* **18**, 1355–1360 (1984).

32. F. Li, S. Li, C. Zhang, and H. Zhao, Application of corrosive cell process in treatment of printing and dyeing wastewater, *Chem. Eng. Environ. Protec.* **15**, 157–161 (1995).

33. M. Qiu, *Water Purification by Electrocoagulation*, Chinese Translation from Russian of the book by L. A. Kul'skii, P. P. Strokach, V. A. Slipchenko, and E. I. Saigak, Kiev, Budivel'nik, 1978. Shanghai Jiaotong University Press, 1988.

34. T. Ya. Pazenko, T. I. Khalturina, A. F. Kolova, and I. S. Rubailo. Electrocoagulation treatment of oil-containing wastewaters. *J. Appl. USSR*, **58**, 2383–2387 (1985).

35. X. Chen, G. Chen, and P. L. Yue, Modeling the Electrolysis Voltage of Electrocoagulation Process Using Aluminum Electrodes, *Chem. Eng. Sci.* **57**(13), 2449–2455 (2002).

36. P. E. Ryan, T. F. Stanczyk, and B. K. Parekh, Solid/liquid separation using alternating current electrocoagulation, *1989 International Symposium on Solid/Liquid Separation: Waste Management and Productivity Enhancement*, pp. 469–478, 1989.

37. V. A. Matveevich, Electrochemical methods of natural and waste water purifying, *Elektronnaya Obrabotka Materialov*, **5**, 1030114 (2000).

38. S. H. Lin and C. F. Peng, Treatment of textile waste-water by electrochemical method. *Water Res*. **28**(2), 277–282 (1994).

39. S. H. Lin and C. F. Peng, Continuous treatment of textile wastewater by combined coagulation, electrochemical oxidation and activated sludge. *Water Res.* **30**, 587–592 (1996).

40. S. H. Lin and M. L. Chen, Treatment of textile waste-water by chemical methods for reuse, *Water Res*. **31**(4), 868–876 (1997).

41. L. J. Gao and Y. F. Cheng, Treatment of printing and dyeing wastewater using pulsed high voltage electrocoagulation flocculation method, *Environ. Pollut. Control* **14**(5), 10–13 (Chn) 1992.

42. G. Chen, X. Chen, and P. L. Yue, Electrocoagulation and Electroflotation of Restaurant Wastewater, *J. Envir. Eng.* **126**(9), 858–863 (2000).

43. R. R. Renk, Electrocoagulation of tar sand and oil shale wastewaters, *Energy Prog.* **8**, 205–208 (1988).

44. T. R. Demmin and K. D. Uhrich, Improving carpet wastewater treatment, *Am. Dyestuff Rep.* **77**, 13–18, 32 (1988).

45. M. F. Pouet and A Grasmick, Urban wastewater treatment by electrocoagulation and flotation, *Water Sci. Technol*. **31**, 275–283 (1995).

46. S. H. Lin and C. S. Lin, Reclamation of wastewater effluent from a chemical fiber plant, *Desalination* **120**, 185–195 (1998).

47. G. V. Sleptsov, A. I. Gladkii, E. Ya. Sokol, and S. P. Novikova, Electrocoagulation treatment of oil emulsion wastewaters of industrial enterprises, *Elektronnaya Obrabotka Materialov* **6**, 69–72 (1987).

48. U. B. Ogutveren and S. Koparal, Electrocoagulation for oil-water emulsion treatment, *J. Environ. Sci. Health* A **32**(9–10), 2507–2520 (1997).

49. J. Szynkarczuk, J. Kan, T. A. T. Hassan, and J. C. Donini, Clays, *Clay Miner*. **42**, 667 (1994).

50. N. S. Abuzaid, Z. Al-Hamouz, A. A. Bukhari, and M. H. Essa, Electrochemical treatment of nitrite using stainless steel electrodes, *Water Air and Soil Poll.* **109**, 429–442 (1999).

51. U. B. Ogutveren and S. Koparal, Electrochemical treatment of water containing dye-stuffs: anodic oxidation of congo red and xiron blau 2RHD, *Int. J. Environ. Studies*, **42**, 41–52 (1992).

52. R. S. Yeh, Y. Y. Wang, and C. C. Wan, Removal of Cu-EDTA compounds via electrochemical process with coagulation, *Water Res.* **29**(2), 597–599 (1994).
53. G. B. Raju and Khangaonkar, Electroflotation–A critical review, *Trans. Indian Inst. Metals* **37**(1), 59–66 (1984).
54. Y. Fukui and S. Yuu, Removal of colloidal particles in electroflotation, *AIChE J.* **31**(2), 201–208 (1985).
55. V. A. Glembotskii, A. A. Mamakov, A. M. Ramanov, and V. E. Nenno, 11th International Mineral Processing Congress, Caglairi, 562–581, 1975.
56. C. Llerena, J. C. K. Ho, D. L. Piron, Effect of pH on electroflotation of sphalerite, *Chem. Eng. Commun.* **155**, 217–228 (1996).
57. D. R. Ketkar, R. Mallikarjunan, and S. Venkatachalam, 1988, Size determination of electrogenerated gas bubbles, *J. Electrochem. Soc. India* **37**(4), 313 (1996).
58. D. R. Ketkar, R. Mallikarjunan, and S. Venkatachalam, Electroflotation of quartz fines, *Int. J. Miner. Proc.* **31**, 127–138 (1991).
59. S. E. Burns, S. Yiacoumi, and C. Tsouris, Microbubble generation for environmental and industrial separations, *Separ. Pur. Technol.* **11**, 221–232 (1997).
60. C. P. C. Poon, Electroflotation for groundwater decontamination, *J. Hazard. Mater.* **55**, 159–170 (1997).
61. A. Y. Hosny, Separating oil from oil-water emulsions by electroflotation technique, *Separ. Technol.* **6**, 9–17 (1996).
62. X. Chen, G. Chen, and P. L. Yue, A Novel Electrode System for Electro-flotation of Wastewaters, *Environ. Sci. Technol.* **36**(4), 778–783 (2002).
63. D. G. Stevenson, *Water Treatment Unit Processes*, Imperial College Press: London, 1997.
64. C. Tsouris, D. W. Depaoli, J. Q. Feng, O. A. Basaran, and T. C. Scott, Electrostatic spraying of nonconductive fluids into conductive fluids, *AIChE J.* **40**(11), 1920–1923 (1994).
65. V. I. Il'in and O. N. Sedashova, An electroflotation method and plant for removing oil products from effluents, *Chem. Petrol. Eng.* **35**(7–8), 480–481 (1999).
66. M. Y. Ibrahim, S. R. Mostafa, M. F. M. Fahmy, and A. I. Hafez, Utilization of electroflotation in remediation of oily wastewater, *Separ. Sci. Technol.* **36**(16), 3749–3762 (2001).
67. L. Alexandrova, T. Nedialkova, I. Nishkov, Electroflotation of metal ions in waste water, *Int. J. Miner. Process.* **41**, 285–294 (1994).
68. C. C. Ho and C. Y. Chan, The application of lead dioxide-coated titanium anode in the electroflotation of palm oil mill effluent, *Water Res.* **20**, 1523–1527 (1986).
69. F. Hine, M. Yasuda, T. Noda, T. Yoshida, and J. Okuda, Electrochemical behavior of the oxide-coated metal anodes, *J. Electrochem. Soc.* **126**, 1439–1445 (1979).
70. V. A. Alves, L. A. D. Silva, E. D. Oliveira, and J. F. C. Boodts, Investigation under conditions of accelerated anodic corrosion of the effect of TiO_2 substitution by CeO_2 on the stability of Ir-based ceramic coatings, *Mater. Sci. Forum* **289–292**, 655–666 (1998).
71. J. Rolewicz, Ch. Comninellis, E. Plattner, and J. Hinden, Characterisation des electrodes de type DSA pour le degagement de O_2-I. l'electrode Ti/IrO_2-Ta_2O_5, *Electrochim. Acta* **33**, 573–580 (1988).
72. Ch. Comninellis and G. P. Vercesi, Problems in DSA® coating deposition by thermal decomposition, *J. Appl. Electrochem.* **21**, 136–142 (1991).
73. Ch. Comninellis and G. P. Vercesi, Characterization of DSA-type oxygen evolving electrodes: choice of a coating, *J. Appl. Electrochem.* **21**, 335–345 (1991).
74. G. P. Vercesi, F. Rolewicz, and Ch. Comninellis, Characterization of DSA-type oxygen evolving electrodes: choice of base metal, *Thermochim. Acta* **176**, 31–47 (1991).
75. V. A. Alves, L. A. D. Silva, J. F. C. Boodts, and S. Trasatti, Kinetics and mechanism of oxygen evolution on IrO_2-based electrodes containing Ti and CE acidic solutions, *Electrochim. Acta* **39**, 1585–1589 (1994).

76. R. Mraz and J. Krysa, Long service life IrO_2/Ta_2O_5 electrodes for electroflotation, *J. Appl. Electrochem.* **24**, 1262–1266 (1994).

77. X. Chen, G. H. Chen, and P. L. Yue, Stable Ti/IrO_x-Sb_2O_5-SnO_2 anode for O_2 evolution with low Ir content, *J. Phys. Chem. B* **105**, 4623–4628 (2001).

78. G. Chen, X. Chen, and P. L. Yue, Electrochemical behavior of stable Ti/IrO_x-Sb_2O_5-SnO_2 anodes for oxygen evolution, *J. Phys. Chem. B* **106** (17), 4364–4369 (2002).

79. V. K. Makarenko and A. Yu. Klimov, An electroflotation device for extracting suspended particles from liquids, *Elektronnaya Obrabotka Materialov* **4**(106), 89–90 (1982).

80. V. I. Il'in, V. A. Kolesnikov, and Yu. I. Parshina, Purification of highly concentrated industrial sewage from the porcelain and faience industry by the electric flotation method, *Glass and Ceramics* **59**(7–8), 242–244 (2002).

81. V. D. Gvozdez and B. S. Ksenofontov, Waste water treatment in an electroflotation apparatus with a fluidized media, *Khimiya I Tekhnologiya Vody* **8**(4), 70–72 (1986).

82. I. A. Zolotukhin, Effect of built-in partitions and electrode systems on the operating efficiency of an electroflotation unit, *Khimiya i Tekhnologiya Vody* **10**(4), 342–344 (1988).

83. C. Camilleri, Electroflottation et flotation al'air disous, *Indus. Miner. Les Techniques* **67**(1), 25–30 (1985).

84. V. A. Kolesnikov, V. I. Il'in, S. O. Varaksin, and V. T. Shaturov, Electroflotation method and equipment for removing metals and organic contaminants from waste waters, *Russian J. Heavy Machinery* **1**, 37–38 (1996).

85. N. V. Tyabin, G. L. Dakhina, A. G. Golovanchikov, and A. A. Mamakov, Design of ideal displacement reactos for the separation of fine suspensions by electrolytic gases, *Theoretical Foundations of Chem. Eng.* **13**(6), 757–761.

86. V. E. Nenno, V. I. Zelentsov, E. V. Mel'nichuk, A. M. Romanov, T. Ya. Datsko, and T. M. Radzilevich, Experience in operating a device for concentration of mineral raw material combining electroflotation and separation in a froth layer, *Electronnaya Obrabotka Materialov* **6**, 77–79 (1988).

87. W. Chen and N. J. Horan, The treatment of a high strength pulp and paper mill effluent for wastewater re-use—III) Tertiary treatment options for pulp and paper mill wastewater to achieve effluent recycle, *Environ. Technol.* **19**, 173–182 (1998).

88. C. J. Huang and J. C. Liu, Precipitate flotation of fluoride-containing wastewater from a semiconductor manufacturer, *Wat. Res.* **33**, 3403–3412 (1999).

89. P. Lafrance and D. Grasso, Trajectory modelling of non-Brownian particle flotation using an extended Derjaguin-Landau-Verwey-Overbeek approach, *Environ. Sci. Technol.* **29**, 1346–1352 (1995).

90. N. T. Manjunath, I. Mehrotra, and R. P. Mathur, Treatment of wastewater from slaughterhouse by DAF-UASB system, *Water Res.* **34**, 1930–1936 (2000).

91. R. L. Vaughan, B. E. Reed, G. W. Roark, and D. A. Masciola, Pilot-scale investigation of chemical addition-dissolved air flotation for the treatment of an oily wastewater, *Environ. Eng. Sci.* **17**, 267–277 (2000).

92. L. M. Balmer and A. W. Foulds, Separation oil from oil-in-water emulsions by electroflocculation/electroflotation. *Fil. Separ.* **23**(11/12), 366–369 (1986).

93. V. I. Il'in, Unit for sewage cleaning from petroleum products, *Khimicheskoe i Neftyanoe Mashinostroenie* **5**, 41–42 (2002).

94. M. F. Prokop'eva, V. N. Tkacheva, and E. Yu. Kirshina, A gas chromographic investigation of the composition of spent cooling lubricants and the products formed during their electroflotation-coagulation treatment, *Khimiya i Tekhnologia Vody* **10**(4), 335–337 (1988).

95. I. V. Aleksandrov, O. I. Rodyushkin, and K. S. Ibraev, Electroflotation treatment of wastewaters from by-product coke production to remove tars and oils, *Koks I Khimiya* **7**, 41–44 (1992).

96. B. J. Hernlem and L. S. Tsai, Chlorine generation and disinfection by electroflotatioin, *J. Food Sci.* **65**, 834–837 (2000).

97. O. R. Shendrik, E. E. Andreeva, M. I. Ponomareva, and I. B. Ivanenko, Electroflotation treatment of fat containing solutions, *Khimiya i Tekhnologiya Vody* **15**(1), 54–56 (1993).

98. T. D. Kubritskaya, I. V. Drako, V. N. Sorokina, and R. V. Drondina, Use of electrochemical methods to purify the waste water from the production of concentrates in the food industry, *Surface Engineering and Applied Electrochemistry* **6**, 62–68 (2000).

99. M. N. Rabilizirov and A. M. Gol'man, Treatment of diary waste waters by foam electroflotation-separation, *Khimiya i Tekhnologiya Vody* **8**(4), 87–88 (1986).

100. M. Krofta and L. K. Wang, Development of innovative flotation-flitration systems for water treatment, part c: an electroflotation plant fro single families and institutions, *Proceedings of the American Water Works Association Water Reuse Symposium III* Vol. **3**, 1251–1264 (1984).

101. M. Krofta and L. K. Wang, *Investigation of water treatment alternative fro single families and small communities in rural areas*, US Dept. of Commerce, National Information Service, Springfield, VA. Technical Report Nos. PB86-175312/AS, p. 38 and PB85-207595/AS, p. 52, 1984.

102. L. K. Wang, *Treatment of septic tank effluent by electroflotation and filtration*, Lenox Institute of Water Technology, Lenox, MA. Technical Reports Nos. LIR/03-88-290S, p. 21 and LIR/03-88290L, p. 92, 1988.

103. I. A. Zolotukhin, V. A. Vasev, and A. L. Lukin, Electroflotation purification of the pit waters of the Kuzbass, *Khimiya i Tekhnologiya Vody* **5**(3), 252–255 (1983).

104. V. Srinivasan and M. Subbaiyan, Electroflotation studies on Cu, Ni, Zn, and Cd with ammonium dodecyl dithiocarbamate, *Separ. Sci. Technol.* **24**(1–2), 145–150 (1989).

105. G. Ramadorai and J. P. Hanten, Removal of molybdenum and heavy metals from effluents by flotation, *Miner. Metall. Processing*, 149–154 (1986).

106. V. I Zelentsov and K. A. Kiselev, An investigation of separation of valuable components from solutions with electrical flotation, *Elektronnaya Obrabotka Materialov* **4**, 50–54 (1986).

107. V. E. Nenno, V. I. Zelentsov, T. Ya, Datsko, E. E. Dvornikova, and T. M. Radzilevich, Gold and silver sorption from cyanide solutions by activated coal and metal isolation by electroflotation, *Electronnaya Obrabotka Materialov* **3**, 42–44 (1994).

108. A. T. Kuhn, Electrolytic decomposition of cyanides, phenols and thiocyanates in effluents streams—a literature review, *J. Appl. Chem. Biotechnol.* **21**, 29–34 (1971).

109. M. O. Azzam, Y. Tahboub, and M. Al-Tarazi, Effect of counter electrode material on the anodic destruction of 4-Cl phenol solution, *Trans. IChemE* **77**, Part B, 219–226 (1999).

110. L. Szpyrkowicz, J. Naumczyk, and F. Zilio-Grandi, Application of electrochemical processes for tannery wastewater treatment, *Toxicol. Environ. Chem.* **44**, 189–202 (1994).

111. S. J. Allen, K. Y. H. Khader, and M. Bino, Electrooxidation of dyestuffs in waste waters, *J. Chem. Tech. Biotechnol* **62**, 111–117 (1995).

112. J. Naumczyk, L. Szpyrkowicz, and F. Z. Grandi, Electrochemical treatment of textile wastewater, *Water Sci. Tech.* **34** (11), 17–24 (1996).

113. J. Naumczyk, L. Szpyrkowicz, M. D. D. Faveri, and F. Zilio-Grandi, Electrochemical treatment of tannery wastewater containing high strength pollutants, *Trans IChemE, B* **74**, 59–68 (1996).

114. A. G. Vlyssides and C. J. Israilides, Detoxification of tannery waste liquors with an electrolysis system, *Environ. Pollut.* **97**(1–2), 147–152 (1997).

115. A. G. Vlyssides, C. J. Israilides, M. Loizidou, G. Karvouni, and V. Mourafeti, Electrochemical treatment of vinasse from beet molasses, *Water Sci. Tech.* **36** (2–3), 271–278 (1997).

116. S. H. Lin and C. L. Wu, Electrochemical nitrite and ammonia oxidation in sea water, *J. Environ. Sci. Health A*, **32**, 2125–2138 (1997).

117. L. C. Chiang, J. E. Chang, and T. C. Wen, "Electrochemical oxidation process for the treatment of coke-plant wastewater," *J. Environ. Sci. Health A*, **30**, 753–771 (1995).
118. L. C. Chiang, J. E. Chang, and T. C. Wen, Indirect oxidation effect in electrochemical oxidation treatment of landfill leachate, *Water Res.*, **29**, 671–678 (1995).
119. A. G. Vlyssides and C. J. Israilides, Electrochemical oxidation of a textile dye and finishing wastewater using a Pt/Ti electrode, *J. Environ. Sci. Health A*, **33**, 847–862 (1998).
120. T. Matsue, M. Fujihira, and T. Osa, Oxidation of alkylbenzenes by electrogenerated hydroxyl radical, *J. Electrochem. Soc.* **128**, 2565–2569 (1981).
121. E. Brillas, R. M. Bastida, and E. Llosa, Electrochemical destruction of aniline and 4-chloroaniline for wastewater treatment using a carbon-PTFE O_2-fed cathode, *J. Electrochem. Soc.* **142**, 1733–1741 (1995).
122. E. Brillias, E. Mur, and J. Casado, Iron(II) catallysis of the mineralization of aniline using a carbon-PTFE O_2-fed cathode, *J. Electrochem. Soc.* **143**, L49–53 (1996).
123. E. Brillas, R. Sauleda, and J. Casado, Peroxi-coagulation of aniline in acidic medium using an oxygen diffusion cathode, *J. Electrochem. Soc.* **144**, 2374–2379 (1997).
124. E. Brillas, R. Sauleda, and J. Casado, Degradation of 4-chlorophenol by anodic oxidation, electro-Fenton, photoelectro-Fenton, and peroxi-coagulation processes, *J. Electrochem. Soc.* **145**, 759–765 (1998).
125. E. Brillas, E. Mur, R. Sauleda, L. Sanchez, F. Peral, X. Domenech, and J. Casado, Aniline mineralization by AOP's: anodic oxidation, photocatalysis, electro-Fenton and photoelectro-Fenton processes, *Appl. Catal. B: Environ.* **16**, 31–42 (1998).
126. S. Stucki, H. Baumann, H. J. Christen, and R. Kotz, Performance of a pressurized electrochemical ozone generator, *J. Appl. Electrochem.* **17**(4), 773–778 (1987).
127. W. El-Shal, H. Khordagui, O. El-Sebaie, F. El-Sharkawi, and G. H. Sedahmed, Electrochemcial generation of ozone for water treatment using a cell operating under natural convection, *Desalination* **99**, 149–157 (1991).
128. J. C. Farmer, F. T. Wang, R. A. Hawley-Fedder, P. R. Lewis, L. J. Summers, and L. Foiles, Electrochemical treatment of mixed and hazardous wastes: oxidation of ethylene glycol and benzene by silver (II), *J. Electrochem. Soc.* **139**, 654–662 (1992).
129. J. C. Farmer and F. T. Wang, Electrochemical treatment of mixed and hazardous wastes: oxidation of ethylene glycol by cobalt (III) and iron (III), *IChemE Symp. Series*, **127**, 203–214 (1992).
130. R. G. Hickman, J. C. Farmer, and F. T. Wang, Mediated electrochemical process for hazardous waste destruction, ACS symposium Series 518, Emerging Technologies in Hazardous Waste Management III, *Am. Chem. Soc.* 430–438 (1993).
131. F. Bringmann, K. Ebert, U. Galla, and H. Schmieder, Electrochemical mediators for total oxidation of chlorinated hydrocarbons: formation kinetics of Ag(II), Co(III), and Ce(IV), *J. Appl. Electrochem.* **25**, 846–851 (1995).
132. V. Cocheci, C. Radovan, G. A. Ciorba, and I. Vlaiciu, Mediate electrochemical wastewater treatment, *Revue Roumaine de Chimie* **40**, 615–619 (1995).
133. A. Paire, D. Espinoux, M. Masson, and M. Lecomte, Silver (II) mediated electrochemical treatment of selected organics: hydrocarbon destruction mechanism, *Radiochim. Acta* **78**, 137–143 (1997).
134. Ch. Comninellis, Electrocatalysis in the electrochemical conversion/combustion of organic pollutants for wastewater treatment, *Electrochim. Acta* **39**, 1857–1862 (1994).
135. M. Gattrell and D. W. Kirk, The electrochemical oxidation of aqueous phenol at a glassy carbon electrode, *Can. J. Chem. Eng.* **68**, 997–1003 (1990).
136. O. J. Murphy, G. D. Hitchens, L. Kaba, and C. E. Verostko, Direct electrochemical oxidation of organics for wastewater treatment, *Wat. Res.* **26**, 443–451 (1992).
137. G. Rajalo and T. Petrovskaya, Selective electrochemical oxidation of sulphides in tannery wastewater, *Environ. Technol.* **17,** 605–612 (1996).

138. N. N. Rao, K. M. Somasekhar, S. N. Kaul, and L. Szpyrkowicz, Electrochemical oxidation of tannery, *J. Chem. Tech. Biotechnol.* **76**, 1124–1131 (2001).

139. J. L. Boudenne, O. Cerclier, J. Galea, and E. V. Vlist, Electrochemical oxidation of aqueous phenol at a carbon black slurry electrode, *Appl. Catal. A: General*, **143**, 185–202 (1996).

140. J. L. Boudenne and O. Cerclier, Performance of carbon black-slurry electrodes for 4-chlorophenol oxidation, *Water Res.* **33**, 494–504 (1999).

141. A. M. Polcaro and S. Palmas, Electrochemical oxidation of chlorophenols, *Ind. Eng. Chem. Res.* **36**, 1791–1798 (1997).

142. J. Manriquez, J. L. Bravo, S. Gutierrez-Granados, et al., Electrocatalysis of the oxidation of alcohol and phenol derivative pollutants at vitreous carbon electrode coated by nickel macrocyclic complex-based films, *Anal. Chim. Acta* **378**, 159–168 (1999).

143. C. S. Hofseth and T. W. Chapman, Electrochemical destruction of dilute cyanide by copper-catalyzed oxidation in a flow-through porous electrode, *J. Electrochem. Soc.* **146**, 199–207 (1999).

144. X. Chen, G. Chen, and P. L. Yue, Anodic oxidation of dyes at novel Ti/B-Diamond electrode, *Chem. Eng. Sci.* **58**, 995–1001 (2003).

145. I. Troster, L. Schafer, and M. Fryda, Recent developments in production and application of DiaChem-electrodes for wastewater treatment, *New Diam. Front. C. Tec.* **12**(2), 89–97 (2002).

146. Ch. Comninellis and E. Plattner, Electrochemical wastewater treatment, *Chimia* **42**(7/8), 250–252 (1988).

147. Y. M. Awad and N. S. Abuzaid, Electrochemical treatment of phenolic wastewater: efficiency, design considerations and economic evaluation, *J. Environ. Sci. Health*, A **32**, 1393–1414 (1997).

148. N. Kannan, S. N. Sivadurai, L. J. Berchmans, and R. Vijayavalli, Removal of phenolic compounds by electrooxidation method, *J. Environ. Sci. Health. A* **30**, 2185–2203 (1995).

149. L. Marincic and F. B. Leitz (1978), Electro-oxidation of ammonia in wastewater, *J. Appl. Electrochem.* **8**, 333–345.

150. C. C. Ho, C. Y. Chan, and K. H. Khoo, Electrochemical treatment of effluents: a preliminary study of anodic oxidation of simple sugars using lead dioxide-coated titanium anodes, *J. Chem. Tech. Biotechnol.* **36**, 7–14 (1986).

151. S. Stucki, R. Kotz, B. Carcer, and W. Suter, Electrochemical wastewater treatment using high overvoltage anodes part II: Anode performance and applications, *J. Appl. Electrochem.* **21**, 99–104 (1991).

152. Ch. Comninellis, Electrochemical treatment of wastewater containing phenol, *Trans Ichem E. B* **70**, 219–224 (1992).

153. J. D. Rodgers, W. Jedral, and N. J. Bunce, Electrochemical oxidation of chlorinated phenols, *Environ. Sci. Technol.* **33**, 1453–1457 (1999).

154. C. Pulgarin, N. Adler, P. Peringer, and Ch. Comninellis, Electrochemical detoxification of a 1,4-benzoquinone solution in wastewater treatment, *Water Res.* **28**, 887–893 (1994).

155. Ch. Comninellis and E. Plattner, The preparation and behaviour of Ti/Au/PbO$_2$ anodes, *J. Appl. Electrochem.* **10**, 399–404 (1982).

156. D. W. Kirk, H. Sharifian, and F. R. Foulkes, Anodic oxidation of aniline for waste water treatment, *J. Appl. Electrochem.* **15**, 285–292 (1985).

157. I. H. Yeo and D. C. Johnson, Electrocatalysis of anodic oxygen–transfer reactions: effect of groups IIIA and VA metal oxides in electrodeposited β-lead dioxide electrodes in acidic media, *J. Electrochem. Soc.* **134**, 1973–1977 (1987).

158. J. Feng and D. C. Johnson, Electrocatalysis of anodic oxygen-transfer reaction: Titanium substrates for pure and doped lead dioxide films, *J. Electrochem. Soc.* **138**, 3329–3337 (1991).

159. J. Feng, L. L. Houk, and D. C. Johnson, Electroatalysis of anodic oxygen-transfer reactions: the electrochemical incineration of benzoquinone, *J. Electrochem. Soc.* **142**, 3626–3631 (1995).

160. A. M. Polcaro, S. Palmas, F. Renoldi, and M. Mascia, On the performance of Ti/SnO$_2$ and Ti/PbO$_2$ anodes in electrochemical degradation of 2-chlorophenol for wastewater treatment, *J. Appl. Electrochem.* **29**, 147–151 (1999).

161. A. Nanthakumar and N. R. Armstrong, in *Studies in physical and theoretical chemistry* 55, Semiconductor Electrodes, H. O. Finklea, (Ed.), New York, Elsevier Science Publishing Company Inc., p. 203, 1988.

162. C. A. Vincent and D. G. C. Weston, Preparation and properties of semiconducting polycrystalline tin oxide, *J. Electrochem. Soc.* **119**, 518–521 (1972).

163. J. A. Aboaf and V. C. Marcotte, Chemical composition and electrical properties of tin oxide films prepared by vapor deposition, *J. Electrochem. Soc.* **120**, 701–702 (1973).

164. Z. M. Jarzebski and J. P. Marton, Physical properties of SnO$_2$ materials I. Preparation and defect structure, *J. Electrochem. Soc.* **123**, 199C–205C (1976).

165. Y. S. Hsu and S. K. Ghandhi, The preparation and properties of arsenic-doped tin oxide films, *J. Electrochem. Soc.* **126**, 1434–1435 (1979).

166. Y. S. Hsu and S. K. Ghandhi, The effect of phosphorus doping on tin oxide films made by the oxidation of phosphine and tetramethyltin I: Growth and etching properties, *J. Electrochem. Soc*. **127**, 1592–1595 (1980).

167. Y. S. Hsu and S. K. Ghandhi, The effect of phosphorus doping on tin oxide films made by the oxidation of phosphine and tetramethyltin II: Electrical properties, *J. Electrochem. Soc*. **127**, 1595–1599 (1980).

168. R. Kotz, S. Stucki, and B. Carcer, Electrochemical wastewater treatment using high overvoltage anodes part I: physical and electrochemical properties of SnO$_2$ anodes, *J. Appl. Electrochem*. **21**, 14–20 (1991).

169. E. Giani and R. Kelly, A study of SnO$_2$ thin films formed by sputtering and by anodising, *J. Electrochem. Soc*. **121**, 394–399 (1974).

170. B. Correa-Lozano, Ch. Comninellis, and A. D. Battisti, Preparation of SnO$_2$-Sb$_2$O$_5$ films by the spray pyrolysis technique, *J. Appl. Electrochem.* **26**, 83–89 (1996).

171. J. P. Chatelon, C. Terrir, E. Bernstein, R. Berjoan, and J. A. Roger, Morphology of SnO$_2$ thin films obtained by the sol-gel technique, *Thin Solid Films* **47**, 162–168 (1994).

172. L. Lipp and D. Pletcher, The preparation and characterization of tin dioxide coated titanium electrodes, *Electrochim. Acta* **42**, 1091–1099 (1997).

173. B. Correa-Lozano, Ch. Comninellis, and A. D. Battisti, Physicochemical properties of SnO$_2$-Sb$_2$O$_5$ films prepared by the spray pyrolysis technique. *Electrochem. Soc.* **143**, 203–209 (1996).

174. F. Grimm, D. Bessarabov, W. Maier, S. Storck, and R. D. Sanderson, Sol-gel film-preparation of novel electrodes for the electrocatalytic oxidation of organic pollutants in water, *Desalination* **115**, 295–302 (1998).

175. R. Cossu, A. M. Polcaro, M. C. Lavagnolo, M. Mascia, S. Palmas, and F. Renoldi, Electrochemical treatment of landfill leachate: oxidation at Ti/PbO$_2$ and Ti/SnO$_2$ anodes, *Environ. Sci. Technol.* **32**, 3570–3573 (1998).

176. B. Correa-Lozano, Ch. Comninellis, and A. Debattisti, Service life of Ti/SnO$_2$-Sb$_2$O$_5$ anodes, *J. Appl. Electrochem.* **28**(8), 970–974 (1997).

177. X. Chen and G. Chen, Comparison of BDD and with SnO$_2$ electrodes, *J. Environ. Sci. Technol.* submitted (2003).

178. R. Hutchings, K. Muller, F. Kotz, and S. Stucki, A structural investigation of stabilized oxygen evolution catalysts, *J. Mater. Sci.* **19**, 3987–3994 (1984).

179. O. Weres and M. R. Hoffmann, Electrode, electrode manufacturing process and electrochemical cell, US patent 5,419,824 (1995).

180. J. M. Kesselman, O. Weres, N. S. Lewis, and M. R. Hoffmann, Electrochemical production of hydroxyl radical at polycrystalline Nb-doped TiO_2 electrodes and estimation of the partitioning between hydroxyl radical and direct hole oxidation pathways, *J. Phys. Chem. B* **101**, 2637–2643 (1997).

181. J. R. Smith and F. C. Walsh, Electrodes based on magneli phase titanium oxides: the properties and applications of Ebonex® materials, *J. Appl. Electrochem.* **28**, 1021–1033 (1998).

182. G. Chen, E. A. Betterton, and R. G. Arnold, Electrolytic oxidation of trichloroethylene using a ceramic anode, *J. Appl. Electrochem.* **29**, 961–970 (1999).

183. M. A. Prelas, G. Popovici, and L. K. Bigelow, *Handbook of industrial diamonds and diamond films*, New York, Marcel Dekker, Inc., 1023–1147, 1998.

184. G. M. Swain, The use of CVD diamond thin films in electrochemical systems, *Adv. Mater.* **6**, 388–392 (1994).

185. G. M. Swain, The electrochemical activity of boron-doped polycrystalline diamond thin film electrodes, *Anal. Chem.* **65**, 345–351 (1993).

186. J. Isberg, J. Hammersberg, E. Johansson, et al., High Carrier Mobility in Single-Crystal Plasma-Deposited Diamond, *Science* **297**, 1670–1672 (2002).

187. J. Asmussen and D. K. Reinhard, Diamond Film Handbook, Michigan State University East Lansing, Michigan (2002).

188. W. G. Eversole, Synthesis of Diamond, US patents 3,030,187, and 3,030,188 (1962).

189. J. C. Angus, H. A. Will, and W. S. Stanko, Growth of diamond seed crystals by vapor deposition, *J. Appl. Phys.* **39**, 2915–2922 (1968).

190. B. V. Derjaguin, D. V. Fedoseev, B. V. Spitzyn, D. V. Lukyanovich, B. V. Ryabov, and A. V. Lavrntev, Filamentary diamond crystals, *J. Cryst. Growth*, **2**, 380–384 (1968).

191. B. V. Derjaguin and D. V. Fedoseev, Vapor growth of diamond on diamond and other surfaces, *Scientific Am.* **233**(5), 102–109 (1975).

192. S. Matsumoto, Y. Sato, M. Kakmo, and N. Setaka, Growth of diamond particles from methanae-hydrogen gas, *J. Mater. Sci.* **17**, 3106–3112 (1982).

193. S. Matsumoto, Y. Sato, M. Kakmo, and N. Setaka, Vapor deposition of diamond particles from methane, *Jpn. J. Appl. Phys.* **2**, L183–L185 (1982).

194. M. Kamo, S. Sato, S. Matsumoto, and N. Setake, Diamond synthesis from gas phase microwave plasma, *J. Cryst. Growth.* **62**, 642–644 (1983).

195. K. Suzuki, A. Sawabe, H. Yasuda, and T. Inuzuka, Growth of diamond thin films by DC plasma chemical vapor deposition, *Appl. Phys. Lett.* **50**, 728–729 (1987).

196. P. K. Bachmann, Microwave plasma CVD, and related techniques for low pressure diamond synthesis, *in Thin Film Diamond*, A. Lettington and J. W. Steeds (ed.), London, Chapman and Hall, 31–53, 1994.

197. J. Mort, D. Kuhman, M. Machonkin, et al., Boron doping of diamond thin-films, *Appl. Phys. Let.* **55**(11), 1121–1123 (1989).

198. N. Fujimori, H. Nakahata, and T. Imai, Properties of boron-doped epitaxial diamond films, *Jpn. J. Appl. Phys.* **29**, 824–827 (1990).

199. J. G. Ran, C. Q. Zheng, J. Ren, and S. M. Hong, Properties and texture of B-doped diamond films as thermal sensor, *Diam. Relat. Mater.* **2**, 793–796 (1993).

200. M. Fryda, D. Herrmann, L. Schafer, et al., Properties of diamond electrodes for wastewater treatment, *New Diam. Front. C. Technol.* **9**, 229–240 (1999).

201. S. A. Grot, G. S. Gildenblat, C. W. Hatfield, C. R. Wronski, A. R. Badzian, T. Badzian, and R. Messier, The effect of surface treatment on the electrical properties of metal contacts to boron-doped homoepitaxial diamond film, *IEEE Electron Device Lett.* **11**, 100–102 (1990).

202. J. J. Carey, J. C. S. Christ, and S. N. Lowery, Method of electrolysis employing a doped diamond anode to oxidize solutes in wastewater, US patent 5,399,247 (1995).

203. H. B. Martin, A. Argoitia, U. Landau, A. B. Anderson, and J. C. Angus, Hydrogen and oxygen evolution on boron-doped diamond electrodes, *J. Electrochem. Soc.* **143**, L133–L136 (1996).

204. R. Tenne, K. Patel, K. Hashimoto, and A. Fujishima, Efficient electrochemical reduction of nitrate to ammonia using conductive diamond film electrodes, *J. Electroanal. Chem.* **347**, 409–415 (1993).

205. J. Iniesta, P. A. Michaud, M. Panizza, and Ch. Comninellis, Electrochemical oxidation of 3-methylpyridine at a boron-doped diamond electrode: application to electroorganic synthesis and wastewater treatment, *Electrochem. Commun.* **3**, 346–351 (2001).

206. X. Chen, G. Chen, and P. L. Yue, High performance Ti/BDD electrodes for pollutant oxidation, *J. Environ. Sci. Technol.* **37**, 5021–5026 (2003).

207. I. Troster, M. Fryda, D. Herrmann, et al., Electrochemical advanced oxidation process for water treatment using DiaChem (R) electrodes, *Diam. Rela. Mater.* **11**(3–6), 640–645.

208. L. Schafer, M. Fryda, T. Matthee, et al., Investigation of DiaChem electrodes for industrial applications, *in Proc. 6th Applied Diamond Conference/2nd Frontier Carbon Technology Joint Conference (ADC/FCT 2001)*, Y. Tzeng et al., (ed.), (NASA Center for Aerospace Information, Hanover, 2001, NASA/CP-2001-210948) p. 158, 2001.

209. A. Perret, W. Haenni, N. Skinner, et al., Electrochemical behavior of synthetic diamond thin film electrodes, *Diam. Relat. Mater.* **8**, 820–823 (1999).

210. D. Gandini, E. Mahe, P. A. Michaud, W. Haenni, A. Perret, and Ch. Comninellis, Oxidation of carboxylic acids at boron-doped diamond electrodes for wastewater treatment, *J. Appl. Electrochem.* **30**, 1345–1350 (2000).

211. F. Beck, B. Kaiser, and H. Krohn, Boron doped diamond (BDD)-layers on titanium substrates as electrodes in applied electrochemistry, *Electrochim. Acta* **45**, 4691–4695 (2000).

212. W. Hanni, A. Perret, and Ch. Comninellis, Electrolytic cell with bipolar electrode including diamond, US Patent No. 6,306,270 (2001).

213. S. Wodiunig, F. Bokeloh, and Ch. Comninellis, Electrochemical promotion of bipolar electrodes: an estimation of the current bypass, *Electrochimica Acta* **46**, 357–363 (2000).

214. H. Sharifian and D. W. Kirk, Electrochemical oxidation of phenol, *J. Electrochmem. Soc.* **133**, 921–924 (1986).

215. C. L. K. Tennakoon, R. C. Bhardwaj, J. O'. M. Bockris, Electrochemical treatment of human wastes in a packed bed reactor, *J. Appl. Electrochem.* **26**, 18–29 (1996).

216. E. A. El-Ghaoui, R. E. W. Jansson, and C. Moreland, Application of the trickle tower to problems of pollution control. II. The direct and indirect oxidation of cyanide, *J. Appl. Electrochem.* **12**, 69–73 (1982).

217. U. B. Ogutveren, N. Gonen, and S. Koparal, Removal of dye stuffs from wastewater: electrocoagulation of acilan blau using soluble anode, *J. Environ. Sci. Health*, A **27**(5), 1237–1247 (1992).

218. A. Lopez-lopez, E. Exposito, J. Anton, F. Rodriguez-Valera, and A. Aldaz, Use of Thiobacillus ferrooxidans in a coupled microbiological-electrochemical system for wastewater detoxification, *Biotechnol. Bioeng.* **63**, 79–86 (1999).

219. K. B. Holt, J. D. Campo, J. S. Foord, R. G. Compton, F. Marken, Sonoelectrochemistry at platinum and boron-doped diamond electrodes: achieving fast mass transport for slow diffusers, *J. Electroanal. Chem.* **513**, 94–99 (2001).

220. R. H. De Lima Leite, P. Cognet, A. -M. Wilhelm, H. Delmas, Anodic oxidation of 2,4-dihydroxybenzoic acid for wastewater treatment: study of ultrasound activation, *Chem Eng. Sci.* **57**, 767–778 (2002).

221. M. Kuroda, T. Watanabe, and Y. Umedu, Simultaneous oxidation and reduction treatments of polluted water by a bio-electro reactor, *Water Sci. Tech.* **34**(9), 101–108 (1996).

222. G. M. Swain, B. A. B. Anderson, and J. C. Angus, Applications of diamond thin films in electrochemistry, *MRS Bulletin* **23**(9), 56–60 (1998).

223. M. Panizza, I. Duo, P. A. Michaud, G. Cerisola, and Ch. Comninellis, Electrochemical generation of Silver (II) at boron-doped diamond electrodes, *Electrochem. Solid-state Lett.* **3**(12), 550–551 (2000).

224. F. Bonfatti, S. Ferro, F. Lavezzo, M. Malacarne, G. Lodi, and A. Debattisti, Electrochemical incineration of glucose as a model organic substrate I—Role of the electrode material, *J. Electrochem. Soc.* **146** (6), 2175–2179 (1999).

225. J. P. Chen, S. Y. Chang, and Y. T. Hung. Electrolysis. In: *Physicochemical Treatment Processes*. L. K. Wang, Y. T. Hung, and N. K. Shammas (eds.). Humana Press, Totowa, NJ, pp. 359–378.

226. L. K. Wang, Y. T. Hung, H. H. Lo, and C. Yapijakis (eds.). *Waste Treatment in the Food Processing Industry.* CRC Press, NY, 2006, pp. 119–192.

227. TWRI. Field Demonstration of Performance of an Electrocoagulation System to Reduce Phosphorus from Dairy Lagoon Effluent. Eng. Report, Texas Water Resources Institute, College Station, TX, 2006.

<div align="right">

3
Irradiation

</div>

Lawrence K. Wang, J. Paul Chen, and Robert C. Ziegler

CONTENTS

1. INTRODUCTION

1.1. Disinfection and Irradiation

Solid substances described in this chapter will include foods, wastewater sludges, and solid wastes. Disinfection is a process involving the destruction or inactivation of pathogenic organisms in the solid substances. The process is carried out principally to ensure sanitation or to minimize public health concerns. Destruction is the physical disruption or disintegration of a pathogenic organism, although inactivation, as used here, is the removal of a pathogen's ability to infect. An important but secondary concern may be to minimize the exposure of domestic animals to pathogens in the solid substances. At present in the United States, the use of procedures to reduce the number of pathogenic organisms is a requirement before sale of sludges or recycled byproducts to the public as a soil amendment, or before recycling the sludges/byproducts directly to croplands, forests, or parks. Because the final use or disposal of sludges/byproducts may differ greatly with respect to public health concerns, and because a great number of treatment options affecting various degrees of pathogen reduction are available, the system chosen for reduction of pathogens should be tailored to the demands of the particular situation (1,2).

This chapter identifies the major pathogenic organisms found in wastewater sludges; briefly describes the pathogen characteristics, including size, life, and reproductive requirements, occurrence in the solid substances, and survival under different environmental conditions and discusses methods for reducing the number of pathogenic organisms

in the sludges/byproducts. Various processes designed specifically for the reduction of pathogenic organisms in solid substances are briefly discussed in this chapter because they are presented in other chapters of this handbook. However, the high-energy irradiation process, is introduced in this chapter in detail.

1.2. Pathogenic Organisms

A pathogen or pathogenic agent is any biological species that can cause disease in the host organism. The discussions in this chapter are conducted in North America will be confined to pathogens that produce disease and complete their life cycles in man. These organisms or agents fall into four broad categories: viruses, bacteria, parasites, and fungi. Within the parasite category, there are protozoa, nematodes, and helminths. Viruses, bacteria, and parasites are primary pathogens that are present at some level in solid substances as a result of human activities. Fungi are secondary pathogens and are only numerous in solid substances when given the opportunity to grow during some treatment or storage process.

Pathogens enter environmental systems from a number of sources such as: (a) human wastes, including feces, urine, and oral and nasal discharges; (b) contaminated foods and food wastes from homes and commercial establishments; (c) industrial wastes from food processing, particularly meat packing plants; (d) domestic pet feces and urine; and (e) biological laboratory wastes such as those from hospitals. In addition, where combined sewer systems are used, ground surface and street runoff materials, especially animal wastes, may enter the sewers as storm flows. Vectors such as rats that inhabit some sewer systems may also add a substantial number of pathogens.

1.3. Pathogen Occurrence in the United States

Information on pathogen occurrence and associated morbidity and mortality data vary greatly with pathogenic species. Available data, complied by the Center for Disease Control of the United States Public Health Service, indicate that enteric viral, bacterial, and parasitic infections annually affect tens of thousands of people in the United States (3–7). Data on the occurrence of bacterial disease in the United States are scarce. However, the frequent detection of enteropathic bacteria (bacteria which affect the intestinal tract), such as *Escherichia coli, Salmonella*, fecal *streptococci, Shigella*, and others in the contaminated foods, untreated wastewater, and wastewater sludges indicates that these pathogens and their associated diseases are endemic to the United States. More than 12% of stool samples checked by state and territorial public health laboratories were positive for one or more pathogenic parasites. *Ascaris lumbricoides*, which produces a resistant ova, was found in more than 2% of the samples (6,7). The frequent occurrence of enteric pathogens in the US population indicates that pathogens should be expected in all wastewaters and sludges.

1.4. Potential Human Exposure to Pathogens

Man may be exposed to pathogens in wastewater sludge in various ways and at greatly varying concentrations. Figure 1 lays out in simplified form some of the potential pathways. There is no firm scientific evidence to document a single confirmed case in which human disease is directly linked to exposure to pathogens from wastewater
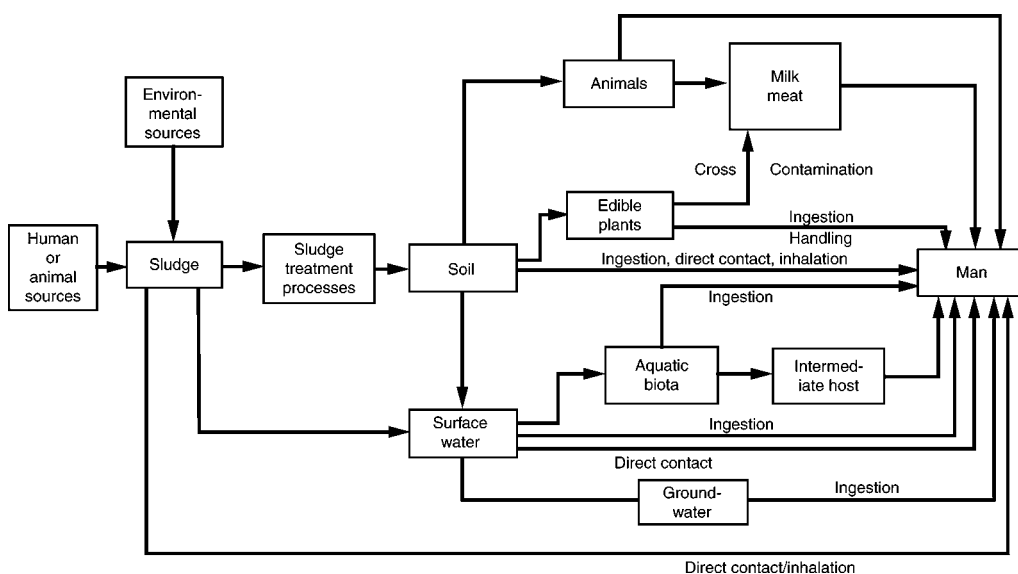
Fig. 1. Potential pathogen pathways to humans.

sludge. Viable pathogens have, however, been isolated from intermediate points in the sludge management system, such as from surface runoff, from sludge-treated fields. These factors should be considered in the selection and design of a process for reducing the number of pathogenic organisms (8–10).

2. PATHOGENS AND THEIR CHARACTERISTICS

Viruses, bacteria, parasites, and fungi differ in size, physical composition, reproductive requirements, occurrence in the US population, and prevalence in wastewater.

2.1. Viruses

Viruses are obligate parasites and can only reproduce by dominating the internal processes of host cells and using the host's resources to produce more viruses. Viruses are very small particles whose protein surface charge changes in magnitude and sign with pH. In the natural pH range of wastewater and sludges, most viruses have a negative surface charge. Thus, they will adsorb to a variety of materials under appropriate chemical conditions. Different viruses show varying resistance to environmental factors such as heat and moisture. Enteric viruses are acid resistant and many show tolerance to temperatures as high as 140°F (600°C). Many of the viruses that cause disease in man enter the sewers with feces or other discharges and have been identified, or are suspected of being in sludge. The major virus subtypes transmitted in feces are as follows:

a. Adenoviruses.
b. Coxsackie virus, Group A.
c. Coxsackie virus, Group B.
d. ECHO virus, (30 types).
e. Poliovirus (three types).
f. Reoviruses.

g. Hepatitis virus A.
h. Norwalk agent.

Viruses are excreted by man in numbers several orders of magnitude lower than bacteria. Typical total virus concentrations in untreated wastewaters are 1000–10,000 plaque-forming units (PFU)/100 mL; effluent concentrations are 10–300 PFU/100 mL. Wastewater treatment, particularly chemical coagulation or biological processes followed by sedimentation, concentrates on viruses in sludge. Raw primary and waste-activated sludges contain 10,000–100,000 PFU/100 mL.

2.2. Bacteria

Bacteria are single-celled organisms that range in size from slightly less than 1 μm diameter to 5 μm wide by l5 μm long. Among the primary pathogens, only bacteria are able to reproduce outside the host organism. They can grow and reproduce under a variety of environmental conditions. Low temperatures cause dormancy, often for long periods. High temperatures are more effective for inactivation, although some species form heat-resistant spores.

Pathogenic bacterial species are heterotrophic and generally grow best at a pH between 6.5 and 7.5. The ability of bacteria to reproduce outside a host is an important factor. Although solid substances may be disinfected, it can be reinoculated and recontaminated. Bacteria are numerous in the human digestive tract; man excretes up to 10^{13} coliform and 10^{16} other bacteria in his feces every day. The most important of the pathogenic bacteria are listed as follows:

a. *Arizona hinshawii.*
b. *Bacillus cereus.*
c. *Vibrio cholerae.*
d. *Clostridium pérfringens.*
e. *C. tetani.*
f. *E. coli.*
g. *Leptospira* spp.
h. *Mycobacterium tuberculosis.*
i. *S. paratyphi, A, B, C.*
j. *S. seridai.*
k. *Salmonella* spp. (more than 1500 types).
l. *S. typhi.*
m. *Shigella* spp.
n. *Yersinia enterocolitica.*
o. *Y. pseudotuberculosis.*

2.3. Parasites

Parasites include protozoa, nematodes, and helminths. Pathogenic protozoa are single-celled animals that range in size from 8 to 25 μm. Protozoa are transmitted by cysts, the nonactive and environmentally insensitive form of the organism. Their life cycles require that a cyst be ingested by man or another host. The cyst is transformed into an active organism in the intestines, where it matures and reproduces, releasing cysts in the feces. Pathogenic protozoa are listed in Table 1, together with the diseases they cause.

Table 1
Pathogen Occurrence in Liquid Wastewater Sludges

Pathogen	Name or species	Concentration (number/100 mL)	
		Unstabilized raw sludge[a]	Digested sludge[a,b]
Virus	Various	2.5×10^3–7×10^4	100–10^3
Bacteria	*Clostridia* spp.	6×10^6	2×10^7
Bacteria	Fecal coliform	10^9	3×10^4–6×10^6
Bacteria	*Salmonella* spp.	8×10^3	BDL[c]–62
Bacteria	*S. faecalis*	3×10^7	4×10^4–2×10^6
Bacteria	Total coliforms	5×10^9	6×10^4–7×10^7
Bacteria	*M. tuberculosis*	10^7	10^6
Parasites	*A. lumbricoides*	200–1000	0–1000
Parasites	Helminth eggs	200–700	30–70

[a]Type of sludge usually unspecified.
[b]Anaerobic digestion; temperature and detention times varied.
[c]BDL is less than the detection limits (<3/100 mL).

Nematodes are roundworms and hookworms that may reach sizes up to 14 in. (36 cm) in the human intestines (1). The more common roundworms found in man are as follows:

1. Protozoa:
   a. *Acanthamoeba* spp.
   b. *Balantidium coli.*
   c. *Dientamoeba fragilis.*
   d. *Entamoeba histolytica.*
   e. *Giardia lamblia.*
   f. *Isosiora bella.*
   g. *Naegleria fowleri.*
   h. *Toxoplasma gordii.*
2. Nematodes:
   a. *Ancyclostoma dirodenale.*
   b. *Ancyclostoma* spp.
   c. *A. lumbricoides.*
   d. *Enterobius vermicularis.*
   e. *Necator americanus.*
   f. *Strongyloides stercoralis.*
   g. *Toxocara canis.*
   h. *T. cati.*
   i. *Trichusis trichiura.*
3. Helminths:
   a. *Diphyllobothrium latum.*
   b. *Echinococcus granulosis.*
   c. *E. multilocularis.*
   d. *Hymenolepis diminuta.*
   e. *Tymenolepis nana.*
   f. *Taenia saginata.*
   g. *T. solium.*

They may invade tissues other than the intestine. This situation is especially common when man ingests the ova of a roundworm common to another species such as the dog. The nematode does not stay in the intestine but migrates to other body tissue such as the eye and encysts. The cyst, similar to that formed by protozoa, causes inflammation and fibrosis in the host tissue. Pathogenic nematodes cannot spread directly from man to man. The ova discharged in feces must first embryonate at ambient temperature, usually in the soil, for at least 2 wk.

Helminths are flatworms, such as tapeworms, that may be more than 12 in. (30 cm) in length. The most common types in the United States (listed earlier) are associated with beef, pork, and rats. Transmission occurs when man ingests raw or inadequately cooked meat or the eggs of the tapeworm. In the less serious form, the tapeworm develops in the intestine, maturing and releasing eggs. In the more serious form, it localizes in the ear, eye, heart, or central nervous system.

2.4. Fungi

Fungi are single-celled nonphotosynthesizing plants that reproduce by developing spores, which form new colonies when released. Spores range in size from 10 to 100 μm. They are secondary pathogens in wastewater sludge, and large numbers have been found growing in compost (2). The pathogenic fungi, listed later, are most dangerous when the spores are inhaled by people whose systems are already stressed by a disease such as diabetes, or by immunosuppressive drugs. Fungi spores, especially those of *Aspergillus fumigatus*, are ubiquitous in the environment and have been found in pasture lands, hay stacks, manure piles, and the basements of most homes (2). The pathogenic fungi potentially in wastewater sludge are the following:

a. *Actinomyces* spp.
b. *Aspergillus* spp.
c. *Candida albicans.*

3. SOLID SUBSTANCES DISINFECTION

3.1. Long-Term Storage

Pathogen reduction has been recognized for years as a side benefit of sludge storage in lagoons. Hinesley and others have reported 99.9% reduction in fecal coliform density after 30 d storage (11). For an anaerobically digested sludge stored in anaerobic conditions for 24 wk at 39°F (4°C), Stern and Farrell reported major reductions in fecal coliform, total coliform, and *Salmonella* bacteria (11). In similar tests at 68°F (20°C), the same bacteria could not be measured after 24 wk. Viruses were reduced by 67% at 39°F (4°C) and to below detectable limits at 68°F (20°C) in the same time period. Recent work by Storm and others showed fecal coliform reductions of 1–3 orders of magnitude during long-term storage of an anaerobically digested mixture of primary and waste-activated sludge (WAS) in facultative lagoons (12).

3.2. Chemical Disinfection

A number of chemicals used for wastewater sludge stabilization, including lime and chlorine, also reduce the number of pathogenic organisms in sludge.

3.2.1. Lime

Lime treatment of wastewater and sludge is a common practice (44). Plant-scale liming of wastewater sludge was evaluated at Lebanon, OH (15). Two chemical primary sludges, one with alum and one with ferric chloride, were limed to pH 11.5 and placed on drying beds. After 1 mo, *Salmonella* spp. and *Pseudomonas aeruginosa* were undetectable. Bench testing was also conducted on ferric chloride-treated wastewater raw sludges that were limed to pH 10.5, 11.5, and 12.5; these sludges were sampled after 0.5 and 24 h and bacterial tests were performed (15). Pathogenic bacteria reduction improved with time and was substantially better at pH values of 11.5 and 12.5. Qualitative checks for higher life forms such as *Ascaris* ova indicated that they survived 24 h at a pH more than 11.0. Virus studies on limed sludges have not been reported, but a pH in excess of 11.5 should inactivate known viruses (11).

3.2.2. Chlorine

Chlorine is a strong oxidizing chemical used for disinfecting drinking water and wastewater effluents (16). It is effective for bacteria and virus inactivation if applied in sufficient quantity to develop a free chlorine residual in the solution being treated. Chlorine is less effective in disinfecting solutions with a high suspended solids concentration. Cysts and ova of parasites are very resistant to chlorine. Few data are available on the potential of chlorine for reducing the number of pathogenic organisms in sludge. Some samples of sludge treated with large doses of chlorine in South Miami, Florida, and Hartland, Wisconsin, showed large reductions in bacteria and coliphages (24). Chlorine doses of 1000 mg/L applied to WAS with a 0.5% solids concentration reduced total bacteria counts by 4–7 logs and coliform bacteria and coliphage to below detection limits. Primary sludge with a 0.5–0.85% solids concentration was treated with 1000 mg/L chlorine, and total and fecal coliform counts were reduced to less than the detectable limits.

3.2.3. Quaternary Ammonium Compounds and Ozone

Other organic disinfectants, such as quaternary ammonium compounds (18–26), and strong oxidizing chemicals such as ozone (17–20,25–28) are sometimes used for solid substances disinfection. Today, quaternary ammonium compounds have been widely used in household kitchen, bathroom, and swimming pool disinfection. Oxygenation and ozonation have been proven useful for sludge disinfection in both pilot plant and full-scale municipal operations (11,25,27,28).

3.3. Low-Temperature Thermal Processes for Disinfection

The number of pathogenic organisms in wastewater sludge can be effectively reduced by applying heat to untreated or digested sludges. Heat may be used solely for pathogen reduction as in pasteurization or as one step in a process designed to stabilize sludge, improve treatability, or reduce mass. The focus of this section will be on sludge pasteurization. Other heating processes, such as thermal processing and incineration, are developed in other chapters of this handbook and will only be reviewed briefly here.

3.3.1. Sludge, Milk, and Foods Pasteurization

Man has recognized for many years that heat will inactivate microorganisms as well as the eggs and cysts of parasites. Different species and their subspecies show different

sensitivities to elevated temperatures and duration of exposure. Roediger, Stern, and Ward and Brandon have determined the time and temperature relationships for disinfection of wet sludges with heat (29–31). Their results indicate that pasteurization at 158°F (70°C) for 30 min inactivates parasite ova and cysts and reduces population of measurable pathogenic viruses and bacteria below detectable levels. For bacteria, Ward and Brandon found that fecal *streptococci* were most heat resistant, followed by coliforms and then *Salmonella* (31). Wang indicates that a higher temperature for a shorter time period (195°F, 10 min) also destroys all pathogens (32).

3.3.2. Heat Conditioning

Heat conditioning includes processes in which wet wastewater sludge is pressurized with or without oxygen and the temperature is raised to 3500–4000°F (177°C–240°C) and held for 15–40 min. These processes destroy all pathogens in sludge, and are discussed in another chapter in detail.

3.3.3. Heat Drying

Heat drying is generally done with a flash drier or a rotary kiln. Limited data from analyses on Milwaukee, Wisconsin's dried sludge, Milorganite, produced with a direct–indirect rotary counter-flow kiln-type dryer, indicate that it is bacteriologically sterile (12). Data on samples of flash-dried sludge taken in Houston, Chicago, Baltimore, and Galveston, showed no coliform bacteria in the Houston sludge and not more than 17 most probable number (MPN)/g dry sludge in the other sludges. Total nonconfirming lactose fermenters (spore formers) ranged from 14 MPN to 240,000 MPN/g (33). No tests were made for viruses or parasites; other pathogens may also survive if some bacterias do.

Data for the Carver–Greenfield process gathered during testing by LA/OMA showed a seven order of magnitude reduction for total and fecal coliform, to a detectable level of less than one organism per gram (34). Fecal *streptococci* were reduced six orders of magnitude to 2 MPN/g and *Salmonella* from 50,000 MPN/g to less than 0.2 MPN/g. *Ascaris* ova were reduced to less than 0.2 ova/g.

3.4. High-Temperature Thermal Processes for Disinfection

High-temperature processes include incineration, pyrolysis, or a combination thereof (starved air combustion). These processes raise the sludge temperature to more than 930°F (500°C) destroying the physical structure of all sludge pathogens and effectively sterilizing the sludge. The product of a high-temperature process is sterile unless short-circuiting occurs within the process. The readers are referred to another chapter of this handbook series for details.

3.5. Composting

Composting is considered here as a heat process because a major aim of sludge composting operations is to produce a pathogen-free compost by achieving and holding a thermophilic temperature. Available data indicate that a well-run composting process greatly reduces the numbers of primary pathogens (24,35–38,40,41). However, window or aerated pile operations have not achieved a sufficiently uniform internal temperature to inactivate all pathogens. Adverse environmental conditions, particularly heavy rains,

can significantly lower composting temperatures. Another chapter of this handbook series introduces the theory, principles, design considerations, operational considerations, and applications of the composting process.

3.6. High-Energy Radiation

The use of high-energy radiation for solid substances disinfection has been considered for more than 25 yr. Two energy sources, β- and γ-rays, offer the best potential system performance. β-rays are high-energy electrons, generated with an accelerator for use in disinfection, whereas γ-rays are high-energy photons emitted from atomic nuclei. Both types of rays induce secondary ionizations in sludge as they penetrate. Secondary ionizations directly inactivate pathogens and produce oxidizing and reducing compounds that in turn attack pathogens. Sections 4 and 5 introduce the technologies in detail.

4. DISINFECTION WITH ELECTRON IRRADIATION

4.1. Electron Irradiation Systems and Process Description

4.1.1. Electron Irradiation Systems for Sludge Treatment

High-energy electrons, projected through wastewater sludge by an appropriate generator, are being pilot tested as a means for inactivating or destroying pathogens in sludge at the Deer Island Wastewater Treatment Plant in Boston, MA, USA (39). The electrons produce both biological and chemical effects as they scatter off material in the sludge. Direct ionization by the electrons may damage molecules of the pathogen, particularly the DNA in bacteria cell nuclei and the DNA or RNA of the viruses. The electrons also cause indirect action by producing hydrated electrons and H and OH free radicals that react with oxygen and other molecules to produce ozone and hydroperoxides. These compounds then attack organics in any solid substances, such as waste sludges—including pathogens—promoting oxidation, reduction, dissociation, and other forms of degradation.

The pathogen-reducing power of the electron beam (e-beam) depends on the number and the energy of electrons impacting the sludge. E-beam dose rates are measured in rads; 1 rad is equal to the absorption of 4.3×10^{-6} Btu/lb (100 ergs/g) of the material. Because the radiation distributes energy throughout the volume of material regardless of the material penetrated, the degree of disinfection with an irradiation system is essentially independent of the sludge solids concentration within the maximum effective penetration depth of the radiation. The penetrating power of electrons is limited, with a maximum range of 0.2 in. (0.5 cm) in water or sludge slurries, when the electrons have been accelerated by a potential of 1 MeV.

For e-beam disinfection to be effective, some minimum dosage must be achieved for all sludge being treated. This effect is attained by dosing above the average dosage desired for disinfection. One method used to ensure adequate disinfection is to limit the thickness of the sludge layer radiated so that ionization intensity of electrons exiting the treated sludge is about 50% of the maximum initial intensity. For the 0.85 MeV electrons used in the existing facility, this constraint limits the sludge layer thickness to about 0.08 in. (0.2 cm). Accelerated electrons can induce radioactivity in substances which they impact. However, the electron energy levels for sludge irradiation, up to about 2 MeV, are well below the 10 MeV needed to induce significant radioactivity with electrons.

High voltage cable

Electron
beam
power
supply

Electron
accelerator

Concrete
shielding

Electron
beam
scanner

Viewing
window

Feed
sludge

Sludge
screen

Sludge
grinder

Sludge
feed
pump

Sludge
spreader

Sludge
removal
pump
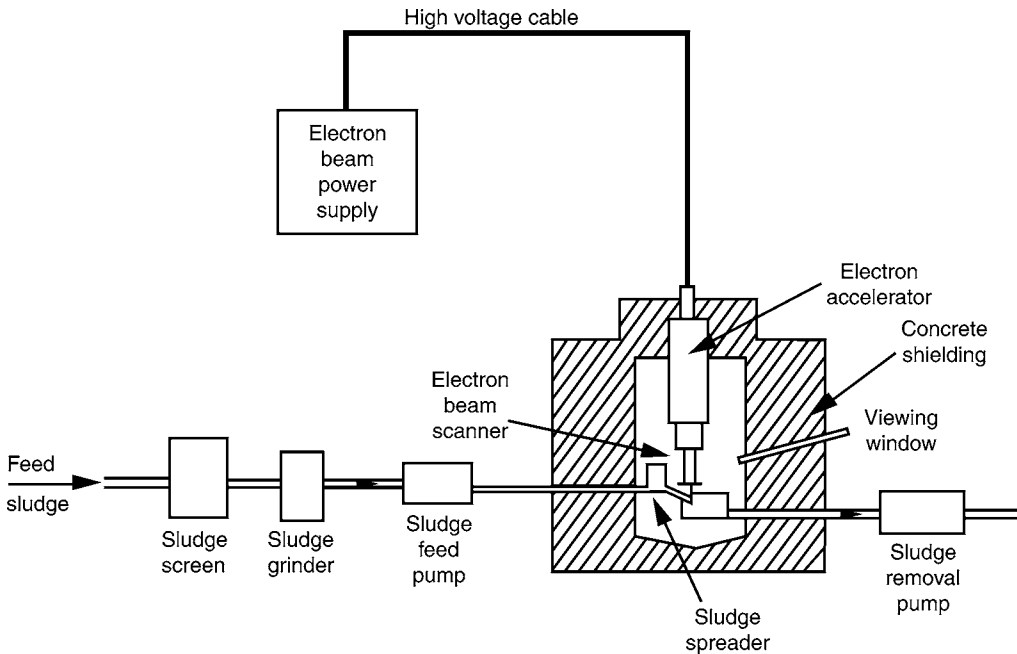
Fig. 2. E-beam facility (*Source:* US EPA).

4.1.2. Electron Irradiation Systems for Food Disinfection

Electron beam facilitates the generation of e-beams with an e-beam linear accelerator. It works on the same principle as a television tube. The electrons are concentrated and accelerated to 99% of the speed of light and energies of up to 10 MeV for food disinfection.

Because e-beams are generated electrically, they offer certain advantages: (a) they can be turned on only as needed, (b) they do not require replenishment of the source as does cobalt-60 (Co-60), and (c) there is no radioactive waste. However, e-beam technology also has disadvantages when it is used for food disinfection: (a) shallow depth of penetration, (b) e-beams must be converted to X-rays to penetrate large items such as carcasses, (c) high electric power consumption, and (d) complexity and potentially high maintenance (47).

4.1.3. Process Description

Disinfection with an e-beam has been proposed for use on both untreated and digested sludges. The major system components of the Deer Island facility shown in Fig. 2 includes the sludge screener, sludge grinder, sludge feed pump, sludge spreader, e-beam power supply, electron accelerator, e-beam scanner, and sludge removal pump. A concrete vault houses the e-beam, providing shielding for the workers from stray irradiation, especially X-rays. X-rays are produced by the interaction of the electrons with the nucleus of atoms in the mechanical equipment and in the sludge. The pumps must be progressive cavity or similar types to assure smooth sludge feed. Screening and grinding of sludge prior to irradiation is necessary to assure that a uniform layer of sludge is passed under the e-beam. At Deer Island, sludge from the feed pump discharges into the constant
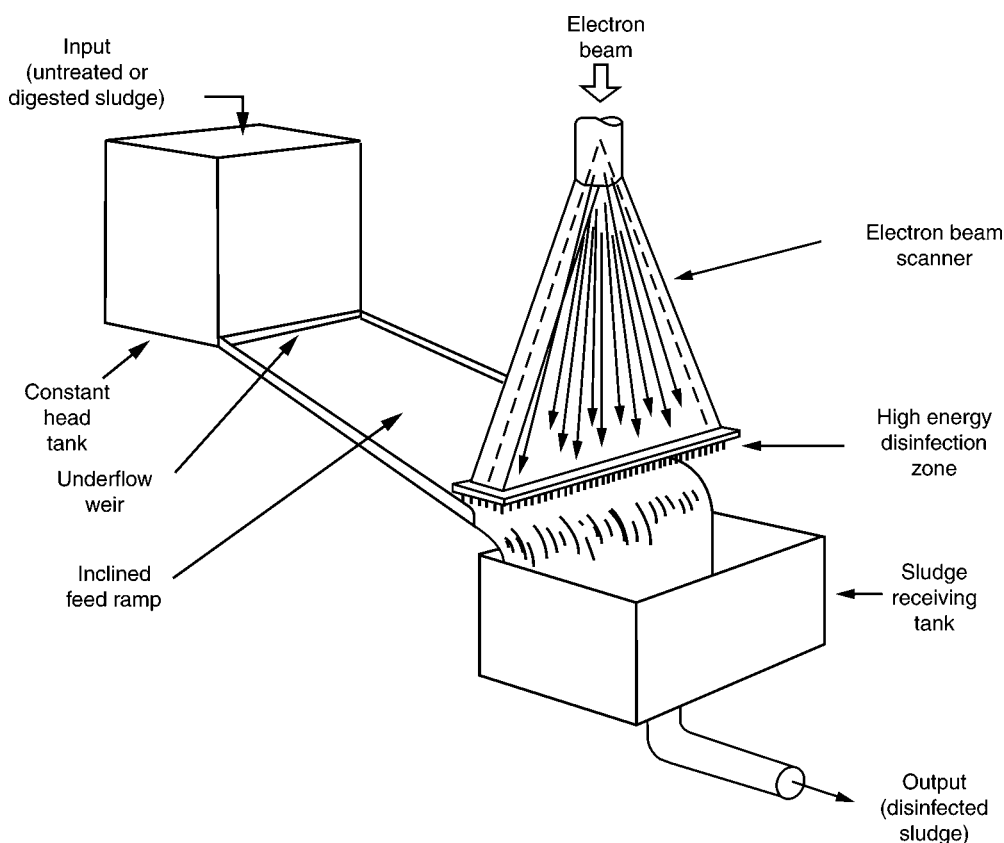
Fig. 3. E-beam scanner and sludge spreader (*Source:* US EPA).

head tank (*see* Fig. 3), which is equipped with an underflow discharge weir. Sludge is discharged under the weir in a thin stream and then flows down an inclined ramp. At the bottom of the ramp, it moves by free fall into the receiving tank.

The electrons are first accelerated. They leave the accelerator in a continuous beam that is scanned back and forth at 400 times/s across the sludge as it falls free in a thin film from the end of the inclined ramp. The dosage is varied by adjusting the height of the underflow weir and hence the sludge flow rate. E-beam sludge irradiation must be considered as a developing technology. The Deer Island irradiation facility is used for sludge disinfection. This project is designed to treat 0.1 MGD (4 L/s) sludge at up to 8% solids with a dosage of 400,000 rads. According to Shah, the facility has been operated for about 700 h, since it was brought on line in 1976, with the longest continuous on-line time being 8 h (40).

4.2. Electron Irradiation Design Considerations

Design criteria for an e-beam sludge facility are difficult to establish because operational data are available from only one pilot facility. However, the work at Deer Island provides good baseline information. A minimum level of electron irradiation should be 400,000 rads, which can best be supplied with a 1–2 MeV electron accelerator.

This energy level provides good penetration for 0.2 in. (0.5 cm) thick sludge layers, making the achievement of a uniform sludge layer less important than with lower energy electrons. However, screening and grinding of sludge before disinfection are still necessary to ensure uniform spreading by this feed mechanism. The high-energy electrons, combined with a short spacing of about 2.75 in. (7 cm) between the scanner window and the sludge film, ensure efficient energy transfer in the system. Only digested sludge has been irradiated at Deer Island. Nonstabilized sludge disinfection by e-beam irradiation still requires pilot-scale testing before any design is considered. Owing to the limited penetrating power of high-energy electrons, this method of treatment is probably only feasible for liquid sludge disinfection. Piping pumps, valves, and flow meters should be specified as equal to those used for anaerobic sludge digestion systems.

4.3. Electron Irradiation Operational Considerations

Instrumentation needed for an e-beam facility should include flow measurement of and temperature probes in the sludge streams entering and leaving the irradiator. Alarms as well as monitoring should be used to indicate variation in sludge flow and high or low radiation doses. Sludge disinfection by e-beam irradiation has large inherent flexibility. The radiation source (the e-beam) can be switched on and off as easily as an electric motor. The unit can be run as needed, up to its maximum throughput capacity. Electron accelerators have a proven record for reliability over at least 20 yr in industrial applications and should prove dependable in wastewater treatment applications. The reliability of the e-beam generator and associated electronics presently used for medical and industrial applications is comparable to that for the microwave radar systems at major airports (41). Accelerators for sludge disinfection would use the same basic components and would have similar reliability. Other system components, such as, pumps, screens, and grinders, are all in common use in waste treatment plants. Cooling air for the scanner must be provided at several hundred cfm (about 10 m³/s). This constant introduction of cooling air leads to the generation of ozone in the shielding vault around the accelerator. If the ozone were vented into the plant or into the atmosphere, some air pollution would result. At Deer Island, this problem is avoided by venting the cooling air through the sludge, in which the ozone is consumed by chemical reduction. These reactions provide a small amount of additional disinfection and COD reduction.

Energy use for e-beam facilities has been estimated for the equipment used at Deer Island. A facility with a 50-kW (50-kJ/s) beam would require about 100 kW (l00 kJ/s) of total electrical power including 25 W (25 kJ/s) for screening, grinding, and pumping, 10 kW (10 kJ/s) for window cooling, and 12 kW (12 kJ/s) for electrical conversion losses. Energy requirements for 0.1 MGD are 6 kWh/t (24 MJ/T) of wet sludge at 5% solids or 120 kWh/dry t (480 MJ/T) (39,40). Here 1 t = 2000 lb; 1 T = 1000 kg.

4.4. Electron Irradiation Performance

For untreated primary sludge, a dose of 400 krads with 3 MeV electrons reduced total bacteria count by 5 logs, total coliform by more than 6 logs, below detectable limits, and total *Salmonella* by more than 4 logs, also below detectable limits. Fecal *streptococci* were only reduced by 2 logs with data indicating that some fecal *streptococci* are sensitive to radiation, whereas others are resistant. For samples of anaerobically digested

sludge irradiated at Deer Island with 0.85 MeV electrons, total bacteria were reduced by 4 logs at a dose of 280 krads, total coliform by 5–6 logs at a dose of 150–200 krads; a dose of 400 krads reduced fecal *streptococci* by 3.6 logs.

Virus inactivation has also been measured. A dose of 400 krads will apparently reduce the total virus measured as PFU by 1–2 logs. Laboratory batch irradiation of five enteric viruses showed about 2 logs reduction at a dose of 400 krads; Coxsackie virus was most resistant, whereas Adeno virus was least resistant. These results correlate directly with virus size. Larger viruses are larger targets and hence more susceptible to electron "hits" (39,40).

Data for parasite reduction are scarce but 400 krads will apparently destroy all *Ascaris* ova (39). Comparing these performance data with information from Table 1 on the quantity of pathogens in sludge indicates that a dose of 400 krads may be adequate to disinfect anaerobically digested sludge, but raw sludge or aerobic sludge may require higher doses.

Odor problems are dramatically lower for irradiated sludge as compared with pasteurized sludge (40). Irradiation of digested sludge with an e-beam may also improve sludge dewaterability and destroy some synthetic organic chemicals, as well as reduce pathogen levels. Irradiation has reduced specific resistance of sludge by up to 50% at a dose of 400 krads (40). Because specific resistance is normally measured on a log scale, a 50% reduction may indicate minimal improvement in sludge dewaterability.

The energy requirements (fuel and electricity) for an irradiation system are estimated to be 90–98% less than those for heat pasteurization.

5. DISINFECTION WITH γ-IRRADIATION

5.1. γ-Irradiation Systems and Process Description

5.1.1. γ-Irradiation Systems for Liquid Sludge

γ-irradiation produces effects similar to those from an e-beam. However, γ-rays differ from electrons in two major ways. First, they are very penetrating; a layer of water 25 in. (64 cm) thick is required to stop 90% of the rays from a Co-60 source; in comparison, l MeV electron can only penetrate about 0.4 in. (1 cm) of water. Second, γ-ray result from decay of a radioactive isotope. Decay from a source is continuous and uncontrolled; it cannot be turned off and on. The energy level (or levels) of the typical γ-ray from a given radioactive isotope is also relatively constant. Once an isotope is chosen for use as a source, the applied energy can only be varied with exposure time. Two isotopes, Cs-137 and Co-60, have been considered as "fuel" sources for sludge irradiators. Cs-l37 has a half-life of 30 yr and emits a 0.660 MeV γ-ray. It has been available in the United States as a byproduct from the processing of nuclear weapons wastes. If the United States establishes a nuclear reactor spent-fuel rod reprocessing program, it would also be available at a rate of about 2 lb/t (1 kg/T) of fuel. Co-60 has a half-life of 5 yr and emits two γ-rays with an average energy of 1.2 MeV. It is made by bombarding normal cobalt metal, which is stable cobalt isotope 59, with neutrons.

Two general types of γ-ray systems have been proposed for wastewater sludge disinfection. (40) The first is a batch-type system for liquid sludge, in which the sludge is circulated in a closed vessel surrounding the γ-ray source. Dosage is regulated by detention and source strength. The second system is for dried or composted sludge. A special
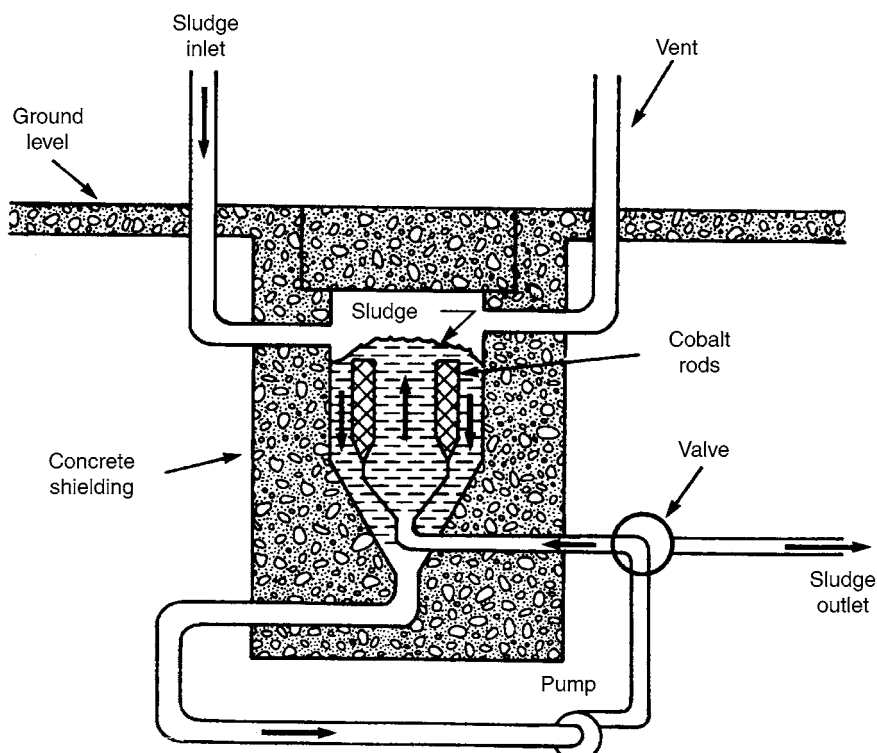
Fig. 4. γ-Irradiation facility (*Source:* US EPA).

hopper conveyor is used to carry the material for irradiation to the γ-ray source. Conveyor speed is used to control the dosage.

One γ-ray system in active operation is a liquid sludge facility at Geiselbullach (near Munich) in West Germany. Sludge has been treated there since 1973. The design capacity is 0.04 MGD (2 L/s) but the initial Co-60 charge only provided radiation to treat 0.008 MGD (0.3 L/s). The basic flow scheme is shown in Fig. 4. Digested sludge is pumped or otherwise moved into the vault with the Co source and circulated until the desired dosage is reached. The chamber is then completely emptied and recharged. Wizigmann and Wuersching (42) reported on the efficiency of the Geiselbullach facility when the applied dose was 260 krads in 210 min. Bacterial tests were made on samples of processed sludge and showed 2 log reduction in total bacterial count, an *Enterococcus* reduction of 2 logs, and an *Enterobacteriaceae* reduction of 4–5 logs. Two of 40 samples were positive for *Salmonella*. Bacterial regrowth was measured in sludge-drying beds in which the sludge was placed after irradiation.

Plastic-encapsulated bacteria samples were also irradiated in the system to a dosage of 260 krads. Two of nine *E. coli* strains were radiation resistant and reduced 5–6 logs; three strains were totally inactivated, and four strains were reduced 6–8 logs. Tests on 10 strains of *Salmonella* in 170 samples showed 4–7 log reduction, with 85% of the samples more than 5 logs and 61% more than 6 logs. *Kiebsiella* were reduced 6–8 logs. Gram-negative species were more sensitive to γ-radiation than gram-positive
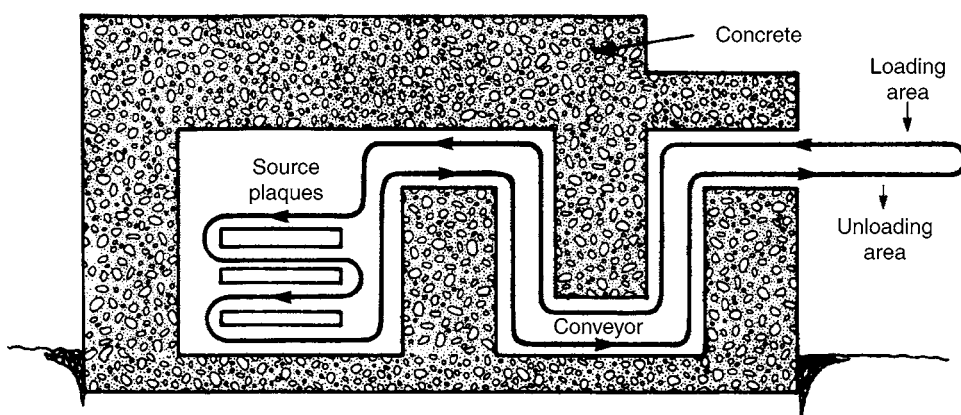
Fig. 5. γ-Irradiation facility for handling 25 t/d or more of dewatered sludge (*Source:* US EPA).

ones, and spores were more resistant than vegetative forms. A comparison of the disinfection results of the real sludge samples and the plastic-encapsulated cultures indicates that circulation in the sludge system apparently did not result in a very uniform dose exposure.

Parasite ova (*Ascaris suum*) circulated through the system in plastic capsules failed to develop during 3 wk of incubation. This observation period was not adequate, however, to assure that long-term recovery would not take place. Land spreading of the sludges treated at Geiselbullach has been well received by local farmers and the general public. No radiation hazards have resulted and the treated sludges satisfy disinfection requirements. The competing system in Germany, heat pasteurization, requires more energy and produces an odorous product that is more difficult to handle.

5.1.2. γ-Irradiation Systems for Dried or Composted Sludge

A dry sludge irradiation system using a γ-source has been developed by Sandia Laboratories in Albuquerque, New Mexico. The 8-T/d (7.2 T/d) facility contains about 1×10^6 Ci of Cs-l37. The facility is used to irradiate bagged composted sludge for agricultural experiments and bagged dried raw primary sludge for testing as a cattle-feed supplement. Owing to the high cost of Co-60, the overall viability of any sludge irradiation facility in the United States depends on Cs-l37 supplies. Cs-l37 will be available in quantity only if the political and technical difficulties associated with power plant fuel rod reprocessing can be resolved. About 200 megaCi of Cs-l37 could be available from processing wastes from weapons manufacture and could be used for further testing. The dry system uses a bucket conveyor to move the sludge past the radiation source as shown in Fig. 5.

5.1.3. γ-Irradiation Systems for Food Irradiation

Food irradiation is a technology for controlling spoilage and eliminating food-borne pathogens, such as *Salmonella*. The result is similar to conventional pasteurization and is often called "cold pasteurization" or "irradiation pasteurization." Like pasteurization, irradiation kills bacteria and other pathogens that could otherwise result in spoilage or

food poisoning. The fundamental difference between the two methods is the source of the energy they rely on to destroy the microbes. Although conventional pasteurization relies on heat, irradiation relies on the energy of ionizing radiation. The US Food and Drug Administration (US FDA) emphasizes that no preservation method is a substitute for safe food handling procedures. (47).

In a food irradiation process, bulk or packaged food passes through a radiation chamber on a conveyor belt. The food does not come into contact with radioactive materials, but instead passes through a radiation beam, like a large flashlight. The type of food and the specific purpose of the irradiation determine the amount of radiation, or dose, necessary to process a particular product. The speed of the belt helps control the radiation dose delivered to the food by controlling the exposure time. The actual dose is measured by dosimeters within the food containers.

Co-60 is the most commonly used radionuclide for food irradiation. However, there are also large cesium-137 (Cs-137) irradiators and the US Army has also used spent fuel rods for irradiation.

The food irradiation process uses three types of ionizing radiation sources: (a) γ-irradiation using Co-60 γ-sources; (b) electron irradiation using e-beam generators; and (c) X-ray irradiation using X-ray generators. This section discusses only the γ-irradiation using Co-60 γ-sources.

Co-60 emits ionizing radiation in the form of intense γ-rays. "γ-facilities" store it in stainless steel capsules (like "pencils" of cobalt), in underwater tanks. Co-60 has several advantages: (a) up to 95% of its emitted energy is available for use, (b) penetrates deeply, (c) yields substantial uniformity of the dose in the food product, (d) decays to non-radioactive nickel, and (e) be considered to pose low risk to the environment. However, its 5.3-yr half-life offers some disadvantages: (a) Co-60 "pencils" require frequent replenishment, and (b) treatment of the food is relatively slow.

Cs-137 is a γ-source that is also used for irradiation. Cs-137 has a less penetrating γ-beam and a longer half-life, making it more suitable under certain circumstances.

5.1.4. Process Description

It is a disinfection process involving the use of γ-facilities to store Co-60 or Cs-137, which emits ionizing radiation in the form of intense γ-rays. When ionizing radiation strikes bacteria and other microbes, its high energy breaks chemical bonds in molecules that are vital for cell growth and integrity. As a result, the microbes die, or can no longer multiply causing illness or spoilage. Breaking chemical bonds with radiation is known as radiolysis.

5.2. γ-Irradiation Design Considerations

5.2.1. General Design Considerations

The design criteria for γ-irradiation facilities depend on the type of wastewater sludge or solid food treated.

The current literature discussions suggest a dose of 400 krads but this level does not ensure complete virus removal (40). The dose level should probably be varied in relation to other treatments that the sludge receive. A composted, bagged product with an 80% solid content needs a lower dose than a mixture of raw primary and WAS because

the dried product already has a reduced pathogen level owing to the drying process. The storage capacity for both untreated and irradiated sludge should be equal to that for a pasteurization facility of similar size.

When a dry system radiation source is not in use, it should be shielded in a steel-lined concrete vault. The vault should be designed to be flooded with water during loading and unloading of the radiation source, to shield workers from radiation. Provision must be made for pool water treatment in the event that the radiation source leaks. Cooling air is circulated around the source both during system operation and down times. This air must be filtered to prevent a radioactive air release. Because the dried sludge is a flammable material, there must be smoke and/or heat detection and a fire suppression system. For a liquid storage system the treatment vessel serves as a radiation source storage vault.

5.2.2. Facility Design Components

5.2.2.1. Liquid Sludge Treatment Facility

The liquid facility may include the following components: (a) insulated concrete building with 25 ft (7.6 m) ceiling; (b) equalization sludge storage tank; (c) emergency water dump tank (for source shielding water); (d) irradiating capsules (radiation source); (e) steel-lined source handling pool; (f) deionizer; (g) data acquisition and control system; (h) oxygen injection facility; (i) pumps, piping, and flow meters; (j) radiation alarm; and (k) a fire suppression system.

The dry sludge treatment system (Fig. 5) uses a bucket conveyor to move the sludge past the radiation source. This dry system may include the following: (a) loading and unloading conveyors; (b) concrete shielding; (c) source handling pool; (d) holder for the Cs-137 capsules; (e) a holder moving mechanism; (f) steel building; (g) pumps; (h) ventilators; (i) hoists; (j) a radiation alarm system; (k) pool water testing tank; and (l) a fire suppression system.

5.2.2.2. Solid Food Disinfection Facility

The Linear Accelerator Facility at Iowa State University is introduced in this section (48). Irradiation kills organisms that cause food-borne illness. As in the heat pasteurization of milk, the irradiation process greatly reduces but does not eliminate all bacteria. Irradiated poultry, for example, still requires refrigeration, but would be safe longer than untreated poultry. The energy source is either γ-rays (produced by a radioactive element such as cobalt) or electrons (produced by electricity). Electron radiation breaks up the bacteria's DNA, making it impossible for the bacteria to reproduce or continue living. The Iowa State University's linear accelerator facility uses electrons, and consists of three major components: (a) the accelerator, (b) the irradiation process unit, and (c) the food laboratory, such as the meat laboratory.

Accelerators work on the same principle as a television tube. Instead of being widely dispersed and hitting a phosphorescent screen at low energy levels, the electrons are concentrated and accelerated to 99% of the speed of light. This produces rapid reactions on the molecules within the product. The e-beam linear accelerator machine generates and accelerates electrons to energies of 5.0, 7.5, or 10.0 MeV with beam power of up to 10 kW.
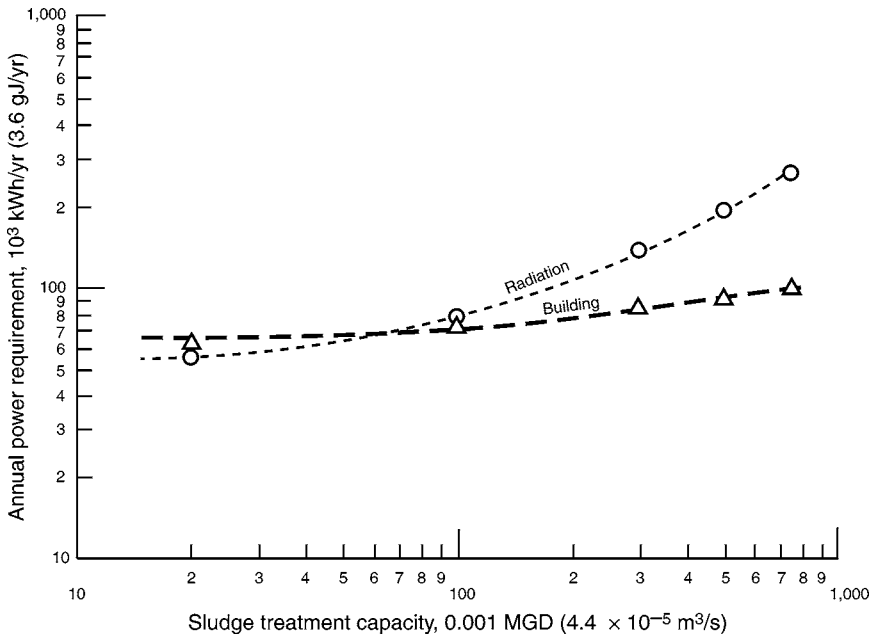
Fig. 6. Annual power requirement for γ-irradiation treatment of liquid sludge (*Source:* US EPA).

A stainless steel plate may be placed under the scanning horn to convert the electrons to X-rays at an energy level of 5 MeV to allow very thick penetration at low doses; however, this increases irradiation time considerably.

The Irradiation process unit is a cart system which moves the products to be irradiated under the e-beam at a predetermined speed to obtain the desired dosage. Multiple carts move products in and out of the irradiation area continuously with a throughput up to 500 lb/h. Maximum product dimensions are 24 in. wide and 36 in. long. Product thickness depends on density and electron energy. For example, 3.5 in. is the maximum thickness for meat. Using X-rays increases thickness to several feet for various products (*see* Section 6).

The meat laboratory, attached to the linear accelerator facility, has complete slaughter, cutting and processing operations with refrigeration and frozen storage. An analytical laboratory may conduct chemical, sensory, microbiological, and physical analyses on the irradiated product. In addition to meat, the irradiation process can be conducted on a wide variety of fresh vegetables, fruits, and spices, as well as some nonfood industrial products.

5.3. γ-Irradiation Operational Considerations

5.3.1. Sludge Treatment

Instrumentation should include radiation detectors and flow metering for the wet sludge system. When either facility is operating, arrangements must be made for periodic radiation safety inspection. The disinfection effectiveness should also be tested by periodic sampling of the sludge before and after disinfection. Ahlstrom and McGuire (43) projected annual energy requirements for both wet and dry γ-irradiation facilities, using a dose rate of 1000 krads. Their results are summarized in Figs. 6 and 7. For a 0.l MGD (4 L/s) facility treating sludge with 5% solids, 300 d/yr, the unit energy use is
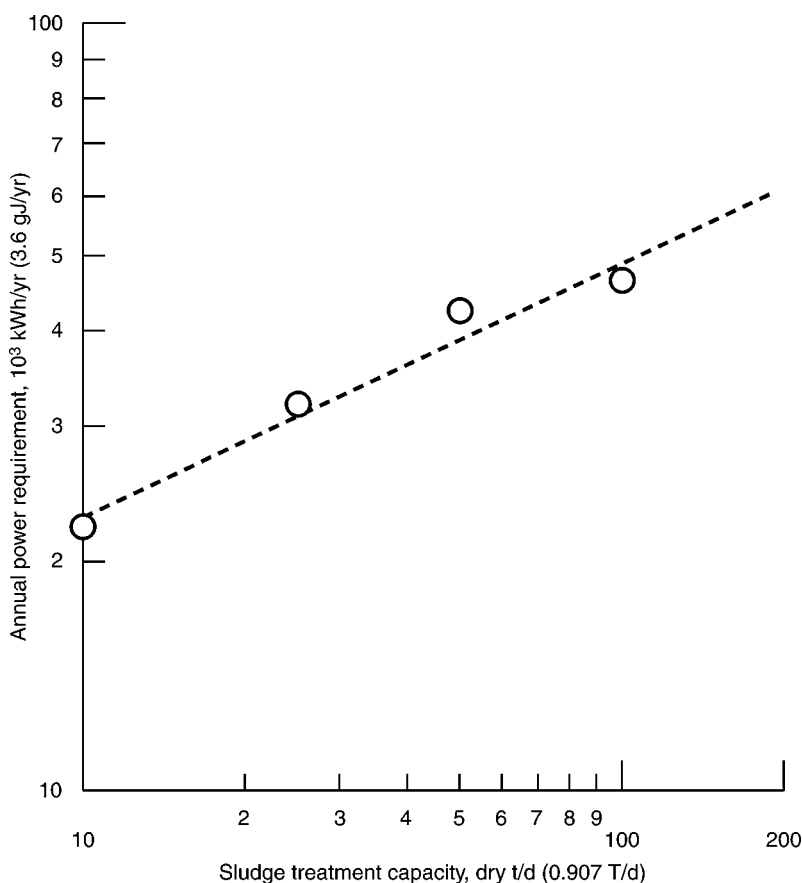
Fig. 7. Annual power requirement for γ-irradiation treatment of dewatered sludge (*Source:* US EPA).

about 5.2 kWh per 1000 gal (5 MJ/m^3) or 25 kWh/t (100 MJ/T) dry solids. For a plant treating 35 t/d (32 T/d) at 60% solids, 300 d/yr, the energy use is 5.6 kWh/T dry (22 MJ/T) solids, almost 80% less than the facility treating solids. These energy uses should be compared with 120 kWh/dry t (450 MJ/T) for an e-beam system. The liquid system requires a much larger Cs-137 charge because it will be treating almost 12 times the volume of material at the same dose level. However, the rod configuration for a dry facility would be much less efficient in terms of radiation transfer than a liquid one.

Figure 8 shows the annual labor requirements for γ-irradiation treatment of liquid sludge, whereas, Fig. 9 shows the annual labor requirements for γ-irradiation treatment of dewatered sludge (43). Here, 1 t = 2000 lb; 1 T = 1 tonne = 1000 kg.

5.3.2. Food Disinfection

The radiation dose to the food must be determined. Radiation doses vary for different foodstuffs. For the vast majority of foods, the limit is less than 10 kiloGrays. The US FDA sets radiation dose limits for specific food types: (a) fruit, 1 kiloGrays; (b) poultry, 3 kiloGrays; and (c) spices and seasonings, 30 kiloGrays. The dose limit for spices and seasons is higher, because they are consumed in very small quantities. Figure 10 shows a linear accelerator facility at the Iowa State University, IA, USA, designed specifically for food disinfection.
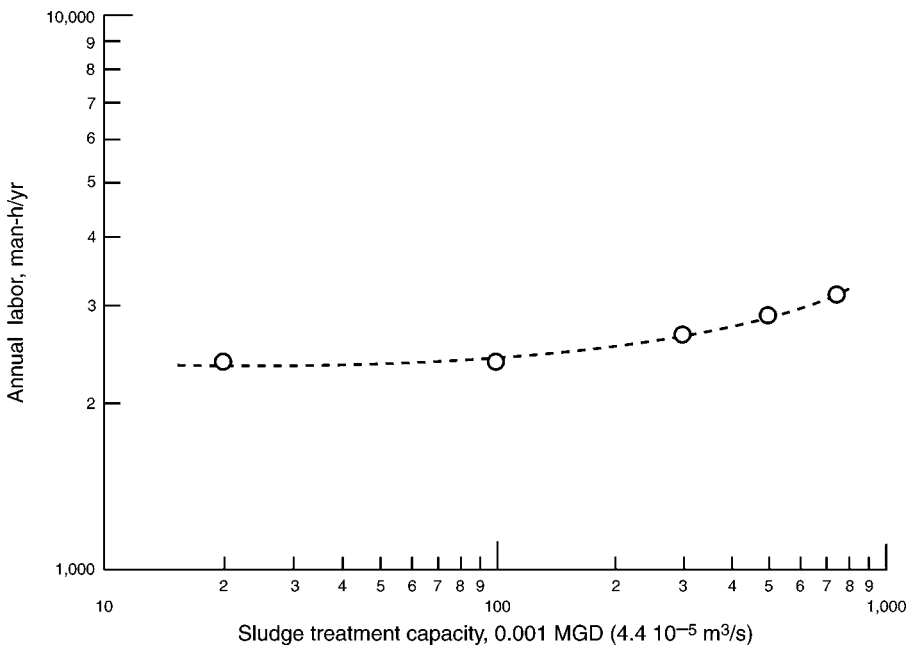
Fig. 8. Annual labor requirement for γ-irradiation treatment of liquid sludge (*Source:* US EPA).

6. X-RAY FACILITIES

It is important to note that X-ray facilities use an e-beam accelerator to target electrons on a metal plate. Although some energy is absorbed, the rest is converted to X-rays. Like γ-rays, X-rays are penetrating, and can be used on food boxes 15 in. thick or more. Accordingly it is suitable for food disinfection because it allows food to be processed in a shipping container. X-rays offer the advantage of high penetration similar to that of γ-irradiation, but share the other e-beam technology disadvantages.

7. NEW APPLICATIONS

7.1. Food Disinfection by Irradiation

Irradiation is known as a cold process, which has been approved for many uses in about 40 countries, but only a few applications are presently used because of consumer concern and because the facilities are expensive to build. The most common application of the process is sludge or biosolids treatment. Recently, the cold process has been successfully used for various applications. The irradiation process itself does not significantly increase the temperature or change the physical or sensory characteristics of most foods. An irradiated apple, for example, will still be crisp and juicy. Fresh or frozen meat can be irradiated without cooking it.

During irradiation, the energy waves affect unwanted organisms but are not retained in the food. Similarly, food cooked in a microwave oven, or teeth and bones that have been X-rayed do not retain those energy waves (47,48).

In the United States, the FDA has approved irradiation for eliminating insects from wheat, potatoes, flour, spices, tea, fruits, and vegetables. Irradiation can also be used to control sprouting and ripening. Approval was given in 1985 to use irradiation on pork to
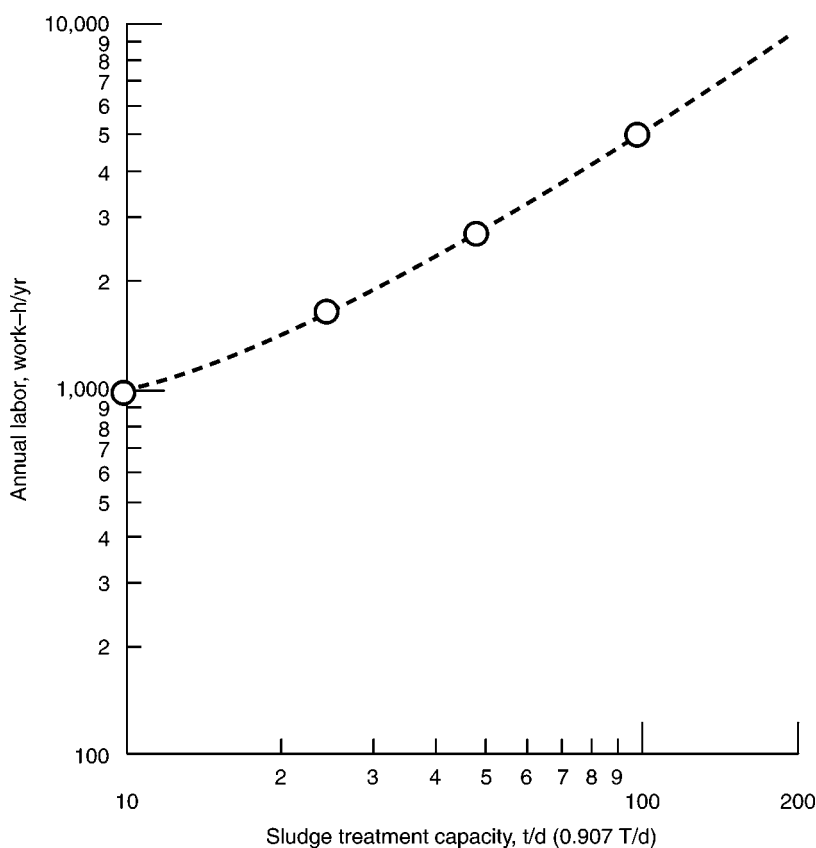
Fig. 9. Annual labor requirement for γ-irradiation treatment of dewatered sludge (*Source:* US EPA).

control trichinosis. Using irradiation to control *Salmonella* and other harmful bacteria in chicken, turkey, and other fresh and frozen uncooked poultry was approved in May 1990. In December l997, FDA approved the use of irradiation to control pathogens (disease causing microorganisms such as *E. coli* and *Salmonella* spp.) in fresh and frozen red meats such as beef, lamb, and pork. Because the irradiation process works with both large and small quantities, it has a wide range of potential uses in the food industry. For example, a single serving of poultry can be irradiated for use on a space flight. Or, a large quantity of potatoes can be treated to reduce sprouting during warehouse storage.

However, irradiation cannot be used with all foods. It causes undesirable flavor changes in dairy products, for example, and it causes tissue softening in some fruits, such as peaches and nectarines. Irradiation is most useful in four areas: (a) preservation, (b) sterilization, (c) control sprouting, ripening, and insect damage, and (d) control of food borne illness. As a preservation process, irradiation can be used to destroy or inactivate organisms that cause spoilage and decomposition, thereby extending the shelf life of foods. It is an energy-efficient food preservation method that has several advantages over traditional canning. The resulting products are closer to the fresh state in texture, flavor, and color. Using irradiation to preserve foods requires no additional liquid, nor does it cause the loss of natural juices. Both large and small containers can be used and food can be irradiated after being packaged or frozen.
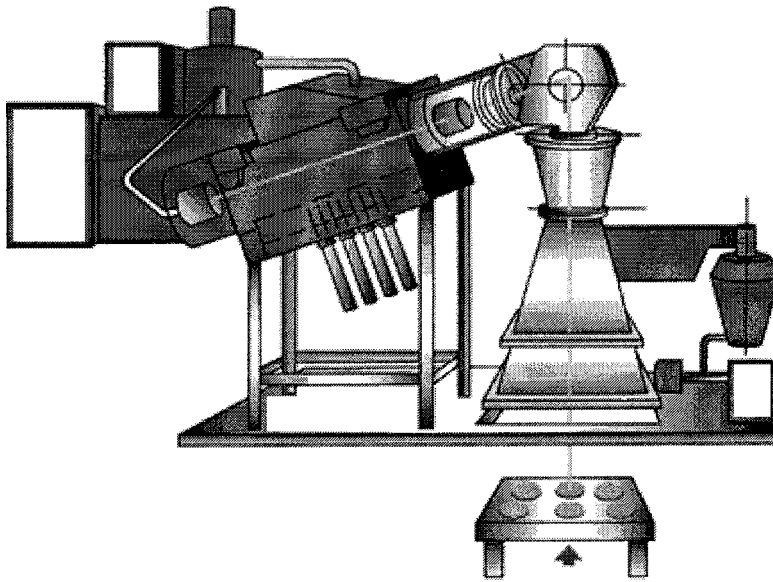
Fig. 10. The linear accelerator facility at Iowa State University, USA (*Source:* ISU).

Irradiation is a typical sterilization process. Foods that are sterilized by irradiation can be stored for years without refrigeration, just like canned (heat sterilized) foods. With irradiation it will be possible to develop new shelf-stable products. Sterilized food is useful in hospitals for patients with severely impaired immune systems, such as some patients with cancer or AIDS. These foods can be used by the military and for space flights.

When irradiation is used for control of sprouting, ripening, and insect damage, it offers an alternative to chemicals for use with potatoes, tropical and citrus fruits, grains, spices, and seasonings. However, because of no residue is left in the food, irradiation does not protect against reinfestation like insect sprays and fumigants do. Irradiation can be used to effectively eliminate those pathogens that cause food-borne illness, such as *Salmonella*. Scientists believe that irradiation produces no more nutrient loss than what occurs in other processing methods, such as canning.

7.2. Hospital Waste Treatment by Irradiation

Medical waste is one of the most problematic types of wastes for solid waste authorities in all countries. When such wastes enter the municipal solid waste streams, pathogens in the wastes pose a great hazard to the environment and to those who come in contact with the wastes. Waste generated within hospital premises has three main components: (a) common wastes, for example, administrative office waste and kitchen waste; (b) pathogenic or infectious wastes (these also contain sharps); and (c) hazardous wastes (mainly those originating in the laboratories containing toxic substances). The quantity of the first type of waste tends to be much larger than the second and third types. Ideally, as recommended in the accompanying box, these three types of waste should be separated. However, separation is possible only when there is significant management commitment, in-depth and continuous training of personnel, and permanent

supervision to ensure that the prescribed practices are being followed. Otherwise, there is always a risk that infectious and hazardous materials will enter the common waste stream.

Sound environmental engineering practices for managing medical wastes are characterized by: (a) source separation within the hospital; (b) take-back systems; (c) tight inventory control over medications; (d) piggy-back systems for nursing homes, clinics, and doctors' offices; (e) treatment of infectious waste through incineration, or by disinfection; and (f) proper disposal of hospital wastes.

The first step for proper disposal of hospital wastes is source separation: (a) that isolates infectious and hazardous wastes from non-infectious and nonhazardous ones, through color coding of bags or containers; (b) that source separates and recycles the large quantities of noninfectious cardboard, paper, plastic, and metal; (c) that source separates compostable food and ground wastes and directs them to a composting facility, if available and (d) that is characterized by thorough management monitoring.

When the take-back system is established in a hospital, vendors or manufacturers are required to take back the unused or out-of-date medications for controlled disposal.

When the policy of the tight inventory control over medication is established in a hospital, the hospital can avoid wastage because of expiration dates (really a form of waste reduction).

The piggy-back systems should be established for nursing homes, clinics, and doctors' offices, so that they can funnel their wastes through hospital waste systems in the vicinity.

Treatment of infectious waste can be done through incineration, or by disinfection (including autoclaving, chemical reaction, microwaves, and irradiation). In the case of incineration this may be done within the hospital premises or in a centralized facility. An incinerator is difficult and expensive to maintain, so it should be located in a hospital only when the hospital is large or where it provides services to other nearby hospitals. Otherwise, a centralized incinerator that provides services to hospitals in one region or city is more appropriate. In the case of disinfection, residues from these processes should still be treated as special wastes, unless a detailed bacteriological analysis is carried out.

Proper disposal of hospital wastes is important in many developing countries because none of the above treatment systems are widely available, so final disposal of infectious and hazardous components of the wastes is necessary. Since in many developing countries there are no landfills specifically designed to receive special wastes, hospital wastes need to go to the local landfill or dump. In this case, close supervision of the disposal process is critical in order to avoid contact with waste pickers. Final disposal should preferably be done in a specially designated cell, which should be covered with a layer of lime and at least 50 cm of soil. When no other alternative is available for final disposal, hospital wastes may be disposed of jointly with regular wastes. In this case, however, hospital wastes should be covered immediately by a meter thickness of ordinary municipal solid waste and always be placed more than 2 m from the edge of the deposited waste (49–52).

Although there are many technologies for treatment, and disposal of medical wastes, only irradiation technologies are discussed in this chapter. The irradiation technologies used for food irradiation can also be adopted for the medical waste irradiation.

7.3. *Mail Irradiation*

In October 2001, the deadly microorganism anthrax was found in mail sent to various news agencies and to the offices of U.S. Congressmen. As a precaution, the U.S. Postal Service, with assistance from FBI and national public health experts, began irradiating mail to kill potentially present anthrax spores (53). Irradiation of mail kills organisms in or on the envelopes and packages, thereby protecting the recipient against possible bacterial or viral releases from that mail. It is a reliable sterilization method that can handle the large flows of mail that come to federal agencies.

Irradiating mail does not make it radioactive. The process is comparable to shining a flashlight on the mail—when the flashlight is turned off, mail does not glow, or radiate back the light it received. However, mail tends to be brittle and discolored and may have an unusual smell after it has gone through the irradiation process (53). Individuals who handle large amounts of irradiated mail have complained of adverse health effects, including skin irritation; eye, nose, and throat irritation; headaches; and nausea. Initially, some workers mistakenly feared these symptoms were due to radiation. It was necessary to ensure they understood the basics of radiation science involved in the process and that the mail itself was not radioactive. The symptoms may have resulted from a combination of factors, including a dry environment, drying effects on the skin from handling irradiated paper, chemicals released from plastics in the mail, and the odor from the irradiated mail.

The irradiation process sterilizes mail by passing it through a high-energy beam—an electron beam or X-ray. This beam is ionizing radiation that delivers in a dose approximately 2 million times more potent than a chest X-ray. The beam penetrates deep into the mail to destroy germs and viruses and is capable of penetrating letter trays and packages (53). To ensure that employees and visitors are not exposed to even low levels of radiation at the irradiation facilities, very thick concrete or lead-lined walls shield the exposure rooms. Radiation levels are closely monitored at these facilities to ensure that workers are safe.

8. GLOSSARY

Bacteria: Bacteria are one-celled microorganisms that can cause illness and spoil food, sometimes without changing the food's taste, smell, or appearance.

Carbohydrates: Carbohydrates are components of food that give us energy. They are made of carbon, hydrogen, and oxygen. Sugars and starches are examples.

Cesium 137: Cs 137 is a metal that, when processed in a certain way, gives off ionizing radiation. It is used in food irradiation.

Cobalt 60: It is a metal that, when processed in a certain way, gives off ionizing radiation. It is used in food irradiation.

Electron irradiation: It is a disinfection process involving acceleration of electrons and producing a continuous beam that is scanned back and forth at 400 times/s across the target material as it falls free in a thin film from the end of the inclined ramp. The dosage is varied by adjusting the height of the underflow weir and hence the flow rate of the target material to be disinfected. The electrons are not penetrating. A 1 MeV electron can only penetrate about 0.4 in. (1 cm) of water.

Enzyme: It is a protein in food that starts a chemical reaction, such as ripening.

Food irradiation: It is the process of exposing food to radiation (rays of energy).

Free radicals: They are atoms or molecules with an unpaired electron. Formation of free radicals is a normal oxidation process in foods and are formed during food treatments such as toasting, frying, freeze drying, and irradiation. They are generally very reactive, unstable structures that continuously react with substances to form stable products. Free radicals disappear by reacting with each other in the presence of liquids, such as saliva in the mouth. Consequently, their ingestion does not create any toxicological or other harmful effects.

Fungi: It is plural of fungus. Fungi are single-celled nonphotosynthesizing plants that reproduce by developing spores, which form new colonies when released. Spores range in size from 10 to 100. They are secondary pathogens in wastewater sludge, and large numbers have been found growing in compost.

Fungus: It is a type of plant with no chlorophyll (green pigment). Examples are yeasts, molds, and mushrooms.

γ-Irradiation: It is a disinfection process producing γ-rays, which are very penetrating. A layer of water 25 in. (64 cm) thick is required to stop 90% of the rays from a Co-60 source. γ-Rays result from decay of a radioactive isotope. Decay from a source is continuous and uncontrolled; it cannot be turned off and on. The energy level (or levels) of the typical γ-ray from a given radioactive isotope are relatively constant. Once an isotope is chosen for use as a source, the applied energy can only be varied with exposure time. Two isotopes, Cs-137 and Co-60, have been considered as "fuel" sources for sludge irradiators. Cs-l37 has a half-life of 30 yr and emits a 0.660 MeV γ-ray.

Gray: It is the unit that measures the radiation dose (Gy). International health and safety authorities have endorsed the safety of irradiation for all foods up to a dose level of 10,000 Gy (10 kGy). One gray equals 1 J of energy absorbed per kilogram of food being irradiated.

Ionizing radiation: It is a process that emits the rays of energy that move in short, fast wave patterns and can penetrate cells.

Irradiate: It means to expose to, or treat, with radiation.

Mold: It is a fungus that can grow in food. It often shows up as a furry growth on food.

Nonionizing radiation: It is a process that emits the rays of energy that move in long, slow wave patterns and do not penetrate cells.

Parasite: It is an organism that lives on or in another organism which is called the "host." It does not help the host. Parasites include protozoa, nematodes, and helminths. Pathogenic protozoa are single-celled animals that range in size from 8 μm to 25 μm. Protozoa are transmitted by cysts, the nonactive and environmentally insensitive form of the organism. Their life cycles require that a cyst be ingested by man or another host. The cyst is transformed into an active organism in the intestines, where it matures and reproduces, releasing cysts in the feces.

Radiation: It is a process that emits the rays of energy.

Radiation dose: It is the quantity of radiation energy absorbed by the food as it passes through the radiation field during processing.

Radiolytic products (RPs): They are the chemicals produced in food when the food is irradiated that are the same as chemicals produced during cooking.

Radura symbol: It is a circular symbol that must appear on all irradiated food unless the food is used as an ingredient in a processed food or is served in a restaurant.

Spore: It is the part of mold that reproduces and causes the mold to spread. It is the mold's version of a seed.

Unique radiolytic products (URPs): They are the chemicals produced in food when the food is irradiated that are different from chemicals produced during cooking.

Viruses: They are obligate parasites and can only reproduce by dominating the internal processes of host cells and using the host's resources to produce more viruses. Viruses are very small particles whose protein surface charge changes in magnitude and sign with pH. In the natural pH range of wastewater and sludges, most viruses have a negative surface charge. Thus, they will adsorb to a variety of materials under appropriate chemical conditions. Different viruses show varying resistance to environmental factors such as heat and moisture. Enteric viruses are acid resistant and many show tolerance to temperatures as high as 140°F (600°C). Many of the viruses that cause disease in man enter the sewers with feces or other discharges and have been identified, or are suspected of being, in sludge.

REFERENCES

1. J. R. Branden, Parasites in Soil/sludge systems. *Proceedings of Fifth National Conference on Acceptable Sludge Disposal Techniques*, Orlando, Florida, January 31 to February 2, 1978. Information Transfer, Inc. Rockville, Maryland, MA, p. 130, 1978.
2. J. R. Oliver, The life and times of *Aspergillus fumigatus*. *Compost Sci./Land Utilization* **20**(2), 1979.
3. US Public Health Service, *Enteric and Neurotropic Viral Diseases Surveillance*, *1971–1975*. US Public Health Service, Center for Disease Control, Atlanta, Georgia, 1977.
4. US Public Health Service, *Shigella Surveillance*, *Annual Summary 1976*. US Public Health Service, Center for Disease Control, Atlanta, Georgia, 1977.
5. US Public Health Service, *Salmonella Surveillance*, *Annual Summary 1977*. US Public Health Service, Center for Disease Control, Atlanta, Georgia, 1979.
6. US Public Health Service, *Intestinal Parasite Surveillance*, *Annual Summary 1976*. US Public Health Service, Center for Disease Control, Atlanta, Georgia, 1977.
7. US Public Health Service, *Intestinal Parasite Surveillance*, *Annual Summary 1977*. US Public Health Service, Center for Disease Control, Atlanta, Georgia, 1978.
8. B. P. Sagik, Survival of pathogens in soils. *Proceedings of Williamsburg Conference on Management of Wastewater Residuals*, Williamsburg, Virginia, November 1975. US National Science Foundation, Washington DC, RANN-AEN74-08082. p. 30, 1975.
9. T. G. Metcalf, "Role of Viruses in Management of Environmental Risks. *Proceedings of Williamsburg Conference on Management of Wastewater Residuals*, Williamsburg, Virginia, November 1975. US National Science Foundation, Washington DC RANN-AEN 74-08082. p. 53.
10. B. F. Moore, B. P. Sagik, and C. A. Sorber, An assessment of potential health risks associated with land disposal of residual sludges. *Proceedings of Third National Conference on Sludge Management*, *Disposal and Utilization*, Miami Beach, Florida. December 14–16, 1976. Information Transfer, Inc. Rockville, Maryland, p. 108, 1976.
11. G. Stern and J. B. Farrell, Sludge disinfection techniques. *Proceedings of National Conference on Composting of Municipal Residues and Sludges.* Washington, DC, August 1977. Information Transfer, Inc., Rockville, Maryland, p. 142, 1977.
12. J. B. Farrell and G. Stern, Methods for reducing the infection hazard of wastewater sludge. *Radiation for a Clean Environment*, *Symposium Proceeding.* International Atomic Energy Agency, Vienna, Austria, 1975.
13. L. K. Wang, A potential organic disinfectant for water purification, *J. N. Engl. Water Works Assoc.* **89**(3), 250–270 (1975).

14. L. K. Wang, Disinfection with quaternary ammonium compounds, *Water Res. Bull.*, *J. Am. Water Res. Assoc.* **11**(5), 919–933 (1975).

15. L. K. Wang, Thickening of sewage sludge with quaternary ammonium compounds and magnetic fields, *Proceedings of the Third National Conference on Complete Water Reuse*, pp. 252–258, June 1976.

16. L. K. Wang, Cationic surface active agent as bactericide, *Ind. Eng. Chem. Product Res. Dev.* **14**(4), 308–312 (1975).

17. L. K. Wang and M. H. S. Wang, General theories of chemical disinfection and sterilization of sludge, part I, *Water and Sewage Works*, **125**(7), 30–32 (1978).

18. L. K. Wang and M. H. S. Wang, General theories of chemical disinfection and sterilization of sludge, part II, *Water and Sewage Works*, **125**(8), 58–62 (1978).

19. L. K. Wang and M. H. S. Wang, General theories of chemical disinfection and sterilization of sludge, part III, *Water and Sewage Works*, **125**(9), 99–104 (1978).

20. L. K. Wang and M. H. S. Wang, *Principles and Kinetics of Oxygenation & Ozonation Waste Treatment System*, US Dept. of Commerce, National Technical Information Service, Springfield, VA, PB83-127704, p. 139, 1983.

21. US EPA, *Agricultural Benefits and Environmental Changes Resulting from the Use of Digested Sludges on Field Crops*. US Environmental Protection Agency, Office of Research and Development, Cincinnati, OH, 45268. Report SW-30d, 1971.

22. Sacramento Regional County Sanitation District, *Sewage Sludge Management Program Final Report, Volume 6, Miscellaneous Use Determinations.* Sacramento Regional County Sanitation District, Sacramento, California, September, 1979.

23. J. B. Farrell, J. E. Smith, S. W. Hathaway, and R. B. Dean, Lime stabilization of primary sludge. *J. Water Poll. Contr. Federation* **46**, 113 (1974).

24. L. K. Wang and N. C. Pereira, *Handbook of Environmental Engineering*, *Vol. 2*, *Solid Waste Processing and Resource Recovery.* Humana Press, Inc., Totowa, NJ, pp. 269–327, 1980.

25. L. K. Wang, *Development of Alternative Sterilization Methods*, US Dept. of Commerce, National Technical Information Service, Springfield, VA, PB83-225052, p. 17, July 1983.

26. L. K. Wang, *Waste Treatment by Innovative Flotation-Filtration and Oxygenation-Ozonation Process*, US Dept. of Commerce, National Technical Information Service, Springfield, VA. PB85-174738-AS, p. 171, 1984.

27. L. K. Wang, *Sludge Treatment by Oxygenation-Ozonation Flotation and Press Dewatering*, Technical Report No. LIR/07-88/311, Lenox Institute of Water Technology, Lenox, MA, July, 1988.

28. L. K. Wang, *Guidelines for Disposal of Solid Wastes and Hazardous Wastes*, *Volumes I to VI*, US Dept. of Commerce, National Technical Information Service, Springfield, VA, PB89-158596/AS, 1988.

29. H. Roediger, The techniques of sewage sludge pasteurization: actual results obtained in existing plants. *InternationalRes Group on Refuse Disposal, Informational Bulletin*, **(21–31)**, 325, August 1974 to December 1976 (1974).

30. G. Stern, Pasteurization of liquid digested sludge. *Proceedings of National Conference on Municipal Sludge Management*, Pittsburgh. June 1974. Information Transfer Inc., Rockville, Maryland, p. 163, 1974.

31. R. L. Ward and J. R. Brandon, Effect on heat on pathogenic organisms found in wastewater sludge. *Proceedings of National Conference on Composting of Municipal Residue and Sludges*, Washington, DC, August 23–25, 1977. Information Transfer Inc., Rockville, Maryland, p. 122, 1977.

32. L. K. Wang, *Method and Apparatus for Purifying and Compacting Solid Wastes*, US Patent No. 5232584, US Patent and Trademark Office, Washington, DC, August 3, 1993.

33. C. H. Connell and M. T. Garrett Jr, Disinfection effectiveness of heat drying at sludge. *J. Water Poll. Contr. Federation* **35**(10), 1963.

34. LA/OMA Regional Wastewater Solids Management Program. *Carver-Greenfield Process Evaluation*. Los Angeles & Orange County Metropolitan Area (LA/OMA Project). Whittier, California, 1978.

35. W. D. Burge, P. B. Marsh, and P. D. Millner, Occurrence of pathogens and microbial allergens in the sewage sludge composting environment. *Proceedings of National Composting Conference on Municipal Residue and Sludges*, Washington DC, August 23–25, 1977. Information Transfer, Inc., Rockville, Maryland, p. 128, 1977.

36. K. Kawata, W. N. Cramer, and W. D. Burge, Composting destroys pathogens in sewage sludge. *Water and Sewage Works* **124**, 76 (1977).

37. County Sanitation Districts of Los Angeles County. *Pathogen Inactivation During Sludge Composting.* Report to US EPA. County Sanitation Districts of Los Angeles County, Whittier, California, 1977.

38. R. C. Cooper and C. G. Colueke, Survival of enteric bacteria and viruses in compost and its leachate. *Compost Sci./Land Utilization*. March, 1979.

39. Massachusetts Institute of Technology, *High Energy Electron Irradiation of Wastewater Liquid Residuals.* Report to US National Science Foundation, Washington, DC, December 31, 1977. Massachusetts Institute of Technology, Boston, MA, 1977.

40. US EPA, *Process Design Manual for Sludge Treatment and Disposal*. US Environmental Protection Agency, Washington, DC, EPA625/1-79-012, 1979.

41. US EPA, *Innovative and Alternative Technology Assessment Manual.* US Environmental Protection Agency, Washington, DC, EPA430/9-80-009, 1980.

42. I. Wizigmann and F. Wuersching, Experience with a pilot plant for the irradiation of sewage sludge: bacteriological and parasitological studies after irradiation. *Radiation for a Clean Environment*, *Symposium Proceedings.* International Atomic Energy Agency. Vienna, 1975.

43. S. B. Ahlstrom and H. E. McGuire, *An Economic Comparison of Sludge Irradiation and Alternative Methods of Municipal Sludge Treatment.* Battelle Northwest Laboratories, Richland, Washington, PNL-2432/UC-23, November 1977.

44. L. K. Wang, J. S. Wu, N. K. Shammas, and D. A. Vaccari, Recarbonation and softening. In: *Physicochemical Treatment Processes*. L. K. Wang, Y. T. Hung, and N. K. Shammas (eds.), Humana Press, Inc., Totowa, NJ, 2005, pp. 199–228.

45. L. K. Wang, P. C. Yuan, and Y. T. Hung, Halogenation and disinfection. In: *Physicochemical Treatment Processes*. L. K. Wang, Y. T. Hung, and N. K. Shammas, (eds.), Humana Press, Inc., Totowa, NJ, 2005, pp. 271–314.

46. N. K. Shammas, J. Yang, P. C. Yuan, and Y. T. Hung, Chemical oxidation. In: *Physicochemical Treatment Processes*. L. K. Wang, Y. T. Hung, and N. K. Shammas, (eds.), Humana Press, Inc., Totowa, NJ, 2005, pp. 229–270.

47. US EPA, *Food Irradiation*. US Environmental Protection Agency, Washington, DC, http://www.epa.gov/radiation/sources/food_irrad.htm. accessed on April 2006.

48. Iowa State University, *The Linear Accelerator Facility.* Iowa State University, Iowa. http://www.extension.iastate.edu/foodsafety/irradiation/top. April 2006.

49. B. Fenger, O. Krogh, K. Krongaard, and E. Lund, *A Chemical*, *Bacteriological*, *and Virological Study of Two Small Biological Treatment Plant*. Fifth Meeting of the North West European Microbiological Group. Bergen, Norway, 1973.

50. G. M. Wesner, *Sludge Pasteurization System Costs.* Battelle Northwest, Richland, Washington, June 1977.

51. J. B. Farrell, High energy radiation in sludge treatment—status and prospects. *Proceedings of the National Conference on Municipal Sludge Management and Disposal*, Anaheim, August 18–20, 1975. Information Transfer Inc., Rockville, Maryland, 1975.

52. Radiation Safety Academy, *Radiation Sterilization Equipment Technical and Training Services.* Radiation Safety Academy, Gaithersburg, MD, 2001. www.radiationsafetyacademy.com.

53. US EPA. *Mail Irradiation.* U.S. Environmental Protection Agency, Washington, DC. EPA 402-F-06-052, 2006.

<div align="right">

4

</div>

Nonthermal Plasma Technology

Toshiaki Yamamoto and Masaaki Okubo

CONTENTS

1. FUNDAMENTAL CHARACTERISTICS OF NONTHERMAL PLASMA

1.1. Definition and Characteristics of Plasma

1.1.1. Definition of Plasma

All substances change from solid to liquid, and from liquid to gas when energy or heat is added. This change is called phase change and occurs at constant temperature. When energy is added to the gas, electrons emerge from the neutral particles and become ions. The state in which many ions and electrons are intermingled is called "plasma" (Fig. 1) (1–4). The change from gas to plasma is based on an ionization reaction. The energy needed for the reaction is in the range of 1–50 eV, which is generally much more than latent heat energy in the phase change (0.01 eV). Therefore, the change from gas to plasma is not strictly classified into the phase change. However, plasma is often called the fourth state, whereas solid, liquid, and gas are the other states of substance.

Plasma is generally defined as an ionization gas, which is electrically neutral macroscopically (the local number density of ion n_i is equal to the number density of electrons n_e). Both ion and electron particles in plasma are moved by the heat. In particular, the speed of electrons is much more than other particles because of their small mass and mobility.

1.1.2. Plasma Parameters

Physical quantities such as density and temperatures in plasma are recognized as plasma parameters and are used to define the characteristics of plasma. Several kinds of densities and temperatures exist in plasma: electron number density n_e, ion number density n_i, and gas molecule number density n_g, electron temperature T_e, ion temperature T_i, and gas temperature T_g. From the definitions of the plasma, n_e is usually equal to n_i. However, the electron temperature is often more than the ion and gas temperatures T_i
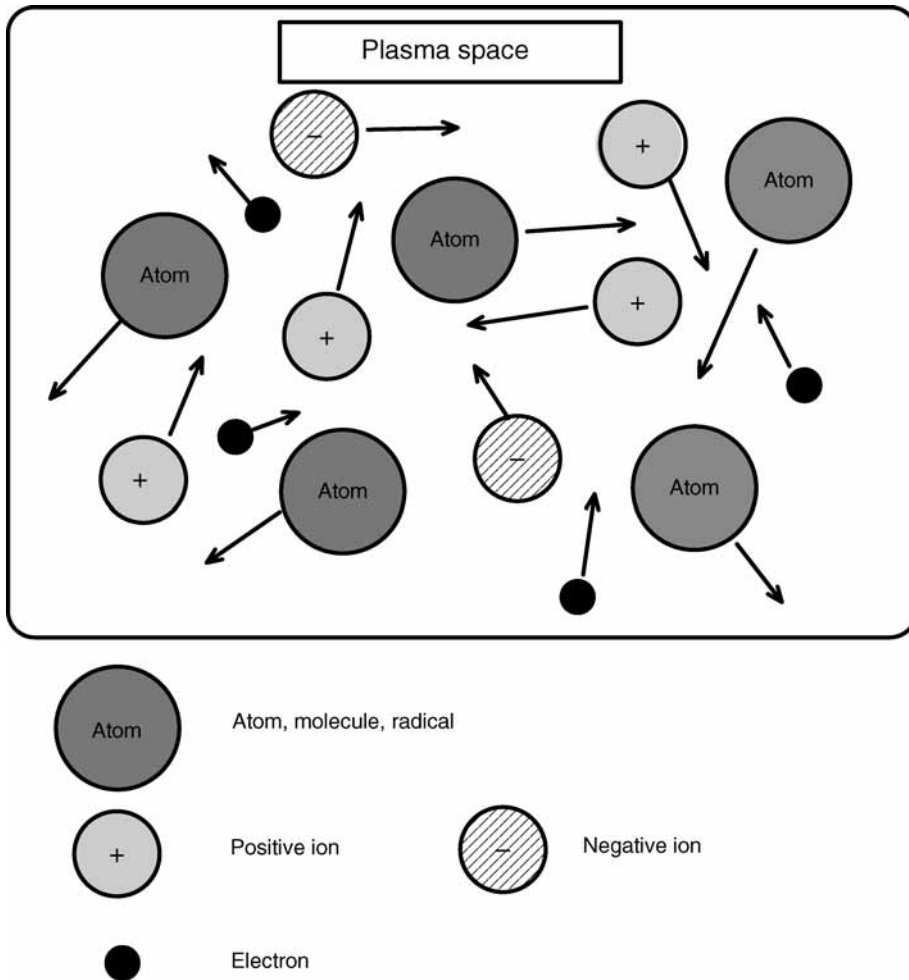
Fig. 1. Various kind of particles and collisions in the plasma space.

and T_g, whereas T_i is nearly equal to T_g. Therefore, this state is called "Nonequilibrium plasma." In general, when the T_g is much lower than the combustion temperature ($T_c \approx 1000°C$), the state is called "nonthermal plasma."

Because the temperature of plasma is defined only when the energy of each particle follows the Maxwell distribution, the energy distribution function of the particles in the plasma $f(v)$ is also very important information in characterizing the plasma. Furthermore, the Debye length, plasma angular frequency, thickness of ion sheath, and plasma space potential are also important parameters for describing the state of the plasma.

This section discusses the definitions of important plasma parameters, Debye length, temperature, and density.

1.1.2.1. DEBYE LENGTH

For sake of simplicity, it is assumed that only electrons are moving, whereas ions stay still in plasma. Let us consider the situation in which an electron moves away from an

ion by thermal motion. The electrostatic field is induced between the ion and the electron, and the ion attracts the electron. The maximum distance for the electron to move away from the ion is determined from the force balance between the kinetic energy of the electron and the electrostatic potential. This situation can also be considered in one-dimensional analysis. The kinetic energy of an electron E_k is expressed as

$$E_k = \frac{kT_e}{2} \tag{1}$$

where k is the Boltzmann's constant and T_e is the absolute temperature. In order to determine the electrostatic potential, one-dimensional Poisson's equation should be solved

$$\frac{d^2V}{dx^2} = \frac{ne}{\varepsilon} \tag{2}$$

where V is the electrical potential, x is the distance, n is the number density of charged particles, e is the magnitude of an electron charge, and ε is the permittivity of the space. This equation determines the electrostatic field induced by the charged particles. This equation can be integrated twice with respect to x, and then the potential V can be obtained. The electrostatic field potential becomes

$$E_p = eV = \frac{ne^2x^2}{2\varepsilon} \tag{3}$$

If it is assumed that E_k is equal to E_p, the maximum distance for the electron to move away from the ion is determined as

$$x_D = \sqrt{\frac{kT_e\varepsilon}{ne^2}} \tag{4}$$

This length is called the Debye length. The macro scale in defining the electrical neutrality of the plasma should be more than the Debye length. In a scale shorter than the Debye length, the electrical neutrality $n_e = n_i$ is not materialized. The Debye length varies with the type of plasma. For example, the Debye length in the plasma induced by an atmospheric-pressure arc discharge is about 10^{-4} mm whereas the Debye length in space plasma is nearly 1 m.

1.1.2.2. DENSITY

Because plasma is a collection of charged particles that moves randomly, it can be considered as a continuous media or a fluid except for the rarefied state. Therefore, the field of a quantity can be defined from an average value in a small volume, which is small macroscopically but includes enough number of particles. Density is the number of particles, which exist in a certain unit volume at a certain moment, therefore ion density, electron density, and neutral particle density (gas density) can be defined. The unit of density is m^{-3}.

The electron number density of the plasma induced by the low pressure (around several approx several 10 Pa) glow discharge has been investigated in detail. The electron density can be changed in the range of 10^8–$10^{11}/cm^{-3}$ by adjusting the electric discharge current from several milliampere to several ampere. The number density of electrons is almost proportional to the electric current. On the other hand, the electron number

density of the plasma in the ionosphere is around 10^4–10^6 cm^{-3}, which is smaller than that of the glow discharge. Further, ionization degree is defined as the ratio of ion number density to the gas particle number density.

1.1.2.3. TEMPERATURE

Generally, the temperature can be defined only when the kinetic energy of each particle follows the Maxwell distribution. The electron temperature for electrons, the ion temperature for ions, and the gas temperature or simply the temperature for heavy particles can be defined respectively. Electrons and heavy particles (neutrals and ions) have respectively kinetic energies and continuously collide with each other. As far as most collisions are considered to be completely elastic collisions, they can be treated like the theory of ideal gas. Therefore, it is considered that the particles as a whole follow a simple law, although, individual particles are moving randomly. The velocity of a particle follows the Maxwell velocity distribution law after many collisions occur.

$$f(v_x) = \left(\frac{m_e}{2\pi kT_e} \right)^{1/2} \exp\left(-\frac{m_e v_x^2}{2kT_e} \right) \tag{5}$$

$$f(v_y) = \left(\frac{m_e}{2\pi kT_e} \right)^{1/2} \exp\left(-\frac{m_e v_y^2}{2kT_e} \right) \tag{6}$$

$$f(v_z) = \left(\frac{m_e}{2\pi kT_e} \right)^{1/2} \exp\left(-\frac{m_e v_z^2}{2kT_e} \right) \tag{7}$$

$$F(v) = 4\pi \left(\frac{m_e}{2\pi kT_e} \right)^{3/2} v^2 \exp\left(-\frac{m_e v^2}{2kT_e} \right) \tag{8}$$

The probability density function of particle velocities is expressed in Eqs (5)–(7) and Eq (8) expresses the cumulative distribution function of particle velocity v. They are defined in the velocity space (v_x, v_y, v_z). Here, the electrons are considered as an example, and the same treatment is possible in the case of ions by replacing the mass and temperature of the electrons with those of the ions.

In order to understand the distribution function $f(v_x)$ and $F(v)$, the following change of variables are conducted:

$$f(x_v) = \frac{1}{\sqrt{\pi}} \exp(-x_v^2) \quad \text{where } x_v = (m_e/2kT_e)^{1/2} v_x \tag{9}$$

$$F(x_v) = \frac{4}{\sqrt{\pi}} x_v^2 \exp(-x_v^2) \quad \text{where } x_v = (m_e/2kT_e)^{1/2} v \tag{10}$$

The Eq. (9) and (10) are plotted in Fig. 2. The shape of the $f(x_v)$ distribution becomes maximum and symmetry at $x_v = 0$. The shape of $F(v)$ distribution is maximum at $x_v = 1$ and zero both at $x_v = 0$ and $x_v =$ infinite. Because v is the absolute value of the velocity,
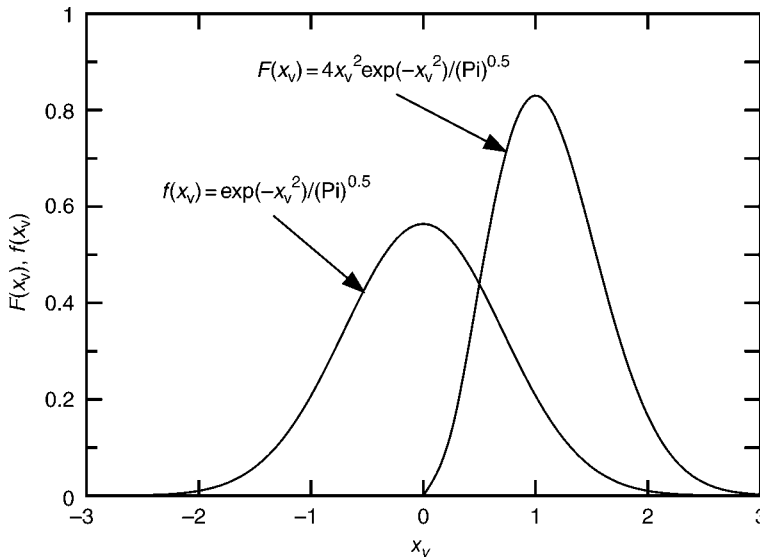
Fig. 2. Shapes of the function $f(x)$ and $F(x)$.

x_v must be positive. Therefore, the distribution of $F(v)$ is not symmetrical. The velocity can be defined as v_p for $x_v = 1$ as the velocity:

$$v_p = \left(\frac{2kT_e}{m_e}\right)^{1/2} \text{ or } \frac{1}{2}m_e v_p^2 = kT_e \tag{11}$$

where the electron exists most probably. This velocity is the most probable velocity. The Eq. (11) defines the electron temperature.

1.1.3. Thermal Equilibrium and Nonequilibrium Plasma

Plasma that is in a fully thermal equilibrium state satisfies the following five conditions.

a. The energy distribution of particles follows the Maxwell–Boltzmann distribution. The average value of the energy distribution is defined as the plasma temperature.
b. The temperature of each particle is equivalent, it is the same as the plasma temperature.
c. The excitation state is close to the Boltzmann distribution.
d. The particle number density becomes the reaction balance composition.
e. The electromagnetic wave is considered as black body radiation.

Except for condition (5), it is relatively easy to realize the conditions of (1)–(4) in the arc discharge at the atmospheric pressure, and so on. The state where the conditions (1)–(4) are satisfied is called local thermodynamic equilibrium (LTE). Generally, the physical properties such as the electrical conductivity and the specific heat of the plasma cannot be defined when the plasma is in a thermally nonequilibrium state.

When pressure is low, electric field is strong, a three-body recombination is active, or if the interface between the plasma and solid exists, the conditions (1)–(4) is often not satisfied and the plasma is in a nonequilibrium state. Especially, it is called the two-temperature nonequilibrium plasma when the electron temperature is different from the heavy particles temperature.

Table 1
Ionization Potentials and Statistical Weights for Various Species

Species	Ionization potentials (ε_i eV)	Statistical weights	
		g_o	g_i
He	24.6	1	2
Li	5.39	2	1
Na	5.14	2	1
K	4.34	2	1
Cs	3.89	2	1
Ne	21.56	1	6
Ar	15.76	1	6
H_2	15.6	–	–
O_2	12.05	3	4
O	13.61	9	4
N_2	15.6	1	2
NO	9.26	8	1
CO	14.1	1	2
CO_2	14.4	–	–
H_2O	12.6	–	–
OH	13.8	–	–

1.1.4. Governing Equation of Ionization

1.1.4.1. EQUATION OF NUMBER DENSITY

When gas becomes plasma, the ionization phenomenon where the electron comes out of the neutral particle occurs. The ionization follows a mass action law like any chemical reaction. The energy of the ionization reaction, expressed in electron volts (eV), is called the ionization potential. The ionization potential of main atoms and molecules are shown in Table 1. It is known from this table that the ionization energy of most atoms and molecules is in the range of 10–15 eV. Most common gases such as air, N_2, O_2, CO, CO_2, or the noble gases such as Ar, He, and Xe, have a relatively high ionization potential and hence they do not ionize thermally until temperatures more than 4000 K. However, if vapor of the alkali metals, which have low ionization potential, is added to a gas in small fraction (on the order of 10^{-6} or less), sufficient thermal ionization can be obtained at temperatures of 2000–2500 K. This process, called seeding, will result in temperatures low enough to be withstood by some solid materials, and can be produced in furnaces. On the other hand, these temperatures are difficult to produce even in a solid-core nuclear reactor. As a result, considerable effort has been directed toward the understanding of nonequilibrium ionization. This state can be easily produced and is widely used in practical devices.

The ionization is often caused by the collision of a high-speed particle and a neutral particle. This process is called the ionization reaction. Various kind of ionization reactions exist. The main ionization reactions are shown as follows:

$$\text{(Ionization by electron collision)} \quad A + e \rightarrow A^+ + e + e \tag{12}$$

$$\text{(Ionization by ion collision)} \quad A + M^+ \rightarrow A^+ + M^+ + e \tag{13}$$

$$\text{(Ionization by neutral particle collision)} \quad A + M \rightarrow A^+ + M + e \tag{14}$$

$$\text{(Ionization by photon)} \quad A + h\nu \rightarrow A^+ + e \tag{15}$$

$$\text{(Ionization by excited atom collision)} \quad A + M^* \rightarrow A^+ + M + e \tag{16}$$

$$\text{(Ionization by electron attachment)} \quad A + e \rightarrow A^- \tag{17}$$
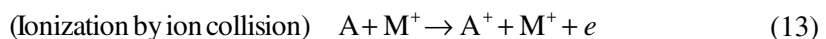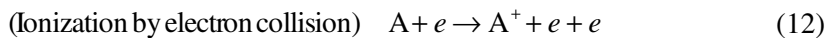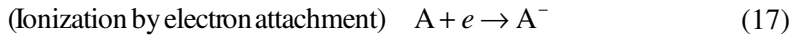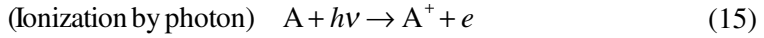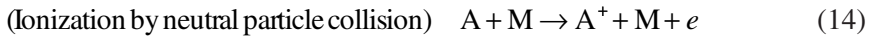
In these reactions, the ionization by electron collision in Eq. (12) mainly occurs in the plasma. The ionization process involves the collision of a high-speed electron with a neutral particle. In this type of ionization, the following rate equation is materialized assuming that the increase rate of ion number density is proportional to the product of the number densities of neutral particles and electrons.

$$\frac{dn_i}{dt} = k_i n_n n_e \tag{18}$$

where n_i, n_n, and n_e are the number densities of ions, neutrals, and electrons, respectively. k_i is the velocity coefficient in the collision ionization reaction explained later.

On the other hand, the reaction, where the ion and electron are combined together and becomes a neutral atom, is called a recombination reaction. This is the reverse reactions of the ionization reactions as shown in Eqs. (12)–(17). The reverse reaction of the ionization reaction (12) is called the three-body recombination reaction:

$$\text{(Three-body recombination)} \quad A^+ + e + e \rightarrow A + e \tag{19}$$
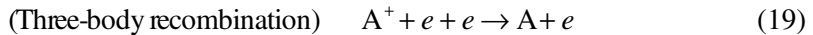
The following equation is materialized on the decrease rate of the ion number density n_i, assuming in the reaction (19) that the decrease rate of ion number density is proportional to the product of the ion number density n_i, and the second power of the electron number density n_e,

$$\frac{dn_i}{dt} = -k_r n_i n_e^2 \tag{20}$$

where k_r is named the rate coefficient in the three-body recombination. There are other various types of recombination reactions such as dissociative recombination, radiative recombination, ion-to-ion recombination, and so on.

From the Eq. (18) and Eq. (20), we obtain the rate equation on the increase in the ion number density for the field is obtained where only the collision ionization and the three-body recombination occur simultaneously.

$$\frac{dn_i}{dt} = k_i n_n n_e - k_r n_i n_e^2 \tag{21}$$

When the ionization reaction and the recombination reaction occur at the same rate, we can put the right-hand side of the Eq. (21) can be assumed to be zero so that the ion number density does not change. This state is called the ionization equilibrium. The coefficient of the ionization equilibrium K is obtained by applying the mass action law to the reaction as shown in Eq. (12),

$$K_i = \frac{n_e n_i}{n_n} = \frac{(2\pi m_e kT)^{3/2}}{h^3} \frac{2g_i}{g_0} \exp\left(-\frac{e\varepsilon_i}{kT}\right) \tag{22}$$

where h is the Planck's constant, ε_i is the ionization potential of the species, g_i is the statistical weight of the ground state of the ion, and g_0 is the statistical weight of the ground state of the neutral species. The statistical weight factor and the ionization potential of a number of materials are given in Table 1. The equation determines the n_e and n_i in the ionization equilibrium. In the nonequilibrium ionization, the temperature T may be considered to be T_e. On the other hand, we obtain the next equation is obtained by putting the right-hand side of the Eq. (21) as zero:

$$K_i = \frac{n_e n_i}{n_n} = \frac{k_i}{k_r} \tag{23}$$

Therefore, k_i can be determined from k_r and K using the Eq. (22) and Eq. (23). Although there are not so many examples of k_r measurement, the following empirical formula was proposed for a nonequilibrium ionization of noble gas by Hinnov and Hirschberg (5):

$$k_r = 1.09 \times 10^{-20} T_e^{9/2} \tag{24}$$

Although, the aforementioned treatment is the simplest one considering only collision ionization and three-body recombination, the degree of ionization in plasma can be estimated with high accuracy, where the ionization degree is defined as $n_i/n_0 \times 100\%$, (n_0 is the number density of the neutral species before ionization). In a more exact analysis, Eq. (20)–(24) and the reverse reaction of them for multicomponents gases should be considered. For example, the electrically neutral condition for two-component gas mixture is given as:

$$n_e = n_{i1} + n_{i2}$$

1.1.4.2. EQUATION OF ELECTRON TEMPERATURE

For the sake of simplicity, this discussion (1,2) is restricted only to the so-called two-temperature nonequilibrium plasma. In plasma, electrons gain and lose kinetic energy by being accelerated by the electric field and with atoms and molecules. In order to determine the kinetic energy of an electron or the electron temperature T_e, this energy balance of the electron is considered. When an electron having charge e, receives the force eE, from the electric field E, and moving with the velocity V_d, it obtains the energy of eEV_d per unit time. On the other hand, the average kinetic energy of an electron becomes $3kT_e/2$. The energy loss per unit time by the collision with a neutral particles is $3k(T_e - T_g)\kappa\nu_c/2$, where κ is the energy loss efficiency during collision named collision loss factor, and ν_c is the collision frequency or the reciprocal of a collision cycle. Therefore, the energy equation of an electron is:

$$\frac{d}{dt}\left(\frac{3}{2}kT_e\right) = eEV_d - \frac{3}{2}k(T_e - T_g)\kappa\nu_c \tag{25}$$

In an elastic collision, κ is almost equal to $2m_e/M$, where M is either the mass of a neutral molecule or that of an atom. The k-value becomes significantly higher with increase in the electron energy because many types of excitation and nonelastic collisions occur in the plasma. Many experimental and theoretical formulas have been proposed to determine the κ- and ν-value for various gases. In many cases, the magnitude

of the left-hand side of the Eq. (14) is negligibly small and considered as a steady state. Therefore, to determine T_e, the equation,

$$\frac{3}{2}k(T_e - T_g)\kappa \nu_c = eEV_d \tag{26}$$

is often used, where T_g is the heavy particle or gas temperature. The unit of T_e is either eV or K. Traditionally, the equation $kT_e = eV$ is used to convert the unit of K from that of eV. Therefore, 1 $eV (= 1.60218 \times 10^{-19}$ J) is equivalent to 11,600 K.

In order to determine plasma parameters in the plasma fluid, the conversion of a Lagrangian coordinate to an Eulerian one is required for the Eq. (21) and Eq. (25) using

$$\frac{d}{dt} = \frac{\partial}{\partial t} + v \cdot \nabla v \tag{27}$$

The other fluid dynamic equation such as the continuity, momentum, and energy equations should be solved simultaneously. The details of this procedure are beyond the scope of this book and are thus referred to in the other literatures (1,6).

1.1.5. Classification of Plasma

Plasma exists around us in nature in a variety of forms such as thunder, sun, aurora, ionosphere, stars, as well as in human environments such as arc welding, electrical discharge machining, pale light in the pantograph of train, flame, fluorescent light, and neon bulbs. There are several ways to classify these plasmas. One is based on the ionization degree. The ionization degree is defined as the number density of ions divided by the number of neutral particles. All neutral particles are ionized in the plasma when the ionization degree is one. On the other hand, no neutral particles are ionized when the ionization degree is zero. The plasma is classified according to the difference in ionization degrees:

- *Fully ionized plasma:* The ionization degree is >90%. Neutral particles have little effect on the plasma.
- *Weakly ionized plasma:* The ionization degree is <1%. Effects of electrons are dominant.
- *Partially ionized plasma:* It has the middle character of fully ionized plasma and weakly ionized plasma.

Although partially ionized plasma and weakly ionized plasma are realized in many cases, fully ionized plasma is artificially established in a few cases: nuclear fusion and nonequilibrium MHD generation plasma. In nature, it is known that the full ionization plasma of hydrogen occupies the most part of space.

In artificially generated plasma, there are other methods to classify the plasma based on the generation methods. Among many plasma generation methods, the following classifications can be considered roughly.

a. Electrical discharge plasma.
b. Microwave-induced plasma.
c. Shock wave-induced plasma.
d. Magneto hydrodynamic (MHD)-induced plasma.
e. High energy particle beam (electron and ion)-induced plasma.
f. Combustion-induced plasma.
g. Laser-induced plasma.

The details of some of these plasmas are explained later in the Section 1.2.

Plasma is also classified as being in an equilibrium state or not. The equilibrium is defined as the state in which the temperatures of electron, ion, and natural particles are equal and the ionization equilibrium is established. In nonequilibrium plasma, the electron temperature is usually more than the neutral particle temperature.

- *Equilibrium plasma.* For example, The atmospheric pressure arc discharge thermal plasma.
- *Nonequilibrium plasma.* For example, The low-pressure glow discharge plasma, the atmospheric pressure high voltage pulse plasma.

Plasma is also classified depending on whether the gas temperature of the plasma T_g is as high as the combustion temperature ($T_c > 500°C$) or not.

- *Thermal plasma.* $T_g \geq T_c$ For example, Plasma spraying arc discharge, flame and the plasma for garbage incineration.
- *Nonthermal plasma.* $T_g << T_c$ For example, Discharge lamp, plasma display monitor, corona, and exhaust gas treatment plasma, and so on.

1.1.6. Characteristics of Plasma and Its Applications

Plasma differs from unionized ordinary gas which result from on several points:

1. Highly chemical activation.
2. Electrical conductivity.
3. High energy and high temperature (gas or electron).
4. Electromagnetic radiation and light emission.

In characteristic 1, the plasma produces radicals easily when the reactive gas is inserted into it, and extremely reactive state can be obtained with the high energy of the plasma. The fields of plasma chemistry, plasma environmental improvement, and plasma processing such as chemical vapor deposition (CVD) make use of these characteristic. Most applications are classified into this group and used in this practical aspect.

In characteristic 2, the plasma is affected by the electric and magnetic field, and the electric current can pass there because many electric charged particles exist in the plasma such as ions and electrons. Using this feature, the plasma parameters can be controlled and the plasma can be heated to a high temperature. There is a possibility to control the heat transfer of the plasma by electromagnetic filed.

In characteristic 3, the plasma with 10–100 million°C will make a nuclear fusion reaction possible. It is expected that this type of energy source be used in 21st century. Also, materials can be heated rapidly at high temperature using 10,000°C plasma. In the region of lower temperature, it is used in the mechanical processing such as plasma welding, cutting, electrical discharge machining, plasma spraying, and so on.

In characteristic 4, many kinds of strong electromagnetic waves are emitted from the plasma because of the high temperature ionization. It can be used as a light source, a display, and an optical analysis.

1.1.7. Contents of This Chapter

This chapter, mainly focuses on the nonthermal plasma generated by a high voltage power supply and mainly reviewed research on applications of environmental protection and surface modifications. In these applications, the characteristics of highly chemical activations are utilized. In most of these types of nonequilibrium plasma, high-speed

electrons are generated by the pulsed high voltage having a high-speed rise time discharge and the chemical bonds such as covalent bond, ionic bond, hydrogen bond, and so on, are cleavaged to decompose the hazardous material in the environment. In addition, the chain reactions that never advance at the normal conditions can be advanced at low temperature. In an ordinary chemical reaction apparatus, high pressure of 50 atm hydrogen reduction environments and temperature of 300°C are required for reduction of very stable global warming gas CO_2 which is always produced by combustion. However, CO_2 can be reduced to CO by nonthermal plasma on the atmospheric pressure and temperature condition to certain degree. In order to reduce similar global warming gas CH_4, the high temperature of 600°C is required in ordinary atmospheric-pressure chemical reaction. However, the reduction to CH and CH_2 is observed in the nonthermal plasma on the atmospheric-temperature condition. The reaction, which is normally not proceeded easily, can be advanced under the nonthermal plasma environment. Furthermore, since the temperature of heavy particles is not increased, low power consumption can be achieved.

The energy of the chemical bonds per molar and that per a single bond is shown for various species in Table 2. Because the bond energy differs for various kinds of molecules, the average bond energies are shown in this table. The chemical reaction rates in the plasma can be predicted by the plasma parameters, such as T_e and n_e. Either measurement or simulation is used to predict the parameters. One of the measurement methods is explained in the Section 1.3.1.

Nonthermal plasma enhances not only the decomposition reaction, but also the oxidization and the reduction reactions with saved energy. Further, it has the ability of low temperature catalyst activation, combination of a thin film deposition to the surface, surface cleaning, and low temperature incineration of carbon soot and hydrocarbons. Examples of some applications are described in the Sections 2 and 3.

The detailed explanations of plasma science cannot be treated in this chapter. The authors recommended the books of plasma science (6–11) for further reading.

1.2. Generation of Plasma

In order to generate plasma, the electron must be removed from the neutral gas particle. The energy required for electric discharges is generally used to ionize the gas. There are many other methods to generate the plasma, which are described in the following section.

1.2.1. Steady DC Plasma

The direct current (DC) discharge (12–14) is induced by applying the DC voltage between the electrodes and realizing the ionization of the gas by breaking down the gas insulation. The DC electrical discharges are classified mainly into the corona discharge, the glow discharge, and the arc discharge ordered with the degree of current. Sparks is another type of electrical discharge, which generates the plasma with a short period.

1.2.1.1. DC CORONA DISCHARGE

The corona discharge consists of relatively low power electrical discharges that take place at or near atmospheric pressure. The corona is invariably generated by strong electric fields associated with small diameter wires, needles, or sharp edges from the

Table 2
Averaged Bond Energy Per Single Bond

Bonds	Energy per mol (kcal/mol)	Energy per single bond (eV/bond)
H–H	104.2	4.5
I–I	36	1.6
H–I	71	3.1
H–Cl	103	4.5
Cl–Cl	57.8	2.5
O–O	118.3	5.1
C–H	99.5	4.3
C–Cl	78.5	3.4
C–C	83.1	3.6
O–H	110.7	4.8
C–F	116	5
OH–H (water)	–	4.7
N–O	–	6.1
N–N	–	9.1
O–H (hydrogen bond)	–	0.25

electrodes. This is usually induced with high voltage of several or several 10 kV. The current is usually in the range of 1–100 µA/cm^2. Corona takes its name (Crown) from mariner's observation of discharges from their ship's masts during electrical storms. The corona appears as a faint filamentary discharge radiating outward from the discharged electrode. The plasma region for the corona is limited in the immediate vicinity of electrodes.

Because the corona is relatively easy to establish, it has wide application in a variety of processes. Application for corona discharge processes has existed for more than a 100 yr, dating to the first electrostatic precipitator (ESP) of Lodge ([1]). Since then, corona has been extensively used in several commercial ways and is gaining attention for use in other applications.

Two primary conditions for corona generation are:

a. The distribution of the electric field is nonuniform and its (dV/dr) strength is more than the corona initiation electric field.
b. The maximum gradient of the electric potential (dV/dr) decreases by the generation of the corona.

In a nonuniform electric field, the strength of the electric field is at its maximum in the space near the electrode, therefore the corona is induced there first. The corona near the anode is called positive corona, and the corona near the cathode is called negative corona. For a typical ESP employing the negative corona, the positive ions are produced in the vicinity of the high voltage electrode, whereas the negative ions exist most of the interelectrode space.

Corona discharge exists in several forms, depending on the polarity of the field and the electrode geometrical configurations. For positive corona in the needle-plate electrode configuration, discharges start with a burst pulse corona and proceed to the streamer
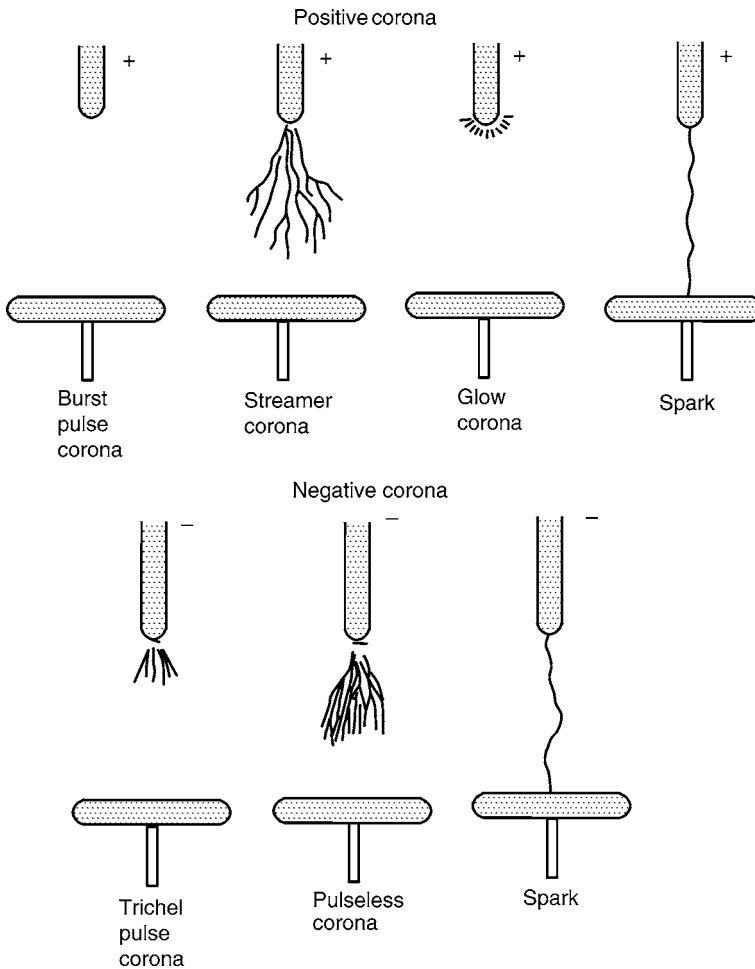
Fig. 3. Various kind of discharge in positive and negative coronas (© 1991 IEEE).

corona, glow corona, and spark discharge as the applied voltage increases (Fig. 3). For negative corona in the same geometry, the initial form will be the Trichel pulse corona, followed by pulseless corona and spark discharge as the applied voltage increases.

When AC voltage is applied to the needle-to-plate configuration, positive and negative coronas are generated from each electrode every half cycle. When both electrodes consist of the needles, both positive and negative coronas are generated from each electrode, its polarity changing every half cycle. The corona initiation voltage is similar to DC or AC corona. The positive polarity has been employed because the positive streamer corona tends to extend more in the interelectrode space than the negative streamer corona. It is also known that the ionic wind (sometimes called electric wind or secondary flow) is generated from the high electric field electrode (the needle) to the plate electrode for both DC and pulsed corona. This phenomena are applied for the electrohydrodynamic (EHD) pumping, instrumentation device, enhancing the heat transfer, and so on. The detailed discussion can be found elsewhere.
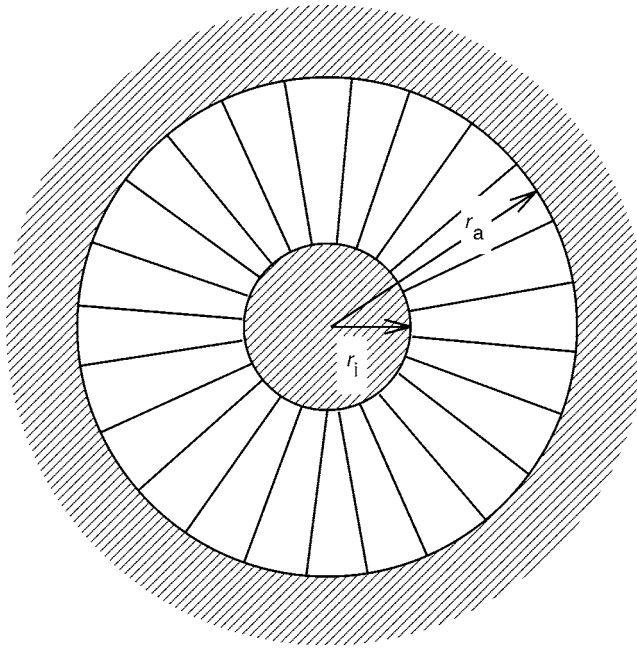
Fig. 4. Coaxial type plasma reactor with infinite length.

Let us consider a corona discharge in a coaxial-type reactor of infinite length as shown in Fig. 4. Only a radical component of the electric field exists and is a function of the radius *r* not depending on the azimuthal coordinate θ The electric filed *E* is obtained by solving an asymmetric Laplace equation in the cylindrical coordinate:

$$E = \frac{V}{r \ln(r_a/r_i)} \qquad (28)$$

where *E* is the strength of the electric field, *V* is the voltage between the electrodes and *r* is the radial distance. The strength of the electric field *E* is inversely proportional to the radial distance *r*. The strength of the electric field is at its maximum near the surface of the center electrode and equal to

$$E_{max} = \frac{V}{r_i \ln(r_a/r_i)} \qquad (29)$$

The onset of the corona discharge in this case is discussed in the following section.

1.2.1.2. Design Example: Calculation of Onset of Corona Discharge

Problem
For the wire-cylinder ESP, find the condition of r_a/r_i required for the corona initiation (14). Here, r_i, is the outer cylinder radius, r_a is the wire radius and the applied voltage is set constant.

Solution
The condition (1) of the corona initiation is satisfied because the electric field distribution is nonuniform in the radial direction as shown in Fig. 4. Therefore, the condition (2)

should be checked, where the maximum gradient of the electric potential decreases by the generation of the corona. We can assume that the apparent radius of the inner electrode slightly decreases from r_i to $r_i + r_0$ ($r_i \gg r_0$) because the corona is first induced near the surface of the inner electrode. The condition (ii) is expressed as

$$\left(\frac{dE_{max}}{dr} \right)_{r=r_i} < 0 \tag{30}$$

By differentiating the Eq. (28), the following equation is obtained

$$\frac{dE_{max}}{dr_i} = \frac{V}{r_i^2 [\ln(r_a/r_i)]} [1 - \ln(r_a/r_i)] \tag{31}$$

If this Eq. (30) is put zero, the following equation is obtained

$$\ln \frac{r_a}{r_i} = 1 \quad \therefore \frac{r_a}{r_i} = e = 2.718 \tag{32}$$

Therefore, when $r_a/r_i > 2.718$, the corona is initially induced and the spark discharge occurs with increase in the applied voltage. On the contrary, when $r_a/r_i < 2.718$, the corona is not induced and the spark discharge is initially induced. It is known from the experiment that the corona is induced for $r_a/r_i > 3$ and not induced for $r_a/r_i < 3$.

1.2.1.3. DC GLOW DISCHARGE

Two parallel plates are installed in a container in which the pressure is in the range of 10–100 Pa. When the voltage of 100–1000 V is applied between the plates, the discharge occurs and is called as a DC glow discharge. The corresponding current is in the range of mA/cm². This discharge is sustained by the discharge caused by the secondary electron impaction to the media, which is triggered by the ions or photon's impact on the cathode. This device is simple to build in generating the plasma. This plasma is called a nonequilibrium or nonthermal plasma, where electron temperature is high, and the ions and neutral particles' temperature are low.

1.2.1.4. DC ARC DISCHARGE

When the voltage of the range of 10 V is applied for the two rod-type electrodes in which initially two electrodes are in contact and detached, extremely intense discharge occurs almost in atmospheric pressure. This discharge is called the arc discharge. The arc discharge is characterized by low voltage and extremely high current as high as 10–1000 A. This discharge is sustained by thermal electrons emitted from the cathode. The device requires a large capacity, but the device is extremely simple. The device is used for the generation of thermal plasma where gas and ion temperatures are in equilibrium condition. Thermal plasma jet can be obtained when the anode for arc discharge is designed in a nozzle type shape. An extremely high-energy plasma jet is able to heat, treat, and generate the substances. There are many methods to increase the gas temperature to even higher levels. One method is to utilize the magnetic field to increase the plasma density.

1.2.2. Unsteady Plasma

1.2.2.1. AC OR PULSE CORONA DISCHARGE

There are other methods to generate the plasma by the intermittent discharge or AC discharge. Low frequency AC discharge behaves like DC discharge. Lately, such plasma is
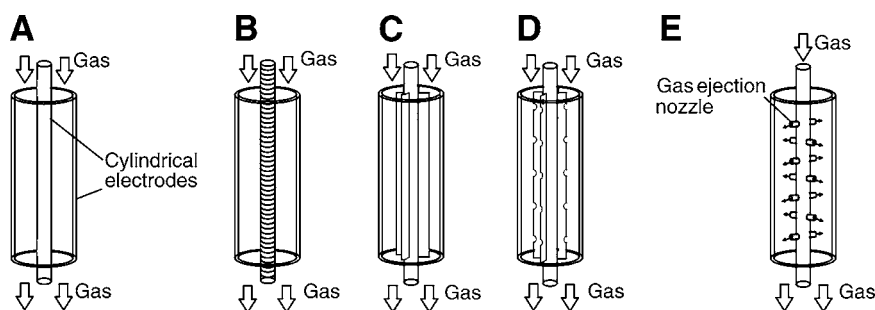
Fig. 5. Various kind of coaxial type nonthermal plasma reactors.
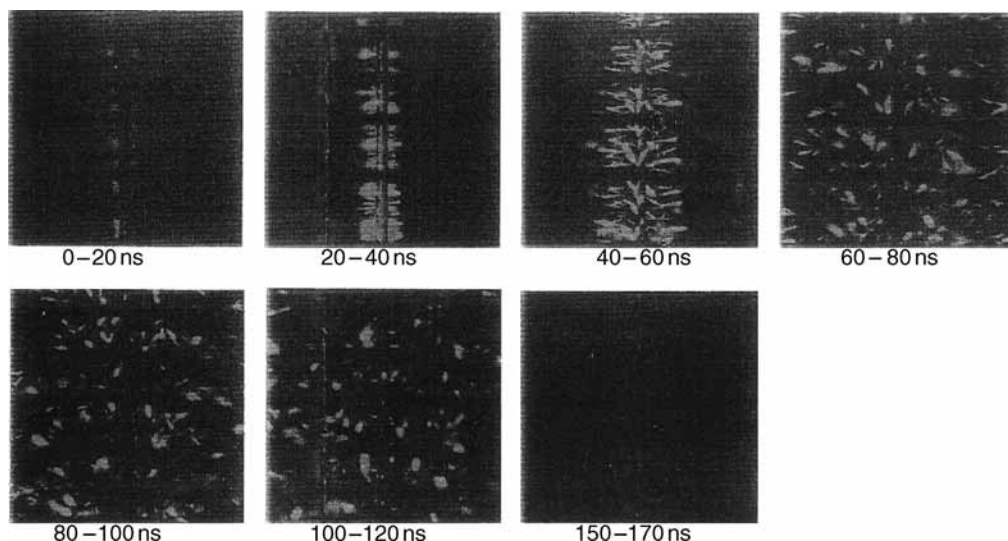
Fig. 6. Photographs of the discharge structures in a coaxial type pulse corona plasma reactor.

widely used for the application of environmental protection. Examples using this type of plasma are described in Sections 2 and 3. A variety of plasma reactors have been investigated by many researchers and typical reactors and discharges are shown in Figs. 5–19.

Figures 5A–E show several types of the coaxial-type plasma reactors. A high voltage AC or pulse voltage is applied between outer and inner electrodes in which the plasma is generated and hazardous air pollutants are decomposed. Figure 5A is the most standard coaxial-type plasma reactor. Figure 5B shows a bolt-shape reactor. The plasma is generated from the sharp edges from the bolt. Figures 5C and D shows the vane-type and scallop-type center electrodes, respectively, in which the plasma is generated from the sharp edges of these electrode. Figure 5E shows the corona-shower-type electrode in which the treated gases are injected out from the center electrode nozzle. Figure 6 shows the photos for streamer corona for the wire-type electrode (wire-to-cylinder distance is 10 cm), similar to Fig. 5(A). The time-dependent streamer propagation is initiated from the center electrode and moves away from the wire electrode. After 150 ns, streamers reach the ground electrode. The speed of streamer propagation can be estimated as 7×10^7 m/s from these photos.
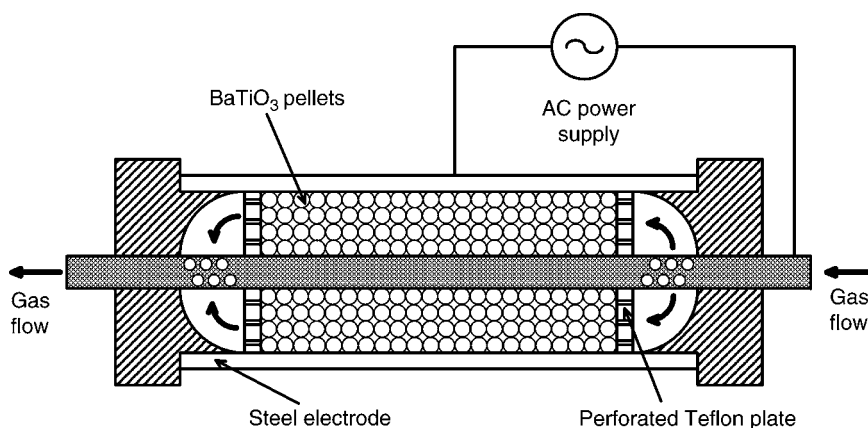
Fig. 7. Coaxial-type packed-bed nonthermal plasma reactor.
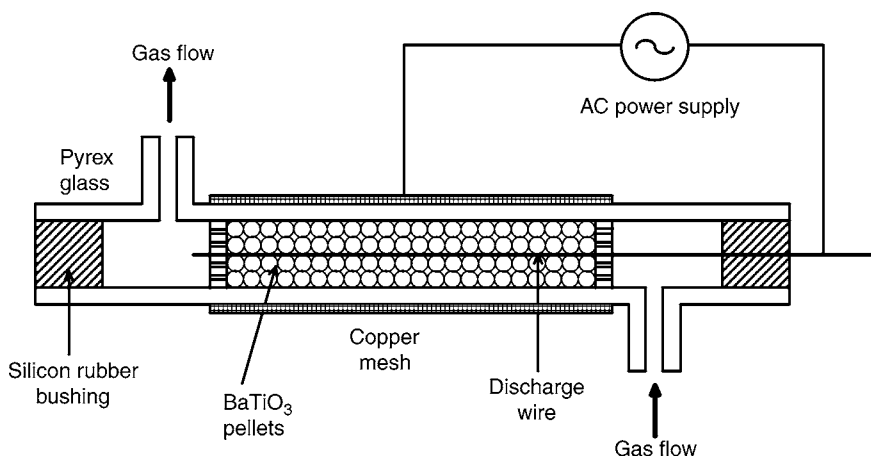
Fig. 8. Coaxial and barrier-type packed-bed nonthermal plasma reactor.

Figures 7 and 8 show a so-called the packed-bed plasma reactors used for the experiment in the Section 2. These reactors are tubular reactors packed with a ferroelectric (high dielectric ceramic) pellet layer such as $BaTiO_3$, $SrTiO_3$, $NbTiO_3$, or $PbTiO_3$. Especially, in the reactor in Fig. 8, the grounded electrode is covered with a glass barrier. This reactor is called the barrier-type packed-bed plasma reactor. A high-voltage AC power supply energizes the reactors. When an AC field is applied, an intense electric field is formed around each dielectric pellet contact point, producing high-energy free electrons as well as air molecular ions throughout the cross-section of the reactor. The spherical pellets enhance the electric fields in the contact regions between adjacent pellets and lead to micro breakdowns in the gaps. The high dielectric constant of the ceramic enhances the effect; when glass pellets, with much lower dielectric constant are substituted, sparking between the contact electrodes occurs before any significant micro-spark activity. However, the pressure drop of the bed reactors is much larger compared with other reactors discussed in this section. Catalysis or adsorbent particles are also used to enhance the plasma effects.
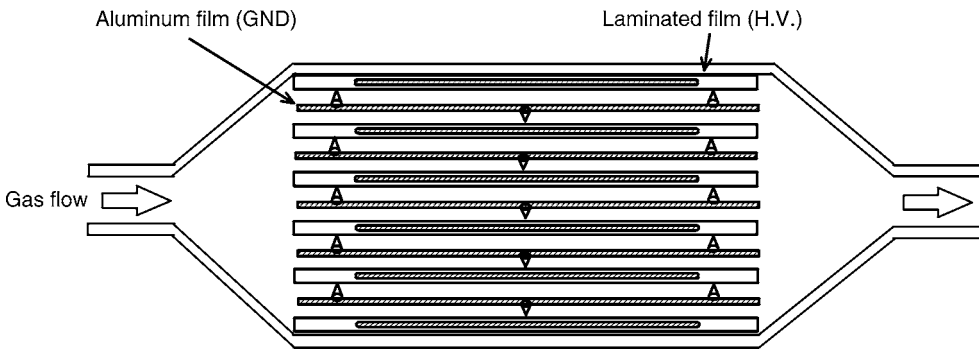
Fig. 9. Film-type plasma reactor consisted of laminated parallel steel plate electrodes.
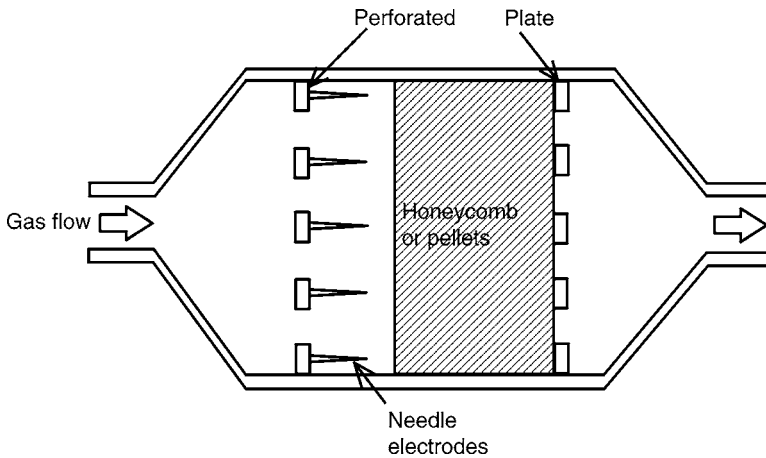
Fig. 10. Needle-to-perforated plate type nonthermal plasma reactors with honeycomb or pellets.

Figure 9 shows the multiplates type nonthermal plasma reactor used in the novel indoor electric air cleaner explained in the Section 2.4. This reactor consists of many aluminum plates with sharp projections and ones covered with polyester film as a barrier. The gap distance is several mm. Because this nonthermal plasma reactor is a kind of honeycomb channel, it has a small pressure drop and can be energized by relatively low voltage (approx several kV) with high energy efficiency.

Figure 10 shows a needle to plane type plasma reactor which is used for diesel engine flue gas emission after treatment explained in the Section 2.7.3. This reactor can process the flue emission at a large flow rate because the cross-sectional area can be made larger keeping distance between the electrodes. Further, it can be used to activate the catalysts coated inside the honeycomb or on the pellets. Figure 11 shows the plasma reactor having a similar structure but the flow direction is different.

Figure 12 shows the structures of the electrode in an electric discharge ozonizer explained in the Section 2.5. In this ozonizer, large amount of ozone with high concentration can be
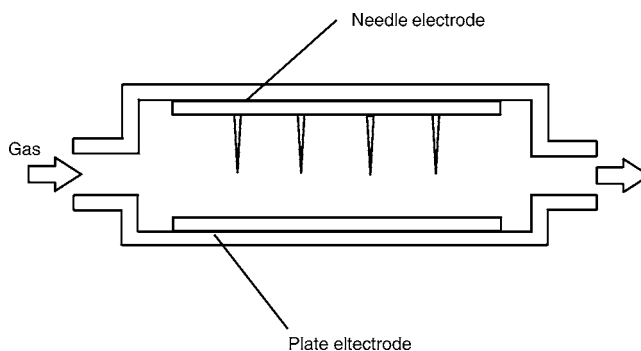
Fig. 11. Needle-to-plate type plasma reactor.
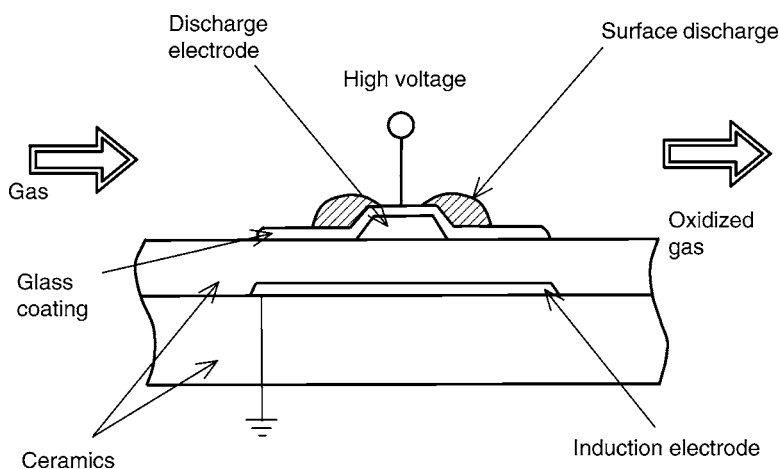
Fig. 12. Ceramics surface discharge type plasma reactor for high performance ozonizer (courtesy by Masuda research Inc.).

generated using a surface discharge. Figure 13 shows another electrical discharge ozonizer or NO_x redaction system using a silent discharge (15). Very high performance can be achieved using a very short gap of around 50 μm.

Figure 14 shows a nonthermal plasma reactor with a wire-to-coil electrode that is used for the combustion exhaust gas treatment. Large-scale equipment was tested for cleaning exhaust gas from a garbage incinerator (16). Figure 15 shows a photograph of the discharge.

1.2.2.2. RF PLASMA

When the discharge frequency increases in the range of MHz, both ions and electrons change the direction of the motion before reaching the other electrode, trapping them in the interelectrode space. These trapped ions and electrons will form plasma to excite the gas molecules. This is called a high frequency or radio frequency (RF) discharge (17). The electrodes generated by the RF plasma do not contact with the contaminated gases so that only clean plasma can be obtained. The RF plasma can be generated by either inductively coupled plasma or capacitive coupled plasma.
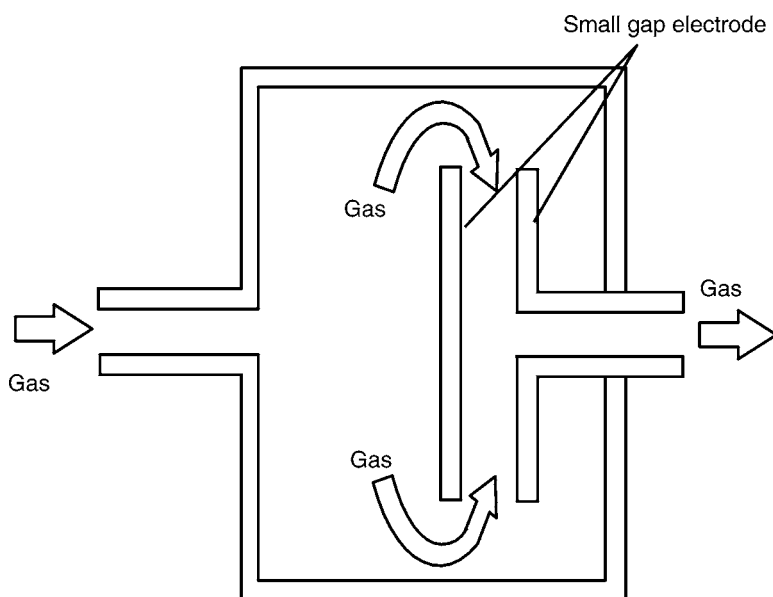
Fig. 13. Nonthermal plasma reactors with small gap electrodes.
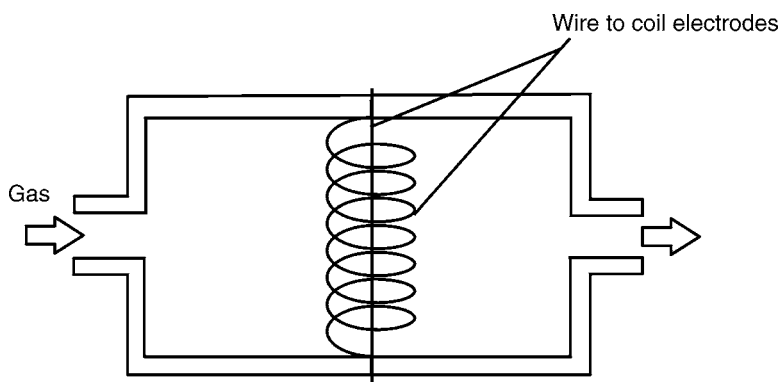
Fig. 14. Nonthermal plasma reactors with wire-to-coil electrodes.

The inductively coupled plasma shown in Fig. 16A uses the coil outside of the dielectric barrier reactor tube in which high frequency current is applied to induce the magnetic flux. The plasma can be generated in the azimuthal direction within the tube reactor. The most widely used frequency is 13.56 MHz but 4 MHz or 2 MHz RF power supply is occasionally employed. The inductively coupled plasma is widely used because the reactor is simple to build. The nonthermal plasma generated at low pressure has a wide range of applications such as CVD, polymerization, etching, surface modification, and environmental protection. When the plasma is generated at atmospheric pressure, thermal plasma can be obtained. Applications are for ultrafine particles generation and plasma torch for plasma spraying.
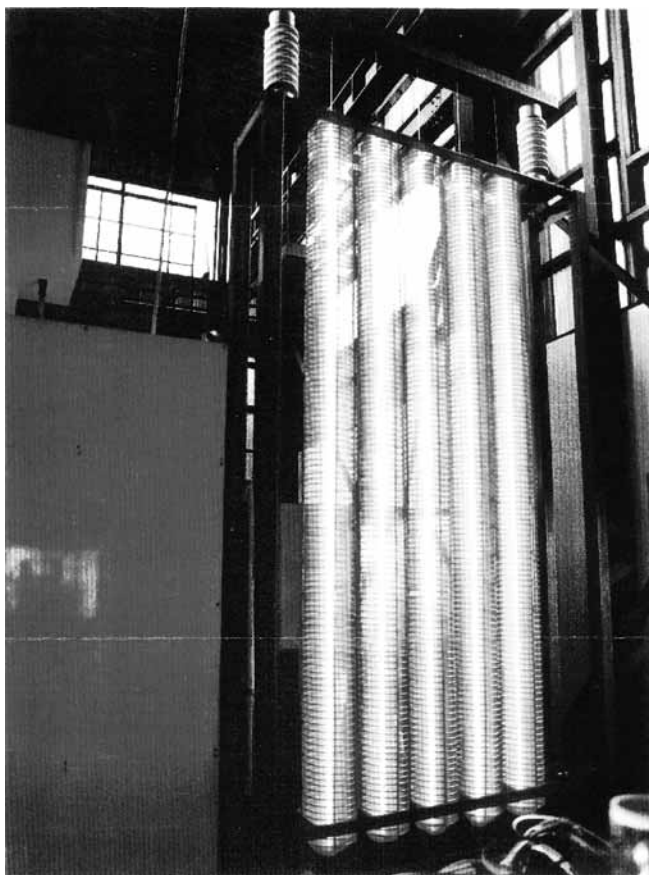
Fig. 15. Photographs of the discharge of nonthermal plasma reactors with wire-to-coil electrodes.

On the other hand, the plasma generated by the capacitively coupled plasma uses high frequency and high voltage. The electrode can be placed on either outside or inside of the reactor. Figure 16B shows the electrode placed outside of the reactor. When the electrode is placed inside of the reactor, the electrode can be wrapped by the dielectric material. The frequency used is a commercially available 13.56 MHz. The capacitively coupled plasma has less power consumption compared with the inductively coupled plasma.

1.2.2.3. Microwave-Induced Plasma

Microwave generated by a magnetron oscillator is introduced to the chamber using a microwave waveguide. The chamber is usually made from insulating material such as quartz or alumina tube. The plasma is induced inside the chamber by radiation of the microwave. Typical frequency of the microwave is 2.45 GHz.

When a transverse magnetic field is applied to the electric field, the electrons rotate around the magnetic field lines. When the frequency of the rotation (cyclotron frequency) is adjusted to that of the applied electric field, the rotation of the electron is accelerated because of resonance. This phenomenon is called "electron cyclotron resonance (ECR)." The initiation voltage of the discharge decreases at this state. The resonance frequency is generally 10^9–10^{12} Hz (Fig. 17).
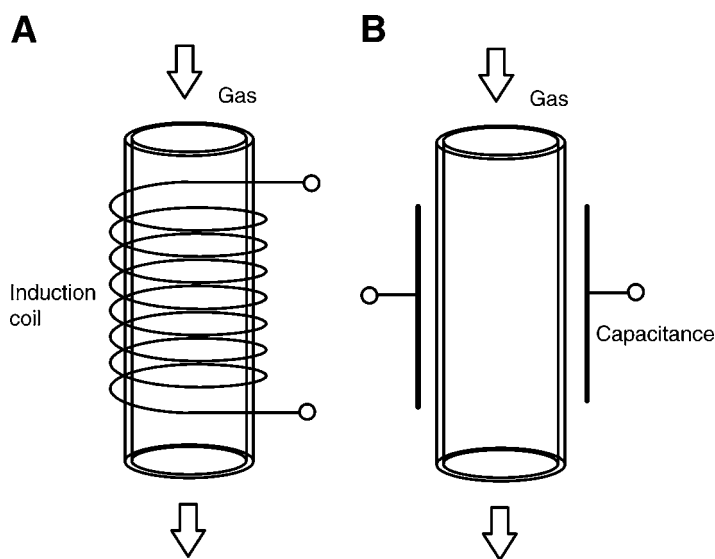
Fig. 16. Radio frequency plasma reactors. **(A)** Inductively coupled plasma (ICP) reactor. **(B)** Capacitively coupled plasma (CCP) reactor.

1.2.2.4. Shock Wave-Induced Plasma

When gas is rapidly compressed and its temperature is raised using a shock tube, the thermal ionization occurs in the gas by the shock waves. The structure of the shock tube is very simple. A thin plate separates the gas inside the tubes which are 4–5 m in length. The area on one side is filled with a high-pressure gas. Inhomogeneous pressure waves are generated by breaking the thin plate instantaneously. These pressure waves are called "Shock waves" which compress the gas (usually noble gas) rapidly filled in the other areas thus generating the plasma. Because the generation and disappearance of the shock waves are performed for a very short period (approx ms), the induced plasma is usually in the nonequilibrium state. This plasma is often used to determine the fundamental characteristics of the nonequilibrium plasma. For example, it has been used to investigate the performance of MHD (magnetohydrodynamic) power generator (18). Figure 18 shows the test apparatus for investigating the performance of a MHD power generator (19).

1.2.2.5. High Energy Particle Beam Induced Plasma

High intensity laser, ion beams, electron beams, and heavy ion beams can be exposed to the gases to generate the plasma. The electron beam technology has been especially used for the decomposition of Freon and the treatment of combustion flue gas. Figure 19 shows an experimental setup for an exhaust gas treatment system (20). Ammonia is injected upstream of the electron beam generator and NO_x and SO_x are converted to NH_4NO_3 and $(NH_4)_2SO_4$ aerosols which are collected in the ESP or bag filter.

1.2.2.6. Combustion Induced Plasma

The high-temperature combustion emission gas is emitted from the incinerator in which fossil fuels such as oil is burned at temperatures of 2000–3000 K. When some vapor of alkali metal such as potassium (K) or cesium (Cs) that have low ionization
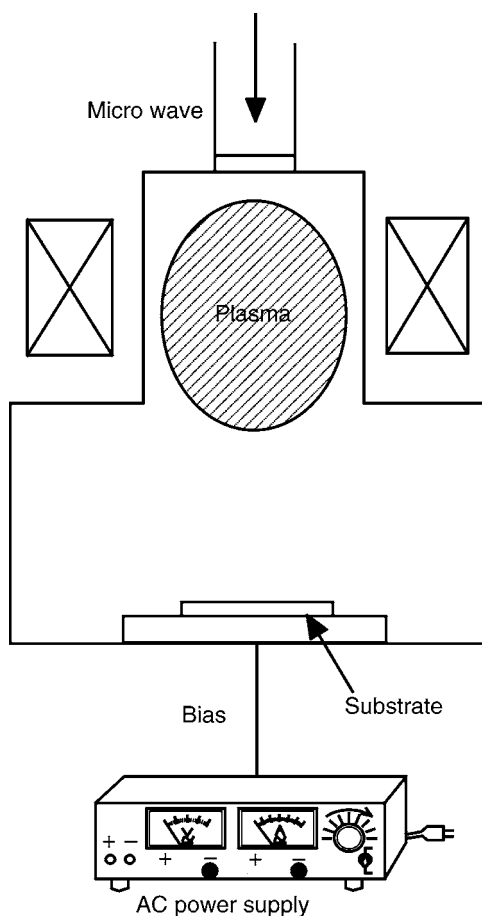
Fig. 17. Microwave induced plasma reactor for substrate surface modification.

potential is injected into the gas, weakly ionized plasma of 1–2% ionization degree can be obtained. This procedure is called "seeding" and the additives are called "seed material." In the 1980s, the combustion gas plasma was investigated by many researchers in many countries for the application of open cycle MHD electrical power generation system (2). Recently, studies have ceased because it is very difficult to understand the characteristics and behavior of MHD plasma.

1.2.3. Power Supply System for the Generation of Discharge Plasma

Although there is a case such as the DC arc discharge which is generated by relatively low voltage, the high voltage is usually used to generate the discharge plasma. Although it is impossible to review all methods in this chapter, some examples of plasma induced by high voltage discharge (especially corona discharge) used for environmental improvements are reviewed.

1.2.3.1. AC AND DC HIGH VOLTAGE SUPPLY

In order to generate high-voltage discharge plasma, the voltage of commercial electric power (100–240 V) must be raised using coil-winding type transformer as shown
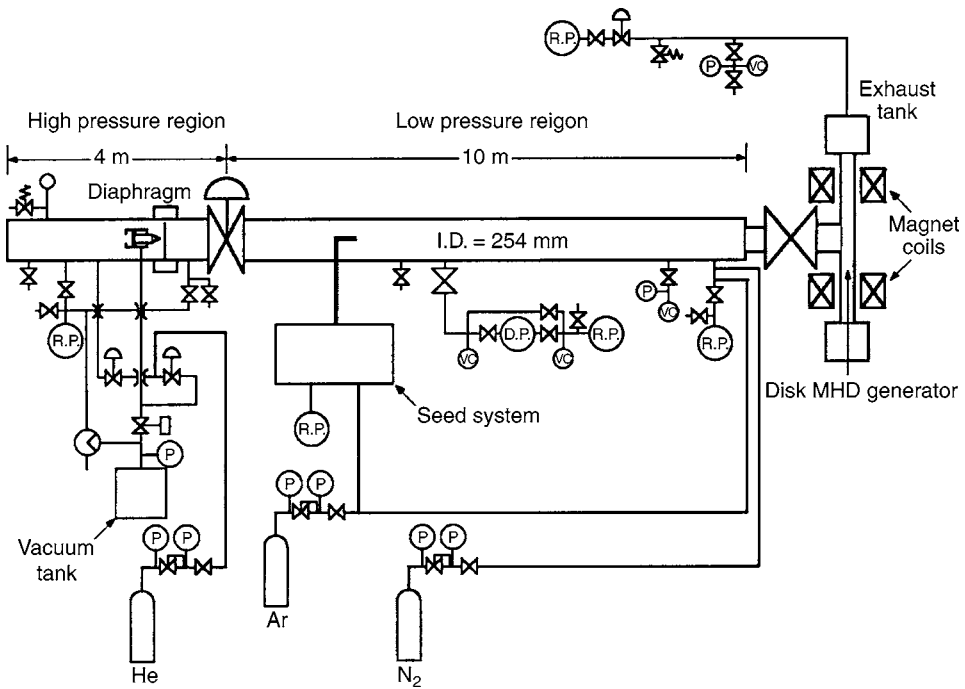
Fig. 18. Shock tube for generating nonequilibrium plasma in disk MHD generator.
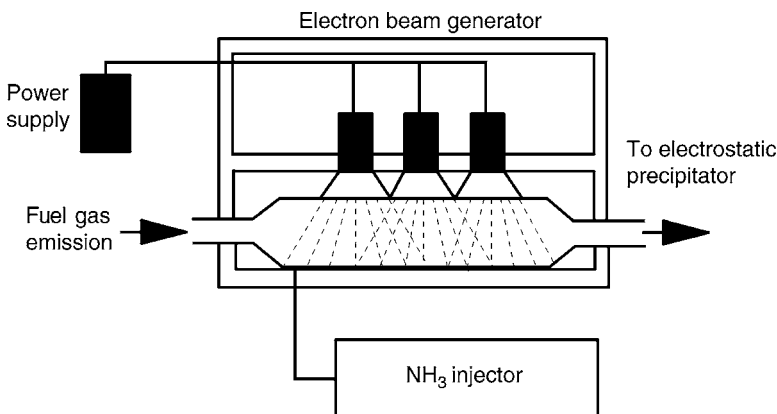
Fig. 19. Reactors with electron beam generator for combustion flue emission treatment.

with T in Fig. 20 (21). The increased ratio of the voltage is proportional to the ratio of the numbers of primary winding and secondary winding. For example, in most ESPs, the DC corona is induced using the combination of the transformer and rectifier circuit. Figures 20(A)–(C) show the fundamental electrical circuit of a rectifier. Either half-wave or full-wave rectification is carried out using either the diode D or the diode bridge D1–D4. The smoothing capacitor removes the ripples in the voltage waveforms. As a load Z_r, the ESP or the electrical discharge tube is connected.
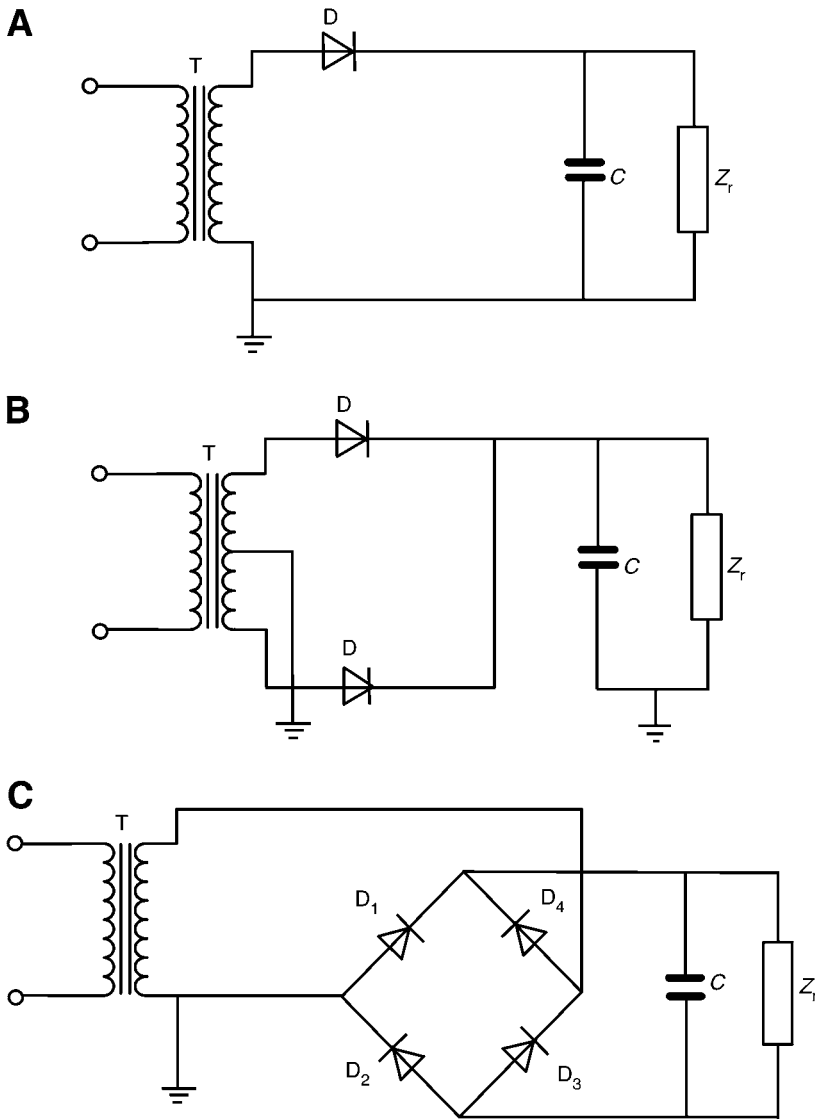
Fig. 20. Examples of rectification electrical circuits. **(A)** Half-wave rectification circuit. **(B)** Double voltage rectification circuit. **(C)** Full wave rectification circuit.

1.2.3.2. PULSE POWER SUPPLY WITH SEMICONDUCTOR SWITCHING ELEMENTS

It is possible to make the high-voltage pulse with short width and high frequency by turning the current on and off of the primary winding of the transformer using semiconductor switching elements. It is believed that rapid switching of high voltage is important because the strong nonequilibrium plasma can be generated with small power consumption by fast switching with small rise time. If we were to raise the voltage using a pulse transformer with a large ratio of windings (secondary/primary), a sharp increase in the voltage cannot be obtained. Recent development in semiconductor switching elements makes the switching voltage higher. Figures 21 and 22 show the examples of
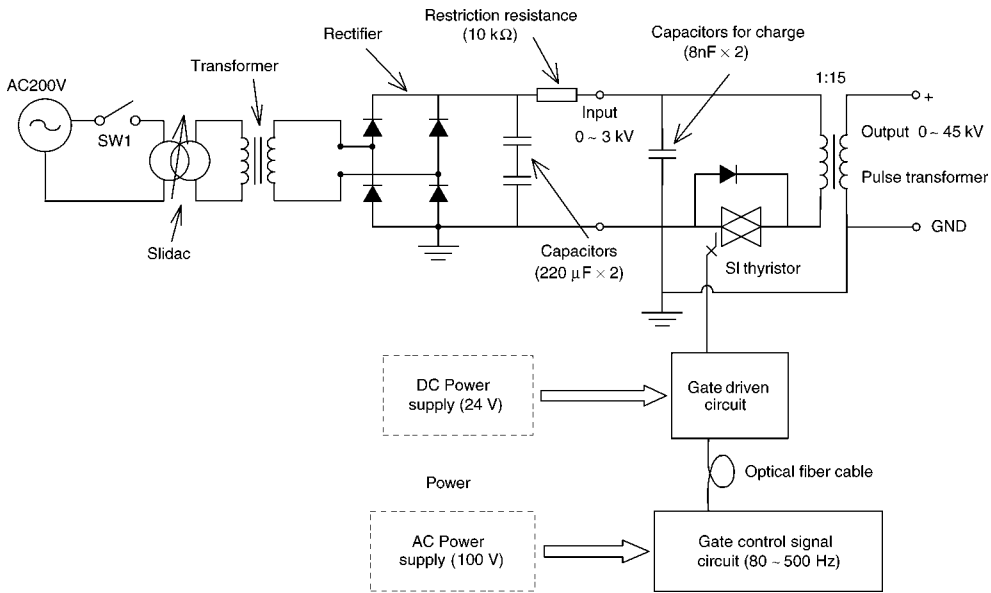
Fig. 21. Electric circuit for high voltage pulse power supply using SI thyristor switching.
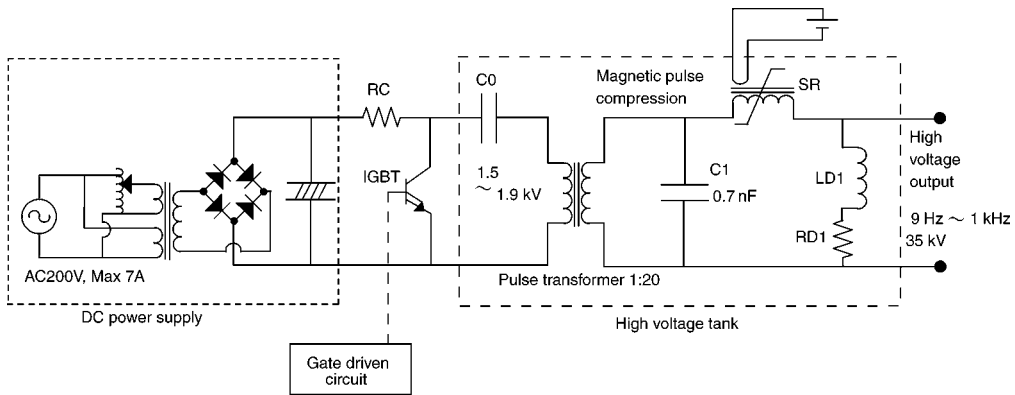
Fig. 22. Electric circuit for high voltage pulse power supply using IGBT switching.

such types of electric circuits for the pulse high voltage power supply used in the experiments in the Section 2.7.3. Figure 21 shows a circuit using Static Induction (SI) thyristor switching. In this circuit, after the 3 kV DC voltage is switched to induce the sharp rising pulse, it is boosted by a pulse transformer (1:15) up to around 45 kV. Figure 22 shows the circuit using IGBT elements switching. In this circuit, the DC voltage of 1.5–1.9 kV is switched to induce the sharp rising pulse, and is raised by a pulse transformer (1:20) up to 35 kV. Figure 23 shows an example of a voltage and current waveform induced by the SI thyristor electric circuit as shown in Fig. 21. The rise time of the pulse is around 100 ns. In order to obtain the pulse with a smaller rise time, the price of the power supply becomes higher. The price of the power supply as shown in Fig. 22 is roughly 300,000 USD in the year 2003.
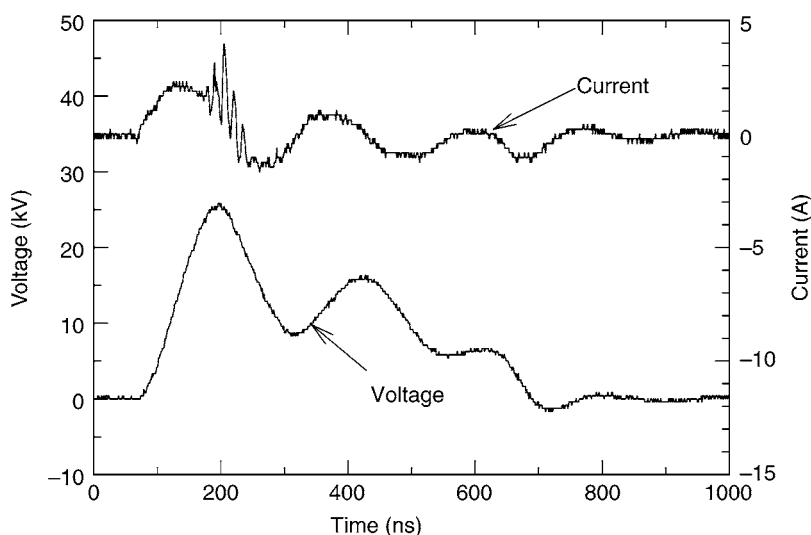
Fig. 23. Voltage and current waveforms induced by the pulse power supply using SI thyristor switching (f = 420 Hz).

1.2.3.3. FUEL IGNITION SYSTEM FOR AUTOMOBILE ENGINE

Figure 24A shows an electrical circuit for a fuel ignition system (spark plug) of an automobile gasoline engine. This circuit is considered as a kind of pulse high voltage power supply for the spark and glow discharges. In this diagram, the contact point is made to open and close mechanically in the primary windings of the transformer using a rotating comb mechanism. When the contact point is open, around 20 kV of high voltage is induced instantly in the second winding because of the reverse electromotive force. A glow discharge followed by a spark discharge is generated by this high voltage pulse. The effects of this discharge on the stability of the fuel ignition system have been investigated in details for various kinds of spark plugs by many researchers (22).

In a mechanical contacting on/off system, the secondary voltage decreases with increase in the rotation speed because the contact period becomes shorter. Therefore, in recent automobile ignition system, the on/off of the primary current is performed electronically using a semiconductor switching element such as transistors or thyristors as shown in Fig. 24(B). As a result, high secondary voltage can be assured in the wide range of rotation speeds (22).

1.2.3.4. PULSE POWER SUPPLY WITH A ROTARY SPARK-GAP SYSTEM

As explained in the Section 2.2., combustion flue emission gas from factories including NO_x and SO_x can be cleaned effectively by use of a pulse corona discharge that is generated by switching the DC high voltage with the frequency of several ten to several hundred Hz.

Pulsed DC with pulse durations less than 1 ms has the advantage of generating electrons with limited movement of ions. As a result, much higher electric fields can be applied during the duration of the pulse without causing spark breakdown in the reactor. The nanosecond pulsar generally employs a DC power supply that is used to charge a
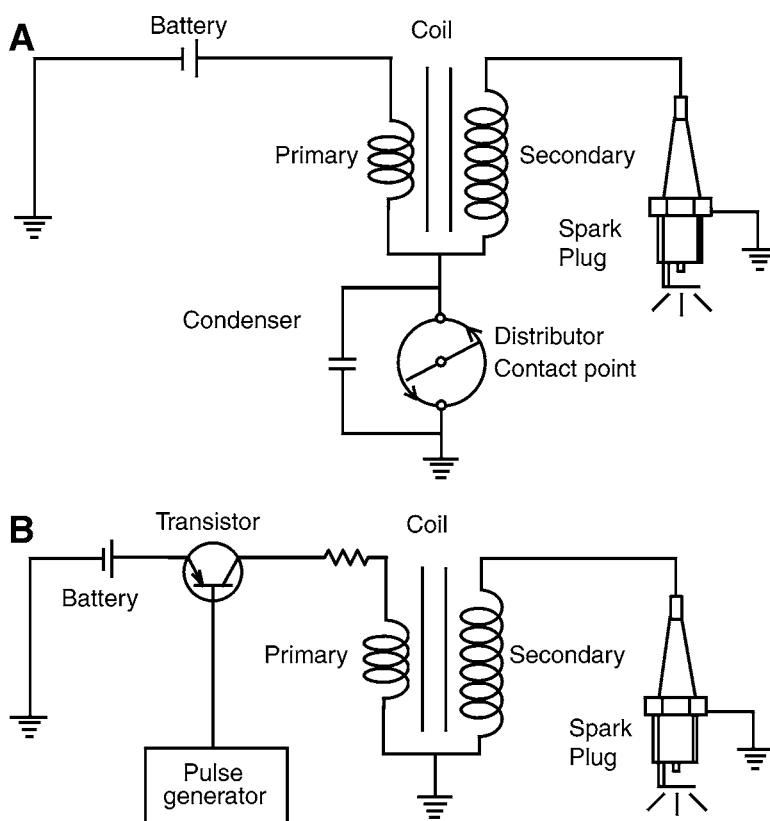
Fig. 24. Electrical circuit for energizing a spark plug in an automobile engine. **(A)** Type of mechanical contact points. **(B)** Type of semiconductor switching.

low inductance capacitor. The discharge of this capacitor through a spark gap gives the short rise time required. The pulse length can be determined by the load resistance that is coupled to the reactor, such as the one shown schematically in Fig. 25 as used in the experiment in the Section 2.8. The spark gap discharge is currently required to produce the short rise time. Conventional thyristor switching cannot produce such a short-rise pulse. The fast rise time of the pulse also allows the electric field at the corona onset to become much higher than in the DC corona, because statistical time lags govern the initial formation of the corona. The electron energies in the pulse corona are correspondingly higher than that for DC current.

There are several additional advantages of nanosecond pulsing over DC energization. The brief application of voltage allows the production of electrons without raising the ion temperature (which forms various radicals) at atmospheric pressure. This means that less energy goes into heating the gas for a given electron concentration. The electron concentration can be orders of magnitude more than under DC conditions because of the higher electric field at corona onset. Because of the higher concentration, space charge effects disperse the electrons more uniformly throughout the reactor volume. The reactors can be designed with larger volumes because of the greater range of the energetic
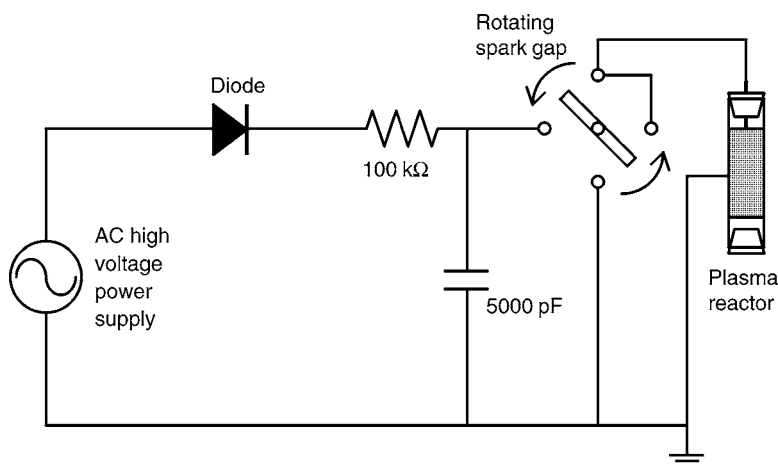
Fig. 25. Electric circuit for high voltage pulse power supply using rotating spark gap high voltage switching.

electrons and filling efficiency. This allows the mechanical tolerances to be relaxed, for most geometries. Finally, the high over voltage of the pulse for corona onset means that many reactors can be driven in parallel with the differences in their individual onset thresholds not affecting the operation.

In Fig. 25, the rotating switch is rotated driven by an electric motor and a matching condenser is chosen to adjust the electrical impedance of the reactor and the circuit. Because the mechanical switching of the secondary or high voltage line is possible, a very sharp pulse with a small rise time (approx several ns) can be generated as shown in Fig. 26. Further, the cost of this apparatus is not very expensive. However, there are several problems to this method:

a. The lifetime of the contact point is short.
b. The width of the pulse is relatively large.
c. It is difficult to generate the pulse with large amplitude and frequency.
d. The large space is required.
e. Electromagnetic interference must be considered.

1.2.3.5. HIGH FREQUENCY AC POWER SUPPLY

High frequency (several kHz to several ten MHz) power supply has often been used for the manufacturing process of semiconductor chips. Recently, it is also used for post processing or decomposition of flue gases from the semiconductor manufacturing equipment. The material gases such as CF_4, NF_3, and SF_6, and so on, generally have larger global warming coefficients compared with CO_2. The frequency of 13.56 MHz is often used for the industrial power supply. Either an inductor coil or capacitance is used as a load for the power supply. The current in the inductor load (ICP reactor) decreases with increase in the frequency because the impedance of the inductance increases. Generally, several times the winding coil or large capacitance is used as the load. For example, the electrical circuits with variable condensers as shown in
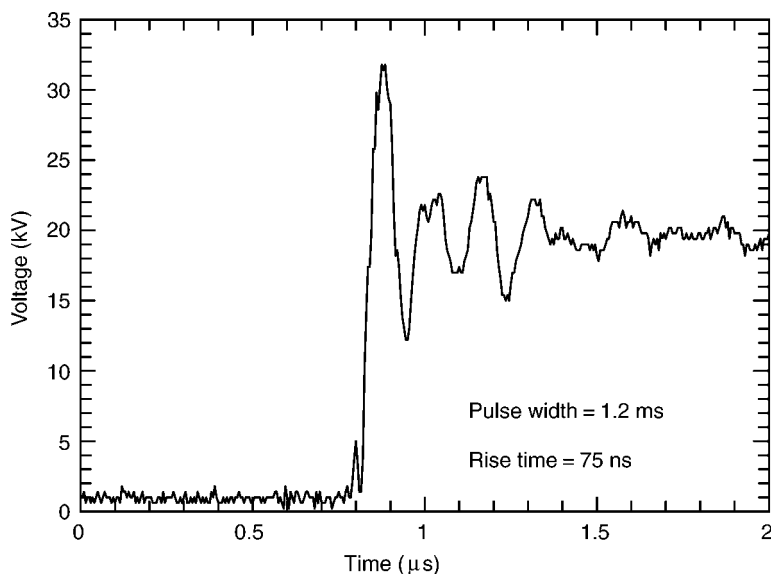
Fig. 26. Voltage waveforms induced by the pulse power supply using rotating spark gap switching ($f = 210$ Hz).
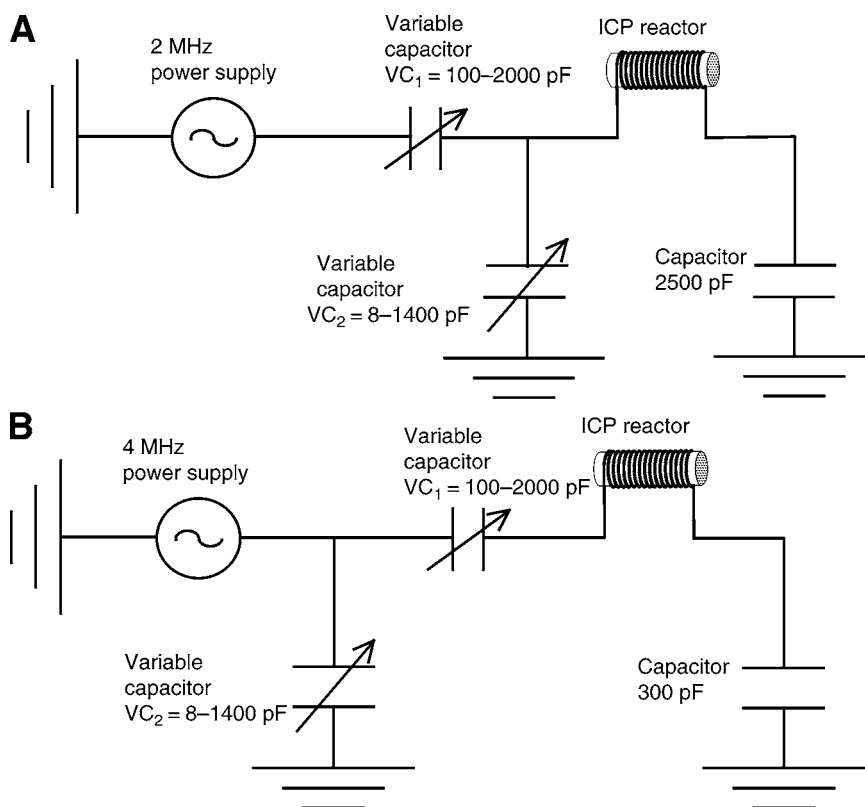
Fig. 27. Electrical circuits for impedance matching RF plasma discharge reactors (coil diameter = 75 mm, coil length = 150 mm, the number of coil windings = 15). **(A)** For frequency = 2 MHz. **(B)** For frequency = 4 MHz.

Figs. 27A,B are used for impedance matching. The induction of plasma changes the matching or resonance point of *L* and *C* because the impedance of the plasma reactor changes. The electrical circuits are used in the experiments in the Section 2.9. More precise plasma analysis is required to determine the resonance point when the plasma is generated.

1.3. Analysis and Diagnosis of Nonthermal Plasma

1.3.1. Plasma Diagnosis Using Langmuir Probe

1.3.1.1. PROBE METHOD AND ELECTROMAGNETIC WAVE METHOD

Quantitative physical properties for electron temperature (electron energy) and electron density may be measured using one of two methods (4). The probe method inserts a probe in the interelectrode space in the plasma region and to measure the current so that plasma parameters can be diagnosed. The second method is to use the microwave or laser, i.e., the electromagnetic method, which is radiated into the plasma region. Plasma parameters can be obtained by the refractive light or its interaction resulting from the light emission in plasma.

Because the probe is inserted into the plasma, it is possible to determine the particle energy density by capturing the charged particles, although it is limited for low plasma temperature and density. This probe method has been widely accepted because of its superiority in determining the space-dependent plasma characteristics and it is easy to use. However, the disadvantage exists in terms of the response time and interference of the probe itself. On the other hand, the electromagnetic method is suited for relatively high temperature and high plasma density. In addition, the response time and interference problem are held to a minimum and the measurement of ion temperature instead of the plasma energy distribution can be measured. However, the resolution of the interelectrode space is rather difficult and the equipment cost can become significant.

The diagnosis method should be selected depending on the type of plasma. Because the nonthermal plasma described in this section is low-temperature and low-density plasma (number density of electron n_e of less than 10^{16} cm^{-3} and electron temperature T_e of less than few 10 eV), the probe method should be considered as the primary method amongst many experimentalists. For these reasons, the discussion focuses on the probe method, especially for the single probe method. The electromagnetic method and the other two or three probe methods for unsteady plasma are described elsewhere (4).

1.3.1.2. PRINCIPLE OF SINGLE PROBE METHOD

Figure 28 shows the fundamental electrical circuit setup for the single probe method. A low-pressure glow discharge is considered as an example. In general, the probe made out of a small piece of metal consists of a flat plate, and a circular tube or sphere so that the surface area can be calculated easily for the purpose of analysis. The probe is usually covered by a quartz glass and only the tip is exposed to the plasma. The bipolar power supply is connected to the probe and the potential V_{pr} is applied to the probe. Referring to the example shown in Fig. 28, the voltage V_{pr} is applied to the probe and varied in a wide range. The probe current I_{pr} is recorded accordingly and their results are shown in Fig. 29. When the current I_{pr} is in the direction shown in Fig. 28, it is assumed to be positive. This is called the voltage-current characteristics of the single probe method (4).
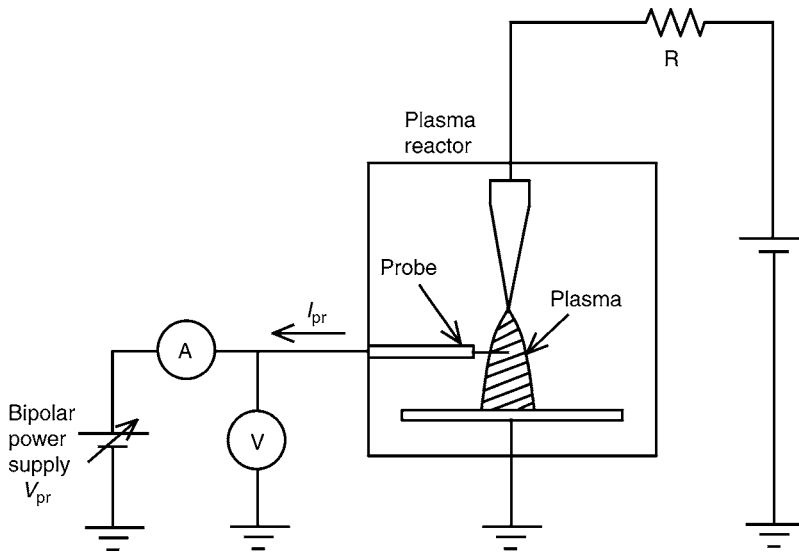
Fig. 28. Fundamental electrical circuit and plasma and probe for the single Langmuir probe method.
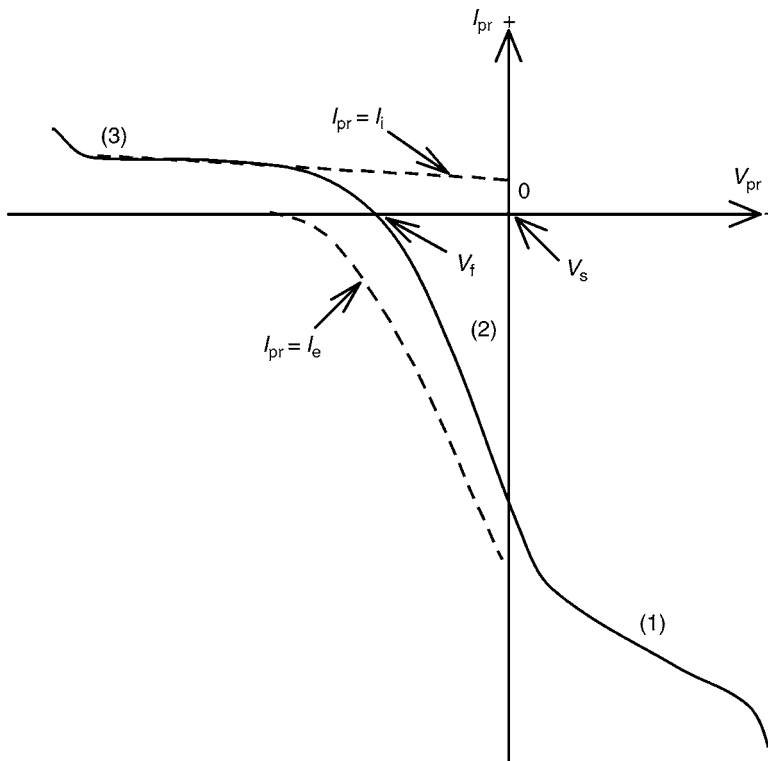
Fig. 29. V_{pr}-I_{pr} characteristics curve in the single probe method.

When the potential of the probe is equal to the space potential V_s, the thermal diffusive current because of the thermal motion is flowing into the probe. As for electrons, the following equation can be expressed as:

$$I_{e0} = -\frac{1}{4}n_e e\bar{v}_e S = \frac{1}{4}n_e e\left(\frac{8kT_e}{\pi m_e}\right)^{1/2} S \tag{33}$$

As for positive ions,

$$I_{i0} = +\frac{1}{4}n_i e\bar{v}_i S = \frac{1}{4}n_i e\left(\frac{8kT_i}{\pi m_i}\right)^{1/2} S \tag{34}$$

where S is the probe surface area, k is the Boltzmann's constant, e is the elemental charge, m_e and m_i are the mass of electrons and ions, and $\bar{v}_e$ and $\bar{v}_i$ are the average thermal velocities of electrons and ions, respectively. Although, both I_{e0} and I_{i0} flow into the probe, the probe reads as a negative current $I_{pr} = I_{e0} + I_{i0}$ because $|I_{e0}| \gg |I_{i0}|$ and $I_{e0} < 0$, $I_{i0} > 0$. The voltage and current characteristics for the single probe method is divided into three regions which are divided by the space potential V_s and the floating potential to show the zero current V_f.

Region 1 in Fig. 29: When the probe potential exceeds V_s, ions are expelled from the probe, although electrons are attracted to the probe, resulting in the formation of an electron sheath. As the probe potential increases further, the current increases because of electrons ($|I_e| > |I_i|$: saturated electron current).

Region 2 in Fig. 29: When the probe voltage is less than the V_s, electrons are repelled from the probe and positive ions are attracted to the probe to form an ion sheath. I_{pr} becomes zero at the floating potential V_f. At this point, the magnitude of the current are equal because of ions and electrons ($|I_e| = |I_i|$).

Region 3 in Fig. 29: When the probe potential is further reduced to a negative value with respect to V_f, the current because of electrons are further reduced, whereas the current owing to ions increase. As a result, significant amount of positive ions are attracted to the probe as V_{pr} further decreases ($|I_e| < |I_i|$, saturated ion current).

Under collisionless plasma, the disturbance resulting from thermal motion by the probe can be neglected by assuming that the electron mean free path is more than the probe dimension or the ion sheath, and the electron energy distribution follows the Maxwell distribution. The current owing to electrons in the range of $V_s < 0$ can be expressed as:

$$I_e(\Delta V) = I_{e0}\exp\left(-\frac{e\Delta V}{kT_e}\right) \tag{35}$$

where ΔV is the probe potential based on V_s and can be expressed as $\Delta V = V_s - V_{pr}$.

1.3.1.3. Cautions for Conducting Experiments

In order to obtain the voltage and current relationship as illustrated in Fig. 29, the following must be considered:

a. In general, the voltage should be varied from a negative to positive direction with a constant sweep. For many cases, the current should be measured by setting the voltage constant.
b. It is important to record the precise current measurement in the vicinity of zero current.

c. Once the saturated current is reached, the voltage should not be increased beyond this level to protect the probe.
d. It is convenient to use a bipolar power supply. However, if one is not available, the polarity of the power supply can be switched during these experiments.
e. The grounding will affect the voltage and current readings. It should be noted that a good grounding is essential to minimize the noise of the voltage and current.

After heeding the general cautions described earlier, the electron temperature T_e and the electron number density n_e as shown in Fig. 29 can be obtained.

1.3.1.4. DETERMINATION OF ELECTRON TEMPERATURE AND ELECTRON NUMBER DENSITY

The following equation can be derived from Eq. (34):

$$\frac{d \ln I_e(V)}{dV} = -\frac{e}{kT_e} \tag{36}$$

The electron temperature T_e can be obtained by the slope when the electron current $I_e(V)$ is plotted against voltage V in a logarithmic graph. Here, it is essential to estimate I_e based on the measured I_{pr}. As a common practice, I_{pr} can be extrapolated from the tangential line at $I_{pr} = I_i$ in the region of $V_p < 0$ as illustrated in Fig. 29. The current I_i does not depend on the probe geometry but can be obtained based on the linear relationship between I_i and V_{pr}. The electron number density n_e (cm^{-3}) can be obtained by substituting T_e and I_{e0} into the Eq. (33).

$$n_e(\text{cm}^{-3}) = 4.03 \times 10^{13} \frac{|I_{e0}|(\text{Amp})}{S(\text{cm}^2)[T_e(\text{K})]^{0.5}} = 3.73 \times 10^{11} \frac{|I_{e0}|(\text{Amp})}{S(\text{cm}^2)[T_e(\text{eV})]^{0.5}} \tag{37}$$

where the units of T_e, I_{e0}, and S is K or eV (1 eV = 11,600 K), ampere, and cm^2, respectively. The probe surface area S should be measured in advance. Care must be taken for S because S, might change during the experiments especially when the current rapidly decreases.

1.3.2. Estimation of Discharge Power

It is important to estimate the power consumption of the plasma reactor accurately for the cost estimation of the scale-up process. However, a high-resolution oscilloscope, which is rather expensive, is essential to measure a short rise-time pulse or the microdischarge. In general, the input power of the high voltage power supply as shown in Figs. 21, 22, and 25 can be measured on AC 100/200 V line using a power meter. The actual energy consumed for the reactor is approx 30% of the total input energy without adjustments but it is theoretically possible to input 100% of the input energy to the reactor with proper adjustment.

Generally, the discharge power consumption of the plasma reactor is obtained by the Lissajou's method using the circuit as shown in Fig. 30 (23). The Lissajou's figure in the V–I plane is drawn in a high-speed oscilloscope. The discharge power can be obtained from the area of the figure. The values of the condenser C_1 and the resistance $R_{1\,is}$ are calculated by trial and error. For Fig. 30, the values are shown in the ref. 23.

The authors evaluated the discharge power using the method as shown in Fig. 31 (24). In the figure, the applied voltage V and the current waveforms I of the reactor were measured using a digital oscilloscope (Yokogawa Electric Corp., Japan, DL1740-1GS/s)
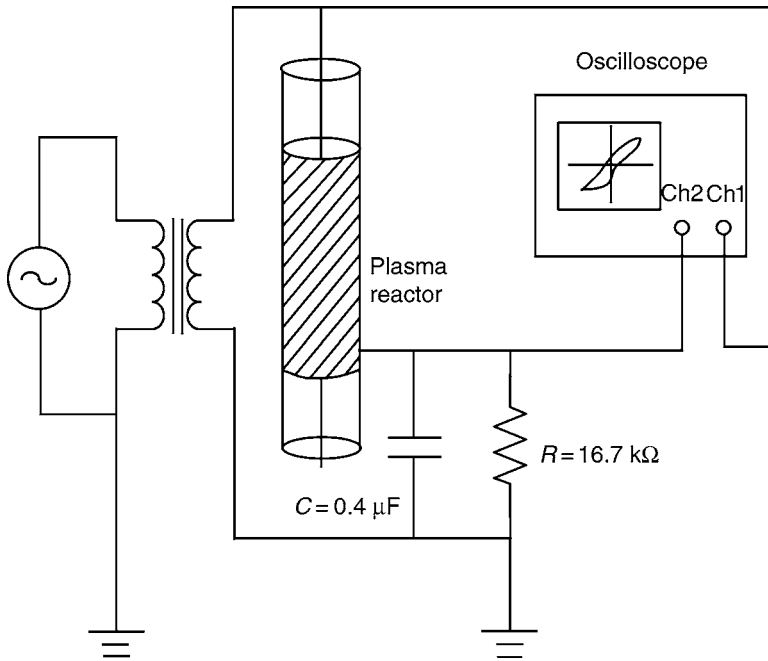
Fig. 30. Electrical circuit for measuring the discharge power of the plasma reactor using Lissajou's method.
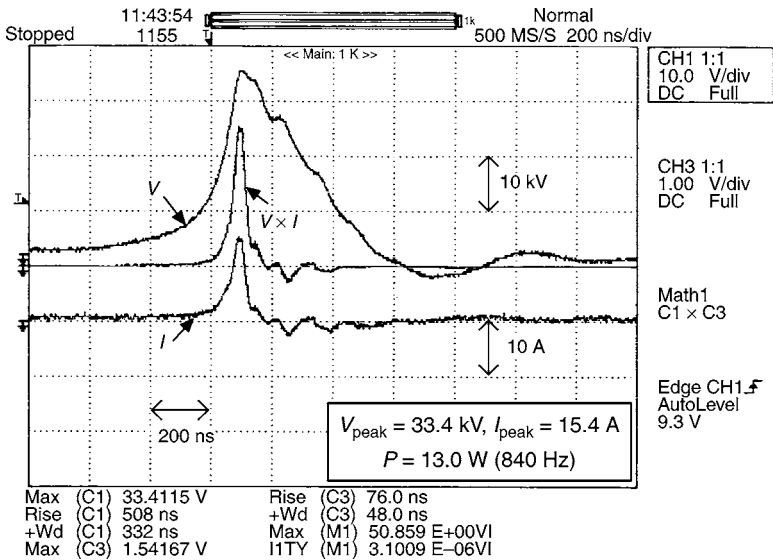
Fig. 31. Voltage, current and instantaneous power waveforms for measuring the discharge power of the reactor.

through the voltage and the current dividers (Sony Tektronix, Japan, P6015A and P6021). The discharge power of the reactor was obtained by averaging the product of the voltage and current waveforms on the oscilloscope. In this figure, the instantaneous discharge power $V \times I$ curve is also shown. The time-averaged discharge power P is calculated from the product of the positive area ($I1TY$ [$M1$]), which the $V \times I$ curve and the horizontal axis surround, with a conversion factor (*factor* $= 10^4 \times 10/20 = 5000$) and the pulse frequency of $f = 840$ Hz; $P = I1TY(M1) \times factor \times f$.

1.3.3. Gas Concentration Measurement

The efficiency is determined by measuring the concentration of gas constituents. There are various types of instruments available. In this section, the principal of the instruments used for decomposition of hazardous air pollutants using nonthermal plasma technologies are described.

1.3.3.1. CHEMILUMINESCENCE METHOD

A portion of NO is oxidized by ozone to form NO_2 of which a portion of NO_2 becomes the excited state. When the excited state of NO_2 goes back to the base NO_2, the light emission called chemical luminescence occurs as follows:

$$NO + O_3 \rightarrow NO_2{}^* + O_2 \tag{38}$$

$$NO_2{}^* \rightarrow NO_2 + hv_p \tag{39}$$

This reaction occurs very quickly. This reaction is not influenced by other compounds but only NO. In addition, this light emission is proportional to the concentration. This is the principle for NO measurement by utilizing the chemical luminescence method (25).

As for the NO_x measurement instruments used in the Section 2.2., gas samples are divided into two sections: one line is to use the reduction catalyst, which converts from $NO_2 \rightarrow NO$ so that NO_x ($NO_2 + NO$) can be measured. The other line is measured as NO. These gases are switched every 0.5 s by the magnetic valves and transported into the reaction chamber. On the other hand, the filtered air is humidified by the electron cooling device, reacted with the ozone, and then introduced into the reaction chamber. In the reaction chamber, the sample and ozone react, and its light emission is detected by the photo diode and the light intensity will determine the concentration of NO, NO_2, and NO_x, respectively.

1.3.3.2. INFRARED ADSORPTION

It is known that gaseous molecules adsorb certain frequencies of the infrared (IR) band and its adsorption is proportional to the concentration of gaseous molecules under constant pressure. Based on this principal, the gaseous molecule concentration can be measured continuously. In an infrared spectroscopy, the intermittent IR light is produced by the rotating chopper from the light source and IR radiation is passed through a sample of gaseous molecules. Some of this radiation is transmitted through, whereas the rest is absorbed by the sample, producing an infrared spectrum or "molecular fingerprint." Because each molecular structure has a unique combination of atoms, each produces a unique infrared spectrum. From this, identification (qualitative analysis) and analysis (quantitative measurement) of the gases such as CO, CO_2, N_2O, and SO_2 are possible using IR adsorption (26).

1.3.3.3. Gas Chromatographys

Chromatography is the science of separation, which uses a diverse group of methods to separate closely related components of complex mixtures. During gas chromatographic separation, the sample is transported through an inert gas called the mobile phase. The mobile phase carries the sample through a coiled tubular column where analytes interact with a material called the stationary phase. For separation to occur, the stationary phase must have an affinity for the analytes in the sample mixture. The mobile phase, in contrast with the stationary phase, is inert and does not interact chemically with the analytes. The only function of the mobile phase is to sweep the analyte mixture through the length of the column. Gas chromatography (GC) can be divided into two categories, (1) gas–solid and (2) gas–liquid chromatography. Gas–liquid GC, developed in 1941, is the primary GC technique used for environmental applications. Gas–solid GC is not widely used for environmental applications (27).

The sample stream elutes from the column through the detector's reaction chamber in which it is continuously irradiated with high-energy ultraviolet light. When compounds that have a lower ionization potential than that of the irradiation energy (10.2 eV with standard lamp) are present, they are ionized. The ions formed are collected in an electric field, producing an ion current that is amplified and outputted by the GC's electrometer.

1.3.3.4. Fourier Transform-Infrared

A Fourier transform infrared (FT-IR) spectrometer is simply a technical variant of a common infrared spectrometer, which yields an intensity signal as a function of wavelength or "spectral color" (28). The setup differs from a classical grating or prism spectrometer in that way, that it does not record the spectral intensity directly as a function of the wavelength, but an interferogram is taken instead as shown in Fig. 32. The central component of an FT-IR spectrometer is a Michelson interferometer and the signal is recorded as a function of the optical path difference between the fixed and movable mirror. From this interferogram the spectrum as a function of wavelength is calculated by applying a Fourier Transform (FT), which gives the instrument its name. The advantages of these techniques are, for example, the higher spectral resolution achievable and a typically higher throughput in intensity (no slit aperture required).

As an initial task, the background data by using nitrogen gas is essential. The gas sample is obtained from the infrared adsorption spectrum by subtracting it from the background data. Care must be taken for the presence of moisture in the sample gas because moisture adsorbs infrared signals in the wide spectrum and often interfered with other gas molecules. Table 3 shows the accuracies in the measurement of various gas concentrations in a specific FT-IR apparatus with light pass length of 2.4 m (29).

1.3.3.5. Gas Detection Tube

Gastec gas detector (Gastec, Co.) tubes are thin glass tubes with calibration scales printed by which you can directly read the concentrations of the substances (gases and vapors) to be measured (Fig. 33A). Each tube contains detection reagents that are especially sensitive to the target substance and quickly produces a distinct layer of color change. The tubes are hermetically sealed. For use, both ends must be broken off first, and then the tube must be connected to the Gas Sampling Pump with the directional
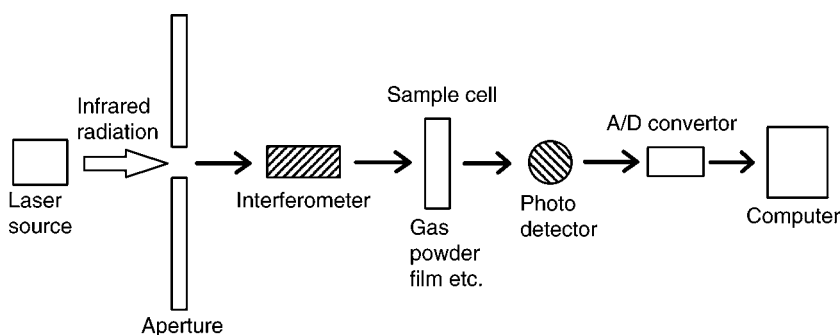
Fig. 32. Schematic diagram of FT-IR apparatus.

Table 3
Maximum Measurable Concentrations and Measurement Accuracy
for FT-IR With the Light Path Length of 2.4 m

Names of species	Analysis wave number (cm^{-1})	Maximum concentration (ppm)	Measurement accuracy of concentration (ppm)
CO_2	2360.38	165	0.08
CO	2169.43	811	0.41
CH_3OH	1033.36	470	0.23
HCHO	1745.81	357	0.18
H_2O	1653.47	2304	1.15
N_2O	2235.73	245	0.12
NO_2	1630.57	205	0.10
NO	1890.96	1504	0.75
O_3	1055.06	891	0.45
CH_4	3017.87	588	0.29
C_2H_6	2987	656	0.33
HNO_3	1325.82	304	0.15
NH_3	967.058	230	0.11
CH_3CHO	1762.21	932	0.47
COF_2	1255.43	94	0.05
CF_4	1283.15	2	0.001
HCOOH	1105.11	405	0.20

arrows pointing toward the pump as shown in Fig. 33B. To assure a high precision indication, the Gastec gas detector tube's inner diameter are tightly controlled and detection reagents with long-term stability (many have 3-yr shelf life) are strictly selected. All tubes undergo stringent quality control. Individual production lots are tested and calibrated independently of each other to ensure the highest calibration accuracy for each lot. Each tube has its quality control number printed on it. Today over 545 kinds of applications are available. The other type of gas detection tube is also made by Komyo Rikagaku Kogyo.
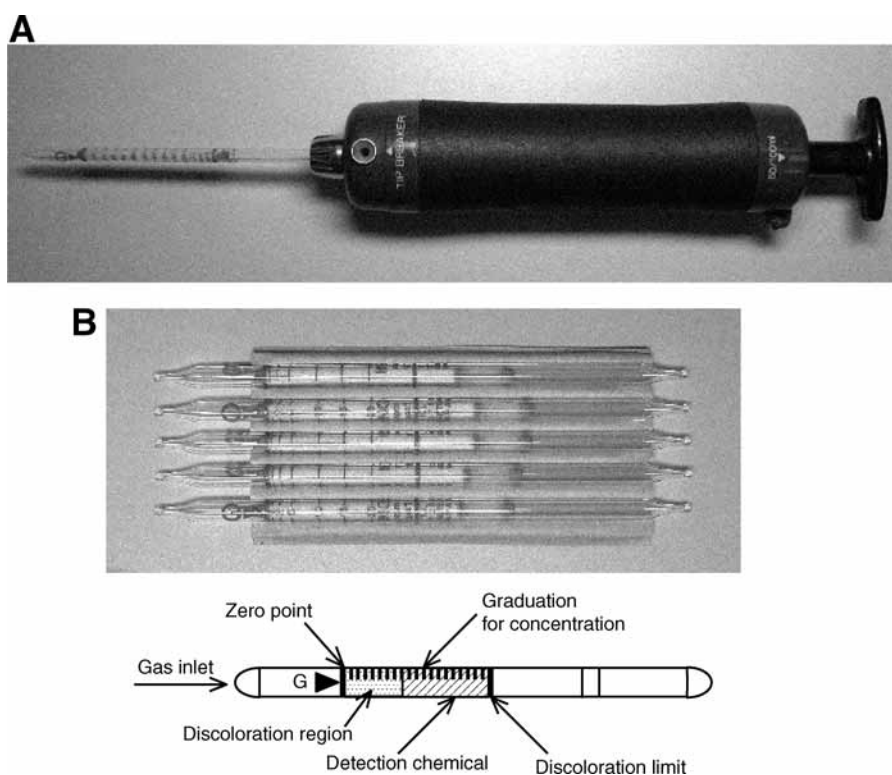
Fig. 33. Gas detection tube. **(A)** Detection tube connected with sampling pump. **(B)** Detection tubes.

2. ENVIRONMENTAL IMPROVEMENT

2.1. Electrostatic Precipitator

2.1.1. Principle of Electrostatic Precipitator

The ESP is the most prevalent application for the corona as an ion source (12,30–35). Although, the plasma region for the DC corona is limited in the immediate vicinity of wire electrodes, the majority of negative ions for the typical industrial ESP which used the negative polarity, exist in the interelectrode space. The dust particles are charged in the corona region so effectively that the charged particles are collected on the grounded positive electrode.

An industrial ESP was first developed by Cottrell in 1907 as an apparatus for collecting mist of sulfuric acid in the combustion flue emission. Since then, precipitators have been operated at an industrial scale for collecting the particulate emissions in the utility, iron/steel, paper manufacturing, and cement and ore-processing industries. The electrostatic precipitators have greatly contributed to the atmospheric environment protection. The typical structure of the ESP is shown in Fig. 34. Corona discharge in the ESP is generated at high voltage electrodes, commonly round discharge wires, which are centered between flat collecting plates. The plasma occupies only a small volume near the wire; the rest of the interelectrode space is filled with ions from the corona. In this region, charging and movement of particles to the collecting plate takes place.
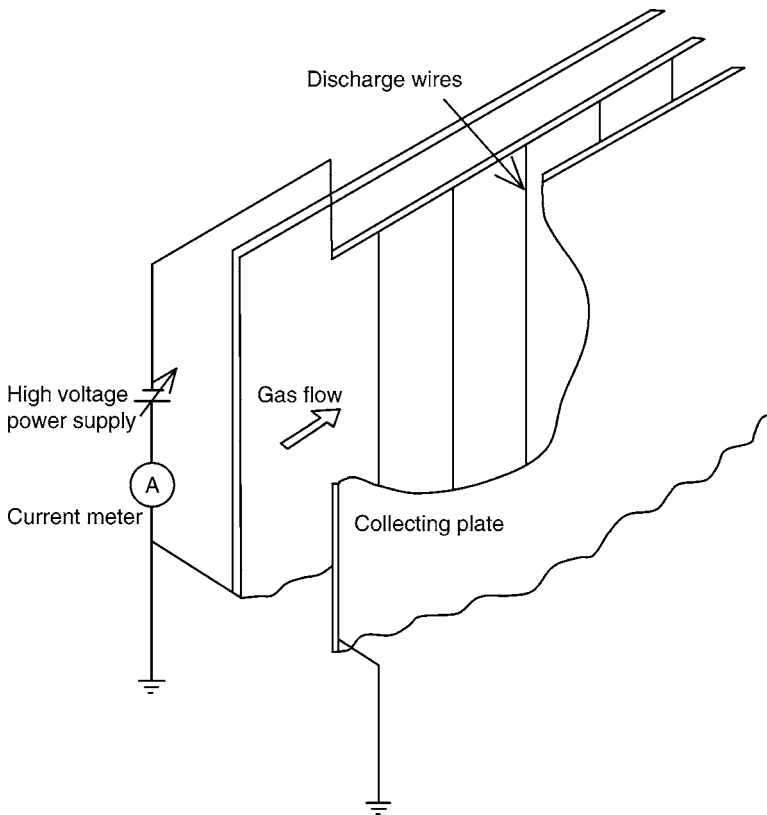
Fig. 34. Typical structure of industrial electrostatic precipitator (ESP).

For the best dust particle-charging environment with the least power consumption, the industrial precipitator operates in the negative corona to avoid the formation of streamers and the lower sparking potential associated with them. When the particle diameter is in the field charging regime (>0.1 μm), the collection efficiency of the ESP is proportional to the square of the electric field between electrodes. Consequently, maximizing the field strength is a major goal of designers.

Precipitators are also used in buildings and domestic ventilation systems for control of particles in the indoor environment. Many kinds of small ESP's are marketed for about several hundred dollars for the improvement of sick house. The indoor air cleaner operates with the positive corona to reduce the production of ozone. The charging of particles is usually separated from the collection (two-stage ESP). A typical structure of two-stage ESP is shown in Fig. 35. This is a commercial indoor small ESP energized by DC 5 kV power supply. The price is around 500 USD. In the first stage (ionizer), particles are charged and they are collected in the second stage (collector). The wire to plate distance of the ionizer is 11.5 mm, length of the ionizer is 18 mm, plate to plate distance of the collector is 2.5 mm, length of the collector is 40 mm. The collection efficiency often exceeds 99.9% in this type of ESP. This allows both processes to be optimized and results in somewhat better performance than would be achieved in a standard
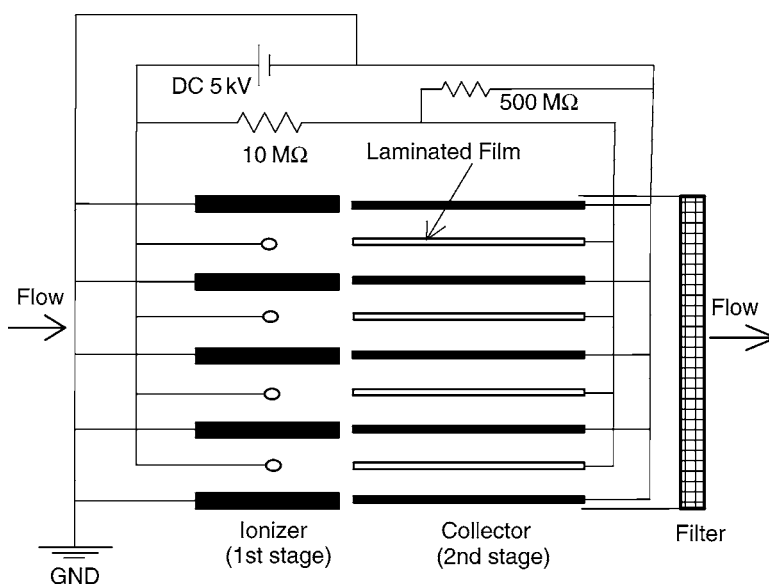
Fig. 35. Two-stage ESP for indoor air cleaning.

single-stage design. The small volume of gas treated also allows the indoor cleaner to be sized more conservatively than the industrial unit. The full description of an ESP requires many more considerations than can be given here (36–40).

2.1.2. Characteristics of ESP

Electrostatic precipitators have several advantages and disadvantages in comparison with other particulate control devices.

Advantages include:

a. Very high efficiencies, even for very small particles.
b. Very large gas volumes can be handled with a low pressure drop (10–20 mmAq) and low power consumption of fan energy.
c. Dry collection of valuable materials, or wet collection of fumes and mists.
d. Can be designed for a wide range of gas temperatures.
e. Low operating costs, except at very high efficiencies.
f. Few mechanical moving parts, high reliability.

Disadvantages are:

a. High capital coats.
b. Will not control gaseous emissions.
c. Not very flexible, once installed, to changes in operating conditions.
d. Occupies more space.
e. Poor collection for high and low resistive dusts.

It is generally difficult for the ESP to collect low resistivity dust such as carbon particles whose electrical resistivity is less than 10^4 Ω cm because the collected dusts easily lose their charges instantly on the grounded electrode and move into the flow field again. This phenomenon is called as re-entrainment and decreases the collection efficiency

of the ESP. This is often observed in the cleaning system of flue emission from heavy oil-fired electric power plant as well as the collection of carbon soot emitted from diesel engine exhaust gas.

On the other hand, fly ash generated by the incineration of imported coal has so high electrical resistance that streamer discharges are extended from the collected dust layer and breakdown often occur. As a result, the collection efficiency decreases. It especially decreases in the range of the resistivity more than 5×10^{10} Ω cm. This phenomenon is called "back corona." In order to avoid the back corona and extend the field of the application of the ESP, the following methods have been proposed:

a. Resistivity of the dust is decreased by the temperature control (hot or cold side ESP) and/or the addition of conditional agents such as S or Na.
b. The current or charge in the dust layer is controlled using pulse high voltage power supply with variable duty ratio.
c. The dust layer having a high resistance on the collecting electrode is removed by the rotating brushes and hoppers.

2.1.3. Theory of ESP

Consider a dusty airflow in a rectangular channel defined by two parallel plates as shown in Fig. 36. Also consider only the half-channel between the charging wires and the plate, with width $D/2$ and height H, where D is the distance between the plates, H is the height of the collecting electrode, L is the length of the collecting plate and u is the average velocity. With certain assumption, we can derive the basic equation used in ESP design—the Deutsch–Anderson equation that was first derived in 1922 (30). The assumptions are

a. Gases and particles move in the x direction at constant velocity u, with no longitudinal mixing.
b. Particles velocities are uniformly distributed in the y and z directions at every x location.
c. Charging and collecting fields are constant and uniform; the particles quickly attain terminal velocity w_e in the y direction.
d. Re-entrainment of collected particles can be negligible.

The concentration of particles will decrease with x because of the net migration of particles to the plate. We consider a material balance on particles flowing into and out of a very short cross-section of the channel (located at x and $x + dx$ and width of $D/2$) Assuming that the difference between the mass of particles flowing into and out of the slice must be equal to the mass of particles removed at the plate, the following equation is obtained.

$$uH\frac{D}{2}C_x - uH\frac{D}{2}C_{x+\Delta x} = wC_{x+\Delta x/2}H\Delta x \tag{40}$$

where u is the gas velocity (m/s); H is the plate height (m); D is the channel width (m); C is the particle concentration or loading (kg/m³); and w is the terminal or drift velocity in the y direction (m/s). Dividing both sides of the Eq. (40) by Δx and taking $\Delta x \rightarrow 0$, the following equation is obtained.

$$\frac{-uHD}{2}\frac{dC}{dx} = wHC \tag{41}$$

Solving this differential equation of separated variables types, we obtain

$$\ln\left(\frac{C_L}{C_0}\right) = \frac{-wA_p}{Q_c} \tag{42}$$
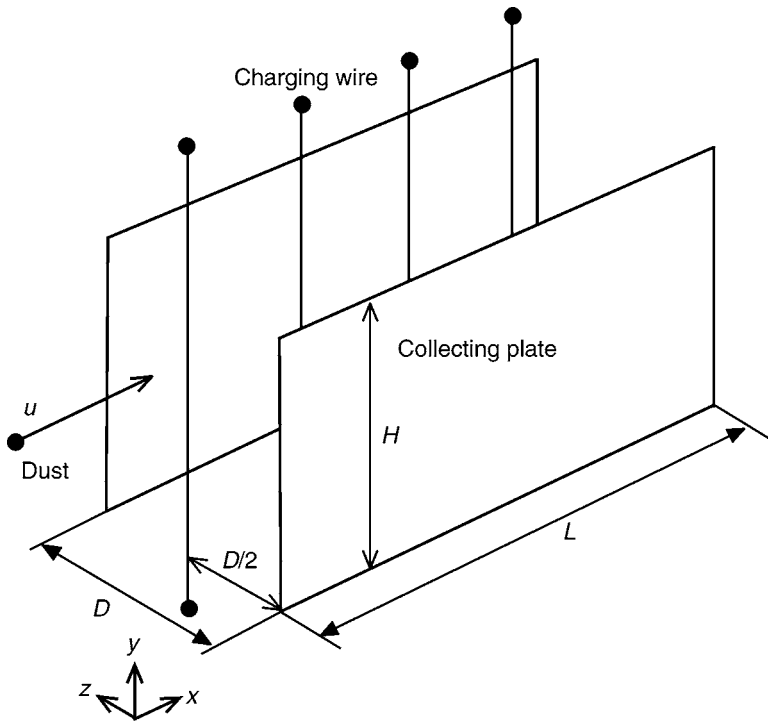
Fig. 36. Analysis model for electrostatic precipitator.

where A_p is the area of one plane (two sided) (m²) (= $2HL$), and Q_c is the volumetric gas flow rate in one channel (m³/s) (= uHD). For the whole ESP, we can consider A_p and Q_c to be the total collection area A and the total gas flow rate Q. Thus, Eq. (42) can be written as

$$\frac{C_L}{C_0} = e^{-wA/Q} \tag{43}$$

Using the usual definition of collection efficiency, the Deutsch–Anderson equation can be obtained from the Eq. (43)

$$\eta \equiv 1 - \frac{C_L}{C_0} = 1 - e^{-wA/Q} \tag{44}$$

2.1.4. Design Example: ESP Design

Problem

a. Calculate the total plate area for a 98% efficient ESP that is treating 20,000 m³/min of air. The effective drift velocity is assumed to be 7 m/min (30).
b. Assuming the plates are 7 m high and 4 m long, calculate the number of plates required.

Solution

a. From the Deutsch–Anderson Eq. (44),

$$A = -\frac{Q}{w}\ln(1-\eta) \tag{45}$$

Because of $\eta = 0.98$, $Q = 20{,}000$ m³/min and $w = 6$ m/min, the following equation is obtained.

$$A = -\frac{20{,}000}{7}\ln(1 - 0.98) \cong 11{,}177.2 \text{ m}^2 \qquad (46)$$

b. The total area of the N collecting plates having a height of H and length of L is $A = 2\,H\,L$ (N–1). Therefore,

$$N = \frac{A + 2HL}{2HL} \qquad (47)$$

Substituting the result in Eq. (47) that $A = 11{,}177.2$ m², $H = 7$ m, and $L = 4$ m, the following equation is obtained.

$$N = \frac{11{,}177.2 + 2\times7\times4}{2\times7\times4} = 200.6 < 201\,\text{plates} \qquad (48)$$

2.1.5. Equation of Motion for a Charged Particle

When the ESP is designed using the Eq. (44), the migration velocity of the particle w_e should be determined (20,41). It is generally difficult to determine the effective migration velocity because it depends on particle size, electric field, fuel gas characteristics, and so on. Therefore, it must be determined from experiments, experiences or precise numerical simulations. When a high performance ESP must be designed, the measurement of the effective value of the migration (or terminal) velocity w_e is obtained from the experiment with a smaller scale pilot plant. In this section, the theoretical method to determine the trajectories and terminal velocities of a particle is explained using the two-dimensional (2D) Lagrangian method. From the numerical results, the approximate value of w_e can be determined in a simple case.

Consider that a particle of velocity $v = (u, 0)$ moves into the ESP at the position $x = (0, y_0)$ that consists of the discharge wire and the ground electrode. Considering the electrostatic force and the fluid resistance force (Stokes drag force) as the body force, the equation that determines the motion of the particle is

$$F_e - F_D = M_p \frac{dv}{dt} = M_p \frac{d^2x}{d^2t} \qquad (49)$$

where d_p is the diameter of the particle; F_e is the electrostatic force; F_D is the fluid drag force; M_p is the mass of the particle; and q is the charge of the particle. The electrostatic force is expressed by

$$F_e = qE \qquad (50)$$

where E is the electric field vector that is generally the function of the coordinate.

The fluid drag force F_D is expressed using the drag coefficient C_D as

$$F_D = C_D A_{pr} \frac{\rho}{2}\left|v_r\right|v_r \qquad (51)$$

where A is the projected area of a particle in the flow direction, and $v_r = v - v_f$ (v_f is the velocity of the fluid). The drag coefficient C_D depends on the particle Reynolds number of a spherical particle,

$$Re = \frac{\left|v_r\right|d_p}{\nu} \qquad (52)$$

and given by the equations:

a. Laminar flow ($Re < 2$)

$$C_D = \frac{24}{Re} \tag{53}$$

b. Transient flow ($2 < Re < 500$)

$$C_D = \frac{24}{\sqrt{Re}} \tag{54}$$

$$\text{or } C_D = \frac{24}{\sqrt{Re}}\left(1 + \frac{Re^{2/3}}{6}\right) \tag{55}$$

c. Turbulent flow ($500 < Re < 2 \times 10^5$)

$$C_D = 0.44 \tag{56}$$

For most aerosols having the diameter d_p of around 10 μm, the following Stokes drag force expressed by the Eq. (53) is applicable because the particle Reynolds number is much smaller than one:

$$\boldsymbol{F}_{\mathrm{DST}} = 3\pi\mu d_p(\boldsymbol{v} - \boldsymbol{v}_f) \tag{57}$$

When the diameter of the particle is much more than the mean free path of the surrounding fluid, formula (57) is applicable for laminar region as it is. However, the slip between the gas and the particle occurs when the particle diameter is too small approx 1 μm or in the same order as the mean free path λ. In such a case, the drag force becomes small and the Eq. (57) should be corrected using the correction factor $C_c > 1$ as follows:

$$\boldsymbol{F}_D = \boldsymbol{F}_{\mathrm{DST}} / C_c = 3\pi\mu d_p(\boldsymbol{v} - \boldsymbol{v}_f) / C_c \tag{58}$$

where C_c is called the Cunningham's correction factor usually calculated by the following equations:

$$C_c = \begin{cases} 1 + 2.52\dfrac{\lambda}{d_p} \\ 1 + \dfrac{\lambda}{d_p}\left[2.5 + 0.8\exp\left(-0.55\dfrac{d_p}{\lambda}\right)\right] \end{cases} \tag{59}$$

The values are given in Table 4. When the diameter of the particle d_p is more than 0.5 μm, C_c is almost equal to one. From the Eq. (49), Eq. (50), and Eq. (58), the following equation is obtained:

$$\frac{d^2\boldsymbol{x}}{dt^2} = \frac{d\boldsymbol{v}}{dt} = \frac{q\boldsymbol{E}}{M_p} - \frac{18\mu}{C_c\rho_p d_p^2}(\boldsymbol{v} - \boldsymbol{v}_f) \tag{60}$$

where ρ_p is the density of the spherical particle and M_p is the mass of the spherical particle ($= \rho \pi d_p^3/6$). It is assumed that air flows into the ESP uniformly and with a constant velocity $\boldsymbol{v}_f = (u, 0)$, The x and y components of the Eq. (60) becomes

$$\frac{d^2x}{dt^2} = \frac{dv_x}{dt} = \frac{qE_x}{M_p} - \frac{v_x - u}{\tau'} \tag{61}$$

Table 4
Cunningham's Correction Coefficient

d_p μm	C_c
0.10	2.89
0.30	2.112
0.50	1.334
0.60	1.300
1	1.166
2	1.083
3	1.066
5	1.033
10	1.017

$$\frac{d^2 y}{dt^2} = \frac{dv_y}{dt} = \frac{qE_y}{M_p} - \frac{v_y}{\tau'} \tag{62}$$

respectively, where

$$\tau' = C_c \tau = C_c \tau \frac{\rho_p d_p^{\,2}}{18\mu} \tag{63}$$

is the characteristic time of the particle corrected considering slips, where μ is the viscosity of the air (approx 1.71×10^{-5} Pa·s).

The 2D trajectories (x,y) of the particle's motion can be obtained from the given distribution of q and E by integrating these Eq. (61) and Eq. (62). In order to obtain the distributions of q, E, and v inside the ESP, the basic equations of fluid flow and electric field (Maxwell equation) must be analyzed simultaneously. The detailed explanation of the numerical analysis is beyond the scope of this chapter. The detailed calculations are found in ref. 42, 43.

In the simplest case, the Eq. (62) can be easily integrated when it can be assumed that the charge q and the electric field E are specially uniform, In the condition of $v_y = 0$ at $\tau = 0$, the result becomes as follows:

$$v_y = \tau' \frac{qE}{M_p}[1 - \exp(-t/\tau')] \tag{64}$$

When time reaches infinity ($t \rightarrow \infty$), the terminal velocity or the migration velocity is

$$v_y = \tau' \frac{qE}{M_p} = \frac{qEC_c}{3\pi\mu d_p} \tag{65}$$

Equation (65) gives the theoretical value of the migration velocity of the particle in the ESP.

2.1.6. Particle Electric Charges

The magnitude of particle charging q is greatly dependent on the method of charging. Charging by the corona discharge, which is the most popular method in the ESP consists of two types of charging mechanisms (31). One is fielding charging in which the monotonic ions in the corona are driven by the electric field and attached with dust particles. The other is diffusional charging, in which the induced ions are driven by the thermal energy and

attached to the surface of dust particle. In the range of the particle diameters more than 1 μm, field charging is the dominant mechanism. In the range of diameter less than 0.1 μm, diffusional charging is dominant. Both charging mechanisms occur for the range of 0.1–1 μm.

In each charging mechanism, the amount of particles charging after t is expressed as

1. Field charging

$$q_f = q_\infty \frac{t/\tau_c}{1+t/\tau_c} \tag{66}$$

$$q_\infty = \pi\varepsilon_0 \frac{3\varepsilon_r}{\varepsilon_r+2} d_p^2 E \ : \text{(saturation charge)} \tag{67}$$

$$\tau_c = \frac{4\varepsilon_0 E}{i_c} \tag{68}$$

where ε_0 is the permeability in vacuum ($= 1/[4\pi \times 10^9]$); ε_r is the relative permeability of the particle (typical value approx 5); E is the strength of the electric field (V/m); and i_c is the ion current density (A/m^2)

2. Diffusional charging

$$q_{\text{th}} = q^* \ln(1+t/\tau_c') \tag{69}$$

$$q^* = \frac{2\pi\varepsilon_0 d_p kT}{e} \tag{70}$$

$$\tau_c' = \frac{8\varepsilon_0 kT \mu_i E_c}{d_p C_i e i_c} \ : \text{Charging time constant} \tag{71}$$

where k is the Boltzmann's constant = 1.3804×10^{-23}(J/K), T is the absolute temperature, e is the charge of an electron (= 1.602×10^{-19}[C]), C_i is the root mean square of the velocity of the ion's thermal motion (= $3kT/m_i)^{1/2}$(m/s), m_i is the mass of an ion, μ_i is the mobility of the ion (m^2/V·s), and E_c is the strength of the electric field in the charging part (V/m).

The total amount of charge given to the particle is approximately expressed as the sum of the charging amounts in both mechanisms:

$$q = q_f + q_{\text{th}} \tag{72}$$

assuming that both mechanisms occur independently.

The charging of the particulates creates a nearly immobile space charge, at least compared with the high motilities of the ionic carriers. The space charge always influences the corona generation, often causing the voltage to rise several kilovolts more than the value with no particles present at the same current. For extremely fine particulate fumes, the particulate density may be sufficient to absorb all ions before they reach the counter electrode. The ESP appears to operate with no current in such a case, even though many particles are being charged and removed.

2.1.7. Design Examples: Particle Motion in the ESP

Problem

We consider a two-stage ESP as shown in Fig. 35. In the first stage, a particle is charged and flows into the second stage of many parallel plates with the velocity of
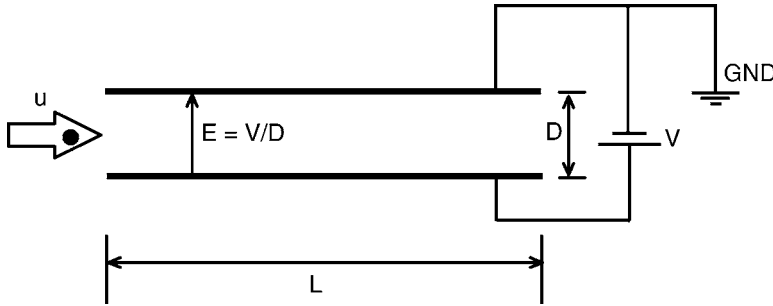
Fig. 37. Second stage of Two-stage ESP.

Table 5
Amount of Charge in a Particle

Diameter of particle (μm)	Charge (q C)
0.1	1.08×10^{-18}
0.3	8.89×10^{-18}
0.5	2.42×10^{-17}
1	9.54×10^{-17}

u as shown in Fig. 37. The calculation conditions are as follows: $V = 4.7$ kV, $L = 30$ mm, $D = 2.5$ mm, $u = 1$ m/s and charging amounts of a particle are shown in Table 5.

a. Calculate the characteristic time constant τ' of the Eq. (63) and show that the velocity of the particle having the diameter less than 1 μm terminates after times of less than 10^{-3} s. and the trajectory of the particle motions is almost linear.

b. Draw the trajectories of the particle's motions having the diameters of 0.1, 0.3, 0.5, and 1 μm. It is assumed that these particles are first charged by the upper-sided electrode, and collected on the lower sided grounded electrode.

Solution

a. The velocity of the charged particle moving to the collecting plate v_y is given by the Eq. (65). Furthermore, τ' is given by Eq. (63). The Cunningham's correction coefficient C_c becomes 1.166 for a particle with a diameter of $d = 1$ μm. From the Eq. (63),

$$\tau' = 9.747 \times 10^6 \times 1.166 \times (1 \times 10^{-6})^2 = 1.137 \times 10^{-5} \text{ (s)} \qquad (73)$$

Therefore, in Eq. (64),

$$1 - \exp\left(-\frac{t}{\tau'}\right) = 1 - \exp\left(-\frac{10^{-3}}{1.137 \times 10^{-5}}\right) = 1 \qquad (74)$$

for $t = 10^{-3}$ (s). This result indicates that the velocity terminates instantaneously.

b. From the result of solution 1, the velocity v_y reaches terminal velocity almost instantaneously. Therefore, the trajectory is almost linear with the velocities

$$v_x = u = \text{const}. \qquad (75)$$

$$v_y = \tau' \frac{qE}{M_p} = \frac{qEC_c}{3\pi\mu d_p} = \text{constant} \qquad (76)$$

The electric field is calculated as

$$E = \frac{V}{d} = \frac{4.7 \times 10^3 (\text{V})}{2.5 \times 10^{-3} (\text{m})} = 1.88 \times 10^6 \ (\text{V/m}) \tag{77}$$

By substituting the values into the equations, the termination velocity $v_{y0.1}$, the time taken to collect $t_{0.1}$ and the horizontal distance $l_{0.1}$ at which the particle moves are calculated as

$$v_{y0.1} = 0.367 \, (\text{m/s}), \quad t_{0.1} = 6.81 \times 10^{-3} \, (\text{s}), \quad l_{0.1} = 6.81 \, (\text{mm}) \tag{78}$$

For particles of different diameters (0.1, 0.3, 0.5, and 1 μm), these values are calculated as follows:

$$v_{y0.3} = 0.730 \, (\text{m/s}), \quad t_{0.3} = 3.42 \times 10^{-3} \, (\text{s}), \quad l_{0.3} = 3.42 \, (\text{mm}) \tag{79}$$

$$v_{y0.5} = 0.754 \, (\text{m/s}), \quad t_{0.5} = 3.32 \times 10^{-3} \, (\text{s}), \quad l_{0.5} = 3.32 \, (\text{mm}) \tag{80}$$

$$v_{y1.0} = 1.299 \, (\text{m/s}), \quad t_{0.3} = 1.92 \times 10^{-3} \, (\text{s}), \quad l_{1.0} = 1.92 \, (\text{mm}) \tag{81}$$

2.2. Combustion Flue Gas Treatment from Power Plant

2.2.1. Principle of Gas Cleaning Systems

There are several methods to decompose hazardous air pollutants such as combustion flue gases, volatile organic compounds, global warming gases, odorous gases, toxic gases utilizing nonthermal plasma technology. The plasma chemical process produces various forms of radicals, atomics, and ions such as OH, HO_2, O, O^-, O_3 induced by the high-energy electron impaction through unsteady pulse and AC discharges. Basically, the oxidation is the principal decomposition mechanisms. As for plasma chemical decomposition, it is important to confirm the final products to make certain that the reaction does not end up with partial oxidation.

Although, many processes are proposed for treating the combustion flue gases using nonthermal plasma, the following methods are the main plasma processes for removing flue gas emission, primarily, NO_x and SO_x, from electric power stations, various industrial processes, and diesel emission from automobiles.

1. Aerosolization by plasma and ESP or bag filter capture.
2. Plasma chemical hybrid process.
3. Plasma assisted catalytic process.
4. Selective catalytic reduction.

Here, two processes 1 and 2 are focused on and processes 3 and 4 are described elsewhere (44–46). The principal reactions for NO_x and SO_x by the plasma are first described.

2.2.1.1. CHEMICAL REACTION OF NO_X AND SO_X IN A NONTHERMAL PLASMA PROCESS

Nonthermal plasma reactors can generate chemically activated nonequilibrium plasma with lower power input under the atmospheric pressure and temperature. It can decompose hazardous air pollutants and volatile organic compounds effectively compared with ordinary high-temperature thermal plasma. In this section, the main chemical reactions in the removal of NO_x and SO_x using nonthermal plasma are shown. In air activated by plasma, not only high-speed electrons, but also the activated oxygen (O),

nitrogen (N), HO_2, O_3, and OH radicals are generated. These radicals advance the following chemical reactions:

[NO_x]

$$NO + e \rightarrow N + O + e \tag{82}$$

$$NO + O + M \rightarrow NO_2 + M \tag{83}$$

$$NO + N \rightarrow N_2 + O \tag{84}$$

$$NO + OH + M \rightarrow HNO_2 + M \tag{85}$$

$$NO + O_3 \rightarrow NO_2 + O_2 \tag{86}$$

$$NO_2 + O + e \rightarrow NO_3 \tag{87}$$

$$NO_2 + N \rightarrow N_2O + O \tag{88}$$

$$NO_2 + OH + M \rightarrow HNO_3 + M \tag{89}$$

$$NO_2 + O_3 + e \rightarrow NO_3^- + O_2 \tag{90}$$

[SO_x]

$$SO_2 + O + M \rightarrow SO_3 + M \tag{91}$$

$$2SO_2 + 4OH \rightarrow 2H_2SO_4 \tag{92a}$$

$$2SO_2 + 4OH \rightarrow 2H_2SO_4 \tag{92b}$$

$$SO_2 + O^- \rightarrow SO_3^- \tag{93}$$
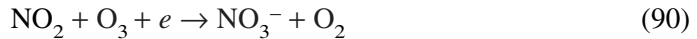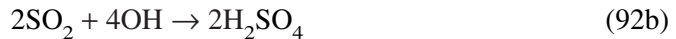
where M is the third material and expresses N_2 or O_2 for the case of air, and e represents the high-speed electron. The chemical reaction like Eq. (83), (85), (86), and Eqs. (91)–(93) advance and most of the NO and SO_2 in the flue emission are converted to NO_2, HNO_2, and SO_3, SO_3^- respectively with increase in the input power of the plasma reactor. With further increase in the input power, the reductions of NO and SO_2 partially occur. It is known that the reduction scarcely occurs under oxygen rich environment, especially, in the reaction of NO. The oxidation reactions such as Eq. (83), Eq. (85), and Eq. (86) progress rapidly and the reaction byproducts such as N_2O, NO_3^-, HNO_3 are induced greatly. From these reasons, effective NO_x reduction using the non-thermal plasma alone is restricted under the oxygen rich environment. Therefore, the combinations of additive agents, catalysts, and nonthermal plasma (44–46) have been investigated to reduce the NO_x. However, with these combinations, there are some practical limitations in terms of low efficiency, the generation of the hazardous byproducts, and increased cost. In order to overcome these problems, the following effective methods were proposed.

2.2.1.2. PLASMA ESP HYBRID METHOD (PPCP METHOD)

In this method, after the ammonia NH_3 gas is injected into the gas emission, NO and SO_2 are oxidized and converted to the NH_4NO_3 and $(NH_4)_2SO_4$ aerosols by radicals and activated ions such as OH, HO_2, O, O^-, O_3 and so on induced by the pulse corona discharge of the frequency = several ten to several hundred Hz. The induced aerosols are
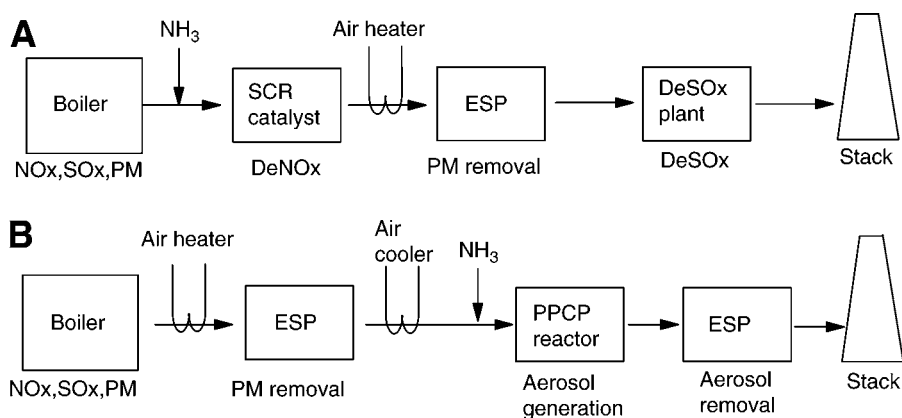
Fig. 38. Comparison of SCR and PPCP methods. **(A)** SCR method. **(B)** PPCP method.

collected by the ESP located downstream. The induced NH_4NO_3 and $(NH_4)_2SO_4$ aerosols are used as the originator of the chemical fertilizers. The principle of this method is similar to the electron beam method in which the radicals induced by the high-speed electrons progress the removal of NO and SO_2. In the electron beam method, there is a safety problem on the X-ray generated by the very high-energy electrons (approx 100 keV). On the other hand, the generation of the X-ray is negligible in the nonthermal plasma method because the energy of the electrons is significantly smaller than 100 eV. This method was named as Pulse Corona Induced Plasma Chemical Process (PPCP) method by Prof. Sen-ichi Masuda because the pulse corona is used in the plasma chemical process (20,47–49).

Figure 38A shows a typical environmental protection equipment for after treatment of combustion flue gas emission from coal-fired or heavy oil-fired boiler. Figure 38B shows the schematics of the PPCP process. The flue exhaust gas first passes through the heat exchanger and the gas temperature decreases to temperatures of less than 200°C for the cold side ESP operation, where large particles such as fly ash are removed. The flue gas is again cooled down to about 90°C. After the injection of NH_3, the flue gas passes through the plasma reactor, whose structure is similar to the ordinary ESP. The high-voltage pulse corona is generated by the electrical circuit using a rotary spark gap switch. The induced radicals and the ions are used for the oxidization of NO and SO_2 to induce HNO_3 and H_2SO_4.

The induced HNO_3 and H_2SO_4 react with NH_3 to generate NH_4NO_3 and $(NH_4)_2SO_4$ aerosols according to the following chemical reactions:

$$HNO_3 + NH_3 \rightarrow NH_4NO_3 \tag{94}$$

$$H_2SO_4 + 2NH_3 \rightarrow (NH_4)_2SO_4 \tag{95}$$
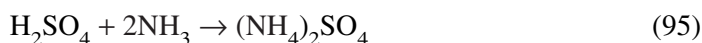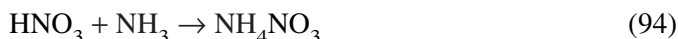
The induced aerosols are collected by the second ESP. After these processes, the cleaned gas is discharged to the atmosphere from the stack. The PPCP is a new dry simultaneous removal method of NO_x and SO_x based on the principle that the radicals and the ions have a very high chemical activity and can progress the oxidization of NO_x

and SO_x. In order to develop this method in a practical application, the problem must be solved. Because the power consumption for plasma generation is too high, the cost should be less than 5% of the power generation.

2.2.1.3. PLASMA–CHEMICAL HYBRID METHOD

The authors have proposed a new plasma–chemical hybrid NO_x reduction method (50–52). In this method, after the NO is oxidized to NO_2 using nonthermal plasma, the induced NO_2 is reduced to N_2 by a wet chemical process using the strong reduction chemicals such as Na_2SO_3 water solution. The following chemical reaction takes place very effectively.

$$2NO_2 + 4Na_2SO_3 \rightarrow N_2 + 4Na_2SO_4 \qquad (96)$$
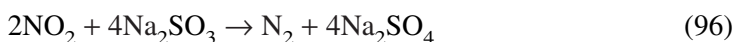
In this technology, the nonthermal plasma process is combined with the wet-chemical process. In the nonthermal plasma process, the oxidization reactions such as Eq. (83) and (85) can take place effectively with significantly lower power consumption. In the chemical process using the Na_2SO_3 water solution, the reduction reaction Eq. (96) of NO_2 can be achieved with low cost. The chemical reactions Eq. (85), (88)–(90) of the byproducts generation does not proceed so much because the input power to the plasma reactor is restricted to as little amount as possible. The induced part of the NO_2 reacts with moisture and generates NO_2^-, NO_3^- ions as follows:

$$2NO_2 + H_2O \rightarrow HNO_2 + HNO_3 \rightarrow 2H^+ + NO_2^- + NO_3^- \qquad (97)$$
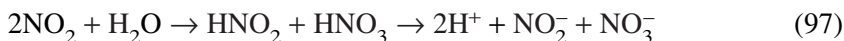
However, the induced products produced are small quantity and easily processed, and neutralized with the addition of a small amount of alkali. The total operating cost of this plasma–chemical hybrid process is less than 1/4 of the conventional selective catalytic reduction (SCR) process. The details of discussion are described in later section.

2.2.2. Two-Stage Plasma Chemical Hybrid Process

2.2.2.1. PRINCIPLE

Nitrogen oxides (NO_x) [the sum of nitric oxide (NO) and nitrogen dioxide (NO_2)] are mixtures of compounds of nitrogen and oxygen generally found in effluents from combustion sources (50). NO_x is a precursor to ozone or smog in atmosphere, greenhouse effect gas, and is believed to be a major contributor to acidic deposition of acid rain. With the passage of the 1990 Clean Air Act Amendments, many chemical and metal industries and utilities were required to limit their production. Various types of corona-induced nonthermal plasma technologies have been studied to achieve economical feasibility in contrast to the conventional techniques for the removal of NO_x. However, nonthermal plasma alone cannot convert nitrogen dioxide (NO_2) to nitrogen (N_2) effectively but, rather, generates a significant amount of nitrous oxides (N_2O), nitrate (NO_3^-), and nitric acid (HNO_3). In addition, the power consumption for nonthermal plasma for decomposing NO_x is extremely high (70–780 eV/molecule) and the NO_x removal efficiency was up to 80% (53,54). It was known that the O species generated by the plasma process serve to trap NO_x in the oxidation–reduction cycle between NO and NO_2 (54). Part of the NO_2 will be converted into N_2O, HNO_2, and HNO_3. In the nonthermal plasma process without additives, NO can be effectively converted to NO_2 but NO_2 cannot effectively be reduced to N_2. For these reasons, the removal of NO_x (the sum of NO and NO_2) by nonthermal plasma alone has practical limitations.

Recent trend is to use reducing agents, chemicals, and catalysts in combination with the nonthermal plasma process. The addition of hydrocarbons such as ethylene has been investigated for the removal of NO_2 but conversion efficiency was approx 60% (44,45). A three-way catalyst used for automobile emission control, such as the copper coated zeolite catalyst (Cu-ZSM5), was investigated combined with nonthermal plasma, but NO_x conversion was insignificant even at an elevated temperature of 250°C (45). When the pulsed corona discharge plasma was combined with the addition of hydrocarbon and the catalysts, conversion of as much as 90% of NO_x was reported (45,55) but N_2O and CO generation were not discussed. The use of water vapor and a $Ca(OH)_2$ catalyst showed some promising NO_x conversion in the range of 80% (44).

The effect of hydrocarbon additives was investigated for lowering the energy consumption of NO_x removal using a pulsed corona reactor. It was also reported that nonthermal plasma techniques were effective for high NO_x concentrations but ineffective for low NO_x concentrations (56). A dielectric barrier discharge reactor with film coating on the ground electrode was investigated to remove NO_x, CO_x, SO_x, and soot. The NO_x reduction was limited to approx 70% (57).

Because NO_2 is the direct product, most researchers tend to convert NO_2 to nitric acid by injecting water vapor, then neutralizing the nitric acid with ammonia to form ammonium nitrate. Compared with NO, NO_2 is highly soluble and reactive with water, aqueous solutions, or alkalis. Gaseous NO, on the other hand, is slightly soluble in water and is not very reactive with typical aqueous solutions. Thus, the plasma oxidation followed by sodium sulfite (Na_2SO_3) absorption was adapted.

A more economical and innovative technology for integrated NO_x control is essential because of the need to develop alternative technologies that can meet the provisions of the Clean Air Act Amendment of 1990. However, the operating cost of the nonthermal plasma technology is far higher than for most of the other technologies (58,59). Our approach is to use the plasma process for NO to NO_2 oxidation because the plasma process is effective and inexpensive, and to use the chemical process for NO_2 reduction because the plasma process is expensive and chemical process is inexpensive. Sodium sulfite (Na_2SO_3), which is one of the strongest reducing chemicals, was used to convert NO_2 to N_2 ($2NO_2 + 4Na_2SO_3 \rightarrow N_2 + 4Na_2SO_4$). The end product of Na_2SO_4 is a nontoxic water soluble compound. The other reaction products such as HNO_2 and HNO_3 in aqueous solution ($2NO_2 + H_2O \rightarrow HNO_2 + HNO_3$) were easily neutralized by the chemical process. In the present study two types of plasma reactors: an ordinary packed-bed reactor and a barrier type packed-bed plasma reactor were compared, and the reaction products and NO_x removal efficiency were measured to optimize the plasma–chemical hybrid process.

2.2.2.2. EXPERIMENTS

The traditional packed-bed plasma reactor was a coaxial type: the inner cylindrical electrode was 16.6 mm and the outer electrode was 47.3 mm in diameter, resulting in a gap distance of 15.4 mm. The ferroelectric $BaTiO_3$ pellets (the relative dielectric constant of 10,000 at room temperature) were packed between the two concentric electrodes with a high AC voltage applied in the radial direction. The $BaTiO_3$ pellets having 1–3 mm in diameter were held by a perforated Teflon plate at both ends. The effective reactor length was 127 mm. The gas steam passes through the entry tube (6.4 mm in diameter) and dispersed into the plasma zone as shown in Fig. 39. On the other hand,
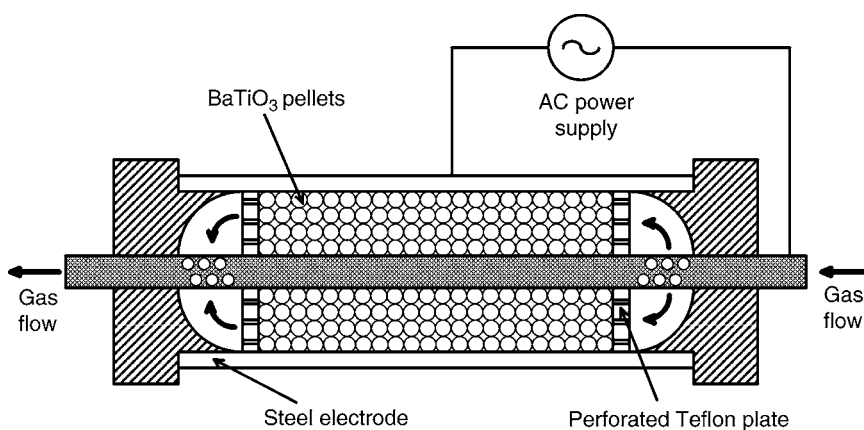
Fig. 39. Ordinary packed-bed plasma reactor.
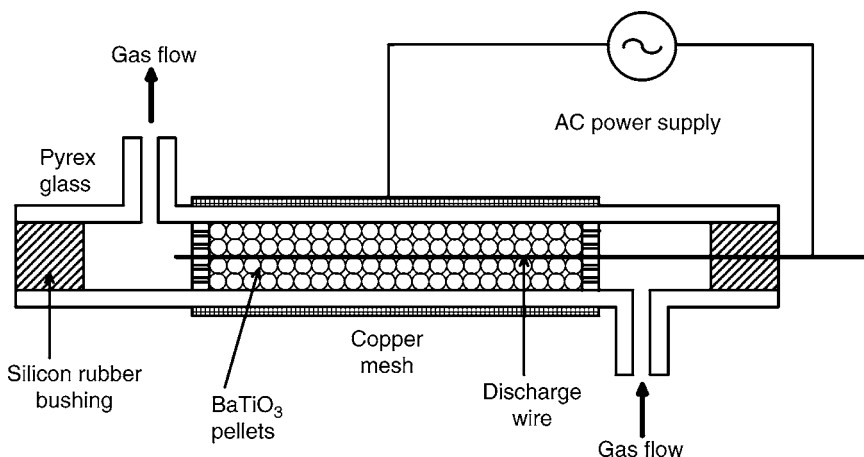
Fig. 40. Barrier-type packed-bed plasma reactor.

the barrier-type plasma reactor consists of a 5 mm diameter wire and a cylindrical glass (20 mm inner diameter Pyrex and 27 cm effective length) as dielectric barrier around which the copper screen was wrapped as a ground electrode, as shown in Fig. 40. Both reactors were energized by a 60 Hz AC power supply (15 kV and 30 mA).

A schematic diagram of this experimental set-up is shown in Fig. 41. The 2% NO balanced with the N_2 in the cylinder was prepared and the dry air was supplied by the compressor through the dryer. The desired NO concentration and flow rate were obtained with the mass flow controller. The gas was then passed through a plasma reactor and a chemical reactor in two stages. The NO, NO_2, NO_x, CO, CO_2, and N_2O concentrations were measured before and after the chemical reactor. The concentrations of these compounds were measured by a Horiba gas analyzer (PG-235, chemiluminescence NO–NO_2–NO_x analyzer, Infrared absorption for CO and O_2 for zirconia method, VIA-510, infrared absorption for N_2O and CO_2). The applied voltage, and the voltage and current wave forms were measured by an oscilloscope (Tektronix TDS380P)
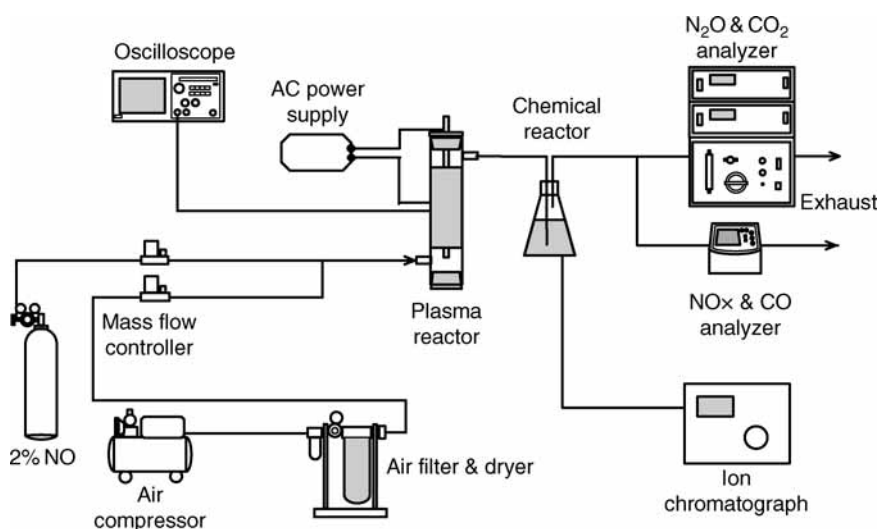
Fig. 41. Schematic diagram of the experimental set-up.

through the voltage divider (Tektronix P6015A) and the current probe. The concentration of HNO_2 and HNO_3 in an aqueous solution were measured by the ion chromatograph (Dionex 2000i/sp).

2.2.2.3. RESULTS AND DISCUSSIONS

2.2.2.3.1. Ordinary Plasma Reactor: Figure 42A shows the NO, NO_2, NO_x, CO, CO_2, and N_2O concentrations when 200 ppm of NO was introduced into the ordinary plasma reactor with the flow rate of 2 L/min. The NO, NO_2, and N_2O increased with increased voltage as observed for the air. However, the NO_2 concentration dropped initially but increased again at a voltage level of 7 kV. This was attributed to the oxidation of air. When these gases passed through the chemical reactor, only NO_2 was reduced to zero, as shown in Fig. 42B. Although, N_2O concentration remained the same, the NO (accordingly NO_x) concentration was decreased from 250 to 190 ppm. The CO_2 concentration was unchanged with voltage. It is clear that the ordinary packed-bed plasma reactor is not superior in relation to NO oxidation and byproducts formation.

Figure 43 shows the NO, NO_2, NO_x, CO, CO_2, and N_2O concentrations in air when the ordinary ferroelectric packed-bed plasma reactor was used with a flow rate of 2 L/min, which corresponds to 2.6 s in residence time. The residence time was calculated without taking the void fraction into account. The NO, NO_2, NO_x, CO, and N_2O increased with increased voltage beyond 5 kV. The NO, NO_2, CO, and N_2O generation from air reaches 180, 250, 50, and 130 ppm at a voltage level of 7 kV, respectively. Note that the voltage indicated here is the peak-to-peak voltage (V_{p-p}). It is known that additional NO_x is induced by the plasma.

2.2.2.3.2. Barrier-Type Plasma Reactor: When the plasma was applied to the air with a flow rate of 2 L/min by a barrier-type ferroelectric packed-bed plasma reactor, the NO, NO_2, NO_x, CO, CO_2, and N_2O concentrations were illustrated in Fig. 44. The CO and N_2O increased with voltage and reached 30 and 5 ppm, respectively, at 2.6 W (16 kV). However, there is no NO formation from air irrespective of residence time and
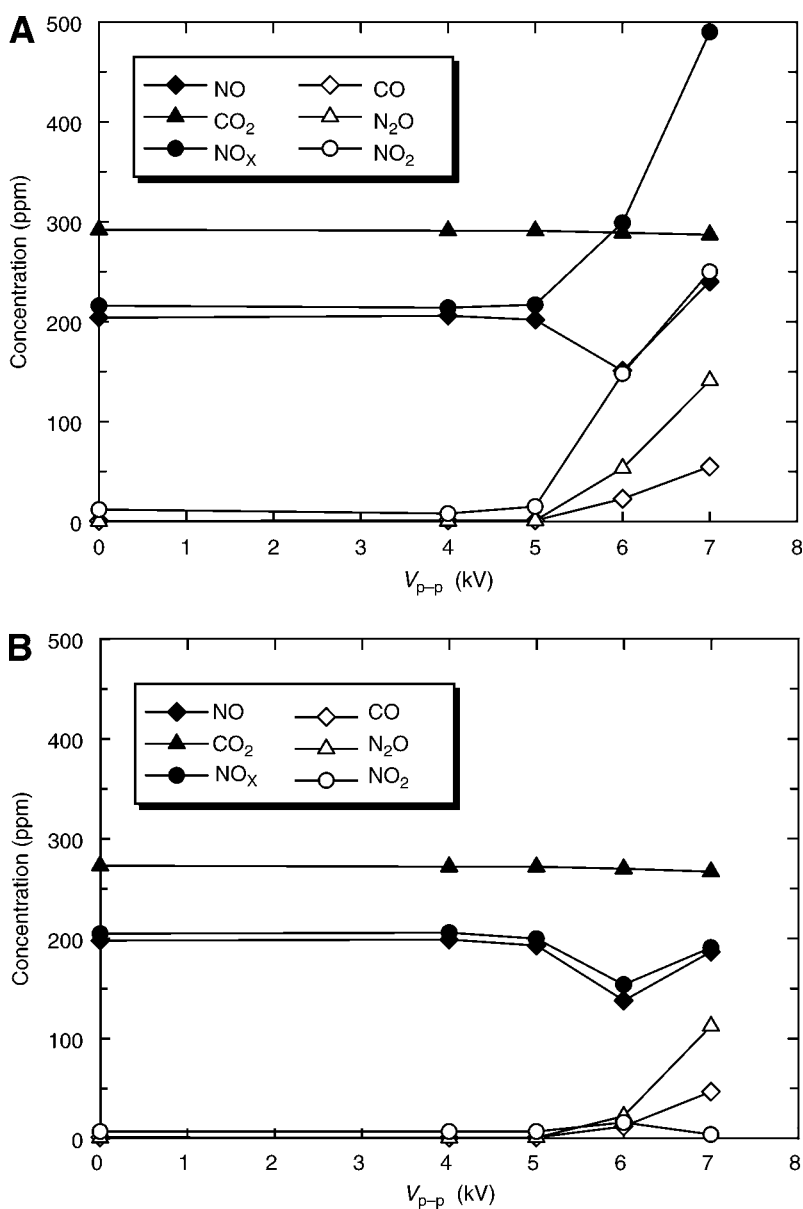
Fig. 42. Byproducts concentrations for decomposition of 200 ppm NO using the ordinary plasma reactor (flow rate = 2 L/min). **(A)** Without chemical reactor. **(B)** With chemical reactor.

applied power (voltage). Note that the power indicated was the power at the reactor. It is observed that the concentration of CO was increased, but NO_x did not increase. This plasma reactor is suitable for NO_x processing.

Figure 45A,B show the NO, NO_2, NO_x, CO, CO_2, and N_2O concentrations before and after the chemical reactor when the flow rate was set at 4 L/min (residence time of 0.8 s). The NO concentration was reduced to 55 ppm at 16 kV, whereas the NO_2
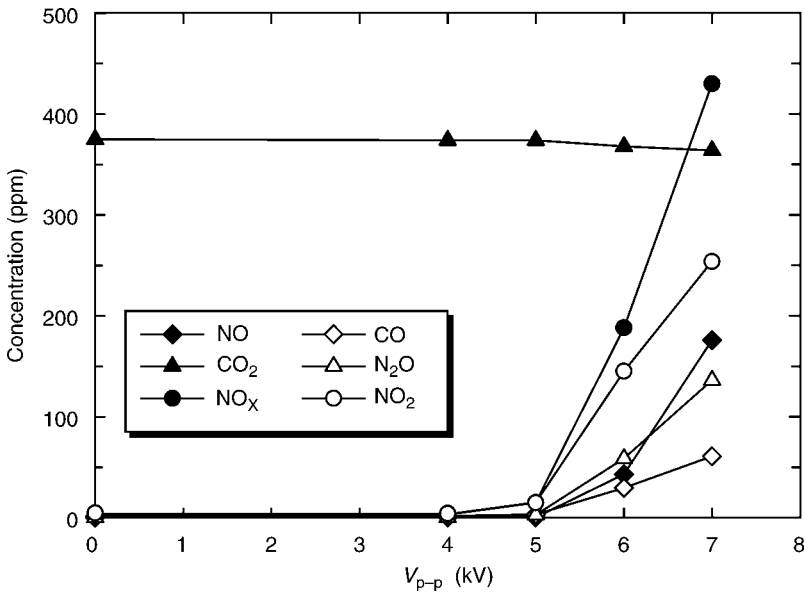
Fig. 43. Byproducts concentrations for decomposition of air using the ordinary plasma reactor without chemical reactor (flow rate = 2 L/min).
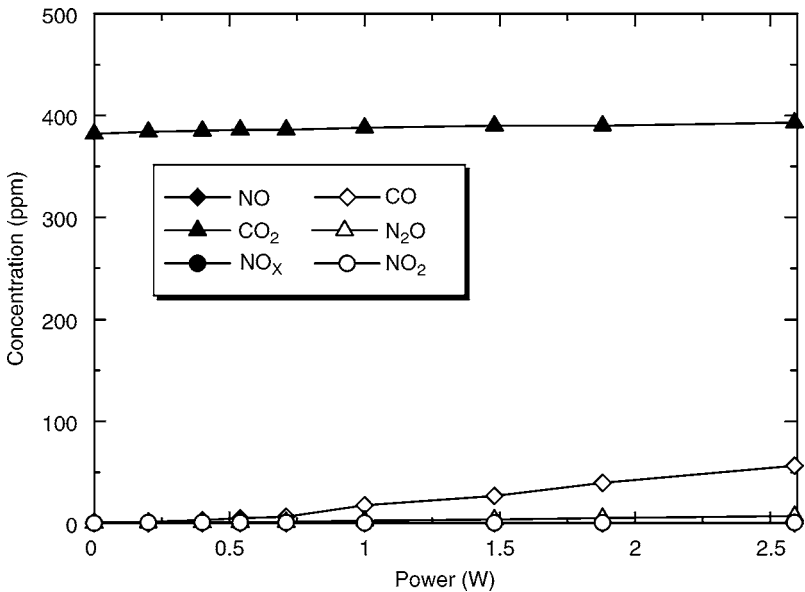
Fig. 44. Byproducts concentrations for decomposition of air using the barrier-type plasma reactor without chemical reactor (flow rate = 2 L/min).

concentration increased to 144 ppm at 2.7 W before the chemical reactor. The CO concentration was 6 ppm and the CO_2 concentration remained at 327 ppm at 2.6 W. These concentrations are expected to further reduce at higher voltage because the spark-over voltage was about 22 kV. After the chemical reactor, the CO and N_2O
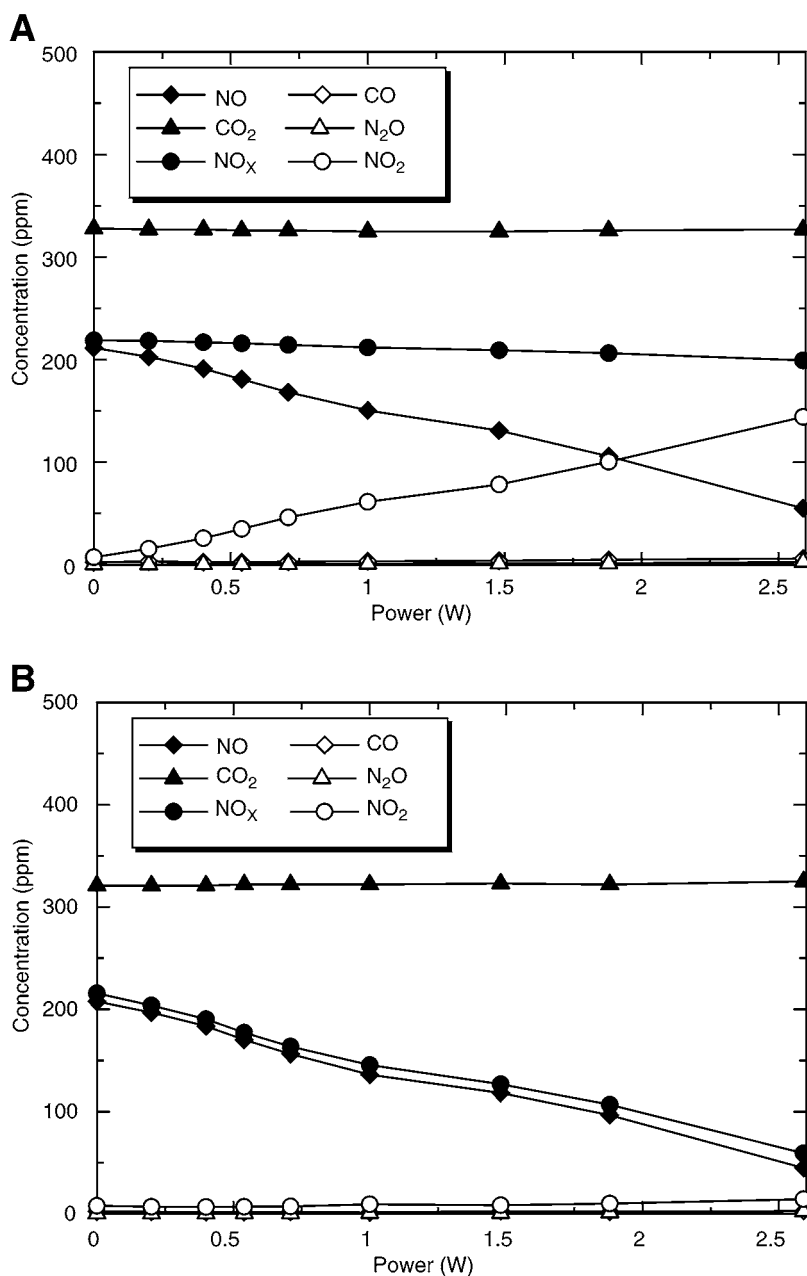
Fig. 45. Byproducts concentrations for decomposition of 200 ppm NO (flow rate = 4 L/min). **(A)** Without chemical reactor. **(B)** With chemical reactor.

concentrations reached near zero at 2.6 W, the NO and NO_x were reduced to 50 ppm level and the CO_2 concentration was slightly increased.

The effect of $BaTiO_3$ relative dielectric constant was investigated on NO to NO_2 oxidation. The dielectric constants used were 870, 1600, 2600, and 5000 and the amount of NO oxidation was not significantly affected by the dielectric constant used in this
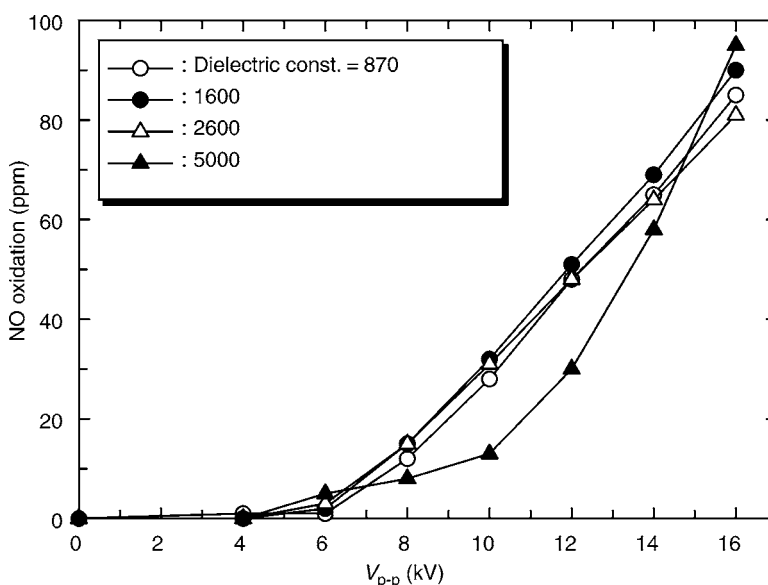
Fig. 46. Effect of $BaTiO_3$ relative dielectric constant on NO oxidation.

experiment as shown in Fig. 46. However, a dielectric constant of less than 10 showed a significant difference (60,61).

2.2.3. Design Example: Cost Calculation of the Hybrid Process

According to our experimental results (51), the power consumption for the barrier-type plasma reactor is 3.3 W for 20°C. When the flow rate is 10 L/min, the specific energy density becomes 18.4 J/L or 23 eV/mole. Because the operating cost for the plasma reactor becomes 1440 USD for NO oxidation (0.05 USD/kWh was assumed) and the operating cost for the chemical reactor is 509 USD/t of NO_2 reduction (0.48 USD/kg was used for Na_2SO_3), the total operating cost of the hybrid process becomes around 2000 USD/t which is more than four times economical than the conventional SCR process.

2.2.4. Dioxin Control

2.2.4.1. DIOXIN

Dioxin is the most toxic substance that a human has ever created. When a guinea pig takes dioxin of only 1 ng/1 g, half of them die (62,63). This toxicity was widely recognized and linked to the deformed child in the "Agent Orange" which contains dioxin, and was used during the Vietnam War. Later, Olie et al. has reported in 1977 that dioxin was found in the vicinity of the incinerator plant. Since then, the dioxin was considered as one of the most important substances of hazardous air pollutants especially in European countries. Many researches have been conducted research related to the generation and formation of dioxin, mechanisms to in entering the human being, and control methods. As a result, the emission guidelines for the incinerator plants were established in 1987.

2.2.4.2. STRUCTURES OF DIOXIN

The structures of dioxin are shown in Fig. 47A,B. Dioxin has the structure in which two aromatic rings are partially replaced with chlorine and are connected with oxygen.
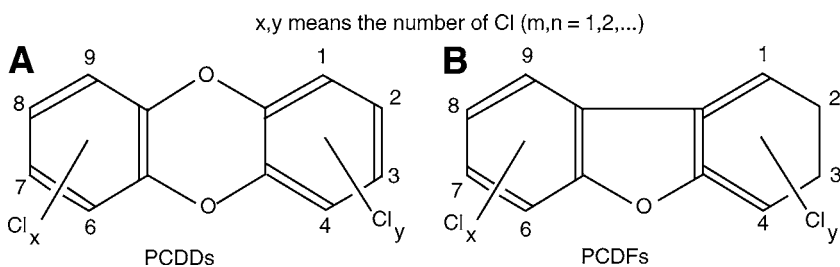
Fig. 47. Chemical structures of dioxin. **(A)** PCDDs. **(B)** PCDFs.

They are called polychlorinated dibenzo dioxines (PCDDs). There are 75 isomers having similar structures but with different positions and numbers of Cls. In these isomers, 2, 3, 7, 8-T4 is most toxic compound in which the positions of 2, 3, 7, 8 are replaced with Cls. On the other hand, furans (polychlorinated dibenzofurans [PCDFs]) have a similar structure to dioxin as shown in Fig. 47B. They have 135 isomers. Dioxin and furans are ordinarily called "dioxin race."

Because the toxicity of a dioxin greatly depends on its chemical structure, the toxicity conversion factors are defined for many isomers based on the toxicity of the most toxic 2, 3, 7, 8-T4 CCD. The toxicity equivalency quantity (TEQ) is defined for each isomer by the product of the toxicity conversion factor and its concentration. For example, the equivalent concentration is expressed as 0.1 ng TEQ/m^3.

Because the dioxins are thermally decomposed at temperature of 800°C, they are not generated so much in the combustion process. Most of them are generated in the low-temperature postprocessing process which is located in the downstream of the incinerator. In order to repress the generation of dioxins, the perfect combustion should be realized in the incinerator by combustion improvements, and the generations of antecedent materials such as chloro benzene (CC), chloro phenol (CP) and carbon should be avoided.

It is also important to remove the fly ash attached to the inner wall of the environmental protection apparatus frequently and keep the gas temperature less than 200°C. Dioxins are also classified into the groups: the gaseous dioxin and the particulate dioxin. Although, particulate dioxins are relatively easily collected by the ESP, it is difficult to remove the gaseous dioxins. The plasma process is one of the promising ways to remove gaseous dioxin. In the next section, the experimental results of gaseous dioxin decomposition by high-energy electrons generated by the nonthermal plasma are discussed.

2.2.4.3. Dioxin Control Using NTP

The bench scale test (50 Nm^3/h) was carried out to demonstrate the decomposition effect of DXNs (64–66) and then the pilot plant scale test (2000 Nm^3/h) followed (67–69). In these tests, the rotating spark gap whose pulse generation rate was up to 200 pps were used, and the moisture content of the exhaust gas was about 20%. The decomposition efficiency of dioxins was obtained to exceed 80% when the corona injection power was more than 5–6 Wh/Nm^3 and the gas residence time in the PPCP reactor was approx 2 s.

Next, a pilot plant facility of the PPCP gas treatment system was installed adjacent to an existing incineration plant (70,71). The PPCP reactor consisted of wire-to-cylinder configuration, energized by the PPCP pulser with the thyristor switch and the magnetic pulse compression circuit. The flow rate of the test gas branched from the outlet duct of the existing electrostatic precipitator, was varied up to 6700 Nm^3/h. The decomposition efficiency for gas-phase dioxins (DXNs) in TEQ base was more than 85% (the best result was 92.4%) when the corona power injection rate exceeded approx 4 Wh/Nm^3. The decomposition characteristics of DXNs were highly affected by the molecular structure and chlorination degrees. The decomposition efficiency of PCDDs with two oxygen atoms between two benzene rings was always higher PCDFs with one oxygen atom. PCBs with no oxygen atom showed the lowest decomposition efficiency among these three chemical families of DXNs. When the chlorination degrees (65,67–70) were larger, the decomposition efficiency became higher. The main components of residual toxic DXNs after the PPCP reactor were PCDFs with five and six chlorines (P5CDFs and H6CDFs). It was confirmed through a series of the pilot plant experiments from the incinerator plant, that the PPCP gas treatment was effective for controlling the gas-phase DXNs, even when the moisture content was approx 35% by volume although the decomposition efficiency drops to approx 73%.

Figure 48 shows the decomposition efficiencies in relation with power injection rate normalized to the gas flow rate. There is the tendency of improvement in decomposition efficiencies with the increase of power injection rate. However, the effect of the power injection rate in the range of 3–6 Wh/Nm^3 seemed to be saturated. There is a big difference in decomposition efficiencies between three different families of DXNs. The highest decomposition efficiency was achieved with PCDDs, followed by PCDFs. The worst was PCBs. With increase in the number of oxygen atoms, the decomposition efficiencies increase. This fact leads to the assumption that the decomposition process is caused by the dissociation of C–O bond between two benzene rings. This assumption, of course, needs further verification. It is also clear from the figure that more than 95% of NO$_x$ reduction was obtained when the inlet NO concentration was in the range of 119–152 ppm, gas flow rate of 20–50 Nm^3/h, and the gas temperature of 180°C.

The total TEQ reduction is affected by the decomposition efficiencies of PCDFs because in this particular incineration plant, about 2/3 of the total TEQ at the inlet of the PPCP reactor attributed to PCDFs, as shown in Fig. 49 in which TEQ distribution of individual components is indicated both at the inlet and outlet of PPCP reactor. Most of the total TEQ at the outlet were from T4CDFs, P5CDFs, and H6CDFs whose chlorination degrees are 4, 5, and 6, respectively. Even in the inlet these three components showed high concentrations and the decomposition efficiencies of these three components are lower than the other components. The distribution of DXNs components differ from each incineration plants, but it is important to raise the decomposition efficiencies of the PCDFs components with lower chlorination degrees.

The gas treatment systems of the incineration plants are combinations of dust collection and decomposition/separation of gaseous pollutants. In the case of DXNs removal in exhaust gases from the incineration plants, the dust collector removes more than 90%. However, the removal of DXNs in dust is not sufficient, and the removal of gaseous DXNs becomes important. It is confirmed through this pilot plant tests that
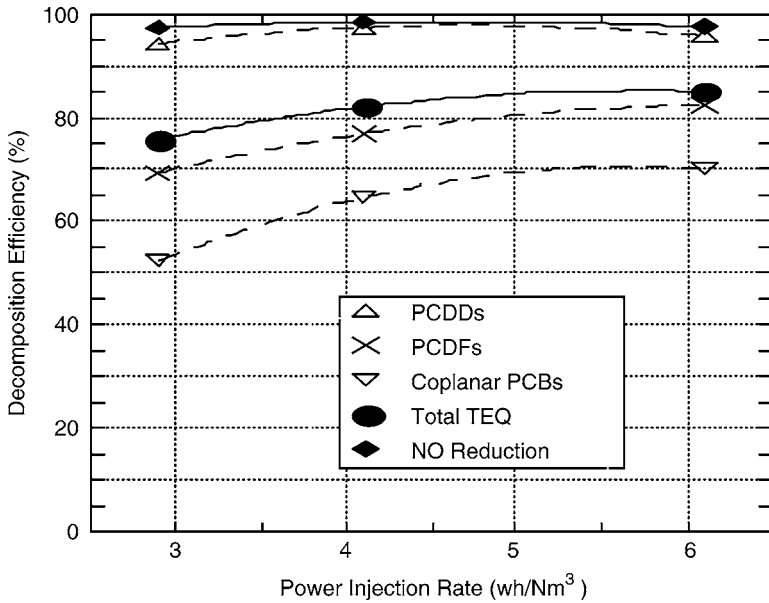
Fig. 48. Decomposition efficiencies in relation with power injection rate normalized to the gas flow rate.
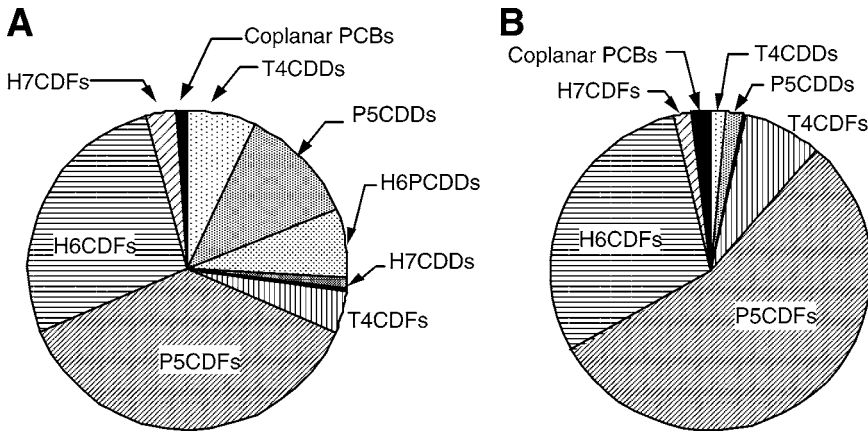
Fig. 49. Distribution of TEQ attributed to individual chlorination degrees. **(A)** Inlet of PPCP reactor. **(B)** Outlet of PPCP reactor.

DXNs decomposition efficiency by the PPCP gas treatment system is in the level applicable to the real plants (9,10).

2.3. Nonthermal Plasma Application for Detoxification

The first nonthermal plasma application was reported by Masuda in early 1980 for NO_x and SO_x removal using an extremely short pulse power supply, which was called the pulsed corona induced plasma chemical process (PPCP) (64,65,72). The details were discussed in application on the section of NO_x and SO_x removal. The electron

beam technology is one of the nonthermal plasma technologies and significant development has been made since 1970. This technology was shortly explained in the Section 1.2.2.5.

In the early 1980s during the Cold War, air purification study was necessitated to protect humans from chemical warfare (CW) agents. Initially, individual respiratory protection is provided through the use of gas mask with CW agent removal for the air stream accomplished with particulate filters and charcoal beds. Charcoal has been the primary candidate for use to remove CW agent vapors, although, other concepts such as alternative sorbents, chemical reactions, and combustion (direct or catalytic) have been considered. However, practical limitations have been recognized as life-time, deposition of other contaminant, frequent replacement, logistic problem, effect of humidity, weight, and disposal. A potential alternative to charcoal absorption was to use the corona discharge.

2.3.1. Detoxification With DC Corona Discharge

The DC corona device to handle a 30 cfm (cubic feet per minutes) was constructed to decompose a simulant CW gas, i.e., dimethyl methyl phosphonate (DMMP). The DC corona reactor consists of a narrow-gap, multiple point-to-plane geometry in which the gas passes through a corona discharge at high velocity (approx 100 m/s) as shown in Fig. 50 (73). Ozone was thought to be the primary agent in the gas destruction. Experiments have shown that more ozone can be generated with an increased current density (or voltage) and that increasing the gas velocity will increase the spark-over potential considerably. The experimental results showed that the average field strength and current per needle sustained as high as 18 kV/cm and 1 mA/needle, respectively. The ozone generation rate was approx 250 ppm/kW of the corona power and the destruction efficiency was proportional to the ozone generation. However, the decomposition efficiency was in the range of 15%. It was not additive in respect to the number of corona points and reactor length, and it was further reduced by increasing the needle-to-plane distance (73).

For detoxification, it is likely that the radicals and excited atomic species resulting from electron activation in the discharge region have the greatest impact. Kondo and Miyoshi (74) reported that spectroscopic evidence estimated a temperature in of 1000 K near the point corona. It is speculated that the active zones for either a high electron activity or high temperature are in a very narrow confined region near the corona point which results poor decomposition efficiency.

2.3.2. Model Study

Yamamoto et al. (75) conducted a model study for Townsend avalanche mechanisms and the results were incorporated into a narrow-gap three-dimensional (3D) corona discharge model for the multiple-points to plane geometry. The Townsend avalanche model generate ion and electron concentrations as a function of distance from the corona point. The results are sufficiently conclusive to show that few electrons are found more than 3 mm from the corona point. Thus, if the electron concentration is an important factor in chemical reaction, then the 3 mm gap devices should work much better than devices with a larger gap. The 3D ion flow simulation showed that, although, the low electron-force density region can be minimized by reducing the point-to-plate spacing,
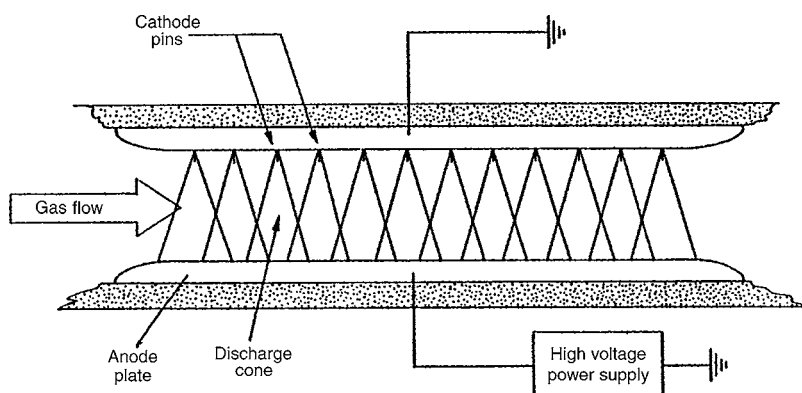
Fig. 50. Glow discharge flow channel (© 1991 IEEE).

there is still a considerable fraction of nonactive zones, resulting in electrical sneakage. If high temperatures are significant contributors to the agent destruction, then the model assumes that the zone of the high temperature zone is less than 1 mm. This is in accordance with both the magnified observations of the active region of the corona and the spectroscopic measurements (74).

Figure 51 shows the single-stage triangle-shaped DC corona device which was selected to reduce the electrical sneakage because the triangular shape seems a good approximation of the visual shape of the corona in air. The laboratory DC corona device was designed with the reactor housing constructed of Teflon for both chemical inertness and electrical resistance. Standard 0.32 cm (1/8 in.) tubing fittings were used for the gas flow into and out of the device. A high-voltage power supply was connected through for 20 MΩ high voltage ballast resistors to stabilize the corona discharge. The corona current was collected on a flat stainless-steel plate. The electrode used was a sewing needle with a point diameter of about 100 μm. The distance from the needle electrode to the ground plate in the two cases was 0.4 cm and 0.7 cm, respectively, and the reactor length in the direction of gas flow was only 0.64 cm (1/4 in.) for both devices. A flow rate of 75 cm^3/min was maintained throughout the tests.

The decomposition efficiency achieved was $42 \pm 8\%$ for 0.4 cm spacing and $72 \pm 8\%$ for 0.7 cm spacing. The maximum efficiency was achieved at the highest electric field of approx 12 kV/cm for a 0.4 cm device and 13 kV/cm for 0.7 cm. The corresponding residence times in these devices were 0.04 s for 0.4 cm spacing and 0.14 s for 0.7 cm spacing. Two levels of DMMP concentration (5 and 10 μg/L) and moisture content (approx 0 and 10%) were examined. However, the decomposition efficiency did not show a significant difference in these parameters. Another factor affecting the efficiency would be the ionic wind (or electric wind) caused by the corona discharge that enhances the turbulence or mixing in the gas stream.

The 3D numerical simulation for determining the electrical force density distribution was also performed to obtain the optimum reactor configuration. Based on the experimental and numerical modeling results, the optimum shape of the triangle corona device has an equilateral and apex angle of about 60° with a point-to-plane
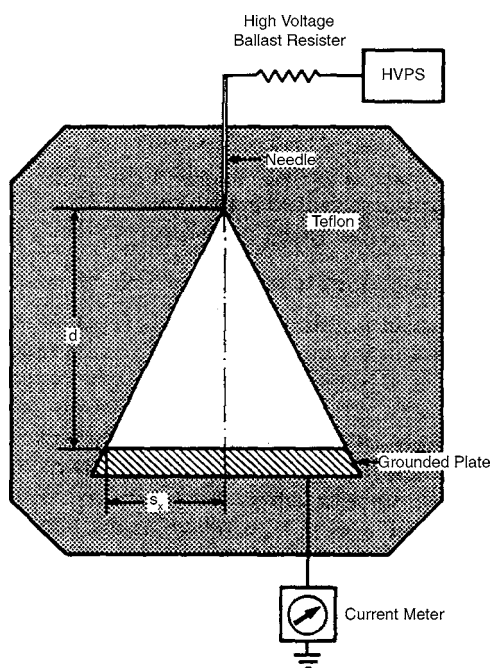
Fig. 51. Schematic diagram of inner electrode configuration (© 1991 IEEE).

distance of approx 0.7 cm (76). The reactor was further improved to adapt the afore-mentioned design requirement: the circular cylinder, which was divided into six sections by the dielectric material. The center has six needles for each housing. This design was accomplished to minimize the electrical sneakage across the entire reactor zone but the experimental results were not obtained.

2.4. Air Cleaner for Odor Control

Nonequilibrium plasma can be defined as an electrically neutral and chemically activated ionization state in which the electron temperature is significantly higher than the gas or ion temperature. Using an AC high voltage or a pulse high voltage with sharp rising time of several to several hundred nanoseconds, nonthermal plasma can be induced at atmospheric-pressure and temperature. The hazardous air pollutants can be cleaned with nonthermal plasma. A barrier electric discharge, glow discharge or surface discharge is mainly used for nonthermal plasma treatment. The nonthermal plasma can be generated with lower energy than the thermal plasma. The plasma is able to promote chemical reactions such as oxidization or decomposition when exposed to odorous gases. The nonthermal plasma in which the average electron temperature is in the range of 4–5 eV, the electron density is $10^{10}/m^3$ is often used. This technology was commercialized as the PPCP system for treating hazardous air pollutants. Applications of the nonthermal plasma to odor control have been reported on the deodorization from sewage disposal plant, refuse disposal plant, and livestock farm near the human environment (77,78). In this section, the research on indoor air purification or odor control technology using plasma is described in the following section.
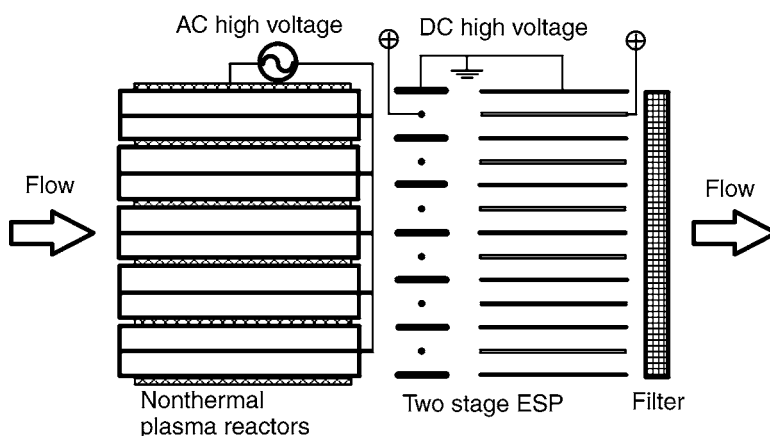
Fig. 52. Electric air cleaner composed of nonthermal plasma reactor, two stage ESP and functional filter (© 2001 IEEE).

2.4.1. Indoor Air Cleaner Using Nonthermal Plasmas

Odor control from living environment has become an increased concern. One of the main odor sources in living environment is cigarette smoke. More than 4000 chemical components are identified in the cigarette smoke (79). These are roughly classified into two groups; gaseous compounds such as acetaldehyde (CH_3CHO) and ammonia (NH_3), and particulate matter such as tar. Recently, various kinds of indoor electric air cleaners using the application of electrostatic precipitators (ESP, *see* Section 2.1.) have been manufactured to improve the living environment. Although, a wide range of airborne particles can be removed effectively with an ordinary electrostatic air cleaner, it is impossible to remove gaseous compounds from cigarette smoke using the ESP. Using nonthermal plasma, experimental studies or new electric air cleaners have been reported on the removal of these gaseous compounds (80–85). An example of a new type of indoor electric air cleaner which realizes simultaneous removal of airborne particles and odors was developed (86). It is made up of a nonthermal (nonequilibrium) plasma reactor followed by a two-stage ESP as illustrated in Fig. 52.

The experimental results on CH_3CHO, NH_3, and cigarette smoke removals are reported in detail (87). Two kinds of AC nonequilibrium plasma reactors are employed: one is the packed-bed plasma reactor, the other is the film-type plasma reactor consisted of laminated parallel steel plate electrodes. In this reactor, the electrically grounded plates are wrapped with a thin film of high dielectric material. The results are shown in the next section.

2.4.2. Odor Removal Using the Packed Bed Plasma Reactor

A barrier-type packed-bed plasma reactor as shown in Fig. 53 is used for the removal of gaseous CH_3CHO and NH_3. It consists of a 1.6 mm diameter wire electrode and a Pyrex glass tube (20 mm inner diameter and 24 mm outer diameter) as dielectric barrier around which the copper screen is wrapped as the other electrode. The 1.7–2 mm in diameter $BaTiO_3$ pellets (the relative dielectric constant of 10,000 at room temperature)
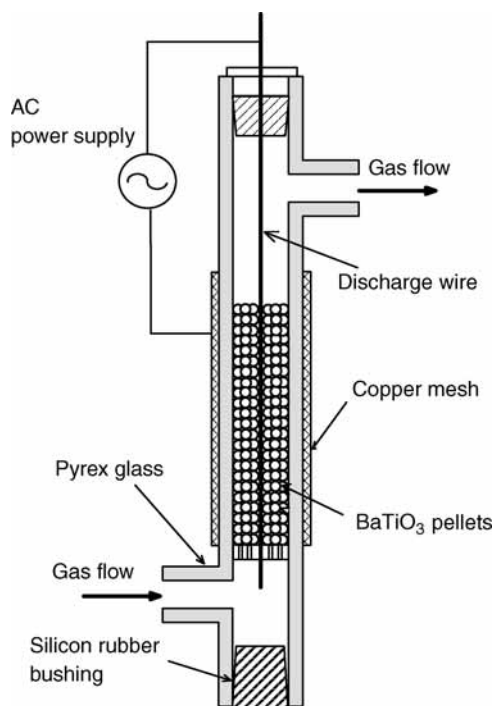
Fig. 53. Barrier-type packed-bed plasma reactor (© 2001 IEEE).

are packed inside the tube. The width of the copper mesh electrode H_m is set at a length of 260 mm. The AC high voltage (max 20 kV) of 60 Hz is applied to the reactor using a neon transformer. Nonequilibrium plasma is induced between the pellets. The experimental setup is shown in Fig. 54. The 1020 ppm CH_3CHO and 950 ppm NH_3 balanced with N_2 are prepared in the cylinders and the dry air (relative humidity = 4%) is supplied by the compressor through the dryer. The desired CH_3CHO and NH_3 concentrations are obtained with the mass flow controller on each line. The flow rates are varied at 1, 2, and 4 L/min. The removal efficiency of CH_3CHO and NH_3 are evaluated using an FID (flame ionization detector) GC, and the gas detection tubes, respectively. The concentrations of byproducts such as CO, CO_2, NO, NO_2, and N_2O are measured using a set of gas analyzers. The concentration of ozone was measured using the gas detection tubes.

Figure 55 shows the removal efficiency of 100 ppm acetaldehyde balanced with dry air when the flow rate is at 1, 2, and 4 L/min in the packed bed-plasma reactor. The specific energy density, SED based on the discharge power in the plasma reactor (SED = discharge power/flow rate) is used for the horizontal axis. At a fixed SED, the removal efficiency increases with the increase in the flow rate. When the flow rate is 1 L/min, the concentration becomes minimum at SED of 146 J/L (V_{p-p} = 16 kV). This optimum value of SED decreases with increased flow rate and becomes 94.5 J/L at a flow rate of 4 L/min. More than 95% of removal efficiency is obtained with the flow rate of 4 L/min. The concentration of byproducts, such as CO and CO_2 increase with increase in SED as CH_3CHO is removed. However, the concentrations of NO, NO_2, and N_2O are relatively
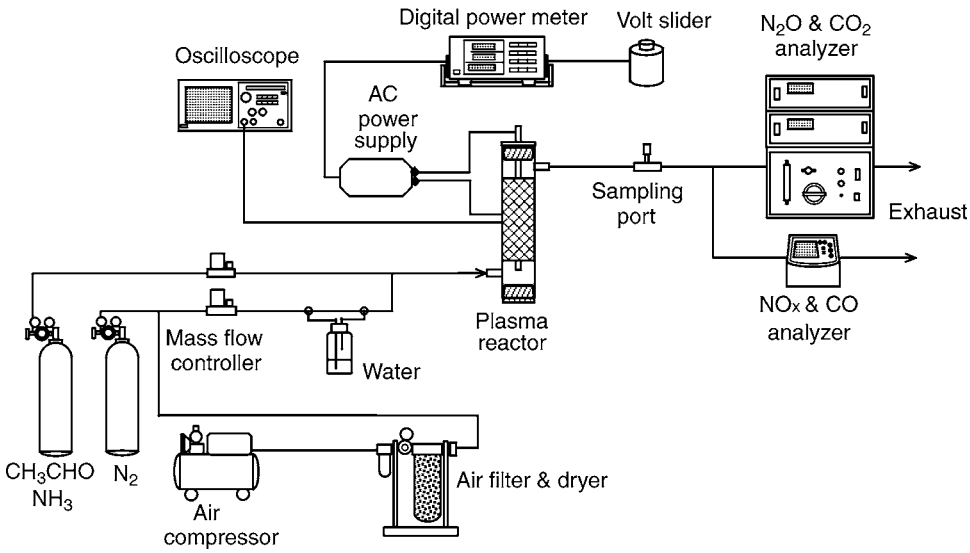
Fig. 54. Experimental setup for acetaldehyde and ammonia removal using the packed-bed plasma reactor (© 2001 IEEE).
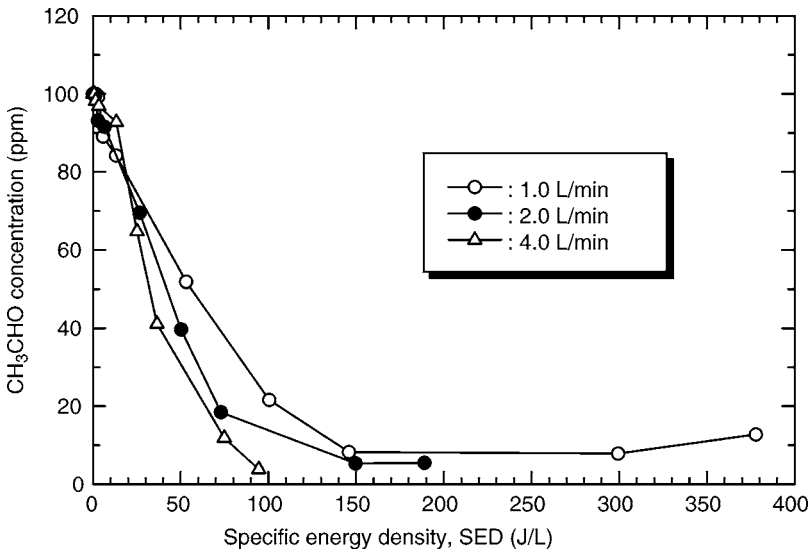
Fig. 55. Acetaldehyde concentration vs specific energy density under dry air using the packed-bed plasma reactor (initial concentration of $CH_3CHO = 100$ ppm) (© 2001 IEEE).

low. Considering the carbon balance, acetaldehyde is effectively converted to CO, CO_2, and other hydrocarbons by nonthermal plasma. It is clarified that radical species such as active oxygen (O), nitrogen (N), and (OH) play a key role than O_3 in CH_3CHO removal.

Figure 56 shows the removal efficiency of 20, 60, and 100 ppm NH_3 balanced with dry air when the flow rate is set at 1 L/min. 100% NH_3 removal is achieved at SED = 265 J/L. The concentration of N_2O is about 10 ppm at SED = 219 J/L (V_{p-p} = 16 kV)
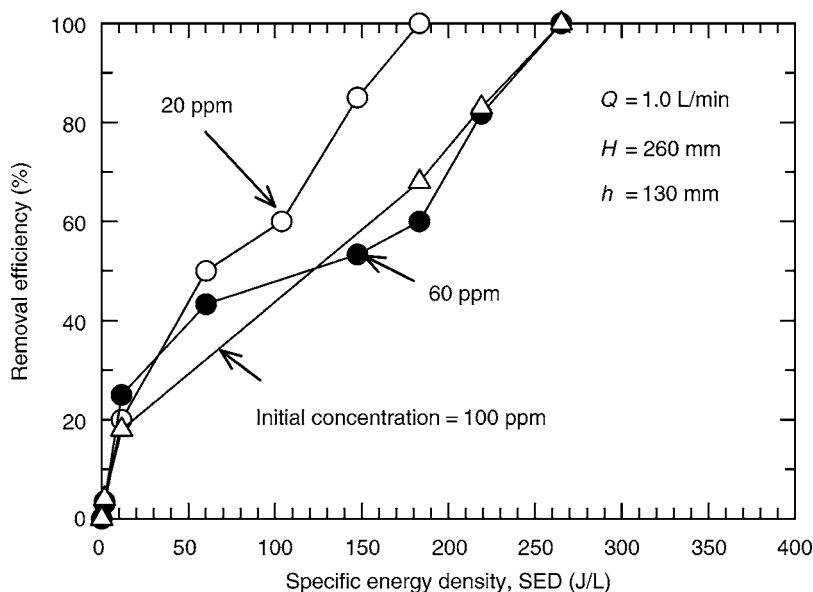
Fig. 56. Effect of initial concentration on ammonia removal (© 2001 IEEE).

but, the concentrations of NO_x and CO are low. A large amount of white powder observed inside the wall of the plasma reactor, is identified as NH_4NO_3 aerosol produced as the reaction of induced HNO_3 and NH_3.

2.4.3. Odor and Cigarette Smoke Removal Using the Dielectric Barrier Plasma Reactor

The plate-type, dielectric-barrier discharge plasma reactors are widely used for ozone generation, odor, and VOC removal. A film-type plasma reactor shown in Fig. 57 is used for the removal of gaseous CH_3CHO, NH_3, and cigarette smoke (87). It consists of aluminum electrodes with many sharp projections and the other aluminum electrodes wrapped with polyester film. The 60 Hz AC high voltage (max 8 kV) is applied to the wrapped electrode and the other electrode is grounded. The effective reactor length is 40 mm and the gap between the two electrodes is 2.5 mm. The 90 ppm CH_3CHO and 100 ppm NH_3 are balanced with dry air (relative humidity = 4% at 25°C). The flow rate is set at 5, 10, and 20 L/min, and the corresponding residence times are 7.5, 3.8, and 1.9 s, respectively. The removal efficiency of CH_3CHO is evaluated with the sample using the GC. The removal efficiency of NH_3 is measured using the gas detection tubes and an FT-IR (Fourier transform infrared) analyzer. The concentrations of byproducts such as O_3, HNO_3, HCOOH, CO, and N_2O were also measured using the FT-IR.

Experiments are carried out using the cigarette smoke. A Japanese cigarette (Mild Seven) is burned using the dry air with a flow rate of 1 L/min. The particulates in the cigarette smoke are first removed with the glass fiber filter. After the plasma treatment, the concentrations of CH_3CHO and NH_3 in the smoke are measured using a GC and the gas detection tube.

Figure 58 shows the removal efficiency of acetaldehyde in dry air when the flow rate was set at 5, 10, and 20 L/min, respectively. At a fixed SED, the removal efficiency increases with increase in the flow rate. The maximum removal efficiencies are 88% for
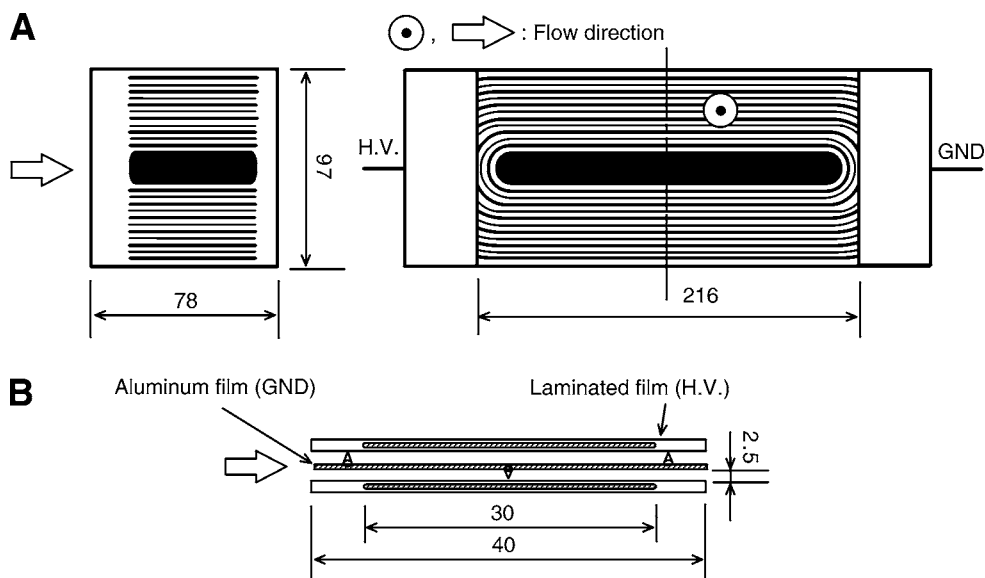
Fig. 57. Film-type plasma reactor (© 2001 IEEE). **(A)** Frontal and cross sectional views. **(B)** Details of the film electrode section.
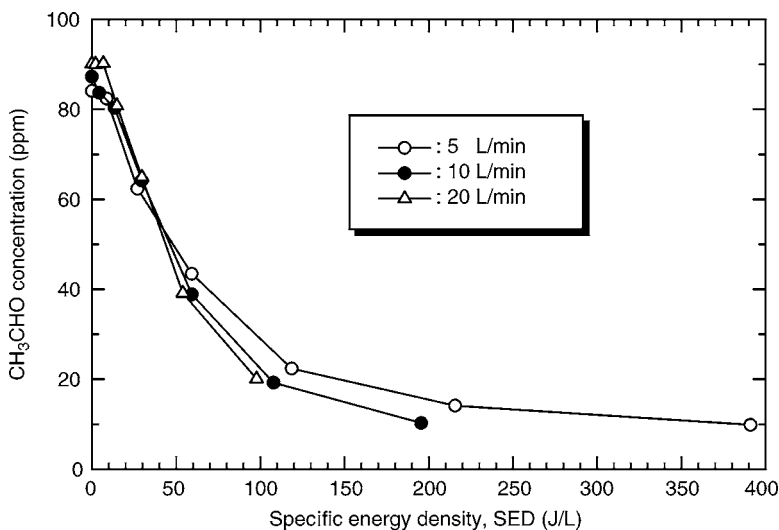
Fig. 58. Acetaldehyde concentration vs specific energy density in dry air using the film-type plasma reactor (© 2001 IEEE).

5 L/min, 87% for 10 L/min and 78% for 20 L/min. It is known from the byproducts measurement using a FT-IR analyzer that O_3, HNO_3, $HCOOH$, CO, CO_2, and N_2O are induced when CH_3CHO is removed.

Figure 59 shows the removal efficiency of 100 ppm NH_3 in dry air when the flow rate is set at 5, 10, and 20 L/min. In this figure, 100% removal is accomplished at the applied voltage 8 kV for the flow rate of 5 and 10 L/min (SED = 196 and 391 J/L). The removal
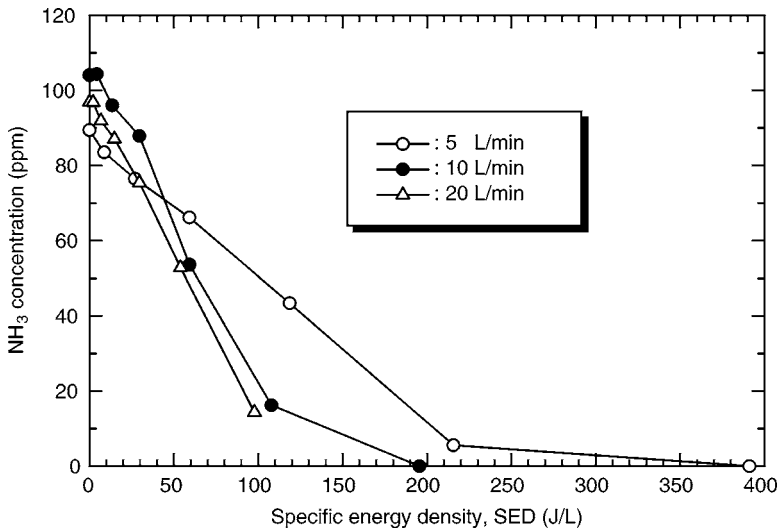
Fig. 59. Ammonia concentration vs specific energy density under dry air using the film-type plasma reactor (© 2001 IEEE).

efficiency is 85% with the flow rate of 20 L/min. The reaction byproducts such as gas components of O_3, CO, CO_2, N_2O, HNO_3, and HCOOH, and aerosol of NH_4NO_3 are identified when NH_3 is removed. A large amount of NH_4NO_3 white powder is observed on the grounded electrodes after the experiment. This aerosol is induced by the reaction between the NH_3 and the induced HNO_3. Those aerosols can be easily removed by the ESPs or filters.

The experiments are further carried out using real cigarette smoke. In the result, one of the components, NH_3 is completely removed at SED of 150 J/L with the efficiency of over 90%. However, removal efficiency of CH_3CHO is reduced to 50% because of its low concentration.

2.4.4. Design Example: Indoor Air Cleaner Using Nonthermal Plasma

Problem

The system as shown in Fig. 52 is designed in which odorous gas including NH_3 and CH_3CHO are decomposed or converted into aerosol by the plasma reactor in the first stage of the system, and in the second stage the induced aerosols are completely collected by the electrostatic force. The volumetric flow rate is assumed to be 10 m³/min (25°C, 1 atm). Determine the specification of the air cleaner system.

Solution

In the first stage or the plasma reactor, the distance between the discharge wire and the outer grounded electrode is usually taken as $r_a = 1$–3 cm in order to produce the stronger plasma possible. Here, $r_a = 3$ cm is assumed. The residence time should be taken around $t_r = 0.5$ s for more than 90% removal efficiency. When the length of the plasma reactor L_p is assumed to be equal to 50 cm, the following equations hold:

$$t_r = \frac{L_p}{v_{ave}}, \quad v_{ave} = \frac{Q_s}{\pi r_a^2} \tag{98}$$

where v_{ave} is the mean velocity inside the reactor and Q_s is the volumetric flow rate for a single reactor. The flow rate of a single reactor is

$$Q_s = \frac{\pi r_a^2 L_p}{t_r} = \frac{3.14 \times 0.03^2 \times 0.5 \times 60}{0.5} = 0.170 \text{ (m}^3/\text{min)} \tag{99}$$

Therefore, the number of the annular type plasma reactor $10/0.170 = 59$ is required for parallel connection. For a single reactor, square cross-section of $6 \times 6 = 36$ cm² is needed. It can attain with the square of every direction $6 \times 8 = 48$ cm. Moreover, the power consumption is calculated with SED = 1 J/L = 1 kJ/m³

$$P = \frac{1 \left(\dfrac{\text{kJ}}{\text{m}^3}\right) \times 10 \left(\dfrac{\text{m}^3}{\text{min}}\right)}{60 \left(\dfrac{\text{s}}{\text{min}}\right)} = 170 \text{ (W)} \tag{100}$$

Unfortunately, the SED of nonthermal plasma reactor is in the order of 10 J/L in the current status. It is necessary to attain the further optimization of the energy efficiency in the nonthermal plasma reactor. In addition, the design of the second stage of an electric precipitator system is discussed in the Section 2.1. and the books on the ESP (30) and aerosols (41,88).

2.5. Ozone Synthesis and Applications

2.5.1. Principle of Ozone Synthesis

The ozone generation system by corona discharges was developed by Simens (89) approx 100 yr ago. A silent discharge, as shown schematically in Fig. 60, is generally used in which the implementation of silent discharge corresponds to a capacitor that has two dielectrics between its plates. This system is one of the more famous applications of corona discharge. In ordinary ozonizer using a silent discharge, the gap distance is 2–3 mm. Recently, the generation amount of ozone has improved greatly by making the gap distance as 0.05–0.2 mm (90,91).

To obtain a higher efficiency, a surface discharge type ozonizer was recently developed. Figure 61 shows an example of high concentration ozone generating equipment by adapting the principle of the surface discharge induced plasma chemical process (SPCP) (81,92,93) and the cross-section of the surface discharge electrode. Because the discharge electrode is protected with the glass coating, it has good reliability and durability as previously shown in the Fig. 12. It is useful for ozone water processing. In addition, there are many other applications, such as semiconductor manufacturing, surface treatment, medical application, and food processing. Table 6 shows the main specification of these ozonizers.

Commercial ozonizers usually have an energy yield of 90 and 150 g/kWh for dry air and pure oxygen gas, respectively. Because the theoretical limit of energy yield is 1200 g/kWh, 92.5% of the energy in a silent discharge is lost as heat. The ozone generated in a discharge is a two-step process as follows:

a. Generation of oxygen-free radicals by O–e collision processes:

$$O_2 + e \rightarrow O_2^+ + 2e \quad \text{direct ionization} \tag{101}$$
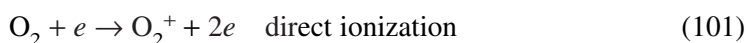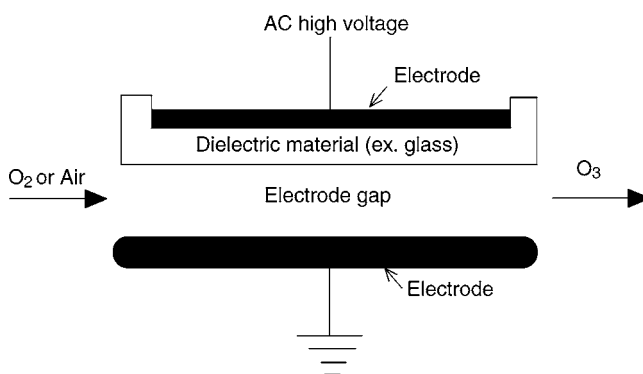
Fig. 60. Typical silent discharge ozonizer.
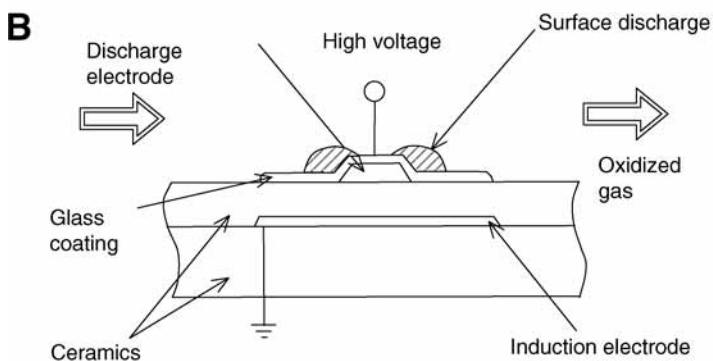
Fig. 61. Commercially used ozonizers and the shapes of surface discharge electrode for high voltage (courtesy of Masuda research inc.).

$$O_2 + e \rightarrow O^+ + O + 2e \quad \text{dissociative ionization} \tag{102}$$

$$O_2 + e \rightarrow O + O + e \quad \text{dissociation} \tag{103}$$

$$O_2 + e \rightarrow O^- + O \quad \text{dissociative attachment} \tag{104}$$
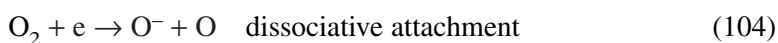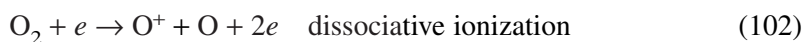
Table 6
Specification of the High Performance Ozonizers

Model	OZS-MC702D-4WJ	OZS-FC-2/10-AC
Ozone concentration	140 g/Nm^3 (10 NL/min)	90 g/Nm^3 (1 NL/min)
Ozone production	150 g/h (25 NL/min)	15 g/Nm^3 (5 NL/min)
Gas flow rate (NL/min)	10–25	<5
Material gas	Oxygen	Oxygen
Operation pressure	0.12 MPa (12 kgf/cm^2)	0–0.05 MPa
Cooling water	6 L/min (at 15°C)	Air cooling
Power supply and power	AC200V, 50/60Hz, 2.7 KVA	AC100V, 50/60Hz, 0.8 KVA
Environmental condition	Indoor, 5–35°C	Indoor, 20°C (5–35°C)
Size	W600 × D700 × H1100 mm^3	W300 × D500 × H700 mm^3
Mass	About 130 kg	About 45 kg

Courtesy of Masuda Research Inc.

b. Generation of ozone by free radical reactions:

$$O + O_2 + M \rightarrow O_3 + M; \ \ M = O_2 \text{ or } N_2 \tag{105}$$
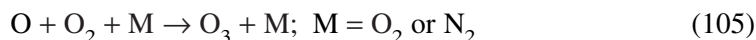
where the details of other secondary reactions are explained in the ref. 90,94. The reaction (101) is induced by a number of electrons having an energy level higher than 12.2 eV. The reactions in Eqs. (102)–(105) occur by the electrons having energy of 5–8 eV. Except for dissociative attachments, the reactions in the first step a are not significantly influenced by gas temperature. However, the reaction rate of the second step b appears to be significantly influenced by gas temperatures, in which reaction rate, hence, ozone generation rate decreases with increasing gas temperature. The ozone generation processes are substantially reduced by increasing gas temperature, although the ozone loss processes are significantly enhanced by increasing gas temperature. Therefore, if we operate an ozonizer in lower temperature conditions, substantial enhancement of ozone generation can be expected.

2.5.2. *Application of Ozonizer*

There are many industrial applications of ozone such as the cleaning of semiconductor chip, whiting of pulp, killing the virus from drinking water, wastewater treatment, and odor removal, and so on. Because it is impossible to cover all applications here, several examples of applications are discussed.

2.5.2.1. Small Ozonizer for Indoor Air Cleaning

It is known that odor components are oxidized or decomposed by injecting ozone or chemically activated radicals such as O, N, OH, H$_2$O$_2$, which is produced by the discharge reactor. This is one of the application as an ozonizer. Figure 62 shows the photographs of a small ozonizer for indoor and automobile odor control (93). Very small amounts of ozone lower than safety standards concentration (<1 ppm) and nitrogen radicals are continuously supplied by the ozonizer only with several 10 W of power consumption. Offensive odor and uncomfortable gas components suspended inside the room or automobile are decomposed or removed to achieve a comfortable environment. The target odors are smells of cigarette smoke, sickroom,
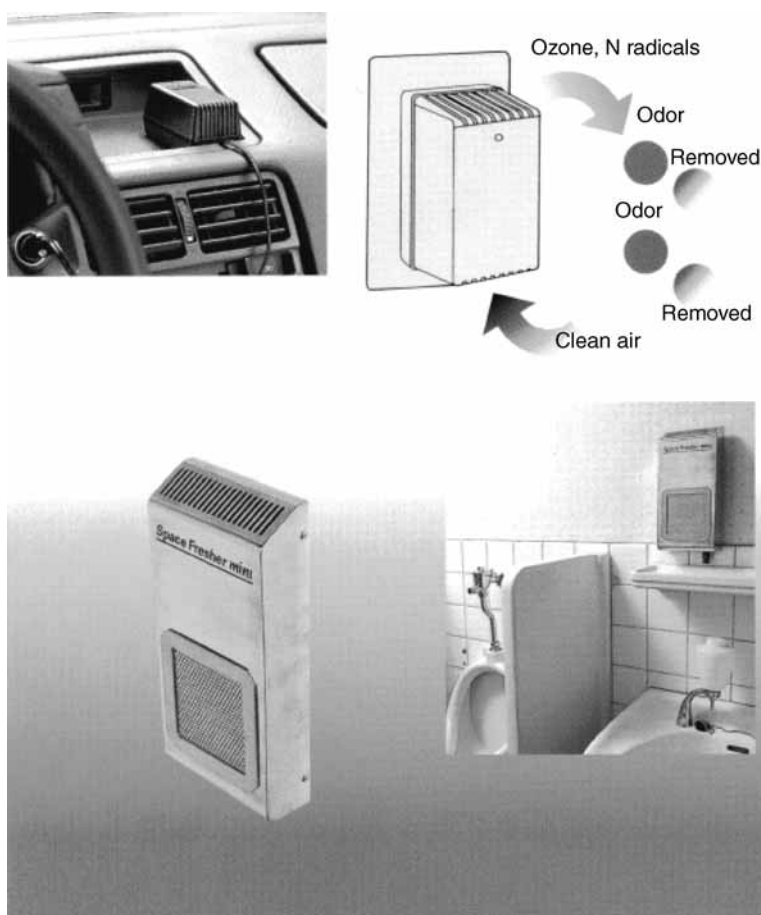
Fig. 62. Small ozonizers and principle of odor removal by ozone or radical injections (Courtesy of Masuda research inc.).

pet, toilet, exhaust gas, mold and so on. Moreover, it will be useful for the sterilization of air.

2.5.2.2. COMMERCIAL PLANT FOR ODOR REMOVAL USING OZONE INJECTION

Ozone water is formed by an ozonizer, and odorous gas passes through the chemical scrubber. In these procedures, odorous gas from factories and wastewater treatment plants can be processed.

The schematics of ozone and radical injection commercial plant is shown in Fig. 63 (95). Because ozone generally becomes more reactive under humidified condition, a water-washing scrubber is additionally built and water-soluble components are absorbed simultaneously (96,97). In addition, ozone is easily decomposed at the outlet of the system to a level that does not have influence in the human body by installing decomposition equipment with activated carbon or a heating furnace ($T = 300°C$) after the chemical scrubber.

Odor control using ozone is an excellent method from the standpoint of energy efficiency. This method is especially effective for ammonia, trimethyl amine, dimethyl
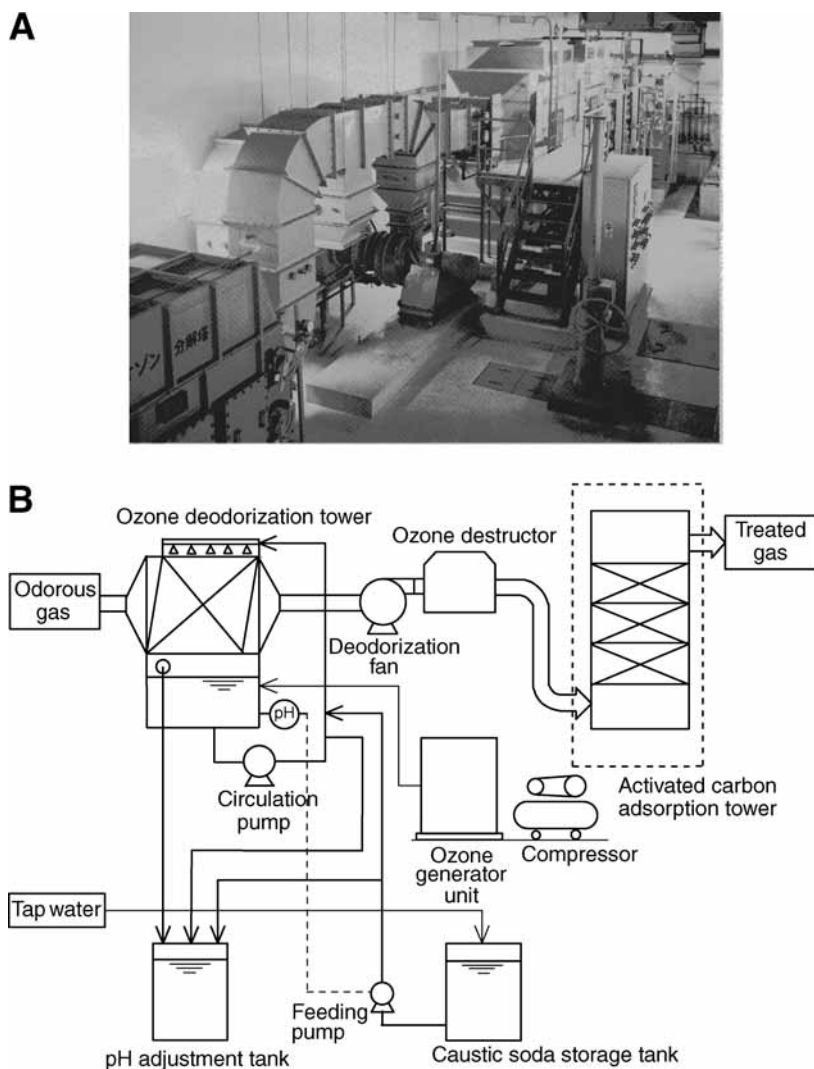
Fig. 63. Ozone deodorization system (courtesy of NGK Insulators, LTD). **(A)** Photograph of the facility. **(B)** Schematic diagram.

disulfide, and so on. The following chemical reactions mainly proceed when odor components are removed by ozone.

$$\text{Ammonia:} \quad 2NH_3 + O_3 \rightarrow N_2 + 3H_2O \tag{106}$$

$$\text{Trimethyl amine:} \quad 3(CH_3)_3N + O_3 \rightarrow 3(CH_3)_3NO \tag{107}$$

$$(CH_3)_3N + 3O_3 \rightarrow CH_3NO_2 + 2CO_2 + 3H_2O \tag{108}$$

$$\text{Dimethyl sulfide:} \quad 3(CH_3)_2S + O_3 \rightarrow (CH_3)_2SO \tag{109}$$

$$(CH_3)_2S + O_3 \rightarrow (CH_3)_2SO_3 \tag{110}$$

Dimethyl disulfide: $2(CH_3)_2S_2 + H_2O + O_3 \rightarrow 2CH_3SO_3H$ (111)

$$3(CH_3)_2S_2 + H_2O + 5O_3 \rightarrow 3(CH_3)_2S_2O_5$$ (112)
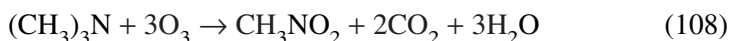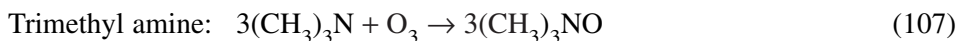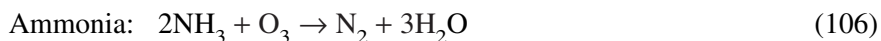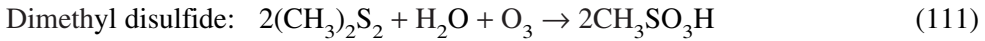
There are many unknown mechanisms in the reaction of radicals and odor components. It is known that radicals work for the decomposition of odor ingredients. When high performance of odor control cannot be obtained, the process combined with NaClO scrubbing method is recommended.

2.5.2.3. DESIGN EXAMPLE: OZONE OXIDIZATION SYSTEM FOR ODOR REMOVAL

Problem

In order to remove odor exhaust gas from a disposal plant, ozone water is formed by an ozonizer and odorous gas passes through the chemical scrubber in which ozone water flows. Objective odorous gases are ammonia, trimethyl amine, dimethyl sulfide, and dimethyl disulfide. It is assumed that the initial concentrations of these odorus gases are 5, 0.1, 0.3, and 0.3 respectively. Calculate the capacity of the ozonizer (g/h) to make the concentrations of these gases 0.7, 0.002, 0.003, and 0.003 ppm, respectively. It is assumed that the total flow rate of the gas is $Q = 11,000$ Nm^3/h and the chemical reactions in Eqs. (106)–(112) progress with the same rate.

Solution

From the reactions in Eqs. (106)–(112), the amount of required ozone can be calculated as follows:
For ammonia:

$$M_1 = 11,000 \left(\frac{Nm^3}{h} \right) \times (5 - 0.7) \times 10^{-6} \times \frac{48 \left(\frac{kg}{kmol} \right) \times 0.5}{22.4 \left(\frac{Nm^3}{kmol} \right)} = 0.0507 \left(\frac{kg}{h} \right)$$ (113)

For trimethyl amine:

$$M_2 = 11,000 \times (0.1 - 0.002) \times 10^{-6} \times \frac{48}{22.4} = 0.0023 \left(\frac{kg}{h} \right)$$ (114)

For dimethyl sulfide:

$$M_3 = 11,000 \times (0.3 - 0.003) \times 10^{-6} \times \frac{48 \times 0.5}{22.4} = 0.0035 \left(\frac{kg}{h} \right)$$ (115)

For dimethyl disulfide:

$$M_4 = 11,000 \times (0.3 - 0.003) \times 10^{-6} \times \frac{48 \times 1.2}{22.4} = 0.0084 \left(\frac{kg}{h} \right)$$ (116)

A total amount of needed O_3:

$$M_t = M_1 + M_2 + M_3 + M_4 = 65 (g/h)$$ (117)

Therefore, the type OZS-MC702D-4WJ ozonizer (capacity = 150 g/h) shown in Table 6 has enough capacity.

2.6. Decomposition of Freon and VOC

2.6.1. VOC Decomposition

As the results of the Clean Air Act Amendments of 1990, emissions of volatile organic compounds (VOCs) into air became an increasing environmental concern. The understanding and subsequent development of technologies for controlling these streams has been mandated. Conventional technologies for VOC control are carbon adsorption, catalytic oxidation, and thermal incineration. These technologies are widely accepted but have practical limitations with respect to concentration, compounds treated, energy requirements, and cost. For these reasons, nonthermal plasma technology was investigated as an alternative technical approach. The first investigation was performed by Yamamoto et al. (61) using the ferroelectric packed-bed and pulsed corona plasma reactors. Successful demonstration was reported for toluene, methylene chloride, and trichloro-trifluoroethane (known as CFC-113) using the nonthermal plasma device. The conversion was dependent on the mean energy (or peak pulse voltage and pulse repetition rate) in the reactor and was also related to how strongly halogen species were bonded with carbon.

Since then, many researchers have investigated the various VOCs with different operating ranges and different plasma reactors (12,61,76,82,98–188).

2.6.2. Decomposition of Freon or Hard-to-Decompose VOCs

The decomposition of VOCs has been described by using the ratio of power input to flow rate of energy to gas flow rate, which was defined as a specific energy density (SED) in W/L/s or J/L. However, VOC decomposition was not constant for a given SED but rather depends on SED, especially hard-to-decompose VOCs such as freon, CF_4, halons, and other strongly bonded molecules. A new approach to deal with hard-to-decompose VOCs was proposed (186) and experimental data were presented (181).

The work described here represents a new way of looking at VOC decomposition. Previous theoretical work has considered only the balance of force acting on VOC. In contrast, this approach recognizes the influence of the transfer of electron impact to the VOC molecule. According to this new concept, energy maintains the VOC molecular structure in motion within a potential well. The VOC molecule is decomposed when it accumulates enough energy to overcome the potential well and to form radicals, which leads to the VOC decomposition homolitically via their excited states. The hypothesis is that VOC decomposition is not instantaneous but is a statistical process. This approach recognizes the influence of the transfer of electron impact to a VOC molecule in plasma. Such a transfer takes place through the agency of the plasma, which fluctuates randomly in time because of the physical nature of microdischarges. Thus, VOC is exposed to a constant state of vibration, building up energy until this energy is sufficient to break the VOC bond force. The excited VOC and surrounding molecules proceed homolitically, leading to decomposition. Experimental data support that decomposition was affected with time.

For example, the decomposition efficiency for 1000 ppm CFC-113 in dry air using the packed-bed plasma reactor, varying the flow rate and voltages whereas maintaining SED at a constant value (SED = 2700 J/L) is shown in Fig. 64. With the applied voltage of 6.6 kV and flow rate of 2.2 L/min (2 s in residence time), CFC-113 decomposition efficiency was in the range of 25.9–28.5%. As the flow rate was decreased to 1 L/min and the applied voltage was decreased to 6 kV to achieve the same SED, the decomposition efficiency improved significantly ranging from 51.7 to 53.5%. When the
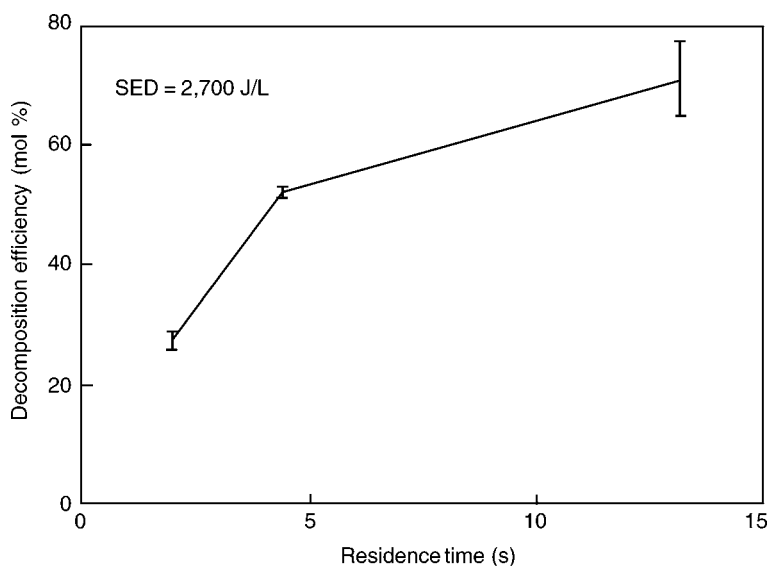
Fig. 64. CFC-113 decomposition in dry air (© IEEE).
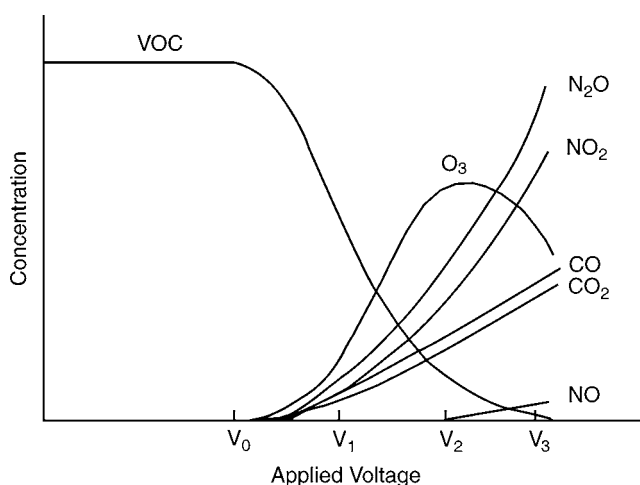
Fig. 65. Typical VOC decomposition and concentration of inorganic byproducts (© IEEE).

applied voltage was reduced to 5.2 kV with the lower flow rate whereas maintaining the same SED, the decomposition efficiency was further increased to 65.4 to 77.3%. These results indicate that decomposition efficiency is affected by treatment time even when SED is maintained at the same level. As a consequence, CFC-113 molecules are decomposed more easily than when the force required for CFC-113 molecule cleavage is applied, which supports the new theory (186). The similar experimental trends were observed for halon, TCE, CH_4, C_2H_6, C_2H_4, C_4H_{10}, and Cl_3CCH_3 in both air and N_2 backgrounds. The operation with low voltage and longer residence operation is superior to that with high voltage and shorter residence, i.e., soft plasma. It is also advantageous that reaction byproducts such as CO, NO, NO_2, N_2O, and O_3 are also significantly smaller for the soft plasma operation as shown in Fig. 65 (181).

Table 7
Major Byproducts of 1000 ppm CFC-113 (CCl_2F-$CClF_2$)
for Various Background Conditions

Dry H_2	Dry N_2	Wet N_2	Dry Air	Wet Air
CHClF–$CClF_2$	CCl_2F_2	CHClF–$CClF_2$	C_2H_5Cl	C_2H_5Cl
$CHCl_2F$	CH_2ClF	$CHCl_2F$	$CClF = CF_2$	$CClF = CF_2$
$CHCl_2$	CCl_3F	CCl_2F_2	–	–
$CHClF_2$	–	CH_2ClF	–	–

Source: © IEEE.

Regarding the reaction mechanisms by nonthermal plasma, the first step of CFC-113 decomposition is breaking the C–C bond and forming CCl_2F_2 radicals. Table 7 indicates that product distributions were affected by background gas and humidity. Both hydrogen and moisture produced more reaction byproducts than dry air and nitrogen, implying more complicated reaction processes. The byproducts are the highest for dry H_2, followed by dry N_2, wet N_2, wet air, and dry air. It is interesting to note that no oxygen-containing compounds were found for air. Reaction byproducts were minimal with aerated condition. The detailed reaction pathways for CFC-113 with various background gas was described in ref. 180.

2.6.3. Aerosol Generation

In volatile organic compounds (VOCs) decomposition by nonthermal plasma, gas-phase byproducts and aerosols are likely to be formed, depending on the type of plasma reactor, the energy level, the background gas, and the type of VOCs to be treated (180,189–191). The plasma chemical decomposition will cause either a recombination or an elimination reaction. The former reaction will lead to cluster formation and aerosolization, and the latter reaction will lead to lower molecular-weight hydrocarbon compounds and, finally, to the formation of carbon monoxide (CO), carbon dioxide (CO_2), water (H_2O), and halogenated compounds (HCl and HF). Identifying the gas phase reaction byproducts and the conditions of aerosolization are important not only for understanding the reaction mechanisms but for successful application for nonthermal plasma processing.

Experiments were carried out in a laboratory-scale ferroelectric packed-bed plasma reactor (180), the barrier type plasma (191), and the pulsed corona reactor (189). Aerosol generation was measured by the Laser Aerosol Spectrometer (PMS Model LAS-X) and condensation nuclei counter (CNC), which were used to obtain a full spectrum of aerosol generation: the CNC measures a total count for particle size more than 0.013 μm and the LAS-X measures the particle-size-dependent aerosol density ranging from 0.09 to 3.0 μm. Aerosol generation for dry air measured by the LAS-X was shown in Fig. 66.

Figure 67 shows the aerosol formation of 1000 ppm CFC-113 in air and in dry air alone. The aerosolization of 1000 ppm CFC-113 in air and was one order of magnitude more than that of dry air alone and also more than that of N_2 background. Most of the aerosols produced under plasma were of particle size much less than 0.1 μm and aerosol generation by CFC-113 was 10 particles/cm^3 (180). In the case of benzene decomposition using the barrier plasma, both the size of aerosol and number concentration increased with the increase of specific energy. Peak size and the corresponding number
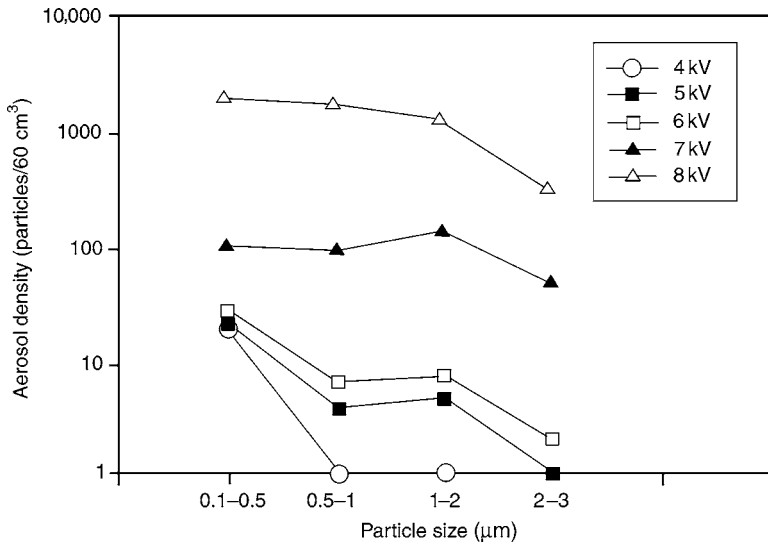
Fig. 66. Aerosol generation for dry air measured by the LAS-X (© IEEE).
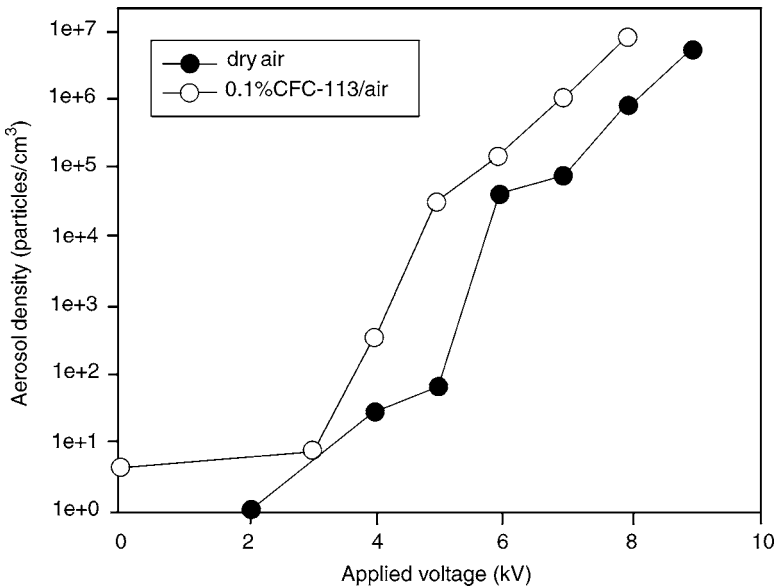
Fig. 67. Aerosolization of 1000 ppm CFC-113 in air (© IEEE).

concentration reached 19 nm and 1.19×10^5 particles/cm^3 at 550 J/L, respectively. In the packed-bed plasma reactor peak size was 14.3 nm at the same conditions. Number concentration at the peak size was 3.7×10^3 particles/cm^3 (191).

2.7. Diesel Engine Exhaust Gas Treatment

2.7.1. Introduction

In recent years, stricter emission standards of diesel engine exhaust have been established because of its effects on global warming, acid rain and health damage. Diesel

engine emissions are roughly classified into two groups: particulate matter (PM) or diesel exhaust particle (DEP) and gaseous emissions. These two have the following subdivisions and characteristics:

Particulate matter or diesel exhaust particle

- *Carbon soots*. It is usually called black smoke. Carbon is the main component. In PMs, incineration is most difficult.
- *Soluble organic fraction*. The components which are solvable in organic solvents. Because these components remain vapor in high temperature, it can be incinerated enough using the oxidization catalyst. However, these components increase the diameter of a carbon soot particle when the temperature of the emission decreases.
- *Oil ash*. The residual component after the incineration of engine oil. It is generated mostly by the deterioration and age of engine.
- *Mist of sulfate or sulfuric acid* (H_2SO_4). The gaseous emission SO_2 is changed to sulfate by the catalytic oxidization system. The sulfate is changed to sulfuric acid by the existence of moisture. This causes the acid rain.
- *Mist of nitrate or nitric acid* (HNO_3). The gaseous emission NO is changed to nitrate by catalytic oxidization system. The sulfate is changed to nitric acid by the existence of moisture. It also causes the acid rain.

Gaseous emission

- *Carbondioxide* (CO_2). It is always induced by incinerations, and causes the global warming effect (GWE).
- *Carbonmonoxide* (CO). It is a very hazardous emission component and causes human poisoning.
- *Nitrous oxide* (N_2O). It causes the global warming effect greatly. The coefficient of GWE is about 310.
- *Oxide of sulfur* (SO_x). Most sulfur in light fuel is changed to SO_x inside diesel engine combustion. Generally, the concentration of SO_2 is highest. It causes sulfuric acid rain. The induced amount becomes small by conducting enough predesulfurization of fuel.
- *Oxides of Nitrogen* (NO_x). NO, NO_2, NO, and N_2O_5 are included. Generally, the concentration of NO is highest. It causes acid rain, photochemical smog and health damage.
- *Hydrocarbons* (HC): General term for organic compound (chemical compound of hydrogen and carbon). It causes acid rain and photochemical smog. It is easily resolved at high temperature.

In these emissions, black smoke such as carbon soot has attracted attention especially because it is the main visible emission from the exhaust pipe of diesel automobile and causes human health damage, and the installation of diesel particulate filter (DPF) is about to be imposed as a duty for the collection of carbon soot in large city suburbs. The most typical DPF structure is a wall filter type made from honeycomb ceramics (cordierite or SiC). The flow passes through the wall of porous filter because plugs alternately close the passes. Carbon soots are trapped at the wall of the porous filter. Other types of DPFs such as fibrous filter type, mat type, foam type, and multi-plate type are also proposed. The trapped carbon soot must be removed periodically because the increase in the pressure of the exhaust gas leading to engine power decrease and halting at worst case. Methods to regenerate the DPF by incineration are classified into the two categories: active methods such as heat addition with an electric heater, after burner, fuel addition, and passive method (self-regenerating method) such as continuously regenerating trap (CRT) or nonthermal plasma regeneration.

Although, the conventional regulation concerns the total mass of the PM (unit is g/km or g/kW), it has recently been noted that the number of emitted small particles such as PM 2.5 (particulate matter smaller than 2.5 μm) is another important problem. These particles are called SPM (suspended particulate matter). Such particles are easily suspended in the air, and can get inside the human lung through the human respiratory system. This will lead to health damage directly. There is a possibility that such a very small particle may pass through the DPF. Many studies have been reported on such small particles in the diesel engine emission.

On the other hand, not only particulate matter, but also emission of nitrogen oxide (NO_x) is also an important problem to be addressed. As reduction technologies, burning improvement techniques such as the control of fuel injection timing, Exhaust Gas Recirculation (EGR) and so on have been investigated primarily (192). However, it is difficult to satisfy the future more severe NO_x emission standard only with burning improvement techniques. The establishment of low-cost and effective post process NO_x removal technology is desired. Generally several to several 10% oxygen is comprised in diesel engine emission, the three-way catalyst which is usually used in the gasoline engine purification may not work. Therefore, many NO_x reduction methods have been proposed. At present, the leading method is selective catalytic reduction (SCR), which was explained in the previous section. A high performance reduction catalyst is required in this system. Further, the preparation of the infrastructure for supplying urea or ammonia is needed.

Figure 68 shows the diesel emission treatment equipment proposed by Johnson Matthey Inc. The CRT system consists of oxidation catalyst and diesel particulate filter (DPF) (193–195). The DPF is regenerated by NO_2 induced by the oxidation catalyst. The CRT is followed by SCR catalyst and ammonia slip catalyst. The injected urea water solution is resolved to NH_3 at high temperature before the SCR catalyst. Using this system, HC, CO, PM, NO_x, and slipped NH_3 can be simultaneously removed. Although there are several problems to be solved in this system, the near future utilization is expected especially in Europe, which has a high number of diesel cars.

In this section, the new application of the nonthermal plasma to the NO_x removal and self-regeneration of DPF investigated mainly by the authors are explained.

2.7.1.1. NO_x Removal In Diesel Engine Emission Using Plasma–Chemical Hybrid Process

Section 2.2.2. described the hybrid NO_x (= $NO + NO_2$) removal technology in which atmospheric pressure nonequilibrium low temperature plasma and a wet-type chemical reaction process are combined (196,197). This method was first applied to the real exhaust of a small-sized diesel engine and removal of NO_x was investigated. Generally, an output load of the diesel engine changes greatly during the operation and exhaust gas is in high temperature and humidity. Therefore, the effects of the diesel engine load, gas temperature, and gas humidity on NO removal characteristics by the plasma were examined in detail. Moreover, it was confirmed that NO_2 could be removed with high efficiency using Na_2SO_3 as the reducing chemical in the chemical reactor.

2.7.1.2. Experimental Apparatus and Method

2.7.1.2.1. Plasma Reactor: A barrier-type packed-bed plasma reactor shown in Fig. 69 was used for the removal of NO_x in the diesel engine exhaust. As explained in
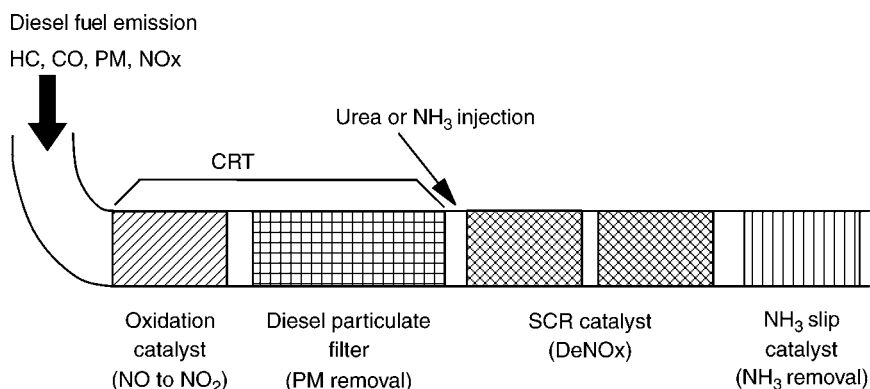
Fig. 68. Final diesel engine treatment system.
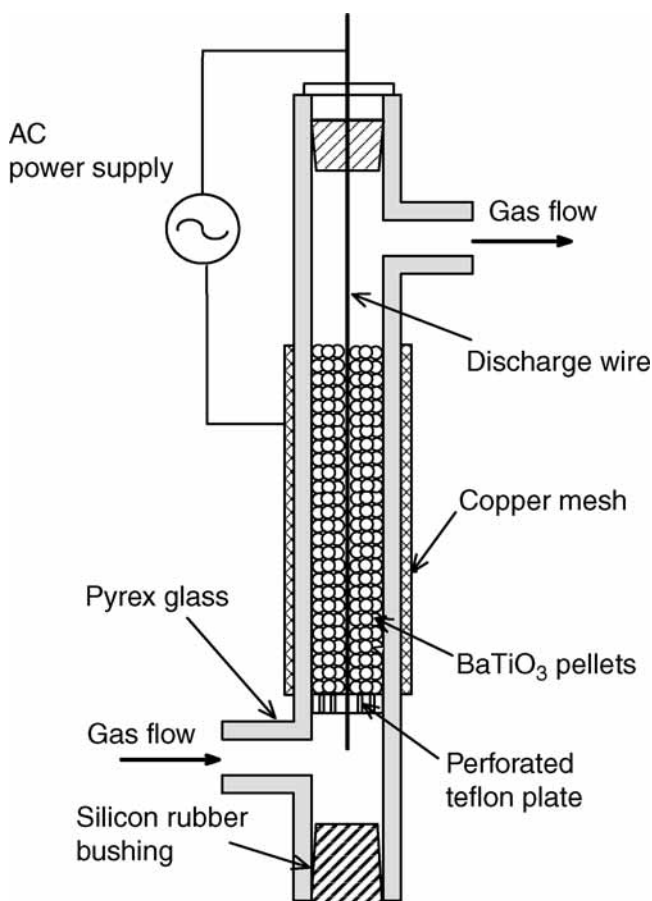
Fig. 69. Barrier type packed-bed plasma reactor.

previous papers, this reactor could oxidize NO to NO_2 with high efficiency. It consisted of a 1.5 mm diameter wire electrode and a Pyrex glass tube (20 mm inner diameter and 24 mm outer diameter) as a dielectric barrier around which the copper screen was wrapped as the other electrode. The 1.7–2 mm in diameter titanium acid barium ($BaTiO_3$) pellets
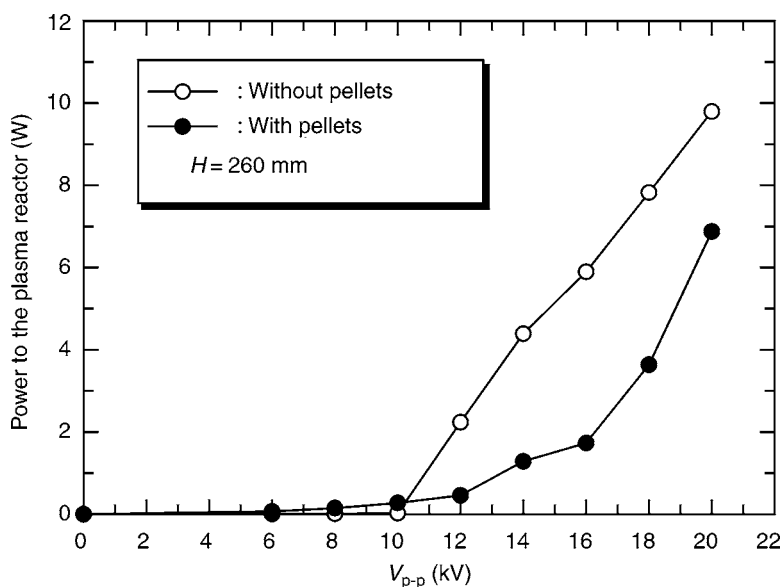
Fig. 70. Power to the plasma reactors vs applied voltage.

(the relative dielectric constant of 10,000 at room temperature) were packed inside the tube. The pellets were held by a perforated Teflon plate at the bottom end. The height of pellet layer h_p was the same as the width of the copper mesh electrode H_m (= 260 mm). The gas passes through the reactor as shown with arrows in the figure. The AC high voltage (max. 20 kV) of 60 Hz was applied to the reactor using a neon transformer. As a result, the periodic micro electric discharge of a nano second order was induced between the pellets and the exhaust gas was processed in the reactor.

The applied voltage and current waveforms were measured by an oscilloscope (Sony Tektronix TDS380P-2GS/s) through the voltage and current dividers (Sony Tektronix P6015A). The power consumption in the reactor was obtained by averaging the product of the voltage and current waveforms. The voltage to the reactor represented was the peak-to-peak voltage V_{p-p} in the following results. Figure 70 shows the measurement results of the discharge powers to the reactor with and without $BaTiO_3$ pellets. A higher removal efficiency of hazardous gas was obtained with smaller discharge power consumption at the same voltage when the pellets were used.

2.7.1.2.2. Experimental Apparatus and Method: A schematic diagram of the experimental setup is shown in Fig. 71. The specification of the tested diesel engine driven AC power generator was as follows: single cylinder, direct fuel injection, volume of cylinder = 200 cc, rotation speed = 3600 rpm, output voltage AC 100 V, maximum (regular) electric power output = 2 kW (Yammer diesel Co., YDG200SS-6E). Output electric power was regulated by changing the resistance of an electric heater in five steps which was used as the generator load. A part of the exhaust gas was sampled with a pump from the exhaust pipe and larger particles such as carbon soot were first removed by a glass filter.

Under low humidity conditions, moisture and smaller particles were removed using a silica gel layer and a drain pot in which hollow-fiber membranes filters (pore size = 0.01 mm) were used. As a result, absolute humidity AH = 0.4 mg/L, relative humidity
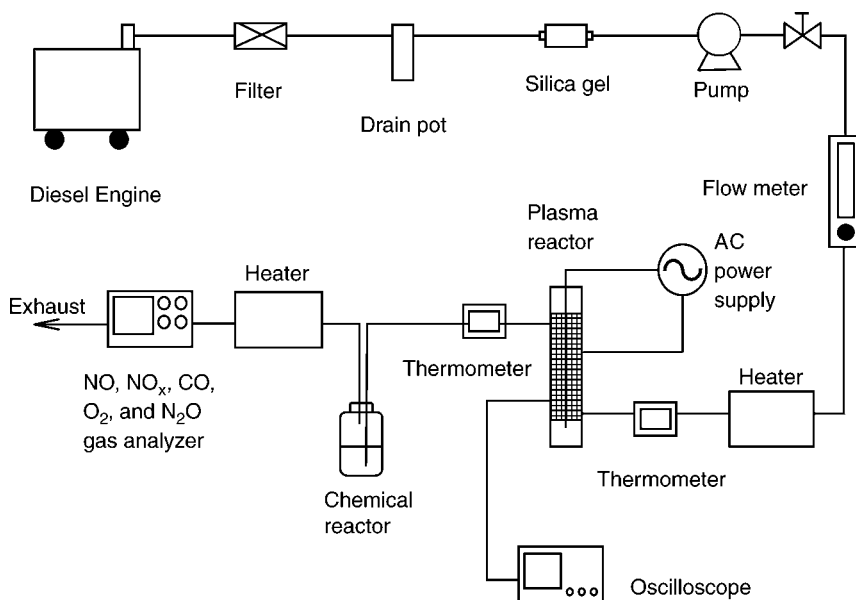
Fig. 71. Schematic diagram of the experimental setup.

RH = 2.6% were obtained in room temperature $T = 22°C$. The flow rate was controlled using a valve and a float-type flow meter. Under elevated temperature conditions, exhaust gas passed through a tubular-type electric furnace (Inner temperature = 300°C) to increase gas temperature. Exhaust gas temperatures were measured before and after the plasma reactor using thermo-couple thermometers. Exhaust gas temperature is represented by the averaged value of the temperature before and after the plasma reactor.

Exhaust gas was passed through the packed-bed plasma reactor and AC high voltage was applied. The NO_2 in the exhaust gas was first oxidized to NO by the nonequilibrium plasma. Next NO_2 was reduced to N_2 by the bubble injection-type chemical reactor in which Na_2SO_3 aqueous solution (mass concentration = 1%) was used.

The concentrations of gas components such as CO, CO_2, NO, NO_2, N_2O, and O_2 were measured using a set of gas analyzers (Horiba Co. Ltd., PG-235, Chemiluminescence for NO, NO_x, CO, Infra-red absorption for CO and O_2 for zirconia method, measurement accuracy: NO, NO_x, CO: 0.1 ppm, O_2: 0.1%, and Horiba Co. Ltd., VIA-50, Infra-red absorption for N_2O and measurement accuracy: 0.1 ppm). The concentration of CO_2 and humidity were measured using gas detection tubes (Gastec Co.).

The exhaust gas passed through the tubular-type electric furnace again before the gas analyzers in order to remove ozone of high concentration produced by the plasma reactor, because a large amount of ozone often interrupted the diaphragms of pumps in the gas analyzers especially at high voltage.

2.7.1.3. EXPERIMENTAL RESULTS AND DISCUSSIONS

2.7.1.3.1. Basic Characteristics of Diesel Engine Exhaust Gas: To understand the basic characteristics of the tested diesel engine exhaust gas, the concentrations of several components in the exhaust gas were directly measured changing the diesel engine
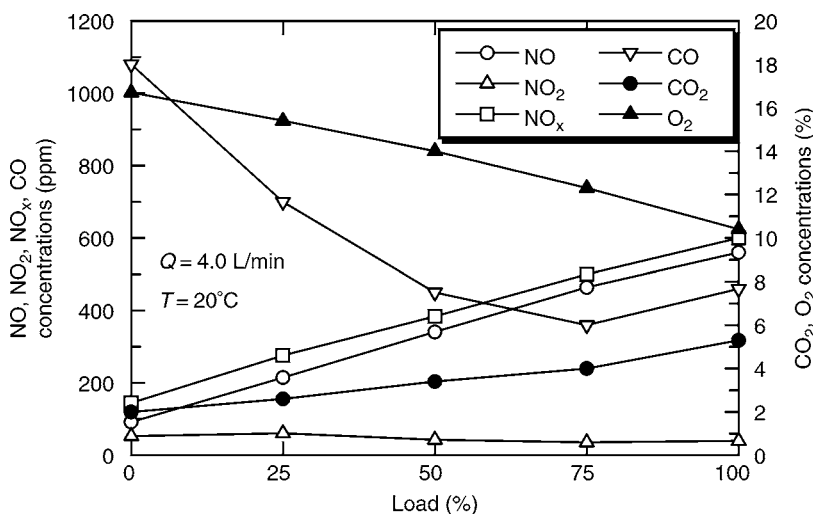
Fig. 72. Exhaust gas concentration characteristics of tested diesel engine.

load from 0 to 100%. The measurement result as shown in Fig. 72. Regular (maximum) power output 2 kW is correspond to a full load of $K = 100\%$. As for NO_x, NO, NO_2, and CO concentrations, the unit is ppm referring to the left vertical axis. On the other hand, a unit for CO_2 and O_2 is volume % referring to the right vertical axis.

In this graph, when the load K is changed from 0 to 100%, NO concentration increased from 92 to 560 ppm and NO_x concentration increased from 145 to 600 ppm. They were almost proportional to the load factor K. On the other hand, NO_2 concentration was almost a constant 40–60 ppm. The concentration of CO reached maximum 1080 ppm at the load factor 0%, decreased with an increase in K and became a minimum value 360 ppm when the load factor is 75%. It increased again and reached about 460 ppm when K was 100%. The concentration of CO_2 increases from 2 to 5.3% with increase in the load factor. The concentration of O_2 decreased from 16.7 to 10.4% with an increase in the load factor.

2.7.1.3.2. NO Removal Characteristics at Room Temperature and Byproducts: An experiment concerning removal or oxidation characteristics of NO only by a plasma reactor was performed under the following representative operating conditions: gas temperature $T = 20°C$, load factor $K = 50\%$ (NO concentration in the exhaust gas = 325 ppm), gas flow rate $Q = 2$ L/min, absolute humidity $AH = 0.4$ mg/L.

Figure 73 shows the experimental result in the relation between gas concentrations and the applied voltage V_{p-p}. In this figure, the concentration of NO decreased from 325 ppm to 7 ppm and the concentration of NO_2 increasing up to 258 ppm at the voltage $V_{p-p} = 18$ kV. The oxidation or removal efficiency of NO was 98%. In this result, the oxidization of NO to NO_2 was performed effectively using the plasma reactor. The total NO_x concentration decreased from 360 ppm to 265 ppm and the concentration of N_2O increased from 0 to 34 ppm. Therefore, it was concluded that NO_3^-, NO_2^-, HNO_2, and HNO_3 of $(360–265) – (34–0) = 61$ ppm was induced. The NO_2 can be reduced using the chemical reactor with Na_2SO_3 aqueous solution at low cost.
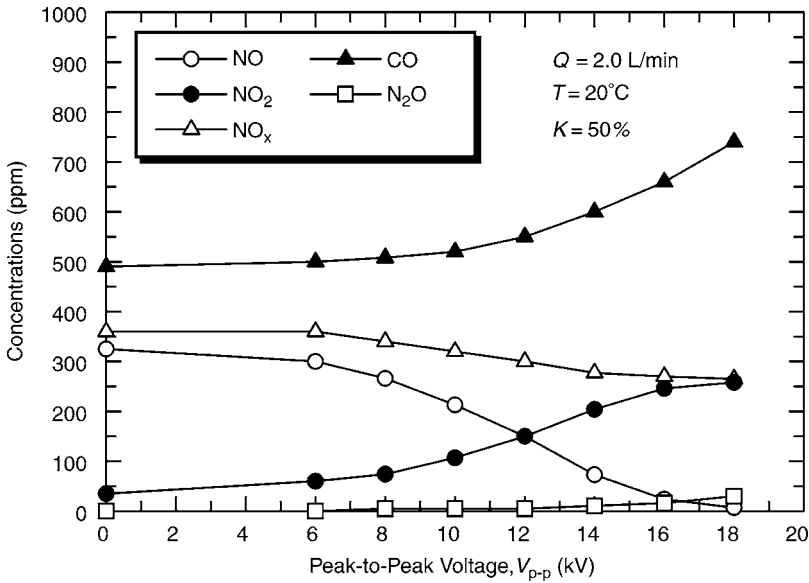
Fig. 73. Products concentration in NO removal process using the plasma reactor under dry and room temperature conditions ($K = 50\%$).

As a result, the concentration of CO increased with an increase in voltage. The amount of induced CO was more than that of a previous experiment using a simulated exhaust gas. This may have been caused by the oxidization of small amount of resident carbon soot and/or plasma reduction for CO_2. The detailed mechanism is unknown. Furthermore, the result was omitted in the graph, and the concentration of O_2 was almost a constant 14.2% throughout the voltage.

2.7.1.3.3. Effects of Gas Temperature and Humidity on NO Removal Efficiency: Figure 74 shows the relation between NO removal efficiencies and the applied voltage for various T and AH conditions. It is known from this graph that NO removal efficiency at 22 kV reached a maximum (about 92%) under room and dry gas condition and decreased with increases in gas temperature and humidity.

2.7.1.3.4. Effect of Residence Time on NO Removal Characteristics: In order to determine the optimum flow rate for the plasma reactor, experiments were carried out for various gas flow rates = 2, 3, 4, and 5 L/min, under the following condition; T = 20°C, low humidity condition (AH = 0.4 g/kg), K = 50% (initial NO concentration = 320 ppm) and V_{p-p} = 18 kV. For these flow rates, the corresponding residence times are 2.4, 1.6, 1.2, and 0.9 s respectively when the void fraction inside the reactor is not considered.

Figure 75 shows the experimental result in the relation between NO removal efficiency and the residence time. For the range of residence time 0.9–1.6 s, NO removal efficiency increases almost proportionally to the residence time. However, for the range of residence time 1.6–2.4 s, it is almost constant. About 95% NO can be removed in this range of residence time. Generally, since a generation of byproducts can be suppressed for smaller residence time, the flow rate Q = 3 L/min (residence time 1.6 s) is the best condition for the present plasma reactor.
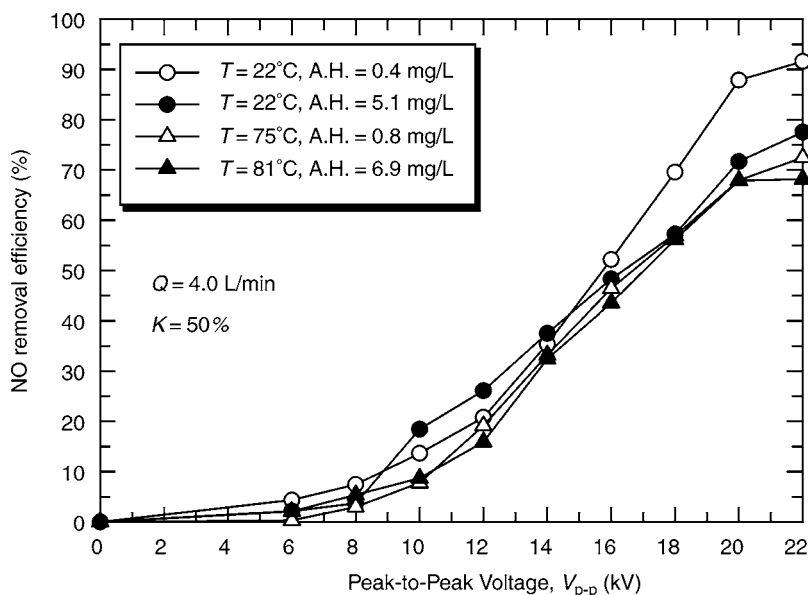
Fig. 74. Effects of gas temperature and humidity on NO removal efficiency.

2.7.1.3.5. Removal Characteristics of NO_x Using Plasma–Chemical Hybrid Process: Figure 76 shows the experimental results of NO_x removal by plasma–chemical hybrid process. This experiment was performed when $K = 50\%$, optimum flow rate = 3 L/min, room temperature, and low humidity. These were optimum conditions for oxidizing NO to NO_2 by the plasma reactor as shown previously.

It is known from the above figure that 87% NO_x (= NO + NO_2) can be removed at voltage 20 kV (specific energy density SED = 140 J/L) using a plasma–chemical hybrid process. In this process, NO is oxidized to NO_2 by the plasma and NO_2 reacts with Na_2SO_3 aqueous solution to produce N_2 and nontoxic aqueous solution of Na_2SO_4 in the chemical reactor. Moreover, small amounts of reaction byproducts such as HNO_2 and HNO_3 is easily neutralized by, for example, NaOH scrubbing.

According to a new hybrid NO_x removal concept proposed by the authors, an experiment was carried out to remove NO_x in diesel engine exhaust gas. In this method, the nonequilibrium plasma is used to oxidize NO to NO_2 and the resulting NO_2 was reduced in a wet-type chemical reaction process. The main results are summarized as follows:

a. Using a barrier-type packed-bed plasma reactor, NO in exhaust gas can be oxidized efficiently to NO_2. The efficiency of NO removal of 98% was achieved on the condition of $K = 50\%$ (NO concentration = 325 ppm), flow rate = 2 L/min, room temperature and low humidity.
b. Though N_2O, HNO_3, and CO were induced as byproducts, the concentration of N_2O was not very high, and generally, HNO_2, and HNO_3 are easily neutralized by neutralizing chemicals.
c. When the engine load, exhaust gas temperature or humidity increase, the NO removal efficiency tended to decrease.
d. For the size of this reactor (inner diameter = 20 mm and length = 260 cm), it was known that the flow rate of $Q = 3$ L/min (residence time 1.6 s) was the optimum operating condition.
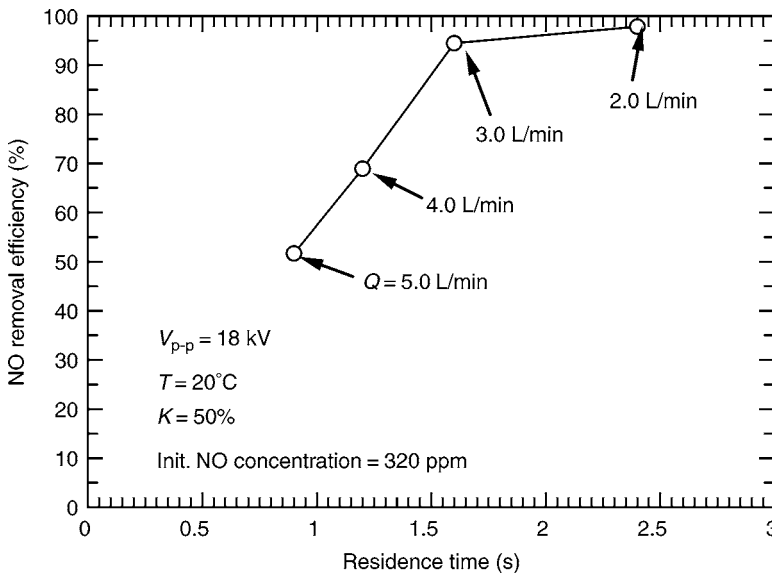
Fig. 75. Effect of the residence time on the amount of NO removal efficiency ($K = 50\%$, $V_{p-p} = 18$ kV).

e. 87% NO_x can be removed by the plasma–chemical hybrid process under the condition of engine load $K = 50\%$, gas flow rate = 3 L/min, applied voltage 20 kV, room temperature and low humidity.

2.7.2. NO_x, SO_x and PM Simultaneous Removal Using Single-Stage Plasma–Chemical Hybrid Process

2.7.2.1. NO_x, SO_x, PARTICULATE SIMULTANEOUS REMOVAL

Nitrogen oxides (NO_x) and sulfur oxides (SO_x) are the major contributors to acid rain, and particulates such as soot are emitted from the power plants from coal fired boilers and diesel engines. In these power plants, NO_x is typically treated using the selective catalytic reduction (SCR) system, the particulates are collected by electrostatic precipitators (ESP), cyclones or the bag filters, the SO_x are then removed by chemical adsorption (magnesium hydroxide or calcium carbonate). Generally, the SO_x removal is easy because SO_x is soluble in water and reacts with alkalis. On the other hand, the NO_x removal is difficult, especially because NO hardly reacts with water, solutions, or alkalis.

In the present study, we applied the plasma–chemical hybrid process to the simultaneous removal of NO_x, SO_x and particulates in the diesel engine exhaust gas using a new single-stage wet-type plasma reactor.

2.7.2.2. PLASMA–CHEMICAL HYBRID PROCESS

NO_x removal using nonthermal plasma has been investigated by many researchers as explained in the Section 2.2. However, nonthermal plasma alone cannot remove NO_x effectively; instead, it generates a significant amount of byproducts such as N_2O, NO_3^-, and CO as the input power is increased. For these reasons, the authors proposed a plasma–chemical hybrid process, which consists of the plasma reactor followed by a chemical reactor using Na_2SO_3 or Na_2S solutions. NO_x can be reduced almost completely
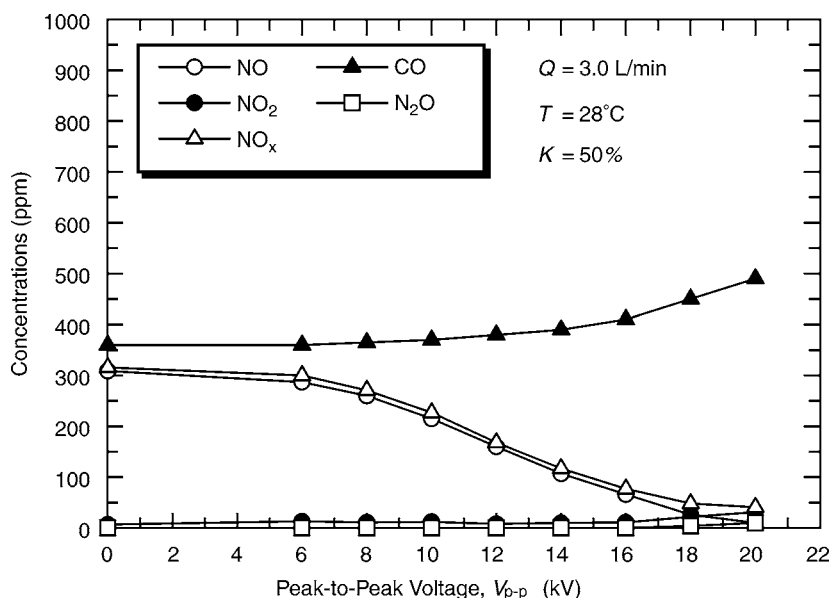
Fig. 76. Result of NO$_x$ removal in the diesel engine exhaust using the plasma reactor and the chemical reactor under dry and room temperature conditions ($T = 28°C$, $AH = 0.4$ mg/L).

with low cost using this method. This process is based on the following principle. In the nonthermal plasma process, NO can be effectively converted to NO$_2$ with low energy but NO$_2$ cannot effectively be reduced to N$_2$. On the other hand, in a wet chemical process, NO cannot be effectively removed but NO$_2$ can effectively be reduced to N$_2$.

2.7.2.3. EXPERIMENTAL APPARATUS

A single-stage wet-type plasma reactor is shown in Fig. 77 (198). This reactor consists of a 2 mm diameter stainless discharge wire and Pyrex cylinder, wrapped by the copper mesh of 26 cm length in which water or Na$_2$SO$_3$ and NaOH solutions flow along the inner wall of the cylinder from the top to bottom of the reactor. The electrodes were energized by a pulsed power supply (SI thyristor switching, frequency 210 Hz, max. voltage 45 kV, rising time 30–70 ns). Particulates can be collected by an electrostatic force on the inner wall of the cylinder and removed by solutions flow. The chemical reactions occur at the surface of solutions flowing on the inner wall.

A schematic diagram of the experimental set-up is shown in Fig. 78. In order to prepare a simulated exhaust gas, 2% NO and 2% SO$_2$ gases balanced with N$_2$ in the cylinder were mixed with the dry air supplied by the compressor through the dryer. The desired NO and SO$_2$ concentrations and the flow rate were obtained with the mass flow controllers. In the experiments for the treatment of diesel engine exhaust gas, a small diesel engine generator (200 cc, 2 kW) was used. The exhaust gas was sampled from the exhaust pipe and the gas passed through the reactor. The SO$_2$, NO, NO$_2$, NO$_x$, CO, N$_2$O concentrations and removed particulates mass were measured after the reactor. Concentrations of these compounds were measured by a set of gas analyzers (Horiba Co., PG-235, VIA-510).
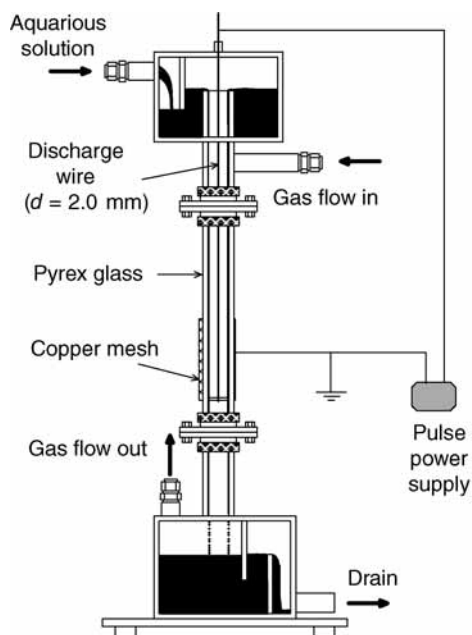
Fig. 77. Schematic diagram of experimental setup.
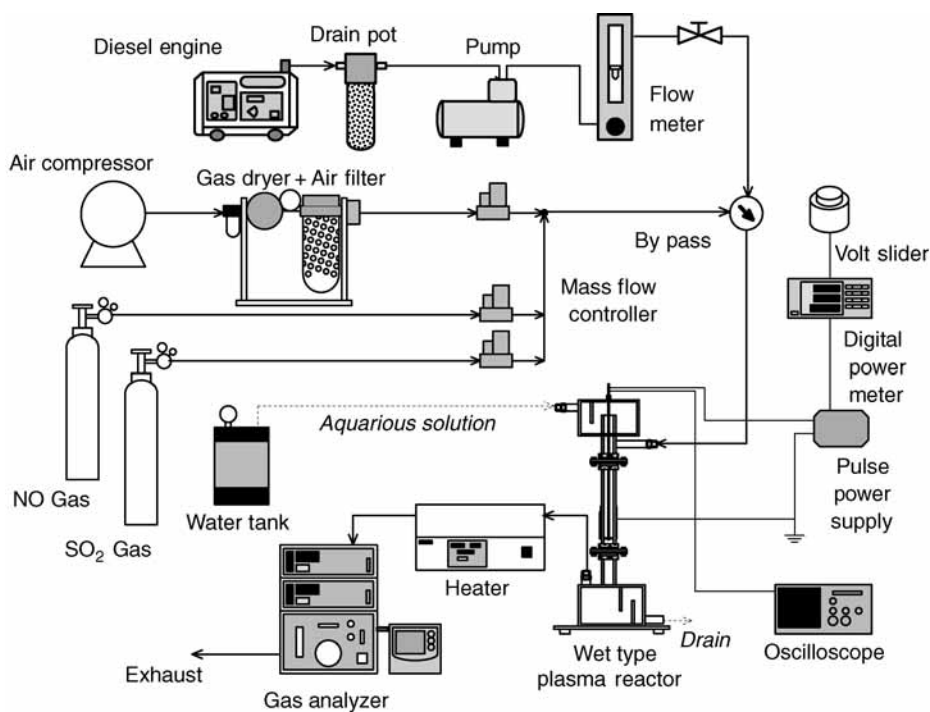
Fig. 78. Wet type plasma reactor.
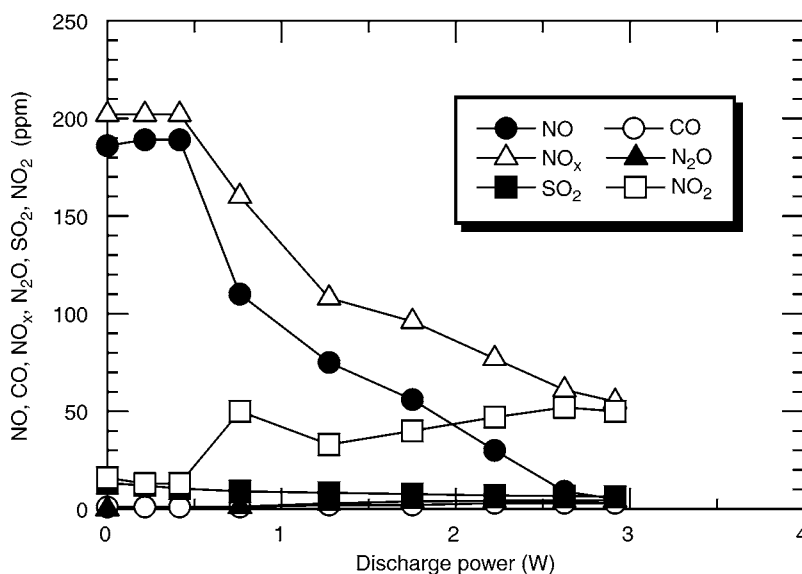
Fig. 79. Gases concentration after treatment by the wet-type plasma reactor (NO, SO$_x$ = 200 ppm).

2.7.2.4. EXPERIMENTAL RESULTS AND DISCUSSIONS

2.7.2.4.1. NO$_x$ and SO$_x$ Removal: Figure 79 shows experimental results of NO$_x$ and SO$_x$ removal. In this graph, gases concentrations are plotted as a function of plasma discharge power on the condition of the gas flow rate, Q = 4 L/min and the solutions flow rate q = 0.2 L/min including Na$_2$SO$_3$ (0.869 g/L) and NaOH (0.298 g/L). The amount of these chemicals was sufficient to react with NO$_2$ and SO$_2$. NO concentration decreased with an increase in discharge power and reached 5 ppm at 2.9 W. 98% NO and 75% NO$_x$ removal efficiency were achieved. Byproducts such as CO and N$_2$O stayed less than 4 ppm at 2.9 W. The SO$_2$ concentration decreased less than 13 ppm and more than 93% of SO$_2$ was removed.

In experiments on real exhaust gas from a diesel engine, around 60% NO$_x$ can be removed for the flow rate of 4 L/min. Further experiments are now in progress to achieve higher efficiency.

2.7.2.4.2. Particulate Matter Removal: Figures 80A,B show the photographs of high efficiency particulate air (HEPA) filters with the deposited soot before and after the reactor when discharge power was 2.9 W (voltage = 24 kV). The mass increases of the HEPA filters after the experiments for 20 min were measured using an electronic analytical mass balance (detection limit is 0.001 mg). The mass increase was 0.505 mg for Fig. 80A and 0.059 mg for Fig. 80B. From this result, 88% of diesel particulates were removed using the plasma–chemical hybrid reactor with the electrostatic force effect.

The single-stage wet-type plasma reactor achieved NO$_x$ removal of 75% and SO$_2$ removal of 95% were achieved with negligible reaction byproducts such as N$_2$O and CO. Regarding the removal efficiency of diesel soot, around 88% particulate removal efficiency was achieved.
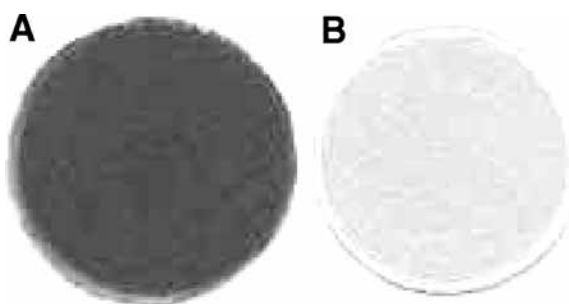
Fig. 80. Photographs of Hepa filters with soot before and after the reactor in the diesel exhaust gas cleaning. **(A)** Before the reactor. **(B)** After the reactor.

2.7.3. Nonthermal Plasma Regeneration of Diesel Particulate Filter

2.7.3.1. DIESEL PARTICULATE FILTER (DPF)

Regulation of automotive diesel engine emission becomes increasingly stringent every year, and it is difficult to meet the emission requirement only by combustion improvements (199) or EGR in the near future. Various types of postprocessing technologies for reduction of nitrogen oxides (NO_x) using catalyst (200,201) and nonthermal plasma process (44–59,196,197,202–205) have been investigated as explained in the Sections 2.2. and 2.7. However, more effective postprocessing technology is desired especially on particulate matter (PM), such as carbon soots.

Ceramics diesel particulate filter (DPF) made from SiC or cordierite has been widely used for the collection of carbon soot (194,206–209). A typical structure of DPF is shown in Fig. 81 (206,207). It is made from honeycomb ceramics. Black arrows denote a dusty gas and white arrows denote a clean gas. The flow passes through the wall of the porous filter because plugs alternately close the passes. Carbon soots are trapped at the wall of the porous filter. Although the use of DPF is now a leading technology for PM removal in diesel engines, the problem of soot incineration or regeneration exists, especially in a cold emission or an engine brake operation. Because engine power decreases as back pressure caused by the deposited soot increases, it must be removed periodically or continuously. This operation is called regeneration.

2.7.3.2. NONTHERMAL PLASMA REGENERATION METHODS

Various methods of DPF regeneration are illustrated in Fig. 82. The most typical regeneration process is shown in Fig. 82A. Soot removal or incineration is carried out under the oxygen rich environment using an electric heater or high temperature afterburner. However, since high temperatures around 600°C are needed for regeneration, melting or cracking of the DPF occurs.

Recently a regeneration method of NO_2 catalytic incineration system proposed by Johnson Matthey Inc. was given attention as shown in Fig. 82B (194,195). Incineration of soots begins with a low temperature of around 200°C if sufficient amount of NO_2 is available. Initially, NO, which occupies most diesel engine exhaust gases, is oxidized to NO_2 with the oxidation catalysts using noble metals. Then, the carbon soots deposited on the DPF react with generated NO_2 and are removed by the incineration. However, as shown in Fig. 83, a high temperature of around 300–400°C is required in order to activate
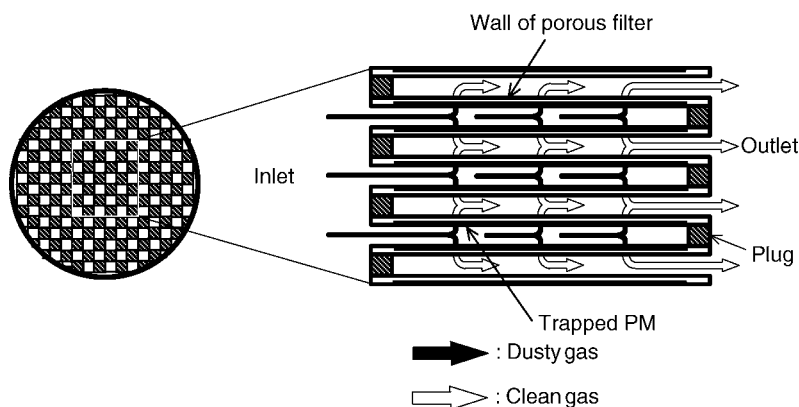
Fig. 81. Structure of the diesel particular filter (DPF).
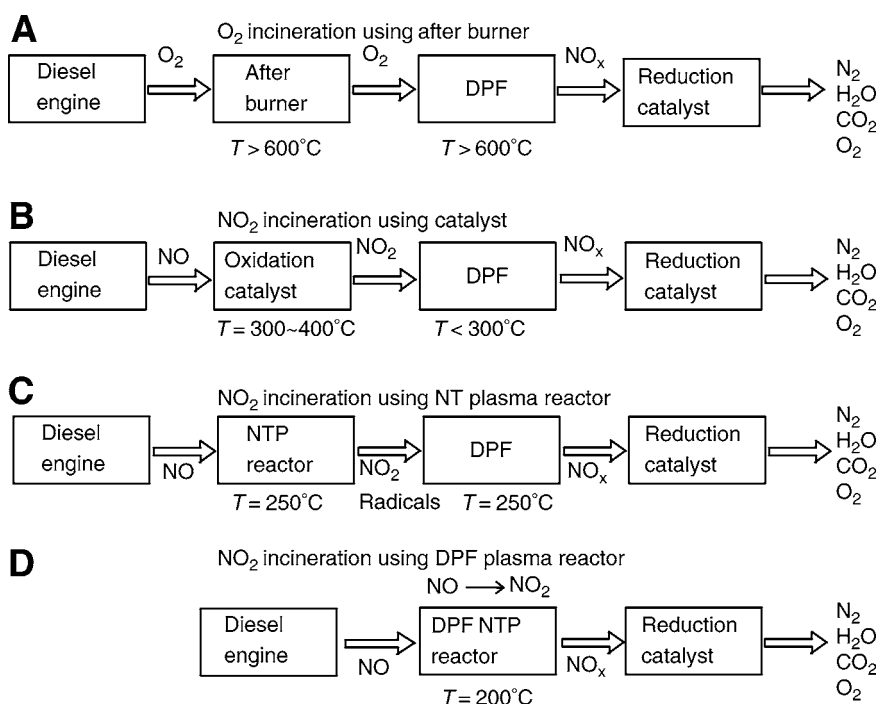
Fig. 82. Methods of DPF regeneration.

the oxidation catalysts enough. Moreover, the maximum efficiency of the oxidation catalyst is around 50%, and the problem exists on degradation of the oxidization catalyst under the influence of sulfur in light fuel.

More recently, a new concept of the regeneration method using nonthermal plasma (NTP) was proposed (194,210–216). This method is shown in Fig. 82C. The oxidation catalyst is replaced with a nonthermal plasma reactor generally exhibiting excellent performance of NO oxidation under low temperature (52,197). The emitted NO_2 and radicals induced by the plasma reactor incinerate carbon soot deposited inside DPF at lower
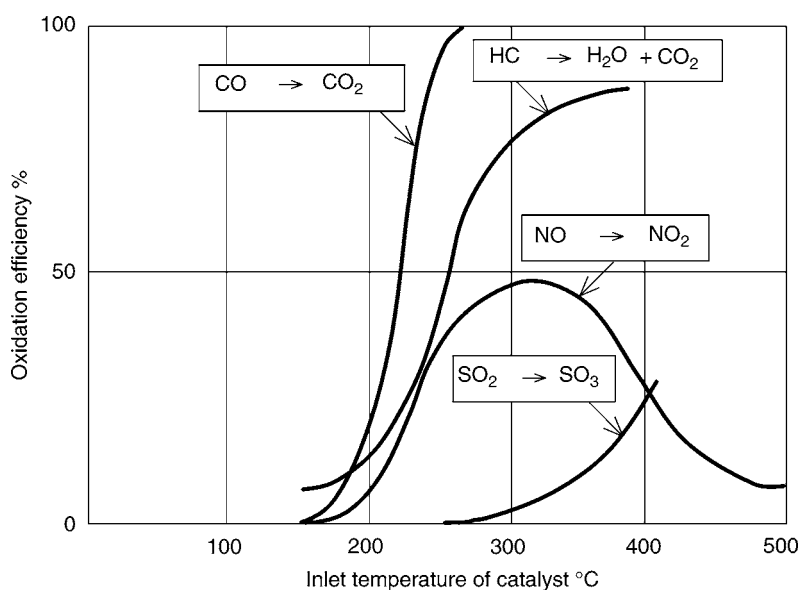
Fig. 83. Effect of inlet gas temperature on oxidation catalyst efficiency.

temperature less than 300°C. Because the oxidization catalyst is not used, there is no problem regarding catalyst degradation.

Further, from a viewpoint of a compact system, a new nonthermal plasma regeneration system was investigated in which DPF and a plasma reactor are unified as shown in Fig. 82D. In this system, the nonthermal plasma induced inside the honeycomb path of the DPF oxidize NO to NO_2, and the induced NO_2 and radicals incinerate trapped carbon soot simultaneously.

In this section, the nonthermal plasma regenerations of DPF conducted by the authors are reviewed. First, the experiment of DPF regeneration was shown using the barrier type pulse corona plasma reactor (indirect plasma) (214,216). Next, the experiment of DPF regeneration was conducted using the needle to plate pulse corona plasma reactor. In this plasma reactor called honeycomb nonthermal plasma reactor the DPF and the high voltage electrodes are unified (direct plasma) (215). It was confirmed that the pressure drop decreased when the plasma was applied and the regeneration of DPF with PM was observed at 200–300°C.

2.7.3.3. PLASMA REACTORS

The structure of the plasma reactors both in the direct plasma method and in the indirect plasma method is shown. Experiments were carried out in order to confirm the regeneration of DPF with collected carbon soots under low temperature condition (less than 250°C) by oxidizing NO to NO_2 using nonthermal plasma. A barrier type pulse corona plasma reactor shown in Fig. 84 was used. The inner diameter was 20 mm and the effective electrode length was 260 mm. The pulse high voltage power supply using a SI thyrister was used as the power supply. The frequency of the pulse was 210 Hz.

Prior to the regeneration experiment, NO oxidation performance of this plasma reactor was examined. The test of plasma oxidation was carried out with the simulated
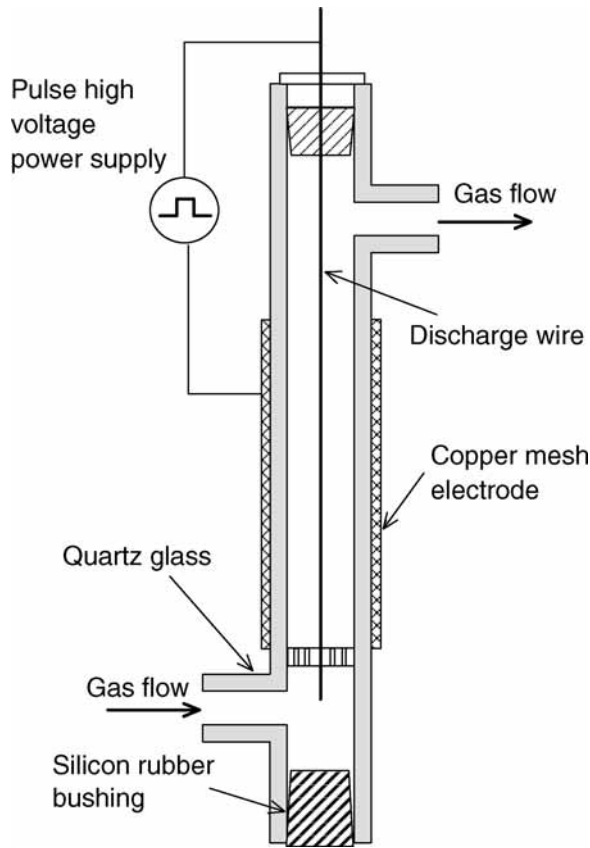
Fig. 84. Pulse corona plasma reactor for indirect DPF regeneration.

exhaust gas of NO = 316 ppm, NO_x = 348 ppm prepared by mixing the NO in the cylinder and dry air (RH = 10% at 20°C). The flow rate was Q = 3 L/min. The applied voltage and discharge power consumption was 45 kV and 2 W respectively. The results shows that NO = 95 ppm, NO_x = 348 ppm, CO = 10 ppm, O_2 = 20.50%, CO_2 = 414 ppm, and N_2O = 0 ppm. Seventy percent of 316 ppm NO could be oxidized to NO_2 at room temperature.

The cross-section of the direct DPF nonthermal plasma reactor is shown in Fig. 85. The reactor consists of a needle to perforated plate type. The gap distance between the needle and the grounded electrode is 33 mm and the length of the needle was 7 mm. A cordierite ceramics DPF (diameter of 50 mm, length of 25 mm, electrical resistivity of $10^{12}\Omega\cdot$cm, the number of cells of 100 cpsi and the thickness of porous filter wall of 17 mil) is located between the needles and the plate. Because of the high resistance of DPF, the nonthermal plasma is induced inside each honeycomb path of the DPF by applying a pulse high voltage between the electrodes. It was observed that the nonthermal plasma was actually induced inside each path of DPF. Therefore, this plasma reactor was named the honeycomb nonthermal plasma reactor.

Prior to a regeneration experiment, NO oxidation performance of this plasma reactor was examined. The plasma oxidation was carried out using simulated gas of 320 ppm
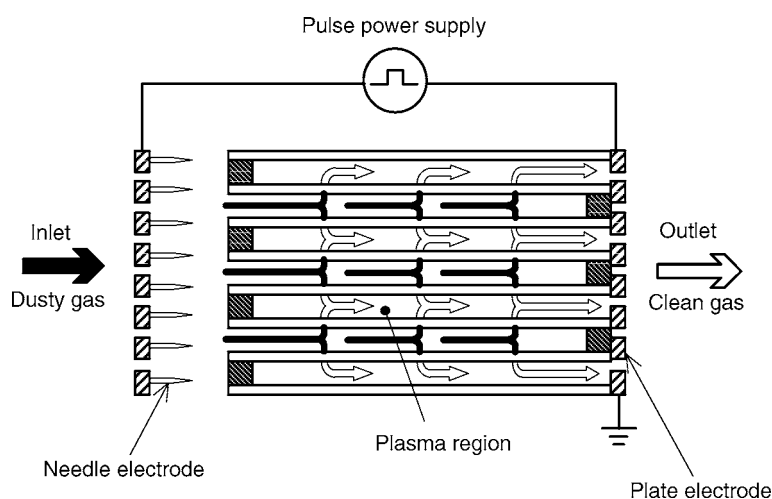
Fig. 85. Honeycomb nonthermal plasma reactor for direct regeneration of DPF.

of NO, and 349 ppm of NO_x, prepared by mixing the NO in the cylinder with dry air (RH = 10%, 20°C). The flow rate was set at $Q = 3$ L/min. The applied voltage, frequency and discharge power was maintained at 45 kV, $f = 15$ Hz, and 1.4 W, respectively. When the pulse high voltage was applied, the concentration of NO_x increased with increase in the frequency at gas temperature of 200°C. Therefore, the frequency was set at a lower value of $f = 15$ Hz. The results show that NO = 201 ppm, $NO_x = 349$ ppm, CO = 11 ppm, $O_2 = 20.83\%$, $CO_2 = 410$ ppm, and $N_2O = 1.5$ ppm, respectively. 63% of 320 ppm NO was oxidized to NO_2 at room temperature.

2.7.3.4. EXPERIMENTAL SETUPS

Figure 86 illustrates the experimental setup for indirect regeneration of DPF. After the gas passes through the plasma reactor, the NO_2 and radicals (O, N, OH) were induced. The activated gas flowed into the quartz tube (inner diameter = 50 mm) in which the cordierite DPF with deposited carbon soots was inserted and heated at constant temperature with a tubular electric furnace. The gas temperature is monitored and kept constant (250°C) using a thermo controller and an optical fiber temperature sensor (Anritsu Meter Co., Japan, AMOTH FL-2000) inserted near the DPF. The dimensions of the DPF are as follows: diameter = 46 mm, length = 50 mm, and cell density = 100 cpsi. The mass of the deposited carbon soots per unit volume of DPF was 2.1 g/L. The pressure difference before and after the DPF was monitored and recorded using a semiconductor-type small pressure difference transducer (Kyowa Electronic Instruments Co., Japan, Ltd, PDV-25GA) and a digital recorder (Yokogawa electric corp., OR100E). The decrease in the carbon soot or regeneration was determined from the decrease in pressure difference.

Figure 87 shows the apparatus used for the direct regeneration of DPF using DPF honeycomb nonthermal plasma reactor. After the gas passed through the DPF plasma reactor, radicals (O, N, OH), and NO_2 were induced. The activated gas flowed into another DPF with deposited carbon soots downstream. The gas temperature monitored was kept constant (200°C) using a thermo controller and an optical fiber temperature
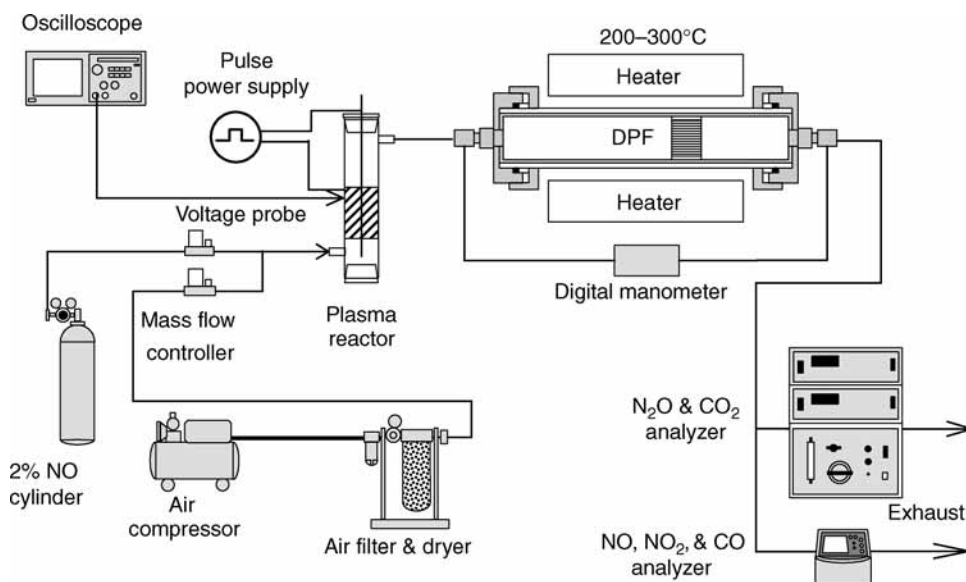
Fig. 86. Experimental setup for indirect regeneration test of DPF.
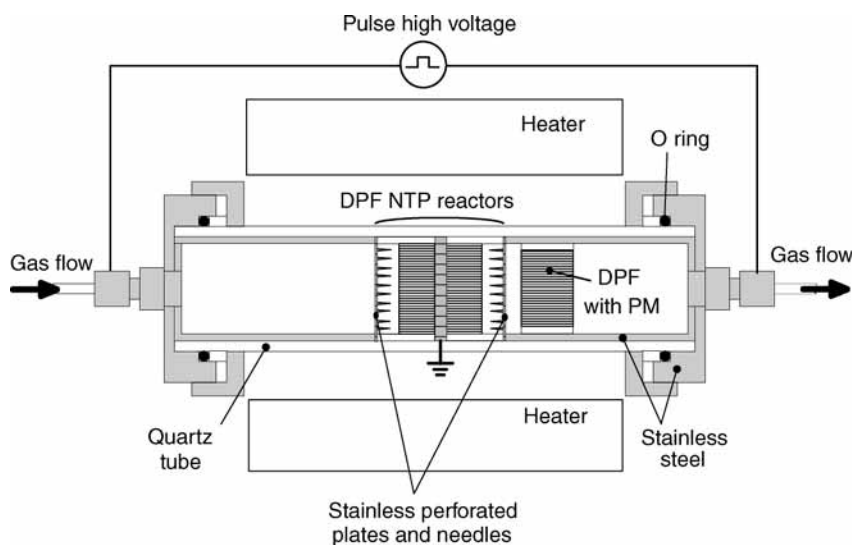
Fig. 87. Apparatus for direct regeneration test of DPF.

sensor (Anritsu meter Co., AMOTH FL-2000) inserted near the honeycomb NTP reactor. The total mass of deposited particulate matter per unit volume of DPF was initially estimated as 4.1 g/L (total mass is 0.33 g). This value is slightly more than the value of an ordinary automobile diesel engine. The pressure difference before and after the DPF was monitored and recorded using the semiconductor-type small pressure difference transducer (Kyowa electronic instruments Co., Ltd, PDV-25GA) and a digital recorder (Yokogawa Electric Corp., OR100E). The removal of carbon soots or regeneration
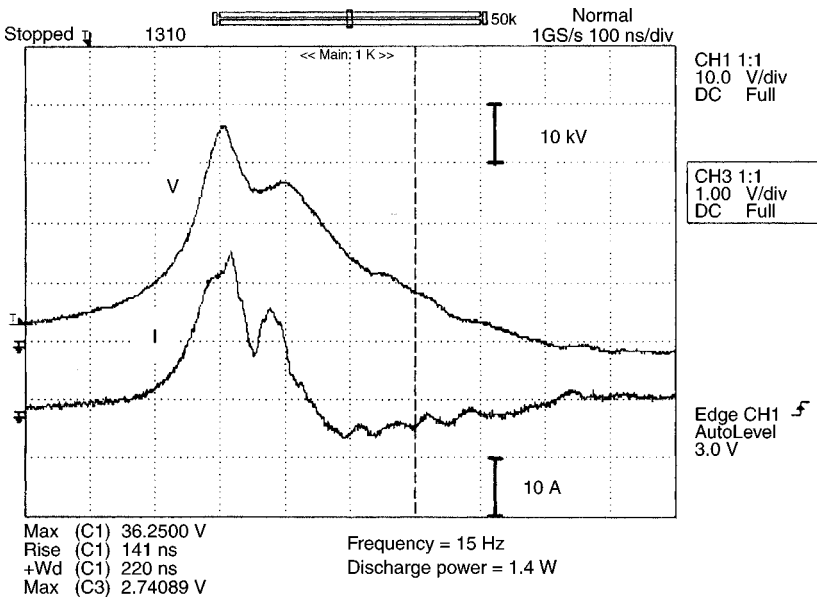
Fig. 88. Voltage and current waveforms of the honeycomb nonthermal plasma reactor.

can be known from the decrease in the pressure difference when the flow rate and gas temperature are kept constant. The voltage and current waveforms are shown in Fig. 88.

2.7.3.5. RESULTS OF INDIRECT REGENERATION EXPERIMENT

The experiment result of pressure difference against elapsed time t is shown in Fig. 89A. It is confirmed from the graph that the pressure difference decreases with time when the plasma is turned on and the plasma regeneration occurs. The temperature at the surface of the DPF inside the channel was 250°C.

Figure 89B shows the relation of gas concentrations vs elapsed time during the regeneration. The performance of the plasma reactor at room temperature is shown at the point of $t = 0$ when the plasma is turned on. When the regeneration starts at $t > 1$ (h), the concentrations of CO_2 and CO increase due to the incineration of carbon soots. The NO_2 and oxygen radicals induced by the plasma reactor are used to incinerate the carbon soot deposited inside the DPF, and the nearly 100% of it is reduced to NO according to the following chemical reactions:

$$C + 2NO_2 \rightarrow CO_2 + 2NO \tag{118}$$

$$C + NO_2 \rightarrow CO + NO \tag{119}$$

Incineration of oxygen radicals also occurs.

$$C + O^* \rightarrow CO \tag{120}$$

$$C + O_2^* \rightarrow CO_2 \text{ and so on.} \tag{121}$$
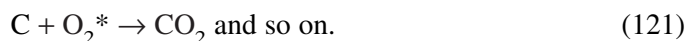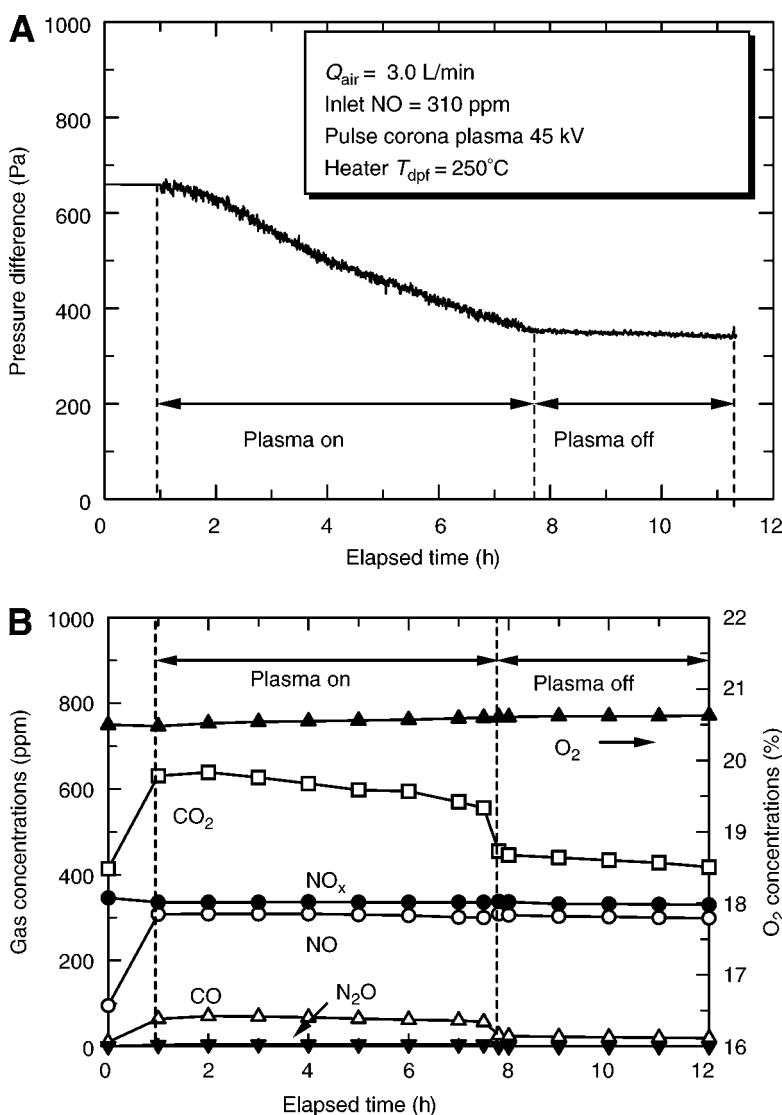
Fig. 89. Result of the indirect regeneration using the barrier type pulse corona plasma reactor. **(A)** Pressure difference vs elapsed time. **(B)** Gas concentrations during DPF regeneration.

For the regeneration, sufficient amounts of NO and O_2 are needed in the exhaust gas. The ratio of C/NO and C/O_2 can be controlled by adjusting the operation mode of the diesel engine. In the present experiment, the balance of carbon mass was fair. The mass of the incinerated carbon calculated from CO and CO_2 increased by 135 mg although the total mass of the deposited sediment on the DPF was around 170 mg. Approximately 75% of soot removal was achieved.

2.7.3.6. RESULTS OF DIRECT REGENERATION EXPERIMENT

In the direct DPF regeneration experiment, the experimental result of pressure difference vs elapsed time is shown in Fig. 90A. It is confirmed from the graph that
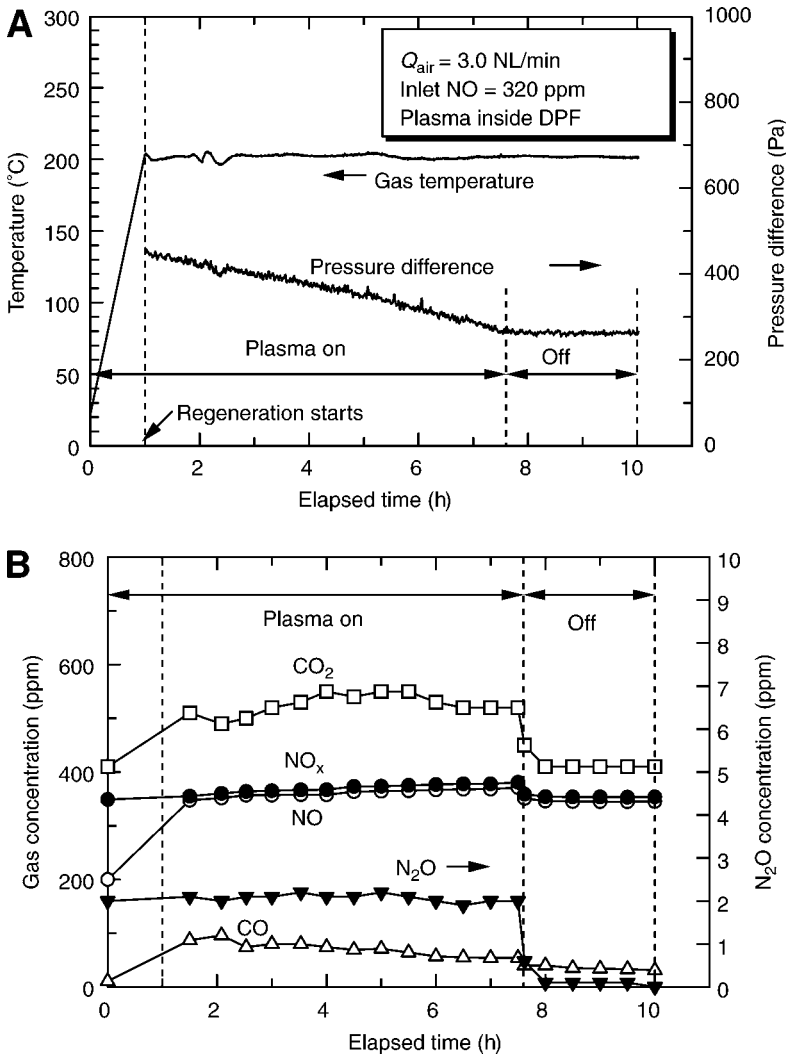
Fig. 90. Result of the direct regeneration using the honeycomb nonthermal plasma reactor. **(A)** Pressure difference vs elapsed time. **(B)** Gas concentrations during DPF regeneration.

the pressure difference decreases with time when the plasma is turned on and plasma regeneration occurs. The temperature at the surface of the DPF inside the channel was 200°C.

Figure 90B shows the relation of gas concentrations vs elapsed time during regeneration. The performance of the plasma reactor at room temperature is shown at point of $t = 0$ when the plasma is turned on. When regeneration starts at $t = 1$ (hour), the concentrations of CO_2 and CO increase due to the incineration of carbon soot. The NO_2 and oxygen radicals induced by the plasma reactor is used to incinerate the carbon soot deposited inside the DPF, and nearly 100% of NO_2 was reduced to NO according to the chemical reactions in Eqs. (118) and (119):
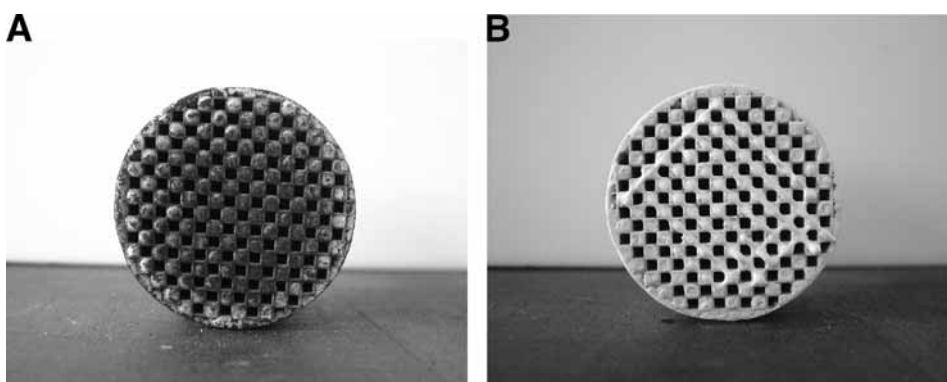
Fig. 91. Photographs of DPF before and after regeneration. **(A)** Before regeneration (mass = 55.2525 g). **(B)** After regeneration (mass = 55.0044 g).

The photograph of the DPF before and after regeneration is shown in Fig. 91. Most black carbon soots were burned and removed. It is confirmed from these results that the regeneration of DPF at a temperature of 200°C using the honeycomb nonthermal plasma reactor. It was known from the carbon mass balance that approx 80% of soot removal was achieved in 6.6 h. Initial loaded carbon mass was 330 mg and decreased carbon mass was 247 mg.

2.7.3.7. DESIGN EXAMPLE: ENERGY EFFICIENCY AND REGENERATION RATE IN NONTHERMAL PLASMA REGENERATION

Problem

As a measure of effective plasma treatment, the removal mass of carbon per unit time (regeneration rate) and the energy efficiency (*SED*) can be considered. The regeneration rate is obtained by dividing the removal amount of carbon mass by the regeneration time. The SED is defined as $60 \times$ Input power (W)/flow rate (L/min), which expresses the energy efficiency of plasma. In the left column of Table 8, speculation for a 3 l class automobile diesel engine, the concentration of carbon soot, and dimensions of DPF are shown. In the right column of this table, the most recent experimental results in the authors' laboratory are shown in Eq. (215). Complete the blanks (i)–(viii) in Table 8 according to the following procedures.

1. Calculate SV (surface velocity) value for the automobile engine and the regeneration experiment, where SV (1/h) is defined as the volume of the exhaust gas per unit time and unit DPF volume.
2. For the automobile diesel engine, calculate the minimum and maximum the volumetric densities of carbons or the carbon mass per unit exhaust gas volume (mg/Nm^3). Here, minimum and maximum masses of trapped soot were 400 and 4000 g, respectively.
3. Calculate the volumetric density of removed carbons (mg/Nm^3) in the experiment.
4. Calculate the specific energy density (*SED*) (J/L) in the experiment.
5. When the DPF is used in the 3 L engine, estimate the power required for the regeneration of the DPF from the experimental data. When the total power of the engine is 117 kW, what percent of it is required for the plasma power?
6. If SED =10 J/L is achieved, estimate the power required for the regeneration of the DPF. What percent of the total power 117 kW is required for the plasma power?

Table 8
Data for Automobile Real Diesel Engine and Plasma Regeneration Experiment

Data for an automobile diesel engine with DPF		Data of present plasma regeneration experiment	
Engine displacement volume (L)	3	Regeneration time (h)	4.6
Mileage (km)	1000	–	
Average velocity (km/h)	50	–	
Running time (h)	20	–	
Average rotation speed (rpm)	2000	–	
Min. mass of trapped soot (g)	400	–	
Max. mass of trapped soot (g)	4000	Mass of trapped soot (g)	0.18
Flow rate (Nm^3/min)	4	Flow rate (NL/min)	10
Total exhaust gas volume (Nm^3)	4800	Total exhaust gas volume (Nm^3)	2.8
Diameter of DPF (cm)	20	Diameter of DPF (cm)	4.6
Length of DPF (cm)	40	Length of DPF (cm)	5
Volume of DPF (cc)	12560	Volume of DPF (cc)	83
SV value (1/h)	(i)	SV value (1/h)	(ii)
Min soot mass per unit gas volume (mg/Nm^3)	(iii)	Soot mass per unit gas vol. (mg/Nm^3)	(v)
Max soot mass per unit gas volume (mg/Nm^3)	(iv)	–	
–		Discharge power of plasma (W)	13
–		SED (J/L)	(vi)
–			
		Power for 3 L engine (present) (kW)	(vii)
–		Power for 3L engine (aimed value) (kW)	(viii)

Solution

1. From the definition of SV and Table 8, the values of SV are calculated as

$$\text{Automobile diesel engine SV, (a)} = \frac{4\left(\dfrac{Nm^3}{min}\right) \times 60\left(\dfrac{min}{h}\right)}{12560\,(cc) \times 10^{-6}\left(\dfrac{m^3}{cc}\right)} = 19,108\,(1/h) \qquad (122)$$

$$\text{Regeneration experiment SV, (b)} = \frac{10\left(\dfrac{NL}{min}\right) \times 60\left(\dfrac{min}{h}\right)}{83\,(cc) \times 10^{-3}\left(\dfrac{L}{cc}\right)} = 7229\,(1/h) \qquad (123)$$

2. In the automobile diesel engine operation for 20 h, total exhaust gas volume is 4800 Nm^3, minimum and maximum mass of trapped soot are 400–4000 g. Therefore,
Mass of the trapped soot per unit exhausts gas volume,(c)–(d)

$$= \frac{400 - 4000\,(g)}{4800\,(Nm^3)} = 83 - 833\left(\frac{mg}{Nm^3}\right) \qquad (124)$$

3. In the regeneration experiment for 4.6 h, total exhaust gas volume is 2.8 Nm^3 and mass of incinerated carbon soot is 180 mg. Therefore,
   Mass of the incinerated soot per unit exhaust gas volume, (e)

$$= \frac{180\,(\text{mg})}{2.8\,(\text{Nm}^3)} = 64\left(\frac{\text{mg}}{\text{Nm}^3}\right) \tag{125}$$

This value is the same order as the soot concentration in real diesel engines with lighter loads obtained in the Eq. (124). Therefore, nonthermal plasma regeneration is possible at the same order rate as that at which soot deposit in the DPF.

4. In the experiment, power consumption of the plasma is 13 W and the flow rate is 10 NL/min. Therefore,

$$\text{SED, (f)}\ 1 = \frac{60 \times 13\,(\text{W})}{10\left(\dfrac{\text{NL}}{\text{min}}\right)} = 78\left(\frac{\text{J}}{\text{NL}}\right) \tag{126}$$

5. Required plasma power, (g)

$$= 78\left(\frac{\text{J}}{\text{NL}}\right) \times 4000\left(\frac{\text{NL}}{\text{min}}\right) \times \frac{1}{60}\left(\frac{\text{min}}{\text{s}}\right) \times \frac{1}{1000}\left(\frac{\text{kW}}{\text{W}}\right) = 5.2\,(\text{kW}) \tag{127}$$

$$\text{Plasma power/total engine power} = \frac{5.2\,(\text{kW})}{117\,(\text{kW})} \times 100 = 4.4\% \tag{128}$$

Further improvement of energy efficiency or decrease in SED is required.

6. Required plasma power, (h)

$$= 10\left(\frac{\text{J}}{\text{NL}}\right) \times 4000\left(\frac{\text{NL}}{\text{min}}\right) \times \frac{1}{60}\left(\frac{\text{min}}{\text{s}}\right) \times \frac{1}{1000}\left(\frac{\text{kW}}{\text{W}}\right) = 0.67\,(\text{kW}) \tag{129}$$

$$\text{Plasma power/total engine power} = \frac{0.67\,(\text{kW})}{117\,(\text{kW})} \times 100 = 0.57\% \tag{130}$$

This is considered to be in a practical level.

2.8. Gas Concentration Using Nonthermal Plasma Desorption

2.8.1. Adsorption and Nonthermal Plasma Desorption

In hazardous air pollutant (HAP) emissions or flue exhaust gases from factories, power stations and automobiles, the gas flow rates are generally high and their concentrations are low (in ppm levels). When exhaust gas with a large flow rate and low concentration is treated directly, the size of the equipment necessary becomes large, resulting in high operation costs. As a more economical technology, the exhaust gas is initially adsorbed to the absorbent for a long time and then, desorbed from it in a short time period so that exhaust gas with a large flow rate and low concentration may be converted to the one with a small flow rate and high concentration. The concept for this process is explained in Fig. 92. Concentrated exhaust gas can be treated later by, for example, SCR, electron beams or by reported plasma–chemical techniques with high efficiency. In the adsorption process, activated carbon, activated alumina, or molecular sieve (217–219) is generally used as absorbent materials and incinerated or disposed
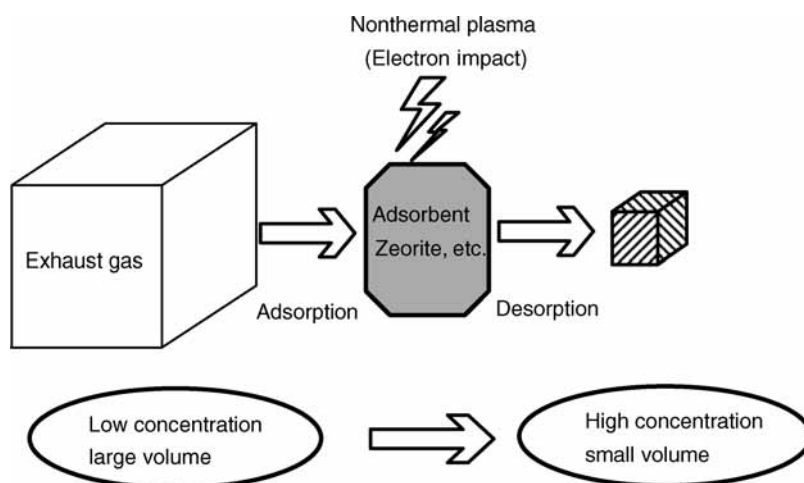
Fig. 92. Concept of concentrating exhaust gas using adsorption and nonthermal plasma desorption (© 2002 IEEE).

after use. Some adsorption materials can be used repeatedly and regenerated by heat or steam additions, or by the pressure and temperature swing adsorption (PSA and TSA) (220), However, this entails the additional costs of preparing high temperature gas, steam, low pressure state, apparatus, and energy.

The process we have developed may be characterized as using the nonthermal plasma for desorption from the absorbent material by high-energy electron impacts. Because the nonthermal plasma is used, the system can be operated at room temperature and atmospheric pressure. If this process is combined with nonthermal plasma gas cleaning technology, there is a possibility to decrease the specific energy density further. This new concept, nonthermal plasma desorption or regeneration was successfully demonstrated for methyl ethyl ketone (MEK, $CH_3CH_2COCH_3$) (221), Benzene (172), and NO_x (222,223). In other related studies, odor components adsorption using the functional fabrics prepared by plasma–graft polymerization as explained in the Section 3.4., and gas-phase contaminant removals from material surfaces using low-pressure glow discharge plasma (224,225) were reported. In the present section, we focused on one of the difficulties in desorbing the hazardous pollutant NO_x. The methods for adsorption and concentrating desorption of NO_x using this unique nonthermal plasma technology were demonstrated.

2.8.2. Plasma Reactor and High-Voltage Power Supplies

A barrier-type packed-bed plasma reactor shown in Fig. 93 was used for adsorption and desorption. This reactor consisted of a 1.6 mm diameter stainless-steel wire electrode and a Quartz glass tube (20 mm inner diameter and 24 mm outer diameter) as a dielectric barrier around which the copper screen was wrapped as the other electrode. Around 2 mm in diameter molecular sieve pellets (MS-13X, pore size of 1 nm, relative dielectric constant = 4–5, made of zeolite) were packed inside the tube. It was reported in the papers (222,223) that molecular sieve pellets with a pore size of 1 nm was best
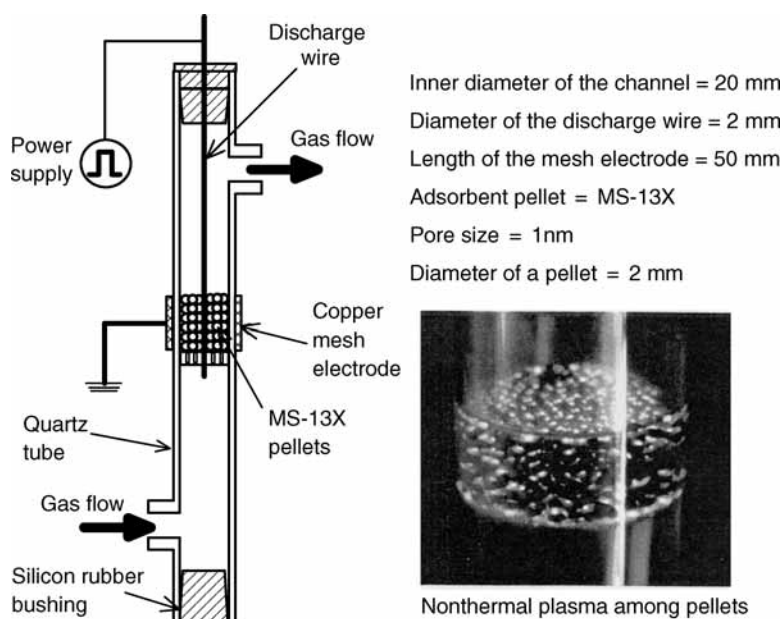
Fig. 93. Pulse corona packed-bed plasma reactor for plasma desorption and photograph of plasma among pellets.

for NO adsorption compared with those with pore sizes of 0.3, 0.4, 0.5 nm. The pellets were held by a perforated Teflon plate at the bottom end. The reactor contained 15.7 mL (5 cm high) of these pellets. The width of the copper mesh electrode was the same as the height of pellets′ layer. The nonthermal plasma induced among the pellets desorbed NO from the pellets.

Any one of AC 60 Hz high voltage (Peak-to-peak voltage $V_{p–p}$ = 20 kV) induced by a neon transformer, or AC 20 kHz high voltage ($V_{p–p}$ = 10 kV) induced by a semiconductor-type transformer or 210 Hz pulsed high voltage (rise time = 75 ns, pulse width = 1.2 ms, peak voltage $V_{p–0}$ = 32 kV) induced by an electric circuit (Fig. 94) with a rotary spark gap switch was applied to the plasma reactor. Because a rapid and sharp voltage rise could be obtained with lower power using the pulse power supply compared with an AC power supply, more effective plasma desorption could be expected when using the pulse power supply.

The discharge power of the reactor was obtained by averaging the product of the voltage and current waveforms. The values of the discharge power of the reactor for a fixed voltage are shown in Table 9 for three kinds of the power supplies. The following experiments on the desorption process were carried out under these conditions.

2.8.3. Experimental Apparatus and Method

The layout of the experimental setup is shown in Fig. 95. In order to prepare the simulated exhaust gas, 2% NO balanced with N_2 in a cylinder was mixed with dry clean air (relative humidity–10%) from a compressor through a filter and dryer. The desired concentration and flow rate were obtained using the mass flow control valve on each line.
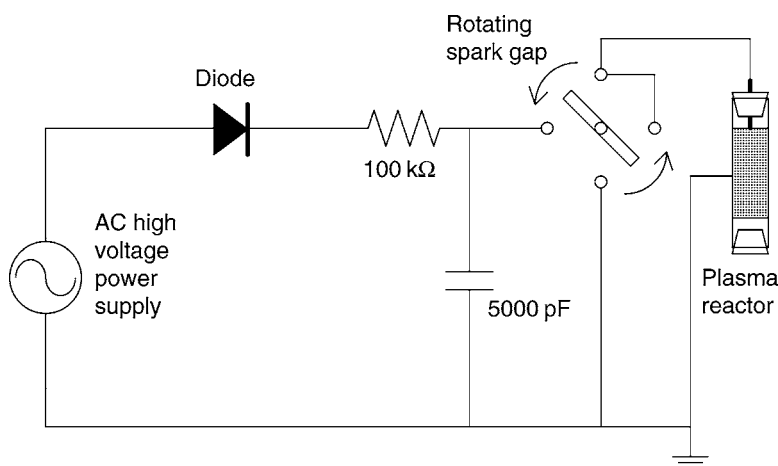
Fig. 94. Circuit with rotary spark gap switch for applying high voltage pulse power to the reactor (© 2002 IEEE).

Table 9
Voltage vs Discharge Power for Tested
High Voltage Power Supplies

Power supply	V_{p-p}, V_{p-o} (kV)	Discharge power (W)
AC 60 Hz	20	9.3
AC 20 kHz	10	8.9
Pulse 210 Hz	32	2.1

© 2002 IEEE.

The gas passed through the reactor in which the adsorption and plasma desorption were performed. The surface temperature of the reactor, which refers to the local temperature of a 5×5 mm^2 area painted black on a copper mesh surface, was monitored with an infrared radiation thermometer. The accuracy of the temperature measurement was to 1°C. The NO concentration and reaction byproducts such as NO_x (= NO + NO_2), CO and N_2O were measured by gas analyzers (Horiba, Ltd., Japan, PG-235: chemilumines-cence NO–NO_2–NO_x, infrared absorption for CO and Horiba, Ltd., VIA-510: infrared absorption for N_2O). In order to remove high concentration ozone (–400 ppm) that was induced by the plasma and often damaged the diaphragm of gas pumps inside the gas analyzer, the gas was passed through a tubular-type heater (Isuzu Co., Japan, AT-58) before the gas analyzer. The inner temperature of the heater was kept at 300°C. Verifications were made so that the heater did not induce any additional NO_x and byproducts during the experiment.

2.8.4. Experimental Results and Discussions

2.8.4.1. ADSORPTION AND DESORPTION CHARACTERISTICS OF NO_x WITH AN AC 60Hz POWER SUPPLY

Adsorption is generally classified as physical or chemical. The physical adsorption is based on van der Waals' attraction force on surfaces, whereas chemical adsorption is
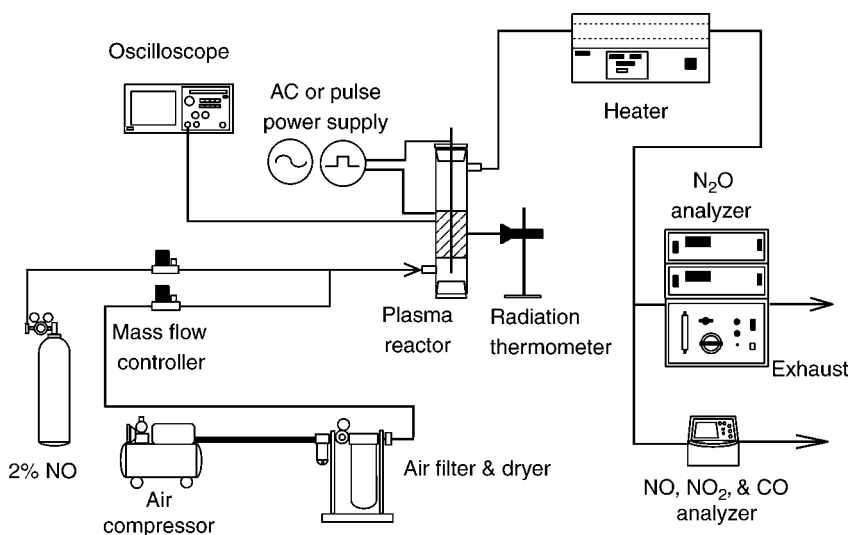
Fig. 95. Layout of the experimental setup for adsorption and plasma desorption (© 2002 IEEE).

related to the chemical reaction or the transfer of electrons and ions between adsorbent surface and molecules. In the present study, it is considered that the adsorption occurred physically because NO was reversibly removed with large heat addition.

First, NO adsorption and plasma desorption characteristics of MS-13X pellets were investigated using an AC 60 Hz high voltage power supply. The 4000 ppm NO was adsorbed by the MS-13X pellets inside the reactor for 30 min. with a flow rate of 2 L/min. In order to adsorb large amounts of simulated gas into the pellets for a short time, the concentration was set at a high value of 4000 ppm in this case. The investigation of the adsorption/desorption with low concentration NO_x is another important theme because normal concentration of NO_x is around 200–300 ppm in stationary sources. After adsorption, the NO was desorbed from the pellets by applying a high voltage with fresh dry air of 1.2 L/min. This adsorption/desorption process was repeated three times. Figure 96A shows the relation between the NO concentration at the reactor exit and the elapsed time in the adsorption process. In this result, over 85% of NO was adsorbed for 30 min. Figure 96B shows the time-dependent plasma desorption characteristics for 30 min. In this graph, the concentration of NO_x (= NO + NO_2) is taken in the vertical axis because the part of desorbed NO was oxidized to NO_2 by the plasma. In the result, all the NO_x adsorbed on the molecular sieve was not fully desorbed in each process. Some amount of NO remained inside the pellets in each process. When all the NO_x was desorbed in a single desorption process with longer periods, the concentrating desorption was difficult using plasma. During the experiment, the surface temperature of the reactor was 40°C at maximum. Furthermore, in the desorption process, only a little amount of the byproducts (CO and N_2O) were detected (CO < 10 ppm, N_2O < 5 ppm). It was known from Fig. 96B that the concentration became high by repeating the adsorption/desorption process. The amount of desorbed NO for 30 min in the second adsorption was three times more than that in the first adsorption.
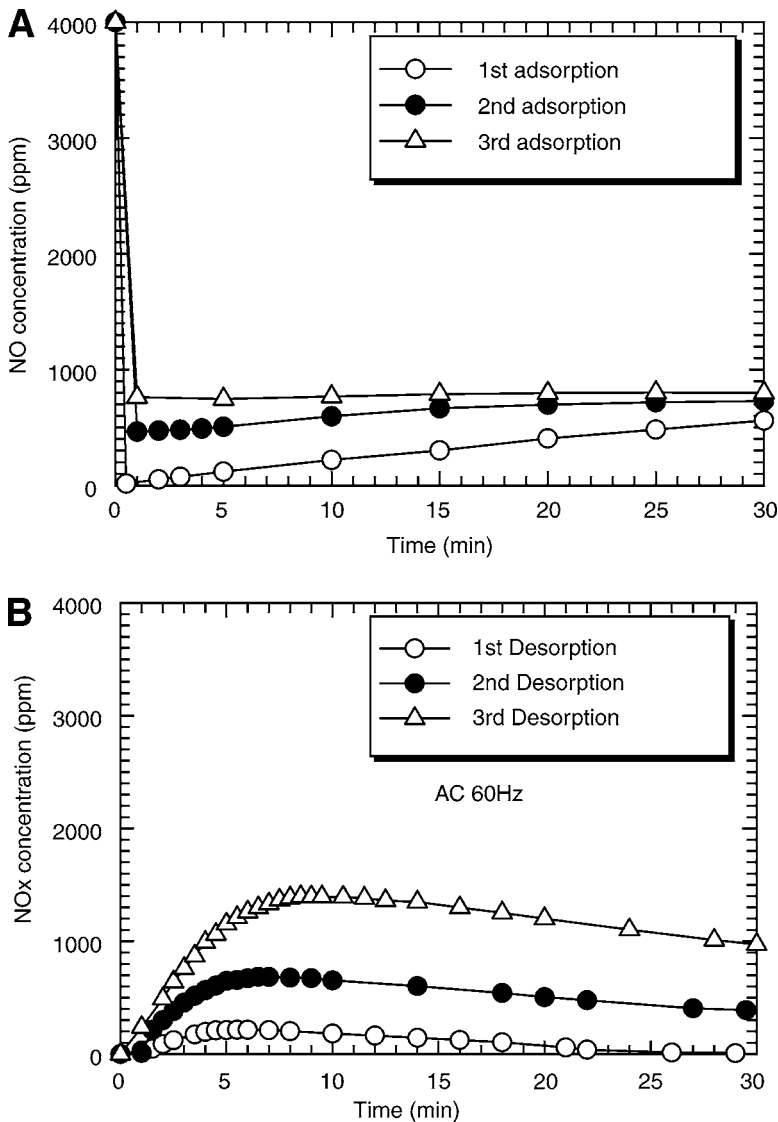
Fig. 96. Adsorption and plasma desorption of NO_x with AC 60 Hz power supply (© 2002 IEEE). **(A)** Adsorption processes (gas flow rate = 2 L/min, inlet NO concentration = 4000 ppm). **(B)** Desorption processes (air flow rate = 1.2 L/min, V_{p-p} = 20 kV).

2.8.4.2. CONCENTRATING DESORPTION CHARACTERISTICS OF NO_x WITH AN AC 20 KHZ POWER SUPPLY

Next, desorption was attempted using plasma induced by a higher frequency, the AC 20 kHz high voltage power supply. After the simulated exhaust gas of 1 L/min and 100 ppm NO was adsorbed in the MS-13X pellets for 10 h, the adsorbed NO was desorbed by applying the plasma using an AC 20 kHz power supply. In order to demonstrate the conversion of gas with a large flow rate and low concentration to the

one with a small flow rate and higher concentration using the adsorption/desorption process, relatively lower concentration 100 ppm of NO gas was adsorbed to the pellets for a longer period. The results of this adsorption and desorption process is shown in Fig. 97A,B. In Fig. 97A, the 100 ppm NO was adsorbed efficiently for 10 h. The maximum concentration of NO after the reactor was 13 ppm. In the desorption process shown in Fig. 97B, high voltage was applied to the reactor as fresh air was flowed at 1.2 L/min. In this result, large amount of NO desorption was observed. After 3 min, the concentration in desorption reached 2500 ppm which is the limitation value of the NO_x analyzer. Further, as soon as the high voltage was turned on, the reactor emitted thin purple light and the reactor surface temperature began to increase.

Because it was considered that the gas temperature was higher than the surface one, NO_x may be additionally induced by the oxidation of air (a kind of thermal NO_x). The amount of the induced NO and the surface temperature were measured using new unadsorbed pellets. The surface temperature increased up to 190°C and the concentration of the induced thermal NO_x was 70 ppm after 4 min since the voltage was turned on. From these results, the desorption with AC 20 kHz took place not only by the electron impacts or plasma but also by addition of heat. However, the amount of the thermal NO_x was relatively small compared with the desorption amount.

2.8.4.3. CONCENTRATING DESORPTION CHARACTERISTICS OF NO_x
WITH A PULSE POWER SUPPLY

It was known from the aforementioned results that the repetition of adsorption /desorption and the process of closing the reactor are effective in obtaining a high concentration of the desorbed NO_x. According to these results, the following experiments were carried out in order to demonstrate the NO_x of high concentration exceeding the concentration at the time of adsorption with little gas temperature rise. The concentration of NO at the time of adsorption was 1000 ppm and nonthermal plasma desorption was tried with a pulse power supply and air flow of 1.2 L/min. For the first 10 min in the adsorption process, the reactor was closed without air flow. The adsorption/desorption process was repeated 20 times. The results of the 1st, 5th, 10th, 15th, and 20th adsorption process, and the 1st, 5th, 10th, 15th, and 20th plasma desorption processes are shown in Figs. 98A,B respectively. The surface temperature during the experiment was under 50°C. In Fig. 98A, although the adsorption efficiency was not so high until the 10th adsorption, it became stable after the 10th. It was known from the result in Fig. 98B that the maximum concentration in desorption process increased as adsorption/desorption was repeated. After the 12th desorption, over 1000 ppm of NO_x, which excelled the concentration at the time of adsorption was detected. The maximum NO_x concentration in the desorption was nearly twice as high as that in the adsorption process.

Although the concentrating efficiency is not enough at the present time, the conversion to the NO_x of high concentration by nonthermal plasma is successful. After the 16th desorption, the concentration became smaller than the maximum value. This may have been caused by the complete removal of the NO layer on the surface of a pellet in
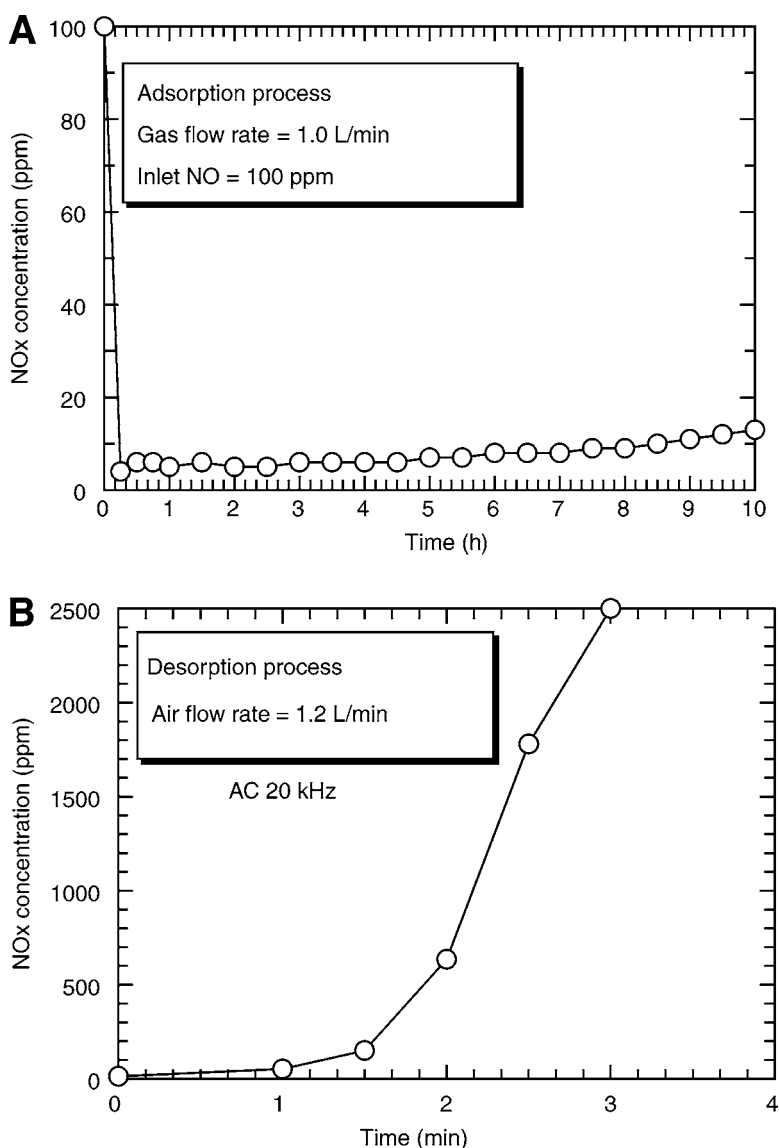
Fig. 97. Adsorption and plasma desorption of NO_x with AC 20 kHz power supply (© 2002 IEEE). **(A)** Adsorption process. **(B)** Desorption process.

the 16th desorption and the 17th desorption with lower concentration after a new NO layer was formed in the 17th adsorption.

In order to increase the efficiency of NO_x treatment using nonthermal plasma, a basic study was carried out for converting the exhaust gas with a large flow rate and low concentration into the one with a small flow rate and high concentration using the adsorption and nonthermal plasma desorption. In the industrial application of nonthermal plasma desorption, multiadsorbent tubes switching system or honeycomb adsorbent rotor
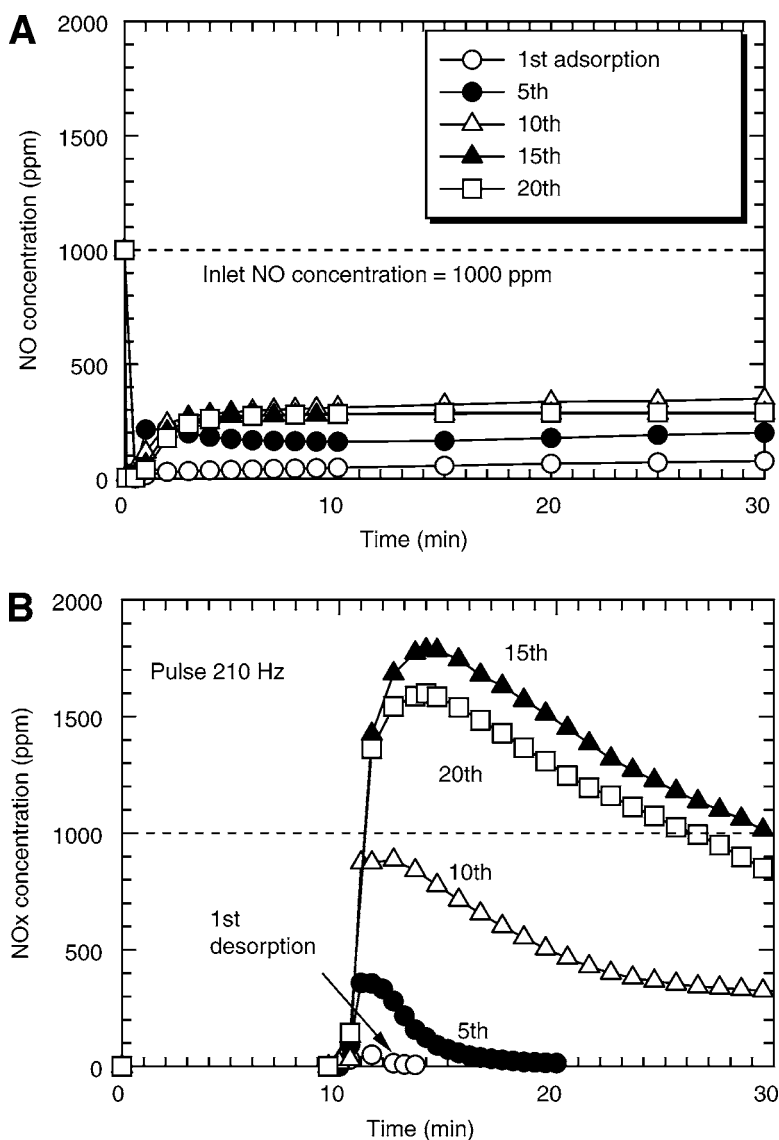
Fig. 98. Concentrating nonthermal plasma desorption with repeated adsorption/desorption (© 2002 IEEE). **(A)** The 1st, 5th, 10th, 15th, and 20th adsorption processes (gas flow rate = 2 L/min, inlet NO = 1000 ppm. **(B)** The 1st, 5th, 10th, 15th, and 20th plasma desorption processes (air flow rate = 0 L/min for time = 0–10 min. and 1.2 L/min for time = 10–30 min).

system should be combined with the plasma reactors. The concept of these systems is illustrated in Figs. 99 and 100.

2.9. Emission Gas Decomposition in Semiconductor Manufacturing Process

2.9.1. PFC Decomposition Using Nonthermal Plasma

Perfluorinated carbons (PFCs, not including hydrogen) and hydrofluorinated carbons (HFCs) such as CF_4, C_2F_6, and CHF_3, and SF_6, NF_3, are emitted from semiconductor
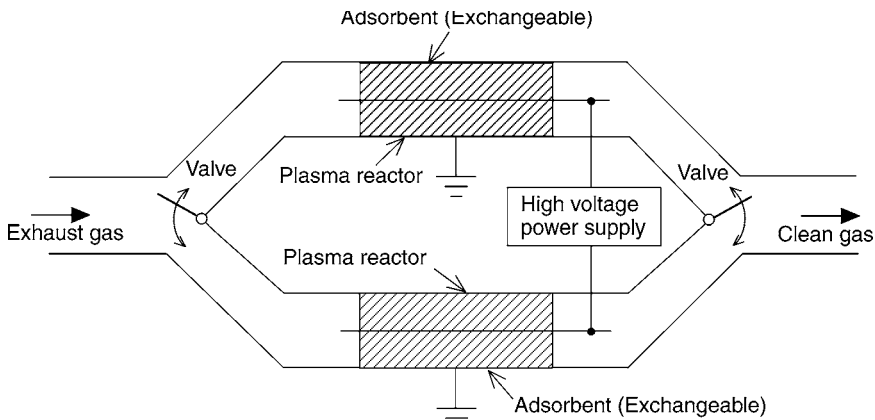
Fig. 99. Multiadsorbent tubes switching system combined with the plasma reactors.
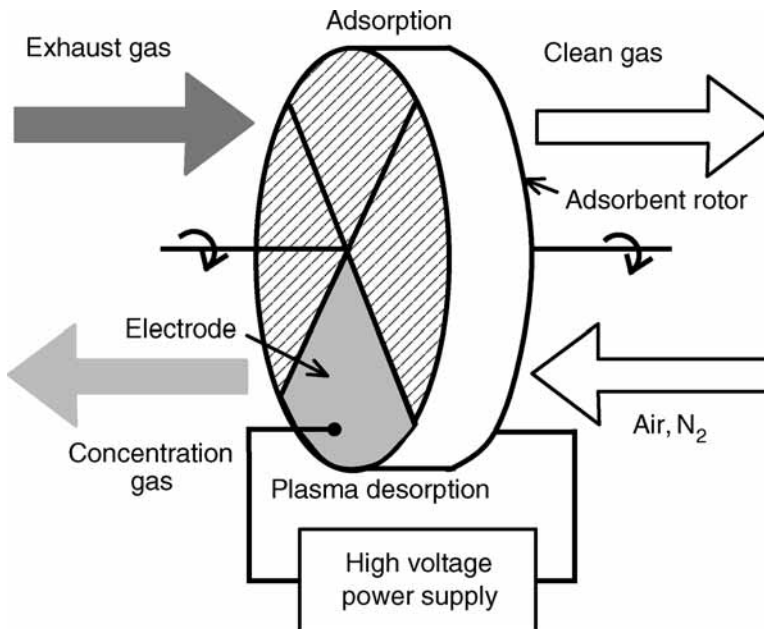
Fig. 100. Honeycomb adsorbent rotor system combined with the plasma reactor.

industries because these gases are used as the wafer etching and clean-up of CVD chambers. These gases are stable and have an extremely large global warming potential (GWP, Table 10) and a long life time in stratosphere. Therefore, it has been confirmed in the material of a regulation subject at the Kyoto conference (COP3) held in 1997 (226,227). It was agreed that the total amount of the exhaust must be reduced more than 10% in comparison with that of 1995 until 2010 in the World Semiconductor Council (WSC) in 1999. For these reasons, the emission of these gases has to be reduced worldwide. The total amount (unit million tons, CO_2 equivalent) of global warming emissions

Table 10
Global Warming Potential (GWP) and Lifetime
of Various Kinds of Gases

Gases	Global warming potential (GWP)	Lifetime (yr)
CO_2	1	50–200
CF_4	6500	50,000
C_2F_6	9200	10,000
SF_6	23,900	3200
NF_3	8000	700
CFC-11($CFCl_3$)	3400	65
CFC-12(CF_2Cl_2)	10,600	130
COF_2	≈ 1	–
CH_4	21	10
N_2O	310	150
CHF_3	11,700	264

Table 11
Amount of Typical Global Warming Gases' Emission in Japan (1995–2000)

Gases	GWP	1995	1996	1997	1998	1999	2000
Carbon dioxide (CO_2)	1	1217.8	1236.2	1233.5	1187	1225	1237.1
Methane (CH_4)	21	29.5	28.9	27.7	27.3	27	22
Dinitrogen oxide (N_2O)	310	21.8	22.8	23.5	22.3	16.5	36.9
Hydrofluorinated carbons (HFCs)	HFC-134a: 1300	20	19.7	19.6	19	19.5	18.3
Per-fluorinated carbons(PFCs)	PFC-14: 6500	11.4	11.2	14	12.4	11	11.5
Sulfur hexafluoride (SF_6)	23,900	16.7	17.2	14.4	12.8	8.4	5.7
Total amount		1317.3	1335.9	1332.7	1280.8	1307.4	1331.6

Data of Japan National council on environment (Cyuo kankyo shingikai).

in the year of 2000 in Japan is shown in Table 11. Although, the emitted total volumes of HFC_S and PFC_S are much smaller than CO_2, their contributions to the global warming effect can not be ignored because they have very large GWP.

To control the emission of PFCs and HFCs, the optimization of the processes such as the selection of alternative gas, the development of high efficiency abatement systems and capture-recycle systems were investigated (226). For the abatement technologies of PFCs and HFCs, catalytic decomposition, thermal decomposition or combustion, and chemical adsorption have been used conventionally. However, no significant economical and convenient technologies were available.

Recently, the PFCs abatement system using using plasma are remarkable (227–239). The plasma abatement system for PFCs removal is so compact that it was easily

attached to existing equipment. There are two types of plasma abatement systems: one is located downstream of the dry pump and is driven at atmospheric pressure, the other is located upstream of the dry pump and is driven at low pressure. For the former, because an exhaust gas is diluted a hundreds times by N_2 purge gas of a dry pump, the amount of exhaust gas increases and concentration reduces. Moreover, NO_x could be produced if the thermal plasma is used. The plasma abatement systems driven at low pressure is able to decompose exhaust gas from the process chamber directly without N_2 dilution of the dry vacuum pump.

In the present study, we investigated the CF_4 decomposition, which is one of the most stable gases and extremely difficult to decompose among PFCs, at low pressure (40 Pa). We investigated to employ the inductive coupled RF plasma (ICP) reactor (240), which can be used to generate the remote plasma in wafer etching process and chamber cleaning so that the wafer processing and CF_4 decomposition can be used by the same power supply. Many of the PFCs abatement systems using the plasma convert F to HF for the purpose of improvement in removal efficiency using H_2O. The produced HF reacts with calcium, and then is collected as CaF_2 using the scrubber. However, HF has a high potential of corrosion on pipes and other components, so our aim is to improve CF_4 decomposition efficiency without H_2O.

2.9.2. *Experimental Apparatus and Method*

The ICP reactor and RF power supply system are shown in Fig. 101 consists of alumina (Al_2O_3) tube. The length of tube is 300 mm and the diameter is 31 mm. The reactor tube is coiled with the two pipes which the diameters are 5 mm (10 turns × 2). The cooling water flows in one pipe. The cooling section is covered by silicone in order to cool the reactor tube uniformly. The two pipes are connected with a lead wire in series. The series pipes were energized by a high frequency power supply (Pearl Kogyo Co., Ltd, RP-2000-2M, frequency 2 MHz, max power 2 kW).

A schematic diagram of this experimental set-up is shown in Fig. 102. CF_4, O_2, Ar, He, and N_2 gases were prepared to simulate the exhaust gas from semiconductor manufacturing equipment. The desired flow rates and concentration were obtained with the mass flow controllers (MFC). The reactor was vacuumed by a dry pump (Ebara Co., A30W). The pressure in line was regulated by valves. The PIRANI-vacuum meter (ULVAC, Inc., GP-1000H) was used for the pressure measurement. The CF_4 concentration was measured using a GC with thermal conductivity detector (TCD) (Shimadzu Co., GC-8AI) after diluted with N_2 using a dry pump. Byproducts were analyzed using a Fourier Transform Infrared Spectrophotometer (FT-IR) with mercury cadmium telluride (MCT) detector (Biorad Co. FTS3000).

2.9.3. *Results and Discussions*

Figure 103 shows the relationship between the total flow rate and the CF_4 decomposition efficiency whereas maintaining the ratio of O_2 to CF_4 constant (O_2/ CF_4 = 0.9). The pressure and the power were set at 40 Pa and 1.2 kW, respectively. From this figure, the complete CF4 removal was achieved with the total flow rate of 0.189 NL/min which corresponds to the actual residence time of 0.01 s at reactor operating conditions. However, CF_4 decomposition efficiency decreased when the total flow rate increased.
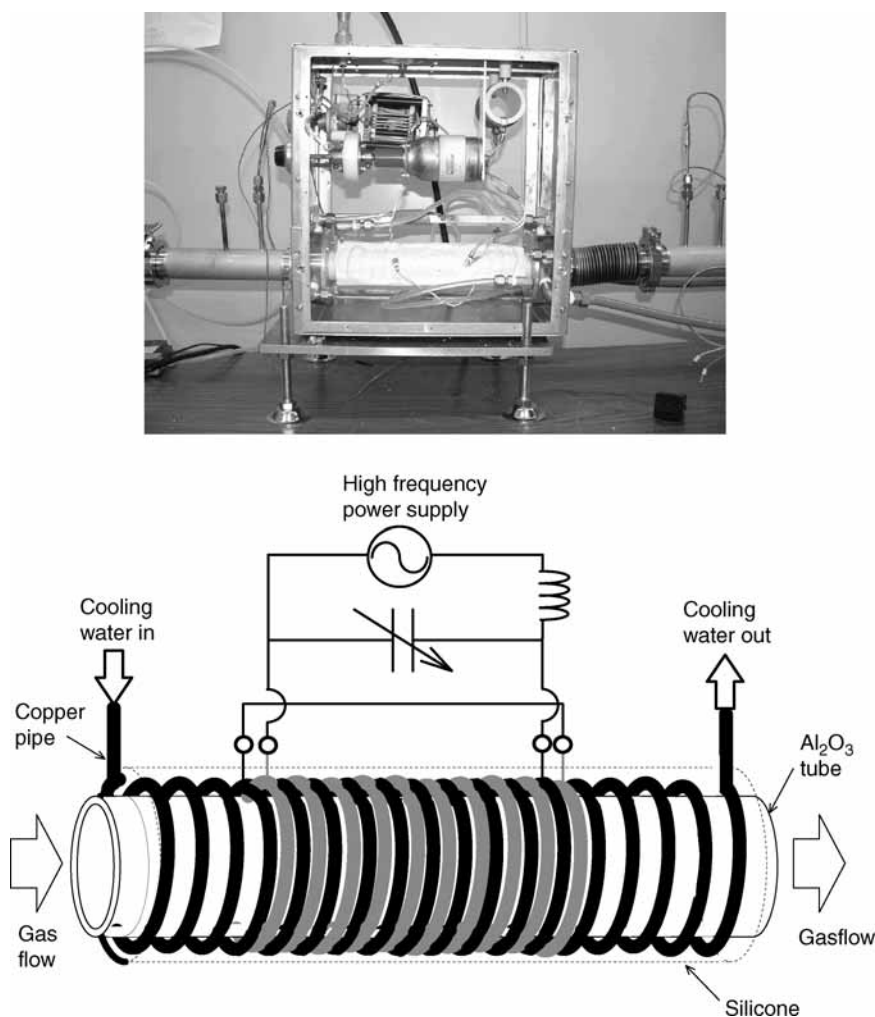
Fig. 101. ICP reactor for CF_4 decomposition.

Figure 104 shows the relationship between the power and the CF_4 decomposition efficiency. The pressure was set at 40 Pa and the flow rate of CF_4 and O_2 were set at 0.115 and 0.105 NL/min, respectively (here "NL/min" indicates the flow rate of 20°C and 1 atm). This result indicated that the power of more than 1.25 kW was required to decompose CF_4 completely when the total flow rate was 0.22 NL/min.

The experiments using argon (Ar), helium (He), and nitrogen (N_2) were investigated with the aim of enhancing CF_4 decomposition. The CF_4 flow rate was fixed at 0.115 NL/min. The ratio of CF_4 to these gases was changed with the fixed total flow rate in order to prevent the influence of change of the total flow rate to CF_4 decomposition efficiency.

Figure 105 shows the CF_4 decomposition efficiency as a parameter of the ratio of Ar, He, and N_2 to CF_4. The pressure and the power were set at 40 Pa and 1.2 kW, respectively. The total flow rate was fixed at 0.373 NL/min. From this figure, for Ar addition, as the ratio of Ar to CF_4 increased, the CF_4 decomposition efficiency increased. For He addition,
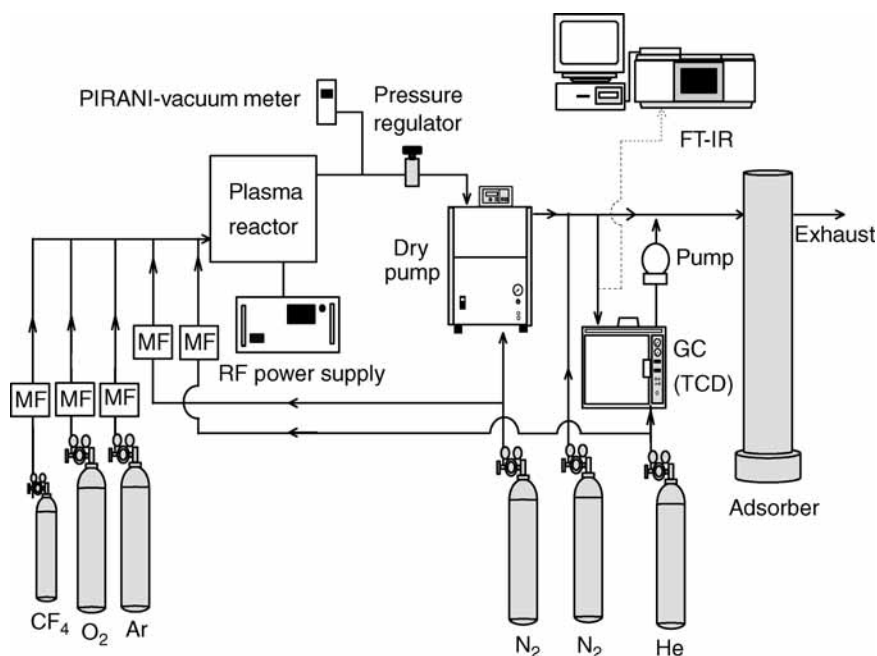
Fig. 102. Schematic diagram of the experimental setup.
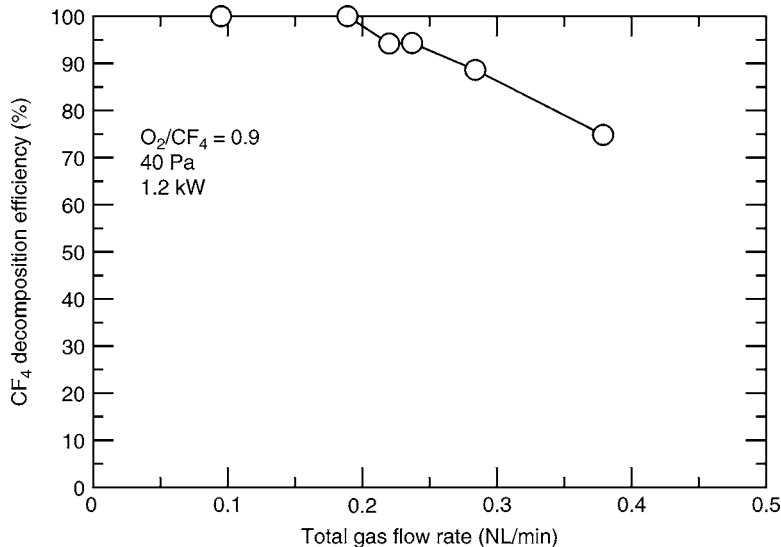
Fig. 103. Relation between the total flow rate and CF_4 decomposition efficiency.

it was indicated that there was no influence on CF_4 decomposition efficiency by changing He/CF_4. For N_2 addition, the CF_4 decomposition efficiency decreased as N_2 was added. Therefore, it is insignificant to add He and N_2 in the system, and the minimum amount of Ar to achieve the best decomposition efficiency was 0.65 times of CF_4.
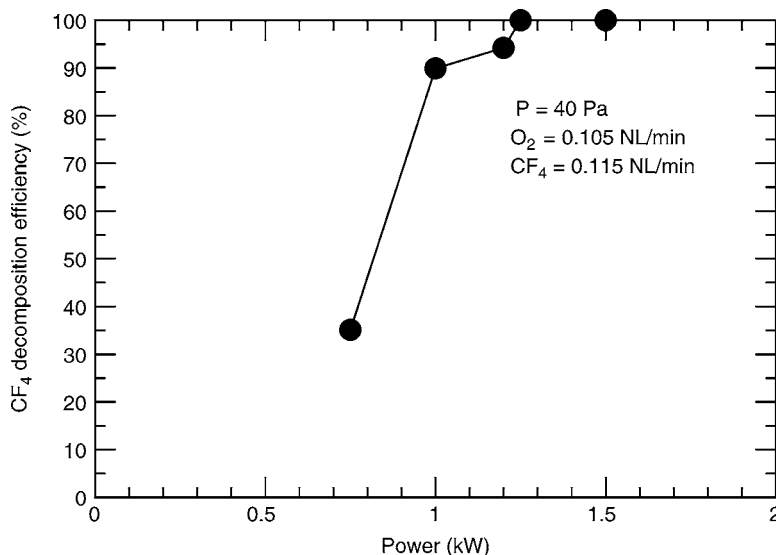
Fig. 104. Relation between power and CF_4 decomposition efficiency.
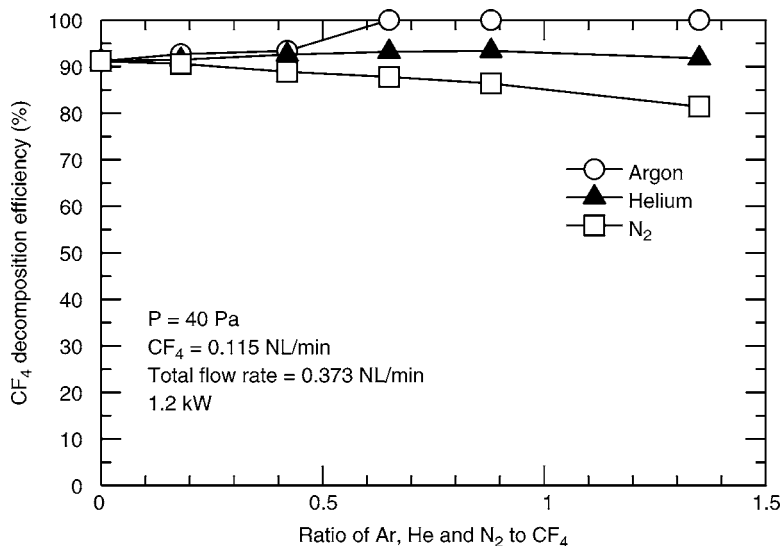
Fig. 105. CF_4 decomposition efficiency as a parameter of the ratio of Ar, He, and N2 to CF4.

Next, byproducts were analyzed using a FT-IR system. When gases which were treated by the plasma, they were sampled using a gas cell with and without the power of 1.2 kW after the dry pump, the spectra analysis were shown in Figs. 106A,B, respectively. The flow rate of CF_4 and O_2 were set at 0.115 and 0.105 NL/min. The pressure was set at 40 Pa. It is clear from these figures that CO and carbonyl fluoride (COF_2) and CO_2 are major byproducts. From these results, CF_4 was removed mainly according to the following chemical reactions:
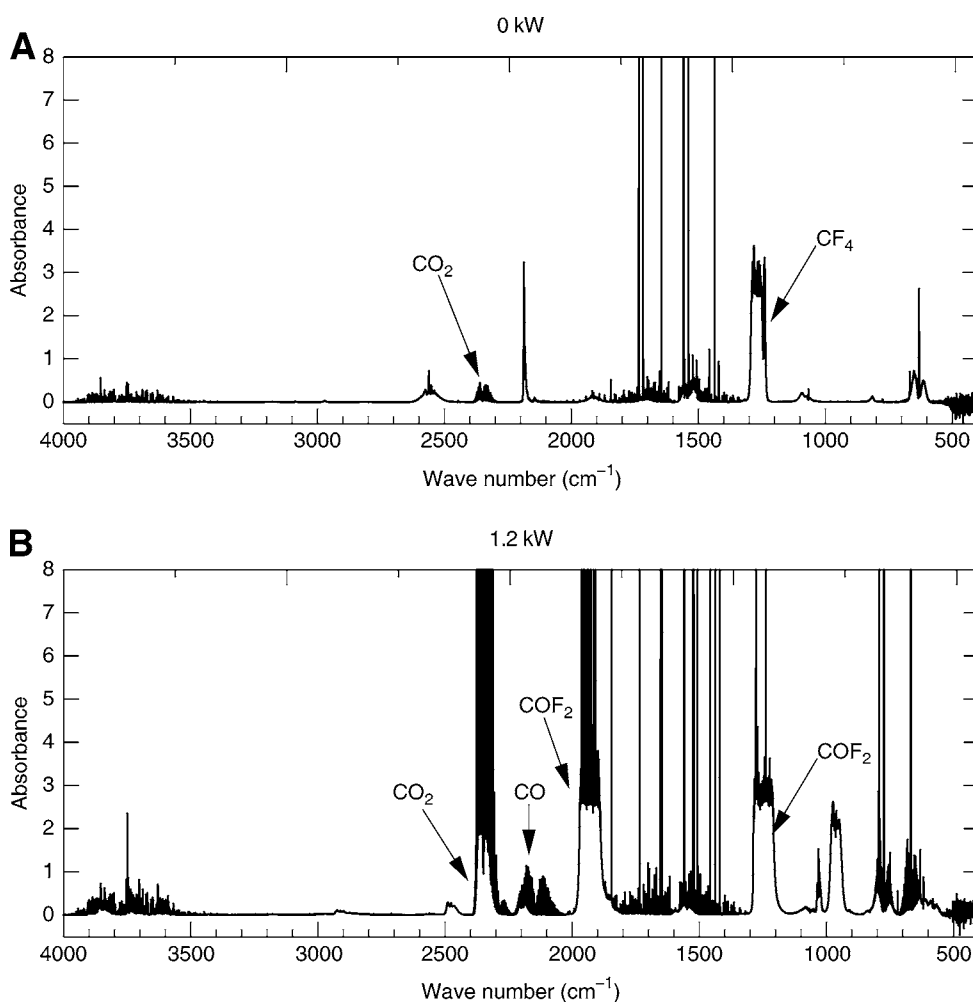
Fig. 106. FT-IR absorbance spectra ($CF_4 = 0.115$ NL/min, $O_2 = 0.105$ NL/min, pressure = 40 Pa). **(A)** 0 kW. **(B)** 1.2 kW.

$$CF_4 + O_2 \rightarrow CO_2 + 2F_2 \tag{131}$$

$$2CF_4 + O_2 \rightarrow 2COF_2 + 2F_2 \tag{132}$$

$$2CF_4 + O_2 \rightarrow 2CO + 4F_2 \tag{133}$$
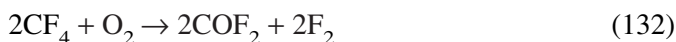
It is very interesting future work to know which reaction is most dominant and what is the molar ratio of the induced CO_2, COF_2, and CO. Note that the GWP of COF_2 is nearly one.

2.9.4. Design Example: PFC Plasma Decomposition System

Problem

In Fig. 103, the decomposition rate reaches 100% when the effective power is 1.2 kW in the condition that the absolute pressure is 40 Pa and the total flow rate is $Q = 0.1$ NL/min at 20°C, 1 atm. The inner diameter of the reactor is 31 mm and the effective length is 0.3 m.

1. Calculate the residence time of the gas inside the plasma reactor. The atmospheric pressure is 1.01325×10^2 kPa.
2. In designing the plasma reactor which can decompose the $CF_4 + O_2$ gases mixture (molar ratio: $O_2/CF_4 = 0.9$) of the total flow rate 0.13 NL/min using a quartz tube having the diameter of 40 mm when the input power is 1.2 kW and the absolute pressure is 60 Pa, determine the length of the plasma reactor having the same residence time as one calculated in the question 1.
3. When the plasma reactor in the question 1 is connected with three-set parallel, operated with the flow rate of $Q = 0.3$ NL/min and the total operating time is 3600 h/yr, calculate the total amount of CF_4 to be processed (mol/yr) and the electric bill needed for 100% decomposition (USD). It is assumed that the electric bill per unit power is 0.05 USD/kWh.
4. In the question 3, it is assumed that all electric power for the plasma is generated by a thermal electric plant and CO_2 is emitted in the rate of 670 g/kWh. Estimate the efficiency of the reduction in GWP (%). It is also assumed that the GWP of CF_4 is 6500, and that of COF_2 and CO is the same as CO_2 (= 1).

Solution

1. The total flow rate at 20°C and 40 Pa is

$$Q = \frac{1.01325 \times 10^5 \, (\text{Pa})}{40 \, (\text{Pa})} \times 0.1 \left(\frac{\text{NL}}{\text{min}} \right) = 253.3 \left(\frac{\text{L}}{\text{min}} \right) \tag{134}$$

The residence time is obtained by dividing the volume of the reactor *Vol* by *Q*.

$$t_r = \frac{Vol}{Q} = \frac{\frac{\pi}{4}(31 \times 10^{-3})^2 \, (\text{m}^2) \times 0.3 \, (\text{m})}{253.3 \left(\frac{\text{L}}{\text{min}} \right) \times \frac{1}{1000} \left(\frac{\text{m}^3}{\text{L}} \right) \times \frac{1}{60} \left(\frac{\text{min}}{\text{s}} \right)} = 5.36 \times 10^{-2} \, (\text{s}) \tag{135}$$

2. The total flow rate at 25°C and 60 Pa is

$$Q = \frac{1.01325 \times 10^5 \, (\text{Pa})}{60 \, (\text{Pa})} \times 0.13 \left(\frac{\text{NL}}{\text{min}} \right) = 219.5 \left(\frac{\text{L}}{\text{min}} \right) \tag{136}$$

In order to make the residence time the same value as that in Eq. (1), the length of the reactor L_p (m) should be determined from the equation:

$$t_r = \frac{\frac{\pi}{4}(40 \times 10^{-3})^2 \, (\text{m}^2) \times L_p \, (\text{m})}{219.5 \left(\frac{\text{L}}{\text{min}} \right) \times \frac{1}{1000} \left(\frac{\text{m}^3}{\text{L}} \right) \times \frac{1}{60} \left(\frac{\text{min}}{\text{s}} \right)} = 5.36 \times 10^{-2} \, (\text{s}) \tag{137}$$

From this Eq. (137), it is obtained, $L_p = 0.156$ m.

3. The total volume of CF_4 processed for a year is

$$V_t = 0.3 \left(\frac{\text{NL}}{\text{min}} \right) \times 60 \left(\frac{\text{min}}{\text{h}} \right) \times 3600 \left(\frac{\text{h}}{\text{yr}} \right) = 64{,}800 \left(\frac{\text{NL}}{\text{yr}} \right) \tag{138}$$

By the unit conversion to mol/yr,

$$m_{CF4} = \frac{64{,}800 \left(\frac{\text{NL}}{\text{yr}} \right)}{\frac{(273 + 20)}{273} \times 22.4 \, (\text{L})} = 2695 \left(\frac{\text{mol}}{\text{yr}} \right) \tag{139}$$

Because three reactors of 1.2 kW are used in series, the electric bill for a year is

$$\text{Bill} = 3 \times 1.2(\text{kW}) \times 3600 \left(\frac{\text{h}}{\text{yr}} \right) \times 0.05 \left(\frac{\text{USD}}{\text{kWh}} \right) = 648 \left(\frac{\text{USD}}{\text{yr}} \right) \quad (140)$$

4. The total amount of the electric energy for a year is

$$E_{\text{year}} = 3 \times 1.2\,(\text{kW}) \times 3600 \left(\frac{\text{h}}{\text{yr}} \right) = 12{,}960 \left(\frac{\text{kWh}}{\text{yr}} \right) \quad (141)$$

The amount of emitted CO_2 (mol/yr) to generate the electric energy E_{yr} (141) is

$$m_{CO_2} = 12{,}960 \left(\frac{\text{kWh}}{\text{yr}} \right) \times \frac{670 \left(\dfrac{\text{g}}{\text{kWh}} \right) \times 12{,}960 \left(\dfrac{\text{kWh}}{\text{yr}} \right)}{44 \left(\dfrac{\text{g}}{\text{mol}} \right)} = 1.97 \times 10^5 \left(\frac{\text{mol}}{\text{yr}} \right) \quad (142)$$

where the molecular weight of CO_2 is 44. On the other hand, the amount of decomposed CF_4 (mol/yr) equivalent to CO_2 effect

$$m_{CF_4(CO_2 \text{ eqivalent})} = 2695 \left(\frac{\text{mol}}{\text{yr}} \right) \times 6500 = 1.75 \times 10^7 \left(\frac{\text{mol}}{\text{yr}} \right) \quad (143)$$

From these calculations, the efficiency of the reduction in GWP (%) becomes

$$\eta_r = \left(1 - \frac{m_{CO_2} + m_{CF_4}}{m_{CF_4(CO_2 \text{ equivalent})}} \right) \times 100 = \left(1 - \frac{2.00 \times 10^5}{1.75 \times 10^7} \right) \times 100 = 98.9\% \quad (144)$$

From these results, the global warming effect can be reduced greatly. Note that when the electric power generation is fully carried out by a nuclear electric power plant, the efficiency becomes

$$\eta_r' = \left(1 - \frac{m_{CO_2}}{m_{CF_4(CO_2 \text{ equivalent})}} \right) \times 100 = \left(1 - \frac{2.695 \times 10^3}{1.75 \times 10^7} \right) \times 100 = 99.98\% \quad (145)$$

3. SURFACE MODIFICATION

3.1. RF Plasma CVD

3.1.1. Characteristics of Plasma CVD

When plasma is induced in material gas with a constant pressure by the electrical discharge, using DC, RF, or micro wave electrical powers, chemically activated radicals and ions are generated. In plasma CVD (P-CVD) technologies, thin films for semiconductor chips are manufactured on the substrate in which many kinds of chemical reactions are spurred by particles activated in the plasma.

Compared with thermal CVD technologies in which the material gases are thermally activated and decomposed, the nonthermal plasma CVD has the following features:

a. Uniform and fine thin film can be generated compared with the thermal CVD technologies.
b. Some kind of material that cannot be deposited using the thermal process can be deposited with proper speed to make thin film on the substrate.

c. The mixture of several kinds of materials that have different temperatures for thermal decomposition can be deposited on the substrate with various mixing ratio.
d. It is possible to reduce thermal damage, mutual diffusion, and chemical reaction between the material gases and the substrate.

In particular, P-CVD using the RF glow discharge between the two parallel plates is often used in the finalized process of ultra fine LSIs for surface protection, the manufacturing of solar battery panels and thin-film transistors with glass substrates for the active-matrix type liquid crystal display.

There are many kinds of plasma generation method in P-CVD that can be classified by these types of input electric power or power supply methods. The next section discusses the characteristics and equipment of the typical P-CVD (RF plasma CVD).

3.1.2. Reactors of RF Plasma CVD

The RF (–MHz, industrial frequency = 13.56 MHz) plasma is usually induced by the discharge generated with a high frequency power supply (17). In this type of plasma reactor, the reactor is usually pumped down and the pressure is reduced to make the plasma stable. These RF plasma reactors are classified into two types: inductively coupled plasma reactor (ICP, Fig. 107), in which a capacitor is used as plasma electrodes (17); and capacitance coupled plasma reactor (CCP, Fig. 108), in which a coil is used as plasma inductor. Other classifications include the inner electrode-type plasma reactor, which positions the electrode inside the vacuum chamber and the outer electrode type plasma reactor, which positions the electrode outside the chamber.

In the inner electrode type plasmas, the glow discharge between two parallel plates is often applied to many industrial fields as written before, because it can produce the high-quality and large thin film at relatively low temperature (150–300°C). In this type of CVD apparatus as shown in Fig. 107, thin film transistors of LCD and solar battery of amorphous silicon are manufactured. The substrate is usually attached on the grounded electrode. In order to make the thickness of the film uniform, the material gas is generally injected from the pinholes in the high frequency voltage electrode and impinges on the substrate. In another type pf CVD apparatus shown in Fig. 108 (ICP reactor), the substrate is processed by the plasma inside the coil. The P-CVD system consists of the gas supplying system (gas cylinders, pressure reducer valve, flow stop valves, purge lines and mass flow control valves), plasma generation system (plasma reactor, vacuum chamber and power supply), vacuum pumping system and emission gas processing system. Figures 107 and 108 show schematics of laboratory scale simple P-CVD system. In an industrial scale equipment, there are many chambers connected in series as shown in Fig. 109. Using this system, many kinds of thin films having multi layers can be deposited continuously.

The RF plasma and the corona discharge are also used for etching and cleaning of the substrate. In the next section, some experimental results on surface treatment using the pulse corona nonthermal plasma are reviewed. Most of these technologies are still on a laboratory scale, but hold much promise for future industrial applications.

3.2. Surface Modification for Substrate

3.2.1. Nonthermal Plasma Technology for Surface Modification

A laboratory-scale atmospheric-pressure plasma reactor, using a nanosecond pulsed corona was constructed to demonstrate potential applications ranging from modification
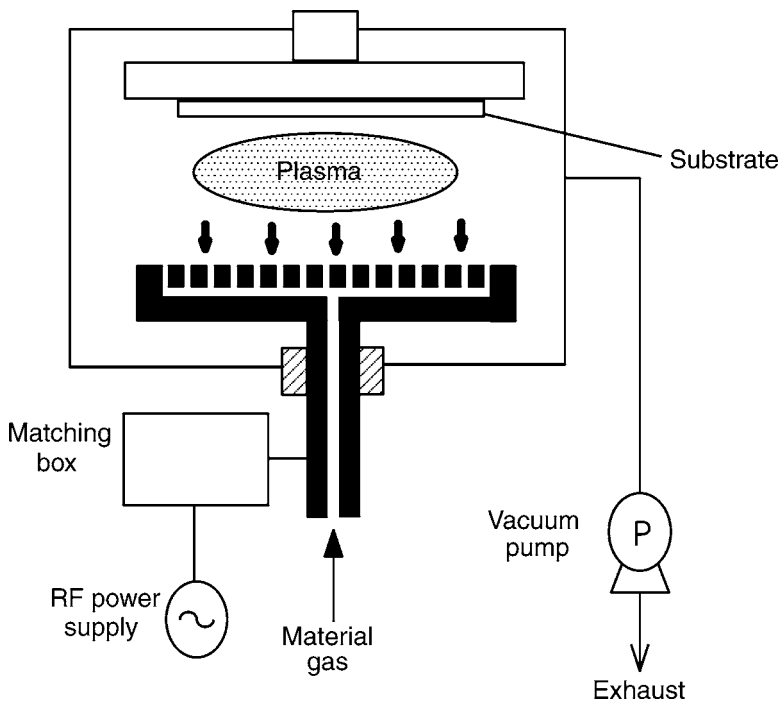
Fig. 107. Capacitively coupled RF plasma semiconductor manufacturing process reactor.
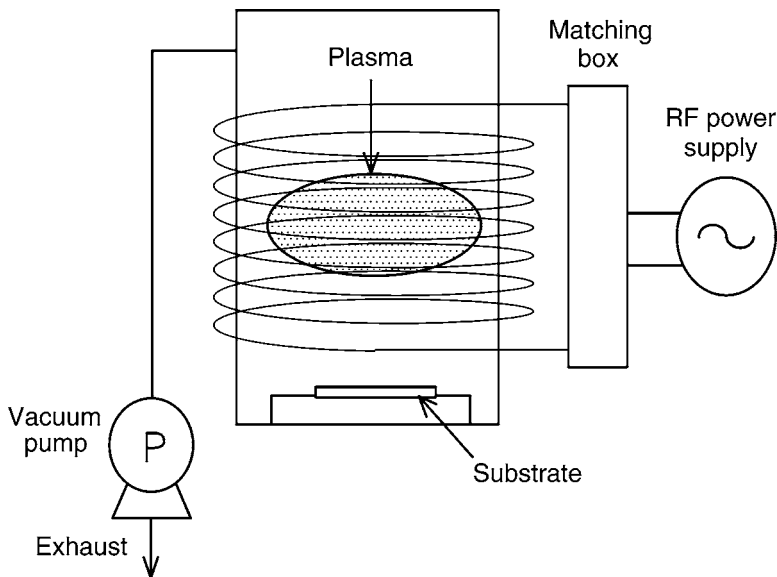
Fig. 108. Inductively coupled RF plasma manufacturing process reactor.

of surface energy to removal of surface organic films (241). For surface modification studies, three different substrates were selected to evaluate the surface energies: bare aluminum, polyurethane, and silicon coated with photoresist. The critical surface energy for all materials studied significantly increased after the plasma treatment.
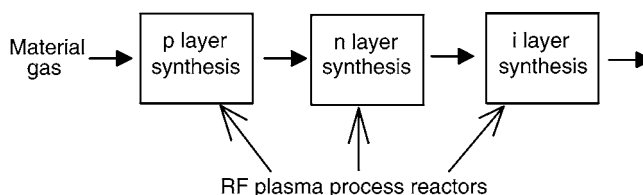
Fig. 109. Series connection of RF plasma reactor for manufacturing different layer.

The effects of gas composition and plasma treatment time were also investigated. Photoresist, ethylene glycol, and Microsurfactant were used as test organic films. The etching rate of a photoresist coating on silicon was 9 nm/min. Organic film removal using atmospheric pressure plasma technology was shown to be feasible.

3.2.2. *Experimental Apparatus and Procedure*

A laboratory-scale atmospheric pressure pulsed-corona plasma reactor was designed and constructed for the purpose of surface modification and organic film removal. The plasma reactor consisted of wire in the cylinder section and bottom section designed to hold the sample. A centered discharge wire was attached to a source of pulsed high voltage, and a stainless-steel cylinder was grounded, as shown in Fig. 110. The wire-to-cylinder distance was 11.5 mm and the effective tube length was 127 mm. The discharge wire was 0.2 mm in diameter and 100 mm in length. A grounded stainless disk was placed downstream of the plasma reactor for mounting the substrate to be treated or cleaned. The distance between the electrode wire and the substrate could be adjusted by moving the stem of the disk.

The pulsed corona reactor employed a positive DC power supply that was altered to produce a short pulse with an extremely fast rise time (approx 20 ns) through a rotating spark gap. The advantage of this arrangement is that a sharp-rise pulsed corona produces streamer corona, which generates radical species and free electrons while producing a limited number of ions. A detailed description of this power supply appears in the Section 1.2.3.

The plasma reactor could be operated in either direct or remote-plasma modes. To achieve remote-plasma mode, the high-voltage discharge electrode was raised by about 20 mm above the bottom of the grounded cylinder so that the electric field terminated within the reactor zone, resulting in no electron or ion bombardment on the substrate. On the other hand, direct-plasma mode could be achieved by lowering the wire electrode to the same level or below the bottom of the grounded cylinder. The electric field from the tip of the discharge wire then terminated on the substrate surface so that electrons and ions as well as radicals bombarded the substrate surface.

A schematic of the experimental setup is shown in Fig. 110. The gas flow rate was calibrated with a soap bubble flow meter and maintained at a total of 500 cc/min with 10% argon, and 90% dry air or oxygen by volume. This corresponds to 1.87 cm/s flow velocity and 3.1 s residence time in the plasma reactor. The pulse rate was maintained at 400 Hz and the peak voltage was approx 30 kV.

3.2.3. *Experimental Results*

Table 12 shows gravimetric data for aluminum and polycarbonate samples before and after plasma treatment. The first column of numbers shows the weight before coating,
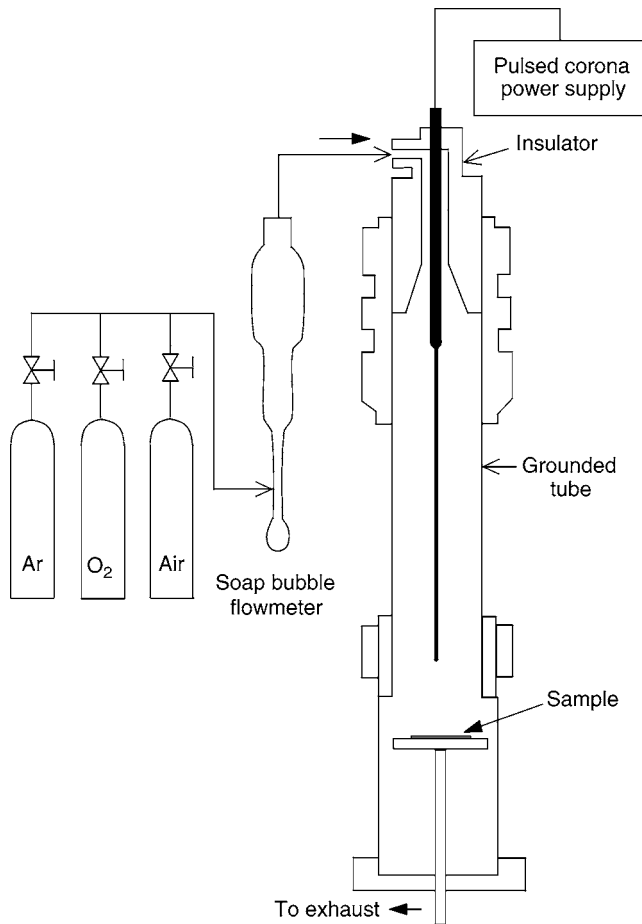
Fig. 110. Surface treatment pulse nonthermal plasma reactor (© 1995 IEEE).

the second column shows the weight after coating, and the third column is the weight after remote plasma exposure. The weight change between each step is also shown in parentheses. Note that polycarbonate materials easily absorb water, resulting in weight gain. Based on the gravimetric data of Table 12, organic film removal using APPT appears marginally feasible. The direct plasma appears to be more effective in removing organic films than the remote plasma. This suggests that the electron energy and/or high-energy-state radicals are more important in organic removal than the lower-energy radicals.

   Three major conclusions were drawn from this work: First, a dry plasma etching of photoresist on silicon is feasible. Second, organic film removal by APPT appears to be feasible, based on gravimetric data. This seems clear even though we could not measure the organic film removal rate by the ESCA method because of the difficulty in depositing a thin organic film on the substrate. And third, the direct-plasma method appears to be more effective in removing organic films than the remote-plasma method.

Table 12
Gravimetric Data for Aluminum and Polycarbonate Samples
Before and After Plasma Treatment

	Before coating	After coating with micro surfactant	Plasma treated
Aluminum			
Direct plasma	1.19638 g	1.20593 g (+9.55 mg)	1.20509 g (−0.84 mg)
Remote plasma	1.21387 g	1.22300 g (+9.13 mg)	1.22288 g (−0.12 mg)
Control	1.20400 g	–	1.20400 g
Polycarbonate			
Direct plasma	0.64887 g	0.64794 g (−0.93 mg)	0.64586 g (−2.08 mg)
Control	0.64148 g	0.64151 g (+0.03 mg)	0.64155 g (+0.04 mg)

3.3. Surface Modification for Glass

3.3.1. Surface Modification by Nonthermal Plasma

The field of surface modification by plasma treatment has undergone enormous expansion in recent years (242). Particularly in the surface modification of polymeric materials, there now exist numerous industrial applications such as enhancement of paint adhesion, improved bonding, surface cleaning, and so on (225, 243–246).

Conventional plasma technologies use a RF or microwave frequency power supply and require reduced pressure for some applications, necessitating pump-down and subsequent repressurization of the parts to be treated. In addition, the cooling system is often required because of gas heating. This result in extremely high-power consumption, slow processing time, and lower throughput. An atmospheric-pressure nonthermal plasma technology (APNPT) system (241) is simple to build, does not require reduced pressure, and consumes very little power, thereby overcoming many of the drawbacks associated with the conventional plasma processing

In this section, some experimental results are shown on modification of glass surface using the nonthermal plasma technique. The objective is to eliminate the windshield wiper from automobiles by making improvements on hydrophobic and hydrophilic properties of glass surface.

3.3.2. Principles of Surface Modification

Figure 111 shows a typical liquid droplet placed on the glass substrate. The force balance for liquid droplet and glass substrate can be expressed in the following Young's equation.

$$\gamma_L \cos\theta = \gamma_S - \gamma_{SL} \tag{145}$$

where γ_S is the surface tension of the glass, γ_L is the surface tension of liquid, γ_{SL} is the surface tension between liquid droplet and glass, and θ is the contact angle. The contact angle θ of a liquid droplet on the glass is closely related to the work of adhesion, W_{SL}, required to remove the droplet from the glass plate (Young-Dupré equation).

$$W_{SL} = \gamma_L (1 + \cos\theta) \tag{146}$$
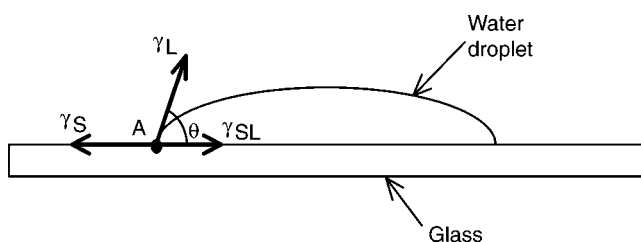
Fig. 111. Contact angle between glass surface and liquid droplet.

Therefore, the contact angle provides a mean of calculating liquid–glass adhesion.

It is known from the Eq. (145) and (146) that when the surface tension (or surface energy) between liquid droplet and glass, γ_{SL}, increases, the contact angle θ increases, resulting in decrease of adhesion energy, W_{SL}, or hydrophobic characteristics. On the other hand, when surface tension of the glass γ_S, increases, the contact angle decreases resulting in the increase of W_{SL} or hydrophilic characteristics. The application of plasma is known to increase the surface energy, adhesion energy wet-ability or hydrophilic property (241). The sol–gel methods on glass surface have been used to obtain the hydrophobic property of the glass (247). In this section, the fundamental properties of glass surface on plasma exposure and the extended durability using nonthermal plasma in combination with hydrophobic chemicals are introduced.

3.3.3. Experiments

Among various types of atmospheric pressure nonthermal plasma technologies, the silent corona was employed because the plasma can be applied on the glass surface easily and uniformly. A schematic diagram of the experimental set-up is shown in Fig. 112. The silent corona plasma reactor consists of two parallel cylindrical aluminum disks. A top disk electrode of 73 mm diameter is hollowed with 30 pinholes of 2 mm diameter. The bottom disk electrode having the same diameter is covered with the dielectric material (acrylic plate with a thickness of 1mm) in which a glass sample (width = 38 mm, length = 26 mm, and thickness = 1 mm) is placed. The electrode to the glass surface distance is maintained at 3 mm. As a background gas, dry air with a relative humidity of 4% and 20°C was primarily used by the compressor through the dryer. Pure nitrogen (N_2) and helium (He) in cylinders were also tested. The desired flow rate is obtained by a mass flow controller. The gas is supplied from the top shaft, passed through 30 holes and impinged uniformly to the glass sample. Then, the gas is dispersed outward and discharged to the holes of the bottom shaft. The electrodes are energized by a 60 Hz AC power supply (15 kV and 30 mA max.) to generate microdischarges between the electrodes.

The effects of background gas, flow rate Q, plasma treatment time and peak-to-peak applied voltage V_{p-p} on the contact angle were investigated to understand the fundamental characteristics of the glass surface by plasma, and plasma and chemical combined process. The contact angle of the glass sample was measured with a goniometry (Kyowa Kaimen Kagaku Co., CA-DT). For the durability test, the windshield wiper for automobile was applied to the glass sample continuously with a frequency of 33 rpm for one
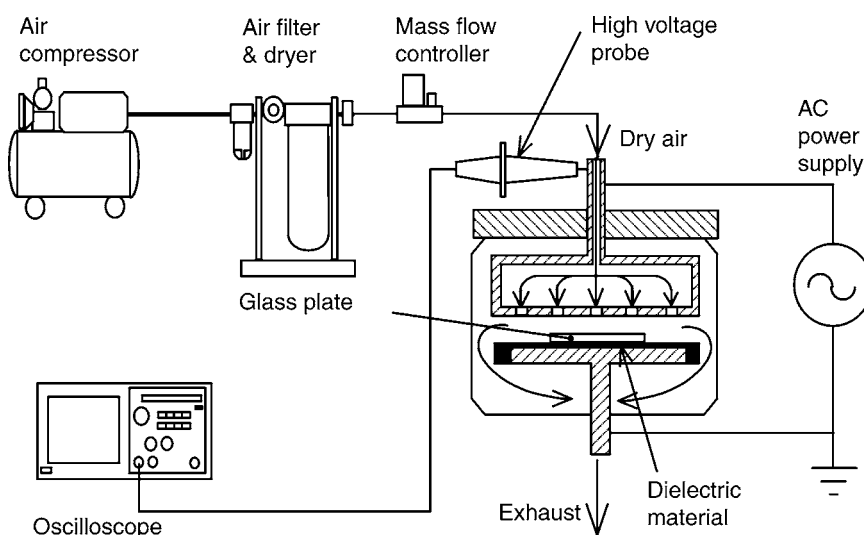
Fig. 112. Schematic of the experimental setup.

and half hours. Then, the glass sample was exposed to ambient condition (January through February) for the rest of the day. During the windshield wiper operation, water was applied to simulate a rainy day. This procedure was repeated for a couple of days. The applied voltage and current waveforms were measured with an oscilloscope (Tektronix TDS380P) through a voltage divider (Tektronix P6015A) and current probe.

3.3.4. Results and Discussion

Two approaches were undertaken for modifying the glass surface: one is a hydrophilic approach using plasma alone and the other is hydrophobic approach using the combination of hydrophobic chemical and plasma.

3.3.4.1. HYDROPHILIC APPROACH

Although experiments were also carried out at voltage more than 13 kV using air, nitrogen, and helium as test gases, the results were almost the same. Therefore, the condition was fixed in the following experiment: $V_{p-p} = 15$ kV and the working gas is air. The plasma exposure time was varied from 0 to 60 s. The contact angle decreased from 45° to 10° with 10 s of plasma exposure time, 5° with 30 s and less than 4° with 60 s of plasma exposure time. The contact angle of the glass sample does not change beyond 60 s of plasma treatment time which was consistent with previous findings for aluminum, photoresist on silicon and polymer (241).

The experimental conditions were set the same, while the flow rate was varied from 0 to 5 L/min. As a result, the flow rate did not affect the contact angle at all.

Durability of the plasma treated glass samples was investigated. Three different plasma treated glass samples ($V_{p-p} = 13$ kV, 15 kV, and 17 kV) were exposed outdoors for 5 d without windshield wiper operation. At the end of each day, the sample was taken and the contact angle was measured. The results are shown in Fig. 113. It is clear that the contact angle increases from 3.3° to 15°–20° for all three samples even after 1 d. In fact, the contact angle exceeds 10° after 7 h. After 5 d, hydrophilic property is totally
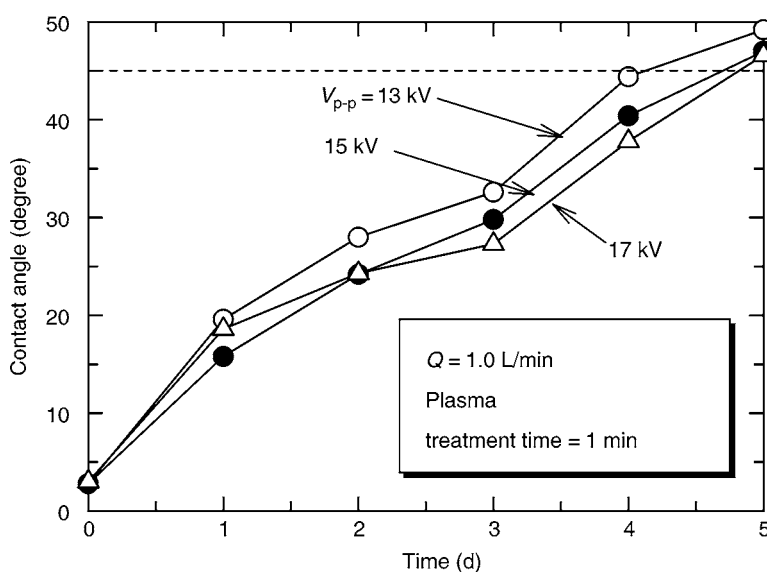
Fig. 113. Voltage dependent durability test on glass sample (background gas: dry air, flow rate Q = 1 L/min, plasma treatment time = 1 min).

lost for all samples. In order to maintain the low contact angle, plasma induced graft polymerization (248–250) was considered but was not performed at the present time because the visibility problem of glass still exists.

3.3.4.2. HYDROPHOBIC APPROACH

A commercially available hydrophobic chemical solution used to replace the automobile windshield wiper, Tri Alkoxy Silane (TAS) was used as the hydrophobic approach. Four kinds of glass samples were prepared. As a control sample 1, a hydrophobic TAS was coated on the glass surface and wiped off with a cloth and the contact angle was measured to obtain the baseline data.

As sample 2, the plasma was applied first and the TAS was coated next. Then, the sample was wiped off to remove any TAS coating. The plasma condition was the same conditions as in the other experiments (flow rate of 1 L/min and plasma treatment time of 1 min) except with the applied voltage of 20 kV. As for sample 3, the process was reversed as from the case in sample 2, i.e., TAS was coated first followed by the plasma treatment. Then, the glass surface was wiped off with a cloth to remove the liquid. For sample 4, the TAS was first coated and the coating then removed. After that, the plasma was exposed to the sample.

The durability test was conducted with the procedures mentioned earlier. All the samples were placed outdoors and continuously rubbed by the automobile windshield wiper with a frequency of 33 rpm for one and a half hours, while the water was continuously applied to the sample. Then, the sample was again exposed to the outside for the rest of the day in January or February (Osaka, Japan). This procedure was repeated for a couple of days. The results are shown in Fig. 114.

Sample 1 shows the baseline data and indicates that the contact angle is 108° initially after TAS application, and it is dropped to 90° after 70 min of windshield wiper operation.
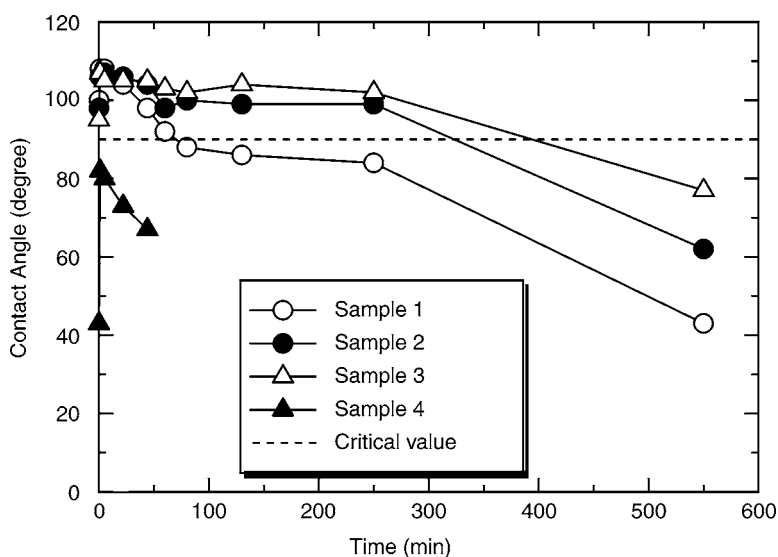
Fig. 114. Durability test using an automobile wiper for hydrophobic TAS coating combined with plasma (background gas: dry-air, flow rate $Q = 1$ L/min, plasma treatment time = 1 min, $V_{p-p} = 20$ kV).

Here, the contact angle of 90° is set as the critical hydrophobic property. On the other hand, the durability of sample 2 increases to 330 min to reach the critical hydrophobic property which is 4.7 times more durable compared with that of sample 1 (TAS coating alone). The durability test for sample 3 reaches 400 min in which the durability increased 5.7 times more. Sample 4 shows that the effectiveness of durability is totally faded away. The glass sample was totally exposed to plasma resulting in the enhancement of hydrophilic property.

It is clear from these results that with the proper combination of hydrophobic chemicals, TAS coating and plasma are able to increase the durability of glass coating at least five times longer. In addition, the visibility of plasma and chemical treated glass is excellent.

Now, the role of plasma on hydrophobic coating (TAS) is considered. The molecular structure of sodium silicate glass was proposed by Schloze (251). In the glass manufacturing process, the water in molten silicates exists as OH, which is either combined with an hydrogen atom or stands by itself. When the plasma is applied, the O–OH bond with the longer distance (0.79 nm) is divided up by electron impact and atomic oxygen O and OH radials will appear on the glass surface as shown in Fig. 115. A similar phenomenon was observed for different materials and was identified as the oxygen peak (O 1 s) by an electron spectroscopy for chemical analysis (ESCA) spectra evaluation (8). When TAS coating is applied after the plasma treatment, the molecular structure of the glass surface will be shown in Fig. 116. Here, H_2SO_4 solution is used as a catalyst for TAS coating. The chemically stable Si-O will be formed on the glass surface which will be the main cause of increased hydrophilic property. At the same time, the solution of MeOH is removed.
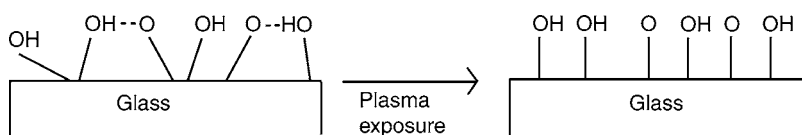
Fig. 115. Molecular structure of the glass surface after plasma treatment.

$R = CH_3(CH_2)_{10}, CH_3(CH_2)15, CF_3(CF_2)_7CH_2CH_2$
$OM_2 = OCH_3, OCH_2CH_3$
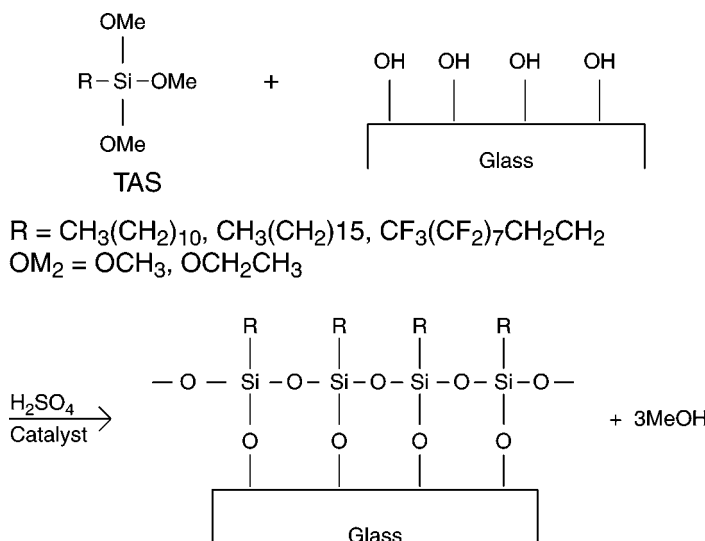
Fig. 116. Molecular structure of the glass surface on TAS coating after plasma treatment.

When the plasma is exposed, after TAS is coated on the sample (sample 3), the molecular structure on the glass surface will end up with the same structure as sample 2. The mechanisms of increased durability will be explained by the stable Si-O structure on the glass (the same as sample 2). However, when TAS is applied and the surface is wiped off, the surface structure is totally exposed to the plasma and becomes hydrophilic as for the case in sample 4.

3.4. Surface Modification for Polymer or Cloth

High functional air filters are used to clean up the exhaust gas from factory and indoor environments have reported on the improvements in odor removal properties using the plasma–chemical treatment. In this subsection, the manufacturing process, measurement result of the functional properties and applications are described in ref. 248–250.

3.4.1. Plasma Processed Functional Cloth

Nonthermal plasma is first applied and hydrophilic monomers are next graft-polymerized to the surface of the cloth. The morphology of the cloth has been dramatically changed to breathe moisture and to absorb offensive odor, simultaneously. The process of a new plasma graft-polymerization is shown in Fig. 117. Schematic and photo of a continuous manufacturing system of such kind of cloth is shown in Fig. 118. As a plasma source, the atmospheric pressure (RF),13.56 MHz glow discharge using
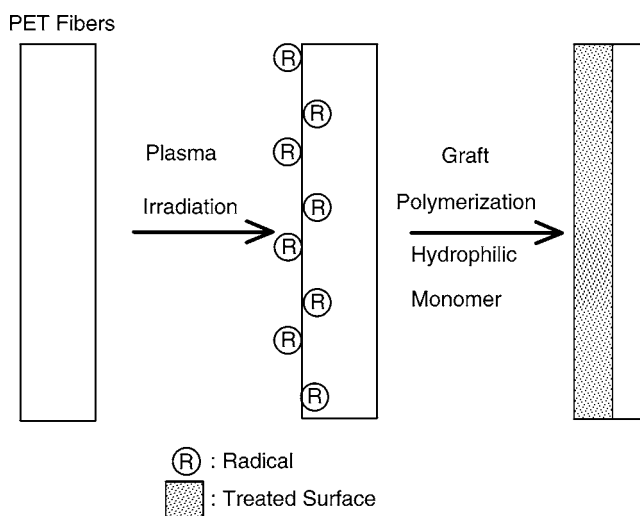
Fig. 117. Plasma graft-polymerization process.

argon and helium mixed gas is applied uniformly on the surface of the high-polymer cloth (for e.g., PET fiber). The surface of the cloth is modified to generate many radicals. Next, aerosols of the hydrophilic monomer (acrylic acid) are sprayed on the surface to proceed a graft-polymerization. The surface morphology of the cloth is modified to become porous (Fig. 119) and the cloth promotes to adsorb moisture and offensive odor simultaneously.

The features of this process are as follows:

1. The carboxyl (–COOH) is not generated.
2. Heat decomposition process of carboxyl is not necessary in the graft-polymerization process.
3. The process proceeds under room temperature and atmospheric pressure condition.

From these features, this process has many advantages compared with the conventional one. The manufacturing system in Fig. 118 has been already commercialized by Pearl Kogyo Co, Osaka, Japan. In the next section, the measurement results on the characteristics of the manufactured cloth are reported.

3.4.2. Experimental Apparatus and Methods

Experiments were carried out to investigate odor control properties of the functional cloth. The experimental setup is shown in Fig. 120. The NH_3 balanced with N_2 was prepared in the cylinders and the dry air (relative humidity = 4%) was supplied by the compressor through a dryer. The desired concentration (= 50 ppm) and flow rate (= 1 L/min) of NH_3 were obtained with the mass flow controller on each line in which the gas passed through the test section. In the test section, a porous polyethylene tube was wrapped with the tested cloth (51×42 cm^2). The gas flowed out of the holes in the tube and passed through the cloth. The adsorption characteristics of NH_3 were evaluated by measuring the concentrations of NH_3 before and after the test section using gas detection tubes.
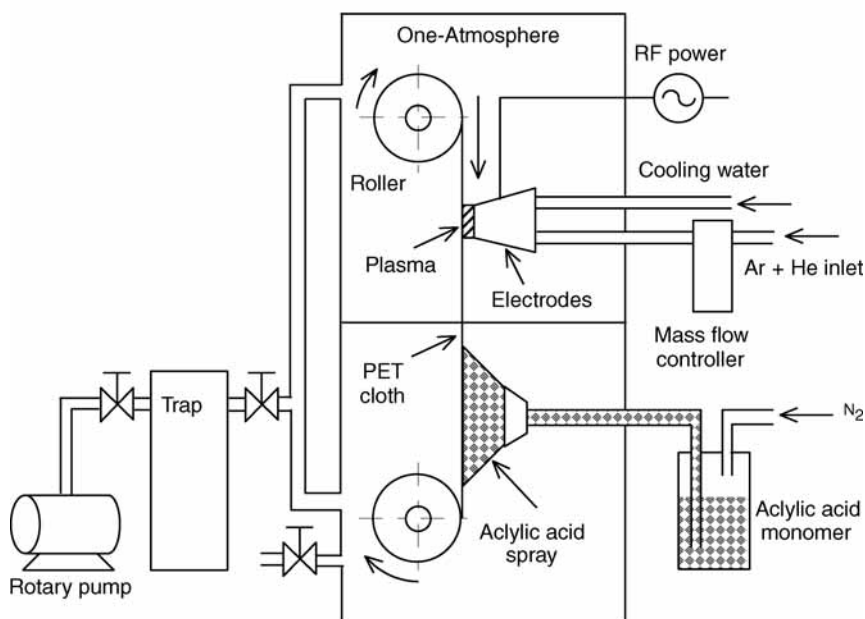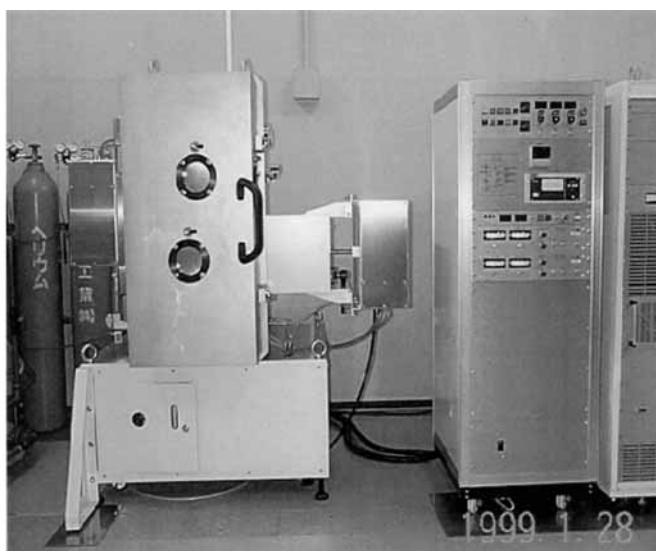
Fig. 118. New system for plasma graft-polymerization process.

3.4.3. Experimental Results

Adsorption characteristics of three different functional cloths are shown in Fig. 121. For the untreated cloth, the concentration of the cloth was 15 ppm in 5 min. It reached 50 ppm in 60 min and the adsorption to the cloth was saturated. A total volume of adsorption became 0.68 mL. On the other hand, for the cloth treated on both sides, 100% of the NH_3 was adsorbed for the first 30 min and the concentration reached
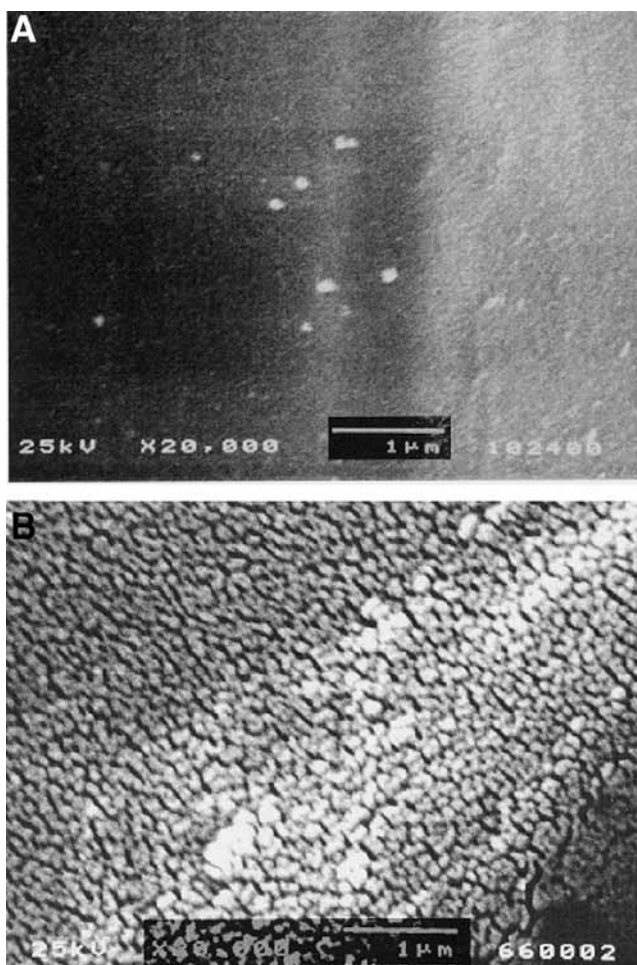
Fig. 119. Scanning electron microscope photograph of the PET cloth surface before and after the plasma-graft polymerization process. **(A)** Before processing. **(B)** After processing.

22 ppm after 210 min. A total volume of adsorption was about 10 mL. For the cloth treated one-side, over 90% of the NH_3 was adsorbed for 20 min and was saturated for 120 min, resulting in a total adsorption amount of 3.4 mL. Further, for the cloth treated single side, the change of the gas adsorption efficiency was measured after washing the cloth by hand. Fig. 122 shows the result. Although the total adsorption amount decreases about 60% just after the first washing, it scarcely changed after the second washing. Further, the performance of the moisture breath also scarcely changed after washing 50 times (248–250). It was confirmed from these results that the regeneration of the functional cloth is possible.

Various potential applications of this functional cloth have been proposed: underwear that allows moisture to breathe and odor control (Fig. 123), seat covers of automobile, partitions in hospital, bag filters for dust and odor. Using a single-sided processed cloth, the sweat and odor from human body disperses to outside effectively.
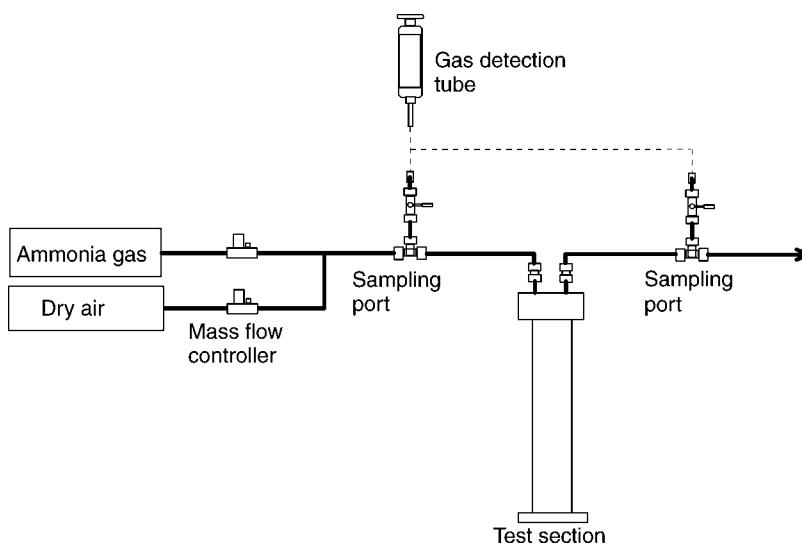
Fig. 120. Experimental apparatus for NH$_3$ adsorption characteristics.
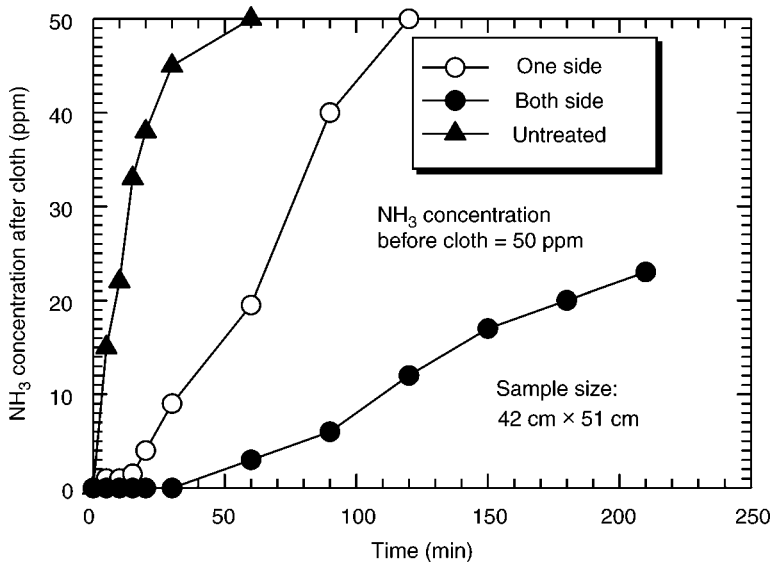
Fig. 121. Time-dependent NH$_3$ adsorption characteristics.

In summary, it is confirmed that the cloth processed by the atmospheric-pressure plasma graft-polymerization using the acrylic acid exhibit the durable functions of moisture breath and odor control. In order to increase the performance of this cloth, it is required to clarify the detail of the adsorption mechanism, choose more proper monomers and find the optimum conditions (temperature, pressure, and so on) in the plasma graft polymerization.
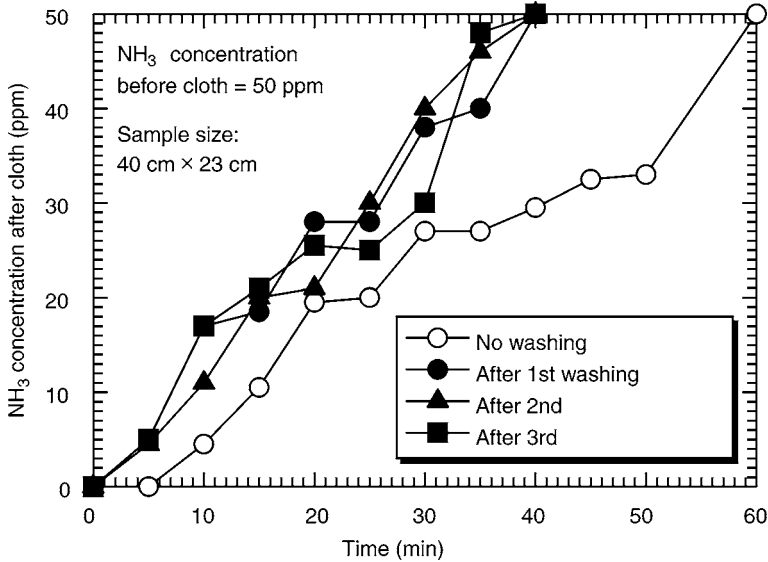
Fig. 122. Change of NH_3 adsorption characteristics after washings.
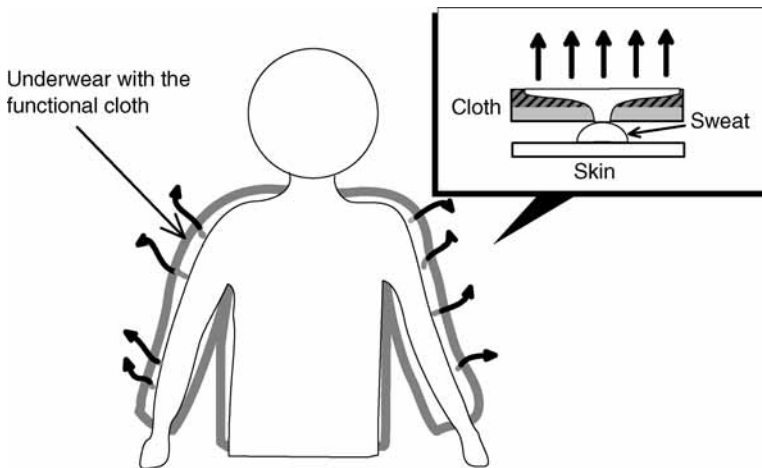
Fig. 123. Application of the functional cloth to underwear.

3.5. Surface Modification for Metal

3.5.1. Plasma-Assisted Dry Chemical Process

Aluminum coil as received from the manufacturer uses grease on aluminum surface in order to enhance the detachment of aluminum coil (252,253). The surface of the aluminum plate having hydrophilic and corrosion-resistant property is often required for various mechanical parts or systems after receiving as an aluminum coil. The conventional process for treating aluminum surfaces employs a series of wet processes as shown in Fig. 124: grease removal from the uncoiler followed by the drying process at 200ºC, chromate process followed by drying at 200ºC, and finally chemical treatment to achieve
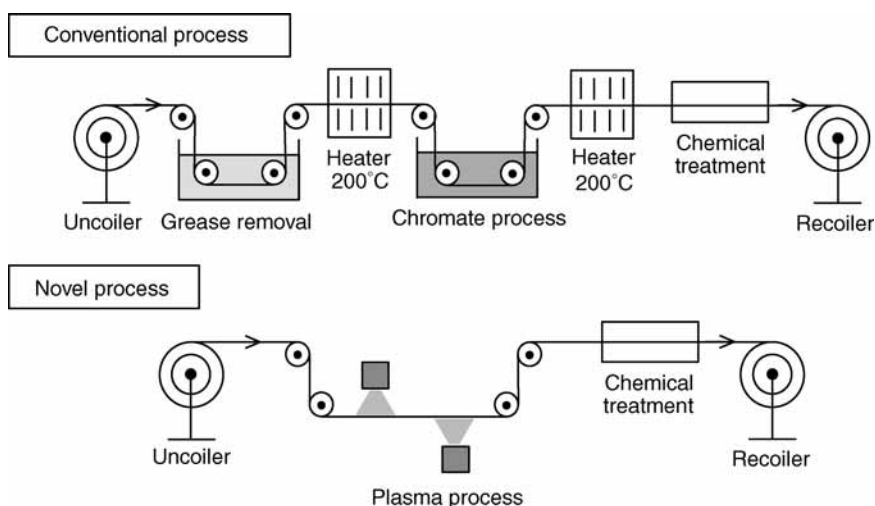
Fig. 124. Conventional process and novel process for treating aluminum surfaces.

hydrophilic property before the recoiler. However, the use of chromium (Cr^{+6}) in the chromate process, which is widely used for aluminum treatment, creates an environmental problem. Here, we explored a simple dry cleaning process to replace the conventional aluminum wet surface treatment, i.e., nonthermal plasma followed by a chemical process so that several stages for surface preparation can be eliminated as shown in Fig. 124. The cross-section view of the final aluminum surface is illustrated in Fig. 125.

The use of nonthermal plasma on surface modification was reported elsewhere (254–259) but very limited studies were conducted for aluminum surface treatment (241,260). Among several nonthermal plasma processes, two types of plasma jets (60 Hz AC plasma and RF plasma) and pulsed-corona plasma were investigated to remove the grease or contaminated organics and were used to create an excited state on aluminum surface. The adhesive characteristics between the aluminum surface and the corrosion-resistant epoxy resin coating were evaluated by employing the accelerated corrosion test.

3.5.2. Experiments

Three kinds of plasma jets were used for nonthermal plasma surface modification. The first is a plasma jet energized by a 60 Hz AC power supply (10 kV, 0.06 A) in which air was used as a feeding gas (Corotec Co., model PJ-1). The plasma jet to the aluminum surface distance was maintained at 10 mm. The second is a RF plasma jet (Pearl Kogyo Co.) in which plasma was generated between the jet nozzle and aluminum surface as illustrated in Fig. 126. The flow rate of helium was set at 1 L/min and 250 W of the RF power, which was rated at 3 kVA and 13.56 MHz, was injected during the experiments. The RF power supply consists of a matching box and tuner controller to minimize the power reflection. The plasma jet to the aluminum surface was maintained at 5 mm. As a third plasma device, an insulated gate bipolar transistor (IGBT) pulse power supply (Masuda Research, Inc., PPCP Pulser SMC-30/1000) in combination with a magnetic pulse compression was used. The schematic diagram of the experimental setup was shown in Fig. 127. This pulse power supply can generate 200 ns pulse width
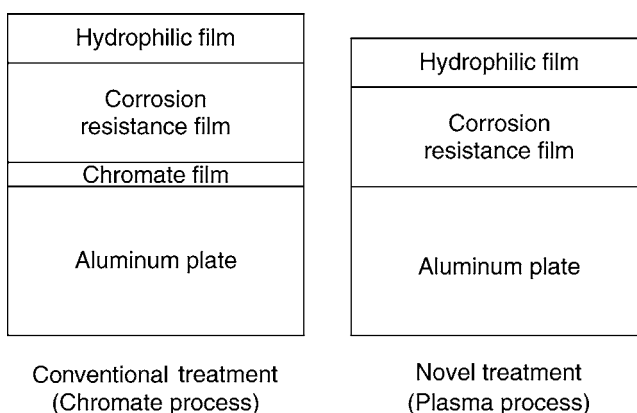
Fig. 125. Cross-section of the aluminum surfaces in conventional and plasma processes.
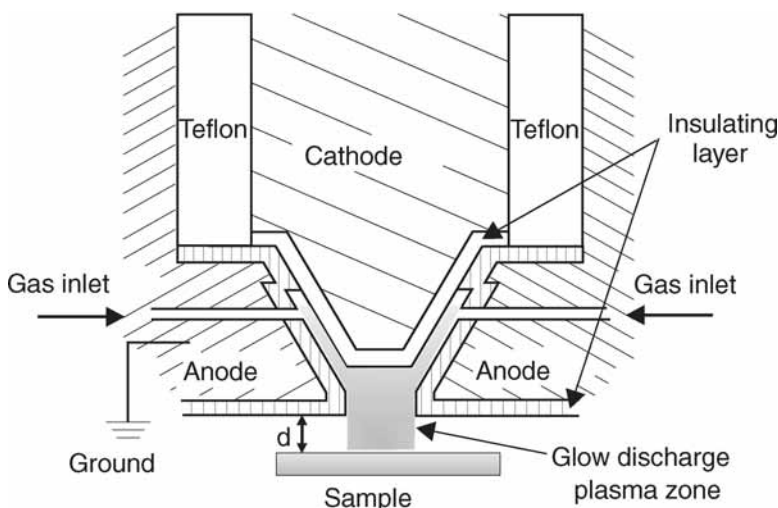
Fig. 126. RF plasma jet apparatus for surface treatment.

at 30 kV. The reactor consists of 10 knife edges which were contained in 104 mm in diameter and 120 mm high acrylic housing. The aluminum sample was placed on either 3 mm thick barrier surface or on knife edges. The jet nozzle to the aluminum surface distance was set at 5 mm. Either air or helium was used as a feeding gas with a flow rate of 1 L/min. The power of 4.5 W with the pulse repetition rate of 300 Hz was supplied.

The grease removal on aluminum surface was evaluated by the contact angle measurement using a goniometry (Kyowa Kaimen Kagaku, CA-DT). After plasma exposure, the corrosion resistant chemical (epoxy resin) was coated using a specific roller, which provides an approx 2.5 µm thick coating. The corrosion resistance and adhesion force were evaluated by the pressure cooker test, where samples were placed in the chamber under 130ºC, 100% RH, and 2.755 kg/cm^2 environments. As a more stringent and more rapid test, copper-accelerated acetic acid salt spray test, which was specified as Japan industrial
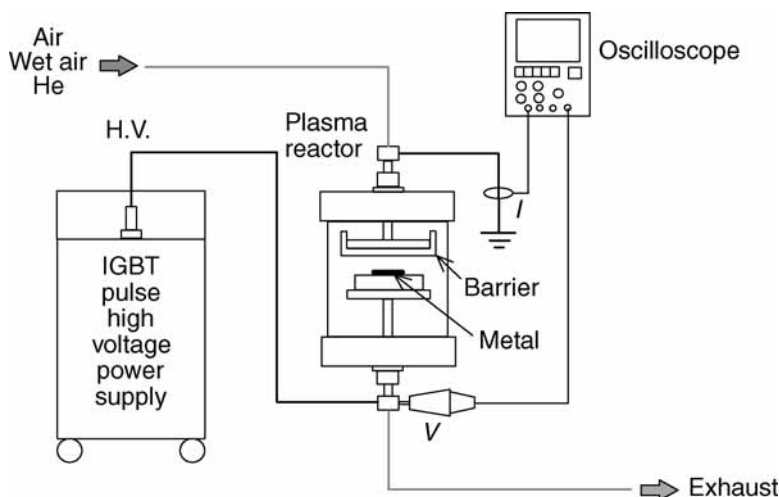
Fig. 127. Experimental setup for pulse nonthermal plasma reactor for surface treatment.

standard (JIS) H8520, was performed. This test procedure was recommended for the corrosion resistance evaluation for plating. The test chamber was sustained at extremely strong acid environment for 8 h: NaCl and $CuCl_2$ were sprayed into the chamber to maintain pH value of 3.0 and the temperature was set at $63 \pm 2^\circ C$. All samples were cut at 80×30 mm². The aluminum surface was evaluated using a scanning electron microscope and the corrosion area was scanned and analyzed by the computer.

3.5.3. Corrosion Tests

The following six cleaning methods were performed for organic removal:
500°C for 10 min in oven

a. Alkali cleaning.
B. AC plasma cleaning.
c. RF plasma cleaning.
d. Alkali and AC plasma cleaning.
e. Pulsed corona cleaning.
f. Conventional chromate cleaning.

The epoxy-type film thickness using the combined chromate process and the corrosion resistance used for the conventional process was approx 2.5 µm. The corrosion resistance epoxy film thickness after plasma cleaning was selected at approx 2.4 µm throughout the plasma experiments. Three samples were prepared for each condition and a total of 21 samples were prepared.

The pressure cooker test indicated no distinct corrosion for all samples. Therefore, the copper-accelerated acetic acid salt spray test, which is a more severe test condition, was performed for 8 h and the surface pictures were incorporated into the computer and the corroded area was evaluated by the computer to 600 mm². The results were shown in Table 13.

It is clear that RF plasma showed the least corrosion area. It implies that the corrosion resistance using the RF plasma cleaning was significantly higher than the conventional

Table 13
Total Corroded Area and Ratio of Corroded Area of 600 mm² on Each Condition

	Total corroded area (mm²)	Corroded area ratio (%)
At 500°C for 10 min in oven	2.33	0.39
Alkali cleaning	2.77	0.46
AC plasma cleaning	2.22	0.37
RF plasma cleaning	0.67	0.11
Alkali cleaning + AC plasma cleaning	1.71	0.29
Pulsed corona cleaning	1.31	0.22
Conventional chromate treatment	1.35	0.22

Exclude corroded points under 0.01 mm².
Total inspected area is 600 mm².

method and at the same time the adhesion force between aluminum surface and corrosion resistance coating was improved. The pulsed corona process was nearly equal to the conventional process. Alkali cleaning followed by AC plasma was the next, followed by AC plasma alone and alkali cleaning alone.

Since RF plasma cleaning followed by an epoxy treatment showed the best performance on the corrosion resistant test, the exposure time was varied to obtain the optimum operating condition. The plasma exposure was varied at 10, 28, and 45 s. The results were shown in Table 14 in which the data for the conventional chromate wet process was also comprised. It is apparent from the table that the corrosion area decreases with increased plasma exposure time. RF plasma with more than 30 s of exposure followed by an epoxy-type corrosion-resistant coating showed the best performance over the conventional wet process. Therefore, the conventional wet chemical process for aluminum treatment can be replaced by the newly developed plasma-assisted chemical process, thus making the whole process more simplified and economical.

3.5.4. Design Example: Comparison of Surface Treatment Process Costs

Problem

Calculate the process costs per 100 m aluminum plate in RF plasma, pulse plasma and ordinary chromate processing. The process speed is calculated from the data in Table 13. In the ordinary process, the moving of the plate is about 50 cm/min because drying time of 1 min is required using two electric heaters of 1.5 kW and 50 cm long. It is also assumed that the width of the plate is 10 cm and the electric bill is 0.05 USD/kWh.

Solution

RF plasma process:

Because the area of the sample is 32 cm³ and the plasma treatment time is 180 s, the area which can be processed for 1 s is 0.178 cm²/s. Therefore, the velocity of the plate which can be processed by the single reactor u is calculated as

$$u_p = \frac{0.178\left(\dfrac{cm^2}{s}\right) \times 60\left(\dfrac{s}{min}\right)}{10\,(cm)} = 1.07 \text{ cm/min} \tag{147}$$

Table 14
Total Corroded Area and Ratio of Corroded Area of 600 mm²
on RF Plasma Exposure Time

	Total corroded area (mm²)	Corroded ratio (%)
RF plasma exposure time 10 s	1.74	0.29
RF plasma exposure time 28 s	0.67	0.11
RF plasma exposure time 45 s	0.11	0.07
Conventional chromate treatment	1.35	0.22

Exclude corroded points under 0.01 mm².
Total inspected area is 600 mm².

Because the power consumption in the reactor is 0.25 kW, two sets of the reactors and the power of 0.5 kW are required in order to treat both the side. Therefore, the cost per 1 m is

$$\frac{0.05\left(\dfrac{\text{USD}}{\text{kWh}}\right) \times 0.5\,(\text{kW}) \times 100\left(\dfrac{\text{cm}}{\text{m}}\right)}{1.07\left(\dfrac{\text{cm}}{\text{min}}\right) \times 60\left(\dfrac{\text{min}}{\text{h}}\right)} = 0.0389 \ \text{USD/m} \tag{148}$$

Pulse plasma process:
Because the area of the sample is 6 cm², and the plasma treatment time is 180 s, the area which can be processed for 1 s is 0.033 cm²/s. Therefore, the velocity of the plate is calculated as

$$u_p = \frac{0.0333\left(\dfrac{\text{cm}^2}{\text{s}}\right) \times 60\left(\dfrac{\text{s}}{\text{min}}\right)}{10\,(\text{cm})} = 0.200 \ \text{cm/min} \tag{149}$$

Because the power consumption in the reactor is 0.33 W, two sets of the reactors and the power of 0.66 W are required in order to treat both the side. Therefore, the cost per 1 m is

$$\frac{0.05\left(\dfrac{\text{USD}}{\text{kWh}}\right) \times 0.0066\,(\text{kW}) \times 100\left(\dfrac{\text{cm}}{\text{m}}\right)}{0.200\left(\dfrac{\text{cm}}{\text{min}}\right) \times 60\left(\dfrac{\text{min}}{\text{h}}\right)} = 0.0275 \ \text{USD/m} \tag{150}$$

Ordinary chromate process:
Because the two electric heaters of 1.5 kW are used to dry the surface, the electric bill per 1 m for the two heaters is

$$\frac{0.05\left(\dfrac{\text{USD}}{\text{kWh}}\right) \times 1.5\,(\text{kW}) \times 2 \times 100\left(\dfrac{\text{cm}}{\text{m}}\right)}{50\left(\dfrac{\text{cm}}{\text{min}}\right) \times 60\left(\dfrac{\text{min}}{\text{h}}\right)} = 0.0500 \ \text{USD/m} \tag{151}$$

Additionally, further cost is required such as chemicals required for alkali washing and chromate process, and waste water solution processing.

In summary, the costs are:

RF plasma: 3.9 USD/100 m.
Pulse plasma: 2.8 USD/100 m.
Ordinary chromate process: 5 USD/100 m + (Large environmental protection cost).

In these treatments, the cost of the pulse plasma process is lower. In order to increase the process speed, the number of the plasma reactors should be increased. The process cost does not change.

NOMENCLATURE

A	Total area of plates (m^2)
A_{pr}	Projected area of a particle in the flow direction (m^2)
AH	Absolute humidity
A_p	Area of one plane (two sided) (m^2)
Bill	Electric bill for a year (USD/yr)
C	Particle concentration or loading (kg/m^3)
C_c	Cunningham's correction factor (dimensionless)
C_D	Drag coefficient (dimensionless)
C_i	Root mean square of the velocity of the ion's thermal on = $(3kT/m_i)^{1/2}$ (m/s)
C_L	Particle concentration at exit (kg/m^3)
C_0	Particle concentration at inlet (kg/m^3)
d	Distance between the electrodes (m)
d_p	Diameter of a particle (m)
D	Distance between the plates (m)
e	Charge of an electron = 1.602×10^{-19}(C)
E	Strength of the electric field (V/m)
E	Electric field vector (V/m)
E_c	Strength of the electric field in the charging part (V/m)
E_k	Kinetic energy of an electron (J)
E_{max}	Maximum strength of the electric field (V/m)
E_p	Electrostatic field potential (V/m)
E_x, E_y	Components of electric field (V/m)
E_{yr}	Total amount of the electric energy for a year (kWh/yr)
f	Frequency (Hz)
$f(v)$	Energy distribution function of the particles in the plasma (s/m)
$F(v)$	Cumulative distribution function of particle velocity (dimensionless)
F_e	Electrostatic force vector (N)
F_D	Fluid drag force vector (N)
F_{DST}	Stokes' fluid drag force vector (N)
g_i	Statistical weight of the ground state of the ion (dimensionless)
g_0	Statistical weight of the ground state of the neutral atom (dimensionless)
h	Planck's constant = 6.6261×10^{-34}(J·s)
h_p	Height of pellet layer (m)
H	Height of the collecting electrode (m)
H_m	Width of the mesh electrode (m)

i_c	Ion current density (A/m^2)
I	Current (A)
I_{e0}	Probe current by electrons (A)
I_{i0}	Probe current by ions (A)
I_{pr}	Total probe current (A)
$IITY$	Positive area which the $V \times I$ curve and the horizontal axis surround (W)*(M1)*
k	Boltzmann's constant $= 1.3806503 \times 10^{-23}$(J/K)
k_i	Rate coefficient in the collision ionization reaction (m^3/s)
k_r	Rate coefficient in the three-body recombination (m^6/s)
K	Ratio of engine load (%)
K_i	Coefficient of the ionization equilibrium (1/m^3)
l	Horizontal distance (m)
L	Length of the collecting plate (m)
L_p	Length of the plasma reactor (m)
m_{CF_4}	Total mol of CF$_4$ processed for a year (mol/yr)
m_{CO_2}	Total mol of emitted CO$_2$ for a year (mol/yr)
m_e	Mass of an electron (kg)
m_i	Mass of an ion (kg)
M	Either the mass of a neutral molecule or that of an atom (kg)
M_p	Mass of the particle (kg)
M_t	Total mass of required ozone per unit time (kg/h)
M_1–M_4	Masses of required ozone per unit time (kg/h)
n	Number density of charged particles (1/m^3)
n_n	Number densities of neutrals (atoms and molecules) (1/m^3)
N	Number of collecting plates (dimensionless)
n_e	Number density of electrons (1/m^3)
n_g	Number density of gas molecules (1/m^3)
n_i	Number densities of ions (1/m^3)
P	Discharge power or power consumption of plasma reactor (W)
q	Charge of the particle (C)
q_f	Charge by field charging (C)
q_{th}	Amount of diffusional charging (C)
q_∞	Amount of saturation charge (C)
Q	Volumetric gas flow rate (m^3/s)
Q_c	Volumetric gas flow rate in one channel (m^3/s)
Q_s	Volumetric flow rate for a single reactor (m^3/s)
r	Radial distance or coordinate (m)
r_a	Radius of outer cylinder (m)
r_i	Radius of inner cylinder (m)
r_0	Distance between the discharge wire and the outer grounded electrode (cm)
Re	Particle Reynolds number of a spherical particle (dimensionless)
RH	Relative humidity (%)
S	Probe surface area (m^2)
SED	Specific energy density (J/L)
SV	Surface velocity (1/h)

t	Time (s)
t_r	Residence time (s)
T	Temperature (K)
T_c	Combustion temperature (K)
T_e	Electron temperature (K)
T_i	Ion temperature (K)
T_g	Gas temperature (K)
u, v	Velocity components (m/s)
u_p	Velocity of the moving plate (m/s)
v	Velocity vector of a particle (m/s)
v_e	Average thermal velocity of electrons (m/s)
v_f	Velocity vector of the flow field (m/s)
v_i	Average thermal velocity of ions (m/s)
v_p	Most probable velocity in energy distribution function of the particles in the plasma (m/s)
v_r	Relative velocity vector of a particle ($= v - v_f$) (m/s)
v_x, v_y	Velocity components (m/s)
V	Voltage or electrical potential (V)
V_{ave}	Mean velocity inside the reactor (m/s)
V_f	Floating potential to show the zero current (V)
V_d	Velocity of electrons (m/s)
Vol	Volume of the reactor (m³)
V_{p-p}	Peak-to-peak voltage (kV)
V_{pr}	Potential of the probe (V)
V_s	Space potential of probe (V)
V_t	Total volume of CF_4 processed for a year (NL/yr)
w_e	Terminal velocity (m/s)
W_{SL}	Work of adhesion (N/m)
x, y, z	Cartesian coordinates (m)
x	Position vector of a particle (m)
x_D	Debye length (m)
ΔV	Probe potential based on V_s (V)
ε	Permeability of the space (dimensionless)
ε_i	Ionization potential of species (eV)
ε_r	Relative permeability of the particle (dimensionless)
ε_0	Permeability in vacuum ($= 1/[4\pi \times 10^9]$) (dimensionless)
γ_L	Surface tension of liquid (N/m)
γ_S	Surface tension of the glass (N/m)
γ_{SL}	Surface tension between liquid droplet and glass (N/m)
η	Collection efficiency (%)
η_r	Efficiency of the reduction in GWP (%)
η_r	Efficiency of the reduction in GWP only with a nuclear electric power generation (%)
κ	Elastic collision loss factor (dimensionless)
λ	Molecular mean free path (m)

μ	Viscosity of fluid (Pa·s)
μ_i	Mobility of an ion (m^2/V·s)
ν	Kinetic viscosity of fluid (m^2/s)
ν_c	Collision frequency (Hz)
ν_p	Frequency of photon (Hz)
θ	Contact angle (degree)
ρ	Density of fluid (kg/m^3)
ρ_p	Density of a particle (kg/m^3)
τ	Characteristic time of the particle corrected considering slips (s)
τ_c, τ_c	Charging time constant (s)

REFERENCES

1. J. Kanzawa, *Plasma Dennetsu (English Translated Title: Heat Transfer in Plasma)*. Shinzan-sha Saitek Publ. Co., Tokyo, (in Japanese), 1992.
2. R. J. Roza, *Magnetohydrodynamic Energy Conversion*. McGraw-Hill Book Company, New York, NY, 1968.
3. M. Mitchner and C. H. Kruger, *Partially Ionized Gas*. John Wiley and Sons, New York, NY, 1973.
4. S. Teii, *Plasma Kiso Kogaku (English Translated Title: Basic Plasma Engineering)*. Uchida Rokakuho Publishing Co. LTD., (in Japanese), 1997.
5. E. Hinnov and J. Hirschberg, Electron-ion recombination in dense plasmas. *Phys. Rev.* **125**(3), 795–801 (1962).
6. F. F. Chen, *Introduction to Plasma Physics*. Plenum Press, New York, NY, 1974.
7. E. M. Lifshits, *Physical Kinetics (Course of Theoretical Physics)*. Butterworth-Heinemann Publication 1981.
8. N. G. Van Kampen and B. U. Felderhof, *Theoretical Method in Plasma Physics*. North-Holland Publ. Co., 1967.
9. D. R. Nicholson, *Introduction to Plasma Theory*. John Wiley & Sons, Inc. New York, NY, 1986.
10. A. B. Cambel, *Plasma Physics and Magnetohydrodynamics*. McGraw-Hill Inc. New York, NY, 1963.
11. J. S. Chang and T. Kaneda, *Denri Kitai No Gensi Bunsi Katei (English Translated Title: Atoms and Molecular Processes of Ionized Gases)*. Tokyo Denki Daigaku Publ. Co., (in Japanese), 1982.
12. J. S. Chang, P. A. Lawless, and T. Yamamoto, Corona discharge processes. *IEEE T. Plasma Sci.* **19**(6), 152–1166 (1991).
13. D. K. Cheng, *Field and Wave Electromagnetics* (2nd ed.). Addison-Wesley Publishing Company, Reading, MA, 1992.
14. K. Kanaya and A. Iijima, *Kodenatsu Kogaku Ensyu (English Translated Title: Problems on High Voltage Engineering)*. Maki Syoten Publishing Co. LTD., 7 and 37 (in Japanese), 1989.
15. A. Gal, M. Kurahashi, and M. Kuzumoto, An energy-consumption and byproduct-generation analysis of the discharge nonthermal plasma NO-reduction process. *J. Phys. D. Appl. Phys.* **32**, 1–6 (1999).
16. T. Yamamoto, K. Sonoyama, and S. Hosokawa, Gas-phase dioxins and NO$_x$ control from incinerator plant using the pilot-scale PPCP. *Proc. of ESCAMPIG16/icrp5*, **2**, 373–374 (2002).
17. T. Hirao, T. Yoshida, and S. Hayakawa, *Hakumaku Gijyutsu no Shin Choryu (English Translated Title: New Trend in Thin film Manufacturing Technologies)*. Kogyo Chosakai Publishing Co. LTD., (in Japanese), 1997.

18. H. Yamasaki, K. Hayakawa, Y. Nagasaki, et al., Performances of closed cycle disk MHD generator with Ar/Cs. *Proc. of 31st Intersociety Energy Conversion Eng. Conf.* **2,** Washington DC, pp. 854–859 (1996).

19. K. Wada, *Performance and Transient Characteristics of Closed Cycle Disk MHD Generator.* Master Course Thesis, Graduate School of Nagatsuta, Tokyo Institute of Technology, Yokohama, Japan, 1998.

20. M. Sadakata, *Taiki Kuriin Kano Tameno Kagaku Kougaku (English Translated Title: Chemical Engineering for Atmospheric Clean-up).* Baifukan Publishing Co., 75–78, (in Japanese), 1999.

21. Y. Nakano, *Daigaku Katei Koudenatsu Kogaku (English Translated Title: Undergraduate Course, High Voltage Engineering)* 2nd ed. Ohmsha Publishing Co., Vol. **132**, 1991.

22. T. Murayama and H. Tsunemoto, *Jidosya Engine Kogaku (English Translated Title: Automobile Engine Engineering).* San-kai do Publ., 79–81 (in Japanese), 1997.

23. T. Oda, S. Kozuma, and T. Takahashi, Dilute trichloroethylene decomposition by using non-thermal discharge plasma cooperation with catalysis. *Proc. of 1998 Annual Meeting of the Institute of Electrostatics Japan*, 1–4, (in Japanese), 1998.

24. M. Okubo, T. Kuroki, Y. Miyairi, and T. Yamamoto, Low temperature soot incineration of DPF using non-thermal plasma induced radical injection. *Proc. of ESA-IEEE Joint Meeting on Electrostatics*, 416–430, 2003.

25. NO_x analyzer, Horiba Corp. *Portable Gas Analyzer PG-200 Series*. Product manual, 58, 2003.

26. Horiba Corp., *Analyzer of CO, CO_2 and N_2O Gas Analyzer Unit for General Purpose VIA-510*, Product manual, **2**, 2003.

27. Shimazu, Co. *Instruction Manual of GC-14 Gas Chromatograph.* **12**(1) (1997).

28. M. Takuma, (ed.) *Fundamentals and Applications of FT-IR*. 2nd ed., Tokyo Kagaku Dojin Publ. Co., 3–16 (in Japanese), 1994.

29. Biorad Laboratories, Inc. *Spectrometer Manual of EXCALIBUR* (1998).

30. C. D. Cooper and F. C. Alley, *Air Pollution Control* (*A Design Approach*). 2nd ed*.*, Chapter 5, Waveland Press, Inc. 1994.

31. Japan Society of Electrostatics *Electrostatics Handbook*. Chapter 9, Ohm Sya Publ. (1981).

32. S. Oglesby and G. B. Nichols, *A Manual of Electrostatic Precipitator Technology*. National Technical Information Service, Springfield, VA, 1970.

33. H. J. White, *Industrial Electrostatic Precipitation*. Addison-Wesley, Reading, MA, 1963.

34. W. T. Davis (ed.), *Air Pollution Engineering Manual*. Air and Waste Management Association, Van Nostrand Reinhold, New York, NY.

35. A. D. Moore (ed.), *Electrostatics and Its Applications*. John Wiley, 1973.

36. G. W. Penny, A new electrostatic precipitator. *Electr. Eng.* **56**, 159–163 (1937).

37. H. Lim, K. Yatsuzuka, and K. Asano, Fundamental characteristics of a two-stage electrostatic precipitator. *J. Institute of Electrostat. Jpn*. (in Japanese) **22**(3), 145–152 (1998).

38. Y. Kawada, T. Kubo, Y. Ehara, et al., Development of high collection efficiency ESP by barrier discharge system. *Proc. of IEEE/IAS Annual Meetings*, 1130–1135 (1999).

39. S. Jayaram, G. S. P. Castle, J. S. Chang, et al., Semipilot plant pulse energized cold-precharger electrostatic precipitator tests for collection of moderately high resistivity fly-ash particles. *IEEE T. Ind. Appl.* **32**(4), 851–857 (1996).

40. A. Zukeran, P. C. Looy, A. Chakrabarti, et al., Collection efficiency of ultrafine particles by an electrostatic precipitator under DC and pulse operating modes. *IEEE T. Ind. Appl.* **35**(5), 1184–1191 (1999).

41. W. C. Hinds, *Aerosol Technology*. John Wiley & Sons, Inc, USA (Chapters 3 and 5), 1982.

42. T. Yamamoto and H. R. Velkoff, Electrohydrodynamics in an electrostatic precipitator. *J. Fluid Mech*. **108**, 1–18 (1981).

43. T. Yamamoto, M. Okuda, and M. Okubo, Three-dimensional ionic wind and electrohydro-dynamics of tuft/point corona electrostatic precipitator. *IEEE T. Ind. Appl.* November/December (in printing) 2003.

44. A. Mizuno, K. Shimizu, K. Yanagihara, et al., Effect of additives and catalysts on removal of nitrogen oxides using pulsed discharge. *Proc. of 1996 IEEE/IAS Annual Meeting* 3, October 6–10, San Diego, CA, 1808–1812 (1996).

45. T. Oda, T. Kato, T. Takahashi, and K. Shimizu, Nitric oxide decomposition in air by using non-thermal plasma processing-with additives and catalyst. *IEEE T. Ind. Appl.* **34**(2), 268–272 (1998).

46. H. H. Kim, K. Tsunoda, S. Katsura, and A. Mizuno, A novel plasma reactor for NO_x control using photocatalyst and hydrogen peroxide injection. *Proc. of 1997 IEEE/IAS meeting*, New Orleans, October **5–9**, 1937–1941 (1997).

47. S. Masuda, Pulse corona induced plasma chemical process: a horizon of new plasma chemical technologies. *Pure Appl. Chem.* **60**, 727–731 (1988).

48. S. Masuda, S. Hosokawa, X. Tu, and Z. Wang, Novel plasma chemical technologies—-PPCP and SPCP for control of gaseous pollutants and air toxics. *J. Electrostat.* **34**, 415–438 (1995).

49. R. Hackam and H. Akiyama, Application of pulsed power for the removal of nitrogen oxides from pollution air. *IEEE Electr. Insul. M.* **17**(5), 8–13 (2001).

50. T. Yamamoto, M. Okubo, K. Hayakawa, and K. Kitaura, Towards ideal NO_x control technology using a plasma-chemical hybrid process. *IEEE T. Ind. Appl.* **37**(5), September/October, 1492–1498 (2001).

51. T. Yamamoto, M. Okubo, T. Nagaoka, and K. Hayakawa, Simultaneous removal of NO_x, SO_x, and CO_2 at elevated temperature using a plasma-chemical hybrid process. *IEEE T. Ind. Appl.* **38**(5), 1168–1173 (2002).

52. T. Kuroki, M. Takahashi, M. Okubo, and T. Yamamoto, Single-stage plasma-chemical process for particulates, NO_x and SO_x simultaneous removal. *IEEE T. Ind. Appl.* **38**(5), 1204–1209 (2002).

53. B. M. Penetrante, Non-thermal plasma reactors for treatment of NO_x and other hazardous gas emissions. *Task 1.1 Report for CRADA T No. 336-92-1-C*, October 1993.

54. B. M. Penetrante, Plasma chemistry and power consumption in non-thermal plasma DeNO$_x$. *Non-thermal Plasma Techniques for Pollution Control, NATO ASI Series* 34, Part A, B. M. Penetrante (ed.), 65–89 (1993).

55. T. Oda, T. Kato, T. Takahashi, and K. Shimizu, Nitric oxide decomposition in air by using non-thermal plasma processing. *Proc. of IEJ-ESA 1996 Joint Symposium on Electrostatics*, Univ. of Tokyo, Tokyo, Japan, October, 30–31 1996, 17–28.

56. G. E. Vogtlin and B. E. Penetrante, Pulsed corona discharge for removal of NO_x from flue gas. *Non-Thermal Plasma Techniques for Pollution Control, NATO ASI Series* G34, Part B, B. M. Penetrante (ed.), 187–198 (1993).

57. K. Fujii, M. Higashi, and N. Suzuki, Simultaneous removal of NO_x, CO_x, SO_x, and soot in diesel engine exhaust. *Non-Thermal Plasma Techniques for Pollution Control, NATO ASI Series* G34, Part B, B. M. Penetrante (ed.), 257–279, 1993.

58. H. Shaw, Aqueous solution scrubbing for NO_x control in munitions incineration. *The Amr. Soc. of Mechanical Engineers*, August (1976).

59. T. Yamamoto, C. L. Yang, Z. Kravets, and M. Beltran, Plasma assisted chemical reactor for NO_x decomposition. *IEEE T. Ind. Appl.* **36**(3), 923–927, May/June (2000).

60. A. Ogata, N. Shintani, K. Mizuno, S. Kushiyama, and T. Yamamoto, Decomposition of benzene using non-thermal plasma reactor packed with ferroelectric pellet. *Proc. of 1997 IEEE/IAS Annual Meeting*, New Orleans, LA, October 6–9, 1975–1982, 1997.

61. T. Yamamoto, K. Ramanathan, P. A. Lawless, et al., Control of volatile organic compounds by an ac energized ferroelectric pellet reactor and a pulsed corona reactor. *IEEE T. Ind. Appl.* **28**(3), 528–534 (1992).

62. M. Sadakata, *Taiki Kuriin Kano Tameno Kagaku Kougaku (English Translated Title: Chemical Engineering for Atmospheric Clean-up).* Baifukan Publishing Co., Tokyo, Japan, (in Japanese), p. 140 (1999).

63. Z. Kiji and N. Kato, *Kankyo Kaizen no Kagaku (English Translated Title: Chemical Engineering for Environmental Improvement).* Dai Nippon Tosyo Publ. Co., Tokyo, Japan, (in Japanese), p. 9 (1986).

64. S. Masuda, S. Hosokawa, X. Tu, and Z. Wang, Novel cold plasma technologies for pollution control. *Proc. of 2nd International Conf. on Applied Electrostatics*, Beijing, China 1–24 (1993).

65. A. Tamaki and S. Hosokawa, Reduction of chemical pollutants in the exhaust gas of the municipal waste incinerator by PPCP. *Proc. of 6th International Conf. on Electrostatic Precipitation*, Budapest, Hungary 544–549 (1996).

66. H. H. Kim, I. Yamamoto, K. Takashima, S. Katsura, and A. Mizuno, Incinerator flue gas cleaning using wet-type electrostatic precipitator. *J. Chem. Eng. Jpn.*, **33**(4), 669–674 (2000).

67. S. Hosokawa, A. Tamaki, and K. Sonoyama, Application of PPCP for reduction of gaseous pollutants exhausted from incineration plant. *Proc. of NEDO Symposium on Non-Thermal Discharge Plasma Technology for Air Pollution Control*, Beppu and Oita, Japan, 109–114 (1997).

68. S. Hosokawa, Application of PPCP as gas treatment system in incineration plants. *Proc. of The Asia-Pacific Workshop on Water and Air Treatment by Advanced Oxidation Technologies: Innovation and Commercial Applications*, Tukuba, Japan, 182–183, 1998.

69. S. Hosokawa, Application of PPCP for exhaust gases from incineration plants. *Electrical Discharges for Environmental Purposes*, E. M. VanVeldhuizen (ed.), NOVA Science Publishers, Inc. New York, NY, pp. 377–404 (1999).

70. S. Hosokawa, K. Sonoyama, and T. Yamamoto, PPCP pilot plant experiments for decomposition of dioxins. *Proc. of Third International Symp. on Nonthermal Plasma Technology for Pollution Control*, Cheju Island, Republic of Korea, April 23–27 (2001).

71. T. Yamamoto, K. Sonoyama, and S. Hosokawa, Emission control from incinerator plant using non-thermal plasma-chemical process. *Proc. of Third International Symp. on Nonthermal Plasma Technology for Pollution Control*, Cheju Island, Republic of Korea, April 23–27 (2001).

72. S. Masuda, Y. Wu, T. Urabe, and Y. Ono, (1987) Pulse corona induced plasma chemical process for $DeNO_x$, $DeSO_x$ and mercury vapour control of combustion gas. *Proc. of Third International Conf. on Electrostatic Precipitation*, 667–676, Abono-Padova, Italy, October. It also appears in J. S. Chang and T. Oda (eds.), *Applied Electrostatic Studies of Senichi Masuda* (2002).

73. P. M. Castle, I. E. Kanter, P. K. Lee, and L. E. Kline, *Corona Glow Detoxification Study.* Westinghouse Corporation, final report, contract DAAA09-82-C-5396.

74. Y. Kondo and Y. Miyoshi, Pulseless corona in negative point to plane gap. *Jpn. J. Appl. Phys.* **17**, 643–649 (1978).

75. T. Yamamoto, P. A. Lawless, and L. E. Sparks, Narrow-gap point-to-plane corona with high velocity flows. *IEEE T. Ind. Appl.* September/October, **24**(3), 934–939 (1988).

76. T. Yamamoto, P. A. Lawless, and L. E. Sparks, Triangle-shaped DC corona discharge device for molecular decomposition. *IEEE Tran. Ind. Appl.* July/August, **35**(4), 743–749 (1989).

77. K. Hinokiyama, *Jiturei ni Miru Datsusyu Gijyutu (English Translated Title: Odor Control Technologies with Industrial Applications).* Kogyo Chosa Kai Pub. Co., Tokyo, Japan (in Japanese), 1999.

78. R. Zhang, T. Yamamoto, and D. S. Bundy, Control of ammonia and odors in animal houses by a ferroelectric plasma reactor. *IEEE T. Ind. Appl.* **32**(1), 113–117 (1996).

79. Ishiguro, S. and Sugawara, S. (1981) Tobacco smoke and tobacco smoke flavor. *Koryo* (in Japanese), **130**, 31–39 (1996).

80. A. Mizuno, Y. Yamazaki, H. Ito, and H. Yoshida, AC energized ferroelectric pellet bed gas cleaner. *IEEE T. Ind. Appl.* **28**(3), 535–540 (1992).

81. S. Masuda, S. Hosokawa, X. L. Tu, et al., The performance of an integrated air purifier for control of aerosol, microbial, and odor. *IEEE T. Ind. Appl.* **29**(4), 774–780 (1993).

82. A. Mizuno, Y. Kisanuki, M. Noguchi, et al., Indoor air cleaning using a pulsed discharge plasma. *IEEE T. Ind. Appl.* **35**(6), 1284–288 (1999).

83. H. Yoshida, Z. Marui, M. Aoyama, J. Sugiura, and A. Mizuno, Removal of odor gas component utilizing plasma chemical reactions promoted by the partial discharge in a ferroelectric pellet layer. *J. Institute of Electrostat. Jpn.* (in Japanese), **13**(5), 425–430 (1989).

84. Y. Kisanuki, M. Yoshida, K. Takashima, et al., Study on indoor air cleaning using plasma reactor combined with catalyst—experimental study on activation mechanism of TiO_2— *J. Institute of Electrostat. Jpn.* (in Japanese), **24**(3), 153–158 (2000).

85. H. Suda, T. Ueno, T. Yamauchi, and Y. Sainomoto, Plasma discharge deodorizing system. Matsushita Electric Works, Ltd. *Technical Report*, December 2001, 58–63 (in Japanese), 2001.

86. M. Okubo, T. Yamamoto, T. Kuroki, and H. Fukumoto, Electric air cleaner composed of non-thermal plasma reactor and electrostatic precipitator. *IEEE T. Ind. Appl.* **37**(5), 1505–1511 (2001).

87. M. Okubo, T. Kuroki, H. Kametaka, and T. Yamamoto, Odor control using the ac barrier-type plasma reactors. *IEEE T. Ind. Appl.* **37**(5), 1447–1455 (2001).

88. S. K. Friedlander, *Smoke, Dust, and Haze—Fundamental of Aerosol Dynamics*—Oxford University Press, NY, 2000.

89. M. Horvath, *Ozone*. Amsterdam The Netherlands: Elsevier Science, 1980.

90. M. Kuzumoto, Extremely narrow discharge gap ozone generator. *J. Plasma and Fusion Research* (in Japanese), **74**(10), 1144–1150 (1998).

91. Y. Kamase, T. Mizuno, and M. Sakurai, Development of ozone sterilization system for pharmacy plant. *Ishikawajima-Harima Engineering Review* (in Japanese), **40**(1), 3–6 (2000).

92. Masuda Research Inc. *Plasma Deodorization System—ADO Series*—Products catalog, Tokyo, Japan, (in Japanese), 2002.

93. Masuda Research Inc., *Ceramic Ozonizer and Small Ozonizers*. Products Catalog, Tokyo, Japan, 2002.

94. N. Tabata, Ozone generation and generation efficiency. *J. Plasma and Fusion Research* (in Japanese), **74**(10), 1119–1126 (1998).

95. NGK Insulators, LTD. *NGK Deodorization Systems*. Products Catalog, Environmental Systems & Equipment Division, Nagoya, Japan, 2002.

96. J. A. Libra and A. Saupe, *Ozonation of Water and Wastewater: A Practical Guide to Understanding Ozone and Its Application.* John Wiley & Sons Inc., 2000.

97. J. J. McKetta (ed.), *Encyclopedia of Chemical Processing and Design: Wastewater Treatment with Ozone to Water and Wastewater Treatment*. 66, Marcel Dekker Publisher, 1999.

98. A. Kanazawa, H. Sekiguchi, and T. Honda, Destruction technologies of substances that deplete the stratospheric ozone layer. Ed. Japanese Committee of Technologies for Destruction of Substances that Deplete the Stratospheric Ozone Layer, *JICOP*, November, **53**, 1991.

99. D. J. Helfritch, Plasma technologies applied to air pollution control. *IEEE T. Ind. Appl.* **29**(5), 882–886 (1993).

100. E. Odic, M. Paradisi, M. Rea, L. Parissi, A. Goldman, and M. Goldman, Treatment of organic pollutants by corona discharge plasma. *The Modern Problems of Electrostatics*

with Application in Environment Protection, NATO Science Series, 2. Environmental Security, I. I. Inculet, F. T. Tanasescu, and R. Cramariuc, (eds.), **63**, 143–160 (1999).

101. E. N. Ruddy and L. A. Caroll, Select the best VOC control strategy. *Chem. Eng. Progress* **89**(7), 28–35 (1993).

102. J. J. Sudnick and D. L. Corwin, VCR control techniques. *Hazard. Waste Hazard.* **11**(1), 129–143 (1994).

103. K. L. L. Vercamnen, A. A. Berezin, F. Lox, and J. S. Chang, Destruction of volatile organic compounds by non-thermal plasmas, a critical review. *J. Adv. Oxid. Technol.* **2**(2), 312–329 (1997).

104. K. Mizuno, Stratospheric ozone depletion and its countermeasures. *J. Institute of Electrostat. Jpn.* **17**(4), 251–258 (1993).

105. T. Yamamoto, Control of NO_x and volatile organic compounds using catalyst/chemical combined packed-bed plasma reactor. *OYO BUTURI* **69**(3), 284–289 (2000).

106. C. Lahousse, A. Bernier, P. Grange, et al., Evaluation of γ-MnO_2 as a VOC removal catalyst: comparison with a nobel metal catalyst. *J. Catal.* **178**, CA982148, 214–225 (1998).

107. A. Czernichowski, Gliding arc. applications to engineering and environment control. *Pure Appl. Chem.* **66**(6), 1301–1310 (1994).

108. J. Teply, M. Dressler, J. Janca, and C. Tesar, Destruction of organic compounds in a high-frequency discharge plasma at reduced pressure. *Plasma Chem. Plasma P.* **15**(3), 465–479 (1995).

109. J. Arno, J. W. Bevan, and M. Moisan, Acetone conversion in a low-pressure oxygen surface wave plasma. *Environ. Sci. Technol.* **29**(8), 1961–1965 (1995).

110. T. Yokoyama, M. Kogoma, T. Moriwaki, and S. Okazaki, The mechanism of the stabilization of glow plasma at atmospheric pressure. *J. Phys. D. Appl. Phys.* **23**, 1125–1128 (1990).

111. D. G. Storch and M. J. Kushner, Destruction mechanisms for formaldehyde in atmospheric pressure low temperature plasmas. *J. Appl. Phys.* **73**(3), 51–55 (1993).

112. J. S. Chang and F. Kaufman, Kinetics if the reactions of hydroxyl radicals with some halocarbons: $CHFCl_2$, CHF_2Cl, CH_3CCl_3, C_2HCl_3 and C_2Cl_4. *J. Chem. Phys.* **66**(11), 4989–4994 (1997).

113. J. S. Chang, Energetic electron induced plasma processes for reduction of acid and green-house gases in combustion flue gas. *Non Thermal Plasma Techniques for Pollution Control, NATO ASI Series, Series G: Ecological Sciences* G34, Part A, B. M. Penetrante, and S. E. Schulthis (ed.), Springer-Verlag, Berlin, 1–32 (1993).

114. A. W. Miziolek, J. T. Herron, W. G. Mallard, et al., Importance of chemistry in non-thermal plasma control of volatile organic compounds and air toxics. *Proc. of ELMECO94*, Lublin, 65–71 (1994).

115. B. M. Penetrante, M. C. Hsiao, J. N. Bardsley, et al., Electron bean and pulsed corona processing of carbon tertachloride in atmospheric pressure gas streams. *Phys. Lett.* (A) **209**(1 and 2), 69–77 (1995).

116. H. Matzing, K. Woletz, and H. R. Paur, Abscheidung von fluchtigen organischen verbindungen (VOC) aus abluft durch elektronenstrahl. *Statuskolloquium des PEF:9.* Karlsruhe vom 9-11. Maerz, Vorhanden in Kernforschungzentrum Karlsruhe: KfK-PEF **104**, 445–455 (1993).

117. H. Matzing, K. Hirota, W. Baumann, and H. R. Paur, Abscheidung von organischen verbindungen (VOC) aus abluft durch elektronenstraahl. *Statuskolloquium des PEF:10.* Karlsruhe vom 15–17. Maerz, Vorhanden in Kemforschungzenturm Karlsruher: KfK-PBF **118**, (1994).

118. H. Matzing, W. Baunann, and H. R. Paur, Abscheidung von fluchtigen orsanischen verbindungen (VOC) aus abluft durch elektronenstrahl. Vorhanden in Kernforschungzenturn, Karlsruhe, PEF11 (1996).

119. H. R. Paur, H. Matzing, and K. Woletz, Removal of volatile organic compounds from industrial off gas by irradiation induced aerosol formation. *J. Aerosol Sci.* **22**, 509–512 (1991).

120. L. Bromberg, D. R. Cohn, M. Koch, R. M. Patrick, and P. Thomas, Decomposition of dilute concentrations of carbon tetrachloride in air by an electron-bean generated plasma. *Phys. Lett.* (A), **173**, 293–299 (1993).

121. M. C. Hsiao, B. T. Merritt, B. M. Penetrante, G. E. Vogtlin, and P. H. Wallman, Plasma-assisted decomposition of methanol and trichloroethylene in atmospheric pressure air streams by electrical discharge processing. *J. Appl. Phys.* **78**(5), 3451–3456 (1995).

122. C. M. Nunez, G. H. Ramsey, W. H. Ponder, J. H. Abbott, L. E. Hamel, and R. H. Kariher, Corona destruction: an innovative control technology for VOCs and air toxics. *Air & Waste* **43**, 242–247 (1993).

123. M. B. Chang and C. C. Chang, Destruction and removal of volatile organic compounds (VOCs) from gas streams with dielectric barrier discharge plasmas. In *88th Annual Meeting & Exhibition, Air and Waste Management*, 95-WP77 B.05, 1995.

124. D. Evans, L. A. Rosocha, G. K Anderson, J. J. Coogan, and M. J. Kushner, Plasma remediation of trichloroethylene in silent discharge plasmas. *J. Appl. Phys.* **74**(9), 5378–5386 (1993).

125. M. B. Chang and C. C. Lee, Destruction of formaldehyde with dielectric barrier discharge plasmas. *Environ. Sci. Technol.* **29**, 181–186 (1995).

126. M. B. Chang and C. C. Chang, Destruction and removal of toluene and MEK from gas streams with silent discharge plasmas. *AICHE J.* **43**(5), 1325–1330 (1997).

127. Z. Falkenstein, Proceeding of C_3H_7OH, C_2HCl_3 and CCl_4 in flue gases using silent discharge plasmas (SDPs), enhanced by (V)UV at 172 nm and 253.7 nm. *J. Adv. Oxid. Technol.* **2**(1), 223–237 (1997).

128. A. Sjoberg, T. H. Teich, E. Heinzle, and K. Hungerbuhler, Oxidation products of toluene in a dielectric barrier plasma reactor. *J. Adv. Oxid. Technol.* **4**(3), 319–327 (1999).

129. S. Yamaguma, A. Osawa, T. Kodama, and Y. Tabata, Detoxification of hazardous gaseous substances by discharge plasma-decomposition of aromatic organic solvents by surface discharge plasma. *Res. Rep. of the Res. Inst. Industrial Safety in Japan*, R11 S-RR-**92**, l57–166 (1993).

130. T. Oda, R. Yamashita, I. Haga, T. Takahasi, and S. Masuda, Decomposition of gaseous organic contaminants by surface discharge induced plasma chemical processing-SPCP. *IEEE T. Ind. Appl.* **32**(1), 118–124 (1996).

131. T. Oda, R. Yamashita, K. Tanaka, T. Takahasi, and S. Masuda, Atmospheric pressure discharge plasma decomposition for gaseous air contaminants—trichlorotrifuluorethane and trichloroethylene. *IEEE T. Ind. Appl.* **32**(2), 227–232 (1996).

132. T. Oda, T. Takahashi, and K. Tada, Decomposition of dilute trichloroethylene by non-thermal plasma. *IEEE T. Ind. Appl.* **35**(2), 373–379 (1999).

133. T. Oda, T. Takahashi, H. Nakano, and S. Masuda, Decomposition of fluorocarbon gaseous contaminants by surface discharge induced plasma chemical processing. *IEEE T. Ind. Appl.* **29**(1), 787–792 (1993).

134. S. Masuda, S. Hosokawa, X. L. Tu, K. Sakakibara, S. Kitoh, and S. Sakai. Destruction of gaseous pollutants by surface-induced plasma chemical process (SPCA). *IEEE T. Ind. Appl.* **29**(4), 781–786 (1993).

135. A. Mizuno, Y. Yamazaki, S. Obama, E. Suzuki, and K. Okazaki, Effect of voltage waveform on partial discharge in ferroelectric pellet layer for gas clearing, *IEEE T. Ind. Appl.* **29**(2), 262–267 (1993).

136. R. A. Korzekwa and L. A. Rosocha, Treatment of a multicomponent VOC mixture in air using a dielectric barrier discharge. *J. Adv. Oxid. Technol.* **4**(4), 390–399 (1999).

137. S. Futamura and T. Yamamoto, Byproduct identification and mechanism determination in plasma chemical decomposition of trichloroethylene. *IEEE T. Ind. Appl.* **33**(2), 447–453 (1997).
138. S. Futamura, A. Zhang, G. Prieto, and T. Yamamoto, Factors and intermediates governing byproduct distribution for decomposition of butane in nonthermal plasma. *IEEE T. Ind. Appl.* **34**(5), 967–974 (1998).
139. T. Yamamoto, J. S. Chang, A. A. Berezin, H. Kohno, S. Honda, and A. Shibuya, Decomposition of toluene, *o*-xylene, trichloroethyelen and their mixture using a $BaTiO_3$ packed-bed plasma reactor. *J. Adv. Oxide. Technol.* **1**(1), 67–78 (l996).
140. T. Yamamoto, P. A. Lawless, M. K. Owen, D. S. Ensor, and C. Boss, Decomposition of volatile organic compounds by a packed-bed reactor and a pulsed-corona plasma reactor. In: *Nonthermal Plasma Techniques for Pollution Control, NATO ASI Series, Series G: Ecological Sciences* G34, Part B, B. M. Penetrante and S. E. Schultheis (eds.), Springer-Verlag, Berlin, 223–237, 1993.
141. J. D. Skalny, V. Sobek, and P. Lukac, Negative corona induced decomposition of CCl_2F_2. In: *Now-ThermaI Plasma Techniques for Polluion Control, NATO ASI Series, Series G: Ecological Sciences* G34, Part A, B. M. Penetrante and S. E. Schultheis, (eds.), Springer-Verlag, Berlin, 151–165, 1993.
142. H. Kohno, M. Tamura, S. Honda, et al., Generation of aerosol particles during the destruction of xylene and trichloroethylene from air stream by a pulse corona discharge. *J. Aerosol Sci.* **26**(Suppl.1), S585–S586 (1995).
143. J. S. Chang, T. Yamamoto, H. Kohno, et al., Removal of xylene, trichloroethylene and their mixtures from air stream by a pulsed corona discharge induced plasma reactor. *J. Adv. Oxi. Technol.* **2**(2), 346–352 (1997).
144. H. Kohno, A. A. Berezin, J. S. Chang, et al., Destruction of volatile organic compounds used in a semiconductor industry by a capillary tube discharge reactor. *IEEE T. Ind. Appl.* **34**(5), 953–966 (1998).
145. J. S. Chang, A. Chakrabarti, T. A. Myint, and A. W. Miziolek, The effect of corona wire geometries on the destruction of volatile organic compounds in air by a pulsed corona discharge plasma reactor—adsorbent hybrid system. *J. Adv. Oxid. Technol.* **4**(3), 297–304 (1999).
146. J. S. Chang, K. Urashima, T. Ito, and T. Misaka, Removal of volatile organic compounds by an electrical discharge/activated carbon filter hybrid system. *Electrostatic 95. IOP Press, Bristol, Inst. Phys, Conf. Ser.* **143**, 183–186 (1995).
147. T. Yamamoto, K. Mizuno, I. Tamori, et al., Catalysis-assisted plasma technology for carbon tetrachloride destruction. *IEEE T. Ind. Appl.* **32**(1), 100–105 (1996).
148. K. Urashima, J. S. Chang, T. Ito, and T. Misaka, Destruction of volatile organic compounds in air by a superimposed barrier discharge plasma reactor and activated carbon filter hybrid system. *Proc. of IEEE/LAS Annual Meeting*, 1969–1974, 1997.
149. J. S. Chang, K. Urashima, and T. Ito, Mechanism of non-thermal plasma treatment of volatile organic compounds in dry air. *Emerging Technologies in Hazardous Waste Management*, D. W. Tedder (ed.), ACS Press, Atlanta, 203–206, 1994.
150. S. Futamura, A. Zhang, and T. Yamamoto, The dependence of nonthermal plasma behavior of VOCs on their chemical structures. *J. Electrostat.* **42**, 51–62 (1997).
151. A. Zhang, S. Futamura, and T. Yamamoto, Nonthermal plasma chemical processing of bromomethane. *J. Air & Waste Manage. Assoc.*, **49**, 1442–1448 (1999).
152. S. Futamura, H. Einaga, and A. Zhang, Comparison of reactor performance in the nonthermal plasma chemical processing of hazardous air pollutants. *IEEE T. Ind. Appl.* **37**(4), 978–985 (2001).
153. H. Einaga, T. lbusuki, and S. Futamura, Perfomance evaluation of hybrid system comprising silent discharge plasma and manganese oxide catalysts for benzene decomposition. *IEEE T. Ind. Appl.* **37**(5), 1476–1482 (2001).

154. S. Futamura, H. Einaga, A. Zhang, and H. Kabashima, Involvement of catalyst materials in nonthermal plasma chemical processing of hazardous air pollutants. *Catal. Today* **72**, 259–265 (2002).

155. M. B. Chang and S. J. Yu, An atmospheric-pressure plasma process for C_2F_6 removal. *Environ. Sci. Technol*. **35**, 1587–1592 (2001).

156. S. J. Yu and Chang, M. B. Oxidative conversion of PFC via plasma processing with dielectric discharge. *Plasma Chem. Plasma P*. **21**, 311–327 (2001).

157. D. A. Li, D. Yakushiji, S. Kanazawa, T. Ohkubo, and Y. Nomoto, Decomposition of toluene by streamer corona discharge with catalyst. *J. Electrostat*. **55**, 311–319 (2002).

158. M. Kang, B. J. Kim, S. M. Cho, et al., Decomposition of toluene using an atmospheric pressure plasma/TiO_2 catalytic system. *J. Mol. Catal. A-Chem.* **180**, 125–132 (2002).

159. T. Oda, T. Takahashi, and K. Yamaji, Nonthermal plasma processing for dilute VOCs. *IEEE T. Ind. Appl*. **38**, 873–878 (2002).

160. D. W. Park, S. H. Yoon, G. J. Kim, and H. Sekiguchi, The effect of catalyst on the decomposition of dilute benzene using dielectric barrier discharge. *J. Ind. Eng. Chem*. **8**, 393–398 (2002).

161. U. Roland, F. Holzer, and F. D. Kopinke, Improved oxidation of air pollutants in a non-thermal plasma. *Catal. Today* **73**, 315–323 (2002).

162. X. Chen, J. Rozak, J. C. Lin, S. L. Suib, Y. Hayashi, and H. Matsumoto, Oxidative decomposition of chlorinated hydrocarbons by glow discharge in PACT reactors. *Appl. Catal. A-Gen.* **219**, 25–31 (2001).

163. T. Oda, T. Takahashi, and S. Kohzuma, Decomposition of dilute trichloroetylene by using nonthermal plasmas processing-frequency and catalyst effects. *IEEE T. Ind. Appl.* **37**, 965–970 (2001).

164. H. Holzer, U. Roland, and F. D. Kopinke, Combination of non-thermal plasma and heterogeneous catalysis for oxidation of volatile organic compounds, Part1. Accessibility of intra-particle volume. *Appl. Catal. B-Environ.* **38**, 163–181 (2002).

165. A. Gervasini and V. Ragaini, Catalytic technology assisted with ionization/ozonization phase for the abatement of volatile organic compounds. *Catal. Today* **60**, 129–138 (2000).

166. Y. H. Song, S. J. Kim, K. I. Choi, and T. Yamamoto, Effect of adsorption and temperature on a nonthermal plasma process for removing VOCs. *J. Electrostat*. **55**, 189–201 (2002).

167. K. P. Francke, H. Miessner, and R. Rudolph, Cleaning of air stream from organic pollutants by plasma-catalytic oxidation. *Plasma Chem. Plasma P.* **20**, 393–403 (2000).

168. H. Sekiguchi, Catalysis assisted plasma decomposition of benzene using dielectric barrier discharge. *Can. J. Chem. Eng*. **79**, 512–516 (2001).

169. A. Gervasini, G. C. Vezzoli, and V. Ragaini, VOC removal by synergic effect of combustion catalyst and ozone. *Catal. Today* **29**, 449–455 (1996).

170. K. P. Francke, H. Miessner, and R. Rudolph, Plasmacatalytic processes for environmental problems. *Catal. Today* **59**, 411–416 (2000).

171. V. Demidiouk, S. I. Moon, and J. O. Chae, Toluene and butyl acetate removal from air by plasma-catalytic system. *Catal. Commun*. **4**, 51–56 (2003).

172. A. Ogata, D. Ito, K. Mizuno, S. Kushiyama, and T. Yamamoto, Removal of dilute benzene using a zeolite-hybrid plasma reactor. *IEEE T. Ind. Appl.* **37**, 959–964 (2001).

173. A. Ogata, K. Yamanouchi, K. Mizuno, S. Kushiyama, and T. Yamamoto, Decomposition of benzene using alumina-hybrid and catalyst-hybrid plasma reactor. *IEEE T. Ind. Appl.* **35**, 1289–1295 (1999).

174. A. Ogata, K. Yamanouchi, K. Mizuno, S. Kushiyama, and T. Yamamoto, Oxidation of dilute benzene in an alumina hybrid plasma reactor at atmospheric pressure. *Plasma Chem. Plasma P.* **19**, 383–394 (1999).

175. T. Ohkubo, D. Li, D. Yakushiji, S. Kanazawa, and Y. Nomoto, Decomposition of VOC in air using a streamer corona discharge reactor combinated with catalyst. *J. Adv. Oxi. Technol.* **6**, 75–79 (2003).

176. B. Penetrante and S. E. Schultheis, *Edited, Non-Thermal Plasma Techniques for Pollution Control,* Springer-Verlag, NATO ASI Series 34, Part B, 223–237 (1993).
177. A. Ogata, D. Ito, K. Mizuno, S. Kushiyama, A. Gal, and T. Yamamoto, Effects of coexisting components on aromatic decomposition in a packed-bed plasma reactor. *Appl. Catal. A-Gen.* **236**, 9–15 (2002).
178. G. Saithamoorthy, B. R. Locke, W. C. Finney, R. C. Clark, and T. Yamamoto, Halon destruction in a gas phase pulsed streamer corona reactor. *J. Adv. Oxi. Technol.* **4**(4), 375–379 (1999).
179. S. Futamura, A. Zhang, and T. Yamamoto, Mechanisms for formation of inorganic byproducts in plasma chemical processing of hazardous air pollutants. *IEEE T. Ind. Appl.* **35**(4), 760–766 (1999).
180. T. Yamamoto and B. L. Jang, Aerosol generation and decomposition of CFC-113 by the ferroelectric plasma reactor. *IEEE Tran. Ind. Appl.* **35**(4), 736–742 (1999).
181. T. Yamamoto, Optimization of nonthermal plasma for the treatment of gas streams. *J. Hazard. Mater.* B**67**, 165–181 (1999).
182. T. Yamamoto and S. Futamura, Nonthermal plasma processing for controlling volatile organic compounds. *Combust. Sci. Tech.* **133**, 117–133 (1998).
183. H. Kohno, M. Tamura, A. Shibuya, et al., Destruction of volatile organic compounds used in a semiconductor industry by a capillary tube discharge reactor. *IEEE Tran. Ind. Appl.* **34**(5), 953–966 (1998).
184. A. Ogata, K. Mizuno, S. Kushiyama, and T. Yamamoto, Methane decomposition in a barium titanate packed-bed nonthermal plasma reactor. *Plasma Chem. Plasma P.* **18**(3), 363–373 (1998).
185. G. Prieto, O. Prieto, C. R. Gay, K. Mizuno, I. Tamori, and T. Yamamoto, Decomposition of carbon tetrachloride by a packed-bed plasma reactor. *J. Adv. Oxi. Technol. for Water and Air Remediation* **2**(2), 330–336 (1997).
186. T. Yamamoto, VOC decomposition by nonthermal plasma processing—a new approach. *J. Electrostat.* **42**, 227–238 (1997).
187. T. Yamamoto, VOC decomposition technology using electrical discharge. *Proc. of Institute of Electrostat. Jpn.* **19**(4), 301–305 (1995).
188. K. Jorgan, A. Mizuno, T. Yamamoto, and J. S. Chang, The effect of residence time on the CO_2 reduction from combustion flue gases by an ac ferroelectric packed bed reactor. *IEEE T. Ind. Appl.* **29**(5), 876–882 (1993).
189. H. Kohno, S. Honda, J. S. Chang, T. Yamamoto, and A. A. Berezin, Generation of aerosol particles by spark discharges in a capillary tube under air flow with trace organic compounds. *J. Aerosol Sci.* 25 (Suppl. 1), S41–S42 (1994).
190. J. S. Chang, The role of H_2O and NH_3 on the formation of NH_4NO_3 aerosol particles and De-NO$_x$ under the corona discharge treatment of combustion flue gases. *J. Aerosol Sci.* **20**, 1087–1097(1989).
191. H. H. Kim, H. Kobara, A. Ogata, and S. Futamura, Nono-sized aerosol formation from benzene decomposition using non-thermal plasma. *J. Institute of Electrostat. Jpn.* **27**(1), 45–46 (2003).
192. T. Murayama and H. Tsunemoto, *Jidosya Engine Kogaku (English Translated Title: Automobile Engine Engineering)*. Sankai-do Publ. Corp., 142 (in Japanese), 1997.
193. B. J. Cooper, The catalytic control of motor vehicle emissions. *Preprint of Commemorative Lecture at the Twenty-third Honda Prize Awarding Ceremony,* 15th November, Tokyo 2002.
194. M. Okubo and T. Yamamoto, Recent studies on regeneration of DPF using nonthermal plasma. *J. Institute of Electrostat. Jpn.* (in Japanese), **26**(6), 254–255 (2002).
195. N. Kajiwara, (ed.) *Particle Removal Technologies of Diesel Car Exhaust Gas*. CMC books Corp., 203 (in Japanese) 2001.

196. M. Okubo, T. Miyashita, K. Kitaura, and T. Yamamoto, NO_x removal characteristics in diesel engine exhaust using plasma-chemical hybrid process, *Proc. 4th ESA/IEJ Joint Symposium in Electrostatics*, Kyoto, Japan, September 25–26, 341–354 (2000).

197. T. Yamamoto, M. Okubo, T. Miyashita, and K. Kitaura, NO_x removal in diesel engine exhaust using nonequilibrium plasma and chemical process, *Trans. of Jpn. Society of Mech. Eng.* (in Japanese), **67B**, 663, 2891–2897 (2000).

198. M. Okubo, M. Takahashi, K. Kuroki, and T. Yamamoto, Simultaneous removal of NO_x, SO_x and soot particles in diesel engine exhaust gas using corona plasma-chemical hybrid process, *Proc. of ESCAMPIG16/icrp5 2*, Grenoble, France, 363–364, 2002.

199. T. Murayama, and H. Tsunemoto, *Jidosya Engine Kogaku* (*English Translated Title: Automobile Engine Engineering*). Sankai do Publ. (in Japanese) 1997.

200. N. Miyoshi, T. Tanaka, and S. Matsumoto, Development of NO_x storage-reduction catalysts. *TOYOTA Technical Rev.* (in Japanese) **50(2)**, 28–33 (2000).

201. T. Hirayama and T. Uekusa, Aftertreatment technologies for diesel engines. *Engine Technol* (in Japanese) **2(2)**, 13–17 (2000).

202. S. E. Thomas, A. R. Martin, D. Raybone, J. T. Shawcross, K. L. Ng, and P. Beech, Non thermal plasma aftertreatment of particulates—theoretical limits and impact on reactor design. Presented at International Spring Fuels & Lubricants Meeting & Exposition, Paris, France, June 19-22, 1–13 (2000).

203. K. Fujii, Plasma treatment of the exhaust gas from vehicles. *J. Plasma and Fusion Research* (in Japanese) **74**(2), 151–154 (1998).

204. B. R. Locke, A. Ichihashi, H. H. Kim, and A. Mizuno, Diesel engine exhaust cleanup with a pulsed streamer corona reactor equipped with reticulated vitreous carbon electrodes. *IEEE T. Ind. Appl.*, 1111–1116 (1999).

205. A. Mohammadi, Y. Kaneda, T. Sogo, Y. Kidoguchi, and K. Miwa, Study of NO into NO_2 conversion by high-frequency dielectric barrier discharge plasma for diesel exhaust aftertreatment. *Preprints of 17th JSAE Internal Combustion Engine Symposium*, (in Japanese) pp. 257–262, 2002.

206. S. Yamada, *Honeycomb Ceramics for Air Pollution Control*. Nihon Ceramics Kyo-kai, 27th Kosyukai shiryo (in Japanese), 1995.

207. H. Ogawa, and T. Ogasawara, *Honeycomb Ceramics,Past, Present and Future*. Ceramics data book 99, Kogyo to Seihin, (in Japanese) **27–81**, 219–224 (1999).

208. P. Kojetin, F. Janezich, L. Roth, and D. Tuma, Production experience of a ceramic wall flow electric regeneration diesel particulate trap. *SAE paper*, 930129, Febraury 1993.

209. Y. Ichikawa, S. Yamada, and T. Yamada, Development of wall-flow type diesel particulate filter system with efficient reverse pulse air regeneration. *SAE paper*, 950735, Febraury 1995.

210. J. Kupe, D. Goulette, M. Hemingway, et al., Non-thermal plasma approach to simultaneous removal of NO_x & particulate matter. Presented at Diesel Engine Emission Reduction 2000 Workshop, SanDiego, CA., August 20–24, 2000.

211. J. Kupe, J. Bonadies, D. Goulette, et al., Delphi enhanced NTP emission solution tested on light-duty vehicle. Presented at Diesel Engine Emission Reduction 2001 Workshop, Portsmouth, Virginia, August 5–9, 2001.

212. S. Müller, J. Conrads, and W. Best, Reactor for decomposing soot and other harmful substances contained in flue gas. *Proc. of Int. Symp. High Pressure Low Temperature Plasma Chemistry* (Hakone VII) **2**, 340–344 (2000).

213. M. Okubo, T. Miyashita, T. Kuroki, S. Miwa, and T. Yamamoto, Regeneration of diesel particulate filter using nonthermal plasma without catalyst. *Proc. of 2002 IEEE/IAS Annual Meeting*, CD-ROM, 2002.

214. T. Yamamoto, M. Okubo, T. Kuroki, and Y. Miyairi, Nonthermal plasma regeneration of diesel particulate filter. *SAE paper*, 2003-01-1182, presented at 2003 SAE World Congress, Detroit, Michigan, March 3–6, 2003.

215. M. Okubo, T. Kuroki, T. Yamamoto, and S. Miwa, *SAE paper,* 2003-01-1886, *JSAE* 20030309 presented at JSAE/SAE International Spring Fuels & Lubricants Meetin*g*, Yokohama, Japan, May 19–22, 2003.

216. M. Okubo, T. Yamamoto, and S. Miwa, Exhaust gas cleaning system. Japanese patent pending, No. 2002-227920, August 5, 2002, PCT international patent pending, July 29, 2002.

217. P. C. Wankat, Cyclic separation processes (review). *Separation Sci.* **9**,(2), 85–116 (1974).

218. D. Diagne, M. Goto, and T. Hirose, New PSA process with intermediate feed inlet position operated with dual refluxes: application to carbon dioxide removal and enrichment. *J. Chem. Eng. Jpn.* **27**, 85–89 (1994).

219. H. Tominaga, *Zeolite no Kagaku to Ouyo* (*English Translated Title: Science and Applications of Zeolite*), Kodansha LTD., 1 (in Japanese), 1987.

220. M. Suzuki, *Adsorption Engineering*, Kodansha LTD. and Elsevier Science Publishers, p. 245, 1990.

221. T. Yamamoto and C. L. Yang, Plasma desorption and decomposition. *Proc. of IEEE/IAS Annual Meeting*, St. Louis, MO, 12–16, pp. 1877–1883, (1998).

222. T. Yamamoto, M. Okubo, and T. Kuroki, Nonthermal plasma desorption for NO_x control. *Trans. of the Institute of Fluid-Flow Machinery* **107**, 111–120 (2000).

223. T. Yamamoto, M. Okubo, and M. Fujimoto, Desorption and regeneration of NO using non-equilibrium plasma. *J. Institute of Electrostat. Jpn.* **24**(3), 161–162 (2000).

224. K. L. Mittal, and W. J. Ooji van (eds.), Special Issue on Plasma Surface Modification. *J. Adhesion Sci. and Technol.* **7**(10), 1 (1993).

225. W. W. Balwanz, Plasma Cleaning of Surfaces. *Surface Contamination: Genesis. Detection and Control* **1**, 255–269 (1979).

226. Y. Matsushita, Activities of PFCs emission reduction by EIAJ CVD & dry etching working group. *OYO BUTURI* (in Japanese), **69**(3) 305–309 (2000).

227. M. Yamamoto, Q. Li, M. Nishioka, and M. Sadakata, Decomposition of CF_4 and C_2H_6 by gas-phase ion-molecule reaction. *Proc. of 6th World Congress of Chemical Engineering*, (September 23–27, Melbourne, Australia), 2001.

228. J. S. Chang, K. G. Kostov, K. Urashima, et al., Removal of NF_3 from semiconductor-process flue gases by tandem packed-bed plasma and absorbent hybrid system. *IEEE T. Ind. Appl.* **36**(5), 1251–1259 (2000).

229. T. Yamamoto, J. S. Chang, K. Yoshimura, S. Okayasu, T. Iwaizumi, and T. Kato, NF_3 treatment by ferroelectric packed bed plasma reactor. *J. Adv. Oxid. Technol.* **4**, 454–457 (1999).

230. T. Oda and M. Itoh, Dilute PFC decomposition by the non-thermal plasma. *Proc. of 2001 Annual Meeting of the Institute of Electrostatics Japan*, (Tokyo, Japan, September 11–12), 25–26 (in Japanese), (2001).

231. R. Itatani, M. Deguchi, T. Toda, and H. Ban, Abatement of CF_4 using atmospheric pressure discharge plasma. *Proc. of Second Asia-Pacific International Symposium on the Basis and Application of Plasma Technology*, (Kaohsiung, Taiwan, April 30–31), 37–38 (2001).

232. M. Kogoma, PFC abatement System with using the atmospheric pressure glow plasma. *Proc. of Second Polish-Japanese Hakone Group Symposium on Nonthermal Plasma Processing of Water and Air*, 49–54 (2001).

233. H. H. Sawin, Abatement of PFC's in a plasma reactor using O_2 as an additive gas. *B. Am. Phys. Soc.* **43**, 475 (1998).

234. J. D. Crip, Microwave PFC treatments. presented at the NIST Work-shop on Pollution Control Technol., Washington, DC, 1995.

235. E. J. Tonnis, V. Vartanian, L. Beu, T. Lii, R. Jewett, and D. Graves, Evaluation of a litmas "Blue" point-of-use (POU) plasma abatement device for perfluorocompound (PFC) destruction. Technology Transfer No. 98123605A-ENG, International SEMATECH, 1998.

236. V. Vartanian, L. Beu, T. Stephens, et al., Long-term evaluation of the litmas "Blue" plasma device for point-of-use (POU) perfluorocompound and hydrofluorocarbon abatement. Technology Transfer No. 99123865B-ENG, International SEMATECH, 2000.

237. K. Urashima, K. G. Kostov, J. S. Chang et al., Removal of C_2F_6 from a semiconductor process flue gas by a ferroelectric packed-bed barrier discharge reactor with an adsorber. *IEEE T. Ind. Appl.* **37**(5), 1456–1463 (2001).

238. Y. Inanaga, K. Ohta, N. Wada, M. Doi, K. Yoshida, and M. Kuzumoto, Destruction of perfluoro compounds by atmospheric pressure plasma. *Proc. of 2002 Annual Meeting of The institute of Electrostatics Japan*, (Toyohashi, Japan, August 29–30), (in Japanese), 79–82 (2002).

239. N. Hayashi, K. Yamamoto, S. Ihara, S. Satoh, and C. Yamabe, Treatment of fluorocarbon using non-thermal plasma produced by atmospheric discharge. *Proc. of 8th International Symposium on High Pressure Low Temperature Plasma Chemistry*, (Pühajärve, Estonia, July 21–25), 361–362 (2002).

240. H. Nishiyama and M. Shigeta, Numerical simulation of an RF inductively coupled plasma for functional enhancement by seeding vaporized alkali metal. *Eur. Phys. J. Appl. Phys.*, 125–133 (2002).

241. T. Yamamoto, J. R. Newsome, and D. S. Ensor, Modification of surface energy, dry etching, and organic film removal using atmospheric-pressure pulsed corona plasma. *IEEE T. Ind. Appl.* **31**(3), 494–499 (1995).

242. T. Yamamoto, M. Okubo, N. Imai, and Y. Mori, Improvement on hydrophilic and hydrophobic properties of glass surface treated by nonthermal plasma induced by silent corona discharge. *Plasma Chem. Plasma P.* **24**, (1) (in printing), (2003).

243. H. Yasuda, Glow discharge polymerization. *J. Polymer Sci.: Macromolecular Reviews* **16**, 199–293 (1981).

244. M. Yekta-Fard and A. B. Ponter, Surface treatment and its influence on contact angles of water drops residing on polymers and metals. *Phys. Chem. Liq.* **15**, 19–30 (1985).

245. Y. Qiu, S. Deflon, and P. Schwartz, Plasma surface treatment of poly (*p*-phenylenebenzobisthiozol) fibers. *J. Adhesion Sci. and Tech.* (K. L. Mittal, and W. J. Ooji, eds., Special Issue on Plasma Surface Modification) **7**(10), 1041–1049 (1993).

246. N. Inagaki, S. Takasa, and H. Kawai, Surface modification of Kevlar© fiber by a combination of plasma treatment and coupling agent treatment for silicone rubber composite. *J. Adhesion Sci. and Tech.* K. L. Mittal and W. J. Ooji, (eds.), Special Issue on Plasma Surface Modification **7**(10), 279–291 (1993).

247. T. Minami and S. Tadanaga, Preparation of functional thin films by sol-gel method. *Surf. Technol.* **48**(3), 298–303 (1997).

248. New energy and industrial technology development organization (NEDO) report, Development of comfortable cloth with moisture breath prepared by plasma process. *Nedo report* (*Heisei 10 Nendo Chi-iki Konsosiam Kenkyu Kaihatu Jigyou*), (Researchers: Kataoka, S. and Saeki, N. et al.), 1 (in Japanese), 1999.

249. M. Okubo, J. Mine, T. Kuroki, T. Yamamoto, N. Saeki, and S. Kataoka, Preparation of functional cloth with moisture breath and odor control properties using atmospheric-pressure plasma-graft polymerization. *Proc. of 2nd Asia Aerosol Conf.*, Pusan, Korea, July 1–4, 361–362 (2001).

250. M. Okubo, T. Yamamoto, T. Kuroki, J. Mine, N. Saeki, and S. Kataoka, Odor control and moisture breath of functional cloth prepared by plasma-graft polymerization. *J. Institute of Electrostat. Jpn.* **25**(6), 328–329 (2001).

251. S. Sakuhana, *Fundamentals and Applications for Glass Surface*. Uchida Rokaku-Ho Publ., Tokyo, (in Japanese), 103–107 (1985).

252. T. Yamamoto, A. Yoshizaki, T. Kuroki, and M. Okubo, Aluminum surface treatment using plasma-assisted dry chemical process. *Proc. of ESA-IEEE Joint Meeting on Electrostatics*, 846–857 (2003).

253. T. Kuroki, T. Yamamoto, and M. Okubo, Surface treated metal, its manufacturing method and equipment. Japanese patent pending, no. 2003-173519, June 18, 2003.

254. T. Karube and R. Haku, Cr^{+6} free surface treatment technology. *Surf. Technol.* (in Japanese), **53**(6), 368–371 (2002).

255. S. Wolf and R. N. Tauber eds., Silicon processing for the VLSI. Era. Vol. 1 *Process Technology*. Sunset Beach, CA: Lattice, 1986.

256. I. Jacob and N. Israelachvili, *Intermolecular and Surface Forces*, Academic Press Ltd (1992).

257. T. Okamoto and K. Inoue, *Corrosion and Protection*. Dainippon Tosho Publ., (in Japanese), 150 (1987).

258. J. M. Kogoma, The characteristics of atmospheric pressure non-equilibrium plasma processing. *Surf. Technol.* **51** (2), 21 (2000).

259. H. F. Webster and J. P. Wrightman, Effects of oxygen and ammonia plasma treatment on polyphenylene sulfide thin films and their interaction with epoxy adhesive. *J. Adhesion Sci. Technol.* **5**(1), 93–106 (1991).

260. H. P. Godard, Oxide film growth over five years on some aluminum sheet alloys in air of varying humidity at room temperature. *J. Electrochem. Soc.* **114**(4), 354–356 (1967).

5

Thermal Distillation and Electrodialysis Technologies for Desalination

J. Paul Chen, Lawrence K. Wang, and Lei Yang

1. INTRODUCTION

Water is one of the scarce resources in the world. Naturally occurring freshwater sources are rainwater, surface water, and groundwater. After conventional treatment, most of the water can be directly used for various purposes. The demand for water to serve the world continues to increase; however, freshwater supplies are finite, it is becoming more difficult to develop them on a renewable basis. In addition, water pollution is becoming increasingly serious as a result of which water sources are greatly affected.

Water has a great impact on the economic development of all countries. It is estimated that one-fifth of the world's population does not have access to safe drinking water. Water is particularly important in an arid region such as the Middle East, where water is not only an economic issue, but also a key political issue (1). The scarcity of water and the high cost of its development have long been globally recognized. Water for direct human use could become more important than oil in the near future.

In many countries, as water shortages have already been exploited and full utilization is reached, searching for water sources has become extremely important. The available solutions include: reclamation of used water, recycle of used water, optimization of water usage, and desalination.

About 97% of the water in the world is salty as its chief sources are sea and brackish areas. Less than 1% of the world's water sources are considered potable. Desalination is a term used to describe the process involved in the removal of dissolved mineral salts,

organic substances, bacteria and viruses, and solids from seawater to obtain freshwater. The major function of the process is to essentially remove salt content or salinity of water. The salinity of water source is measured in terms of the "total dissolved solids" (TDS), which is commonly reported in milligrams per liter (mg/L). Freshwater normally has less than 1000 mg/L TDS. The raw water for desalination can be seawater from the ocean or from shallow beach wells, brackish water (surface or aquifer), wastewater, and even waters produced by oilfields. Water can be classified into four categories based on the salt content in it. They are:

- Recycled water with less than 1500 mg/L TDS.
- Slightly saline water with 1000–3000 mg/L TDS.
- Moderately saline water with 3000–10,000 mg/L TDS.
- Highly saline water with over 10,000 mg/L TDS.

Brackish water normally refers to water with salinities between 1000 and 10,000 mg/L TDS. The salinity of seawater is in the order of 35,000 mg/L TDS. The US Environmental Protection Agency (US EPA) and the World Health Organization (WHO) established a TDS guideline of 500 and 1000 mg/L, respectively, for drinking water. In addition, silt density index (SDI) is another important parameter. SDI is a measure of the amount of 0.45-μm filter plugging that is caused by passing a sample of water through the filter for 15 min. It must be determined for water that is considered for reverse osmosis (RO) and electrodialysis (ED)/electrodialysis reversal (EDR) treatments. SDI is also used for evaluation of product water.

Total world capacity is approaching 30 million m³/d of potable water, in some 15,000 plants. Half of these are in the Middle East, where water resource is extremely limited, whereas energy (oil) is widely available. Approximately 25% is located in Saudi Arabia. More than two-thirds of the world's desalting capacity is located in the arid, oil-rich areas of North Africa and Western Asia, or the Middle East (3). Figure 1 illustrates the distribution of desalination capacity in the world. About 10% of Israel's water is desalinated. In the United Kingdom, 150,000 m³/d RO plant is proposed for the lower Thames estuary, utilizing brackish water. Around 800 desalination plants are operated in the United States, producing fresh water with a capacity of 225 MGD (approx 1.4% of total water consumption). Most of them are in Florida, California, and Texas.

The general process of producing useable water from the water with high salt content is illustrated in Fig. 2. The desalination technologies are normally developed for treating large quantities of water (e.g., 100–1000 MGD) at a central location. However, some have been recently adapted for small-scale water supply at home.

Modern desalination practices are broadly categorized into distillation or membrane processes. The distillation process involves phase changes and usually utilizes thermal energy and mechanical energy. It includes the multistage flash (MSF) distillation, the multieffect distillation (MED or ME), and vapor compression (VC). The membrane process involves no phase changes and the separation is mainly carried out using semipermeable membranes. This requires mechanical or electric energy. The commonly used techniques are RO and ED (EDR).

About 70% of the world's desalination capacity is dependent on the distilling process. However, in the United States, the distribution is different; RO and ED (EDR)
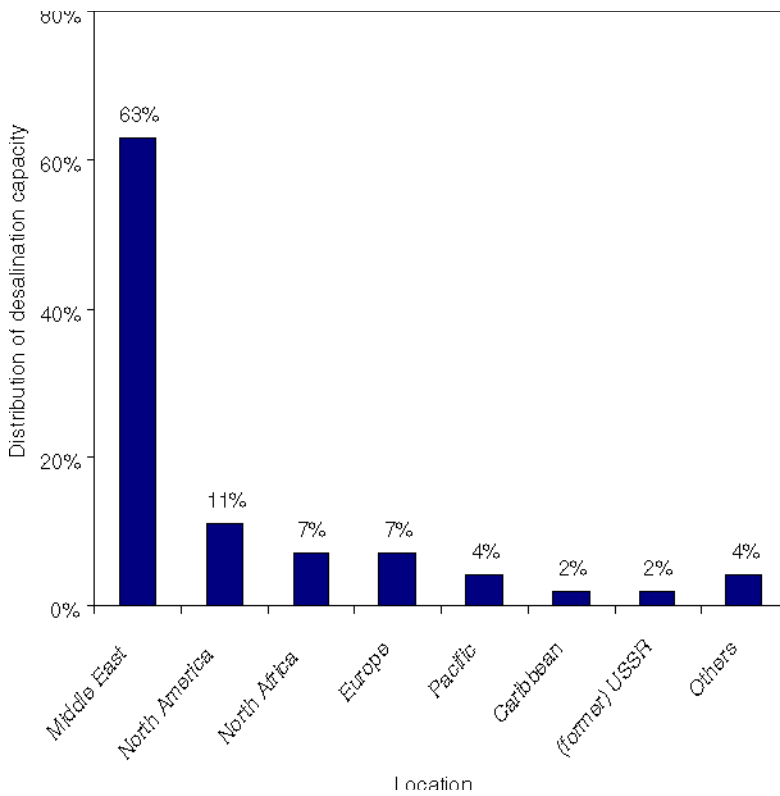
Fig. 1. Distribution of desalination capacity in the world.
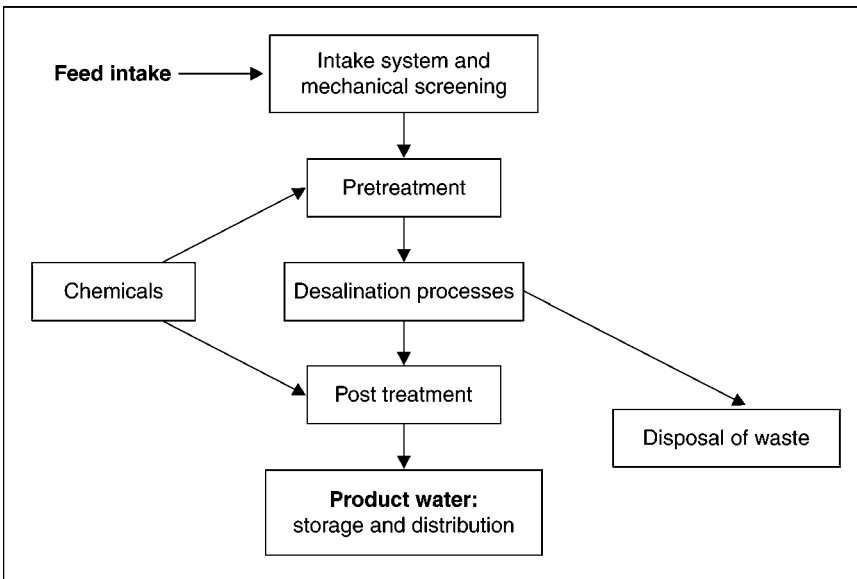
Fig. 2. General process for production of freshwater by desalination processes.

Table 1
Comparison of Major Desalination Technologies

Item	MSF	MED	ED/EDR	RO
Preferred water source	Seawater—brine	Seawater—brine	Brackish	Any
Final product salinity	5 mg/L < TDS < 50 mg/L	5 mg/L < TDS < 50 mg/L	TDS < 500 mg/L	TDS < 500 mg/L
Land usage	Large area	Large area	Small area	Small area
Capital costs	High	High	Medium	Medium
Operating temperature	High (~100°C)	Moderate (~70°C)	Not applicable	Not applicable
Energy cost	High	High	Moderate	Moderate
Feed-to-product ratio	7–12:1	6–10:1	1.2–2:1	2–2.5:1
Pretreatment	Not required	Not required	Required	Required
Influent requirement	Not required	Not required	SDI < 12	SDI < 4
Quality of water produced	Pure	Pure	TDS of 350–500 mg/L	TDS of 20–50 mg/L
Susceptibility to scaling	Low	Low	Low	High
Bacterial contamination	Unlikely	Unlikely	Post-treatment needed	Possible
Waste	High salt content and corrosive	High salt content and corrosive	High salt content	Low salt content

occupy around 80% of the market. The freshwater production capacity normally follows the descending sequence of MSF > RO > ED (EDR) > MED > VC. Table 1 gives the key factors for the different desalination operations. Other processes, like freezing and membrane distillation are seldom used. Of the aforementioned five main desalination technologies, MSF, MED, and VC thermal processes are generally used in the following applications:

- To treat highly saline waters (predominantly seawater).
- Where large volumes of product water are required.
- In locations where energy costs are low or where a waste heat source is available.

Membrane processes of RO and ED (EDR), on the other hand, are more favorable for treating brackish waters (under most conditions) or highly saline wastes for which energy costs are high or the flow rates are low.

In addition to the thermal and membrane processes, ion exchange (IX), freezing, and membrane distillation can be used for removal of salt in the water. IX is presented in another chapter of this handbook series. In the freezing process, saline water is frozen to form ice crystals under controlled conditions. Before the water is completely frozen, the mixture is usually rinsed to remove the salts in the remaining water or those adhering to the ice crystals. The ice is then melted to produce freshwater. Lower energy requirement, lower potential for corrosion, and lesser scaling or precipitation problems are the advantages; however, the disadvantage is the difficulty in operations (e.g., handling huge ice crystals). Membrane distillation process combines the use of distillation and membranes (4,5). Saline water is warmed to enhance vapor production, and this vapor is exposed to a membrane that can pass water vapor but not liquid water. After the vapor passes through the membrane, it is condensed on a cooler surface to produce freshwater. In its liquid form, freshwater cannot pass back through the membrane; hence it is trapped and collected as the output of the plant. The advantages lie in its simplicity and the need for only small temperature differentials for its operation. However, when the process is run with low temperature differentials, large amounts of water must be used, which affects its overall energy efficiency. A recent development is adopting solar-powered membrane distillation technology for production of pure water from brackish water (5). Solar energy is collected for the operation of membrane distillation system.

Before the raw water enters the aforementioned treatment systems, it is normally pretreated by various technologies, such as filtration, chemical coagulation, softening, and pH adjustment. Selection of these technologies is dependent upon the water quality of the influent and the desalination process that is to be applied.

The cost of desalting saline water ranges from USD 0.4 to 2.2/m^3 of product water, which depends on the quality of the raw water and the technologies applied. Table 2 shows a comparison of capital and operational costs of desalination processes. The membrane technologies are cost-effective for low salinity sources (brackish water), whereas distillation-based technologies make sense only for higher salinity courses, such as seawater. The RO process can be regarded as the optimum choice for desalination of low-salinity water, regardless of plant capacity. The optimum choice for desalination of higher salinity feed depends on the required capacity. The MSF process would be the technology of choice for capacities more than 25,000 m^3/d; whereas the MED

Table 2
Capital and Operational Costs of Desalination Processes

Nature of technologies	Technologies	Capital cost (USD/m³/d)	Operational cost (USD/m³)
Thermal technologies	MSF	1200–3000	0.7–1.5 (with waste heat)
	MED	1000–3900	0.4–0.8 (with waste heat)
	VC	1000–1300	0.5–1.2
Membrane technologies	RO	500–1200 (brackish water)	1000–2500 (seawater)
		0.2–1.2 (brackish water)	0.2–1.7 (seawater)
	ED (EDR)	400–2500	0.6–2.1

process should be chosen for capacities in the order of 10,000 m³/d. VC is good for capacities in the order of 3000 m³/d (6). When a desalination plant with a larger capacity is built, the capital cost per unit of product water is lower. The daily operational cost, however, is not significantly affected by the size of the plant. It is advisable to build a larger plant instead of several smaller plants. Cost analysis must be conducted even before design is initiated. Computer models such as ARIMA model can be used (7).

The cost for treating sea and brackish water by RO decreased by almost 50% from 1980 to 2005, because the cost of membrane materials had dropped and prevention technologies of membrane fouling were well developed. For example, desalination of seawater costs approx USD 1.5/m³ production water in 1980, whereas the figure dropped to USD 0.8 in 2005. Over the last 50 yr, the cost of freshwater production by MSF has decreased by an average of 44% per decade (8).

Large-scale desalination projects are extremely expensive and often require some degree of public financing. To build 25-MGD plant it costs 70–100 million USD. Thus, it becomes more common that contractual arrangements of selling/purchasing water between governments and suppliers are made. The suppliers build and operate the plant. "Build, own, operate, and transfer" and "build, operate, and transfer" are two typical arrangements. The first one becomes more popular in developing countries, such as China.

Factors influencing selection of desalination technologies are many. The applicability of desalination is very site specific. Site-specific conditions will also determine the type of desalination technology selected (9). Financial issue is the first one to be solved. Both capital investment and cost of daily operations are essential. As desalination requires high-energy input, energy requirement is an important issue. Selection of desalination process is highly dependent on source water characteristics; the quality and the quantity of product water rely on them. Desalination plants should be close to the raw water source (e.g., sea) to obtain a steady flow of raw water and be able to discharge its byproducts easily. Limited land space can be a major concern in selection of desalination process. Desalination plants are usually big and their accommodation could be the main cost factor that needs to be considered. The plants that are built must have a large capacity in order to provide substantial amounts of water. Environmental factors and waste disposal options are also important. The wastewater with high salt content is
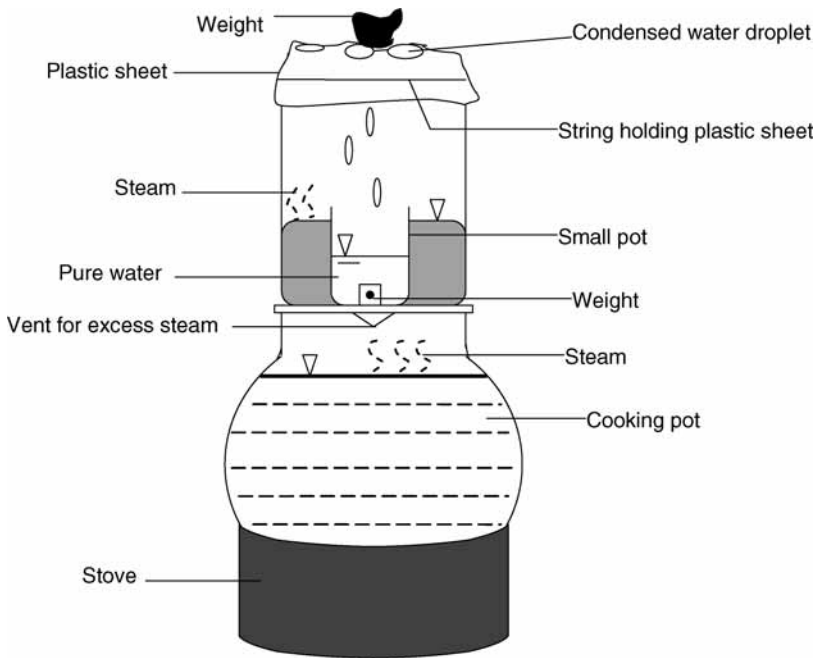
Fig. 3. Illustration of simple distillation for desalination.

produced. Handling the environmental problems is a great challenge and principles of pollution prevention can be implemented. Finally, operational and maintenance (O&M) issues must be considered. Training of operators is highly recommended.

Laws and regulations of federal, state, and local agencies play important roles in the design and operation of desalination projects. "Water Desalination Act of 1996," "Pollution Prevention Act of 1990," and "Clean Water Act of 2002" regulate the projects at the federal level. In addition, government policies have a great impact on costs of desalination.

In this chapter, the thermal distillation and ED (EDR) technologies for desalination are presented and the working mechanisms of the same are illustrated. RO process is also briefly presented. A comparison of these desalination technologies is given. Other important issues, such as pre- and post-treatment processes, energy, and environmental aspects are discussed.

2. THERMAL DISTILLATION

2.1. Introduction

Distillation is a thermal process. It is the oldest and most commonly used method of desalination. A simple distillation process for desalination is illustrated in Fig. 3. The world's first desalination plant operated in the mode of a multiple-effect distillation with a capacity of 60 m³/d. This was installed on Curaçao, Netherlands Antilles, in 1928. Further, commercial development of the seawater distillation units took place in the late 1950s (10). Distillation relies on the technology developed for industrial evaporation operation. The MSF, MED, and VC processes have successfully led to the widespread use of distillation to desalinate seawater.

The product water recoveries by distillation range from 15 to 45%, depending on the operation. The water is nearly mineral-free, with very low TDS content. TDS of less than 25 mg/L is quite common and it normally ranges from 5 to 50 mg/L. However, this water must have been subjected to proper posttreatment, as it is too corrosive to meet the corrosivity standards. The water can be stabilized by chemical treatment or by blending with other potable water.

2.2. Working Mechanisms

Distillation is a phase separation method. The saline water is heated to produce water vapor, which is then condensed to produce freshwater (e.g., Fig. 3). The distillation processes are generally operated on the principle of reducing the vapor pressure of water within the unit to permit boiling to occur at lower temperatures, without the use of additional heat. Distillation units routinely use designs that conserve as much thermal energy as possible by interchanging the heat of condensation and heat of vaporization within the units. The major energy requirement in the distillation process is to provide the heat for vaporization to the saline feed.

The "distillation process" used for the desalination can be analyzed as the "evaporation," which is commonly adopted for concentration of substances in chemical and biochemical industries (11). The basic equation for solving for the capacity of an evaporator can be written as:

$$q = U \times A \times \Delta T = U \times A \times (T_s - T_L) \tag{1}$$

where q (W) is the rate of heat transfer, U (W/m^2 K) is the overall heat-transfer coefficient, A (m^2) is the heat-transfer area, ΔT (K) is the difference in temperature between the condensing steam (T_s,K) and the boiling liquid (T_L,K) in the evaporator.

The evaporation process can be determined by heat and material balance as shown in Fig. 4. The feed to the evaporator F (kg/h) has a solid content of X_F (mass fraction), temperature (T_F, K), and enthalpy (h_F, kJ/kg). The concentrated liquid leaving the evaporator (L, kg/h) has a solid content of X_L (mass fraction), temperature of T_L (K), and enthalpy of h_L. The vapor (V, kg/h) is given off as pure solvent having a solid content of $Y_V = 0$, temperature of T_V (K), and enthalpy of H_V. The vapor (V) is in equilibrium with the liquid (L) and both have the same temperature, or $T_V = T_L$. The pressure (P_1) is the saturation vapor pressure of the liquid of composition (X_L) at its boiling point (T_L).

During the operation, a saturated steam (S, kg/h) must be added to the evaporator to provide heat to the feed solution. The steam has a temperature of T_s (K) and an enthalpy of H_s. The condensed steam leaving the system (S, kg/h) has a temperature of T_s (K) and an enthalpy of h_s. The steam gives off its latent heat (λ) as follows:

$$\lambda = H_s - h_s \tag{2}$$

The latent heat of steam at the saturation temperature (T_s) can be obtained from the steam tables. As the system is operated at steady state, the rate of mass coming to the evaporator is equal to that leaving the evaporator. Thus,

$$F = L + V \tag{3}$$

The mass balance on the solute (solids) is:
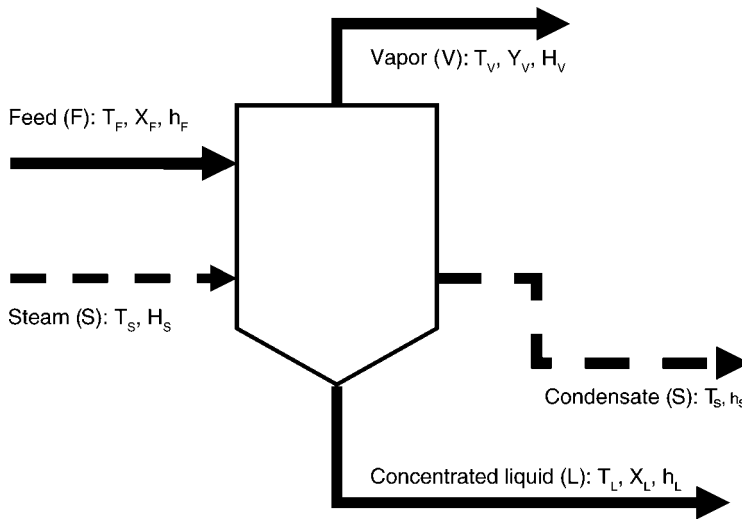
Fig. 4. Heat and mass balance for single-effect evaporator.

$$F\,(X_F) = L\,(X_L) \tag{4}$$

In the heat balance, the total heat entering the system is equal to the total heat leaving the system. Assuming that there is no heat lost by radiation or concentration.

Heat in feed + heat in steam = heat in concentrated liquid + heat in vapor
+ heat in condensed steam (5)

$$F \times h_F + S \times H_s = L \times h_L + V \times H_v + S \times h_s \tag{6}$$

Substituting Eq. (2) into Eq. (6) yields:

$$F \times h_F + S \times \lambda = L \times h_L + V \times H_v \tag{7}$$

The heat q transferred to the evaporator can be determined by:

$$q = S \times (H_s - h_s) = S \times \lambda \tag{8}$$

Example

A continuous evaporator is used for treatment of a salt solution that has a flow rate of 9000 kg/h, 1% of salt, and a temperature of 37.8°C or 310.8K. The concentrated liquid that leaves the evaporator has 1.5% of salt. The vapor space of the evaporator is at 1 atm, whereas the steam supplied is at 1.414 atm. The overall coefficient is 1700 W/m$^{2\cdot}$ K. Determine the amounts of vapor and liquid leaving the system, the amount of steam added, and the rate of heat transfer.

Solution
According to the given conditions, $F = 9000$ kg/h, $X_F = 1\%$, and $X_L = 1.5\%$. Thus,
$F = L + V$, $9000 = L + V$, $F \times X_F = L \times X_L$, $9000 \times 0.01 = L \times 0.015$.
On solving these equations, $L = 6000$ kg/h and $V = 3000$ kg/h.
The operation produces freshwater of 3000 kg/h (after condenser).

The boiling point of the solution in the evaporator is assumed to be that of water at 1 atm and 100°C (i.e., T_L = 373.2 K). The heat capacity of the feed is assumed to be that of water (c_{pF} = 4.14 kJ/kg K). H_v of water at 100°C is 2257 kJ/kg. The latent heat of steam at 1.414 atm is 2230 kJ/kg. The saturation temperature [T_s] is 110°C. The enthalpy of feed is: $h_F = c_{pF} \times (T_F - T_L)$, $h_L = 0$.

From Eq. (7), $9000 \times 4.14 \times (310.8 - 373.2) + S \times 2230 = 6000 \times 0 + 3000 \times 2257$. S = 4076 kg/h steam.

The rate of heat transfer (q) can be determined by:

$q = S \times \lambda = 4076 \times 2230 \times 1000/3600 = 2.52 \times 10^6$ W.

2.3. Multistage Flash Distillation

MSF distillation is currently the most common and simple technique that is in use. Since 1950s, it has been commercially used. The largest MSF plant, also the world's largest desalination plant, is the Al Jubail plant in Saudi Arabia. It was completed in 1985 and has a capacity of 208 MGD.

MSF is essentially a method whereby seawater is spontaneously boiled through a series of chambers, at progressively lower pressures. Figure 5 demonstrates this process. When the atmospheric pressure is lowered, the seawater will boil at a lower boiling temperature. As such, this will hasten the process of obtaining pure water. The water vapor given off is condensed into pure water at each chamber. The remaining seawater that is not evaporated is then moved on to the next chamber at a lower pressure. The sample process is subsequently repeated until the seawater leaves all the chambers.

A large amount of flashing brine is normally required in the MSF operation (10). As a result, 50–75% of the brine from the last stage is often mixed with the incoming feed, recirculated through the heat recovery sections of the brine heater, and flashed again through all of the subsequent stages. This "brine recycle" operation can reduce the amount of water-conditioning chemicals that must be added, which can significantly affect operational costs. It can increase the salinity of the brine at the product end of the operation, raise the boiling point, and increase the danger of corrosion and scaling in the plant. In order to maintain a proper brine density in the system, a portion of the concentrated brine from the last stage is discharged to the ocean.

MSF is energy-intensive and the cost of energy often constitutes a large portion of its water costs. An MSF plant also requires a large space area owing to its numerous chambers. The condenser tubes of the majority of the operating units are made of Cu–Ni alloys (12). The corrosion of the alloys usually leads to tube failure and hence checking of the tubes is important during maintenance. Protective measures should also be adopted.

2.4. Multieffect Distillation

MED is actually a modification of the MSF process. Figure 6 demonstrates an MED process. Like MSF, seawater is heated into vapor and subsequently condensed to produce freshwater. The main difference lies in the arrangements of its chambers or pipes. MED usually operates on horizontal or vertical pipes. The steam is condensed on one side of the tube wall, whereas the saline water is evaporated on the other side. This is similar to the VC process.
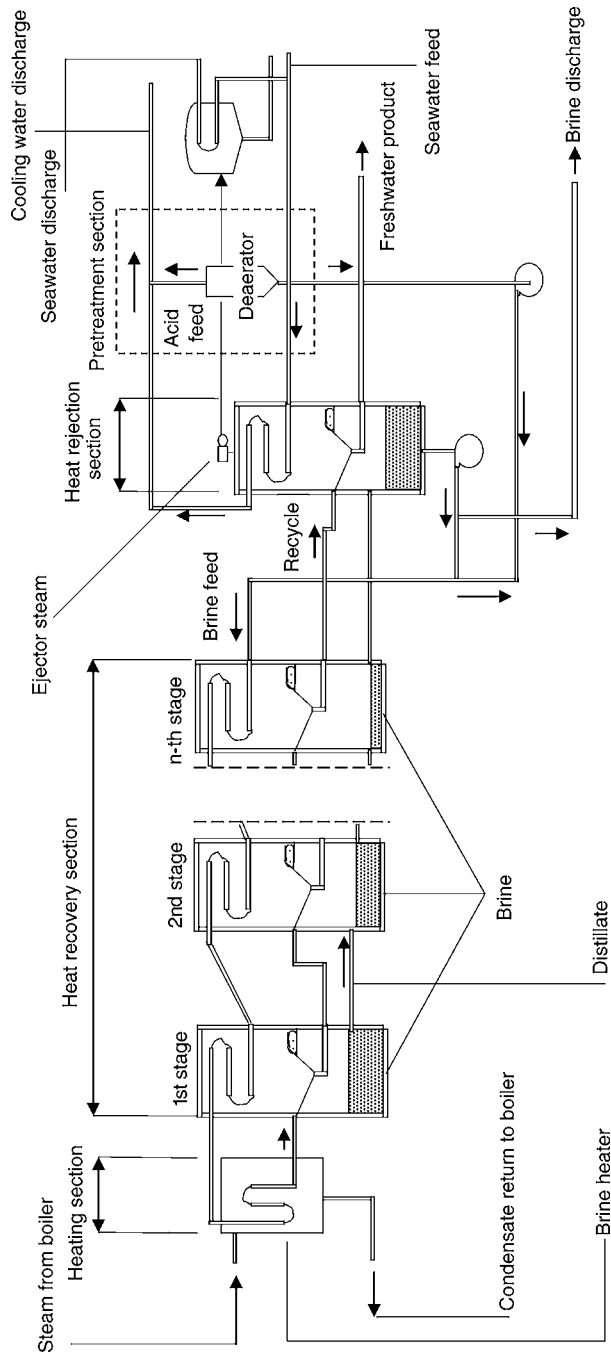
Fig. 5. Schematic of a multistage-flash distillation process.

305
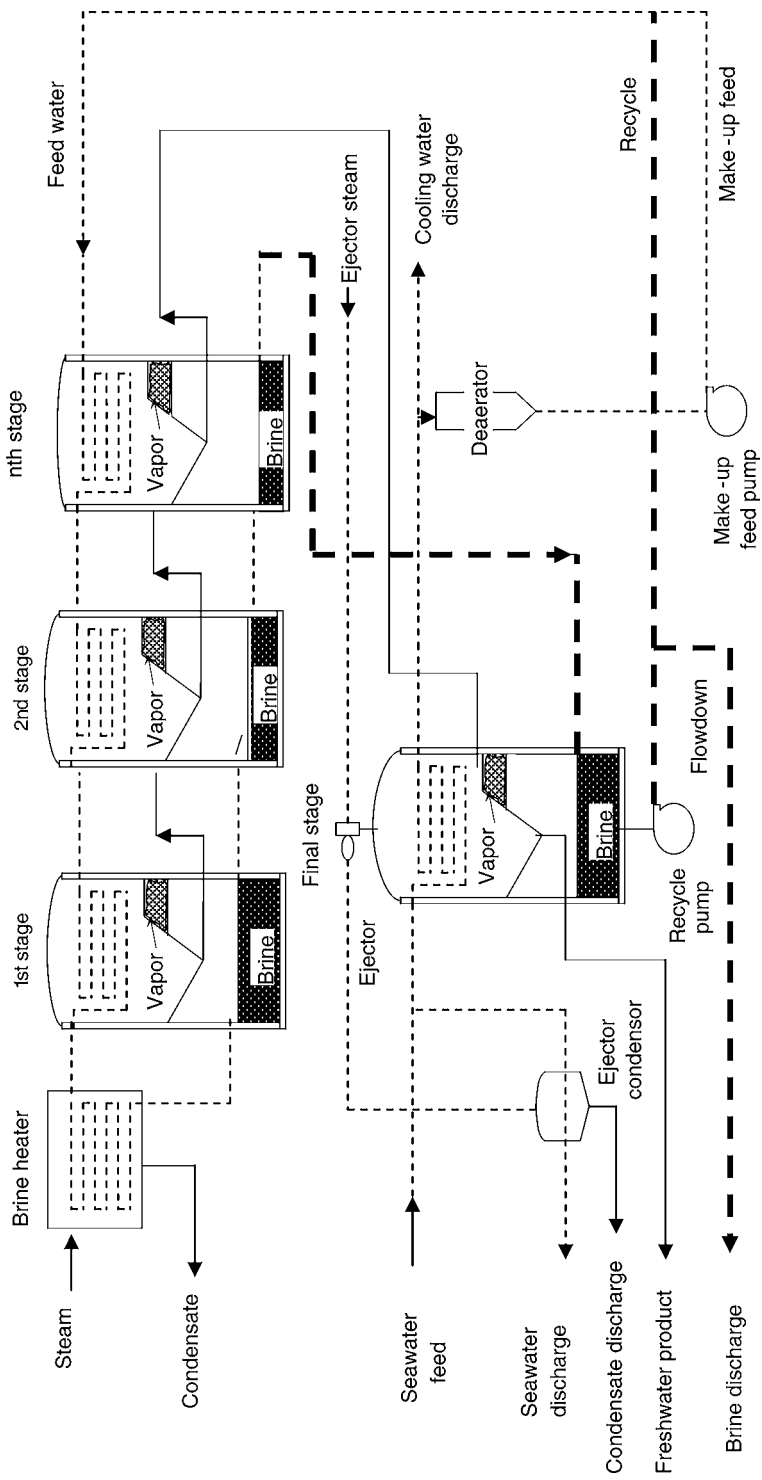
Fig. 6. Schematic of a multieffect distillation process.

306

In the MED operation, some of the feed water is flash-evaporated, but most of the sea-water is dispersed over an evaporator tube bundle and boiled. Steam then condenses to produce freshwater and this process is continuously repeated. As the evaporation takes place in a vacuum, the sprayed seawater is able to reach boiling point even at low temperatures. As MED uses a progression of stages with ever-dwindling temperatures (60–70°C), it is comparatively smaller than MSF in terms of output. Unlike the MSF technique where water is produced by turning heat into latent heat of evaporation, the MED technique uses latent heat to produce secondary latent heat in each chamber. This use of double condensing–evaporation heat transfer mechanisms is highly efficient and energy saving.

MED was developed earlier than MSF; however, it has not been extensively utilized for water production. A new type of low-temperature, horizontal-tube MED process has been successfully developed and used in the Caribbean. These plants appear to be very rugged, easy to operate, and economical, as they can be made of aluminum or other low-cost materials (10). The cost for O&M of MED is slightly higher than RO.

2.5. Vapor Compression

VC process uses mechanical energy rather than direct heat as a source of thermal energy. Figures 7 and 8 demonstrate the VC process. Water vapor is drawn from the evaporation chamber by a compressor. Except in the first stage, the vapor is condensed on the outside of the tubes in the same chambers. The heat of condensation is used to evaporate a film of saline water applied to the inside of the tubes within the evaporation chambers. VC normally has a low fresh water production capacity, i.e., <100 m^3/d, and is used at resorts and industrial sites (10).

2.6. Solar Desalination

Solar energy is always available and thus can be used to desalinate saltwater. Its usage can be classified into two types: (a) direct usage: solar distillation and (b) indirect usage: energy from the sun rays used to operate desalination processes.

Solar desalination is the simplest survival technique that is used to collect small quantities of drinkable water. It does not require any additional energy to run the operation. As shown in Fig. 9, a hole is dug in the ground, a sheet of plastic is placed on the floor, and a cup is placed at the bottom of the hole. Seawater is then added into the hole. A plastic sheet is covered on the hole and a small stone is placed in the center. Seawater evaporates from the hole and condenses on the underside of the plastic sheet and collects in the cup. This system can temporarily solve the shortage for drinking water in remote areas.

Solar energy can be used to evaporate water from saltwater for household or small community water supplies by building sealed units covered by glass as shown in Fig. 10. The water production rate ranges from 7 to 18 kg/m^2/d (13). The temperature of water from the outlets of the collectors increase from 70°C at 9.00 AM to 95°C at 1.00 PM, then decrease to 65°C at 4.00 PM (14). The quality of water before and after the solar desalination is given in Table 3. As shown, the product water is free of any impurities. This water, however, cannot be used as potable water. Mineral substances must be added.

Growth of algae on the underside of the units is normally observed. Effective sealing of the units and regular checking and clearing can efficiently control this problem.
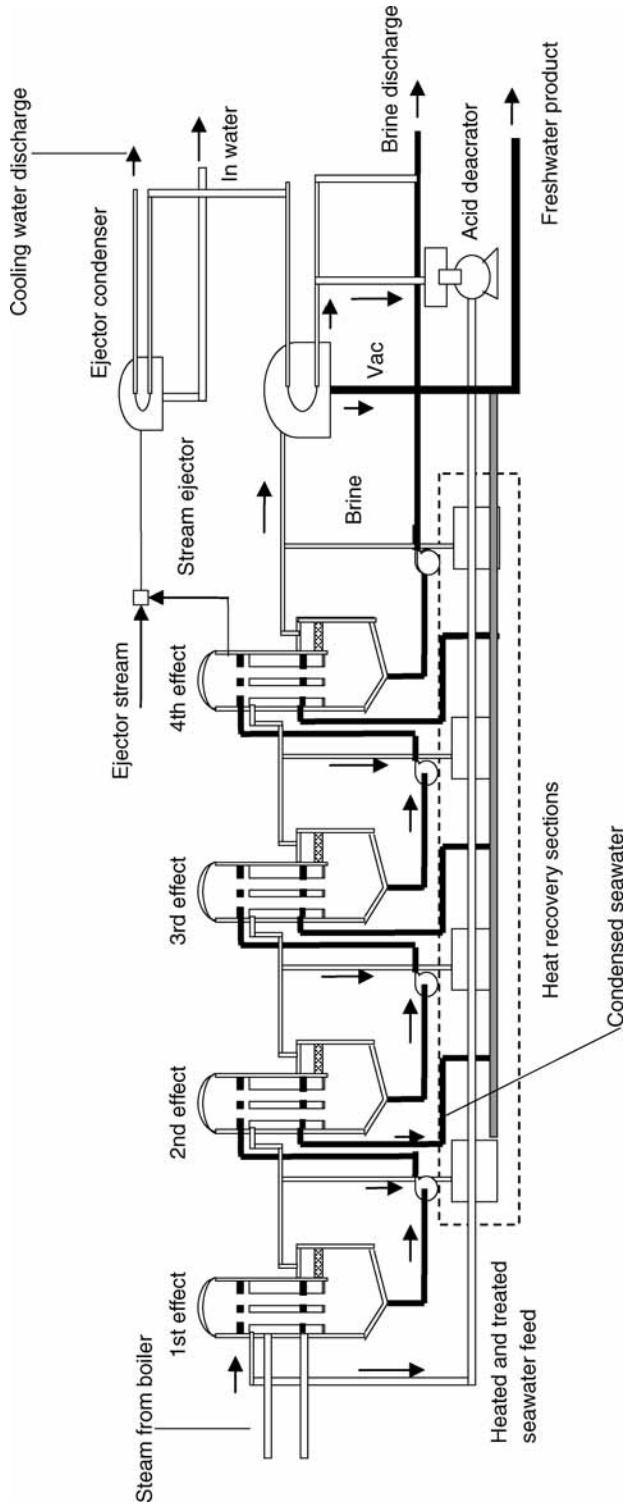
Fig. 7. Schematic of a vapor compression process.
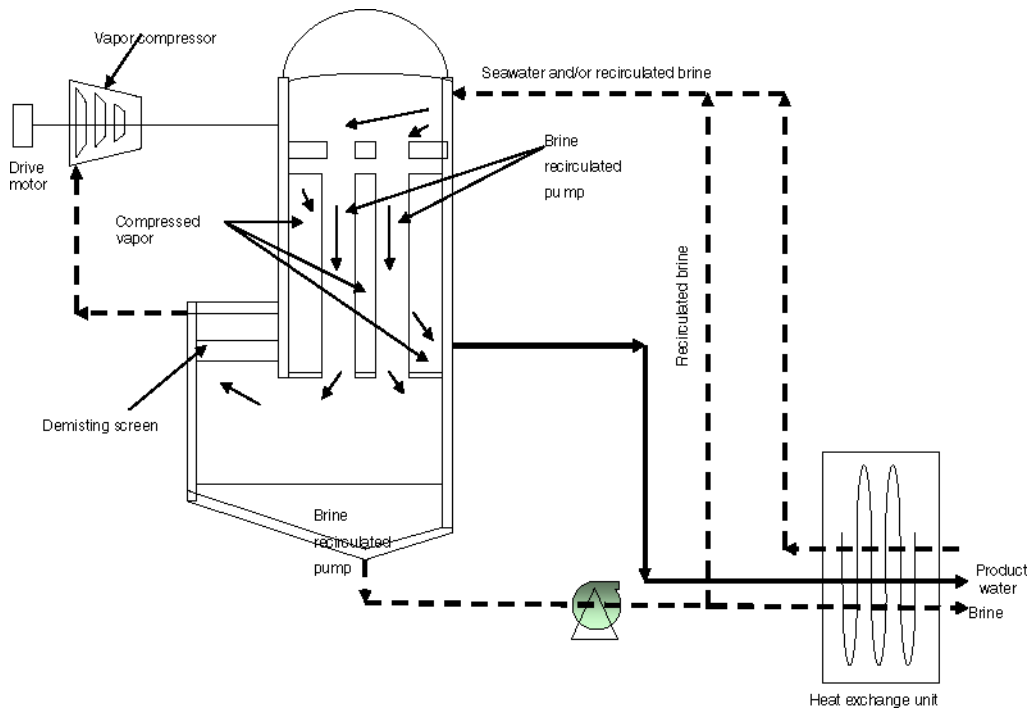
Fig. 8. Schematic of a single-stage vapor compression process.
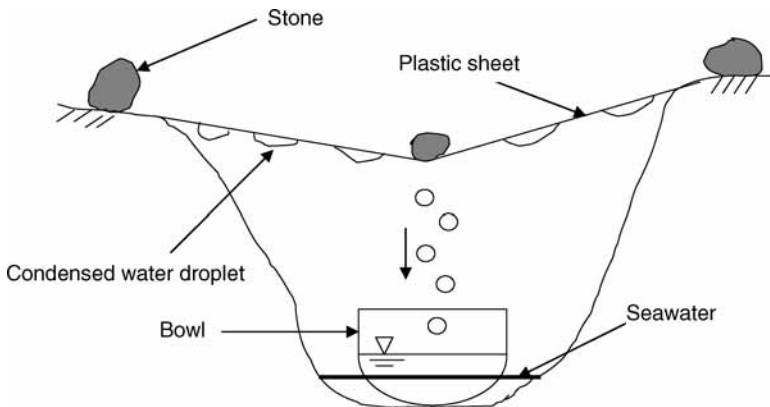
Fig. 9. Schematic of the simplest solar distillation for desalination.

Small-scale solar stills are operated by families or small villages in many parts of the world. Solar-powered desalination plants are used in isolated parts of the world on a small scale, but the high capital cost, fragility, and complexity of operation have discouraged extensive use.

Figure 11 illustrates the Rosendahl System for desalination. This system was developed by Wilfried Rosendahl of Germany in the 1980s. The energy from sunlight increases the temperatures in the distillation collector to 80–90°C. About 50% of the raw
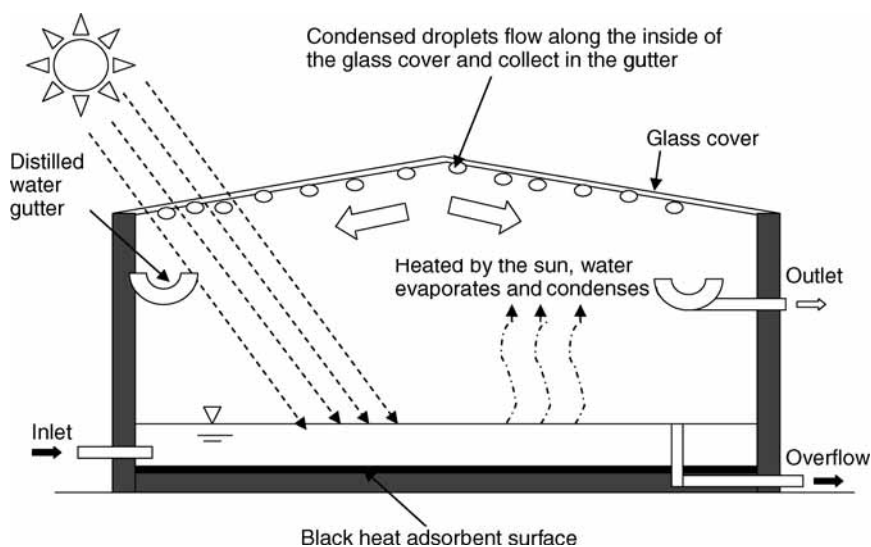
Fig. 10. Schematic of solar desalination.

Table 3
Comparison of Water Quality in a Single-Stage Solar Desalination System

Parameter	Quality in desalinated water[a]	Quality in seawater[a]	US EPA/WHO standard
Conductivity	50 μS/cm	49,000	–/–
pH	6.8	8	6.5–8.0/–
Calcium	4 mg/L	411 mg/L	–/–
Magnesium	1 mg/L	1290 mg/L	–
Sodium	5 mg/L	10,760 mg/L	–/200 mg/L
Potassium	1 mg/L	400 mg/L	–/–
Bicarbonate	12 mg/L	142 mg/L	–/–
Carbonate	0 mg/L	370 mg/L	–/–
Sulfate	0 mg/L	2710 mg/L	250 mg/L/250 mg/L
Chloride	11 mg/L	19,350 mg/L	250 mg/L/250 mg/L
Nitrate	2 mg/L	120 mg/L	–/–
Total dissolved solids	30 mg/L	35,000 mg/L	500 mg/L/1000 mg/L
Total hardness	15 mg/L as $CaCO_3$	4300 mg/L as $CaCO_3$	–/–
Total alkalinity	10 mg/L as $CaCO_3$	2150 mg/L as $CaCO_3$	–/–
Dissolved oxygen	7.6 mg/L	13 mg/L	–/–

[a]Adapted from ref. 14.

water evaporates and condenses under the cool glass cover, which subsequently flows into a condensation channel and is channeled to the reservoir. The remaining untreated water (i.e., waste) that has a high salt content is collected and sent out for final disposal. As the system is exposed to sunlight, the ultraviolet can cause a certain degree of disinfection of freshwater. Its effect can be enhanced in the high temperature in the system.
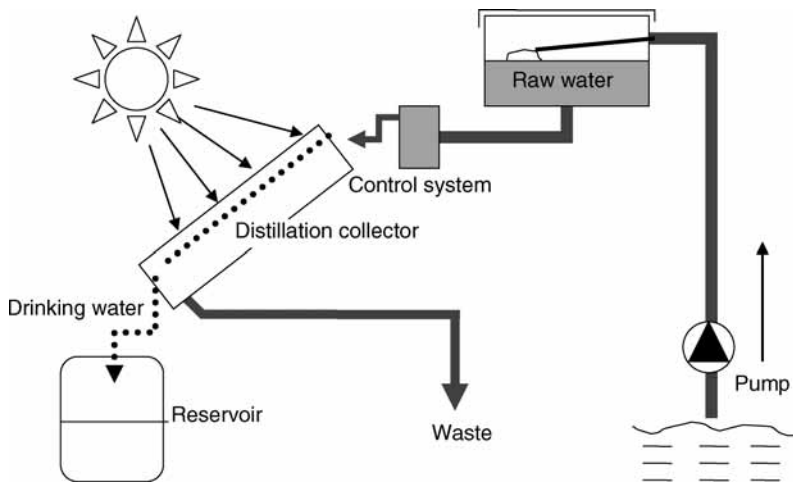
Fig. 11. Rosendahl system for desalination.

A water production rate of >2–7 L/d/m^2 of still area can be achieved on a day (15). Water production varies at different time periods. Normally, it reaches its maximum at 1.00 PM– 3.00 PM. More water production is achieved when the water depth is 0.1–0.15 m (16).

In indirect usage, a solar collector is used to concentrate solar energy to produce high temperature in the thermal desalination process. The electrical energy, which is used to operate desalination processes, such as RO or ED can also be produced by sunlight.

2.7. Important Issues in Design (O&M)

When a distillation plant for desalination is designed and operated, all the flowering issues must be taken into consideration.

2.7.1. Thermal Discharge

A common problem resulting from the desalination operations is thermal discharge of liquids. Older high-temperature facilities produce brine at very high temperatures. Cooling towers, heat exchangers, or similar equipments must be considered in the design and construction so that the waste heat from the facilities can properly be handled and the water pollution is minimized. For the newly built distillation systems, the thermal discharge is not a major concern because the brine water with high temperatures is cooled by the raw feed water.

2.7.2. Materials of Construction

The corrosive nature of high-temperature brines, acid pretreatments, and chemical scaling can cause plant failure. Presently, the only acceptable construction material for wetted surfaces in high-temperature systems is an austenitic stainless steel. Anodized aluminum and many thermoplastic materials are acceptable for use in low-temperature systems.

2.7.3. Energy for Operation

Operation of distillation is mainly energy-driven. The crude oil prices have been increased by almost 100% in the last 2 yr. It is therefore important to consider the energy cost for operations and a sound forecast of the same is essential.

2.7.4. Characteristics of Raw Water

The important parameters of raw water are TDS, salt contents, organic contents (TOC), and temperature. The availability of raw water is also important.

2.7.5. Final Disposal of Waste Brine

The waste brine has high temperatures and TDS. Thus, it must be properly treated before it is discharged to the nearby waters. Cooling and IX are recommended for its treatment.

3. ELECTRODIALYSIS

3.1. Introduction

ED was commercially introduced in the early 1960s, about 10 yr before the introduction of RO. The development of ED provides a cost-effective technology to remove salt from seawater. ED is also used in water and wastewater treatment, food processing, and chemical and pharmaceutics manufacturing.

In ED, ionic components are removed from aqueous solutions through the IX membranes using the driving force of an electric field. The membrane is selective and semipermeable and it only allows the passage of either the anions or the cations. The separation is because of the nature of the charged substances rather than the differences in their sizes. In seawater desalination, the dissolution of salt leads to the formation of positively charged cations, such as Na^+, Ca^{2+} and Mg^{2+} and negatively charged anions, such as Cl^-. The cations and the anions are attracted to the anode and the cathode, respectively, which are subsequently removed. As a result, the water after treatment carries less ionic substances. A typical ED plant operates at 50–90% conversion and this conversion value is determined by the brine recirculation rate. An ED system can operate over a wide pH range (pH 1.0–13.0) as well as a wide temperature range (up to 43°C). The cost for O&M of ED (EDR) is slightly higher than RO.

The drawback of this process is that the surfaces of membranes can be easily fouled. Thus, a modified process of EDR was developed. By intermittently reversing the polarity, the membranes' surfaces can be cleaned. Standard EDR operates for 15 min on each polarity. Electrodeionization (EDI) is a modification of conventional ED systems with IX resins installed in the ED stacks. The resins reduce the electrical resistance of the unit and the direct current potential splits water into hydrogen and hydroxyl ions that continuously regenerate a portion of the IX resins. EDI is particularly suited for the production of ultrapure water.

3.2. Mechanisms

The working mechanism of ED is demonstrated in Fig. 12. The IX membranes are arranged alternately with an anion-selective membrane followed by a cation-selective membrane. A cell is a space that is bounded by the two different membranes; it is arranged as anion exchange membrane, space, and cation exchange membrane. A unit cell or cell pair is made up of two cells. The ion-depleted cell is used for the passage of freshwater (the freshwater channel or desalted water channel), whereas the ion-concentrated cell is used for the passage of brine (the brine channel). The cells alternate between the freshwater channel and the brine channel. Each cell is connected by
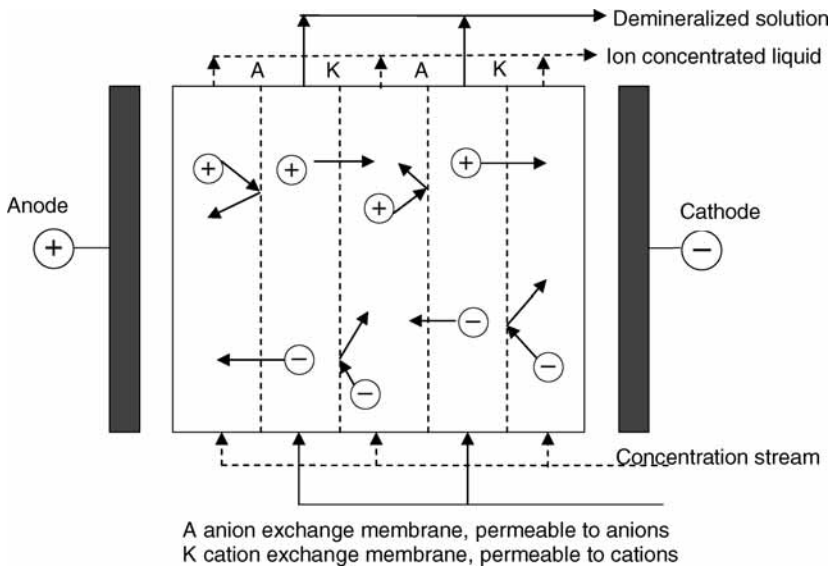
Fig. 12. Demonstration of mechanism of electrodialysis process.

its own feed/product stream and brine stream. The unit cells and electrodes are arranged horizontally or vertically and the entire unit is called a stack. An ED system requires huge amounts of direct current (DC); a rectifier is usually used to transform the alternating current (AC) to DC.

The feed solution containing both positive and negative ions enters in a parallel path through all the cells, where an electric potential is maintained across the electrodes. This causes the ions to migrate to their respective electrodes. The positively charged cations in the solution will move toward the cathode and the negatively charged anions will move toward the anode. Cations can pass through the negatively charged cation exchange membrane but are retained by the positively charged anion exchange membrane. Similarly, anions pass through the positively charged anion exchange membrane but are retained by the negatively charged cation exchange membrane.

In the freshwater channel, the anions are attracted and diverted toward the cathode, whereas the cations are attracted and diverted toward the anode in a direction opposite to the movement of anions. The cations pass through the cation-selective membrane into the brine channel and are trapped in the brine channel as the next membrane is anion-selective. Likewise, the anions pass through the anion-selective membrane into the brine channel but cannot pass through the next membrane because it is a cation-selective membrane. Consequently, the freshwater channel is depleted of both cations and anions through migration across the membranes, whereas the brine channel next to the freshwater channel becomes enriched with cations and anions. In other words, the alternating channels contain streams of dilute ion concentration and streams rich in ion concentration.

The quality of freshwater is dependent on the following factors: (a) wastewater temperature, (b) amount of electrical current passed, (c) type and amount of ions, (d) permselectivity of the membrane, (e) fouling and scaling potential of the wastewater, (f) wastewater flow rates, and (g) number and configuration of stages.
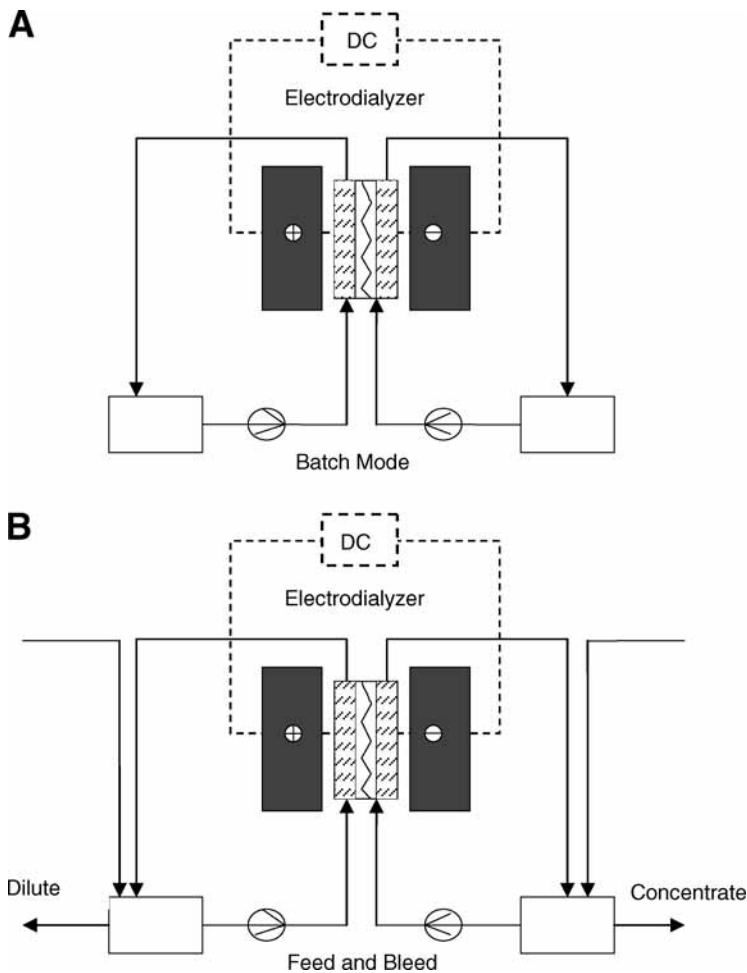
Fig. 13. Operation of electrodialysis process: **(A)** batch mode; **(B)** continuous mode.

3.3. Important Issues in Design

ED process may be operated in either a continuous or a batch mode as shown in Fig. 13. The units can be arranged either in parallel or in series in order to achieve the desired degree of demineralization.

A typical ED plant is made up of the following components: a pretreatment system for the feed, membrane stack, power supply (AC–DC), process control unit, solution pumping system, and post-treatment system.

3.3.1. Pretreatment System

Pretreatment is usually required to remove the large particles in the water before applying ED. The presence of suspended solids, microorganism, organic ions, and metal oxides can cause serious problems during operations as they can damage the membranes and alter their chemical properties.

Particles that do not carry an electrical charge are not removed. Suspended solids with a diameter that exceeds 10 mm need to be removed, or else they will plug the membrane

pores. Large organic anions, colloids, iron oxides, and manganese oxides can neutralize the membrane, which disturb the selective effect of the membrane. The type and complexity of the pretreatment depends on the nature of the feed water to be treated. Pretreatment methods for these impurities are active carbon filtration (for organic matter), flocculation (for colloids), and filtration techniques. It has been demonstrated that filtration helps to remove the large, charged organic molecules and colloids such as humic acid because these molecules are too large to be removed through the membranes during ED.

The growth of microorganisms is another type of problem as it can cause fouling of the membrane. Chlorine should be used for disinfection to kill them so that they cannot grow on the membrane. However, chlorine must be removed from the feed water before it enters the ED stack as chlorine can cause damage to the membranes. Sodium meta-hexaphosphate can be added to prevent fouling of the membrane surface by precipitation of sparingly soluble salts such as calcium sulfate.

After pretreatment, the feed water can be pumped through the ED stack, which usually contains more than 100 membrane cell pairs each with a membrane area of 1–2 m^2.

3.3.2. Membrane Stack

In a membrane stack, spacer gaskets separate the membranes sheets. A simple cell pair is made up of two membranes and two spacer gaskets. The spacers are turbulence-promoting support mesh used to create the channels through which the solutions flow. The holes in the spacer gaskets are aligned with the holes in the membrane sheets to form the manifold channels that distribute the feed to the proper channels and remove the product and brine streams.

The distance between the membranes (i.e., the cell thickness) needs to be as small as possible in order to minimize the electrical resistance and save energy consumption. The spacer maintains the shape of the membranes, controls the solution flow distribution in the stack, and reduces the film thickness on the membrane which in turn limits the effects of concentration polarization. It is important to have a uniform flow distribution in the manifold channels to prevent internal leakage, particularly from the ion-concentrating cell to the ion-depleting cell. The feed water (wastewater) is usually retained for about 10–20 d in a single stack or stage. Both sheet flow and tortuous path designs are used in ED.

In the sheet flow design, the solution flows in a relatively straight line from the entrance to the exit ports, which are located on opposite sides. Therefore, the supply ducts for the dilute and brine must be in line with the holes in the spacer gaskets, the membranes, and the electrode cell. An array of membranes is held between the electrodes and the process streams are kept separated. If the length-to-width ratio of the spacer is large enough, the entrance and exit ports can be located at the corners.

In the tortuous path design, a spacer gasket creates a labyrinthine flow and extends the path length within the cell. The solution takes several 180° turns between the entrance and exit ports located in the middle of the spacer. The main objective is to provide a long residence time for the solution in the cell despite the requirement of high linear velocity to limit the polarization effect. A tortuous path spacer gasket is shown next.

The end plate of the stack is a hard and plastic frame that contains the electrode compartment. The anode is made of stainless steel and the cathode is made of platinum-coated

tantalum, niobium, or titanium. The whole set-up is compressed together with bolts between the two end flow plates. The perimeter gaskets of the gasket spacers are tightly pressed into the membranes to form the cells.

The membranes of ED units are subject to fouling and scaling, and thus some pretreatment of the feed water is usually necessary. Precipitation of scale can be facilitated in the ED process by changes in pH that occur near the membranes as a result of the transport of H^+ and OH^- ions. However, as there is no flux of water through the membranes, ED can treat water with a higher level of suspended solids than RO. As nonionic solids, e.g., silica, are not concentrated by this process, these components are of less concern. Thus, inorganic acids such as H_2SO_4 can be fed to the concentrate stream to maintain a low pH and thus minimize scaling and fouling.

3.3.3. Ion-Exchange Membrane

In the ion-exchange membranes, the charged groups are attached to the polymer backbone of the membrane material. A cationic membrane with fixed negative groups will exclude the anions but is permeable to the cations. Similarly, an anionic membrane with fixed positive groups will exclude the cations but is permeable to anions. Cation-selective membranes consist of sulfonated polystyrene, whereas anion-selective membranes consist of polystyrene with quaternary ammonia. There are two types of IX membranes: homogeneous and heterogeneous membranes.

3.3.3.1. HOMOGENEOUS MEMBRANE

Charged groups are uniformly distributed through the membrane matrix. The cation-selective membranes are often made up of crosslinked polystyrene (with divinyl benzene) that has been sulfonated to produce sulfonate that is attached to the polymer. The anion-selective membranes are made of crosslinked polystyrene containing quaternary ammonium groups.

3.3.3.2. HETEROGENEOUS MEMBRANE

The IX groups are contained in small domains distributed throughout an inert support matrix that provides the mechanical support. The simplest form has very finely powdered cation or anion exchange particles uniformly dispersed in polypropylene. A much finer heterogeneous dispersion of IX can be made from polyvinylchloride plastisol.

3.3.4. Solution Pumping System

The low-pressure pump helps to circulate the feed water through the stack. The pump must have enough power to overcome the resistance of water because it passes through narrow passages. The energy required for the solution pumping system increases as the average salt concentration of the feed decreases. This can be significant when the feed concentration drops to a very low value. The pressure drop per stack varies from 15 to 30 psi for flow cells and 7 to 90 psi for tortuous cells. Depending on the extent of separation required, the water is pumped through 2–4 cells in a series. Therefore, interstage pumps may be required.

3.3.5. Posttreatment

Posttreatment includes stabilizing the water and preparing it for distribution. Removal of unwanted gases such as hydrogen sulfide and adjustment of the pH are normally
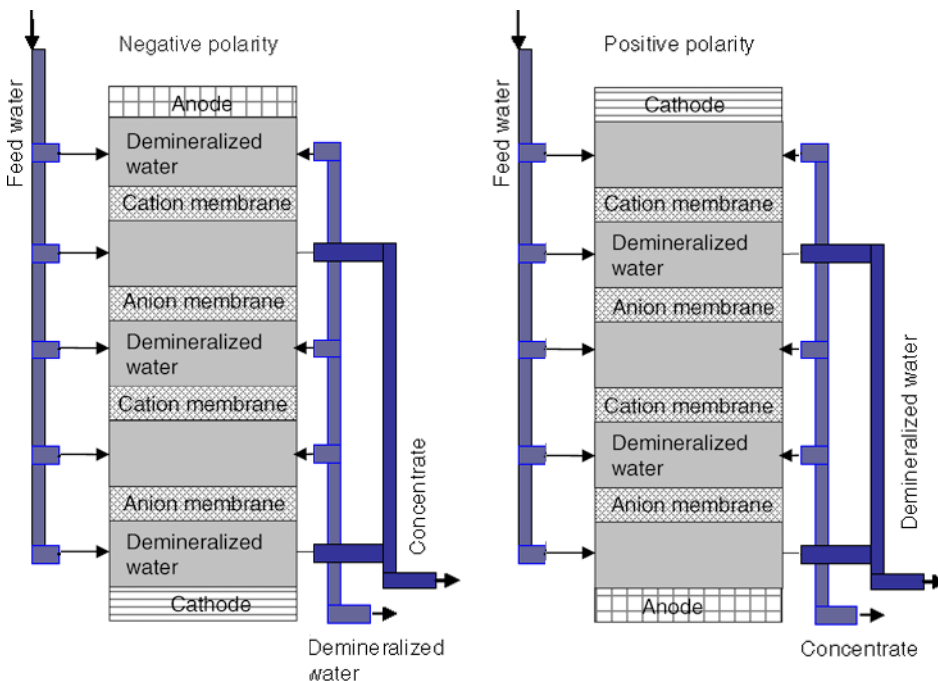
Fig. 14. Demonstration of electrodialysis reversal process.

conducted. If the salt content in the water is still too high, other processes such as IX and RO can be used.

3.4. Electrodialysis Reversal

As the membranes used in ED easily become fouled, efforts have been made to overcome the problem. EDR process was developed to help eliminate membrane fouling. In the early 1970s, an American company commercially introduced the EDR process for ED. EDR is a continuous self-cleaning ED process (17,18).

EDR was developed with ED technology as the basis. In the EDR process, the membrane polarity is reversed several times an hour as shown in Fig. 14. The brine stream becomes the product water stream and vice versa. As a result, the ions are now attracted in the reverse direction across the membrane stack. Immediately following the reversal of polarity and flow, the product water is dumped until the stack and lines are flushed out, and the desired water quality is restored. This flush takes about 1 or 2 min, and then the unit can resume producing water. The reversal process is useful in breaking up and flushing out scales, slimes, and other deposits in the cells before they can buildup and create a problem. Flushing allows the unit to operate with fewer pretreatment chemicals and minimizes membrane fouling. The EDR systems operate with higher concentrations in the brine or concentrate the streams with less flow to waste (19).

The major advantage of EDR is its ability for cleaning colloidal particulates that are formed on the membrane during the operation the mechanism of which is better explained by Fig. 15. The particulates interact with water to form an effective negative charge at the surface of their bound water layer. The DC applied to ED stacks is a driving
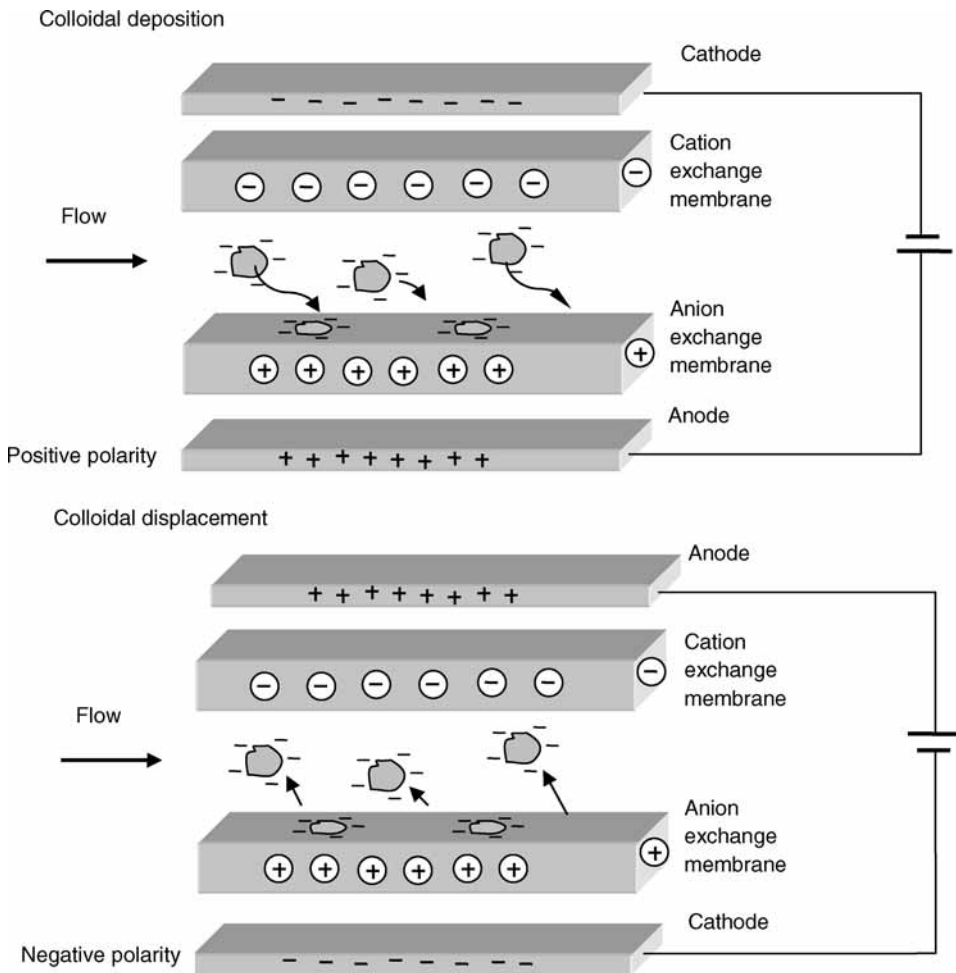
Fig. 15. Deposition and displacement of colloidal particulates during electrodialysis reversal operation.

force that moves the negatively charged colloids toward the anion exchange membrane (20). When the particles reach the membrane surface, the electric field and electrostatic attraction to the IX sites at the membrane surface tend to hold the deposit in place. The periodic DC power polarity reversal in an EDR system reverses the driving force for this deposition and tends to remove the deposit.

The EDR systems offer the following benefits:

- Automatic cleaning cycle every 10–20 min reduces scales, fouling, and slimes.
- Freshwater production is high.
- The systems can be either land-based or mobile.
- The membrane life of the EDR systems ranges between 5 and 10 yr.
- The EDR membrane stacks can easily be cleaned.
- The systems are less sensitive than RO to particulates and metal oxides.
- The systems do not have silica limitation.
- The systems are stable and perform continuously.
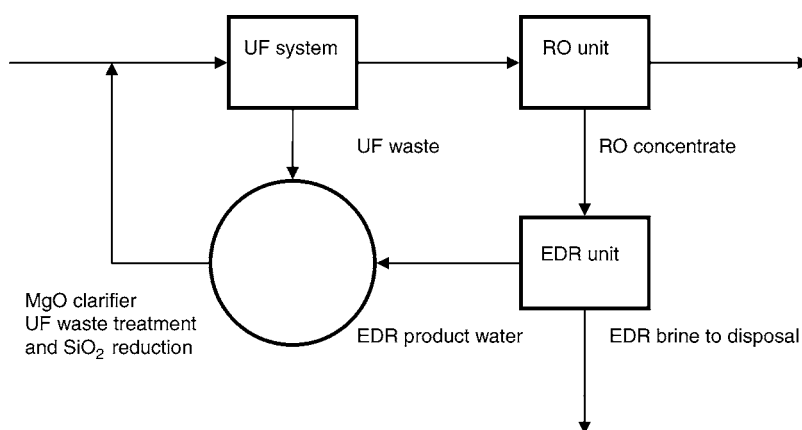
Fig. 16. Combination of UF, reverse osmosis, and electrodialysis reversal for desalination.

• The systems can be operated with effective residuals of chlorine, chloramines, and chlorine dioxide to prevent biological fouling.
• Average free chlorine residuals up to 0.5 mg/L and chloramine (total chlorine) residuals up to 1 mg/L have no effect on membrane life.

The EDR system has a wide flow capacity ranging from 500 gal/d up to 1.6 million gal/d. By using multiple stages (stacks in series), systems are designed to handle a wide range of treatment needs. It is able to reduce TDS with an efficiency of 50–95%.

The major advantage of EDR over RO is that it is not necessary to feed chemicals at remote water treatment sites in the Middle East. EDR and RO compete with one another on many desalting projects. EDR offers advantages over RO on some applications. It can be applied to reclaim the RO concentrate of approx 8000 mg/L TDS. The combined RO–EDR system in Fig. 16 can yield up to 96% of recovery (18). EDR is not affected by as many feed water constituents as RO. The EDR can take raw water with turbidity of up to 2 nephlometric turbidity unit (NTU), whereas the RO cannot function well if the turbidity is above 1 NTU. The oil and grease (O&G) of raw water to EDR is up to 1 mg/L, whereas the raw water to RO must be O&G-free.

Particles and microorganisms are not removed by EDR (also ED). Hence, post-treatment of the product water becomes necessary. Filtration and disinfection by chlorination can be used. Remineralization of product water is seldom required. However, when recalcification is deemed desirable, it is suggested that calcium carbonate be added.

3.5. Electrodeionization

EDI theory and practice have been advanced by a large number of researchers throughout the world. EDI process was first described in a publication by a group of scientists at Argonne Labs in early 1955 as a method for removal of trace radioactive materials from water (21). EDI technology was first fully commercialized in early 1987 by a division of Millipore that is now part of US Filter Corporation (22). Several thousand commercial EDI devices are now manufactured by a number of companies, such as Ionpure, Ionics, GE, and Electropure for the production of high-purity water at capacities ranging from <0.1 to >250 m³/h.
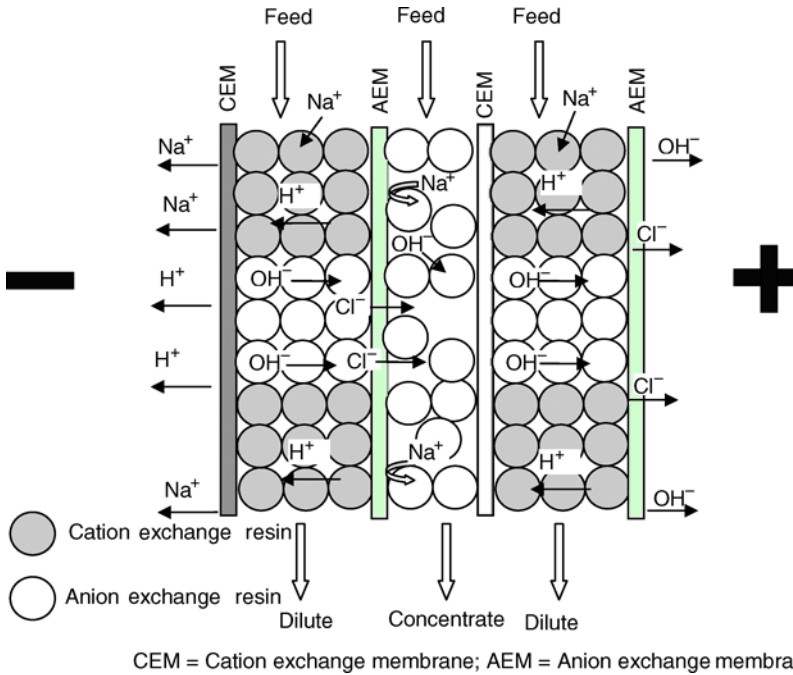
Fig. 17. Schematic of electrodeionization for ultrapure water production.

EDI process is a continuous process, which has very high water recovery. The reject stream of the EDI is usually of better quality than the feed to the RO system, which can be completely reused by pumping it back to the pre-treatment section of the RO system. RO/EDI systems may achieve overall water recoveries of greater than 90%. The electrical requirements are nominal. When 1 kWh of electricity is used to deionize 1000 gal of raw water, the conductivity can typically be reduced from 50 μm MΩ/cm in the feed to 10 MΩ/cm in the product water. As the EDI concentrate (or reject) stream contains only the feed water contaminants at 5–20 times higher concentration, it can usually be discharged without treatment, or used for another process. The process is particularly good for production of ultrapure water.

The operation mechanism of EDI is shown in Fig. 17. The process uses a combination of ion-selective membranes and IX resins sandwiched between two electrodes (anode [+] and cathode [−]) under a DC voltage potential to remove ions from pretreated water. Compartment sets are called cell pairs and form the basic element in a module. Ion-selective membranes operate using the same principle and materials as IX resins. Anion-selective membranes are permeable to anions but not to cations, whereas cation-selective membranes are permeable to cations but not to anions. The membranes are not water-permeable. Two complete EDI processes are given in Fig. 18.

By spacing alternating layers of anion-selective and cation-selective membranes within a plate-and-frame module, a "stack" of parallel purifying and concentrating compartments are created. The "stack" of cell pairs is positioned between the two electrodes, which provide the DC potential to the module. Under the influence of the applied DC voltage potential, some of the ions across the respective membranes are captured by
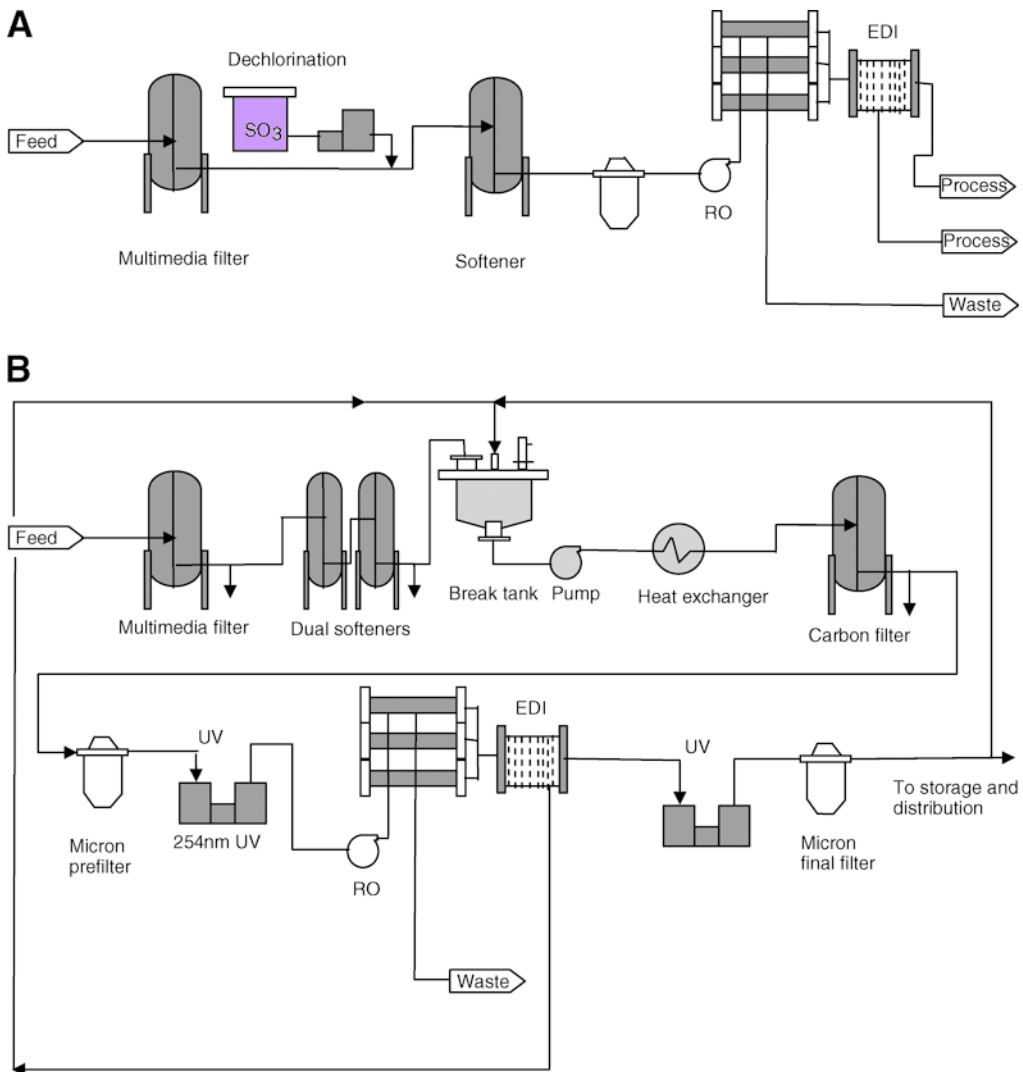
Fig. 18. Production of ultrapure water by electrodeionization (EDI) process: **(A)** pretreatment-single-pass reverse osmosis/EDI; **(B)** USP purified water system with EDI.

the IX resins. The remaining ions are transported across the membranes and migrated into the concentrating chambers. As a result, the salt content in the dilute compartments is very low (free of ions in most operations). The resins in the devices are continuously regenerated by the electric current; therefore, they do not become exhausted. This continuous electroregeneration enables continuous EDI systems to produce pure water without chemical regeneration.

4. REVERSE OSMOSIS

RO is one of the most important desalination processes. It is estimated that more than USD 10 billion will be spent for construction of RO plants over the next 5 yr and over
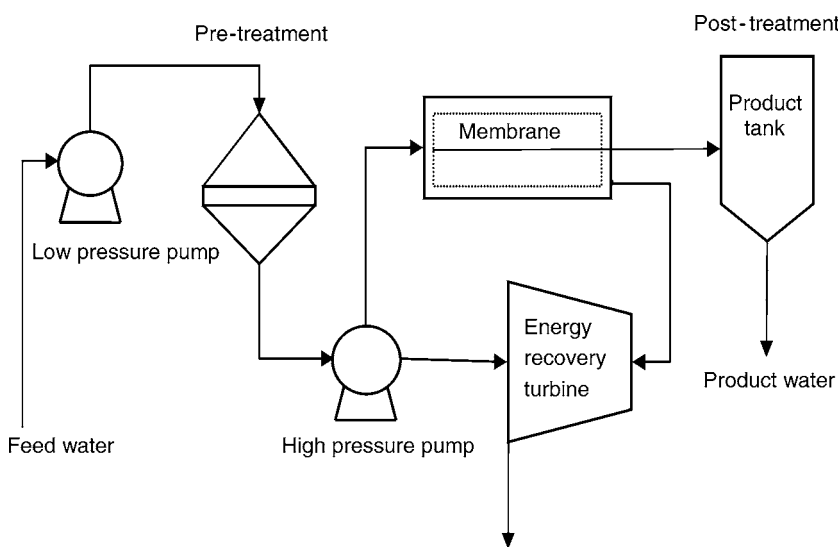
Fig. 19. Schematic presentation of a reverse osmosis desalination plant.

USD 70 billion over the next 20 yr. RO becomes a popular choice as the price of membranes has decreased significantly since 1980. For example, the relative cost of spiral-wound membranes has declined by more than 60% in the past 25 yr (23).

In RO, saltwater on one side of a semipermeable membrane is subjected to high pressure (24). Pure water diffuses through the membrane, leaving behind a more salty concentrate containing most of the dissolved organic and inorganic contaminants. The pressure ranges from 15 to 25 bar for brackish water and from 55 to 85 bar for seawater. Two of the most commercially successful RO configurations are spiral-wound and hollow fiber. Brackish water RO plants can typically recover 50–80% of the feed water, with 90–98% of salt rejection. For seawater, recovery rates vary from 20 to 40%, with 90–98% of salt rejection. The feed must have undergone pretreatment so that the solid and organic contents are below a certain level. The pretreatment usually consists of chemical coagulation, filtration (fine filtration, ultrafiltration or microfiltration), scaling control (e.g., softening), and acidification for regulating pH. Post-treatment of production water is needed for its distribution, which includes disinfection, removing gases (e.g., H_2S), and pH balancing. Interesting readers can refer to the literature (25–32) for details. A complete RO system is shown in Fig. 19.

5. ENERGY

In desalination, energy must be applied to drive the operations. The energy can be in the form of heat, pressure, and electricity. Its sources can be many, such as sunlight. Desalination is very energy-intensive as illustrated in Fig. 20 (8). RO needs about 6 kWh of electricity per cubic meter of water, whereas MSF and MED require heat at 70–130°C (25–200 kWh/m^3). A variety of low-temperature heat sources may be used, including solar energy. The choice of the process generally depends on the relative economic values of freshwater and the particular energy source (e.g., fuel).
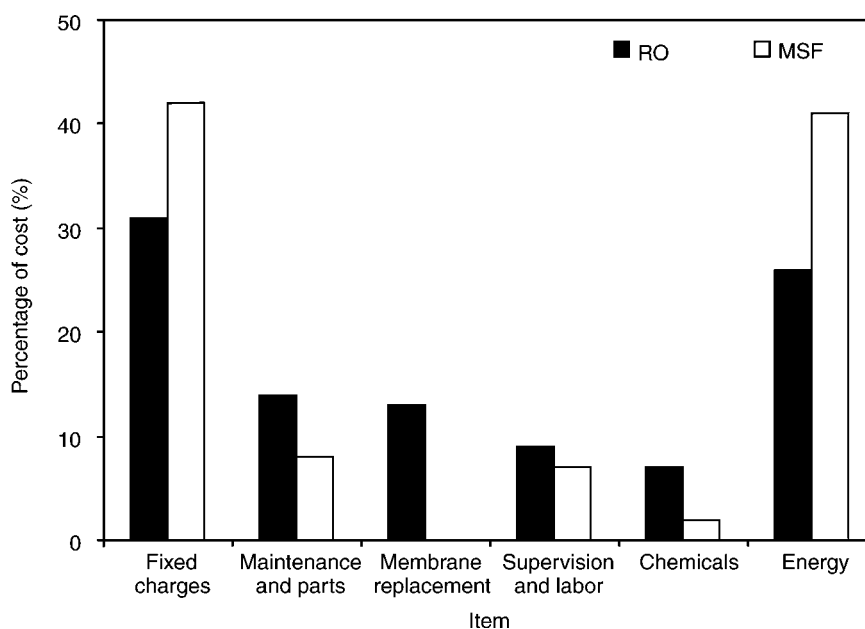
Fig. 20. Cost composition for representative reverse osmosis and multistage flash seawater desalination plants.

Traditionally, fossil fuels have been used for most desalination, which contributes to increased levels of greenhouse gases. The crude oil price has been dramatically increased in the last 2 yr. Thus, alternative energy sources must be sought.

Nuclear energy is becoming an important energy source as it is more cost-effective (2), clean, and efficient. Nuclear energy is already being used for desalination, and has the potential for much greater use.

Small- and medium-sized nuclear reactors are suitable for desalination, often with cogeneration of electricity using low-pressure steam from the turbine and hot seawater feed from the final cooling system. The main opportunities for nuclear plants have been identified as the 80–100,000 m^3/d and 200–500,000 m^3/d ranges.

Large-scale deployment of nuclear desalination on a commercial basis will depend primarily on economic factors. The United Nation's International Atomic Energy Agency has been fostering research and collaboration on the issue, and more than 20 countries are involved.

Instead of using the energy produced by nuclear reactions, the waste heat produced by the nuclear reactors can be directly used for running desalination operations. The reactors can be designed to couple with desalination systems. It can be expected to enable further cost reductions of nuclear desalination. Safety and reliability are of course the key requirements. There are many successful cases.

In Japan, some 10 desalination facilities linked to pressurized water reactors operating for electricity production have yielded 1000–3000 m^3/d each of potable water. An MSF was initially employed, but an MED and an RO have been found to be more efficient. India has been engaged in desalination research since the 1970s and is about to set up a demonstration plant coupled to few nuclear power reactors at the Madras

Table 4
List of Disposal Alternatives for Water Pollution in DWTP

Technology	Brief description
Ocean disposal	Ocean disposal is typically done several miles offshore with diffusers. Dilution by seawater can reduce the contents of the waste. The treatment plant outfall location may be affected by water quality rules and regulation
Discharge to sewer and surface waters	Sewer discharge is simplest; however, it depends on the ability of the wastewater treatment plant to accept high salinity discharge. Surface water discharge involves discharge to a point of outfall such as tidal lake or brackish canal. Dilution by surface waters can reduce the contents of wastes. The location of the discharge and the pretreatment requirement are determined by state and regulatory agencies; water quality testing (e.g., bioassay toxicity) is required
Land application	Irrigation is sometimes used for the waste streams with relatively lower salinity. Saline tolerant vegetation and habitat are required. This is usually determined by site-specific soil and drainage characteristics
Evaporation pond	Desalting concentrate is discharged to ponds and evaporated to dryness for final disposal. It is land-intensive and requires relatively dry climates. Dry salt is the final waste product, which must be characterized and disposed off accordingly as solid waste. This is generally applicable only in arid environments and then usually in an inland location
Deep well injection	In deep well injection, the waste streams are injected to the ground and are permanently stored in the injection zone. It is very commonly used by the DWTP
Zero-discharge and industrial reuse	Zero-discharge of wastes can be achieved by thermal processes, which greatly reduce or eliminate the waste stream. The thermal processes are energy-intensive and very costly. Wastes must be characterized and disposed off accordingly. Marketable salts for generally industrial uses can be recovered. This is still in the development stages, but past attempts indicate that recovery of marketable byproducts is economically difficult

Atomic Power Station, Kalpakkam. This project will be a hybrid RO/MSF plant; RO and MSF produce freshwater of 1800 and 4500 m^3/d, respectively. The plant will deliver water of 45,000 m^3/d by both kinds of desalination technologies. China is looking at the feasibility of a nuclear seawater desalination plant in the Yantai area producing 160,000 m^3/d by an MED process.

6. ENVIRONMENTAL ASPECT OF DESALINATION

Absolute environmental impacts of desalination plants and the respective processes are largely unknown owing to limited public attentions (8,25). One impediment to the growing demand for desalting technologies is the environmental pollution that every

desalination water treatment plant (DWTP) must face. Most environmental concerns that are raised relate to saltwater, air, and noise emissions.

Air emissions are a result of the desalination industry's heavy energy consumption and involve the commonly named pollutants carbon dioxide and sulfur dioxide. In light of their substantially higher energy consumption, thermal processes are inferior to membrane processes when it comes to air pollution. Noise pollution is very often associated with equipments such as high-pressure pumps in RO process, which produce noise during operations. Various technological measures can be utilized to reduce noise levels so that the risk to the operators can be minimized (26). The operations should be kept away from population centers.

The more important form of emission from desalination that raises environmental concerns comprises the discharge of concentrated saltwater after the desalination process is completed (27). The TDS of wastewater from a conventional DWTP is approx 3–5 times higher than that in the feed; the flow rate is 20–50% of feed flow. The waste also contains chemicals used in the pre-treatment of feed water, such as antiscalants, surfactants, and acid.

Major disposal alternatives for the water pollution are given in Table 4. Each method varies in complexity and costs. Sewer discharge is commonly the least complex and least costly. Zero-discharge is the most complex and the thermal processes are costly. The salt produced can be reused by other industries, thus, the approach can be considered more environmental-friendly according to the pollution prevention principles (28–32). It can help to improve public acceptance. The cost can be offset by beneficial use of byproducts (brine or specific salts).

NOMENCLATURE

ΔT Difference in temperature between the condensing steam (T_s) and the boiling liquid (T_1) in the evaporator (K)

A Heat-transfer area (m^2)

C_{PF} Heat capacity of the feed (kJ/kg-K)

F Feed to the evaporator (kg/h)

h_F Enthalpy (kJ/kg) of the feed to the evaporator (kJ/kg)

h_L Enthalpy of the concentrated liquid leaving the evaporator (kJ/kg)

h_s Enthalpy of condensate (kJ/kg)

H_s Enthalpy of steam (kJ/kg)

H_v Enthalpy of vapor (kJ/kg)

L Concentrated liquid leaving the evaporator (kg/h)

P_1 Saturation vapor pressure of the liquid of composition (X_L) at its boiling point (T_L)

q Rate of heat transfer (W)

S Condensed steam leaving the system (kg/h)

T_L Temperature of the concentrated liquid leaving the evaporator (K)

T_F Temperature of the feed to the evaporator (K)

T_s Temperature of the condensed steam leaving the system (K)

T_V Temperature of the vapor (K)

U Overall heat-transfer coefficient (W/m^2 K)

V	Vapor given off as pure solvent (kg/h)
X_F	Solid content of the feed to the evaporator (mass fraction)
X_L	Solid content of the concentrated liquid leaving the evaporator (mass fraction)
Y_v	Solid content of the vapor = 0
λ	Latent heat given off by steam (kJ/kg)

REFERENCES

1. M. Murakami, *Managing Water for Peace in the Middle East: Alternative Strategies*, United Nations University Press, Tokyo, New York, Paris, 1995.
2. World Nuclear Association, *Nuclear Desalination*, London, 2004.
3. O. K. Buros, *The ABCs of Desalting, International Desalination Association*, Topsfield, MA, 2000.
4. A. M. Alkaibi and N. Lior, Membrane-distillation desalination: status and potential. *Desalination* **171**, 111–131 (2004).
5. Z. W. Ding, L. Y. Liu, M. S. El-Bourawi, and R. Y. Ma, Analysis of a solar-powered membrane distillation system. *Desalination* **172**, 27–40 (2005).
6. H. M. Ettouney, H. T. El-Dessouky, R. S. Faibish, and P. J. Gowin, Evaluating the economics of desalination. *Chem. Eng. Prog.* **98**, 32–39 (2002).
7. M. H. I. Dore, Forecasting the economic costs of desalination technology. *Desalination* **172**, 207–214 (2005).
8. U. Ebensperger and P. Isley, *Review of the Current State of Desalination*, Environmental Policy Program, Georgia State University, Atlanta, GA, 2005.
9. Department of Natural Resources and Mines, *Desalination in Queensland, Final report*, The State of Queensland, Australia, 2004.
10. UNEP *Source Book of Alternative Technologies for Freshwater Augmentation in Latin America and the Caribbean*, UNEP, International Environmental Technology Centre, Osaka/Shiga, Japan, 1997.
11. C. J. Geankoplis, *Transport Processes and Separation Process Principles*. 4th ed., Pearson Education, Inc., 2003, pp. 700–702.
12. A. M. S. El Din, M. E. El-Dahshan, and H. H. Haggag, Carbon-induced corrosion of MSF condenser tubes in Arabian Gulf water. *Desalination* **172**, 215–226 (2005).
13. M. Abu-Arabi and Y. Zurigat, Year-round comparative study of three types of solar desalination units. *Desalination* **172**, 137–143 (2005).
14. J. Joseph, R. Saravanan, and S. Renganarayanan, Studies on a single-stage solar desalination system for domestic applications. *Desalination* **173**, 77–82 (2005).
15. A. A. Badran, A. A. Al-Hallaq, I. A. Eyal Salman, and M. Z. Odat, A solar still augmented with a flat-plate collector. *Desalination* **172**, 227–234 (2005).
16. R. Tripathi and G. N. Tiwari, Effect of water depth on internal heat and mass transfer for active solar distillation. *Desalination* **173**, 187–200 (2005).
17. US Department of Army, *Water Desalination Army TM 5-813-8*, Washington, DC, 1986.
18. E. R. Reahl, *Half a Century of Desalination with Electrodialysis*, Technical Paper, Ionics Inc., 2004.
19. P. Tsiakis and L. G. Papageorgiou, Optimal design of an electrodialysis brackish water desalination plant. *Desalination* **173**, 173–186 (2005).
20. R. P. Allison, Electrodialysis reversal in water reuse applications. *Desalination* **103**, 11–18 (1995).
21. W. R. Walters, D. W. Weiser, and L. J. Marek, Concentration of aqueous radioactive wastes. *Indus. Eng. Chem.* **47**, 61–67 (1955).

22. G. C. Ganzi, Y. Egozy, A. J. Giuffrida, and A. Jha, High purity water by electro-deionization. *Ultrapure Water J.* **4**, 3 (1987).
23. R. Semiat, Desalination: present and future. *Water Int.* **25**, 54–65 (2000).
24. N. Kahraman, Y. A. Cengel, B. Wood, and Y. Cerci, Energy analysis of a combined RO, NF, and EDR desalination plant. *Desalination* **171**, 217–232 (2004).
25. R. Einav and R. Lokiec, Environmental aspects of a desalination plant in Ashkelon. *Desalination* **156**, 79–85 (2003).
26. D. A. Crowl and J. F. Louvar, *Chemical Process Safety, Fundamentals with Applications.* 2nd ed., Prentice Hall, NJ, 2002.
27. J. E. Miller, *Review of Water Resources and Desalination Technologies*, Sandia National Laboratories, SAND 2003-0880, Albuquerque, NM, 2003.
28. J. P. Chen, T. T. Shen, Y. T. Hung, and L. K. Wang, Pollution prevention, In: *Handbook of Industrial and Hazardous Wastes Treatment*. 2nd ed., CRC Press & Marcel Dekker, NY, 2004, pp. 971–1004.
29. AWWA. *Desalination of Seawater and Brackish Water.* American Water Works Association, Denver, CO, 2006.
30. L. K. Wang, Y. T. Hung and N. K. Shammas (eds.) *Advanced Physicochemical Treatment Processes.* Humana Press Inc., Totowa, NJ. pp. 549–580, 2006.
31. California Coastal commission, *Seawater Desalination in California*, http://www.coastal.ca.gov/desalrpt/dsynops.html (2006).
32. Texas A&M University, 2nd Annual short course on the future of desalination in Texas, August 6–8, College Station, TX, (2006).

Reverse Osmosis Technology for Desalination

**Edward S. K. Chian, J. Paul Chen, Ping-Xin Sheng,
Yen-Peng Ting, and Lawrence K. Wang**

Contents

1. INTRODUCTION

Desalination technologies are intended for the removal of dissolved salts that cannot be removed by conventional treatment processes. Thermal distillation technologies have been used in some ships for more than 100 yr. Desalination was used on a limited scale for municipal water treatment in the late 1960s. The past four decades can be divided into three phases of development: (1) 1950s was the time for discovery; (2) 1960s was concerned with research; and (3) 1970s and 1980s has been the time for commercialization. In the beginning of the 1970s, the industry began to concentrate on commercially viable desalination applications and processes.

The first commercial plant for the production of potable water from a saline source using electrodialysis was put into operation in 1954. At that time, this process was not received favorably because of its inability to reduce dissolved solids to a desired extent. The first reverse osmosis (RO) water treatment plant was constructed in 1970s in Florida. Significant advances in membrane materials and technologies for the past 20 yr have greatly improved the cost effectiveness and performance capabilities of the processes. RO membrane processes are increasingly used worldwide to solve a variety of water treatment problems. In the desalination industry of the United States, RO membrane technology is most popular.

In this chapter, mechanisms of membrane separation are first illustrated. Membrane materials are presented. Several mathematical models are given for the membrane processes used in desalination. Pre- and post-treatment processes are given. Examples and case studies are also provided.
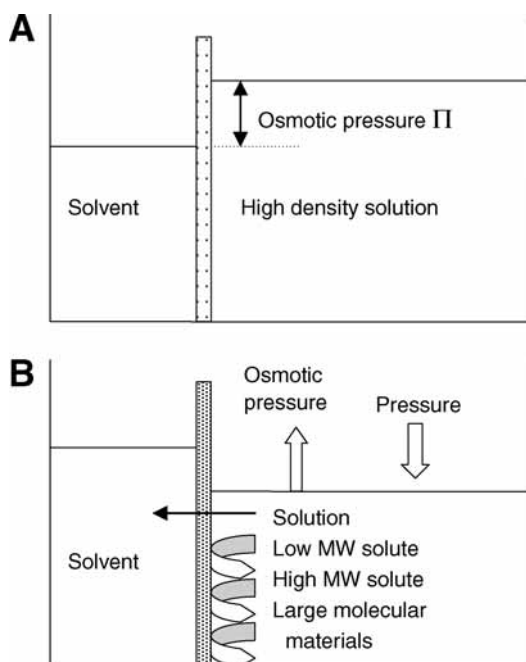
Fig. 1. Schematic of reverse osmotic equilibrium (**A**) and reverse osmosis membrane (**B**).

2. MEMBRANE FILTRATION THEORY

2.1. Osmosis and RO

Osmosis is the phenomenon of water flowing through a semipermeable membrane that blocks the transport of salts or other solutes through the membrane. It is applied to water purification and desalination, waste material treatment, and many other chemical and biochemical processes. When two aqueous solutions (or other solvents) are separated by a semipermeable membrane, water will flow from the side of low solute concentration to the side of high solute concentration. The flow is stopped, or even reversed by applying external pressure on the side of higher concentration. In such a case the phenomenon is called RO as shown in Fig. 1. If there are solute molecules only on one side of the system, then the pressure that stops the flow is called the osmotic pressure Π, which is given by the Van't Hoff equation:

$$\Pi = C_S RT \tag{1}$$

where Π is the osmotic pressure (force/length^2); C_S is the summation of molalities of all dissolved ions (moles/length^3); R is the ideal gas constant (force-length/mass-temperature); and T is the absolute temperature (K). The magnitude of the osmotic pressure, even in very dilute solution, is very large.

For instance, with a solute of 0.01 M at room temperature (298 K), the osmotic pressure would be:

$$\Pi = C_S RT = \left(\frac{0.010 \, \text{mol}}{1 \, \text{L}} \right) \times \left(\frac{0.0821 \, \text{L} \cdot \text{atm}}{\text{mol} \, \text{K}} \right) \times 298 \, \text{K} = 0.24 \, \text{atm}$$

This pressure is sufficient to support a column of water 8.1 ft high.

For applications of the RO of seawater, an approximate expression is

$$\Pi = 1.12T\sum \overline{m_i} \tag{2}$$

where Π is in psia; T is in K; and $\sum \overline{m_i}$ is the summation of molarities of all dissolved ions and nonionic species in the solution (*M*).

RO membrane has an anisotropic (also called asymmetric) structure: it consists of an extremely thin skin layer (100–500 nm thick) with very fine microporous texture (1) and on the top of a much thicker, spongy, supporting sublayer with much larger pore size. In the case of cellulose acetate (CA) RO membranes of the Loeb-Sourirajan type (2), for example, the pores of the skin layer have been estimated, based on the results of titrated water diffusion experiments, to be less than 0.8 nm (8 Å) in diameter (3), and the pore size of the substructure is in the range 100–400 nm (4).

Because of its peculiar physicochemical properties and porous texture (5,6), an RO membrane is much more permeable to solvent molecules than to solute particles (ions and/or molecules). Thus, when a sufficiently pressurized solution (feed solution) is applied to the membrane, the solvent flux through the membrane is usually much greater than the solute flux, i.e., the solute is partially rejected. It is believed that the separation between solvent and solute occurs at the membrane skin layer (7).

Because the feed solution loses solvent, the resulting solution on the high-pressure side of the membrane (concentrate) becomes more concentrated, whereas the solution on the opposite side (permeate) has a lower concentration of solute. The process is used to separate solutes of low molecular weight (usually molecules and/or ions with diameters <100 nm) from their solvents. One of its most important applications is water (seawater included) desalination, whose schematic flow diagram is shown in Fig. 2. In this case, the operating pressure must exceed the effective osmotic pressure of the feed solution in order to get any water throughput from the RO membrane. The resultant hydrostatic pressure difference is represented by the transmembrane pressure difference ΔP

$$\Delta p = \frac{P_{\text{feed}} + P_{\text{concentrate}}}{2} - P_{\text{permeate}} \tag{3}$$

where P_{feed}, $P_{\text{concentrate}}$, and P_{permeate} are the hydrostatic pressure of the feed, concentrate, and permeate flows, respectively.

The effectiveness of the RO process for water desalination largely depends on the permeability and selectivity of the membrane. Characteristics that define the membrane performance can be quantified for a set of given operating conditions by the permeate flux through the membrane and the ratio between the permeate flow rate and the effective area of the membrane.

The solute rejection *R* of each solute of interest is defined by:

$$R = \frac{C_s^I - C_s^{II}}{C_s^I} = 1 - \frac{C_s^{II}}{C_s^I} \tag{4}$$
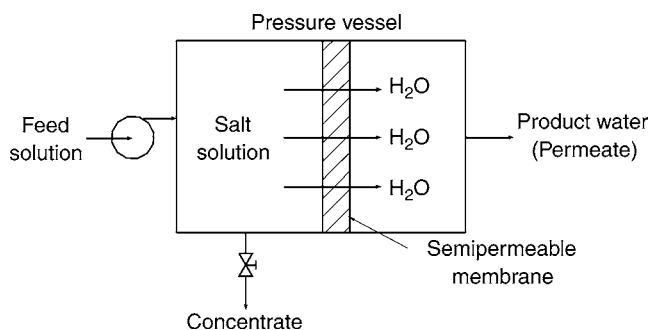
Fig. 2. Simplified RO flow diagram.

where C_s^I is the solute concentration at the feed solution–membrane interface; C_s^{II} is the solute concentration in the permeate. The desalination ratio D_r is defined by:

$$D_r = \frac{C_s^I}{C_s^{II}} \tag{5}$$

Some important requirements for an RO membrane to be used in water desalination are listed next

- High permeate flux.
- High solute rejection.
- Mechanical strength to withstand elevated operating pressures.
- Chemical stability for wide range temperature and pH.
- Operating capability over a broad range of ionic species present in the feed solution.
- Resistance to biological attack.

2.2. Membranes

A wide variety of membrane types, sizes, construction options, and techniques are available for removing salt from water. There are basically two types of commercial membranes used in RO applications to date: CA and thin film (TF). The former is considered as an integral membrane and the latter a composite membrane. Membrane manufacturing, operating conditions, and performances differ significantly for each group of polymeric material.

2.2.1. CA Membranes

The CA membrane originally consists of cellulose diacetate polymer (2). Current CA membrane is usually made from a blend of cellulose diacetate and triacetate. A TF acetone-based solution of CA polymer with swelling additives is first cast onto a non-woven polyester fabric. Part of the solvent is evaporated during casting. After the casting step, the membrane is immersed into a cold waterbath to remove the remaining acetone and other leachable compounds. Following the cold bath, an annealing step is followed by immersing the membrane into a hot waterbath at a temperature of 60–90°C. The annealing step improves the semipermeability of the membrane with a decrease of water transport and a significant decrease of salt passage. The resulting cellulose membrane has an asymmetric structure with a dense surface layer of about 0.1–0.2 μm which rejects the salt. The substructure of the membrane film is spongy and porous and has

high water permeability. Semipermeability of a CA membrane is largely dependent on the temperature and duration of the annealing step.

The superior chlorine and fouling resistance of CA makes it as the membrane of choice for many applications. In desalination, applications are mainly limited for brackish water because of the compressibility of the membrane itself under the high pressures required for operation.

2.2.2. TF Membranes

Two distinct steps are used to manufacture TF composite polyamide (PA) membranes. First, a support layer is formed by casting polysulfone solution onto a nonwoven polyester fabric. The support layer is very porous and hence does not reject the salt. In the following separate manufacturing step, a semipermeable membrane skin is formed on the polysulfone substrate by interfacial polymerization of monomers containing amine and carboxylic acid chloride functional groups.

In the 1970s, Cadotte prepared a composite membrane that consisted of a thin layer of PA formed *in situ*, by condensation of branched polyethyleneimine and 2,4-diisocyanate on a porous polysulfone membrane (8). The effect of surface modification on the performance of an aromatic PA–TF composite membrane has been studied (9). After soaking in solutions of various concentrations of hydrofluoric acid (HF), fluorosililic acid, and their mixtures at the controlled temperature for various times, the membrane was rinsed with deionized (DI) water and tested for their RO performances. For membranes soaked in 15 wt% HF solution for 7 d, the flux increased from 3.5 to 18 L/m^{2}h, whereas NaCl separation increased from 94.5 to 95.3% under the same operating pressure of 250 psig. For membrane soaked in 15 wt% HF solutions for 4 d, X-ray photoelectron spectroscopy showed that the fluorine ratio on the membrane surface increased from 0 on the fresh membrane to 0.012. The value increased to 0.044 for the membrane immersed in 15 wt% HF solution for 75 d. Thus, surface chemical modification contributed to the dramatic increase of the flux as well as the thinning of the selective skin layer, whereas NaCl separation was practically unchanged.

The discovery of TF membrane is a breakthrough in achieving flows and rejections suitable for seawater desalination. In some cases, three-layer configurations are used for extra durability and performance. Some characteristics of the two membranes are listed in Table 1.

TF composite (TFC) membranes are subject to continuous development. Membranes with chlorine resistance, low energy, and low fouling have been produced. Recently, about 60% of seawater recovery has been reported for some extra high-rejection TF membranes. RO systems originally designed using flat CA or hollow fiber membranes that were retrofitted with TFC membranes of polyurea and PA. The TFC, PA membranes have many advantages in comparison with CA or hollow fiber membranes. These include wider chemical and physical tolerance ranges, higher silt density index (SDI) tolerance, feasibility of operation at higher temperatures, and higher pH tolerance. These make pretreatment easier and less expensive, and operation easily controlled. Furthermore, the introduction of the TFC, PA membrane is helpful to better combat biofouling and to raise the effective plant availability in view of the higher resistance of the spiral wound configuration to mechanical blocking and of the PA polymer to biodegradation. Particularly

Table 1
Characteristics of Cellulose Acetate and Thin-Film Membranes

Parameters	Cellulose acetate	Thin film
Temperature	Up to 30°C	Up to 50–90°C
Operating pressure (psi)	Up to 450 typically; up to 800 occasionally	100–1200
pH	3.0–9.0	1.0–12.0
Chlorine tolerance	Fair	Poor
Oxidization tolerance	Good	Poor
Rejection (%)	Good	Excellent

in seawater desalination, higher RO process efficiency and recovery rates are realized, by the development of the very high-rejection TFC membranes, which are resistant to compaction at high applied pressures and enable brine recovery in two-stage systems. Consequently, operation and project cost has been decreased significantly resulting from the application of TFC PA membranes.

2.3. Membrane Filtration Theory

2.3.1. Membrane Transport

Even if the transport in the solution circulating in the space between the membranes is important, it is the ion and water transport in the membranes that determine the performance of the membrane process. Theories used to characterize transport in the skin layer of membrane have been reviewed (10–16). Mechanistic and mathematical models proposed can be divided into three types: irreversible thermodynamics models; nonporous or homogeneous membrane models (such as the solution diffusion [SD], SD-imperfection, and extended SD models); and pore models (such as the finely porous, preferential sorption-capillary flow [PSCF], and surface force-pore flow models [SFPF]). Some of these descriptions rely on relatively simple concepts, whereas others are more complex and require sophisticated solution techniques. Models that adequately describe the performance of RO membranes are very important because these are needed in the design of RO processes. Models that predict separation characteristics also minimize the number of experiments that must be performed to describe a particular system. The transport models focus on the top thin skin of asymmetric membranes or the top thin skin layer of composite membranes because these determine fluxes and selectivities of most membranes (17). Also, most of the membrane models assume equilibrium (or near equilibrium) or steady-state conditions in the membrane.

2.3.2. Irreversible Thermodynamics Models

Irreversible thermodynamics lead to the following expressions for solvent and solute flow:

$$J_w = L_p \cdot \left(\Delta P - \Delta \Pi \right) \tag{6}$$

$$J_s = C_s \left(1 - \sigma \right) J_w + D \varepsilon \Delta C \tag{7}$$

where ΔP and $\Delta \Pi$ are the transmembrane pressure and osmotic pressure across membrane, respectively; C_s and ΔC are average concentration of solute and solute concentration

difference across membrane, respectively; D is the diffusivity and ε is the porosity of the membrane; L_p is the coefficient; σ is the measure of the solute–water coupling within the membrane and may often be treated as 1. The theory then characterizes the membrane by the parameters L_p and $D\varepsilon$, which may be measured by other than RO experiments and then used to quantify the performance of the membrane. A particular strength of this approach is its extension to multicomponent systems, in which it can be used to predict membrane behavior. However, it does not elucidate the actual transfer mechanisms within the membrane.

2.3.3. Homogeneous Models

The homogeneous models assume that the membrane is nonporous. The extent of separation of the solvent and solute by the membrane depends on the difference in the solubilities and diffusivities of the solvent and solute in the membrane phase. In other words, when the solvent and solute molecules come into contact with the membrane surface, the solvent and the solute molecules will dissolve in the surface layer. The solubilities of the solute molecules depend on their respective solute distribution coefficient between the solution and the membrane phase. Once in the membrane phase, the solvent and solute molecules will diffuse across the membrane. The flux of these molecules depends on the transmembrane pressure difference and their respective concentration difference across the membrane (collectively known as the molecular species' individual chemical potential gradient).

The most commonly applied homogeneous model is the SD model. The model gives the following relationships for flux of solvent:

$$J_w = \frac{P_w}{\Delta x}\left(\Delta P - \Delta \Pi\right) = A_w\left(\Delta P - \Delta \Pi\right) \tag{8}$$

where $A_w = P_w/\Delta x$, P_w is the solvent permeability; Δx is the thickness of the membrane; A_w is the solvent permeability constant. Although J_w depends mainly on the difference between ΔP and $\Delta \Pi$, the solute flux, J_s, depends mainly on the solute concentration difference between the feed and permeate sides of the membrane as shown in Eq. (9):

$$J_s = \frac{D_s K_s\left(C_s^I - C_s^{II}\right)}{\Delta x} = A_s\left(C_s^I - C_s^{II}\right) \tag{9}$$

where $A_s = D_s K_s/\Delta x$, D_s is the diffusivity of the solute, K_s is the solute distribution coefficient between the solution and membrane phase, C_s^I is the concentration of the solute in the feed solution on the membrane surface, C_s^{II} is the concentration of the solute in the permeate solution, and A_s is the solute permeability constant.

A comparison between the aforementioned two equations shows that the flow of the solvent and the flow of the solute through the membrane do not affect each other and are indeed separate flows affected only by their own chemical potential gradient as described by the SD model. The intrinsic membrane solute rejection for this model is given by:

$$R = \left[1 + \left(\frac{\rho_w A_s}{A_w}\right)\left(\frac{1}{\Delta P - \Delta \Pi}\right)\right]^{-1} \tag{10}$$

where R is the solute rejection and ρ_w is the density of the solvent.

Example

A RO membrane to be used at 25°C for a 5.0 kg/m^3 NaCl feed solution has a water permeability constant of $A_w = 5.32 \times 10^{-4}$ kg/s.m^2 and a solute (NaCl) permeability constant of $A_s = 4.89 \times 10^{-7}$ m/s. ΔP is 27.2 atm. Calculate the water flux and solute flux through the membrane, the solute rejection R, and C_s^{II} of the product solution.

Solution

In the feed solution, $C_s^I = 5.0$ kg/m^3 (5.0 g/L), then substituting into Eq. (1):

$$\Pi_1 = C_s^I RT = \left(\frac{5.0\,\text{g}/\text{L}}{58.45\,\text{g}/\text{mol}} \right) \times \left(\frac{0.0821\,\text{L}\cdot\text{atm}}{\text{mol}\,\text{K}} \right) \times 298\,\text{K} = 2.09\,\text{atm}$$

Because the product solution C_s^{II} is unknown, a value of $C_s^{II} = 0.1$ g NaCl/L will be assumed, then $\Pi_2 = 0.08$ atm, $\Delta\Pi = \Pi_1 - \Pi_2 = 2.09 - 0.08 = 2.01$ atm. Also, because permeate is quite dilute, a value of $\rho_w = 997$ kg/m^3 is assumed.

Substituting into Eq. (8):

$$J_w = A_w\left(\Delta P - \Delta\Pi\right) = 5.32 \times 10^{-4}\left(27.20 - 2.01\right) = 1.341 \times 10^{-2}\ \text{kg}\ \text{H}_2\text{O/s}\cdot\text{m}^2$$

For calculation of R, substituting into Eq. (10):

$$R = \left[1 + \left(\frac{\rho_w A_s}{A_w}\right)\left(\frac{1}{\Delta P - \Delta\Pi}\right)\right]^{-1} = \left[1 + \left(\frac{997 \times 4.89 \times 10^{-7}}{5.32 \times 10^{-4}}\right)\left(\frac{1}{27.20 - 2.01}\right)\right]^{-1} = 0.965$$

Using this value of R in Eq. (4):

$$R = 0.965 = 1 - \frac{C_s^{II}}{C_s^I} = 1 - \frac{C_s^{II}}{5.0}$$

Solve, $C_s^{II} = 0.175$ kg/m^3 for the product solution. This is not close enough to the assumed value of $C_s^{II} = 0.10$ kg/m^3. At least one more iteration should be conducted until the solved C_s^{II} is very close to another assumed value of C_s^{II}, and Π_2 will not change significantly on another trial. For the purpose of illustration only, it is assumed that the final value of C_s^{II} is 0.175 kg/m^3.

Substituting into Eq. (9):

$$J_s = A_s\left(C_s^I - C_s^{II}\right) = 4.89 \times 10^{-7}\left(2.5 - 0.175\right) = 1.137 \times 10^{-6}\ \text{kg}\,\text{H}_2\text{O/s}\cdot\text{m}^2$$

As transmembrane pressure increases, Eq. (8) suggests that the solvent flux will increase proportionally. Solute flux (Eq. [9]) will rise less rapidly, giving an improvement in solute rejection as is observed experimentally. Similarly the model correctly predicts the decrease in rejection that occurs with increased solvent recovery. As a consequence of increased solvent recovery the concentration of retained solute increases, and by Eq. (9), a greater passage of solute (low rejection) is expected. A transport model based on the solution–diffusion (SD) model incorporating concentration polarization has been successfully used to interpret the experimental results and predict rejection over a range of operating conditions (18). However, the SD model is limited to membranes with low water content, and for many RO membranes and

solutes, particularly organics, the SD model does not adequately describe water or solute flux (12,13). Possible causes for these deviations include imperfections in the membrane barrier layer, pore flow (convection effects), and solute–solvent–membrane interactions (12,13).

2.3.4. Solution-Diffusion-Imperfection Model

Although the SD model assumes the absence of pores on the membrane surface layer, there will inevitably be imperfections (pores) on the surface of the membrane. These pores can provide pathways by which the solvent and solute molecules can diffuse through the membrane. The SD-imperfection model extends the SD model by accounting for the existence of these pores and the flowthrough them.

This model gives the solvent flux as:

$$J_w = \frac{P_w}{\Delta x}\left(\Delta P - \Delta \Pi\right) + \frac{P_3}{\Delta x}\Delta P \qquad (11)$$

where $P_3/\Delta x$ is a coupling coefficient. Comparing Eq. (8) and Eq. (11), it is clear that the second term in Eq. (11) accounts for solvent flowthrough the imperfections in the membrane surfaces, in addition to diffusion as accounted for by the first term in the same equation.

Existence of pore flow is also accounted for in the second term of the extended solute flux equation:

$$J_s = \frac{P_2\left(C_s^I - C_s^{II}\right)}{\Delta x} + \frac{P_3}{\Delta x}\Delta P C_s^I \qquad (12)$$

where $P_2/\Delta x$ is a solute permeability coefficient equivalent to $P_s/\Delta x$ in Eq. (9).

The corresponding intrinsic membrane solute rejection for this model is:

$$R = \left[1 + \left(\frac{P_2}{P_w}\right)\left(\frac{1}{\Delta P - \Delta \Pi}\right) + \left(\frac{P_3}{P_w}\right)\left(\frac{\Delta P}{\Delta P - \Delta \Pi}\right)\right]^{-1} \qquad (13)$$

Extended SD model is mainly used for organic solutes by an introduction of the pressure-dependent term (19). However, the model has two major disadvantages: it contains three parameters that must be determined by nonlinear regression in order to characterize the membrane system and the parameters describing the system are usually functions of both feed concentration and pressure (12).

2.3.5. Preferential Sorption Capillary Flow Model

An early pore model was the preferential sorption capillary flow (PSCF) model proposed by Sourirajan. In contrast to the SD model, the membrane is assumed to be microporous (1,20). Therefore, membrane surface properties and transport phenomena in the membrane pore determine the mechanism for the separation of solute and solvent molecules. According to the model, on contact of the feed solution with the membrane, chemical properties of the barrier layer allow for the preferential sorption of the solvent molecules and subsequently the formation of a solvent layer on the surfaces and in the pores of the membrane. The solute molecules, on the other hand, are rejected by the membrane and, therefore cannot form any surface layer. The solvent molecules in the solvent layer are then forced, under hydrostatic pressure, through the membrane capillary pores to the permeate side.

Solvent flux, J_w, as given by this model is:

$$J_w = A\left\{\Delta P - \left[\Pi\left(C_s^I\right) - \Pi\left(C_s^{II}\right)\right]\right\} \tag{14}$$

where A is the pure solvent permeability constant, $\Pi(C_s)$ is the osmotic pressure of a solution with solute mole fraction C_s. Unlike solvent flux, the applied pressure does not influence the solute flux:

$$J_s = \frac{K_s D_s}{\Delta x}\left(C_s^I - C_s^{II}\right) \tag{15}$$

A comparison between Eq. (9) and Eq. (15) shows that they are identical. Thus in the PSCF model, the transport of solute molecules takes place only by diffusion through the membrane surface layer and not partly by pore flow as suggested by the SD-imperfection model. The model has been utilized to analyze transport for a large number of solutes and membranes (20).

2.3.6. Finely Porous Model

The finely porous model assumes that transport of solvent takes place by viscous flow through uniform membrane pores and that transport of solute occurs by both diffusion and convection in these pores. It can provide valuable insight into parameters such as pore size, solute–membrane interaction (friction parameter), and solute distribution coefficient that affect solute transport (12). However, for some solute systems such as dilute organics, the model does not adequately describe decreases in water flux compared with the pure water flux unless a correction is made in the pore size; it is usually necessary to reduce the pore size in order for the measured and predicted water fluxes to agree. This disadvantage limits the applicability of the finely porous models for water flux prediction in these systems.

2.3.7. Surface Force Pore Flow Model

The surface force pore flow (SFPF) model is a two-dimensional extension of the finely porous model (20,21). Although the finely porous model considers only axial solute concentration gradients, the SFPF model recognizes that the solute concentration in an RO membrane pore may be a function of radial as well as axial positions (15,17,20). The model gives excellent predictions of solute separation for a wide range of inorganics and organics under varying operating conditions (22–24). However, for some dilute organics that cause substantial decreases in water flux, this model does not adequately predict the water flux ratio. The pore radius must be reduced in order to force the predicted and measured water flux ratio into agreement for these systems.

2.4. Concentration Polarization

This phenomenon describes the increase in retained solids or solute concentration on the membrane surface. According to a simple stagnant film theory, there will be a concentration gradient over the thickness of the stagnant film. Thus on the membrane surface, the concentration will be highest and will decrease to bulk concentration in the well-mixed liquid. This will cause a diffusion of solids in the direction opposite to the main flux and, therefore a reduction in the overall flux. Other negative results include

an increase of solute flux resulting from the increased concentration gradient across the membrane, and scaling or particle scaling induced by the precipitation of solute. Consequently, the separation properties of membrane are reduced. The extent of concentration polarization can be reduced by promoting good mixing of the bulk feed solution with the solution near the membrane wall. Mixing can be enhanced through membrane module optimization of turbulence promoters, spacer placement, hollow fiber diameter, and so on, or by simply increasing axial velocity to promote turbulent flow (16,17,25,26).

Concentration polarization complicates the modeling of membrane systems because it is very difficult to experimentally determine the solute wall concentration, which is used in most RO transport models and not the bulk concentration. For very high-feed flow rates, enough mixing near the membrane surface occurs so that the wall concentration can be assumed equal to the bulk concentration. Similarly at low permeation rates, the extent of concentration polarization is likely to be limited. Thus, for example, Du Pont hollow fiber permeators, because of the intrinsic low permeability of the membrane, can be operated under essentially backmixed conditions on the shell (feed) side (27). The presence of a mesh in spiral wound modules promotes feed side mixing and minimizes the effect of concentration polarization on the membrane surface. However, at lower feed flow rates, the difference between the wall and bulk concentration can be substantial and so the wall concentration must be calculated.

The simplest relationship for the membrane surface concentration (C_m) is provided by:

$$J_w = k \cdot \ln \frac{\left(C_m - C_s^{II}\right)}{\left(C_b - C_s^{II}\right)} \tag{16}$$

where k is the mass transfer coefficient, dependent on the extent of cross flow and physical properties prevailing on the surface of the membrane; C_b is the concentration of solute in bulk feed; and C_m is the concentration of solute on the membrane surface.

More complete solutions which account for diffusion effects in the axial direction and loss of solvent along the flow channel have been provided (28,29). All of them broadly show a greater level of polarization than predicted by Eq. (16) and would encourage the use of effective mixing on the feed side of an RO membrane.

2.5. Compaction

Compaction is another phenomenon in membrane mass transport. When a polymeric membrane is put under pressure, the polymers are slightly reorganized and the structure is changed. This results in lowered volume porosity, increased membrane resistance, a dense structure with smaller pores, and eventually a lowered flux. For example, after long-term compaction of the asymmetric CA membranes, the selectivity was found to be unchanged but the flux decreased (30). The flux loss could be attributed to a compaction of the porous sublayer and the unchanged skin. It was concluded that under all circumstances, compaction results in a notable membrane permeability loss. Thus the correct application of pressure is very important.

Table 2
Commercially Available RO Membranes and Modules

Membrane material	Module type	Company
Asymmetric aramid	Spiral wound	Du Pont (USA)
Asymmetric cellulose acetate	Spiral wound	Toray (Japan)
	Spiral wound	Desalination system (USA)
	Plate and frame	DDS (Denmark)
	Tubular	Paterson Candy (UK)
Asymmetric poly(acrylonitrile)	Spiral wound	Sumitomo (Japan)
Cellulose acetate	Hollow fiber	Toyobo (Japan)
	Hollow fiber	Osmonics (USA)
	Spiral wound	Hydranautics/Nitto Denko (USA/Japan)
Composite aramid	Spiral wound	Du Pont (USA)
Composite cellulose acetate	Spiral wound	Du Pont (USA)
Composite PEC	Spiral wound	Toray (Japan)
Composite polyamide	Hollow fiber	Filmtec/DOW (USA)
	Spiral wound	Fluid system/UOP
	Spiral wound	Desalination system (USA)
	Plate and frame	DDS (Denmark)
	Tubular	Paterson Candy (UK)
	Spiral wound	Hydranautics/Nitto Denko (USA/Japan)

3. MEMBRANE MODULES AND PLANT CONFIGURATION

3.1. Membrane Modules

Basically, the RO process is a modular scale process wherein scale up beyond a certain size is not economically advantageous (3). The modules are packaging devices of the membranes and their supports, designed in such a way that the pressurized feed solution can be applied to the surface of the membrane skin layer and the permeate can be collected without being contaminated by the concentrate.

At present, there are basically four RO module designs commercially available, namely, tubular, hollow-fiber, spiral-wound, and flat configuration. For RO applications, the most commonly used configurations are hollow fiber and spiral wound modules. Some commercial RO membranes and corresponding modules are summarized in Table 2.

3.1.1. Hollow Fiber

This configuration consists of a very large number of hollow membrane fibers, which are asymmetric in structure and are as fine as a human hair (Fig. 3). The membrane fibers are assembled into a cylindrical bundle evenly spaced about a central feed distributor tube. The ends of the fibers are epoxy sealed to form a sheet-like permeate tube. In some cases, half-fold bundles are used. The hollow fiber membrane bundle is contained in a cylindrical housing or shell. The assembly is called a permeator. During operation, the pressurized feed water enters the permeator feed end, through the center distributor tube, passes through the tube wall, and flows radially around the fiber bundle toward the outer
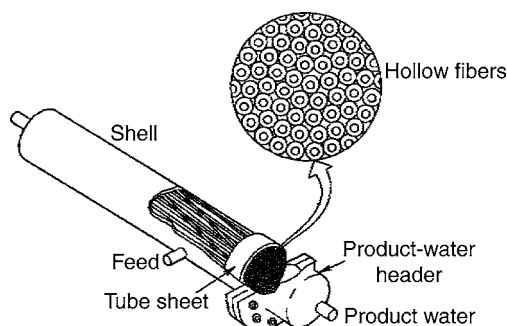
Fig. 3. Schematic drawing of a hollow fiber module.

permeator pressure shell. Water permeates through the outside wall of the fibers into the hollow fiber bore, and is removed from the tube sheet end of the fiber bundle.

An increase in permeate flux will increase the delivery rate of ions to the membrane surface and increases salt concentration on the membrane surface, whereas an increase of feed flow increases turbulence and reduces the thickness of the high concentration layer near the membrane surface. For a hollow fiber module, the permeate water flow per unit area of membrane is generally low, and therefore, the concentration polarization is not high on the membrane surface. Furthermore, the feed water flow must exceed a minimum reject value in order to minimize concentration polarization and maintain even flow distribution through the fiber bundle. Typically, a single hollow fiber permeator can be operated at up to half recovery and meet the minimum reject flow required.

Systems based on this configuration are extremely compact and require relatively little space because of its extremely high packing density. Its primary disadvantage is that the configuration is highly susceptible to fouling and is difficult to clean effectively because of the very small spacing between fibers in the bundle. Thus, extensive pretreatment is required even on relatively clear feedwaters.

3.1.2. Spiral Wound

The spiral wound configuration (Fig. 4) consists of several flat membranes separated by the permeate collector channel materials to form a leaf. The edges of the leaf are sealed on three sides with the fourth side left open for permeate to exit. A number of these permeate assembles or leaves are wound around a central plastic permeate tube. This tube is perforated to collect the permeate from the multiple leaf assemblies.

Spiral systems are usually staged with three to six membrane elements connected in series in a pressure tube. The feed stream from the first element becomes the feed to the following element, and so on, for each element within the pressure tube. The feed flows through the element in a straight axial path from the feed end to the opposite end, running parallel to the membrane surface. The turbulence induced by the feed channel spacer helps to reduce concentration polarization. The brine stream from the last element exits the pressure tube to waste. The permeate from each element enters the permeate collector tube and exits the vessel as a common permeate stream. A single pressure vessel with four to six membrane elements connected in series can be operated at up to half recovery under normal design conditions.
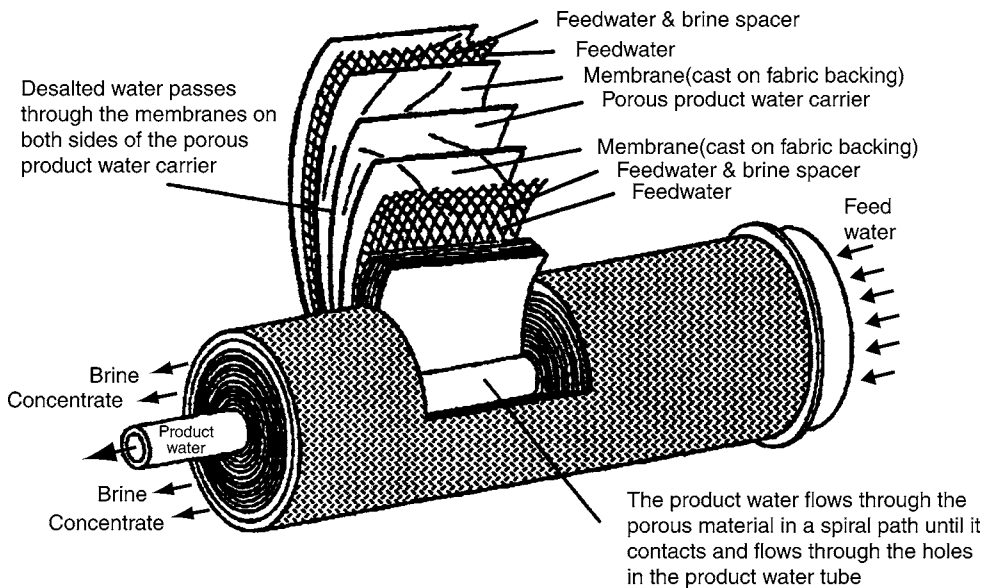
Fig. 4. Schematic drawing of a spiral wound module.

The spiral configuration makes better use of space than tubular or flat-sheet types. Furthermore, it has low manufacturing cost, and can be cleaned both chemically and hydraulically with relative ease. Extensive pretreatment is necessary for highly turbid feed waters because the quite small flow passages are subject to clogging.

3.1.3. Tubular Module

The tubular configuration (Fig. 5) is conceptually the simplest of all the configurations. Membrane is either cast on the inner surface of, or placed within, a porous tube and sealed into place. During operation, pressurized feedwater is circulated through tubes in series or parallel. Purified water passes through the membrane, through the porous tube, and drops off into a convenient collection receptacle for removal from the system.

The tubular system has the advantage that it can be operated on extremely turbid feedwaters and can be cleaned either mechanically or hydraulically with ease. It has the disadvantage of very high capital costs when compared with either the spiral or hollow fine fiber for water treatment applications.

3.1.4. Flat Configuration

In the plate and frame design (Fig. 6), membranes are attached to both sides of the rigid plate. The plate may be constructed of solid plastic with grooved channels on the surface, porous fiberglass materials, or reinforced porous paper. The plate/frame membrane units are placed in a pressurized vessel in a configuration, which allows feedwater to contact all sides of the plates. Feedwater under pressure is fed through the vessel and concentrated brine is removed from the other end.

Each plate in the vessel is at low pressure so that water passes through the membrane which is in contact with the high pressure brine and is collected in the porous media. Fresh water is collected from all the plates. This design is useful for chemical process
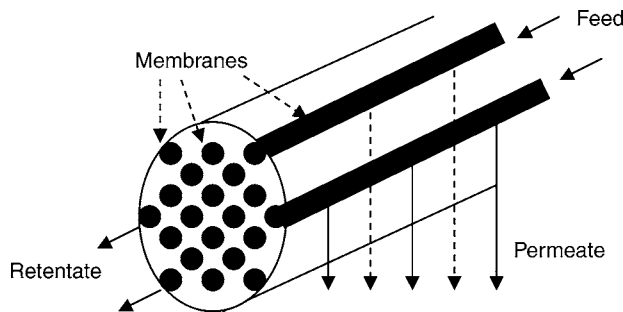
Fig. 5. Schematic drawing of a tubular module.
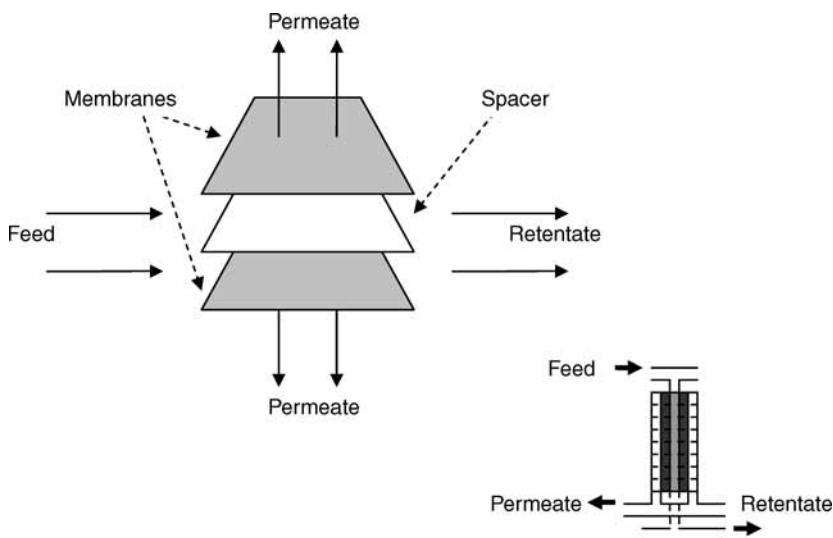
Fig. 6. Schematic drawing of a flat configuration module.

applications but, because of its complexity, is very expensive to operate for large-scale operations.

3.2. Plant Configuration of Membrane Modules

3.2.1. Plant Configuration

A typical RO plant configuration generally includes raw water pumps, pretreatment, membrane units, disinfection units, storage, and distribution elements. For desalination application, membrane units are often configured into a multistage continuous process. In such a system, the concentration of the feed stream increases gradually along the length of several stages of membrane modules arranged in series (Fig. 7). The feed only reaches its final concentration at the last stage. Variations in water temperature and fouling degree of the feed water are compensated by adjustments of the feed pressure. In some case, concentrate recirculation is used to achieve a high enough system recovery. Part of the concentrate is directed back to the feed water side of the module. The recycled
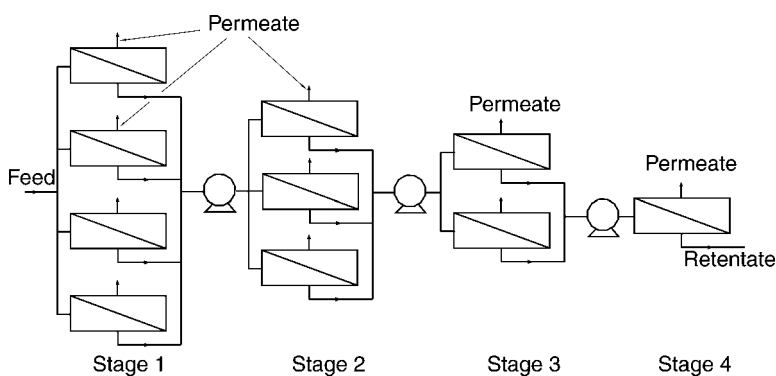
Fig. 7. Schematic flow-diagram of a multistage continuous RO process.

concentrate mixes with the feed water and will be treated once more. Other design considerations for membrane units are discussed next.

3.2.1.1. FEED WATER PRESSURE

The feed pressure is determined by the flux, the energy loss in the system, and the osmotic pressure in the membrane system. The required feed pressure will increase when the membrane elements become contaminated with time. A feed pump that enables a higher flow than the theoretically required flow will then be preferred to keep the feed pressure continual. Generally, a feed pump that increases the feed pressure by 25% will be satisfactory in practice. Typical feed pressures range from 5 to 24 bars. RO systems rated at less than 17 bars are classified as low-pressure units, whereas those operating more than 24 bars are classified as high pressure units. Although high operating pressure can cause noise, vibration, and corrosion problems, these systems are more effective. More recently, new models have been developed to perform well at low pressures.

3.2.1.2. MEMBRANE TYPE AND PORE SIZE

Two types of membrane modules are usually selected for RO systems: spiral wound and hollow fiber. The spiral wound unit clogs less frequently, whereas the hollow fiber membrane has much greater surface area per unit volume. In the early days, membranes were usually made of CA. These days, membranes are also made of aromatic PA and thin-filmed polymer composites. Different materials will have distinct characteristics, such as hydraulic resistance, pH range, temperature range, chlorine tolerance, and biodegradation tolerance.

3.2.1.3. PRETREATMENT REQUIREMENTS

Pretreatment requirements consist of the following major factors: (1) influent suspended solid concentration; (2) ionic size of the contaminants; and (3) membrane type. Other characteristics such as contaminant concentration, water temperature, and presence of competing ions are also important. Pretreatment is most commonly used to prevent fouling of the membrane during operation. Typical pretreatment for RO includes particle removal by filtration, sequestering hardness ions by precipitation, and pH control to prevent clogging.

3.2.1.4. PRODUCT CONVERSION RATE

This is the ratio of rejected water to finished water and it depends on several factors, mainly ionic charge and ionic size. The higher the ionic charge and the larger the ionic size of the contaminant, the more easily the ion is removed and the more finished water is recovered relative to the amount of rejected water.

3.2.1.5. ENERGY SAVING

Application of a pressure exchanger can be used to win back energy from the concentrate flow released under high pressure. The concentrate flow from the membranes is directed through the pressure exchanger, where it directly transfers energy to part of the incoming feed water with maximum affectivity. In an RO system that uses a pressure exchanger, it not only saves more than half the total energy but also saves purchase costs of high-pressure pumps. An RO design software is illustrated in detail in Judd and Jefferson (31).

Although a considerable amount of work has been done to improve membrane performance, there are several limitations that inherent the membrane separation processes. Therefore, engineers have begun to design hybrid systems in which one of membrane separation processes is combined with a more conventional separation process (32). The cost associated with a hybrid separation process is often lower than each individual separation process. According to General des Eaux and USFilter, there are a number of ways to combine distillation process and various membrane separation processes in hybrid desalination systems. For example, the energy consumption is thus reduced by feeding the cooling water from the distillation process to an RO unit; ultrafiltration (UF) and microfiltration (MF) are used to pretreat feed stream; and the upstream of a distillation process is softened by nanofiltration to reduce scale-forming ions, then the productivity of the distillation process is increased by operating at high temperature.

3.2.2. Energy Saving

Energy saving is mainly to recover the energy carried over by the brine leaving the RO system at high pressure. For a seawater RO system operating at 55–69 bar with 15–40% conversion, the brine leaves the RO modules at a pressure of 51–65 bar. When a hydraulic turbine is used to convert the brine stream to power, a major part of the energy of the high pressure brine can be recovered. Without energy recovery, the use of RO for seawater conversion consumes 35–45 kWh/1000 gal depending on feed salinity and other operating conditions. With an energy recovery turbine (ERT), the above energy consumption can be reduced to 20–25 kWh/1000 gal (20).

Consequently, the most important part in any RO plant, as far as the energy consumption is concerned, is the energy recovery system. Basically, there are two different approaches for energy recovery. First, the energy recovery technologies are commonly referred to as the positive displacement systems such as Energy Recovery, Inc.'s Pressure Exchanger, Desalco's Work Exchanger Energy Recovery system, Siemag's system, and RO Kinetic's System. All of these technologies use the principle of positive displacement to transfer the energy contained in the reject stream directly into a new stream (Fig. 8). Positive displacement pumps typically offer lower flow rate and higher discharge pressure capabilities than centrifugal pumps. The efficiencies of all these devices can be quantified as the hydraulic energy out divided by the hydraulic energy in.
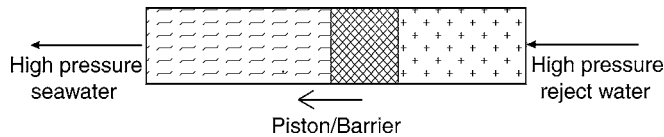
Fig. 8. Simple schematic of energy recovery with a positive displacement device.
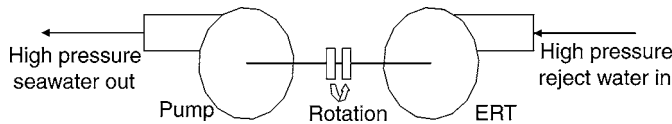
Fig. 9. Simple schematic of energy recovery with energy recovery turbine and pump.

Most of these devices achieve relatively similar net energy transfer efficiencies between 91 and 96%. The energy saving is achieved by reducing the volumetric output of the high pressure pump.

These constituents provide the onset of membrane fouling (58):

- Particulate deposition (colloidal fouling).
- Adsorption of organic molecules (organic fouling).
- Inorganic deposits (scaling).
- Microbial adhesion and growth (biofilm formation).

A pressure exchange system from Siemag was applied in a 5000 m^3/d seawater desalination plant INALSA I, Spain. The results proved that this system contributed to reduce the energy demand for RO units in the range of 25–30% when compared with plants equipped with usual energy recovery devices based on turbines. The direct transfer of the fluid pressure from the concentrate to the fluid pressure in the feed stream with an efficiency of approx 98% allows for short amortization times for the system itself if installed in new plants as well as for retrofitting of existing plants (33).

Another energy recovery technology is to convert the hydraulic energy in the reject stream into rotational energy, in the form of mechanical shaft power, by an ERT. In an RO system, this rotational mechanical energy must then be transferred into another pumping device that pressurizes the incoming stream (Fig. 9). The efficiency of centrifugal ERT is typically in the range 80–88% in converting hydraulic energy into rotational mechanical power which is converted back to hydraulic energy. Therefore, when the efficiency losses of the pump are accounted for the real net energy transfer efficiencies are about 35–75% for these devices even when operating at their optimum efficiency design points

4. PRETREATMENT AND CLEANING OF MEMBRANE

4.1. Mechanisms of Membrane Fouling

The pretreatment system that is used is highly dependent on the feed water quality. A complete and exact analysis of source water is thus important for the design of a pretreatment system and the entire RO system because this often determines the type and size of the pretreatment. The source of water may contain various concentrations of suspended

solids and dissolved matter. Suspended solids may consist of inorganic particles, colloids, and biological debris including bacteria and algae. Dissolved matter may consist of highly soluble salts, such as chlorides, and sparingly soluble salts, such as carbonates, sulfates, and silica. During operation, the concentration of suspended particles and dissolved ions increases with a decreasing volume of feed water. The settled suspended particles on the membrane surface may block feed channels and increase pressure drop across the system. The precipitated soluble salts from the concentrate stream may create scale on the membrane surface and thus decrease water permeability through the RO membranes. The process of forming a deposited layer on the membrane surface is called membrane fouling. Membrane fouling remains the most difficult obstacle in membrane operation. The consequence of membrane fouling is reduction of permeate production rate and/or an increase in solute passage across the membrane with time. Fouling may also cause increase in energy consumption as transmembrane pressure can increase substantially because of fouling. In addition, fouling increases downtime and may shorten membrane life-span. There is also a high level of biological activity resulting from biological treatment.

Colloidal fouling is caused by accumulation of particles and macromolecules on, in, and near a membrane. Materials accumulated on the membrane surface create an additional layer of resistance to permeation. Early work on colloidal fouling of RO membrane used to treat feedwater indicated that subparticles of 5 μm contribute more substantially to fouling than larger particles (34). It was postulated that particles are subjected to higher velocity and shear force on the membrane surface as particle size increases. Therefore, larger particles tend to be swept away in bulk flow rather than deposits on the membrane surface. In addition to surface deposition, some particles may be small enough to penetrate and remain within the pores of the membrane (35). In a study on the influence of colloidal fouling on salt rejection of thin-film composite RO, a sharp decrease in permeate flux and significant decline in salt rejection with increasing concentration factor were observed under conditions in which colloidal fouling occurred (36).

The adsorption of organic matter on membrane surfaces is detrimental to permeate flux and affects the salt rejection of membranes. The negatively charged functional groups on organic foulants have an affinity for the charged membrane surface, thereby forming a permeate-resistant layer. Organic foulants also interact with colloidal foulants. Polyphenolic compounds, proteins, and polysaccharides bind colloids and particles and increase their cohesion to the membrane surface (35). In addition, the biochemical interaction between organics and microorganisms promote biofilm formation and growth. Insufficient knowledge on the composition of dissolved organics in water makes the control of organic fouling difficult (37).

Inorganic fouling is caused by deposit of iron, silica, aluminum, calcium, phosphorus, and sulfate. The fouling mechanism on the membrane surface can be caused by the concentration polarization effect. A concentrated boundary layer is created on the separation surface as product water passes through the membrane. Within this boundary layer, the high concentration causes the salts to precipitate and suspended solids initiated the deposition on the membrane surface, thereby leading to scaling and fouling (35). Scale deposition on and into RO membranes impairs the hydrodynamic conditions of the feed flow. When fouling conditions are not controlled properly, scaling becomes

a self-sustaining phenomenon. Under severe concentration polarization, channeling, failure of RO performance, and damage to membrane surface occur.

Biofouling is the term given to the adhesion of microorganisms and growth of biofilm on the membrane surface. In addition to the detrimental effects of increasing transmembrane pressure and decreased permeate flux, biofouling may cause chemical degradation of the membrane material. This could result from direct enzymatic biodegradation of the membrane surface or by generation of extreme local pH that may hydrolyze the membrane polymer (38). Such fouling can significantly reduce the membrane lifetime.

The ratio of carbon/nitrogen/phosphorus has important influences on the rate of biofilm development (39). It has been reported that membranes that suffered severe biofouling were found to contain a high percentage (typically >60%) of organics. Laboratory characterization of membrane biofilms found that a typical biofilm contains

- 90% moisture.
- 50% total organic matter.
- Up to 40% humic substances.
- Low inorganic content.
- High microbiological counts including bacteria and fungi.

Biofouling is perhaps the most difficult fouling threat to overcome. No system operator can afford to ignore the potential for biofouling. Biological organisms include bacteria, algae, and fungi. Of these, bacteria cause the majority of problems in membrane treatment systems for a variety of reasons. Many bacteria can easily adapt to the environment inside the membrane treatment system. With the organic compounds concentrated on the membrane surface, the bacteria multiply rapidly and are rejected by the membrane. These bacteria have a number of defense mechanisms. For example, some have fimbriae, which stick out from all sides of the cell. These allow the bacteria to attach themselves, and remain attached, to the surface of the membrane or feed space. In addition, bacteria may secrete a mucous capsule, or slime, which coats the cell and protects them from any harsh elements entering their environment.

The susceptibility of membranes to biological fouling is significantly dependent on the membrane composition. CA membranes are easily attacked by bacteria. Disinfection of feed water is required for such membranes. PA membranes are also susceptible to bacterial attack, but TFC membranes are generally quite resistant. Chlorination can be used for CA membrane, but must be followed by dechlorination for PA and other membranes, usually by addition of sodium metabisulfate. In ultrapure water production, sterility is often maintained by ultraviolet (UV) sterilizers (66).

A recent study has shown that some RO membranes are more prone to biofouling than others. The study involved a bioadhesion assay which utilizes a model bacterium, SW 8, known to adhere to membranes. Examination of bacteria adhered to the membranes using optical microscopy revealed that membranes that are less susceptible to bioadhesion are hydrophilic in nature (38). Further investigation carried out on RO simulators that consist of flat sheet membranes to simulate spiral wound module revealed biofilm characteristics under field emission scanning electron microscope. Microorganisms cover the surface of all types of RO membranes used in the experiment to a density of about 2.25×10^8 cells/cm^2 (38). Bacteria of different shapes (mostly rod

shaped) with dimensions between 1 and 3 µm were observed. The organisms appeared to excrete extracellular polymeric substances (EPS).

Understanding membrane fouling creates the foundation for researchers to devise an approach to counter or minimize fouling in order to maintain high RO performance. One strategy to alleviate membrane fouling is feed pretreatment to reduce or remove fouling constituents in the feed. A proper membrane cleaning and regeneration protocol to periodically remove foulants from the membrane surface is also essential in maximizing RO efficiency.

4.2. Feed Pretreatment

The success of RO process is highly dependent on appropriate feed pretreatment. Pretreatment must be effective in reducing RO fouling potential in a reliable and consistent manner. Feed pretreatment continues to be extensively studied. In the development of a pretreatment program, the focus is on removing as many fouling constituents in the feed water as possible before RO processing. The feedwaters are pretreated to extend the lifetime of the membrane, prevent fouling of the membranes, and maintain performances (i.e., salt rejection and recovery) of the system (40).

There are some important indicators related to membrane fouling and feedwater pretreatment. Among them, turbidity and salt density index (SDI) are often used in the RO industry as the indicator of suspended particles. The recommended limitation values are 1 NTU and 4 for turbidity and SDI, respectively. Continuous operation of an RO system with feed water, which has turbidity or SDI values near the limits of these values may result in significant membrane fouling. For long-term reliable operation of the RO unit, the average values of turbidity and SDI in the feed water should not exceed 0.5 NTU and 2.5 SDI units, respectively. Langelier saturation index (LSI) and the saturation ratios are the indicators of saturation levels of sparingly soluble salts in the concentrate stream. The LSI provides an indication of the calcium carbonate saturation. Negative LSI values indicate that the water is undersaturated with respect to calcium carbonate. Undersaturated water has a tendency to remove existing calcium carbonate protective coatings in pipeline and equipment. Positive LSI values indicate that the water is supersaturated with respect to calcium carbonate and scaling may occur. The LSI was originally developed by Langelier for potable water of a low salinity. For high salinity water encountered in RO applications, the LSI is an approximate indicator only. The saturation ratio is the ratio of the actual concentration of the ions in the concentrate stream to the theoretical solubilities of the salts at given conditions of temperature and ionic strength. These ratios are applicable mainly to sparingly soluble sulfates of calcium, barium, and strontium.

4.2.1. Conventional Pretreatment

RO desalination was pioneered using conventional treatment processes to upgrade product water quality. Generally, the conventional pretreatment process for RO application usually includes many interdependent pretreatment stages such as disinfection, coagulation/flocculation, sedimentation/filtration, dechlorination, and scale control.

4.2.2. Disinfection

The goal of disinfection is to prevent and/or control the colonization of microorganisms within the membrane modules and other parts of the RO desalination process from

the intake to the discharge. Chlorination, sodium hypochlorite, formaldehyde, iodine, ozone, copper sulfate, and UV light have been used in disinfection. On the choice of the disinfectant to use, it is best, in theory, to alternate between different disinfectants in case a resistant strain of bacteria develops. A better reason for opting to use different chemical agents is for their individual characteristics. For example, one may be more aggressive at attacking biofilm and result in a gelatinous material secreted by bacteria in order to protect themselves from chemicals and to create an endless food supply whereas another can prevent growth of bacteria in RO systems. Disinfection is also partially accomplished by using conventional water pretreatment processes such as coagulation/flocculation, sedimentation, and filtration.

4.2.3. Coagulation/Flocculation

The process of coagulation and flocculation is applied to separate suspended solids (colloids) in water when small particles are combined into larger particles, which settle out of the water as sediments. This is usually achieved by addition of chemicals such as alum, ion salts, and high-molecular weight polymers. For example, aluminum sulfate and ferric chloride as coagulants were examined for seawater (41). Results showed that the best clarification was found using aluminum sulfate dosages of 20–30 mg/L with an anionic polyelectrolyte flocculant aid at 0.025–0.1 mg/L. Another study showed that the seawater turbidity could be effectively removed by all tested coagulants of aluminum sulfate, ferric chloride, and electrolytic aluminum. Ferric chloride was recommended in the pretreatment of seawater because less of it remains in the treated seawater than aluminum over a wide pH range. Similarly, electrolytic aluminum was found to be ideal for turbidity removal of brackish water (42).

Although coagulation/flocculation is a very effective pretreatment for removing colloidal and suspended matter, the process is expensive as chemical dosage is required. The process is also difficult to operate because optimum dosage depends on influent quality. Furthermore, the coagulation–clarification process generates solid waste that requires additional handling and disposal. In cases where overdosage occurs, high metal salt content of the pretreatment water may result in metal hydroxide precipitation on the subsequent RO membranes (43).

4.2.4. Sedimentation and Filtration

In sedimentation, suspended solids in the water are removed by gravitational settling. The settling rate of particle depends on their size and density as well as the density of the water. Filtration is the most common pretreatment to reduce membrane fouling by particular matters. The most common media filters are silica sand and crushed coal (anthracite). The selection of filter design depends very much on the required quality of effluent.

4.2.5. Dechlorination

Because of high sensitivity of polymide membranes to chlorine, dechlorination is usually achieved by addition of sodium bisulfite ($NaHSO_3$). The problem related with this approach is that the solution itself becomes an incubator of bacteria, causing biofouling of the membranes. In some cases, granular-activated carbon is used to remove chlorine, whereas it can also serve as an incubator of bacteria because of their porous structure and nutrient-rich environment. Recently, UV treatment has become an increasingly popular

dechlorination technology with none of the aforementioned drawbacks. UV light produces photochemical reactions between 180 and 400 nm that dissociate free chlorine to form hydrochloric acid. The peak wavelengths for dissociation of free chlorine range from 180 to 200 nm, whereas the peak wavelengths for dissociation of combined chlorine range from 245 to 365 nm. The UV dosage required for dechlorination depends on adsorption of UV in the water, total chlorine level, ratio of free vs combined chlorine, background level of organics, and target reduction concentrations.

4.2.6. Scale Control

Scaling potential salts often encountered in RO are calcium carbonate, calcium sulfate, silica, calcium fluoride, and strontium sulfate. Calcium carbonate scaling can be controlled by addition of acid such as sulfuric acid. Sodium hexametaphosphate (SHMP) is commonly used to inhibit calcium sulfate. Silica is usually controlled either by decreasing the recovery ratio or by chemical pretreatment. In seawaters and most brackish waters, the concentration of Sr^{2+} is quite low compared with Ca^{2+}. In situations, where there is a potential for both calcium-based and strontium-based scales formation, the amount of $CaSO_4/CaCO_3$ scale formed is so large compared with $SrSO_4/SrCO_3$ scale that the latter is not a significant factor in scale inhibition.

The efficiency of SHMP as scale inhibitor to prevent calcium sulfate scale growth has been evaluated (44). It was shown that SHMP at 5 ppm resulted in a significant increase in the calcium sulfate solubility. However, increasing the SHMP dosage to 20 ppm did not result in a corresponding increase in the solubility. The effectiveness of a polyelectrolyte-based antiscalant, commercially known as AF-400, with SHMP for the control of calcium sulfate scale was compared (45). It was shown that the induction period increased with the increase of AF-400 dose level. At 2 ppm, the crystallization of calcium sulfate was completely inhibited for at least 2 h. At 0.5 ppm, the induction period achieved with AF-400 was about twice as long as that with SHMP.

The effectiveness of four scale inhibitors (ethylene maleic anhydride, acrylate, acrylic acid, and phosphonate) was studied in modifying crystal growth of $CaCO_3$. The presence of these inhibitors in ppm quantities significantly altered crystal growth of $CaCO_3$; the normal rhombohedral form was changed to a needle-like structure. The inhibitor was believed to have inhibited the crystal growth by adsorbing on to the fast growing crystal face. In another study, hydroxyethylidene diphosphonate was found to be most effective against $CaCO_3$ scale among four phosphonate-based scale inhibitors (46).

Another pilot scale study showed that the conventional $SHMP + H_2SO_4$ inhibitor outperformed a so-called advanced antiscalant, consisting of a polyacrylate and hydroxyethylidene diphosphonate, for the treatment of brackish water (47). The study was carried out in two identical hollow fine fiber RO units under the same feed pressure (27.6 bar) and product water recovery (70%). The pumping energy and scale control treatment costs (as USD/m^3 of water produced) were the same for the two treatment units. However, in terms of salt rejection, product TDS, and output, the performance of the advanced antiscalant was inferior. After 3000 h the salt rejection of unit with the advanced antiscalant was about 81 vs 94% for unit with $H_2SO_4 + SHMP$. Similarly, in 3000 h the former unit produced 20% less water of unacceptable quality (620 ppm) whereas the latter unit produced more water of excellent quality (180 ppm).
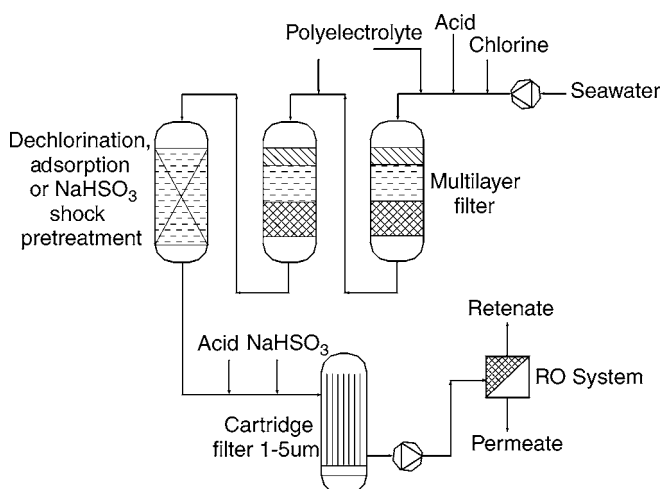
Fig. 10. Pretreatment flow scheme for seawater RO plant.

An example of a complete pretreatment flow scheme for seawater RO plant is shown in Fig. 10 in which water is controlled for pH, scale, particulates, and biological fouling.

4.2.7. Membrane Pretreatment

Conventional pretreatment methods have been used in RO desalination plants for many years. This system is less expensive than the membrane separation system, although the quality of the filtrate is inferior and highly inconsistent. In comparison with conventional pretreatment, MF and UF membrane processes consistently can produce filtrate of a better quality. The membrane separation system is also able to remove viral or microbial contaminants and micropollutants such as agricultural chemicals that conventional pretreatment system is unable to deal with. The ease of operation of the membrane pretreatment processes is also a major advantage. Moreover, membrane pretreatment systems generally require less space and fewer chemicals compared with a conventional pretreatment system. Together with improved maintenance procedures such as filtrate backwashing and air scouring, complete flux and pressure recoveries are achievable with minimal use of chemicals. The RO desalination pretreatment systems that utilize MF and UF membranes have started to take the place of conventional pretreatment in public water supply systems and the benefits of these systems are being felt.

The performance of conventional media-filtration and membrane filtration techniques were studied in an RO desalination process (48). For the membrane filtration techniques, two UF and one MF pilot plants were used in the experimental study. During the experiments, the SDI of the filtrate samples was regularly measured to quantify the performance of pretreatment systems in rejecting colloidal particles. Measurements of other important parameters consist of filtrate flux, transmembrane pressure, total suspended solids, colloidal silica, and total organic carbon. The results showed that the quality of the filtrate produced by the conventional media-filtration technique was inferior and highly inconsistent. SDI of the filtrate varied from 2.8 to 3.8 and spikes as high as 6.3 were frequently observed. Membrane pretreatment produced

filtrate of a better quality; SDI of the filtrate produced was consistently less than 3, a prerequisite for proper operation of an RO desalination plant.

The competitiveness of UF pretreatment over conventional pretreatment was assessed by evaluating the impact on RO hydraulic performances (49). The study showed that UF provided permeate water with high and constant quality resulting in a higher reliability of the RO process than with a conventional pretreatment. The surface seawater of 13–25 SDI was reduced to less than 1, whereas the conventional pretreatment failed to reduce it to less than 2.5. The combination of UF with a precoagulation at low dose helped in controlling the UF membrane fouling and providing filtered water in steady-state conditions. The performance of RO membranes, downstream UF, exceeded the usual operating conditions encountered in seawater desalination. The combined effect of higher recovery and higher flux rate significantly reduced the RO plant costs.

A study was performed to investigate MF and UF pretreatment performances in treating a broad range of water for RO desalination (50). The results of 2 yr testing showed that MF gave the best solution for the pretreatment of raw water to produce infiltration water. The effective mean filtrate production of the pilot plant is higher than for the other systems that were tested, and the amount of chemicals needed in the process is much lower owing to the effectiveness of the air backwash system. The quality of the filtrate produced with UF membranes was slightly better compared with the filtrate produced with MF membranes. A demonstration experiment using 35 pilot scale MF and UF plants showed that there is no significant difference in membrane filtrate quality and energy consumption between MF and UF membranes. No coliforms were found in the filtrates (42).

MF and UF are capable of reducing biofouling tendency in RO membrane as they pose a physical barrier to these microorganisms. MF is capable of removal of protozoa (approx 10 μm), coliform (approx 1 μm), and cysts (approx 0.1 μm). The pore size of UF is smaller and thus can further remove viruses (approx 0.01–0.1 μm) (51). It has been shown that the indicator organisms *Escherichia coli* and spores of sulfite reducing *Clostridia*, present in conventionally treated water, could be reduced by UF to values below the detection limit (52). The application of membranes thus reduces the used dosage of aggressive chemicals such as chlorine and ozone, thereby minimizing or avoiding the production of undesirable disinfection byproducts. The interest in using membrane as part of the disinfection process has intensified with the emergence of chlorine-resistant pathogens. Chlorine-resistant *Cryptosporidium parvum* has been reported to cause outbreak of diarrhoea epidemic in United States and United Kingdom. Water supply authorities are looking to UF and MF application to act as an absolute barrier to *Cryptosporidium oocysts*, which range from 4 to 6 μm (53).

The use of MF membrane as pretreatment also allows the use of TFC RO membrane instead of CA RO membrane. TFC membranes are anisotropic membranes with a porous sublayer supporting a very thin top layer ranging from 0.1 to 0.5 μm in thickness. Such membranes have higher flux compared with thicker isotropic membranes, as flux is inversely proportional to the thickness of the membrane (54). TFC membranes have higher solute rejection capability and can be operated at lower pressure (55).

Chlorination of feed water prior to membrane pretreatment may extend membrane run times between clean. Over 90 h of MF operation was achieved with prechlorinated feed water compared with 42 h operation reported when feed water was not chlorinated (56).

Similar observation was reported with dosage of chloramine prior to MF pretreatment (50). It was speculated that preoxidation resulting from chlorination altered the chemistry of EPS produced by the microorganisms in the feed water. This could weaken the attachment of the EPS on the membrane and thus offset the detrimental effect on the membrane flux. However, care must be taken to verify the compatibility of membrane with chlorination as some membranes are not tolerant to the aggressive action of chlorine.

4.3. Membrane Cleaning and Regeneration

Fouling is almost an inevitable consequence of the nature of the RO process itself even when good pretreatment is employed. Furthermore, the high operating pressures compress the membrane and cause a further loss of membrane properties. During operation, symptoms of fouling would include one or all of the following conditions:

a. Normalized water flow has decreased by 10–15% from startup (reference) conditions.
b. Pressure drop over a stage or the system has increased by 10–15%.
c. Salt rejection has decreased significantly over time.

The challenge is therefore to reduce and control fouling sufficiently to minimize the rate of RO flux decline and prolong membrane lifetime. This can be accomplished by a combination of good feed pretreatment as aforementioned and membrane cleaning programs.

Periodic cleaning is essential to improve the performance and to prolong the life of RO membranes. Cleaning methods used for RO membrane restoration could be broadly categorized into two types: chemical and physical.

4.3.1. Chemical Cleaning Methods

Most membrane manufacturers recommend chemical methods for membrane cleaning and regeneration. Chemical cleaning methods depend on chemical reactions to weaken the cohesion forces between the foulants and the adhesion forces between the foulants and the membrane surface. Chemical reactions involved in cleaning include hydrolysis, peptization, saponification, solubilization, dispersion, chelation, sequestering, and suspending. The choice of chemical cleaning agents not only depends on the type of foulants present in the membrane system but also on the chemical resistance of the membrane material and the whole system. Caution must be taken in applying these chemicals as the aggressive nature of these chemicals may adversely affect the system or membrane integrity when not applied properly. This is especially true for aromatic PA membranes, which are less robust than CA and polysulfone membranes. For example, some cationic and nonionic surfactant may be adsorbed onto PA membranes and cause a flux decrease. PA membranes are also not resistant to the strong oxidizing actions of disinfectants such as hydrogen peroxide and hypochlorite. Acid used to clean the membrane system must be rinsed out thoroughly before application of hypochlorite for disinfection because hypochlorite at low pH can cause corrosion in stainless steel. The pH of the chemical cleaning solution must fall within the tolerable range of pH 1.0–13.0 for polysulfone membranes and pH 3.0–8.0 for CA membranes (57). Generally, chemicals used for cleaning membranes should ideally posses the following desirable properties:

a. Loosen and dissolve foulants from membrane surface.
b. Keep foulants in dispersed and soluble form.

   c. Avoid fresh fouling.
   d. Do not cause damage to membrane material.
   e. Easily rinsed away after cleaning.
   f. Chemically stable before, during, and after use.
   g. Cost effective.

Table 3 summarizes common fouling factors and cleaning and control methods. The cleaning procedures may vary depending on the situation, but the basic steps of chemical cleaning are:

   a. Make up the cleaning solution as per the manufacturer's instructions.
   b. Perform a low-pressure flush with permeate water or cleaning solution to displace the solution in the vessels, the process water can be dumped to drain until the cleaning solution has filled the vessels.
   c. Recycle the solution through the elements and back to the tank. During operation, part of the cleaning solution is dumped to drain before returning back to the RO cleaning tank. Readjust the pH to the target when it changes more than 0.5 pH units.
   d. An optional soak and recirculation sequence can be used. The soak time can be from 1 h to overnight depending on the manufacturer's recommendations. Additional recirculation of cleaning solutions at a high flow will help to displace the foulants from the membrane.
   e. A low-pressure cleaning rinse with permeate water is required to remove all traces of chemical from the cleaning skid and the RO skid.

Once all the stages of a strain are cleaned, the RO can be placed back into service. It is usual for it to take from a few hours to a few days for the RO permeate quality to stabilize, especially after high pH cleanings.

Frequent and appropriate cleaning procedures are vital in order to maintain the performance of RO membranes. Although the procedures may be similar, in many cases, the cleaning solution concentrations, volumes of solution, and stages of cleaning will differ. The frequency of cleaning will be determined by the rate of fouling. The main factors which influence the effectiveness of membrane cleaning are (58):

   • Type of cleaning chemicals used.
   • Cleaning solution volume (it must be appropriate for the size of plant).
   • Contact time (soaking of membranes in solution can aid cleaning).
   • Temperature (cleaning chemicals are most effective at warm temperatures).
   • Design of the cleaning circuit and operating parameters.

Although chemical cleaning agents are categorized with respect to their action on different types of foulants, their combined effects are much more complex. These cleaning agents may interfere with the cleaning effects of each other. Some may provide efficient control over particular foulants while adversely affecting fouling control of another foulants. For example, some cationic polymer whereas effective in silica scale inhibition, reduces calcium carbonate scale inhibition by 30–40% (59). Humic and fulvic acid act as good calcium scale inhibitor but they promote biofouling in the membrane system.

A membrane restoration program was conducted at the site of a large (>3 MGD) RO brackish water desalting plant (60). The procedure applied consisted of low pressure flushing with acidic (pH 4.0) solution of 2% citric acid with ammonia followed by alkaline (pH 10.5) flush with NaOH solution. Before and after applying each cleaning solution, the elements were thoroughly flushed with product water. After that a tannic acid solution

Table 3
Summary of Fouling Factors and Methods to Clean and Control

Fouling factors	Effects on RO performances	Methods for cleaning and controlling fouling
Scales		
Precipitation of soluble salts (minerals), for example, $CaCO_3$, $CaSO_4$, $MgCO_3$, $MgSO_4$, $BaSO_4$, $SrSO_4$, SiO_2, $Fe(OH)_3$	Major loss of salt rejection Moderate increase in differential pressure Slight to moderate flow loss Effects usually occur in last stage or element	Clean with citric acid or EDTA-based solution Clean silicate-based foulants with ammonium bifluoride solutions Reduce recovery Adjust pH Use antiscalant
Colloids		
Agglomeration of suspended matter on the membrane surface, for example, clay or silt particles, often organic and inorganic constituents	Significant increase in differential pressure Moderate flow loss Moderate loss of rejection Effects usually occur in first stage or element	Clean with chelants or detergents at high pH Clean silicate-based foulants with ammonium bifluoride solutions Improve prefiltration Increase feed flow Reduce recovery
Organics		
Attachment of organics, for example, fats, oils, grease, hydrocarbon compounds, synthetic coagulants, and flocculants	Rapid and significant flow loss Stable or moderate increase in salt rejection Generally, no or slight increase in differential pressure	Difficult to clean Prefiltrate with granular active carbon High pH soaks effective for some organic types
Biological		
Formation of bio-growth on membrane surface, for example, sulfur reducing bacteria, mycobacterium	Rapid and major loss of production Moderate but rapidly increasing differential pressure Slight to moderate increase in passage Effects occurs slowly	Clean with commercial detergents or EDTA-based solutions at high pH Add solution bisulfate Chlorinate with or without activated carbon filtration

(100 ppm) was applied at the pressure of 300 psi for hollow fiber elements and 400 psi for spiral wound elements. The average salt passage of hollow fiber elements was about 14% before cleaning. Following the restoration it was reduced to 6–10% and was maintained at that level for several thousand operating hours by applying continuous online treatment. The reduction of salt passage was accompanied by a decrease of about 10% in productivity. Similar treatment results were observed with the PA, spiral wound elements, which had a salt passage in the range of 14–24%. As a result of the treatment, an average decrease in salt passage of 40%, accompanied with a tolerable (approx 10%) decrease of productivity, was obtained. The treated spiral wound elements were reinstalled in the desalting unit and operated for over a 1000 h with no significant increase of salt passage.

The 28,800 gal/d RO system consisting of five cellulose triacetate hollow fine fiber permeators in a 3/2 array was cleaned by the combination of FLOCLEAN 103, a low pH liquid formulation for removal of carbonates and metal hydroxides, and FLOCLEAN 107, a neutral pH liquid formulation designed to remove organic, silt, and other particulates from CA membranes. It was found that differential pressure of the membrane system could be reduced by 42% and the permeate flow was increased by 6.4%. The TFC membrane can withstand the higher pH of this formulation without concern about hydrolytic degradation, and a high pH is generally conducive to removal of colloidal soils. Another RO system equipped with the TFC membrane was cleaned by FLOCLEAN 411, a high pH formulation designed to remove organics, silt, and other particulate deposits from PA, polysulfone, and TFC membranes. It resulted in an excellent improvement in permeate flow. After cleaning, the membrane produced desired recovery at a lower feed pressure. The differential pressure was reduced by 16.7% and the permeate flow was increased by 23.8% (61). Another pilot scale study demonstrated the outperformance of some commercial cleaners over the membrane manufacturer's recommended recipe of 2% citric acid at pH 4.0 for cleaning seawater RO membranes (62). For example, percentage improvement in nominal product flow achieved with Floclean 403 and 411 from Pfizer was 11.6–30.8% higher than those with citric acid.

Systems with chlorination prior to the membrane processes were easier to clean because of the presence of chloramines, which act as a disinfectant and reduce the tendency of biofouling. However, membranes in such a system are more susceptible to structural damage because of prolong exposure to the aggressive action of the combined chlorine. CA membranes are reported to become more brittle when chlorine dosage was in the range 15–20 mg/L (63). It was also suggested that certain organochlorine derivatives might modify the molecular structure of the membranes, thus resulting in flux decline and decreased salt rejecting efficiency.

4.3.2. Physical Cleaning Methods

Physical cleaning methods depend on mechanical forces to dislodge and remove foulants from the membrane surface. Physical methods used include forward flushing, backward flushing, backwashing, vibrations, air sparge, and CO_2 back permeation.

4.3.2.1. FORWARD FLUSHING

The purpose of a forward flush is the removal of a constructed layer of contaminants on the membrane through the creation of turbulence. A high hydraulic pressure gradient

is in order during forward flush. When forward flush is applied in a membrane, the barrier that is responsible for dead-end management is opened. At the same time the membrane is temporarily performing cross-flow filtration, without the production of permeate.

4.3.2.2. Backward Flushing

Permeate is always used for a backward flush and the backward flush pressure is about 2.5 times more than the production pressure. The pressure on the permeate side of the membrane is higher than the pressure within the membranes. The pores of a membrane are flushed inside out resulting from the higher pressure on the permeate side of the membrane than that within the membranes.

4.3.2.3. Air/Water Flush

Air is added to the forward flush to form air bubbles causing turbulence which removes the fouling from the membrane surface. The benefit of the air flush over the forward flush is that it uses a smaller pumping capacity during the cleaning process.

4.3.2.4. Permeate Back Pressure

The pressure added on the product side reverses the normal water transport across the membrane. At the same time, the materials dislodged from the surface are carried away by the feed to brine flush simultaneously.

4.3.2.5. Vibration

The permeator is vibrated by a pneumatic hammer device attached to the pressure vessel. The materials dislodged from the surface are carried away by the feed to brine flush simultaneously.

4.3.2.6. CO_2 Back Permeation

This method is suitable for hollow fiber configuration. A high-pressure CO_2 gas is introduced into product side through the internal fiber bores and removed through the fiber walls. The foulants lifted from the surface are carried away by a flush stream.

Seven RO cleaning methods were compared for cleaning a hollow fiber: simple forward flush, reverse flow, permeate back pressure, vibration, air drain and water refill, air sparge, and CO_2 back permeation (64). The results showed that the reverse flow technique (in which a permeator flush stream was periodically switched from a feed-to-brine to a brine-to-feed flow direction) was the most effective of the methods tested. The cleaning effectiveness of all the cleaning methods could be improved by an average of 55% with the addition of surfactants to the cleaning flush stream. Three brackish RO units using TFC membranes were studied (65).

The literature review reveals that even though some of the above physical methods, such as forward flushing and reverse flushing, seem to be economically very attractive, physical methods are not implemented widely in the RO industry. Only forward flushing with permeate water is used between cleanings, when more than one chemical cleaning agent is applied. MF and UF used in pretreatment to RO are more frequently cleaned by physical cleaning and less frequently by chemical cleaning. Chemical cleaning may be required, as physical cleaning (e.g., backwashing) does not restore the flux to the initial value and, therefore gradually the flux would decline to a level requiring a chemical wash, although chemical wash would not necessarily restore the original flux either. A study showed that MF/UF water recovery (in several stages) could be restored

between 80 and 90% by backwashing for every 40 min and chemically cleaning every 6 mo (59). In another case, a gas backwash was performed periodically to remove the particle fouling and restored the pressure of a pretreatment MF. Consequently, the period between backwash cycles varied typically from 5 to 20 min with different source water. By a rapid flow of gas through the membrane wall (from inside to outside), the solids were removed from the outer surface of the membrane. However, a gradual accumulation of foulants still occurred over time. A periodic chemical cleaning of the membranes was performed every 2–7 d. This comprised an acid and caustic clean every 2–7 d. It was found that the mean recovery during the whole period of testing was 80–83% (50).

5. CASE STUDY

The Cape Coral water treatment system is one of the largest reuse systems for residential use in the United States (64,65). The total system includes two RO plants with total production capability of 15 MGD. The design features of the RO facilities are listed in Table 4. Well water is used as the feed water with quality listed in Table 5. The water treatment system treats the raw well water to meet the drinking water standards of both the US Environmental Protection Agency, and the Florida Department of Environmental Protection. The unit operations and unit processes include: acidification, scale prevention, cartridge filtration, RO, degasification, disinfection, and neutralization (64,65).

5.1. Acidification and Scale Prevention for Pretreatment

With applications of sulfuric acid for acidification, and a scale inhibitor (Flocon-100 Antiscalant) for scale prevention, certain impurities in raw well water can be kept in the liquid form prior to the subsequent water treatment processes. Sulfuric acid feed systems are designed to directly apply a 98% solution to the raw well water through a metering system that includes standby metering pumps. Complete dispersion of scale inhibitor (Flocon-100) is accomplished in very little time (in seconds) and with appropriate velocity gradients. The velocity gradient is related to the amount of energy imparted to the water during mixing of water and scale inhibitor (65).

5.2. Cartridge Filters for Prefiltration

After pretreatment by acidification and scale prevention, the raw well water becomes the feed water. The feed water then passes through a series of cartridge filters for removing suspended particulates, such as microbes, dirt, sand, silt, and turbidity. Cartridge filtration is considered as an emerging technology suitable for removing suspended matter from water. These cartridge filters are similar to the swimming pool filters and are mechanically simple for easy operation.

The cartridge filters use ceramic or polypropylene microporous filter elements that are packed into pressurized housings. They are operated by the physical process of straining the water through porous filter elements and can exclude particles down to less than 1 μm. The ease of operation and maintenance of cartridge filters makes them very attractive for small water systems with treatment capacity equal to or below 15 MGD (65).

5.3. Reverse Osmosis

In the Cape Coral RO operations, spiral membranes are used in all 18 production units (Table 4). Ten of these production units operate at 234 psi. Eight of the newer generation

Table 4
Design Features of the Cap Coral Water Treatment System

Plant data	PLANT 1	PLANT 2
Production capability	6 MGD	9 MGD
Raw water supply	Lower Hawthorn aquifer	Lower Hawthorn aquifer
	Brackish water	Brackish water
	10 Wells (approx 700 ft deep)	12 Wells (approx 700 ft deep)
Production unit data		
Number of production units	10	8
Operating RO pressure	250 psi	160 psi
Recovery (%)	75	85
Pressure vessel array	10 (first stage)	16 (first stage)
	7 (second stage)	8 (second stage)
	4 (third stage)	
Number of elements/vessel	4	7
Number of elements/production unit	84	168
Membrane element data		
Manufacturer	Fluid systems	Hydranautics
Model number	8021 LP	8040-LSY-CPA2
Configuration	Spiral wound	Spiral wound
Type	Thin film composite	Thin film composite polyamid
Minimum salt rejection (%)	97.5	99

Adapted from refs. 64 and 65.

Table 5
Water Quality in the Cape Coral Water Treatment System

Parameters	Raw water	RO reject	Plant effluent
pH	7.7	6.8	8.8
Total hardness as calcium carbonate	500 ppm	2500 ppm	80 ppm
Calcium hardness as calcium carbonate	190 ppm	850 ppm	30 ppm
Magnesium hardness as calcium carbonate	310 ppm	1650 ppm	50 ppm
Conductivity	2400 ms/cm	9000 ms/cm	575 ms/cm
Total dissolved solids	1534 ppm	6390 ppm	313 ppm
Chlorides	600 ppm	2550 ppm	150 ppm
Fluorides	2 ppm	1.6 ppm	0.7 ppm
Residual chlorine			1.82 ppm
Turbidity			0.66 NTU

Adapted from refs. 64 and 65.

spiral membranes operate at 160 psi. About 12.6% of the cartridge filter effluent becomes the "bypass stream," which bypasses the RO units and goes to the posttreatment facilities directly. The remaining about 87.4% of the cartridge filter effluent becomes the "feed water," which is fed to the RO units for RO membrane filtration and subsequent posttreatment. The average pH of the cartridge filter effluent or the feed water (after pretreatment and cartridge filtration) is 5.9 (65).

The capability of RO for removal of 97–99% of salts, color, bacteria, virus, colloidal suspensions, and other toxic organic and inorganic substances has been demonstrated. The RO units at the Cape Coral water treatment system are mainly used to remove chlorides (salts), total hardness, and many other undesirable substances. The average chlorides are reduced from 600 to 62 ppm. The product water is then blended with influent feed water, bringing the chlorides up to 150 ppm. It is important to note that finished water is blended with 10–15% influent feed water. Normal drinking water should not have more than 250 ppm of chlorides as mandated by the Florida Department of Environmental Regulation. Therefore, the chloride concentration at the level of 150 ppm (15 mg/L) is acceptable. The total hardness can be reduced from 500 ppm (as calcium carbonate) to 80 ppm (as calcium carbonate) after blending.

After RO treatment, between 15 and 25% of the influent feed water becomes the RO reject which is discharged into a receiving salt water lake. The average characteristics of the RO reject or brine concentrate are listed in Table 5. This highly concentrated RO reject is discharged from the RO system by way of the brine line, and is also called the "waste stream." The brine concentrate, treated with chlorine and oxygen to maintain environmental standards, although highly concentrated with impurities, sustains a concentration lower than that of the salt water lake it empties into. The brine is evenly diffused throughout the lake using an intricate series of submersed spray nozzles. The brine or RO reject is not drinkable nor is suitable for irrigation because of the high salt and impurity concentration (65).

After RO treatment, between 75 and 85% of the feed water becomes the RO product water which has low concentrations of total hardness, conductivity, total dissolved solids (TDS), chlorides, and fluorides. The RO product water is also called "permeate stream" (65).

5.4. Neutralization and Posttreatment

The RO product water (i.e., the permeate stream) and the bypass stream are both further treated with an air stream by degasification for removing hydrogen sulfide and carbon dioxide gases at low pH. The principal design considerations for the degasification process (also known as the "aeration" process) are air-to-water ratio, number of degasifiers, and hydraulic loading rate. Removal efficiency of degasification improves with increases in air-to-water ratios and increasing number of degasification units.

Finally, chlorine (10 ppm) and sodium hydroxide (40 ppm) are dosed as the disinfectant and neutralizing agent, respectively. Chlorine is an excellent disinfectant and oxidant. It provides a stable residual for the water distribution system. Average free residual chlorine and average plant effluent turbidity are 1.82 ppm and 0.66 NTU, respectively. The City's RO Water Treatment Facility has been designed to use liquid

Table 6
Water Production Cost (1996) (65)

Items	Cost (USD/1000 gal)
Sulfuric acid (130 ppm)	0.03
Scale inhibitor (3 ppm [Flocon-100])	0.03
Chlorine (10 ppm)	0.01
Sodium hydroxide (40 ppm)	0.03
Electricity power	0.34
Labor cost	0.19
Miscellaneous	0.1
Total	0.73

sodium hydroxide for finished water neutralization. The plant feeds a premixed 50% solution containing 6.38 pounds of sodium hydroxide/gal.

The average characteristics of the finished water (the plant effluent) after the post-treatment of degasification, chlorination, and neutralization are listed in Table 5. However, it should be noted that the TDS removal efficiency of RO is very high. Average TDS concentration of the RO produced water (i.e., permeate stream) is only 111 ppm. The higher TDS concentration (313 ppm average) in the finished water (i.e., plant effluent) is mainly contributed by the bypass stream as well as the chemical addition in the post-treatment steps (65). Recent RO and NF developments can be found in the literature (66–68).

5.5. Total Water Production Cost and Grand Total Costs

In 1996, the average water production cost is estimated to be USD 0.73 per 1000 gal of water produced (Table 6). Its cost includes chemical treatment, operating labor, power consumption, and miscellaneous plant administration. Typical chemicals required include 130 ppm of sulfuric acid, 3 ppm of scale inhibitor (Flocon-100), 10 ppm of chlorine, and 40 ppm of sodium hydroxide. Normally between 10 and 20 full-time employees (Chief operators, technician, analyst, supervisor, mechanic, and electricians) are needed to work on site at the plant (65).

The grand total cost includes water production, RO membrane replacement, and capital investment, and it is estimated to be USD 1.25/1000 gal of water produced.

NOMENCLATURE

ΔC	Solute concentration difference across membrane
$\Delta \Pi$	Osmotic pressure across membrane (atm)
ρ_w	The density of the solvent (kg/m^3)
Δp	The transmembrane pressure difference
Δx	The thickness of the membrane
ΔP	Transmembrane pressure
σ	A measure of the solute–water coupling within the membrane and may often be treated as 1
Π	Osmotic pressure (force/length^2) (psia or atm)

ε	Porosity of the membrane
$\sum \overline{m}_i$	The summation of molalities of all dissolved ions and nonionic species in the solution, M
A_s	The solute permeability constant $= D_s K_s / \Delta x$
A_W	The solvent permeability constant $= P_w / \Delta x$ (m/s)
C_S	Average concentration of solute = summation of molalities of all dissolved ions, moles/length^3
C_s^I	The concentration of the solute in the feed solution on the membrane surface (kg/m^3)
C_s^{II}	The concentration of the solute in the permeate solution (kg/m^3)
D	Diffusivity
D_s	The diffusivity of the solute
J_s	Solute flux (kg/s–m^2)
J_w	Solvent flux (kg/s–m^2)
K_s	The solute distribution coefficient between the solution and membrane phase
L_p	A coefficient
$P_{\text{concentrate}}$	The hydrostatic pressure of the concentrate
P_{feed}	The hydrostatic pressure of the feed
P_{permeate}	The hydrostatic pressure of the permeate flow
P_w	The solvent permeability
R	The ideal gas constant force-length/mass-temperature
R	The solute rejection value, dimensionless
T	The absolute temperature (K)

REFERENCES

1. S. Sourirajan, *Reverse Osmosis,* Academic Press, New York, 1970.
2. S. Loeb and S. Sourirajan, Sea water demineralization by means of a semipermeable membrane. UCLA engineering report 60-60, University of California, Los Angeles, LA, 1960.
3. H. E. Podall, Reverse osmosis, in *Recent Developments in Separation Science*, Vol. 2, N. N. Li (ed.), CRC Press, Cleveland, Ohio, pp.171–203 (1972).
4. H. Sun-tak and K. Kammermeyer, Membrane in separations, in *Techniques of Chemistry*, Vol. 7, John Wiley and Sons, New York, 1975.
5. T. Matsuura, P. Blais, L. Pageau, and S. Sourirajan, Parameters for prediction of reverse osmosis performance of aromatic polyamide-hydrazide (1:1) copolymer membranes. *Indus. Eng. Chem. Process Design Dev.* **16**, 361–372 (1977).
6. S. Sourirajan, Reverse osmosis—a new field of applied chemistry and chemical engineering, Plenary lecture at ACS symposium on synthetic membranes and their applications. San Francisco, California, CA, 1980.
7. E. D. Howe, *Fundamentals of Water Desalination*, Marcel Dekker, Inc., New York, NY, 1974.
8. L. T. Rozelle, J. E. Cadotte, K. E. Cobian, and C. V. Kopp, Nonpolysaccharide membranes for reverse osmosis: NS-100 membranes, in *Reverse Osmosis and Synthetic Membranes, Theory-Technology-Engineering*, S. Sourirajan (ed.), National Research Council, Canada, pp. 249–312 (1977).
9. D. Mukherjee, A. Kulkami, and W. N. Gill, Flux enhancement of reverse osmosis membranes by chemical surface modification. *J. Membr. Sci.* **97**, 231–249 (1994).
10. R. D. Noble and S. A. Stern, *Membrane Separations Technology: Principles and Applications*, Elsevier, Amsterdam, New York, NY, 1995.

11. G. Jonsson, Overview of theories for water and solute transport in UF/RO membranes, *Desalination* **35**, 21–28 (1980).
12. M. Soltanieh and W. Gill, Review of reverse osmosis membranes and transport models. *Chem. Eng. Commun.* **12**, 279–287 (1981).
13. M. Mazid, Mechanisms of transport through reverse osmosis membranes. *Sep. Sci. Technol.* **19**, 357–364 (1984).
14. W. Pusch, Measurement techniques of transport through membranes, *Desalination* **59**, 105–115 (1986).
15. J. Dickson, Fundamental aspects of reverse osmosis, in *Reverse Osmosis Technology,* B. Parekh (ed.), Marcel Dekker, Inc., New York, NY, pp.1–51 (1998).
16. R. Rautenbach and R. Albrecht, *Membrane Processes,* John Wiley & Sons, New York, NY, 1989.
17. D. Bhattacharyya and M. Williams, Theory—reverse osmosis, in *Membrane Handbook,* W. Ho and K. Sirkar (eds.), Van Nostrand Reinhold, New York, NY, pp. 269–280 (1992).
18. S. Lee and R. M. Lueptow, Reverse osmosis filtration for space mission wastewater: membrane properties and operating conditions. *J. Membr. Sci.* **182**, 77–90 (2001).
19. H. Burghoff, K. Lee, and W. Pusch, Characterization of transport across cellulose acetate membranes in the presence of strong solute–membrane interactions. *J. Appl. Polymer Sci.* **25**, 323–329 (1980).
20. S. Sourirajan and T. Matsuura, *Reverse Osmosis/Ultrafiltration Principles,* National Research Council of Canada, Ottawa, Canada, 1985.
21. T. Matsuura and S. Sourirajan, Reverse osmosis transport through capillary pores under the influence of surface forces. *Indus. Eng. Chem. Process Design and Dev.* **20**, 273–279 (1981).
22. H. Mehdizadeh, J. Dickson, and P. Eriksson, Temperature effects on the performance of thin-film composite, aromatic polyamide membranes. *Indus. Eng. Chem. Res.* **28**, 814–819 (1989).
23. D. Bhattacharyya, M. Jevtitch, J. Schrodt, and G. Fairweather, Prediction of membrane separation characteristics by pore distribution measurements and surface force-pore flow model. *Chem. Eng. Commun.* **42**, 111–123 (1986).
24. M. Jevtitch, Reverse osmosis membrane separation characteristics of various organics: prediction of separation by surface force-pore flow model and solute surface concentration by finite element method, Dissertation, D. Bhattacharyya, Director, Department of Chemical Engineering, University of Kentucky, Lexington, Kentucky, 1986.
25. E. Matthiasson and B. Sivik, Concentration polarization and fouling. *Desalination* **35**, 59–65 (1980).
26. V. Gekas and B. Hallstrom, Mass transfer in the membrane concentration polarization layer under turbulent cross flow. *J. Membr. Sci.* **30**, 153–161 (1987).
27. W. N. Gill, M. R. Matsumoto, A. L. Gill, and Y. T. Lee, Flow patterns in radial flow hollow fiber reverse osmosis systems. *Desalination* **68**, 11–28 (1988).
28. S. Kimura and S. Sourirajan, Mass transfer coefficients for use in reverse osmosis process design. *Indus. Eng. Chem. Process Design Dev.* **7**, 539–547 (1968).
29. K. K. Sirkar and G. H. Rao, Additivity between donnan salt and ion-exchanged salt in the specific conductance of membranes. *Desalination* **48**, 25–31 (1983).
30. G. Jonsson, The influence of pressure in the compaction of asymmetric cellulose acetate membranes. *Proceedings of the 6th International Symposium in Fresh Water from Sea*, Athens, 1978.
31. S. Judd and B. Jefferson, *Membrane for Industrial Wastewater Recovery and Re-use*, Elsevier Advanced Technology, Oxford, 2003.
32. T. Matsuura, Progress in membrane science and technology for seawater desalination a review. *Desalination* **134**, 47–54 (2001).

33. P. Geisler, W. Krumm, and T. A. Peters, Reduction of the energy demand for seawater RO with the pressure exchange system PES. *Desalination* **135**, 205–210 (2001).
34. B. A. Winfield, A study of the factors affecting the rate of fouling of reverse osmosis membranes treating secondary sewage effluent. *Water Res.* **13**, 565–569 (1979).
35. M. R. Weisner and P. Aptel, Mass transport and permeate flux and fouling in pressure-driven processes, in *Water Treatment Membrane Processes*, P. E. Odendaal, M. R. Wiesner, and J. Mallevialle (eds.), McGraw-Hill Company, New York, pp. 4.1–4.30 (1996).
36. S. Lee, J. Cho, and M. Elimelech, Influence of colloidal fouling and feed water recovery on salt rejection of RO and NF membranes. *Desalination* **160**, 1–12 (2004).
37. H. Winter, Control of organic fouling at two seawater reverse osmosis plants. *Desalination* **66**, 319–325 (1987).
38. S. B. Sadr Ghayeni, P. J. Beatson, R. P. Schneider, and A. G. Fane, Water reclamation from municipal wastewater using combined microfiltration-reverse osmosis (ME-RO): preliminary performance data and microbiological aspects of system operation. *Desalination* **116**, 65–80 (1998).
39. J. S. Baker and L. Y. Dudley, Biofouling in membrane systems—a review. *Desalination* **118**, 81–90 (1998).
40. S. Bou-Hamad, M. Abdel-Jawad, S. Ebrahim, A. Al-Mansour, and A. Al-Hijji, Performance evaluation of three different pretreatment systems for seawater reverse osmosis technique. *Desalination* **110**, 85–92 (1997).
41. A. Adin and C. Klein-banay, Pretreatment of seawater by flocculation and settling for particulates removal. *Desalination* **58**, 227–241 (1986).
42. Y. Taniguchi, An overview of pretreatment technology for reverse osmosis desalination plants in Japan. *Desalination* **110**, 21–36 (1997).
43. S. Ebrahim, Cleaning and regeneration of membranes in desalination and wastewater applications: state-of-the-art. *Desalination* **96**, 225–238 (1994).
44. L. B. Yeatts, P. M. Lantz, and W. L. Marshall, Calcium sulfate solubility in brackish water concentrates and applications to reverse osmosis processes; polyphosphate additives. *Desalination* **15**, 177–192 (1974).
45. Z. Amjad, Applications of antiscalants to control calcium sulfate scaling in reverse osmosis systems. *Desalination* **54**, 263–276 (1985).
46. M. M. Reddy and G. H. Nancollas, Calcite crystal growth inhibition by phosphonates. *Desalination* **12**, 61–73 (1973).
47. F. H. Butt, F. Rahman, and U. Baduruthamal, Pilot plant evaluation of advanced vs. conventional scale inhibitors for RO desalination. *Desalination* **103**, 189–198 (1995).
48. K. T. Chua, M. N. A. Hawlader, and A. Malekb, Pretreatment of seawater: results of pilot trials in Singapore. *Desalination* **159**, 225–243 (2003).
49. A. Brehant, V. Bonnelyeb, and M. Perez, Comparison of MF/UF pretreatment with conventiotial filtration prior to RO membranes for surface seawater desalination. *Desalination* **144**, 353–360 (2002).
50. E. Van Houtte, J. Verbauwhede, F. Vanlerberghe, S. Demunter, and J. Cabooter, Treating different types of raw water with micro- and ultrafiltration for further desalination using reverse osmosis. *Desalination* **117**, 49–60 (1998).
51. A. G. Fane, Membranes for water production and wastewater reuse. *Desalination* **106**, 1–9 (1996).
52. J. C. Kruithof, J. C. Schippers, P. C. Kamp, H. C. Folmer, and J. A. M. H. Hofman, Integrated multi-objective membrane systems for surface water treatment: pretreatment of reverse osmosis by conventional treatment and ultrafiltration. *Desalination* **117**, 37–48 (1998).
53. P. Hills, M. B. Padley, N. I. Powell, and P. M. Gallegher, Effects of backwash conditions on out-to-in membrane microfiltration. *Desalination* **118**, 197–204 (1998).

54. P. Aptel and C. A. Buckley, Categories of membrane operations, in *Water Treatment Membrane Processes*, P. E. Odendaal, M. R. Wiesner, and J. Mallevialle, (eds.), No. 2.1–2.24, McGraw-Hill Company, New York, 1996.

55. C. A. Buckley and Q. E. Hurt, Membrane applications: a contaminant-based perspective, in *Water Treatment Membrane Processes*, P. E. Odendaal, M. R. Wiesner, and J. Mallevialle, (eds.), No. 3.1–3.24, McGraw-Hill Company, New York, 1996.

56. D. Jolis, R. A. Hirano, P. A. Pitt, A. Müller, and D. Mamais, Assessment of tertiary treatment technology for water reclamation in San Francisco, California. *Water Sci. Technol.* **33**, 181–192 (1996).

57. G. Trägårdh, Membrane cleaning. *Desalination* **71**, 325–335 (1989).

58. L. Y. Dudley, Membrane autopsies for reversing fouling in reverse osmosis. *Membr. Technol.* **95**, 9–12 (1998).

59. R. Sheikholeslami, Fouling mitigation in membrane processes. *Desalination* **123**, 45–53 (1999).

60. M. Wilf and P. Glueckstern, Restoration of commercial reverse osmosis membranes under field conditions. *Desalination* **54**, 343–350 (1985).

61. S. I. Graham, R. L. Reitz, and C. E. Hickman, Improving reverse osmosis performance by periodic cleaning. *Desalination* **74**, 113–124 (1989).

62. S. Ebrahim and H. El-Dessouky, Evaluation of commercial cleaning agents for seawater reverse osmosis membranes. *Desalination* **99**, 169–188 (1994).

63. H. F. Ridgway, C. A. Justice, C. Whittaker, D. G. Argo, and B. H. Olson, Biofilm fouling of RO membranes—its nature and effect on treatment of water reuse. *J. Am. Water Works Assoc.* **76**, 94–102 (1984).

64. J. Johnson and M. Leahy, *Development of New Cleaning Techniques for Reverse Osmosis Membranes.* OWRT Contract 14-340-001-8519. Office of Water Research and Technology, Washington, DC, 1982.

65. L. K. Wang and S. P. Kopko, *City of Cape Coral Reverse Osmosis Water Treatment Facility.* Technical report No. NTIS-PB97-139547. US Department of Commerce, National Technical Information Service, Springfield, VA 22161, 1997.

66. L. K. Wang, *Innovative Ultraviolet, Ion Exchange, Membrane and Flotation Technologies for Water and Waste Treatment,* National Engineers Week Seminar, Training Manual, National Association of Professional Engineers and Practicing Institute of Engineers, Albony, NY, February 12–14, 2006.

67. K. Benko, J. Pellegrino, and M. K. Price, Measurement of water permeation kinetics across reverse osmosis and nanofiltration membranes—apparatus development, *J. Membr. Sci.* **270**, 187–195 (2006).

68. AWWA, *Desalination of Seawater and Brackish Water,* American Water Works Association, Denver, CO, 2006.

Emerging Biosorption, Adsorption, Ion Exchange, and Membrane Technologies

J. Paul Chen, Lawrence K. Wang, Lei Yang, and Soh-Fong Lim

Contents

INTRODUCTION
EMERGING BIOSORPTION FOR HEAVY METALS REMOVAL
MAGNETIC ION EXCHANGE PROCESS
LIQUID MEMBRANE PROCESS
EMERGING TECHNOLOGIES FOR ARSENIC REMOVAL
NOMENCLATURE
REFERENCES

1. INTRODUCTION

In the last 20 yr, the water industry has been faced with a series of great challenges. Industries have discharged wastewater that contains various new compounds. In addition, the demand for high-quality water has been significantly increasing. As a result, new water treatment technologies have been developed. In this chapter, three novel technologies are introduced. The emerging technologies for the removal of heavy metals, disinfection by-products, total organic carbons (TOC), and arsenic are illustrated.

2. EMERGING BIOSORPTION FOR HEAVY METALS REMOVAL

Sorption or adsorption is a gas–solid or liquid–solid phenomenon defined as the accumulation of particular component(s) at the surface between the two phases. Unbalanced forces of attraction between the gas or liquid and solid phases result in an increase of concentration of the particular component(s) on the solid phase. Sorption can be categorized into physical sorption and chemisorption based on the strength of these forces. Physical sorption involves only relatively weak forces, whereas in chemisorption a chemical bond is formed between the sorbate components and the sorbent components on the solid surface. In the past several decades, a dramatic increase of metal contaminant volume has posed many serious environmental problems. The most common treatment process such as precipitation and ion-exchange are usually effective in reducing the extent of contamination, but are not economical. Removal by various sorbents, such as activated carbon, has emerged as one of the most effective technologies for removing organic and inorganic pollutants from water and wastewater. The manufacture of sorbents

as well as the disposal and/or regeneration of used sorbents are always associated with higher costs. Searching for cost-effective sorbents, and modeling of the sorption process, have become the focus of attention of many researchers. One promising technique to accumulate metals is by using biopolymers and nonliving organisms as biosorbents. Biopolymers are extracted form and have similar chemical properties as nonliving organisms. The nonliving biosorbents include fungi, bacteria, and fermentation waste. The sorption process for metal removal and recovery by using biosorbents is often called biosorption.

It has been well documented that biosorbents possess a high potential to sequester and accumulate rapidly inorganic ions present in aqueous solutions. The cost is low and the process does not generate waste sludge. Furthermore, used biosorbents, after being contacted with a weak acidic solution, can be reused, and their effectiveness for metal ion removal is comparable to that of fresh biosorbents. The biosorption mechanisms include complexation, coordination, surface precipitation, chelating, and ion exchange (1–14).

2.1. Biosorption Chemistry

Biosorbents are originally from living organisms, which live in sea and fresh water. They are rich in carbon, hydrogen, oxygen, nitrogen, and phosphorus. The ligands or the functional groups in biosorbents play a dominant role in the removal of various contaminants. These representative functional groups are carboxyl, hydroxyl, sulfate, phosphate, and amine groups. Generally, the performance of a biosorption system is determined by the character of raw wastewater (e.g., pH, ionic strength, temperature, and metal species), type of biomass (e.g., capacity, kinetics, selectivity, immobilization, size, and structure), and operation factors of process (e.g., stirring speed).

Because of the presence of the functional groups, the physisorption (i.e., physical interactions) such as electrostatic abstraction can lead to the removal of some pollutants. These interactions play an important role in sorption of organic substances. It is reported that the biosorbents can remove organics, such as dyes, phenols, and pesticides. For example, active sludge, bacteria, and fungi are able to remove dyes with a capacity ranging from 100 to 300 mg dyes/g biosorbents (15). Biosorption of soluble and colloidal organic wastes by activated sludge has been reported (16).

In the metal biosorption, the chemosorption plays a key role. Many factors can influence on biosorption performances, such as pH, pollutant concentration, biomass concentration, temperature, biomass particle size, mixing conditions, and competitive components. Formation of metal surface complexes, ion exchange, and chemical reduction are major chemical interactions, leading to the metal sorption. First, the organic functional groups in the biosorbents are similar to weak acids; thus, the metal complexes can be formed among the metal ions and the functional groups. Second, many biosorbents are initially saturated with light metal ions such as calcium ions, which can exchange with heavy metal ions. As a result, the heavy metals can be sorbed. The light metal ions at the same time are released into the bulk solution. Third, some of the functional groups are reductive, which can reduce metal ions with higher valence. For example, CrO_4^{2-} can be reduced to Cr^{3+} by a marine algal biomass.

Many studies point out that pH is the most critical factor that can affect biosorbents capacity as illustrated in Fig. 1. The pH effect is often determined by metal species and different functional groups on biosorbents. Ionic strength is an indication of the presence
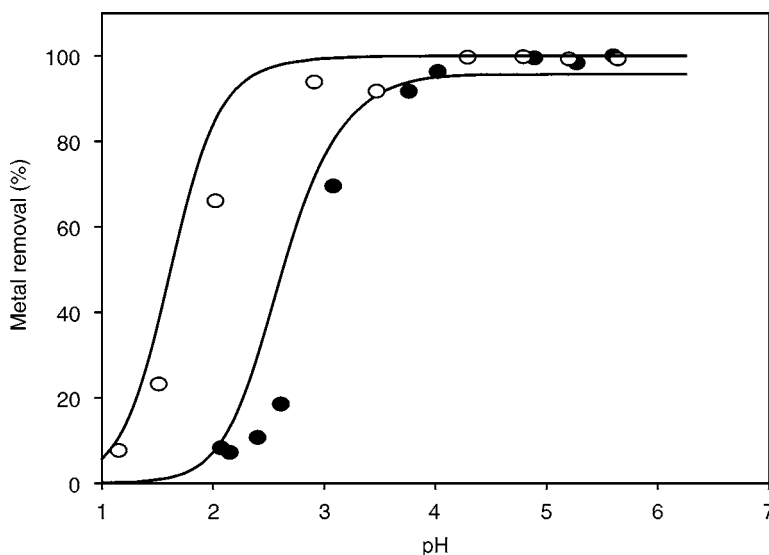
Fig. 1. pH effect on metal removal. Condition: $[Pb]_o = 1 \times 10^{-4}$ *M*, $[Cu]_o = 1.0 \times 10^{-4}$ *M*, calcium alginate = 0.15 g/L. Illustration: •, experimental (Cu); ○, experimental (Pb)—modeling.

of inert ions such as sodium and chloride, which are not involved in the metal sorption. Studies show that with an increase in ionic strength, the biosorption decreases. The presence of competitive ions may affect the metal biosorption, which is dependent on the strength of the interactions among the ions and the organic functional groups on the biosorbents. The temperature does not have a significant influence on heavy metal biosorption at the range of 20–40°C. Most of biosorbents have great metal removal capacity. Table 1 shows Langmuir constants of metal sorption on four important seaweeds. The metal sorption capacities (q_{max}) are much larger than the most commercially available activated carbons and ion exchange resins.

2.2. Biosorption Process

Several factors should be considered when selecting an appropriate biosorbent. First, it should be of low cost in both acquisition (e.g., harvesting and manufacturing) and recycle. Second, the biosorbent should have a high capacity, high selectivity, and fast kinetics. These properties ensure the compact contactor and longer regeneration intervals. Third, the biosorbent should have stable mechanical properties in order to be used in various reactors such as column operation.

Figure 2 describes the biosorbent preparation (1). Dependent on the requirement of treated water and the influent characteristics, different preparation approaches for biosorbents can be used. If the treated water is required to be free of organic substances, chemical pretreatment must be adopted, which can minimize organic leaching during the operation. However, this will not have to be adopted if the treated streams are discharged to sewage work as the organic substances can subsequently be treated biologically.

Biosorption is liquid–solid interaction. Similar to ion exchange and adsorption processes, the biosorption can be operated in batch, semicontinuous or continuously modes.

Table 1
List of Langmuir Constants Used In Metal Biosorption

	Pb			Cu		
	q_{max} (mmol/g)	b (L/mmol)	r^2	q_{max} (mmol/g)	b (L/mmol)	r^2
Padina spp.	1.25	9.31	0.97	1.14	8.39	0.99
Sargassum spp.	1.16	14.23	0.95	0.99	8.78	1
Ulva spp.	1.46	1.11	0.91	0.75	4.14	0.99
Gracillaria spp.	0.45	6.99	0.90	0.59	10.25	0.94
	Cd			Zn		
	q_{max} (mmol/g)	b (L/mmol)	r^2	q_{max} (mmol/g)	b (L/mmol)	r^2
Padina spp.	0.75	5.65	1	0.81	2.57	0.99
Sargassum spp.	0.76	11.34	0.94	0.50	13.63	0.95
Ulva spp.	0.58	1.45	0.98	0.54	1.15	0.97
Gracillaria spp.	0.30	21.11	0.81	0.40	12.68	0.83
	Ni					
	q_{max} (mmol/g)	b (L/mmol)	r^2			
Padina spp.	0.63	1.98	0.99			
Sargassum spp.	0.61	4.69	0.99			
Ulva spp.	0.29	1.58	0.98			
Gracillaria spp.	0.28	9.71	0.86			

Note: pH were controlled at 5.0 for lead and copper, and at 5.5 for cadmium, zinc, and nickel.

They can be upflow/downflow fixed bed reactor, fluidized bed reactor or continuously stirred treatment reactor.

2.2.1. Stirred Tank Reactor

The operation of stirred tank reactor can be batch or continuous. An amount of biosorbent can be added at the inlet of reactor or initially added into the reactor. The solid/liquid separation process can be accomplished either by gravity sedimentation in the same tank or by filtration by an additional unit. Operation of stirred tank reactor is simpler than fixed and fluidized bed reactors; however, the operation cost is often higher. Figure 3 demonstrates a stirred tank reactor for metal biosorption.

2.2.2. Fixed Bed Reactor

Like ion exchange or adsorption fixed bed system, the biosorption process can be implemented by operating a series of fixed beds. Some of the beds are operated for metal uptake, whereas the other beds are for regeneration of used biosorbents. A minimum requirement of column number is two. One is for biosorption for metal uptake and the other is for desorption for regeneration of metal-loaded biosorbents. An auto-switch system is needed for the operation. Figure 4 demonstrates a fixed bed reactor for metal biosorption.
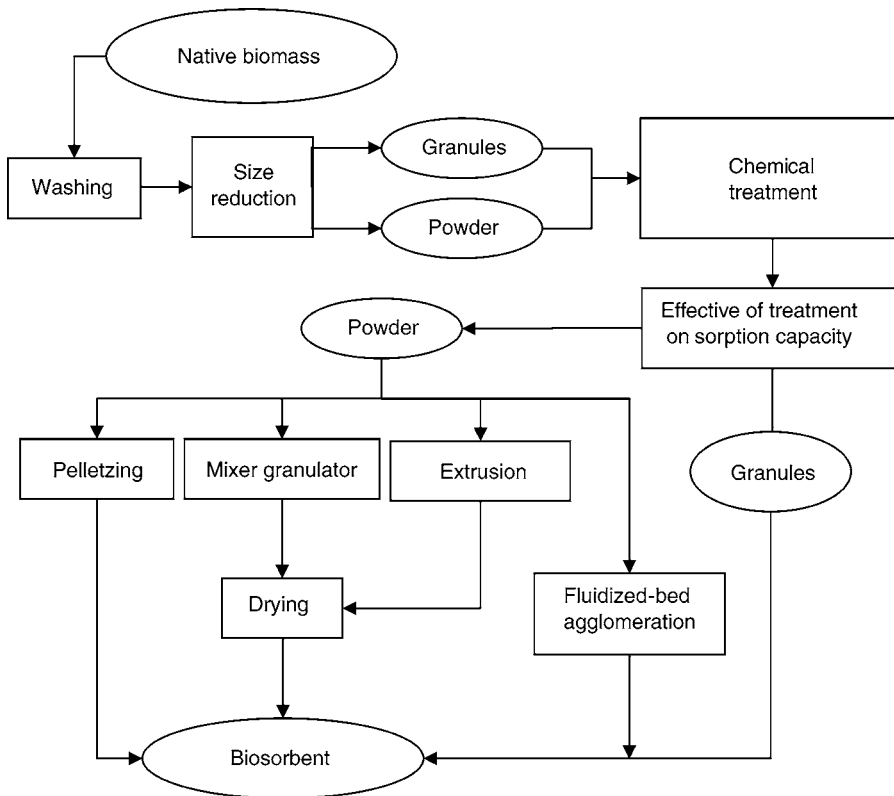
Fig. 2. Schematic diagram of biosorbent preparation.
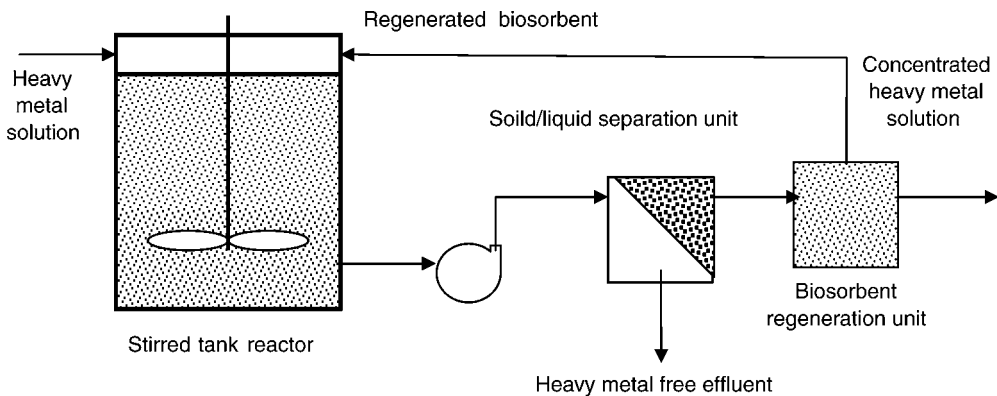
Fig. 3. Stirred tank reactor based biosorption process.

If metal waste streams contain suspended solids, these solids can deposit on or between biosorbent particles and increase the pressure drop along the column. The uptake of metal can increase as high as 20% of biosorbent weight, which reduces the porosity of the bed, and decrease the flow rate. The biosorbents with small sizes are not desirable since a high level pressure drop builds up and thus the operation cost is increased. However, too
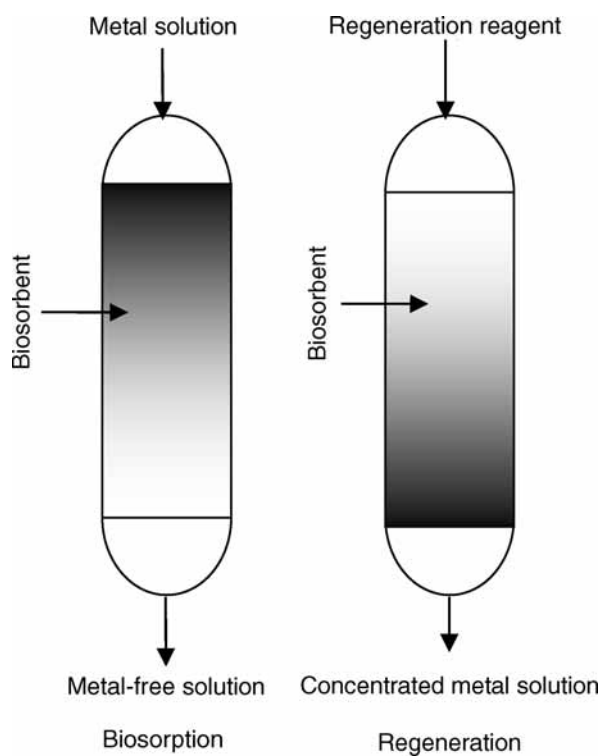
Fig. 4. Fixed bed based biosorption process.

large particles can decrease the biosorption rate as the external mass transfer resistance is increased. Thus, selection of appropriate size is important for operation of biosorption in fixed bed reactor. In application, a biosorbent diameter of 2 mm is often adopted to meet this requirement.

2.2.3. Fluidized Bed Reactor

Biosorbent can be packed in a column and waste stream is pumped upflow. When the flow rate reaches the fluidizing critical value, the biosorbent packed bed begins to expand, and fluidized. This is fluidized bed operation. Generally, a fluidized bed reactor causes less clogging than a fixed bed reactor. The higher degree of mixing enables faster sorption kinetics. The disadvantage is the bed expansion in the operation. Meanwhile, a more stable hydraulic condition must be maintained. Figure 5 demonstrates a fluidized bed reactor for metal biosorption.

2.3. Biosorption Mathematical Modeling

Biosorption mathematical modeling includes both equilibrium and kinetic modeling. Equilibrium models describe the sorption capacity as a function of chemistry; whereas kinetic models describe the sorption history.

In the equilibrium modeling, empirical models such as Langmuir and Freundlich isotherms and theoretical models are used.

Langmuir isotherm model is expressed by the following equation:

$$q_e = \frac{q_{max}bC_e}{1+bC_e} \tag{1}$$
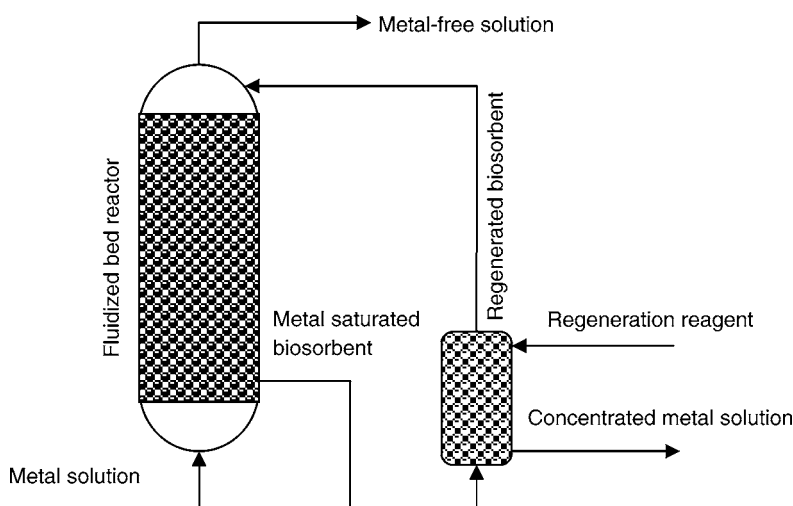
Fig. 5. Fluidized bed reactor-based biosorption process.

where q_e is the amount of contaminant adsorbed at equilibrium (mg/g or mmol/g), C_e is the equilibrium concentration of contaminant in solution (mg/L or mmol/L), q_{max} is the maximum adsorption capacity (mg/g or mmol/g), b is the Langmuir constant related to heat of adsorption (L/mg or L/mmol). The Langmuir constants of metal biosorption onto four important seaweeds are given in Table 1.

The Freundlich isotherm model is expressed as:

$$q_e = K_f C_e^{1/n} \qquad (2)$$

where K_f is the Freundlich adsorption constant, $1/n$ is the measure of adsorption intensity.

Equations (1) and (2) are used to describe the sorption of single component. For multiple components, modified Langmuir and Freundlich isotherms can be used (1,17). The major advantage of these empirical models is their great simplicity; however, they fail to predict the effects of several important factors, such as pH and ionic strength. If the model parameters are obtained based on the experiments under one set of conditions, the models cannot give accurate predictions for another set of conditions. For example, it has been shown that metal ion sorption increases dramatically in a short pH range. If the parameters of the empirical equations are based on experiments at a certain pH in this short range, these parameters cannot be used to calculate sorption equilibrium at a different pH. In addition to the pH effect, it is experimentally shown that the type and concentration of electrolytes, and complexing agents play important roles in sorption as discussed earlier. Empirical equations fail to predict accurately sorption equilibrium under varying ionic strengths. Additionally, the empirical models cannot give a fundamental understanding of ion sorption. An ion exchange model developed by Chen and coworkers is illustrated later, which can be used to describe biosorption in many cases such as seaweeds and calcium alginate for metal removal (7).

It is assumed that there is one generalized type of functional group (represented as R^{2-}) in the metal ion removal process. Most of functional groups are complexed with calcium ions (CaR). Ion exchange is the main pathway through which metal ions are

stripped away. When the biosorbents are immersed in an aqueous solution, calcium ions can be replaced by hydrogen ions according to the following reaction:

$$2H^+ + [CaR] = Ca^{2+} + [H_2R] \tag{3}$$

Similarly, in an aqueous solution of metal salts, exchange between metal ions and calcium ions inside the resin takes place according to the following reaction:

$$M^{2+} + [CaR] = Ca^{2+} + [MR] \tag{4}$$

A greater affinity of R^{2-} to M^{2+} is the driving force for pushing the equilibrium to the right.

In addition, there may be some 'free/unreacted' functional groups in the fresh biosorbent, leading to the formation of an ion-pair ($M^{2+} R^{2-}$)

$$M^{2+} + R^{2-} = [MR] \tag{5}$$

In addition, precipitation and aqueous solution reactions were considered according to the refs. 10 and 13.

It is assumed that a metal-contained system had M_x aqueous species with concentrations x_i, and M_p precipitated species with activities of unity. One can describe the concentrations or activities of the two types of species in terms of N_a aqueous components with concentrations c_j. The equilibrium relationships that give the concentrations or activities of the two types of species are as follows:

$$x_i = K_i^x \prod_{k=1}^{N_a} c_k^{a_{ik}^x} \quad i = 1, 2, \ldots, M_x \tag{6}$$

$$K_i^p \prod_{k=1}^{N_a} c_k^{a_{ik}^p} = 1 \quad i = 1, 2, \ldots, M_p \tag{7}$$

where K_i^x denotes the equilibrium constant of the ith aqueous species; a_{ik}^x, the stoichiometric coefficient of the kth aqueous component in the ith aqueous species; K_i^p, the modified equilibrium constant of the ith precipitated species; a_{ik}^p, the stoichiometric coefficient of the kth aqueous component in the ith precipitated species.

Based on the aforementioned equations and mass balances, the distribution of ions in both solid and liquid phases can be easily obtained by using equilibrium models such as the MINEQL+ and FITEQL 4.0 (18,19). There is always no information available on the chemistry of biosorbents in the literature (e.g., Eq. [3]–Eq. [5], and their equilibrium constants). Therefore, a series of titration and sorption isothermal experiments has to be carried out to provide input data for the model. Figure 1 shows a successful modeling study for metal biosorption by a calcium alginate biosorbent.

Kinetics of biosorption can be calculated by surface diffusion control models. In order to simplify the calculation, the empirical models such as Langmuir Equation are often used. Fixed bed biosorption calculation can be performed by using the models for organic adsorption in fixed bed columns reported in the literature (17).

3. MAGNETIC ION EXCHANGE PROCESS

A magnetic ion exchange resin has both magnet and ion exchange properties (20–24). Orica Watercare of Victoria, Australia successfully developed a resin called
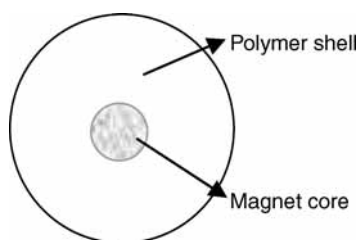
Fig. 6. Structure of magnetic ion exchange resin.

MIEX®. It can specifically remove dissolved organic carbon (DOC) from natural water. This product is probably the only one available commercially and has been used in several water treatment plants in the United States and elsewhere.

The magnetic ion exchange resin has traditional ion exchange resin properties. More importantly, it has magnetized iron oxide incorporated into the polymer matrix. The magnetic component aids agglomeration and settling of the resin, allowing the resin beads to be smaller so that they can be applied to raw water in a slurry form (25).

The MIEX® functions like anionic exchange resin, which has a polyacrylic matrix in the chloride form, a macroporous structure, and strong-base functional groups. The magnet cores are inorganic magnet materials such as Fe_3O_4, Fe_2O_3, nickel, and cobalt (26). Figure 6 demonstrates the basic structure of the MIEX®. The resin has a size of about 150–180 μm, which is 2–5 times smaller than the traditional ion exchange resins. Such a small resin has low resistance to external mass transfer (11,12,17).

Owing to the small size of MIEX®, it cannot be used in a fixed-bed column like the traditional ion exchange resins because the pressure drop can be pretty high. However, the resin is particularly suitable to be used in a suspended manner in a stirred tank reactor by using continuous or batch modes. This increases the turbulence around the resin and decreases resistance to liquid-phase mass transfer. Because the kinetics of ion exchange is governed by solid- and liquid-phase mass transfer, MIEX® is able to remove negatively charged contaminants such as DOC much faster than traditional ion exchange resins (22,27). The resin can also remove sulfide, sulfate, nitrate, arsenate, and chromate ions from aqueous solutions. Figure 7 shows process flow diagram for magnetic ion exchange.

Like other anionic exchange resins, the chemical reactions can be simplified as follows:

$$\overline{R - Cl^-} + An^- \Leftrightarrow \overline{R - An^-} + Cl^- \tag{8}$$

where $\overline{R - Cl^-}$ and An^- represent fresh MIEX® and anions to be removed such as DOC. In the regeneration, concentrated chloride ions (e.g., NaCl) can be used. The resins undergo a reversed ion exchange reaction. The chloride ions substitute the anions (e.g., DOC) on the active site of the resins.

Magnetically driven separation of used resin from aqueous solutions is the major advantage of using the MIEX® resin. The separation is achieved by using magnetic action. An external magnetic coil system is normally adopted as shown Fig. 8. The magnetic field is created from the outer surface of the reactor, which leads to the formation of aggregation of magnetic resins.
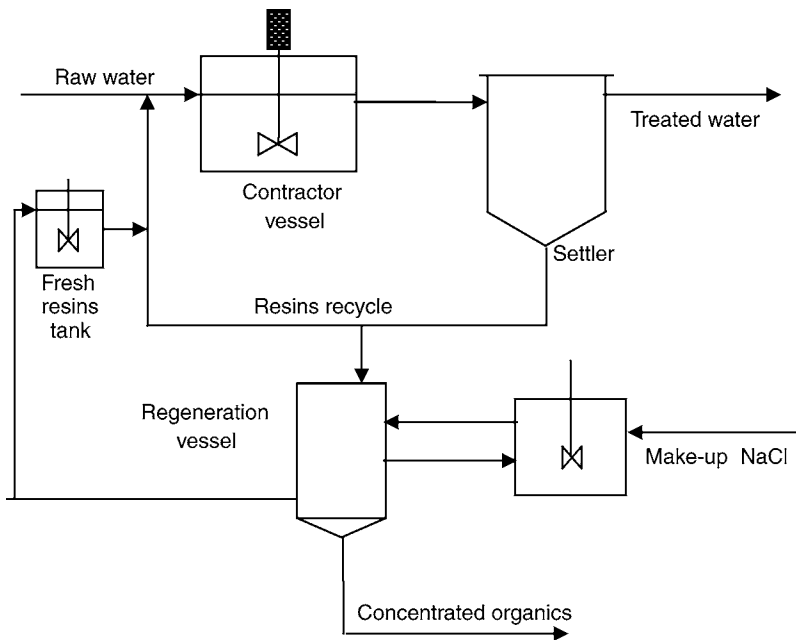
Fig. 7. Process flow diagram for magnetic ion exchange process.
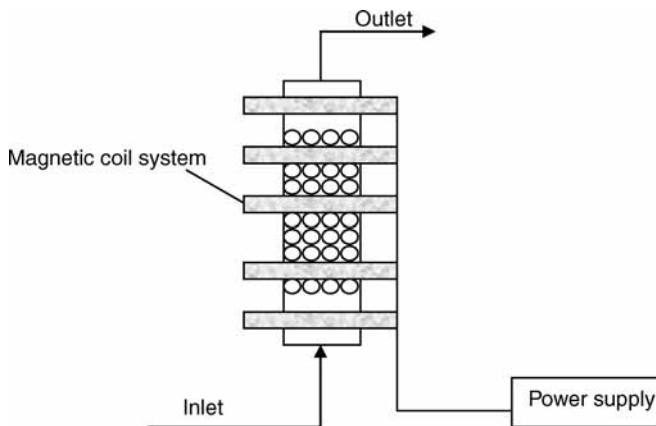
Fig. 8. Magnetically fluidized bed.

The MIEX® is a relatively new technology in full-scale engineering applications. There are not many studies that have been carried out on the MIEX®. The removal of disinfection byproduct and TOC using MIEX® process has been reported on Danville Water Filtration Plant in Kentucky, USA. In addition to the advantage of magnetic separation, the resin has good adsorption kinetics. The equilibrium time of 15 min is required for DOC and bromide removal (21).
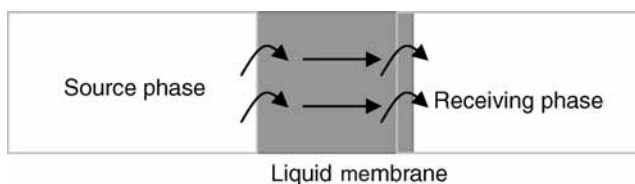
Fig. 9. Liquid membrane principle.

4. LIQUID MEMBRANE PROCESS

4.1. Introduction

Liquid membrane process is one of the membrane technologies. The liquid membrane system involves an immiscible liquid that serves as a semipermeable barrier between two liquid- and gas-phases. The liquid membranes are media consisting of liquid films or membranes through which selective mass transfer of gases, ions, and molecules occur via permeation and transport process as shown in Fig. 9. The mass transfer processes are largely governed by permeation, dissolution, diffusion, active and passive transport phenomena. Only slight external energy is needed for rotation, stirring, and pumping. The use of a mobile carrier, a transport catalyst, or a mediator, which dissolves only in liquid membrane facilitates the transport thus further increases the separation efficiency (28–33). The substrate first needs to react with the carrier to form a complex that is soluble in liquid membrane, but insoluble in adjacent solutions. After diffusing across the membrane, this complex disintegrates into free carrier and the original substrate.

There are several benefits using carriers in the liquid membrane (28).

a. The flux of liquid membrane is higher than that of conventional polymer membrane.
b. Good selective separation can be achieved.
c. Passive transport against the concentration gradient can be achieved.

Liquid membrane can be prepared in two different configurations: the emulsion liquid membrane (ELM) and the immobilized liquid membrane. There are several liquid membrane configurations. Figure 10 demonstrates four typical liquid membrane modules.

4.2. Mechanism

There are two basic operation principles for liquid membrane process: unfacilitated transport and facilitated transport. Figure 11 illustrates the liquid membrane working mechanisms. In facilitated transport, because of its larger solubility in the organic phase, permeate is transferred from the source phase into the membrane, and then from the membrane into the receiving phase (Fig. 11A). The diffusing species react with a chemical regent in the receiving phase, forming a product that is incapable for diffusing back, of which conditions prevent back-extraction of the permeate.

The facilitated transport mechanism can be further cataloged to countertransport and cotransport mechanism as illustrated in Figs. 11B and 11C. There is a specific and reversible reaction between permeate and a carrier molecule, to form a permeate carrier complex. The carrier is dissolved in the membrane phase and is totally insoluble in both the source and the receiving phases.
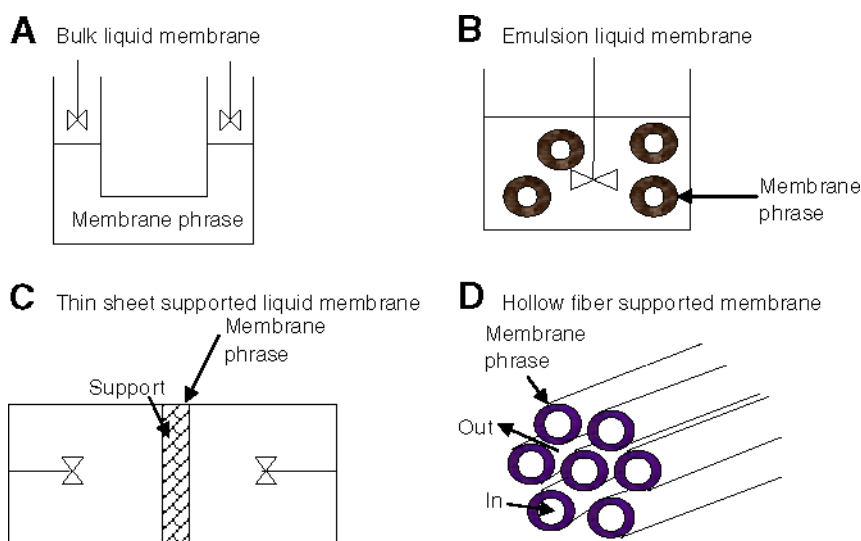
Fig. 10. Several specific setups of liquid membrane process.

In counter-transport mechanism (Fig. 11B), the transport of permeate (A) is coupled with the transport of the counter ion (D) in the opposite direction. Permeate can be transported uphill by providing a much higher concentration of counter ions against the concentration of permeate. In cotransport mechanism (Fig. 11C), the driving force for the transport of permeate is provided by the difference in concentration of the counter-ion (D) between the source and receiving solutions. If the concentration of the co-ion is much higher than the concentration of permeate (A), permeate can be transported uphill.

4.3. Applications

Despite all the research and development activity in recent years on liquid membranes, there are very few reported applications of the technology at a commercial level or at an industrial pilot scale level. However, interest in liquid membranes is high and should be commercially forthcoming especially in the areas of wastewater treatment, hydrometallurgy and well control fluids.

4.3.1. Treatment of Inorganic Wastewater

Liquid membrane separation is favorable for treatment of inorganic wastewater. It has been well-documented that it can effectively remove heavy metals and ammonium from aqueous solutions. The ions to be removed have various concentrations. The advantage of using liquid membrane is its great selectivity and capacity to treat highly concentrated metal wastewater. The mass flux can be as high as 100 m mol/m$^2 \times$ h (28). pH is important in the treatment as it can affect the formation of metal complexes. For example, copper ions often react with ammonium solution to form a complex in the operation. At lower pH, there is a decrease of the ammonium concentration for exchanging a proton with Cu^{2+} at the interface of the source/membrane phases. Therefore,
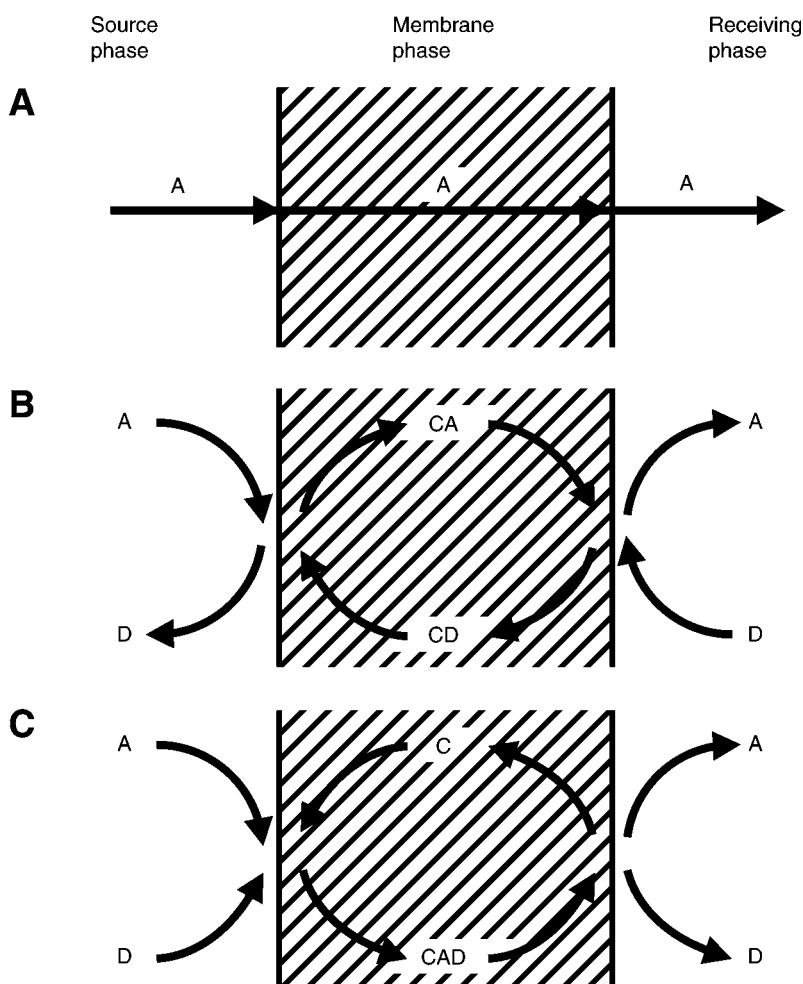
Fig. 11. Schematic representation of solute transport through liquid membrane: **(A)** unfacilitated transport **(B)** countertransport and **(C)** cotransport.

there is a decrease in copper (II) ion transport. At higher pH, the efficiency is decreased because of the complex formation of copper (II) and ammonia. It is found that for the source phase, maximum copper transport occurs at pH 7.0–8.0 and the selectivity is higher at pH 8.0.

4.3.2. Treatment of Organic Wastewater

Most of organic wastes are ionic and soluble in solvent; thus, they can be treated by using liquid membrane separation. The technology has been reportedly used for the removal of phenol from wastewater and also for the treatment of formulated and real wastewater containing *O*-nitrophenol (*O*-NP) and *p*-nitrophenol (*p*-NP) (33). Luan and Plaisier reported that nitrophenol concentration was reduced from 255 to 4.1 mg/L using a simple ELM set up as shown in Fig. 12 (33). The COD in wastewater can be reduced
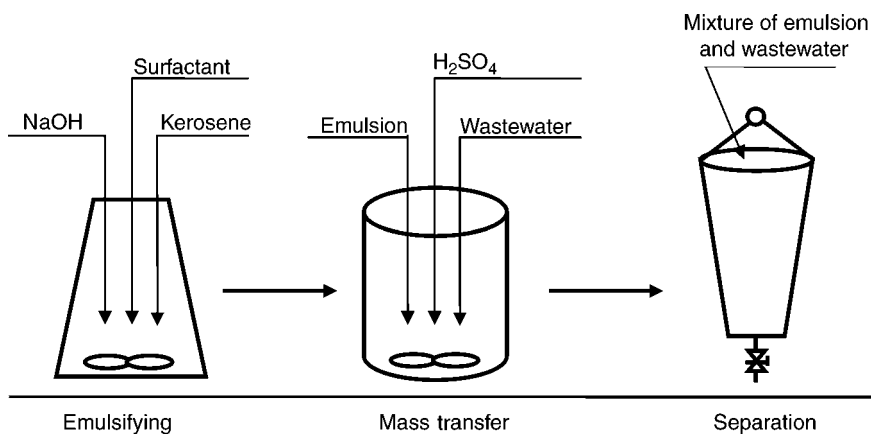
Fig. 12. Experiment device and flow diagram of batch liquid membrane treatment for nitrophenol wastewater.

from 1601 to 154 mg/L. The emulsion solution made up of expolyamine surfactant (industrial pure), kerosene (industrial pure), NaOH, and H_2SO_4. Aniline was successfully treated from wastewater (32) by an ELM with removal efficiency of 98% (32).

5. EMERGING TECHNOLOGIES FOR ARSENIC REMOVAL

Arsenic pollution is a serious environmental problem because of its mobility and toxicity. Consequently, more strict regulations have been made to limit its discharge to sewers and water bodies. The Safe Drinking Water Act requires US Environmental Protection Agency (US EPA) to revise the existing 50 ppb standard for arsenic in drinking water. On January 22, 2001 US EPA adopted a new standard, and public water systems must comply with the 10 ppb standard beginning January 23, 2006 (34). The more strict regulations bring a big challenge to conventional heavy metal treatment technologies, such as chemical precipitation, ion exchange, and membrane filtration (35–40). Arsenate (As[V]) and arsenite (As[III]) are primary forms of arsenic in soils and natural waters. As(III) is more mobile in groundwater and 25–60 times more toxic than As(V). At low pH and mildly reducing environment (>100 mV), As(III) is stable and exists as arsenious acid. On the other hand, under oxidizing conditions, As(V) is the predominant species in a form as arsenic acid (35).

5.1. Precipitation–Coagulation, Sedimentation, and Flotation

Coagulation is a treatment process, by which the physical or chemical properties of dissolved, colloidal and suspended matters are changed. Thus, agglomeration is enhanced to an extent that the resulting particles can settle down by gravity or can be removed by filtration. Coagulants such as aluminum and ferric salts change the surface properties of solids; the stable particles become unstable particles, by which larger particles are formed. Coagulation process is not restricted to the removal of particles. Metal precipitates such as $Al(OH)_3$ are produced; hence, dissolved substances such as phosphates, heavy metals, humic substances, and color can be removed.

When aluminum and ferric salts are used in coagulation, arsenic can be removed because of two mechanisms: First, the insoluble aluminum and ferric hydroxides are formed, which can act as adsorption sites for the arsenic ions. Second, the arsenic ions can form precipitates together with aluminum or ferric ions.

Solution chemical conditions such as pH, initial concentration, and the presence of competitive ions are important in the removal of arsenic. The operational conditions such as dosage of coagulants are also important (35–38). Alum and ferric salts are often used in water treatment. They are able to reduce the contaminants from the water solutions.

Edwards (36) reported that, more than 90% removal of As(V) was achieved at dosage of ferric chloride >20 mg/L or alum >40 mg/L (36). At lower coagulant dosages, the removal did not follow a trend because of poor particle removal, high initial As(V) concentrations, and possible interference from other anions in the different waters tested. The optimum removal of As(V) by ferric salts and alum is achieved at pH of 5.0–7.2 and 5.0–7.0, respectively (37). The solids formed can be removed by direct filtration. The final concentration can be less than 10 ppb. As(III) removal efficiency is not as good as As(V) when coagulation is used. The removal of As(III) is normally 40–50%. Thus, oxidation of As(III) to As(V) is recommended for enhancement of removal.

Presence of inorganic substances is common in natural water. It was reported that, at pH < 7.0, As(III) removal was significantly decreased in the presence of sulfate. However, only a slight decrease in As(V) was observed. At higher pH, removal of As(V) was increased in the presence of calcium (38).

Effect of initial arsenic concentration is different in the removal of arsenic (38,39). With ferric chloride dose of 4.9 mg/L at pH 7.0 and varied initial arsenic concentration from 0.002 mg/L to 0.1 mg/L, both As(III), and As(V) removal efficiencies are independent of the initial concentrations (37). For initial As(V) concentrations between 0.1 mg/L and 1 mg/L, a dosage of 30 mg/L of either alum or ferric sulfate in the optimum pH range removed more than 95% of As(V). More than an initial concentration of 1 mg/L, the removal decreases with an increasing concentration. For concentrations of As(III) greater than 0.1 mg/L, neither alum nor ferric sulfate dosed at 30 mg/L could remove As(III) to concentrations less than 0.05 mg/L.

Preozonation may be used as one of first steps. Oxidation of As(III) to As(V) can therefore be achieved. A survey of several drinking water tertiary treatment plants show that soluble As(V) is converted to particulate As(V) by adsorption during rapid mixing, and is removed along with naturally occurring particulate arsenic predominantly by sedimentation (40). Soluble As(III) tracks through the treatment processes and is converted to soluble As(V) during the chlorination.

Lime is also effective for removal of both As(V) and As(III) (37). More than 90% removal for As(V) with an initial concentration of 0.4 mg/L is achieved at pH > 10.5. As(III) can be removed by 75% at pH > 11.0. After precipitation–coagulation, soluble arsenic would be converted to insoluble suspended solids, which can be separated by either sedimentation or dissolved air flotation (DAF).

5.2. Electrocoagulation

Electrocoagulation (EC) is reportedly used to treat arsenic (35). The EC process can treat organic waste and disinfect wastewater (41). In the EC process, oxidation, formation of metal hydroxides, and coagulation occur simultaneously.

In the EC process, an electrolytic cell is used. It contains both anode and as well as cathode, where separate oxidation and reduction reactions occur (41).

In the anode, there are the following oxidation reactions:

$$Me_1(\text{insoluble1}) = Me_1^{m+}(\text{soluble}) + Me^- \qquad (9a)$$

$$4OH^- = 2H_2O + O_2 + 4e \qquad (9b)$$

$$2Cl^- = Cl_2 + 2e^- \qquad (9c)$$
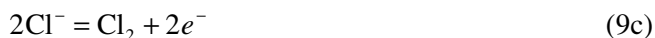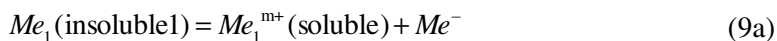
where Me_1 is metal in the anode and it can be sacrificial metal such as iron or aluminum. The electrode metal enters into the reaction, losing a flow of electrons to the electrode. In the cathode, the following reduction reactions occur:

$$2H^+ + 2e = H_2(g) \qquad (10)$$

The EC offers possibility of anodic oxidation and *in situ* generation of metal hydroxide and metal oxides such as hydrous ferric oxides and hydroxides of aluminum. The removal mechanism of As(III) can be oxidized to As(V). Both species are removed by coagulation of the metal hydroxides and adsorption of the metal oxides.

Three electrode materials such as: iron, aluminum, and titanium, can be used for the removal of arsenite and arsenate (35). A research shows that the iron electrodes perform the best removal of arsenic with the final arsenic concentration of less than 10 ppb. In the direct current density range of 0.65–1.53 mA/cm^2, higher current density results in faster arsenic removal. As(III) removal by the EC is reportedly much better than that by the chemical coagulation (40), although As(V) treatment by both approaches is virtually the same. The improvement by the EC is probably because of the reduction of As(III) to As(V).

5.3. Adsorption

Adsorption can concentrate arsenic onto other sorbents. This process is widely studied and still abstracts great interests from academics and industries. It is easy in operation and the waste may be recovered (42–58). The reactors can be in batch or continuous. They can be completely stirred, fixed-bed, or fluidized bed reactors. Adsorbents used for arsenic treatment are either based on organics like activated carbons or inorganic substances like iron oxides.

5.3.1. Activated Carbon

Key elements in activated carbons are carbon, oxygen, hydrogen, nitrogen, and phosphorous. Activated carbons are unique adsorbents because of their extended surface area, microporous structure, high adsorption capacity for gaseous species, and high degree of surface reactivity. Adsorption of anionic species such as arsenic is very much dependent on the chemical properties of the carbons and the solution chemistry.

There are only a few publications dealing with the adsorption of arsenic species onto activated carbons (42–46). The arsenic adsorption ranges from 1 to 4 mg-As/g-carbon. Higher ash content in carbons enhances the adsorption (42). pH is important and the optimum adsorption is achieved at pH 5.0–6.0. Lower or higher pH significantly decreases the arsenic uptake.

Activated carbons are made from different sources. Adsorption ability for As(V) follows the descending sequence of activated carbon from coal> from coconut shell> from wood (43). The effects of coexisting anions have the following order on the As(V) adsorption: $ClO_4^- > SO_4^{2-} > NO_3^- > Cl^-$. Darco carbons showed better As(V) removal capacity, although Nuchar and Filtrasorb brands exhibited little in comparison.

Adsorption of arsenic by activated carbon is quite fast. It can reach equilibrium within 3–6 h (42). Surface complex formation models can be used to describe the arsenic adsorption onto the activated carbons (10,44). The models are based on assumptions that the organic functional groups in carbons can be treated as a generalized weak acid and complex formation reactions between the arsenic species and the acid occurs.

The commercially available activated carbons are not favorable for adsorption of arsenic compounds (44,45). Thus, it is recommended that chemical modification can be applied for enhanced sorption reactions. The modification can be done either by organic surface treatment or impregnation of metal oxides. Reed and coworkers have developed an impregnated technique for activated carbon. Iron oxide is used for the modification as it has good arsenic adsorption capacity (44). The modified carbon is much better than commercial carbons. For example at pH 5.5 and with a dosage of 0.2 g/L, the arsenic removal efficiencies of Fe-modified carbon and commercial carbon are 100%, and 5%, respectively, when the initial As(V) concentration is 1 mg/L.

5.3.2. *Activated Alumina*

Activated alumina (AA) is a granulated form of aluminum oxide with very high specific surface area. The available adsorption sites are the oxide. AA is usually prepared through dehydration of $Al(OH)_3$ at high temperatures and consists of amorphous and γ-alumina oxide (46–48). The mechanisms of arsenic removal are similar to those of a weak base ion exchange resin, and are often collectively referred as "adsorption," though ion exchange is technically more appropriate term (46).

AA is used primarily in fixed bed reactors to remove anionic contaminants such as fluoride, arsenic, selenium, and natural organic matter. To remove contaminants, feed water is passed continuously through one or more AA beds. When all available adsorption sites are occupied, the AA media may be regenerated with a strong base such as NaOH or simply disposed of. Factors such as arsenic oxidation state, pH, competing ions, and flow rate affect arsenic removal. Spent regenerant disposal and alumina disposal are important issues in operations. After it is used, the AA must be replaced and the spent AA must pass the Toxicity Characteristic Leaching Procedure of the US EPA in order to be disposed of as a nonhazardous waste.

As(III) is found to be more difficult to treat than As(V). Thus, preoxidation of As(III) to As(V) is often recommended when treating water containing As(III). Adsorption of As(V) is much faster than the adsorption of As(III).The adsorption occurs rapidly during the first few hours and follows by a slower process.

pH has a significant effect on arsenic removal with activated alumina. pH 8.2 is significant as the isoelectric point of AA occurs at pH 8.2. When pH is less than this value, AA has a net positive charge resulting in a preference for adsorption of anions, including arsenic (46). Acidic conditions are considered suitable for arsenic removal with activated

alumina. Several studies have shown that the optimum pH for arsenic removal ranges from 5.5 to 6.0. The arsenic capacity of AA deteriorates as the pH increases from 6.0 to 9.0. The adsorption capacity ranges from 2 to 8 mg/g.

AA is considered as one of the best treatment options for arsenic by the US EPA (47,48). Its cost is about one-third of granular ferric hydroxide. Treatment of 1 million gal/d water requires about 1 million USD in capital costs and 200,000–250,000 USD in annual operation and maintenance costs (47).

Like any other ion exchange process, AA process exhibits preferences for certain ions. However, the order of preference can be quite different from those of IX resins. AA appears to have a higher preference for arsenic than for the most competing ions in water (including sulfate). Further, as indicated by the general selectivity sequence shown next (46,48), AA preferentially adsorbs

$$SO_4^{2-} > NO_3^- > HAsO_4^{2-} > NO_2^- > Cl^- > H_2AsO_4^- > HCO_3^-$$

5.3.3. Iron Oxides and Hydroxides

Iron oxides and hydroxides in particular are good for arsenic removal. Amorphous iron hydroxide, hydrous ferric oxide (HFO), and amorphous FeOOH always appear in literatures. The adsorption capacity is much higher than other adsorbents (49–55). Amorphous FeOOH can be prepared by mixing Fe(III) salt (e.g., $FeCl_3$ and $Fe[NO_3]_3$) and caustic solution according to the reaction (49):

$$Fe^{3+} + 3OH^- = FeOOH + H_2O \qquad (11)$$

After drying, amorphous FeOOH powders are obtained. It can be further converted to goethite (α-FeOOH) and/or hematite (α-Fe_2O_3), which is dependent on the aging time. pH is important in the arsenic adsorption. The adsorption of arsenite increases from pH 4 and reaches its maximum value at pH 7.0 and then starts to drop (50). Figure 13 shows the maximum adsorption capacity as a function of pH.

MnO_2-loaded resin was reportedly used to adsorb arsenic from waters. A research shows that this metal oxide has slightly higher adsorption capacity than iron oxide. The maximum adsorption capacity can be as high as 60 mg-As/g. MnO_2 is a good oxidant, it can oxidize As(III) to As(V), and both of them are then adsorbed onto the oxide.

Iron oxide can be coated onto the surface of sands for the removal of both arsenite and arsenate. As(V) adsorption is much faster than As(III). Both sulfate and chloride do not affect the As(V) removal. Organic matter, however, can cause some competition in the arsenic adsorption. The presence of 4 mg/L TOC reduces As(V) adsorption by about 50%. Metal oxides can be impregnated onto activated carbons, polymers and biomaterials for enhanced arsenic removal (44,56,57). Ghimire et al. (56) used the phosphorylation approach to modify cellulose and orange waste. The sorbents were further loaded with iron. It was reported that maximum adsorption capacities of 68 mg/g for both arsenate and arsenite were achieved by the iron-loaded sorbents. A contact time of 20 h was sufficient for a complete adsorption. Dambies et al. (57) used molybdate to modify chitosan gel beads for arsenic removal. They found that the modified sorbents significantly adsorb arsenic from aqueous solutions. The adsorption capacities were 230 mg/g and 70 mg/g for As(V) and As(III), respectively.
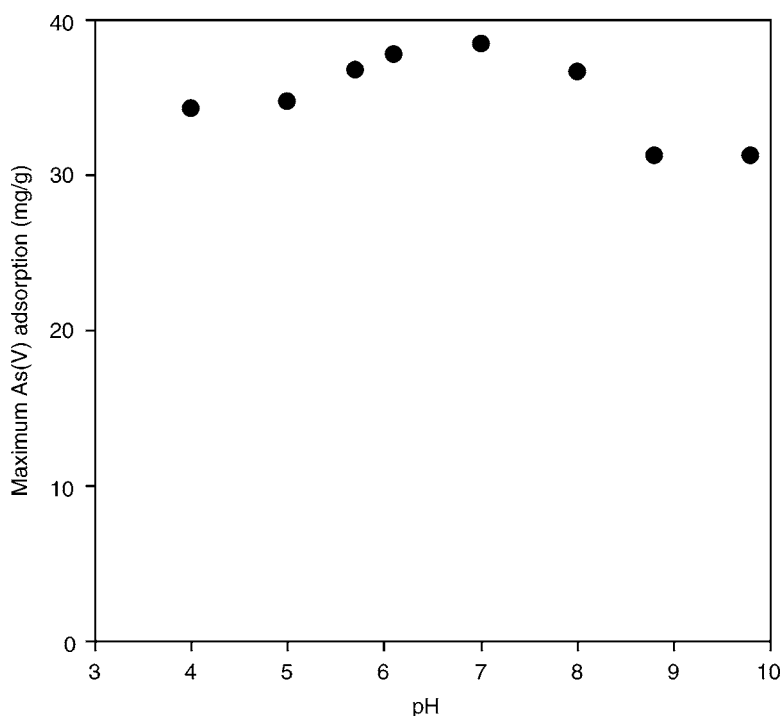
Fig. 13. Adsorption of As(V) as a function of pH. Amorphous iron hydroxide is used.

Several proprietary iron-based adsorbents have been developed recently. Granular ferric hydroxides are being used in full-scale systems in Germany, and similar materials have been developed both in Canada and the United States (58–60). These materials generally have high removal of efficiency and capacity.

The first commercial-scale arsenic removal system in the United States was installed in Phoenix, Arizona by US Filter in 2003 (60). Like many communities in the desert southwest, Phoenix's water supply includes well with arsenic concentrations exceeding 10 ppb. The bench and pilot scale studies were conducted for arsenic removal. AA, ion exchange, coagulation-assisted microfiltration, and adsorption were tested. The adsorption technology by granular ferric hydroxide (GFH™) developed by US Filter finally selected based on the consideration of cost, ease of operation, lower required operator attention, and reduced waste generation. The GFH™ is operated as a fixed bed column and is installed in two 14-ft diameter pressure vessels to allow a single pumping stage for the treatment system. Simplified operation is an important benefit of the system, which will operate without the need for chemical prefeed or pH correction. Once the media reach their adsorption capacity, they are removed, and replaced with new media. Spent media are stored in a storage area before being Toxicity Characteristic Leaching Procedure-tested and hauled away to landfill. After a year of operation since 2003, more than 35,000 bed volumes have passed through the GFH™ with an effluent arsenic concentration remaining less than the detection level. In addition, there have been no back-wash events based on headloss buildup during this time.

5.3.4. Biomaterials

Biosorption by cheap or low-cost natural biomaterials provides an alternative solution for arsenic removal (56,57,61,62). The adsorption capacity is similar to that of activated carbons. For example, chitosan can adsorb As(V) with a capacity of 6.2 mg/g; however, this biomaterial does not remove As(III) from aqueous solutions (56).

Chemical modification could be adopted for enhancement of arsenic removal. Loukidou et al. (61) reported that common surfactants (amines) and cationic polyelectrolyte were used to modify *Penicillium chrysogenum*. The modified biomaterial was found to be effective in removing relatively low concentrations of arsenic. The process was mainly affected by pH and also the modification procedure. At pH 3.0, the removal capacities of modified biomaterials were 37 mg/g for HDTMA-Br-modified Mycan biomaterial, 56 mg/g for Magnafloc-modified biomaterial, and 33 mg/g Dodecylamine-modified biomaterial.

5.4. Ion Exchange

Ion exchange is one of well-known technologies for arsenic removal. Both natural and synthetic resins can be used; the synthetic resins are often chosen to preferentially adsorb the contaminant (63–72). Water quality parameters such as pH, competing ions, resin type, alkalinity, and influent arsenic concentration should be considered in the applicability of the ion exchange process. Other factors include the affinity of the resin for the contaminant, spent regenerant, and resin disposal requirements, secondary water quality effects, and design operating parameters.

Typically, strong-base anion exchange resins are used in arsenic removal. The resins tend to be more effective over a larger range of pH than weak-base resins (46). Several studies have found that sulfate-selective resins tend to be superior to nitrate-selective resins for arsenic removal. The presence of Fe(III) in feed water can affect arsenic removal. When it is present, arsenic can form complexes with the iron oxides. Ion exchange resins do not remove these complexes, and hence, arsenic is not completely removed. Source waters with a high Fe(III) content would have to be treated by alternative technologies for arsenic removal. Wang, Kurylko, and Wang (72) developed a sequencing batch ion exchange process for removal of inorganic contaminants including arsenic. Recently Wang (71) developed sequencing batch magnetic ion exchange process for the same purpose.

5.5. Membrane Filtration

Arsenic found in groundwater is typically less than 10% particulate whereas, arsenic found in surface waters can vary from 0% to as much as 70% particulate (66). The percentage of particulate arsenic does not seem to be related to specific water types. In order to increase removal efficiency, filtration such as microfiltration or ultrafiltration is recommended to use in most of the cases. However, both of microfiltration and ultrafiltration are not viable for complete arsenic removal in surface waters and groundwater.

Through size exclusion, nanofiltration (NF) can remove both dissolved As(V) and As(III) (67,68). The NF is able to remove divalent ions, but not monovalent ions. The NF can remove more than 90% of dissolved arsenic from groundwater. Extensive pretreatment for particle removal is required before the application of NF as the membranes are more prone to fouling by the organic substances and particles.

Reverse osmosis (RO) is another effective arsenic removal technology proven through several bench-scale and pilot-scale studies, and is very effective in removing dissolved constituents (69). It is a suitable technology for arsenic removal in groundwater. As with other processes, RO removes As(V) to a greater degree than As(III). The pilot-scale studies show As(V) removal at 88–99% and As(III) removal of 46–84% (69). Thus, maintaining oxidation conditions is important to the process. Like NF, the water streams must be pretreated before entering the RO system.

NOMENCLATURE

$1/n$	Measure of adsorption intensity
a_{ik}^p	The stoichiometric coefficient of the kth aqueous component in the ith precipitated species
a_{ik}^x	The stoichiometric coefficient of the kth aqueous component in the ith aqueous species
An^-	Anions to be removed such as DOC (Dissolved organic carbon)
b	The Langmuir constant related to adsorption
C_e	The equilibrium concentration of contaminant in solution (mg/L or mmol/L)
K_f	Freundlich adsorption constant
K_i^x	The equilibrium constant of the ith aqueous species
K_i^p	The modified equilibrium constant of the ith precipitated species
Me_1	Metal in the anode and it can be sacrificial metal such as iron or aluminum
q_e	The amount of contaminant adsorbed at equilibrium (mg/g or mmol/g)
q_{max}	The maximum adsorption capacity (mg/g or mmol/g)
$\overline{R - Cl^-}$	Represent fresh MIEX® to be used

REFERENCES

1. B. Volesky, *Biosorption of Heavy Metals.* CRC Press, Inc., 1990.
2. P. X. Sheng, L. H. Tan, J. P. Chen, and Y. P. Ting, Biosorption performance of two brown marine algae for removal of chromium. *J. Dispersion Sci. Technol.* **25**(5), 681–688 (2004).
3. P. X. Sheng, Y. P. Ting, J. P. Chen, and L. Hong, Sorption of lead, copper, cadmium, zinc and nickel by marine algal biomass: characterization of biosorptive capacity and investigation of mechanisms. *J. Colloid Interf. Sci.* **275**(1), 131–141 (2004).
4. J. P. Chen and S. N. Wu, Copper adsorption behaviors of acid/base treated activated carbons. *Langmuir* **20**(6), 2233–2242 (2004).
5. J. P. Chen and L. Wang, Characterization of metal adsorption kinetic properties in batch and fixed-bed reactors. *Chemosphere* **54**(3), 397–404 (2004).
6. S. B. Deng, R. B. Bai, and J. P. Chen, Aminated polyacrylonitrile fibers for lead and copper removal. *Langmuir* **19**(12), 5058–5064 (2003).
7. J. P. Chen, L. Hong, S. N. Wu, and L. Wang, Elucidation of interactions between metal ions and ca-alginate based ion exchange resin by spectroscopic analysis and modeling simulation. *Langmuir* **18**(24), 9413–9421 (2002).
8. J. P. Chen and L. L. Lim, Key factors in chemical reduction by hydrazine for recovery of precious metals. *Chemosphere* **49**(4), 363–370 (2002).
9. J. P. Chen, D. Lie, L. Wang, S. N. Wu, and B. P. Zhang, Dried waste activated sludge as biosorbents for metal removal: adsorptive characterization and prevention of organic leaching. *J. Chem. Technol. Biotechnol.* **77**(6), 657–662 (2002).

10. J. P. Chen and M. S. Lin, Equilibrium and kinetics of metal ion adsorption onto a commercial H-type granular activated carbon: experimental and modeling studies. *Water Res.* **35**(10), 2385–2394 (2001).

11. J. P. Chen and L. Wang, Characterization of a ca-alginate based ion exchange resin and its applications in lead, copper and zinc removal. *Sep. Sci. Technol.* **36**(16), 3617–3637 (2001).

12. J. P. Chen and J. Peng, Uptake of toxic metal ions by novel calcium alginate beads. *Adv. Environ. Res.* **3**(4), 439–449 (1999).

13. J. P. Chen, F. Tendeyong, and S. Yiacoumi, Equilibrium and kinetic studies of copper ion uptake by calcium alginate. *Environ. Sci. Technol.* **31**(5), 1433–1439 (1997).

14. J. P. Chen and S. Yiacoumi, Biosorption of metal ions from aqueous solutions. *Sep. Sci. Technol.* **32**(1–4), 51–69 (1997).

15. Z. Aksu, Application of biosorption for the removal of organic pollutants: a review. *Process Biochem.* **40**(3–4), 997–1026 (2005).

16. W. Zhao, Y. P. Ting, J. P. Chen, C. H. Xing and S. Q. Shi, Advanced primary treatment of wastewater using a bio-flocculation-adsorption sedimentation process. *Acta Biotechnol.* **20**(1), 53–64 (2000).

17. C. Tien, *Adsorption Calculations and Modeling*. Butterworth-Heinemann, Boston, MA, 1994.

18. W. D. Schecher and D. C. McAvoy, MINEQL+ chemical equilibrium modeling system, version 4.5 for windows. *Environ. Res. Software* Hallowell, ME, 2001.

19. A. Herbelin and J. Westall, *FITEQL: A Computer Program for Determination of Chemical Equilibrium Constants from Experimental Data. Ver. 4.0. Technical Report*. Department of Chemistry, Oregon State University, Corvallis, Oregon, 1999.

20. R. Hausmann, C. Hoffmann, M. Franzreb, and W. H. Holl, Mass transfer rates in liquid magnetically stabilized fluidized bed of magnetic ion-exchange particles. *Chem. Eng. Sci.* **55**, 1477–1482 (2000).

21. H. Humbert, H. Gallard, H. Suty, and J. Croué, Performance of selected anion exchange resins for the treatment of a high DOC content surface water. *Water Res.* **39**(9), 1699–1708 (2005).

22. C. J. Johnson and P. C. Singer, Impact of a magnetic ion exchange resin on ozone demand and bromate formation during drinking water treatment. *Water Res.* **38**(17), 3738–3750 (2004).

23. D. A. Fearing, Combination of ferric and Miex® for the treatment of a humic rich water. *Water Res.* **38**(10), 2551–2558 (2004).

24. P. C. Singer and K. Bilyk, Enhanced coagulation using a magnetic ion exchange resin. *Water Res.* **36**(16), 4009–4022 (2002).

25. T. H. Boyer and P. C. Singer bench-scale testing of a magnetic ion exchange resin for removal of disinfection by-product precursors. *Water Res.* **39**, 1265–1275 (2005).

26. Y. Lee, J. Rho, and B. Jung, Preparation of magnetic ion exchange resins by the suspension polymerization of styrene with magnetite. *J. Appl. Polymer Sci.* **89**, 2058–2067 (2003).

27. R. S. Summers, Assessing DBP yield: uniform formation conditions. *J. Am. Water Works Assoc.* **88**(6), 80–93 (1996).

28. R. Molinari, P. Argurio, and F. Pirillo, Comparison between stagnant sandwich and supported liquid membranes in copper(II) removal from aqueous solutions: flux, stability and model elaboration. *J. Membr. Sci.* **256**(1–2), 158–168 (2005).

29. W. Furst and R. Marr, Separation of metal species by emulsion liquid membranes. *J. Membr. Sci.* **38**, 281–293 (1988).

30. W. S. Winston Ho and K. K. Sirkar, *Membrane Handbook*. Van Nostrand Reinhold, New York, 1992.

31. M. Ma, Study on the transport selectivity and kinetics of amino acids through Di(2-ethylhexyl) phosphoric acid-kerosene bulk liquid membrane. *J. Membr. Sci.* **234**, 101–109 (2004).

32. S. Datta, P. K. Bhattacharya, N. Verma, Removal of aniline from aqueous solution in a mixed flow reactor using emulsion liquid membrane. *J. Membr. Sci.* **226**, 185–201 (2003).

33. J. Luan and A. Plaisier, Study on treatment of wastewater containing nitrophenol compounds by liquid membrane process. *J. Membr. Sci.* **229**, 235–239 (2004).

34. US EPA, *Arsenic Rule Benefits Analysis: An SAB Review*. EPA-SAB-EC-01-008. US Environmental Protection Agency, Washington, DC, August 2001.

35. P. R. Kumar, S. Chaudhari, K. C. Khilarand, and S. P. Mahajan, Removal of arsenic from water by electrocoagulation. *Chemosphere* **55**(9), 1245–1252 (2004).

36. M. A. Edwards, Chemistry of arsenic removal during coagulation and Fe-Mn oxidation. *J. Am. Water Works Assoc.* 64–77 (1994).

37. T. J. Sorg and G. S. Logsdon, Treatment technology to meet the interim primary drinking water regulations for inorganics. Part 2 *J. Am. Water Works Assoc.* **70**, 379–393 (1978).

38. J. G. Hering, P. Chen, J. A. Wilkie, M. Elimelech, and S. Liang, Arsenic removal by ferric chloride. *J. Am. Water Works Assoc.* **88**(4), 155–167 (1996).

39. G. S. Logsdon, T. J. Sorg, and J. M. Symons, Removal of heavy metals by conventional treatment, *Proc. 16th Water Quality Conference-Trace Metals In Water Occurrence, Significance, and Control. University Bulletin*. U. of Illinois. No. 71 (1974).

40. J. Gregor, Arsenic removal during conventional aluminium-based drinking-water treatment. *Water Res.* **35**(7), 1659–1664 (2001).

41. J. P. Chen, S. Y. Chang and Y. T. Hung, Electrolysis. In: *Physicochemical Treatment Processes,* L. K. Wang, Y. T. Hung, and N. K. Shammas, (eds.), Humana Press, Totowa, NJ, 359–378, 2005.

42. L. Lorenzen, J. S. J. Deventer and W. M. Landi, Factors affecting the mechanism of the adsorption of arsenic species on activated carbon. *Miner. Eng.* **8**(4–5), 557–569 (1995).

43. G. S. Gupta, G. Prasad and V. N. Singh, Removal of chrome dye from aqueous solutions by mixed adsorbents: fly ash and coal. *Water Res.* **24**, 45–50 (1990).

44. R. L. Vaughan, Jr. and B. E. Reed, Modeling As(V) removal by a iron oxide impregnated activated carbon using the surface complexation approach. *Water Res.* **39**(6), 1005–1014 (2005).

45. B. Daus, R. Wennrich, and H. Weiss, Sorption materials for arsenic removal from water: a comparative study. *Water Res.* **38**(12), 2948–2954 (2004).

46. D. Clifford, Ion exchange and inorganic adsorption. In: *Water Quality and Treatment*, American Water Works Association, McGraw Hill, New York. 1999.

47. US EPA, *Case Study—Arsenic Treatment Technologies, Tucson, AZ,* EPA 816-F-03-015, US Environmental Protection Agency, Washington DC, 2003.

48. US EPA, *Arsenic Removal from Drinking Water by Ion Exchange and Activated Alumina Plants,* EPA 600-R-00-088, US Environmental Protection Agency, Washington DC, 2000.

49. L. Zeng, A method for preparing silica-containing iron(III) oxide adsorbents for arsenic removal. *Water Res.* **37**(18), 4351–4358 (2003).

50. M. L. Pierce and C. B. Moore, Adsorption of arsenite and arsenate on amorphous iron hydroxide. *Water Res.* **16**(7), 1247–1253 (1982).

51. A. Sperlich, A. Werner, A. Genz, G. Amy, E. Worch and M. Jekel, Breakthrough behavior of granular ferric hydroxide (GFH) fixed-bed adsorption filters: modeling and experimental approaches. *Water Res.* **39**(6), 1190–1198 (2005).

52. M. Badruzzaman, P. Westerhoff and D. R. U. Knappe, Intraparticle diffusion and adsorption of arsenate onto granular ferric hydroxide (GFH). *Water Res.* **38**(18), 4002–4012 (2004).

53. J. A. Wilkie and J. G. Hering, Adsorption of arsenic onto hydrous ferric oxide effects of adsorbate/adsorbent ratios and co-occurring solutes. *Colloids Surf. A Physicochem. Eng. Aspects.* **107**, 97–110 (1996).

54. Y. Zhang, M. Yang and X. Huang, Arsenic(V) removal with a Ce(IV)-doped iron oxide adsorbent. *Chemosphere* **51**(9), 945–952 (2003).

55. V. Lenoble, C. Chabroullet, R. al Shukry, B. Serpaud, V. Deluchat and J. Bollinger, Dynamic arsenic removal on a MnO_2-loaded resin. *J. Colloid Interf. Sci.* **280**(1), 62–67 (2004).

56. K. N. Ghimire, K. Inoue, H. Yamaguchi, K. Makino and T. Miyajima, Adsorptive separation of arsenate and arsenite anions from aqueous medium by using orange waste. *Water Res.* **37**(20), 4945–4953 (2003).

57. L. Dambies, T. Vincent and E. Guibal, Treatment of arsenic-containing solutions using chitosan derivatives: uptake mechanism and sorption performances. *Water Res.* **36**(15), 3699–3710 (2002).

58. Editor, Filtration media shown to effectively remove arsenic, *Filtration & Separation,* **42**(3), 14 (2005).

59. Editor, Dow licenses arsenic removal technology, *Filtration & Separation,* **41**(3), 8 (2004).

60. Filtration & Separation, First commercial-scale arsenic removal system In USA. *Filtration & Separation,* **40**(6), 13 (2003).

61. M. X. Loukidou, K. A. Matis, A. I. Zouboulis and M. Liakopoulou-Kyriakidou, Removal of As(V) from wastewaters by chemically modified fungal biomass. *Water Res.* **37**(18), 4544–4552 (2003).

62. S. N. Kartal and Y. Imamura, Removal of copper, chromium, and arsenic from CCA-treated wood onto chitin and chitosan. *Bioresou. Technol.* **96**(3), 389–392 (2005).

63. N. K. Lazaridis, A. Hourzemanoglou and K. A. Matis, Flotation of metal-loaded clay anion exchangers. Part II: The Case of Arsenates. *Chemosphere* **47**(3), 319–324 (2002).

64. S. Shevade and R. G. Ford, Use of synthetic zeolites for arsenate removal from pollutant water. *Water Res.* **38**(14–15), 3197–3204 (2004).

65. M. H. Polyák and J. Hlavay, Removal of pollutants from drinking water by combined ion exchange and adsorption methods. *Environ. Int.* **21**(3), 325–331 (1995).

66. L. S. McNeill and M. Edwards, Arsenic removal during precipitative softening. *J. Environ. Eng.* **125**(5), 453 (1997).

67. T. Urase, J. Oh, and K. Yamamoto, Effect of pH on rejection of different species of arsenic by nanofiltration. *Desalination* **117**(1–3), 11–18 (1998).

68. Y. Sato, M. Kang, T. Kamei and Y. Magara, Performance of nanofiltration for arsenic removal. *Water Res.* **36**(13), 3371–3377 (2002).

69. R. Y. Ning, Arsenic removal by reverse osmosis. *Desalination* **143**(3), 237–241 (2002).

70. F. W. Pontius, N. Renouf, and R. McCutchen. Magnetic ion exchange solves problems. *Opflow* **32**(8), 28–30 (2006).

71. L. K. Wang. *Innovative Ultraviolet, Ion Exchange, Membrance and Flotation Technologies for Water and Waste Treatment.* National Engineers Week Seminar, Traning Manual. Practicing Institute of Engineers, Albany, NY. February 12–14, 2006.

72. L. K. Wang, L. Kurylko, and M. H. S. Wang. *Sequencing Batch Liquid Treatment.* US Patent No. 5354458, US Patent and Trademark Office, Washington, DC, 1996.

Fine Pore Aeration of Water and Wastewater

Nazih K. Shammas

CONTENTS

1. INTRODUCTION

The supply of oxygen for aeration is the single largest energy consumer at activated sludge wastewater treatment plants, representing 50–90% of total plant energy requirements (1,2). Replacement of less-efficient aeration systems with fine pore aeration devices can save up to 50% of aeration energy costs and has resulted in typical simple payback periods of 2–6 yr (3). As a result of these very impressive cost savings, a very large number, 1000–2000 municipal and industrial wastewater treatment facilities in the United States and Canada now use fine pore aeration.

Fine pore aeration technology remains relatively new in North America, and new materials and configurations continue to be developed. This chapter provides designers, end users, and regulators information on the nature of fine pore aeration devices and their performance to promote the intelligent application of fine pore aeration technology.

Standardized testing of oxygen transfer devices in both clean and processed waters is a major advancement in the field. A consensus standard for testing aeration devices in clean water has been adopted by a large segment of the industry (4). Extensive testing of aeration equipment using this standard has led to the development of a large database on the performance of aeration devices in clean water. In addition, the development of improved (more precise and accurate) field test methods has permitted the generation

of data that can be used to better characterize the translation of clean water test results to process conditions (5).

Experiments on wastewater aeration in England date back to as early as 1882 (6). In these experiments, air was introduced through open tubes or perforations in air delivery pipes. In the early years, patents were granted for a variety of diffusers, including perforated metal plates, porous tubes with fibrous materials, and nozzles (7). As activated sludge process investigations progressed, greater oxygen transfer efficiency (OTE) was sought with the production of smaller bubbles created by passing compressed air through porous media of various types. Experiments conducted in the United Kingdom seeking a better porous material consists of evaluations of limestone, firebrick, sand and glass mixtures, pumice, and other materials. The first porous plates were made available as early as 1915 in the United Kingdom. In the following years, several US companies offered porous plates that became the most popular method of aeration in this country in the 1930s and 1940s (3).

Shortly after the emergence of porous diffusers it became clear that media clogging could be a problem. Work in Chicago between 1922 and 1924 prompted the use of coarse media to avoid clogging (8). Clogging was attributed to liquid-side fouling and airside clogging because of dirt and oil in the air delivery system. Emphasis at that time was on improving air filtration (9–11). Substantial experimentation was performed to develop effective air filtration devices (10,11), and the results of that early work have led to the high-efficiency air filters used today in many porous diffused air systems (9).

Mechanical aeration was one answer to the clogging problem. Since the introduction of Archimedean screw-type aerators in 1916, a multitude of mechanical aeration devices has been developed and used. Today, mechanical aeration devices serve as an important function in many applications for treatment of industrial and municipal wastewaters.

Another approach to the clogging problem emerged with the development of large orifice-type (coarse bubble) diffusers. Updated versions of the first marketed diffusers (as early as 1904 in the United Kingdom) evolved in the 1950s in an effort to improve on earlier perforated pipe devices and were designed for easy access and maintenance. In general, the principles that resulted in easily maintained and accessible aeration systems also produced low-oxygen transfer efficiencies (3).

With the renewed emphasis on more energy efficient aeration systems in the 1970s, North America again turned to European technology for more efficient oxygen transfer devices. As a result, newer generation porous diffusers, producing fine bubbles with accompanying high-oxygen transfer efficiencies, became popular. Yet, considerable concern has been registered regarding the performance and maintenance of these porous diffusers owing to their historical susceptibility to clogging.

2. DESCRIPTION

Fine pore diffusion is a subsurface form of aeration where air is introduced in the form of very small bubbles. Since the energy crisis in the early 1970s, there has been increased interest in fine pore diffusion of air as a competitive system because of its high OTE. Smaller bubbles result in more bubble surface area per unit volume and greater OTE (12,13).

The term "fine bubble" diffused aeration is elusive and difficult to define and includes a wide variety of diffuser types. The term "fine pore" was adopted by US Environment protection Agency (US EPA) (14) to more nearly reflect the porous characteristics of one class of high-efficiency diffusers marketed today. Typically, fine pore diffusers will produce a head loss because of surface tension in clean water of greater than about 5 cm (2 in.) water gauge.

Coarse bubble diffusers normally produce a bubble diameter of 6–10 mm (1/4–3/8 in.) in clean water. Although the actual orifice may be much larger, the bubbles produced tend to shear and break into smaller bubbles as they are produced and rise to the surface. For this type of device, as long as the mixing intensity stays roughly the same, bubble size is usually independent of the airflow rate through the diffuser. However, mixing intensity increases with increasing airflow, which most likely shears the bubbles into bubbles with smaller diameters. This may explain the apparent gradual increase in OTE with increasing airflow rate for some coarse bubble systems.

When new, fine bubble diffusers produce bubbles with a diameter of approx 2–5 mm (0.08–0.20 in.) in clean water (15–19). The bubble size produced by fine pore devices is affected by airflow, becoming somewhat larger as airflow increases.

Some advantages and disadvantages of various fine pore diffusers are as follows (12):

Advantages

a. Exhibit high OTEs.
b. Exhibit high aeration efficiencies (mass oxygen transferred per unit power per unit time).
c. Can satisfy high-oxygen demands.
d. Are easily adaptable to existing basins for plant upgrades.
e. Result in lower volatile organic compound emissions than nonporous diffusers or mechanical aeration devices.

Disadvantages

a. Fine pore diffusers are susceptible to chemical or biological fouling, which may impair transfer efficiency and generate high head loss. As a result, they require routine cleaning. (Although cleaning may not be totally free of cost, but does not need to be expensive or troublesome.)
b. Fine pore diffusers may be susceptible to chemical attack (especially perforated membranes). Therefore, care must be exercised in the proper selection of materials for a given wastewater.
c. Because of the high efficiencies of fine pore diffusers at low airflow rates, airflow distribution is critical to their performance and selection of proper airflow control orifices is important.
d. Because of the high efficiencies of fine pore diffusers, required airflow in an aeration basin (normally at the effluent end) may be dictated by mixing—not oxygen transfer.
e. Aeration basin design must incorporate a means to easily dewater the tank for cleaning. In small systems in which no redundancy of aeration tanks exists, an *in situ*, nonprocess-interruptive method of cleaning must be considered.

3. TYPES OF FINE PORE MEDIA

Although several materials capable of serving as effective fine pore diffusion media exist, few are being used in the wastewater treatment field because of cost considerations,

specific characteristics, market size, or other factors. Fine pore media in use today can be divided into the following three general categories:

a. Ceramics.
b. Porous plastics.
c. Perforated membranes.

3.1. Ceramics

Ceramics are the oldest, and currently most common, porous media on the market. Ceramic media consist of irregular or spherically shaped mineral particles that are sized, blended together with bonding materials, compressed into various shapes, and fired at an elevated temperature to form a ceramic bond between the particles. The result is a network of interconnecting passageways through which air flows. As air emerges from the surface pores, pore size, surface tension, and flow rate interact to produce the characteristic bubble size (20). Ceramic diffusers have been manufactured from alumina, aluminum silicate, and silica.

Alumina (aluminum oxide) media used for fine pore diffusers are produced from bauxite, a naturally occurring ore consisting primarily of aluminum hydroxide. Calcination followed by electrorefining produces a material that exceeds 80% alumina. The refined molten mineral is allowed to solidify and is subsequently crushed and screened to select the desired sizes (21). This raw material is called regular or brown fused aluminum oxide.

Other materials used for fine pore media that are similarly crushed and then sized are produced from either man-made or naturally occurring aluminum silicates such as cyanotic. All these minerals are combinations of alumina (aluminum oxide) and silica (silicon oxide) with an alumina content of 50% to slightly over 70%. On heating at high temperatures, they tend to form the equilibrium species of the mineral (mullite) and a siliceous glass. Mullite consists of three parts alumina to two parts silica.

Silica used in the manufacture of fine pore diffusers is a mined material with limited particle size range. As a result, the pore sizes that can be produced are restricted to naturally occurring grain sizes. Some sources of silica are less angular than the jagged crushed alumina or aluminum silicate particles. It has been claimed that the silica material may be more resistant to fouling and more easily cleaned (16). Although this claim has not been well-documented based on controlled experiments, silica plates have been used for years.

No studies have been published, which suggest that there is a difference in process performance between diffusers made with either alumina or aluminum silicate media. Experience would seem to indicate that the two materials might have been used interchangeably (3). As a raw material, alumina is more abrasion resistant than either silica or aluminum silicate; however, actual strength and abrasion resistance also depend on the nature of the ceramic bond itself. Silica porous media, as manufactured, are generally considered to have the lowest overall strength, and their thickness is usually increased to compensate for this weakness.

Sources of ceramic diffuser media are made up of primarily of companies supplying industrial abrasives or refractory materials. In the past, these basic porous media

manufacturers have both marketed diffusers directly and supplied various media shapes to aeration equipment manufacturers. The aeration equipment manufacturers, in turn, marketed the diffuser, holder, piping, and other ancillary equipment. Today, the basic porous media manufacturers will market finished diffuser assemblies directly to the end user with warranties covering only mechanical specifications for materials, dimensions, and permeability. They will not warranty oxygen transfer performance (3).

Ceramic diffusers have been in use for a long period and their advantages, as well as operational problems, are well documented. Because of this longevity of the ceramic materials it has become the standard for comparison. Each new generation of fine pore media reportedly offers some advantage, either in performance or cost, over ceramic diffusers. In the past, the new devices have often not lived up to their expectations. As a result, ceramic diffusers continue to capture a significant share of the fine pore aeration market.

3.2. Porous Plastics

The next development in the fine pore diffuser field is the use of porous plastic materials. As with ceramics, a medium is created consisting of several interconnecting channels or pores through which compressed air can travel. The manufacturing process can be controlled to produce different pore sizes. Some of the advantages of plastic materials over ceramics are (3):

  a. Ease of manufacture.
  b. Lighter weight (which makes them especially suited to liftout applications).
  c. Durability.
  d. Cost-effectiveness.
  e. Greater resistance to breakage (depending on the type of manufacturing material).

  Some disadvantages include:

  a. Lower strength.
  b. Greater susceptibility to creep.
  c. Lower environmental resistance.

To provide further definition, porous plastics are classified as either rigid or nonrigid. The basic difference between the two is that a nonrigid porous plastic requires some form of internal structural support.

3.2.1. Rigid Porous Plastics

Rigid porous plastics are made from several thermoplastic polymers including polyethylene, polypropylene, polyvinylidene fluoride, ethylene-vinyl acetate, styrene-acrylonitrile (SAN), and polytetrafluoroethylene (22). Besides their application in the aeration field, these materials are used extensively as filtration media (air, water, chemicals). When used as a fine pore aeration device, the two most common types of plastic media are high-density polyethylene (HDPE) and SAN.

HDPE is relatively inexpensive and easy to process when compared with other thermoplastics. In addition, shrinkage is low, a uniform quality product can be obtained, and small pore sizes can be produced. HDPE diffusers are manufactured by proprietary

extrusion processes. A HDPE diffuser is usually made from a straight homopolymer (not a blend), is nonpolar, and contains no additives or binders.

A European manufacturer produces a double-layer HPDE material (23). It consists of a grainy, open-pore structure approx 6 mm (1/4 in.) thick covered by a thinner 3 mm (1/8 in.) thick, less porous layer. The manufacturer claims that the double layer results in a filtering effect that decreases maintenance. Allegedly, this lower maintenance would result from a reduction in airside fouling of the diffuser. However, recent studies have demonstrated that airside fouling does not appear to be an important fine pore diffuser operation and maintenance (O&M) factor (24,25). The manufacturer also claims that the thin outer layer is potentially beneficial in helping to produce a small diameter bubble uniformly over the diffuser surface. The manufacturer further suggests that the thin film layer may act as a barrier in preventing precipitates from forming deep within the media. If the foulants are restricted to the surface, they can be more easily removed (23). Any tendency for increased external fouling in such diffusers is unknown. The major advantages of HDPE media compared with other plastic media are their lighter weight, approx 560 kg/m^3 (35 lb/ft^3), inert composition, and resistance to breakage, even under freezing conditions.

SAN diffusers are manufactured from a copolymer. The raw material is a mixture of four different molecules. Physically, SAN media are made up of very small resin spheres fused together under pressure. SAN has a density only slightly more than HDPE. However, the presence of styrene makes the material brittle and the media can break if dropped, even at room temperature. A major advantage of the SAN material is that it has been successfully used for about 30 yr.

Although rigid plastic media diffusers (especially the HDPE material) were installed in several wastewater treatment plants in the early 1980s, they are no longer popular. SAN diffusers, which seemed to work well, are no longer being actively marketed. HDPE diffusers, on the other hand, were plagued by several problems that contributed to their decline in popularity. These included media fouling, lack of quality control in the manufacturing process (diffusers did not always produce uniform air distribution), and the emerging cost competitiveness of other fine pore diffusion products.

3.2.2. Nonrigid Porous Plastic

Only one type of diffuser material is being marketed that could be considered as a nonrigid porous plastic (26). This material, which is extruded from a combination of rubber and HDPE, is soft and somewhat flexible. When air is applied at normal pressures, this type of media does not expand. However, some expansion will occur at higher pressures. It has been demonstrated that a high-pressure water flush can be used to remove foulants that may have become trapped in the pores (25).

3.3. Perforated Membranes

Membrane diffusers differ from the first two groups (ceramics and porous plastics) in that the diffusion material does not contain the network of interconnecting passageways through which air must travel. Instead, mechanical means are used to create preselected patterns of small, individual orifices (perforations) in the membrane to allow passage of air through the material.

Membrane diffusers have been in use for about 50 yr. They initially were called sock diffusers and were made from materials such as plastic, synthetic fabric cord, or woven cloth. A metallic or plastic core material was required with the woven sheaths to provide structural support. Although sock diffusers were capable of achieving high-oxygen transfer rates, fouling problems were often severe. Today, there is essentially no market for the early sock design (3).

Another type of perforated diffuser has been introduced in the early 1980s. It consists of a thin flexible membrane made from either a thermoplastic material or an elastomer. Because of their physical properties, the current literature usually describes diffusers made from these materials as "flexibles" or "flexible membrane" diffusers. However, because the patterned orifices in the membrane material are intentionally made during the manufacturing process, this generation of membrane diffusers is referred to as perforated membrane diffusers.

ASTM (27) defines a thermoplastic as "a plastic that repeatedly can be softened by heating and hardened by cooling through a temperature range characteristic of plastic, and, in the softened state, can be shaped by flow into articles by molding or extrusion." The most common thermoplastic material is polyvinyl chloride (PVC). Plasticizers are added to produce a soft and flexible membrane.

The term elastomer includes the complete spectrum of elastic or rubber-like polymers that are sometimes randomly referred to as rubbers, synthetic rubbers, or elastomers (28). Rubber is a natural material, whereas all other elastomers are synthetic. ASTM (27) defines an elastomer as "macromolecular material that returns rapidly to approximately the initial dimensions and shape after substantial deformation (defined as twice its length) by a weak stress and release of the stress."

Most elastomer membranes are made from ethylenepropylene dimer. Although the main ingredient may be ethylenepropylene dimer, proprietary additives are usually included to enhance the material characteristics. As a result, it may not always be possible to establish media characteristics or physical properties simply by consulting a table in a reference text or handbook.

After the membrane material is produced, air passages are created by punching or cutting minute holes or slits in the membrane. When the air is turned on, the material expands. Each hole acts as a variable aperture opening; the higher the airflow rate, the greater the size of the opening. When the air is turned off, the membrane relaxes down against the support base and a seal is formed between membrane and support in systems in which the membrane area conforms to the support. This closing action will reportedly eliminate or at least minimize the backflow of liquid into the diffuser (29–36).

Perforated membrane diffusers have been developed over the last 30 yr in the United States and Europe. The most significant advantage claimed for the perforated membrane diffuser is that its smooth surface and apertures may be more resistant to fouling than are other types of media (29,30,37). Formation of biological and chemical foulants has been, however, noted on the surfaces of the thermoplastic media (24). One of the disadvantages of the perforated membrane diffusers is that thermoplastic and elastomer materials can experience physical property changes with time. These changes depend on varying degrees, the materials used, their shape and dimensions, and environmental conditions.

4. TYPES OF FINE PORE DIFFUSERS

There are four general types (shapes) of fine pore diffusers on the market: plates, tubes, domes, and discs. Each is discussed in detail next.

4.1. Plate Diffusers

The original fine pore diffuser design was a flat rectangular ceramic plate. These plates are usually 30 cm (12 in.) square and 25–38 mm (1–1.5 in.) thick. They are manufactured from either glass-bonded silica or ceramically bonded aluminum oxide and aluminum silicate. The plates are installed by grouting them into recesses in the basin floor, cementing them into prefabricated holders, or clamping them into metal holders. Of the three, the metal holders are the least attractive because corrosion of some of the holders may result in fouling of the underside of the diffusers. A chamber underneath the plates acts as an air plenum. The number of plates fixed over a common plenum is not standard and can vary from a single plate to 500 or more. Individual control orifices are normally not provided for this original plate design.

Fine pore ceramic plates were almost used exclusively as the method of air diffusion in the early activated sludge plants through the 1920s. Other than retrofits or expansions of existing plants in Milwaukee, WI (38) and Chicago, IL (39), the original ceramic plate design is seldom specified today. Some possible explanations for its decline in popularity include:

a. Problems obtaining uniform air distribution with several plates attached to the same plenum.
b. Inconvenience of removing plates that are grouted or cemented in place.
c. Difficulty in adding diffusers to meet future increases in plant loading.
d. Lack of active marketing by any equipment supplier or media manufacturer.

Some of the advantages of plate diffusers are:

a. Documented service life.
b. High oxygen transfer.
c. Ease of *in situ* cleaning.

A recently developed plate design offers both ceramic and porous plastic media options (40). Both these alternatives are marketed in sizes of 30×61 cm^2 (12×24 in.^{2}) and 30×122 cm^2 (12×48 in.^{2}); although other specialty sizes are also available. The ceramic plates, made of ceramically bonded aluminum oxide, are 19 mm (3/4 in.) thick, whereas the porous plastic (35-μm HDPE) design uses a media thickness of only 6 mm (1/4 in.). Both the ceramic and plastic media are mounted on top of vacuum-formed, ABS plastic plenums. The undersides of the plenums are filled with concrete at the job site to provide position stability on the basin floor and adequate ballast to prevent floating of the diffusers. The porous HDPE media sheets are sealed to their individual plenums by 25 mm (1 in.) wide stainless steel frames bolted into the concrete ballast, whereas the ceramic plates are mastic bonded to ledges set into the inner periphery of their plenums.

Air is fed to each diffuser of this generation plate design through a separate 3.8 cm (1.75 in.) diameter rubber hose. The hoses are connected by saddles to common air

Legend
1. S.S. eye-anchor
2. Ceramic plate (HDPE media also available)
3. S.S. retainer clip
4. PVC air inlet
5. PVC hose adapter
6. S.S. hose clamp
7. Feeder airline
8. S.S. anchor bolt
9. Air plenum
10. Concrete ballast
11. Optional side inlet
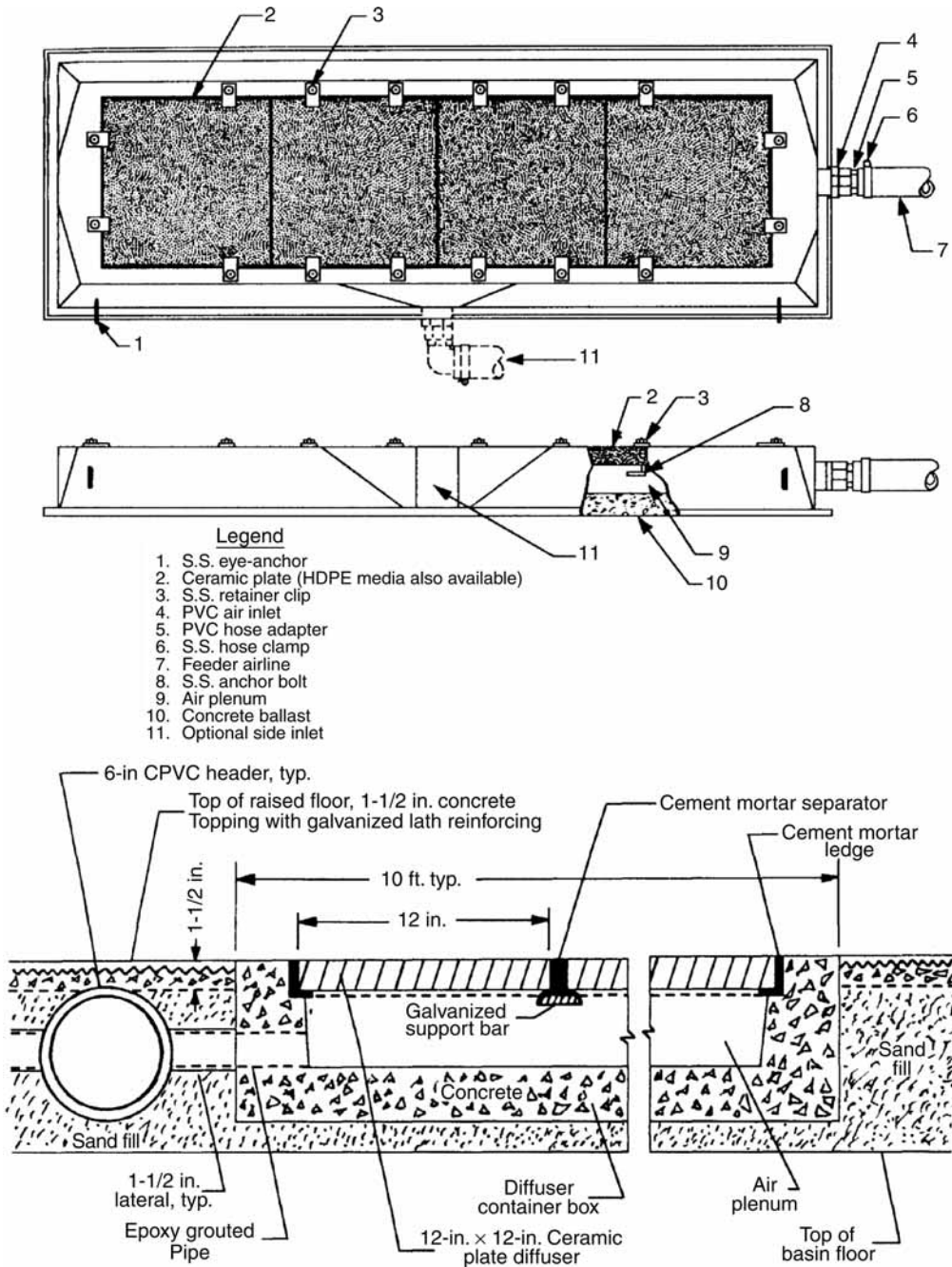
Fig. 1. Ceramic plate diffusers (*Source*: US EPA).

delivery headers. Individually drilled orifices are inserted into the feed nipple of each plate, promoting improved air distribution control compared with the original plate design. Typical plate diffusers of both the original and newer designs are shown in Fig. 1.

4.2. Tube Diffusers

Like plates, fine pore tubes have been used in wastewater treatment for many years (26,31,36,41–45). The early tubes, Saran wound or made from aluminum oxide, have been followed by the introduction of SAN copolymer, porous HDPE, and the new generation of perforated membranes and nonrigid porous plastic.

Most tube diffusers on the market are of the same general shape. Usually, the media portion is 51–61 cm (20–24 in.) long and has an outer diameter (O.D.) of 6.4–7.6 cm (2.5–3 in.). A tee assembly is sometimes placed in the middle, increasing total length to nearly 100 cm (40 in.). The thickness of the media is variable. Perforated membranes are very thin, commonly 0.6–2.5 mm (0.025–0.1 in.). HDPE media are usually supplied at a thickness of 6.4 mm (1/4 in.), SAN media at approx 15 mm (0.6 in.), and fused ceramic media at 9.5–12.7 mm (3/8–1/2 in.).

The dimensions of the rubber-HDPE (nonrigid porous plastic) tube diffuser differ from those just mentioned. This diffuser has an O.D. of 25 mm (1 in.), comes in lengths of up to 91 cm (36 in.), and has a media thickness of approx 3 mm (1/8 in.). The holder designs for the ceramic and rigid porous plastic media are very similar. Most consist of two end caps held together by a connecting rod through the center. The rod is threaded into the feed end of the holder, the media and outer end cap installed, and a hex nut placed on the threaded rod to secure the assembly. When ceramic media are used, the end caps and connecting rod are usually metallic S. S. (stainless steel). With HDPE media, because of their lighter weight, PVC, polypropylene, or some other thermoplastic are often used. When plastic holders or pipe connectors are used, the effects of creep should be considered. Threaded plastic connectors are also susceptible to failure unless properly designed.

In another slightly different version, the feed end cap and inner support are one piece with the assembly held together by a bolt installed through the outer end cap and threaded into the support frame. For both designs, gaskets are placed between the media and the end caps to provide an airtight seal. Sometimes, a gasket or O-ring is also used with the retaining bolt or hex nut. A typical rigid porous plastic (or ceramic) tube diffuser assembly is shown in Fig. 2.

Because of their flexible nature, perforated membrane diffusers require an internal support structure. The frame is made from plastic (e.g., PVC or polypropylene) and has a tubular shape. The tube provides support either around the entire circumference or, in one modification, only the bottom half. With the full tubular frame, holes in the inlet connector or slots in the tube itself allow distribution of the air below the membrane surface. The membrane is usually not perforated at the air inlet point. Thus, when the air is turned off, the liquid head collapses the membrane against the support frame. With the cutaway support frame, an internal flap prevents backflow into the piping system. The ends of the support frame are plugged, and stainless-steel hose clamps are used on each end to secure the membrane tightly to the frame. Typical perforated membrane diffusers are illustrated in Fig. 3.

With the rubber-HDPE (nonrigid porous plastic) diffuser, either a permanent (crimped) stainless steel or a removable acetal clamp is provided on the feed end only. The opposite end of the media is bonded to itself and requires no clamp. The tubular support frame is made from either stainless steel or fiberglass reinforced plastic. To prevent
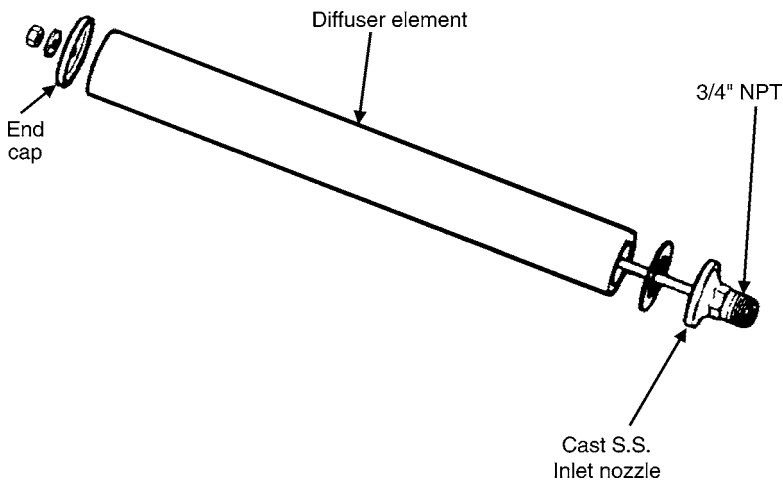
Fig. 2. Ceramic or rigid porous plastic tube diffuser (*Source*: US EPA).
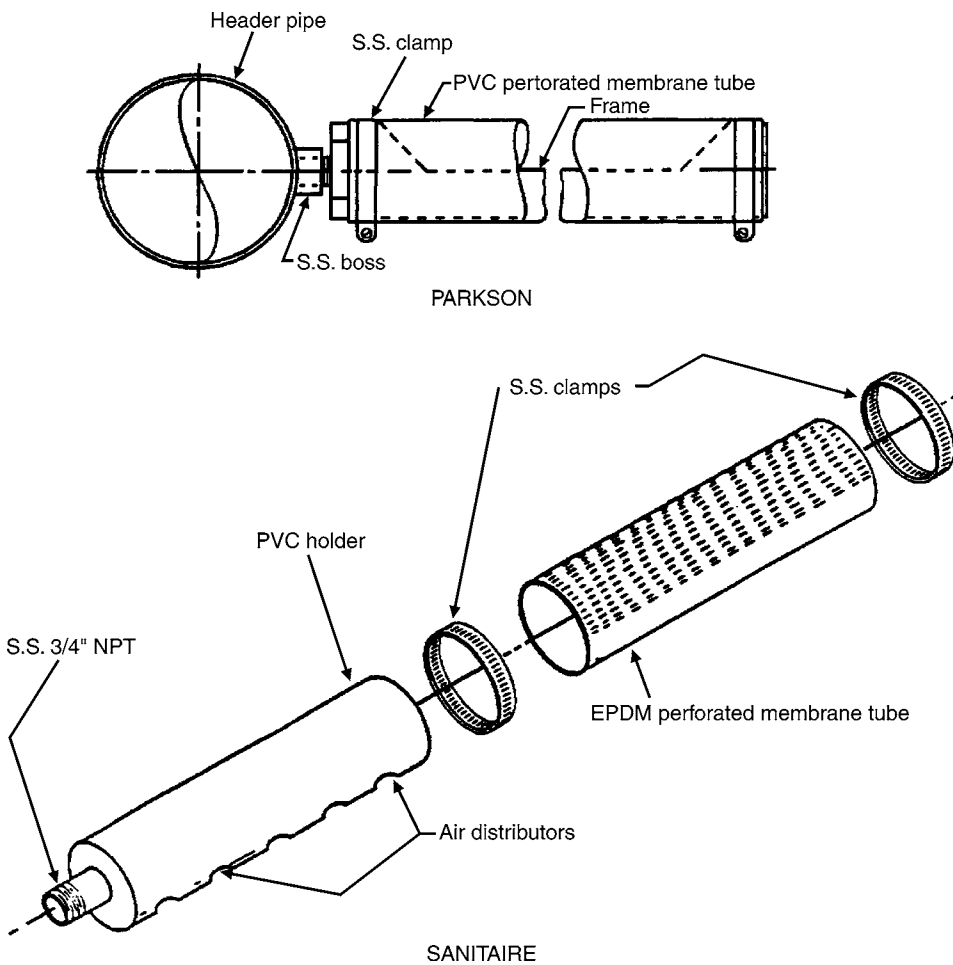
Fig. 3. Perforated membrane tube diffusers (*Source*: US EPA).
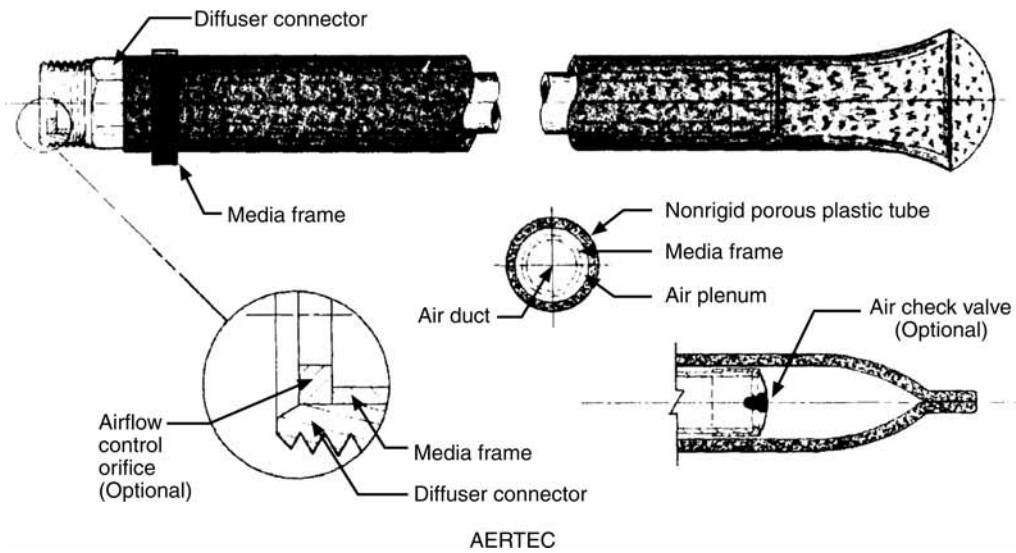
Fig. 4. Nonrigid porous plastic tube diffuser (*Source*: US EPA).

liquid backflow into the air distribution piping, a rubber check valve can be provided. A nonrigid porous plastic diffuser is shown in Fig. 4.

To avoid corrosion problems, most components of the various tube assemblies are made of either stainless steel or durable plastic. The gaskets are usually of a soft rubber material. Tube assemblies with a length of 51–61 cm (20–24 in.) are generally designed to operate in the airflow range of 0.5–4.7 L/s (1–10 scfm)/diffuser. To obtain maximum OTE, the diffusers are usually operated near the lower end of this range, 0.5–2.4 L/s (1–5 scfm)/diffusers. Because of their inherent shape, it is sometimes difficult to obtain air discharge around the entire circumference of the tube. The air distribution pattern will vary with different types of diffusers. The extent of the inoperative area will normally be a function of airflow rate and head loss across the media. As a rule-of-thumb, flow distribution around the tube will improve as head loss increases. Laboratory- or pilot-scale tests should be conducted before selecting a particular tube design because dead areas can provide sites for foulant development. Some tube assemblies are fitted with an airflow rate control orifice inserted in the inlet nipple to aid in air distribution. The orifice is normally about 13 mm (0.5 in.) in diameter, although different sizes can be used for various design airflow rates.

4.3. Dome Diffusers

The fine pore dome diffuser was developed in Europe in the 1950s and introduced in the United States market in the early 1970s (46). Long considered the standard in England and some parts of Europe, domes are now installed in a large number of US plants (47).

The dome diffuser is a circular disc with a downward-turned edge (48–50). These diffusers are 18 cm (7 in.) in diameter and 38 mm (1.5 in.) high. Media thickness is approx 15 mm (5/8 in.) on the edges and 19 mm (3/4 in.) on the top or flat surface. Domes are now being made predominately of aluminum oxide.

The dome diffuser is mounted on either a PVC or mild steel saddle-type baseplate and attached to the baseplate by a bolt through the center of the dome. The bolt can be made from a number of materials including brass, plastics, and stainless steel. Care must be taken when specifying the bolt material and installing the dome to prevent overtightening of the center bolt. Applying too much force can lead to immediate diffuser breakage or future air leakage because of compression set of gaskets and bolt stretching or failures if a plastic bolt is used. A soft, rubber gasket is placed between the diffuser and the baseplate. Ideally, the gasket material should not take excessive permanent compression set with the specified torque. A washer and gasket are also used between the bolt head and the top of the diffuser. Schematics of several dome diffusers are shown in Fig. 5.

Usually, the PVC saddles are solvent cemented to the air distribution piping at the factory. This minimizes bonding, joining, and assembly problems that could occur in the field. For one alternative design (48), the baseplate includes an expansion plug that is inserted into a hole drilled into the air header. It is easier with this design to replace damaged supports than with the solvent-cemented base, but it is more difficult to level or align the baseplates.

The slope of a head loss vs airflow rate curve for a ceramic diffuser is very flat. A variation from the average of ±10% in the specific permeability of a diffuser can result in a 200% change in airflow rate for the same head loss under operating conditions (51). To distribute the air better throughout the system, control orifices are placed in each diffuser assembly to create additional head loss and balance the airflow. The fastening bolt is hollowed out and a small hole is drilled in the side, or the orifice is drilled in the base of the saddle. The size of the orifice is normally 5 mm (0.2 in.).

Dome diffusers are usually designed to operate at an airflow rate of 0.5 L/s (1 scfm)/ diffuser with a range of 0.24–1.2 (0.5–2.5 scfm)/diffuser. Operation more than 1.2 L/s (2.5 scfm)/diffuser is possible, but may not be economical. Increasing the airflow rate more than 0.9 L/s (2 scfm) results in a continuing increase in backpressure and decrease in OTE and may require a larger control orifice.

4.4. Disc Diffusers

4.4.1. Ceramic and Rigid Porous Plastic Media

Disc diffusers are a more recent development. Discs are flat, or relatively so, and are differentiated from dome diffusers in that they do not include a downward-turned peripheral edge. Whereas, the dome design is relatively standard, available disc diffusers differ in size, shape, method of attachment, and type of material (23,19,20). Schematics of typical ceramic and porous plastic diffusers are presented in Fig. 6. One design can be equipped with either ceramic or glass bead media.

Disc diffusers are available in diameters of approx 18–24 cm (7–9.5 in.) and thicknesses of 13–19 mm (1/2–3/4 in.). Except for one design, all discs consist of two flat parallel surfaces. For this exception, a raised ring slopes slightly downward toward both the outer edge and center of the disc. It is claimed that the uniform profile aids in producing uniform air discharge across the entire disc surface (52).

Two disc designs include a step on the outer edge for the purpose of improving uniformity of air flux and effectiveness of the seal at the diffuser edge. The step also facilitates the use of an O-ring seal that is less subject to the adverse effects of compression set of the seal element.
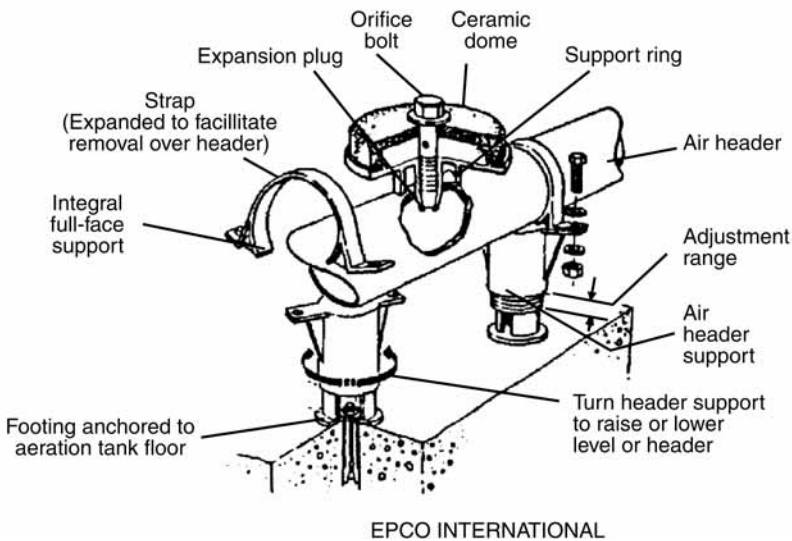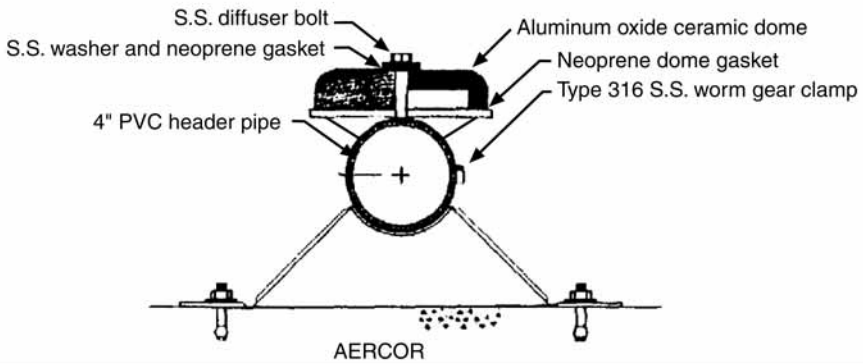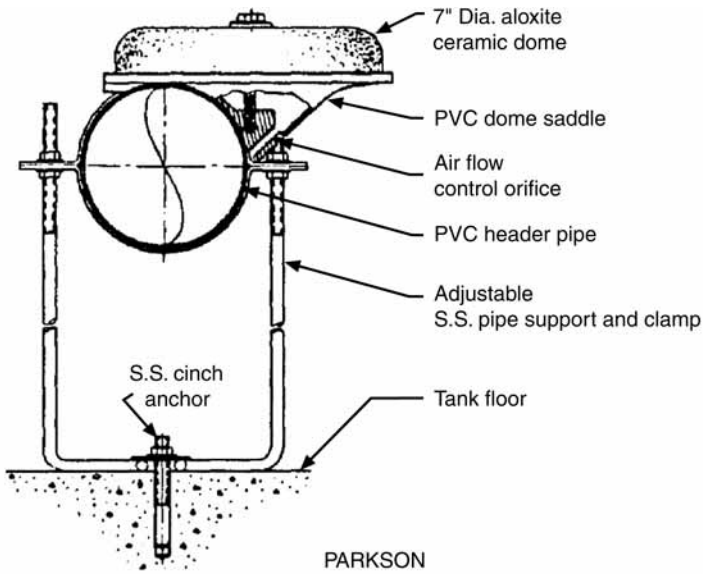
Fig. 5. Ceramic dome diffusers (*Source*: US EPA).

Fig. 6. Ceramic and rigid porous plastic disc diffusers (*Source*: US EPA).

The disc, as with dome diffusers, is mounted on a plastic (usually PVC) saddle-type baseplate. Two basic methods are used to secure disc media to the holder: a center bolt or a peripheral clamping ring. The center-bolt method is similar to that used with domes. A soft, rubber gasket is placed between the diffuser and baseplate. The bolt assembly includes a washer and a gasket. The same precautions should be taken for bolt and gasket materials, as described earlier for domes.

The more common method of attaching the disc to the holder is to use a screw-on retainer ring. Several different gasket arrangements are used with the threaded collar. They include a flat gasket placed below the disc, a U-shaped gasket that covers a small portion of the top and bottom and the entire edge of the disc, and an O-ring gasket placed between the top of the outer periphery of the disc and the retainer ring. The latter arrangement provides a seal between the vertical outer surface of the diffuser and the vertical inner surface of the holder. The baseplate normally includes small raised ribs to aid in obtaining an airtight seal between the gasket and the baseplate.

The retainer ring method of attaching the diffuser to the holder has potential advantages over the center-bolt method. As diffusers become fouled, excessive amounts of air are discharged from the edges and the area around the center-bolt washer (53). Although not specifically documented for discs under controlled conditions, this nonuniform airflow could reduce system OTE. The retainer ring is likely to minimize these problems. In addition, breakage of diffusers from overtightening the bolt, or air leakage problems from gasket compression set or stretching of a nonmetallic bolt can be eliminated.

Two methods are used to attach disc diffusers to air piping. The first is to solvent cement the baseplate to the PVC header prior to shipment to the job site. To avoid future additional costs associated with replacing sections of pipe, the original design should include all the baseplates needed to meet future design requirements for the system. During the early life of the treatment plant, not all the diffusers are installed and plugs are simply inserted in the unused baseplates.

The second disc diffuser attachment method uses mechanical means. Either a bayonet-type holder is forced into a saddle on the pipe, or a wedge section is placed around the pipe and clamps the holder to the pipe. Except for one manufacturer that employs the wedge clamp method of attachment and ships units preassembled, the pipe arrives at the job site with only the holes drilled. This technique makes shipping the pipe somewhat easier (less bulky) and can reduce damage that may occur during shipment or installation. With these types of designs, holes for additional diffusers can be predrilled and plugged or drilled later.

Disc diffusers also include individual control orifices in each diffuser unit. Designs employing the bolt method of attachment usually use a hollow bolt with an orifice drilled in its side. The other designs use either an orifice drilled in the bottom of the diffuser holder or a threaded inlet in the base in which a small plug containing the desired orifice can be inserted. The diameter of the orifice is similar to that used with dome diffusers.

Ceramic and plastic media disc diffusers usually have a design airflow of 0.24–1.4 L/s (0.5–3 scfm)/diffuser. However, the most economical operating range will depend on diffuser size. The smaller 18 cm (7 in.) diameter discs are usually operated at airflow rates of 0.24–0.9 L/s (0.5–2 scfm)/diffuser, similar to those used for dome diffusers. For the larger discs, with diameters of 22–24 cm (8.5–9.5 in.), typical lower and upper airflow

limits are 0.26–0.43 L/s (0.6–0.9 scfm)/diffuser and 1.2–1.4 L/s (2.5–3 scfm)/diffuser, respectively. Prolonged operation at flow rates <0.24 L/s (0.5 scfm)/diffuser is not desirable with discs because insufficient air is available to ensure good distribution across the entire surface of the media. In those applications in which operation above 0.9 L/s (2 scfm)/diffuser is desirable, the control orifice should be sized so that the head loss produced does not adversely affect the economics of the system.

4.4.2. Perforated Membranes

Like their ceramic and rigid porous plastic media counterparts, several different sizes and shapes of perforated membrane disc diffusers are available (32,34–36). They range in diameter from approx 20 to 51 cm (8–20 in.). Although one design uses a convex shape, most are flat in the air-off position. The convex shape reportedly helps in preventing the media from wrinkling (35). Figure 7 shows schematics of several perforated disc diffusers.

As with perforated membrane tube diffusers, perforated membrane discs requires support. The support base is made from a number of different types of thermoplastic materials including polyamide, PVC, and polypropylene. The membrane is usually secured to the base around the periphery by a clamping ring or wire, or a screw-on retaining ring. However, in one case the elasticity of the membrane is enough to secure it to the base. When the air is applied, the membranes will flex upward approx 6–64 mm (0.25–2.5 in.). If the membrane flexes in excess of the manufacturer's recommendations, difficulty could be experienced in maintaining good airflow distribution. Therefore, some designs include an additional means of support in the center to prevent overflexing or ballooning. This center support can consist of a piston-type arrangement or a retaining bolt. The piston type is designed to prevent backflow.

It is common with the disc design to feed air through one or several small holes in the center of the support base. The membrane is normally not perforated near these holes. When the air is turned off, the liquid head forces the unperforated section of the membrane down over the air inlet ports. This provides an additional means of closure to that of the perforations that form a seal against the support member.

The base of the support frame is usually threaded. Common practice is to use a special saddle that is either glued or clamped to the air header for attaching the diffuser. In Europe, where rectangular stainless-steel piping is often used for the air header, a nipple is welded to the pipe for attaching the diffuser.

One membrane disc diffuser utilizes a holder identical to that used for a ceramic disc (32), whereas another utilizes a holder identical to that used for a rigid porous plastic disc (23). By replacing the ceramic or porous plastic disc medium with a membrane disc subplate and the membrane itself, a ceramic or rigid porous plastic system can be converted to a membrane system, or vice versa (Fig. 7).

For the smaller diameter, 20–30 cm (8–12 in.), perforated membrane disc diffusers, the recommended airflow range is approx 0.5–4.7 L/s (1–10 scfm)/diffuser. For the larger diameter, 51 cm (20 in.) disc, the recommended range is 1.4–9.4 L/s (3–20 scfm)/diffuser.

5. DIFFUSER LAYOUT

Figure 8 presents schematics of typical diffuser layouts. These layouts are discussed next as they apply to each of the fine pore diffuser types described earlier.
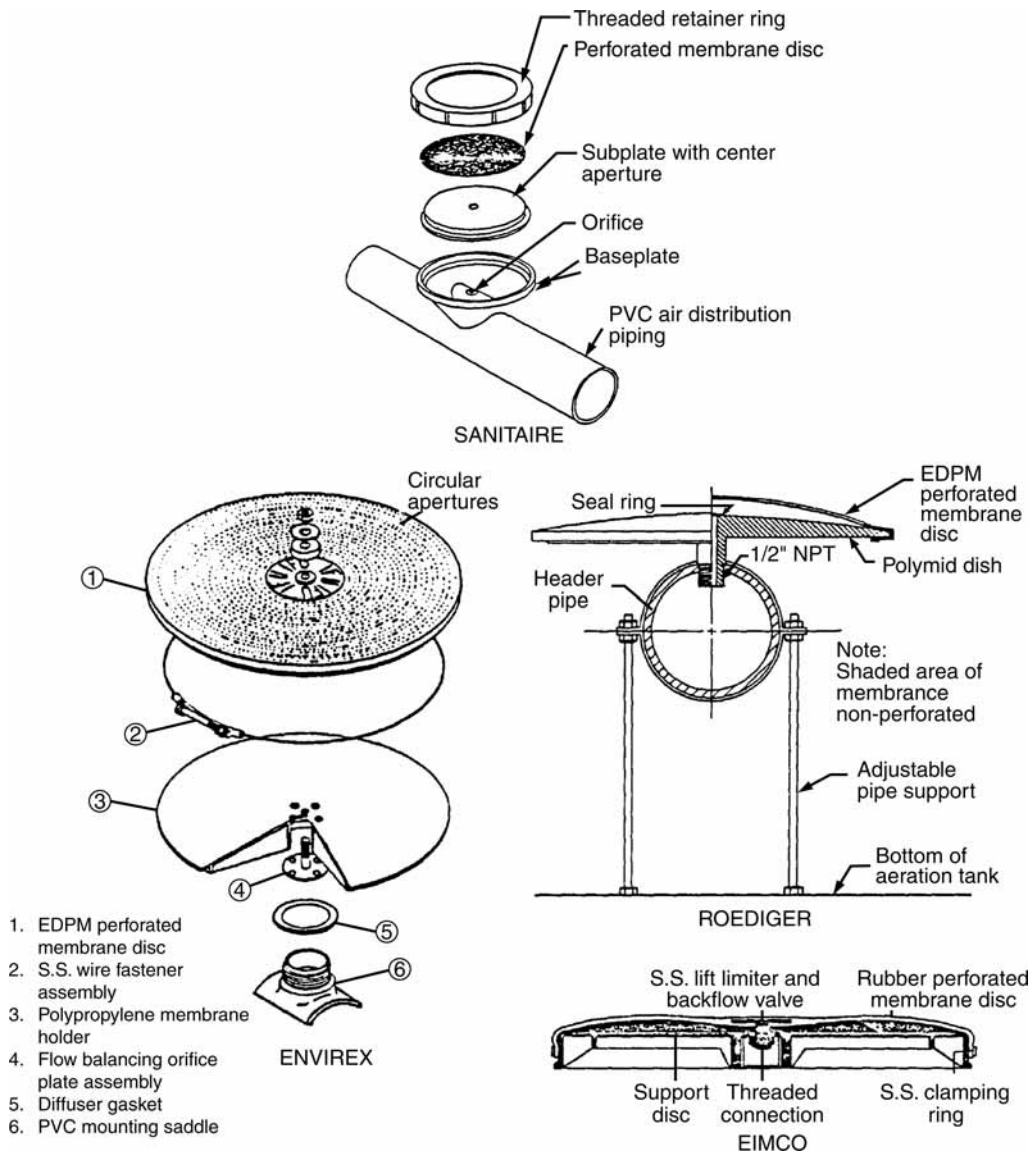
Fig. 7. Perforated membrane disc diffusers (*Source*: US EPA).

5.1. Plate Diffusers

Fine pore ceramic plates of the original 30-cm (12-in.) square design (38,39) are most often grouted into the basin floor. Downcomer pipes deliver the air to open concrete channels below the plates. The channels act as distribution manifolds.

The original plate diffusers can be installed in either a total floor coverage or spiral roll pattern. Total floor arrangements may include closely spaced rows of diffusers running either the width (transverse) or length (longitudinal) of the basin or incorporated into a ridge and furrow design (38). Spiral roll arrangements include rows of plate diffusers typically located along one or both sidewalls of aeration basins. The total floor layout will

Wastewater Flow

Single spiral roll   Mid-width (Center)   Dual spiral roll

Cross roll   Total floor coverage
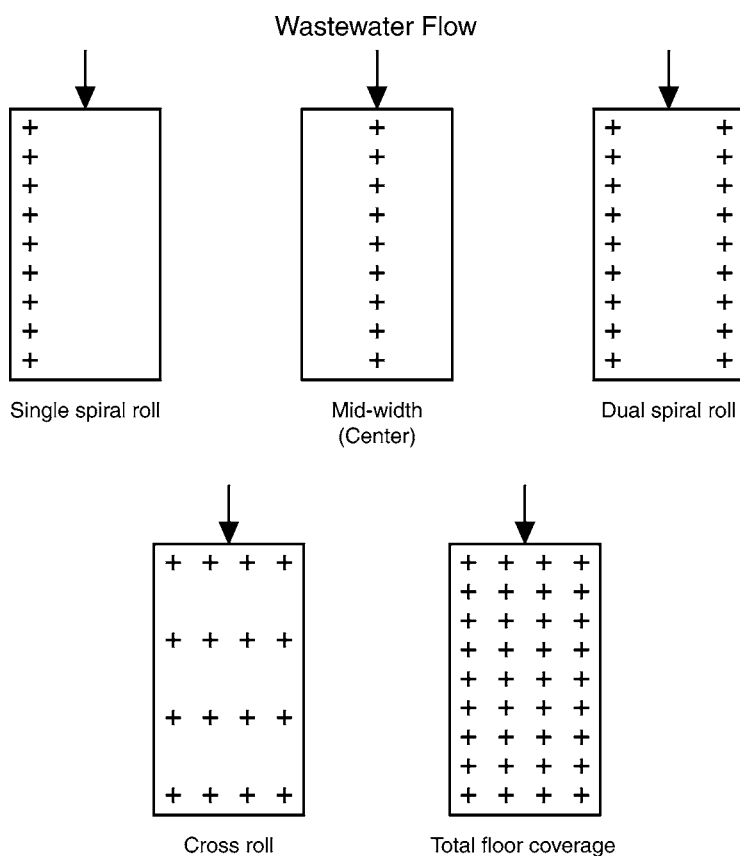
Fig. 8. Typical diffuser layouts (*Source*: US EPA).

produce a higher OTE, whereas the spiral roll pattern will produce more effective bulk mixing of the mixed liquor.

The newer 30×61 cm^2 (12×24 in.^{2}) and 30 cm $\times$ 122 cm^2 (12 in. $\times$ 48 in.^{2}) ceramic and porous plastic plate diffusers (40) are not attached to the basin floor. With the flexibility afforded by their individual rubber air feed hoses, they can be moved, within limits, about the basin floor to form different layout configurations. If a change to a significantly different configuration is desired, new hoses may have to be provided to accommodate the revised diffuser positions.

5.2. *Tube Diffusers*

Most tube diffuser assemblies include a 19 mm (3/4-in. NPT) threaded nipple (stainless steel or plastic) for attachment to the air piping system. This design makes the tubes especially well suited for retrofit or upgrade applications because many coarse bubble diffuser systems use the identical method of attachment.

The air headers on which the tubes are mounted are usually fabricated from PVC, CPVC, stainless steel, or fiberglass reinforced plastic. Carbon steel is sometimes used but is less desirable because of corrosion inside the pipe. Thus, threaded adapters or saddles are glued, welded, or mechanically attached to the pipe at the points in which the

tubes are to be connected. The actual diameter of the air headers will vary depending on the number of diffusers to be installed and the design airflow rate.

The depth of tube submergence in the basin varies depending on the application. In new installations, the tubes are usually placed to the floor as close as possible, typically within 30 cm (1 ft) of the bottom. In retrofit applications, the discharge pressure of the existing blowers may control the depth of submergence. The tubes are normally installed at either the same elevation as the original system or possibly at a somewhat greater distance off the floor to compensate for any increase in head loss incurred through the fine pore media compared with the coarse bubble devices they are replacing. The air headers are usually secured to the basin floor with adjustable height, stainless steel pipe supports.

Tube diffusers are often installed down the center or along one or both long sides of the aeration basin (midwidth, single spiral roll, or dual spiral roll pattern, respectively). In some cases, the headers are mounted on mechanical lifts to allow removal of air headers and diffusers for inspection and cleaning without dewatering the basin. On the header itself, the tubes can be installed along either one side (narrow band) or both sides (wide band) of the pipe.

Tubes can also be installed in either a cross roll or total floor coverage pattern. In the cross roll design, the headers are placed across the basin width and the spacing between diffusers, 30–91 cm (12–36 in.), is small in comparison with the spacing between headers, 3–9 m (10–30 ft). In the total floor coverage pattern, in which the headers can be placed either across the basin width or along its length, the distance between headers and the spacing between diffusers on the headers approach the same value. Total floor coverage will usually achieve higher OTEs than the other configurations.

Spiral roll configurations normally provide better bulk mixing throughout the basin than either total floor coverage or cross-roll patterns. Some designers believe that cross-roll patterns may not provide adequate mixing. One potential disadvantage of the cross roll and total floor coverage designs is that the location and amount of piping required usually makes the use of mechanical liftouts impractical. There is only one known installation in the United States (54) where a total floor coverage liftout system has been installed.

5.3. Disc and Dome Diffusers

Although their shape and operating characteristics may differ, the typical air piping and diffuser layout is identical for both disc and dome diffuser systems. The air distribution manifold should preferably be PVC that should be ultraviolet-stabilized with 2% minimum TiO_2, or equivalent. The specifications, dimensions, and properties of the pipe should conform to either ASTM D-2241 or D-3034 (27), depending on the outside pipe diameter.

The piping network usually has a nominal 10 cm (4 in.) diameter, with an actual O.D. of 10.7–11.4 cm (4.2–4.5 in.). The wall thickness is also variable, typically 3–4.3 mm (0.12–0.17 in.). Sections of pipe are connected with gusseted, mechanical expansion joints to allow for expansion and contraction of the PVC, appropriate to climatic temperature extremes anticipated. Pipe supports, usually made from PVC or stainless steel, are provided to secure the system to the basin floor. The support consists of a cradle or saddle and a holddown strap. The strap is either secured with a bolt or snaps into place.

Pipe supports are adjustable to compensate for variations in the basin floor elevation. Extreme variations in basin floor elevation can cause problems in using standard pipe supports. The pipe support is attached to the basin floor with one or two stainless steel bolts and concrete anchors. The PVC strap and pipe support have experienced some breakage problems in the past. To eliminate these problems, or in cases in which the diffusers are to be mounted a significant distance above the basin floor, i.e., 61 cm (24 in.), stainless steel pipe supports can be used.

Discs and domes are generally installed in a total floor coverage or grid pattern. In some cases in which oxygen demand is low and mixing may control the design (near the end of long narrow basins), the diffusers can be placed in tightly spaced rows along the side or middle of the basin to create a spiral or midwidth mixing pattern, respectively (55). The diffusers are usually mounted to the basin floor as close as possible, within 23 cm (9 in.) of the highest point of the floor being typical. As mentioned in the discussion of tube diffusers, the depth of submergence in some retrofit applications may be controlled by the available blower discharge pressure.

6. CHARACTERISTICS OF FINE PORE MEDIA

Many properties can be used to characterize fine pore media. Knowledge of these characteristics promotes a better aeration system design for a specific set of site conditions (56,57). Appropriate attention to these characteristics in the design phase may also lead to reduced O&M problems during the life of the system. Many of these characteristics are not routinely defined or available for specific media. Reasons for defining media characteristics as thoroughly as possible include providing (3):

a. A means of short-term (batch-to-batch) and long-term (year-to-year) quality control.
b. Baseline performance and a basis for determining changes in media properties under process conditions overtime.
c. Quantitative information needed in design specifications.
d. An indirect indication of changes in field performance.

6.1. Physical Description

For each specific aeration medium, a raw material description should be provided. Usually, the equipment supplier (in conjunction with the manufacturer) selects the optimum materials. By knowing what these materials are, the designer can ascertain whether any unique constituents in the wastewater or cleaning chemicals will be incompatible with the diffusion media. Materials that should be specified include the grit and type of binder for ceramic media, and the chemical composition of the principal constituents comprising porous plastic media and perforated membranes.

6.2. Dimensions

For each type of diffuser element, all critical dimensions should be stated. Other than the obvious reason of assuring compatibility with the mounting base or holder, these dimensions also serve to establish a baseline. After a certain period of operation, the dimensions can be checked to determine whether changes have occurred. It is possible that some materials may warp, expand, or stretch with time. Only if baseline dimensions have been established can these changes be detected.

6.3. *Weight and Specific Weight*

The weight of the diffuser and its apparent specific weight (calculated) should also be determined. These two characteristics can be used for quality control. A wide range in weight or specific weight between several apparently similar diffusers could indicate an unacceptable product (38). In this situation, it is likely that a variance in weight will also result in a variance in some of the other parameters such as dynamic wet pressure (DWP), bubble release vacuum (BRV), or uniformity.

Initial or clean media weight and specific weight should also be determined to establish baseline conditions. Changes in media weight and specific weight, as with media dimensions, can occur with time. These changes can result from absorption of liquids, leaching of certain resins or additives, or dissolution of the base material. A single weight measurement should usually detect any changes. However, a better approach is to obtain a series of measurements over the time. Also, if media weight is determined in conjunction with other physical or mechanical testing (e.g., tensile strength), an indication of any degradation can be determined.

6.4. *Permeability*

The permeability test may have some application for quality control. However, because permeability is such an inexact parameter, it is of little practical significance in characterizing even ceramic-type diffusers. The following discussion is included to define the term because it is often mentioned in regard to fine pore aeration media and points out some of the many shortcomings of the test.

Ceramic diffuser media are usually available in a number of different grades. Grades are distinguished by pore size, which is controlled by the size of the grit material, binder type and content, and firing temperature. Because measurement of pore size was not practical for a large number of samples, the ceramic manufacturing industry developed a simple but somewhat arbitrary test to differentiate between grades of media. This test was referred to as the permeability rating.

Permeability is a measure of a porous medium's frictional resistance to airflow. It is an empirical rating that relates flux rate to pressure loss and pore size or pore volume. Permeability is usually defined as the amount of air at standard conditions that will pass through 929 cm^2 (1 ft^2) of 25-mm (1 in.) thick dry porous media under a differential pressure equivalent to 5 cm (2 in.), w.g. when tested at room temperature. The airflow value obtained (scfm) under these conditions is called the permeability (perm) rating (3).

Unfortunately, the permeability measurement does not provide a true basis for comparison of media performance. The same permeability rating could be obtained from a diffuser with a few relatively large pores or a multitude of small pores. Also, two diffusers with the same pore structure would have different ratings if they have different thicknesses.

Most ceramic and some plastic media specifications now include a test for permeability. Unfortunately, the ceramic industry has not "standardized" this test procedure. The early specifications were developed for 30 × 30 cm^2 (12 × 12 in.^{2}) plates, 25 or 38 mm (1 or 1.5 in.) thick. Today, specifications are needed for products of various shapes, densities, and thicknesses, often of poorly defined effective area. Attempts have been made to apply the principles of the test through a parameter known as specific permeability (58). The procedure for determining specific permeability generally consists of mounting

and sealing the test diffuser in a fixture similar to the manner in which it is mounted in the field. Sufficient air is then passed through the dry element to produce a pressure differential of 5 cm (2 in.) w.g. This measurement and the geometry of the diffusers is then used to estimate what the airflow would have been had the dimensions of the test diffuser been $30 \times 30 \times 25$ mm^3 ($12 \times 12 \times 1$ in.^{3}).

The specific permeability procedure has served to improve the utility of this test to a degree. However, it still suffers from the following deficiencies (3):

a. Clamping and sealing details are not defined well enough to provide acceptable precision.
b. Depending on the degree of complexity of the media geometry, effective diffuser area, and effective air path length cannot always be easily defined and accounted.
c. Correction factors to account for pressure, temperature, and humidity of the air have not been developed.
d. The effects of surface tension are not accounted for since the test is conducted on a dry basis.

6.5. Perforation Pattern

Each perforated membrane diffuser manufacturer uses a slightly different perforation pattern. In fact, the same manufacturer may use one type for a disc diffuser and a different one for a tube assembly. One reason for changing the perforation pattern between diffuser types is that the various shapes result in different stresses and resulting strains on the membrane. Thus, a pattern is developed that will best be able to withstand the magnitude and direction of the loads that will be applied (3).

Perforations can differ in regard to type (holes or slits), size, orientation, and density (number perforations/diffuser surface area). Usually, the specific pattern has been developed over the time and is not a feature that changes from job to job. It is important, however, to detect any changes that may occur to the membrane over time. Measurements or photomicrographs can be made and compared to baseline conditions to determine if the perforations have either expanded or taken on a permanent set. Also, in situations in which replacement diffusers are purchased, the perforations should be similar to the original diffusers to ensure compatibility.

6.6. Strength

Structural or physical strength is also an important media characteristic. Strength, as described in this section, applies only to rigid diffusion media (ceramic and porous plastic). The diffusion media must be strong enough to withstand (3):

a. The static head of the water above the diffuser (in cases in which the air supply is shut off).
b. The forces applied when attaching the media to the diffuser holder.
c. Stresses and shocks of reasonable handling, shipping, and maintenance.

For discs and domes, measurement of strength usually involves supporting the diffuser in a fashion similar to that used for the final assembly and then applying a load to a 25 mm (1 in.) diameter area in the center of the diffuser. Using this method, developed primarily for ceramic diffusers, acceptable loads for the ceramic material are 270–455 kg (600–1000 lb). Diffusers that use a peripheral clamping method do not require the same flexural strength as those that utilize the center bolt method of attachment. Slightly different techniques have been developed to evaluate the strength of nonrigid diffusion material.

6.7. *Hardness*

Hardness is an important media characteristic for perforated membranes because it is an index of the resistance of an elastomer to deformation. It is measured by pressing a ball or blunt point into the surface of the material (27). The most commonly used instrument to measure hardness is the durometer.

Different types of instruments are available that produce a range of overlapping scales. Shore A durometer readings are the most common, although Shore D readings are sometimes specified. For each range, the higher the durometer reading, the harder is the material.

Hardness can be used to detect changes in membranes. Softening or hardening of the membrane material may be indicative of environmental attack. A softening, for instance, may indicate the absorbency of a solvent into a thermoplastic. On removal from the wastewater, the solvent may evaporate and the plastic may resume its original hardness. Hardening, on the other hand, may indicate the loss of an additive or plasticizer over time or attack by some type of acid. In any regard, changes in hardness should be noted and other characteristics (BRV, DWP, and OTE) are evaluated to determine if media performance has been affected. In some cases, changes in hardness may denote a change in media characteristics that will not necessarily shorten service life (3).

6.8. *Environmental Resistance*

The constituents found in typical domestic wastewater are usually not excessively harmful to fine pore diffuser media. Some industrial wastes, however, may contain compounds that will result in physical degradation of the media, especially for the porous plastics and perforated membranes. Some compounds of potential concern include mineral and vegetable oils, organic solvents, and strong oxidizing agents.

It is common practice to use chemicals to clean fine pore diffusers when they become fouled. Although hydrochloric acid is the most common cleaning chemical (either as a liquid or gas), other compounds have been used. These include inorganic acids (sulfuric and nitric), bases (sodium hydroxide, potassium hydroxide, and ammonium hydroxide), carboxylic acids (formic and acetic), detergents, and organic solvents (3).

Air-phase foulants including oxidants such as ozone are also of concern. Ambient concentrations of these oxidants are aggressive to a number of elastomers used in wastewater treatment (e.g., nitrile, styrene butadiene rubber, polyisoprene, and natural rubber). The effect is intensified when the materials are under stress. Ozone-resistant membrane materials should be developed. In all cases, assurance should be obtained (from the literature, supplier, or tests) that the material selected has the requisite resistance to these oxidants in the concentrations expected in service. The same assurances should be obtained for those applications in which fine pore devices are used to disperse ozone.

Most ceramic diffusers have been marketed for many years and, except for some slight degradation when acids are used for cleaning, appear to be quite resistant to chemical attack. Porous plastics and perforated membranes have been developed in the past 10–15 yr. Testing has shown that wide variations exist among the generic groups of plastics in their chemical resistance and physical and mechanical properties (28).

Even within a generic classification, different formulations may result in a wide variation in performance in a particular environment. To enhance the physical properties of plastics and elastomers, manufacturers often incorporate additives into their membrane formulations. Therefore, the actual material may differ in composition from published data. As a result, environmental resistance testing should be conducted with the actual diffuser media in both stressed and unstressed conditions. Much of such testing may serve as a qualification rather than a routine requirement.

In conducting these tests, several of the media characteristics discussed in this section can be used to establish if any chemical degradation is occurring. Some of the more important include changes in dimensions, weight, strength, and DWP.

6.9. Miscellaneous Physical Properties

Several additional physical properties can be used to characterize fine pore aeration media. A partial list of those properties that may be of importance, especially for porous plastics and perforated membranes is (3):

a. Tensile strength (stress and strain).
b. Elongation at failure.
c. Modulus of elasticity.
d. Creep.
e. Compression set.
f. Tear resistance.
g. Strain corrosion.
h. Solvent extraction.
i. Ozone resistance.

Because most of these properties are temperature dependent, data should be developed over the expected range in temperature. Definitions and procedures can be found in the ASTM Standard (27).

Because very little information exists regarding the above items, it is premature to attempt to place guidelines on what would be considered acceptable. However, it is possible to use these parameters for assessing the effects of field operation. Any changes over time may be an indication of degradation of the media or impending problems (e.g., significant creep with a polyethylene tube diffuser may eventually lead to air leaks at the end caps). These properties may also be important in evaluating the general quality of a membrane material. For example, the ratio of the tensile strength at design operating conditions and at failure could be calculated. The higher the ratio, the greater is the safety factor (3).

6.10. Oxygen Transfer Efficiency

The OTE that can be achieved with fine pore diffuser media over their design life is likely their most important characteristic. Most projects require a shop or field oxygen transfer test to verify diffuser performance regarding OTE. OTE information can also be obtained in using laboratory (bench-scale) apparatus to aid in characterizing the media. Laboratory tests are not intended to be a substitute for shop or field testing, or for predicting field OTE. Rather, they should be used to evaluate relative differences in performance between two or more diffusers.

A typical laboratory set up will consist of a small column, 61–91 cm (2–3 ft) in diameter and 2–3 m (7–10 ft) high (3). The diffuser(s) to be tested is installed in the column and clean water OTE is determined over a range of airflows (ideally two or three different rates).

Clean water OTE is usually determined by the nonsteady-state test procedure described in an ASCE Standard (59). A second procedure that also seems to produce excellent results involves a steady-state test (24,60). With this technique two diffusers are usually placed in the test basin. The airflow to the first diffuser is set at the desired rate; a very low airflow rate (<5% of the first) is set for the second diffuser. The basin is covered, sodium sulfite is added at a constant rate to achieve steady-state DO conditions, and the off gas is analyzed for oxygen content. After sufficient data is obtained on one diffuser, the air supply is rapidly switched, causing the second diffuser to operate at the specified rate and the air to the first diffuser to be reduced to maintain only a slight positive pressure. By repeating the cycle several times, the relative oxygen transfer performance of the two diffusers can be obtained. Details of this test procedure are presented in the US EPA manual (3).

Both techniques (steady- and nonsteady-state) produce acceptable results. If an off-gas analyzer is available, the steady-state procedure is more desirable. Data can be generated more quickly, and the ability to compare two diffusers on a side-by-side basis is an additional advantage.

It must be emphasized that OTE values determined in laboratory tests are for comparison purposes only. They can be used as a quality control techniques, for detecting changes in performance that may occur during field operation, or for assessing the effectiveness of various cleaning agents. Ideally, laboratory OTE tests will be conducted in conjunction with other media characterization tests (e.g., DWP and BRV) to examine what correlations might exist.

6.11. Dynamic Wet Pressure

Dynamic wet pressure (DWP) is a very important characteristic in evaluating and selecting porous media. DWP, the pressure differential (head loss) across the diffusion element when operating in a submerged condition, is expressed in cm (in.) w.g. at some specified airflow rate (53). As a general rule, the smaller the bubble size, the higher the DWP. Whereas small bubbles may increase OTE, the additional power required to overcome the higher head loss may negate any potential savings.

DWP can be measured in the laboratory or in the field. Accurate field measurements are often more difficult to obtain. Figure 9 presents a schematic of a typical field set up for *in situ* monitoring of DWP. This particular arrangement includes a bubbler or static line (Tap 3), a line to sense pressure in the air header (Tap 1), and a connection in the body of the diffuser holder immediately below the media (Tap 2). Tap 2 is considered optional because the physical design of some diffusers makes it very difficult or impossible to locate this connection.

Using the three taps shown in Fig. 9, it is possible to measure the head loss across the diffusion media (Taps 1 and 3) as well as estimate the airflow rate through the diffuser based on the head loss across the control orifice (Taps 1 and 2). If Tap 2 is omitted the DWP measured will include inlet losses as well as media losses.
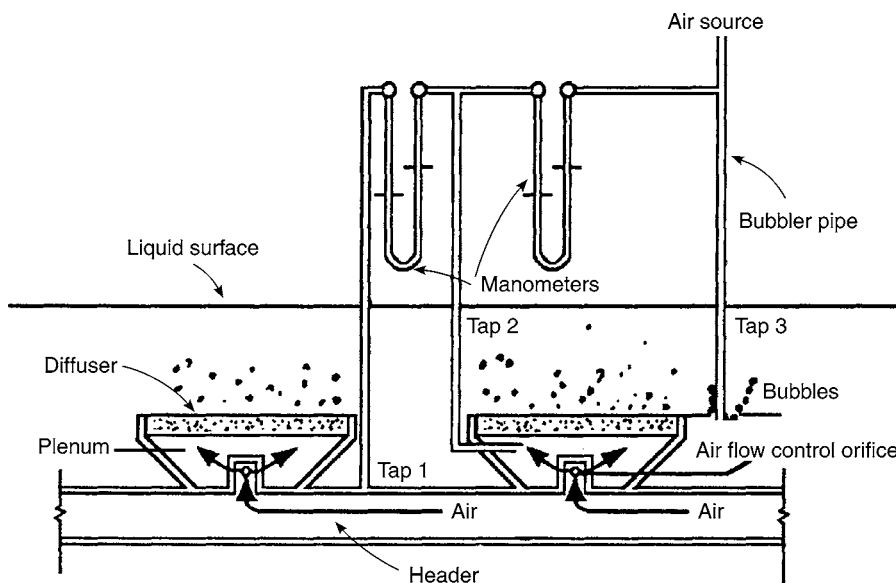
Fig. 9. On-Line device for monitoring DWP of fine pore diffusers (*Source*: US EPA).

Extreme care must be taken to purge all moisture from both pressure sensing lines and set the airflow through the bubbler tube at the lowest possible rate that will not induce a significant head loss. Also, because of the relationship between standard and actual airflow rates, the head loss in the field will be a function of diffuser submergence. If a field measurement of DWP is made the units used in describing the flow (standard or actual) must be known and corrections are made before different media are compared.

An alternative to measuring DWP in the field is laboratory measurement of DWP for selected diffusers removed from the aeration basin. A supply of test diffusers may be provided from removable test headers. Test headers having four diffusers have been used in several plants (24,61,62). A typical test header is shown in Fig. 10. To reduce the weight of the test header assembly so that diffusers can be more easily removed, a two-diffuser arrangement may be used in place of the four-diffuser assembly.

The removable headers can be equipped with pressure taps for *in situ* monitoring of DWP. These field readings can be supplemented with more precise measurements of DWP in the laboratory. It is imperative that the test header be operated at airflow rates similar to the full-scale system. Airflow rates to individual diffusers can be easily determined for units having fixed-size flow control orifices by measuring the pressure drop across the orifice. Airflow rates can also be measured using one or more rotameters. The use of removable headers requires significant operator attention and commitment if the data collected is to be of value.

Although the diffusers must first be removed from the aeration basin, laboratory measurement of DWP will usually be more accurate. However, the diffusers must be kept wet and rapidly transported to the laboratory (ideally, within 24 h) to prevent changes in the characteristics of the foulant from occurring. In determining DWP, it is important that porous diffusers (ceramic and plastic) be allowed to soak for several
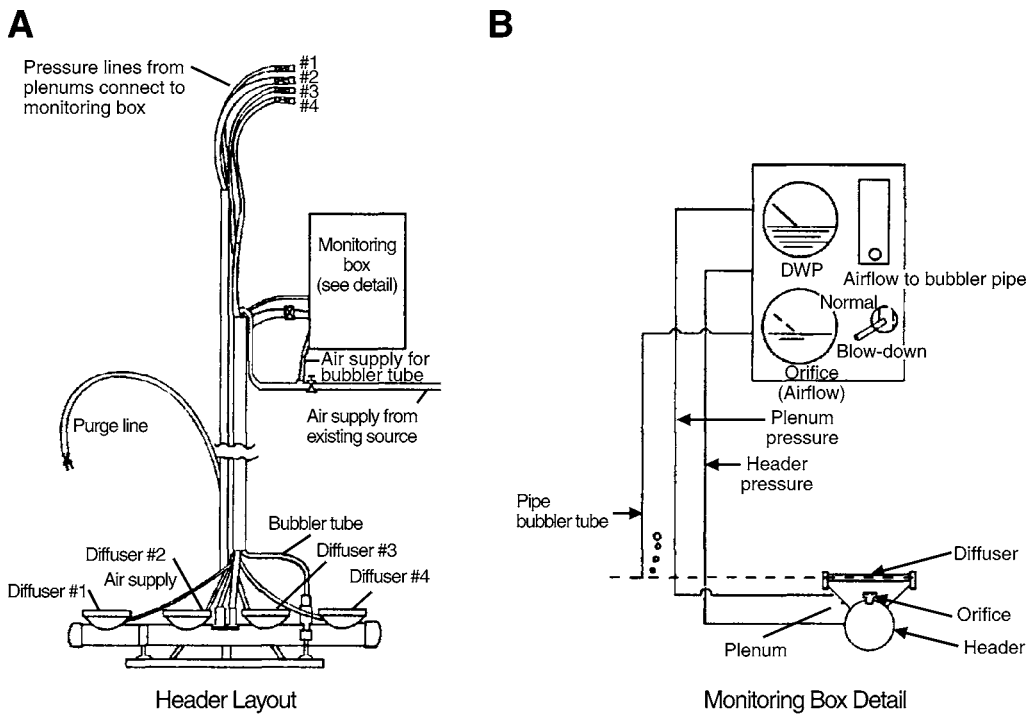
Fig. 10. Removable test header (*Source*: US EPA).

hours (plastic materials may require a much longer period) prior to testing, to completely saturate all the pores. Because the actual head loss will be a function of the degree of water saturation in the diffusers, a slightly different curve will be obtained if the air is started at a low flow rate and is increased, or vice versa. Standard practice is to purge the media at the upper airflow rate for a predetermined interval (5–10 min), then record subsequent head loss values as the airflow rate is decreased. At least three different airflow rates should be used to define DWP adequately (3).

DWP testing can be conducted in an aquarium or similar small basin using an apparatus depicted in Fig. 11. Usually, the diffuser holder will contain a control orifice to aid in airflow distribution throughout the system. In conducting the DWP test, the apparatus should be set up so that the losses across the orifice are not included in the DWP determination. Orifice losses, depending on the airflow rate, can become quite high. This may mask the losses associated with the media that represents the main purpose of the DWP test.

The porous media now in use have a DWP of about 8–51 cm (3–20 in.) w.g. when operated within the typical or specified airflow ranges. The specific value depends on the type of material, surface properties, airflow rate, and diffuser thickness. For ceramic and porous plastic materials the head loss vs airflow curve is linear over the typical operating range and the slope is relatively flat. For these two types of material, most of the DWP is associated with the pressure required to form bubbles against the force of surface tension. Only a small fraction of the DWP is required to overcome frictional
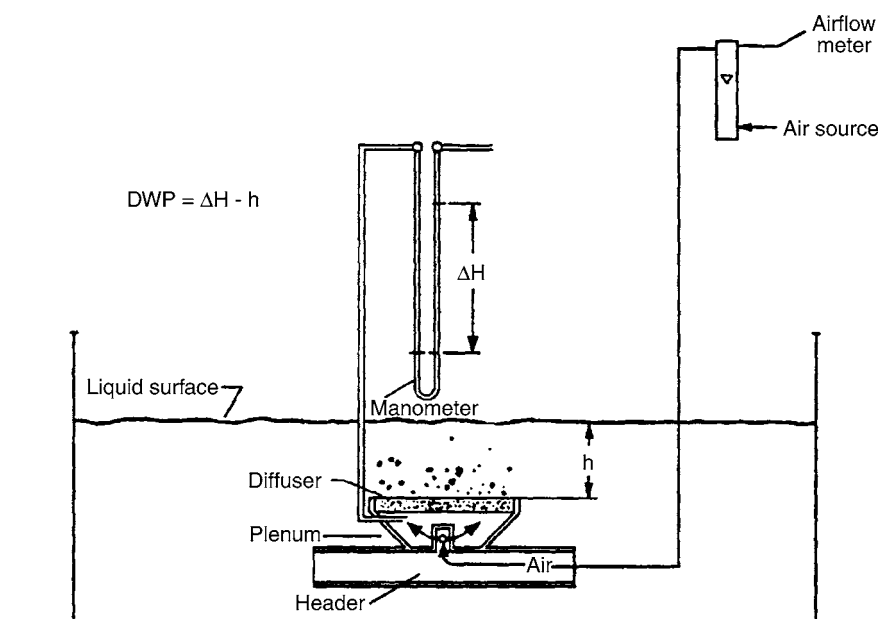
Fig. 11. Apparatus for measuring DWP in the laboratory (*Source*: US EPA).

resistance. Because surface tension is not affected significantly by material thickness or airflow rate, these two factors are only minor contributors to the overall DWP (53).

6.12. Bubble Release Vacuum

The bubble release vacuum (BRV) test provides a means of determining the BRV at any point on the surface of a diffuser element relative to other points on its surface. Normally, BRV denotes the average of the point BRV values for a specific diffuser. This test procedure is useful for assessing the uniformity of pores on the surface of diffusers under clean as well as fouled conditions (63). For details of test the readers are referred to the US EPA manual (3).

BRV, as suggested by the name, is a measure of the negative pressure in cm (in.) w.g. required to form and release bubbles in tap water from a localized point on the surface of a thoroughly wet porous diffuser element. This is accomplished by applying a vacuum to a small area on the working surface of a wet diffuser and measuring the differential pressure when bubbles are released from the diffuser at the specified air flux at the point in question. The air flux is usually set quite low, 10 L/s/m^2 (2 scfm/ft^2), which is within the range of flux values used for porous diffusers to minimize frictional drop in the BRV measurement and, in cases in which the diffusers are fouled, to avoid removing the fouling material during the BRV test.

The BRV test was initially developed for use on ceramic and porous plastic diffusers. It can also be used on perforated membrane diffusers if the test equipment is modified to account for the greater distance between pores and holes or slots in this case (24).

Both DWP and BRV provide a measure of the bubble release pressure. For the DWP test, the measurement is made across the entire diffuser. In cases in which the diffuser

is partially fouled, air may simply short circuit the fouled area. Thus, DWP may not indicate the true condition of the media. The BRV test on the other hand, measures the pressure at a small localized area. For this reason, BRV has been found to be the more sensitive test. In studies evaluating diffuser fouling, the use of BRV data, averaged for the entire diffuser, permits significant shortening of the test period required to obtain definitive conclusions regarding diffuser fouling (63).

It should also be noted that it might be possible to combine various measurement parameters in characterizing fine pore diffusion media. It has been suggested that the ratio of DWP to BRV, when measured at the same air flux, may be a better indicator of diffuser fouling than either parameter alone (61,63,64). DWP measures the overall pressure that forms bubbles at a specific air flux over the entire diffuser surface. BRV measures the average negative pressure required to form bubbles at a specific air flux over a limited region of the diffuser surface.

The ratio of DWP to BRV is closely related to the fraction of the diffuser area that is actually emitting bubbles. As the ratio decreases, less of the diffuser area is operating for the same airflow rate. This means that the active areas are operating at higher localized air fluxes potentially causing the formation of larger bubbles and resulting in lower OTEs. A DWP/BRV of 1 (both measured at the same air flux) suggests clean uniform media, whereas fouled diffusers frequently exhibit DWP/BRV values substantially lower than 1.

The relationship between permeability and BRV is of interest from specification and quality control point of view. Many specifications require that permeability tests be conducted to control uniformity, effective pore size, and backpressure of the diffuser elements in service. There is no recognized standard procedure for determining permeability. Furthermore, because the test measures only an overall resistance to flow, it gives no indication of uniformity within an individual diffuser being tested.

On the other hand, the BRV test, which is conducted at air fluxes and pressure differences comparable to service values and includes the effects of surface tension, is not subject to the deficiencies of the permeability test. Additionally, the coefficient of variation of this measurement provides a measure of diffuser uniformity. It has been suggested, therefore, that the BRV test is a far more applicable and meaningful field test than the permeability test as presently practiced for specifying diffuser uniformity and effective pore size (65).

In reasonably uniform diffusers of a given geometric shape, a relatively good correlation exists between the new or original BRV (BRV_0) and specific permeability. Fig. 12A presents data obtained from four ceramic disc diffusers of equal size having a specific permeability of 14–50 (65). Because BRV is a measure of diffuser pore size, it is reasonable to assume that as pore size increases and BRV decreases, standard OTE (SOTE) decreases. Using a laboratory oxygen transfer test procedure, the relationship between relative SOTE and specific permeability and BRV shown in Fig. 12B was developed (65). It is apparent for these diffusers that little difference in relative SOTE exists for specific permeabilities between 14 and 38, $BRV_0 = 23$–10 cm (9–4 in.) w.g.

6.13. Uniformity

Uniformity of individual diffusers and the entire aeration system is important if high OTEs are to be attained. On an individual basis, the diffuser must be capable of delivering
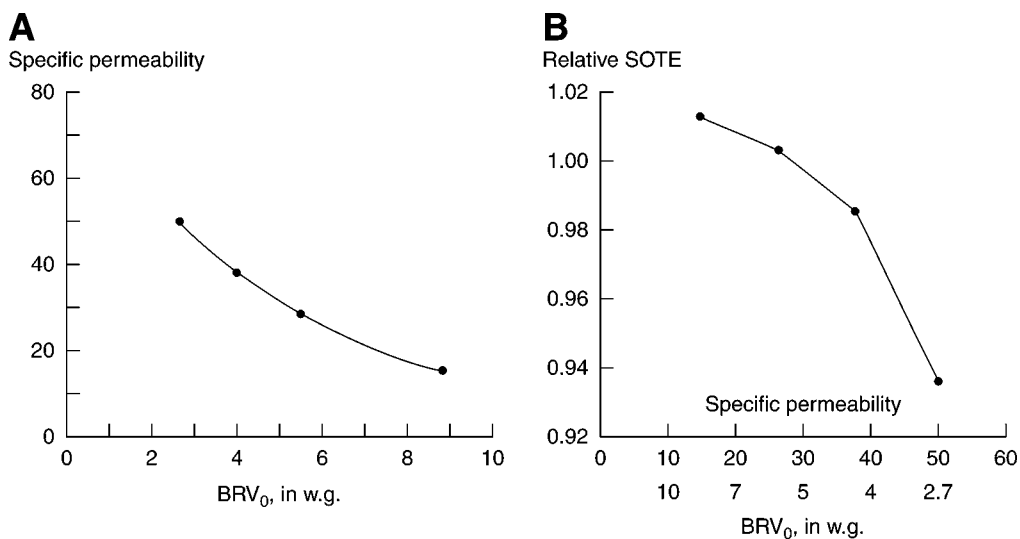
Fig. 12. BRV relationships (*Source*: US EPA).

uniform air distribution across the entire surface of the media. If dead spots exist, chemical or biological foulants may form and eventually lead to premature fouling of the diffuser. Also, if small areas of extremely high air flux are present, larger bubbles may form and OTE will decrease.

Most system designers recognize the importance of uniformity and, as a result, will include a uniformity testing procedure as part of the job specification. A common practice has been to select random samples of media from each batch during the manufacturing run. The diffusers are placed in water for a fixed period to saturate them and then tested in a shallow basin at a predetermined airflow rate. Usually, a visual observation is the basis for the test. This type of qualitative method is obviously quite arbitrary. Two people are likely to have somewhat different definitions for what constitutes uniform airflow. In other cases, a high airflow from around the periphery may tend to mask the view of the center of a diffuser that is completely dead. Because of these problems, a visual test is not considered an acceptable method of characterizing fine pore media for uniformity.

The use of quantitative techniques is a much better approach for measuring uniformity. These procedures actually measure the rate of air release from different areas of the diffuser (53). With the diffuser submerged in 5–20 cm (2–8 in.) of water and at an airflow rate of approx 10 L/s/m^2 (2 scfm/ft^2) (or at the recommended design rate), the rate of air release is determined by measuring the displacement of water from an inverted cylinder. Based on air volume, time, and area of the collection cylinder, an air flux rate is calculated.

Air flux may be expressed in several ways. Apparent flux is the airflow rate per diffuser divided by the effective diffuser area. For planer diffusers, the exposed surface area is considered the effective area. For dome and tube diffusers, the projected area has normally been used to calculate apparent flux. Local flux is the local airflow rate per unit area of a small-defined segment of a given diffuser. Effective flux is the

weighted average (based on area) of the local flux measurements for one or more diffusers.

For diffusers that provide uniform air release (i.e., all local flux values are equal), the effective flux and apparent flux are equal and the ratio of effective flux to apparent flux, the effective flux ratio (EFR), is unity. If air is released unevenly, the EFR would be more than one. High values of EFR may produce poor OTE values and promote fouling.

In measuring air flux, the same or varying size collection cylinders can be used. With varying size cylinders (sometimes referred to as the three bucket catch), air flux is determined for progressively larger rings on the surface. This method involves a certain degree of averaging and as a result may not be very sensitive. For example, results obtained using this technique could indicate that air flux is uniform even though one quadrant of the surface could be discharging no air at all (3).

A more effective procedure is to use a relatively small diameter cylinder and test several points on the media surface. These individual points can be plotted to produce a flow profile or simply compared. It is also useful to calculate s/x, in which s is the sample standard deviation and x is the average of the individual readings. In this case, the smaller the s/x value, the more uniform the diffuser.

Besides measuring flux, BRV values can also be used as a measure of uniformity. Based on individual point values, s/x can be calculated. The smaller the value, the more uniform the specific diffuser.

The previous paragraphs have presented several procedures for establishing uniformity. Unfortunately, no well-defined guidelines have been developed concerning the variations between points that can be tolerated before the diffuser should be rejected as nonuniform. The calculated values should be used only for comparison purposes.

7. PERFORMANCE IN CLEAN WATER

The following discussion summarizes clean water performance data for fine pore diffusion devices. The clean water performance data presented in most of the tables and graphs in this section were generated using the ASCE recommended clean water Standard (59). Data has been screened to best depict the trends and ranges of performance of representative types of fine pore diffusers. It must be emphasized that the information presented in this section provides general trends in clean water performance; these data should only be used with caution in the final design calculations for a particular type of diffusers.

The results of clean water oxygen transfer tests are reported in a standardized form as standard oxygen transfer rate (SOTR), SOTE, or standard aeration efficiency (SAE) as shown in Table 1. The standard conditions for reporting clean water tests are also delineated in this table. All data reported in this section are given as standard transfer values unless otherwise noted.

The performance of diffusers under clean water test conditions is dependent on several factors. Among the important factors are (3,66,67):

a. Diffuser type (material, shape, and size).
b. Diffuser placement and density.
c. Gas flow rate per diffuser.
d. Basin geometry.
e. Diffuser submergence.
f. Uniformity of air flux.

Table 1
Standard Equations for Clean Water Oxygen Transfer Tests

Standard Oxygen Transfer Rate (SOTR), lb/h:
  $SOTR = 8.34 \, K_L a_{20} \, C_{\infty 20} \, V$

Standard Oxygen Transfer Efficiency (SOTE), percent:
  $SOTE = 100 \, (\text{Mass transferred/mass supplied}) = SOTR/W_{O_2}$

Standard Aeration Efficiency (SAE), lb/hp-h:
  SAE = SOTR/power input (specified as delivered, brake, wire, or total wire)
  $K_L a$ = apparent volumetric mass transfer coefficient in clean water at temperature T, 1/h
  $K_L a_{20} = K_L a$ @ 20°C, l/h
  V = clean water volume, MG
  W_{O_2} = mass rate of oxygen, lb/h
  $C_{\infty 20}$ = steady-state DO saturation concentration attained at infinite time at 20°C
        and 1 atm, mg/L
  T = clean water temperature, °C

Standard Conditions:
  DO = 0.0 mg/L α = 1.0
  Water temperature = 20°C β = 1.0
  Pressure = 1.00 atm   F = 1.0
  α = (process water $K_L a$ of a new diffuser)/(clean water $K_L a$ of a new diffuser)
  β = (process water C_∞)/(clean water C_∞)
  F = (process water $K_L a$ of a diffuser after a given time in service)/($K_L a$ of a new diffuser in
      the same process water)

The information that follows is presented to illustrate the effects of these factors.

7.1. Steady-State DO Saturation Concentration (C_∞)

An examination of Table 1 indicates that one of the critical parameters required in the calculation of oxygen transfer rate is the steady-state DO saturation concentration, C. For submerged aeration applications, C is significantly greater than the surface saturation value, C_s, tabulated in most standard tables. Therefore, it is necessary to either measure C (59) during clean water tests or to calculate it based on comparable full-scale test data. The value of C is primarily dependent on diffuser submergence and diffuser type. Typical results of clean water test measurements are presented in Figs. 13 and 14. Suppliers of aeration equipment should be able to provide appropriate clean water test data.

Alternatively, C_∞ can be estimated for design purposes from the surface saturation concentration and effective saturation depth, d_e, by (3):

$$C_\infty = C_s \, [(P_b - P_{vT} + 0.007\gamma_w d_e)/(P_s - P_{vT})] \tag{1}$$

where C_∞ is the steady-state DO saturation concentration attained at infinite time at water temperature T and field atmospheric pressure P_b, mg/L; C_s is the tabular value of DO surface saturation concentration at water temperature T and standard atmospheric pressure P_s, mg/L; d_e is the effective saturation depth, ft; P_s is the atmospheric pressure at standard conditions, 14.7 psia or 1 atm at 100% relative humidity; P_b is the field atmospheric

Tank: 20 ft. × 20 ft.
Power: ~ 1 hp delivered/1,000 ft.^{3} for rigid porous plastic tubes
Power: ~ 5 hp delivered/1,000 ft.^{3} for ceramic domes
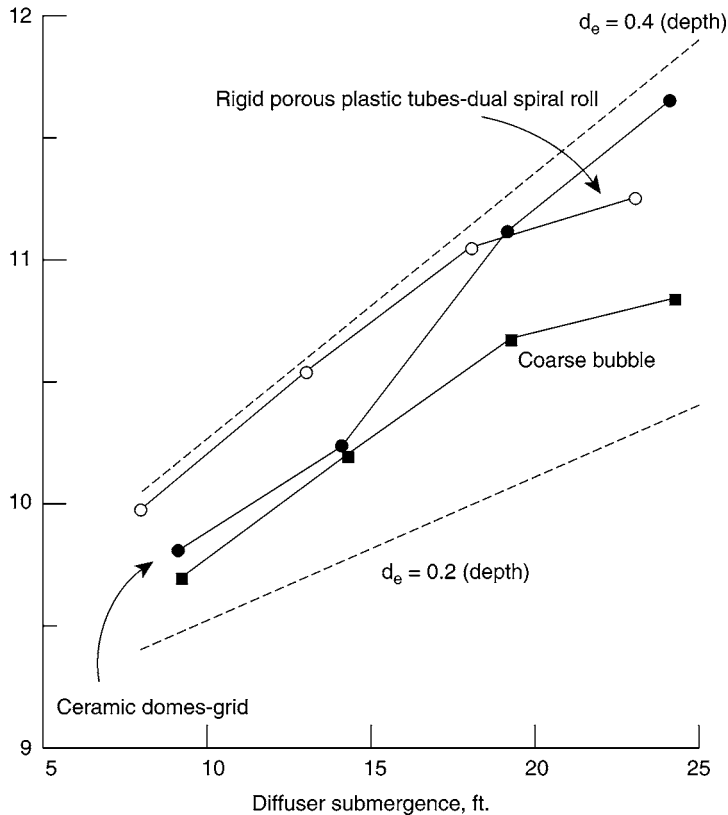
Fig. 13. Effect of diffuser submergence on $C_{\infty 20}$ for three diffuser types (*Source*: US EPA).

pressure, psia; P_{vT} is the saturated vapor pressure of water at temperature T, psia; γ_w is the specific weight of water at temperature T, lb/ft^3; T is the water temperature, ºC.

The effective saturation depth, d_e, represents the depth of water under which the total pressure (hydrostatic plus atmospheric) would produce a saturation concentration equal to C_∞ for water in contact with air at 100% relative humidity. The value of d_e is usually calculated, using Eq. (1), based on a spatially averaged value of C_∞ from a clean water test. For design purposes, d_e can be estimated from clean water test results on similar systems. For diffusers submerged to about 90% or more of basin depth, d_e is normally 21–44% of basin liquid depth for fine pore systems (68).

7.2. Oxygen Transfer

Typical SOTEs for fine pore diffused air systems are presented in Table 2 for a diffuser submergence of 4.6 m (15 ft). The effects of diffuser type, placement, and

$C_{\infty 20}$, mg/L

Most points correspond approximately to:

$d_e = 0.4$ (depth)

Diffuser submergence, ft.
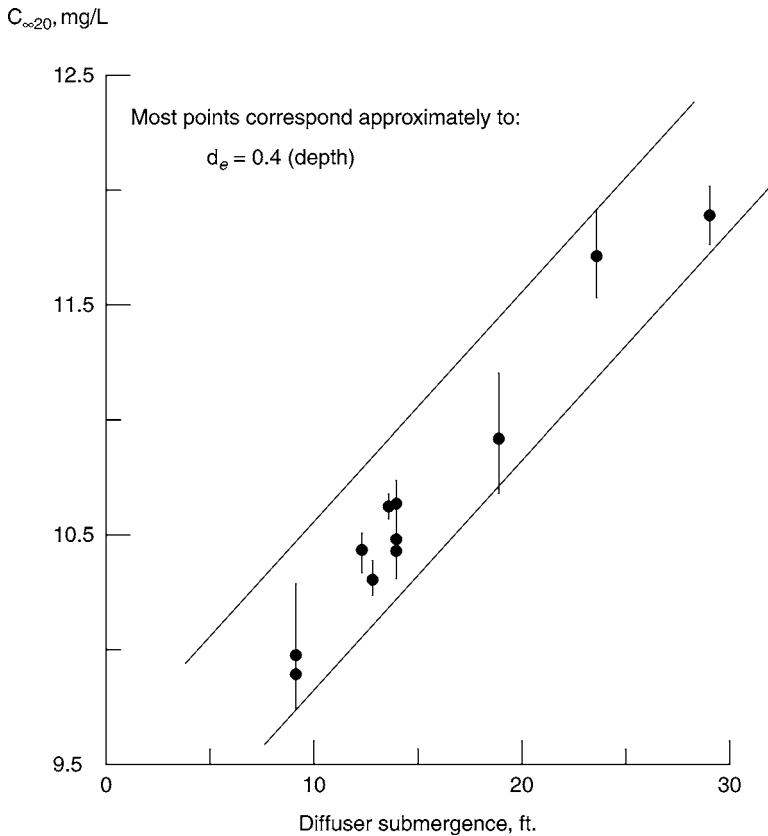
Fig. 14. $C_{\infty 20}$ vs diffuser submergence for perforated membrane disc and tube diffusers (*Source*: US EPA).

airflow rate per diffuser are delineated from this summary of different clean water studies. With the increasing number of materials and shapes being marketed as fine pore diffusers, it is becoming increasingly difficult to make generalizations about diffuser performance. For example, Table 2 presents data for perforated membrane discs that are available in a wide range of diameters. This accounts for the corresponding wide ranges in airflow rate and SOTE for these devices. It would appear, based on Table 2, that there is little difference between the oxygen transfer performance of disc/dome and tube fine pore devices. However, it is evident that the clean water oxygen transfer performance of all fine pore diffusers shown in Table 2 is superior to that of coarse bubble diffusers.

For a given diffuser type, spreading the diffusers more uniformly along the basin bottom area (moving from a single spiral roll to a dual spiral roll to a grid configuration) tends to improve clean water performance (69). The effects of basin and diffuser geometry on diffuser performance have been reported by many investigators. One of the early, notable studies (70) conducted in a 1.2×7.3 m^2 (4×24 ft^2) test basin using coarse bubble spargers and fine pore Saran tubes, demonstrated similar effects of placement.

Table 2
Clean Water Oxygen Transfer Efficiency Comparison for Selected Diffusers

Diffuser type and placement	Airflow rate, scfm/diffuser[a]	SOTE at 15-ft. submergence (%)
Ceramic plates–grid	2.0–5.0 scfm/ft^2	26–33
Ceramic discs–grid	0.4–3.4	25–40
Ceramic domes–grid	0.5–2.5	27–39
Porous plastic discs–grid	0.6–3.5	24–35
Perforated membrane discs–grid	0.5–20.5	16–38
Rigid porous plastic tubes		
Grid	2.4–4.0	28–32
Dual spiral roll	3–11	17–28
Single spiral roll	2–12	13–25
Nonrigid porous plastic tubes		
Grid	1–7	26–36
Single spiral roll	2–7	19–37
Pertorated membrane tubes		
Grid	1–4	22–29
Mid-width	2–6	16–19
Mid-width	2–12	21–31
Single spiral roll	2–6	15–19
Coarse bubble diffusers		
Dual spiral roll	3.3–9.9	12–13
Mid-width	4.2–45	10–13
Single spiral roll	10–35	9–12

[a]Except for plates.

The OTEs produced by fine pore diffusers in clean water generally decrease as the airflow rate per diffuser increases. Over the normal range of operation for a given diffuser submergence, type, density, and geometry, the relationship between SOTE and diffuser airflow rate, q, can be described by the following empirical relationship (3):

$$(SOTE_a/SOTE_b) = [(q_a)/(q_b)]^m \tag{2}$$

where $SOTE_a$ is the SOTE at a diffuser airflow rate of q_a; $SOTE_b$ is the SOTE at a diffuser airflow rate of q_b; m is a constant for a given diffuser and system configuration (usually a fractional negative number for fine pore diffusers).

It is convenient to select q_b at a rate of 0.47 L/s (1 scfm) so that

$$SOTE_a = SOTE_1 (q_a)^m \tag{3}$$

where $SOTE_1$ is the SOTE at diffuser airflow rate of 0.47 L/s (1 scfm).

Data from a number of clean water studies have been used to estimate the value of m in Eq. (3). Table 3 represents the results of these clean water tests.

Table 4 and Fig. 15 demonstrate the effect of unit airflow rate on SOTE for tube diffusers. SOTEs decrease with increased airflow per diffuser, whereas coarse bubble SOTEs are relatively unaffected by unit airflow rate with some indication of a slight

Table 3
SOTE vs Airflow for Selected Fine Pore Diffusers in Clean Water

Diffuser type	Layout	Diffuser submergence, ft	Diffuser density, no./100 ft^2	SOTE$_1$, (%)	m
Ceramic dome	Grid	14	32	29.6	−0.150
Ceramic disc	Grid	12.3	26	31.7	−0.133
Ceramic disc	Grid	12.3	15	26.0	−0.126
Rigid porous plastic disc	Grid	13	34	27.9	−0.097
Rigid porous plastic tube	Double spiral roll	13	10.5	26.7	−0.240
Nonrigid porous plastic tube	Spiral roll	15	8.6	27.1	−0.276
Perforated membrane disc	Grid	14	8.8	29.2	−0.195
9-in perforated membrane disc	Grid	10	20[a]	18.9	−0.110
EPDM perforated membrane tube	Grid	10	20[b]	21.0	−0.150

Data fit to: SOTE = SOTE$_1$ (q)^m *see* Eq. (3).
[a]One 9-in diameter disc in a 30-in diameter column.
[b]One 24-in long tube in a 30-in diameter column.

Table 4
Clean Water Oxygen Transfer Efficiencies of Fine Pore Tube Diffuser Systems

Diffuser type and placement	Airflow, scfm/diffuser	SOTE at following water depth (%)		
		10 ft	15 ft	20 ft
Rigid porous plastic tubes				
Grid[a]	2.4–4.0	–	28–32	–
Dual spiral roll	3–7	10–16	16–24	22–32
	9–11	10–14	15–17	21–26
Single spiral toll	2–7	12–15	15–20	22–25
	8–12	10–15	10–17	22
Perforated membrane tubes				
Floor cover (grid)	1–4	14–18	21–27	29–35
Quarter points	2–6	13–15	18–22	24–29
Mid-width	2–6	9–11	15–18	23–27
Mid-width	2–12	15–21	21–31	27–36
Single spiral roll	2–6	7–11	14–18	21–28
Nonrigid porous plastic tubes				
Grid[a]	1–7	–	20–34	–
Spiral roll	1–7	–	18–35	–

[a]Diffuser density = 13.0 tubes/100 ft^2 basin floor. Basin is 14.4 × 108.2 ft.
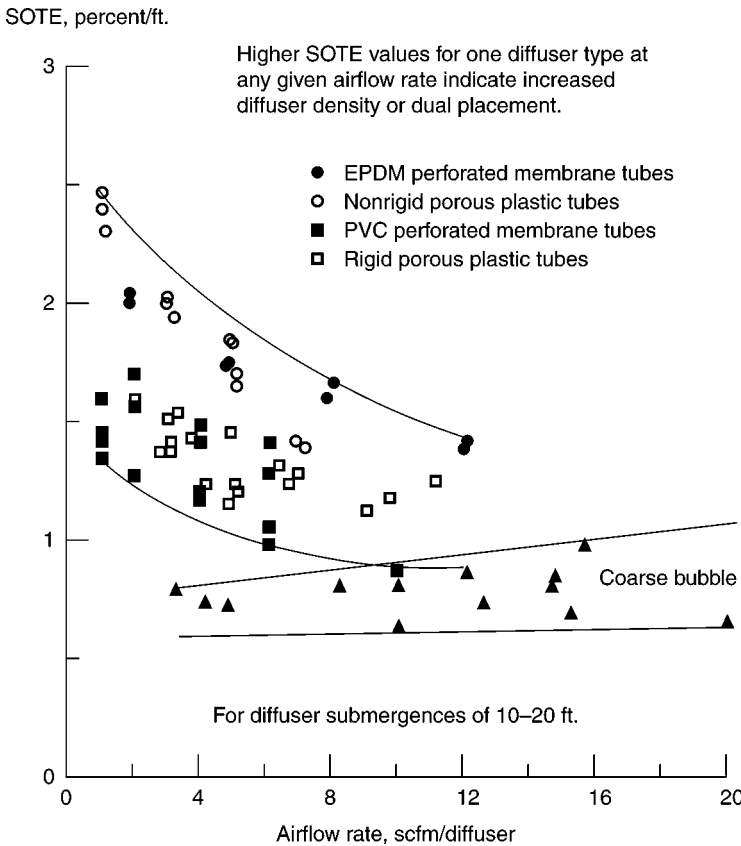
Fig. 15. Effect of unit airflow rate on SOTE for fine pore tube diffusers (*Source*: US EPA).

increase in SOTE at higher airflows. Very similar patterns were reported for coarse bubble spargers and fine pore tubes (70).

Figure 15 demonstrates that there are some overlapping regions of similar SOTE performance for the various tube diffusers represented, especially in the typical design region of 1.4–2.6 L/s (3–6 scfm)/diffuser. These data is for a number of diffuser placements and diffuser densities.

In this book, diffuser density is defined as the number of installed diffusers per 100 ft^2 of tank floor area. Another expression used as an indicator of diffuser density is the total projected media surface area of the installed diffusers (AD) divided by the area of the tank floor (AT).

Table 5 and Figs. 16 and 17 illustrate the effect of airflow rate on SOTE for disc/dome grid systems. SOTE decreases with increasing airflow rate per disc/dome diffuser. At rates >0.9 L/s (2 scfm)/diffuser, SOTE is less sensitive to airflow rate changes.

The effect of diffuser density on SOTE for disc/dome grid configurations is shown in Table 5 and Fig. 18. Generally, an increase in disc/dome diffuser density (or AD/AT) results in an increase in SOTE (71–74). However, there is some indication that a maximum value of AD/AT exists above which little improvement in SOTE occurs. The upper limit is dependent on diffuser size, airflow, and spacing. For example, a 23 cm (9 in.)

Table 5
Clean Water Oxygen Transfer Efficiencies of Fine Pore Disc/Dom Grid Systems

Diffuser type	Diffuser density, no./100 ft.^{2}	Airflow scfm/diffuser	SOTE at following water depth (%)		
			10 ft.	15 ft.	20 ft.
Ceramic disc–9.4 in.	15.6	0.9–3.0	20–22	27–33	34–37
	24.4	0.8–2.9	21–24	30–34	35–41
	31.3	0.7–2.6	22–25	31–34	38–41
Ceramic disc–8.7 in.	14.7–15.4	1.5–3.2	–	25–29	32–38
	16.9–18.9	0.6–2.5	–	26–30	33–40
	21.3–25.0	0.6–3.4	–	27–34	31–40
	29.4–31.3	0.4–2.8	–	25–36	34–39
	40.0–52.6	0.7–3.1	–	27–38	31–38
Ceramic dome–7 in.	17.9	0.5–2.0	–	25–31	28–40
	22.7–23.8	0.5–2.5	16–23	25–32	30–41
	30.3–31.3	0.5–2.5	20–24	27–37	31–44
	40.0–45.4	0.5–2.5	17–23	27–35	33–47
	66.7	0.5–2.5	18–26	27–34	–
Porous plastic disc–7 in.	14.5–14.7	0.6–3.5	15–18	22–27	–
	21.7	0.6–3.5	16–21	24–28	–
	25.6	0.5–2.3	–	25–31	–
	34.5	0.4–1.5	19–22	26–32	–

ceramic disc diffuser at a submergence of 4.3 m (14.2 ft.) exhibited SOTE values that did not increase at AD/AT values more than 0.14 for airflows of 0.5 L/s (1 scfm)/diffuser (75).

As can be seen from Figs. 16 and 17, the oxygen transfer performance of ceramic dome/disc diffusers and rigid porous plastic disc diffusers is similar throughout the range of airflows presented. However, the ceramic diffusers demonstrate a higher upper limit of oxygen transfer performance throughout the airflow range and are generally more efficient at airflows less than about 0.7 L/s (1.5 scfm)/diffuser.

An OTE increase of 5–15%, varying with depth, for a 24 cm (9.4 in.) diameter ceramic disc compared with an 18 cm (7 in.) diameter ceramic disc has been reported (72). This increase was attributed to a 70% higher effective surface area for the 24 cm (9.4 in.) disc. A similar relationship between dome/disc diameter and oxygen transfer per diffuser has also been reported (46,76).

Table 6 and Fig. 19 demonstrate the performance of perforated membrane discs. At airflows of 0.24–3.8 L/s (0.5–8 scfm)/diffuser, SOTE significantly decreases with increasing airflow in a manner similar to other fine pore diffusers. At higher airflow rates, SOTE is less sensitive to airflow. Perforated membrane discs are usually larger than ceramic and porous plastic dome/disc units. As a result, they are often operated at higher airflows per diffuser than ceramic/porous plastic diffusers. In addition, density of perforated membrane discs is normally lower than for ceramic/plastic units.

The effect of density and placement of perforated membrane discs on SOTE appears to be variable as indicated in Table 6. Results of field testing on 51 cm (20 in.) discs indicate OTE increases with increasing diffuser density or increasing AD/AT, at least to

SOTE, percent/ft.
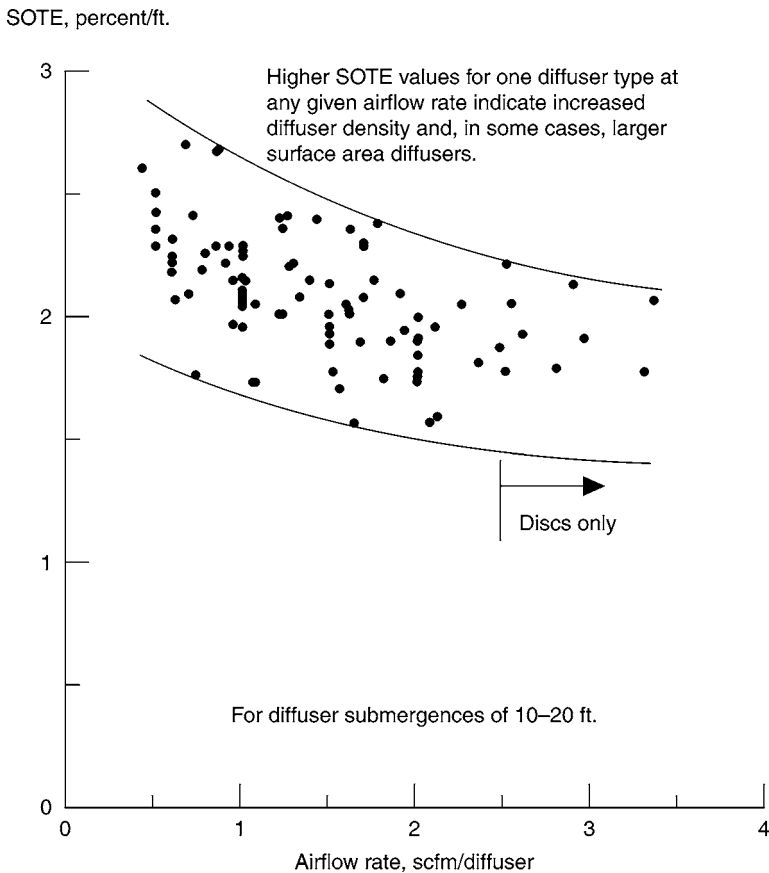
Fig. 16. Effect of unit airflow rate on SOTE for ceramic dome/disc diffusers (*Source*: US EPA).

an AD/AT of 0.26 (77). The data suggests, however, that, at the same airflow rate per diffuser, OTE approaches a limiting value as diffuser density increases. A 40% increase in the number of diffusers (producing an increase in AD/AT from 0.18 to 0.26) resulted in an increase in OTE of only about 5%. Prior pilot-scale testing on 51 cm (20 in.) perforated membrane discs up to an AD/AT of 0.59 also indicated OTE approaches a maximum value with increasing density or increasing AD/AT at the same airflow rate per diffuser (78).

As discussed earlier for ceramic disc/dome diffusers, SOTE of perforated membrane disc diffusers is also affected by airflow per diffuser, diffuser spacing, and diffuser density. Thus, it is evident diffusers of different size will exhibit different maximum densities or AD/AT values above which little improvement in SOTE will be achieved.

As described earlier, the specific permeability (or BRV_0) of a ceramic diffuser will have some effect on OTE; as pore size increases (permeability usually increases), bubble size increases, SOTE may decrease. Figure 20 depicts the results of a clean water test series using ceramic discs with specific permeabilities of 14–50 [BRV_0 = 22.4–7.1 cm (8.8–2.8 in.) w.g.] (65). The results of this study indicate that, for specific permeabilities
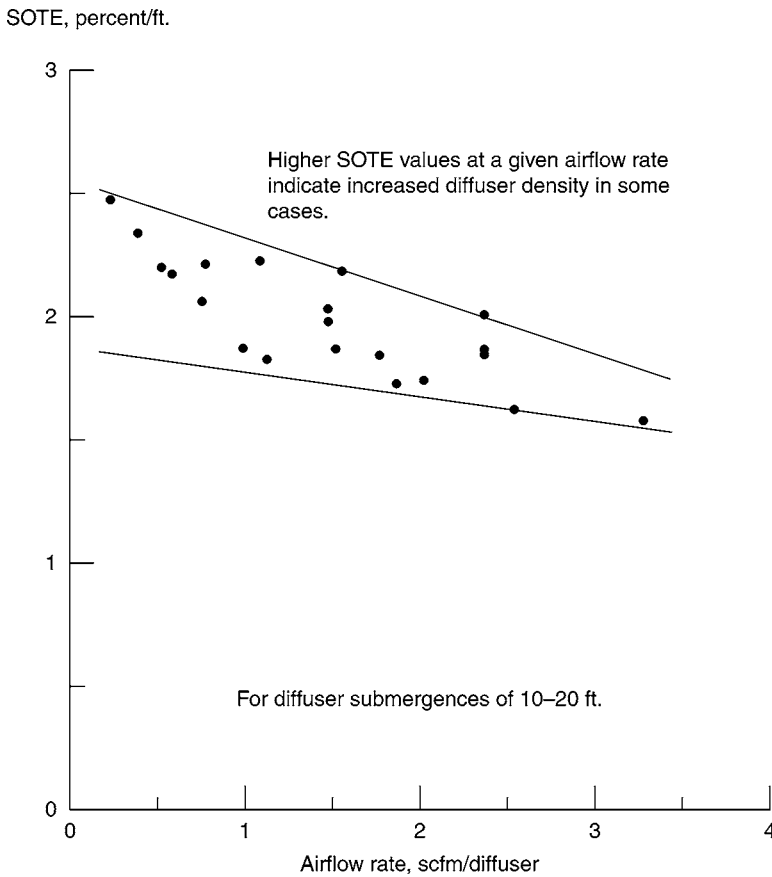
Fig. 17. Effect of unit airflow rate on SOTE for rigid porous plastic disc diffusers (*Source*: US EPA).

of 14–38 [BRV_0 = 22.4–10.4 cm (8.8–4.1 in.) w.g.], SOTE is relatively unaffected. However, at a specific permeability of 50 [BRV_0 = 7.1 cm (12.8 in.) w.g.], there appears to be a significant decline in SOTE, especially at the lower airflow rates.

The effects of water depth on SOTE and SAE for several types of diffusers are illustrated in Figs. 21 and 22, respectively. Although these data are for one specific test basin and airflow rate (79), they represent the typical effects of depth on performance. In general, SOTE values increase with increasing depth because mean oxygen partial pressure is higher (thereby resulting in a greater driving force) and opportunity is present for longer bubble residence time in the aeration basin. SAE; however, remains relatively constant or may increase slightly (46,80) for fine pore diffusers as depth increases because power requirements to drive the required air through diffusers may increase at the greater depths. In contrast, coarse bubble diffusers exhibit a gradually increasing SAE with increasing depth, though not reaching the overall efficiencies demonstrated by fine pore systems.
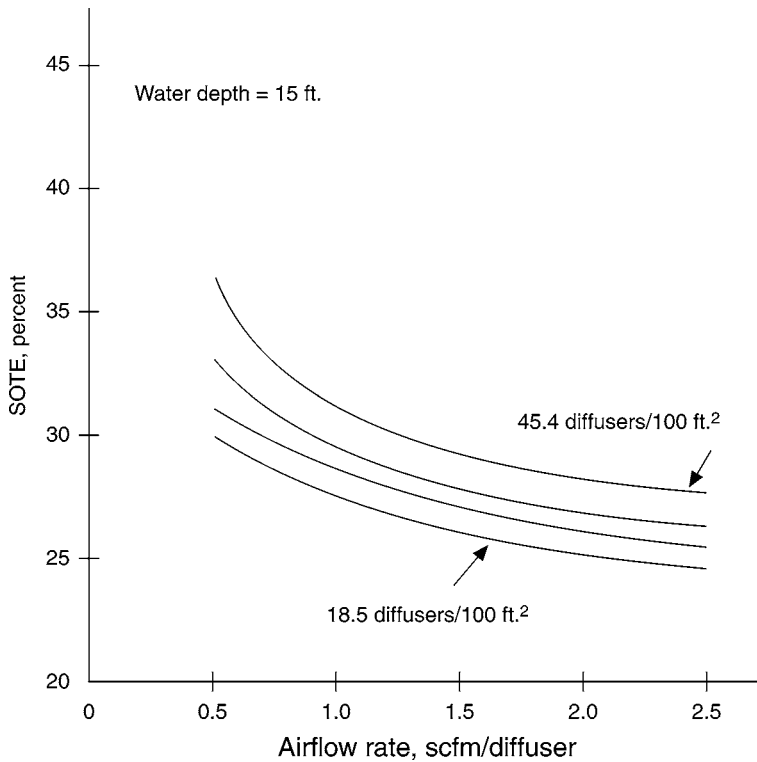
Fig. 18. Effect of diffuser density on SOTE for ceramic disc/dome grid configurations (*Source*: US EPA).

Table 6
Clean Water Oxygen Transfer Efficiencies of Perforated
Membrane Diffuser Systems

Diffuser type	Diffuser density, no./100 ft^2	Airflow scfm/diffuser	SOTE at following water depth (%)		
			10 ft	15 ft	20 ft
20-in. disc	3.0	3.3–20.5	11–16	19–25	24–29
	8.8	2.9–19.4	12–19	21–29	27–38
12–13-in. discs	6.3	1.9–12.0	11–15	19–26	28–37
	8.7–9.3	2.0–12.9	16–23	20–31	34–48
	11.1	1.5–10.3	9–21	24–36	27–43
	17.2	2.0–5.9	18–24	25–30	31–36
9-in. disc	4.0	0.5–7.1	–	15–36	–
	8.0	0.5–6.2	–	21–31	–
	14.1–18.5	05–6.8	–	23–29	–
7–8.5-in. discs	18.5–22.2	0.9–4.7	–	23–26	–

8. PERFORMANCE IN PROCESS WATER

8.1. Performance

As described earlier, a substantial database exists on the performance of fine pore diffusers in clean water. In designing aeration systems to operate under process

SOTE, percent/ft.

Higher SOTE values at a given airflow rate indicate increased diffuser density in some cases.

20-in. Disc only

For diffuser submergences of 10–20 ft.

Airflow rate, scfm/diffuser
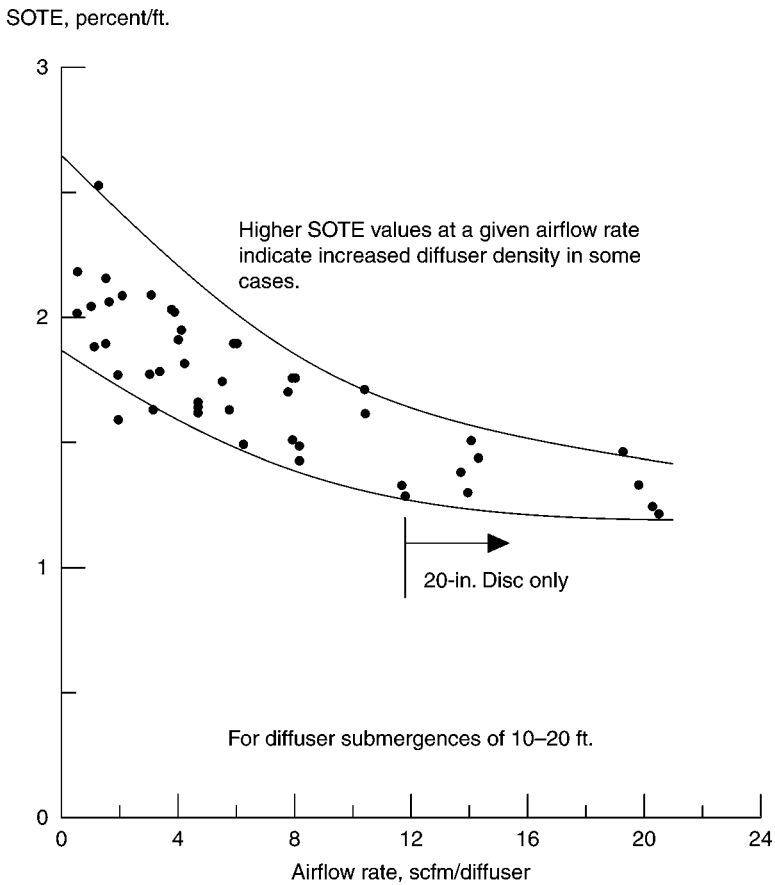
Fig. 19. Effect of unit air flow rate on SOTE for perforated membrane disc diffusers (*Source*: US EPA).

conditions, clean water data is corrected to account for the influences of wastewater characteristics, temperature, and pressure (81,82). Throughout this chapter, the term "process water" is used to refer to mixed liquor under aeration (83,84). The corrections to clean water performance are made using the following Eq. (4):

$$\text{ORT}_f = 8.34\, K_L a_{20}\, \alpha F\, \theta^{(T-20)}\, (\iota\beta\Omega C_{\infty 20} - C)\, V \tag{4}$$

where OTR_f is the oxygen transfer rate under process conditions (lb/h); $K_L a_{20}$ is the apparent volumetric mass transfer coefficient in clean water at 20°C (1/h); V is the process water volume (MG); $C_{\infty 20}$ is the steady-state DO saturation concentration attained at infinite time at 20°C and 1 atm (mg/L); C is the process water DO concentration (mg/L); α is the (process water $K_L a$ of a new diffuser)/(clean water $K_L a$ of a new diffuser); β is the (process water C_{∞})/(clean water C_{∞}); C_{∞} is the steady-state DO saturation concentration attained at infinite time at water temperature T and field atmospheric pressure P_b (mg/L); P_b is the field atmospheric pressure (psia); $\theta^{(T-20)} = K_L a/K_L a_{20}$; $K_L a$
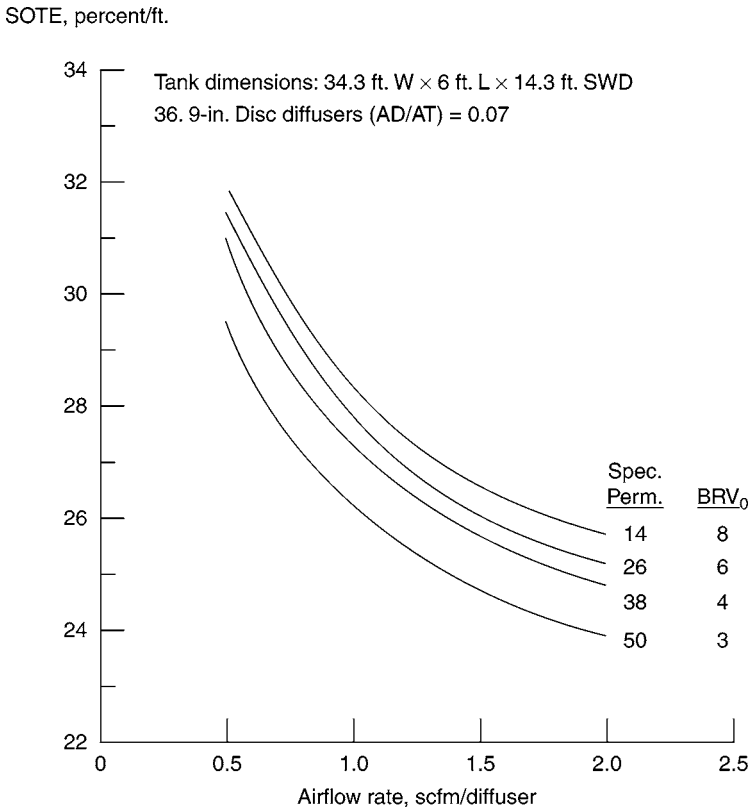
Fig. 20. Clean water disc data—Monroe, WI (*Source*: US EPA).

is the apparent volumetric mass transfer coefficient in clean water at temperature T (1/h); T is the process water temperature (°C); $\Omega = (P_b + 0.007\, \gamma_W\, d_e - P_{vT})/(P_s + 0.007\, \gamma_W\, d_e - P_{vT})$; $\Omega \sim P_b/P_s$ [for basin depths <6.1 m (20 ft) and for elevations <600 m (2000 ft)]; γ_W is the specific weight of water at temperature T (lb/ft^3); P_s is the atmospheric pressure at standard conditions, 14.7 psia or 1 atm at 100% relative humidity; P_{vT} is the saturated vapor pressure of water at temperature T (psia); d_e is the effective saturation depth at infinite time (ft); $\iota = C_\infty/C_{\infty 20} = C_s/C_{s20}$; C_s is the tabular value of DO surface saturation concentration at water temperature T, standard atmospheric pressure and 100% relative humidity (mg/L); F is the (process water $K_L a$ of a diffuser after a given time in service)/($K_L a$ of a new diffuser in the same process water)

Because SOTR is

$$\text{SOTR} = 8.34\, K_L a_{20}\, C_{\infty 20}\, V, \tag{5}$$

Equation (4) and Eq. (5) may be combined to calculate the process water oxygen transfer rate, OTR$_f$:

$$\text{OTR}_f = \alpha F(\text{SOTR})\theta^{(T\text{-}20)}\, (\iota \beta \Omega C_{\infty 20} C)/C_{\infty 20} \tag{6}$$

Tank: 20 ft. × 20 ft.
Power: 1 hp delivered/1000 ft.³ for rigid porous plastic tubes
Power: 5 hp delivered/1000 ft.³ for ceramic domes
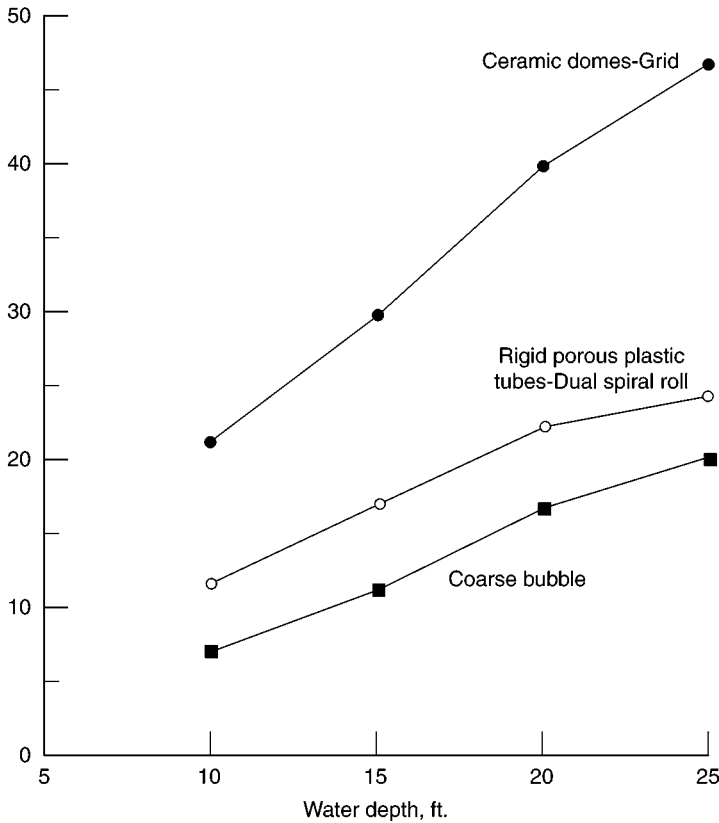
Fig. 21. Effect of water depth on SOTE for three diffuser types (*Source*: US EPA).

This equation can be rearranged as follows:

$$\alpha F(\text{SOTR}) = (\text{OTR}_f C_{\infty 20}\, \theta^{(T-20)})/(\iota\beta\Omega C_{\infty 20} - C). \qquad (7)$$

The term $\alpha F(\text{SOTR})$, or $\alpha F(\text{SOTE})$, is often used to express oxygen transfer under field conditions corrected to standard temperature and pressure and a driving force of $C_{\infty 20}$ (i.e., $C = 0$).

Further, because SOTE (%), is:

$$\text{SOTE} = 100\,(\text{SOTR}/W_{O_2}) \qquad (8)$$

where W_{O_2} is the mass rate of oxygen supplied (lb/h). Equation (6) may also be used to describe OTE under field conditions, OTE_f, by direct substitution.

Although employing clean water SOTR values to estimate oxygen transfer rates in process water (85) is conceptually straightforward, the estimate of OTR_f is subject to

Tank: 20 ft. × 20 ft.
Power: 1 hp delivered/1000 ft.^{3} for rigid porous plastic tubes
Power: 5 hp delivered/1000 ft.^{3} for ceramic domes

SAE, lb O$_2$/hp-hr (wire-to-water)
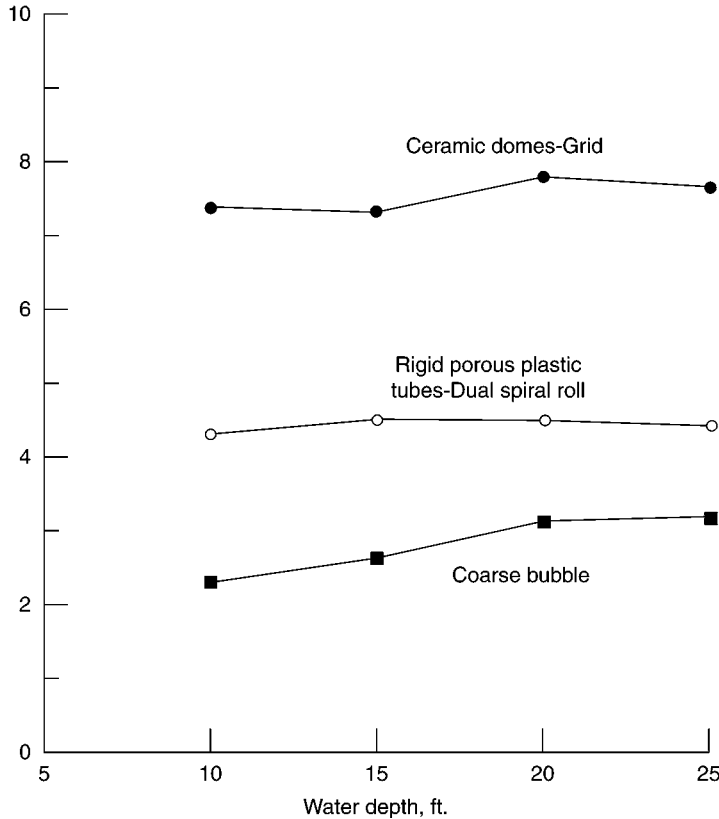
Fig. 22. Effect of water depth on SAE for three diffuser types (*Source*: US EPA).

considerable doubt because of the uncertainties contained in α and *F*. These uncertainties are magnified when the process water application is based on basin geometry and process temperatures that differ from those of the clean water test.

Table 7 is a guide for applying Eq. (6) and indicates the information for the parameters needed to estimate OTR$_f$. Values of $C_{\infty20}$ and SOTR must be calculated from the clean water oxygen transfer test. The average DO value, *C*, should represent the desired process water DO concentration averaged over the entire aeration volume. The temperature correction factor, ι, and pressure correction factor, Ω, are estimated using the definitions given earlier.

α is the ratio of the process water K_La of a new diffuser to the clean water K_La of a new diffuser. It is probably the most controversial and investigated parameter used in translating clean water oxygen transfer data to anticipated field performance. Variables affecting α include aerator type, nature of the wastewater contaminants, position within the treatment scheme, process loading rate, bulk liquid DO, and airflow rate. Reliable

Table 7
Guide to Application of Eq. (6)

Parameter	Source of information
$C_{\infty 20}$	Clean water test results
SOTR	Clean water test results
d_e	Clean water test results
C	Process water conditions
T	Process water conditions
ι	Calculated based on tabulated DO surface saturation values
Ω	Calculated based on site barometric pressure and effective depth data
α	Estimated based on experience or on measured values of $K_L a$ in clean and process waters using a clean diffuser
β	Calculated based on total dissolved solids measurements
θ	Taken as 1.024 unless experimentally proven different
F	Estimated based on field experience, field measurements, or laboratory analysis of diffusers taken from the field

data on α for various aeration devices are limited. Much of the reported data were obtained from bench-scale units that did not properly simulate mixing and $K_L a$ levels, aerator type, water depth, or the geometry effects of their full-scale counterparts. Reliable full-scale test procedures for use under process conditions, coupled with clean water performance data, are required to overcome these deficiencies. Several references provide further information on α and its measurement (86–88).

In the past, the effects of fouling as well as process water effects on $K_L a$ were included in α. The term apparent α', was used to indicate the effects of fouling on OTE (14,89,90). In this chapter, fouling is defined as an impairment of diffuser performance caused by material attached to the diffuser and deterioration of diffuser materials or appurtenances. Examination of the data collected during conduct of the EPA/ASCE Fine Pore Aeration Project has led to the elimination of the term α'. The term αF, in which α continues to describe the process water effects on $K_L a$ as before and a new term, F, describes the impairment of diffuser performance caused by material attached to the diffuser and/or deterioration of diffuser materials or appurtenances, is used in its place. In most cases, it is believed that impairment of diffuser performance is caused by attached material. In some cases, however, deterioration of diffuser materials or appurtenances may have a significant impact on F.

F is the ratio of $K_L a$ (or αF[SOTR] or αF[SOTE]) of a fouled diffuser to the $K_L a$ (or αF[SOTR] or αF[SOTE]) of a new diffuser, both measured in the same process water. F generally decreases from 1 with time of service in the process water. The characteristics of fouling dynamics are site and diffuser specific. Hypothetical fouling patterns are depicted in Fig. 23.

Data on the decrease in F with service time is limited, and what data is available generally consist of only a few points along the F vs time profile. Although this limited data is consistent with the hypothetical profiles shown (Fig. 23), the data points are too few and imprecise to accurately define a fouling profile. For simplicity, and because the precision of the data does not justify a complex model, the fouling profile is approximated at this time by the linear model shown in Fig. 23.
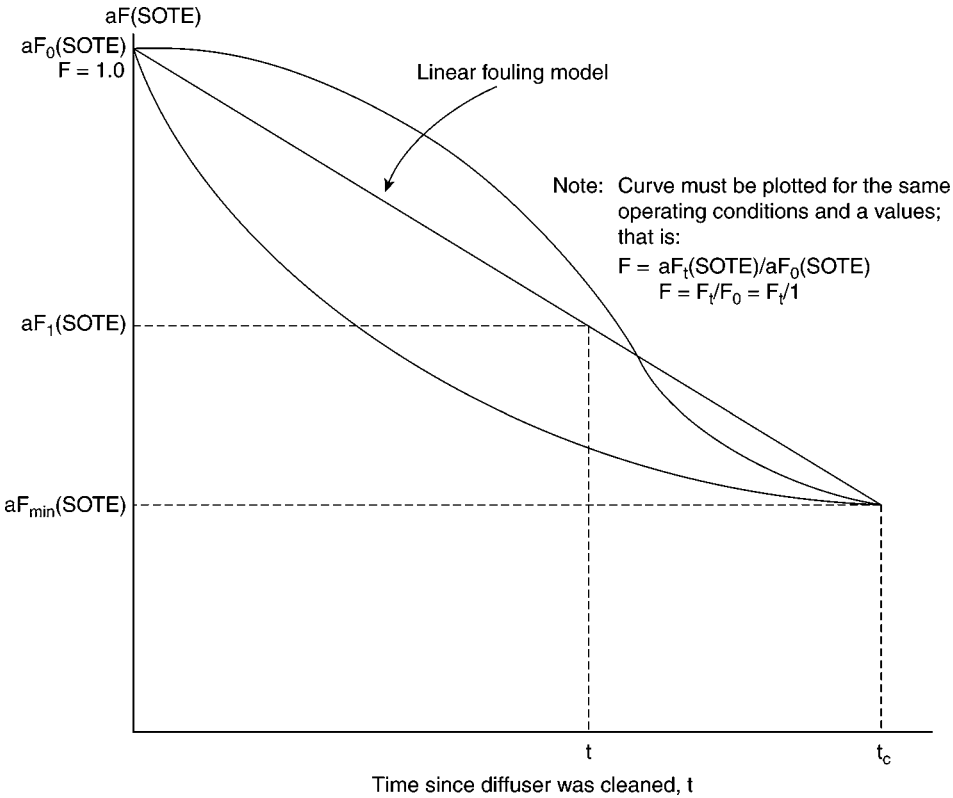
Fig. 23. Hypothetical fouling patterns (*Source*: US EPA).

The conceptual model is illustrated in Fig. 24. The plot of *F* vs time is developed from a linearized plot of an oxygen transfer function such as $\alpha F(SOTE)$, $\alpha F(SOTR)$, or $K_L a$ vs time (e.g., Fig. 23). The slope of the *F* vs time curve represents the fouling rate, f_F, expressed in terms of a unit decrease per month. Note that f_F is also equal to the slope of the linearized curve in Fig. 23 divided by SOTE, i.e. (3)

$$f_F = (1 - F)/t$$

$$= [\alpha F_0(SOTE) - \alpha F_t(SOTE)]/[t(\alpha F_0)(SOTE)]. \tag{9}$$

F relationships are described by the following equations:

$$F = 1 - t(f_F) \qquad \text{for } t \le t_c \text{ and } F > F_{min} \tag{10}$$

and,

$$F = F_{min} \qquad \text{for } t \ge t_c$$

This model assumes that there is a minimum value of *F*, F_{min}, that occurs after some critical service period, t_c. It may be reasonable to assume F_{min} for a system unusually susceptible to fouling approaches the ratio of the oxygen transfer performance of a coarse bubble diffuser to that of an unfouled fine pore diffuser in question, with both diffusers in the same physical basin configuration and operating under the same process loadings. This model is applied to the design and operation of fine pore aeration systems.
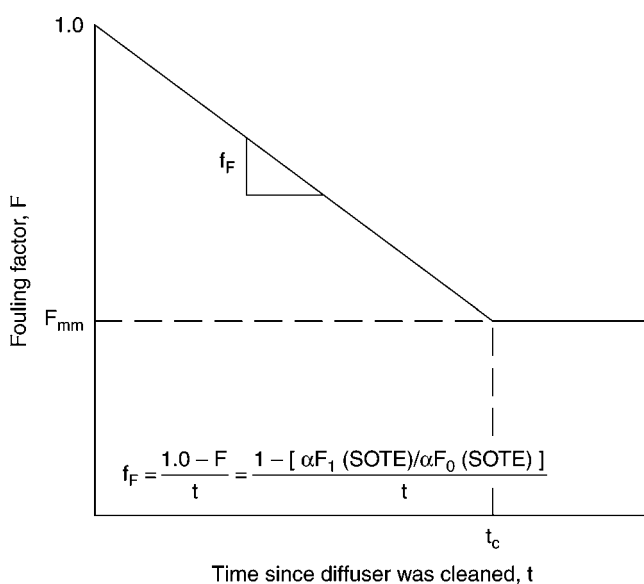
Fig. 24. Linear fouling factor model (*Source*: US EPA)

β is the ratio of the average saturation concentration, C_∞, in process water to the corresponding value in clean water. β can vary from approx 0.8 to 1 and is generally close to 1 for municipal wastewaters. β cannot be measured by a membrane probe and many wastewaters contain substances that interfere with the Winkler method of DO measurement. Therefore, the value of β for use in Eq. (6) may be calculated as the ratio of the DO surface saturation concentration in process water to the DO surface saturation concentration in clean water. The corresponding surface saturation concentrations can be interpolated from DO saturation tables (Table 8) based on the total dissolved solids contents of the process water and clean water.

θ is employed to correct $K_L a$ for changes in temperature. Values of θ range from 1.008 to 1.047 and are influenced by geometry, turbulence level, and type of aeration device (91). θ is usually taken as equal to 1.024. Little consensus exists regarding the accurate prediction of θ, and, for this reason, clean water testing for the determination of SOTR values should be at temperatures close to 20°C (68°F) (59).

8.2. Factors Affecting Performance

The performance of diffused aeration systems under normal operating conditions is directly related to the following parameters (13):

a. Fouling, aging, fatigue, and so on.
b. Wastewater characteristics.
c. Loading conditions.
d. Process type and flow regime.
e. Basin geometry and diffuser placement.
f. Diffuser type, size, shape, density, airflow rate, and performance characteristics.
g. Mixed liquor DO control and air supply flexibility.
h. Mechanical integrity of the system.

Table 8
Solubility of Oxygen (mg/L) in Water Exposed to Water-Saturated Air
at Atmospheric Pressure = 101.3 kP, (14.7 psia)

T (°C)	Chlorinity[a]			T (°C)	Chlorinity[a]		
	0	5.0	10.0		0	5.0	10.0
0.0	14.62	13.73	12.89	21.0	8.91	8.46	8.02
1.0	14.22	13.36	12.55	22.0	8.74	8.30	7.87
2.0	13.83	13.00	12.22	23.0	8.58	8.14	7.73
3.0	13.46	12.66	11.91	24.0	8.42	7.99	7.59
4.0	13.11	12.34	11.61	25.0	8.26	7.85	7.46
5.0	12.77	12.02	11.32	26.0	8.11	7.71	7.33
6.0	12.45	11.73	11.05	27.0	7.97	7.58	7.20
7.0	12.14	11.44	10.78	28.0	7.83	7.44	7.08
8.0	11.84	11.17	10.53	29.0	7.69	7.32	6.96
9.0	11.56	10.91	10.29	30.0	7.56	7.19	6.85
10.0	11.29	10.66	10.06	31.0	7.43	7.07	6.73
11.0	11.03	10.42	9.84	32.0	7.31	6.96	6.62
12.0	10.78	10.18	9.62	33.0	7.18	6.84	6.52
13.0	10.54	9.96	9.41	34.0	7.07	6.73	6.42
14.0	10.31	9.75	9.22	35.0	6.95	6.62	6.31
15.0	10.08	9.54	9.03	36.0	6.84	6.52	6.22
16.0	9.87	9.34	8.84	37.0	6.73	6.42	6.12
17.0	9.67	9.15	8.67	38.0	6.62	6.32	6.03
18.0	9.47	8.97	8.50	39.0	6.52	6.22	5.93
19.0	9.28	8.79	8.33	40.0	6.41	6.12	5.84
20.0	9.09	8.62	8.17				

[a]Chlorinity = Salinity/1.80655.

    i. Operator expertise.
    j. Quality of preventive operation and maintenance program.

Manual of Practice FD-13 (92) is a good general reference on the importance of the previous factors. To minimize life-cycle costs of an aeration system, all these factors must be considered during design and some must be controlled during operation.

The areas of greatest concern in process water oxygen transfer performance are wastewater characteristics, process type and flow regime, loading conditions, and diffuser fouling and material deterioration. In a given case, any combination of these factors can have a significant effect on the α profile of a system, DO control, and changes in aerator performance with time because of diffuser fouling.

All fine pore diffusers are susceptible to buildup of biofilms and/or deposition of inorganic precipitates that can alter the operating characteristics of the diffusers (93). Porous diffuser media are also susceptible to airside clogging of pores because of particles in the supply air. Therefore, practical and cost-effective preventive maintenance designed to keep diffusers as clean and efficient as possible is very important. The appropriate preventive maintenance procedure and frequency depend on the system provided, service conditions, and trade-offs between operating costs and cleaning costs.

The effects of fouling on DWP and OTE should not be confused with changes in the air diffusion media or the integrity of the installation. These types of changes, which include alteration of diffuser media properties over time and leaks in the air piping or around diffuser gaskets, may be caused by poor equipment design, improper installation, or inadequate inspection and maintenance.

Various types of foulants were identified by early investigators, and the list has been expanded by recent studies to include the following (53):

Airside

a. Dust and dirt from unfiltered air.
b. Oil from compressors or viscous air filters.
c. Rust and scale from air pipe corrosion.
d. Construction debris from poor cleanup.
f. Wastewater solids entering through broken diffusers or pipe leaks.

Liquidside

a. Fibrous material attached to sharp edges.
b. Inorganic fines entering media at low or zero au pressure.
c. Organic solids entering media at low or zero air pressure.
d. Oils or greases in wastewater.
e. Precipitated deposits, including iron and carbonates.
f. Biological growths on diffuser media.
g. Inorganic and organic solids trapped by biological growths on diffuser media.

Fouling is generally classified as one of two types: type I and type II. Characteristics of type I fouling are clogging of the diffuser pores, either by airborne particulates clogging the air side, or metal hydroxides and carbonates clogging the liquid side. Type II is characterized by a biofilm layer forming and growing on the surface of the diffuser. In practice, it can be difficult to distinguish between the two types because they occur together, with one or the other dominating.

The presence of constituents such as surfactants, dissolved solids, and suspended solids can affect bubble shape and size and result in diminished oxygen transfer capability. In general, ceramic domes and discs yield slightly higher clean water transfer efficiencies than typical porous plastic tubes or flexible sheath tubes in a grid placement. Other key parameters that have an effect on the performance characteristics of a fine pore media diffuser are permeability, uniformity, DWP, and strength.

Effective long-term process control depends on appropriate selection and integration of the solids' retention time, the food-to-microorganisms loading, and the wastewater flow regime. Short-term, day-to-day variables at the disposal of the operator include control of diffuser airflow rate and mixed liquor DO concentration. It is essential to understand how each of these parameters affects aeration efficiency in order to develop optimum short- and long-term operating procedures.

8.3. Operation and Maintenance

The main operational objective is to achieve acceptable effluent quality while maximizing the aeration efficiency. It is essential that diffusers be kept clean through cost-effective preventive maintenance procedures. Preventive maintenance can virtually eliminate airside (blower filtration system) particulate fouling of fixed fine pore diffusers.

Filtration equipment maintenance entails cleaning and changing filter media. Calibration and/or zeroing of meters is necessary as part of preventive maintenance because accurate airflow and DO measurements are a critical part of monitoring aeration systems.

Preventive maintenance is needed to keep an aeration system operating at the required level of performance and to decrease the need for corrective maintenance. In addition, preventive maintenance will reduce the number of interruptions in the air supply, thus preventing solids from entering the air distribution system.

The cleaning methods used to restore diffuser efficiency are either process interruptive (aeration basin out of service) or process noninterruptive (access to basin not needed). Diffusers can be cleaned by removing them from the basin (*ex situ*) or onsite inside the basin (*in situ*). Some cleaning techniques used are acid washing (94), alkaline washing, gas injection, high-pressure water jetting, and air bumping (12).

When placing an empty aeration basin into service, all recommended operational steps for start-up and shutdown should be followed. If a basin is put into service during cold weather, care must be exercised to prevent any damage from buoyant forces exerted by ice trying to float. Aeration basins must not be drained during freezing weather unless absolutely necessary because ice and frost can cause serious damage. In the event that an aeration basin should stand idle for more than 2 wk, it should be drained and cleaned thoroughly.

The responsibilities of the manufacturer, designer, and owner for obtaining and sustaining an efficient aeration system are detailed by Stenstrom and Boyle (95). Operational costs are determined in part by the OTE of the fine bubble aeration system being used, as well as the characteristics of the influent wastewater. Aerator cleaning costs depend on the aerator type; how easily the aerators can be removed, cleaned, or replaced; and the plant's O&M procedures (96–98).

NOMENCLATURE

AD	Total projected media surface area of diffusers (ft^2)
AT	Area of tank floor (ft^2)
C	Process water DO concentration (mg/L)
C_s	Tabular value of DO surface saturation concentration at water temperature T, standard atmospheric pressure and 100% relative humidity (mg/L)
C_∞	Steady-state DO saturation concentration attained at infinite time at water temperature T and field atmospheric pressure P_b (mg/L)
$C_{\infty 20}$	Steady-state DO saturation concentration attained at infinite time at 20°C and 1 atm (mg/L)
d_e	Effective saturation depth at infinite time (ft)
F	(Process water $K_L a$ of a diffuser after a given time in service)/($K_L a$ of a new diffuser in the same process water)
F_{min}	Minimum value of F
f_F	Fouling rate, expressed in terms of a unit decrease per month
$K_L a$	Apparent volumetric mass transfer coefficient in clean water at temperature T (1/h)
$K_L a_{20}$	Apparent volumetric mass transfer coefficient in clean water at 20°C (1/h)

m	A constant for a given diffuser and system configuration (usually a fractional negative number for fine pore diffusers)
OTE	Oxygen transfer efficiency
OTE_f	Oxygen transfer efficiency under field conditions
OTR	Oxygen transfer rate (lb/h)
OTR_f	Oxygen transfer rate under process conditions (lb/h)
P_b	Field atmospheric pressure (psia)
P_s	Atmospheric pressure at standard conditions, 14.7 psia or 1 atm at 100% relative humidity
P_{vT}	Saturated vapor pressure of water at temperature *T* (psia)
q	Diffuser airflow rate, scfm (L/s)
s	Sample standard deviation
SAE	Standard aeration efficiency
SOTE	Standard oxygen transfer efficiency
$SOTE_a$	SOTE at a diffuser airflow rate of q_a
$SOTE_b$	SOTE at a diffuser airflow rate of q_b
SOTE1	SOTE at diffuser airflow rate of 0.47 L/s (1 scfm)
SOTR	Standard oxygen transfer rate
t	Service period
t_c	Critical service period
T	Water or process water temperature (°C)
V	Process water volume (MG)
x	Average of individual readings
α	(Process water K_La of a new diffuser)/(clean water K_La of a new diffuser)
β	(Process water C_∞)/(clean water C_∞)
γ_w	Specific weight of water at temperature T (lb/ft^3)
θ	Employed to correct K_La for changes in temperature
ι	$C_\infty/C_{\infty 20} = C_s/C_{s20}$
Ω	$(P_b + 0.007\, \gamma_W\, de - P_{vT})/(P_s + 0.007\, \gamma_W\, de - P_{vT})$
Ω	P_b/P_s [for basin depths <6.1 m (20 ft) and for elevations <600 m (2000 ft)]

REFERENCES

1. K. Carns, Bringing energy efficiency to the water and wastewater industry: how do we get there? *Water and Wastewater Energy Roadmap Workshop*, Washington, DC, July 29, 2004.
2. G. M. Wesner, L. J. Ewing, T. S. Jr. Lineck, and D. J. Hinrichs, *Energy Conservation in Municipal Wastewater Treatment*, EPA-430/9-77-011, National Technical Information Service (NTIS) No. PB81-165391, US Environmental Protection Agency, Washington, DC, 1977.
3. US EPA, *Design Manual: Fine Pore Aeration Systems,* EPA/625/1-89/023, Center for Environmental Research Information, US Environmental Protection Agency, Cincinnati, OH, 1989.
4. American Society of Civil Engineers, *ASCE Standard: Measurement of Oxygen Transfer in Clean Water,* ISBN 0-87262-430-7, New York, NY, July, 1984.
5. J. A. Mueller and W. C. Boyle, Oxygen transfer under Process conditions, *J. Water Pollut. Control Fed.* **60**(3), 341–342 (1988).
6. A. J. Martin, *The Activated Sludge Process,* MacDonald and Evans, London, England, 1927.

7. FSIWA, *Air Diffusion in Sewage Work,* Manual of Practice 5, Federation of Sewage and Industrial Wastes Associations, Champaign, IL, 1952.

8. R. S. Busheeand and S. I. Zach, Tests on pressure loss in activated sludge plants*, Engineering News Record,* **93**, 21 (1924).

9. WPC, *Aeration in Wastewater Treatment,* Manual of Practice 5. Water Pollution Control Federation, Washington, DC, 1971.

10. N. E. Anderson, Tests and studies on air diffusers for activated sludge*, Sewage and Industrial Wastes,* **22**, 461 (1950).

11. P. R. Morgan, Maintenance of Fine Bubble Diffusion*, J. San. Eng. Dlv. ASCE,* 84(SA2), 1609 (1958).

12. US EPA, *Fine Bubble Aeration Wastewater Technology Fact Sheet,* EPA 832-F-99-065, US Environmental Protection Agency, Office of Water, Washington, DC, September, 1999.

13. NSFC, *Fine Bubble Aeration*, National Small Flows Clearing House, Fact Sheet WWF-SOM23, Environmental Technology Initiative, West Virginia University, Morgantown, WV, 1998.

14. US EPA, *Summary Report: Fine Pore (Fine Bubble) Aeration Systems*. EPA/625/8-85/010, Water Engineering Research Laboratory, US Environmental Protection Agency, Cincinnati, OH, 1985.

15. W. W. Jr. Eckenfelder, *Water Quality Engineering for Practicing Engineers*, Professional Engineering Career Development Series, Barnes & Noble, New York, NY, 1970.

16. H. J. Schmidt-Holthausen and B. C. Bievers, 50 years of experience in Europe with fine bubble aeration, *53rd Annual Conference of the Water Pollut. Control Fed.* Las Vegas, NV, October, 1980.

17. Filtros, *Product information bulletin*, Ferro Corporation, Refractories Division, East Rochester, NY, May, 1984.

18. K. Hosokawa, Characterization of various diffusers and its application. In: *Proceedings of the 11th United States/Japan Conference on Sewage Treatment Technology,* EPA-600/9- 88,010, NTIS No. PB88-214986, US Environmental Protection Agency, Cincinnati, OH, April, 1988.

19. H. R. King, *Sewage and Industrial Wastes*, 27, 10, August (1955).

20. G. L. Bartholomew, Type of aeration devices. In: *Aeration of Activated Sludge in Sewage Treatment*, D. L. Gibbon, (ed.), Pergamon Press, 1974.

21. Carborundum Company, *Carborundum Aloxite Porous Products for Filtration, Aeration, and Diffusion*, Product information bulletin, Bonded Abrasives Division, Niagara Falls, NY, May, 1970.

22. Oy AB Airam, *Porex Porous Plastic Materials,* Product information bulletin, Helsinki, Finland, 1988.

23. Nokia Metal Products, *Nopol Aeration Systems*, Product information bulletin, Vantaa, Finland (undated).

24. Donohue & Assoc., Inc., *Fine Pore Diffuser System Evaluation for the Green Bay Metropolitan Sewerage District*, Study conducted under Cooperative Agreement CR812167, Risk Reduction Engineering Laboratory, US Environmental Protection Agency, Cincinnati, OH, 1990.

25. M. K. Stenstrorn and G. Masutani, *Fine Bubble Diffuser Fouling: The Los Angeles Studies*. Study conducted under Cooperative Agreement CR8121 67, Risk Reduction Engineering Laboratory, US Environmental Protection Agency, Cincinnati, OH, 1990.

26. Aeration Technologies, Inc., *AERMAX TPD High Efficiency Product Bulletin*, North Andover, MA (undated).

27. ASTM, *1988 Annual Book of ASTM Standards*, Sections 8 and 9, Volumes 8.04 and 14.02, American Society of Testing and Materials, Philadelphia, PA, 1988.

28. C. A. Harper (Editor-in-chief), *Handbook of Plastics and Elastomers*, Westinghouse Electric Corporation, McGraw-Hill, New York, NY, 1975.

29. Aerostrip Corp., *Aerostrip Membrane Diffusers, Fine Bubble Aeration,* Old Saybrook, CT, Web Site: http://www.enquip.com/Aerostripp.html (2006).

30. Koch/Infinity, *Microporous Diffusion Membrane, Fine Bubble Aeration System Specifications*, http://www.koch-water.com/aeration.html (2006).

31. Sanitaire, *Flexible Membrane Tube Diffusers*, Product information bulletin, Sanitaire-Water Pollution Control Corp., Milwaukee, WI, 1987.

32. Sanitaire, *Flexible Membrane Disc Diffusers*, Product information bulletin, Sanitaire-Water Pollution Control Corp., Milwaukee, WI, 1987.

33. Eimco, *Eimco Elastox-T Non Clog Fine Bubble Rubber Diffuser*, Product Bulletin 1335.2T, Eimco Process Equipment Co., Salt Lake City, UT, 1986.

34. Eimco, *Eimco Elastox-D Non Clog Fine Bubble Rubber Diffuser*, Product Bulletin 1335.1, Eimco Process Equipment Co., Salt Lake City, UT, 1985.

35. Roediger Pittsburgh, *Roeflex Diaphram Diffuser*, Product Bulletin RDD 100/5M, Roediger Pittsburgh, Inc., Pittsburgh, PA, 1986.

36. Envirex, *Fine Bubble Membrane Diffusers for Non-Clogging Energy Efficient Aeration*, Product Bulletin No. 315-14C1, Envirex Inc., Waukesha, WI, 1986.

37. Waterworks/Alpac, *Airmax Fine Pore High Efficiency Diffusers*, http://www.wate works.ca/airmax.html (2005).

38. L. A. Ernest, *Case History Report on Milwaukee Ceramic Plate Aeration Facilities, Study Conducted Under Cooperative Agreement* CR812167, Risk Reduction Engineering Laboratory, US Environmental Protection Agency, Cincinnati, OH, 1990.

39. C. Lue-Hing, D. R. Zenz, and B. Sawyer, Case history: aeration system design, operation, control, and maintenance at the Metropolitan Sanitary District of Greater Chicago, *Aeration Systems Operations, Control and Testing Conference*, Georgia Water Pollution Control Association, Atlanta, GA, March, 1984.

40. Environmental Dynamics, *Reef Aeration Mixing Systems*, Product information bulletin, Environmental Dynamics, Inc., Columbia, MD (undated).

41. Sanitaire, *Fine Bubble Tube Diffuser,* Product Bulletin TD 4/85, Sanitaire—Water Pollution Control Corp., Milwaukee, WI, 1985.

42. Parkson, *WYSS Flex-A-Tube Diffuser*, Product Bulletin WD800, Parkson Corp., Ft. Lauderdale, FL (undated).

43. Endurex, *Engineering Data-Endurex Airline Diffusers*, Product Bulletin 5M835, Endurex Corp., Loveland, OH (undated).

44. Envirex, *REX Fine Bubble Tube Diffusers*, Product Bulletin 315-14A3, Envirex Inc., Waukesha, WI, 1982.

45. FMC, *Pearlcomb Air Diffusers*, Product Bulletin 7824, FMC Corporation, Chicago, IL, 1973.

46. D. H. Houck and A. G. Boon, *Survey and Evaluation of Fine Bubble Dome Diffuser Aeration Equipment*, EPA-600/2-81-222, NTIS No. PB82- 105578, US Environmental Protection Agency, Cincinnati, OH, September, 1981.

47. D. H. Houck, *Survey and Evaluation of Fine Bubble Dome and Disc Diffuser Aeration Systems in North America*, EPA-600/2-88/001, NTIS No. PB88-243886, US Environmental Protection Agency, Cincinnati, OH, August, 1988.

48. EPCO, *Fine Bubble Air Diffusers*, Product Bulletin 106, EPCO International, Victoria, Australia (undated).

49. Norton, *Dome Diffuser Aeration System,* Product information bulletin, Norton Industrial Ceramics Division, Worcester, MA (undated).

50. Parkson, *Diffused Aeration Products: Fine Air Ceramic Diffuser*, Product Bulletin FA1001, Parkson Corp., Ft. Lauderdale, FL (undated).

51. J. D. Wren, Diffused Aeration Types and Applications. In: *Proceedings of Seminar Workshop on Aeration System Design, Testing, Operation, and Control*, EPA-600/9-85- 005, NTIS No. PB85-173896, US Environmental Protection Agency, Cincinnati, OH, January, 1985.

52. L. Ewing and D. T. Redmon, *US Patent No. 4,261,933*, April 14, 1981.
53. W. C. Boyle and D. T. Redmon, Biological fouling of fine bubble diffusers: state-of-art. *J. Env. Eng. Div. ASCE,* 109(EE5) 991-1005, October, 1983.
54. Renton Plant Gets Into the Swing of Conservation, *Monitor,* January (1986).
55. A. G. Boon and B. Chambers, Design protocol for aeration systems - UK perspective. In: *Proceedings of Seminar/Workshop on Aeration System Design, Testing, Operation, and Control*, EPA-600/9-85-005, NTIS No. PB85-173896, US Environmental Protection Agency, Cincinnati, OH, January, 1985.
56. US EPA, *Technological Assessment of Fine Pore Aerators,* EPA-600/2-82-003, US Environmental Protection Agency, 1995.
57. K. Egan-Benck, G. McCarty, and W. Winkler, Choosing diffusers, *Water Environ. Technol.* **5**(2), 54–59 (1993).
58. D. T. Redmon, Operation and maintenance! troubleshooting. In: *Proceedings of Seminar/Workshop on Aeration System Design, Testing, Operation, and Control*, EPA-600/9-85- 005, NTIS No. PB85-173896, US Environmental Protection Agency, Cincinnati, OH, January, 1985.
59. American Society of Civil Engineers, *ASCE Standard: Measurement of Oxygen Transfer in Clean Water*, ISBN 0-87262-430-7, New York, NY, July, 1984.
60. J. D. Wren, *Transcript of Biofouling Seminar*, New York Water Pollution Control Association, New York, NY, January, 1985.
61. C. R. Baillod and K. Hopkins, Fouling of fine pore diffused aerators: An Interplant Comparison, Study conducted under Cooperative Agreement CR812167, Risk Reduction Engineering Laboratory, US Environmental Protection Agency, Cincinnati, OH, 1990.
62. W. W. Winkler, Fine bubble ceramic diffuser maintenance, *Annual Meeting of the New England Water Pollution Control Association*, Boston, MA, January 25, 1984.
63. W. B. Danly, *Biological Fouling of Fine Bubble Diffusers*, MS Thesis, Dept. of Civil and Environmental Engineering, University of Wisconsin, Madison, WI, 1984.
64. M. G. Rieth and R. C. Polta, A test protocol for aeration retrofit to fine bubble diffusers, *60th Annual Conference of the Water Pollution Control Federation*, Philadelphia, PA, October, 1987.
65. Ewing Engineering Co., *The Effect of Permeability on Oxygen Transfer Capabilities, Fouling Tendencies, and Cleaning Amenability at Monroe, WI*, Study conducted under Cooperative Agreement CR812167, Risk Reduction Engineering Laboratory, US Environmental Protection Agency, Cincinnati, OH, 1990.
66. ASCE, *Guidelines for Quality Assurance of Installed Fine-Pore Aeration Equipment*, Standards No. 01-035, American Society of Civil Engineers, *Reston, VA,* 2005.
67. Brother Wastewater Engineering, *Features of Fine Bubble Diffuser,* Brother Wastewater Engineering Co. http://www.allproducts.com/manufacture3/diso/02.html (2006).
68. C. R. Baillod, W. L. Paulson, J. J. McKeown, and H. J. Jr. Campbell, Accuracy and precision of plant scale and shop clean water oxygen transfer tests. *J. Water Pollut. Control Fed.* **58**(4), 290–299 (1986).
69. T. C. Rooney and G. L. Huibregtse, Increasing oxygen transfer efficiency with coarse bubble diffusers, *J. Water Pollut. Control Fed.* **52**(9), 2315–2326 (1980).
70. J. K. Bewtra and W. R. Nicholas, Oxygenation from Diffused Air in Aeration Tanks. *J. Water Pollut. Control Fed.* **36**(10), 1195–1224 (1964).
71. K. Y. Maillacheruvu, *Analysis of Oxygen Transfer Performance on Dome-Disc Fine Pore Diffuser Systems*, MS Thesis, Dept. of Civil and Environmental Engineering, University of Iowa, Iowa City, IA, July, 1987.

72. G. L. Huibregtse, T. C. Rooney, and D. C. Rasmussen, Factors affecting fine bubble diffused aeration, *J. Water Pollut. Control Fed.* **5**(8), 1057–1064 (1983).

73. A. G. Gilbert and R. C. Sullivan, The significance of oxygen transfer variables in sizing dome diffuser aeration equipment. In: *Scale-up of Water and Wastewater Treatment Processes*, Schmidtke, N. W. and D. W. Smith, (eds.) Ann Arbor Press, Ann Arbor, ML, 1983.

74. K. A. Yaeger, *The Effects of Tank Geometry on Performance of Fine Pore Diffusers*, MS Thesis, Dept. of Civil and Environmental Engineering, University of Iowa, Iowa City, IA, May, 1986.

75. Sanitaire, *Oxygen Transfer-Ceramic Disc Diffuser System Reports*, Sanitaire-Water Pollution Control Corp., Milwaukee, WI, 1976–1986.

76. F. W. Yunt and T. O. Hancuff, *Relative Number of Diffusers for the Norton and Sanitaire Aeration Systems to Achieve Equivalent Oxygen Transfer Performance*, Internal report, Los Angeles County Sanitation Districts, Whittier, CA, December 14, 1979.

77. G. L. Huibregtse, *Evaluation of the IFU Fine Bubble Membrane Disc Diffuser*, Internal project reports, Envirex Inc., Waukesha, WI, January and April, 1987.

78. H. J. Popel, *Oxygen Feed Capacity and Oxygen Yield of the IFU Membrane Aerator*, Report submitted to K. H. Schussler, Bad Homburg, Germany, November, 1986.

79. F. W. Yunt and T. O. Hancuff, *Aeration Equipment Evaluation: Phase 1 - Clean Water Test Results*, EPA-600/2-88/022, NTIS No. PB88-1 80351, US Environmental Protection Agency, Cincinnati, OH, March, 1988.

80. Eimco, *Evaluation of the Oxygen Transfer Capabilities of the Eimco Elastox-D Fine Bubble Rubber Diffuser*, Eimco Process Equipment Co., Salt Lake City, UT, August, 1986.

81. L. K. Wang, Y. T. Hung, and N. N. K. Shammas, (eds.) *Physicochemical Treatment Processes,* The Humana Press, Inc., Totowa, NJ, 2005.

82. L. K. Wang, Y. T. Hung and N. K. Shammas (eds.), *Advanced Physicochemical Treatment Processes,* The Humana Press, Inc., Totowa, NJ, 2006.

83. L. K. Wang, N. C. Pereira, and Y. T. Hung (eds.), *Biological Treatment Processes*, The Humana Press, Inc., Totowa, NJ, 2007.

84. L. K Wang, N. K. Shammas, and Y. Y. T. Hung (eds.), *Advanced Biological Treatment Processes,* The Humana Press, Inc., Totowa, NJ, 2007.

85. R. Iranpour, Y. J. Shao, B. K. Ahring, and M. K. Stenstrom, Case study of aeration performance under changing process conditions, *Environ. Eng.* **128**(6), 562–569, June (2002).

86. M. Stenstrom and G. Gilbert, Effects of Alpha, Beta and theta factors on design of aeration systems, *Water Res.* **15**(6), 643 (1981).

87. M. Doyle and W. C. Boyle, Translation of clean to dirty water oxygen transfer rates. In: *Proceedings of Seminar/Workshop on Aeration System Design, Testing, Operation, and Control,* EPA 600/9-85-005, NTIS No. PB85-173896, US Environmental Protection Agency, Cincinnati, OH, January, 1985.

88. H. J. Huang and M. K. Stenstrom, Evaluation of fine bubble alpha factors in near full-scale equipment. *J. Water Pollut. Control Fed.* **57**(12), 1143–1151 (1985).

89. V. Mahendraker, D. S. Mavinic, and K. J. Hall, Comparative evaluation of mass transfer of oxygen in three activated sludge processes operating under uniform conditions, *J. Environ. Eng. Sci.* **4**(2), 89–100, 1 March (2005).

90. S. Cameron and A. Burgoyne, *A Field Based Investigation into the Fouling of Fine Bubble Aeration Diffusers in Activated Sludge,* www.iwaponline.com/wio/2002/07/wio200207043.htm, Water Intelligence Online © IWA Publishing (2002).

91. ASCE Oxygen Transfer Standards Subcommittee. *Development of Standard Procedures for Evaluating Oxygen Transfer Devices*. EPA 600/2-83-102, NTIS No. PB84-147438, US Environmental Protection Agency, Cincinnati, OH, October, 1983.

92. WPCF, *Aeration,* Manual of Practice FD-13, Water Pollution Control Federation, Washington, DC, 1988.
93. R. Iranpour and M. K. Stenstrom, Relationship between oxygen transfer rate and airflow for fine-pore aeration under process conditions, *Water Environ. Res.* **73**(3), 266–275, May–Jun (2001).
94. C. H. Hung and W. C. Boyle, The effect of acid cleaning on a fine pore ceramic diffuser aeration system, *Water Sci. Technol.* **44**(2–3), 211 (2001).
95. M. K. Stenstrom and W. C. Boyle, Aeration systems - responsibilities of manufacturer, designer and owner. *Environ. Eng.* May (1998).
96. APCTT, *Fine Pore Tubular Aeration Devices,* Asian and Pacific Center for Transfer of Technology (APCTT), http://www.technology4sme.net/techofferDetail.aspx?offid=4586 (2006).
97. Eandix Equipment, *Aerostrip Membrane Diffuses Fine Bubble Aeration,* http://www.enquip.com (2006).
98. Munkguard Engineering, *Fine Bubble Disk Diffusers,* http://www.munk-eng.dk/dair.htm (2006).

Emerging Flotation Technologies

Lawrence K. Wang

CONTENTS

1. MODERN FLOTATION TECHNOLOGIES

This chapter introduces and reviews typical applications of improved air flotation clarifiers for groundwater decontamination, resources recovery, septic tank effluent treatment, industrial effluent treatment, oil–water separation, shidge thickening, and water purification. Treatment data, process efficiency, energy consumption, and construction costs of flotation process equipment are selectively presented.

Flotation processes are used to remove suspended solids in a flotation clarifier by rising gas bubbles, and to remove soluble iron, volatile organic compounds (VOCs), oils, and surface-active agents by oxidation, air stripping, and surface adsorption. Various modern flotation technologies have been developed by many research engineers around the world, and have become important environmental technologies for groundwater decontamination, industrial effluent treatment, domestic waste treatment, and water purification (1–32). This chapter introduces modern dissolved air flotation (DAF) and flotation–filtration (DAFF) technologies developed by various manufacturers. It is important to note that the results of DAF technical feasibility studies completed by any engineer for a specific DAF/DAFF can be equally applied to other DAF and/or DAFF process equipment. The only difference between each DAF and DAFF is the flotation rate (gallon per minute per square foot, gpm/ft^2; or cubic meter per minute per square meter, m^3/min/m^2). The author of this chapter introduces the DAF and DAFF technologies from a technical point of view, and is not promoting any specific manufacturer's DAF or DAFF product, because they all perform in a similar manner. The differences among various DAF/DAFF process equipment to be considered by the buyer's design engineer are usually the footprints, costs, product reliability, and manufacturer's reputation.

A typical DAF consists of saturating a portion or all of the influent feed or a portion of recycled effluent with air at a pressure of 25–70 lb/in^2 (1.70–4.76 atm). The pressure as high as 90 lb/in^2 has been operated by some plant engineers. The pressurized influent is held at this pressure for 0.2–3 min in a pressure vessel and then released to atmospheric pressure in the flotation chamber. The sudden reduction in pressure results in the release of microscopic air bubbles that oxidize the soluble ferrous iron (Fe^{2+}) to form insoluble ferric iron (Fe^{3+}) and attach themselves to volatile organic compounds (VOCs), surfactants, oil, and suspended particles in the influent water in the flotation chamber. This results in agglomeration, air stripping, and surface adsorption because of the generated air bubbles. The VOCs are removed by air stripping and discharged to a granular activated carbon (GAC) adsorber for purification; whereas the floated materials (oil, surfactants, TSS) rise to the surface with vertical rise rates of about 0.5–2 ft/min (15.24–60.96 cm/min) to form a scum layer. Specially designed sludge scoops, flight scrapers, or other skimming devices continuously remove the scum. The clarified effluent that is almost free of suspended solids and oils is discharged near the bottom of a flotation chamber.

The retention time in the flotation chambers was usually about 20–60 min but has been reduced to 3–15 min by innovative design. The effectiveness of DAF depends on efficient air oxidation and the attachment of bubbles to the oil, VOCs, surfactants, and other particles, which are to be removed from the influent liquid stream. Flotation phenomena can occur in at least three ways: (a) the air bubbles adhere to the insoluble solids by electrical attraction, (b) the air bubbles become physically trapped in the insoluble solids' original or flocculent structure, and (c) the air bubbles chemically adsorb to

the insoluble solids' original or flocculent structure. The attraction between the air bubble and contaminants is believed to be primarily a result of the particle surface charges and bubble size distribution. The depth of the flotation unit depends a uniform distribution of water and microbubbles. Generally, the depth of effective flotation units is only between 3 and 9 ft (91.44–274.32 cm). Flotation units can be round, square, or rectangular. Gases other than air can be used. The petroleum industry has used nitrogen, with closed vessels, to reduce the possibilities of fire. Ozone can be fed through with air for more efficient reduction of soluble iron, VOCs, and so on (25). Ozone–ultraviolet (UV) flotation is another alternative for groundwater decontamination.

Several high-rate air flotation clarifiers (both DAF and dispersed air flotation) with less than 15 min of detention time have been developed for groundwater decontamination, industrial effluent treatment, resources recovery, and water reclamation. Both insoluble and soluble impurities such as VOCs, activated sludge, fibers, free oil and grease (O&G), emulsified oil, lignin, protein, humic acid, tannin, algae, biochemical oxygen demand (BOD), total organic carbon (TOC), iron ions, manganese ions, hardness, titanium dioxide, phosphate, heavy metals, and so on can be separated from a target liquid stream.

Design equations and examples of modern high-rate DAF clarifiers can be found elsewhere (1,2,32). For flotation of dissolved pollutants, addition of flotation aids to a flotation clarifier is required. Flotation aids include, but will not be limited to aluminum sulfate, ferric chloride, organic polymer, poly aluminum chloride, calcium chloride, ferrous sulfate, calcium hydroxide, ferric sulfate, powdered activated carbon (PAC), sodium aluminate, surfactants, and pH adjustment chemicals. This chapter introduces DAF and DAFF, their history, development, process equipment, operational procedures, energy consumption, and various applications. Special emphasis is placed on groundwater decontamination, industrial effluent pretreatment, resources recovery with primary flotation, improved biological process with secondary flotation, and water purification. The treatment, case studies, and new technologies in refs. 1–56 are selectively summarized in this chapter, such as:

a. Textile mills effluents.
b. Pulp and paper mills effluents.
c. Petroleum refinery wastewaters.
d. Auto and laundry wastewater.
e. Storm water runoff contaminated by industrial waste.
f. Industrial effluent treatment.
g. The first North America DAFF water treatment plant built in 1981 in Lenox, MA.
h. Once largest DAFF water treatment plant in the world, built in 1986 in Pittsfield, MA.
i. The largest DAFF plant in North America with 75-MGD capacity.
j. Emerging AquaDAF™ plants.
k. First full-scale anaerobic biological flotation plant in Kassel, Germany.
l. Emerging dissolved gas flotation sequencing batch reactor (SBR).
m. Combined primary flotation clarification and secondary flotation clarification applications.
n. Various recent DAF developments.

DAF is an excellent process for sludge thickening. A DAF thickening clarifier is commonly used before sludge digestion and/or dewatering, or after digestion. The common practice of DAF thickening is introduced in another chapter of this handbook series (57).

2. GROUNDWATER DECONTAMINATION USING DISSOLVED AIR FLOTATION (DAF)

Groundwater contamination is an international major concern. In the United States, which is an industrialized country, about 70% of potable water is supplied by groundwater. The percentage of potable water supplied by groundwater in the developing and underdeveloped countries will be much higher. Groundwater contamination in the United States is about 71% caused by industrial accidents (chemical spills, underground storage tank leaks, and so on), 16% by railroad or truck's chemical accidents and 13% by leachates from lagoons or dumpsites.

a. Potable use (approx 39%).
b. Cleanup of aquifer to prevent spread of contamination (approx 48%).
c. Industrial and commercial use of the treated groundwater (approx 13%).

In any case, the potentially hazardous VOCs must be removed. Timely cleanup of an aquifer to prevent spread of groundwater contamination is extremely important because the damage can be beyond repair if the spread of groundwater contamination becomes too wide.

Toxic organic compounds commonly found in groundwater include, but will not be limited to, the compounds presented in Table 1. Other toxic organic compounds (representing 1% of occurrences) are PCBs, CFCs, 2,4-D, 2,4,5-TP (silvex), toxaphene, methoxychlor, lindane, endrin, and so on, of which 2,4-D and silvex are commonly used for killing aquatic and land weeds. Inorganic toxic substances commonly found in groundwater include lead, arsenic, copper, cadmium, barium, chromium, mercury, selenium, silver, nitrate, and so on.

In a typical groundwater decontamination project, additional impurities that are non-toxic but require pretreatment for their removal include iron, manganese, total dissolved solids, and color. The state-of-the-art technologies for groundwater decontamination are:

a. Pretreatment by aeration, chemical coagulation, sedimentation and filtration for removal of heavy metals, color, TDS, iron and manganese coliforms, and hardness.
b. Air stripping for VOCs removal.
c. Ozonation with UV light for VOCs removal.
d. Liquid-phase GAC for VOCs removal.
e. Hydrogen peroxide for VOCs removal.
f. Gas-phase GAC for air purification.
g. Biological processes for removal of various organic contaminants and nitrate.

Recently innovative air flotation technologies have been developed (1–30) for more cost-effective groundwater decontamination in comparison with the state-of-the-art technologies. DAF is very efficient and cost-effective for groundwater pretreatment where heavy metals, color, TDS, iron, manganese, coliforms, and hardness can all be significantly removed to meet the need State Government's. It aims not only at the decontamination of groundwater but also elimination of biological and chemical fouling for the subsequent processes. Furthermore, many VOCs can be removed by DAF as well. Table 2 presents the US Environmental Protection Agency (US EPA)'s removal data for DAF process in general. The capability of DAF for treatment of various liquid streams has been well established (3–30) although its application for decontamination of groundwater is comparatively new. For pretreatment of a contaminated groundwater, DAF serves the purpose well even when using conventional chemicals (*see* Table 2).

Table 1
Toxic Organic Compounds Commonly Found in the US Groundwater

Organic compounds in groundwater	Occurrences (%)	Concentration range
Carbon tetrachloride	5	130 µg/L–10 mg/L
Chloroform	7	20 µg/L–3.4 mg/L
Dibromochloropropane	1	2–5 mg/L
DDD	1	1 µg/L
DDE	1	1 µg/L
DDT	1	4 µg/L
Cis-1,2-Dichloroethylene	11	5 µg/L–4 mg/L
Dichloropentadiene	1	450 µg/L
Diisopropylether	3	20–34 µg/L
Tertiary methyl-butylether	1	33 µg/L
Diisopropyl methyl phosphonate	1	1250 µg/L
1,3-Dichloropropene	1	10 µg/L
Dichlorethylether	1	1.1 mg/L
Dichloroisopropylether	1	0.8 mg/L
Benzene	3	0.4–11 mg/L
Acetone	1	10–100 µg/L
Ethyl acrylate	1	200 mg/L
Trichlorotrifloroethane	1	6 mg/L
Methylene chloride	3	1–21 mg/L
Phenol	3	63 mg/L
Orthochlorophenol	1	100 mg/L
Tetrachloroethylene	13	5 µg/L–70 mg/L
Trichloroethylene	20	5 µg/L–16 mg/L
1,1,1-Trichloroethane	8	60 µg/L–25 mg/L
Vinylidiene chloride	3	5 µg/L–4 mg/L
Toluene	1	5–7 mg/L
Xylenes	4	0.2–10 mg/L
EDB	1	10 µg/L
Others	1	Not available

Special chemicals may be required for complete groundwater treatment. For instance, powdered activated carbon (PAC) may be dosed into a DAF system for enhancement of VOC removal efficiency. In such a case, it is also termed as adsorption flotation process (i.e., PAC–DAF process). In a recent pilot plant study (6), a process system consisting of adsorption flotation and sand filtration has been proven to be feasible for groundwater decontamination. PACs initially are dosed as adsorbents for removal of color, odor, ethylene dibromide, total trihalomethane (TTHM), and other toxic substances from groundwater. Subsequently, the spent PACs are flocculated by coagulants, and floated to the water surface by DAF. Finally, the flotation-clarified water is polished by automatic backwash filtration (ABF). The results of both bench-scale study and pilot plant study indicate that 250 mg/L of PAC (Hydrodarco B) at 15 min of detention time reduced 100% color (from 25 CU), 100% iron (from 25 µg/L), 98% humic acid (from 3200 µg/L), 100% ethylene dibromide (from 1.2 µg/L), 98% TTHM (from 1265 µg/L), 99.6% odor (from 500 TON), 100% mercaptans (from 730 µg/L), 100% lead (from 6 µg/L),

Table 2
Control Technology Summary for Dissolved Air Flotation

| Pollutant | Effluent concentration | | % Removal |
	Range	Median	
Classical pollutants (mg/L)			
BOD (5-d)	140–1000	250	68
COD	18–3200	1200	66
TSS	18–740	82	88
Total phosphorus	<0.05–12	0.66	98
Total phenols(a)	>0.001–23	0.66	12
Oil and grease	16–220	84	79
Toxic pollutants (µg/L)			
Antimony	ND–2300	20	76
Arsenic	ND–18	<10	45
Xylene	ND–1000	200	97
Cadmium	BDL–<72	BDL	98[a]
Chromium	2–620	200	52
Copper	5–960	180	75
Cyanide	<10–2300	54	10
Lead	ND–1000	70	98
Mercury	BDL–2	BDL	75
Nickel	ND–270	41	73
Selenium	BDL–8.5	2	NM
Silver	BDL–66	19	45
Zinc	ND–53000	200	89
Bis(2-etHylhexyl) phthalate	30–1100	100	72
Butyl benzyl phthalate	ND–42	ND	>99
Carbon tetrachloride	BDL–210	36	75
Chloroform	ND–24	9	58
Dichlorobromomethane		ND	>99
Di-*N*-butyl phthalate	ND–300	20	97
Diethyl phthalate		ND	>99
Di-*N*-octyl phthalate	ND–33	11	78
N-nitrosodiphenylamine		620	66
2,4-Dimethylphenol	ND–28	14	>99
Pentachlorophenol	5–30	13	19
Phenol	9–2400	71	57
Dichlorobenzene	18–260	140	76
Ethylbenzene	ND–970	44	65
Toluene	ND–2100	580	39
Naphthalene	ND–840	96	77
Anthracene/phenanthrene	0.2–600	10	81

Source: US EPA.
BDL, below detection limit.
ND, not detected.
NM, not meaningful.
[a]Approximate value.

and 100% arsenic (from 1000 µg/L). A continuous pilot plant was operated at 40 L/min (10.56 gpm) for separation of 250 mg/L of spent PAC (note: 1 mg/L = 1000 µg/L). Nearly 100% of spent PAC (from 250 mg/L) and total coliform (from three colonies per 100 mL) and more than 95% of turbidity (from 4.5 NTU) were removed when 1.5 mg/L of anionic polymer and 2.5 mg/L of coagulant, were dosed to DAF at neutral pH. More than 95% of all target pollutants in the influent water were removed by the innovative process system. DAF was controlled at 30% of recycle water flow, and 0.5 cubic ft/h (0.01416 m^3/h) of air flow. The sand filter was packed with 27.94 cm (11 inches) of quartz sand (E = 0.36 mm, U = 1.65) and operated at 2.5 gpm/ft^2 (0.1 m^3/min/m^2). It appears that the PAC–DAF–ABF process system involving the use of PAC and coagulants is technically feasible for groundwater decontamination. Alternatively a DAF–GAC process system involving the use of plain DAF (without PAC) and GAC has been proven to be equally effective for complete groundwater decontamination for the same influent water mentioned earlier. Furthermore DAF can be enhanced by ozonation without additional process equipment such as an ozone contactor. A dissolved air–ozone flotation system has been successfully tested for treatment of cooling tower water (25), and will be available for decontamination when necessary. Of course, UV can easily be added to a dissolved air–ozone flotation without any difficulty.

For treatment of a contaminated groundwater source containing high concentration of hardness, DAFF is also an excellent pretreatment process system for reduction of scale formation and biological fouling in the subsequent processes. In a separate study, a groundwater having 12 units of color, 13 NTU of turbidity, and 417 mg/L of calcium harness in terms of $CaCO_3$, was successfully treated by a continuous DAFF plant consisting of a static hydraulic flocculation, a DAF clarifier, a recarbonation facility, and three sand filters. When the groundwater was dosed with 42.3 mg/L of magnesium carbonate as coagulant and small amount of lime was used for pH adjustment (to pH 11.3), the plant's treatment efficiency in terms of percent removal became color, 100%; turbidity, 98%; and total hardness, 62%. Recarbonation with CO_2 (as needed) maintained the effluent pH at 7.2. The plant's operational conditions were flocculation detention time = 5.63 min; DAF detention time = 3 min; flotation clarification rate = 2.5 gpm/ft^2 = 0.1 m^3/min/m^2; sand depth = 27.94 cm of quartz sand; sand filtration rate = 2.5 gpm/ft^2 = 0.1 m^3/min/m^2; continuous influent/effluent water flow rates = 12 gpm = 45.42 L/min; continuous recycle water flow rate = 3 gpm = 11.36 L/min, and continuous air flow rate 1 ft^3/h at 90 psig = 0.02832 m^3/h at 6.12 atm. Soda ash (Na_2CO_3) will be needed only if permanent hardness $CaSO_4$ is present.

(a) $$Ca(HCO_3)_2 + Ca(OH)_2 \rightarrow 2\ CaCO_3 + H_2O$$

(b) $$Mg(HCO_3)_2 + Ca(OH)_2 \rightarrow CaCO_3 + H_2O + MgCO_3$$

(c) $$MgCO_3 + Ca(OH)_2 \rightarrow Mg(OH)_2 + CaCO_3$$

(d) $$CaSO_4 + MgCO_3 \rightarrow CaCO_3 + MgSO_4$$

(e) $$MgSO_4 + Ca(OH)_2 \rightarrow Mg(OH)_2 + CaSO_4$$

(f) $CaSO_4 + Na_2CO_3 \rightarrow CaCO_3 + Na_2SO_4$

(g) $CO_2 + Ca(OH)_2 \rightarrow CaCO_3 + H_2O$

(h) $CO_2 + Mg(OH)_2 \rightarrow MgCO_3 + H_2O$ (coagulant regeneration)
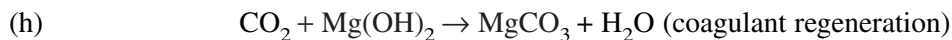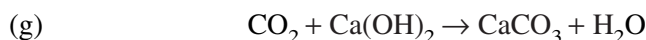
DAF is controlled under laminar flow conditions using only about 1–3% of air flow in comparison with the influent groundwater flow, and its gas bubbles are extremely fine (i.e., less than 80 µm). Although, DAF is an excellent pretreatment process for groundwater decontamination, DAF alone can remove TDS, turbidity, color, coliforms, iron, manganese, hardness, heavy metals, and many VOCs, but not all VOCs. DAF only requires 3–5 min of detention time; therefore it is a low-cost pretreatment process.

Another innovative process, dispersed air flotation, is controlled under turbulent flow condition using about 400% of air flow in comparison with the influent groundwater flow, and its gas bubbles are coarse similar to the air bubbles in an activated sludge plant's aeration basin. Dispersed air flotation requires only 4–10 min of detection time, therefore, it is also a very cost-effective process. Dissimilar to DAF, dispersed air flotation is not an effective pretreatment process for removal of heavy metals, color, turbidity, TDS, hardness, and coliforms, but it is as efficient as conventional aeration process and air stripping process for iron and manganese removal and for VOCs removal, respectively. Dispersed air flotation itself is an aeration process, so soluble iron and manganese ions may be oxidized to form insoluble suspended particles, which can then be separated easily from the liquid phase. The aeration efficiency of dispersed air flotation is higher than that of DAF. If groundwater's soluble ferrous iron content is 8 mg/L or less, DAF alone using conventional coagulants will be able to remove the soluble iron (8). When groundwater's soluble ferrous iron is higher than 8 mg/L, either dispersed air flotation or oxidizing agents (ozone, potassium permanganate, and so on) will be required for its removal.

Conventional air stripping process introduces the target groundwater into a gas phase for stripping VOCs; whereas dispersed air stripping introduces air bubbles into the groundwater, which is a liquid phase. A conventional air stripping tower is very tall (>10 ft or 3 m), and a dispersed air stripping cell can be as shallow as 3 ft (0.91 m). The most important feature of an enclosed dispersed air stripping cell for VOC reduction is its capability of recycling and reuse of its purified air streaming thus totally eliminating any possibility of air pollution. Actual process data for groundwater decontamination cannot be disclosed at present, but will be allowed for public release soon. In summation, both DAF and dispersed air stripping are recent developments for more efficient and more cost-effective decontamination of groundwater. Conventional and innovative groundwater treatment systems for a typical 150 gpm (568-L/min) groundwater decontamination project in New Jersey are presented in Figs. 1 and 2, respectively, for the purpose of process illustration and comparison. The pretreatment unit shall remove mainly arsenic, cadmium (up to 240 µg/L), chromium (up to 150 µg/L), iron, lead (up to 108 µg/L), manganese, selenium (up to 210 µg/L), copper (up to 410 µg/L), zinc (up to 1400 µg/L), TDS, and color from the contaminated groundwater. The groundwater treatment units shall treat the pretreatment unit's effluent for removal of benzene (up to 368 µg/L), chloroform (up to 17 µg/L), 1,1-dichloroethylene (up to 42 µg/L), 1,2-trans-dichloroethylene (up to 542 µg/L),

Contaminated groundwater

Well field

Flow collection tank

Water

Flow equalization tank

Water

Flocculation, sedimentation, & filtration

Sludge

Wastewater

Groundwater pretreatment

Water

Air stripping units (2)

Air

GAC air filter

Air → To atmosphere

Air emission control

Water

GAC polishing filter

Water

Holding tank

Water

Purified water -- to discharge or recharge

Groundwater treatment

Groundwater post-treatment

Flocculation, sedimentation, & filtration: metals, solids removal
Air stripping unit: voc removal - 99%
GAC polishing filter: residual voc removal
GAC air filter: voc removal from exhaust air - 99%

457

Fig. 2. Flow sheet for innovative groundwater treatment system.
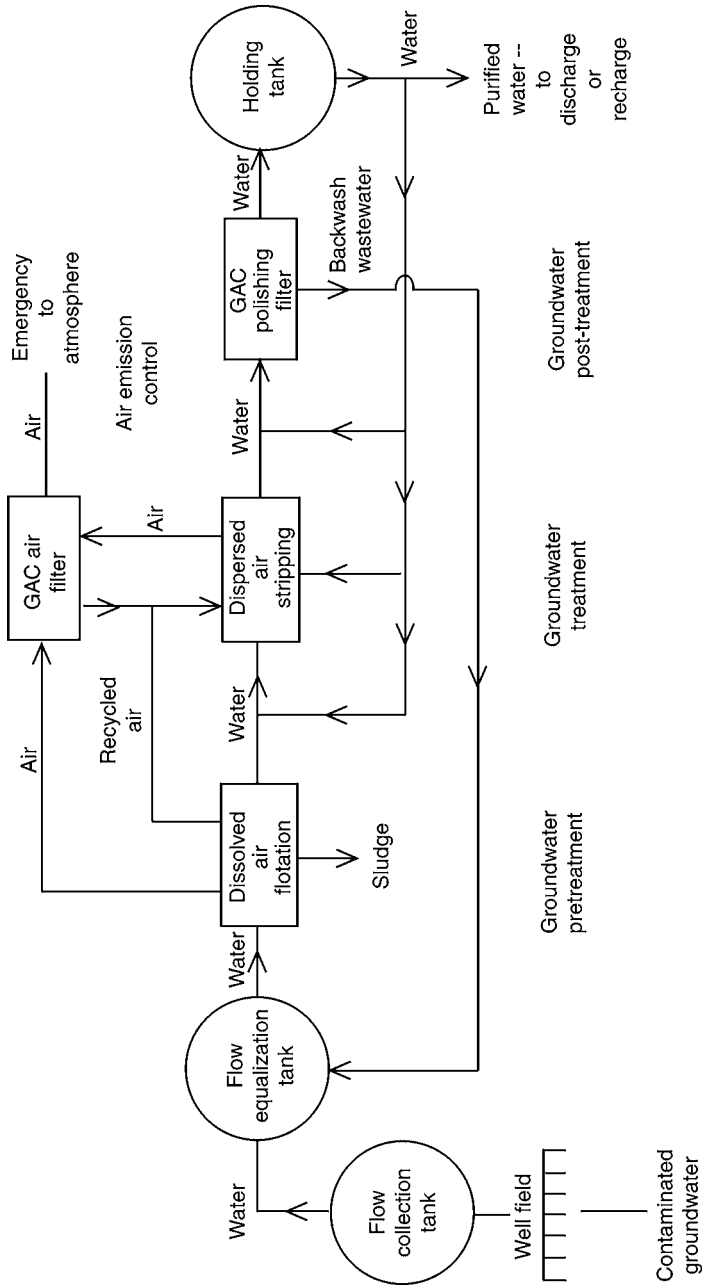
Dissolved air flotation: metals, solids removal
Dispersed air flotation: voc removal - 99%
GAC polishing filter: residual voc removal

methylene chloride (up to 48 μg/L), tetrachloroethylene (up to 70 μg/L), toluene (up to 21,000 μg/L), trichloroethylene (up to 25,200 μg/L), 1,1,1-trichloroethane (up to 165 μg/L), 1,1-dichloroethane (up to 37.5 μg/L), Freon 113 (up to 255 μg/L), and phenols (up to 340 μg/L). It should be noted that the following NJDEP established effluent limits are very stringent:

Benzene	5 μg/L
Chloroform	100 μg/L (as THM)
1,1-Dichloroethylene	42 μg/L
1,2-Trans-dichloroethylene	5 μg/L
Trichloroethylene	5 μg/L
1,1,1-Trichloroethane	200 μg/L
1,1-Dichloroethane	7 μg/L
Others	To be determined by NJDEP

The required efficiencies for both conventional air stripping units and gas phase GAC purifier are set to be 99%.

3. TEXTILE MILLS EFFLUENT TREATMENT USING DAF

The US EPA has conducted a survey and compiled data on treatment of various industrial effluents by DAF. Table 3A indicates the removal data of DAF for treatment of a textile mill effluent. The treated wastewater was from a woven fabric operation with a flow rate of 1730 m³/d. Cationic polymer was dosed as the flotation aid. It is important to know that BOD removal was more than 50%. Suspended solids and phenol removals were 84% and 72%, respectively. The removals of lead, *bis*(2-ethylexyl) phthalate, di-*N*-butyl phthalate, and naphthalene were all more than 92%.

Table 3B indicates that a small DAF pilot plant (diameter = 4 ft = 1.2 m; depth = 6 ft = 1.8 m) which was installed at a textile mill in Seoul, Korea, performed extremely well in terms of high chemical oxygen demand (COD) reduction (66.8–71.0%) and high total suspended solids (TSS) reduction (95–96.3%). The DAF effluent CODs were always the effluent limit of 100 mg/L when the influent CODs were 318 mg/L. Generally DAF performed better than the existing textile mill's conventional wastewater treatment system consisting of primary sedimentation clarifier, activated sludge aeration basins, secondary sedimentation clarifier, sand filters, and GAC filters.

Table 4 (*Source:* US EPA) represents the removal data on flotation treatment of paper and pulp wastewater containing nonintegrated tissue, high COD, and various toxic pollutants. In a 3-d, 24-h composite and grab sampling and analysis, it was found that more than 96% of COD, butyl benzyl phthalate, diethyl phthalate, ethylbenzene, toluene, chloroform, and xylene were removed. Removals of chromium and lead were all more than 82%.

Recycling of paper fibers by flotation for reuse is presented in Section 9. Additional technical data and information on treatment of paper and pulp mill effluent by DAF and dispersed air flotation can be found elsewhere (18,29).

4. PETROLEUM REFINERY WASTEWATER TREATMENT USING DAF

A 3.2-MGD (12,112 m³/d) petroleum refinery effluent was pretreated by an American Petroleum Institute gravity oil–water separator and then treated by a DAF clarifier.

Table 3A
Treatment of Textile Mills Effluent by Dissolved Air Flotation

	Concentration		
Pollutant/parameter	Influent	Effluent	% Removal
Classical pollutants (mg/L)			
BOD$_5$	400	<200	>50
COD	1000	300–720	28–70
TSS	200	32	84
Total phenol	0.092	0.026	72
Toxic pollutants (µg/L)			
Copper	320	81	75
Lead	14	ND	>99
Bis(2-ethylhexyl) phthalate	570	45	92
Di-*N*-butyl phthalate	13	ND	>99
Pentachlorophenol	37	30	19
Phenol	94	26	72
Benzene	18	12	33
Ethylbenzene	460	160	65
Toluene	320	130	59
Naphthalene	250	ND	>99

Source: US EPA.
ND, not detected.

Table 5 (*Source:* US EPA) shows that without any chemical addition, DAF can only remove a small fraction of chromium, lead, zinc, anthracene, and naphthalene. The phenol and copper removals were still more than 50% even without chemical addition. Flotation treatment of petroleum refinery wastewater with chemical addition is highly recommended. Successful application of a high-rate flotation clarifier for secondary flotation clarification of a petrochemical plant's effluent in Texas has been documented in Section 8.

5. AUTO AND LAUNDRY WASTEWATER TREATMENT USING DAF

Table 6A (*Source:* US EPA) documents the results of auto and laundry effluent treatment by DAF (50% recycle flow pressurization). Design or operating parameters were wastewater flow rate = 0.27 m³/min; design flow rate = 0.57 m³/min; hydraulic loading rate = 0.038 m³/min/m²; air-to-solids ratio = 0.0097; sludge overflow = 0.0076 m³/min; sludge concentration = 5%; chemical dosage = 1800 mg/L of calcium chloride and 2 mg/L of polymer; pH = 11.6 in flotation chamber. The pretreatment prior to DAF includes screen, equalization, and oil–water separation. The removal data in Table 6A are for influent and effluent of flotation clarifier only.

Table 6B (*Source:* US EPA) represents additional removal data for auto and laundry wastewater treatment by DAF (50% recycle flow pressurization). In this case, only 60 mg/L of polyelectrolyte was dosed to treat 341 m³/d of laundry effluent. Pretreatment prior

Table 3B
Performance of a Dissolved Air Flotation Pilot Plant
at a Textile Mill in Seoul, Korea (December, 1990)

Time vs parameter	Influent characteristics[a]	Effluent characteristics[b]	Reduction (%)
12/19/90 (1st)			
Flow	80 m^3/d	<80 m^3/d	–
COD	280 mg/L	93 mg/L	66.8
pH	7.2 unit	7.3 unit	–
TSS	800 mg/L	40 mg/L	95
12/19/90 (2nd)			
Flow	100 m^3/d	<100 m^3/d	–
COD	310 mg/L	90 mg/L	71
pH	7.6 unit	7.5 unit	–
TSS	1200 mg/L	45 mg/L	96.3
12/20/90 (1st)			
Flow	120 m^3/d	<120 m^3/d	–
COD	305 mg/L	92 mg/L	69.8
pH	7.0 unit	7.6 unit	–
TSS	1000 mg/L	46 mg/L	95.4
12/20/90 (2nd)			
Flow	160 m^3/d	<160 m^3/d	–
COD	300 mg/L	89 mg/L	70.3
pH	7.5 unit	7.5 unit	–
TSS	1000 mg/L	40 mg/L	96
12/21/90			
Flow	180 m^3/d	<180 m^3/d	–
COD	310 mg/L	92 mg/L	70.3
pH	7.8 unit	7.5 unit	–
TSS	1000 mg/L	38 mg/L	96.2
12/22/90			
Flow	200 m^3/d	<200 m^3/d	–
COD	318 mg/L	96 mg/L	69.8
pH	8.0 unit	7.2 unit	–
TSS	1000 mg/L	39 mg/L	96.1

[a]Wastewater temperature range = 27–30°C.
[b]Chemical dosages for wastewater treatment = 350 mg/L of alum and 5 mg/L of polymer.

to flotation includes screen and equalization. Other operation parameters comprised pH = 10.3–10.6 in flotation chamber; hydraulic loading rate = 0.11 m^3/min/m^2; gas-to-solid ratio = 0.5; sludge overflow = 0.11 m^3/d; and floated sludge concentration = 7.5%.

The different results in Tables 6A and 6B indicate the effect of chemical application on the treatment efficiency of DAF processes. It can be seen that the removal data in Table 6A (using both calcium chloride and polymer) are much better than that in Table 6B (using polymer only). In summation, more than 80% removal of O&G, arsenic, *bis*-(2-ethylhexyl) phthalate, anthracene–phenanthrene, and naphthalene can be achieved by flotation. For removal of total phosphorus, cadmium, lead, zinc, butyl benzyl phthalate, 2,4-dimethylphenol, and 1,1,1-trichloroethane, more than 90% removal can be achieved.

Table 4
Treatment of Pulp and Paper Mills Effluent by Dissolved Air Flotation

Pollutant/parameter	Concentration		Removal (%)
	Influent	Effluent	
Classical pollutants (mg/L)			
COD	400	18	96
Toxic pollutants (µg/L)			
Chromium	15	2	87
Copper	45	19	58
Lead	11	2	82
Butyl benzyl phthalate	800	ND	>99
Diethyl phthalate	12	ND	>99
Ethylbenzene	13,000	ND	>99
Toluene	130	ND	>99
Chloroform	3	ND	>99
Xylene	14,000	ND	>99

Source: US EPA.
ND, not detected.
Sampling: 3-d, 24-h composite and grab
Analysis: data sets 1

Table 5
Treatment of Petroleum Refining Wastewater by Dissolved Air Flotation

Pollutant/parameter	Concentration		Removal (%)
	Influent	Effluent	
Toxic pollutants (µg/L)			
Chromium	720	570	21
Copper	16	5	69
Lead	250	210	16
Zinc	110	83	22
Phenol	4900	2400	51
Anthracene/phenanthrene[a]	1100	600	45
Naphthalene	1100	700	36

Source: US EPA.
[a]Concentration represent sums for these two compounds which elute simultaneously and have the same major ions for GC/MS.
Sampling: 3-d grab composite
Analysis: data sets 1

6. SEAFOOD PROCESSING WASTEWATER TREATMENT USING DAF

A system consisting of a microstrainer, a DAF clarifier, and a GAC column was proven to be feasible for treatment of the 200 gpm Homer Smith scallop processing wastewater containing 2600 mg/L COD, 1325 mg/L TSS, 1238 mg/L BOD$_5$, 224 µg/L copper, 114 µg/L cadmium, 346 µg/L zinc, 145 mg/L TKN, 50 mg/L total phosphorus, 14/100 mL total coliforms, and 37.5 mg/L ammonia nitrogen. DAF alone removed

Table 6A
Treatment of Auto and Laundry Wastewater by Dissolved Air Flotation

Pollutant/parameter	Concentration		Removal (%)	Detection limit
	Influent	Effluent		
Classical pollutants (mg/L)				
COD	6400	3200	50	
TOC	1700	690	59	
TSS	390	98	75	
Oil and grease[a]	700	140	80	
Total phosphorus	42	1.7	96	
Toxic pollutants, (µg/L)				
Antimony	94	BDL	95[b]	10
Arsenic	10	2	80	1
Cadmium	110	BDL	>99[b]	2
Chromium	480	270	44	4
Copper	1500	500	67	4
Cyanide	57	54	5	
Lead	4800	130	97	22
Nickel	350	250	29	36
Zinc	3700	230	94	1
Bis(2-ethylhexyl) phthalate	1200	220	82	0.04
Butyl benzyl phthalate	310	ND	>99	0.03
Di-*N*-butyl phthalate	92	19	79	0.02
Di-*N*-octyl phthalate	150	33	78	0.89
2,4-Dimethylphenol	460	ND	>99	
Phenol	98	42	57	0.4
Dichlorobenzene	1100	260	76	
Anthracene/phenanthrene	380	66	83	0.01
Naphthalene	4800	840	83	0.007
Methylene chloride	2	2	0	0.4
1,1,1-Trichloroethane	18	14	22	2

Blanks indicate data not available.
BDL, below detection limit.
ND, not detected.
[a]Average of four samples.
[b]Approximate value.
Chemical dosages = 1800 mg/L CaCl$_2$ and 2 mg/L polymer.
Sampling: 2-d composite and grab
Analysis: data sets 1

68.5% COD, 96.2% TSS, 54.1% ammonia nitrogen, 58.8% cadmium, 88.2% zinc, 54.8% BOD, 100% coliform, 64.1% TKN, and 96.3% total phosphorus when alum, activated sodium aluminate, and polymer 2PD-462 were dosed to DAF. DAF chemical cost is estimated to be 0.81 46 USD/1000 gal (1000 gal = 3785 L). Bioassay testing indicates that the DAF effluent was not toxic to fish. With additional sodium carbonate and H$_3$PO$_4$ at pH 6.9, removals of cadmium and zinc by DAF were increased to 82% and 92.5%,

Table 6B
Treatment of Auto and Laundry Wastewater by Dissolved Air Flotation

Pollutant/parameter	Concentration		Removal (%)	Detection limit
	Influent	Effluent		
Classical pollutants (mg/L)				
COD	500	460	8	
TOC	140	87	38	
TSS	50	32	36	
Oil and grease[a]	39	16	59	
Total phenol	0.43	0.39	9	
Toxic pollutants (µg/L)				
Copper	55	50	9	4
Cyanide	29	25	14	
Zinc	290	240	17	1
Bis(2-ethylhexyl) phthalate	82	74	10	
Butyl benzyl phthalate	17	ND	<99[b]	0.03
Di-*N*-butyl phthalate	2	ND	<99	0.02
Di-*N*-octyl phthalate	28	11	61	0.89
Anthracene/phenanthrene	0.9	0.2	78	0.01
Naphthalene	0.9	0.6	33	0.007
Pyrene	0.3	0.3	0	0.01
Chloroform	41	24	41	5
Methylene chloride	57	22	61	0.40
Tetrachloroethylene	2	2	0	
1,1,1-Trichloroethane	2	ND	>99	2

Source: US EPA.
Blanks indicate data not available.
ND, not detected.
[a]Average of four samples.
Chemical dosage = 60 mg/L polymer.
[b]Approximate value.
Sampling: 2-d composite and grab
Analysis: data sets 1

respectively. Combined DAF–GAC treatment gave 97.5% COD removal and 94.6% ammonia nitrogen removal. Free chlorination removes 100% bacteria and ammonia nitrogen. Table 7 presents some typical treatment results.

7. STORM RUNOFF TREATMENT USING DAF

The feasibility of removing hazardous soluble arsenic (+5) and other conventional pollutants from combined storm runoff and process wastewater by oil–water separation, DAF filtration, and GAC adsorption was fully demonstrated for an oil blending company in New Jersey (3,4). The oil separated from the raw combined wastewater by the American Petroleum Institute oil–water separators was virgin, and was, therefore, skimmed off, dried, and reused.

Table 7
Treatment of Sea Food Processing Wastewater by Dissolved Air Flotation and Adsorption

Wastewater parameters (mg/L except as noted)	Raw seafood wastewater	DAF effluent	DAF and GAC effluent
Flow (gpm/sq. ft.)	NA	2	2
pH (unit)	7.0	6.9	NA
TSS	1325	50	NA
COD	2600	820	182
BOD (5-d)	1238	560	NA
NH_3–N	37.5	17.2	NA
No. of coliforms/100 mL	14	0	NA
As	ND	ND	ND
Cd	0.114	0.047	0.012
Zn	0.346	0.041	0.030
Cu	0.224	0.058	0.028
Turbidity (NTU)	THTM	10	NA
Color (unit)	THTM	80	NA
Total phosphorus (P)	50	1.85	NA
TKN	145	52	NA

Notes: 70 mg/L alum, 70 mg/L ASA (both as Al_2O_3) and 8 mg/L Polymer 2PD-462, 0.5 mg/L sodium carbonate and 0.5 mg/L phosphoric acid were dosed to DAF with 75% recycle flow. GAC detention time was 30 min. 1 gpm/sq. ft. = 0.0407 m^3/min/m^2.

The oil–water separator effluent containing 1.01 mg/L of arsenic, 3 NTU of turbidity, 50 units of color, 28.5 mg/L of O&G, and 83 mg/L of COD was fed to a DAF clarifier for removal of arsenic by 90.1%, turbidity by 30%, color by 43%, O&G by 43.2%, and COD by 32.5%. Either ferric chloride or ferric sulfate was an effective coagulant for arsenic removal. The same oil–water separator effluent was also successfully treated by a DAF-filtration clarifier. Reductions of arsenic, turbidity, color, O&G, and COD were 90.6, 93.3, 98, 74.7, and 51.8%, respectively.

Although both DAF and DAF-filtration (DAFF) demonstrated to be excellent pre-treatment processes, GAC post-treatment removed 100% of soluble arsenic. Table 8 presents some important operational data generated at the oil blending company. Under Contract 14-12-40, the US EPA has concluded that the combination of screening and flotation is one of the most efficient process systems for treatment of combined sewer overflows (33). There are many prefabricated, highly efficient commercial screening structures available (34). There are also many DAF and DAFF manufacturers (34).

8. INDUSTRIAL EFFLUENT TREATMENT BY BIOLOGICAL PROCESS USING DAF FOR SECONDARY FLOTATION CLARIFICATION

The recent and accelerating emphasis on industrial waste treatment has necessitated the rapid development of improved biological waste treatment systems to aid in cost and energy savings. The use of secondary flotation clarification in the place of, or in assisting secondary sedimentation clarifications in the activated sludge process system is a recent advancement in this basic process. The potential of this development, in terms of

Table 8
Treatment of Storm Runoff by Dissolved Air Flotation and Sand Filtration

Treatment efficiency	Test one	Test two	Test three
Influent arsenic (mg/L)	0.0015	0.518	1.010
Removal by flotation (%)	33.3	79.5	90.1
Removal by flotation/filtration (%)	100	90.3	90.6
Influent turbidity (NTU)	3.4–3.6	3.5	3
Removal by flotation (%)	35.7	45.7	30
Removal by flotation/filtration (%)	93	93.7	93.3
Influent color (unit)	48–49	49	50
Removal by flotation (%)	50.5	40.8	43
Removal by flotation/filtration (%)	98.9	97.9	98
Influent O&G (mg/L)	29.2	29.3	28.5
Removal by flotation (%)	52.7	51.5	43.2
Removal by flotation/filtration (%)	69.2	61.1	74.7
Influent COD (mg/L)	85	86	83
Removal by flotation (%)	37.6	46.5	32.5
Removal by flotation/filtration (%)	58.8	53.5	51.8
Influent pH (unit)	7–7.1	7.1–7.1	7.2–7.2
After flotation (unit)	6.9–7	7.1–7.2	6.9–7.1
After flotation/filtration (unit)	6.9–7	7–7.1	7–7.1

[a]Chemical flotation treatment: Sodium aluminate, 15 mg/L as Al_2O_3, and either ferric chloride or ferric sulfate, 15 mg/L as Fe.
[b]Sand specification: ES = 0.85 mm, UC = 1.55, depth = 11 in. = 28 cm.

higher suspended solids and BOD removals from existing plants and expansion of hydraulic capacity at significantly reduced cost, is expected to result in extremely rapid acceptance by municipalities and industry.

The primary distinguishing feature of the improved activated sludge treatment system is that high-rate DAF is the secondary clarifier for separation of suspended solids from the aeration basin effluent, as opposed to secondary sedimentation alone in conventional activated sludge systems. Secondary flotation can be applied for improving treatment efficiency of an existing overloaded activated sludge plant, or handle additional wastewater flow. The concept and theory of secondary flotation have been presented elsewhere (21). It was concluded that a high-rate DAF clarifier can be applied in series between the aeration basin and secondary sedimentation in a conventional activated sludge process to separate the living microorganisms before settling in the existing secondary sedimentation basins. This results in the following improvements in the existing plant: (a) solids and hydraulic loadings on an overloaded secondary sedimentation are reduced resulting in increasing clarification efficiency and saving construction cost on expansion of secondary sedimentation facilities; (b) A reduction in recycle sludge volume because of higher solids content in the recycled sludge reduces the hydraulic loading on an aeration basin thus increases retention time without increasing aeration basin size; (c) Higher solids content in the waste sludge represents cost saving and improved operation of sludge thickening, dewatering, and disposal; (d) The living microorganisms, separated by the DAF, are returned to the aeration basin quickly (in less than 15 min) in aerobic condition

and are more active than comparable settled microorganisms, and the oxygen requirement for the mixed liquor suspended solids is also significantly reduced; and (e) The problems of sludge rising and sludge bulking owing to industrial effluent's nutrient imbalance or toxicity can be totally solved when using secondary flotation.

This section describes the 9-yr case history of a secondary flotation clarifier (diameter = 49 ft = 14.9 m) at a petrochemical plant in Texas for improving the operation of their existing biological treatment system, and increasing the capacity to allow bringing additional production on-line. The MLSS level in the existing activated sludge aeration basin has been as high as 6000 mg/L thus causing a large volume of recirculation of return sludge and overload of the existing wastewater treatment plant. Sludge rising and bulking have been the added problems to the existing secondary sedimentation clarifier.

The 49 ft (14.9 m) circular DAF clarifier has been installed between the aeration basin and the sedimentation clarifier for clarification of aeration basin effluent. At the recycle flow pressurization mode, the effluent TSS of flotation clarified water is always 150 mg/L. The healthy floated sludge at 2% consistency is recycled to the aeration basin. About 10–20 mg/L of low-cost liquid polymer is dosed to enhance flotation. The TSS solids removal rate is about 60 lbs/d/ft^2 (293 kg/d/m^2). Special features of this installation include (a) short flotation retention time at 3–5 min; (b) low-cost shallow flotation concrete tank construction; (c) outdoor installation at grade level; (d) special aerated flow feed with double rotary joint increases aeration efficiency; (e) increased hydraulic capacity at about 25% the capital cost estimated for expanded aeration and settling tank; (f) dewatering of floated sludge by sludge press, thus bypassing the sludge thickener. Figures 3 and 4 show the flow diagrams of original and improved, biological wastewater treatment system at the petrochemical plant in Texas respectively. Although a DAF makes an excellent secondary clarifier, a more expensive flotation–filtration (DAFF) clarifier will be even better because of its added tertiary filter (24).

9. INDUSTRIAL RESOURCE RECOVERY USING DAF FOR PRIMARY FLOTATION CLARIFICATION

Industry makes decisions about the type of effluent clarification in about two-thirds of the cases through their own employed engineers. These engineers are generally well informed about their problems with the industrial effluent and are dynamic and eager to use the most up to date effluent clarification technologies to recover their resources and to keep installation and operational costs to a minimum.

When DAF is used as the very first clarifier for wastewater clarification, this flotation process unit is termed as primary flotation. Sedimentation–flotation clarifiers are frequently used for effluent's primary clarification and fiber recovery in large papermills. Sedimentation–flotation clarifier which has a DAF cell on the top of a sedimentation tank is specifically designed for clarification of an industrial effluent containing both heavy and light weight of suspended solids. Clarification is effected by both sedimentation and flotation. The denser particles, specifically sand and grit, settle at the bottom; those less dense float on the top.

The slightly higher power cost of a sedimentation–flotation clarifier is more than offset by the installation and financing cost of a more expensive conventional sedimentation clarifier. One very important factor is that the recovered floated sludge from a
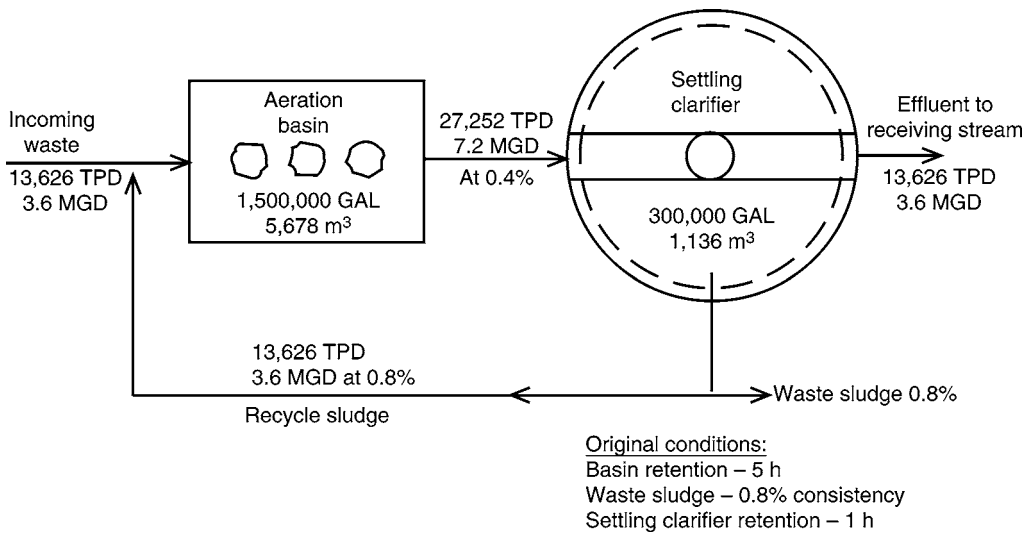
Fig. 3. Original biological wastewater treatment system of a chemical plant in TX.
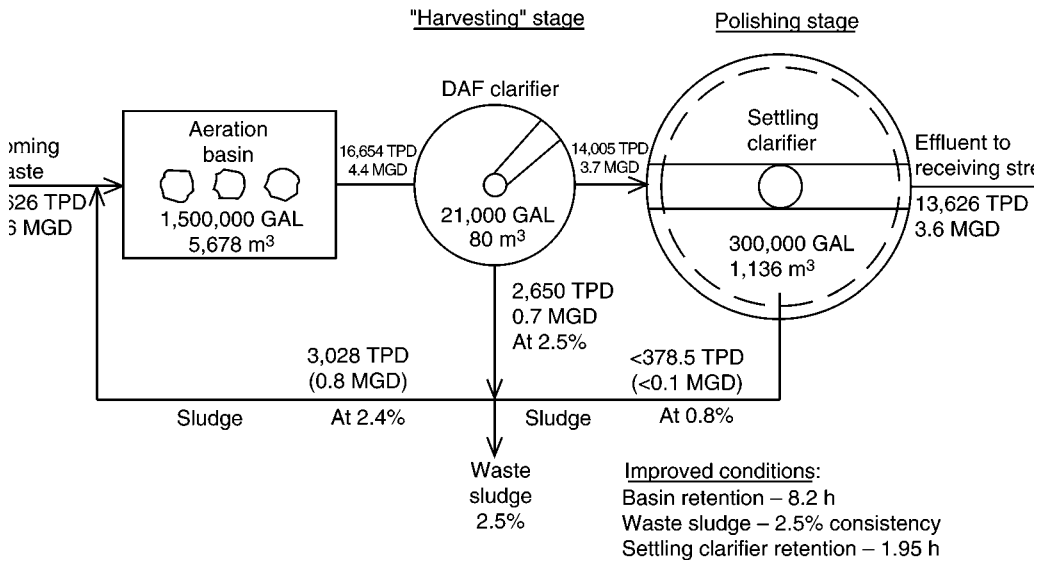
Fig. 4. Improved biological wastewater treatment system of a chemical plant in TX.

sedimentation–flotation clarifier maintains its papermaking qualities and can be reused or sold. The sludge from a conventional sedimentation clarifier is not reusable and is of lower consistency.

The space requirement of the sedimentation–flotation clarifier is only one-fourth of the conventional sedimentation clarifier. All these facts shall be taken into consideration by a plant engineer. Although a sedimentation–flotation clarifier is ideal for primary clarification, a DAF alone can also be used for primary clarification (23).

10. FIRST AMERICAN FLOTATION–FILTRATION PLANT FOR WATER PURIFICATION—LENOX WATER TREATMENT PLANT, MA, USA

An innovative potable flotation–filtration plant with a design capacity of 1.2 MGD (4542 TPD) has been faithfully serving 10,000 residents and tourists in the Town of Lenox, MA, USA, since July, 1982 (26,27). Its process system consisting of chemical flocculation, DAF, and automatic backwash sand filtration, substantially improves on the conventional flocculation, sedimentation, and filtration system in performance, capability, operation, maintenance, and energy use. The detention time of the Lenox flotation–filtration system including flocculation, flotation, filtration, and clearwell is only 15 min in comparison with the conventional system's 6–9 h of long detention time. Because of the Lenox plant's compact design (diameter = 22 ft = 6.7 m; depth = 6 ft = 1.8 m) its equipment installation cost, housing cost, heating cost, land requirement, and so on are all significantly reduced. It is important to note that the entire Lenox Water Treatment Plant including one 1.2-MGD (4542-TPD) potable flotation–filtration clarifier, three 8 ft (2.4 m) alum storage tanks, one compact water quality laboratory, one sanitary facility, and one sludge flotation thickener, is housed in a small building with dimensions of 30×60 ft^2 (9.1×18.2 m^2). The plant's building is smaller than the flocculation basin of a comparable conventional water purification plant with the same hydraulic capacity. The newly installed Lenox flotation–filtration plant (Fig. 5) includes the following unit operations for water purification: (a) chemical feeding/mixing, (b) flocculation, (c) filtration. The filter effluent is chlorinated in a pumping/chlorination station. Specific design criteria for the Lenox flotation plant are listed:

a. Flotation retention time = 5.5 mm.
b. Flotation unit loading = 3.1 gpm/ft^2 (0.13 m^3/min/m^2) or less.
c. Filter area = 335.78 ft^3 (31.19 m^2).
d. Filtration rate = 2.5 gpm/ft^2 (0.10 m^3/min/m^2) or less.
e. Filter bed depth = 11 in. (28 cm) of fine sand.
f. Filter media = ES 0.35 mm; UC 1.6.
g. Filter backwash rate = 15 gpm/ft^2 (0.61 m^3/min/m^2) or more.
h. Effluent handling = to chlorination station.

The only difference between the Lenox flotation–filtration plant (DAFF plant) and a conventional water treatment plant is the clarifiers used for separation of alum flocs (or alum-polymer flocs) from the flocculated water. The Lenox plant uses a DAF clarifier (with up to only 5.5 min of detention time) in comparison with a conventional plant using a sedimentation clarifier (with 2–4 h of detention time). Both the Lenox plant and the conventional plant use the same approved chemicals for potable water treatment, and both types of plants produce product effluents meeting the US EPA Drinking Water Standards. However, the Lenox plant substantially improves on the conventional plants in performance capability, operation, maintenance, and energy use. Several advantages of a potable flotation–filtration plant over a comparable conventional plant (consisting of chemical feeding, mixing, flocculation, sedimentation, filtration, and disinfection) are listed as follows:

a. The Lenox flotation–filtration plant can remove not only all common pollutants that a conventional system can handle, but also the tough pollutants that the conventional system cannot
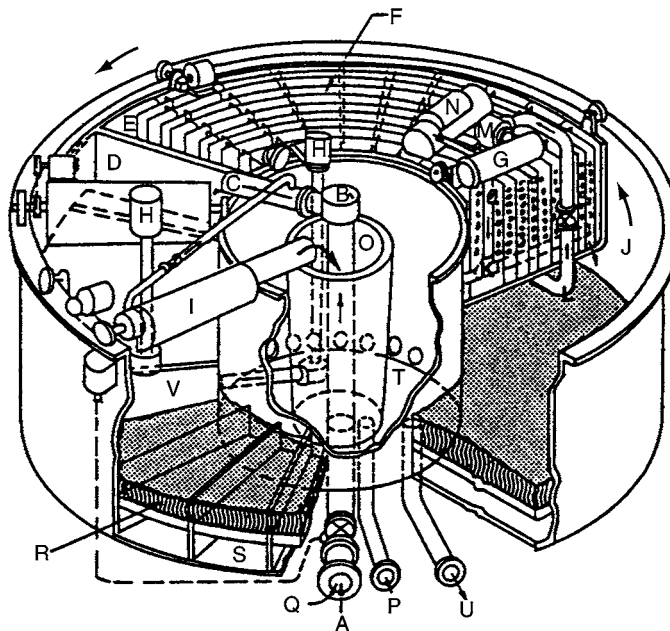
A – Raw water inlet
B – Hydraulic joint
C – Inlet distributor
D – Rapid mixing
E – Moving section
F – Static hydraulic flocculator
G – Air dissolving tube
H – Backwash pumps
I – Spiral scoop
J – Flotation tank
K – Dissolved air addition
L – Bottom carriage
M – Pressure pump
N – Air compressor
O – Center sludge collector
P – Sludge outlet
Q – Chemical addition
R – Sand filter beds
S – Individual clear wells
T – Center clear well
U – Clear effluent outlet
V – Traveling hood

Fig. 5. Bird's eye view of a package flotation–filtration clarifier.

handle, such as, VOCs, floating algae, taste and odors, O&G, surfactants, iron, manganese, and so on.

b. Adoption of static rapid mixer and static baffled flocculator at the Lenox plant significantly conserves energy use.

c. Complete automation (including flow control, level control, proportional chemical feed, and timer-controlled filter backwash) of Lenox plant significantly simplifies the plant's O&M. Only two part-time operators have been operating the plants since July, 1982.

d. The capital and total annual costs of the Lenox plant are less than one-third of comparable conventional systems with the same flow capacity.

e. The Lenox plant recycles all filter backwash wastewater to the intake section for reproduction of potable water, therefore the Lenox plant produces no wastewater, except a very small volume of highly concentrated sludge. Not only the problem of wastewater treatment is eliminated, the Lenox plant conserves about 10% of the total water pumpage, which is normally required for filter backwash in conventional water treatment plants.

f. Direct recycling of filter backwash wastewater at the Lenox flotation plant also eliminates the need of an intermediate decanting basin (or setting basin) which is required for a conventional plant to recycle its filter backwash wastewater.

g. The small Lenox plant (diameter = 22 ft = 6.7 m) can increase the influent flow rate from approx 70 gpm to >800 gpm (265 L/min to > 3028 L/min) in a few minutes, thus eliminates the need of a flow equalization tank. Continuous automatic backwash of filters eliminates the need of an elevated water storage tank required by conventional plants.

h. The Lenox plant can remove all floating algae, most of the pathogenic bacteria, and so on, thus eliminates the need for prechlorination, in turn, reduces the potential for formation of TTHM. The dosage of chlorine in postchlorination is also significantly reduced by DAF.

i. Chemical dosages of alum and polymer for potable water treatment by Lenox flotation plant are much lower than that required for a comparable conventional system. The Lenox flotation–filtration plant can be manually operated, or completely automated with the level control, which operated the inlet flow valve. Filter backwashing is also automated by time and/or head loss control. Tables 9 and 10 present the typical operational data and O&M data of the first potable flotation–filtration plant in America.

11. ONCE THE WORLD'S LARGEST POTABLE FLOTATION–FILTRATION PLANT—PITTSFIELD WATER TREATMENT PLANT, MA, USA

Because of the excellent Pittsfield pilot study results on potable flotation and excellent performance of Lenox flotation–filtration plant, the City of Pittsfield, MA, USA, has built two new potable water treatment plants: Cleveland Water Treatment Plant and Ashley Water Treatment Plant. Cleveland Plant is equipped with four flotation–filtration clarifiers (diameter = 49 ft = 14.9 m; Depth = 6 ft = 1.8 m; design capacity = 6.25 MGD = 23,656 TPD per clarifier) and treats raw Cleveland Reservoir water containing high alkalinity, moderate color, and low turbidity. Ashley Plant is equipped with two identical flotation–filtration clarifiers and treats mainly raw Farnham Reservoir water containing extremely low alkalinity, extremely high color, and moderate turbidity. Ashley Reservoir water containing sufficient alkalinity, high color, and moderate turbidity, is a supplemental source of water supply to Ashley Plant with only limited availability. Both Cleveland Plant and Ashley Plant serve the same Pittsfield water distribution system for 55,000 residents and many industrial plants. The entire Pittsfield water treatment facilities include: four major reservoirs, chemical feed equipment, six flotation–filtration clarifiers, two chlorination stations, two flow control stations and distribution pipes, one hydroelectric plant, one 5-MG (18,925 m^3) concrete water storage tank, one hydroelectric plant, one 5-MG (18,925 m^3) concrete water storage tank, one standpipe, two pumping stations, and one central/data acquisition system.

Two flotation–filtration clarifiers at Ashley Water Treatment Plant were started up for on-line service to the City of Pittsfield in October, 1986. All four flotation–filtration clarifiers at Cleveland Plant were started up on January 29, 1987 for on-line service.

Table 9
Operational Data of the First US Flotation–Filtration Clarifier
at Lenox Water Treatment Plant, MA, USA (26,27,54,55)

Parameters	Testing frequency	Data range	Data average
Clarifier influent			
Flow, gpm	365	148–760	377
Temperature (°F)	362	37–75	51.8
Turbidity (NTU)	365	0.65–7.35	1.6
pH (unit)	352	6.7–8.6	7.6
Alkalinity (mg/L, $CaCO_3$)	352	60–92	73.5
Color (unit)	4	0–15	6
Aluminum (mg/L)	4	0.01–0.08	0.06
Chemical treatment			
Alum (mg/L)	365	0–73.6	23
Polymer 8109 (mg/L)	365	0–66	25.7
Clarifier effluent			
Turbidity (NTU)	365	0.02–0.53	0.08
pH (unit)	352	6.6–8	7.05
Alkalinity (mg/L, $CaCO_3$)	353	48–86	66
Color (unit)	9	0	0
Aluminum residue (mg/L, Al)	9	0.01–0.13	0.06

Note: 1 gpm = 3.785 L/min.

Table 10
Lenox Water Treatment Plant Operation and Maintenance Cost Breakdown (26,27,54,55)

Cost data	7/19–12/31/82 166 d	7/1/86–6/19/87 354 d
Chemical cost	13.31 USD/d	50.04 USD/d
Electricity cost	43.33/d	21.23/d
Gas heat cost	3.33/d	–3.25/d
Labor cost	32.88/d	–
Overtime cost	–	13.50/d
Call time cost	–	5.10/d
Repair cost	–	1.50/d
Supply cost	–	5.14/d
Total cost:	98.85 USD/d × 166	99.76 USD/d × 354
	(16,409.10 USD)	(35,315.04 USD)
Total gallonage:	129,501,478	249,883,323[a]
Cost/1000 gal	12.67 cents	14.13 cents

[a]Note: Gallonage for 6/1–6/19/87 was estimated to be 15,500,133 gal (1 gal = 3.785 L).
Use ref. 58 to update the cost to the current year.

The top view of Cleveland Plant is similar to Ashley Plant except that Cleveland has four flotation–filtration clarifiers and is two times bigger. Pittsfield's clarifiers are also package water treatment clarifiers each consisting of chemical feeders, mixing chamber, flocculation chamber, DAF tank, ABF, and clearwell.

Cleveland raw water having sufficient alkalinity can be treated satisfactorily using alum, sodium aluminate, and polymer, at a cost of 0.02458 USD/1000 gal (3785 L) of

water treated. Ashley raw water having low alkalinity requires alkalinity supplement at a slightly higher cost. Effluent turbidity from both plants ranges 0.1–0.5 NTU under optimum operational conditions.

Pittsfield water treatment facilities including both Cleveland Plant and Ashley Plant has a peak capacity of 37.5 MGD (141,938 TPD). At the same hydraulic capacity and treatment efficiency, the capital cost of a potable flotation–filtration plant is only about one-third of comparable conventional water treatment plants. Water conservation and chemical cost saving are its added advantages. A potable flotation–filtration plant has been applicable to removal of extremely high color and turbidity (5), PAC (18), arsenic (3,4), VOCs (6,9), algae (9), odor (6), coliform bacteria (8), surfactant (9), hardness (15,16), iron and manganese (9), particle counts and *Giardia* Cysts (5), THM formation potential (5,6), and heavy metal (10). In other words, flotation–filtration plants are feasible for treatment of river water, groundwater (16), lake water (22), or storm runoff water (3,4), adequate for serving large communities (8), small communities (11,12), institutions or even single families (32). Pittsfield Water Treatment System has been faithfully serving the City of Pittsfield, MA, USA, since its startup in December, 1986. (38). The six flotation–filtration clarifiers (each clarifier 6.25 MGD = 23,656 TPD; maximum plant capacity = 37.5 MGD) passed the most stringent operating tests under severe winter conditions using only common inexpensive chemicals. Both the Lenox Water Treatment Plant and Pittsfield Water Treatment Plant are the first-generation DAFF plants, which are package process equipment, designed and built by Krofta Engineering Corporation, and the Lenox Institute of Water Technology (formerly Lenox Institute for Research). Each DAFF plant is self-contained including chemical feeding, mixing, flocculation, flotation clarification, sand filtration, disinfection, and clearwell, similar to the process diagram shown in Fig. 5.

Today there are at least 36 DAF and DAFF manufacturers in the United States alone (34). There are more than 3000 DAF and DAFF units installed around the world for both industrial and domestic applications. Olson (35) and Wang et al. (32) have reviewed various DAF and DAFF plants built in the United States. Figure 6 shows a classical DAF drinking water treatment plant which consists of separate unit processes of chemical feeding, rapid mixing, flocculation, flotation clarification, sand filtration, and disinfection (35).

12. THE LARGEST POTABLE FLOTATION–FILTRATION PLANT IN THE CONTINENT OF NORTH AMERICA—TABLE ROCK AND NORTH SALUDA WATER TREATMENT PLANT, SC, USA

DAF is generally applicable for water with light particles (e.g., algae), low-to-medium turbidity (<100 NTU; preferably <30 NTU), low alkalinity, and high color (36,37). In many cases conventional sedimentation is not very effective for these waters. The first large-scale drinking water DAF-filtration system (37.5 MGD) was built in Pittsfield, Massachusettes in 1986 (32,38). In 2005, the largest DAF water filtration plant in the United States is the 75 MGD Table Rock and North Saluda Water Treatment Plant in Greenville, South Carolina, which is shown in Fig. 6, and has been in operation since June 2000. Presently there are more than 10 full-scale DAF-filtration plants in North America (32,36,39).

Table 9 shows the design criteria and treatment performance of the Table Rock and North Saluda Water Treatment Plant. The full-scale plant performance has thus far
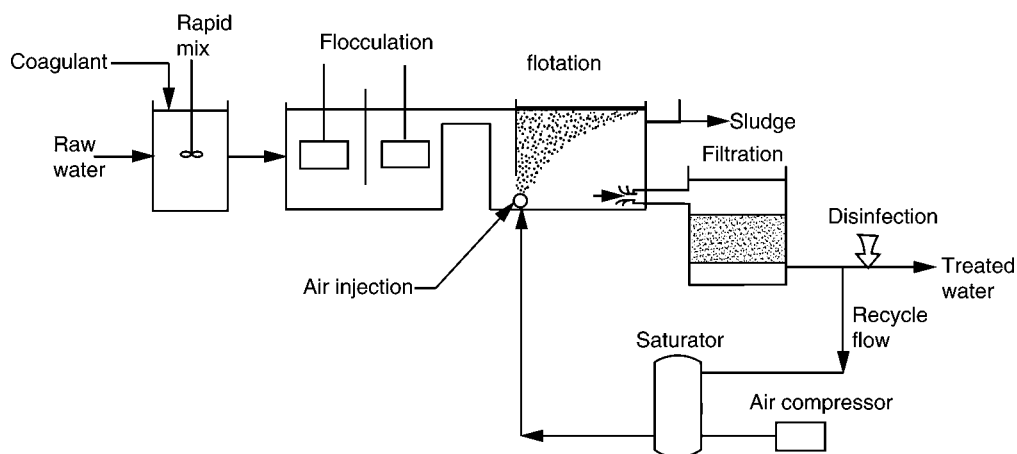
Fig. 6. Flow sheet of a classical dissolved air flotation drinking water treatment plant involving the combination of individual unit processes.

exceeded expectations (from pilot testing), providing effective removal of *Cryptosporidium* (36). On optimization the DAF effluent turbidity was consistently lower than 0.5 NTU with SLR ranging from 4 to 8 gpm/ft^2. With algae concentration in the thousands, the algae removal efficiency was >96% (36).

The advantages of DAF over conventional sedimentation include:

a. More compact because of much higher SLR.
b. More effective for removal of algae, *Giardia* and *Cryptosporidium.*
c. Stable effluent quality without polymer; (d) faster startup time (in minutes).
d. Lower coagulant dosage and flocculation time (no sweep floc required).
e. Can produce thick sludge concentration with a mechanical skimmer (2–4% solids).

The last advantage is not valid when the float is hydraulically removed from the surface of a DAF unit by flooding rather than by mechanical skimming. In this case the solids content of the float is <0.5% and further thickening may be required for subsequent dewatering. The main disadvantages of DAF are that there are more mechanical parts to maintain and the energy cost is higher because of the high pressure water recycling and air compressing. Moreover, the process is limited to relatively low turbidity water (<30–50 NTU) because of the economic recycle ratio as higher turbidity requires higher recycle ratio to be effective (not very economical when recycle ratio >10%).

13. EMERGING DAF PLANTS—AQUADAF™

A new generation of DAF can operate at SLRs of 8–18 gpm/ft^2 that is 2–3 times that of conventional DAF. The process was developed by the Rictor Company in Sweden and licensed to Ondeo Degremont in 2001. The key features of the new DAF system are the internal angled baffle wall and false floor, which create a recirculation effect throughout the DAF basin, ensuring increased bubble density and efficient flotation and removal of the solid/bubble aggregate (float). The clarified water exits the system
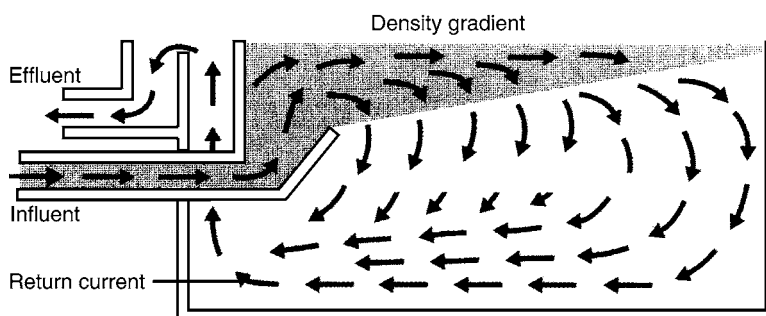
Fig. 7. Improved DAF separator works with density currents to make full use of the DAF reactor volume, improve hydraulic detention time and effectively eliminates short-circuiting.
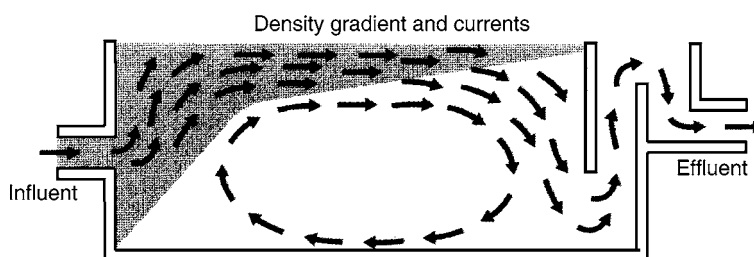
Fig. 8. Density currents developed in a conventional DAF separator lead to inefficient use of available DAF reactor volume and display a greater potential for short circuiting, especially at higher than normal hydraulic loadings.

through the false floor with patented hole-pattern and out an effluent channel as shown in the schematic diagram in Fig. 7. Figure 8 shows a comparison of simulated bubble density between the new DAF and conventional DAF at a very high SLR. The conventional DAF lost its separation performance at the very high SLR.

Although operating at a much higher SLR, the new DAF provides equivalent treatment performance as conventional DAF. The first new DAF system in North America was constructed at the existing Lake DeForest Water Treatment Plant in West Nyack, New York in 2003. The new DAF replaced the existing sedimentation basins as pretreatment to dual media filters. Figure 7 shows a picture of the new DAF basin in the Lake DeForest plant. Table 10 shows the improvements of the plant performance after installation of the 20 MGD new DAF system (40).

A 40-MGD new DAF system is being started up in Manteca, California (June 2005), as pretreatment to a submerged membrane (ZeeWeed®) system for a surface water treatment plant operated by South San Joaquin Irrigation District. The new DAF system is used to optimize the removal of TOC and turbidity with ferric coagulation to facilitate a higher flux for the membrane system. Table 11 shows a comparison of pilot plant treatment performance between plate settler and the new DAF as pretreatment for the submerged membrane system (41). The new DAF outperformed the plate settler while using a lower coagulant dosage (36,39,41).

Table 11
Design Criteria and Treatment Performance of the Table Rock
and North Saluda Water Treatment Plant, Greenville, SC, USA

Design and water quality	Criteria and record
Design Parameters	Design criteria
1. Flow	75 MGD
2. Loading rate	5 gpm/ft^2
3. Units of basins	12 concrete basins
4. Filter media	Leopold dual media
5. Filter run time	144 h (6 d)
Water quality parameters	Process performance record
1. Influent raw water turbidity	1.8 NTU
2. Influent raw water algae count	184 cells/mL
3. DAF effluent turbidity	0.2 NTU
4. DAF effluent algae count	<13 cells/mL
5. Filter effluent turbidity	0.04 NTU
6. Filter effluent algae count	None

Source: From refs. 36,39,41.

The advantages of the "new" DAF and "all other" DAF over conventional sedimentation systems are similar. The new DAF technology is relatively new in North America and it is a proprietary process. There are presently three full-scale new DAF plants in the United States and another one is in progress. As the treatment performance is proven in more full-scale plants, it is believed that the technology will become more popular in North America especially in cases in which algae is a significant raw water concern and site space is limited.

14. EMERGING FULL-SCALE ANAEROBIC BIOLOGICAL FLOTATION—KASSEL, GERMANY

Wang developed the anaerobic biological flotation process in 1974 (42), and pilot studied the process with colleagues at the Lenox Institute of Water Technology (LIWT) and Krofta Engineering Corporation (KEC) in 1981 (9,32,43). Recently LIWT/KEC designed and installed a full-scale 15-ft diameter anaerobic biological flotation clarifier at a paper mill in Germany (44). It was a total success. Because the anaerobic biological flotation was developed by Wang more than 30 yr ago (42), based on anaerobic process reactions for generation of anaerobic gas bubbles, the process is no longer a novelty and therefore not patentable or protected by any valid patents. The author urges the flotation engineers to take advantage of this new process development and to offer solution to similar environmental problems. This section introduces the case history and some operational data. The most common process for anaerobic treatment of municipal primary and secondary sludge is anaerobic digestion, which requires a long retention time of 20–30 d. A number of paper mills in Germany, indeed, treat their high strength wastes by anaerobic digestion process. Anaerobic process may reduce high concentration of dissolved organic matter (BOD$_5$ and COD) in small reactors. The excess sludge generation rate of anaerobic treatment is 10 times lower than that of aerobic treatment. Besides, anaerobic treatment process will deliver biogas as an energy source. Specifically a paper
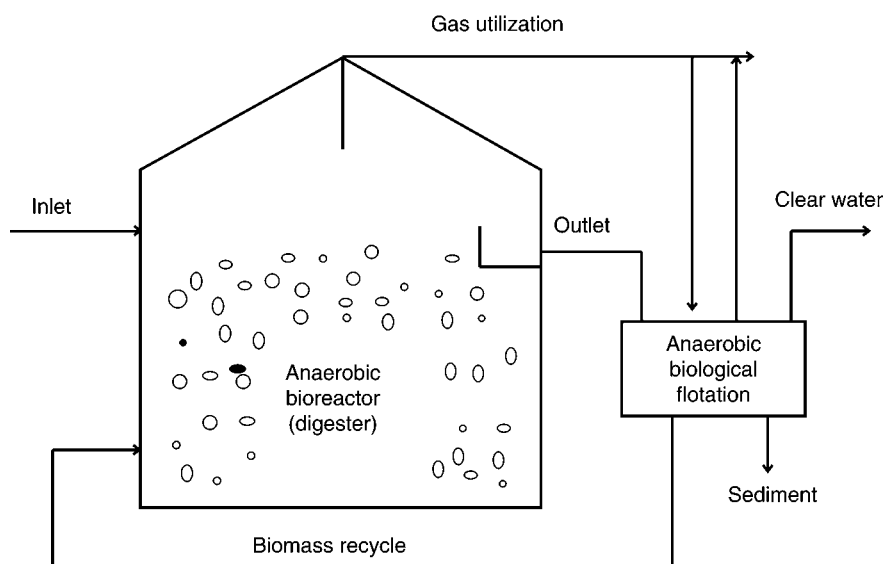
Fig. 9. Flow sheet of an anaerobic digester using an anaerobic biological flotation for harvesting the biomass.

mill near Kassel, Germany had two anaerobic digestors, each with 3000-m^3 reactor volume. The paper mill had an operational problem of loosing the biomass because of inefficient sedimentation clarification following the anaerobic digester. The effluent sludge from the anaerobic digester was full of anaerobically produced gases, such as carbon dioxide, nitrogen, methane, hydrogen sulfide, and so on, in turn, contained gas bubbles, causing the sludge to float. The plant was designed for a COD removal capacity of 14,000 kg/d. In the presence of rising sludge in the existing sedimentation tanks, the performance of sedimentation was poor. The paper mill removed only 2800 kg/d of COD from its raw waste. The COD concentration in the circulated water loop feeding the paper machine increased to 30,000 mg/L and higher, resulting in poor paper quality (i.e., low paper strength and odor of the finished product). It was proposed to take advantage of this "biological flotation" by using a modified commercial flotation clarifier (known as Krofta SUPRACELL™, with 15-ft diameter) with a roof or cover, shown in Figs. 9 and 10.

It was found that by using a modified flotation clarifier, it is possible to float/harvest the anaerobic biomass and returns it to the anaerobic bioreactor. Only very small amount of heavy, inorganic components were removed via the sediment sump (Fig. 10). The biogas, which is consist of about 60% methane, 39% carbon dioxide, and 1% hydrogen sulfide, generated by the anaerobic microorganisms was used in the place of dissolved air in a modified gas dissolving tube (GDT) to ensure that active microorganisms would remain (46). The highlights of the anaerobic biological flotation process reactor are:

a. It is covered airtight unit with water seal.
b. It is explosion proof equipment.
c. The pressure inside the anaerobic biological process reactor is maintained to be positive at 12 mb greater than external pressure, to ensure no oxygen entering the reactor.
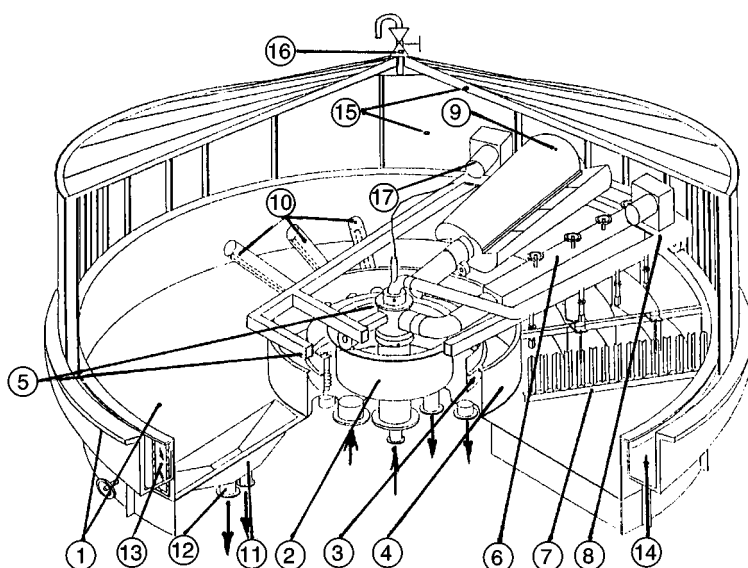
Anaerobic biological flotation with roof

1 = Tank; 2 = Sludge well; 3 = Over flow weir; 4 = Rotating center part;
5 = Electric and hydraulic rotary joint; 6 = Inlet; 7 = Rake mechanism;   8 = Frame;
9 = Spiral scoop; 10 = Clear water outlet; 11 = Sediment sump; 12 = Sediment outlet;
13 = Viewing window; 14 = Water seal; 15 = Cover/roof; 16 = Pressure release valve;
17 = Electric power supply.

Fig. 10. An anaerobic biological flotation reactor with an enclosure on top.

After 6 mo of successful operation, the ash content in the digestor was improved. The specific gas production rate increased from 0.2 mL/g dry matter/h to 2.2 mL gas/g dry matter/h. With this application of anaerobic biological flotation, effective anaerobic treatment by the microorganism in the floated sludge was ensured. This application of anaerobic flotation reduced biomass loss and increased the COD removal efficiency. It is concluded that anaerobic biological flotation has been very effective in separating active and inactive solids in the anaerobic reactor.

15. EMERGING DISSOLVED GAS FLOTATION AND SEQUENCING BATCH REACTOR (DGF–SBR)

Wang, Kurylko, and Wang (45) and their colleagues (46,47) developed DGF–SBR. The process reactor is similar to conventional biological SBR. Except that DGF–SBR uses flotation instead of sedimentation for clarification. DGF–SBR can be a biological process in the presence of microorganisms (either aerobic or anaerobic, or anoxic), or a physicochemical process in the presence of chemicals (coagulants, carbons, ion-exchange resins, and so on), or a combined biological–physicochemical process. Any kind of gases, such as air, nitrogen, anaerobic gases, carbon dioxide, ozone, can be used in DGF–SBR for facilitating the process reactions (46). Because the DGF–SBR process is self-explanatory, the readers are referred to the literature (32,45–48) for the detailed case histories, and the full scale operational experience in Europe.
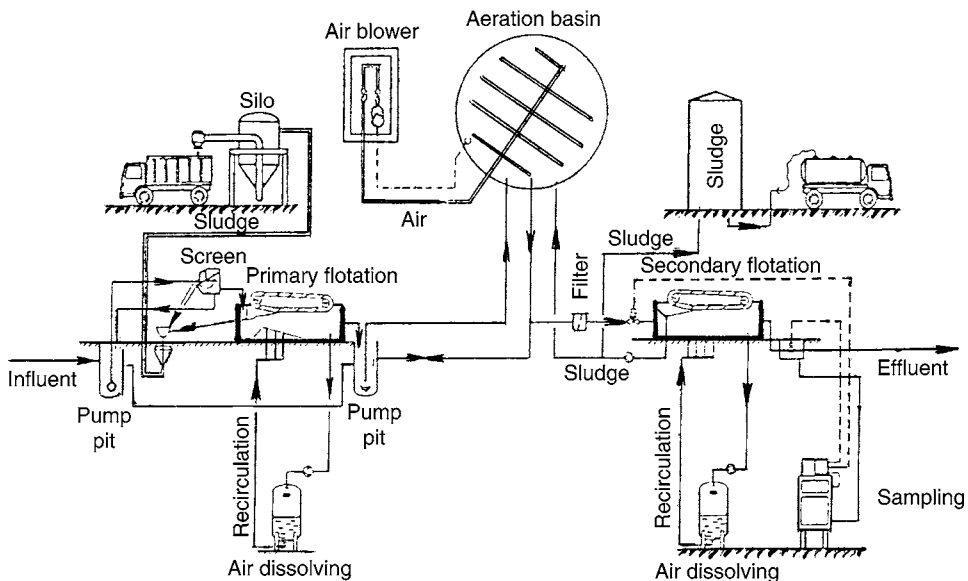
Fig. 11. A flotation activated sludge system involving the use of both primary flotation clarification and secondary flotation clarification for treating dairy effluent.

16. APPLICATION OF COMBINED PRIMARY FLOTATION CLARIFICATION AND SECONDARY FLOTATION CLARIFICATION FOR TREATMENT OF DAIRY EFFLUENTS—A UK CASE HISTORY

Wang, Fahey, and Wu (32) have shown that primary flotation clarification and/or secondary flotation clarification can be successfully used in most of the biological treatment systems (such as activated sludge, rotating biological contactor, trickling filter, lagoon, biological fluidized beds, and so on). When primary flotation and/or secondary flotation are/is used in conjunction with a biological process system, the process name will be slightly changed, such as, flotation activated sludge process, flotation rotating biological contactor, flotation trickling filter, flotation lagoon, flotation biological fluidized beds, and so on (49).

Figure 11 shows a typical, successful flotation activated sludge plant used in the United Kingdom for treating the effluents from dairies (50). The design engineering firm was Stork Engineering, Uxbridge, Middlesex, UK. The advantages offered by Stork Engineering concerning the flotation activated sludge system include:

a. Space saving.
b. Lower volume plant to be housed.
c. High mixing efficiency.
d. Lower sludge volume.
e. Effective water–solids separation.
f. Excellent odor control.
g. More flexible and controllable process.
h. Efficient aeration treatment.
i. High BOD_5/COD reduction.
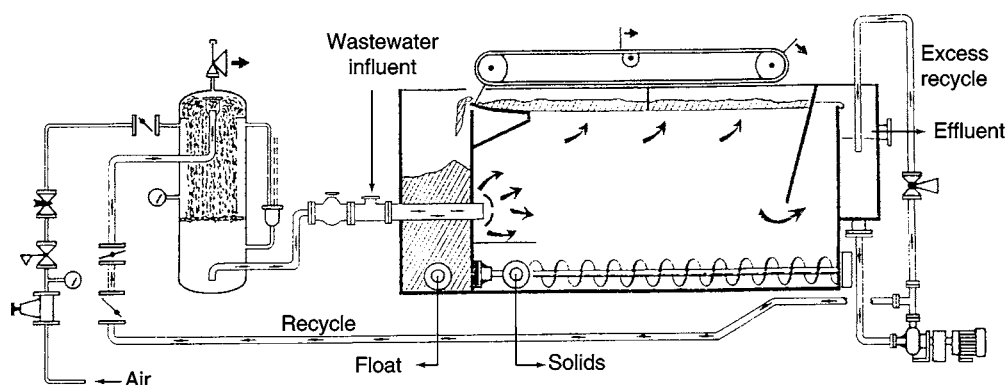
Fig. 12. A rectangular dissolved air flotation clarifier.

It is the author's reminder while Stork Engineering's system is highly efficient for treatment of dairy effluent, any manufacturer's DAF can be used for primary flotation clarification and/or secondary flotation clarification. Figure 12 shows a typical conventional DAF, manufactured by Waterlink Company, Addison, IL.

17. RECENT DAF DEVELOPMENTS

Yeh (51,52) has developed an advanced plug DAF clarifier. Yeh's DAF has been used successfully at a US multiple-oilseeds processing plant in West Fargo, ND, for more than 12 yr. Regulatory compliance management at Marburger Foods Inc., Peru, IN, elected to switch from a lagoon wastewater treatment system to a DAF clarification technology for the company's precooked bacon processing operation (53). As a result, Marburger Foods is able to salvage fat which primarily is sold for livestock and pet food. In addition, the company has ensured continued municipal discharge compliance for a projected wastewater flow increase. Calculations for a projected wastewater flow of 60,000 gal/d over the next 3-yr period indicated that expansion was necessary for continued regulatory compliance. However, there was no room on the property for lagoon expansion. Marburger Foods' customized National Pollutant Discharge Elimination System (NPDES) permit for municipal discharge, developed by the Indiana Department of Environmental Management in consultation with Peru, calls for a pH ranging from 6.5 to 8.5, a TSS limit of 250 mg/L, a carbonaceous BOD limit of 200 mg/L and an O&G limit of 100 mg/L. The new wastewater treatment system includes three DAF clarifiers manufactured by Precision Environmental Systems, Springfield, MO. Two units for the first stage of pretreatment began operation in mid-1996. A special unit for second-stage pretreatment, including a flocculation tube has served the company successfully since its startup in late 1997.

DAF is one of the best processes for removal of algae, TTHM precursors, coliform bacteria, iron, and manganese (54–55). Marvin has reported (56) that the Evitts Creek Water Treatment Plant in WV, USA, converts its 12-MGD plant from a conventional plant to a DAF plant with a great success. The performance of the old, conventional upflow clarification unit compared to the new DAF process at the Evitts Creek Water

Table 12
Plant Operational Improvements After AquaDAF Installation

Parameter	Before installation	After installation
Filter run time (h)	<24	80
Algae removal efficiency (%)	40–60	70–90
Filter loading rate (gpm/ft^2)	2	4
Filter effluent turbidity during algal bloom (NTU)	0.15–0.3	0.15

Source: From refs. 36,39,41.

Table 13
Comparison of Pilot Performance Between Plate Settler and AquaDAF

Parameter	Plate settler	AquaDAF
FeCl$_3$ dosage (mg/L)	15	10
HLR (gpm/ft^2)	0.65	14
Effluent turbidity (NTU)	1–2	0.5
TOC removal (%)	18	>30

Source: From refs. 36,39,41,58.

Table 14
The Performance of the Old Upflow Clarification Unit Compared to the New DAF Process at Evitts Creek Treatment Plant, Cumberland, MD, USA

Parameter	Upflow unit	DAF
Raw water turbidity (NTU)	2–5	2–5
Raw water manganese (mg/L)	0.1–0.17	0.1–0.17
Clarified turbidity (NTU)	1	0.2
Clarified manganese (mg/L)	0.05	0.02
Filter run length (h)	24	72
Filter effluent turbidity (NTU)	0.1	0.04
Filter effluent manganese (mg/L)	0.05	0.02

Source: From refs. 56 and 58.

Treatment Plant is presented in Table 12. Not only algae, turbidity, manganese are successfully removed, but also the filter run time is increased from 24 to 72 h after DAF installation (Tables 13 and 14). The Evitts Creek Water Treatment Plant is similar to the flow diagram shown in Fig. 6.

REFERENCES

1. L. K. Wang and M. H. S. Wang, Bubble dynamics and air dispersion mechanisms of air flotation process systems, Part A: material balances. *Proceedings of the 44th Industrial Waste Conference*, Purdue University, West Lafayette, IN, 505–515, 1989.
2. M. Krofta and L. K. Wang, Bubble dynamics and air dispersion mechanisms of air flotation process systems, Part B: air dispersion. *Proceedings of the 44th Industrial Waste Conference*, Purdue University, West Lafayette, IN, 516–526, 1989.

3. L. K. Wang and W. J. Mahoney, Treatment of storm run-off by oil-water separation, flotation, filtration and adsorption, Part A: wastewater treatment. *Proceedings of the 44th Industrial Waste Conference,* Purdue University, West Lafayette, IN, 655–666, 1989.

4. L. K. Wang, M. H. S. Wang, and W. J. Mahoney, Treatment of storm run-off by oil-water separation, flotation, filtration and adsorption, Part B: waste sludge management. *Proceedings of the 44th Industrial Waste Conference*, Purdue University, West Lafayette, IN, 667–673, 1989.

5. L. K. Wang, *Using Air Flotation and Filtration in Removal of Color, Trihalomethane Precursors and Giardia Cysts*, New York State Department of Health Workshop on Water Treatment Chemicals and Filtration, Ramada Inn, Saratoga Springs, NY, May, 1989. The 1989 American Slow Sand Association Annual Meeting, Thatcher State Park Regional Maintenance Center, NY, October 20, 1989.

6. L. K. Wang and M. H. S. Wang, *Reduction of Color, Odor, Humic Acid and Toxic Substances by Adsorption, Flotation and Filtration*. The 1989 Annual Summer Meeting of American Institute of Chemical Engineers, Symposium on Design of Adsorption Systems for Pollution Control, Wyndham Franklin Plaza Hotel, Philadelphia, PA, August 19–23, 1989.

7. M. Krofta, L. K. Wang, D. B. Aulenbach, and J. P. Van Dyke, *Treatment of Rotating Biological Contactor Effluent by Dissolved Air Flotation.* The Annual Meeting of Engineering Foundation. Symposium on Advances in Coal and Mineral Processing Using Flotation, Sheration Palm Coast Resort, Palm Coast, FL, December 3–8, p. 23, 1989.

8. L. K. Wang and W. L. Forestell, *Air Flotation & Sand Filtration: Pittsfield, Massachusetts*. New England Water Works Associations Annual Conference, September 1990. LeChateau Frontenac, Quebec City, Quebec, Canada.

9. L. K. Wang, *Theory and Applications of Flotation Processes*. US Dept of Commerce, National Technical Information Service, Springfield, VA. Report No. PB-86-1941 98/AS, p. 15, November, 1985.

10. M. Krofta, L. K. Wang, and C. D. Pollman, Treatment of seafood processing wastewater by dissolved air flotation, carbon adsorption and free chlorination. *Proceedings of the 43rd Industrial Waste Conference*, Purdue University, West Lafayette, IN, May, pp. 535–550, 1988.

11. M. Krofta and L. K. Wang, *First Full-Scale Flotation Plant in USA for Potable Water Treatment*, US Dept. of Commerce, National Technical Information Service, Springfield, VA, Report No. PB82-220690, March, p. 67, 1982.

12. M. Krorta and L. K. Wang, *Water Treatment Systems Appropriate and Affordable for Smaller Communities*, US Dept. of Commerce, National Technical Information Service, Springfield, VA, Report No. PB82-201 476, March, p. 30, 1982.

13. M. Krofta and L. K. Wang, *Design. Construction and Operation of Lenox Water Treatment Plant—Project Summary,* US Dept. of Commerce, National Technical Information Service, Springfield, VA, Report No. PB93-1 71264, January, p. 40, 1983.

14. M. Krofta and L. K. Wang, *Design, Construction and Operation of Lenox Water Treatment Plant—Project Documentation*, US Dept. of Commerce, National Technical Information Service, Springfield, VA, Report No. PB83-1 64731, January, p. 330, 1983.

15. L. K. Wang and B. C. Wu, *Water Treatment by Dissolved Air Flotation Using Magnesium Carbonate as Coagulant*, US Dept. of Commerce, National Technical Information Service, Springfield, VA, Report No. PB82-21 1400, April, pp. 25–29, 1982.

16. L. K. Wang and B. C. Wu, *Treatment of Groundwater by Dissolved Air Flotation System Using Sodium Aluminate and Lime as Flotation Aids*, US Dept of Commerce, National Technical Information Service, Springfield, VA, Report No. PB82-21 1400, April, pp. 31–34, 1982.

17. L. K. Wang, O. Barns, P. Milne, B. C. Wu, and J. Hollen, *Removal of Trihalomethane Precursor by Flotation and Filtration*, US Dept of Commerce, National Technical Information Service, Springfield, VA, Report No. PB82-21 1400, April, pp. 22–24, 1982.

18. M. Krofta and L. K. Wang. Total closing of paper mills with reclamation and deinking installations. *Proceedings of the 43rd Industrial Waste Conference*, Purdue University, West Lafayette, IN, May, pp. 673–688, 1988.

19. D. Rogers, Deep aeration & flotation clarification adds a new treatment dimension, *Industrial Wastes*, February, pp. 10–17, 1983.

20. J. R. Bratby, Treatment of raw wastewater overflow by dissolved air flotation, *J. Water Pollut Control Federation*, **54**(12), 1558–1565 (1982).

21. M. Krofta, D. Guss, and L. K. Wang, Improved biological treatment with a secondary flotation clarifier, *Civil Eng. Practicing Design Eng.* **2**, 307–324 (1983).

22. M. Krofta and L. K. Wang, Potable water treatment by dissolved air flotation and filtration, *J. Am. Water Works Assoc.* **74**(6), 304–310 (1982).

23. L. K. Wang, Compact nitrogen removal options for Lake Como, Italy, *Effluent and Water Treatment J.* **22**(11), 435–437, 1982 (England).

24. M. Krofta and L. K. Wang, Tertiary treatment of secondary effluent by dissolved air flotation and filtration. *Civil Eng. Practicing Design Eng.* **3**, 253–272 (1984).

25. M. Krofta and L. K. Wang, Treatment of cooling tower water by dissolved air-ozone flotation, *Proceedings of the Seventh Mid-Atlantic Industrial Waste Conference*, June, 207–216, 1985.

26. M. Krofta and L. K. Wang, Application of dissolved air flotation to the Lenox Massachusetts Water Supply: water purification by flotation. *J. New England Water Works Assoc.* 249–264 (1985).

27. M. Krofta and L. K. Wang, Application of dissolved air flotation to the Lenox Massachusetts Water Supply: sludge thickening by flotation or lagoon. *J. New England Water Works Assoc.* 265–284 (1985).

28. M. Krofta and L. K. Wang, Wastewater treatment by biological-physicochemical two-stage process system. *Proceedings of the 41st Industrial Waste Conference*, Purdue University, West Lafayette, IN, May, pp. 67–72, 1986.

29. M. Krofta and L. K. Wang, Flotation technology and secondary clarification, *Technical Assoc. Pulp Pap. Indus. J.* **70**(4), 92–96 (1987).

30. M. Krofta, D. Guss, and L. K. Wang, Development of low-cost flotation technology and systems for wastewater treatment. *Proceedings of the 42nd Industrial Waste Conference*. Purdue University, West Lafayette, IN, May, 185–190, PA 1987.

31. L. K. Wang, *Treatment of Textile Mill Wastewater by Conventional and Innovative Process Systems*. Zorex Corporation, Newtonville, NY, Technical Report No. 29103-01-91-93, January, 1991.

32. L. K. Wang, E. M. Fahey, and Z. Wu. Dissolved air flotation. In: *Physicochemical Treatment Processes.* Humana Press, Totowa, NJ, 431–500 (2005).

33. US EPA, *Screening/Flotation Treatment of Combined Sewer Overflows*. US Environmental Protection Agency, Washington, DC, Contract 14-12-40, Project 11020FDC, January, 1972.

34. WEF, *Wastewater Technology Buyers Guide–1999-2000*. Water Environment Federation, Alexandria, VA, 1999.

35. S. Olson, Dissolved air flotation, new applications in potable water treatment. *J. New England Water Works Assoc.* 133–151 (1989).

36. J. M. Wong and F. Y. Chang, *Application of High-Rate Clarification Processes to Optimize Drinking Water Treatment*, presented at CA-NV Section, AWWA Fall Conference, San Diego, CA, October 6–9, 2003.

37. J. Edzwald, Principles and applications of dissolved air flotation. *Water Sci. Technol.* **31**(3–4), 1–23 (1995).

38. L. K. Wang, Design and specifications of Pittsfield Water Treatment System consisting of air flotation and sand filtration, *Water Treatment*, **6**, 127–146 (1991).

39. J. M. Wong, W. Faisst, J. Belleci, and V. Darone, *Treating Delta Water Economically with Super High-Rate Clarification and High-Rate Filtration,* presented at CA-NV Section, AWWA Fall Conference, San Diego, CA, October 26–29, 1999.

40. A. J. Capuzzi, R. Raczko, D. Distante, S. Master, and R. Ofeldt, *The First High Rate DAF in The US*, presented at New Jersey Section, AWWA Annual Conference, Atlantic City, NJ, March, 2005.

41. J. M. Wong and J. A. Enson, *Pilot Testing for The Largest Membrane Water Treatment Plant in California,* presented at CA-NV section, AWWA Spring Conference, Las Vegas, CA, April 13–16, 2004.

42. L. K. Wang, Flotation and bubble separation technologies. *Earth Environ. Resour. Conf. Digest of Technical Pap.* **1**(74), 56–57 (1974).

43. M. Krofta and L. K. Wang, *Flotation and Related Adsorptive Bubble Separation Processes*. Lenox Institute of Water Technology, Lenox, MA, Technical Report No. Lenox7-25-1999/348. 1st (ed.) 1981, 4th (ed.), 1999.

44. M. Krofta, and L. K. Wang. *Flotation Engineering*, 1st Edition. Lenox Institute of Water Technology, Lenox, MA, Technical Manual No. Lenox/1-06-2000/368, January, 2000.

45. L. K. Wang, L. Kurylko, and M. H. S. Wang. *Sequencing Batch Liquid Treatment*. US Patent No. 5354458, US Patent and Trade Marks Office, Washington, DC, 1996.

46. L. K. Wang, *Gas Dissolving System and Method*, US Patent No. 5049320, US Patent and Trade Marks Office, Washington, DC, 1991.

47. L. K. Wang, P. Wang, and N. L. Clesceri. Groundwater decontamination using sequencing batch processes. *Water Treatment*, **10**, 121–134 (1995).

48. L. K. Wang, and Y. Li, Sequencing batch reactors. In: *Biological Treatment Processes*. L. K. Wang, N. C. Pereira, and Y. T. Hung (eds.), Humana Press, Totowa, NJ (2007).

49. L. K. Wang, N. K. Shammas, and D. B. Guss. Flotation biological systems. In: *Environmental Biotechnology*. L. K. Wang, J. H. Tay, V. Ivanov, and Y. T. Hung (eds.), Humana Press, Totowa, NJ (2007).

50. Stork Engineering, Treatment of effluent from dairies. *Filtr. Sep.* p. 847, Dec. (1995).

51. G. C. Yeh, Advancing the science of dissolved air flotation. *Environmental Technology*, **6**(6), 26–30, December, 1996.

52. G. C. Yeh, Advanced plug flow dissolved air flotation. *Indus. Wastewater* 30–33, Jan. (1999).

53. Pollution Engineering Editor, Food processor reaps benefits of DAF clarification. *Pollut. Eng.* **32**(4), 53–54, April, 2000.

54. L. K. Wang, and P. J. Kolodziej, *Removal of Trihalomethane Precursors and Coliform Bacteria by Lenox Flotation–Filtration Plant.* US Department of Commerce, National Technical Information Service, Springfield, VA, Technical Report No. PB83-244053, 1983. Proceeding of the Water Quality and the Public Health Conference, Worcester Polytechnic Institute, MA, 17–29, May, 1983.

55. L. K. Wang, M. H. S. Wang, and P. J. Kolodziej, Innovative and cost-effective Lenox Water Purification Plant. *Water Treatment* **7**, 387–406 (1992).

56. R. Marvin, DAF removes algae, eases manganese issues. *Opflow*, **31**(2), 10–12 (2005).

57. L. K. Wang, N. K. Shammas, and Y. T. Hung (eds.) *Biosolids Treatment Processes*. Humana Press, Totowa, NJ (2007).

58. US ACE, *Cost Index Systems Manual*. US Army Corps of Engineers, Washington, DC, manual no. 1110-2-1304, http://www.nww.usace.army.mil/cost.2006.

Endocrine Disruptors

Properties, Effects, and Removal Processes

Nazih K. Shammas

Contents

1. INTRODUCTION

Endocrine disrupting compounds (EDCs) are defined as "chemicals that either mimic endogenous hormones, interfere with pharmacokinetics, or act by other mechanisms" (1). Adverse effects such as compromised reproductive fitness, functional or morphological birth defects, cancer, and altered immune functions, among others have been reported in the scientific literature (1–3). The term "endocrine disruptors" is used to describe substances that are not produced in the body but act by mimicking or antagonizing natural hormones. It is thought that EDCs may be responsible for some reproductive problems in both women and men as well as for the increases in the frequency of certain types of cancer. EDCs have also been linked to developmental deficiencies and learning disabilities in children. Because hormone receptor systems are similar in humans and animals, effects observed in wildlife species raise concerns of potential human health effects. During fetal development and early childhood, low-dose exposure to EDCs may have profound effects not observed in adults, such as reduced mental capacity and genital malformations. Evaluating potential low-dose effects of environmental estrogenic compounds has been identified as a major research priority.

There is growing evidence that artificial chemicals in the environment can disrupt hormones by sending erroneous signals or blocking legitimate signals. Because the hormones are part of the endocrine system, the hormone disruptors are also called endocrine

disruptors. Because the concern originated with estrogen, the "female" hormone, they are sometimes called estrogen mimics.

The strongest evidence that endocrine disruptors are damaging human or animal health comes from the animal kingdom. In the 1980s and 1990s, fish and beluga whales with horrible malformations showed up in the Great Lakes region, with cancers, ulcers, and other deformations. In the 1990s, an epidemic of misshapen reproductive organs in Florida alligators was blamed on a pesticide spill into the lake. Other reproductive abnormalities in gulls, minks, eagles, and other animals have been blamed on chemicals that mimic hormones. Furthermore, in the laboratory, tiny concentrations of hormone mimics lock onto cell receptors, causing the cells to reproduce in a phenomenon suspiciously like cancer. The controversy about endocrine disrupters began with concern about chemicals that disrupt estrogen, but now it has expanded to cover chemicals that interfere with androgens (male hormones). Keeping in mind that males have female hormones, and vice versa, it is immediately realized that the endocrine story is much more complicated than once thought.

Several studies have found a worldwide lowering of sperm counts, and blamed it on the rising concentrations of estrogen mimics in the environment. Some scientists say estrogen mimics could also explain the growing incidence of breast cancer and perhaps prostate cancer as well (4–6). The putative endocrine disruptors have structures akin to real hormones, and seem to include: breakdown products of several pesticides that are now banned, such as DDT, polychlorinated biphenyls (PCBs), a persistent group of chemicals still found in electrical equipment that pollutes lake and stream sediments in many industrial regions, dioxins, a group of toxic chemical byproducts from paper production and incineration, and chemicals found in the epoxy lining of "tin" cans, plastics used for storing food, dental sealants, and vinclozolin, a fungicide used on fruit.

A growing body of scientific research indicates that man-made industrial chemicals and pesticides may interfere with the normal functioning of human and wildlife endocrine systems. A hormone is defined as any substance in the body that is produced by one organ and then carried by the bloodstream to have an effect on another organ. The primary function of hormones, or the endocrine system, is to maintain a stable environment within the body; this is often referred to as homeostasis. The endocrine system also controls reproduction and growth.

Recently, public concern has focused on the possible hormonal effects of some environmental pollutants on wildlife and humans. These chemicals, referred to collectively as endocrine disruptors, include a wide range of substances, such as pesticides (methoxychlor), surfactants (nonylphenol), plasticizers (diethylphthalate), and organohalogens (PCBs and dioxin). Many industrial chemicals and pesticides have undergone extensive toxicological testing; however, since the purpose of this testing was not to find some subtle endocrine effects, these potential effects may not have been revealed. The persistence of some pesticides in the aquatic environment may pose a threat to the human population, especially, if such substances occur in the nation's drinking water sources. As a result of this growing concern, the 1996 Safe Drinking Water Act (SDWA) amendments and the Food Quality Protection Act require the United States Environmental Protection Agency (US EPA) to develop a screening and

testing program to determine which chemical substances have possible endocrine disrupting effects in humans (7).

Many of the potential EDCs may be present in surface water or groundwater. A number of drinking water treatment processes are available and may be used to remove many of the potential EDCs. This chapter presents treatment processes for large municipalities as well as small communities to remove specific EDCs from drinking water.

2. ENDOCRINE SYSTEM AND ENDOCRINE DISRUPTORS

2.1. The Endocrine System

The endocrine system consists of glands, hormones, and receptors. Endocrine glands include the hypothalamus, pineal, pituitary, thyroid, parathyroid, thymus, adrenal, ovaries, prostate, and testes (8). The pituitary gland acts as the control center, informing the other glands when to send their signals and how much hormones to send. The pituitary gets its cues from the hypothalamus, which acts as a regulator, informing the pituitary to increase hormone production or to slow it down and shut it off. These messages travel back and forth continuously throughout all parts of an organism, keeping everything balanced and coordinated.

The glands produce hormones, such as adrenocorticotropic hormone, corticosteroid, adrenaline, estrogen, testosterone, androgen, insulin, triiodothyronine, and thyroxin. Hormones are involved in just about every biological function. They are better known as the body's chemical messengers because they travel through the bloodstream and cause responses in other parts of the body. The amount of hormone that an animal's body produces depends on the stimuli that its body receives. They also can work at astonishingly low concentrations—in parts per billion or even trillion. Hormones regulate (8):

1. Reproduction and embryo development.
2. Growth and maturation.
3. Energy production, use, and storage.
4. Electrolytes—the balance and maintenance of water and salt.
5. Reaction to stimuli, such as fright and excitement.
6. Behavior of human beings and animals.

Receptors, which are in the cells of various target organs and tissues, recognize and respond to the hormones. Receptors are part of a complex biological feedback system that regulates the response. Any disruption to the balance can cause changes in these reactions.

2.2. Endocrine Disruptors

Endocrine disruptors are synthetic or naturally occurring chemicals that interfere with the balance of normal hormone functions in animals, including humans. This imbalance can cause various abnormalities of the reproductive system, such as the feminization of males and the masculinization of females. Among other abnormalities, they can also cause enlargement of the thyroid gland, birth defects, behavioral changes, depressed immune systems, and an increased vulnerability to disease. An endocrine disrupting chemical can affect the endocrine system of an organism in a number of ways,

but they typically affect animals in three specific ways. They can mimic, block, or trigger a hormone response (8).

2.2.1. Mimic Chemicals

Mimic chemicals respond like normal hormones inside the body. A good example of a mimicking endocrine disruptor is the potent drug diethylstilbestrol (DES), a synthetic estrogen. Prior to DES being banned in the early 1970s, doctors prescribed DES to as many as 5 million pregnant women to block spontaneous abortion. When doctors first began prescribing DES, they believed that it would prevent miscarriage and promote fetal growth. However, researchers discovered that after the children went through puberty, DES affected the development of the reproductive system of the daughters of the mothers given DES and, it caused vaginal cancer. In addition, these women are at an increased risk of developing endometriosis. Sons born to mothers given DES are at an increased frequency of undescended testes (cryptorchidism), congenital birth defects, hypospadias (urethra opening on the underside of the penis), and decreased adult sperm count.

2.2.2. Blocker Chemicals

The second group of disrupting chemicals is hormone blockers. These interfere with naturally occurring hormones function. Blockers bind to the same protein receptors as the real hormone but do not stimulate any action. They sit in the way of the natural hormone and prevent it from sending its message. An example of a blocker is how DDE (a metabolic breakdown product of the pesticide DDT) blocked action of testosterone in male alligators in Lake Apopka, Florida, which led to undersized penises. Testosterone, a male hormone, is needed for proper reproductive development.

2.2.3. Trigger Chemicals

Triggers are the third category of disruptors. They attach to protein receptors, and then trigger an abnormal response in the cell. These triggers cause growth at the wrong time, an alteration of metabolism or synthesis of a different product. The best-known triggers are dioxin and dioxin-like chemicals. Dioxin acts through a hormone-like process to initiate entirely new responses.

3. DESCRIPTIONS OF SPECIFIC EDCs

In this section, the potential EDCs are grouped by chemical class (*see* Table 1). Descriptions of the EDCs provide a brief description of the chemical, its major uses, the major human exposure routes, health effects, water solubility, environmental persistence, occurrence/detection in water sources, drinking water standards, and statutes that regulate the substance in water. The best available technology (BAT), as determined by laboratory testing for removal of specific EDCs from water is indicated when this has been determined.

3.1. Pesticide Residues

A number of pesticides have been implicated as endocrine disruptors, primarily in aquatic and wildlife species. Agricultural runoff is responsible for the presence of most pesticides found in surface waters. The pesticide concentrations in surface waters tends to be highest after the first storm following application. Pesticides may also enter source water from accidental spills, in wastewater discharges, or as runoff

Table 1
Environmental Endocrine Disruptors

Chemical	Group	Source
Polychlorinated dioxins, polychlorinated biphenyls	Polychlorinated compounds	Incineration, landfill and industrial production
DDT, dieldrin, lindane	Organochlorine pesticides	Agricultural runoff and atmospheric transport
Atrazine, trifluralin, permethrin	Pesticides	Agricultural runoff
Tributyltin	Organotins	Harbors (from antifoulants used to paint the hulls of ships)
Nonylphenol	Alkylphenols	Surfactants found in industrial and municipal effluents
Dibutyl phthalate, butylbenzyl phthalate	Phthalates	Plasticizers found in industrial effluents
Estradiol, estrone and testosterone; ethynyl estradiol	Natural hormones and synthetic steroids	Municipal effluents and agricultural runoff
Isoflavones, lignans, coumestans	Phytoestrogens	Plant material found in pulp mill effluents

Adapted from ref. 8.

from urban and suburban areas. Because pesticides are known to be potentially highly toxic compounds, the maximum contaminant level (MCL) has been established for each of these substances. These limits were originally established on the basis of known toxicological effects; however, in future, the MCLs may be set at even lower concentrations if adverse endocrine effects are detected because of their presence (9). Again, this chapter does not infer that the reader is obligated to attain an MCL; rather this information is presented to demonstrate how future research on EDCs may eventually impact some MCLs.

3.1.1. DDT

DDT is an organochlorine insecticide used mainly to control mosquito-borne malaria. It is the common name of the technical product that is a mixture of three isomers of DDT and contains 65–80% *p, p′*-DDT. It is very soluble in fats and most organic solvents and practically insoluble in water. In the United States, DDT is currently used only for public health emergencies as an insecticide under Public Health Service supervision and by the US Department of Agriculture or military for health quarantine. US EPA banned the use of DDT in food in 1972 and in nonfoods in 1988 (9). At present no US companies are producing DDT. The primary supporting evidence for adverse health effects in humans comes from an epidemiological study performed by Rogan in North Carolina (10), in which blood levels of DDE (a metabolite of DDT) were determined in pregnant women. Once the blood level was determined for each woman, neurological testing was then performed on the infants that were born from these pregnancies. A very strong correlation

was found linking increased blood levels of DDE with poor performance of the neurological tests by these infants (10,11). Strong correlation of maternal serum levels of DDE, a metabolite of DDT, with defects in muscular tone and hyporeflexia was observed in these children. More convincing evidence of endocrine effects has been observed in an ecological setting (12–14). The initial reports were of egg shell thinning in bald eagles as well as vitellogenin (a protein that is normally only produced in the livers of female amphibians and fish) production in male African clawed frogs (12). Primary exposure routes for humans are inhalation, ingestion, and dermal contact.

In spite of the 1972 ban of DDT in the United States, human exposure to DDT is potentially high because of its prior extensive use and the persistence of DDT and its metabolites in the environment. DDT has been detected in air, rain, soil, water, animal and plant tissues, food, and the work environment (9). Breakdown products in the soil environment are DDE and DDD, which are also highly persistent. Because of its extremely low solubility in water, DDT is mainly retained by soils and soil fractions with higher proportions of soil organic matter. Although it is generally immobile or only very slightly mobile, DDT may leach into groundwater over a long period of time. DDT may reach surface waters primarily by runoff, atmospheric transport, drift, or by direct application. DDT has been widely detected in ambient surface water sampling in the United States at a median level of 1 ng/L (nanogram per liter equals part per trillion). DDT is regulated by US EPA under the Clean Water Act (CWA). Effluent discharge guidelines and water quality criteria have been set under the CWA (9).

3.1.2. Endosulfan

Endosulfan is a chlorinated hydrocarbon insecticide, which acts as a poison for a wide variety of insects and mites on contact. Although it may be used as a wood preservative, it is used primarily on a wide variety of food crops, including tea, coffee, fruits, and vegetables, as well as on rice, cereals, maize, sorghum, or other grains. Human exposure to endosulfan is primarily through breathing air, drinking water, eating food, or working where endosulfan is used. Exposure to endosulfan mainly affects the central nervous system (15). The effects of long-term/low-dose exposure is unknown. The most convincing evidence of endocrine effects in mammals is taken from laboratory animal studies in which doses of 5 mg/kg/d resulted in reduced sperm counts and altered testicular enzyme levels in male rats (9).

Endosulfan has been found in at least 143 of the 1416 National Priorities List sites identified by the US EPA (9). Although not easily dissolved in water, when released in water, endosulfan isomers hydrolyze readily in alkaline conditions and more slowly in acidic conditions. Endosulfan has been detected at levels of 0.2–0.8 µg/L in groundwater, surface water, rain, snow, and sediment samples. Large amounts of endosulfan can be found in surface water near areas of application. The US EPA recommends that the amount of endosulfan in lakes, rivers, and streams should not be more than 74 µg/L (9). Humans can become exposed to endosulfan by drinking water contaminated with it.

3.1.3. Methoxychlor

Methoxychlor is an organochlorine insecticide that is effective against a wide range of pests encountered in agricultural fields, household, and ornamental plants. It is

registered for use on fruits, vegetables, and forage crops. The use of methoxychlor has increased significantly since DDT was banned in 1972 (9). It is similar in structure to DDT, but it is less toxic and has relatively low persistence in biological systems. Methoxychlor is not highly soluble in water. Methoxychlor is highly toxic to fish and aquatic invertebrates. Levels of methoxychlor can accumulate in algae, bacteria, snails, clams, and some fish, but it is usually transformed into other substances and rapidly released from their bodies. The most probable routes of exposure for humans is inhalation or dermal contact during home use, and ingestion of food or drinking water contaminated with methoxychlor. Short-term exposure above the MCL causes central nervous system depression, diarrhea, and damage to liver, kidney, and heart tissue. Evidence suggests that high doses of technical methoxychlor or its metabolites may have estrogenic effects.

The risk of human exposure via groundwater should be slight, but it may be greater if application rates are very high, or if the water table is very shallow. At present, the strongest evidence of endocrine effects resulting from methoxychlor is taken from laboratory studies in which the relatively low dose of 0.5 µg/kg/d caused reduced fertility in mice (16,17).

In an US EPA pilot groundwater survey, methoxychlor was found in a number of wells in New Jersey and at extremely low concentration in the Niagara River, the James River, and an unnamed Lake Michigan tributary (9). Methoxychlor will most likely reach surface waters through runoff. Methoxychlor was detected in drinking water supplies in rural South Carolina. EPA set a limit of methoxychlor in drinking water at 0.04 mg/L (*see* Table 2). EPA advises that children should not drink water containing >0.05 mg/L for >1 d and that adults should not drink water containing >0.2 mg/L for a longer period of time (9).

3.2. Highly Chlorinated Compounds

3.2.1. Polychlorinated Biphenyls (PCBs)

PCBs are a group of manufactured organic compounds that include 209 different chemical forms known as congeners. This high number of many different chemical forms is possible because from 1 to 10 chlorine atoms can attach to the carbon atoms that make up the basic chemical structure of this family of compounds. PCBs are thermally stable, resistant to oxidation, acids, bases, and other chemical agents. PCBs tend to be more soluble in lipid-based solvents than in water; however, among the 209 congeners there is a wide range of water solubility and lipid solubility with the lesser chlorinated congeners being more water soluble (9).

In the environment, PCBs can be contaminated with dibenzofurans, dioxins, and polychlorinated naphthalenes. Since 1974, all PCB manufacturing has been banned and previous use in electrical capacitors and transformers has been greatly reduced. Because of their chemical-resistant properties, PCBs have persisted in the environment in large quantities despite the manufacturing ban. The primary routes of potential human exposure to PCBs are through ingestion of food and water as well as through dermal contact. There is extensive human data which show a strong association of low birthweights and shortened gestation with PCB exposure in humans (18,19). In addition, extensive neurological testing of children who experienced exposure to PCBs prior to birth revealed

Table 2
Regulated Chemicals That Cause Endocrine Disruption

Chemical	MCLG (mg/L)	MCL (mg/L)	Source	Health effect
Atrazine	0.003	0.003	Runoff from herbicide used on row crops	Cardiovascular system; reproductive problems
Benzo(a)pyrene (PAHs)	0.0	0.0002	Leaching from linings of storage tanks and distribution lines	Reproductive difficulties; increased risk of cancer
Carbofuran	0.04	0.04	Leaching of soil fumigant used on rice and alfalfa	Problems with blood, nervous system and reproductive system
2,4-D	0.07	0.07	Runoff from herbicide used on row crops	Kidney, liver, and adrenal gland problems
1,2-Dibromo-3-chloropropane (DBCP)	0.0	0.0002	Runoff/leaching from soil fumigant used on soybeans, cotton, pineapple and orchards	Reproductive difficulties; increased risk of cancer
Di(2-ethylhexyl) adipate	0.4	0.4	Discharge from chemical factories	General toxic effects; reproductive difficulties
Di(2-ethylhexyl) phthalate	0.0	0.006	Discharge from rubber and chemical factories	Reproductive difficulties; liver problems; increased risk of cancer
Dinoseb	0.007	0.007	Runoff from herbicide used on soybeans and vegetables	Reproductive difficulties
Dioxin (2,3,7,8-TCDD)	0.0	0.00000003	Emissions from incineration; discharge of chemical factories	Reproductive difficulties; increased risk of cancer
Ethylene dibromide	0.0	0.00005	Discharge from petroleum refineries	Problems with liver, stomach, reproductive system, and kidneys; increases the risk of cancer
Glyphosate	0.7	0.7	Runoff from herbicide use	Kidney problems; reproductive difficulties
Hexachloro-benzene	0.0	0.001	Discharge from metal refineries and agricultural chemical factories	Liver or kidney problems; reproductive difficulties; increased risk of cancer
Methoxychlor	0.04	0.04	Runoff/leaching from insecticide used on fruits/vegetables/livestock	Reproductive difficulties

(Continued)

Table 2 *(Continued)*

Chemical	MCLG (mg/L)	MCL (mg/L)	Source	Health effect
Polychlorinated biphenyls	0.0	0.0005	Runoff from landfills; discharge of waste chemicals	Skin changes; thymus gland problems; immune deficiencies; reproductive or nervous system difficulties; increased risk of cancer
Toxaphene	0.0	0.003	Runoff/leaching from insecticide used on cotton and cattle	Kidney, liver, or thyroid problems; increased risk of cancer
1,2,4-Trichloro-benzene	0.07	0.07	Discharge from textile finishing factories	Changes in adrenal glands

Source: US EPA.
Adapted from ref. 8.

impaired motor function and learning disorders (20). Studies have indicated that PCBs concentrate in human breast milk.

PCB releases from prior industrial uses and the persistence of the compounds in the environment have resulted in widespread water and soil contamination. They have been found in at least 383 of the 1430 National Priorities List sites identified by the EPA (9). The PCBs with a high degree of chlorination are resistant to biodegradation and appear to degrade very slowly in the environment. PCB concentrations in water are higher for the lower chlorinated PCBs because of their greater water solubility. PCBs have been found in runoff, sediments, soil, creek water, leachate, underground oil-water layer, and in pond effluents. Concentrations in these locations have ranged from 4 to 440,000 µg/L (9). In water, small amounts of PCBs may remain dissolved, but most adhere to organic particles and sediments. PCBs in water bioaccumulate in fish and marine mammals and can reach levels several orders of magnitude higher than levels found in the water (21–23). US EPA regulates PCBs under the CWA and has established water quality criteria and toxic pollutant effluent standards. Based on the carcinogenicity of PCBs, US EPA published a MCL goal (MCLG) for PCBs at 0 and the MCL of 0.5 µg/L (0.5 ppb) under the SDWA (*see* Table 2).

3.2.2. Dioxin

Dioxin is considered an EDC on the basis of its effects that occur during pregnancy, which result in many malformations, observed in the offspring of many species including humans (24,25). Dioxin is a contaminant formed during the manufacture of 2,4,5-trichlorophenoxyacetic acid (2,4,5-T), an herbicidal compound that includes about 50% of the defoliant Agent Orange, and 2,4,5-T derivatives, as well as other chemicals synthesized using 2,4,5-trichlorophenol. Dioxins may also be formed during incineration of chlorinated industrial compounds such as plastic and medical waste.

Dioxin is one of the most acutely toxic compounds synthesized by modern chemistry. TCDD (2,3,7,8-Tetrachlorodibenzo-p-dioxin) is the most toxic member of the 75 dioxins that exist and is mostly studied. It is almost insoluble in water. TCDD is stable in water, dimethylsulfoxide, 95% ethanol, or acetone. It can undergo a slow photochemical and bacterial degradation. Dioxin is degraded when heated in excess of 500°C or when exposed to ultraviolet radiation under specific conditions. TCDD has no known commercial applications but is used as a research chemical. TCDD has been found in at least 91 of 1467 National Priorities List sites identified by the US EPA (9). Dioxins are widespread environmental contaminants. They bioaccumulate throughout the food web because of their lipophilic properties and slow metabolic destruction. The primary source of dioxin exposure to humans is through food.

3.2.3. Furan

Furan is classified as cyclic, dienic ether; it is colorless and flammable liquid. It is insoluble in water, but is soluble in alcohol, ether, and most common organic solvents. Furan is used primarily as an intermediate in the synthesis and production of other organic compounds, including agricultural chemicals (insecticides), stabilizers, and pharmaceuticals (9). Furan is a carcinogen (26) and its primary route of potential human exposure is through inhalation.

Furan was detected in 1 of 63 industrial effluents at a concentration of less than 10 µg/L (9). Furan was detected in a creek in the Niagara River watershed and in the Niagara River.

3.3. Alkylphenols and Alkylphenol Ethoxylates

Nonylphenol (NP) and octylphenol are the largest volume alkylphenol products manufactured in the United States. Alkylphenols (APs) such as nonylphenol and octylphenol are mainly used to make alkylphenol ethoxylates (APE) surfactants. These surfactants are the primary active ingredients in industrial chemicals that are used as cleaning and sanitizing agents. Nonylphenol ethoxylates (NPE) account for approx 80% of total APE use with total US production exceeding 500 million lb/yr (9). APs are also used as plasticizers, in the preparation of phenolic resins, polymers, heat stabilizers, antioxidants, and curing agents. APEs do not break down completely in wastewater treatment plants or in the environment. The most widely used NPEs have 9- or 10-member carbon chains attached to the ethoxylate group. Thus, the great majority of NPEs in use are easily dissolved in water. Human exposure to APs and APEs may occur through contaminated drinking water that has been extracted from polluted waters. At present there is no conclusive evidence that APs or APEs cause adverse health effects in humans; however, there are many reports of APs causing production of a female-associated liver protein, vitellogenin, in male fish (27).

Investigations of NP levels in rivers have found values varying from 2 µg/L in the Delaware River in Philadelphia to 1000 µg/L in the Rhine, and 1000 µg/L in a tributary of the Savannah River (9,28). Drinking water is frequently taken from rivers and can easily become contaminated with APs. Analysis of many drinking water samples in the United States has found an overall average concentration of alkylphenolic compounds of 1 µg/L. Studies in the United States show NPE removal from wastewater ranging from

92 to 99% with minor seasonal variations. NPE concentrations in discharges after treatment are reportedly low, varying between 50 and 200 µg/L. Draft US EPA water quality guidelines for nonylphenol in freshwater are 6.6 µg/L water (4-d average) and 25 µg/L (1-h average), and in saltwater, they are 1.6 µg/L (4-d average) and 6.2 µg/L (1-d average).

3.4. Plastic Additives

3.4.1. Bisphenol A

Bisphenol A is an industrial chemical used to synthesize epoxy resins or polycarbonate plastic. Human exposure to the potential endocrine disrupting effects of bisphenol A may occur when this chemical leaches out of the plastic resulting from incomplete polymerization, or breakdown of the polymer on heating. Polycarbonates are commonly used for food and drink packaging materials and infants are the subgroup of the population that is most highly exposed to this compound. Bisphenol A is also used in plastic dental fillings.

Bisphenol A is a solid, which has low volatility at ambient temperatures. It has a water solubility of 120–300 mg/L. Its water solubility increases with alkaline pH values. Releases of bisphenol A into the environment are mainly in wastewater from plastic-producing industrial plants and from landfill sites that contain large quantities of plastics. Bisphenol A does not bioaccumulate in aquatic organisms to any appreciable extent. If released into acclimated water, bisphenol A would biodegrade. In untreated water, bisphenol A may biodegrade after a sufficient adaptation period, it may absorb extensively to suspended solids and sediments, or it may break down on exposure to light (9).

3.4.2. Diethyl Phthalate

Diethyl phthalate is a synthetic substance that is commonly used to increase the flexibility of plastics used to make toothbrushes, automobile parts, tools, toys, and food packaging. It is also used in cosmetics, insecticides, and aspirin. Diethyl phthalate (DEP) can be released fairly easily from these products because it is not part of the polymer. Plastic materials containing DEP in waste disposal sites constitute the major reservoir of DEP in the environment. If released to water, DEP is expected to undergo aerobic biodegradation. Humans are exposed to DEP through consumer products and plastics, contaminated air, or contaminated drinking water and foods.

There is evidence which shows a strong correlation with impaired reproductive performance in multigeneration studies in rodents (29); however, endocrine effects associated with DEP exposure in humans have not been reported.

DEP has accumulated and persisted in the sediments of the Chesapeake Bay for over a century. DEP has been detected in surface water samples from Lake Ponchartrain and the lower Tennessee River, as well as other industrial river basins. Surface water samples collected along the length of the Mississippi river contained DEP in significant concentrations. DEP has been detected in groundwater in New York State public water system wells, near a solid waste landfill site in Norman, OK, and at sites in Fort Devens, MA, Boulder, CO, Lubbock, TX, and Phoenix, AZ. DEP has been identified in drinking water in the following cities: Miami, Philadelphia, Seattle, Lawrence, New York City, and New Orleans (9).

3.4.3. Di(2-Ethylhexyl) Phthalate

Di(2-ethylhexyl) phthalate (DEHP) is a manufactured chemical that is used primarily as one of several plasticizers in polyvinyl chloride (PVC) resins that make plastics more flexible. It is the most commonly used of a group of related chemicals called phthalates or phthalic acid esters. DEHP is also used in inks, pesticides, cosmetics, and vacuum pump oil. DEHP is everywhere in the environment because of its use in plastics in large quantities, but it evaporates into air and dissolves in water at very low rates. Colon et al. (30) identified the presence of phthalate esters in the serum of young Puerto Rican girls with premature breast development. The primary routes of potential human exposure to DEHP are through inhalation, ingestion, and dermal contact in occupational settings and from air, from consumption of drinking water, food, and food wrapped in polyvinyl chloride. It is easily dissolved in body fluids, such as saliva and plasma. DEHP is biodegradable, but it tends to partition into sediment in which it is relatively persistent. It also tends to bioconcentrate in aquatic organisms. Because of its low vapor pressure, human exposure to DEHP in either water or through air appears to be minimal.

DEHP has been detected frequently in surface water, groundwater, and finished drinking water in the United States at concentrations in the low μg/L range. Groundwater in the vicinity of hazardous waste sites may be contaminated with DEHP. US EPA regulates DEHP under the CWA and the Safe Drinking Water Act (SDWA). DEHP is included in lists of chemicals for which water quality criteria have been established under the CWA. US EPA (9) classifies DEHP as a water priority pollutant and has set the MCLG at zero. US EPA has set the MCL at six parts DEHP/billion parts of drinking water (6 μg/L).

4. WATER TREATMENTS FOR EDC REMOVAL

Water suppliers use a variety of treatment processes to remove contaminants from drinking water. Individual processes may be arranged as series of processes applied in a sequence. Water utilities select a treatment train that is most appropriate for the contaminants found in the source water (31–35). The most commonly used physicochemical processes include coagulation and flocculation, sedimentation, filtration, and disinfection for surface water (36). Some treatment trains also include ion exchange and adsorption (37). These conventional processes are inefficient for substantially reducing certain pesticide concentrations and other EDCs.

The processes described later and in the following sections can be used for removal of EDCs as specified, either individually or as a class of compounds. The feasibility of using the various techniques will depend on the size of the system and the cost effectiveness. The two major concerns regarding technologies for small systems are affordability and technical complexity (which determine the needed skills for the system operators).

4.1. Granular Activated Carbon

Activated carbon is similar to charcoal in composition, but its surface is altered to enhance its sorption properties. Activated carbon is made from a variety of materials including wood, coal, peat, sawdust, bone, and petroleum distillates. Activated carbon produced from wood and coal is the most commonly used variety in drinking water treatment plants. The base carbon material is dehydrated then carbonized through slow heating in the absence of air. It is then activated by oxidation at high temperatures

(200–1000°C), resulting in a highly porous, high surface area/unit mass material (38). The activation process is considered as a two-step procedure in which amorphous material is burned off and pore size is increased. Typically, granular activated carbons (GACs) have surface areas ranging from 500 to 1400 m²/g.

GAC treatment removes contaminants through the physical and chemical process of sorption. The contaminants accumulate within the pores and the greatest efficiency is attained when the pore size is only slightly larger than the material being adsorbed. Removal efficiencies for many organic contaminants are good to excellent. Water quality parameters, such as dissolved organic matter, pH, and temperature can significantly affect the removal efficiency of GAC. However, for GAC treatment of drinking water it is necessary to reduce the total organic carbon of the treated water through the preliminary steps of coagulation/filtration (39) before treatment with GAC. Its removal efficiencies change drastically once the bed nears exhaustion, as contaminant breakthrough occurs. GAC beds can be reactivated by removing the granular carbon from the water treatment chambers, drying the material, then placing it in large furnaces that heat the material between 1200 and 1400°F. This heating process removes any residual contaminants from the pores and again enlarges the pore size. This feature and the high temperatures needed to attain reactivation should be kept in mind when considering claims of some manufacturers that flushing point-of-use (POU) GAC filters with hot water will reactivate units or increase operating efficiency. The increased temperatures that are reached with hot water do not in any manner achieve reactivation.

The performance of GAC for specific contaminants is determined in the laboratory by trial runs and is performed one chemical at a time. The following description is presented to provide the reader with a basic understanding of how the relative capacity of activated carbon to remove a chemical from water (a liquid phase) is determined. Data are gathered within a laboratory setting and determined on the basis of one chemical at a time. The Freundlich equation can be used to indicate the efficiency of GAC treatment. The Freundlich equation is expressed as:

$$Q_e = K \times C_e^n \qquad (1)$$

where Q_e is the equilibrium capacity of the carbon for the target compound (µg/g); C_e is the equilibrium liquid-phase concentration of the target compound, µg/L; K is the Freundlich coefficient in $(µg/g)(L/µg)^{1/n}$; $1/n$ is the Freundlich coefficient, dimensionless units.

Equation (1) can be converted into a linear form as shown next:

$$\log Q_e = \log K + \frac{1}{n} \log C_e \qquad (2)$$

Plotting of Eq. (2) on a logarithmic paper will yield K-value from the intercept and $1/n$ from the slope of the straight line. The K-values that are determined for each chemical are a means of expressing the "ability" of a particular GAC to remove a chemical. Typically when K-values that are more than 200 are attained the process is considered to be economically feasible (9). In addition, the process of GAC can be fine tuned, i.e., certain basic parameters such as pH, temperature, or choice of carbon source can be altered to increase efficiency of the process when certain critical contaminants such as pesticides must be removed. Careful monitoring and testing are required to ensure that

all contaminants are removed. The carbon media must be replaced regularly. The replacement intervals depend on:

1. Type of contaminant.
2. Concentration.
3. Rate of water usage.
4. Type of carbon used in the system.

There is potential for bacterial growth on the adsorbed organic chemicals; routine maintenance must be performed. When POU devices are used for compliance for small systems, programs for long-term operation, maintenance, and monitoring must be provided by the water utility.

4.2. Powdered Activated Carbon

Powdered activated carbon (PAC) also functions by adsorption of contaminants from water onto a solid-phase material, in this case powdered carbon. PAC differs from GAC in which the powdered carbon is added to the water in a large tank, a period of time is provided for adsorption of the contaminants to occur, and then the powdered carbon is later removed in a filtration process (40). This process also differs from GAC in which, PAC needs to be added continually for the process; however, the process is less expensive and less technically demanding but it is more labor intensive. PAC is more adaptable to short-term applications rather than as a continual use process. For contaminants such as pesticides which are mostly used during a 6-wk period in late spring and summer, PAC may be a particularly useful choice (9). The water being treated comes into contact with much less carbon material per unit volume treated, so the process is not as efficient as GAC. GAC is the BAT for removal of all of the selected EDCs that were discussed in the previous section. However, because other technologies are used in the multistep process of drinking water treatment, a brief discussion is included for those processes that enhance the performance of GAC.

4.3. Coagulation/Filtration

Coagulation/filtration processes involve the addition of chemicals like iron salts, aluminum salts, with and without anionic, cationic, or anionic–cationic polymers that coagulate and destabilize particles suspended in the water (39). The suspended particles are ultimately removed via clarification and/or filtration. Conventional filtration includes pretreatment steps of chemical coagulation, rapid mixing, and flocculation, followed by floc removal via sedimentation or flotation (36). After clarification, the water is filtered using common filter media such as sand, dual media, and tri media. Direct filtration has several effective variations, but all include a pretreatment of chemical coagulation, followed by rapid mixing. The water is filtered through dual or mixed media using pressure or gravity filtration units (31,35,36).

4.4. Lime Softening

In the lime-softening process, the pH of the water being treated is raised sufficiently to precipitate calcium carbonate and, if necessary, magnesium hydroxide to reduce water hardness. Some materials in solution are removed by incorporating them into the particles of calcium carbonate/magnesium hydroxide and coprecipitate, which are then separated by settling, filtration, or flotation (31,35,36).

5. POINT-OF-USE/POINT-OF-ENTRY TREATMENTS

The SDWA identifies both point-of-entry (POE) and POU treatment units as options for compliance technologies for small systems. A POU treatment device treats only the water at a particular tap or faucet, resulting in other taps in the facility serving untreated water. POU devices are typically installed at the kitchen tap. POU devices are listed as compliance technologies for inorganic contaminants, synthetic organic contaminants, and radionuclides (34). POU devices are not listed for volatile organic contaminants because they do not address all routes of exposure. POE treatment units treat all the water entering the facility (household or other building), resulting in treated water from all taps. POE devices are still considered as emerging technologies because of waste disposal and cost considerations.

POE and POU treatment units often use the same technological concepts as those used in central treatment processes, but on a much smaller scale. Technologies that are amenable to the POU and POE scale treatment include activated alumina, GAC, reverse osmosis, ion exchange, and air stripping (37). When POU and POE units are used by a public water system to comply with the National Primary Drinking Water Regulations (NPDWRs), the SDWA requires that the units be owned, controlled, and maintained by the public water system or by a person under contract with the public water system. This is to ensure that the units are properly operated and maintained to comply with the MCL or treatment techniques. This will also ensure that the units are equipped with the required mechanical warnings to automatically alert the customers on the occurrence of operational problems.

6. WATER TREATMENT TECHNIQUES FOR SPECIFIC EDC REMOVAL

The EDCs addressed in this chapter that are included in the NPDWRs as drinking water contaminants are methoxychlor, DDT and DDE, endosulfan, PCBs, DEP, and DEHP. The EDCs in this section are grouped by chemical class. Removal techniques for the EDCs not listed in the NPDWRs will be based on removal of similar contaminants that are listed.

The treatment processes are described with considerations of advantages, limitations, and special considerations. The actual choice of a process to include in a treatment train will ultimately depend on:

1. The source water quality.
2. The nature of the contaminant to be removed.
3. The required quality of the finished water.
4. The size of the drinking water system.

6.1. Methoxychlor

The BAT for removal of methoxychlor from drinking water is GAC. Steiner and Singley (41) have tested a wide range of water treatment processes and found GAC to be the most efficient for removal of methoxychlor. They found that over a broad range of concentrations (ranging from 1 to 25 mg/mL) the GAC process could remove sufficient quantities of methoxychlor so that the finished water met MCL requirements, which is 0.1 mg/mL.

6.2. Endosulfan

The BAT for removal of endosulfan from drinking water is GAC. In the US EPA report, Carbon Adsorption for Toxic Organics (42), the following *K*-values, as determined by the Freundlich equation and actual test were

Type of endosulfan	K $(\mu g/g)(L/\mu g)^{1/n}$
α-endosulfan	6135
β-endosulfan	1990
endosulfan sulfate	2548

For small system compliance, GAC, POU-GAC, and PAC can be used to remove endosulfan from drinking water supplies (*see* Table 3) (9,42–46).

6.3. DDT

The BAT for removal of DDT from drinking water is GAC. In the US EPA report (42), the following *K*-values, as determined by the Freundlich equation and actual test were determined: DDT has a *K*-value of 10,449 µg/g $(L/\mu g)^{1/n}$, which is sufficiently above the cutoff point of 200 µg/g $(L/\mu g)^{1/n}$ to be judged an effective treatment method and DDE (a DDT metabolite with endocrine activity) of 18,000 µg/g $(L/\mu g)^{1/n}$.

6.4. Diethyl Phthalate

The BAT for removal of DEP from drinking water is GAC. In the US EPA report (42), the following *K*-value, as determined by the Freundlich equation and actual test for DEP yielded a *K*-value of 17,037 µg/g $(L/\mu g)^{1/n}$.

6.5. Di-(2ethylhexyl) Phthalate

The BAT for removal of DEHP from drinking water is GAC. In the US EPA report (42), the following *K*-value, as determined by the Freundlich equation and the test was determined. DEHP has a *K*-value of 8308 µg/g $(L/\mu g)^{1/n}$ which is one of the highest values established among the 130 compounds that they tested; GAC is very effective for the removal of DEHP from drinking water.

6.6. Polychlorinated Biphenyls

In the US EPA report (42) two studies were reported for PCB-1221 and PCB-1232. The *K*-value determined for PCB-1221 was 1922 µg/g $(L/\mu g)^{1/n}$ and the *K*-value for PCB-1232 was 4067 µg/g $(L/\mu g)^{1/n}$. Both mixtures are among the lesser chlorinated groups containing 21 and 32% chlorine, respectively. Relative to other PCB mixtures they are more hydrophilic and hence would have lower *K*-values than the commercial PCB mixtures, Aroclor 1242, 1248, 1254, and 1260. The most troublesome PCB environmental mixtures tend to be derivatives of this later group of compounds; therefore, GAC should be a very effective method for removal of environmental PCB compounds from drinking water.

6.7. Dioxin

Dioxin is not water soluble; hence it is not likely to be present in untreated drinking water unless it would be attached to sediment in raw water. Because the most conventional water treatment methodologies such as coagulation–sedimentation and filtration

Table 3
Isotherm Constants for Selected EDCs

| Chemical | Isotherm Constants | | Calculated value |
	K mg/g (L/mg)$^{1/n}$	(1/n)	(μg/g) (L/μg)$^{1/n}$
α-Endosulfan	194	0.50	6135
β-Endosulfan	615	0.83	1990
Endosulfan sulfate	686	0.81	2548
DDT	332	0.50	10,499
DDE	232	0.37	18,000
DEP	110	0.27	17,037
DEHP	11,300	1.50	8308
PCB-1231	242	0.70	1922
PCB-1232	630	0.73	4067
Nonylphenol	250	0.37	19,406

Source: US EPA.
Adapted from ref. 9.

are effective in removing sediment, it is likely that these processes would be very effective in the removal of the contaminant, dioxin.

6.8. Alkylphenols and Alkylphenol Ethoxylates

GAC is the best used for removal of these contaminants from drinking water. Previous laboratory-scale testing for removal of nonylphenol with GAC has yielded a *K*-value of 19,406 at a water pH of 7.0 (9). For consistency of removal of synthetic organic chemicals, GAC, POU-GAC, and PAC are recommended for small system compliance. GAC devices include pour-through for treating small volumes, faucet-mounted for POU, in-line for treating large volumes at several faucets, and high volume commercial units for treating community water supply systems. Careful selection of the type of carbon is based on the specific contaminants in the water and the manufacturer's recommendations. Site-specific conditions may affect the percentage removal using these techniques, including the presence of "competing" contaminants. Source water-specific testing will be needed to ensure adequate removal. For GAC, surface waters may require prefiltration. PAC is the most applicable to those systems that already have a process train including mixing basins, precipitation or sedimentation, and filtration.

NOMENCLATURE

Q_e Equilibrium capacity of the carbon for the target compound (μg/g)
C_e Equilibrium liquid-phase concentration of the target compound (μg/L)
K Freundlich coefficient in (μg/g)(L/μg)$^{1/n}$
$1/n$ Freundlich coefficient, dimensionless units

REFERENCES

1. US FDA, *Endocrine Disruptor Knowledge Base (EDKB)*, US Food and Drug Administration, Web Site http://edkb.fda.gov/ (2006).
2. European Commission, *Endocrine Disruptor,* Web Site, http://europa.eu.int/comm/environment/ endocrine (2006).

3. IPCS, *Summary and Details: Scientific Facts on Endocrine Disruptors, International Program on Chemical Safety*, Green Facts, http://www.greenfacts.org/endocrine-disruptors/ (2006).

4. R. K. Naz (ed.), *Endocrine Disruptors: Effects on Male and Female Reproductive System*, CRC Press, Boca Raton, FL, 1999.

5. G. Chhanda, Reproductive malformation of the male offspring following maternal exposure to estrogenic chemicals, *Proc. of the Society for Experimental Biology and Medicine.* Vol. 224, pp. 61–68 (2000).

6. R. Triendl, Genes may solve hormone-disrupter debate, Robert. *Nature* **209**, January 28, 2001.

7. US EPA, *Endocrine Disruptor Screening and Testing Advisory Committee (EDSTAC) Final Report*, Office of Prevention, Pesticides and Toxic Substances, US Environmental Protection Agency, January (1999). http://www.epa.gov/scipoly/oscpendo/history/finalrpt.htm (2005).

8. K. Jesperson, Endocrine disruptors: what are they doing to you, National Drinking Water Clearing House. *On Tap* **2**, **4**, pp. 16–22 and 49, Winter (2003).

9. US EPA, *Removal of Endocrine Disruptor Chemicals Using Drinking Water Treatment Processes,* Technology Transfer Report No. EPA/625/R-00/015, The National Risk Management Research Laboratory, Office of Research and Development, US Environmental Protection Agency, Cincinnati, OH, March, 2001.

10. W. Rogan, and B. Gladen, et al., Neonatal effects of transplacental exposure to PCBs and DDE. *J. Pediatr.* **109**, 335–341 (1996).

11. P. A. StehrGreen, Demographic and seasonal influences on human serum pesticide residue levels. *J. Toxicol. Environ. Health* **27**, 405–421 (1989).

12. B. O. Palmer and S. K. Palmer, Vitellogenin Production by xenobiotic estrogens in the red-eared turtle and African clawed frog. *Environ. Health Perspect.* **103**(Suppl 4) 19–25 (1995).

13. T. Colborn, F. S. vom Saal, and A. M. Soto, Developmental effects of endocrine-disrupting chemicals in wildlife and humans. *Environ. Health Perspect.* **101**, 378–384 (1993).

14. L. J. Guillette and D. A. Crain, Endocrine-disrupting contaminants and reproductive abnormalities in reptiles. *Comments on Toxicol.* **5**, 381–399 (1996).

15. ATSDR, Agency for Toxic Substances and Disease Registry ToxFAQs. Endosulfan (1995). http://www.atsdr.cdc.gov/tfacts41.html (2006).

16. A. M. Cummings and L. E. Gray, Antifertility effect of methoxychlor in female rats: dose- and time-dependent blockade of pregnancy. *Toxicol. Appl. Pharmacol.* **97**, 454–462 (1989).

17. F. S. vom Saal and S. C. Nagel, Estrogenic pesticides: binding relative to estradiol in MCF-7 cells and exposure during fetal life on subsequent territorial behavior in male mice. *Toxicol. Lett.* **77**, 343–350 (1995).

18. P. R. Taylor, C. E. Lawrence, H. L. Hwang, and A. S. Paulson, Polychlorinated biphenyls: influence in birth weight and gestation. *Am. J. Public Health* **74**, 1153–1154 (1984).

19. S. C. Patandin, M. A. Koopman-Esseboom, N. de Ridder, G. Weisglas-Kuperus, and P. J. Sauer, Effects of environmental exposure to polychlorinated biphenyls and dioxins on birth size and growth in Dutch children. *Pediatr. Res.* **44**, 538–545 (1998).

20. J. L. Jacobson, S. W. Jacobson, and H. E. Humphrey, Intellectual impairment in children exposed to polychlorinated biphenyls *In Utero. New Engl. J. Med.* **335**, 783–789 (1996).

21. B. C. Gladen and W. J. Rogan, Effects of perinatal polychlorinated biphenyls and dichlorodiphenyl dichloroethene on later development, *J. Pediatr.* **113**, 991–995 (1991).

22. M. C. Huisman, V. Koopman-Esseboom, M. Fidler, et al., Perinatal exposure to polychlorinated biphenyls and dioxins and its effect on neonatal neurological development. *Early Hum. Dev.* **41**, 111–127 (1995).

23. A. Brouwer, M. P. Longnecker, L. S. Birnbaum, et al., Characterization of potential endocrine-related health effects at low-dose levels of exposure to PCBs, *Environ. Health Perspect.* **107**(Suppl 4), 639–649 (1999).

24. C. Tohyama, Mechanisms of dioxin toxicity: implications for assessing risk to humans, *Conference on Environmental Endocrine Disruptors,* Colby-Sawyer College, New London, NH, June 6–11, 2004.

25. US Department of Health and Human Services, *2,3,7,8-Tetrachlorodibenzo p-Dioxin (TCDD); DIOXIN*, CAS No.1746-01-6, Public Health Service National Toxicology Program, 9th Report on Carcinogens, January, 2001.

26. US Department of Health and Human Services, *Furan*, CAS No. 110-00-9. 9th Report on Carcinogens, Public Health Service National Toxicology Program, January, 2001.

27. S. Jobling, T. Reynolds, R. White, M. G. Parker, and J. P. Sumpter, A variety of environmentally persistent chemicals, including some phthalate plasticizers, are weakly estrogenic. *Environ. Health Perspect*. **103**(6), pp. 582–587 (1995).

28. R. J. Maguire, Review of the persistence of nonylphenol and nonylphenol ethoxylates in aquatic environments. *Water Qual. Res. J. Can.* **34**(1), 37–78 (1999).

29. R. Hauser, Phthalates: understanding human exposure and health risks, *Conference on Environmental Endocrine Disruptors,* Colby-Sawyer College, New London, NH, June 6–11, 2004.

30. I. Colón, D. Caro, C. J. Bourdony, and O. Rosario, Identification of phthalate esters in the serum of young Puerto Rican girls with premature breast development. *Environ. Health Perspect.* **108**, September 9 (2000).

31. AWWA, ASCE, *Water Treatment Plant Design*, 3rd edn., McGraw-Hill Company, Inc., New York, NY, 1998.

32. US EPA, *Technologies for Upgrading Existing or Designing New Drinking Water Treatment Facilities,* EPA/625/4-89/023, US Environmental Protection Agency, March, 1990.

33. US EPA, *Water on Tap: A Consumer's Guide to the Nation's Drinking Water*, EPA/815/K-97/002. US Environmental Protection Agency, July, 1997.

34. US EPA, *Small System Compliance Technology List for the Non-Microbial Contaminants Regulated Before 1996*, EPA/815/R-98/002, US Environmental Protection Agency, September, 1998.

35. US EPA, *Drinking Water Treatment*, EPA/810/F-99/013, US Environmental Protection Agency, December, 1999.

36. L. K. Wang, Y. T. Hung, and N. K. Shammas (eds.), *Physicochemical Treatment Processes,* The Humana Press, Inc., Totowa, NJ, 2005.

37. L. K. Wang, Y. T. Hung, and N. K. Shammas (eds.), *Advanced Physicochemical Treatment Processes,* The Humana Press, Inc., Totowa, NJ, 2006.

38. Y. T. Hung, H. H. Lo, L. K. Wang, J. R. Taricska, and K. H. Li, Granular activated carbon adsorption, in *Physicochemical Treatment Processes,* L. K. Wang, Y. T. Hung, and N. K. Shammas (eds.), The Humana Press, Inc., Totowa, NJ, 2005.

39. N. K. Shammas, Coagulation and flocculation, in *Physicochemical Treatment Processes,* L. K. Wang, Y. T. Hung, and N. K. Shammas (eds.), The Humana Press, Inc., Totowa, NJ, 2005.

40. Y. T. Hung, J. R. Taricska, H. H. Lo, L. K. Wang, and K. H. Li, Powdered activated carbon adsorption, in *Advanced Physicochemical Treatment Processes,* L. K. Wang, Y. T. Hung, and N. K. Shammas (eds.), The Humana Press, Inc., Totowa, NJ, 2006.

41. J. Steiner and J. Singley, Methoxychlor removal from potable water. *J. Am. Water Works Assoc*. **17**, 284–286 (1979).

42. Dobbs and Cohen, *Carbon Adsorption for Toxic Organics*, Report NO. EPA/ 600/8-80/023, US Environmental Protection Agency, Cincinnati, OH, 1980.

43. M. Kamrin, N. Hayden, B. Christian, D. Bennack, and F. D'Itri, *Water Quality: Home Water Treatment Using Activated Carbon*, WQ-13, Cooperative Extension Service, Purdue University, 1991.

44. EUROPA, *Endocrine Disruptors Website,* http://ec.europa.eu/environment/endocrine/index_en.htm July (2006).
45. Green Facts, *Scientific Facts on Endocrine Disruptors* Website: http://www.greenfacts.org/endocrine-disruptors/links/index.htm (2006).
46. Gordon Research Conferences, Environmental endocrine disruptors, *The Fifth Gordon Research Conference on Environmental endocrine disruptors* Barga, Italy, June 4–9 (2006).

Filtration Systems for Small Communities

Yung-Tse Hung, Ruth Yu-Li Yeh, and Lawrence K. Wang

CONTENTS

1. INTRODUCTION

There are about 54,367 community water systems in the United States, which serve about 253 million people. Approximately 93% of community water systems are small water systems serving fewer than 10,000 persons and serve just about 20% of the population served by community water systems (1). Ownership type and system size are closely related. Most water systems serving 500 or less people are ancillary or privately owned systems, whereas most of the larger systems are publicly owned systems. This chapter discusses the operating characteristics of small water systems and the effect of Safe Drinking Water Act (SDWA) amendments implementation on small systems. The main focus of the chapter is on the filtration systems of small water systems, which serve communities less than 10,000 persons. The application of sand filters for treatment of wastewater treatment effluents from septic tanks and lagoons for small communities is also discussed in this chapter.

2. OPERATING CHARACTERISTICS

The smallest water systems, serving less than 501 persons, have experienced little growth in the service population between 1990 and 1994. Growth was only found in the systems serving 101–500 persons, which increased by only 2.5% in median connections during the same period. The largest growth in service population among small systems was found in those systems serving 3301–10,000 persons. Between 1990 and 1994, systems in this size category experienced a 10% increase in the number of connections and

an 11.1% increase in the number of customers. The water source for the water system is a major factor in determining operating characteristics, and the water source corresponds closely to the system size. Larger systems are more likely to use surface water or purchased water as their primary source, whereas most small systems use ground water as their source of water supply.

Production per connection increases as the size of water system increases. This increase in production per connection is indicative of the differences between the customer bases of larger and smaller systems. Large water systems serve higher percentage of industrial, commercial, and agricultural customers, whereas small water systems serve primarily residential customers with lower water consumption rate. Publicly owned systems serving less than 500 persons generally receive more technical assistance than privately owned or ancillary systems of the same size. With proper source, water protection, and well-head protection programs, water systems can improve their water quality, decrease the likelihood of water-borne disease outbreaks, and can reduce the need for future capital expenditures for treatment facilities and equipment. Source water protection is important because 93% of groundwater systems serving 1001–3300 persons and 83% of those serving less than 1001 persons have a potential source of contamination within 2 miles of their wells (1).

3. SDWA IMPLEMENTATION

The SDWA amendments were signed by the President on August 6, 1996. The 1996 SDWA Amendments specifically require US Environmental Protection Agency (US EPA) to make technology assessments relevant to the three categories of small systems for both existing regulations (e.g., Surface Water Treatment Rule [SWTR] and Total Coliform Rule) and future requirements. The three population-based size categories of small systems are 10,000–3301 persons, 3300–501 persons, and 500–25 persons (2).

The 1996 SDWA amendments identified two classes of technologies for small systems; i.e., compliance technologies and variance technologies. A compliance technology may refer to either a technology or other means that is affordable and that achieves compliance with the maximum contaminant level (MCL) and to a technology or other means that satisfies a treatment technique requirement. The listing of a compliance technology for a size category/source water combination prohibits the listing of variance technologies for that combination. Although variance technologies may not achieve compliance with the MCL or treatment technique requirement, they must achieve the maximum reduction or inactivation efficiency that is affordable considering the size of the system and the quality of the source water. Variance technologies must also achieve a level of contaminant reduction that is protective of public health.

4. FILTRATION TREATMENT TECHNOLOGY OVERVIEW

Two common types of water treatment systems used in small communities include filtration plants and deferrization plants. Filtration plants are used for surface water treatment to remove turbidity, whereas the deferrization plants are used for ground water treatment to remove iron and manganese (1–38). The treatment processes of filtration plants include rapid mix with the addition of coagulants, slow mix, clarification,

filtration, and disinfection. The treatment processes for deferrization plants include aeration for iron and manganese removal, clarification, filtration, and disinfection.

Both types of water treatment plants use filtration processes to reduce turbidity and microorganism levels in a community's water supply. Filtration can be very effective in removing pathogenic microorganisms, including *Giardia* cysts and viruses. Conventional filtration processes are normally preceded by coagulation, flocculation, and clarification. Coagulation is the complex process of particle aggregation, which includes coagulant formation, particle destabilization (surface charge alteration of suspended particles), and interparticle collisions. Flocculation is considered as a part of the coagulation process and is the process of promoting interparticle collisions and thus the aggregation of larger particles. Larger suspended particles may be removed by simple filtration, and clarification (gravity sedimentation, or dissolved air flotation). Direct filtration processes are preceded only by coagulation and flocculation; the floc is removed directly by the filters. Common water filtration processes involve passing pretreated water through a filter media to remove suspended substance, colloidal and dissolved contaminants. Examples of suspended particulates include clay and silt, microorganisms, humic and other aggregated organic materials, and aluminum and iron oxide precipitates. Typical filter media include silica sand, diatomaceous earth, garnet, or ilmenite, and a combination of coarse anthracite coal overlaying finer sand. Filtration may involve single media, dual media (coal–sand), and trimedia (an added third layer of sand). Filtration may be rapid or slow, depending on the application, and may involve different removal processes, cleaning methods, and operation methods (3–5).

In the case of slow sand filtration, which does not involve the addition of coagulants, colloidal and dissolved organic materials may be removed by biological processes in the schmutzdecke, which is the black layer or biologically active layer, and in the filter medium below. In the case of direct filtration, which is used for raw water with low turbidity, the coagulation and flocculation steps are immediately followed by filtration. Because there is less aggregated material to remove, sedimentation or flotation is not required to prolong the filter cycle. Some dissolved chemicals may be removed by chemical sorption at the surface of the filter media, especially in the cases of higher surface area filter media (e.g., fine sand and diatomaceous earth), but these processes account for much less of the bulk contaminant removal compared to physical sorption processes (3–6). For meeting the performance criteria under the SWTR and for protecting public health, disinfection treatment is applied following filtration.

5. COMMON TYPES OF WATER FILTRATION PROCESSES FOR SMALL COMMUNITIES

Three common types of water filtration processes used in small communities are

a. Slow sand filters.
b. Rapid filters.
c. Diatomaceous earth (DE) filters.

Process description of these three types of filtration, operation and maintenance (O&M) requirements, technology limitations, and financial consideration will be discussed in this section.
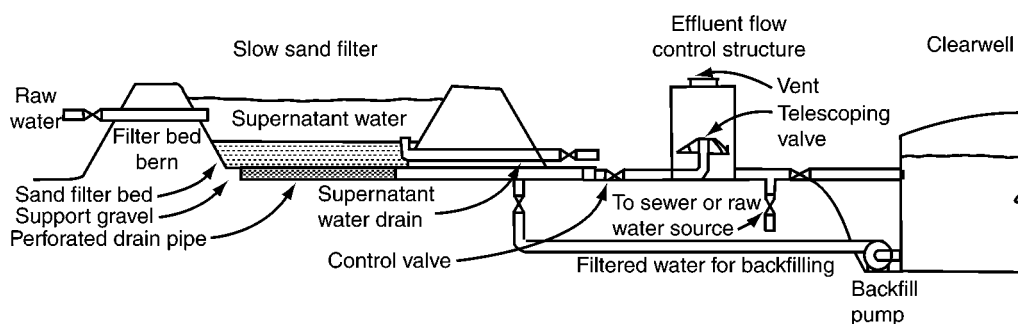
**Fig. 1.** Typical unhoused slow sand filter installation (7).

5.1. Process Description

5.1.1. Slow Sand Filters

Slow sand filters (Fig. 1) consist of a bed of fine sand approx 3–4 ft deep, a 1 ft layer of gravel for support, and an underdrain system to collect treated water (7). The effective size of the sand media ranges from 0.25 to 0.35 mm, with a uniformity coefficient of 2–3. Slow sand filters are designed to operate at very low application rates (0.03–0.10 gpm/ft^2 of filter bed area) and, therefore have relatively extensive land requirements. Slow sand filters are operated under continuous, submerged conditions maintained by adjusting a control valve located on the discharge line from the underdrain system. Slow sand filters are limited to treat surface waters with turbidity levels less than 20 nephelometric turbidity units (NTU) because of the surface biological mat which forms during the process and as well as the small void spaces in the bed. Generally, water applied to slow sand filters are not pretreated by coagulation/flocculation and sedimentation processes.

Slow sand filters are simple, easily used by small systems, and have been adapted to package plant construction (8,9). Slow sand filters are similar to single media rapid-rate filters in some respects, but there are crucial differences in the mechanisms employed (other than the obvious difference in flow rate). The schmutzdecke, the top-most, biologically active layer of filter, removes suspended organic materials and microorganisms by biodegradation and other processes, rather than relying solely on simple filter straining or physico-chemical sorption. Advantages of slow sand filtration include its low maintenance requirements (because it does not require backwashing but requires less frequent cleaning) and the fact that its efficiency does not depend on actions of the operator. However, slow sand filters do require time for the schmutzdecke to develop after each cleaning: during this "ripening period," however, filter performance steadily improves. The ripening period can last from 6 h to 2 wk, but typically requires less than 2 d. A 2-d filter-to-waste period is recommended for typical sand filters (4). Because few remedies are available to an operator when the process is ineffective, particularly if a system has little storage capacity, slow sand filtration should be used with caution and should not be used without pretreatment or process modifications (e.g., granular activated carbon layer addition) unless the raw water is low in turbidity, algae, and color (10).

Package plants with a granular activated carbon layer located beneath the slow sand can adsorb organic materials that are resistant enough to biodegradation to pass through
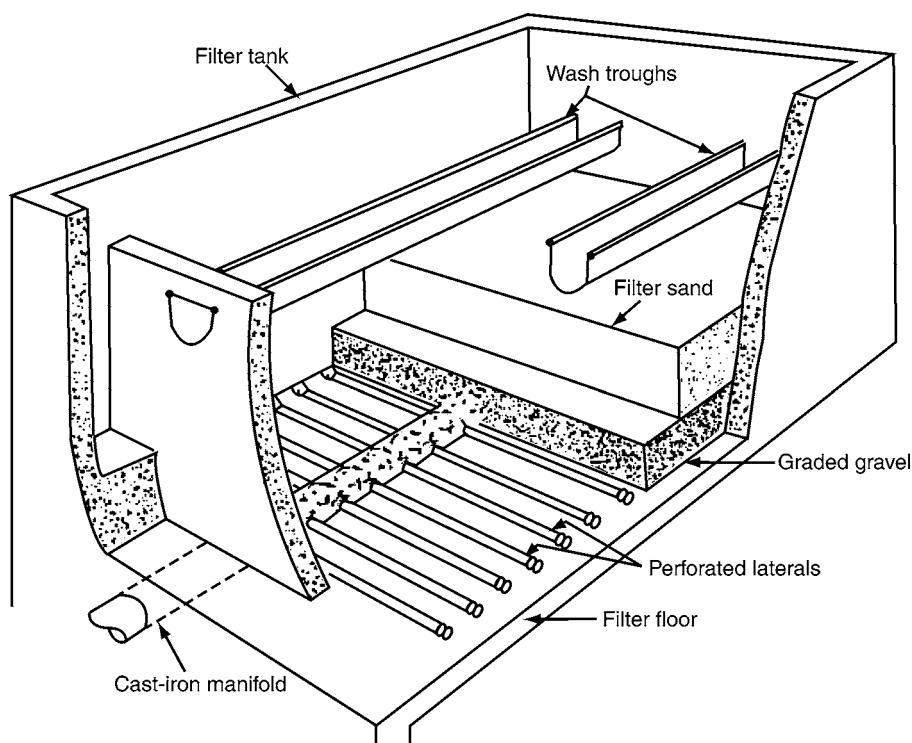
Fig. 2. Cutaway view of typical rapid sand filter (7).

the schmutzdecke. When used with source water of the appropriate quality, slow sand filtration may be the most suitable filtration technology for small systems (7). Slow sand filtration has achieved removal efficiencies in the range of 90–99.9999% for viruses and >99.99% for *Giardia lamblia* (6). Recent studies have demonstrated that certain modifications to slow sand filters can result in improved performance and possibly extend the application range to more turbid waters. Some of these modifications require further full-scale investigations to support the results of these studies and to develop more comprehensive design criteria. Slow sand filter modifications investigated include several pretreatment steps, such as roughing filters and preozonation, to extend the application range to lower quality waters; filter mats to increase filter runs, and simplify cleaning procedures; surface amendments to remove organic precursors and control disinfection byproduct formation; and techniques to reduce cleaning costs and filter ripening periods (7).

5.1.2. Rapid Sand Filters

Rapid sand filters (Fig. 2) can treat raw water with high or variable turbidities at filtration rates up to 2 gpm/ft^2 (7). The filter components (except for the control panel) are contained in a watertight tank. The effective size of the sand media ranges from 0.4 to 0.6 mm; this results in larger void spaces, which do not fill and clog as quickly as in slow sand filters. The filter bed is usually 24–36 in. deep and rests on top of a layer of gravel 6–18 in. deep. The sand and gravel bed is supported by an underdrain system, which collects the filtered water and also evenly distributes the backwash water. Rapid
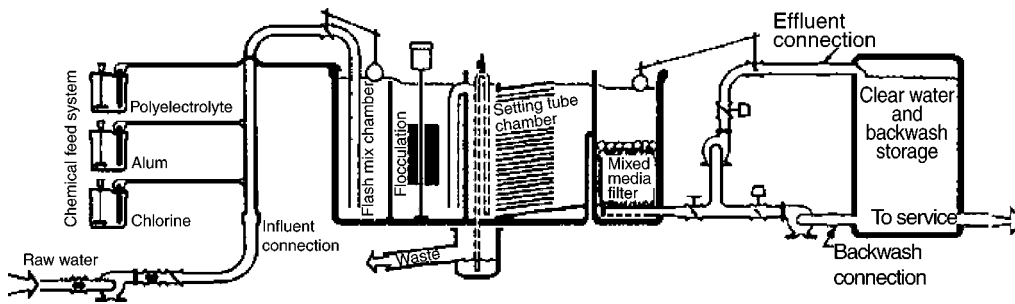
Fig. 3. Flow diagram of a package plant (7).

sand filters are highly automated and are usually included in package plant systems (Fig. 3) (7). Package plants usually consist of coagulation/flocculation, clarification, and filtration components. Occasionally, the clarification step may be omitted. The filters are backwashed automatically at a predetermined head loss or at a predetermined turbidity of the filtered water. On-line turbidimeters are used to continuously monitor and record the turbidity of the filtered water. Head loss indicators are provided to continuously measure the filter head loss (7).

Rapid sand filtration or conventional filtration includes chemical coagulation, rapid mixing, and flocculation, followed by floc removal through sedimentation or flotation. The clarified water is then filtered. Common filter media includes sand, dual media, and tri media. Design criteria for specific sites are influenced by site-specific conditions and thus individual components of the treatment train may vary in design criteria between systems. Conventional treatment has demonstrated removal efficiencies more than 99% for viruses and 97–99.9% (rapid filtration with coagulation and sedimentation) for *G. lamblia* (6).

There are a variety of coagulation/filtration package plants applicable to small systems (4,8,9,11). In package plants that utilize sedimentation, the sedimentation step usually occurs in tube settlers. In dual stage filtration, the sedimentation step is replaced by a passive flocculation/clarification step that occurs in an initial depth clarifier tank (11,12). The clarified water is then passed through a depth filter. Other modes of clarification are possible, including the use of the various upflow and downflow flocculation/filtration processes, also known as roughing filter processes. Typically, roughing filters are not as versatile as sedimentation or flotation, but some varieties may perform comparably. One example of a package plant of this type uses a buoyant crushed plastic medium used in an upflow mode as a contact flocculator and roughing filter ahead of a downflow triple-media bed (4). Coagulation/filtration package units have demonstrated the ability to effectively remove turbidity, color, disinfection byproduct precursors, viruses, bacteria, and protozoa (e.g., *Cryptosporidium* and *Giardia* cysts) (8,9,11,12).

The dissolved air flotation (DAF) process includes coagulation and flocculation, but instead of gravity sedimentation, the floc is carried up to the water surface by rising air bubbles, where the floc can be skimmed off (4,8,13). DAF may be more applicable than other conventional filtration systems for removing particulate matter that does not readily settle, for example, algae-rich waters, highly colored waters, low turbidity/low alkalinity waters, and cold waters. DAF is less appropriate for very turbid waters because of their higher silt and clay contents. The National Research Council suggests an upper turbidity

limit of 50 NTU for small systems using DAF (8). For lower turbidity waters, DAF performance is comparable with conventional filtration employing sedimentation (38).

Rapid sand filtration or conventional filtration is the most widely used technology for treating surface water supplies for turbidity and microbial contaminants, but may be less applicable to the smallest water system size category (those serving 25–500 persons) because of relatively high costs and technical complexity. Although conventional filtration has the advantage that it can treat a wide range of water qualities, it has the disadvantage that it requires advanced operator skill and has high monitoring requirements. Thus, small systems without access to a skilled operator should not use conventional treatment, beacuse the disruption of chemical pretreatment can lead to pathogen introduction to the distribution system (4,8,12). The performance of conventional filtration is extremely sensitive to the proper operation of chemical coagulation and flocculation. If the coagulation step is disrupted or improperly executed, the removal efficiencies for turbidity and microbiological contaminants decrease dramatically. For this reason, US EPA suggests that only those systems with full-time access to a skilled operator use conventional filtration.

One type of rapid sand filters is high rate filter, which operates at filtration rates ranging from 3 to 10 gpm/ft^2. They are well-suited to treating raw water supplies with high or variable turbidities. High rate filters include dual media and multimedia filters. Dual media filters consist of an upper layer of coarse coal (anthracite) and a lower layer of sand; both layers are supported by a gravel bed. Multimedia filters consist of three types of media: coarse coal, sand, and garnet, from top to bottom. High rate filters are highly automated and contain components similar to those found in rapid sand filters. High rate filters are also included in package plant systems (7).

5.1.3. DE Filters

DE filters, also known as precoat or diatomite filtration, can be used directly to treat low turbidity raw water supplies or chemically coagulated more turbid water sources. They have been used extensively for filtering swimming pool water; they may also be applicable for some small-community systems. DE filters are compact pressure filters capable of removing *Giardia* cysts and algae from water supplies. However, they are most suited for water supplies with low turbidities (less than 10 NTU) and low bacteria counts.

DE filters consist of a precoat layer of DE, approx 1/8-in. thick, supported by a septum or filter element. To properly maintain the DE precoat layer, and to maintain porosity, treatment is supplemented by a continuous-body feed of diatomite and recycled filtered water. Intermittent operation of DE filters is not advised unless the system recycles water through the filter during production down times. This will optimize performance, extend the filtration cycle, and lower filter maintenance requirements (39).

Normally the DE filter is backwashed and the septum cleaned after each break in filtration. Then a fresh layer of precoat is applied. If changes in water quality occur, body feed rates may be adjusted immediately and/or a re-precoat may be applied. DE filtration plants can be designed to make such adjustments automatically.

DE filtration is very effective for removing *Giardia* cysts, but filtration studies with plain DE have not indicated a marked capability to remove very small particles, for example, viruses (4,8,14). Some research has shown that specific modifications can lead

to 99% virus removal ([4]). In addition, recent studies have indicated excellent removal rates (e.g., 6 log) of *Cryptosporidium* oocysts for DE grades commonly used by smaller systems ([15]).

Because chemical coagulation is not required, DE filtration is very attractive as small systems technology and it has been used successfully by small systems for many years. Waters that are low in turbidity, color, and other organic matter (disinfection byproduct precursors) are most suitable for direct application of DE technology ([8]).

5.2. Operation and Maintenance Requirements

5.2.1. Slow Sand Filters

Slow sand filters are the simplest to operate. Daily operation consists of checking the raw water temperature and turbidity, filter effluent turbidity, and filter head loss. The filter effluent control valve should be periodically adjusted to maintain a constant discharge rate. Slow sand filter runs may last from 20 to 90 d depending on raw water quality before cleaning is necessary. Slow sand filters are not backwashed. Instead, the top 1–2 in. of sand are manually removed from the surface of the filter bed. The removed sand may be either washed and then stored for future use, or simply discarded. After cleaning, a ripening period of 1–2 d is required to allow the schmutzdecke or surface biological mat to redevelop. The filtered water is typically wasted during this period owing to the poor water quality. New or washed sand should be added to the filter when the bed depth reaches 24 in. ([7]).

5.2.2. Other Filters

Rapid sand filters, high rate filters, and package plants, can be highly automated. However, these systems require the presence of a properly trained operator on a daily basis to ensure continuous and reliable operation. The temperature and turbidity of the raw water should be checked daily. In addition, the filter flow rate, filter run time, filter head loss, backwash cycles, and filtered water turbidity should also be monitored on a daily basis. The duration of the typical filter run will range from 12 to 36 h depending on the filter influent quality. The operator should periodically observe the filter backwash cycles to verify adequate cleaning of the filter and to check for excessive loss of filter media during the backwash cycle.

The effluent turbidity from filters should be checked periodically. The application of additional DE should be adjusted according to the measured turbidity levels. When the filter head loss reaches a predetermined level, the filter must be backwashed. After backwashing, a new precoat layer of DE must be formed on the filter elements before filtration can resume ([7]).

5.3. Technology Limitations

5.3.1. Slow Sand Filters

Slow sand filters are not recommended for waters with high or variable turbidities; water with high turbidity or algae levels will result in short filter runs. Generally, the raw water turbidity should be <20 NTU and the color should be <30 units. Slow sand filters do not remove any synthetic organic compounds, disinfection byproduct precursors, or inorganic chemicals. These filters also have relatively extensive land area requirements. Filters installed in cold climates must be housed ([7]).

Table 1
Slow Sand Filter Construction and O&M Costs

Capacity (gpd)	Construction costs (USD)	Annual O&M costs (USD)
50,000	207,900	6800
100,000	271,100	8100

Costs in 1992 USD.
Adapted from ref. 7.

5.3.2. Rapid Sand Filters

Rapid sand filters, high rate filters, and package plants, require daily attendance by properly trained water treatment plant operators. Inadequate coagulant dosages and/or poor sedimentation can result in filter blinding and reduced filter runs. Excessive levels of turbidity and color in the raw water may exceed package plant design specifications; in these cases, the flow capacity of the plant must be decreased to produce an acceptable water quality (7).

5.3.3. DE Filters

DE filters do not effectively remove viruses unless the water is pretreated with coagulants and filter aids. Also, DE filters do not remove dissolved substances, such as color-causing materials (7).

5.4. Financial Considerations

5.4.1. Slow Sand Filters

Estimated construction and annual O&M costs are presented in Table 1 for uncovered slow sand filters. All cost data is based on 1992 USD (7). Construction costs include clay-liner, earthen berms, polyvinyl chloride (PVC) piping, steel tank reservoir, effluent flow control structure, effluent flow meter, and pump for filter backfilling. The filter loading rate is 70 gpd/ft^2 (7).

5.4.2. Mixed Media Filters

Estimated construction costs for prefabricated, steel package filter units designed for flows less than 100,000 gpd and filtration rates between 2 and 5 gpm/ft^2 and range from 55,000 to 95,000 USD. O&M costs are dependent on the filter size and the number of backwashes performed per day. Annual O&M costs are estimated to range between 4200 and 9500 USD for flows less than 100,000 gpd (7).

5.4.3. Complete Package Treatment Plants

Estimated construction costs for package plants consisting of coagulation/flocculation, sedimentation, and multimedia gravity filtration range from 98,000 to 160,000 USD for flows between 14,000 gpd and 144,000 gpd. The filtration rate is assumed to be 5 gpm/ft^2. Annual O&M costs are projected to range from 10,100 to 14,400 USD for the same range of flows (7).

5.4.4. DE Filters

Estimated construction costs for package pressure DE filters with design capacities of 28,000 gpd and 86,000 gpd are 71,000 and 80,000 USD, respectively. O&M costs for

both systems (exclusive of DE filter aid cost) are estimated to be 10,000 USD/yr. The annual DE filter aid cost for each filter is estimated to range from 225 (28,000 gpd) to 700 USD (86,000 gpd) at an application rate of 15 mg/L (7).

6. OTHER FILTRATION PROCESSES

This section presents other filtration processes which are not commonly used in the small water systems. However, they may have potential application in the small water systems.

6.1. Direct Filtration

Direct filtration has several effective variations; all direct filtration systems include a chemical coagulation step followed by rapid mixing, and all exclude the use of a sedimentation or other clarification step prior to filtration. Following chemical mix, water is filtered through dual or mixed media filters using pressure or gravity units. Pressure units, which are used primarily by small systems (4), have the advantage of not requiring repumping for delivery of the filtrate to the point of use. Gravity units have the advantage of allowing easy visual inspection of the filter medium during and after backwash. In addition to the mode of filtration, variations of direct filtration include filter media type and mixing requirements. In-line filtration (16) is the simplest form of direct filtration and consists of filters preceded by direct influent chemical feed and static mixing. In general, direct filtration usually requires low turbidity raw water and is attractive because of its low cost relative to conventional treatment (16,17). The National Research Council (8) has suggested that small systems not use direct filtration for waters with average turbidities more than 10 NTU or maximum turbidities more than 20 NTU. Two other important considerations are color and algae. Beacuse color removal requires coagulant additions in proportion to the degree of color, an upper limit of color is appropriate for direction filtration. An American Water Works Association Committee report (18) suggests an upper limit of 40 color units. Algae removal must be evaluated on a case by case basis. Direct filtration has demonstrated removal efficiencies of 90–99% for viruses, 50% for *G. lamblia* without coagulation, and 95–99% for *G. lamblia* with coagulation pretreatment (6).

Direct filtration has the disadvantage that it requires advanced operator skill and has high monitoring requirements. Thus, small systems without access to a skilled operator should not use direct filtration, given that waterborne pathogens are acute contaminants and that the disruption of chemical pretreatment can lead to pathogen introduction into the distribution system (4,5,8). The performance of direct filtration is extremely sensitive to the proper management of the coagulation chemistry involved; if the coagulation step is disrupted or improperly executed, the removal efficiencies for turbidity and microbiological contaminants decrease dramatically in a matter of minutes. For this reason, US EPA suggests that only those systems with full-time access to a skilled operator use direct filtration.

6.2. Membrane Processes

The four treatments listed later are membrane processes, which make use of pressure-driven semipermeable membrane filters. Membranes are manufactured in a variety

of configurations, materials, and pore size distributions. The selection of membrane treatment for a particular drinking water application would be determined by a number of factors, such as: targeted material(s) to be removed, source water quality characteristics, treated water quality requirements, membrane pore size, molecular weight cutoff (MWCO), membrane materials, and system treatment configuration (19).

The membrane technologies listed next have been historically employed for specific drinking water uses:

a. Reverse osmosis (RO) treatment in a high pressure mode, in removal of salts from brackish water and seawater.
b. Nanofiltration (NF) also referred to as membrane softening or low pressure RO, in removal of calcium and magnesium ions (hardness) and/or natural organics and disinfection byproducts control.
c. Ultrafiltration (UF), characterized by a wide band of MWCO and pore sizes, for removal of specific dissolved organics (e.g., humic substances, for control of disinfection byproducts in finished water) and for removing particulates.
d. Microfiltration (MF) as with UF utilizing low operating pressures, for removal of particulates including pathogenic cysts (19,20).

Prefiltration and scale-inhibiting chemical addition may be utilized to protect membranes from plugging effects, fouling and/or scaling, and to reduce operational and maintenance costs. For the purpose of meeting the performance criteria under the SWTR and as a safety measure, a disinfectant is commonly applied following membrane treatment to protect distributed water quality.

Stakeholders have requested that US EPA include the following information as part of the listing of these technologies:

a. The degree of operator skill level, which often depends on water quality and amount of pre- and post-treatment required.
b. Higher operator skills are often needed for chemical cleaning of membranes.
c. Test piloting of membrane filtration systems may be required.
d. Monitoring of membrane integrity, as well as alarm and back-up systems, may be required but that state reviewers should have latitude to decide on such requirements.
e. Although the first two listed membrane treatments are absolute barriers to viruses, it should be noted that UF and microfiltration are not, therefore the latter two should not be given credit for viral reductions.
f. No distinction is made in terms of membrane configuration type, for example, spiral bound or other, in this guidance.
g. Regarding other treatment goals, microfiltration will pass all organic compounds in water whereas UF will capture some organics.
h. Because designations of membrane absolute or nominal pore size have often been irregularly specified, causing some confusion in interpreting a membrane's exclusion capability, state reviewers may wish to request specific information from manufacturers or suppliers for particular applications.

The following membrane processes are listed SWTR technologies for all three categories of small public water systems

6.2.1. RO Filtration

RO is a listed technology for all three categories of small public water system. Because of typical RO membrane pore sizes and size exclusion capability (in the metallic ion and

aqueous salt range), RO filtration is effective for removal of cysts, bacteria and viruses (20,21); however, RO produces the most wasted water, at between 25 and 50% of the feed. Disinfection is also recommended to ensure safety of water.

6.2.2. Nanofiltration

NF is a listed technology for all three categories of small public water systems. Because of typical NF membrane pore sizes and size exclusion capability (1 nm range, e.g., organic compounds), NF is effective for removal of cysts, bacteria, and viruses. Disinfection is also recommended to ensure safety of water.

6.2.3. Ultrafiltration

UF is a listed technology for all three categories of small public water systems. Because of typical UF membrane pore sizes and size exclusion capability (0.01 µm, molecular or macromolecular range), UF is effective for absolute removal of *Giardia* cysts and partial removal of bacteria and viruses, and when used in combination with disinfection appears to control these microorganisms in water (22,23). Tests have also shown that filtrate turbidity may be kept consistently at or less than 0.1 NTU (24). Because of the importance of disinfection providing a second barrier to contamination, EPA stresses the need for disinfection in conjunction with membrane treatment.

6.2.4. Microfiltration

MF is a listed technology for all three categories of small public water systems. Because of typical membrane pore sizes and size exclusion (e.g., 0.1–0.2 µm, macromolecular/ microparticle range), is effective for absolute removal of *Giardia* cysts and partial removal of bacteria and viruses, and when used in combination with disinfection appears to control these microorganisms in water (22,23). Tests have also determined that filtrate turbidity may be kept below 0.2 NTU (25), typically at or less than 0.1 NTU (24). Because of the importance of disinfection providing a second barrier to contamination, US EPA stresses the need for disinfection in conjunction with membrane treatment.

6.3. Bag and Cartridge Type Filtration

6.3.1. Bag Filtration

Bag filtration systems remove particles in water by physical screening. If the pore size of the bag filter is small enough, it could also remove parasite (26). In bag filtration systems, raw water passes through a bag-shaped filter in which the particulates are collected allowing treated water to pass to the outside of the bag (27). Bag filters are manufactured by a variety of companies. Bags are available in a variety of material and pore size ratings (typically from 1 to 40 µm). The size of the bag depends on the raw water quality, including the amount of particulate matter and level of turbidity (28). Pretreatment is not required for raw water of good quality. If pretreatment is required, the treatment processes will include sand or multimedia filters, followed by preliminary bag or cartridge filters of 10 µm or larger pore size, and the use of 1–5 µm filters as final filters. Pretreatment will increase particulate removal efficiencies and to extend the life of the filter (27,29). Bag filters are used for raw water with turbidity units from 0.1 to 10 NTU and flow rate between 10 and 50 gpm (29). The bag filters will only last a few hours when turbidity of raw water consistently exceeds 1 NTU.

Bag filters in combination with cartridge filtration systems have been used to remove *G. lamblia* from raw water supply serving small systems (28,30). Bag filters have shown mixed results in the removal of *Cryptosporidium*, with 70–99.9% removal efficiency. Studies of various membranes using beads as surrogates for *Cryptosporidium* oocysts have showed variability in the removal efficiency (31).

Field study using bag filtration has shown poor to excellent removal regarding turbidity. This variability might be because of improper installation of the bag filtration units, leaks or tears in the systems, or raw water quality conditions, or problems with prefilters (27,29). The general trends in field study has indicated that the smaller the pore size, the better the filter efficiency.

Stakeholders emphasized that bag filtration systems have been successfully used in water supply systems across the country. On-site pilot study has been used to determine applicability at individual water systems. The stakeholders also reported two additional factors that can cause variability in bag filter performance. The bag filter must fit the housing, and bag filters from different manufacturer may not be interchangeable. Some bag filters use nominal pore size ratings instead of absolute pore size ratings. Because nominal pore size ratings are the average pore size rather than the largest pore size, particles larger than the nominal pore size may pass through the bag filter.

Stakeholders have also reported that bags may be fragile and that care must be taken during installation of replacements of filters in order to minimize bag tearing. They also noted that monitoring of filter integrity may be necessary, but that State reviewers should have the latitude to decide on such requirements. To further inactivate microorganisms, the final filter effluent would require disinfection to meet the SWTR requirements.

Bag filters have been used successfully in water systems in United States. This is because of the preliminary pilot testing of the process to ensure adequate removal of contaminants. Pilot testing prior to installation of a bag filter is recommended to determine any performance variability factors. Bag filters are best suited for systems in the first two small water supply system size categories (i.e., systems serving up to 3300). Bag filters are listed as a compliance technology for all three system size categories.

6.3.2. Cartridge Filtration

Cartridge filtration removes particles using simple physical screening process. They are different from bag filters regarding materials used and the direction of flow. Small pore size openings prevent passage of contaminants through the cartridge filter (26). Typical cartridge filters are pressure filters with ceramic membranes or glass fiber, or strings wrapped around a filter element, housed in a pressure vessel (33). The pleating results in higher surface area for filtration. Cartridge filters are manufactured and supplied by a variety of companies with different materials (16,28) or pore size ratings (0.3–80 µm). Similar to bag filtration, these units are very compact and do not require much space.

The pore size rating of the cartridge filtration depends on the raw water quality, including the amount of particulate matter and the turbidity level (28). Depending on the quality of the raw water, pretreatment of the raw water using sand or multimedia filter, followed by bag or cartridge filters of 10 µm or larger pore size as preliminary filter, and the use of 1–5 µm filters as final filters are recommended to increase particulate removal efficiencies and to extend the life of the filter (27,29). Cartridge filters can

be used to remove *G. lamblia* (16,28,30). Filtration studies to determine *Cryptosporidium* removal using beads as surrogates showed that cartridge filtration with 2-μm rated units achieved log removals of 3.51 and 3.68 (31).

Stakeholders emphasized that cartridge filters have been successfully used in water systems in the United States. On-site pilot testing was used to determine applicability at individual systems. The stakeholders also identified a factor that causes variability in filter performance. Some products use nominal pore size ratings rather than absolute pore size ratings. Because nominal pore size ratings are the average pore size rather than the largest, particles larger than the nominal pore size may pass through the filter.

Stakeholders have noted that cartridge filter seals are subject to damage, and that the housing material may be improperly specified, resulting in leakage and/or other treatment malfunctions. They also have observed that monitoring of filter integrity may be necessary, but that State reviewers should have the latitude to decide on such requirements. To further inactivate the microorganisms, the final filter effluent would need disinfection to meet the SWTR requirements.

Cartridge filters have been used successfully in water system across the country for more than 10 yr. This may be because of the upfront pilot testing of the process to ensure adequate contaminant removals. Pilot testing prior to installation of a cartridge filter is recommended to ensure adequate performance. Cartridge filters are best suited for water systems in the first two small system size categories (i.e., those serving up to 3300 people). However, cartridge filters are listed as a compliance technology for all three water system size categories.

6.3.3. Backwashable Depth Filtration

Operation of backwashable depth filters is similar to cartridge filters in that water flows radially inward resulting in particle screening. In one system, bundles of fibers (the filter medium) are rotated and compressed during the filtration mode. Monitoring of pressure is used to indicate clogging, which triggers a reverse flow of washwater under pressure. During the backwash cycle the fibers are relaxed, stretched and squeezed to allow for the release of trapped deposits. Studies in Europe have indicated more than 2 log removal of *Cryptosporidium* (32,33). According to National Sanitation Foundation, the backwashable depth filters technology may include a bag filter, cartridge filter, or granular media filter intended to filter uncoagulated water and designed to be backwashed when terminal head loss is attained or turbidity breakthrough occurs (34). Backwashable depth filters are most suitable for treatment of surface waters of high quality. Raw water turbidity may not be an adequate indicator of suitability for this treatment. Particulate matter may consist of incompressible and compressible substances such as algae or other biological matter. Compressible particles may result in frequent filter backwashing. The quantity of water treated prior to backwashing may vary greatly depending on the type of particulate matter present in raw water. National Sanitation Foundation also reported that disinfection is required for destruction of virus for backwashable depth filters, because backwashable depth filters are not designed to remove viruses.

EPA reported that backwashable depth filters, whereas not used and tested extensively in the United States, have similar characteristics as bag and cartridge filters. These filters may be best suited for water systems in the first two small system size

categories (i.e., those serving up to 3300 people). However, backwashable depth filters are listed as a compliance technology for all three small system size categories.

6.4. Summary of Compliance Technologies for the SWTR

Tables 2 and 3 summarize the current listing of small water system compliance technologies for the SWTR for disinfection, and filtration treatments, respectively (2). The filtration and the disinfection treatment tables each are split into parts 1 and 2 to accommodate the information categories presented. The technologies are listed for all three of the subject size categories unless otherwise indicated. Filtration technology plays a very important role in water treatment and produces high-quality drinking water, safe for human consumption by some of the most susceptible populations. Understanding the limitations of various filtration technologies, at a specific point in the conventional water treatment train, will allow the consumers to evaluate individual needs for advanced point of use (POU) treatment applications (35).

7. CASE STUDIES OF SMALL WATER SYSTEMS

7.1. Case Study of Westfir, OR

7.1.1. Background

Westfir is a small community in Lane County and is located about 40 miles southeast of Eugene, OR (7). The current population of city is approx 310. The community was originally established to house workers from a nearby lumber mill. The City was incorporated in 1981 to improve its ability to provide municipal services to the community's residents.

The lumber company built a water supply system for the city in 1946. The water system uses surface water supply and includes chlorination for treatment, a storage reservoir, and a distribution system. Although the original water system provided the city with a sufficient amount of water, it was noted during the late 1970s that the original water treatment system could not consistently meet requirement of the turbidity MCL of the SDWA.

Violation notices issued by the Oregon Drinking Water Program (DWP) and later by the USEPA culminated in the City agreeing to a compliance schedule to address the turbidity MCL violations. This case study describes the actions the City of Westfir took to comply with the turbidity MCL of the SDWA.

7.1.2. Community Response

As in most small communities, Westfir did not have the financial or technical resources to select an appropriate treatment processes and to obtain adequate funding to comply with the compliance schedule. Therefore, the city asked help from the Lane County Housing Authority and Community Services Agency (HACSA) to identify suitable treatment processes and apply for financial assistance. The Rural Community Assistance Corporation also provided funding to Westfir through a small project development grant that enabled the community (with HACSA's assistance) to prepare an engineering report and an application for a Community Development Block Grant (CDBG). No local funds were available to prepare the application for the CDBG.

Table 2
Surface Water Treatment Compliance Technology Table—Disinfection Technologies

Unit technologies	Disinfection byproducts: concerns	Other limitations
Free chlorine	Trihalomethanes, haloacetic acids, aldehydes, inorganic byproducts, others.	Fe and Mn demand, pH and other factors influence dose. DBP (disinfecting byproducts) production should be monitored where precursors occur. Providing adequate CT (concentration–contact time) may be a problem for some supplies. Chlorine gas requires special caution in handling and storage, and operator training.
Ozone	Organic acids, aldehydes, AOC, and others. If bromide present, brominated organics and bromate.	Ozone leaks represent hazard: air monitoring required. Ozone used as primary disinfectant (i.e., no residual protection). Biodegradable organics may affect distributed water quality. Personnel time requirements for system cleaning may be fairly substantial.
Chloramines		Long CT. Requires care in monitoring of ratio of added chlorine to ammonia.
Chlorine dioxide		Storage and handling precautions: exposure to heat, sunlight, or UV light may decrease product strength; spillage would require rapid recovery/sumps, and access to water for cleanup.
On-site oxidant generation	Chlorate (ClO_3), bromate (BrO_3), and chlorinated THMs	Research will determine CT values appropriate for electolyzed salt brine. Other oxidants (other than chlorine) not detected in solution by significant research effort.
Ultraviolet radiation	NA	No disinfectant residual protection for distributed water. Periodic calibration of UV sensors and other special maintenance may be required.

Adapted from ref. 2.

The City was successful in obtaining a 294,000 USD CDBG to upgrade the existing water treatment system. Lane County HACSA entered into contract with City of Westfir to provide assistance for the duration of the project. These services include preparation of

Table 3
Surface Water Treatment Compliance Technology Table—Filtration Technologies

Unit technologies	Removals: log *Giardia* and log virus	Raw water, pretreatment and other water quality issues
Conventional filtration and specific variations on convention	2–3 Log *Giardia* and 1-log virus	Wide range of water quality. DAF more applicable for removing particulate matter that doesn't readily settle: algae, high color, low turbidity (up to 30–50 NTU) and low-density turbidity. Prior to filtration: chemical coagulation, rapid mix, flocculation, sedimentation or flotation (depth clarifiers or roughing filters may replace sedimentation).
Direct filtration	0.5 Log *Giardia* and 1–2 Log viruses and 1.5–2 Log *Giardia* with w/coagulation	Suggested limits: average turbidity 10 NTU; maximum turbidity 20 NTU; 40 color units; algae on a case-by-case basis4. Prior to filtration: chemical coagulation and rapid mixing.
Slow sand filtration	4 Log *Giardia* and 1–6 log viruses	"Schmutzdecke" formation prerequisite. Pretreatment or process modifications required if raw water high in turbidity, color, and/or algae.
DE filtration	Very effective for *Giardia* (2–3 log) and *Cryptosporidium* (up to 6 log); low bacteria and virus removal	Low turbidity, low color water; low organic DBP precursors. Pretreatment may be used to decrease turbidity and DBP precursors, although chemical coagulation is not typically necessary.

Adapted from ref. 2.

the Request for Proposals (REP) for engineering services, development of bid documents and specifications, construction oversight, and grant closeout functions. The involvement of the Lane County HACSA from project inception to completion was a key element to ensure the successful completion of this project within the available funding allotment.

7.1.3. Evaluation of Alternatives

The engineering report submitted with the CDBG application had selected a package pressure filtration system to meet the turbidity requirement. However, this design was not acceptable because of the following reasons:

a. For small community systems, the Oregon DWP favored a treatment system that could be more readily observable visually rather than the proposed closed pressure filters.
b. The proposed pressure filtration system would require regular attendance by certified operators. Experience with similar types of systems in Oregon's rural communities indicated that this will be difficult because of limited financial resources and high rates of operator turnover.

An alternative source of water supply, which is groundwater, was not feasible owing to limited groundwater resources in the area and the potential for natural arsenic contamination from volcanic rock formations. Unable to use a groundwater supply, the

consulting engineer retained by the City proposed a slow sand filter to meet Westfir's requirements. The consultant had prior experience with both small communities and slow sand filter applications. Slow sand filters do not have complex O&M requirements; similarly, they do not have complicated design requirements. During the early 1980s, however, slow sand filters were still a relatively unproven technology. Therefore, the State approved the project contingent on the results of a pilot filter study. The compliance schedule was renegotiated with the US EPA to permit adequate time for the pilot study. The Oregon DWP, which had decided in the early 1980s to encourage the use of alternative and simpler treatment technologies for small communities, assumed an active role in the study. The DWP supplied a pilot apparatus previously used in another study as well as technical assistance and analytical support. The pilot study was conducted during an 8-mo period. The duration of the study ensured that the pilot system was subjected to any potential seasonal fluctuations in water quality, such as temperature, turbidity, color, and suspended solids. The pilot system was monitored daily for temperature, turbidity, filter head loss, and flow. The weather and river conditions were also monitored. Periodically, samples for total and fecal coliform analyses were collected and shipped to the state laboratory in Portland. The filter media utilized in the pilot study was slightly "out-of-spec." However, the engineer decided to use it because abundant supplies were available locally and at a reasonable cost. The results obtained at the end of the pilot study indicated that the proposed system would consistently achieve the turbidity MCL of 1NTU, and construction approval was granted by the Oregon DWP.

7.1.4. Design Criteria

Figures 4 and 5 present plan and cross-sectional diagrams of the installed treatment system (7). The total cost of the treatment system and distribution system improvements was 217,483 USD (1986 USD), exclusive of engineering and grant administration fees.

The main treatment system components consist of the following:

1. The raw water intake consists of two, 2 horsepower, submersible, 100 gal/min pumps at a total dynamic head of 50 ft. The pumps were installed in an infiltration-type wet well located immediately adjacent to the Willamette River.
2. Filtration is provided by two 45 ft^2 slow sand filters designed to operate at 70 gal/d/ft^2. To control costs, the filters were constructed with earth berms and elastomeric membrane liners rather than with reinforced concrete walls and bottoms. The filter underdrain system is made up of 4-in. PVC pipe. The filter bed consists of a 30-in. graded gravel support layer and a 3-ft layer of filter sand. The filter sand media has a uniformity coefficient of 2.32, an effective size of 0.315 mm. A control manhole distributes filtered water either to the chlorine contact tank or during periods of low demand, to the river. An overflow weir inside the control manhole maintains a minimum water level just above the surface of the sand. This prevents accidental dewatering of the filter, which could adversely affect the microbiological population present at the surface of the filter.
3. Filtered water is chlorinated by feeding sodium hypochlorite solution prior to the chlorine contact tank.
4. Two 100 gpm centrifugal pumps were installed to pump treated water to the distribution system. Storage is provided by an existing 200,000 gal redwood reservoir.

In addition to the treatment system project, a portion of the grant funds were used to replace some of the distribution system steel water mains to reduce water loss from leaking mains.
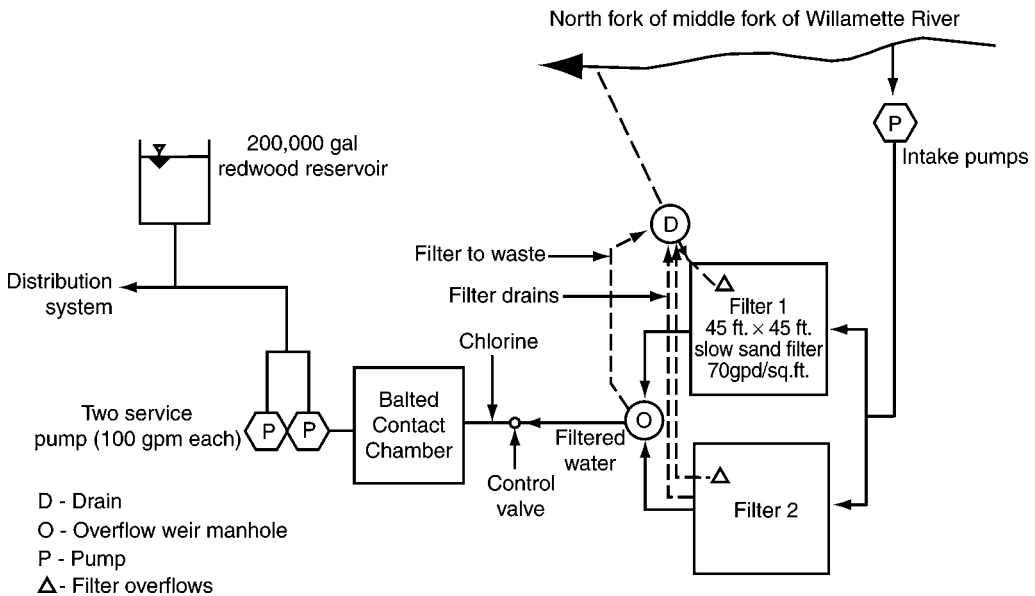
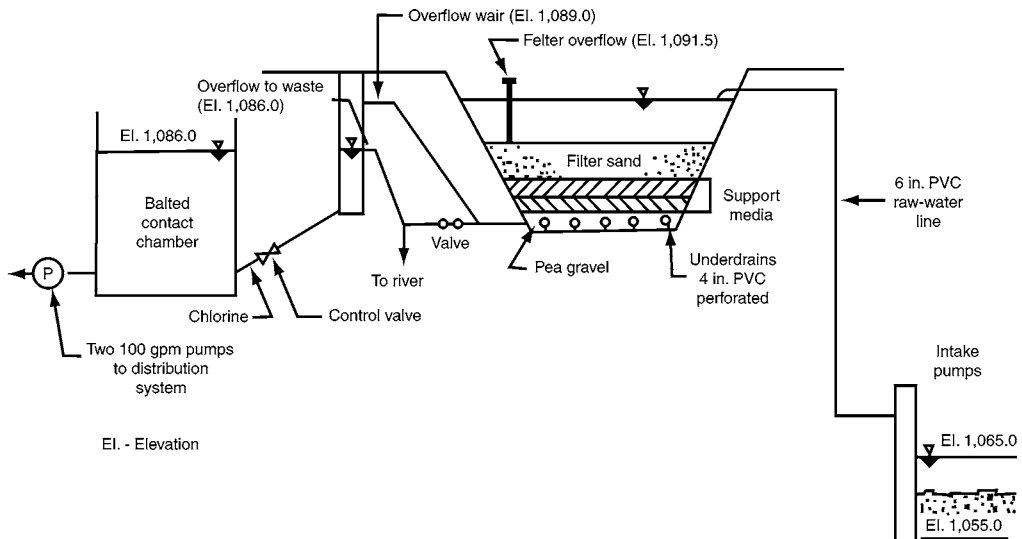**Fig. 4.** Westfir slow sand filtration plant schematic plan (7).

Fig. 5. Westfir slow sand filtration plant schematic profile (7).

7.1.5. Results and Summary

Operation of the water treatment system commenced in November 1986. During the first year of operation, filtered water had slightly higher turbidity levels than the raw water. This was because of the presence of excessive fine particles in the sand media. This problem demonstrated the need to thoroughly wash the sand media prior to installation. Operating requirements have been minimal. Daily equipment and process control checks, including turbidity, chlorine residual, are performed by the operator in

about 60 min. The turbidity of the river was also measured daily. If the river turbidity levels became excessive, the raw water intake pumps were shut down until the turbidity levels subside or the reservoir level became too low. The reservoir had a storage capacity for about 3-d supply of water for the community. Each filter was cleaned once in every 6 mo. One filter remained in service whereas the other one was cleaned. It took about 36 h to drain and dry out the filter. Flat-bladed shovels were used manually to scrape the filter in about 7 h. About 1 in. of sand was removed during the cleaning. The removed sand was not cleaned for reuse. It was disposed of onsite.

The raw water submersible intake pumps were replaced by a single 200 gpm centrifugal pump. The intake screens to the submersible pumps required frequent cleaning because of debris in the river. During periods of high river water, it was not possible to raise the pumps to remove the debris. Pump removal was also a problem because of limited manpower resources.

The requirements of the US EPA compliance schedule were met by the installation of a slow sand filter system. The capital cost for slow sand filter system was similar to package filtration plants. The O&M requirements were significantly less for slow sand filters. Westfir currently charged water system users 20.00 USD/mo to cover O&M expenses, utility charges, and water analyses. The rate was recently increased from 12.50 USD/mo because of the additional testing requirements.

The design features of the Westfir, OR, slow sand filtration system includes the following:

1. Raw water intake pumps— two, 2 horsepower, 100 gpm submersible pumps.
2. Slow sand filters:
   a. Two 45 ft^2 filters.
   b. Hydraulic loading of 70 gpd/ft^2.
   c. Sand media (uniformity coefficient of 2.32 and effective size of 0.315 mm).
3. Sodium hypochlorite chlorination system.
4. Treated water supply pumps—two 100 gpm centrifugal pumps.

7.2. Mockingbird Hill, Arkansas, Case Study

7.2.1. Background

Mockingbird Hill is a very small, unincorporated community is located in Newton County within the Ozark National Forest in northwestern Arkansas. Tourism is the dominant industry in this region (7). By the early 1970s, the community had grown to include approx 90 residences and businesses. The main impediment to development was the limited drinking water supply. In order to foster further development, the residents of Mockingbird Hill decided to establish a centralized water supply system and formed the Mockingbird Hill Water Association (MHWA). They obtained Farmer's Home Administration grant and loan to drill a 3200 ft deep well and constructed a water distribution system. The total project cost was about 1.6 million USD.

Since the beginning of the service, the quality of water produced by the Association's well was a problem. The well water contained high hydrogen sulfide, dissolved and suspended solids, and color. To remove odors from groundwater, high chlorine dosages were routinely applied. The poor water quality of raw water coupled with the high chlorine dosage made water unsuitable for consumption. The residents of Mockingbird Hill

generally used bottled water for drinking purpose until their homes were connected to the water supply system of nearby Deer-Wayton Water Association. The connection was made in 1982, and the MHWA was absorbed into the Deer-Wayton Water Association. However, joining the Deer-Wayton Water Association did not solve Mockingbird Hill's water supply problems. Water quality was improved significantly, but drought conditions in 1983–1985 resulted in serious water shortages for the Deer-Wayton water supply system. This case study describes the steps taken by Mockingbird Hill community to address their water supply problem and evaluates the performance of the water treatment system.

7.2.2. Community Response

The drought-related shortages that occurred after the connection to the Deer-Wayton Water Association supply resulted from a series of shallow wells of less than 200 ft depth that supplied Deer-Wayton's water system. These shortages caused a number of actual shutdowns of the supply from Deer-Wayton to Mockingbird Hill, which convinced numerous residents of Mockingbird Hill that Deer-Wayton was not the solution to their water supply problem. As a result, several of the residents took the lead in re-establishing the MHWA.

The reborn Association hired a consulting engineer to test the water in the original deep well to determine if it could be economically treated to meet the drinking water standards. The Association and the consulting engineer also evaluated the condition of the well pumping system. The MHWA received significant assistance from a circuit rider with the Arkansas Rural Water Association.

When the results of the engineering evaluation were received, the MHWA held a series of public meetings that comprised the Association Board, the consulting engineer, and the County Health Department. As a result of these meetings, it was recommended that the MHWA would rehabilitate the existing well and construct a water treatment system to address the raw water quality problems. The president of MHWA, with the support of several local congressmen and senators, lobbied successfully to secure 600,000 USD in grant funding from Farmer's Home Administration. An additional 350,000 USD of long-term, low-interest loans were obtained. In addition, the MHWA Board, the consulting engineer, and the County Board of Health held discussions to determine the required degree of treatment.

7.2.3. Evaluation of Alternatives

Mockingbird Hill's engineer did not formally evaluate multiple alternative water treatment systems. Instead, the engineer made recommendations based on recent experiences in dealing with low-quality drinking water sources. Onsite testing at Mockingbird Hill well water revealed a 20 mg/L of hydrogen sulfide concentration. The consulting engineer recommended that the hydrogen sulfide be removed using an air stripping tower. In addition, high concentration of iron and manganese were present. The engineer recommended alum coagulation and precipitation and filtration to remove their removal. Because of the very small flow to be treated and the minimum operator requirement, a package-type water treatment system was recommended. The consulting engineer recently had a very positive experience with this proprietary water treatment system.

7.2.4. Selection of Distribution and Treatment Systems

Mockingbird Hill's recommended water treatment system includes:

a. Air stripping system.
b. Degassed water storage.
c. Package precipitation/filtration treatment system.

7.2.5. Design Criteria

The design characteristics of the selected treatment system include the following:

1. Air stripping tower: 100 gpm, 1300 cfm air throughput.
2. Stripped water storage: 13,000 gal.
3. Package precipitation system:
   a. Automatic chemical feed system.
   b. Alum and polymer.
   c. Upflow adsorption clarifier.
   d. Downflow filter, 20 ft^2.
   e. Effluent turbidimeter.

The air stripping system was designed to remove 85% of hydrogen sulfide. The design capacity was 100 gpm, with a design air throughput of 1300 cfm (cubic feet per minute). The air stripping tower, which is about 3 ft in diameter and 10 ft height, is situated on top of a stripped water storage tank. The proprietary skid mounted treatment system incorporates chemical feed and mixing, an upflow adsorption clarifier, and gravity multimedia filtration. The nominal capacity rating by the manufacturer is 100 gpm. However, the rating by the State is 60 gpm, which is based on a filtration rate of 3 gpm/ft^2 instead of 2 gpm/ft^2. Figure 6 depicts the Mockingbird Hill's water treatment system.

7.2.6. Cost Reduction

Cost-reduction efforts seem to have been limited in Mockingbird Hill's attempt to address its water supply problem. This can probably be because of the severity of the water shortage problem and to the technical difficulties encountered in treating Mockingbird Hill's water supply.

7.2.7. Results and Summary

The main elements of Mockingbird Hill's response to solve its drinking water problem are listed below:

a. Effort championed by a concerned citizen.
b. Assistance provided by Arkansas Rural Water Association.
c. All available financial assistance options successfully pursued.
d. Engineer knowledgeable of local water conditions.
e. Effective treatment technologies and equipment selected.

Since start-up, hydrogen sulfide removals averaged 90%. The operator noted that at the present time, alum and polymer were not added to the degassified water. Instead, chlorine is injected into the degassified water as it was pumped from the storage tank to the package treatment system. The chlorine dosage was 4 mg/L. This chlorine dosage resulted in additional removal of hydrogen sulfide and the oxidation of iron and manganese. The insoluble precipitate resulting from the oxidation of iron and manganese was removed
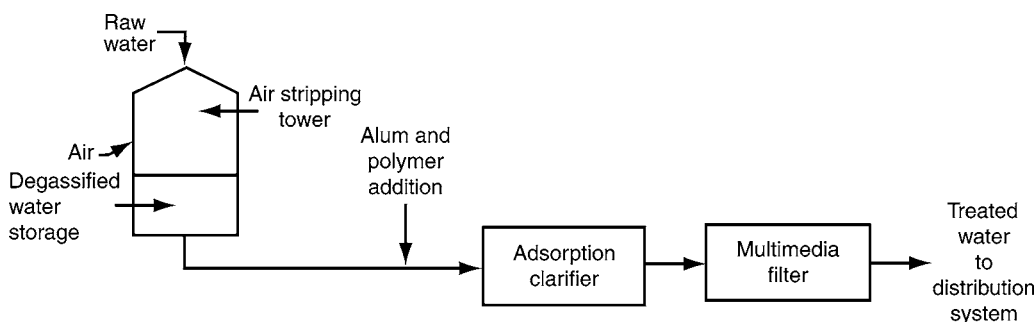
Fig. 6. Plant schematic for Mackingbird Hill Water Association (7).

by sedimentation and filtration in the package treatment plant. An on-line turbidimeter monitored the quality of the treated water. The turbidimeter regulated the application rate of coagulants when used. At preset turbidimeter levels, the package system will either automatically initiate a backwash cycle or shutdown, if excessive turbidity levels are determined after the completion of backwash cycle.

Since the installation of the package treatment system, the service area has been expanded to 165 customers. Nonetheless, the debt service associated with the nongrant funded portion of the capital cost of the treatment system was quite high for the community. The present monthly user charge is 16.25 USD for the first 1000 gal and 2.75 USD for each additional 1000 gal used. The average water used per customer is 3000 gal/mo. In addition to the financial difficulties, radium was detected in Mockingbird Hill's treated water after the treatment system was installed. Although ongoing tests showed that a concentration of radium was less than the threshold levels, this issue has caused a significant concern of the consumers.

8. INTERMITTENT SAND FILTERS FOR WASTEWATER TREATMENT

Other application of sand filter includes the polishing of wastewater treatment plant effluent from septic tanks and lagoons for small communities. This section discusses technology application, process description, O&M requirements, technology limitations and financial considerations.

8.1. Technology Applications

Intermittent sand filters are most often used to provide further treatment of lagoon or septic tank effluent. These filters are ideally suited for populations of less than 1000 people and in which flow is less than 100,000 gpd. These filters can achieve high removals of 5-d biochemical oxygen demand (BOD_5) and total suspended solids removal with effluent concentrations normally in the range of 5–10 mg/L. High levels of nitrification of 90–95% can also be obtained with proper operation. Intermittent sand filters are especially applicable to small communities because of low cost and minimal operator requirements (36).

8.2. Process Descriptions

Intermittent sand filters (Fig. 7) are variations of fixed film biological treatment systems. They consist of two types of processes: single-pass (where wastewater travels through the
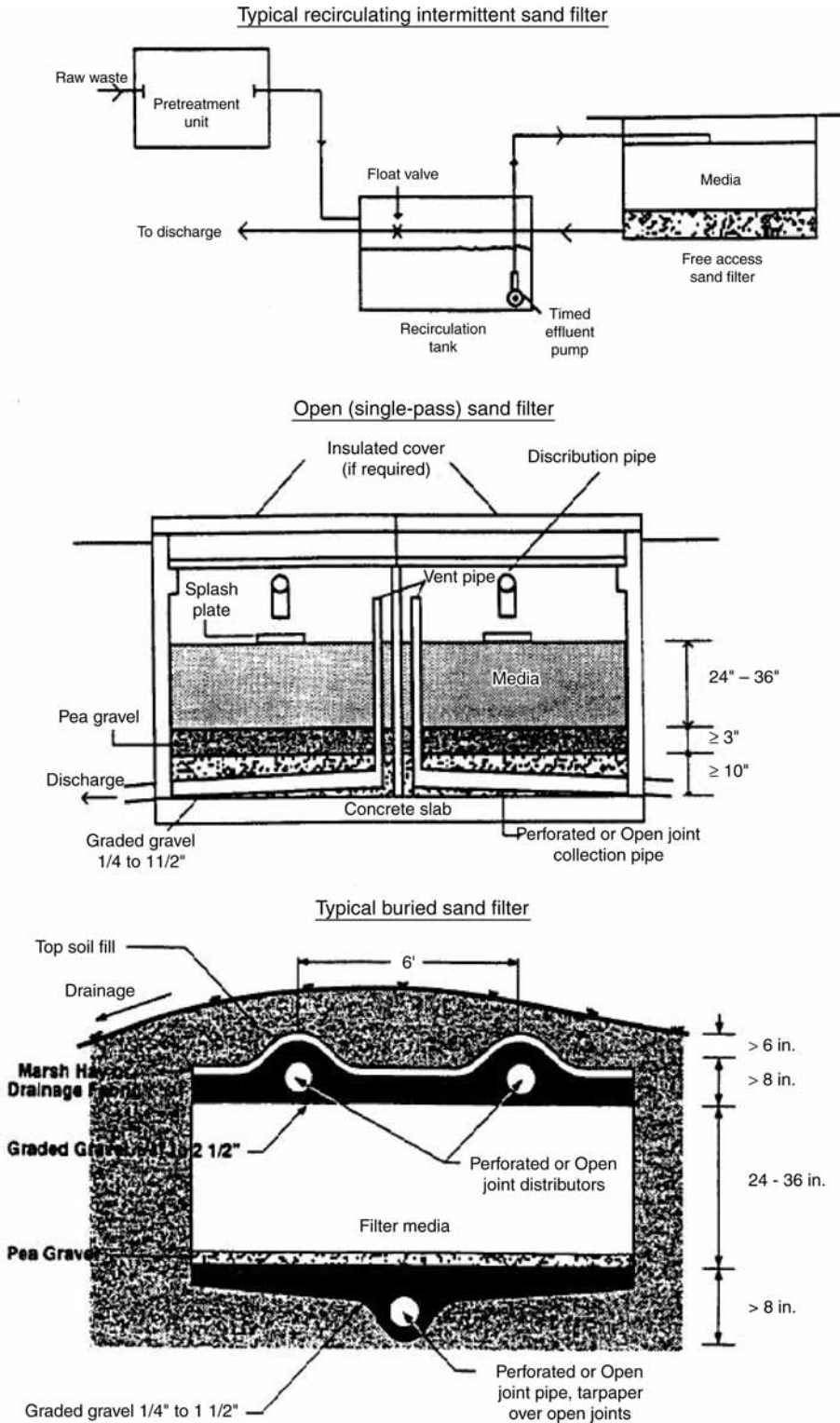
Typical recirculating intermittent sand filter

Open (single-pass) sand filter

Typical buried sand filter

Fig. 7. Schematic showing the three types of intermittent sand filters (36).

filter once) and recirculating (where the wastewater travels through the filter several times). Single-pass filters can be further divided into buried and open types. Recirculating filters are similar in design to the open types except a coarser media is used and a portion of the filtered effluent is returned to the dosing tank and reapplied to the filter.

An open intermittent sand filter consists of a bed of sand, usually 30–36 in. deep, resting on a layer of gravel containing an under drainage system of open joint/perforated pipe. The filter floor (usually earthen) is graded and sloped to provide necessary drainage. Sidewalls extend approx 18 in. above the sand filter surface. The total filter bed area is usually divided into two or more smaller filters. Each individual filter is dosed on an alternating cycle. This allows the filter to drain completely after each dose, which is necessary to maintain aerobic conditions for effective biological treatment.

The recirculating intermittent sand filter uses a recirculation tank in which most of the discharge from the sand filter is returned and mixed with pretreated wastewater to be reapplied to the filter. This system dilutes the wastewater stream being applied to the filter while improving filter performance and decreasing clogging. A recirculating filter has a design hydraulic loading rate of 2–3 gpd/ft^2. Open single-pass filters are operated at rates as high as 10 gpd/ft^2.

8.3. Operation and Maintenance (O&M) Requirements

This section pertains to open and recirculating sand filters because buried filters are not readily accessible. The hydraulic loading to the filters should be checked daily. To maintain aerobic conditions, the filters should drain completely before the next dosing cycle begins. Hydraulically overloaded filters will typically exhibit anaerobic conditions and decreased treatment efficiency and reduced effluent quality. For recirculating filters, a recirculation ratio of 3:1–5:1 should be maintained for proper operation. The dosing interval should be adjusted so that each dose results in about 2–4 in. of wastewater uniformly distributed across the filter.

Maintenance of sand filters includes keeping the filter inlet distribution channels clear of any debris, cleaning or raking the upper layer of the filter bed, and replenishing sand lost from the filter bed. The filter surface should be cleaned whenever the top layer of sand begins to show signs of clogging. Weeds and grasses should not be allowed to grow in the filter. Sand should be replaced periodically to maintain a sand depth in excess of 24 in. Some sludge will be generated whenever the surface of the filter is cleaned. The sludge and sand removed should be properly disposed of in accordance with state regulations.

8.4. Technology Limitations

Intermittent sand filters are easily upset by excessive hydraulic loading. These filters are also unable to handle excessive solids levels in the influent wastewater. Cold weather can have an adverse effect on intermittent sand filters; sometimes, removable covers are installed to prevent freezing condition. Intermittent sand filters have intermediate land requirements, lower than land treatment systems but much more than mechanical treatment plants.

8.5. Financial Considerations

The costs for intermittent sand filter systems are broken down in Table 4 (43) into construction and O&M costs. The capacity of the plants ranges from 10,000 to 100,000 gpd.

Table 4
Intermittent Sand Filters Construction and O&M Cost

Capacity (gpd)	Construction costs (USD)	Annual O&M costs (USD)
10,000	42,000	3500
50,000	200,000	10,000
100,000	450,000	12,500

Note: Costs in 1992 (USD).
Adapted from ref. 36. Use ref. 37 to update the cost to current year.

The construction costs include the following components: concrete, sand, gravel, distribution system, and pumps. They do not include the cost of land, engineering, legal and financing, pretreatment, and disinfection costs. O&M costs include labor, utilities, maintenance materials, and associated chemicals.

8.6. Case Studies

8.6.1. Case Study of Mapleton, OR

8.6.1.1. BACKGROUND

Mapleton is located on the west bank of the Siuslaw River in Lane County, Oregon, approx 10 miles inland from Oregon's Pacific coast. This small community has a population of approx 800, which is located in the Siuslaw National Forest (36).

Mapleton is an unincorporated Village, a region dependent on the timber and timber products industry. The commercial area of Mapleton covers approx 30 acres of area and consists of three residences and approx 16 commercial/industrial establishments. Because of its location on the bank of the Siuslaw River, local topography, and hydrogeology, this area experiences seasonal, very high groundwater levels. This condition excluded the use of onsite wastewater disposal systems by the properties in this area.

Prior to the construction of the Mapleton Sewerage Facility, wastewater treatment and disposal for all commercial establishments and residences includes:

a. Utilized onsite septic systems.
b. Discharged sewage untreated to the soil through cesspools.
c. Discharged directly to the Siuslaw River.

Septic tank systems usually provided an acceptable means of handling wastewater in all but the riverside commercial area. Several buildings in this area had direct discharges to the river, and septic systems in this area were subject to seasonal surface and lateral leakage. In the early 1980s, the severity of Mapleton's sewage disposal problem became apparent to the County Board of Health and to the Oregon Department of Environmental Quality (DEQ). Sanitary surveys of Mapleton's commercial area convinced DEQ and Lane County officials that the situation in Mapleton's commercial area warranted serious attention. To encourage response from Mapleton, a building permit moratorium was imposed on the commercial area until appropriate alternative sewage handling could be provided by the Village.

This case study describes the technical and financial problems Mapleton encountered and discusses how a joint effort by the state, local businesspersons, Lane County, and

Mapleton led to the construction of an innovative and effective wastewater collection and treatment system.

8.6.1.2. COMMUNITY RESPONSE

In an effort to find a solution to this problem, the property owners in the commercial area of Mapleton sought the assistance of a number of agencies. These agencies includes the Rural Communities Assistance Corporation, the Oregon DEQ, the Oregon Rural Communities Assistance Program (ORCAP), and Lane County. ORCAP and DEQ conducted sanitary surveys that indicated that onsite treatment was not suitable in the commercial area and that some form of centralized treatment with offsite disposal would be required for Mapleton.

Since Mapleton was unincorporated, it was recommended that a legal entity would need to be created to make decisions, pursue funding, and ultimately build and operate a centralized wastewater treatment system. The owners of the commercial properties formed the Mapleton Commercial Area Owners' Association (Association). An agreement was reached between Lane County and the Association for the County to sponsor a request for an Oregon Community Block Grant. Once the treatment facility was constructed, the Association will be responsible for O&M of the sewage treatment facilities.

Lane County and ORCAP remained actively involved in the project both throughout the pursuit of funding and the construction of the collection and treatment systems. The Siuslaw Port District, which is a state-established port management agency with authority over a substantial part of the Siuslaw River, provided legal assistance in the formation of the Association and ultimately acted as title holder to the property on which the sewage treatment plant was built to provide the benefits of public rather than private ownership of the property.

The Association was actively involved in all phases of this project. For example, the local bank made both staff time and the bank's physical resources available to the Association during the project. Members of the Association perceived the successful elimination of this problem, will enhance the economic growth for Mapleton.

The first application for block grant funding submitted by Lane County was not successful. With the continued assistance of Lane County, a second application was prepared and submitted. This ultimately resulted in the award of a grant in the amount of 319,000 USD.

8.6.1.3. EVALUATION OF ALTERNATIVES

A consulting firm was hired by Lane County to assess the situation and to recommend possible solutions. The consulting engineer determined that centralized treatment with offsite disposal would only be necessary for the commercial area, with the effluent to be disposed of by land application.

Early in the evaluation process, several important factors were considered:

  a. The limited number of connections made the selection of a treatment system extremely sensitive to capital cost and the availability of state funds.
  b. The isolated location of Mapleton in conjunction with the financial limitations made any system requiring the routine attention of experienced operations personnel unattractive.
  c. Very small wastewater flows are difficult to treat effectively in conventional biological wastewater treatment systems.

As a result of these considerations, the consulting engineer initially recommended the use of a recirculating gravel filter with land disposal of the treated effluent. Oregon requires that all treatment facilities use nonsurface discharge options whenever possible. As the Association and the engineer further pursued the initial proposal, several major impediments to the use of land application became apparent. This includes the following:

   a. Difficulties in obtaining right-of-way for installation of the necessary pipeline to the potential application sites.
   b. Unacceptably high-projected pumping costs because of the significant difference in elevation between the commercial area and the proposed application sites.

These considerations prompted the pursuit of a surface discharge permit from DEQ. In addition to Oregon's general bias against surface water discharges, DEQ had apparently not approved surface water discharges for many recirculating filter systems. As a result, Mapleton was required to evaluate the potential impact of proposed wastewater treatment system on Siuslaw River.

The results of this study in conjunction with review of National Pollutant Discharge Elimination System monitoring data for other Oregon recirculating filters ultimately prompted DEQ to grant a surface water discharge permit to the Association.

8.6.1.4. SELECTION OF COLLECTION AND TREATMENT SYSTEMS

Lane County and the Association ultimately decided to construct a recirculating gravel filter on a site in the middle of the commercial area. In addition, because of the condition of the existing septic systems in the commercial area, new septic tanks and piping were installed for every connection served by the new system. The cost of the collection and treatment systems together was approx 400,000 USD.

8.6.1.5. DESIGN CRITERIA

The main features of the septic/gravity sewer collection system and filter treatment system are presented in Table 5.

8.6.1.5.1. Collection System: New building services, laterals, septic tanks, and mains were installed for the service area. PVC piping was used for branches and mains. The topography of the commercial area allowed the use of a gravity sewer system, with no pumping stations required. Septic tanks installed were of prefabricated concrete construction and ranged in size from 1000 to 3000 gal.

8.6.1.5.2. Treatment System: A two-cell recirculating filter was constructed on a 1.5-acre site located in the commercial area. Each cell is 35 ft wide and 70 ft long and has a pea gravel media depth of 3 ft. Cell construction is bermed earth with concrete retaining walls and a PVC membrane liner. The distribution manifold is constructed of 2-in. perforated PVC pipe; the underdrains are perforated 4-in. PVC pipe. Two recirculation tanks are provided, each consisting of 60 ft of 72-in. diameter reinforced concrete pipe. Two recirculation pump stations are provided; each station consists of one 250 gpm (gallon per minute) at 22 ft total dynamic head submersible pump of 250 gpm flow rate at 22 ft total dynamic head. Effluent is chlorinated using sodium hypochlorite and dechlorinated using sulfur dioxide. Effluent is pumped to the Siuslaw River by a discharge pump station, which consists of two submersible pumps of 100 gpm flow rate at 15 ft total dynamic head. A small chemical feed/control/lab building was also constructed. A schematic of the system is provided in Fig. 8.

Table 5
**Key Design Features of the Selected Collection System and Treatment System, Mapleton, OR**

Collection system
- All new service, laterals, mains; laterals and mains of 6-in. PVC
- Installation of new septic tanks with concrete construction capacities from 1000 to 3000 gal
- Laterals and mains gravity drain to plant

Treatment plant
- Recirculating filter
- Pea gravel media (3–5 mm effective diameter, uniform coefficient <2)
- Two cells, each 35×70 ft. media depth
- Two recirculation tanks; total capacity of 25,000 gal
- 25,000 gpd design capacity

Adapted from ref. 36.
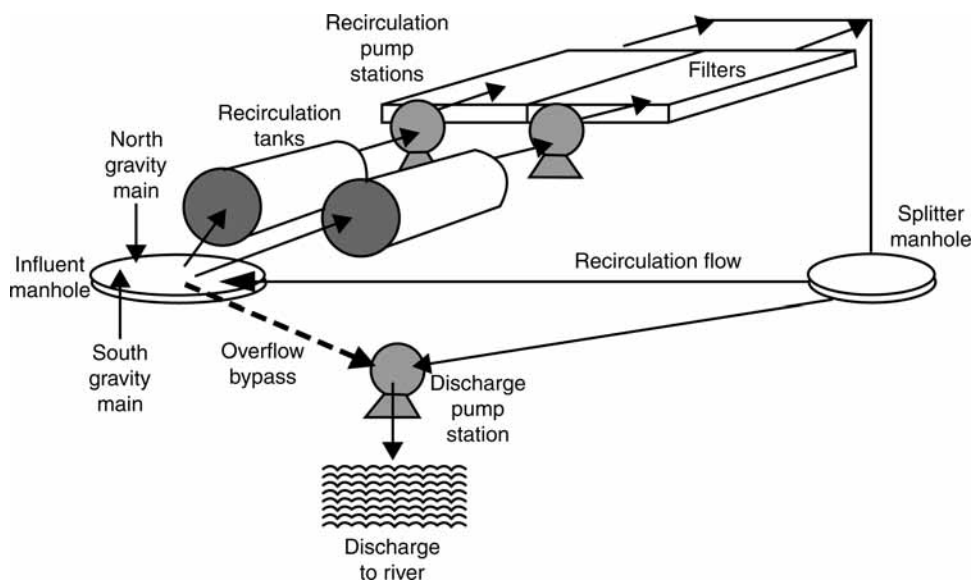
Fig. 8. Plant schematic for Mapleton, Oregon (36).

8.6.1.6. REDUCTION OF COSTS

8.6.1.6.1. *Adoption of a Low Capital/Operating Cost Treatment System:* The selection of a septic/recirculating filter treatment system has provided Mapleton with a cost-effective method for treatment of their wastewater. Installation costs of the gravity sewers were somewhat higher than if Small Diameter Pressure Sewers (SDPS) had been used; however, the elimination of the grinder pumps associated with SDPS provided an offset savings. In addition, maintenance costs of the installed collection system are expected to be significantly less than if a SDPS system had been used.

As in the case of the collection system, the major cost savings associated with the treatment system are operations and maintenance cost rather than capital cost. The

recirculating filters do not require regular solids disposal, which eliminates a major conventional treatment operating cost. It should be noted that to a certain extent, this cost has been picked up directly by the customers in the form of septic tank cleanout costs. Another significant savings is minimum operation cost of the treatment systems. Mapleton has retained a local water distribution system operator on a part-time basis, thereby eliminating the need to hire an operator from outside the area.

8.6.1.6.2. Reliance on Lane County and Other Agencies: Mapleton made full use of the various types of assistance available to it from the State, County, and various community outreach programs. This reduced project costs in two ways. The most obvious was that these agencies provided technical and organizational guidance and services for which Mapleton might otherwise have obtained by contract. Examples of this include both Lane County's hiring of the consulting engineer and the provision of county resources to carry out improvements on the treatment plant access road. Less obvious is the impact that the guidance had in keeping Mapleton on the right track. Had Mapleton's citizens made decisions regarding this project with less guidance, they might have selected inappropriate and more costly design option.

8.6.1.6.3. Limitation of Funding Sources to Impacted Parties: In addition to the block grant, funding for this project was obtained directly from the affected parties. The total local funding was approx 100,000 USD. Mapleton incurred no debt with this project.

The direct funding of this project was to a large extent made possible by the local bank's decision to provide loans at very attractive terms to businesses and residents affected by the project. In addition, the bank paid the connection fees of one or more senior citizens. Monthly sewer fees for businesses are 64 USD/mo and the fees for residences are 20 USD/mo.

8.6.1.7. Results and Summary

The collection and treatment systems have been in service since 1989 and both have generally performed very well. A summary of recent sewage treatment plant performance data is provided in Table 6.

The Village has retained an operator from the local Water District on a part-time basis; this individual has received the additional state training necessary to be type-certified for the Mapleton plant. Relatively minor problems have surfaced because the plant went online. Settlement of the plant site has required the addition of media to eliminate a low area on the level upper surface of the filter. As a result of the successful start-up of the treatment system, DEQ lifted the building moratorium. Several new businesses have opened in the downtown area, and the Florence Regional Library recently opened a branch in the commercial area. Progress is also now being made to restore several commercial area buildings of historical significance.

In conclusion, Mapleton has overcome a number of technical and institutional barriers to solve a serious sewage treatment and disposal problem. This success was achieved through the cooperative effort of the Village and a number of agencies and through thoughtful consideration of Mapleton's resource limitations when evaluating various design alternatives. The key elements and strategies are as follows:

a. Community involvement.
b. Local business championed the project.

Table 6
Performance Summary, Mapleton, OR, Wastewater Treatment Plant

Parameter	BOD$_5$ (mg/L)	TSS (mg/L)
Permit limits	10	10
June 1991	6	7
July 1991	10	6
August 1991	7	7
September 1991	–	–
October 1991	34	7
November 1991	3	5
December 1991	4	10
January 1992	8	6
February 1992	14	8

Adapted from ref. 36.

c. Employment of an engineering firm with experience in small system design.
d. Selection of a low O&M cost treatment alternative.
e. Successful pursuit of state funding.

8.6.2. Case Study of Portville, NY

8.6.2.1. BACKGROUND

The Village of Portville, Cattaraugus County, is located in the southwestern portion of the State of New York, and is approx 7 miles east of Olean on the north bank of the Allegheny River (36). The population of this bedroom community is approx 1100. Prior to 1988, the Village of Portville operated a primary wastewater treatment system consisting of an Imhoff tank and sand sludge drying beds. Because Portville's Imhoff tank provided only primary treatment, the New York State Department of Environmental Conservation (NYDEC) had applied increasing pressure on Portville for more than a decade to upgrade the Village's wastewater treatment facilities. This pressure ultimately took the form of a formal enforcement action against the Village. Finally, on New Year's Day in 1988, the Imhoff tank suffered a major structural failure. As a result, the Village was faced with the need to replace the existing treatment system with the one that would consistently meet secondary treatment standards or it would face further enforcement actions.

This case study describes the challenges encountered by the Village of Portville in upgrading its wastewater treatment plant, and examines how the Village ultimately elected to construct a type of treatment system rarely used in the Northeast, and evaluates how well the Village has been served by that decision.

8.6.2.2. COMMUNITY RESPONSE

The Village government consists of the Mayor and four trustees. Together, these individuals made all the decisions concerning selection of both consulting engineers and a wastewater treatment system. Efforts to involve the general citizenry were somewhat limited; notification of Village residents was limited to those within 500 ft of the proposed plant site (which was the site of the former treatment plant). General community involvement was largely limited to the resolution of a post-startup odor problem.

In response to the NYDEC enforcement action, the Village retained a consulting engineer to design a new treatment plant, to handle the completion and submission of applications for the necessary permits, and to complete various grant and loan applications. As a result of the consulting engineer's success in pursuing available funding, the Village received a grant of approx 1.5 million USD, which is 82.7% of the estimated cost of the treatment system first proposed.

After the receipt of funding approval, the consulting engineer revised the original cost estimates for the proposed treatment system. These revisions had higher than expected capital and operating costs. In conjunction with evaluation of the experiences of other area towns that had recently upgraded their treatment systems, these higher cost estimates convinced the Mayor and the trustees that the Village would not be financially capable of constructing and operating the proposed treatment system. This was a "Catch-22" situation for the Village, in that failure to upgrade the treatment plant would place the Village at risk of further enforcement action by NYDEC, as would failure to operate the proposed treatment plant properly.

In an effort to resolve this conflict, the Village retained a second consulting engineer, who in turn retained a treatment process design engineer with experience in alternative small-scale treatment technologies. This engineer's recommendation was ultimately accepted and constructed. Coincidentally, the capital cost of this second recommended technology was very close to that of the original more conventional recommendation.

NYDEC originally had concerns regarding the Village's revised proposal and did not immediately approve the change. After review of the additional information regarding this technology, NYDEC allowed the Village and its engineers to proceed. The cost of the new facility and attendant equipment was approximately the same as originally estimated for the more conventional plant (1.8 million USD). Funding for the remaining 17.5% of capital costs was met by the Village through long-term loans.

8.6.2.3. Selection of Treatment System

In the early 1980s, the Village inspected portions of the collection system to evaluate the feasibility of reducing infiltration. At that time, rehabilitation was judged to be economically infeasible. Based on this earlier evaluation, the possibility of rehabilitating the collection system was not considered when the need to upgrade treatment capability was addressed in the late 1980s.

The Village's first consulting engineer recommended a rotating biological contactor (RBC) treatment system. The operating cost estimates for this original system convinced the Mayor and trustees that the Village could not carry the debt service necessary to fund the Village's share of the construction cost and at the same time cover the expected annual operations and maintenance costs for the treatment system. Therefore, the Mayor and trustees decided to have a re-evaluation of treatment alternatives.

A second consulting engineering team retained by the Village recommended a recirculating stone filter (RSF) treatment system. This recommendation was made on the basis of the following:

a. This type of system's ability to handle wide ranges of hydraulic loading, which is important because of the high rate of infiltration and inflow experienced by Portville's collection system.
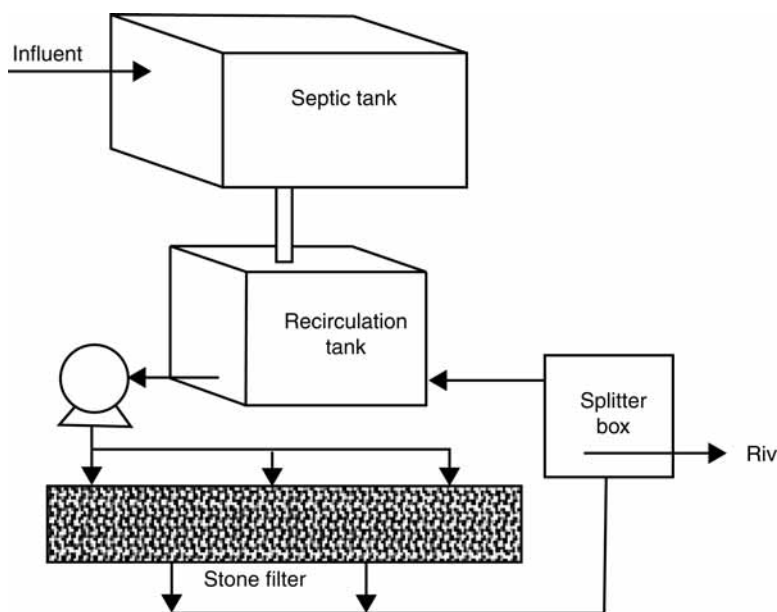b. Its low O&M requirements and costs.

Fig. 9. RSF system schematic (36).

8.6.2.4. DESIGN CRITERIA

The design criteria for the Village of Portville's RSF system are as follows:

a. Design capacity of 400,000 gpd.
b. Septic tank volume of 70,000 gal.
c. Filter area of 54,000 ft.^{2}
d. Media depth of 1.5 ft.
e. Media consists of 1.5–2.5 mm pea gravel.
f. Recirculation by four 970 gpm pumps.

A schematic of the system is shown in Fig. 9.

The RSF design was chosen for its low O&M costs and its ability to treat widely fluctuating flows and waste strengths. The system ultimately constructed by the Village consists of three major components:

1. One 700,000 gal capacity "communal" septic tank.
2. One 28,000 gal recirculation dosing tank (with associated recirculation pumps and controls).
3. One 54,000 ft.^{2} pea gravel media filter. In order to handle septic tank solids.
4. The Village also purchased an all-terrain sludge hauling/application vehicle, constructed a separate septage holding facility, and secured the use of a 30-acre application site.

8.6.2.5. REDUCTION OF COSTS

Capital cost reduction was not significant in Portville's wastewater treatment plant upgrade project. The constructed cost of 1.8 million USD was in fact little high compared with the expected cost for a similarly sized, package extended aeration treatment system. This is because of several factors. First, RSF systems cannot treat raw wastewaters effectively. The solids content of typical raw sanitary wastewater will quickly plug the filter media and significantly reduce the life of the filter. Therefore, it is essential

Table 7
Portville, NY, Wastewater Treatment Plant
Performance Summary

Parameter	BOD_5 (mg/L)	TSS (mg/L)
Influent	85	85
Effluent	6.8	1.7
Removal (%)	92	98

Adapted from ref. 36.

that the raw wastewater receive adequate pretreatment using gravity settling in either septic tanks, Imhoff tanks, or primary settling tanks. For the Portville treatment system, a communal septic tank was constructed to provide the necessary pretreatment and equalization. This 700,000 gal septic tank system increased capital costs substantially.

The Village also made a large investment in the septage storage facility and transport/disposal truck. This capital cost was motivated by both concern regarding disposal of material from the communal septic system and an interest in developing septage handling capability as a revenue-generating operation.

The impetus for selecting the system ultimately constructed was its expected low operating costs. The actual annual operating costs through late 1990 averaged about 1.93 USD/1000 gal of sewage treated, including debt service (which represents more than 50%). Labor costs are somewhat higher than normal for this type of system because the Village employed a full-time operator. Nonlabor, nondebt service operating costs were low, with pumping costs averaging about 0.10 USD/1000 gal. The average resident paid approx 12 USD/mo or 144 USD/yr for sewer charge.

8.6.2.6. RESULTS AND SUMMARY

In general, the selected wastewater treatment system has provided a high quality effluent meeting and the requirements of the National Pollutant Discharge Elimination System permit. Table 7 summarizes the RSF plant performance from January 1989 through August 1990. During that time period, plant effluent BOD_5 averaged about 7 mg/L and effluent TSS averaged about 2 mg/L. The plant has also achieved high degree of nitrification, with effluent ammonia concentrations of less than 1 mg/L.

The plant has also experienced and had to overcome operational difficulties related to high flow, odors, and industrial discharges. Higher than expected the flow rates initially caused difficulties in meeting the filter bed's dosing and resting requirements. The pump supplier modified the recirculation system to allow it to function properly under the entire range of flows being experienced.

Odor control was one of the major community and regulatory concerns. Following startup, odor from the dosing tank has become a problem. The addition of an aeration system to this tank did not provide the expected relief, and the Village was required to install an odor control system.

In June 1991, a local pulp and paper mill significantly changed its production processes. This substantially changed the characteristics of the suspended solids in its wastewater. This change in characteristics resulted in significant amounts of suspended

solids passing through the septic tank to the filter. This in turn resulted in the plugging of the dosing pumps and clogging of the pea gravel filter media. This rendered the filters inoperable. The pulp and paper mill was ordered to cease its discharge to the plant. The mill has since achieved zero discharge. Rehabilitation of the system was carried out by the Village, which is currently attempting to recover the costs from the mill. An overview of both positive and negative aspects of Portville's experience in upgrading its treatment system is listed next:

1. Positive elements
   a. Willingness to step back and change direction.
   b. Selection of an engineering firm with small system experience.
   c. Successful pursuit of funding assistance.
   d. Selection and construction of a treatment technology which under most conditions has easily met its permit requirement.
2. Negative element
   a. Overpurchase of O&M staffing and equipment.
   b. Failure to consider effects of industrial wastewater source.

REFERENCES

1. US Environmental Protection Agency, *National Characteristics of Drinking Water Systems Serving Populations Under 10,000*; EPA 816-R-99-010; US Environmental Protection Agency, 1999.
2. US Environmental Protection Agency, *Small System Compliance Technology List for the Surface Water Treatment Rule and Total Coliform Rule*; EPA-815-R-98-001; US Environmental Protection Agency, 1998.
3. US Environmental Protection Agency, *Technologies and Costs for the Removal of Microbiological Contaminants from Potable Water Supplies,* US Environmental Protection Agency, October, 1988.
4. J. L. Cleasby, Filtration, In: *AWWA, Water Quality and Treatment: A Handbook of Community Water Supplies*, F. W. Pontius, (ed.), 4th ed., McGraw-Hill, Inc. New York, NY, 1990.
5. R. D. Letterman, *Filtration Strategies to Meet the Surface Water Treatment Rule.* American Water Works Association. Denver, Colorado, 1991.
6. US Environmental Protection Agency, *40 CFR Parts 141 and 142. Drinking Water; National Primary Drinking Water Regulations; Filtration, Disinfection; Turbidity, Giardia lamblia, Viruses, Legionella, and Heterotrophic Bacteria; Final Rule. Federal Register*, 27486, V. 54, N. 124, June 29, 1989.
7. US Environmental Protection Agency, *Technologies for Upgrading Existing or Designing New Drinking Water Treatment Facilities*; EPA/625/4-89/023; US Environmental Protection Agency. Cincinnati, Ohio, 1990.
8. National Research Council (NRC), *Safe Water From Every Tap: Improving Water Service to Small Communities.* National Academy Press, Washington, DC, 1997.
9. S. Campbell, B. W. Lykins Jr, J. A. Goodrich, D. Post, and T. Lay, Package plants for small systems: a field study. *J. Am. Water Works Assoc.* **87**, 39–47 (1995).
10. J. L. Cleasby, Source water quality and pre-treatment options for slow sand filters, In: *Slow Sand Filtration*, G. Logsdon, (ed.), American Society of Civil Engineers. New York, NY, 1991.
11. F. A. Brigano, J. P. McFarland, P. E. Shanaghan, and B. Burton, Dual-stage filtration proves cost effective. *J. Am. Water Works Assoc.* **86**, 75–88 (1994).
12. J. B. Horn, D. W. Hendricks, J. M. Scanlan, L. T. Rozelle, and C. Trnka, Removing *Giardia* cysts and other particles from low turbidity waters using dual-stage filtration. *J. Am. Water Works Assoc.* **80**, 68–77 (1988).

13. American Water Works Association, International conference examines flotation technology. *J. Am. Water Works Assoc.* **86**, 26 (1994).

14. G. S. Logsdon, Comparison of some filtration processes appropriate for *Giardia* cyst removal, Presented at the Calgary *Giardia* Conference, Calgary, Alberta, Canada, February 23–25, (1987).

15. J. E. Ongerth and P. E. Hutton, DE filtration to remove *Cryptosporidium. J. Am. Water Works Assoc.* **89**, 39–46 (1997).

16. US EPA, *Very Small Systems Best Available Technology Cost Document*. US Environmental Protection Agency, Washington, DC. 1993.

17. Westerhoff et al., Plant-scale comparison of direct filtration versus conventional treatment of a Lake Erie water. *J. Am. Water Works Assoc.* **72**, 148 (1980).

18. AWWA Committee Report, The status of direct filtration. *J. Am. Water Works Assoc.* **72**, 405 (1980).

19. J. G. Jacangelo, The Development of Membrane Technology. International Report (JR 3). *Water Supply: Review Journal of the International Water Supply Association* **9**(3/4) (1991).

20. J. S. Taylor, S. J. Duranceau, W. M. Barrett, and J. F. Goigel, *Assessment of Potable Water Membrane Applications and Research Needs.* Prepared for AWWA Research Foundation, Denver, Colorado, 1989.

21. US EPA, *Guidance Manual for Compliance with the Filtration and Disinfection Requirements for Public Water Systems Using Surface Water Sources,* US Environmental Protection Agency, Washington, DC. (1989 and 1991).

22. J. G. Jacangelo, S. Adham, and J. M. Lame, *Application of Membrane Filtration Techniques for Compliance With the Surface Water and Groundwater Treatment Rules.* Prepared for AWWA Research Foundation, Denver, Colorado, 1995.

23. J. G. Jacangelo, J. -M. Lame, K. E. Cams, E. W. Cummins, and J. Mallevialle, Low-pressure membrane filtration for removing *Giardia* and microbial indicators. *J. Am. Water Works*. **83**, 97–106 (1991).

24. R. D. Letterman, *Evaluation of Alternative Surface Water Treatment Technologies.* Sponsored by New York State Department of Health, Albany, New York, NY, 1991.

25. V. P. Olivieri, D. Y. Parker, G. A. Willinghan, and J. C. Vickers, Continuous microfiltration of surface water. In: *AWWA Seminar Proceedings: Membrane Technologies in the Water Industry, AWWA Membrane Processes Conference*, Orlando, Florida, FL, 1991.

26. J. A. Goodrich and K. R. Fox, Small system control of cryptosporidium for WQA recertification credit. *Water Conditioning and Purification* **38(2)**, 50–58 (1996).

27. New York State Department of Health Bureau of Public Water Supply Protection, *Alternative Technology Filtration Study;* New York State Department of Health, Albany, NY, 1993.

28. B. Brandt, Remote control used to fight *Giardia*, *J. Am. Water Works Assoc*. **86**, 137–138 (1994).

29. G. G. Smith, *Small Surface Water Systems Alternate Filtration Report;* Minnesota Department of Health, St. Paul, Minnesota, 1994.

30. The Greeley-Polhemus Group, Inc. and Malcolm Pirnie, Inc., *Case Studies Assessing Low-Cost, In-Place Technologies At Small Water Systems;* Prepared for The Association of State Drinking Water Administrators, Washington, DC, 1992.

31. J. A. Goodrich, Cost and performance evaluations of alternate filtration technologies for small systems, In: *Proceedings of the American Water Works Association, Annual Convention*, 1995.

32. K. J. Ives, An evaluation of the effectiveness of the fibrotex filter in removing cryptosporidial oocysts from a surface water supply, In: *Protozoan Parasites and Water*, W. B. Betts, (ed.), University of York, United Kingdom, 1995.

33. H. Bernhardt et al., *Investigations of the Retention Efficiency of Fibrotex Filters for Cryptosporidium Oocysts Applying Low Turbid Waters from a Water Treatment Plant.* Unpublished study by Wahnbacktalsperrenverband Siegburg, Universitat Bonn, and Kalsep Ltd.

34. NSF International, *Draft NSF Equipment Verification Testing Plan: Backwashable Depth Filtration for the Removal of Microbiological and particulate Contaminants;* NSF International, 1998.

35. K. A. Reynolds, Filtration and waterborne microbes. *Water Conditioning Purf.* **47**(4), 32–33 (2005).

36. US EPA, *Small Community Water and Wastewater Treatment;* EPA/625/R-92/010; US Environmental Protection Agency, Washington, DC. 1992.

37. US ACE. Cost Index Systems Manual, US Army Corps of Engineers, Washington DC. Manual No. 1110-2-1304. www.nww.usace.army.mil/cost. (2006).

38. L. K. Wang. Using Air-Flotation and Filtration for Removal of Color, THM Precursors and Giardia Cysts. PB89-158398. US Dept. Commerce, National Technical Information Service, Springfield, VA. (1989).

39. L. K. Wang. Diatomacecus earth precoat filtration. In: *Advanced Physicochemical Treatment Processes.* L. K. Wang, Y. T. Hung and N. K. Shammas. (eds.). Humana Press, Totowa, N.J. p. 155–190 (2006).

Chemical Feeding System

Puangrat Kajitvichyanukul, Yung-Tse Hung,
and Jirapat Ananpattarachai

CONTENTS

1. INTRODUCTION

Generally, in a water treatment plant various number and kinds of chemicals are widely used. The required characteristic of water is the major factor for chemical selection. For example, activated carbon is used for taste and odor control, lime and alum are used for coagulation, chlorine is used for disinfection, and so on. Type of water plant is another factor to consider when choosing specific type of chemicals, for example, sodium hypochlorite in a single well system and gas chlorination in a large conventional treatment plant. List of most chemicals used in water treatment is shown in Table 1. To control the addition of these chemicals to water, chemical feeding systems are necessary. The design of a chemical feed system must consider whether the chemical form is solid, liquid, or gas. Other considerations are the desire for feeding, the physical and chemical characteristics of the chosen chemical, maximum and minimum water flows, and the dependability of the feeding devices.

Figure 1 shows the simple schematic of chemical feeding system which consists of equipment to store the chemical, feed the chemical at controlled dosages, place the chemical(s) in solution or slurry, and feed the solution to the process.

Form of chemicals which is solid, liquid, or gas, is the major consideration to select the chemical feeding systems. The solid form is usually transformed to the solution or slurry form prior to injecting the chemical to the water stream; however, some chemicals are required to feed in a dry form. In either case, solid feeders are usually required. Chemical characteristics, feed rates, and degree of accuracy are essential information to choose the type of feeder. Characteristics of solid chemicals vary significantly and they

Table 1
Chemicals Used in a Water Treatment Plant

	Name	Use
1	Ammonia (anhydrous)	Disinfection
2	Hydroxide ammonium	Disinfection
3	Ammonium sulfate	Disinfection
4	Bromine	Disinfection
5	Chlorine (gas)	Disinfection
6	Chlorine dioxide	Disinfection, oxidation agent
7	Hydrochlorites	
	Calcium hypochlorite (HTH)	Disinfection
	Sodium hypochlorite (household bleach)	Disinfection
8	Ozone	Disinfection
9	Silver nitrate	Disinfection—home units
10	Ultraviolet light	Disinfection
11	Activated carbon	Adsorption material
12	Charcoal (carbon)	Adsorption material
13	Aluminum ammonium sulfate	A metal coagulant, dechlorinator
14	Sulfur dioxide	Dechlorination agent
15	Sodium sulfite	Dechlorination agent
16	Sodium bisulfite	Dechlorination agent
17	Sodium thiosulfate	Dechlorination agent
18	Ion-exchange resins	Water softener media
19	Sodium chloride (salt)	Water softener media
20	Glauconite (greensand)	Water softener media
21	Silica sand	Filter media
22	Anthracite coal	Filter media
23	Aluminum sulfate (alum)	A metal coagulation
24	Ferric sulfate	A metal coagulation
25	Ferrous sulfate	A metal coagulation
26	Ferric chloride	Coagulation
27	Sodium aluminate	Coagulation pH control
28	Aluminum potassium sulfate	Coagulation
29	Calcium oxide (quick lime)	pH control, coagulation
30	Calcium hydroxide (hydrated lime)	pH control, coagulation
31	Clay (bentonite)	Coagulation aid
32	Calcium carbonate	Coagulation aid, pH control
33	Activated silica	Coagulation aid
34	Sodium silicate	Coagulation aid
35	Sodium carbonate (soda ash)	pH control, coagulation
36	Carbondioxide (gas)	pH control
37	Hydrochloric acid	pH control
38	Sodium hydroxide	pH control, corrosion control
39	Sodium bicarbonate ($NaHCO_3$)	pH control
40	Sulfuric acid	pH control
41	Potassium hydroxide	pH control
42	Potassium permanganate	Disinfection, remove color, oxidant,

(Continued)

Table 1 *(Continued)*

	Name	Use
43	Polyelectrolytes	Coagulant aid
44	Polyphospates	
	Calcium polyphosphate	Corrosion control, iron control
	Zinc polyphosphate	Corrosion control, iron control
	Sodium tripolyphosphate	Corrosion control
	Sodium hexapolyphosphate	Corrosion control
45	Sodium fluoride	Fluoridation
46	Sodium fluorosilicate	Fluoridation
47	Fluorosilicic acid	Fluoridation
48	Copper sulfate	Algae control

Adapted from ref. 1–7.
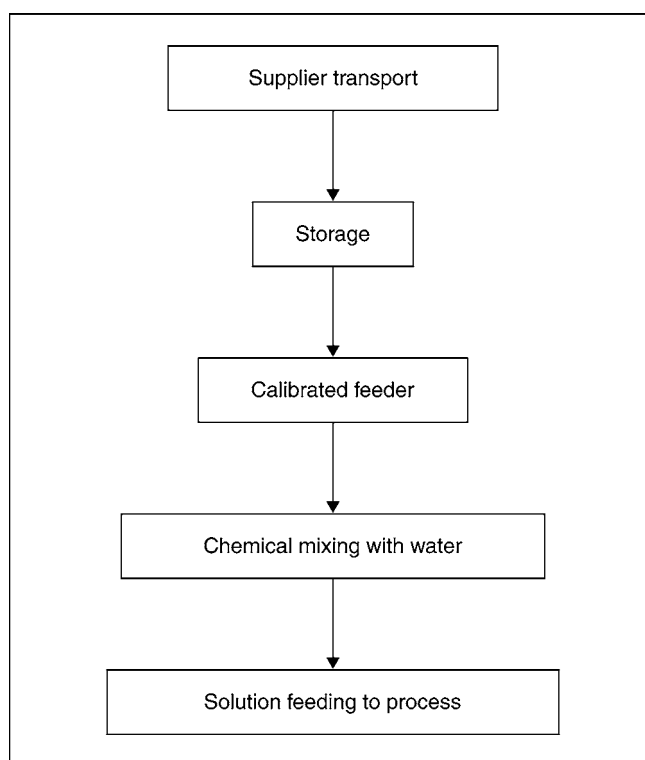
Fig. 1. Chemical feeding system schematic.

are the selection criteria of a feeder that have to be considered carefully. Liquid feeding selection depends mainly on liquid volume and viscosity.

2. CHEMICALS USED IN WATER TREATMENT

Many chemicals are used in the treatment of water. The specific chemicals are used for particular purposes such as coagulants, coagulant aids, disinfecting agents, and

oxidizing agents. The chemicals used for pH adjustment are called general agents such as acids and bases. The details of chemicals frequently used in water treatment are given here (1–8).

2.1. Aluminum Sulfate or Alum

This chemical is frequently used as a coagulant and can be used in either solid or liquid forms. The formula of dry solid form is $Al_2(SO_4)_3 \cdot 14H_2O$. In this dry powder form 14 water molecules are attached to the alum molecule. These water molecules are included in calculating the molecular weight. It is generally defined by its alumina content, expressed as Al_2O_3, which is approx 17%. The apparent density of this solid form is in the region of 1000 kg/m^3. The liquid form is defined by its alumina content, Al_2O_3 which is usually between 8 and 8.5% or 48–49% dry solid equivalent. The aqueous solutions of alum are very acidic with pH in the range of 2.0–3.8 depending on the sulfate/alumina molar ratio. This acidity has to be considered for storage, preparation, and distribution purposes.

In dry alum feeding, noncorrosive dissolving tanks are required. The solution strengths are 0.5 lb of alum to 1 gal of water, or a 6% solution. A minimum detention time of 5 min at the maximum feed rate should be designed. Water meters and mixers are required to control the water/alum mixture ratio. Alum is usually fed by positive displacement metering pumps (8). Dilution water is usually added to alum feed pump discharge line to prevent line plugging and reduce delivery time to the application point. By setting the alum dosage for the maximum flow rate, the output of the pumps can be controlled.

2.2. Ammonia

This chemical is frequently used as a disinfecting agent. Ammonia is usually a liquid-feed gas and is applied with a gas feeder. The formula of ammonia is NH_3. When dissolved in water it forms NH_4OH called ammonium hydroxide or aqua ammonia. Its major use is to form chloramines for disinfection purpose.

2.3. Calcium Hydroxide and Calcium Oxide

Lime is the major chemical used for neutralization, precipitation, coagulation, and carbonate removal. Quicklime and hydrated lime are widely used for this purpose. Quicklime is almost calcium oxide (70–96% CaO). The apparent density varies between 800 and 1200 kg/m^3. Quicklime should not contain less than 90% calcium oxide and insoluble matter content (calcium carbonate, silica) should not be less than 5%.

Quicklime is used in water treatment in powder form. Its advantage over slaked lime area are lower cost, occupies less storage room for an equal quantity of calcium ions. Before use, it has to convert to the hydrated form by adding enough water to quicklime to satisfy its affinity for water. Normally, lime is fed as slurry; thus, the amount of water used in feeding is not necessary to control. However, precautions must be taken when storing and handling because of its caustic nature.

2.4. Carbon Dioxide

This chemical is often used to recarbonate water that has been softened and is saturated with $CaCO_3$, or contains excess $Ca(OH)_2$. It forms a very corrosive water solution containing carbonic acid. Carbon dioxide may be bought as a liquefied gas or produced on site by burning gas or oil.

2.5. Ferric Chloride

Ferric chloride is a chemical used as a coagulant in the coagulation process. The formula of ferric chloride is $FeCl_3$. Ferric chloride has two forms: solid and liquid. The latter form is mostly used in water treatment. The solid form has the appearance of a yellowish-brown deliquescent crystalline mass, with a theoretical formula of $FeCl_3 \cdot 6H_2O$. This form must be kept away from heat because it melts in its water of crystallization at 34°C.

The liquid form contains about 20–40% of pure $FeCl_3$. The aqueous solutions of ferric chloride are rapidly reduced to ferrous chloride, $FeCl_2$, in the presence of iron. When iron salts such as ferric chloride are used for coagulation in soft waters, a small amount of base (such as sodium hydroxide or lime) is needed to neutralize the acidity of this strong acid salt.

2.6. Ferric Sulfate

This chemical is an alternative coagulant to alum in water treatment. It is in a white powder form with a formulation of $Fe_2(SO_4)_3$. It is very soluble in water with an apparent density of 1000 kg/m^3. In aqueous solution, hydrolysis occurs and sulfuric acid forms. In solid form, the dry feeding requirements are similar to those for dry alum. For solution feeding, a water/chemical ratio should be in the range of 2/1–8/1 on a weight basis. The typical ratio is 4:1 with 20 min detention time. The dilution of ferric sulfate solutions to less than 1% can cause hydrolysis and deposition of ferric hydroxide.

2.7. Ferrous Sulfate

This chemical is used as a coagulant in water treatment. It is in the form of green powder with an apparent density of about 900 kg/m^3. The formula of ferrous sulfate is $FeSO_4 \cdot 7H_2O$.

2.8. Phosphate Compounds

Phosphates are generally the limiting nutrient in most growth and can act as a fertilizer on bacterial growth in systems. Polymeta and polyphosphates are good sequestering agents used to tie up hardness and ferrous iron. They, along with zinc, inhibit cathodic reactions in the corrosion cell.

The major phosphate chemical used in water is orthophosphoric acid. Salts of orthophosphoric acid are called orthophosphates. The polyphosphates are widely used in water treatment. By removing water from orthophosphates, polyphosphates are formed. Phosphate compounds used in water treatment include:

1. Orthophosphoric acid (H_3PO_4)
   a. Metaphosphoric acid ($H_3PO_4 \rightarrow H_2O + HPO_3$)
   b. Pyrophosphoric acid ($2H_3PO_4 \rightarrow H_2O + H_4P_2O_7$)
2. The simple orthophosphates:
   a. Monosodium orthophosphate (NaH_2PO_4)
   b. Disodium orthophosphate (Na_2HPO_4)
   c. Trisodium orthophosphate (Na_3PO_4)
   d. Zinc orthophosphate ($ZnHPO_4$)
   e. Zinc sodium orthophosphate ($ZnNaPO_4$)

3. The linear polyphosphates:
   a. Sodium tripoloyphosphate ($Na_5P_3O_{10}$)
   b. Tetra sodium pyrophosphate ($Na_4P_2O_7$)
4. The more complex cyclic polymetaphosphates as a polymer, $(NaPO_3)_X$ with a formula Na_{n+2} P_nO_{3n+1}, for example:
   a. Sodium trimetaphosphate ($Na_5P_3O_{10}[NaPO_3]_3$)
   b. Sodium hexametaphosphate ($Na_8P_6O_{19}[NaPO_3]_6$)

The cyclic metaphosphate can revert to linear polyphosphate and finally to orthophosphate causing the increase of temperature and pH decrease.

2.9. Polymers

This chemical is frequently used in water treatment. It is also called polyelectrolytes. It is mainly used in coagulation and flocculation with various purposes such as to improve coagulation and flocculation (speeding), reduce sludge volume, strengthen, and thicken flocculation. It is also used to improve sludge dewatering and used as the filter aides to lengthen the filter runs.

The polymers can be used in solid (powder) or liquid form. The powdered polymers are suspended at concentrations of 2–10 g/L during a minimum contact time of 30–60 min and fed as suspensions at 0.1–1 g/L (8). This powder form can be kept for less than a week. The liquid polymer can be distributed in the same concentration.

There are three types of polymers:

a. Cationic—has positive charges.
b. Anionic—has negative charges.
c. Nonionic—no charge.

The most often used are the liquid cationics with alum. Doses range from 0.1 to 1 mg/L. A very few plants use a polymer alone as a coagulant.

2.10. Potassium Permanganate

This is a strong oxidizer used to oxidize taste and odor with iron and manganese. It is used in the form of a powdered solid with a formulation of $KMnO_4$. Density is in the range of 800–1200 kg/m³, depending on the extent to which it is compacted. It is poorly soluble as 5 g/L at 20°C after a contact time of 15 min and 30 g/L at 20°C after 1 hr (8). It attacks ferrous metals. Therefore, the containing tanks must be made of a plastic material, or lined with ebonite if made of steel. It should be kept away from glycol, glycerin, and acids to avoid fire.

2.11. Sodium Carbonate

This chemical is generally used to adjust the alkalinity titration in the water treatment. Its formulation is Na_2CO_3 or called soda ash. It is used as a white anhydrous powder, soluble in water, with an apparent density varying between 500 and 700 kg/m³, according to the extent to which it is compacted. Its solubility is rather poor: about 100 g/L at 20°C (8). This chemical is widely used in municipal applications because of superior handling characteristics. The ample dissolver capacity must be provided because of the poor solubility. It is readily decomposed by most acids. Dissolving of soda ash may be hastened by the

Table 2
Properties of Caustic Soda Solution at 60°F

Percentage NaOH	Specific gravity	Density (lbs/gal)	NaOH (lbs/gal)
2	1.023	8.5	0.17
4	1.045	8.71	0.35
6	1.067	8.90	0.53
10	1.112	9.27	0.93
12	1.134	9.45	1.13
14	1.156	9.63	1.35
22	1.245	10.38	2.28
24	1.267	10.56	2.53
26	1.289	10.75	2.79
28	1.310	10.92	3.06
46	1.492	12.44	5.72
48	1.511	12.60	6.04
50	1.530	12.76	6.38

Adapted from ref. 5.

use of warm dissolving water. Mechanical or hydraulic jet mixing should be provided in the dissolver.

2.12. Sodium Chlorite

Sodium chlorite ($NaClO_2$) is used in conjunction with chlorine and hydrochloric acid to form chlorine dioxide. Its solubility is approx 550 g/L at 20°C. It is used in the form of a powdered solid, containing 50–80% $NaOCl_2$, or in liquid form, containing about 24–25% $NaClO_2$ (300 g/L) (8). Sodium chlorite, free from organic matter, will withstand considerable rough handling. It is sensitive to heat, friction, and impact. Both liquid and solid forms must be stored in inert materials: polyvinyl chloride, polyethylene, glass, stoneware, porcelain, or molybdenum stainless steel. The powdered product must not come into contact with reducing material, especially organic materials: fabric, paper, wood, and so on, to reduce the risk of explosion or combustion. Nondiluted sodium chlorite must never be mixed with a concentrated acid. Use of sodium chlorite solutions can minimize these problems.

2.13. Sodium Hydroxide

Liquid sodium hydroxide, or caustic soda, is frequently used for neutralization and for regeneration of anion exchangers. Its formula is NaOH. Caustic soda is used in solid (blocks, flakes) or liquid form (lyes at various concentration). The properties of caustic soda solutions at 60°F are shown in Table 2.

It is usually delivered in bulk shipments and must be transferred to storage. It is often heated and fed by metering pumps as a concentrated solution. Dilution water is usually added after feeding to the pump discharge line. This chemica should be handled with care as when making a solution a considerable amount of heat is generated. Improper handling can lead to dangerous accidents because of its poisonous nature. To avoid spilling, all pumps, valves, and lines should be checked regularly for leaks.

Operators should be properly instructed about precautions related to the safe handling of this chemical.

2.14. Sodium Hypochlorite

This chemical is widely used as a source of free chlorine for disinfection. Its formula is NaClO. This liquid chemical comes in solutions ranging from 3.5% to 16%. The density of sodium hypochlorite solution prepared from chlorine and caustic soda is shown in Table 3. When used, the percentage of available chlorine will decrease with time. It is important to remember that the percentage of sodium hypochlorite is not the same as the percentage of available chlorine.

2.15. Sulfuric Acid

This chemical is used for the regeneration of cation exchangers, pH correction, and the preparation of activated silica. This acid generally used in the water treatment has an average density of 1830 kg/m^3 and contains 92–98% H_2SO_4 by weight. Its viscosity at 20°C is 25 mPa/s (25 centipoises). When diluted with water, a fairly considerable amount of heat is generated, and precautions must be taken. Sulfuric acids diluted in water, attack metals and steels. Special steels or plastic materials should therefore be used. More than a certain degree of concentration, sulfuric acid no longer acts as a strong acid, and may be stored in tanks made of ordinary low-carbon steel, and protected against the entry of damp air. List of chemicals and the suitable handling materials in coagulation, stabilization and corrosion, and softening processes are shown in Tables 4–6. The chemicals used in taste and odor control are listed in Table 7.

3. CHEMICAL STORAGE

Chemical storage is necessary to store and keep the chemicals in a good condition. The advantages of quantity purchase vs the disadvantages of construction cost and chemical deterioration with time should be considered for storage capacity design. The necessary environmental requirements, such as temperature and humidity are the major considerations to be accounted for the storage tank of solid chemicals. Size and slope of feeding lines and their material construction are necessary information for chemical storage design.

In general, requirement of chemical storage is to keep all dry chemicals cool and dry. The equipment used for storing and handling chemicals varies with the type of chemicals used, liquid or dry form of the chemical, quantity of chemicals used, and plant size. Typically, storage requirement may be 15–30 d of use or 150% of the bulk transport capacity, whichever is greater (8). Dust removal equipment should be used at shoveling locations. Bucket elevators, hoppers, and feeders are required for corrosion prevention and safety reasons. Collected chemical dust can be used along with stored chemicals.

3.1. Storage of Powder Chemicals

3.1.1. Unloading Facilities

Generally dry powder chemicals are available in either bagged or bulk form. Bagged chemicals are delivered in loose bags or palletized in trucks or boxcars. They are generally transferred by forklift to storage. Unloading conveyors may be required for loose bags with a long distance between the unloading point and storage area. In some case,

Table 3
Density of Sodium Hypochlorite Solution Prepared
From Chlorine and Caustic Soda

Available chlorine (%)	Sodium hypochlorite (wt %)	Available chlorine (lb/gal)	Specific gravity of finished hypochlorite (at 20°C)
1	1.03	0.083	1.02
2	2.03	0.167	1.04
3	3	0.250	1.05
4	3.94	0.334	1.07
5	4.87	0.417	1.08
5.1	5	0.42	1.08
5.4	5.25	0.45	1.09
5.5	5.32	0.46	1.09
5.7	5.50	0.48	1.09
6	5.76	0.50	1.09
6.3	6	0.52	1.10
6.5	6.21	0.54	1.10
7	6.64	0.58	1.11
7.5	7.07	0.63	1.11
8	7.50	0.67	1.12
8.5	7.93	0.71	1.13
9	8.34	0.75	1.13
9.5	8.76	0.79	1.14
10	9.16	0.83	1.15
10.5	9.56	0.88	1.15
11	10.05	0.92	1.16
11.5	10.36	0.96	1.17
12	10.76	1.00	1.17
12.5	11.14	1.04	1.18
13	11.53	1.08	1.18
13.5	11.91	1.13	1.19
13.6	12	1.13	1.19
14	12.28	1.17	1.20
14.5	12.66	1.21	1.20
15	13.03	1.25	1.21
15.5	13.38	1.29	1.22
16	13.75	1.33	1.22

Adapted from ref. 5.

palletized bag shipments with forklift trucks move the loaded pallets to storage and to the point of use required.

3.1.2. Storage Facilities

Dryness is very important as the chemicals can be absorbed by water. The damped chemicals may become lumpy, viscous, or heavy. For other chemicals, which absorb water less readily, may become sticky from moisture on the surfaces, causing increased arching in hoppers. In addition, moisture can change the density of the chemical resulting in under-feed and reducing the effectiveness of dry chemicals, especially polymers.

Table 4
List of Chemicals in Coagulation Process

Chemical name	Formula	Common or trade name	Suitable handling materials	Available forms
Aluminum sulfate	$Al_2(SO_4)_3 \cdot 14\,H_2O$	Alum, filter alum sulfate of alumina	Dry—iron, steel, solution lead—lined rubber, silicon asphalt, 316 stainless steel	Ivory—colored powder granule lump liquid
Ammonium aluminum sulfate	$Al_2(SO_4)_3 \cdot (NH_4)_2 \cdot SO_4 \cdot 24\,H_2O$	Ammonia alum, crystal alum	Duriron lead rubber silicon iron stoneware	Lump nut pea powdered
Bentonite		Colloidal clay, volclay, wilkinite	Iron, steel	Powder pellet mixed sizes
Ferric chloride (35–45% solution)	$FeCl_3$	"Ferrichlor," chloride of iron	Glass, rubber, stonewater, synthetic resins	Dark brown syrupy liquid
	$FeCl_3 \cdot 6H_2O$	Crystal ferric chloride		Yellow-brown lump
	$FeCl_3$	Anhydrous ferric chloride		Green—black powder
Ferric sulfate	$Fe_2(SO_4)_3 \cdot 9H_2O$	"Ferrifloc," ferrisul	Ceramics, lead, plastic rubber 18—8 stainless steel	Red—brown powder 70—or granule 72
Ferrous sulfate	$FeSO_4 \cdot 7H_2O$	Copperos, green vitriol	Asphalt, concrete lead, tin, wood	Green—crystal granule, lump
Potassium aluminum sulfate	$K_2SO_4 \cdot Al_2(SO_4)_3 \cdot 24H_2O$	Potash alum	Lead, lead—lined rubber, stoneware	Lump, granule, powder
Sodium aluminate	$Na_2O \cdot Al_2O_3$	Soda alum	Iron, plastics, rubber, steel	Brown, powder, liquid (27°Be)
Sodium silicate	$Na_2O \cdot SiO_2$	Water glass	Cast iron, rubber, steel	Opaque, viscous liquid

Adapted from ref. 9.

Table 5
List of Chemicals in Stabilization and Corrosion Control

Chemical name	Formula	Common or trade name	Suitable handling materials	Available forms
Disodium phosphate	$Na_2HPO_4 \cdot 12H_2O$	Basic sodium phosphate, DSP, secondary sodium phosphate	Cast iron, steel	Crystal
Sodium hexametolphosphate	$Na_2(PO_3)_6$	"Calgon" glassy phosphate, vitreous phosphate	Hard rubber, plastics, stainless steel	Crystal, flake, powder
Sodium hydroxide	$NaOH$	Caustic soda, soda lye	Cast iron, rubber, steel	Flake, lump liquid
Sulfuric acid	H_2SO_4	Oil of vitriol, vitriol	Concentrated iron, steel; dilute glass, lead, porcelain, rubber	Solution
Tetrasodium pyrophosphate	$Na_4P_2O_7 \cdot 10H_2O$	Alkaline sodium pyrophosphate TSPP	Cast, iron, steel	White powder
Trisodium phosphate	$Na_3PO_4 \cdot 12H_2O$	Normal sodium phosphate, tertiary sodium phosphate TSP	Cast, iron, steel	Crystal—course medium standard

Adapted from ref. 9.

553

Table 6
List of Chemicals in Softening Process

Chemical name	Formula	Common or trade name	Suitable handling materials	Available forms
Calcium oxide	CaO	Burnt lime, chemical lime, quicklime, unslaked lime	Asphalt, cement, iron, rubber steel	Lump, pebble granule
Sodium carbonate	Na_2CO_3	Soda ash	Iron, rubber, steel	White powder, extra light, light dense
Sodium chloride	$NaCl$	Common salt, salt	Bronze, cement, rubber	Rock, rine
Calcium hydroxide	$Ca(OH)_2$	Hydrated lime, slaked lime	Asphalt, cement, iron, rubber steel	White powder, light dense

Adapted from ref. 9.

Table 7
List of Chemicals in Taste and Odor Control

Chemical name	Formula	Common or trade name	Suitable handling materials	Available forms
Activated carbon	C	"Aqua Nuchor," "Hydrodarco," "Herite"	Dry iron, steel, wet rubber, silicon, iron, stainless steel	Black granules powder
Chlorine	Cl_2	Chlorine gas, liquid chlorine	Dry black iron, copper, steel; wet gas glass, hard rubber, silver	Liquefied gas under pressure lump
Chlorine dioxide	ClO_2	Chlorine dioxide	Plastics, soft rubber (avoid hard rubber)	Yellow–red gas
Copper sulfate	$CuSO_4 \cdot 5H_2O$	Blue vitriol, blue stone	Asphalt, silicon, iron, stainless steel	Crystal lump powder
Ozone	O_3	Ozone	Aluminum, ceramics, glass	Colorless
Potassium permanganate	$KMnO_4$	Purple salt	Iron, steel wool	Purple crystals

Adapted from ref. 9.

In general practice, powder chemicals for medium and large plants are stored in containers, hoppers, or silos. The capacity of those containers is varied with the size of the plant and the length of storage time. In a small plant, the easiest way of storing chemical powders is in bags on a special storage floor. The storage materials are made of metal, reinforced concrete, or polyester reinforced with glass fiber and are round with conical bottoms. In practice, silos, the most frequently used containers, are filled mechanically by air pressure from a supply tank. The chemicals are fluidized and pumped by air pressure and flows into the silo. A belt or conveyor is used for chemical transport in silos. The chemicals are usually carried to the top of the silo, and separated from the air. Dust from

this separation is removed before it is distributed into the atmosphere. The air, which carries or fluidizes the chemicals must have all dust extracted before being returned to the atmosphere. The cloth filters at the top of the silos in a chamber are typically used equipment for this process. Precaution has to be made for handling dust-generating products like lime or activated carbon; the conveyor is not suitable for these chemicals.

The level of the chemicals in the silos can be checked by capacitive system (7). The level can be detected by a membrane that is distorted by the weight of the product that is stored and operated by an electric switch. A freely suspended motor which drives a blade that can rotate in the chemical can be used to monitor the level of the chemical (7). The presence of the chemical sets up an opposing torque, which causes the housing of the drive motor to rotate. In the absence of chemical, the housing returns to its normal position. Piezo-electric devices and strain gauges are also the other means to measure the chemical level in the silos. Because of the complex system of these two methods, they are not widely used. Powder chemicals can also be stored in sealed containers of steel or synthetic rubber. This storage is suitable for small and medium sized plants.

3.2. Storage of Liquid Chemicals

3.2.1. Unloading Facilities

Bulk quantities of liquid chemicals are usually delivered in truck or by rail in boxcars and hopper cars. Bulk unloading facilities usually must be provided at the treatment plant. Rail cars are constructed for top unloading. The required system for this handling includes air supply system and flexible connectors to pneumatically displace the chemical from car. The natural gravity or a truck-mounted pump is usually applied for unloading of liquid chemicals from a tank truck.

3.2.2. Storage Facilities

At small plants, liquid chemicals are usually supplied and stored in drums. At larger plants, they are delivered by road or rail tankers and transferred by gravity, air compressors, or pumps. The storage tanks for these chemicals are made of steel, concrete with or without lining, or plastic material. The corrosive protection is required for the corrosive action of the chemical. Storage tanks have some form of level recorder, ranging from a float and arm system with a pointer moving over a graduated scale, which also transmits the reading for remote display. Liquid storage tanks can be located either at ground level (Fig. 2) or above ground level (Fig. 3). The point of application is the selection criteria in using gravity feed or pressure feed. Normally they stand as a lined concrete leak proof pit, with a capacity at least equal to that of the tank (10).

3.3. Storage of Gaseous Chemicals

3.3.1. Unloading Facilities

In general, most of the gaseous chemicals, including chlorine, ammonia, and sulfur dioxide, are a nonflammable compressed gas. These gaseous chemicals must be packaged in containers that comply with the US Department of Transportation and the US Coast Guard regulations regarding loading, handling, and labeling (10). Various mechanical devices, such as skids, troughs, and upending cradles to facilitate handling of chlorine cylinders are required. When unloading from trucks or platforms, cylinders
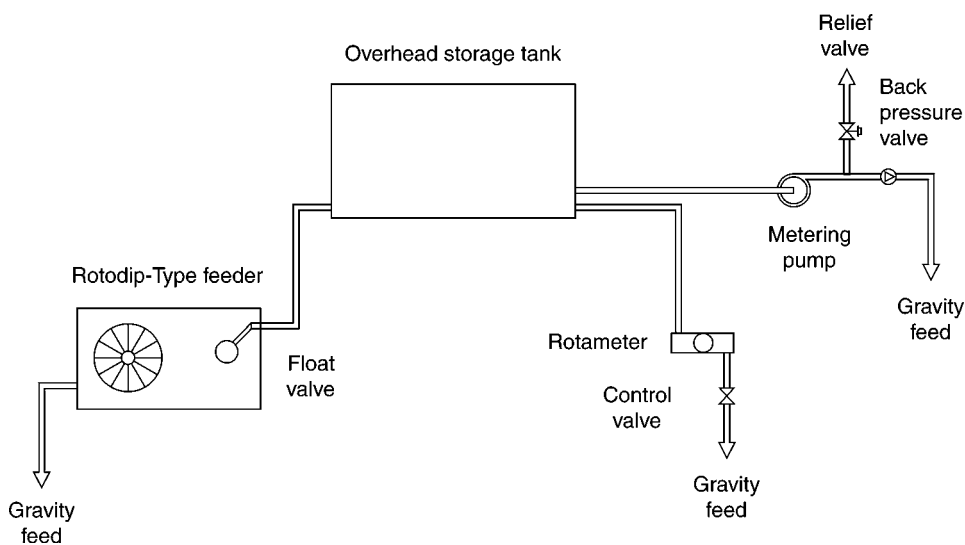
Fig. 2. Alternative liquid feed systems for overhead storage.
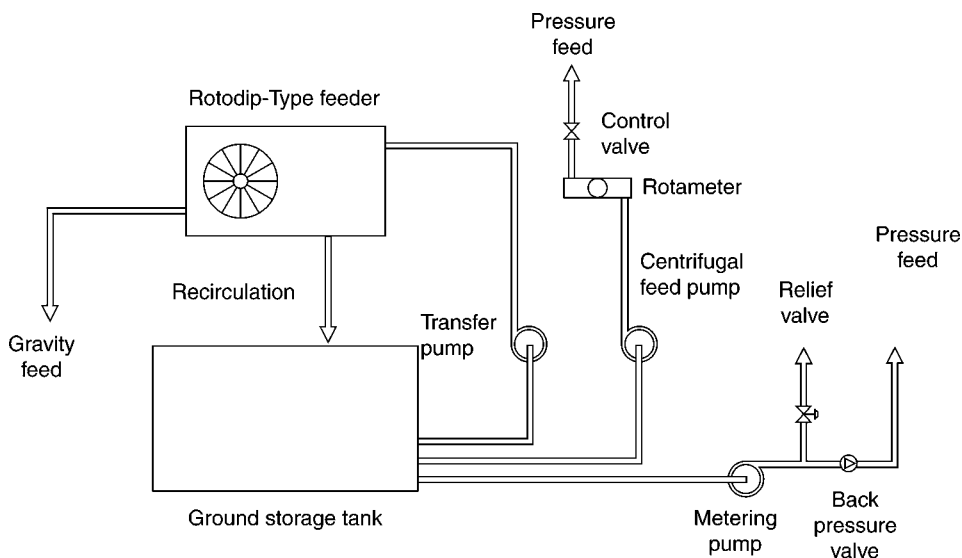
Fig. 3. Alternative liquid feed systems for ground storage.

must not be dropped to ground level. Valve protection hoods in place are required to move those cylinders. These hoods are not designed to hold the weight of cylinders and their contents, and cylinder should never be lifted by this mean (10).

3.3.2. Storage Facilities

Gaseous chemicals, which are normally compressed and stored in the liquid state, include chlorine, sulfur dioxide, and ammonia gas. These liquids are stored in steel cylinders or tanks housed in special premises built and fitted as required by law. Among the gaseous chemicals, chlorine is the most widely used chemical. The precaution of handling
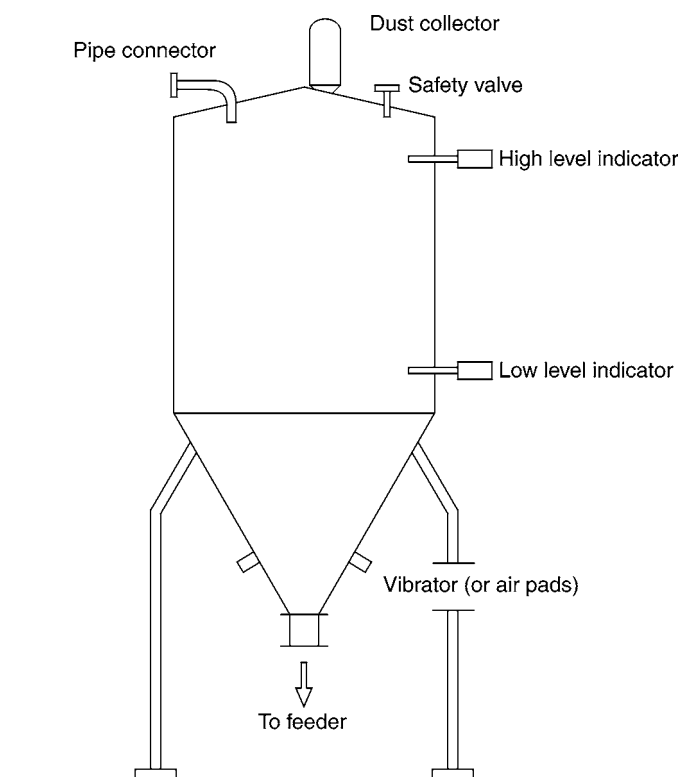
Fig. 4. Typical bulk storage tank.

chlorine has to be taken. All storage premises must be equipped with reliable leak detectors. To deal with chlorine leaks, the neutralizing plant is required. The chlorinated air to be neutralized is extracted by a fan and then expelled into the bottom of a tower in which a backflow of neutralizing solution trickles across contact rings. The neutralized solutions include soda lyes alone or together with sodium hyposulfite. A leak of chlorine gas from a storage tank can continue, if enough heat penetrates into the tank. When leaking out, the pressurized gas expands, the temperature drops and this tends to reduce the leak.

3.4. Storage Facility Requirements

3.4.1. Bulk Storage

A typical bulk storage tank or bin for dry chemicals is shown in Fig. 4. The general requirements for the bulk storage are as follows (10):

- Dust collectors should be provided on manually and pneumatically filled bins.
- Material of construction and the required slope on the bin outlet vary with type of chemical stored. Some dry chemicals such as lime must be stored in airtight bins to keep moisture out.
- Bulk storage bins should have a discharge bin gate so feeding equipment can be isolated for servicing. The bin gate should be followed by a flexible connection and a transition chute or hopper, which acts as a conditioning chamber over the feeder.
- Liquid storage tanks should be sized according to maximum feed rate, shipping time required, and quantity of shipment.

- Total storage capacity should be 1.5 times the largest anticipated shipment, and should provide at least a 10 d to 2 wk supply of the chemical at the design average dose.
- For outdoor tanks, insulating or heating must be provided to prevent crystallization. Storage tanks for some liquids, such as liquid caustic soda, should be provided with an air vent for gravity flow.

3.4.2. Bag and Drum Storage

The general requirement for the bulk storage are as follows (10):

- Bags or drums should be stored in a dry, cool, and low humidity area.
- Bags or drums loaded hoppers should have storage capacity for 8 h at the nominal maximum feed rate.
- Proper chemical rotation, i.e., first in, and first out should be provided.

3.4.3. Cylinder and Ton Container Storage

The general requirements for the cylinder and ton container storage are as follows (10):

- Cylinders should not be permitted to stand unsupported whether in storage or in use. They should be chained to a fixed wall or support.
- Ton containers should be stored horizontally, slightly elevated from ground or floor level, and blocked to prevent rolling.
- Ton containers should not be stacked or racked more than one high unless special provision is made for easy access and removal.
- Chlorine cylinders and containers should be protected from impact, and handling should be kept to a minimum.
- Full and empty cylinders and ton containers should be stored separately.
- Storage areas should be clean, cool, well ventilated, and protected from corrosive vapors and continuous dampness.
- Cylinders and ton containers stored indoors should be in a fire-resistant building, away from heat sources, flammable substances, and other compressed gases. Subsurface storage areas should be avoided, especially for chlorine and sulfur dioxide.
- Cylinders and ton containers stored outdoors should be shielded from direct sunlight and protected from accumulation of rain, ice, and snow.
- All storage, handling, and use areas should be of such design that personnel can quickly escape in emergencies. It is generally desirable to provide at least two ways to exit. Doors should open out and lead to outside platforms, fire escapes, or other unobstructed areas.

4. CHEMICAL PREPARATION OF SOLUTIONS AND SUSPENSIONS

There are many ways to prepare chemicals for the feeding system. In some cases, such as the regeneration of ion-exchange resins or the preparation of activated silica, the chemicals (sulfuric or hydrochloric acid, soda lyes, sodium silicate) are dosed directly in concentrated form and then diluted to the required concentration. In other cases, the chemicals are used in the form of diluted solutions or suspensions prepared from concentrated solutions or solid products. In general, there are three ways to prepare the chemicals which are, preparation of diluted solutions from concentrated solutions, preparation of diluted solutions from solid products, and preparation of suspension.

4.1. Preparation of Dilute Solutions from Concentrated Solutions

Method in preparation of diluted solutions from concentrated solutions is shown in Fig. 5. The concentrated solution, stored in the tank, is pumped to a measuring tank.
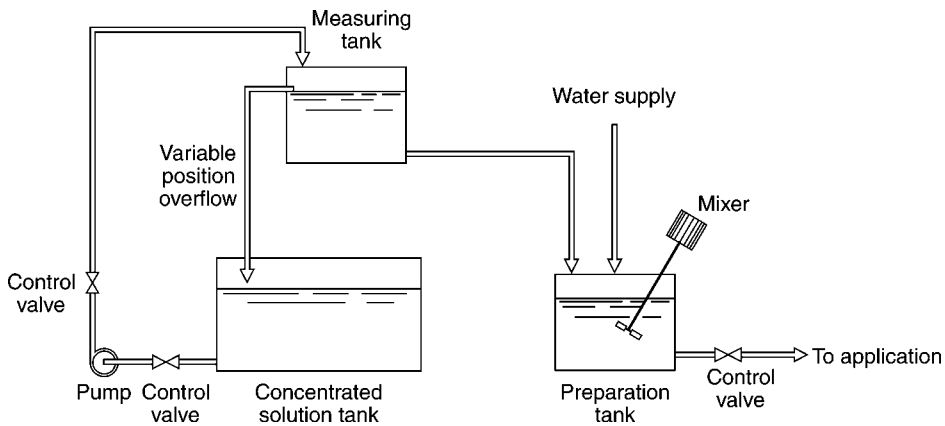
Fig. 5. Preparation of dilute solutions from concentrated solutions.
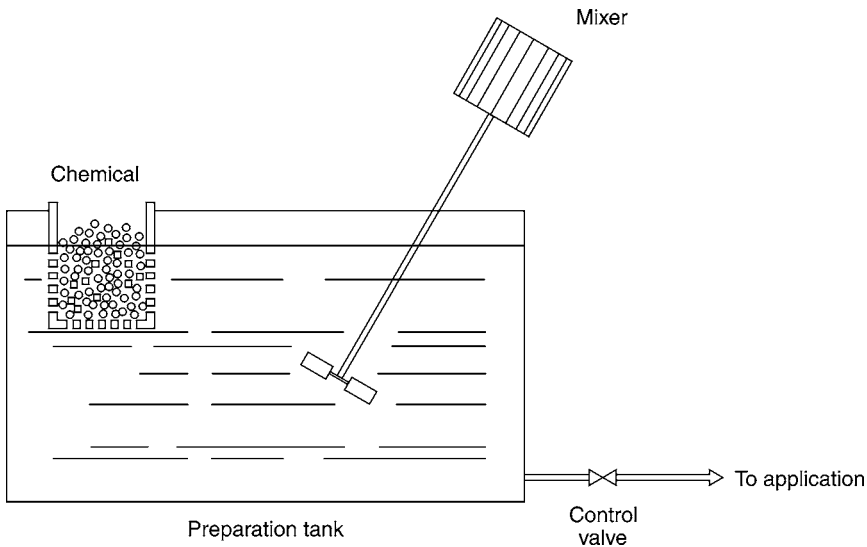
Fig. 6. Preparation of dilute solutions from immersed solid products.

This measuring tank may have a control device to keep the required level of the solution. This can be done either by a variable-position overflow or the level-detecting device. The variable-position overflow will return the liquid to the storage tank when excess and the level-detecting device will stop the pump automatically when the required level is reached. The concentrated solution is then poured into tank and diluted to the required concentration.

4.2. Preparation of Dilute Solutions from Solid Products

When the chemical is in the form of solid products, the equipment as shown in Fig. 6 is used. The chemical is placed in a perforated basket immersed in tank and dissolves gradually in the water. The tank is equipped with agitator for uniform mixing after the
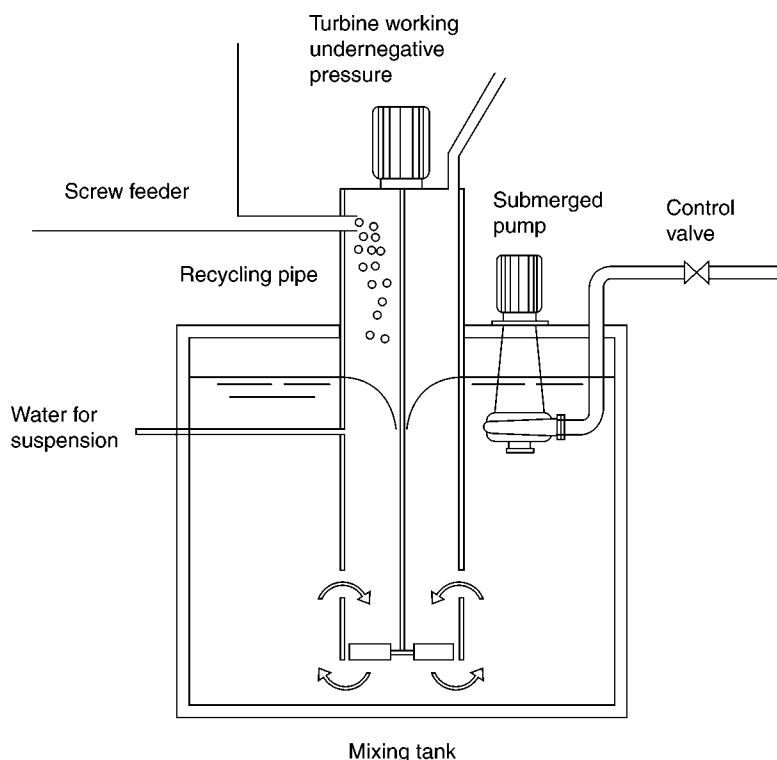
Fig. 7. Mixing tank for preparing solutions and suspensions.

chemical has dissolved. The stirring by compressed air is used for the large treatment plants. For the small treatment plants, the chemical can be directly fed into the tank from bags.

4.3. Preparation of Suspension

In this process, the chemical is held in suspension by a slow mixer in the preparation tank, which is equipped with antivortex partitions. This method is used to prepare milk-of-lime from slaked lime. The required concentration is the parameter, which indicates the time required to slake quicklime and introduce it into suspension. Mixing tank, shown in Fig. 7, is used to dissolve chemicals such as aluminum sulfate, sodium bicarbonate, and polyelectrolytes and to put difficult products such as powdered activated carbon and lime into suspension.

5. CHEMICAL FEEDING SYSTEM

There are three chemical feeding systems: dry feeders, solution feeders, and gas feeders (10). Each type of feeder should have one or more means to adjust the chemical feed rate or dosage easily. The adjustment(s) may be manual or flow pacing and must be accurate, repeatable, and easy to change. They should also provide the broadest possible adjustment span from minimum to maximum feed rate. Types and uses of chemical feeders are shown in Table 8. Troubleshooting guide is provided in Table 9.

Table 8
Types and Uses of Chemical Feeders

Type of Feeder	Use
Dry feeder	
Volumetric	
Oscillating plate	Any material, granules, or powder
Oscillating throat (universal)	Any material, any particle, or size
Rotating disc	Most materials including NaF, granules, or powder
Rotating cylinder (star)	Any material, granules, or powder
Screw	Dry, free flowing material, powder, or granular
Ribbon	Dry, free flowing material, powder, granular, or lumps
Gravimetric	
Continuous-belt and scale	Dry, free flowing, granular material, or floodable material
Loss in weight	Most materials, powder, granular or lumps
Solution feeder	
Nonpositive displacement	
Decanter (lowering pipe)	Most solutions or light slurries
Orifice	Most solutions
Rotameter (calibrated valve)	Clear solutions
Loss in weight (tank with control valve)	Most solution
Positive displacement	
Rotating dipper	Most solution or slurries
Proportioning pump	
Diaphragm	Most solutions, special unit for 5% slurries
Piston	Most solutions, light slurries
Gas feeders	
Solution feed	Chlorine
	Ammonia
	Sulfur dioxide
	Carbon dioxide
Direct feed	Chlorine
	Ammonia
	Carbon dioxide

Adapted from ref. 10.

5.1. Dry Feeders

In general, a dry feed installation consists of a storage bin and/or hopper, a feeder, and a dissolver tank as shown in Fig. 8. Most dry feeders are of the belt, grooved disc, screw, or oscillating plate type. The feeding device (belt, screw, disc, and so on) is usually driven by an electric motor. The powder chemicals can be measured and distributed in dry form by either volumetric or gravimetric feeders.

5.1.1. Volumetric Dry Feeders

Volumetric dry feeders are feasible system when low initial cost and low feed rates are required. These feeders provide a constant amount of chemicals. This type of feeder

Table 9
Troubleshooting Guide

Indicators/Observations	Probable cause	Check or monitor	Solutions
Cake or filtrate solids decreases	Improper chemical dosage (assuming no mechanical problem in dewatering device)	Test for proper dosage (Buchner Funnel test, filter leaf test, or jar test)	Correct dosage according to test results
	Mechanical failure in feed system	Visual inspection	Repair failure
Air slaking occurring during storage of quicklime	Adsorption of moisture from atmosphere when humidity is high	Humidity, storage facility not air-tight	Make storage facilities air-tight, and do not convey pneumatically
Feed pump suction or discharge line clogged	Chemical deposits	Visual inspection Inspect check valves	Provide sufficient dilution water
Grit conveyor or slaker inoperable	Foreign material in the conveyor	Broken shear pin	Replace shear pin and remove foreign material from grit conveyor
Paddle drive on slaker is overloaded	Lime paste too thick	Visual inspection	Adjust compression on the spring between gear reducer and water control valve to alter the consistency of the paste
	Grit or foreign matter interfering with paddle action	Visual inspection	Remove grit or foreign materials or use a better grade of lime
Lime deposits in lime slurry feed lines	Velocity too low	Check velocity in pipelines	Maintain high slurry velocity by use of a return line to the slurry holding tank. Better yet, the slurry should be transported in troughs with removable covers
	Inadequate mixing	Inspect mixing in slurry tank	Provide adequate mixing in slurry tank

Problem	Cause	Check	Solution
Incomplete slaking of quicklime	Too much water is being added	Hydrate particles coarse due to rapid formation of a coating	Reduce quantity of water added to quicklime (ratio to weight of water to lime should be 3/1–5/1 depending on lime and slaker)
"Burning" during quicklime slaking	Insufficient water being added, resulting in excessive reaction temperatures	Some particles left unhydrated after slaking	Add sufficient water for slaking
Chemical feed line ruptures	Positive displacement pump has been started against a closed valve or plugged line	Valves and line	Open valve in feed line before pump is started. Be sure that line is open. A good procedure is to start flow of dilution water first
Chemical concentration changes without varying setting	New load of chemical with different moisture content, density, or chemical content	Analyze moisture content, density, chemical concentration	Recalibrated and adjust feeder accordingly
High turbidity in the settling tank effluent	Improper chemical dosage	Jar test	Correct dosage according to results of jar test
	Mechanical failure in feed system	Visual inspection	Repair Failure in feed system

Adapted from refs. 10 and 11.

563
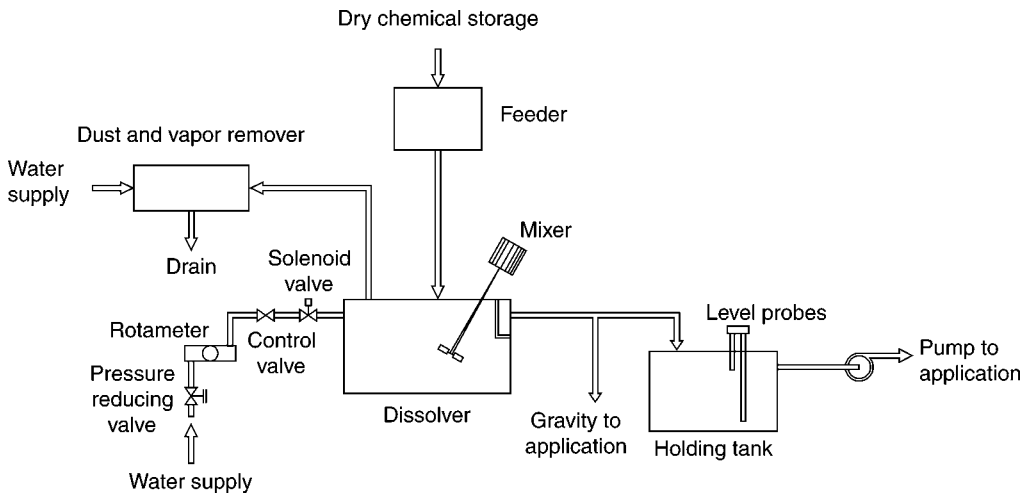
Fig. 8. Typical dry feed system.

must be calibrated by trial and error and readjusted periodically if the density of material changes. In operation, the chemical falls by gravity into the cavity and is enclosed and separated from the hopper's feed. The rate at which the cavity moves and is discharged, together with the cavity size, governs the amount of chemical fed. Most types of volumetric feeders are in the positive displacement category. In addition, the rotating screw, disc, anger, and rotary vane types are also used.

Rotary paddle feeder or rotary vane feeder is used in water treatment plants in which great accuracy is not necessary (7). The vane is controlled by a time-contact or a variable-speed motor. This rotary paddle feeder is especially effective for fine materials that tend to flood. The paddle or vane is located beneath the hopper discharge with variable feed by means of a sliding gate and/or variable speed drive. The feed rate is adjusted by the variable speed drive on the vane shaft. A variant of the rotary paddle feeder is the pocket feeder, also called the star or revolving door feeder, in which the paddle is tightly housed to permit delivery against vacuum or pressure.

Grooved disc feeder (8) provides higher accuracy in chemical feeding than the rotary vane. It is designed to distribute standard chemicals such as aluminum sulfate, lime, calcium, or sodium carbonate. This feeder consists of a grooved horizontal disc, which meters the chemical addition. The disc rotates and the grooves are filled as they pass under the storage hopper, are struck off level, and then a stationary plow removes the material from the groove for metering. The feed rate is varied by changing the speed of disc rotation or by changing the groove size. Typically, these feeders are used for applications requiring small feed rates of dry material.

Anger-type feeder (7) is frequently used to distribute most powdered chemicals including those in very fine powder form. The dry powders can be dosed with reasonable accuracy, provided the capacity of the hopper and the method of feed are clearly defined. The feed hopper may be fitted with a vibrator or an oscillating system, the frequency or amplitude of which can be adjusted. The flow rate is varied either by directly adjusting the mechanical speed variation, which controls the speed of rotation of the
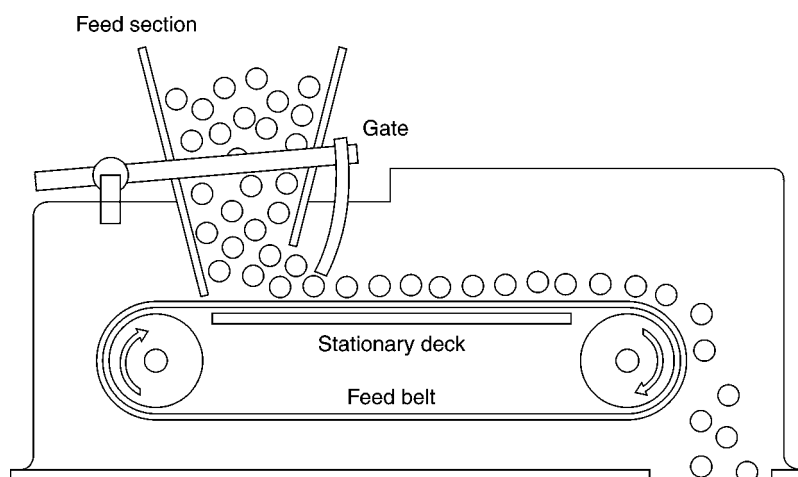
Fig. 9. Volumetric belt-type feeder.

dosing auger. Variable speed motor is another way to adjust the flow rate. The speed of motor for this system is controlled by the flow of water to be treated. The flow rate of this auger-type feeder can be varied from a few liters to a few cubic meters per hour.

Volumetric belt feeder uses a continuous belt of specific width moving from under the hopper to the dissolving tank as shown in Fig. 9. The material falls on the feed belt from the hopper and passes beneath a vertical gate. For a given belt speed, the position of the gate determines the volume of material passing through the feeder.

5.1.2. Gravimetric Dry Feeders

A gravimetric dry feeder has a built-in control system to maintain a constant feed weight. The belt-type gravimetric feeder is the conventional type of gravimetric dry feeder. The feeder consists of a belt fed by a hopper. Its speed is controlled by the flow of water to be treated. For manual feed systems, an operator dosage adjustment is provided as part of this gravimetric control system. The feed belt is weighed continuously. A weighing device under the belt checks whether the weight of chemical corresponds to the product—flow of water to be treated multiplied by chemical dosing rate displayed. This method establishes automatic internal control of gate position to maintain a constant belt weight for a given dosage setting. If there is a deviation, the height of the layer is automatically corrected. Belt-type gravimetric feeders have a wide capacity range and usually can be sized for any use in a wastewater treatment plant. Belt-type gravimetric feeders use a basic belt feeder with a weighing and control system. Feed rates can be changed by adjusting the weight per foot of belt, the belt speed, or both. There are two types of gravimetric belt-type feeders, the pivoted belt type and the rigid belt type.

The pivoted belt feeder consists of a feed hopper, an endless traveling belt mounted on a pivoted frame, an adjustable weight which counterbalances the load on the belt, and a means of continuously and automatically adjusting the feed of material to the belt as shown in Fig. 10. Dry chemical flow to the feeder can be controlled by a gate placed between the feed hopper and the belt or by controlling the amplitude of vibration in a vibrating deck placed between the feed hopper and the belt.
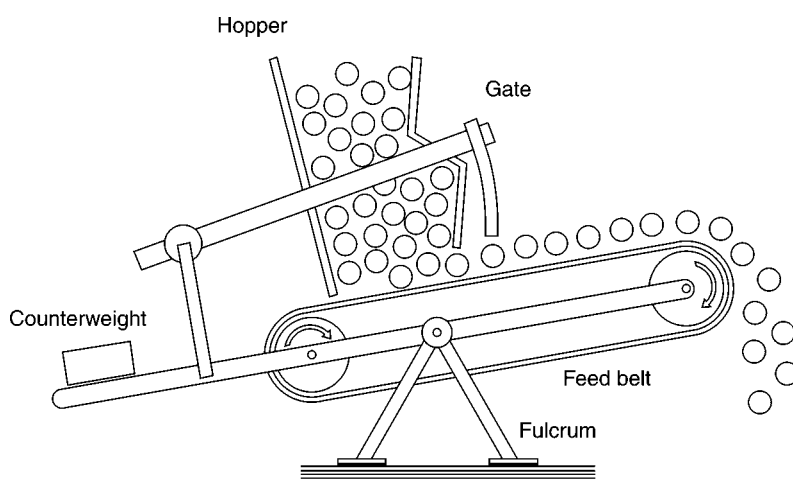
Fig. 10. Pivoted belt gravimetric feeder.

The rigid belt feeder is similar to the pivoted belt feeder except for one main difference. With the pivoted belt filter, adjustment is accomplished through action of the belt tilting up and down, where as with the rigid belt, adjusting occurs through action of the scale beam dependent only on the weight of the belt.

5.2. Solution Feeders

A typical solution feed system consists of a storage tank, transfer pump, dry tank, and liquid feeder as shown in Fig. 11. Some liquid chemicals can be fed directly without dilution and the day tank would not be needed. Dilution water is usually still added to the solution feed pump discharge line after the chemical is metered to prevent plugging, reduce delivery time, and to help mix the chemical with the water being treated. Liquid feed systems are generally recommended for use in the following conditions: when low chemical quantities are required, with less stable chemicals, with chemicals which are fed more easily as a liquid, and in which handling of dusty chemicals or dangerous chemicals is undesirable.

Liquid feeders usually are metering pumps or orifices. These metering pumps usually are of the positive displacement variety, plunger, or diaphragm type. Positive displacement pumps can be set to feed over a wide range by adjusting the pump stroke length. In some cases, control valves and rotameters may be all that is needed, whereas in other cases the rotating dipper type feeder may be satisfactory. For uses like lime slurry feeding, however, centrifugal pumps with open impellers are used. The type of liquid feeder used depends on the viscosity, corrosivity, solubility, suction and discharge heads, and internal pressure relief requirements.

Displacement feeder is suitable for slightly soluble chemicals such as alum, fused sodium carbonate, certain polyphosphates, and so on. The measurement and feed of this system is not particularly accurate, as the concentration of the solution can vary according to the quantity of chemicals left in the tank. It cannot be employed for very soluble chemicals such as aluminum sulfate. Dosing pumps are reciprocating displacement pumps in which flow can be adjusted by modifying cylinder capacity or speed. Many types of dosing pumps are used to distribute the liquid chemical. The piston-operated
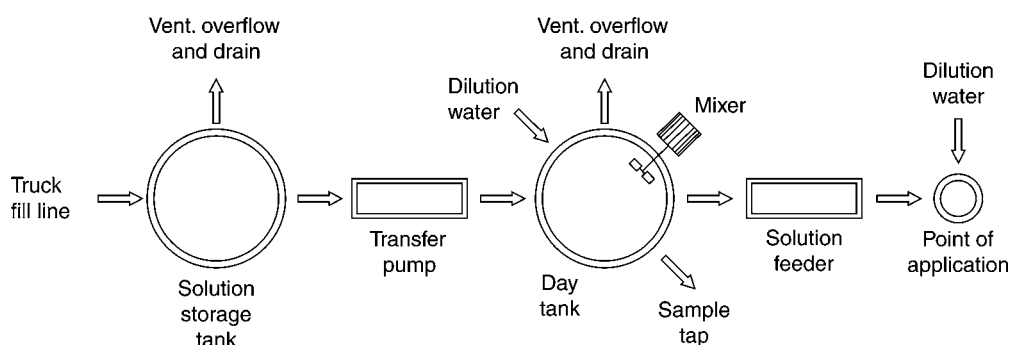
Fig. 11. Typical solution feed system.

dosing pump is very accurate but precautions must be taken when it is used for abrasive or particularly corrosive products (sodium silicate, ferric chloride). The flow rate can vary from some tens of milliliters to as high as several thousands of liters per hour per metering head. For the corrosive, toxic, abrasive, polluted, or viscous liquids, the use of dosing pump with hydraulically operated diaphragm should be considered (12).

5.3. Gas Feeders

Gas feeders can be classified as solution feed or direct feed. The major chemical that is applied to the gas feeders in the feeding systems is chlorine. The solution feed is typically used for chlorination and dechlorination processes. In chlorination, chlorine gas is measured and maintained under a vacuum throughout the apparatus. Vacuum is formed by water flowing through the injector. This moves chlorine from the supply system through the chlorine gas metering devices to the injector. Under vacuum, chlorine gas is mixed with water in an injector to produce a chlorine solution. The chlorine solution is moved to the point of application in the water. In this feeder, the vacuum controls the operation of the chlorine inlet valve. Therefore, the chlorine will not feed unless sufficient vacuum is induced through the apparatus. The flow of chlorine gas is automatically shut off on loss of vacuum, stoppage of the solution discharge line, or loss of operating water pressure. This type of feeder is practical because of its safe operation is assured (8,12).

Only when either water or electricity or both is unavailable direct feed or "dry feed" equipment is infrequently used. In this system, the gas is delivered under pressure directly to the point of application in the water treatment plant. This system is used only when there is no adequate water supply for ejector operation. It is not recommended to use this system as the standard method for chlorination feeding system because it is less safe than solution feed chlorinators.

6. DESIGN EXAMPLES

6.1. Example 1

Chlorine is used for disinfection in one wastewater treatment plant with an average of flow rate of 100 MGD. The average chlorine dosage is 6 mg/L. Chlorine (Cl_2) costs 1.20 USD/lb. Sulfur dioxide (SO_2) is used to dechlorinate the effluent before it is discharged and is consumed at an average dose of 2 mg/L. Its cost is 1.40 USD/lb. Calculate the following items:

1. Daily Cl_2 and SO_2 dosage.
2. Annual operating costs for Cl_2 and SO_2 addition.

[Conversion factor: A dose of 1 mg/L = 8.34 lb/10^6 gal (MG)]

Solution

Calculate the daily Cl_2 and SO_2 dosage rates as follows:

Cl_2 dosage rate	= (100 MGD) (6 mg/L) [(8.34 lb/MG)/(1 mg/L)]
	= 5000 lb/d
SO_2 dosage rate	= (100 MGD) (2 mg/L) [(8.34 lb/MG)/(1 mg/L)]
	= 1670 lb/d

These daily rates are then converted to annual rates:

Annual Cl_2 dosage rate	= (daily Cl_2 rate) (d/yr)
	= (5000 lb/d) (365 d/yr)
	= 1,825,000 lb/yr
Annual SO_2 dosage rate	= (daily SO_2 rate) (d/yr)
	= (1670 lb/d) (365 d/yr)
	= 609,550 lb/yr

The annual costs for Cl_2 and SO_2 addition are calculated as follows:

Annual Cl_2 cost	= (annual Cl_2 dosage rate) (Cl_2 cost in USD/lb)
	= (1,825,000 lb/yr) (1.20 USD/lb)
	= 2,190,000 USD/yr
Annual SO_2 cost	= (annual SO_2 dosage rate) (SO_2 cost in USD/lb)
	= (609,550 lb/yr) (1.40 USD/lb)
	= 853,400 USD/yr
Total operating cost	= Annual Cl_2 cost + Annual SO_2 cost
	= 2,190,000 USD/yr + 853,400 USD/yr
	= 3,043,400 USD/yr

6.2. Example 2

A 0.1 MGD wastewater treatment plant requires sludge treatment. The plant's wastewater contains 10^5 mg/m^3 of suspended solids (ss). The required lime dosage for sludge stabilization is 5% by weight (lime wt./sludge wt.). 80% of the solids are to be captured, calculate the daily and annual lime requirements.

Solution

The sludge flow rate	= (0.1) (10^5) (8.34)/(1000)
	= 83.4 lb/d
The treated sludge	= (0.8) (83.4)
	= 66.72 lb/d
The lime requirement	= (0.05) (66.72)
	= 3.34 lb/d
The lime annual requirement	= (3.34) (365)
	= 1219 lb/yr

6.3. Example 3

Estimate of lime sludge quantities from the following data:

Raw sewage suspended solids	250 mg/L
Raw sewage volatile suspended solids	150 mg/L
Raw sewage PO_4^{3-}	11.5 mg/L as P
Raw sewage total hardness	170.5 mg/L as $CaCO_3$
Raw sewage Ca^{2+}	60 mg/L
Raw sewage Mg^{2+}	5 mg/L
Effluent PO_4^{3-}	0.3 mg/L as P
Effluent Ca^{2+}	80 mg/L
Effluent Mg^{2+}	0 mg/L
Lime dosage	400 mg/L as $Ca(OH)_2$ or
	216 mg/L as Ca^{2+}

Solution:

From: $3PO_4^{3-} + 5Ca^{2+} + OH^- \rightarrow Ca_5OH(PO_4)_3 \downarrow$, $Ca_5OH(PO_4)_3$ formed is 1 mol/3 mol P

$$\frac{11.5}{30.97} = 0.371 \text{ mol P removed}$$

or $\quad \dfrac{0.371}{3} = 0.124$ mol $Ca_5OH(PO_4)_3$ are formed; MW is 502.31

Therefore, weight is $0.124 \times 502.31 = 62.27$ mg/L as $Ca_5OH(PO_4)_3$

From: $Mg^{2+} + 2OH^- \rightarrow Mg(OH)_2 \downarrow$, $Mg(OH)_2$ formed is 1 mol/M Mg^{2+}

$$\frac{5}{24.31} = 0.206 \text{ mol } Mg^{2+}$$

Therefore, $0.206 \times 58.33 = 12.02$ mg/L as $Mg(OH)_2$

From: Σ coagulant in $= \Sigma$ coagulant out, Ca^{2+} in $= Ca^{2+}$ out; Ca^{2+} in $= 60 + 216 = 276$

Ca^{2+} content of $Ca_5OH(PO_4)_3$ formed $= 5 \times 40 \times 0.124 = 24.8$ mg/L

Ca^{2+} lost in effluent $= 80$ mg/L

Therefore, Ca^{2+} not accounted for $= 276 - (80 + 24.8) = 171.2$ mg/L

From: $Ca^{2+} + CO_3^{2-} \rightarrow CaCO_3 \downarrow$, $CaCO_3$ formed is 1 mol/M Ca^{2+}

Therefore, $\dfrac{171.2}{40} = 4.28$ mol $CaCO_3$; MW $= 100.09$

So weight of $CaCO_3 = 428.38$ mg/L

Sludge composition:

Sludge species	Total weight (mg/L)
Raw sewage solids	250
$Ca_5OH(PO_4)_3$	62.27
$Mg(OH)_2$	12.02
$CaCO_3$	428.38
Total	752.67

6.4. Example 4

Estimate of alum sludge quantities from the following data:

Raw sewage suspended solids	250 mg/L
Raw sewage volatile suspended solids	150 mg/L
Raw sewage PO_4^{3-}	11.2 mg/L as P
Raw sewage total hardness	170.5 mg/L as $CaCO_3$
Raw sewage Ca^{2+}	60 mg/L
Raw sewage Mg^{2+}	5 mg/L
Effluent PO_4^{3-}	0.3 mg/L as P
Effluent Ca^{2+}	60 mg/L
Effluent Mg^{2+}	5 mg/L
Effluent Al^{3+}	18.1 mg/L

Solution

Alum dosage 200 mg/L as $Al_2(SO_4)_3 \cdot 14H_2O$, MW = 594.14

From: $Al^{3+} + PO_4^{3-} \rightarrow AlPO_4 \downarrow$, $AlPO_4$ formed is 1 mol per mole of P

$$\frac{11.2}{30.97} = 0.362 \text{ mol P removed}$$

Therefore, 0.362 mol of $AlPO_4$ are formed; MW is 121.95

Therefore, weight is $0.362 \times 121.95 = 44.14$ mg/L

From: Σ coagulant in = Σ coagulant out, Al^{3+} in = Al^{3+} out; Al^{3+} = 18.1 mg/L

$$Al^{3+} \text{ content of } AlPO_4 = 0.362 \times 26.98 = 9.77 \text{ mg/L}$$

$$Al^{3+} \text{ not accounted for} = 18.1 - 9.77 = 8.33 \text{ mg/L}$$

From: $Al^{3+} + 3OH^- \rightarrow Al(OH)_3 \downarrow$, $Al(OH)_3$ formed is 1 mol/M Al^{3+}

$$\text{Therefore, } \frac{8.33}{26.98} = 0.31 \text{ mol } Al(OH)_3; \text{ MW} = 77.98$$

$$\text{So weight of } Al(OH)_3 \text{ is } 0.31 \times 77.98 = 24.17 \text{ mg/L}$$

Sludge composition:

Sludge species	Total weight (mg/L)
Raw sewage solids	250
$AlPO_4$	44.14
$Al(OH)_3$	24.17
Total	318.31

6.5. Example 5

Estimate of iron sludge quantities from the following data:

Raw sewage suspended solids	250 mg/L
Raw sewage volatile suspended solids	150 mg/L
Raw sewage PO_4^{3-}	11.2 mg/L as P

(Continued)

(Continued)

Raw sewage total hardness	170.5 mg/L as $CaCO_3$
Raw sewage Ca^{2+}	60 mg/L
Raw sewage Mg^{2+}	5 mg/L
Effluent $PO_4{}^{3-}$	0.3 mg/L as P
Effluent Ca^{2+}	60 mg/L
Effluent Mg^{2+}	5 mg/L
Effluent Fe^{3+}	28 mg/L
$FeCl_3$ dosage	80 mg/L

Solution

From: $Fe^{3+} + PO_4{}^{3-} \rightarrow FePO_4 \downarrow$, $FePO_4$ formed is 1 mol/mole of P

$$\frac{11.2}{30.97} = 0.362 \text{ mol P removed}$$

Therefore 0.362 mol of $FePO_4$ are formed; MW = 150.18

Therefore weight is $0.362 \times 150.18 = 54.36$ mg/L

From: Σ coagulant in = Σ coagulant out, Fe^{3+} in = Fe^{3+} out; Fe^{3+} in = 28 mg/L

Fe^{3+} content of $FePO_4 = 0.362 \times 55.84 = 20.21$ mg/L

Fe^{3+} not accounted for = $28 - 20.21 = 7.79$ mg/L

From: $Fe^{3+} + 3OH^- \rightarrow Fe(OH)_3 \downarrow$, $Fe(OH)_3$ formed is 1 mol/mole Fe^{3+}

Therefore, $\frac{7.79}{55.84} = 0.140$ mol $Fe(OH)_3$; MW = 106.84

So weight of $Fe(OH)_3$ is $0.140 \times 106.84 = 14.96$ mg/L

Sludge composition:

Sludge species	Total weight (mg/L)
Raw sewage solids	250
$FePO_4$	54.36
$Fe(OH_3)$	14.96
Total	319.32

6.6. Example 6

Estimate of lime feed rates for a plant in which lime is recovered by recalcining of lime sludges from following data:

Plant flow	15 mg/d
Total CaO dosage	400 mg/L
Makeup lime	92% CaO
Recalcined lime	70% CaO
Makeup lime dosage	25% of total
Recalcined dosage	75% of total

Solution

$$Ca(OH) = 1.32 \times CaO;$$

Therefore, 400 mg/L CaO $= 1.32 \times 400 = 528$ mg/L

Makeup lime dosage $= 0.25 \times 400$ mg/L $= 100$ mg/L as CaO

$100 \times 8.34 = 834$ lb of CaO/MG

$834 \times \dfrac{100}{92} = 906$ lb makeup lime at 92% purity/MG

$906 \times 15 = 13,590$ lbs for 15 MG, lb/d of makeup lime

$\dfrac{13,590}{24} = 566$ lb/h of makeup lime (makeup lime feeder setting)

Recalcined lime dosage $= 0.75 \times 400$ mg/L $= 300$ mg/L CaO

$300 \times 8.34 = 2503$ lb of CaO/MG

$2503 \times \dfrac{100}{70} = 3574$ lb of recalcined lime at 70% purity/MG

$3574 \times 15 = 53,614$ lb for 15 MG (lb/d of recalcined lime)

$\dfrac{53,614}{24} = 2234$ lbs/h of recalcined lime (recalcined lime feeder setting)

6.7. *Example 7*

Estimate of alum feed rates for a piston feed pump system. Three alum feed pumps, two dual head, and one single head.

Dual head pumps 0–50 gpm at 100% stroke/head
Single head pump 0–11.5 gph at 100% stroke
Plant flow = 15 MGD
Liquid alum strength = 5.5 lb dry alum/gal
Alum dosage = 18 mg/L

Solution

Alum dosage $= (18$ mg/L$) \times (8.34$ lb/gal$) = 150$ lb/MG

lb/15 MGD $= (150$ lb/MG$) \times (15$ MGD$) = 2250$ lb/d

$$\text{lb/h} = \frac{2250 \text{ lb/d}}{24 \text{ h/d}} = 94 \text{ lb/h}$$

$$\text{gal/h} = \frac{94 \text{ lb/h}}{5.5 \text{ lb/gal}} = 17 \text{ gal/h}$$

One pump (2 heads) $= \dfrac{17 \text{ gal/h}}{100 \text{ gal/h}} \times 100 = 17$ (use 20% stroke setting)

REFERENCES

1. S. R. Qasim, E. M. Motley, and G. Zhu, *Water Works Engineering: Planning, Design, and Operation,* Prentice-Hall, Upper-Saddle River, NJ, USA, 2000.
2. AWWA (5th ed.), *Water Quality and Treatment,* McGraw-Hill Publishing Co., Inc., New York, NY, 1999.

3. ASCE and AWWA (2nd ed.), *Water Treatment Plant Design,* McGraw-Hill Publishing Co., Inc., New York, NY, 1990.
4. S. R. Qasim, (2nd ed.), *Waste Water Treatment Plants: Planning, Design, and Operation,* Technomic Pulishing Co., Inc., Lancaster, PA, 1999.
5. US EPA, *List of Regulated Substanves and Thresholds for Accidental Release Prevention and Risk Management Programs for Chemical Release Prevention; Final Rule and Notice.* Federal Register, Vol. 59, No. 20, US Environmental Protection Agency, Washington DC. January 31, 1994.
6. Matcalf and Eddy, Inc. (3rd ed.), *Wastewater Engineering: Treatment, Disposal and Reuse,* McGraw-Hill Book Co., Inc., New York, NY, 1991.
7. Degremont Company, (5th ed.), *Water Treatment Handbook,* John Wiley & Sons, New York, NY, 1979.
8. US EPA, *Chemical Aids Manual for Wastewater Treatment Facilities,* EPA-430/9-79-018, US Environmental Protection Agency, Washington, DC, 1979.
9. E. Roberts Alley, *Water Quality Control Handbook,* McGraw-Hill, Inc., New York, NY, 2000.
10. US EPA, Performance Evaluation and Trobleshooting at Municipal Wastewater Treatment Facilities, EPA-430/9-78-001, US Environmental Protection Agency, Washington, DC, 1978.
11. US EPA, Sludge Handling and Conditioning, EPA 430/9-78-002, U.S. Environmental Protection Agency, Washington, DC, 1978.
12. MacRae. Chemical Feeders Suppliers Directory. MacRae's Blue Book. www.macraesbluebook.com (2006).

Wet Air Oxidation for Waste Treatment

Linda Y. Zou, Yuncang Li, and Yung-Tse Hung

Contents

INTRODUCTION
CATALYTIC WAO PROCESSES
EMERGING TECHNOLOGIES IN ADVANCED OXIDATION
APPLICATIONS EXAMPLES
REFERENCES

1. INTRODUCTION

Wet air oxidation (WAO) is a technology used to treat the waste streams which are too dilute to incinerate and too concentrated for biological treatment. The WAO process was originally developed by Zimmermann and its first industrial applications appeared in the late 1950s. It can be defined as the oxidation of organic and inorganic substances in an aqueous solution or suspension by means of oxygen or air at elevated temperatures and pressures either in the presence or absence of catalysts. According to this method, the dissolved or suspended organic matter is oxidized in the liquid phase by some gaseous source of oxygen, that may be either pure oxygen, or air. The usual temperature range, 150–320°C, requires high pressure to maintain a liquid phase. Typical conditions for WAO are 150–320°C for temperature, 2–15 MPa for pressure, and 15–120 min for residence time; the preferred chemical oxidation demand (COD) load ranges from 10 to 80 kg/m^3 (1,2). WAO destroys toxics in industrial wastewater by breaking down complex molecular structures into simpler components such as water and carbon dioxide, without emissions of NO$_x$ SO$_2$, HCl, dioxins, furans, and fly ash. It is reported that the WAO process is capable of a high degree of conversion of toxic organics with more than 99% destruction rate; however, some materials are not oxidized completely to carbon dioxide and water, instead, some intermediate compounds are formed, which represent a quarter of the original mass of organic matter. For example, small carboxylic acids: acetic acid and propionic acids, methanol, ethanol, and acetaldehyde. Removal of acetic is usually negligible at temperature less than 300°C. On the other hands, organic nitrogen compounds are easily transformed into ammonia, which is also very stable in WAO process. Therefore, WAO is pretreated of liquid wastes which requires additional treatment processes, for example, a bio-treatment is usually provided for final clean-up (3).

More than 200 WAO plants have been built worldwide. There are two principal categories of applications. One is to treat raw sewage, consisting of a low concentration of sewage in water; another is to treat waste streams from petrochemical, chemical, and pharmaceutical industries. Only a modest amount of oxidation occurs in WAO process for raw sewage sludge as the conditions are mild, for example, 15% reduction in COD. However, sludge has greatly improved settling and drainage properties and is sterile and biologically stable. Toxic materials containing in industrial wastes are not suitable for direct biological treatment. WAO process is demonstrated for successfully treating hazardous industrial wastes such as spent nonhalogenated solvents and still bottoms, sludge from electroplating operations, spent cyanide bath solutions, chemical agent surrogates, and TNT red water (3,4).

1.1. Process Description

WAO is the oxidation of soluble or suspended components in water using oxygen as the oxidizing agent. Air is used as the source of oxygen in the process. Typical conditions for WAO are 150–320°C for temperature, 2–15 MPa for pressure, and 15–120 min for residence time. The WAO process generally involves a number of oxidation and hydrolysis reactions in series that degrade the initial compound into a series of compounds of simpler structure. Complete WAO results in converting of hazardous organic compounds into carbon dioxide, water vapor, and ammonia (for nitrogen containing wastes), sulfate (for sulfur containing wastes), and halogen acids (for halogenated wastes). Partial degradation products may remain in treated wastewaters from WAO and may be given subsequent treatment before being discharged.

The process can convert organic contaminants to CO_2, water, and biodegradable short-chain organic acids. Inorganic constituents such as sulfides and cyanides can also be oxidized. WAO can involve any or of the following reactions:

$$\text{Organics} + O_2 \rightarrow CO_2 + H_2O + RCOOH *$$

$$\text{Sulfur} + O_2 \rightarrow SO_4^{-2}$$

$$\text{Organic Cl} + O_2 \rightarrow Cl^{-1} + CO_2 + RCOOH *$$

$$\text{Organic N} + O_2 \rightarrow NH_3 + CO_2 + RCOOH *$$

$$\text{Phosphorus} + O_2 \rightarrow PO_4^{-3}$$
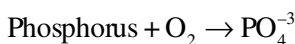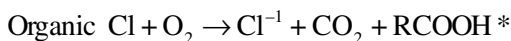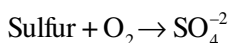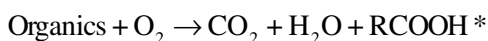
Figure 1 shows a basic flow diagram of a WAO plant, which consists mainly of an air compressor, a high-pressure pump, a heat exchanger as well as a reactor with a relief valve, and a downstream separator. The simplest reactor design is usually a concurrent vertical bubble column with a height-to-diameter ratio in the range of 5–20. An industrial WAO unit is typically run continuously. The raw waste in term of liquid is pumped to the lower part of the reactor, for example, a bubble column reactor through a series of preheaters. The waste is remained in the reactor for sufficient period of time to achieve

---

[*]Short chain organic acids such as acetic acid make up the major fraction of residual organic compounds.
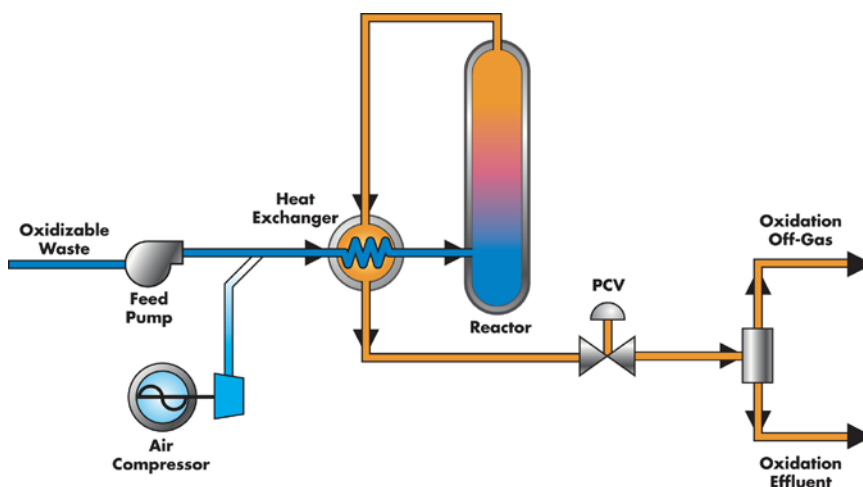
Fig. 1. Diagram of WAO plant (44).

the desired chemical oxidation (15–120 min). Air or oxygen is compressed and is allowed to bubble at the low part of the reactor. The oxygen flow rate is less than 110% of the inlet COD flow rate. Cryogenic oxygen may be used and pumped before vaporization to save shaft work during compression. After starting up, the reactor is normally adiabatic and the temperature can be controlled by changing the total pressure. The heat is absorbed when water vaporizes in gas stream and released when organic contaminants oxidize in the liquid phase. The energy content of the liquid and gas outlet stream is normally sufficient to ensure the preheating of feed. In some cases, WAO applies to very dilute feed (low COD feed) in which the heat release is too small to achieve the desired temperature, additional heat is supplied. With higher concentration feed (high COD feed) some heat release must be removed by cooling or generating high-pressure steam. Typically, the process can run with no additional energy if the oxygen up-take is greater than 15 g/L.

The typical COD removal efficiency seldom exceeds 95% and the stream cannot be discharged into the environment. Most of the WAO units are operated in connection with biological facilities in which a post-treatment is carried out before final release. For example, in Grenzach, Germany and Stignaes, Denmark, the gas stream coming out of a WAO unit contains a limited amount of volatile organic compounds and carbon monoxide (0.5–2.5%) together with CO_2, oxygen in excess, and water. So a simple post-combustion unit ensures the final oxidation of these gases before final release.

Wastewaters including pesticide wastes, petrochemical process wastes, cyanide containing metal finishing wastes, spent caustic wastewaters containing phenolic compounds and some organic chemical production wastewaters can be treated using WAO. WAO is the most applicable for waste streams containing dissolved or suspended organics in the 500–15,000 mg/L range. Less than 500 mg/L, the rates of WAO of most organic constituents are too slow for efficient application of this technology. Wastes containing significant concentrations of metals (approx 2%) can be treated by WAO, whereas biological treatment, carbon adsorption, and chemical oxidation may have difficulty treating

Table 1
WAO of Organic Compounds in Industrial Wastewater^a Concentration (mg/L)

Compound	IEPAluent	Effluent	Removal (%)
COD	56,000	7200	87.1
Methylene chloride	734	0.08	>99.9
Xylene	109	0.11	99.9
MEK	3937	2.3	99.9
Benzene	8.0	0.03	99.6
Carbon tetrachloride	2450	2	99.9

^{a}WAO temperature = 495°F; pressure > 700 psi; residence time = 83 min.

such wastes. Typical results of WAO of organic compounds in industrial wastewaters are presented in the following Table 1: (from US Filter/Zimpro).

1.2. Mechanisms and Kinetics

The oxidation proceeds are presented in Fig. 2 according to a chain reaction mechanism, which highlights the particular role of acetic acid. The series of Reactions 1–5 were recommended by Debellefontaine and Foussard to indicate mechanism of WAO Reaction (2). The reaction is propagated by an organic radical $R^\bullet$ during a compiling with molecular oxygen (*see* Reaction 1). The reaction between oxygen and weakest C–H bonds (Reaction 2) and an attack by the radical $HO_2^\bullet$ (Reaction 3) can normally produce this organic radical. The hydrogen peroxide decomposes rapidity to hydroxyl radical $HO^\bullet$(Reaction 4) because of the temperature. Reaction 5 is a propagation step leading to oxidize species, as hydroxyl radical is the most active oxidation agent.

$$O - O + R^\bullet \rightarrow ROO^\bullet \qquad \text{Reaction 1}$$

$$O_2 + RH \rightarrow R^\bullet + H_2O_2 \qquad \text{Reaction 2}$$

$$HO_2^\bullet + R \rightarrow R^\bullet + H_2O_2 \qquad \text{Reaction 3}$$

$$H_2O_2 + M \rightarrow 2HO^\bullet + M \qquad \text{Reaction 4}$$

$$ROO^\bullet + RH \rightarrow R^\bullet + ROOH \qquad \text{Reaction 5}$$
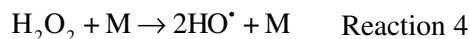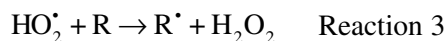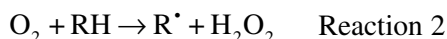
For most of molecules, the Reaction 2 is limiting on and extremely dependent on temperature, with an activation energy, which can be greater than 100 or 200 kJ/mol. This is why WAO becomes fairly rapid at temperature exceeding 250 or 300°C rather than at room temperature. The initial step (Reaction 1) is usually rapid and rate constants are about 10^7–10^9 L/(mol s) (5).

A generalized model according to Fig. 3 is proposed by Lixiong L et al. (6). Group "A" includes all initial and relatively unstable intermediates and group "B" contains the more refractory intermediates represented chiefly by acetic acid. Both groups can lead to oxidation end products, for example, CO_2 and rate of a chemical Reaction is determined by Eq. (1). Equation (2) gives the evolution of the concentration of organic compounds over time in a batch reactor in which the concentration dissolved oxygen remains unchanged over the reaction period.
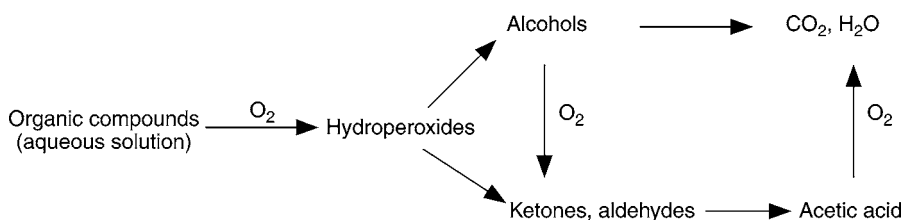
Fig. 2. Simplified diagram for wet air oxidation (45).
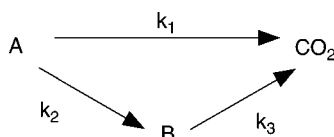
Fig. 3. Generalized kinetic model for wet oxidation of organic compounds (46).

$$r_c = k_0 e^{-E/\mathrm{RT}} C(\mathrm{O}_2)^b \tag{1}$$

$$\frac{(A+B)}{(A+B)_0} = \frac{k_2}{k_1 + k_2 - k_3} e^{-k_3 t} + \frac{k_1 - k_3}{k_1 + k_2 - k_3} e^{-(k_1 + K_2)t} \tag{2}$$

$$k_i = k_{0,i} e^{-E_i/\mathrm{RT}} (\mathrm{O}_2)^{b_i} \tag{3}$$

where B is the partial order of the reaction with respect to the oxidation, C is the actual concentration of an organic compound; E is the activation energy for the chemical reaction; k_0 is the pre-exponential factor coefficient; O_2 is the actual concentration of oxygen dissolved; R is the constant for ideal gases (8.3145 J/mol/K); T is the temperature; t is the time. Subscript i and 0: Subscript for a specific compound and inlet or initial condition, respectively.

Parameter (A + B) is a global indication of the actual value of the organic load such as COD or TOC value. k_1, k_2, and k_3 are apparent constants for chemical reaction rates and they depend on the temperature value and dissolved oxygen concentration according to Eq. (3). For example, a high value of k_2 indicates accumulation of low reactivity intermediates, like acetic acid, and a low value indicates a high global reactivity.

Tow steps exist in the overall WAO mechanism. One is the chemical reaction between the organic matter and oxygen dissolved in liquid phase, produce CO_2. This process can be described by Eqs. (1–3). The other one, a physical step, is transfer of oxygen from the gas phase to the liquid phase and the transfer of CO_2 to the gas from liquid phase. The rate of transfer of a component between the two phases is expressed by Eq. (4).

$$r_{t,i} = w_i \left(Y_i \Phi_i \frac{P}{\gamma_i} H_{i/w} \mathrm{FP}_i - X_i \right) \tag{4}$$

where FP_i is the pointing factor for a specific component "i"; $H_{i/w}$ is the Henry's law constant for the solubility of gas in water; P is the total pressure; $r_{t,i}$ is the rate of transfer of

a component "*i*" between the two phases; W_i is the overall mass transfer coefficient; X_i is the mol fraction of component "*i*" in the liquid phase; Y_i is the mol fraction of component "*i*" in the gas phase; Φ_i is the fugacity coefficient for component "*i*" γ_i is the activity coefficient for component "*i*" in the solution.

1.3. Design

There are many factors need to be considered during the designing stage of a WAO plant (24):

a. The temperature at which WAO is carried out has been found to be the most important parameter in the operation of a WAO plant. The temperature used in WAO range from 180 to 320ºC. The addition of catalysts can lower the operating temperature.
b. The total pressure is critical to the WAO process as it has a function to maintain the liquid phase, which is essential to the oxidation reaction. The operating pressure is often adjusted to a value higher than the saturated water vapor pressure at the operating temperature to prevent the vaporization of the liquid water. At the same time, the partial pressure of oxygen is also important, which is determined by the operation pressure, i.e., total pressure and composition of the gas. If pure oxygen is used instead of air that is normally used in most of industrial installations, safety, for example, explosions may be an issue to be careful.
c. Whether a WAO reaction is controlled by mass transfer in the liquid phase or by kinetics is determined by operating temperature. Sometimes, it is necessary to calculate the mass transfer coefficient of oxygen in the liquid phase to estimate under which mechanism (mass transfer or kinetic) the reaction is controlled, although in most of reactors the oxygen mass transfer resistance both in gas phase or liquid phase is negligible.
d. The design of the reactor itself is the core in designing of a WAO plant. It can affect greatly the oxidation efficiency. The reactor must be designed for carrying out gas–liquid reactions and operating in the kinetic control mode. To achieve this, the resistance between gas phase and liquid phase mass transfer must be minimized. Sectionalized bubble column reactors and the stirred tank cascade reactor are the most common designs of the WAO reactor, not only because of the efficiency but also because of their low fabrication costs.

1.4. Issues and Considerations of Using Wet Air Oxidation

Wastewater with low pH may cause corrosion damage to the metals used in the WAO equipment. Wastewater pH adjustment could provide better materials compatibility results. Care should be taken when handling wastewater. Wastewater can be toxic and/or corrosive. Proper personal protection equipment is highly recommended. Consult your local industrial health specialist, your local health and safety personnel, and the appropriate MSDS before implementing any of these technologies.

A variety of chemical compounds can be treated at the same time in the one step process by WAO. Waste must be in the liquid phase. Wastes are destroyed in liquid phase. As a result, the problems associated with air pollution are reduced. The process is less energy intensive than incineration and is less likely to produce oxides of nitrogen as by-product air pollutants. Wastes are limited to wastewaters containing oxidisable organic and inorganic compounds. For example, WAO cannot destroy PCBs, some halogenated aromatics and some pesticides.

Capital costs for WAO systems depend on the capacity of the system, oxygen demand, reduction of the wastewater, severity of the oxidation conditions required to meet the treatment objectives, and the construction materials. A cost example of a WAO

Table 2
Cost Comparison for WAO System vs Disposal of Wastewater

	WAO (USD)	Disposal (USD)
Capital and installation	12,000,000	0
Operation and maintenance costs	974,000	4500
Waste disposal	0	3,744,000
Annual total (w/o capital)	974,000	3,748,500

system for treating TNT red water is given as the following. The operation and mainte-nance costs for the WAO system are based on estimates from the US Army Construction Engineering Research Laboratories and is based on red water at 3.2 MG/yr (4,7).

Assumptions

a. WAO System for treating TNT red water costs 12 million USD for a 16,000 gal/d system.
b. Operation and maintenance costs 974,000 USD/yr.
c. WAO system runs 200 d/yr.
d. Disposal of hazardous waste costs 1.17 USD/gal.
e. Labor of 100 man-hours a year for disposal of hazardous waste at 45 USD/h.
f. WAO system runs at 340°C and 1 h contact time Table 2.

1.4.1. Economic Analysis Summary

a. Annual savings for WAO: 2,774,500 USD.
b. Capital cost for diversion equipment/process: 12,000,000 USD.
c. Payback period for investment in equipment/process: 4.3 yr.

2. CATALYTIC WAO PROCESSES

2.1. Process Description

Catalytic WAO (CWAO) process is a further development of the WAO process in which a stable and active catalyst is used. Organic and some inorganic contaminants are oxidized in the liquid phase by contacting the liquid with high pressure air at tempera-tures which are typically between 120 and 310°C. In the CWAO process the liquid phase and high pressure air are passed cocurrently over a stationary bed catalyst. Other steps are the similar as the WAO process shown in Fig. 1. The operating pressure is maintained well above the saturation pressure of water at the reaction temperatures (usually about 15–60 bar) so that the reaction takes place in the liquid phase. This enables the oxidation processes to proceed at lower temperatures than those required for incineration. Residence times are from 30 to 90 min, and the chemical oxygen demand removal may typically be about 75–99%. The effect of the catalyst is to provide a higher degree of COD removal than is obtained by WAO at comparable conditions (>99% removal can be achieved), or to reduce the residence time. Organic compounds may be converted to carbon dioxide and water at the higher temperatures; nitrogen and sulphur heteroatoms are converted to to molecular nitrogen and sulphates. The process becomes autogenic at COD levels of about 10,000 mg/L, at which the system will require exter-nal energy only at start-up.

The CWAO process is capable of converting all organic contaminants ultimately to carbon dioxide and water, and can also remove oxidizable inorganic components such as cyanides and ammonia. The process uses air as the oxidant, which is mixed with the effluent and passed over a catalyst at elevated temperatures and pressures. If complete COD removal is not required, the air rate, temperature and pressure can be reduced, therefore reducing the operating cost. CWAO is particularly cost-effective for effluents those are highly concentrated (chemical oxygen demands of 10,000 to over 100,000 mg/L) or, which contain components those are not readily biodegradable or are toxic to biological treatment systems. CWAO process plants also offer the advantage that they can be highly automated for unattended operation, have relatively small plant footprints, and are able to deal with variable effluent flow rates and compositions. The process is not cost-effective compared with other advanced oxidation processes or biological processes for lightly contaminated effluents (COD less than about 5000 mg/L).

The pathways and mechanism of CWAO reactions depend on the compound oxidized. A simple but accepted mechanism for the CWAO of phenol has been proposed by the following reactions, which is the similar to the WAO mechanism (Reactions 1–5, Eqs. [1–4], and Figs. 2 and 3).

$$RH-OH+cat \rightarrow R \cdot H = O + \cdot H - cat \quad \text{Reaction 6}$$

$$R \cdot H = O + O_2 \rightarrow RHO - OO \cdot \quad \text{Reaction 7}$$

$$RHO - OO \cdot + RH - OH \rightarrow ROH - OOH + R \cdot H = O \quad \text{Reaction 8}$$
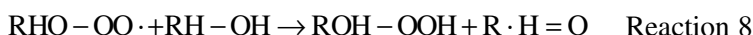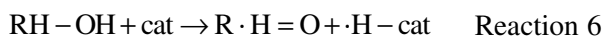
In this mechanism RH–OH corresponds to phenol, R·H = O corresponds to the phenoxy radical and RHO–OO· corresponds to the peroxy radical. Recently efforts are driven to develop more detailed radical reaction networks for the WAO of phenol, involving several tens of radical reactions that should be more reliable in extrapolation beyond the fitted conditions.

2.2. Process Application and Limitation

The most widely spread variation is the noncatalytic Zimpro process, which uses a bubble column reactor, operating at temperatures between 147 and 325°C and pressures of 2–21 MPa. The heterogeneous Catalytic WAO (hereafter stated as CWAO) has scarcely found industrial applications. The NS-LC process uses a vertical monolith reactor with a Pt–Pd/TiO2–ZrO$_2$ catalyst. The operating conditions are 220°C and 4 MPa. The Osaka gas process uses a mixture of precious and base metals on Titania or zirconia-titania supports. Typical operating conditions are 250°C and 6.86 MPa. The Kurita process uses nitrite instead of oxygen, and a similar catalyst (supported Pt), becoming more effective at lower temperatures, around 170°C.

The heterogeneous catalysts that have been employed in CWAO can be divided in two main groups, i.e., metal oxides (as well as mixtures of them) and supported noble metals. Active carbon, without any deposited active phase, has also exhibited catalytic activity.

2.2.1. Noble Metals

Noble metals have been very effective in the treatment of different pollutants such as phenols, carboxylic acids, including refractory acetic acid, and ammonia effluents. Pd, Pt,

Table 3
Process Data of CWAO Using Noble Catalysts

Noble Metal	Support	Substrate	T (°C)	P (MPa)
Pt	$\gamma - Al_2O_3$	Acetic acid	>200	
Ru, Ir, Pd, Ag, base metals	CeO_2, TiO_2, ZrO_2	Acetic acid	200	2
Pt	$\gamma - Al_2O_3$	Maleic acid	>120	>0.4
Ru	CeO_2	Maleic acid	>160	2
Ru	TiO_2	Succinic acid	>150	5
Pt	C	Carboxylic acids	>20	>0.1
Pt	C	Carboxylic acids	200	0.69
Pt	$\gamma - Al_2O_3$, resin	Carboxylic acids	80	0.1
Ir	C	Butyric acid	200	0.69
Pt, Ru, Rh	TiO_2, CeO_2, C	Phenol/acrylic acid	170	2
Pt	$\gamma - Al_2O_3$	Phenol	>155	2
Pt, Ag	MnO_2/CeO_2	Phenol	>80	0.5
Pt-Ru	C	Phenol	>35	
Ru	C, CeO_2/C	Phenol	160	2
Pt	C	p-Chlorophenol	170	2.6
Pt, Ru, Pd, Rh	CeO_2	Ammonia	>150	2
Pd	C	Ammonia	280	2
Pt	SDB resin	Ammonia	>110	<0.28
Pt, Ru, Pd, Ir	TiO_2, CeO_2, C	Ammonia	>150	1.5
Pt-Ru	C	Trichloroethene	>90	>0.2
Ru	TiO_2, ZrO_2	Kraft effluent	190	5.5
Ru	TiO_2	Kraft effluent	190	8
Pd, Pd – Pt	$\gamma - Al_2O_3$, ALON™	Kraft effluent	>80	1.84
Pd –Pt – Ce	$\gamma - Al_2O_3$	Kraft effluent	>130	> 1.5

and Ru have received most attention although Ir or Rh have also been tested. Table 3 summarizes the applications of noble metal catalysts in the CWAO.

From Table 3 it can be deduced that numerous noble metal catalysts are available, but for different pollutants different metals may present optimum results. For example, in the case of acetic acid oxidation, the catalytic activity decreases in the order Ru > Ir > Pd, whereas for the oxidation of *p*-chlorophenol, catalytic activity decreases in a reverse order Pt > Pd > Ru. Occasionally, synergistic effects in bimetallic catalysts improve catalyst activity and/or selectivity. Better N_2 selectivity was achieved during ammonia oxidation when a mixed Ru–Pd/CeO_2 catalyst was used. Promoters have also been used with noble metal catalysts. An Ag promoted Pt over MnO_2/CeO_2 catalyst enhanced the CWAO of phenol compared to the non promoted catalyst.

The noble metal support also influences significantly catalyst performance. Metal oxides, like alumina, ceria, titania, and zirconia, as well as active carbon or high specific area graphite have been mainly studied. In the treatment of Kraft bleach effluents increasing the support surface area had a positive effect on catalyst activity. The dispersion of the active phase was also shown to be important for the CWAO of phenol, as

demonstrated by a comparative study of two Pt/Al_2O_3 catalysts prepared in different manners. Finally, the deposition of noble metals on hydrophobic supports, i.e., certain active carbons, or styrene divinyl benzene copolymer, is very effective for the destruction of volatile pollutants such as ammonia.

2.2.2. Metal Oxides

The other broad family of catalysts used in CWAO is the pure or mixed metal oxides. Copper oxide, alone or combined with other oxides, has received special attention in the CWAO of aqueous effluents. Phenol was successfully oxidized by a commercial Harshaw Cu0803 T1/8 catalyst, comprising 10% copper oxide supported over alumina. A commercial CuO/ZnO catalyst was used to oxidize formic acid. In the early 1990s, other commercial catalysts comprising CuO, ZnO, and Al_2O_3, or CoO were successfully employed to oxidize phenol and substituted phenols. Table 4 summarizes the applications of metal oxide catalysts in the CWAO.

2.2.3. Activated Carbon

Most commonly, activated carbon (AC) has been used as a catalyst support. Only in the last 5 yr, the AC without any additional active phase was shown to possess a long-term catalytic activity in the oxidation of phenol, which could even surpass that of a conventional copper oxide catalyst. The underlying mechanisms those are responsible for the catalytic activity of AC in CWAO are far from being well understood. To bring some light in this open aspect, a recompilation of the existing data of the CWAO of phenol over AC is carried out and an attempt is done to relate these results to other studied systems that employ AC as a catalyst. The most important conclusion is that the phenol oxidation over AC seems to proceed through the formation of a carbonaceous layer on the AC surface. It has been reported that during the CWAO of phenol over powdered AC in a semibatch slurry reactor it was impossible to balance the total carbon mass over the liquid and gas phase.

2.2.4. Catalyst Stability

Till date, the main drawback of CWAO, preventing it from a broad industrial application, consists in the catalyst deactivation, which occurs mainly because of active phase leaching or formation of carbonaceous deposits, during the oxidation process. The most prominent catalysts prone to leaching of the active phase are mixed oxides catalysts. Pintar and Levec (97) performed CWAO of nitrophenol and chlorophenol over a catalyst consisting of CuO, ZnO, and CoO in a liquid full fixed bed reactor and detected metal ions from all the above oxides in the solution. Similar trends were also observed for other copper catalysts like CuO/Al_2O_3, bimetallic copper-containing catalysts, copper on AC or zeolites. Under continuous operation, this decline leads to a continuous activity loss. Thus, the development of more stable metal oxide catalysts can be pointed out as a critical issue in CWAO.

Metal oxide catalysts with promising behavior have been prepared. Mixed copper, nickel, and aluminum oxide catalysts were developed, which performed without any activity loss for 15 d on stream in a Trickle Bed Reactor. Different $CuO–CeO_2$ catalysts in which copper leaching was significantly reduced. For mixed Ce/Mn oxide catalysts, it was found that measurable amounts of Mn could dissolve. Active phase leaching was also reported for noble metal catalysts from during the CWAO of pulp mill effluents over Pd and Pt catalysts.

Table 4
Process Data of CWAO Using Metal Oxide Catalysts

Oxide	Support	Substrate	T (℃)	P (MPa)
Cu/Cr oxides		Phenol	>127	0.32
Cu/Cr/Ba/Al oxides		Phenol	127	0.8
Cu, Fe, Mn, Zn oxides with Cu oxides	γ–Al$_2$O$_3$	Phenol	140	0.9
CuO	γ–Al$_2$O$_3$	Phenol	>120	>0.6
CuO	γ–Al$_2$O$_3$	Phenol	140	0.9
Cu/Ni/Al oxides		Phenol	140	0.9
CuO/ZnO/CoO	Cement	Phenol	>130	7
CuO/ZnO/CoO	Cement	Phenol	>150	(^{a})
CuO/ZnO	γ–Al$_2$O$_3$	Phenol	>105	>0.15
CuO	γ–Al$_2$O$_2$	Phenol	>113	>0.44
CuO/CeO$_2$		Phenol	130	0.73
K–MnO$_2$/CeO$_2$		Phenol	110	0.5
MnO$_2$/CeO$_2$		Phenol	>80	>0.2
CuO	C	Phenol	>160	>2.6
CuO	γ–Al$_2$O3	Phenol	>95	>0.1
MnO$_2$, Co$_2$O$_3$		Phenol	>170	>1.3
Ni–oxide		Phenol	>15	–
Cu/Zn/Cr/Ba/Al oxides		Phenol	>110	>0.1
MnO$_2$, Co$_2$O$_3$		p-Chlorophenol	>170	>1.3
CuO/ZnO/CoO	Cement	p-Chlorophenol p-Nitrophenol	>150	(^{a})
CuO/ZnO	γ–Al$_2$O$_3$	p-Chlorophenol p-Nitrophenol	>105	>0.15
CuO/ZnO		Formic acid	>200	4
Fe$_2$O$_3$		Acetic acid	>252	>6.7
Cu/Mn/La	ZnO–Al$_2$O$_3$	Acetic acid	>250	(^{a})
Ce/Zr/Cu oxides or Ce/Zr/Mn		Acetic acid	>245	>5
MnO/CeO		Acetic acid	247	1
		N-Butilamine	220	
		PEG	220	
		Pyridine	270	
		Ammonia	263	
MnO$_2$/CeO$_2$		Alcohol distilery waste	>180	>0.5

^{a}These tests were performed in a liquid full reactor saturated with oxygen.

Catalyst deactivation caused by the formation of carbonaceous deposit on the catalyst surface has been observed for several types of catalysts. Ceria oxide based catalysts have been found to suffer from this type of catalyst deactivation during tests carried out in agitated tank reactors. Further work demonstrated that carbonaceous deposits could be minimized by promoting the catalyst with Pt and Ag. More recently, it was found that less expensive potassium can also retard such formation. The carbonaceous deposit has

to be related both to the nature of the organic pollutant and the reactor type used. The enhanced formation of such deposits has been confirmed by several authors in slurry reactors, with a characteristic high liquid to catalyst ratio that promotes the homogeneous polymerization reactions. Consequently, comparative studies have shown that the extent of these parallel side reactions in the liquid phase is significantly reduced in Trickle Bed Reactors.

In the case of AC the catalytic activity during the CWAO of phenol at 140°C was shown to be stable only for pressures less than 0.4 MPa, whereas at higher pressures a constant decline was observed. The loss of AC catalytic activity was attributed to the simultaneous burnt out of the AC catalytic bed during the oxidation process. It was demonstrated that the rate of combustion of AC is considerably faster when, instead of the phenolic solution, a pure water solution is fed to the reactor. Obviously the phenol oxidation and the carbon burn out are competitive reactions, and the phenol adsorbed on the AC surface protects the AC from being oxidized, as long as the concentration of O_2 is kept below a certain limit.

A wide range of supported noble metals, mixed metal oxides, as well as active carbon alone have been shown to exhibit catalytic activity for the oxidation of aqueous solutions of organic pollutants. Noble metal catalysts are very effective for the removal of refractory carboxylic acids, although for the less refractory phenolic pollutants, mixed metal oxides, and active carbon yield good results. Catalyst deactivation has been found to occur either resulting from carbonaceous deposit formation, or resulting from active phase leaching. For both noble metal and mixed oxide catalysts analysis of the outlet solution for dissolved metals should be always carried out to measure the degree of stability of the catalyst. Long term runs in continuous reactor should also be tested to validate catalyst stability under continuous operation conditions. Such 10 d tests have shown that AC can yield constant phenol conversions, as long as oxygen partial pressure is less than 0.4 MPa.

2.3. Design Considerations

All design considerations for WAO are suitable to apply in CWAO process. The complexity of multiphase reactor modeling increases when they are used for solid catalyzed reactions between a gaseous and a liquid reactant. This situation is very common in industrially relevant processes, such as hydro treating and hydrogenation, but recent works point out the increasing use of multiphase reactors in selective oxidation, and wastewater treatment processes, i.e., in the CWAO process.

Several reactor types, with different characteristics, can be used to accommodate the solid catalyst and carry out multiphase catalytic reactions. Therefore, reactor type selection has to be examined for each reaction system, considering catalyst type, catalyst activity and stability, reactant and product properties, and interfering reactions.

Four main categories of gas–liquid–solid catalytic reactors can be distinguished: agitated slurry reactors, sparged catalyst reactors, like slurry bubble column and fluidized beds, and finally fixed bed reactors. Mechanically agitated slurry reactors exhibit high heat and mass transfer rates; but stirring leads to high investment and operation costs and energy consumption. Furthermore, these reactors have a very low catalyst to liquid ratio, thus undesired parallel reactions may be enhanced. Sparged catalyst reactors exhibit heat

transfer rates those are still higher than those of fixed bed reactors, but also a higher liquid to catalyst ratio. Furthermore, catalyst particles have to be separated from the exit liquid stream when continuous operation is desired. Fixed bed reactors have the lowest liquid to catalyst ratio; on cost of lower heat and mass transfer rates.

As it was shown earlier, during the CWAO of certain organic pollutants, like phenols, parallel polymerization reactions occur when the liquid to catalyst ratio is high. For this reason agitated slurry and sparged catalyst reactors do not seem to be adequate for the CWAO of phenol.

On the other hand, as the pollutants are diluted the intrinsic reaction rates are low, thus mass and heat transfer limitations should not be as important as in the case of pure reaction systems, for example, for hydrogenation reactions. These facts suggest that fixed bed reactors are the priority choice for the CWAO of phenol. There exist three basic modes of operation of gas–liquid–solid fixed bed catalytic reactors, depending on the direction of the gas and the liquid flow. The Trickle Bed Reactor (TBR) is characterized by the cocurrent downflow of both gas and liquid phases, although the countercurrent operation of liquid downflow and gas upflow, may be advantageous in special cases. The last configuration is that of cocurrent gas and liquid upflow, then termed packed bubble column. The most frequently used in industry is the TBR as it allows a variety of flow regimes making it more flexible. Up flow reactors are used when it is necessary to assure complete external wetting of catalyst. Furthermore, they have been shown to permit better temperature control for extremely exothermic reactions. Countercurrent operation allows to selectively removing byproducts that may inhibit catalyst performance. The large experience on the operation of TBRs in industrial hydro treatment processes makes them the first choice for the performance of CWAO reactions.

Till date, industrial-scale application of CWAO process is limited mainly because of catalyst deactivation problems and high catalyst costs. The recent development of stable catalysts is expected to realm interest for the process. Among the most promising catalysts, AC offers a less expensive alternative with a proven activity in the abatement of several phenol-like compounds. Such pollutants are of special interest, because they are increasingly encountered in effluents that cannot be treated in conventional biological treatment plants.

The pathways leading to the complete mineralization of the treated pollutants during WAO or CWAO processes are complex and far from being well understood. For phenol it has been shown that it is oxidized towards toxic ring compounds, which consequently yield low-molecular weight carboxylic acids. Because of the toxicity of the aromatic compounds formed in the first step of phenol degradation, it is important to monitor their production and destruction for the catalysts used.

3. EMERGING TECHNOLOGIES IN ADVANCED OXIDATION

3.1. Photocatalytic Oxidation (PCO) Process

3.1.1. Mechanism and Kinematic of PCO Process

Advanced oxidize processes (AOPs) are based on the generation of very reactive species such as the hydroxyl radical that oxidation a broad range of organic pollutants quickly and nonselectively. The photocatalytic AOPs is a fast-developing area, in which

the ultraviolet (UV) radiation or UV band in the solar radiation is used to provide the energy to generate the reactive species, which makes the process even more environmentally friendly. Photocatalytic oxidation is a process in which a semiconductor on adsorption of photons acts as a catalyst in producing reactive radicals, mainly hydroxyl radicals, which in turn can oxidize organic compounds and totally mineralize them (8,9). In the process organic molecules are decomposed to form carbon dioxide, water, and mineral acids as terminal products (Fig. 4).

When a semiconductor like TiO_2 is irradiated with light having energy greater than the band gap, an electron is excited from the valence band to the conduction band, creating a hole and an electron. The hole is an oxidizing agent, and the electron is a reducing agent. In the generally accepted mechanisms for the photocatalytic process, the hole can react with water to produce the hydroxyl radical ($OH^\bullet$) and the electron can reduce molecular oxygen, hydrogen peroxide or some other oxidizing agent in the solution. The reactive hydroxyl radicals act as powerful oxidizing agents responsible for removal of the hazardous components from the water (10,11).

The following equations describe the oxidation and reduction reactions

$$TiO_2 \xrightarrow{\quad h\nu \quad} TiO_2\,(e_{cb}^- + hole_{cb}^+) \tag{4a}$$

$$TiO_2\,(e_{cb}^- + hole_{cb}^+) \xrightarrow{\quad recomb \quad} TiO_2 + heat \tag{5}$$

$$H_2O \longrightarrow OH^- + H^+ \tag{6}$$

$$hole_{vb}^+ + OH_{ads}^- \longrightarrow OH^\bullet \tag{7}$$

$$O_2 + e_{cb}^- \longrightarrow O_2^{-\bullet} \tag{8}$$

$$2O_2^{-\bullet} + 2h_{aq}^+ \longrightarrow H_2O_2 + O_2 \tag{9}$$

Oxidation of organism

$$OH^\bullet + Organism + O_2 \longrightarrow Products\,(CO_2,\ H_2O,\ and\ so\ on). \tag{10}$$
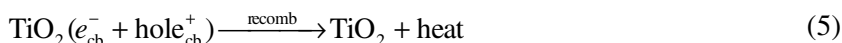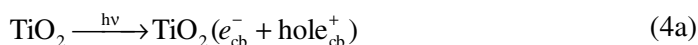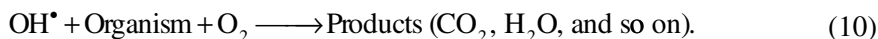
The use of TiO_2 in water detoxification was first demonstrated by Carey et al. in 1976. They used aqueous suspensions of TiO_2 to dechlorinate polychlorinated biphenyl (12). A large number of researches has been conducted by now. They covered many types of contaminant treatment, like ground water, drinking water, herbicide, residential wastewater and industrial wastewater, even pollution in soil and air (13–23).

The rate of photocatalytic degradation depends on several factors including illumination intensity, photocatalyst type, oxygen concentration, pH value, presence of inorganic ions, and the concentration of organic reactant and has been modeled by different kinetic models. Langmuir-Hinshelwood (L-H) kinetics seem to describe many of reactions fairly well. The rate of degradation is given by :

$$-\frac{dC}{dt} = \frac{K_1\,K_2\,C}{1 + K_2\,C} \tag{11}$$

where C is the bulk solution concentration, K_1 is the reaction rate, K_2 is the equilibrium adsorption constant and t represents time. Once the reaction constants K_1 and K_2 have
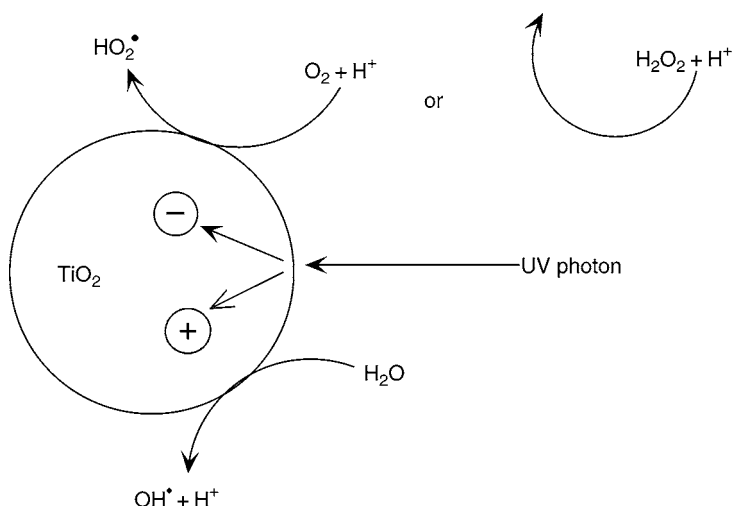
Fig. 4. Illustration of the oxidation and reduction reactions in a semiconductor exposed to UV light (47).

been evaluated, the disappearance of reactant can be estimated if all other factors are held constant. The L-H expression can be reduced to a pseudo-first-order expression Eq. (12) for low solute concentration C.

$$-\frac{dC}{dt} = K_1 K_2 C = kC \tag{12}$$

This equation has been applied to many photocatalytic reactions. As industrial pollutant levels are typically on the order of ppm, the pseudo first-order kinetics describes the process very well. The disappearance of pollutant in a photocatalytic oxidation process can be estimated by Eq. (13) if all other factors are held constant. For the design of a system, the apparent reaction rate constant k can be determined for experimental data.

$$C = C_0 e^{-kt} \tag{13}$$

Figure 5 shows a simplified schematic of a flat-plate reactor (FPR) system. The contaminated liquid from the tank feeds to FPR with the initial concentration of pollutants C_{fi} and is irradiated in FPR and degraded to final concentration C_{fo} when it flows out from the reactor. The liquid out of FPR with the concentration C_{ti} enters the tank and mixes with the liquid of concentration C_t (C_t is the average concentration of pollutants in the tank) in the tank to form a liquid with a concentration C_{to} (tank outlet concentration), which goes to the FPR again. It is reasonable to assume that the degradation only occurs in the FPR under the UV and does not happen in the tank and connecting tubes. Hence, considering $C_{fo} = C_{ti}$, C_{to} can be calculated using the following equation.

The mean liquid velocity on FPR is

$$u = \frac{Q}{dW} = \frac{QL}{V_R} \tag{14}$$

An irradiated time t_1 (the time that liquid stays on FPR during one pass) is
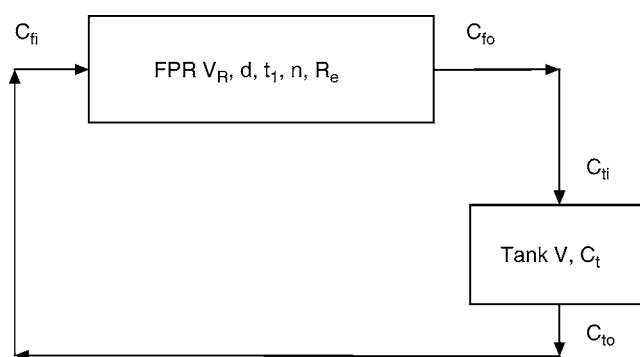
Fig. 5. Model sketch diagram of the FPR system (48).

$$t_1 = \frac{L}{u} = \frac{V_R}{Q} \tag{15}$$

A circulation time t (the time that liquid takes to circulate once from the tank to the FPR, then back to the tank) is:

$$t = \frac{V}{Q} \tag{16}$$

where V is the total volume of liquid in the system; Q is the volumetric flow rate;

The ratio of the irradiated time t_1 to the circulation time t is

$$r_1 = \frac{t_1}{t} = \frac{V_R/Q}{V/Q} = \frac{V_R}{V} \tag{17}$$

As liquid flows passing the FPR, for a liquid point, it is irradiated by UV radiation only when it is in the FPR. Numbers of passing for a liquid particle during the experiment those lasts for t time can be calculated as

$$n = \frac{tQ}{V} \tag{18}$$

Total irradiated time t_1 (the effective time that a liquid particle is irradiated during the experiment, i.e., treatment process) is:

$$T_1 = \frac{T}{V/Q} t_1 = \frac{T V_R}{V} = T r_1 \tag{19}$$

$$C_{to} = \frac{V_R C_{fo} + (V - V_R) C_t}{V_R + (V - V_R)} \tag{20}$$

The dye degradation (in the FPR) obeys a pseudo-order kinetic law, as previously reported in the literature for most of the investigated organic substrates. The liquid concentration at the outlet of the reactor is then calculated using the following equation.

$$C_{fo} = C_{fi}e^{-kt_1} \tag{21}$$

So, Eq. (20) becomes:

$$C_{to} = \frac{V_R C_{fi}e^{-kt_l} + (V - V_R)C_t}{V_R + (V - V_R)} \tag{22}$$

The Eq. (22) actually gives the after-treatment concentration of pollutant in the liquid/solution as a function of irradiated time t_1 in the FPR. If C_{to} is smaller the treatment results in a better manner, i.e., the photocatalytic performance (in the reactor) is better. It can be seen that there is a large volume of liquid V_R (thicker liquid film thickness), then the irradiated time t_1 and is longer reaction rate constant k is apparently large and will result in quicker degradation of pollutants, which means the better performance of FPR is better. However, the apparent reaction rate constant k depends not only on flow status (Re) but also on the intensity of UV light, dosage, and form of photocatalysts applied.

3.1.2. TiO$_2$ Photocatalyst in the PCO Process

Two types of photocatalyst, fixed photocatalyst, and powders (slurry) are typically used in PCO processes. For example, TiO$_2$ powder has been the most commonly used photocatalyst as it is active and cheap, insoluble under most conditions, photo-stable, and nontoxic. However, for slurry reactors the TiO$_2$ particles have to be separated from the treated wastewater after photocatalytic degradation. The photocatalytic activity of TiO$_2$ powder depends on the size of TiO$_2$ particle. Generally, the finer the particles are the higher photocatalytic activity. This makes it very difficult to be separated from the treated wastewater. For example, P25 TiO$_2$ powder are very fine with an average primary particle size of about 21 nm (24). Thus, for the development of the photocatalytic technology, the solid-liquid separation has become an extremely important issue.

The technologies to fix TiO$_2$ photocatalyst on substrates such as glass, metal plate, concrete, or ceramics were developed by many researchers in recent years. The method to coat on substrates comprised the Sol-Gel process (25–27), dip coating method (28,29), electrodeposit method (30), ultrasonic atomization–pyrogenation methods (31), and other methods (32–35). These applications were successful to degrade organisms and pollutants in wastewater (36). However, resulting from a limitation of mass transfer and a loss of photocatalytic activity by the fixation, slurry-reactor systems excel the fixed one with respect to photocatalytic degradation efficiency (37).

Synthesized ultrafine SnO$_2$–TiO$_2$ coupled particles were used for photocatalytic degradation of azo active red X-3B in aerated solution (38). The results show that a very rapid and complete decolorization of the azo can be achieved using such particles under UV irradiation. It results from coupling two semiconductor systems with different energy levels for extending the used UV portion and enhancement in the rat of photocatalytic degradation. A study for improving visible sensitization of nanocrystalline TiO$_2$ doped with metal ions in cosolvent was carried out (39). The experimental results indicated that the vanadium-doped TiO$_2$ photocatalyst showed high photocatalytic activity of 96.9% for decomposition of H$_2$S with an initial concentration of 50 µL/L under visible light.

3.1.3. Photocatalytic Reactors

The photocatalytic reactor is an important component in a photocatalytic oxidation system. The structure will determine the received solar intensity and affect the photocatalytic reaction. A number of different types of photocatalytic reactors have been developed and used in research or pilot plant studies. Examples of these reactors include the annular photoreactor (40–43), the packed bed photoreactor (44), the photocatalytic Taylor vortex reactor (45), the TiO_2 fluidized-bed reactor (46), the TiO_2-coated fiber optic cable reactor (47–52), the falling film reactor (53), the thin-film-fixed-bed slope plate reactor (54,55), and the swirl-flow reactor (56), concentrate reactors (50,57–60), batch reactors (61,62), flat plate reactors (55,63–66), tube reactors or spinning tube reactors (67–71), and bell reactors (72–77).

3.2. Supercritical Water Oxidation

3.2.1. Process Description

It has been discovered that if the usual operation temperature and pressure for WAO were raised above the critical condition of water supercritical condition, the oxidation potential of the process, and consequently the removal efficiency, would increase greatly. Fluids with temperatures and pressures those are above their critical values are called *supercritical fluids*. The critical point of a fluid is defined as the highest temperature and pressure at which it can exist in liquid/vapor equilibrium. A phase is considered a liquid if it can be vaporized by reducing the pressure at constant temperature. A gas can generally be condensed to produce a liquid by reducing the temperature at constant pressure. Supercritical fluids are neither because they do not fit this definition (7), and generally consist of one phase which occupies the entire volume of a vessel (78). Any fluid less than the critical point is generally referred to as a *subcritical fluid*. To produce a liquid from a supercritical fluid above its critical temperature and pressure, at first the temperature must be reduced below the critical temperature and then pressure applied isothermally.

The properties of supercritical fluids are generally between those of liquid and gases in terms of viscosity, density, and diffusion coefficients. Water, on the other hand, shows dramatic changes in physical and chemical properties when in the supercritical state. The critical point of water is 374°C and 221 atm (79). Above these water condition is supercritical water (SCW). As a medium for chemical reaction, has been found very useful for oxidation of organics. Above the critical point of water, water is an excellent solvent for both organic compounds and gases (e.g., oxygen, nitrogen, and carbon dioxide) (80). Dissolving waste in air or oxygen in SCW leads to a homogeneous phase in which oxidation is rapid. For example, at 400–450°C, 99–99.9% conversions (to carbon dioxide, carbon monoxide) can be achieved within 5 min. If the operating temperatures are increased to 600–650°C, 99.999% can be obtained in less than a minute (81).

One physiochemical property that changes as the critical temperature and pressure are approached is the dielectric constant (permittivity relative to vacuum). This property dictates to a large degree the ability of water to act as an organic solvent. At room temperature the dielectric constant of water is about 80. Figure 6 shows the dielectric constant of water along the saturation line (at temperature, *T*, with just enough pressure to maintain
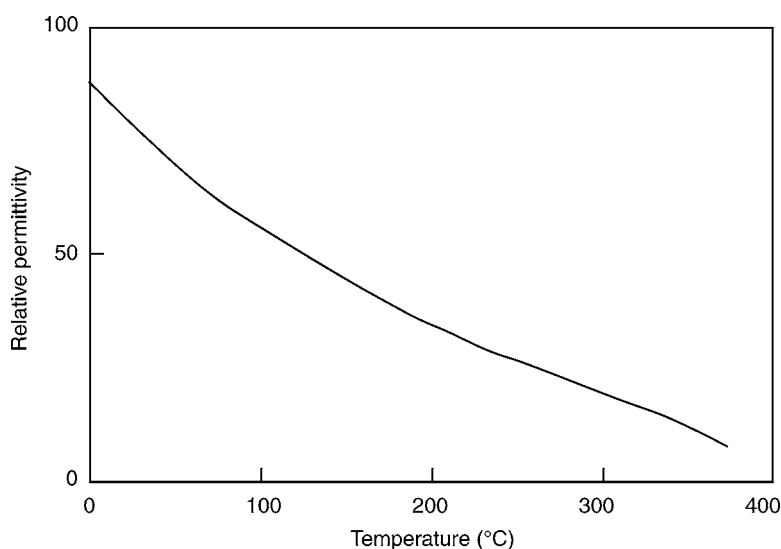
Fig. 6. Dielectric constant of water with increasing temperature (49,84).

liquid state). As the temperature is increased the dielectric constant is reduced to 30.79 at 500 K and 10 MPa, and then 10.34 at 750 K, and 100 MPa (82). Under supercritical conditions the dielectric constant can be reduced to values less than 2, thus making organics order of magnitude more soluble. For example, the solubility of benzo[*a*]pyrene in water at 25°C is 0.004 μg/mL and at 250°C increases to 1100 μg/mL (83).

3.2.2. Removal of Organic Compounds With Supercritical Water

The key parameter in extraction processes is the solvent-solute interaction. This is partly related to the dielectric constant and the polarity. A high dielectric constant favors the solubility and extraction of high polarity compounds. Conversely, a low dielectric constant favors the solubility of low polarity compounds. This section of the report explores the effect of using supercritical water over subcritical water and hence the subsequent decrease in the dielectric constant to achieve extraction.

Removal of various organic compounds from sand and soil using sub- and supercritical water has been well documented by the research of Hartonen et al. (85) and Hawthorne and Yang (86). Sand spiked with various organic pollutants such as alkanes, phenols, amines, and PAHs was extracted by Hawthorne and Yang to determine the extraction efficiency when the conditions are altered from subcritical to supercritical. For the spiked sand mixture, all the spiked elements, except the alkanes were extracted under subcritical condition. However, it has been demonstrated that unlike CO_2, which is very effective at extracting alkanes, water is less effective, and for this reason supercritical conditions are required to achieve extraction. Similar trends were observed for the same organic compounds in soil, which demonstrate that the effect of substrate interaction is not a crucial component of extraction.

The extraction of dioxins such as polychlorinated dibenzo-*p*-dioxins (PCDDs), polychlorinated dibenzofurans (PCDFs) and various PCBs was studied by Hashimoto (87) as part of a soil remediation study. As previously, over 99% extraction was achieved

under subcritical conditions at temperature of 350°C. An important factor to mention in this study was the use of a 240 min extraction time whereas the previous study used much shorter time of 15 min to achieve satisfactory extraction.

Larger scale operations have been reported by Lagadec et al. (83), with pilot scale sized equipment used in the remediation of soils. However, the scaled-up process lacks the response of a laboratory system and heating and extraction times were lengthened, because of the size of the extraction vessel. The extraction time can be reduced by increasing the flow rate of water through the system but not necessarily the amount of water used in the extraction. For example, for the extraction of PCBs in 8 kg of soil 300 mL/min for 120 min extraction is required and is equal to 600 mL/min for 60 min, both achieving complete extraction. Therefore extraction appears to be driven by the volume of water used rather than the flow rate.

3.2.3. Reaction Rates, Mechanisms, and Kinetics

Oxidation of organic compounds is generally higher when supercritical conditions are used rather than subcritical (88). The higher temperatures favor reaction conditions and physiochemical parameters such as activation energy and the reactions proceed with higher yields of destruction. Weber et al. (88), found that the destruction efficiency of PCBs was increased from <20% at 350°C, subcritical conditions, to 99.99% at 450°C, supercritical conditions.

Kinetics and rates of reactions under subcritical and supercritical water conditions are not fully understood. Many researchers aim at producing and optimizing a process that has the highest destruction of organic compounds rather than working with fundamental reaction concepts under strictly controlled conditions. All the research described to this point has taken this approach. It is certainly of great benefit to understand reaction mechanism and kinetics, however in many cases these are specific to reactor configuration (batch vs flow), operating conditions, and the organic involved. Some research has been conducted on the reaction mechanism of basic compounds such as carbon dioxide, methanol, methane, hydrogen, and ammonia (89) and the destruction pathways of more complex organic compounds such as phenol (90) under supercritical conditions.

Reaction mechanisms are complex even for the simple molecules listed above. There exist a number of possible pathways of oxidation with intermediate formation, side reaction, and the possibility of more than one reaction pathway to arrive at the products. Global models have been proposed to simplify the overall mechanisms and allow the calculation of reaction constants and model parameters for process design purposes. Tester et al. (89) found that the destruction of larger molecules often occurs quickly with the partial oxidation to low-molecular weight species. Further oxidation of these smaller species proceeds much slower and it is eventually the oxidation of simple compounds, such as carbon monoxide and ammonia, that is rate limiting.

Portela et al. (90) experimentally studied the reaction kinetics of phenols in both sub- and supercritical water and compared the results to other proposed models. They found that many models do not accurately fit both sets of condition. The study showed that in the subcritical and supercritical region the rate laws are pseudo-first-order with respect to phenol in subcritical water, and nearly first-order for phenol in the supercritical region. Gloyna and Li (91) also state pseudo-first-order oxidation reaction rates are a reasonable

Table 5
Rate Controlling Intermediates in Sub- and Supercritical Water Oxidation

Organic compound category	Key intermediate	Oxidation end product	Conditions
Hydrocarbons and oxygenated hydrocarbons	CH_3COOH	CO_2, H_2O	Subcritical and supercritical
Nitrogen containing organics	NH_3, N_2O	N_2, H_2O	Supercritical
Chlorinated organics	CH_3Cl, CH_3OH	HCl, H_2O	Supercritical

assumption for supercritical water oxidation. Using a number of references they tabulated three categories of organic compounds and identified key intermediates which potentially are rate controlling Table 5.

3.2.4. Issues and Considerations of Using Supercritical Water Oxidation

Generally, SCW oxidation process design must consider the following requirements:

- System integration-feed lines, preheater, reactor, heatexchangers, catalytic conversion units, separators (solid–fluid and gas–liquid), and pressure let-down device;
- Influent pretreatment-waste characterization, waste segregation, possible physical/chemical pretreatment, and appropriate feed tank capacity;
- Pressurization-pumps and piping system for requires unit processes;
- Monitoring for temperature, pressure, flow, process control and appropriate data collector;
- Heat-source of initial heat, heat content of waste, and heat transfer devices;
- Materials-constructability, corrosion, erosion, and repairability;
- Effluent handling-post treatment (pH adjustment, by product recovery, and so on.) and ash disposal-collection, use, disposal;

3.2.4.1. HEAVY METAL SPECIATION AND FORMATION OF INSOLUBLE SALTS

A reduction in the dielectric constant means that nonpolar materials become soluble in sub- and supercritical water and polar materials become less soluble under the same conditions. This is consistent with the reduction in dielectric constant and the dissociation constant and is depicted in Fig. 7 which shows the solubility of common salts in water at elevated temperatures and in the supercritical region (89).

These salts have a high solubility at 25°C and 1bar as seen in Fig. 7 and this is considerably reduced, to values of ppm, as the temperature is increased. The reduced solubility can lead to process operating problems as these salts precipitate in the supercritical phase. The formation of "sticky" salts becomes a problem when particles impinge on surfaces and cause blockages in pipes and sensors as well as changing the heat transfer characteristics of the reaction vessel (92).

Reactor design for supercritical oxidation process involves a continuous flow-type reactor with the feed, oxidant, and water introduced at the top. For example, WAO, and SCW oxidation are proposed to conduct in reactors, which are placed underground in deep, well-like cavities. A schematic diagram of the reactor "downhole" is shown in Fig. 8. In the reactor, oxygen is injected into the liquid organic waste at sufficient pressure and temperature to support liquid state oxidation. The organic waste is converted
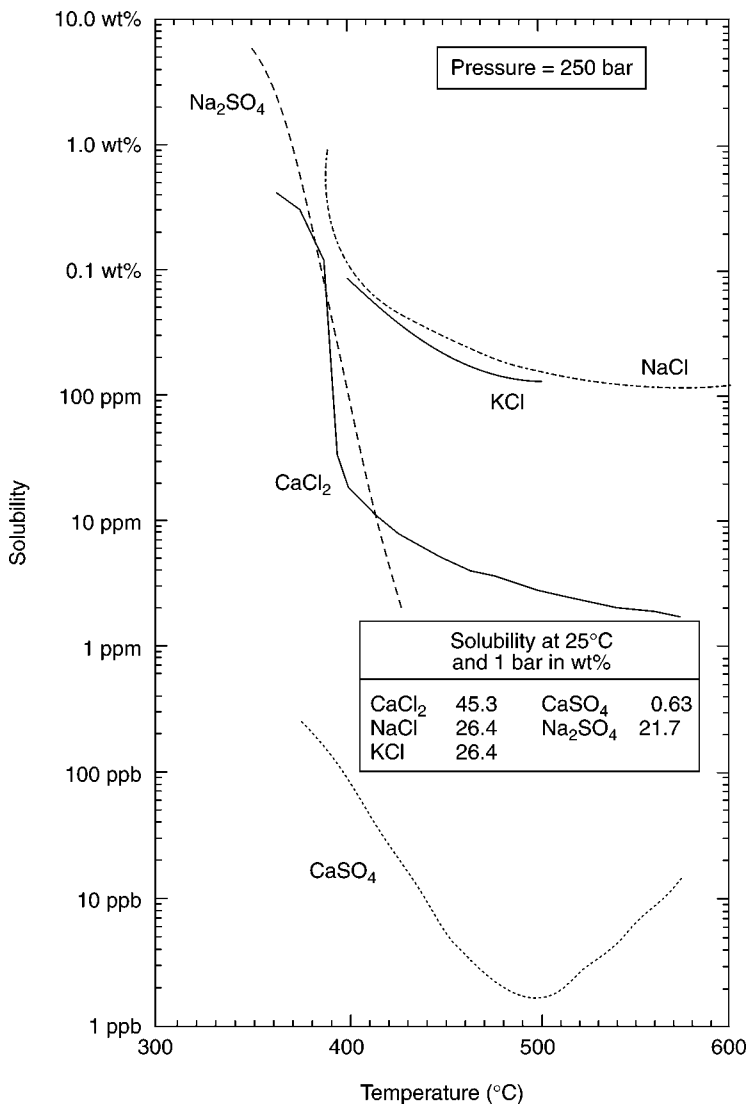
Fig. 7. Solubility of common salts in supercritical water and 250 bar (50,89).

into inert ash, carbon dioxide, and water. The excess heat generated may be recovered at surface for increasing energy efficiency (93).

3.2.4.2. CORROSION AND MATERIALS OF CONSTRUCTION

Supercritical water is very corrosive and subcritical water is to a lesser extent. One of the advantages in using subcritical conditions over supercritical is the reduction in corrosive nature of the fluid, although if reactions are important a reduction in temperature would increase reaction times (94). Corrosion mechanisms also differ between sub- and supercritical conditions and depend on the dielectric constant and the concentration of dissociated ions in solution.
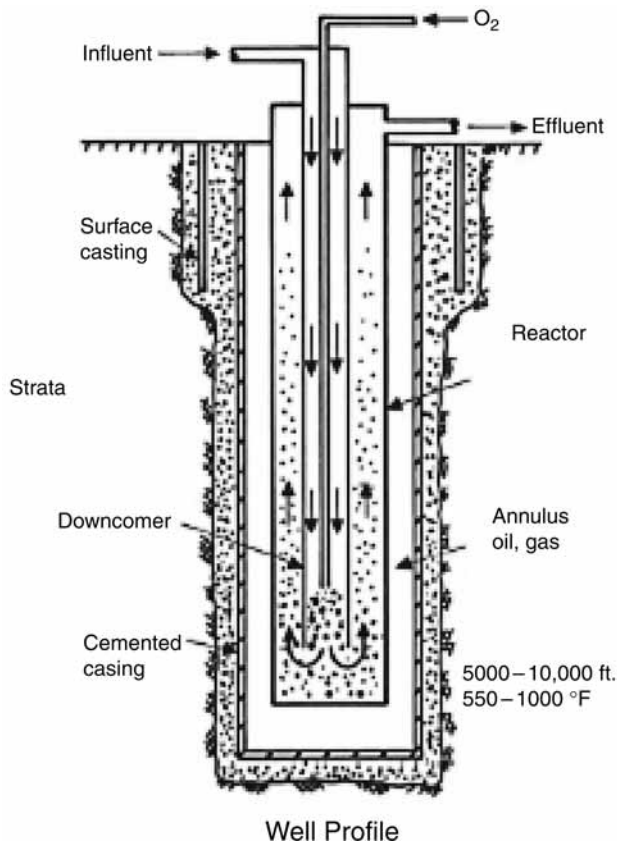
Fig. 8. Schematic diagram of "downhole" oxidation reactor (51).

Controlling corrosion is critical to system uptime since corrosion reaction products can interfere with sensors and also influence the composition of the effluent as demonstrated in the chromium study by Gloyna and Li (91). There are cases in which corrosion has occurred at faster rates in subcritical water with low pH (approx 2) rather than supercritical water. The excess of dissociated ions at subcritical conditions with low pH and a higher dielectric constant can lead to the increase in corrosion rates. Corrosion is likely to occur via electrochemical pathways because inorganic ions are soluble and present in solution because of polar water molecules. Supercritical water corrosion increases with increasing temperature and in most part occurs via chemical pathways. This is largely resulting from the reduction of solubility in inorganic and dissociated molecules (91). As a result materials of construction must be chosen carefully if durability and life expectancy are not to be compromised.

Materials of construction are recommended to be high nickel, high-chromium alloys such as Hastelloy, Inconel, Allcorr or titanium for lower temperatures. Studies on the corrosion resistance of various metals was conducted by Barner et al. (95), and showed that in general higher corrosion rates were observed than would be allowed in the construction of conventional process plants.

Berry documented the corrosion of iron-chromium-nickel alloys in high-temperature water (96) and found that corrosion rates are low with metal consumption being less than 1.25 μ/yr. The corrosion mechanism was diffusion controlled since corrosion rates slowed down with time. Galvanic corrosion was also minimized because these alloy tend to form a thick oxide film which provides insulation against galvanic corrosion. Corrosion products in Fe-Cr-Ni alloys are generally spinels with the chemical formula M_3O_4 in deaerated conditions and M_2O_3 in aerated conditions, in which M is Fe, Ni and Cr in M_3O_4, and Fe and Cr in M_2O_3. The growth of the oxide layer is a diffusion of metal ions outwards to the oxide-water interface and in some cases the diffusion of oxygen inwards at the same time. The diffusion rates are approximately equal for both species. Loose particulate corrosion products are generated by the reaction of metals to form metals hydroxides and then react to form oxides, which escape into the water. These small particulates can foul sensors and also cause blockages of small pipes, similar to insoluble salts.

4. APPLICATION EXAMPLES

4.1. Case 1: WAO of Refinery Spent Caustic: A Refinery Case Study

In 1995, a WAO system was put into operation for treatment of refinery spent caustic from gasoline sweetening, gasoline and liquid petroleum gas prewashing and from gasoline and liquid petroleum gas mercaptans extraction at the Refinaria de Petroleos de Manguinhos, S.A. (RPDM) in Rio de Janeiro (97). Prior to installing a WAO system, the refinery was dependent on off-site disposal of their spent caustic. In considering on-site treatment, there was great concern for odors because the refinery was in a populated area. The refinery concluded that WAO was the best choice for their scenario, allowing for on-site treatment without the production of odorous off-gas.

The use of aqueous caustic washing in order to improve the quality of the product and to aid in the refining process is common. The caustic washings are done to remove sulfidic and acidic components from the relevant hydrocarbons stream. The aqueous spent caustic solution from these treatments is laden with various contaminants including sulfides, mercaptans, naphthenates, and phenols (cresylates), as well as emulsified hydrocarbons. This stream is hazardous and must be treated before discharge. The odor-ous and reactive nature of the spent caustic precludes the use of biological treatment as the primary means of treatment, even with reasonable dilution.

In this application, WAO is a pretreatment technology, and at the refinery the oxidized effluent is routed to the pre-existing biological treatment facilities before discharge to the environment. A summary of the reactions occurring in the reactor can be expressed as:

$$NaHS + 2O_2 \rightarrow NaHSO_4 + H_2O$$
$$NaSR + 2O_2 \rightarrow NaHSO_4 + CO_2 + R'COONa \text{ (unbalanced)}$$
$$[Naphthenics] + O_2 \rightarrow CO_2 + R'COONa \text{ (unbalanced)}$$
$$[Cresylics] + O_2 \rightarrow CO_2 + R'COONa \text{ (unbalanced)}$$
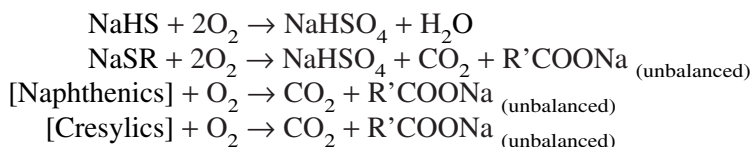
where R' is typically CH_3.

A key point which is illustrated in this reaction summary is that as oxygen is reacted, acids are produced. This is an important consideration as NaOH depletion can lead to
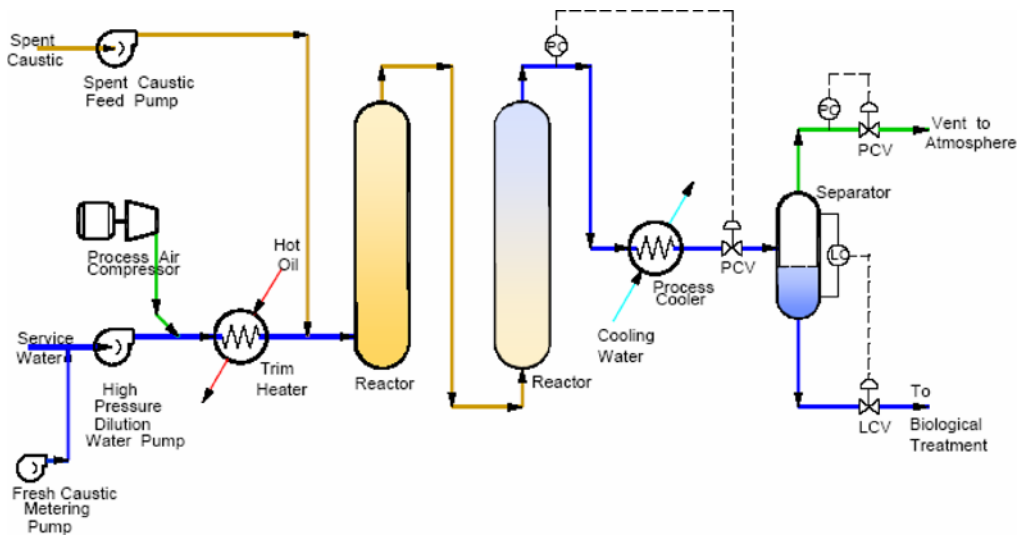
Fig. 9. RPDM WAO flow diagram (52).

Table 6
Design Conditions of RPDM Spent Caustic Oxidation System

Spent caustic feed rate	0.20 m^3/h (0.88 gpm)
Dilution feed water	0.40 m^3/h (1.76 gpm)
Reactor temperature	260°C (500°F)
Reactor pressure	90 bar (1270 psig)

acidic conditions, resulting in slower reactions and corrosion in the reactor. In the RPDM reactor, the COD loading is high enough that additional caustic is added to the system to prevent acidic conditions. The reactor achieves a high COD removal as well as detoxification; with the effluent consisting mostly of sodium sulfate and acetic acid (sodium acetate), which are benign compounds to biological treatment facilities.

The reaction conditions of the RPDM wastewater WAO facility are now typical for refinery spent caustic systems containing cresylic and naphthenic salts, at 260°C (500°F), 88 bar (1270 psig), and a 1 h hydraulic detention time. The flow diagram for the RPDM WAO unit is shown in Fig 9.

The highly concentrated nature of this spent caustic stream called for the addition of dilution water at a 3:1 ratio. This dilution is performed in order to maintain a controllable exotherm in the reactor. The dilution water is preheated, along with the pressurized air, in a hot oil heat exchanger. The cold spent caustic is then injected directly into the bubble column reactor in which the hot inlet water, coupled with the reactor heat from the exothermic reaction, raise the temperature high enough for reaction to commence. The exothermic nature of the reaction causes an increase in reaction temperature as the reactants rise through the vertical bubble reactor. The operating conditions and flow rates are seen in Table 6.

Table 7
RPDM Spent Caustic WAO Performance ($T = 246°C$)

	Reactor inlet	Reactor effluent
COD (mg/L)	72,000	15,000
COD reduction	–	79.2%
BOD/COD	–	0.515
Phenols (mg/L)	1,700	3
Sulfide-S^{2-} (mg/L)	2,700	$<1^a$
Mercaptans-CH_3SH (mg/L)	2,800	2
Thiosulfate-$S_2O_3^{2-}$ (mg/L)	640	$<26^a$
pH	13.43	8.24

[a]Below detection limit.

The hot effluent from the reactor is cooled using a cooling water heat exchanger before it is depressurized. The pressure control valve is a proprietary erosion resistant valve for reducing the pressure from 90 bar inlet to 3 bar. The depressurized effluent is then phase separated in a flash tank with the liquid effluent consisting mainly of sodium sulfate and sodium acetate in water routed to the biological treatment facility. Ultimate discharge is as makeup water for the refinery cooling towers. The off-gas is vented to the atmosphere. The reactor and process sides of the heat exchangers were manufactured out of alloy 600 in order to withstand the corrosive environment during normal operating conditions, as well as during upsets1. The WAO system was skid manufactured by Zimpro in their factory and shipped to Brazil, reducing the on-site installation work required. The reactors were field erected and connected to the skid on-site.

Performance as shown in Table 7, approx 80% destruction of COD is achieved, with near complete phenols (cresylic) destruction and sulphide levels reduced to less than detection limits. Performance and overall reliability over the past 5 yr has been good. The unit was run continuously for the first year of operation in order to treat production as well as stockpiled spent caustic. Now the unit is operated every other week to treat production spent caustic as it accumulates. No dedicated operators are assigned to the WAO unit, but rather operation is performed as necessary by RPDM refinery staff. There have been a few maintenance issues, which for the sake of completeness should be mentioned. The cooler for the system air compressor experienced corrosion resulting from off-spec oil. The corroded radiator was replaced and heat transfer oil quality is now monitored more closely. Compressor performance has been trouble free after these corrections. The occasional instrumentation breakage has also been experienced. An example would be leakage in the seals of the safety Pressure Release Valve (PRV) on the fresh caustic metering pump, calling for the replacement or repair of the PRV. Another example involved the leak detectors on the diagram feed pumps in which two of the detectors needed repair.

Implementation of WAO at RPDM allows the refinery to treat all spent caustics produced at the refinery on-site. On-site WAO has eliminated odor problems and the need to outsource spent caustic waste management. After 5 yr of operation the unit continues to meet design specifications with 80% COD destruction and good detoxification of the waste. Operation of the unit has been relatively trouble free, with the exception of the occasional instrumentation maintenance issue. Sulfidic and hazardous organic compounds
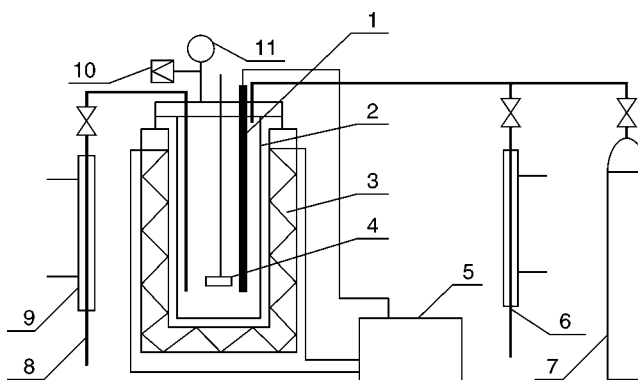
Fig. 10. Scheme of CWAO process (53).

in the wastewater such as mercaptans, naphthenic, and cresylic compounds are destroyed or converted to benign molecules. Additionally, the pH of the effluent is reduced. Reactor effluent is discharged to the on-site biological facilities for final polishing.

4.2. Case 2: CWAO for the Treatment of H-Acid Manufacturing Process Wastewater

H-acid (1-amino-8-naphthol-3, 6-disulfonic acid) is an important dye intermediate and used in chemical industry for the synthesis of direct, acidic, reactive and azoic dye, as well as in the pharmaceutical industry (98). Because the production process of H-acid is complicated and the utilization ratio of raw materials is low, the wastewater from the manufacturing processes is rich in various substituted derivatives of naphthalene compound, and is of dark color and strong acidity. Organic substances in dye intermediate wastewater are often aromatic compounds substituted by some groups, such as $-NH_2$, $-NO_2$, $-SO_3^-$, and so on. They are extremely toxic to organisms. The biological processes cannot effectively degrade these substances and decolorize the H-acid wastewater. As aromatic ring with $-SO_3H$ is easily dissolved in water; the general chemical and physical method is very inefficient. Therefore, H-acid wastewater is one of the most hardly treated wastewaters so far.

CWAO was applied for the treatment of H-acid manufacturing process wastewater by four types of powder catalysts whose main active components are copper (Cu), cerium (Ce), cadmium (Cd), and cobalt-bismuthide (Co-Bi) that were prepared with the method of the codeposition. Experimental apparatus is presented in Fig. 10. The GS-0.5 autoclave equipped with a stirrer and a heating device that keeps the constant temperature was used in experiments. It has a cooling coil and two sampling outlets (liquid- and gas-phase outlet).

All catalysts within the same group have been compared with each other. The best catalyst was selected to be Ce_3Cu1 (weight ratio of Ce and Cu is 3:1, calcination temperature is 6001°C). The results reported in Fig. 2 demonstrate that the Ce_3Cu1 composite catalyst is the best catalyst among the four catalyst groups. The Ce_3Cu1 composite catalyst was selected as the catalyst used in further study on CWAO treatment of dye intermediates.

Table 8
Effects of Ce3Cu1 Catalyst on CWAO Under Different pH Value

Initial pH of wastewater	Amount of dissolved metal (mg/L)		COD removal at 30 min (%)	The lowest pH value in reaction
	Highest	Lowest		
8.0	0.91	0.18	81.8	2.22
10.0	0.48	0.09	71.7	3.00
12.0	0.44	0.08	68.3	5.00

A simulative wastewater was used in CWAO with Ce_3Cu1 catalyst. H-acid wastewater from an actual industry mainly contains intermediates such as H-acid, T-acid (1-naphthylamine-3, 6, 8-trisulfonic acid), chromotropic acid, high concentration of salts and so on. The concentrations of H-acid, T-acid, chromotropic acid, and Na_2SO_4 in the simulative wastewater used in experiments were 10, 10, 2, and 150 g/L, respectively.

In experiments, the temperature was fixed at 200±1°C, the amount of catalyst added was 0.2 g/300 mL, and the pH value was 12.0. The results indicate that COD removal can approach 85 and 91.3% after 10 and 30 min reaction, respectively, and pH value can be kept at high levels. The lowest pH value is about 5.25 (*see* Table 8).

When temperature is 200±1°C, oxygen partial pressure is 3 MPa, pH value is 12.0, reaction time is 30 min, the COD removal by CWAO process with Ce_3Cu1 catalyst is more than 90%, and the lowest pH value of reaction solution during CWAO of H-acid solution is kept at about 6. There are many factors. The most important factors that can influence on the CWAO process of organic compounds are reaction temperature, pH value of wastewater, and catalytic conditions to improve treating effects and reduce treating costs. The pH value of solution can affect CWAO reaction significantly. Low pH value is beneficial for speeding the reaction, but at the same time, higher corrosion resistance of reactor and catalysts are required.

4.3. Case 3: Photocatalytic Decolorization of Lanasol Blue CE Dye Solution in Flat-Plate Reactor

A dye, Lanasol Blue CE was photocatalyticlly degradated using a TiO_2 photocatalyst in a Flat-Plate Reactor (FPR) in the presence of UV light (99). The flat-plate reactor designed and used for this investigation is shown schematically in Fig. 11. The reactor's area is 0.37 m² (1.22 m long and 0.30 m wide). The UV light consists of six 36-watt blacklight blue lamps. The dye solution (e.g., 30 mg/L) to be treated was prepared and stored in a tank. The outlet of the tank fed the suction side of a pump. A flow meter was used to record the system flow rate. From the outlet of the flow meter, fluid was pumped into the reactor in which it trickled through a spray tube. Holes of 1 mm in diameter and separated by 5 mm were drilled along the tube's length. After the solution was treated, it flowed back to the tank.

Results indicated that the photocatalytic oxidation process with a flat-plate reactor is effective in decoloring dyes. First-order kinetics ($C = C_0 e^{-kt}$) is representative for simplified characterizing this process in engineering applications (Fig. 12). Parameters, such as dosages of photocatalyst, flow rate through the flat-plate reactor
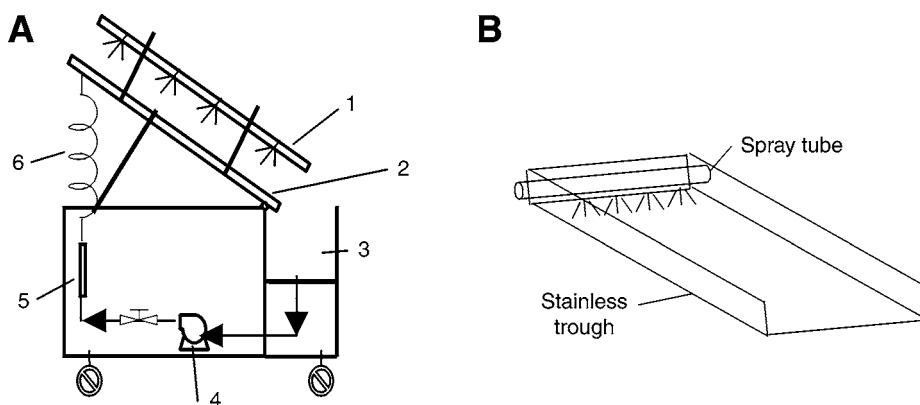
(1. UV source 2. Flat plate photoreactor 3. Tank 4. Circulating pump 5. Flow meter 6. Soft connection tube)

Fig. 11. (A) Experimental rig. **(B)** Flat plate photo-reactor (54).
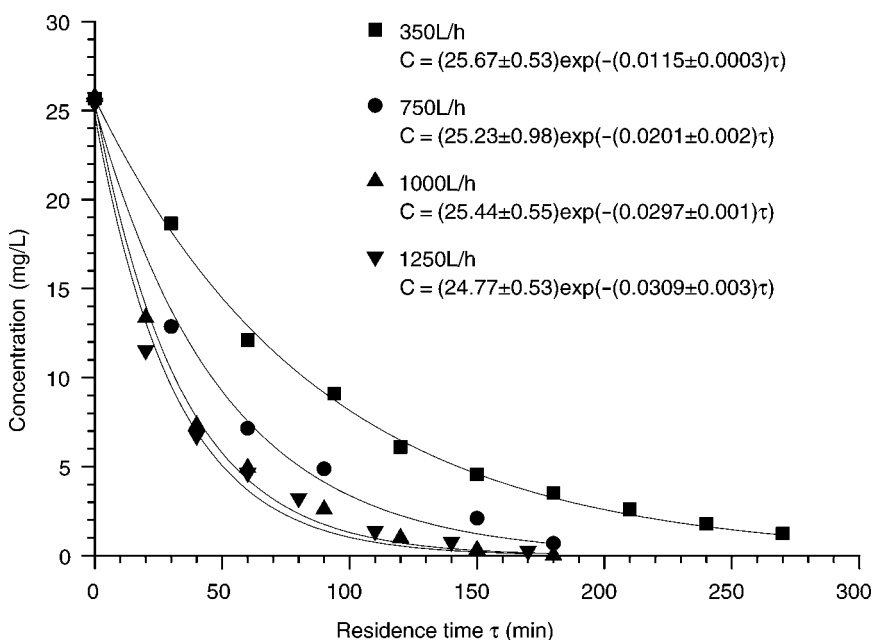
Fig. 12. Concentration vs residence time τ for different flow rate at the initial treated solution of 8 L, $\alpha = 20°$, $TiO_2 = 1$ g/L and mean UV = 36.5 W/m^2 (55).

and UV intensity, were found to significantly influence the process. Operating parameters of the system at the flow rate of 1000 L/h and TiO_2 of 1 g/L were recommended. If the value of T and the UV intensity are more, the rate of constant is more. The relationship among them is linear. The flow rate and the tilted angle were found to influence the mean film thickness of the fluid in the reactor, which in turn also affected the degradation rates in the process.

Table 9
Results and Conditions for SCWO of Real Waste Effluents Using the Tube Reactor

Waste water from	Feed-TOC (ppm)	Conversion (%)	Temperature (°C)	Salt content (wt.%)
Pharmaceutical industry	1	86	450	1
	7	83	410	1
	20	97	550	3
Chemical industry	23	99.99	550	
	4.5	99.98	550	
Paper mill	2	98	450	0.1
	2	99	500	0.1
	11	97	500	0.2
Sewage works	1	85	500	<0.1
	630	98	550	0.1
	5.4	99.8	550	0.1

4.4. Case 4: Oxidation of Industrial Waste Waters in the Pipe Reactor (100)

A continuous SCW oxidation bench scale plants is operated with a pipe reactor system (design data: $T = 630°C$, $p = 32$ MPa, feed rate waste water = 10, and 50 kg/h, air feed rate = 20 kg/h) (99, 100). Suspensions containing up to 5wt% solid material can be fed to the reactor using a membrane pump. With the pipe reactor, efficiencies of up to 99.99% were achieved for the oxidation of model compounds (ethanol, toluene, phenol) as well as real waste effluents (paper, chemical, pharmaceutical industry, sewage works). The use of the pipe reactor is limited to feeds without salt to avoid plugging.

The flow diagram of the installed SCWO bench scale plant (Fig. 9) shows that feed, water, and air are pumped and compressed, typically to 26–30 MPa. After preheating and mixing the reactants are fed into the pipe reactor (PR) or transpiring wall reactor (TWR) in which oxidation takes place. Samples can be taken for analysis (TOC, GC/MSD, and so on). After cooling and gas–liquid separation, water, and off-gas are sent to be analyzed. The SCWO bench scale apparatus is controlled automatically. The pipe reactor coil is made of Inconel 625, 15 m in length with an inner diameter (i.d.) of 8 mm and an outer diameter (o.d.) of 14 mm. It is submerged in a fluidized sand bath, which is electrically heated and acts as a thermostat.

Results and conditions for the oxidation of real waste waters at 26–28 MPa in the PR from the pharmaceutical, chemical and paper industry and our own sewage works are summarized in Table 9. The residence times were calculated with the assumptions mentioned above to be between 10 and 60 s. The feeds cover a broad range with respect to TOC, salt and solid content. The paper mill and sewage works effluents are containing solids of up to 5 wt%. The mean components of these solids are paper fibers with fillers inside. The other effluents are clear solutions. Conversions of at least 97% of the organic chemicals in the feed were achieved. At high salt concentrations the reactor plugs up eventually, but this blockage can be washed out. The influence of temperature is obviously improving the destruction efficiency, although the feed concentration at this level up to 2.3% TOC is not affecting the conversion Fig. 13. Other case histories can be found from the literature (101–102).
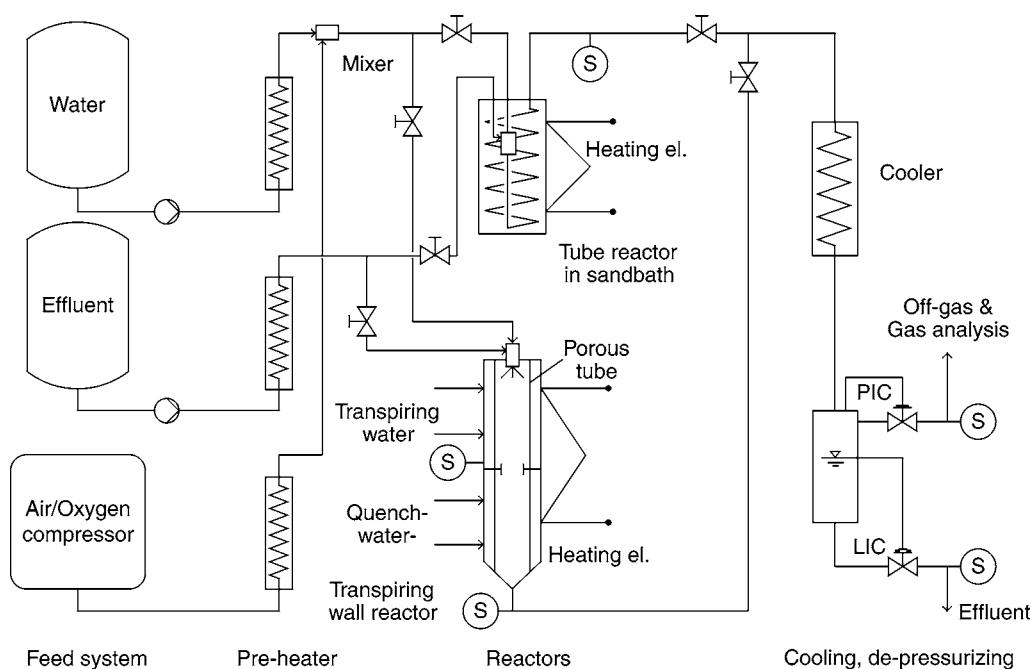
Fig. 13. Flow diagram of the SCWO bench scale apparatus (56).

REFERENCES

1. F. Luck, Wet air oxidation: past, present and future, *Catal. Today* **53**, 81–91 (1999).
2. H. Debellefontaine and J. N. Foussard, Wet air oxidation for the treatment of industrial wastes. Chemical aspects, reactor design and industrial applications in Europe. *Waste Manage.* **20**, 15–25 (2000).
3. W. G. May, *Scientific advances in alternative demilitarization technologies* F. W. Holm (ed.) Dodrechi/Boston/London: Kluwer Academic Publishers, 111–128 (1995).
4. S. W. Maloney et al., *TNT Red Water Treatment by Wet Air Oxidation*, USACERL Technical Report EP-95/01, 1994.
5. M. Jouffret, *Les oxydations radicalaires par l'air ou l'oxyene en phase liquide ou gazeuse. Aspects theoriques et pratique de catalyse d'oxydation.* In *CNRS Conference*, *Lyon France*, May 12–18 (1978).
6. L. Lixiong, P. Chen, and E. F. Gloyna, Generalized kinetic model for wet oxidation of organic compounds. *AICHE J.* **31**(11), 1687–1697 (1991).
7. J. M. Smith, H. C. V. Ness, and M. M. Abbott, *Introduction to chemical engineering thermodynamics.* 5th ed., McGraw Hill, Sydney, 1996.
8. M. I. Cabrera et al., Photocatalytic reactions involving hydroxyl radical attack. *J. Catal.* **172**(2), 380–390 (1997).
9. O. M. Alfano, M. I. Cabrera, and A. E. Cassano, Photocatalytic reactions involving hydroxyl radical attack, *J. Catal.* **172**(2), 370–379 (1997).
10. D. Blake, H. Link, and K. Eber, Solar photocatalytic detoxification of water. *Adv. Sol. Energ.* **7**, 167–210 (1995).
11. D. Y. Goswami, Engineering of solar photocatalytic detoxification and disinfection processes. *Adv. Sol. Energy* **10**, 165–209 (1995).
12. D. Y. Goswami, A review of engineering developments of aqueous phase solar photocatalytic detoxification and disinfection processes. *J. Sol. Energ. Eng.* **119**, 101–107 (1997).

13. M. Romero, J. Blanco, and B. Sanchez, Solar photocatalytic degradation of water and air pollutants: challenges and perspectives. *Sol. Energy* **66**, 169–182 (1999).

14. M. Hamerski, J. Grzechulska, and A. W. Morawski, Photocatalytic purification of soil contaminated with oil using modified Tio$_2$ powders. *Sol. Energy* **66**, 395–399 (1999).

15. N. Z. Muradov, A. T. Raissi, and D. Muzzey, Selective photocatalytic destruction of airborne VOCs. *Sol. Energy.* **56**, 445–453 (1996).

16. E. Alberto and M. Orlando, Reaction engineering of suspended solid heterogeneous photocatalytic reactors. *J. Catal. Today.* **58**, 167–197 (2000).

17. J. Bussi, et al., *Photocatalyric removal of Hg from solid wastes of Chlor-Alkali plant. J. Environ. Eng.* August, 733–738 (2002).

18. D. Y. Goswami, D. M. Trivedi, and S. S. Block, Photocatalytic disinfection of indoor air. *J. Sol. Energ. Eng.* **119**, 92–96 (1997).

19. S. Kaneco, H. Kurimoto, and Y. Shimizu, Photocatalytic reduction of CO$_2$ using TiO$_2$ powders in supercritical fluid CO$_2$ *Energy* **24**, 21–30 (1999).

20. L. Lei, et al., Catalytic wet air oxidation of dyeing and printing wastewater. *Water Sci. Technol.* **35**(4), 311–319 (1997).

21. N. N. Lichtin, M. Avudaithai, and E. Berman, TiO$_2$-photocatalyzed oxidative degradation of binary mixtures of vaporized organic compounds. *Sol. Energy* **56**, 377–385 (1996).

22. J. Lin and J. C. Yu, An investigation on photocatalytic activities of mixed TiO$_2$-rare earth oxides for the oxidation of acetone in air. *J. Photoch. Photobio. A: Chem.* **116**, 63–67 (1998).

23. Q. Wu, P. L. Yue, and X. Liu, *Continuous catalytic wet air oxidation of phenol in a trickle bed reactor.* Proceedings of the Third Asia-Pacific Conference on Sustainable Energy and Environmental Technologies, 3–6 December, 2000, Hongkong, 2000, pp. 45–50.

24. Degussa Company, *Physicochemical data of AEROSIL, Aluminium Oxide C and Titanium Dioxide P25, in AEROSIL, Aluminium Oxide C and Titanium Dioxide P25 for catalysts, Technical Bulletin Pigments*, p. 18 (1991).

25. B. Samuneva, V. Kozhukharov, and C. Trapalis, Sol-gel processing of titanium-containing thin coatings. *J. Mater. Sci.* **28**, 2353–2360 (1993).

26. U. O. Krasovec, et al., The gasochromic properties of sol-gel WO$_3$ films with sputtered Pt catalyst. *Sol. Energy* **68**(6), 541–551 (2000).

27. S. Sun, Z. Kang, and Z. Wei, *Treatment of woolen-dyeing wastewater by TiO$_2$ film-solar photocatalytic oxidation process.* Environmental protection of Chemical Industry, **20**(1), 2000.

28. A. Fujishima, *Photocatalytic and self-cleaning fuctions of TiO$_2$ coatings.* Proceedings of the Third Asia-Pacific Conference on Sustainable Energy and Environmental Technologies, December 3–6, 2000, Hongkong, 2000, pp. 1–5.

29. K. Sunada et al., Bactericidal and detoxification effects of TiO$_2$ thin film photocatalysts, *Environ. Sci. Technol.* **32**, 726–728 (1998).

30. J. He et al., Effect of crystallization phases of titania film on photocatalytic degradation of aniline. *Chinese J. Appl. Chem.* **16**(5), 56–60 (1999).

31. P. Zhang, G. Yu, and Z. Jiang, Review of semiconductor photocatalyst and its modification. *Adv. Environ. Sci.* **5**(3), 2–10 (1997).

32. M. Bekbolet, M. Lindner, and D. Weichgrebe, Photocatalytic detoxification with the thin-film fixed-bed reactor (TFFBR): clean-up of highly polluted landfill effluents using a novel TiO$_2$-photocatalyst. *Sol. Energy.* **56**, 455–469 (1996).

33. J. Yu et al., Study on photocatalytic degradation of organophosphorous insecticide using porous TiO$_2$ nanometer thin films by sunlight. *Acta Energae Solaris Sin.* **21**(2), 165–170 (2000).

34. L. Shivalingappa, J. Sheng, and T. Fukami, Photocatalytic effect in platinum doped titanium dioxide films. *Vacuum* **48**, 413–416 (1997).

35. U. Gesenhues, Al-doped TiO_2 pigments: influence of doping on the photocatalytic degradation of alkyd resins. *J. Photochem. Photobiol. A: Chem.* **139**, 243–251 (2001).
36. H. Wei, D. Xu, and J. Xu, Photo oxidation of humic acid in aqueous solution catalized by TiO_2 Film. *ACTA Scientiae Circumstantiae.* **18**(2), 162–166 (1998).
37. W. Xi and S. -u. Geissen, Separation of titanium dioxide from photocatalytically treated water by cross-flow microfiltration, *Water Res.* **35**(5), 1256–1262 (2001).
38. L. Shi, et al., Morphology and properties of ultrafine SnO_2–TiO_2 coupled semiconductor particles. *Mater. Chem. Phy.* **62**, 62–67 (2000).
39. F. Zhang and Q. Li, Study of visible spectral sensitization of nanocrystalline TiO_2 photocatalyst. *Chinese J. Catal.* **20**(3), 329–332 (1999).
40. A. E. Cassano, et al., Photoreactor analysis and design: fundamentals and applications. *Ind. Eng. Chem. Res.* **34**, 2155–2201 (1995).
41. L. Jakob, et al., *TiO_2 photocatalytic treatment of water. Reactor design and optimization experiments.* In *Photocatalytic Purification and Treatment of Water and Air*, D. F. Ollis and H. Al-Ekabi, eds., Elsevier Science Publishers BV: Amsterdam, The Netherland, 1993, pp. 511–532.
42. O. Legrini, E. Oliveros, and A. M. Braun, Photochemical processes for water treatment, *Chem. Res.* **93**, 671–698 (1993).
43. P. L. Yue, *Modelling, scale-up and design of multiphasic photoreactors.* In: *Photocatalytic Purification and Treatment of Water and Air*. Amsterdam, The Netherland: Elsevier Science Publishers BV, 1993.
44. A. Sclafani, A. Brucato, and L. Rizzuti, *Mass transfer limitations in a packed bed photoreactor used for phenol removal.* In: *Photocatalytic Purification and Treatment of Water and Air*. Amsterdam, The Netherland: Elsevier Science Publishers BV, 1993.
45. J. G. Sczechowski, C. A. Koval, and R. D. Noble, A Taylor votex reactor for heterogeneous photocatasis. *Chem. Eng. Sci.* **50**, 3163–3173 (1995).
46. A. Haarstrick, O. M. Kut, and E. Heinzle, TiO_2-assisted degradation of environmentally relevant organic compounds in wastewater using a novel fluidized bed photoreactor. *Environ. Sci. Technol.* **30**, 817–824 (1996).
47. D. F. Ollis, E. Pelizzetti, and N. Serpone. *Heterogeneous photocatalysis in the environment: application to water purification.* In: *Photocatalysis: Fundamentals and Applications.* New York, Wiley, 1989.
48. N. J. Peill and M. R. Hoffmann, Development and optimization of a TiO2-coated fibre-optic reactor: photocatalytic degradation of 4-chlorophenol, *Environ. Sci. Technol.* **29**, 2974–2981 (1995).
49. N. J. Peill and M. R. Hoffmann, Chemical and physical characterization of a TiO_2-coated fiber optic cable reactor. *Environ. Sci. Technol.* **30**, 2806–2812 (1996).
50. N. J. Peill and M. R. Hoffmann, Solar-powered photocatalytic fiber-optic cable reactor for waste stream remediation. *J. Sol. Energ. Eng.* **119**, 229–236 (1997).
51. N. J. Peill and M. R. Hoffmann, Mathematical model of photocatalytic fiber-optic cable reactor for heterogeneous photocatalysis. *Environ. Sci. Technol.* **32**, 398–404 (1998).
52. O. Zik, J. Karni, and A. Kribus, The trof (tower reflector with optical fibres): a new degree of freedom for Solar energy systems. *Sol. Energy* **67**(1–3), 13–22 (1999).
53. H. C. Yatmaz, C. R. Howarth, and C. Wallis, *Photocatalysis of organic effluents in falling film reacor.* In: *Photocatalytic Purification and Treatment of Water and Air*. Amsterdam, The Netherland: Elsevier Science Publishers BV, 1993.
54. D. Bockelmann et al., *Solar detoxification of polluted water: comparing the efficiencies of a parabolic through reactor and a novel thin-fixed-bed reactor.* In: *Photocatalytic Purification and Treatment of Water and Air*. Amsterdam, The Netherland: Elsevier Science Publishers BV, 1993.
55. Y. Zhang and J. C. Crittenden, Fixed-bed photocatalysts for solar decontamination of water. *Environ. Sci. Technol.* **28**(3), 435–442 (1994).

56. A. K. Ray and A. A. C. M. Beenackers, Novel swirl-flow reactor for kinetic studies if semi-conductor photocatalysis. *AIChE J.* **43**, 2571–2578 (1997).

57. J. I. Ajona and A. Vidal, The use of CPC collectors for detoxification of contaminated water: design, construction and preliminary results. *Sol. Energy* **68**, 109–122 (2000).

58. M. S. Mehos and C. S. Turchi, Field testing solar photocatalytic detoxification of TEC contaminated groundwater. *Environ. Prog.* **12**(3), 194 (1993).

59. M. R. Prairie, J. E. Pacheco, and L. R. Evans, *Solar detoxification of waste containing chlorinated solvents and heavy metals via TiO₂ photocatalysis. Sol. Energy.* 1992 (Proceeding of the ASME international Solar Energy conference). **1**, 1–8 (1992).

60. J. Blanco, et al., Compound parabolic concentrator technology development to commercial solar detoxification application. *Sol. Energy* **67**(4–6), 317–330 (1999).

61. P. Wyness, et al., Performance of nonconcentrating solar photocatalytic oxidation reactors, Part II: shallow pond configuration. *J. Sol. Energ. Eng.* **116**(1), 8–13 (1994).

62. J. F. Klausner, A. R. Martin, and D. Y. Goswami, On the accurate determination of reaction rate constants in batch-type solar photocatalytic oxidation facilities, *J. Sol. Energ. Eng.* **116**(1), 19–24 (1994).

63. W. M. Van, R. H. G. Dillert, and D. W. Bahnemann, A novel nonconcentrating reactor for solar water detoxification. *J. Sol. Energ. Eng.* **119**, 114–119 (1997).

64. M. March, A. Martin, and C. Satiel, Performance modeling of nonconcentrating solar detoxification systems. *Sol. Energy* **54**(3), 143–151 (1995).

65. R. F. P. Nogueira and W. F. Jardim, TiO₂-fixed-bed reactor for water decontamination using solar light, *Sol. Energy* **56**, 471–477 (1996).

66. P. Wyness, J. F. Klausner, and D. Y. Goswami, Performance of nonconcentrating solar photocatalytic oxidation reactors, Part I: flat-plate configuration. *J. Sol. Energ. Eng.* **116**, 2–7 (1994).

67. O. M. Alfano, R. L. Romero, and A. E. Casano, A cylindrical photoreactor irradiated from the bottom–I. Radiation flux density generated by a tubular source and a parabolic reflector. *Chem. Eng. Sci.* **40**(11), 2119–2127 (1985).

68. O. M. Alfano, R. L. Romero, and A. E. Cassano, A cylindrical photoreactor irradiated from the bottom–II. Models for the local volumetric rate of energy absorption with polychromatic radiation and their evaluation. *Chem. Eng. Sci.* **41**(5), 1155–1161 (1986).

69. O. M. Alfano, et al., A cylindrical photoreactor irradiated from the bottom–III. Measurement of absolute values of the local volumetric rate of energy absorption. Experiments with polychromatic radiation. *Chem. Eng. Sci.* **41**(5), 1163–1169 (1986).

70. J. C. Crittenden, et al., Solar detoxification of fuel-contaminated groundwater using fixed-bed photocatalysts, *Water Environ. Res.* **68**(3), 270–277 (1996).

71. D. Y. Goswami. et al., *Solar photocatalytic treatment of groundwater at Tyndall AFB:Field test results.* Solar 1993, Proceedings of the American Solar Energy Society Annual Conference 1993, pp. 235–239 (1993).

72. D. D. Dionysiou. et al., Rotating disk photocatalytic reactor: development, characterization, and evaluation for the destruction of organic pollutants in water. *Water Res.* **34**(11), 2927–2940 (2000).

73. D. D. Dionysiou et al., Effect of ionic strength and hydrogen peroxide on the photocatalytic degradation of 4-chlorobenzoic acid in water. *Appl. Catal. B: Environ.* **26**(3), 153–171 (2000).

74. D. D. Dionysiou et al., Continuous-mode photocatalytic degradation of chlorinated phenols and pesticides in water using a bench-scale TiO2 rotating disk reactor. *Appl. Catal. B: Environ.* **24**(3–4), 139–155 (2000).

75. D. D. Dionysiou et al., Oxidation of organic contaminants in a rotating disk photocatalytic reactor: reaction kinetics in the liquid phase and the role of mass transfer based on the dimensionless Damkohler number. *Appl. Catal. B: Environ.* **38**(1), 1–16 (2002).

76. J. T. Spadaro, L. Isabelle, and V. Ranganathan, Hydroxyl radical mediated degradation of azo dyes: evidence for benzene generation. *Environ. Sci. Technol.* **28**(7), 1389–1393 (1994).

77. J. T. Shama, C. Peppiatt, and M. Biguzz, A novel thin film photoreactor. *J. Chem. Technol. Biotechnol.* **65**, 56–64 (1996).

78. P. W. Atkins, *Physical Chemistry*. 5th ed., Oxford University Press, Melbourne, 1995.

79. G. F. C. Rogers and Y. R. Mayhew, *Thermodynamic and transport properties of fluids.* 5th ed., Blackwell, Cambridge, pp. 1–28 (1996).

80. M. J. Dietrich and A. J. Patarcity, wet air oxidation of hazardous organics in wastewater, *Environ. prog.* **4**(3), 1985.

81. M. Modell, *Supercritical fluid technology in hazardous waste treatment.* In *Conference proceedings of oil waste management alternatives symposium.* Oakland, CA, April 28–29, 1988.

82. D. R. Lide, *CRC Handbook of Chemistry and Physics.* 72nd ed., CRC Press, Boston, pp. 12–18 (1991–1992).

83. A. J. M. Lagadec, et al., Pilot-scale subcritical water remediation of polycyclic aromatic hydrocarbon- and pesticide-contaminated soil. *Environ. Sci. Technol.* **34**(8), 1542–1548 (2000).

84. Critical Processes Ltd., *Introduction to Superheated Water.* Roecliffe (2004).

85. K. Hartonen, et al., Pressurised hot water extraction (PHWE) of n-alkanes and polyaromatic hydrocarbons (PAHs): comparison for PAHs with supercritical fluid extraction. *J. Microcolumn.* **12**, 412–418 (2000).

86. S. B. Hawthorne, Y. Yang, and D. J. Miller, Extraction of organic pollutants from environmental solids with sub- and supercritical water. *Analyt. Chem.* **66**, 2912–2920 (1994).

87. S. Hashimoto et al., Remediation of soil contaminated with dioxins by subcritical water extraction, *Chemosphere* **54**(1), 89–96 (2004).

88. R. Weber, S. Yoshida, and K. Miwa, PCB destruction in subcritical and supercritical water—evaluation of PCDF formation and initial steps of degradation mechanisms, *Environ. Sci. Technol.* **36**(8), 1839–1844 (2002).

89. J. W. Tester, et al., *Supercritical water oxidation technology: process development and fundamental research.* In: *ACS symposium on emerging technologies for hazardous waste management.* Atlanta, USA, 1991.

90. J. R. Portela, E. Nebot, and E. M. D. L. Ossa, Kinetic comparison between subcritical and supercritial water oxidation of phenol, *Chem. Eng. J.* **81**(1–3), 287–299 (2001).

91. E. F. Gloyna and L. Li, Supercritical water oxidation: an engineering update, *Waste Manage.* **13**(5–7), 379–394 (1993).

92. H. E. Barner, et al., Supercritical water oxidation: an emerging technology. *J. Hazard. Mater.* **31**(1), 1–17 (1992).

93. A. P. Jackman and R. L. Powell, *Hazardous Waste Treatment Technologies: Bilogical treatment, Wet Air Oxidation, Chemical Fixation, Chemical Oxidation.* Noyes publications, Park Ridge, New Jersey, USA, 1991.

94. S. Rice and R. Steeper, Oxidation rates of common organic compounds in supercritical water, *J. Hazard. Mater.* **59**, 261–278 (1998).

95. H. E. Barner et al., Supercritical water oxidation: an emerging technology, *J. Hazard. Mater.* **31**(1), 1–17 (1992).

96. W. E. Berry, *The Corrosion Behaviour of Fe-Cr-Ni Alloys in High-Temperature Water. High Temperature*, *High Pressure Electrochemistry in Aqueous Solutions*, 1976, pp. 48–66.

97. T. M. S. Carlos, R. d. P. d. Manguinhos, and C. B. Maugans, *Wet Air Oxidation of Refinery Spent Caustic: A Refinery Case Study.* in *NPRA Conference, San Antonio, Texas,* September 12, 2000.

98. W. Zhu et al., Application of catalytic wet air oxidation for the treatment of H-acidmanufacturing process wastewater. *Water Res.* **36**, 1947–1954 (2002).
99. L. Zou, Y. Li, and E. Hu, Photocatalytic decolorisation of Lanasol Blue CE dye solution using a flat plate reactor. *J. Environ. Eng.* **131**, 102–107 (2005).
100. J. Abeln et al., *Supercritical Water Oxidation (SCWO): A process for the treatment of industrial waste effluents*, Forschungszentrum Karlsruhe, Institut für Technische Chemie, http://www.turbosynthesis.com/summitresearch/bord-paperkorr.pdf. (2006).
101. L. K. Wang, T. T. Hung, H. H. Lo and C. Yapijakis (eds.). *Handbook of Industrial and Hazardous Wastes Treatment*. Marcel Dekker Inc., NY. p. 774–1046 (2004).
102. L. K. Wang, Y. T. Hung, H. H. Lo and C. Yapijakis (eds.). *Waste Treatment in the Food Processing Industry*. CRC Press, NY. p. 156–160 (2006).

14
Lime Calcination

**Gupta Sudhir Kumar, Anushuya Ramakrishnan,
and Yung-Tse Hung**

CONTENTS

1. INTRODUCTION

Lime is one of the most widely used and cheapest alkalizing agents employed worldwide. It is often applied in chemical processes in a slaked or calcium hydroxide or slurry form. The term "calcinations of limestone" refers to the process of thermal decomposition into quick lime and carbon dioxide. It is frequently referred to as "calcinations." Decomposition of limestone is characterized by very simple chemical reactions. Complexity is seen to arise when dealing with dolomite, which is believed to cause a change in crystallography and microstructure. Kinetics of decomposition of granular and lumped limestones has been found to be very complex. This has resulted in a limited validity to produce a unified theory on calcinations. This is controlled by many factors, which includes:

- One of the steps in calcinations may be rate limiting under specific circumstances.
- Differences exist in crystallography and microstructure of limestone, which are very difficult to quantify, can have a marked effect.
- Microstructure and surface morphology of limestone are seen to have a significant effect on calcinations and these are controlled by temperature, impurities, and time of exposure after completion of the reaction.
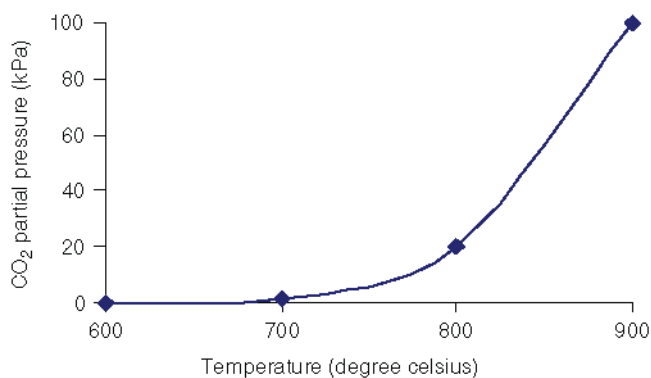
Fig. 1. Variation of the dissociation pressure of calcite with temperature.

2. THE CHEMICAL REACTIONS

2.1. *Calcium Carbonate*

Limestone is calcined to produce unslaked lime, the reaction for the thermal decomposition of calcium carbonate may be expressed as:

$$CaCO_3 + Heat \rightleftharpoons CaO + CO_2 \tag{1}$$

$$100\ g \qquad\qquad 56\ g \quad 44\ g$$
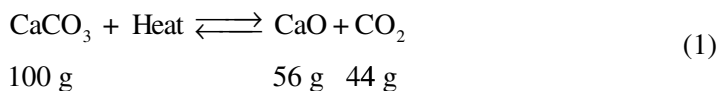
The variation of dissociation pressure of calcite with temperature is shown in Fig. 1. It is seen to reach 1 atm (101.3 kPa) at approx 900°C. Recent work has pointed out a value of 902.5°C unlike the earlier studies, which had reported a value of 898°C.

Calcination of limestone is accompanied by dissociation of heat. The heat of dissociation of calcite relative to 25°C has been reported in the literature to range between 695 and 834 kcal/kg of CaO. An average value of 770 kcal/kg has been reported by Boynton (1), whereas Schwarzkopf (2) has reported a value of 754 kcal/kg.

At 900°C, the heat of dissociation is 723 kcal/kg CaO based on the aforementioned calculation. A difference of 37 kcal/kg CaO is because of the following fact. It should be noted that 1.786 kg of calcium carbonate requires 431 kcal to be heated from 25°C to 900°C, whereas the reaction products—1 kg of CaO and 0.786 kg of CO_2—release 208 and 186 kcal, respectively, on cooling from 900 to 25°C, a total of 394 kcal. Schwarzkopf (2) reports a value of 698 kcal/kg at 900°C.

2.2. *Magnesium Carbonate*

Thermal decomposition of magnesium carbonate is represented as:

$$MgCO_3 + Heat \rightleftharpoons MgO + CO_2 \tag{2}$$

$$84\ g \qquad\qquad 40\ g \quad 44\ g$$
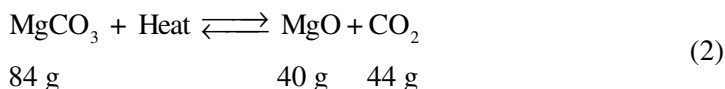
The dissociation pressure of $MgCO_3$ has been reported to range between 402 and 550°C (1,2) at 1 atm. The heat of dissociation of $MgCO_3$ has been reported to be 723 kcal/kg MgO (3).

2.3. Dolomite and Magnesian/Dolomitic Limestone

Dolomite and magnesian/dolomitic limestones are seen to undergo a complex decomposition. The decomposition has been reported to take place via a single stage for some varieties of limestones, whereas some decompose via two discrete stages, whereas others decompose in an intermediate manner (1,3).

$$CaCO_3 \cdot MgCO_3 + Heat_{(1)} \rightleftharpoons CaCO_3 \cdot MgO + CO_2 \uparrow \tag{3}$$
184 g   140 g   44 g

$$CaCO_3 \cdot MgO + Heat_{(2)} \rightleftharpoons CaO \cdot MgO + CO_2 \uparrow \tag{4}$$
140 g   96 g   44 g

$$CaCO_3 \cdot MgCO_3 + Heat_{(1+2)} \rightleftharpoons CaO \cdot MgO + 2CO_2 \uparrow \tag{5}$$
184 g   96 g   88 g
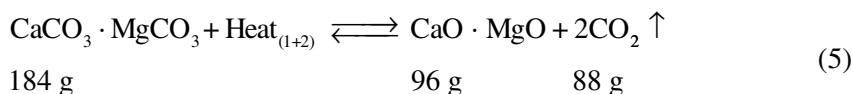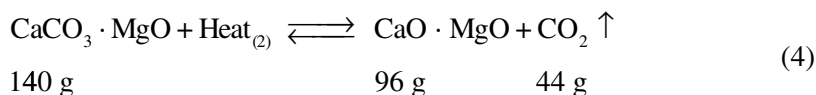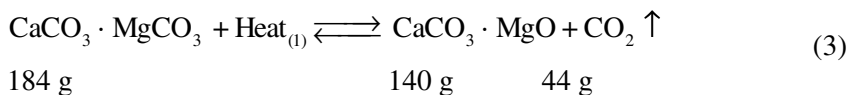
Dolomite and magnesian/dolomitic limestones decompose at higher temperatures than magnesium carbonate. The calcinations temperature during initiation varies from 510 to 750°C (2) and is governed by the crystal structure and the form of the stone (1). Reaction 3 occurs towards the lower end of the range, whereas reaction 4 occurs at about 900°C. Reaction 5 has been reported to occur at the higher end of the range. Differential heat transfer rates govern the discrepancy rather than fundamental differences in the physical chemistry of the various limestones.

The heat of dissociation of dolomite that is heat$_{(1 + 2)}$ is reported to be 723 kcal/kg of (CaO·MgO), relative to 25°C (3). This is seen to be lower than the weighted average of the heats of dissociation of $CaCO_3$ and $MgCO_3$—750 kcal/kg (CaO·MgO). This discrepancy may be related to the difference in the heat of formation of dolomite relative to those of calcite and $MgCO_3$.

3. KINETICS OF CALCINATION

3.1. Stages of Calcinations

The passage of a limestone particle through a lime kiln can be divided into five stages. The following stages have been observed with the high calcium limestone, but this can also be compared with magnesian/dolomitic limestones and dolomite.

 a. The limestone is preheated in the preheating zone from ambient temperature to about 800°C by the kiln gases (i.e., products of combustion plus CO_2 from calcinations and excess air).
 b. At about 800°C, the pressure of carbon dioxide produced by the dissociation of limestone equals the partial pressure of CO_2 in the kiln gases. As the temperature of limestone rises, the surface layer begins to decompose, so that when the temperature of the stone reaches 900°C, the layer of lime may be 0.5 mm thick (corresponding to about 5% by weight of quicklime for a 25 mm particle).
 c. As the temperature of limestone exceeds the "decomposition temperature" of 900°C, the partial pressure exceeds 1 atm and the process of dissociation can proceed beyond the surface of the particles.

   d. The lime begins to sinter, if all of the calcium carbonate dissociates before a given particle leaves the calcining zone. This process occurs to a very limited extent during stage (c); but for most situations, it can be disregarded.
   e. Particles of lime, which may contain residual limestone, leave the calcinations zone at 900°C and are cooled by air used for combustion.

Stages (a), (b), and (e) involve the direct heat transfer between a gaseous medium and particles. As a unit process, the heat transfer mechanism is clear, and not specific to the calcinations of limestone. However, stages (c) and (d), are specific to limestone, are influenced by the design of lime kiln and influence the properties of the quick lime. They are discussed in detail later.

3.2. Dissociation of High Calcium Limestone

Dissociation of limestone always proceeds gradually from the outside surface to inside. Usually the depth of penetration uniformly moves inward on all sides of the stone, like a "growing veneer or shell." Actually, a certain amount of exterior or surface dissociation of carbonate molecules can occur at lower temperatures than the preceding carbonate molecule under favorable conditions, such as low concentrations of carbondioxide with low partial pressures. But for dissociation to penetrate into the interior of the limestone, higher temperatures are necessary and must be further elevated for dissociation to occur in the center or core of the stone. The larger the diameter of the stone, the higher the temperatures required for dissociation of core because of increasing internal pressure as the carbon dioxide gas forces its escape. Thus, with the same stone purity, the difference between dissociation temperatures of the surface and core may be 300–700°F (150–350°C), depending primarily on the stone's diameter. The dissociation of limestone above the decomposition temperature as described earlier can be regarded as consisting of five processes, as illustrated in Fig. 2.

   a. Heat transfer from the kiln gases to the surface of the decomposing particle.
   b. Heat conduction from the surface to the reaction interface through the microporous layer of lime.
   c. Dissociation of calcium carbonate into CaO and CO_2.
   d. Migration of the produced CO_2 from the reaction interface, through the limelayer to the surface of the particle, and is simultaneously heated from the temperature of the reaction zone to that of the surface.
   e. Migration of carbon dioxide away from the surface into the kiln gases.

The processes (a), (b), and (e) are such that their physical and physical chemistry are well understood, but reactions (c) and (d) are complex, because of the effect of the microstructure of the lime layer on these reactions. Further complications arise when changes occur in the structure of the surface layers of the lime, caused by sintering, slagging, and absorption of sulfur dioxide.

Any of the aforementioned steps may become rate limiting under particular circumstances, which causes a difficulty in arriving at a unified theory on calcinations. The major variable affecting the rate of dissociation of limestone are:

   a. The characteristics of the limestone.
   b. The particle size distribution.
   c. The shape of the particles.
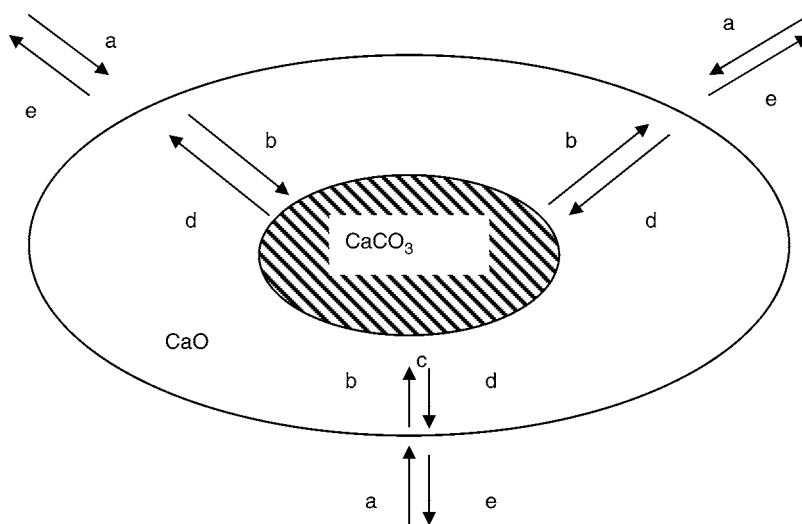
Fig. 2. Illustration of the processes involved in dissociation of limestone.

d. The temperature profile in the calcining zone.
e. The rate of heat exchange between the gases and the particles.

Calcining trial quantities would help in revealing the characteristics of a particular limestone. It is recommended that such trials should be carried out at both laboratory and on the full scale. It has been observed that variations to the extent of two times factor are common and even greater factors have been reported (1). Generally fine-grained limestones are believed to decompose more rapidly than coarse-grained ones.

Complete dissociation of particles with a given shape, but of differing sizes has been found to follow a common curve. Figure 3 shows such a curve for spheres of a dense limestone, and the results are summarized in Table 1.

Figure 4 and Table 2 summarize the combined effects of temperature and size on spheres of the same dense limestone.

The optimum temperature for maximum calcination efficiency (capacity and Btu consumption) varies with different stones and can only be determined with exactitude by experimentation. However, such a temperature must be balanced against the optimum temperature for maximum quality, and the two are usually disconstant. Generally, these two temperatures differ by 200–500°F (100–260°C) and there is often a question on adoption of suitable temperature and this can be resolved through a compromise intermediate temperature. For high calcium and dolomitic temperatures respectively, 2100°F and 1950°F (1149 and 1066°C) might be regarded as a median demarcation line between high and low temperatures in lime burning. Approximate, maximum, and minimum practical calcining temperatures would be depending on the stone's crystallinity and lineal dimensions: high calcium, 2450–1850°F; dolomitic, 2250–1725°F.

It has been reported that for a given shape factor, the calcining time is directly proportional to the square of thickness (in which thickness is defined as the minimum dimension measured through the center of gravity of the particle) (4). A formula has also been derived for the calcining effort of a particular shape. This concludes that the
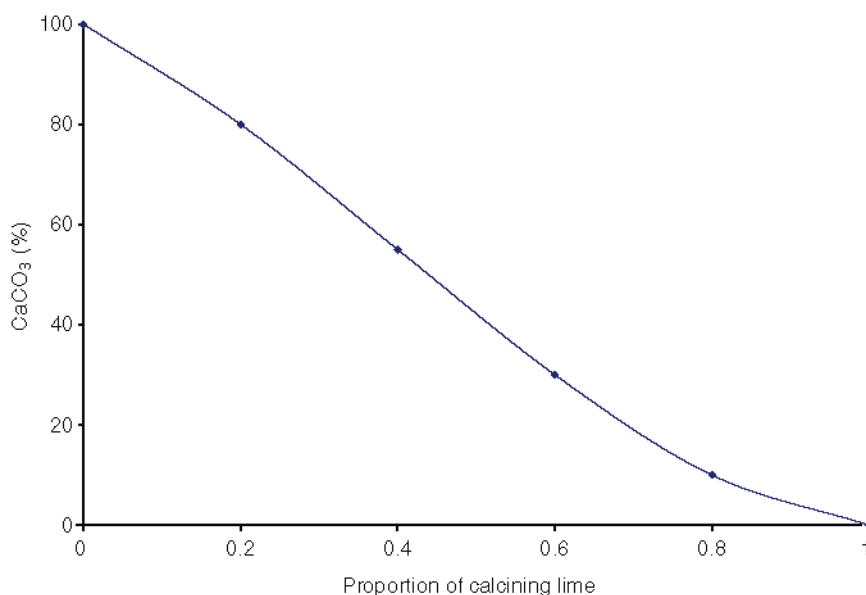
Fig. 3. Normalized dissociation curve for limestone spheres.

Table 1
Dissociation of Limestone[a]

Proportion of dissociation time	Dissociation of original calcium carbonate[b] (%)	Calcium carbonate in sphere[b] (%)
0.16	40	73
0.29	60	54
0.37	70	43
0.48	80	31
0.63	90	17
0.76	95	8.6
0.86	98	3.5
0.90	99	1.8
1.00	100	0

[a]For spheres of dense, high calcium limestone, with a range of diameters.
[b]values are m/m (%).
Adapted from ref. 5.

calcining effort of a long rectangular prism of a given thickness is double that of a cube of the same thickness (3). Calcining times have been reported to be 1 for a given thickness of sphere, 1.5 for a cube, 1.7 for a cylinder, and 3 for a plate (2). Moreover, rapid burning is achieved with the more porous stones or stone with natural cracks or fissures that are either open or filled with moisture or carbonaceous matter. These pores provide more surface area for the evolution of carbon dioxide.

The rate of heating has the greatest influence on lime quality, its shrinkage, porosity, and reactivity, affecting more than temperature or retention time. A gradual rather than
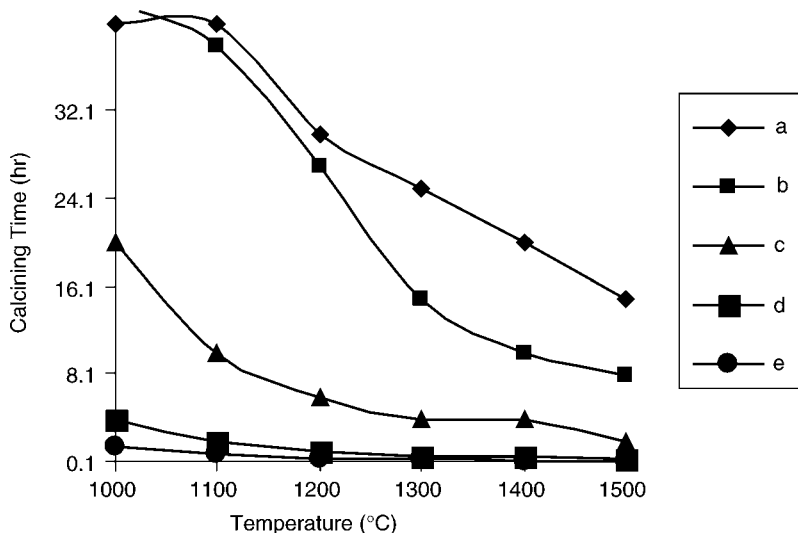
Fig. 4. Variation of calcining time with size and temperature for spheres of a dense, high calcium limestone with diameters of **(A)** 150 mm, **(B)** 125 mm, **(C)** 100 mm, **(D)** 75 mm, and **(E)** 50 mm.

Table 2
Variation of Clacining Time with Size and Temperature

	Dissociation time (h)[a]					
	Temperature (°C)					
Diameter of sphere (mm)	1000	1100	1200	1300	1400	1500
12	0.8	0.3	0.2	–	–	–
19	1.1	0.5	0.3	0.2	–	–
25	1.5	0.6	0.4	0.25	0.2	–
37	2.3	1.0	0.6	0.4	0.3	0.2
50	3.5	1.5	0.8	0.6	0.4	0.3
75	7.9	3.8	2.0	1.4	1.0	0.8
100	19	8.5	4.8	3.5	2.6	1.9
125	43	19	11	8.3	6.3	4.6
150	–	45	26	19	15	11

[a]For a dense high calcium limestone.
Adapted from ref. 5.

shock preheating and a gradual increase in calcination temperature up to the point at which dissociation is complete are most fruitful to pursue for successful calcinations.

3.3. Calorific Requirements for Dissociation of Calcium and Dolomitic Quick Lime

Heat consumed for dissociation may be calculated from the specific heat of high calcium or dolomitic limestone by the formula: specific heat of limestone × 2000 lb × net gain in °F from atmospheric temperature.

Assuming that the specific heat is calculated for calcium carbonate at 0.255 and that the starting temperature of dissociation is 50°F, and that the minimum dissociation temperature is 1648°F, then $0.255 \times 2000 \times 1648 - 50 = 840,430$ Btu/t of high quick lime.

Calorific requirements for dolomitic limestone would be less because of its lower dissociation point (about 1337°F [or 725°C] for a pure equimolar double carbonate). Based on the preceding formula, the same constants and a factor of 1.9 to allow for dolomite's greater carbon dioxide content, the theoretical kinetics would be 656,370 Btu/t of dolomitic stone or 1,247,103 Btu/t of dolomitic limestone.

3.4. Dissociation of Magnesian/Dolomitic Limestones and Dolomite

The processes are described in Section 3.2. that are applicable to limestones containing significant quantities of magnesium carbonate. The calcination of such limestones does not differ significantly from that of high calcium limestones.

3.5. Sintering of High Calcium Quicklime

Sintering is a method for making objects from powder, increasing the adhesion between particles as they are heated. Sintering traditionally serves for manufacturing ceramic objects, and has also found use in calcinations of lime. Sintering relates to diffusion. In most cases the density of a collection of grains increases as material flows into voids, causing a decrease in overall size. Mass movements which occur during sintering consist of the reduction of total porosity by repacking, followed by material transport because of evaporation and condensation with diffusion. In the final stages metal atoms move along crystal boundaries to the walls of internal pores, redistributing mass from the internal bulk of the object and smoothening pore walls. Surface tension serves as the driving force for this movement. A pore, in general, is some form of opening, usually very small. In physics, surface tension is an effect within the surface of a liquid that causes the layer to behave as an elastic sheet.

During the calcination of dense calcitic limestone at temperatures close to 900°C, the volume of individual particles increases very slightly until about 60% of the limestone has dissociated, and then decreases slightly to about 98% of the original volume at the point when calcination is complete (5).

Calcination at very high temperatures has been shown to cause significant sintering of the surface layer of lime, whereas dissociation is still in progress; under extreme conditions this can interfere significantly with the dissociation process (3). The sintering process is of more practical relevance to lime burning because of its effect on the reactivity of lime. Figure 5 shows the effect of temperature and time on sintering as measured by the variation of apparent density, of quicklime produced from a dense, high calcium limestone (5).

An example could illustrate the implications of the sintering process, coupled with the effects of particle size on calcining lime. When 50–150 mm limestone, consisting of spherical particles, is calcined in a furnace at 1300°C, the time required for complete calcinations (from Table 2) are given in Table 3.

The properties of quick lime from a given kiln reflect the average properties of individual lumps, each of which has experienced a particular-time temperature history. Figure 6 compares the distribution of particle densities for a light-burned quick lime
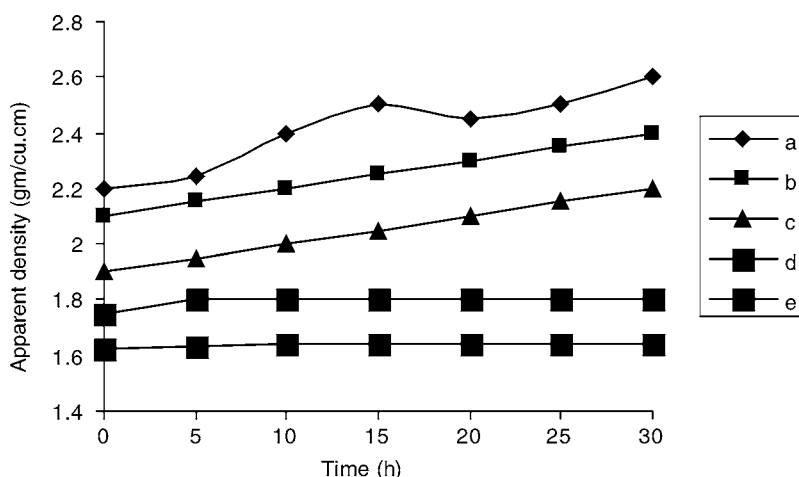
Fig. 5. Variation of apparent density with temperature and time **(A)** 1400°C, **(B)** 1300°C, **(C)** 1200°C, **(D)** 1100°C, and **(E)** 1000°C.

Table 3
Estimated Extent of Dissociation and Sintering after 10 h at 1200°C

Diameter of sphere (mm)	Dissociation time (h)	Expected properties after 10 h	
		$CaCO_3$ (%)[a]	Density (g/mL)
50	0.8	0	2.05
75	2.0	0	2.05
100	4.8	0	1.95
125	11	1.8	1.6
150	26	43	1.5

[a]% by mass.
Adapted from ref. 5.

from an annular shaft kiln, with a mean apparent density of 1.66 g/cm³ with that of a solid-burned quick lime from a coal fired traditional shaft kiln with a mean apparent density of 2.15 g/cm³.

Table 4 provides some typical properties of lime from a gas-fired rotary kiln operated to give "soft," "medium," and "hard" burning. Presence of impurities influences the characteristics of quick limes. Presence of high levels of sodium either in the limestone or added to the stone as a solution of sodium chloride or sodium carbonate, reduces the sintering of some limes (3). The effect on lime reactivity does not appear to have been reported. Addition of finely divided silica, alumina, or iron oxide dispersed in the limestone may increase sintering. Sintering characteristics of very porous limes produced from microporous limestones such as chalk, differ from those of limes made from dense limestones. The MgO component of magnesian/dolomitic limes and dolime (or calcined dolomite) calcines more rapidly and is understood to sinter more readily than the CaO component.
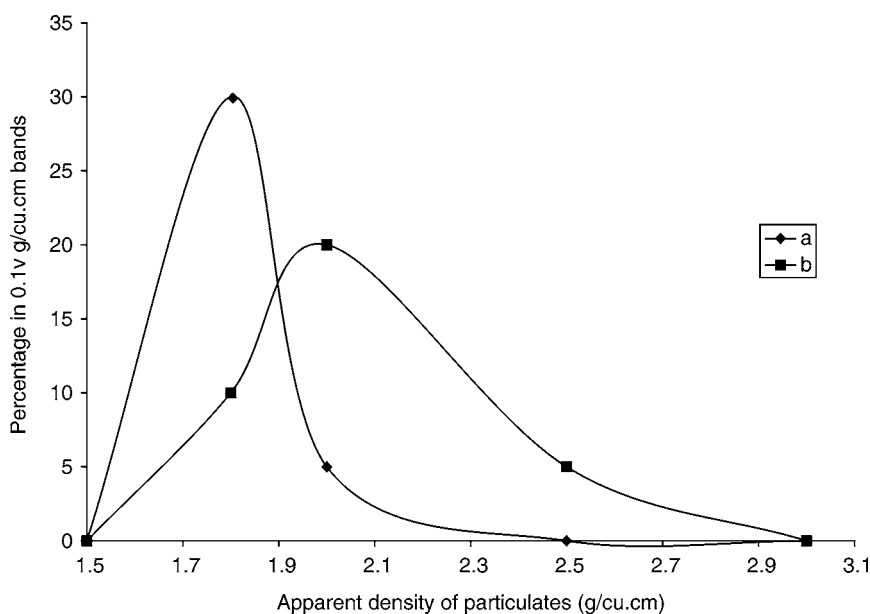
Fig. 6. Distribution of particle densities of quick lime **(A)** from an oil-fired annular shaft kiln. **(B)** From a coal-fired shaft kiln.

Table 4
Typical Properties of Soft-, Medium-, and Hard-Burned Quick Limes

Property	Degree of burning		
	Soft	Medium	Hard
Apparent density (g/mL)	1.5–1.8	1.8–2	>2
Porosity (% v/v)	55–45	45–39	<39
Reactivity (min)	<3	3–9	>9
Calcium carbonate (% mass/mass)	4–1	1–0.5	<0.5

Adapted from ref. 1.

3.6. Sintering of Calcined Dolomite

Sintering of lime occurs during the elevation of calcination temperature from 2800 to 3000°F, when a hard-burned lime undergoes still further shrinkage, increased specific gravity, reduced porosity, reduced surface area, and virtual elimination of any chemical reactivity. Chemically, the product is the same as quick lime, a true oxide of calcium or calcium–magnesium, but it is as inert and stable as its limestone antecedent.

Manufacture of refractory products with mean apparent densities in excess of 3 g/cm^3 requires the sintering of dolomite. This involves heating calcined dolomite at temperatures between 1400 and 1800°C (6,7). Grain size and crystallite size affect the sintering process, but the predominant factor is the amount of impurities present with fluxing properties. A pronounced effect on sintering has been reported to be produced by iron oxide (8). Production of certain grades of sintered dolomite takes place by blending

ground, calcined dolomite with about 0.5% of finely divided ferric oxide, and heating the mixture at temperatures of up to 1600°C.

3.7. Steam Injection

Steam injection has been reported to reduce the dissociation temperature of some limestones and increase the rate of dissociation (3). Steam would act as an inert gas reducing the partial pressure of carbon dioxide in the kiln gases, thereby marginally lowering the dissociation temperature and increasing the rate of dissociation.

The expected effects of steam injection on lime production would be:

a. Moderation of kiln temperatures, particularly if water, rather than steam were added to the combustion zone.
b. Increased usage of heat.

To make soft-burned lime, some producers of dolomite, operate shaft kilns by injecting steam into the combustion gases to moderate kiln temperatures. The resulting lime has a higher reactivity, and is particularly suitable for the production of type S hydrate (3).

3.8. Recarbonation

Recarbonation can occur when large lumps of limestone are calcined. As the higher temperature heat inflow penetrates well into the lump near its center, dissociation in an atmosphere of pure carbon dioxide will start to exert considerable pressure in excess of the atmospheric pressure up to as high as 100 psi in extreme instances. The temperature rises as the pressure increases and causes the already calcined surface to be overburned. This tends to shrink the stone, occluding or narrowing the pores and fissures through which the carbon dioxide must escape, thus generating more pressure. If such lime is discharged into the cooler before all the core is calcined, there is still a faint diffusion of carbon dioxide from the red-hot core that can be reabsorbed on the surface of the cooling lime. This, of course, vitiates the value of the resulting quick lime. So at greater pressure of carbon dioxide, the dissociation temperature is higher. Circumstances that are conducive for excessive recarbonation in the kiln are: excessive calcination temperatures, uneven distribution of combustion gases that envelope the stone in the burning zone, and a resulting disparity in heat exchange, excluding carbon dioxide gases in the cooler with insufficient draft to vent the carbon dioxide up the kiln shaft with exhaust gases, and inordinately long retention of calcined lime in the cooler. Such heavy recarbonation dilutes the concentration of lime oxides, rendering the product unusable for many purposes.

Recarbonation of quick lime takes place through two mechanisms:

Above the dissociation temperature of calcium hydroxide and less than the dissociation temperature of calcite Eq. (1) can proceed to the left with evolution of heat. Porous high calcium limes can absorb over 50% of the theoretical amount of CO_2, whereas dense limes may absorb 3–5% of CO_2. Higher temperature recarbonation can occur in lime kilns under abnormal conditions in which some kiln gases enter the cooling zone. It has been observed during the recirculation of exhaust gases, during the failure of shaft kiln internal structures such as arches, and when crutching has occurred.

The second mechanism occurs at temperatures below the dissociation temperature of calcium hydroxide, and involves:

a. Surface hydration of the quick lime by atmospheric water vapor according to Eq. (6).
b. Carbonation of some of the calcium hydroxide to calcium carbonate plus water which can then hydrate more quick lime:

$$CaO + H_2O \rightleftharpoons Ca(OH)_2 \tag{6}$$

$$Ca(OH)_2 + CO_2 \rightleftharpoons CaCO_3 + H_2O \tag{7}$$
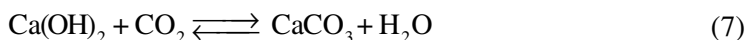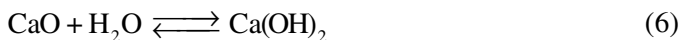
The cooling zone of all lime kilns experiences such slaking and recarbonation, but this does not cause any significant effects. Exposure of quick lime to atmosphere for excessive periods causes "air slaking." Excessive recarbonation by either of the mechanism results in an abnormally low reactivity.

3.9. Calcination of Finely Divided Limestones

Calcination of finely divided limestones (ranging from 5 μm to 5 mm) is applicable for:

a. The production of quick lime in fluidized bed and flash calciners.
b. The production of cement.
c. The use of injected limestone to remove oxides of sulfur from boiler flue gases.
d. Recalcination of precipitated calcium carbonate in a process such as the production of wood pulp.

Some conclusions drawn by various researchers on the calcination of finely divided limestone are as follows:

- The dissociation of particles of 5–10 μm appears to be controlled by chemical kinetics and an Arrhenius activation energy of 46 kcal/mole has been determined. However, at more than 900°C, the apparent activation energy decreases markedly, indicating that chemical kinetics no longer controls the rate of dissociation. The time to achieve 80% calcinations for such particle size varies from 0.55 s at 850°C to 0.03 s at 1250°C (9).
- Literature review relating to particle sizes of 20–30 μm by Muller and Stark (9) concluded that reactors operating below 900°C require residence times ranging from 10 s to several minutes, whereas reactors with temperatures above 900°C require residence times ranging from 10 s to several minutes, whereas reactors with temperatures more than 900°C require residence times ranging from a fraction of a second to a few seconds for 90% calcinations.
- Calcination of precipitated calcium carbonate in the recausting cycle of kraft pulp mill revealed that activation energy of 50 kcal/mole applies to calcinations at temperatures of 1165 and 1240°C (6).
- At 1000°C, the time for complete calcinations of 1, 3, and 5 mm particles are 1, 6, and 13 min, respectively.

4. PROPERTIES OF LIMESTONES AND THEIR CALCINES

Lime stone rock (commercial) is reported to consist of over 90% calcium carbonate and contains 3–35% voids. This voidage is almost exclusively in the form of larger pores, with few micropores, so that the specific surface area ranges from 1 to 10 m^2/g. Most limestones occur as calcite, and in the absence of significant impurities, do not shrink on

Table 5
Some Properties of CaO Prepared by Lime Calcination

Limestone	CaCO$_3$ (%)	Calcination temperature (°C)	Calcine surface area (m^2/g)	Calcine porosity	References
Mequinenza	95.8	–	19.4	0.68	Benedetto et al., 1998 (12)
Massici	96.8	850	–	0.37	
Unspecified	96.1	780	–	–	Khinast et al., 1996 (13)
Fredonia white	96	700	104	–	Borgwardt et al., 1986 (14)
Greener limestone	>95	750	56	0.51	Krishnan et al., 1994 (15)
Georgia marble	>95	850	52	0.51	
Fredonia valley	–	600	87	–	Borgwardt et al., 1986 (14)

Adapted from ref. 11.

calcinations. From his study of 25 limestones, Trikkel (10) noted that impurities such as iron and aluminum oxides tend to lead to lower surface areas in both the limestones and their calcines. He also found that the mass loss vs time curves in a temperature-ramped TGA were of the same shape for different limestones under the same conditions, but displaced in temperature by 10–15 K. Geologically younger stone (e.g., chalk) is reported to exhibit greater initial porosity and greater adsorption capacity for sulfur dioxide (16).

The product of calcinations, calcium oxide weighs only 56% of the parent carbonate. Because the relative molar volumes are 36.9 cm^3/mol for CaCO$_3$ and 16.9 cm^3/mol for CaO, if there is negligible particle shrinkage, the porosity of the product from a pure nonporous carbonate will increase to a theoretical value of 0.55. Hence a lime may have a porosity greater than 0.6. For maximum adsorption efficiency, care must be taken to ensure that calcination is complete, and also that the CaO grains do not get sintered after formation. Measured values for some surface areas of calcined solids reported by various researchers are presented in Table 5. From the perusal of data, it must be concluded that most of the CaO products have suffered some sintering as they exhibit surface areas which are significantly lower than the nascent values.

5. FACTORS AFFECTING LIME CALCINATION

5.1. Effect of Stone Size

Because dissociation always penetrates gradually from the surface into the interior of the stone, the larger stone sizes are more difficult to calcine uniformly and require more time. Large cubical stone sizes of 6 in. (15.2 cm) and more are particularly difficult to calcine. To expel the carbon dioxide from such large stone, high temperatures are necessary to generate sufficient CO$_2$ pressure in the interior of the crystal lattice for the

escape of the gas. Frequently, these high temperatures (2300–2450°F range) overburn the surface layer of the stone, causing excessive shrinkage, which narrows and closes the pores and fissures. Thickness of the stone rather than width or length (in irregularly shaped stone) or total volume in cubic inches is the main criterion in the influence of stone's size on calcination. For example, comparing stone A, that is cubically shaped and 2.5 in. (6.3 cm) in thickness with slab-shaped stone B of the same thickness, but with a dimension of $2.5 \times 7.5 \times 10$ in.^{3} ($6.3 \times 19.1 \times 25.4$ cm^3), they both have the same distance for heat to transfer to the core, in spite of the fact that stone B has about 11 times as much volume. But the calcining effort, according to Azbe (4) is proportionally much less for its size—only about twice as much as for stone B.

The ideal stone to calcine for optimum quality, uniformity, and thermal efficiency, of course would be of small size (–0.5 in. or 1.25 cm) and be of uniform size and shape. Production of such kiln feed would be economically impossible. However, probably the greatest deterrent to high, uniform quality among lime manufacturers is the use of stone gradations, that are too broad and in some cases of an erratic size distribution. Attaining more narrow and consistent gradations can potentially improve overall calcination performance more than any other single factor.

5.2. Effect of Crystal Ion Spacing

Hard burning does not shrink the molecular structures, only there is a decrease of spaces between the intercrystalline matrix. When subjected to X-ray diffraction, sharp, fine X-ray lines indicate clear perfect crystals of impressive impurity. In contrast, broad indistinct X-ray lines indicate the imperfections in the crystal caused by impurities.

5.3. Effect of Salts

Lime manufacturers have experimented for many years with small additions of sodium chloride to limestone or to the fuel preparatory to calcination. Either the salt is added dry (0.2–1.0%) or the limestone is soaked in or doused with brine. Contradictory results have been reported; some claim benefits from improved lime quality and even superior fuel economy. Murray (17) on experimentation with 10% sodium chloride and sodium carbonate solutions in laboratory on calcination in rotary kiln observed that efficiency of the NaCl or Na_2CO_3 solutions averaged about equal, some limes were enhanced more by one or the other of these two salts. He also observed that limestones containing Na_2O as an impurity generally exhibited less shrinkage than those stones with only a trace. Salt additions to dolomites yielded even more profound changes in comparing the same stone with and without salt as determined by differential thermal analysis.

5.4. Influence of Stone Impurities

Purest stone provides the best quality of lime. High purity also generally enhances lime's physical or rheological properties for structural uses. In addition to stone, the other source of impurities is derived from fuel. For a majority of lime uses, the quantity of impurities is more critical than quality. Not only the impurities dilute the availability of the lime, but they also adversely affects its reactivity, particularly when it is calcined at high temperatures of 2200°F (1204°C) and above. Impurities form various calcium compounds such as lime monocalcium and dicalcium silicates on the temperature

increase, which results in a slagging effect, that tends to occlude the pores in the quick lime and mute its reactivity. This results in the pores getting clogged and in turn retards hydration with water encountering more difficulty in penetrating the interior of the lime. As a result, lime that is abnormally high in impurities may react like a hard-burned or recarbonated lime with water.

5.5. *Effect of Steam*

Research has indicted that steam tends to reduce the dissociation temperatures of some stones by 5–15%, thereby catalyzing the rate of dissociation slightly. Knibbs (3) appears to favor the use of steam generally and claims that some steam is almost invariably present in most commercial kilns, derived from the stones, solid fuels, and atmosphere. Application of steam might produce moderately successful results with certain type of stone or with some kiln designs.

5.6. *Effect of Storage and Production*

The influence of storage and production on the reactivity, i.e., the slaking rate of lime in water, has been investigated. It was found that hard burning of the lime during calcinations dramatically decreases its reactivity, as does storing under humid conditions (Table 6). It also seemed that air rehydration during storage precedes recarbonation and there is an evidence to show that the former process catalyses the latter one.

Potgieter et al. (18) measured the rate of lime slaking by monitoring the time that a fixed mass of lime particle size 1–2 mm takes to raise the temperature of a selected mass of water from 20 to 60°C, and furthermore measuring the amount of available lime before and after completion of the slaking reaction. Effect of hard burning stimulated by heating the lime after the initial calcining period of 1 h at 950°C for additional times indicate that there is a considerable drop in the rate of slaking or reactivity of the lime as the degree of hard-burning increases (Table 6). However, the change in available lime of the material before and after slaking stays relatively constant. This indicates that, although the rate of slaking changes, the degree to which it occurs does not. This fact has important practical applications in plant operations.

It is often observed that lime undergoes air slaking and recarbonation after calcining, especially during periods of prolonged storage and in particular under humid atmospheric conditions. It is conceivable that during these processes a thin skin of calcium hydrate and/or calcium carbonate that can impair the slaking of the lime forms on the surface of the lime particles. Calcium carbonate can potentially also be present in the final product if the residence time in the kiln was too short to ensure complete calcinations. To simulate this, calcium carbonate, calcium hydroxide, and combinations of both were added to lime samples before their slaking was evaluated. The results obtained are graphically represented in Fig. 7.

From the data shown in the graph, it can be deduced that the occurrence of both air-slaking and recarbonation reduces the slaking rate of lime, with the former having a more pronounced effect than the latter. When these processes occur simultaneously and result in the presence of both calcium carbonate and calcium hydroxide compounds in the lime, the combined effect is somewhere between the two individual contributions.

Table 6
The Effect of Hard Burning on the Slaking Rate of Lime

Calcination time over 1 h (min)	R_{DIN} (reactivity)	Δ Av CaO (m/v [%])
10	160 ± 1	1.1 ± 0.9
20	158 ± 1	32.6 ± 0.7
30	139 ± 2	34.8 ± 0.9
60	122 ± 2	30.9 ± 1.1
90	118 ± 1	31.4 ± 0.7
12	116 ± 1	33.8 ± 0.3
18	109 ± 2	31.6 ± 0.7
24	106 ± 2	31.2 ± 0.7

Adapted from ref. 18.
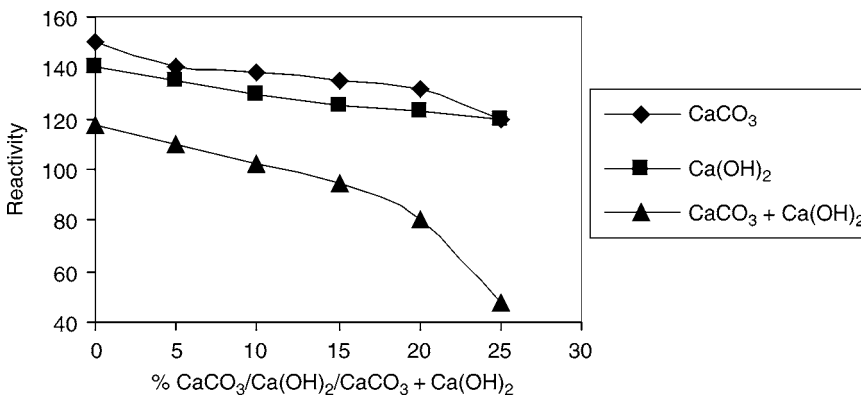
Fig. 7. The effect of $CaCO_3$, $Ca(OH)_2$, and combinations thereof on the slaking rate of lime (16).

The effect of storage time on the change of available lime content before and after slaking is summarized in Table 7.

The numbers presented in Table 7 indicate that the change in available lime content stays relatively constant (average 33.4%) regardless of the drop in slaking rate. Styrdom and Potgieter (19) previously found that lime samples with a high available lime content, which theoretically should slake well and fast, sometimes have low reactivity values or slaking rates, or that the slaking rates decreased dramatically with time, although the available lime value remained fairly constant. This means that the degree to which slaking occurs stays constant, although the rate changes.

5.7. Effect of Calcination Temperature

The effect of calcination temperature on Belbeis clay and Sammlout limestone as well as hydration characteristics of calcined products were investigated. Three mixes 50/50, 60/40, 70/30 wt% clay-limestone were calcined at 700, 800, 900, and 1000°C for 2 h, then hydrated for up to 90 d. The degree of calcination was investigated from the free lime content and the ignition loss for each mixture. Also, the mineralogical composition of the fired mixes was investigated with the aid of X-ray diffractometry.

Table 7
The Effect of Storage Time on the Change in Available Lime Content

Storage time (h)	Δ Av Cao (%)
1	34.0 ± 0.2
2	34.9 ± 0.4
4	32.7 ± 1.0
6	32.6 ± 0.5
24	33.0 ± 0.6
72	33.1 ± 0.4
120	33.7 ± 0.3
240	33.1 ± 0.3

Adapted from ref. [18].

The results revealed that the free lime of each mix increased up to 800°C then decreased gradually up to 1000°C. Mix 60/40 clay-limestone fired at 800°C shows the presence of $Ca(OH)_2$ with quartz. As the firing temperature increased, gehlenite appeared and increased up to 1000°C with the disappearance of lime. Mix 50/50 gave the highest hydration kinetics as measured from determination of free lime and combined water contents. As the limestone decreased, the rate of hydration decreased. The suitable firing temperature of the clay-limestone mixes was 800°C for 2 h [20].

6. CALCINATION OF INDUSTRIAL SOLID WASTES

Recycling and reuse of waste materials and byproducts in construction is always a popular concept because large quantities of various materials are needed by the construction industry. A recent publication by the Transport Research Board in the United States has reviewed the recycling and use of various waste materials and byproducts in highway constriction and maintenance operations [21].

Red mud is a byproduct from the production of aluminum. It is well known that it can be converted into pozzolan through proper calcination. The raw mud from the production of alum consisted mainly of kaolinite, quartz, and anatase. After calcinations of the mud at 750°C for 5 h, the XRD peaks for kaolinite disappeared and amorphous metakaolinite formed, whereas quartz and titanium oxide remained unchanged. Equation below shows the changes taking place during calcinations of red mud:

$$\underset{\text{Kaolinite}}{Al_2(Si_2O_5)(OH)_4} \longrightarrow \underset{\text{Metakaolinite}}{Al_2O_3 \cdot 2SiO_2} + 2H_2O \tag{8}$$
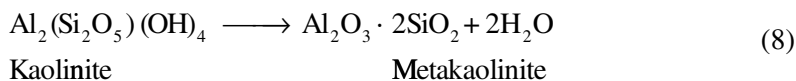
The calcined mud showed very high pozzolanic activity. Compressive strength testing of lime-calcined mud mixtures indicated that the calcined mud appears to be a good pozzolanic material. The addition of chemical activators such as sodium sulfate and calcium chloride accelerated the pozzolanic reaction between lime and calcined mud and increased the strength of lime-calcined mud very significantly [22].

Calcination of paper sludge seems to be a viable solution for land filling in Western Europe. The paper industry in Western Europe generates around 6 million tons/yr of

sludges, which contain about 60% dry matter mainly composed of cellulose fibers, kaolinite, and calcite. Production of metakaolin by calcining paper sludge in the temperature range of 700–800°C has been reported (23). After calcination, pastes containing 50% calcium hydroxide and 50% burnt sludge were hydrated and the lime consumption was investigated by differential thermal analysis. The results show that a very reactive pozzolan is produced by calcining paper sludge at 700°C or 750°C for 2 or 5 h. Despite a smaller kaolinite content, the burnt paper sludge exhibits more pozzolanic activity than commercially available metakaolins, especially at early ages. Thermo-desorption analyses show that this higher activity is because of the presence of superficial defects that occur during the sludge calcination. Pilot scale and industrial tests of calcination are being performed and the production of low cost metakaolin can be expected within a few years.

Recycling sugar-ash for use in lime industry has been explored by Kantiranis (24). Large amounts of sugar-ash, a material rich in calcium carbonate, are produced as a by-product in the Greek Sugar Industry. A representative sample of sugar-ash from the Plati Imathias sugar plant was studied by PXRD, TG/DTG, calcinations experiments at temperatures between 650 and 1150°C and experiments to determine the quality of the quick lime produced at temperatures between 850 and 1150°C. The sugar-ash was found to consist of 90 wt% calcium rich minerals (calcite and monohydro calcide) and 10 wt% amorphous material. Traces of quartz were also detected. The quicklime of highest quality was produced at 950°C. It is concluded that this "useless" material (sugar-ash) can be recycled for use in rotary kilns in the lime industry at calcination temperatures up to 950–1000°C.

7. CARBON DIOXIDE EMISSIONS FROM LIME CALCINATION

Modern cement plants have recorded a carbon dioxide emission at the rate of 0.9 kg CO_2/kg clinker. According to world business council for sustainable development, the cement industry is responsible for 5% global anthropogenic carbon dioxide emissions, of which 50% is derived from the chemical process and 40% from burning fuel. The remainder is split between electricity and transport use. Estimates of the global anthropogenic carbon dioxide emissions from the lime industry are 1% (25). Here the combustion of fossil fuels contributes 20–40% of the plant's carbon dioxide emissions depending on the type of kiln used. A number of strategies have been proposed for mitigating these emissions. Examples include the capturing and sequestering carbon dioxide, fuel switching such as the use of waste products as a fuel source (26), and the use of concentrated solar energy as the source of process heat (27). The use of concentrated solar energy in place of fossil fuels for driving the endothermic calcination reaction $CaCO_3 \rightarrow CaO + CO_2$ at above 1300 K has the potential of reducing CO_2 emissions by 20% in a state-of-the-art lime plant and up to 40% in a conventional cement plant. The cleanliness of the solar process leads to very pure lime. It seems conceivable that a pure product may be advantageous for special niche markets in chemical and pharmaceutical industries.

8. SOLAR LIME CALCINATION

The technical feasibility of the solar thermal decomposition of limestone was experimentally demonstrated. The use of solar energy as a source for high-temperature process
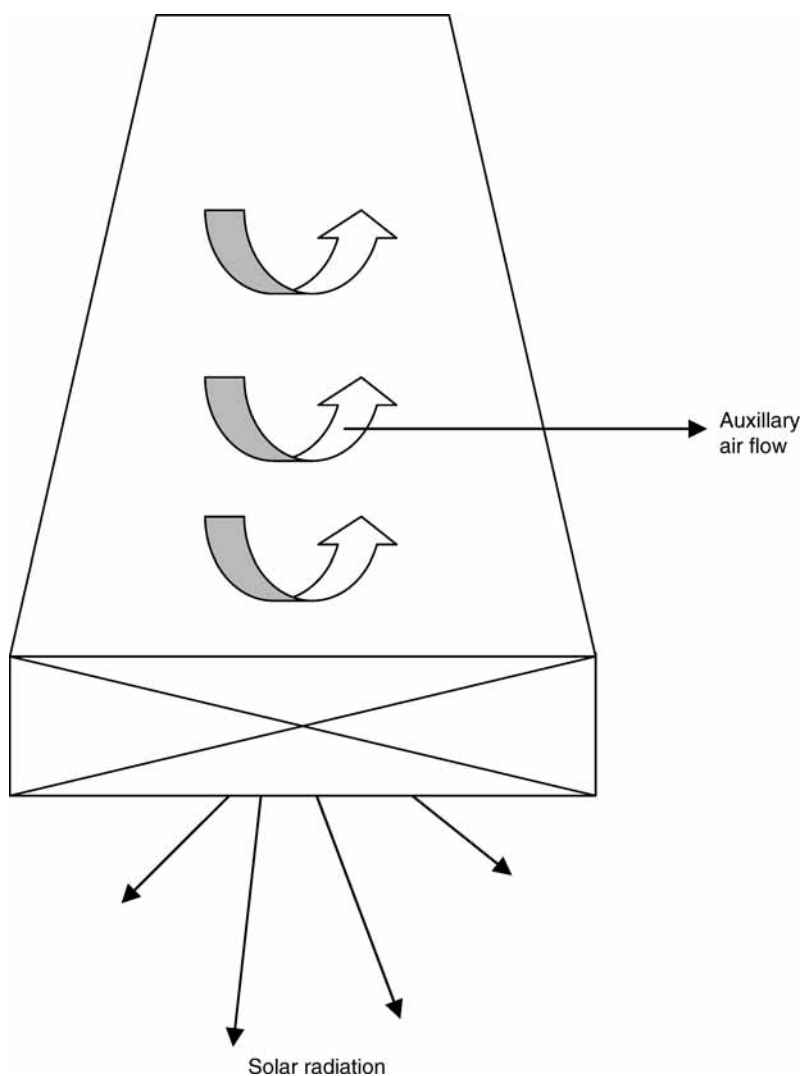
Fig. 8. Scheme of solar cyclone reactor (29).

heat offers the potential of reducing significantly the CO_2 emissions from lime producing plants. Such a solar thermochemical process can find application in sunny rural areas for avoiding deforestation (28).

Many solar thermal devices have been experimentally demonstrated for their technical feasibility.

Imhof (29) has designed a solar cyclone reactor (Fig. 8) for conducting gas solid thermochemical processes. The reactor consists of a conventional cyclone gas/particle separator that has been modified to let concentrated solar energy enter the cavity through an aperture. Its main body is a conical cavity, made of heat-resistant steel. The remainder of the cavity is formed by two concentric cones that form a conduit for the
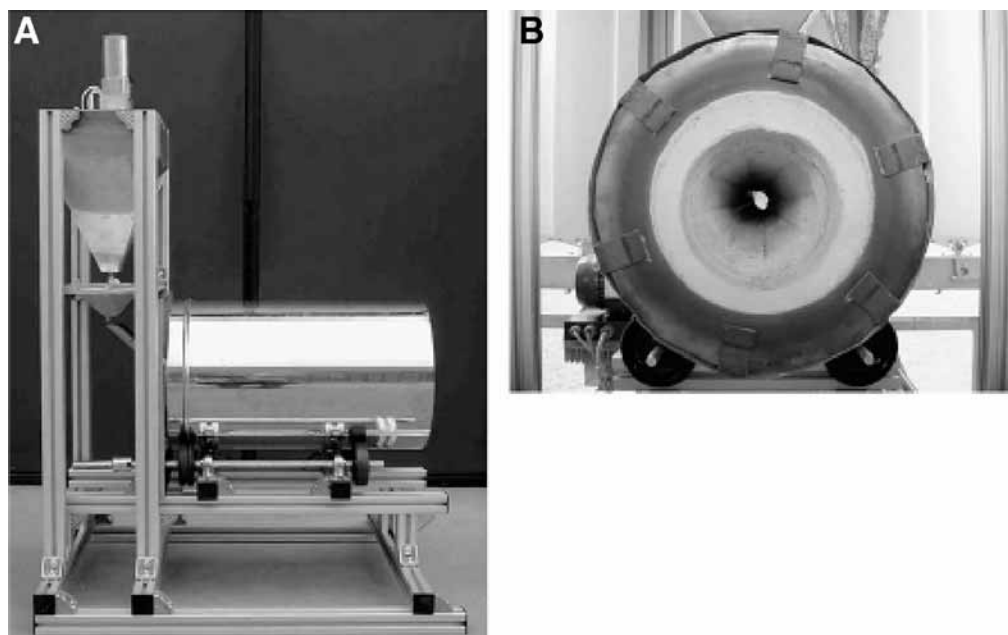
Fig. 9. (A) Side view of solar lime reactor showing the rotary drum and feeding system, pre-assembled and prepared for initial tests. **(B)** Front view of the conical reaction chamber lined with a refractory concrete and insulated with a porous ceramic fiber (30).

gas and particle exhaust. The reactor uses a windowless (atmospheric open) aperture as calcination reaction can be conducted in the presence of air.

The thermal decomposition of limestone has been selected as a model reaction for developing and testing an atmospheric open solar reactor. The reactor consists of a cyclone gas/particle separator which has been modified to let the concentrated solar energy enter through a windowless aperture. The reacting particles are directly exposed to the solar irradiation. Experimentation with a 60 kW reactor prototype was conducted at SI's 90 m^2 parabolic solar concentrator, in a continuous mode of operation. A counter-current flow heat exchanger was employed to preheat the reactants. Eighty five percent degree of calcination was obtained for cement raw material and 15% of the solar input was converted into chemical energy (enthalpy).

A 10-kW solar rotary kiln reactor was designed and tested to effect the calcination reaction: $CaCO_3 \rightarrow CaO + CO_2$. The reactor processes 1–5 mm limestone particles, producing 95% or higher purity lime with a t_{60} reactivity ranging from 14 s to 38 min (30). The solar lime reactor is a rotary kiln of 600 mm length and 350 mm diameter that is operated in a horizontal position (Fig. 9). The solar lime reactor with a conical reaction chamber fixed at a cone angle of 5° works in a continuous mode. The raw material is stored in a hopper that is placed on top of the rear part of the reactor. A simple dozing system is integrated in the hopper structure for controlling the feeding rate of the raw material. The reactants are fed through a bent and tilted stainless steel tube into the conical reaction chamber. A rudimentary discharging system below the front plate collects the end product in bins open to the air. The residence time of the reactants inside the reaction chamber is controlled by properly adjusting the feeding rate and the rotational speed

of the drum. For very slow rotational speed, the particles tend to slide along the walls, but with increasing rotational speed, the transition to a continuous rolling motion takes place, which is the preferred particle flow regime inside the kiln.

The degree of calcination and the reactivity both depend on the reactant's decomposition temperature (1323–1423 K), residence time (3–7 min), and feed rate (10–50 g/min). The reactor's efficiency, defined as the enthalpy of the calcination reaction at a specified temperature divided by the solar energy input, reached 20% for solar flux inputs of about 1200 kW/m² and for quicklime production rates of about 1.3 kg/h. The solar lime reactor operated reliably for more than 100 h for a total of 24 sunny days, withstanding the thermal shocks that occur in solar applications (30).

8.1. Carbon Dioxide Mitigation Potential

By substituting concentrated solar energy for the fossil fuels used to drive the calcinations reaction, carbon dioxide emissions can be reduced between 20% in a state-of-the-art lime plant and 40% in a conventional cement plant. A life cycle analysis concludes that the solar production of lime is ecologically beneficial. About 95% of the green house gas emissions released by the combustion of fossil fuels from an average single shaft kiln can be saved. The carbon dioxide mitigation potential is higher if the conventional shaft kiln is fired with coal or fuel oil instead of natural gas.

9. CONCLUSIONS

Economic assessment indicates that the cost of solar produced lime ranges from 128–157 USD/t for a 25 mW plant to 168–198 USD/t for a 1 mW plant. It is conceivable that the extremely pure solar produced lime will allow for a much higher selling price than the actual market price for lime (at about 60 USD/t). Finally, government subsidies and regulations like the levy of a carbon dioxide tax may help introduce the solar lime technology into the market. As much as 95% of the green house gas emissions released by fossil fuel based production of lime could be avoided by solar based lime production. The solar production of high purity lime for special sectors in the chemical and pharmaceutical industry might be competitive with conventional fossil fuel based calcination processes at current fuel prices (31).

NOMENCLATURE

A	Area (m²)
C	(Current) costs (USD)
$\hat{C}$	Solar concentration ratio
D	Diameter (m)
h	Height (m)
I	Investment (USD)
l	Length (m)
n	Number
S	Savings (USD)
t	Time (s, min, h, d)
LCA	Life cycle analysis

REFERENCES

1. R. S. Boynton, *Chemistry and Technology of Lime and Limestone*. John Wiley & Sons. (1980).
2. F. Schwarzkopf, *Lime Burning Technology – a manual for lime plant operators* (3rd ed.). Svedala Industries Kennedy, Van Saun, 1994.
3. N. V. S. Knibbs and B. J. Gee, *Lime and Limestone. the origin, occurrence, properties, chemistry, analysus and testing of Limestone. Dolomite and their products, and the theory of Lime burning and hydration.* Canada: H.L. Hall Corporation Limited, 1974.
4. V. J. Azbe, *Theory and practice of lime manufacture*. Part II, Rock Products. 1953, pp. 102–104.
5. L. C. Anderson, Resume of ICI work on Limestone calcination, lime reactivity and apparent density, (Internal report) (1973).
6. A. L. Campbell, A. R. Job, and J. F. Robertson, Lime calcination: time and temperature of calcination expressed as a single variable and the effect of selected impurities on lime properties. *Zement Ralk Gips* **9,** 442 (1988).
7. E. J. Koval, G. L. Messing, and R. C. Bradt, Effects of raw material properties and Fe_2O_3 additions on the sintering of dolomites. *Ceremic Bulletin* **9,** 274–277 (1983).
8. G. V. Kukolev and G. Z. Doglina, Study of the properties of difficulty sinterable dolomites in the Abono deposits. *Ogneupory* **13,** 17–21 (1948).
9. A. Muller and J. Stark, Calcination of limestone powders in suspension. *Zement Ralk Gips* **12,** 620 (1989).
10. A. Trikkel, Estonian calcareous rocks and oil shale ash as sorbents for sulphur dioxide, Ph.D Thesis. Tallinn University (2001).
11. H. El-Didamony, K. A. Khalil, and M. S. El-Attar, Physicochemical characteristics of fired clay limestone mixes. *Cem. Concr. Res.* **30,** 7–11 (2000).
12. A. Benedetto Di and P. Salatino, Modelling attrition of limestone during calcination and sulpnation in a fluidized bed reactor. *Powder Technol.* **95,** 119 (1998).
13. J. Khinast, G. H. Krammer, C. H. Brunner, and G. Staudinger, Decomposition of limestone influence of carbon dioxide and particle size on the reaction rate. *Chem. Eng. Sci.* **51(4),** 623–634 (1996).
14. R. H. Borgwardt, K. R. Bruce, and J. Blake, An investigation of product layer and diffusurty for calcium oxide sulpnation. *Ind. Eng. Chem. Res.* **26,** 1993 (1986).
15. S. V. Krishnan and S. V. Sotirehas, Experimental and theoretical investigation of factors affecting the direct sulfation of limestone-hydrogen sulphide reaction. *Ind. Eng. Chem. Res.* **33,** 1444–1453 (1994).
16. K. Dam-Johnson and K. Ostegaard, High temperature reaction between sulphur dioxide and limestone-I. Composition of limestones in two laboratory reactors and a pilot plant. *Chem. Eng. Sci.* **46,** 827–837 (1991).
17. J. A. Murray, Summary of fundamental research on lime. National lime association, 1956.
18. J. H. Potgieter, S. S. Potgieter, S. S. Moja, and A. Mulaba-Bafubiadi, An empirical study of factors influencing lime slaking. Part 1 production and storage conditions. *Miner. Eng.* **15,** 201–206 (2002).
19. C. A. Strydom and J. H. Potgieter, An investigation of chemical reactivity of lime. In *Proceeding of the 10th International Chemistry at Cement Conference. Gothenberg, Sweden*, Vol 2. paper no 21,049 (1997).
20. H. El-Didamony, K. A. Khalil, and M. S. El-Attar, Physicochemical characteristics of fired clay limestone mines. *Cem. Concr. Res.* **30,** 7–11 (2000).
21. Trasportation Research board, Recycling and use of waste materials and by-products in high way construction. NCHRP synthesis 199,Washington DC, National Academy Press, 1994.
22. Canjun Shi, P. E. Gratten Bellew, and J. A. Stegemann, Conversion of a waste mud into a pozzolanic material. *Constr. Build. Mater.* **13,** 279–284 (1999).

23. Jean Pera and Achene Amrouz, Development of Highly reactive metakaolin iron paper sludge. *Adv. Cem. Bas. Mat.* **7,** 49–56 (1998).
24. N. Kantiranis, Recycling of sugar ash—a raw feed material for rotary kilns. *Waste Manage.* **24(10),** 999–1004 (2004).
25. J. A. H. Oates, *Lime and Limestone chemistry and technology, production and uses.* Germany: Weinem Wiley VCH Verlag, GmbH, 1998.
26. E. H. Males, Lime production and the environment: challenges and opportunities. In: *Proc 9th International lime congress*, Yokohama, Japan, October 27-28. P 902-12 (1998).
27. G. Flamant, D. Hernandez, C. Bonet, and J. P. Traverse, Experimental aspects of the thermochemical conversion of solar energy. Decarbonation of calcium carbonate. *Sol. energy* **24,** 383–395 (1980).
28. A. Imhof, Decomposition of limestone in a solar reactor. *Renewable Energy* **10(23),** 239–246 (1997).
29. A. Imhof, The cyclone reactor, an atmospheric open solar reactor. *Sol. Energy Mater.* **24,** 733–741 (1991).
30. A. Meier, B. Bonaldi, G. M. Cella, W. Lipinski, D. Wuillemin, and R. Palumbo, Design and experimental investigation of a horizontal rotary reactor for the solar thermal production of lime. *Energy.* **29,** 811–821 (2004).
31. Columbia University. Calcination. *The Columbia Encyclopedia,* 6th ed. Columbia University, NY, 2006.

Appendix
Conversion Factors for Environmental Engineers

Lawrence K. Wang

CONTENTS

ABSTRACT

With the current trend toward metrication, the question of using a consistent system of units has been a problem. Wherever possible, the authors of this Handbook of Environmental Engineering series have used the British system (fps) along with the metric equivalent (mks, cgs, or SIU) or vice versa. For the convenience of the readers around the world, this book provides a 55-page detailed *Conversion Factors for Environmental Engineers*. In addition, the basic and supplementary units, the derived units and quantities, important physical constants, the properties of water, and the Periodic Table of the Elements, are also presented in this document.

Key Words: Conversion factors, British units, metric units, physical constants, water properties, periodic table of the elements, environmental engineers, Lenox Institute of Water Technology.

I. CONSTANTS AND CONVERSION FACTORS

Multiply	by	to obtain
abamperes	10	amperes
abamperes	2.99796×10^{10}	statamperes
abampere-turns	12.566	gilberts
abcoulombs	10	coulombs (abs)
abcoulombs	2.99796×10^{10}	statcoulombs
abcoulombs/kg	30577	statcoulombs/dyne
abfarads	1×10^{9}	farads (abs)
abfarads	8.98776×10^{20}	statfarads
abhenries	1×10^{-9}	henries (abs)
abhenries	1.11263×10^{-21}	stathenries
abohms	1×10^{-9}	ohms (abs)
abohms	1.11263×10^{-21}	statohms
abvolts	3.33560×10^{-11}	statvolts
abvolts	1×10^{-8}	volts (abs)
abvolts/centimeters	2.540005×10^{-8}	volts (abs)/inch
acres	0.4046	ha
acres	43560	square feet
acres	4047	square meters
acres	1.562×10^{-3}	square miles
acres	4840	square yards
acre-feet	43560	cubic feet
acre-feet	1233.5	cubic meters
acre-feet	325850	gallons (U.S.)
amperes (abs)	0.1	abamperes
amperes (abs)	1.036×10^{-5}	faradays/second
amperes (abs)	2.9980×10^{9}	statamperes

Multiply	by	to obtain
ampere-hours (abs)	3600	coulombs (abs)
ampere-hours	0.03731	faradays
amperes/sq cm	6.452	amps/sq in
amperes/sq cm	10^4	amps/sq meter
amperes/sq in	0.1550	amps/sq cm
amperes/sq in	1,550.0	amps/sq meter
amperes/sq meter	10^{-4}	amps/sq cm
amperes/sq meter	6.452×10^{-4}	amps/sq in
ampere-turns	1.257	gilberts
ampere-turns/cm	2.540	amp-turns/in
ampere-turns/cm	100.0	amp-turns/meter
ampere-turns/cm	1.257	gilberts/cm
ampere-turns/in	0.3937	amp-turns/cm
ampere-turns/in	39.37	amp-turns/meter
ampere-turns/in	0.4950	gilberts/cm
ampere-turns/meter	0.01	amp-turns/cm
ampere-turns/meter	0.0254	amp-turns/in
ampere-turns/meter	0.01257	gilberts/cm
angstrom units	1×10^{-8}	centimeters
angstrom units	3.937×10^{-9}	inches
angstrom unit	1×10^{-10}	meter
angstrom unit	1×10^{-4}	micron or (Mu)
ares	0.02471	acre (US)
ares	1076	square feet
ares	100	square meters
ares	119.60	sq. yards
assay tons	29.17	grams

Multiply	by	to obtain
astronomical unit	1.495×10^8	kilometers
atmospheres (atm)	.007348	tons/sq. inch
atmospheres	76.0	cms of mercury
atmospheres	1.01325×10^6	dynes/square centimeter
atmospheres	33.90	ft of water (at 4°C)
atmospheres	29.92	in. of mercury (at 0°C)
atmospheres	1.033228	kgs/sq cm
atmospheres	10,332	kgs/sq meter
atmospheres	760.0	millimeters of mercury
atmospheres	14.696	pounds/square inch
atmospheres	1.058	tons/sq. foot
avograms	1.66036×10^{-24}	grams
bags, cement	94	pounds of cement
barleycorns (British)	1/3	inches
barleycorns (British)	8.467×10^{-3}	meters
barrels (British, dry)	5.780	cubic feet
barrels (British, dry)	0.1637	cubic meters
barrels (British, dry)	36	gallons (British)
barrels, cement	170.6	kilograms
barrels, cement	376	pounds of cement
barrels, cranberry	3.371	cubic feet
barrels, cranberry	0.09547	cubic meters
barrels, oil	5.615	cubic feet
barrels, oil	0.1590	cubic meters
barrels, oil	42	gallons (U.S.)
barrels, (U.S., dry)	4.083	cubic feet
barrels (U.S., dry)	7056	cubic inches
barrels (U.S., dry)	0.11562	cubic meters
barrels (U.S., dry)	105.0	quarts (dry)

Multiply	by	to obtain
barrels (U.S., liquid)	4.211	cubic feet
barrels (U.S., liquid)	0.1192	cubic meters
barrels (U.S., liquid)	31.5	gallons (U.S.)
bars	0.98692	atmospheres
bars	10^6	dynes/sq cm
bars	1.0197×10^4	kgs/sq meter
bars	1000	millibar
bars	750.06	mm of Hg (0°C)
bars	2,089	pounds/sq ft
bars	14.504	pounds/sq in
barye	1.000	dynes/sq cm
board feet	1/12	cubic feet
board feet	144 sq.in. x 1 in.	cubic inches
boiler horsepower	33475	Btu (mean)/hour
boiler horsepower	34.5	pounds of water evaporated from and at 212°F (per hour)
bolts (U.S., cloth)	120	linear feet
bolts (U.S., cloth)	36.576	meters
bougie decimales	1	candles (int)
Btu (mean)	251.98	calories, gram (g. cal)
Btu (mean)	0.55556	centigrade heat units (chu)
Btu (mean)	1.0548×10^{10}	ergs
Btu (mean)	777.98	foot-pounds
Btu (mean)	3.931×10^{-4}	horsepower-hrs (hp-hr)
Btu (mean)	1055	joules (abs)
Btu (mean)	0.25198	kilograms, cal (kg. cal.)
Btu (mean)	107.565	kilogram-meters
Btu (mean)	2.928×10^{-4}	kilowatt-hr (Kwh)
Btu (mean)	10.409	liter-atm
Btu (mean)	6.876×10^{-5}	pounds of carbon to CO_2
Btu (mean)	0.29305	watt-hours

Multiply	by	to obtain
Btu (mean)/cu ft	37.30	joule/liter
Btu/hour	0.2162	foot-pound/sec
Btu/hour	0.0700	gram-cal./sec
Btu/hour	3.929×10^{-4}	horsepower-hrs (hp-hr)
Btu/hour	0.2930711	watt (w)
Btu/hour (feet)^{o}F	1.730735	joule/sec (m)^{o}k
Btu/hour (feet^2)	3.15459	joule/m^2-sec.
Btu (mean)/hour(feet^2)^{o}F	1.3562×10^{-4}	gram-calorie/second (cm^2)^{o}C
Btu (mean)/hour(feet^2)^{o}F	3.94×10^{-4}	horsepower/(ft^2)^{o}F
Btu (mean)/hour(feet^2)^{o}F	5.678264	joule/sec.(m^2)^{o}k
Btu (mean)/hour(feet^2)^{o}F	4.882	kilogram-calorie/hr(m^2)^{o}C
Btu (mean)/hour(feet^2)^{o}F	5.682×10^{-4}	watts/(cm^2)^{o}C
Btu (mean)/hour(feet^2)^{o}F	2.035×10^{-3}	watts/(in.^{2})^{o}C
Btu(mean)/(hour)(feet^2) (^{o}F/inch)	3.4448×10^{-4}	calories, gram(15^{0}C)/sec (cm^2)(^{o}C/cm)
Btu(mean)/(hour)(feet^2)(^{o}F/in.)	1	chu/(hr)(ft^2)(^{o}C/in.)
Btu(mean)/(hour)(feet^2) (^{o}F/inch)	1.442×10^{-3}	joules (abs)/(sec)(cm^2) (^{o}C/cm)
Btu(mean)/(hour)(feet^2) (^{o}F/inch)	1.442×10^{-3}	watts/(cm^2)(^{o}C/cm)
Btu/min	12.96	ft lb/sec
Btu/min	0.02356	hp
Btu/min	0.01757	kw
Btu/min	17.57	watts
Btu/min/ft^2	0.1221	watts/sq. inch
Btu/pound	0.5556	calories-gram(mean)/gram
Btu/pound	0.555	kg-cal/kg
Btu/pound/^{o}F	1	calories, gram/gram/^{o}C
Btu/pound/^{o}F	4186.8	joule/kg/^{o}k
Btu/second	1054.350	watt(w)
buckets (British, dry)	1.818×10^4	cubic cm
buckets (British, dry)	4	gallons (British)
bushels (British)	1.03205	bushels (U.S.)

Multiply	by	to obtain
bushels (British)	1.2843	cubic feet
bushels (British)	0.03637	cubic meters
bushels (U.S.)	1.2444	cubic feet
bushels (U.S.)	2150.4	cubic inch
bushels (U.S.)	0.035239	cubic meters
bushels (U.S.)	35.24	liters (1)
bushels (U.S.)	4	pecks (U.S.)
bushels (U.S.)	64	pints (dry)
bushels (U.S.)	32	quarts (dry)
butts (British)	20.2285	cubic feet
butts (British)	126	gallons (British)
cable lengths	720	feet
cable lengths	219.46	meters
calories (thermochemical)	0.999346	calories (Int.Steam Tables)
calories, gram(g. cal or simply cal.)	3.9685×10^{-3}	Btu (mean)
calories, gram (mean)	0.001459	cubic feet atmospheres
calories, gram (mean)	4.186×10^{7}	ergs
calories, gram (mean)	3.0874	foot-pounds
calories, gram (mean)	4.186	joules (abs)
calories, gram (mean)	0.001	kg. cal (calories, kilogram)
calories, gram (mean)	0.42685	kilograms-meters
calories, gram (mean)	0.0011628	watt-hours
calories, gram (mean)/gram	1.8	Btu (mean)/pound
cal/gram-^{o}C	4186.8	joule/kg-^{o}k
candle power (spherical)	12.566	lumens
candles (int)	0.104	carcel units
candles (int)	1.11	hefner units
candles (int)	1	lumens (int)/steradian
candles (int)/square centimeter	2919	foot-lamberts
candles (int)/square centimeter	3.1416	lamberts

Multiply	by	to obtain
candles(int)/square foot	3.1416	foot-lamberts
candles (int)/square foot	3.382×10^{-3}	lamberts
candles(int)/square inch	452.4	foot-lamberts
candles (int)/square inch	0.4870	lamberts
candles(int)/square inch	0.155	stilb
carats(metric)	3.0865	grains
carats(metric)	0.2	grams
centals	100	pounds
centares(centiares)	1.0	sq. meters
centigrade heat units (chu)	1.8	Btu
centigrade heat units (chu)	453.6	calories, gram (15°C)
centigrade heat units(chu)	1897.8	joules (abs)
centigrams	0.01	grams
centiliters	0.01	liters
centimeters	0.0328083	feet (U.S.)
centimeters	0.3937	inches (U.S.)
centimeters	0.01	meters
centimeters	6.214×10^{-6}	miles
centimeters	10	millimeters
centimeters	393.7	mils
centimeters	0.01094	yards
cm of mercury	0.01316	atm
cm of mercury	0.4461	ft of water
cm of mercury	136.0	kgs./square meter
cm of mercury	1333.22	newton/meter^{2} (N/m^{2})
cm of mercury	27.85	psf
cm of mercury	0.1934	psi
cm of water (4°C)	98.0638	newton/meter^{2} (N/m^{2})
centimeters-dynes	1.020×10^{-3}	centimeter-grams
centimeter-dynes	1.020×10^{-8}	meter-kilograms

Multiply	by	to obtain
centimeter-dynes	7.376×10^{-8}	pound-feet
centimeter-grams	980.7	centimeter-dynes
centimeter-grams	10^{-5}	meter-kilograms
centimeter-grams	7.233×10^{-5}	pound-feet
centimeters/second	1.969	fpm
centimeters/second	0.0328	fps
centimeters/second	0.036	kilometers/hour
centimeters/second	0.1943	knots
centimeters/second	0.6	m/min
centimeters/second	0.02237	miles/hour
centimeters/second	3.728×10^{-4}	miles/minute
cms/sec./sec.	0.03281	feet/sec/sec
cms./sec./sec.	0.036	kms./hour/sec.
cms/sec./sec.	0.02237	miles/hour/sec.
centipoises	3.60	kilograms/meter hour
centipoises	10^{-3}	kilograms/meter second
centipoises	0.001	newton-sec/m^2
centipoises	2.089×10^{-5}	pound force second/square foot
centipoises	2.42	pounds/foot hour
centipoises	6.72×10^{-4}	pounds/foot second
centistoke	1.0×10^{-6}	meter^2/sec
chains (engineers' or Ramden's)	100	feet
chains (engineers' or Ramden's)	30.48	meters
chains (surveyors' or Gunter's)	66	feet
chains (surveyors' or Gunter's)	20.12	meters
chaldrons (British)	32	bushels (British)
chaldrons (U.S.)	36	bushels (U.S.)
cheval-vapours	0.9863	horsepower
cheval-vapours	735.5	watts (abs)
cheval-vapours heures	2.648×10^6	joules (abs)

Multiply	by	to obtain
chu/(hr)(ft^2)($^\circ$C/in.)	1	Btu/(hr)(ft^2)($^\circ$F/in.)
circular inches	0.7854	square inches
circular millimeters	7.854×10^{-7}	square meters
circular mils	5.067×10^{-6}	square centimeters
circular mils	7.854×10^{-7}	square inches
circular mils	0.7854	square mils.
circumferences	360	degrees
circumferences	400	grades
circumferences	6.283	radians
cloves	8	pounds
coombs (British)	4	bushels (British)
cords	8	cord feet
cords	8' x 4' x 4'	cubic feet
cords	128	cubic feet
cords	3.625	cubic meters
cord-feet	4' x 4' x 1'	cubic feet
coulombs (abs)	0.1	abcoulombs
coulombs (abs)	6.281×10^{18}	electronic charges
coulombs (abs)	2.998×10^{9}	statcoulombs
coulombs (abs)	1.036×10^{-5}	faradays
coulombs/sq cm	64.52	coulombs/sq in
coulombs/sq cm	10^{4}	coulombs/sq meter
coulombs/sq in	0.1550	coulombs/sq cm
coulombs/sq in	1,550	coulombs/sq meter
coulombs/sq meter	10^{-4}	coulombs/sq cm
coulombs/sq meter	6.452×10^{-4}	coulombs/sq in
cubic centimeters	3.531445×10^{-5}	cubic feet (U.S.)
cubic centimeters	6.102×10^{-2}	cubic inches
cubic centimeters	10^{-6}	cubic meters
cubic centimeters	1.308×10^{-6}	cubic yards
cubic centimeters	2.6417×10^{-4}	gallons (U.S.)

Multiply	by	to obtain
cubic centimeters	0.001	liters
cubic centimeters	0.033814	ounces (U.S.,fluid)
cubic centimeters	2.113×10^{-3}	pints (liq.)
cubic centimeters	1.057×10^{-3}	quarts (liq.)
cubic feet (British)	0.9999916	cubic feet(U.S.)
cubic feet (U.S.)	0.8036	bushels(dry)
cubic feet (U.S.)	28317.016	cubic centimeters
cubic feet (U.S.)	1728	cubic inches
cubic feet (U.S.)	0.02832	cubic meters
cubic feet (U.S.)	0.0370	cubic yard
cubic feet (U.S.)	7.48052	gallons (U.S.)
cubic feet (U.S.)	28.31625	liters
cubic feet (U.S.)	59.84	pints (liq.)
cubic feet (U.S.)	29.92	quarts (liq.)
cubic feet of common brick	120	pounds
cubic feet of water (60°F)	62.37	pounds
cubic foot-atmospheres	2.7203	Btu (mean)
cubic foot-atmospheres	680.74	calories, gram (mean)
cubic foot-atmospheres	2116	foot-pounds
cubic foot-atmospheres	2869	joules (abs)
cubic foot-atmospheres	292.6	kilogram-meters
cubic foot-atmospheres	7.968×10^{-4}	kilowatt-hours
cubic feet/hr	0.02832	m³/hr
cubic feet/minute	472.0	cubic cm/sec
cubic feet/minute	1.6992	cu m/hr
cubic feet/minute	0.0283	cu m/min
cubic feet/minute	0.1247	gallons/sec
cubic feet/minute	0.472	liter/sec
cubic feet/minute	62.4	lbs. of water/min
cubic feet/min/1000 cu ft	0.01667	liter/sec/cu m
cubic feet/second	1.9834	acre-feet/day

Multiply	by	to obtain
cubic feet/second	1.7	cu m/min
cubic feet/second	0.02832	m^3/sec
cubic feet/second	448.83	gallons/minute
cubic feet/second	1699	liter/min
cubic feet/second	28.32	liters/sec
cubic feet/second (cfs)	0.64632	million gallons/day (mgd)
cfs/acre	0.07	m^3/sec-ha
cfs/acre	4.2	cu m/min/ha
cfs/sq mile	0.657	cu m/min/sq km
cubic inches (U.S.)	16.387162	cubic centimeters
cubic inches (U.S.)	5.787×10^{-4}	cubic feet
cubic inches (U.S.)	1.0000084	cubic inches (British)
cubic inches (U.S.)	1.639×10^{-5}	cubic meters
cubic inches (U.S.)	2.143×10^{-5}	cubic yards
cubic inches (U.S.)	4.329×10^{-3}	gal (U.S.)
cubic inches (U.S.)	1.639×10^{-2}	liters
cubic inches (U.S.)	16.39	ml
cubic inches (U.S.)	0.55411	ounces (U.S.,fluid)
cubic inches (U.S.)	0.03463	pints (liq.)
cubic inches (U.S.)	0.01732	quarts (liq.)
cubic meters	8.1074×10^{-4}	acre-feet
cubic meters	8.387	barrels (U.S.,liquid)
cubic meters	28.38	bushels (dry)
cubic meters	10^6	cubic centimeters
cubic meters	35.314	cubic feet (U.S.)
cubic meters	61023	cubic inches (U.S.)
cubic meters	1.308	cubic yards (U.S.)
cubic meters	264.17	gallons (U.S.)
cubic meters	999.973	liters
cubic meters	2113	pints (liq.)

Multiply	by	to obtain
cubic meters (m^3)	1057	quarts (liq.)
cubic meters/day	0.183	gallons/min
cubic meters/ha	106.9	gallons/acre
cubic meters/hour	0.2272	gallons/minute
cubic meters/meter-day	80.53	gpd/ft
cubic meters/minute	35.314	cubic ft/minute
cubic meters/second	35.314	cubic ft/sec.
cubic meters/second	22.82	mgd
cubic meters/sec-ha	14.29	cu ft/sec-acre
cubic meters/meters^2-day	24.54	gpd/ft^2
cubic yards (British)	0.9999916	cubic yards (U.S.)
cubic yards (British)	0.76455	cubic meters
cubic yards (U.S.)	7.646×10^5	cubic centimeters
cubic yards (U.S.)	27	cubic feet (U.S.)
cubic yards (U.S.)	46,656	cubic inches
cubic yards (U.S.)	0.76456	cubic meters
cubic yards (U.S.)	202.0	gal (U.S.)
cubic yards (U.S.)	764.6	liters
cubic yards (U.S.)	1616	pints (liq.)
cubic yards (U.S.)	807.9	quarts (liq.)
cubic yards of sand	2700	pounds
cubic yards/minute	0.45	cubic feet/second
cubic yards/minute	3.367	gallons/second
cubic yards/minute	12.74	liters/second
cubits	45.720	centimeters
cubits	1.5	feet
dalton	1.65×10^{-24}	gram
days	1440	minutes
days	86,400	seconds
days(sidereal)	86164	seconds(mean solar)

Multiply	by	to obtain
debye units (dipole moment)	10^{18}	electrostatic units
decigrams	0.1	grams
deciliters	0.1	liters
decimeters	0.1	meters
degrees(angle)	60	minutes
degrees(angle)	0.01111	quadrants
degrees(angle)	0.01745	radians
degrees(angle)	3600	seconds
degrees/second	0.01745	radians/seconds
degrees/second	0.1667	revolutions/min
degrees/second	0.002778	revoltuions/sec
degree Celsius	$^{o}F=(^{o}Cx9/5)+32$	fahrenheit
degree Celsius	$^{o}K=^{o}C+273.15$	kelvin
degree Fahrenheit	$^{o}C=(^{o}F-32)x5/9$	celsius
degree Fahrenheit	$^{o}K=(^{o}F+459.67)/1.8$	kelvin
degree Rankine	$^{o}K=^{o}R/1.8$	kelvin
dekagrams	10	grams
dekaliters	10	liters
dekameters	10	meters
drachms(British,fluid)	3.5516×10^{-6}	cubic meters
drachms(British,fluid)	0.125	ounces(British,fluid)
drams(apothecaries' or troy)	0.1371429	ounces(avoirdupois)
drams (apothecaries' or troy)	0.125	ounces(troy)
drams(U.S.,fluid or apoth.)	3.6967	cubic cm
drams(avoirdupois)	1.771845	grams
drams(avoirdupois)	27.3437	grains
drams(avoirdupois)	0.0625	ounces
drams(avoirdupois)	0.00390625	pounds(avoirdupois)
drams(troy)	2.1943	drams(avoirdupois)

Multiply	by	to obtain
drams(troy)	60	grains
drams(troy)	3.8879351	grams
drams(troy)	0.125	ounces(troy)
drams(U.S.,fluid)	3.6967×10^{-6}	cubic meters
drams(U.S.,fluid)	0.125	ounces (fluid)
dynes	0.00101972	grams
dynes	10^{-7}	joules/cm
dynes	10^{-5}	joules/meter(newtons)
dynes	1.020×10^{-6}	kilograms
dynes	1×10^{-5}	newton(N)
dynes	7.233×10^{-5}	poundals
dynes	2.24809×10^{-6}	pounds
dyne-centimeters(torque)	7.3756×10^{-8}	pound-feet
dynes/centimeter	1	ergs/square centimeter
dynes/centimeter	0.01	ergs/square millimeter
dynes/square centimeter	9.8692×10^{-7}	atmospheres
dynes/square centimeter	10^{-6}	bars
dynes/square centimeter	2.953×10^{-5}	inch of mercury at 0°C
dynes/square centimeter	4.015×10^{-4}	inch of water at 4°C
dynes/square centimeter	0.01020	kilograms/square meter
dynes/square centimeter	0.1	newtons/square meter
dynes/square centimeter	1.450×10^{-5}	pounds/square inch
electromagnetic fps units of magnetic permeability	0.0010764	electromagnetic cgs units of magnetic permeability
electromagnetic fps units of magnetic permeability	1.03382×10^{-18}	electrostatic cgs units of magnetic permeability
electromagnetic cgs units, of magnetic permeability	1.1128×10^{-21}	electrostatic cgs units of magnetic permeability
electromagnetic cgs units of mass resistance	9.9948×10^{-6}	ohms (int)-meter-gram
electronic charges	1.5921×10^{-19}	coulombs (abs)
electron-volts	1.6020×10^{-12}	ergs
electron-volts	1.0737×10^{-9}	mass units

Multiply	by	to obtain
electron-volts	0.07386	rydberg units of energy
electronstatic cgs units of Hall effect	2.6962×10^{31}	electromagnetic cgs units of Hall effect
electrostatic fps units of charge	1.1952×10^{-6}	coulombs (abs)
electrostatic fps units of magnetic permeability	929.03	electrostatic cgs units of magnetic permeability
ells	114.30	centimeters
ells	45	inches
ems, pica(printing)	0.42333	centimeters
ems, pica(printing)	1/6	inches
ergs	9.4805×10^{-11}	Btu (mean)
ergs	2.3889×10^{-8}	calories, gram (mean)
ergs	1	dyne-centimeters
ergs	7.3756×10^{-8}	foot-pounds
ergs	0.2389×10^{-7}	gram-calories
ergs	1.020×10^{-3}	gram-centimeters
ergs	3.7250×10^{-14}	horsepower-hrs
ergs	10^{-7}	joules (abs)
ergs	2.390×10^{-11}	kilogram-calories (kg. cal.)
ergs	1.01972×10^{-8}	kilogram-meters
ergs	0.2778×10^{-13}	kilowatt-hrs
ergs	0.2778×10^{-10}	watt-hours
ergs/second	5.692×10^{-9}	Btu/min
ergs/second	4.426×10^{-6}	foot-pounds/min
ergs/second	7.376×10^{-8}	foot-pounds/sec
ergs/second	1.341×10^{-10}	horsepower
ergs/second	1.434×10^{-9}	kg.-calories/min
ergs/second	10^{-10}	kilowatts
farad (international of 1948)	0.9995	farad (F)
faradays	26.80	ampere-hours
faradays	96500	coulombs (abs)
faradays/second	96500	amperes (abs)

Multiply	by	to obtain
farads (abs)	10^{-9}	abfarads
farads (abs)	10^6	microfarads
farads (abs)	8.9877×10^{11}	statfarads
fathoms	6	feet
fathom	1.829	meter
feet (U.S.)	1.0000028	feet (British)
feet (U.S.)	30.4801	centimeters
feet (U.S.)	12	inches
feet (U.S.)	3.048×10^{-4}	kilometers
feet (U.S.)	0.30480	meters
feet (U.S.)	1.645×10^{-4}	miles (naut.)
feet (U.S.)	1.893939×10^{-4}	miles (statute)
feet (U.S.)	304.8	millimeters
feet (U.S.)	1.2×10^4	mils
feet (U.S.)	1/3	yards
feet of air (1 atmosphere, 60°F)	5.30×10^{-4}	pounds/square inch
feet of water	0.02950	atm
feet of water	0.8826	in. of mercury
feet of water at 39.2°F	0.030479	kilograms/square centimeter
feet of water at 39.2 $^{\circ}$F	2988.98	newton/meter^2 (N/m^2)
feet of water at 39.2°F	304.79	kilograms/square meter
feet of water	62.43	pounds/square feet (psf)
feet of water at 39.2°F	0.43352	pounds/square inch (psi)
feet/hour	0.08467	mm/sec
feet/min	0.5080	cms/sec
feet/min	0.01667	feet/sec
feet/min	0.01829	kms/hr
feet/min	0.3048	meters/min
feet/min	0.01136	miles/hr
feet/sec	30.48	cms/sec
feet/sec	1.097	kms/hr

Multiply	by	to obtain
feet/sec	0.5921	knots
feet/sec	18.29	meters/min
feet/sec	0.6818	miles/hr
feet/sec	0.01136	miles/min
feet/sec/sec	30.48	cms/sec/sec
feet/sec/sec	1.097	kms/hr/sec
feet/sec/sec	0.3048	meters/sec/sec
feet/sec/sec	0.6818	miles/hr/sec
feet/100 feet	1.0	per cent grade
firkins (British)	9	gallons (British)
firkins (U.S.)	9	gallons (U.S.)
foot-candle (ft-c)	10.764	lumen/sq m
foot-poundals	3.9951×10^{-5}	Btu (mean)
foot-poundals	0.0421420	joules (abs)
foot-pounds	0.0012854	Btu (mean)
foot-pounds	0.32389	calories, gram (mean)
foot-pounds	1.13558×10^{7}	ergs
foot-pounds	32.174	foot-poundals
foot-pounds	5.050×10^{-7}	hp-hr
foot-pounds	1.35582	joules (abs)
foot-pounds	3.241×10^{-4}	kilogram-calories
foot-pounds	0.138255	kilogram-meters
foot-pounds	3.766×10^{-7}	kwh
foot-pounds	0.013381	liter-atmospheres
foot-pounds	3.7662×10^{-4}	watt-hours (abs)
foot-pounds/minute	1.286×10^{-3}	Btu/minute
foot-pounds/minute	0.01667	foot-pounds/sec
foot-pounds/minute	3.030×10^{-5}	hp
foot-pounds/minute	3.241×10^{-4}	kg.-calories/min
foot-pounds/minute	2.260×10^{-5}	kw

Multiply	by	to obtain
foot-pounds/second	4.6275	Btu (mean)/hour
foot-pounds/second	0.07717	Btu/minute
foot-pounds/second	0.0018182	horsepower
foot-pounds/second	0.01945	kg.-calories/min
foot-pounds/second	0.001356	kilowatts
foot-pounds/second	1.35582	watts (abs)
furlongs	660.0	feet
furlongs	201.17	meters
furlongs	0.125	miles (U.S.)
furlongs	40.0	rods
gallons (Br.)	3.8125×10^{-2}	barrels (U.S.)
gallons (Br.)	4516.086	cubic centimeters
gallons (Br.)	0.16053	cu ft
gallons (Br.)	277.4	cu. inches
gallons (Br.)	1230	drams (U.S. fluid)
gallons (Br.)	4.54596	liters
gallons (Br.)	7.9620×10^{4}	minims (Br.)
gallons (Br.)	7.3783×10^{4}	minims (U.S.)
gallons (Br.)	4545.96	ml
gallons (Br.)	1.20094	gallons (U.S.)
gallons (Br.)	160	ounces (Br., fl.)
gallons (Br.)	153.72	ounces (U.S., fl.)
gallons (Br.)	10	pounds (avoirdupois) of water at $62^{\circ}F$
gallons (U.S.)	3.068×10^{-4}	acre-ft
gallons (U.S.)	0.031746	barrels (U.S.)
gallons (U.S.)	3785.434	cubic centimeters
gallons (U.S.)	0.13368	cubic feet (U.S.)
gallons (U.S.)	231	cubic inches
gallons (U.S.)	3.785×10^{-3}	cubic meters

Multiply	by	to obtain
gallons (U.S.)	4.951×10^{-3}	cubic yards
gallons (U.S.)	1024	drams (U.S., fluid)
gallons (U.S.)	0.83268	gallons (Br.)
gallons (U.S.)	0.83267	imperial gal
gallons (U.S.)	3.78533	liters
gallons (U.S.)	6.3950×10^{4}	minims (Br.)
gallons (U.S.)	6.1440×10^{4}	minims (U.S.)
gallons (U.S.)	3785	ml
gallons (U.S.)	133.23	ounces (Br., fluid)
gallons (U.S.)	128	ounces (U.S., fluid)
gallons	8	pints (Liq.)
gallons	4	quarts (Liq.)
gal water (U.S.)	8.345	lb of water
gallons/acre	0.00935	cu.m/ha
gallons/day	4.381×10^{-5}	liters/sec
gpd/acre	0.00935	cu m/day/ha
gpd/acre	9.353	liter/day/ha
gallons/capita/day	3.785	liters/capita/day
gpd/cu yd	5.0	l/day/cu m
gpd/ft	0.01242	cu m/day/m
gpd/sq ft	0.0408	cu m/day/sq m
gpd/sq ft	1.698×10^{-5}	cubic meters/hour/sq. meter
gpd/sq ft	0.283	cu. meter/minute/ha
gpm	8.0208	cfh
gpm	2.228×10^{-3}	cfs
gpm	4.4021	cubic meters/hr
gpm	0.00144	mgd
gpm	0.0631	liters/sec
gpm/sq ft	2.445	cu. meters/hour/sq. meter
gpm/sq ft	40.7	l/min/sq m
gpm/sq ft	0.679	liter/sec/sq. meter

Multiply	by	to obtain
gallons/sq ft	40.743	liters/sq. meter
gausses (abs)	3.3358×10^{-4}	electrostatic cgs units of magnetic flux density
gausses (abs)	0.99966	gausses (int)
gausses (abs)	1	lines/square centimeter
gausses (abs)	6.452	lines/sq. in
gausses (abs)	1	maxwells (abs)/square centimeters
gausses (abs)	6.4516	maxwells (abs)/square inch
gausses (abs)	10^{-8}	webers/sq cm
gausses (abs)	6.452×10^{-8}	webers/sq in
gausses (abs)	10^{-4}	webers/sq meter
gilberts (abs)	0.07958	abampere turns
gilberts (abs)	0.7958	ampere turns
gilberts (abs)	2.998×10^{10}	electrostatic cgs units of magneto motive force
gilberts/cm	0.7958	amp-turns/cm
gilberts/cm	2.021	amp-turns/in
gilberts/cm	79.58	amp-turns/meter
gills (Br.)	142.07	cubic cm
gills (Br.)	5	ounces (British, fluid)
gills (U.S.)	32	drams (fluid)
gills	0.1183	liters
gills	0.25	pints (liq.)
grade	.01571	radian
grains	0.036571	drams (avoirdupois)
grains	0.01667	drams (troy)
grains (troy)	1.216	grains (avdp)
grains (troy)	0.06480	grams
grains (troy)	6.480×10^{-5}	kilograms
grains (troy)	64.799	milligrams
grains (troy)	2.286×10^{-3}	ounces (avdp)
grains (troy)	2.0833×10^{-3}	ounces (troy)
grains (troy)	0.04167	pennyweights (troy)

Multiply	by	to obtain
grains	1/7000	pounds (avoirdupois)
grains	1.736×10^{-4}	pounds (troy)
grains	6.377×10^{-8}	tons (long)
grains	7.142×10^{-8}	tons (short)
grains/imp gal	14.254	mg/l
grains/imp.gal	14.254	parts/million
grains/US gal	17.118	mg/l
grains/US gal	17.118	parts/million
grains/US gal	142.86	lb/mil gal
grams	0.5611	drams (avdp)
grams	0.25721	drams (troy)
grams	980.7	dynes
grams	15.43	grains
grams	9.807×10^{-5}	joules/cm
grams	9.807×10^{-3}	joules/meter (newtons)
grams	10^{-3}	kilograms
grams	10^{3}	milligrams
grams	0.0353	ounces (avdp)
grams	0.03215	ounces (troy)
grams	0.07093	poundals
grams	2.205×10^{-3}	pounds
grams	2.679×10^{-3}	pounds (troy)
grams	9.842×10^{-7}	tons (long)
grams	1.102×10^{-6}	tons (short)
grams-calories	4.1868×10^{7}	ergs
gram-calories	3.0880	foot-pounds
gram-calories	1.5597×10^{-6}	horsepower-hrs
gram-calories	1.1630×10^{-6}	kilowatt-hrs
gram-calories	1.1630×10^{-3}	watt-hrs
gram-calories	3.968×10^{-3}	British Thermal Units (Btu)

<u>Multiply</u>	<u>by</u>	<u>to obtain</u>
gram-calories/sec	14.286	Btu/hr
gram-centimeters	9.2967×10^{-8}	Btu (mean)
gram-centimeters	2.3427×10^{-5}	calories, gram (mean)
gram-centimeters	980.7	ergs
gram-centimeters	7.2330×10^{-5}	foot-pounds
gram-centimeters	9.8067×10^{-5}	joules (abs)
gram-centimeters	2.344×10^{-8}	kilogram-calories
gram-centimeters	10^{-5}	kilogram-meters
gram-centimeters	2.7241×10^{-8}	watt-hours
grams-centimeters^2 (moment of inertia)	2.37305×10^{-6}	pounds-feet^2
grams-centimeters^2 (moment of inertia)	3.4172×10^{-4}	pounds-inch^2
gram-centimeters/second	1.3151×10^{-7}	hp
gram-centimeters/second	9.8067×10^{-8}	kilowatts
gram-centimeters/second	0.065552	lumens
gram-centimeters/second	9.80665×10^{-5}	watt (abs)
grams/cm	5.600×10^{-3}	pounds/inch
grams/cu cm	62.428	pounds/cubic foot
grams/cu cm	0.03613	pounds/cubic inch
grams/cu cm	8.3454	pounds/gallon (U.S.)
grams/cu cm	3.405×10^{-7}	pounds/mil-foot
grams/cu ft	35.314	grams/cu meter
grams/cu ft	10^6	micrograms/cu ft
grams/cu ft	35.314×10^6	micrograms/cu meter
grams/cu ft	35.3145×10^3	milligrams/cu meter
grams/cu ft	2.2046	pounds/1000 cu ft
grams/cu m	0.43700	grains/cubic foot
grams/cu m	0.02832	grams/cu ft
grams/cu m	28.317×10^3	micrograms/cu ft
grams/cu m	0.06243	pounds/cu ft
grams/liter	58.417	grains/gallon (U.S.)

Multiply	by	to obtain
grams/liter	9.99973×10^{-4}	grams/cubic centimeter
grams/liter	1000	mg/l
grams/liter	1000	parts per million (ppm)
grams/liter	0.06243	pounds/cubic foot
grams/liter	8.345	lb/1,000 gal
grams/sq centimeter	2.0481	pounds/sq ft
grams/sq centimeter	0.0142234	pounds/square inch
grams/sq ft	10.764	grams/sq meter
grams/sq ft	10.764×10^{3}	kilograms/sq km
grams/sq ft	1.0764	milligrams/sq cm
grams/sq ft	10.764×10^{3}	milligrams/sq meter
grams/sq ft	96.154	pounds/acre
grams/sq ft	2.204	pounds/1000 sq ft
grams/sq ft	30.73	tons/sq mile
grams/sq meter	0.0929	grams/sq ft
grams/sq meter	1000	kilograms/sq km
grams/sq meter	0.1	milligrams/square cm
grams/sq meter	1000	milligrams/sq meter
grams/sq meter	8.921	pounds/acre
grams/sq meter	0.2048	pounds/1000 sq ft
grams/sq meter	2.855	tons/sq mile
g (gravity)	9.80665	meters/sec^2
g (gravity)	32.174	ft/sec^2
hand	10.16	cm
hands	4	inches
hectare (ha)	2.471	acre
hectares	1.076×10^{5}	sq feet
hectograms	100	grams
hectoliters	100	liters
hectometers	100	meters
hectowatts	100	watts

Multiply	by	to obtain
hemispheres	0.5	spheres
hemispheres	4	spherical right angles
hemispheres	6.2832	steradians
henries (abs)	10^9	abhenries
henries	1,000.0	millihenries
henries (abs)	1.1126×10^{-12}	stathenries
hogsheads (British)	63	gallons (British)
hogsheads (British)	10.114	cubic ft
hogsheads (U.S.)	8.422	cubic feet
hogsheads (U.S.)	0.2385	cubic meters
hogsheads (U.S.)	63	gallons (U.S.)
horsepower	2545.08	Btu(mean)/hour
horsepower	42.44	Btu/min
horsepower	7.457×10^9	erg/sec
horsepower	33,000	ft lb/min
horsepower	550	foot-pounds/second
horsepower	7.6042×10^6	g cm/sec
horsepower, electrical	1.0004	horsepower
horsepower	10.70	kg.-calories/min
horsepower	0.74570	kilowatts (g = 980.665)
horsepower	498129	lumens
horsepower, continental	736	watts (abs)
horsepower, electrical	746	watts (abs)
horsepower (boiler)	9.803	kw
horsepower (boiler)	33.479	Btu/hr
horsepower-hours	2545	Btu (mean)
horsepower-hours	2.6845×10^{13}	ergs
horsepower-hours	6.3705×10^7	ft poundals
horsepower-hours	1.98×10^6	foot-pounds
horsepower-hours	641,190	gram-calories
horsepower-hours	2.684×10^6	joules

Multiply	by	to obtain
horsepower-hours	641.7	kilogram-calories
horsepower-hours	2.737×10^{5}	kilogram-meters
horsepower-hours	0.7457	kilowatt-hours (abs)
horsepower-hours	26494	liter atmospheres (normal)
horsepower-hours	745.7	watt-hours
hours	4.167×10^{-2}	days
hours	60	minutes
hours	3600	seconds
hours	5.952×10^{-3}	weeks
hundredweights (long)	112	pounds
hundredweights (long)	0.05	tons (long)
hundredweights (short)	1600	ounces (avoirdupois)
hundredweights (short)	100	pounds
hundredweights (short)	0.0453592	tons (metric)
hundredweights (short)	0.0446429	tons (long)
inches (British)	2.540	centimeters
inches (U.S.)	2.54000508	centimeters
inches (British)	0.9999972	inches (U.S.)
inches	2.540×10^{-2}	meters
inches	1.578×10^{-5}	miles
inches	25.40	millimeters
inches	10^{3}	mils
inches	2.778×10^{-2}	yards
inches^{2}	6.4516×10^{-4}	meter^{2}
inches^{3}	1.6387×10^{-5}	meter^{3}
in. of mercury	0.0334	atm
in. of mercury	1.133	ft of water
in. of mercury (0°C)	13.609	inches of water (60°F)
in. of mercury	0.0345	kgs./square cm.
in. of mercury at 32°F	345.31	kilograms/square meter
in. of mercury	33.35	millibars
in. of mercury	25.40	millimeters of mercury

Multiply	by	to obtain
in. of mercury (60°F)	3376.85	newton/meter^2
in. of mercury	70.73	pounds/square ft
in. of mercury at 32°F	0.4912	pounds/square inch
in. of water	0.002458	atmospheres
in. of water	0.0736	in. of mercury
in. of water (at 4°C)	2.540 x 10^{-3}	kgs/sq cm
in. of water	25.40	kgs./square meter
in. of water (60°F)	1.8663	millimeters of mercury (0°C)
in. of water (60°F)	248.84	newton/meter^2
in. of water	0.5781	ounces/square in
in. of water	5.204	pounds/square ft
in. of water	0.0361	psi
inches/hour	2.54	cm/hr
international ampere	.9998	ampere(absolute)
international volt	1.0003	volts (absolute)
international volt	1.593 x 10^{-19}	joules (absolute)
international volt	9.654 x 10^4	joules
joules	9.480 x 10^{-4}	Btu
joules (abs)	10^7	ergs
joules	23.730	foot poundals
joules (abs)	0.73756	foot-pounds
joules	3.7251 x 10^{-7}	horsepower hours
joules	2.389 x 10^{-4}	kg-calories
joules (abs)	0.101972	kilogram-meters
joules	9.8689 x 10^{-3}	liter atmospheres (normal)
joules	2.778 x 10^{-4}	watt-hrs
joule-sec	1.5258 x 10^{33}	quanta
joules/cm	1.020 x 10^4	grams
joules/cm	10^7	dynes
joules/cm	100.0	joules/meter(newtons)
joules/cm	723.3	poundals

Multiply	by	to obtain
joules/cm	22.48	pounds
joules/liter	0.02681	Btu/cu. ft
joules/m^2-sec	0.3167	Btu/ft^2-hr
joules/sec	3.41304	Btu/hr
joules/sec	0.056884	Btu/min
joules/sec	1×10^7	erg/sec
joules/sec	44.254	ft lb/min
joules/sec	0.73756	ft lb/sec
joules/sec	1.0197×10^4	g cm/sec
joules/sec	1.341×10^{-3}	HP
joules/sec	0.01433	kg cal/min
joules/sec	0.001	kilowatts
joules/sec	668	lumens
joules/sec	1	watts
kilograms	564.38	drams (avdp)
kilograms	257.21	drams (troy)
kilograms	980,665	dynes
kilograms	15432	grains
kilograms	1,000	grams
kilograms	0.09807	joules/cm
kilograms	9.807	joules/meter (newtons)
kilograms	1×10^6	milligrams
kilograms	35.274	ounces (avdp)
kilograms	32.151	ounces (troy)
kilograms	70.93	poundals
kilograms	2.20462	pounds (avdp)
kilograms	2.6792	pounds (troy)
kilograms	9.84207×10^{-4}	tons (long)
kilograms	0.001	tons (metric)
kilograms	0.0011023	tons (short)
kilogram-calories	3.968	British Thermal Units

Multiply	by	to obtain
kilogram-calories	3086	foot-pounds
kilogram-calories	1.558×10^{-3}	horsepower-hours
kilogram-calories	4,186	joules
kilogram-calories	426.6	kilogram-meters
kilogram-calories	4.186	kilojoules
kilogram-calories	1.162×10^{-3}	kilowatt-hours
kg-cal/min	238.11	Btu/hr
kg-cal/min	3.9685	Btu/min
kg-cal/min	6.9770×10^{8}	erg/sec
kg-cal/min	3087.4	ft-lb/min
kg-cal/min	51.457	ft-lb/sec
kg-cal/min	7.1146×10^{5}	g cm/sec
kg-cal/min	0.0936	hp
kg-cal/min	69.769	joules/sec
kg-cal/min	0.0698	kw
kg-cal/min	46636	lumens
kg-cal/min	69.767	watts
kgs-cms.squared	2.373×10^{-3}	pounds-feet squared
kgs-cms. squared	0.3417	pounds-inches squared
kilogram-force (kgf)	9.80665	newton
kilogram-meters	0.0092967	Btu (mean)
kilogram-meters	2.3427	calories, gram (mean)
kilogram-meters	9.80665×10^{7}	ergs
kilogram-meters	232.71	ft poundals
kilogram-meters	7.2330	foot-pounds
kilogram-meters	3.6529×10^{-6}	horsepower-hours
kilogram-meters	9.80665	joules (abs)
kilogram-meters	2.344×10^{-3}	kilogram-calories
kilogram-meters	2.52407×10^{-6}	kilowatt-hours (abs)
kilogram-meters	2.7241×10^{-6}	kilowatt-hours
kilogram-meters	0.096781	liter atmospheres (normal)

Multiply	by	to obtain
kilogram-meters	6.392×10^{-7}	pounds carbon to CO_2
kilogram-meters	9.579×10^{-6}	pounds water evap. at $212°F$
kilograms/cubic meter	10^{-3}	grams/cubic cm
kilograms/cubic meter	0.06243	pounds/cubic foot
kilograms/cubic meter	3.613×10^{-5}	pounds/cubic inch
kilograms/cubic meter	3.405×10^{-10}	pounds/mil. foot
kilograms/m^3-day	0.0624	lb/cu ft-day
kilograms/cu meter-day	62.43	pounds/1000 cu ft-day
kilograms/ha	0.8921	pounds/acre
kilograms/meter	0.6720	pounds/foot
kilograms/sq cm	980,665	dynes
kilograms/sq cm	0.96784	atmosphere
kilograms/sq cm	32.81	feet of water
kilograms/sq cm	28.96	inches of mercury
kilograms/sq cm	735.56	mms. of mercury
kilograms/sq cm	2,048	pounds/sq ft
kilograms/sq cm	14.22	pounds/square inch
kilograms/sq km	92.9×10^{-6}	grams/sq ft
kilograms/sq km	0.001	grams/sq meter
kilograms/sq km	0.0001	milligrams/sq cm
kilograms/sq km	1.0	milligrams/sq meter
kilograms/sq km	8.921×10^{-3}	pounds/acre
kilograms/sq km	204.8×10^{-6}	pounds/1000 sq ft
kilograms/sq km	2.855×10^{-3}	tons/sq mile
kilograms/sq meter	9.6784×10^{-5}	atmospheres
kilograms/sq meter	98.07×10^{-6}	bars
kilograms/sq meter	98.0665	dynes/sq centimeters
kilograms/sq meter	3.281×10^{-3}	feet of water at $39.2°F$
kilograms/sq meter	0.1	grams/sq centimeters
kilograms/sq meter	2.896×10^{-3}	inches of mercury at $32°F$
kilograms/sq meter	0.07356	mm of mercury at $0°C$
kilograms/sq meter	0.2048	pounds/square foot

Multiply	by	to obtain
kilograms/sq meter	0.00142234	pounds/square inch
kilograms/sq mm.	10^6	kgs./square meter
kilojoule	0.947	Btu
kilojoules/kilogram	0.4295	Btu/pound
kilolines	1,000.0	maxwells
kiloliters	10^3	liters
kilometers	10^5	centimeters
kilometers	3281	ft
kilometers	3.937×10^4	inches
kilometers	10^3	meters
kilometers	0.53961	miles (nautical)
kilometers	0.6214	miles (statute)
kilometers	10^6	millimeters
kilometers	1093.6	yards
kilometers/hr	27.78	cm/sec
kilometers/hr	54.68	feet/minute
kilometers/hr	0.9113	ft/sec
kilometers/hr	0.5396	knot
kilometers/hr	16.67	meters/minute
kilometers/hr	0.2778	meters/sec
kilometers/hr	0.6214	miles/hour
kilometers/hour/sec	27.78	cms/sec/sec
kilometers/hour/sec	0.9113	ft/sec/sec
kilometers/hour/sec	0.2778	meters/sec/sec
kilometers/hour/sec	0.6214	miles/hr/sec
kilometers/min	60	kilometers/hour
kilonewtons/sq m	0.145	psi
kilowatts	56.88	Btu/min
kilowatts	4.425×10^4	foot-pounds/min
kilowatts	737.6	ft-lb/sec
kilowatts	1.341	horsepower

Multiply	by	to obtain
kilowatts	14.34	kg-cal/min
kilowatts	10^3	watts
kilowatt-hrs	3413	Btu (mean)
kilowatt-hrs	3.600×10^{13}	ergs
kilowatt-hrs	2.6552×10^6	foot-pounds
kilowatt-hrs	859,850	gram-calories
kilowatt-hrs	1.341	horsepower hours
kilowatt-hrs	3.6×10^6	joules
kilowatt-hrs	860.5	kg-calories
kilowatt-hrs	3.6709×10^5	kilogram-meters
kilowatt-hrs	3.53	pounds of water evaporated from and at 212°F
kilowatt-hrs	22.75	pounds of water raised from 62° to 212°F
knots	6,080	feet/hr
knots	1.689	feet/sec
knots	1.8532	kilometers/hr
knots	0.5144	meters/sec
knots	1.0	miles (nautical)/hour
knots	1.151	miles (statute)/hour
knots	2,027	yards/hr
lambert	2.054	candle/in^2
lambert	929	footlambert
lambert	0.3183	stilb
langley	1	15° gram-calorie/cm^2
langley	3.6855	Btu/ft^2
langley	0.011624	Int. kw-hr/m^2
langley	4.1855	joule (abs)/cm^2
leagues (nautical)	3	miles (nautical)
leagues (statute)	3	miles (statute)
light years	63274	astronomical units
light years	9.4599×10^{12}	kilometers
light years	5.8781×10^{12}	miles

Multiply	by	to obtain
lignes (Paris lines)	1/12	ponces (Paris inches)
lines/sq cm	1.0	gausses
lines/sq in	0.1550	gausses
lines/sq in	1.550×10^{-9}	webers/sq cm
lines sq in	10^{-8}	webers/sq in
lines/sq in	1.550×10^{-5}	webers/sq meter
links (engineer's)	12.0	inches
links (Gunter's)	0.01	chains (Gunter's)
links (Gunter's)	0.66	feet
links (Ramden's)	0.01	chains (Ramden's)
links (Ramden's)	1	feet
links (surveyor's)	7.92	inches
liters	8.387×10^{-3}	barrels (U.S.)
liters	0.02838	bushels (U.S. dry)
liters	1000.028	cubic centimeters
liters	0.035316	cubic feet
liters	61.025	cu in
liters	10^{-3}	cubic meters
liters	1.308×10^{-3}	cubic yards
liters	270.5179	drams (U.S. fl)
liters	0.21998	gallons (Br.)
liters	0.26417762	gallons (U.S.)
liters	16894	minims (Br.)
liters	16231	minims (U.S.)
liters	35.196	ounces (Br. fl)
liters	33.8147	ounces (U.S. fl)
liters	2.113	pints (liq.)
liters	1.0566828	quarts (U.S. liq.)
liter-atmospheres (normal)	0.096064	Btu (mean)
liter-atmospheres (normal)	24.206	calories, gram (mean)
liter-atmospheres (normal)	1.0133×10^{9}	ergs

Multiply	by	to obtain
liter-atmospheres (normal)	74.735	foot-pounds
liter-atmospheres (normal)	3.7745×10^{-5}	horsepower hours
liter-atmospheres (normal)	101.33	joules (abs)
liter-atmospheres (normal)	10.33	kilogram-meters
liter-atmospheres (normal)	2.4206×10^{-2}	kilogram calories
liter-atmospheres (normal)	2.815×10^{-5}	kilowatt-hours
liter/cu m -sec	60.0	cfm/1000 cu ft
liters/minute	5.885×10^{-4}	cubic feet/sec
liters/minute	4.403×10^{-3}	gallons/sec
liter/person-day	0.264	gpcd
liters/sec	2.119	cu ft /min
liters/sec	3.5316×10^{-2}	cu ft /sec
liters/sec	15.85	gallons/minute
liters/sec	0.02282	mgd
$\log_{10}N$	2.303	$\log_e N$ or ln N
$\log_e N$ or ln N	0.4343	$\log_{10}N$
lumens	0.07958	candle-power (spherical)
lumens	0.00147	watts of maximum visibility radiation
lumens/sq. centimeters	1	lamberts
lumens/sq cm/steradian	3.1416	lamberts
lumens/sq ft	1	foot-candles
lumens/sq ft	10.764	lumens/sq meter
lumens/sq ft/steradian	3.3816	millilamberts
lumens/sq meter	0.09290	foot-candles or lumens/sq
lumens/sq meter	10^{-4}	phots
lux	0.09290	foot-candles
lux	1	lumens/sq meter
lux	10^{-4}	phots
maxwells	0.001	kilolines
maxwells	10^{-8}	webers

Multiply	by	to obtain
megajoule	0.3725	horsepower-hour
megalines	10^6	maxwells
megohms	10^{12}	microhms
megohms	10^6	ohms
meters	10^{10}	angstrom units
meters	100	centimeters
meters	0.5467	fathoms
meters	3.280833	feet (U.S.)
meters	39.37	inches
meters	10^{-3}	kilometers
meters	5.396×10^{-4}	miles (naut.)
meters	6.2137×10^{-4}	miles (statute)
meters	10^3	millimeters
meters	10^9	millimicrons
meters	1.09361	yards (U.S.)
meters	1.179	varas
meter-candles	1	lumens/sq meter
meter-kilograms	9.807×10^7	centimeter-dynes
meter-kilograms	10^5	centimeter-grams
meter-kilograms	7.233	pound-feet
meters/minute	1.667	centimeters/sec
meters/minute	3.281	feet/minute
meters/minute	0.05468	feet/second
meters/minute	0.06	kilograms/hour
meters/minute	0.03238	knots
meters/minute	0.03728	miles/hour
meters/second	196.8	feet/minute
meters/second	3.281	feet/second
meters/second	3.6	kilometers/hour
meters/second	0.06	kilometers/min
meters/second	1.944	knots

Multiply	by	to obtain
meters/second	2.23693	miles/hour
meters/second	0.03728	miles/minute
meters/sec/sec	100.0	cms/sec/sec
meters/sec/sec	3.281	feet/sec/sec
meters/sec/sec	3.6	kms./hour/sec
meters/sec/sec	2.237	miles/hour/sec
microfarad	10^{-6}	farads
micrograms	10^{-6}	grams
micrograms/cu ft	10^{-6}	grams/cu ft
micrograms/cu ft	35.314×10^{-6}	grams/cu m
micrograms/cu ft	35.314	microgram/cu m
micrograms/cu ft	35.314×10^{-3}	milligrams/cu m
micrograms/cu ft	2.2046×10^{-6}	pounds/1000 cu ft
micrograms/cu m	28.317×10^{-9}	grams/cu ft
micrograms/cu m	10^{-6}	grams/ cu m
micrograms/cu m	0.02832	micrograms/cu ft
micrograms/cu m	0.001	milligrams/cu m
micrograms/cu m	62.43×10^{-9}	pounds/1000 cu ft
micrograms/cu m	$\dfrac{0.02404}{\text{molecular weight of gas}}$	ppm by volume (20°C)
micrograms/cu m	834.7×10^{-6}	ppm by weight
micrograms/liter	1000.0	micrograms/cu m
micrograms/liter	1.0	milligrams/cu m
micrograms/liter	62.43×10^{-9}	pounds/cu ft
micrograms/liter	$\dfrac{24.04}{\text{molecular weight of gas}}$	ppm by volume (20°C)
micrograms/liter	0.8347	ppm by weight
microhms	10^{-12}	megohms
microhms	10^{-6}	ohms
microliters	10^{-6}	liters
microns	10^{4}	angstrom units
microns	1×10^{-4}	centimeters
microns	3.9370×10^{-5}	inches

Multiply	by	to obtain
microns	10^{-6}	meters
miles (naut.)	6,080.27	feet
miles (maut.)	1.853	kilometers
miles (naut.)	1.853	meters
miles (naut.)	1.1516	miles (statute)
miles (naut.)	2,027	yards
miles (statute)	1.609×10^5	centimeters
miles (statute)	5,280	feet
miles (statute)	6.336×10^4	inches
miles (statute)	1.609	kilometers
miles (statute)	1,609	meters
miles (statute)	0.8684	miles (naut.)
miles (statute)	320	rods
miles (statute)	1,760	yards
miles/hour	44.7041	centimeter/second
miles/hour	88	feet/min
miles/hour	1.4667	feet/sec
miles/hour	1.6093	kilometers/hour
miles/hour	0.02682	kms/min
miles/hour	0.86839	knots
miles/hour	26.82	meters/min
miles/hour	0.447	meters/sec
miles/hour	0.1667	miles/min
miles/hour/sec	44.70	cms/sec/sec
miles/hour/sec	1.4667	ft/sec/sec
miles/hour/sec	1.6093	kms/hour/sec
miles/hour/sec	0.4470	m /sec/sec
miles/min	2682	centimeters/sec
miles/min	88	ft/sec
miles/min	1.609	km/min
miles/min	0.8684	knots/min

Multiply	by	to obtain
miles/min	60	miles/hour
miles-feet	9.425×10^{-6}	cu inches
millibars	0.00987	atmospheres
millibars	0.30	inches of mercury
millibars	0.75	millimeters of mercury
milliers	10^3	kilograms
millimicrons	1×10^{-9}	meters
milligrams	0.01543236	grains
milligrams	10^{-3}	grams
milligrams	10^{-6}	kilograms
milligrams	3.5274×10^{-5}	ounces (avdp)
milligrams	2.2046×10^{-6}	pounds (avdp)
milligrams/assay ton	1	ounces (troy)/ton(short)
milligrams/cu m	283.2×10^{-6}	grams/cu ft
milligrams/cu m	0.001	grams/cu m
milligrams/cu m	1000.0	micrograms/cu m
milligrams/cu m	28.32	micrograms/cu ft
milligrams/cu m	1.0	micrograms/liter
milligrams/cu m	62.43×10^{-6}	pounds/1000 cu ft
milligrams/cu m	$\dfrac{24.04}{\text{molecular weight of gas}}$	ppm by volume (20°C)
milligrams/cu m	0.8347	ppm by weight
milligrams/joule	5.918	pounds/horsepower-hour
milligrams/liter	0.05841	grains/gallon
milligrams/liter	0.07016	grains/imp gal
milligrams/liter	0.0584	grains/US gal
milligrams/liter	1.0	parts/million
milligrams/liter	8.345	lb/mil gal
milligrams/sq cm	0.929	grams/sq ft
milligrams/sq cm	10.0	grams/sq meter
milligrams/sq cm	10^4	kilograms/sq km
milligrams/sq cm	10^4	milligrams/sq meter

Multiply	by	to obtain
milligrams/sq cm	2.048	pounds/1000 sq ft
milligrams/sq cm	89.21	pounds/acre
milligrams/sq cm	28.55	tons/sq mile
milligrams/sq meter	92.9×10^{-6}	grams/sq ft
milligrams/sq meter	0.001	grams/sq meter
milligrams/sq meter	1.0	kilograms/sq km
milligrams/sq meter	0.0001	milligrams/sq cm
milligrams/sq meter	8.921×10^{-3}	pounds/acre
milligrams/sq meter	204.8×10^{-6}	pounds/1000 sq ft
milligrams/sq meter	2.855×10^{-3}	tons/sq mile
millihenries	0.001	henries
milliliters	1	cubic centimeters
milliliters	3.531×10^{-5}	cu ft
milliliters	6.102×10^{-2}	cu in
milliliters	10^{-6}	cu m
milliliters	2.642×10^{-4}	gal (U.S.)
milliliters	10^{-3}	liters
milliliters	0.03381	ounces (U.S. fl)
millimeters	0.1	centimeters
millimeters	3.281×10^{-3}	feet
millimeters	0.03937	inches
millimeters	10^{-6}	kilometers
millimeters	0.001	meters
millimeters	6.214×10^{-7}	miles
millimeters	39.37	mils
millimeters	1.094×10^{-3}	yards
millimeters of mercury	1.316×10^{-3}	atmospheres
millimeters of mercury	0.0394	inches of mercury
millimeters of mercury (0°C)	0.5358	inches of water (60°F)
millimeters of mercury	1.3595×10^{-3}	kgs/sq cm

Multiply	by	to obtain
millimeter of mercury (0^oC)	133.3224	newton/meter^2
millimeters of mercury	0.01934	pounds/sq in
millimeters/sec	11.81	feet/hour
million gallons	306.89	acre-ft
million gallons	3,785.0	cubic meters
million gallons	3.785	mega liters (1×10^6)
million gallons/day (mgd)	1.547	cu ft/sec
mgd	3,785	cu m/day
mgd	0.0438	cubic meters/sec
mgd	43.808	liters/sec
mgd/acre	9,360	cu m/day/ha
mgd/acre	0.039	cu meters/hour/sq meter
mils	0.002540	centimeters
mils	8.333×10^{-5}	feet
mils	0.001	inches
mils	2.540×10^{-8}	kilometers
mils	25.40	microns
mils	2.778×10^{-5}	yards
miner's in.	1.5	cu ft/min
miner's inches (Ariz.,Calif. Mont., and Ore.)	0.025	cubic feet/second
miner's in. (Colorado)	0.02604	cubic feet/second
miner's inches (Ida., Kan., Neb., Nev., N.Mex., N.Dak., S.Dak. and Utah)	0.020	cubic feet/second
minims (British)	0.05919	cubic centimeter
minims (U.S.)	0.06161	cubic centimeters
minutes (angles)	0.01667	degrees
minutes (angles)	1.852×10^{-4}	quadrants
minutes (angles)	2.909×10^{-4}	radians
minutes (angle)	60	seconds (angle)
months (mean calendar)	30.4202	days

Multiply	by	to obtain
months (mean calendar)	730.1	hours
months (mean calendar)	43805	minutes
months (mean calendar)	2.6283×10^6	seconds
myriagrams	10	kilograms
myriameters	10	kilometers
myriawatts	10	kilowatts
nepers	8.686	decibels
newtons	10^5	dynes
newtons	0.10197	kilograms
newtons	0.22481	pounds
newtons/sq meter	1.00	pascals (Pa)
noggins (British)	1/32	gallons (British)
No./cu.cm.	28.316×10^3	No./cu.ft.
No./cu.cm.	10^6	No./cu. meter
No./cu.cm.	1000.0	No./liter
No./cu.ft.	35.314×10^{-6}	No./cu.cm.
No./cu.ft.	35.314	No./cu. meter
No./cu.ft.	35.314×10^{-3}	No./liter
No./cu. meter	10^{-6}	No./cu.cm.
No./cu. meter	28.317×10^{-3}	No./cu.ft.
No./cu. meter	0.001	No./liter
No./liter	0.001	No./cu.cm.
No./liter	28.316	No./cu.ft.
No./liter	1000.0	No./cu. meter
oersteds (abs)	1	electromagnetic cgs units of magnetizing force
oersteds (abs)	2.9978×10^{10}	electrostatic cgs units of magnetizing force
ohms	10^9	abohms
ohms	1.1126×10^{-12}	statohms
ohms	10^{-6}	megohms
ohms	10^6	microhms

Multiply	by	to obtain
OHM (International)	1.0005	OHM (absolute)
ounces (avdp)	16	drams (avoirdupois)
ounces (avdp)	7.2917	drams (troy)
ounces (avdp)	437.5	grains
ounces (avdp)	28.349527	grams
ounces (avdp)	0.028350	kilograms
ounces (avdp)	2.8350×10^{4}	milligrams
ounces (avdp)	0.9114583	ounces (troy)
ounces (avdp)	0.0625	pounds (avoirdupois)
ounces (avdp)	0.075955	pounds (troy)
ounces (avdp)	2.790×10^{-5}	tons (long)
ounces (avdp)	2.835×10^{-5}	tons (metric)
ounces (avdp)	3.125×10^{-5}	tons (short)
ounces (Br. fl)	2.3828×10^{-4}	barrels (U.S.)
ounces (Br. fl)	1.0033×10^{-3}	cu ft
ounces (Br. fl)	1.73457	cu in
ounces (Br. fl)	7.6860	drams (U.S. fl)
ounces (Br. fl)	6.250×10^{-3}	gallons (Br.)
ounces (Br. fl)	0.07506	gallons (U.S.)
ounces (Br. fl)	2.84121×10^{-2}	liters
ounces (Br. fl)	480	minims (Br.)
ounces (Br. fl)	461.160	minims (U.S.)
ounces (Br. fl)	28.4121	ml
ounces (Br. fl)	0.9607	ounces (U.S. fl)
ounces (troy)	17.554	drams (avdp)
ounces (troy)	8	drams (troy)
ounces (troy)	480	grains (troy)
ounces (troy)	31.103481	grams
ounces (troy)	0.03110	kilograms
ounces (troy)	1.09714	ounces (avoirdupois)
ounces (troy)	20	pennyweights (troy)
ounces (troy)	0.068571	pounds (avdp)

Multiply	by	to obtain
ounces (troy)	0.08333	pounds (troy)
ounces (troy)	3.061×10^{-5}	tons (long)
ounces (troy)	3.429×10^{-5}	tons (short)
ounces (U.S. fl)	2.48×10^{-4}	barrels (U.S.)
ounces (U.S. fl)	29.5737	cubic centimeters
ounces (U.S. fl)	1.0443×10^{-3}	cu ft
ounces (U.S. fl)	1.80469	cubic inches
ounces (U.S. fl)	8	drams (fluid)
ounces (U.S. fl)	6.5053×10^{-3}	gallons (Br.)
ounces (U.S. fl)	7.8125×10^{-3}	gallons (U.S.)
ounces (U.S. fl)	29.5729	milliliters
ounces (U.S. fl)	499.61	minims (Br.)
ounces (U.S. fl)	480	minims (U.S.)
ounces (U.S. fl)	1.0409	ounces (Br. fl)
ounces/sq inch	4309	dynes/sq. cm
ounces/sq. inch	0.0625	pounds/sq inch
paces	30	inches
palms (British)	3	inches
parsecs	3.260	light years
parsecs	3.084×10^{13}	kilometers
parsecs	3.084×10^{16}	meters
parsec	19×10^{12}	miles
parts/billion (ppb)	10^{-3}	mg/1
parts/million (ppm)	0.07016	grains/imp. gal.
parts/million	0.058417	grains/gallon (U.S.)
parts/million	1.0	mg/liter
parts/million	8.345	lbs/million gal
ppm by volume (20°C)	$\dfrac{\text{molecular weight of gas}}{24.04}$	micrograms/liter
ppm by volume (20°C)	$\dfrac{\text{molecular weight of gas}}{0.02404}$	micrograms/cu meter
ppm by volume (20°C)	$\dfrac{\text{molecular weight of gas}}{24.04}$	milligrams/cu meter
ppm by volume (20°C)	$\dfrac{\text{molecular weight of gas}}{28.8}$	ppm by weight

Multiply	by	to obtain
ppm by volume (20°C)	$\dfrac{\text{molecular weight of gas}}{385.1 \times 10^6}$	pounds/cu ft
ppm by weight	1.198×10^{-3}	micrograms/cu meter
ppm by weight	1.198	micrograms/liter
ppm by weight	1.198	milligrams/cu meter
ppm by weight	$\dfrac{28.8}{\text{molecular weight of gas}}$	ppm by volume (20°C)
ppm by weight	7.48×10^{-6}	pounds/cu ft
pecks (British)	0.25	bushels (British)
pecks (British)	554.6	cubic inches
pecks (British)	9.091901	liters
pecks (U.S.)	0.25	bushels (U.S.)
pecks (U.S.)	537.605	cubic inches
pecks (U.S.)	8.809582	liters
pecks (U.S.)	8	quarts (dry)
pennyweights	24	grains
pennyweights	1.555174	grams
pennyweights	0.05	ounces (troy)
pennyweights (troy)	4.1667×10^{-3}	pounds (troy)
perches (masonry)	24.75	cubic feet
phots	929.0	foot-candles
phots	1	lumen incident/sq cm
phots	10^4	lux
picas (printers')	1/6	inches
pieds (French feet)	0.3249	meters
pints (dry)	33.6003	cubic inches
pints (liq.)	473.179	cubic centimeters
pints (liq.)	0.01671	cu feet
pints (liq.)	4.732×10^{-4}	cu meters
pints (liq.)	6.189×10^{-4}	cu yards
pints (liq.)	0.125	gallons
pints (liq.)	0.4732	liters
pints (liq.)	16	ounces (U.S. fluid)

Multiply	by	to obtain
pints (liq.)	0.5	quarts (liq.)
planck's constant	6.6256×10^{-27}	erg-seconds
poise	1.00	gram/cm sec
poise	0.1	newton-second/meter^2
population equivalent (PE)	0.17	pounds BOD
pottles (British)	0.5	gallons (British)
pouces (Paris inches)	0.02707	meters
pouces (Paris inches)	0.08333	pieds (Paris feet)
poundals	13,826	dynes
poundals	14.0981	grams
poundals	1.383×10^{-3}	joules/cm
poundals	0.1383	joules/meter (newton)
poundals	0.01410	kilograms
poundals	0.031081	pounds
pounds (avdp)	256	drams (avdp)
pounds (avdp)	116.67	drams (troy)
pounds (avdp)	444,823	dynes
pounds (avdp)	7000	grains
pounds (avdp)	453.5924	grams
pounds (avdp)	0.04448	joules/cm
pounds (avdp)	4.448	joules/meter (newtons)
pounds (avdp)	0.454	kilograms
pounds (avdp)	4.5359×10^5	milligrams
pounds (avdp)	16	ounces (avdp)
pounds (avdp)	14.5833	ounces (troy)
pounds (avdp)	32.17	poundals
pounds (avdp)	1.2152778	pounds (troy)
pounds (avdp)	4.464×10^{-4}	tons (long)
pounds (avdp)	0.0005	tons (short)
pounds (troy)	210.65	drams (avdp)
pounds (troy)	96	drams (troy)

Multiply	by	to obtain
pounds (troy)	5,760	grains
pounds (troy)	373.2418	grams
pounds (troy)	0.37324	kilograms
pounds (troy)	3.7324×10^{5}	milligrams
pounds (troy)	13.1657	ounces (avdp)
pounds (troy)	12.0	ounces (troy)
pounds (troy)	240.0	pennyweights (troy)
pounds (troy)	0.8229	pounds (avdp)
pounds (troy)	3.6735×10^{-4}	tons (long)
pounds (troy)	3.7324×10^{-4}	tons (metric)
pounds (troy)	4.1143×10^{-4}	tons (short)
pounds (avdp)-force	4.448	newtons
pounds-force-sec/ft^{2}	47.88026	newton-sec/meter^{2}
pounds (avdp)-mass	0.4536	kilograms
pounds-mass/ft^{3}	16.0185	kilogram/meter^{3}
pounds-mass/ft-sec	1.4882	mewton-sec/meter^{2}
pounds of BOD	5.882	population equivalent (PE)
pounds of carbon to CO_2	14544	Btu (mean)
pounds of water	0.0160	cu ft
pounds of water	27.68	cu in
pounds of water	0.1198	gal
pounds of water evaporated at 212°F	970.3	Btu
pounds of water per min	2.699×10^{-4}	cubic feet/sec
pound-feet	13,825	centimeter-grams
pound-feet (torque)	1.3558×10^{7}	dyne-centimeters
pound-feet	0.1383	meter-kilograms
pounds-feet squared	421.3	kgs.-cms. squared
pounds-feet squared	144	pounds-ins. squared
pounds-inches squared	2,926	kgs.-cms. squared
pounds-inches squared	6.945×10^{-3}	pounds-feet squared
pounds/acre	0.0104	grams/sq ft

Multiply	by	to obtain
pounds/acre	0.1121	grams/sq meter
pounds/acre	1.121	kg/ha
pounds/acre	112.1	kilograms/sq km
pounds/acre	0.01121	milligrams/sq cm
pounds/acre	112.1	milligrams/sq meter
pounds/acre	0.023	pounds/1000 sq ft
pounds/acre	0.32	tons/sq mile
pounds/acre/day	0.112	g/day/sq m
pounds/cu ft	0.0160	g/ml
pounds/cu ft	16.02	kg/cu m
pounds/cu ft	16.018×10^9	micrograms/cu meter
pounds/cu ft	16.018×10^6	micrograms/liter
pounds/cu ft	16.018×10^6	milligrams/cu meter
pounds/cu ft	$\dfrac{385.1 \times 10^6}{\text{molecular weight of gas}}$	ppm by volume (20°C)
pounds/cu ft	133.7×10^3	ppm by weight
pounds/cu ft	5.787×10^{-4}	lb/cu in
pounds/cu ft	5.456×10^{-9}	pounds/mil-foot
pounds/1000 cu ft	0.35314	grams/cu ft
pounds/1000 cu ft	16.018	grams/cu m
pounds/1000 cu ft	353.14×10^3	micrograms/cu ft
pounds/1000 cu ft	16.018×10^6	microgram/cu m
pounds/1000 cu ft	16.018×10^3	milligrams/cu m
pounds/cubic inch	27.68	grams/cubic cm
pounds/cubic inch	2.768×10^4	kgs/cubic meter
pounds/cubic inch	1728	pounds/cubic foot
pounds/cubic inch	9.425×10^{-6}	pounds/mil foot
pounds/day/acre-ft	3.68	g/day/cu m
pounds/day/cu ft	16	kg/day/cu m
pounds/day/cu yd	0.6	kg/day/cu m
pounds/day/sq ft	4,880	g/day/sq m
pounds/ft	1.488	kg/m

Multiply	by	to obtain
pounds/gal	454 g/3.785 l=119.947	g/liter
pounds/1000-gal	120	g/1000-liters
pounds/horsepower-hour	0.169	mg/joule
pounds/in	178.6	g/cm
pounds/mil-foot	2.306×10^6	gms/cu cm
pounds/mil gal	0.12	g/cu m
pounds/sq ft	4.725×10^{-4}	atmospheres
pounds/sq ft	0.01602	ft of water
pounds/sq ft	0.01414	inches of mercury
pounds/sq ft	4.8824×10^{-4}	kgs/sq cm
pounds/sq ft	4.88241	kilograms/square meter
pounds/sq ft	47.9	newtons/sq m
pounds/sq ft	6.944×10^{-3}	pounds/sq inch
pounds/1000 sq ft	0.4536	grams/sq ft
pounds/1000 sq ft	4.882	grams/sq meter
pounds/1000 sq ft	4882.4	kilograms/sq km
pounds/1000 sq ft	0.4882	milligrams/sq cm
pounds/1000 sq ft	4882.4	milligrams/sq meter
pounds/1000 sq ft	43.56	pounds/acre
pounds/1000 sq ft	13.94	tons/sq mile
pounds/sq in	0.068046	atmospheres
pounds/sq in	2.307	ft of water
pounds/sq in	70.307	grams/square centimeter
pounds/sq in	2.036	in of mercury
pounds/sq in	0.0703	kgs/square cm
pounds/sq in	703.07	kilograms/square meter
pounds/sq in	51.715	millimeters of mercury
pounds/sq in	6894.76	$newton/meter^2$
pounds/sq in	51.715	millimeters of mercury at 0^oC
pounds/sq in	144	pounds/sq foot

Multiply	by	to obtain
pounds/sq in (abs)	1	pound/sq in (gage) + 14.696
proof (U.S.)	0.5	percent alcohol by volume
puncheons (British)	70	gallons (British)
quadrants (angle)	90	degrees
quadrants (angle)	5400	minutes
quadrants (angle)	3.24×10^{5}	seconds
quadrants (angle)	1.571	radians
quarts (dry)	67.20	cubic inches
quarts (liq.)	946.4	cu cms
quarts (liq.)	0.033420	cubic feet
quarts (liq.)	57.75	cubic inches
quarts (liq.)	9.464×10^{-4}	cubic meters
quarts (liq.)	1.238×10^{-3}	cu yards
quarts (liq.)	0.25	gallons
quarts (liq.)	0.9463	liters
quarts (liq.)	32	ounces (U.S., fl)
quarts (liq.)	0.832674	quarts (British)
quintals (long)	112	pounds
quintals (metric)	100	kilograms
quintals (short)	100	pounds
quires	24	sheets
radians	57.29578	degrees
radians	3438	minutes
radians	0.637	quadrants
radians	2.063×10^{5}	seconds
radians/second	57.30	degrees/second
radians/second	9.549	revolutions/min
radians/second	0.1592	revolutions/sec
radians/sec/sec	573.0	revs/min/min
radians/sec/sec	9.549	revs/min/sec
radians/sec/sec	0.1592	revs/sec/sec

Multiply	by	to obtain
reams	500	sheets
register tons (British)	100	cubic feet
revolutions	360	degrees
revolutions	4	quadrants
revolutions	6.283	radians
revolutions/minute	6	degrees/second
revolutions/minute	0.10472	radians/second
revolutions/minute	0.01667	revolutions/sec
revolutions/minute^2	0.0017453	radians/sec/sec
revs/min/min	0.01667	revs/min/sec
revs/min/min	2.778×10^{-4}	revs/sec/sec
revolutions/second	360	degrees/second
revolutions/second	6.283	radians/second
revolutions/second	60	revs/minute
revs/sec/sec	6.283	rads/sec/sec
revs/sec/sec	3600	revs/min/min
revs/sec/sec	60	revs/min/sec
reyns	6.8948×10^{6}	centipoises
rod	.25	chain (gunters)
rods	16.5	feet
rods	5.0292	meters
rods	3.125×10^{-3}	miles
rods (surveyors' means)	5.5	yards
roods (British)	0.25	acres
scruples	1/3	drams (troy)
scruples	20	grains
sections	1	square miles
seconds (mean solar)	1.1574×10^{-5}	days
seconds (angle)	2.778×10^{-4}	degrees
seconds (mean solar)	2.7778×10^{-4}	hours
seconds (angle)	0.01667	minutes

Multiply	by	to obtain
seconds (angle)	3.087×10^{-6}	quadrants
seconds (angle)	4.848×10^{-6}	radians
slugs	14.59	kilogram
slugs	32.174	pounds
space, entire (solid angle)	12.566	steradians
spans	9	inches
spheres (solid angle)	12.57	steradians
spherical right angles	0.25	hemispheres
spherical right angles	0.125	spheres
spherical right angles	1.571	steradians
square centimeters	1.973×10^{5}	circular mils
square centimeters	1.07639×10^{-3}	square feet (U.S.)
square centimeters	0.15499969	square inches (U.S.)
square centimeters	10^{-4}	square meters
square centimeters	3.861×10^{-11}	square miles
square centimeters	100	square millimeters
square centimeters	1.196×10^{-4}	sq yards
square centimeters-square centimeter(moment of area)	0.024025	square inch-square inch
square chains (gunter's)	0.1	acres
square chains (gunter's)	404.7	square meters
square chains (Ramden's)	0.22956	acres
square chains (Ramden's)	10000	square feet
square feet	2.29×10^{-5}	acres
square feet	1.833×10^{8}	circular mils
square feet	144	sq in
square feet	0.092903	square meters
square feet	929.0341	square centimeters
square feet	3.587×10^{-8}	square miles
square feet	1/9	square yards
square feet/cu ft	3.29	sq m/cu m

<u>Multiply</u>	<u>by</u>	<u>to obtain</u>
square foot-square foot (moment of area)	20736	square inch-square inch
square inches	1.273×10^{6}	circular mils
square inches	6.4516258	square centimeters
square inches	6.944×10^{-3}	square feet
square inches	645.2	square millimeters
square inches	10^{6}	square mils
square inches	7.71605×10^{-4}	square yards
square inches-inches sqd.	41.62	sq cms.-cms sqd.
square inches-inches sqd.	4.823×10^{-5}	sq feet-feet sqd.
square kilometers	247.1	acres
square kilometers	10^{10}	sq cms
square kilometers	10.76×10^{6}	sq ft
square kilometers	1.550×10^{9}	sq inches
square kilometers	10^{6}	square meters
square kilometers	0.3861006	square miles (U.S.)
square kilometers	1.196×10^{6}	sq yd
square links (Gunter's)	10^{-5}	acres (U.S.)
square links (Gunter's)	0.04047	square meters
square meters	2.471×10^{-4}	acres (U.S.)
square meters	10^{4}	sq cms
square meters	10.76387	square feet (U.S.)
square meters	1550	square inches
square meters	3.8610×10^{-7}	square miles (statute)
square meters	10^{6}	sq millimeters
square meters	1.196	square yards (U.S.)
square miles	640	acres
square miles	2.78784×10^{7}	square feet
square miles	2.590	sq km
square miles	2.5900×10^{6}	square meters
square miles	3.098×10^{6}	square yards

Multiply	by	to obtain
square millimeters	1.973×10^{3}	circular mils
square millimeters	0.01	square centimeters
square millimeters	1.076×10^{-5}	sq feet
square millimeters	1.550×10^{-3}	square inches
square mils	1.273	circular mils
square mils	6.452×10^{-6}	square centimeters
square mils	10^{-6}	square inches
square rods	272.3	square feet
square yard	2.1×10^{-4}	acres
square yards	8,361	sq cms
square yards	9	square feet
square yards	1296	square inches
square yards	0.8361	square meters
square yards	3.228×10^{-7}	square miles
square yards	8.361×10^{5}	sq millimeters
statamperes	3.33560×10^{-10}	amperes (abs)
statcoulombs	3.33560×10^{-10}	coulombs (abs)
statcoulombs/kilogram	1.0197×10^{-6}	statcoulombs/dyne
statfarads	1.11263×10^{-12}	farads (abs)
stathenries	8.98776×10^{11}	henries (abs)
statohms	8.98776×10^{11}	ohms (abs)
statvolts	299.796	volts (abs)
statvolts/inch	118.05	volts (abs)/centimeter
statwebers	2.99796×10^{10}	electromagnetic cgs units of magnetic flux
statwebers	1	electrostatic cgs units of magnetic flux
stilb	2919	footlambert
stilb	1	int. candle cm^{-2}
stilb	3.142	lambert
stoke (kinematic viscosity)	10^{-4}	$meter^{2}$/second
stones (British)	6.350	kilograms
stones (British)	14	pounds

Multiply	by	to obtain
temp. (degs. C.)+273	1	abs. temp. (degs. K.)
temps (degs. C.)+17.8	1.8	temp. (degs. Fahr.)
temps. (degs. F.)+460	1	abs. temp. (degs. R.)
temps. (degs. F.)-32	5/9	temp. (degs. cent.)
toises (French)	6	paris feet (pieds)
tons (long)	5.734×10^5	drams (avdp)
tons (long)	2.613×10^5	drams (troy)
tons (long)	1.568×10^7	grains
tons (long)	1.016×10^6	grams
tons (long)	1016	kilograms
tons (long)	3.584×10^4	ounces (avdp)
tons (long)	3.267×10^4	ounces (troy)
tons (long)	2240	pounds (avdp)
tons (long)	2722.2	pounds (troy)
tons (long)	1.12	tons (short)
Tons (metric) (T)	1000	kilograms
Tons (metric) (T)	2204.6	pounds
Tons (metric) (T)	1.1025	tons (short)
tons (short)	5.120×10^5	drams (avdp)
tons (short)	2.334×10^5	drams (troy)
tons (short)	1.4×10^7	grains
tons (short)	9.072×10^5	grams
tons (short)	907.2	kilograms
tons (short)	32,000	ounces (avdp)
tons (short)	29,166.66	ounces (troy)
tons (short)	2000	pounds (avdp)
tons (short)	2.430.56	pounds (troy)
tons (short)	0.89287	tons (long)
tons (short)	0.9078	Tons (metric) (T)
tons (short)/sq ft	9765	kgs./sq meter
tons (short)/sq ft	13.89	pounds/sq inch

Multiply	by	to obtain
tons (short)/sq in	1.406×10^6	kgs/sq meter
tons (short)/sq in	2000	pounds/sq inch
tons/sq mile	3.125	pounds/acre
tons/sq mile	0.07174	pounds/1000 sq ft
tons/sq mile	0.3503	grams/sq meter
tons/sq mile	350.3	kilograms/sq km
tons/sq mile	350.3	milligrams/sq meter
tons/sq mile	0.03503	milligrams/sq cm
tons/sq mile	0.03254	grams/sq ft
tons of water/24 hours	83.333	pounds of water/hr
tons of water/24 hours	0.16643	gallons/min
tons of water/24 hours	1.3349	cu ft/hr
torr (mm Hg, $0°C$)	133.322	newton/meter^2
townships (U.S.)	23040	acres
townships (U.S.)	36	square miles
tuns	252	gallons
volts (abs)	10^8	abvolts
volts (abs)	3.336×10^{-3}	statvolts
volts (international of 1948)	1.00033	volts (abs)
volt/inch	.39370	volt/cm.
watts (abs)	3.41304	Btu (mean)/hour
watts (abs)	0.0569	Btu (mean)/min
watts (abs)	0.01433	calories, kilogram (mean)/ minute
watts (abs)	10^7	ergs/second
watts (abs)	44.26	foot-pounds/minute
watts (abs)	0.7376	foot-pounds/second
watts (abs)	0.0013405	horsepower (electrical)
watts (abs)	1.360×10^{-3}	horsepower (metric)
watts (abs)	1	joules/sec
watts (abs)	0.10197	kilogram-meters/second

Multiply	by	to obtain
watts (abs)	10^{-3}	kilowatts
watt-hours	3.415	British Thermal Units
watt-hours	3.60×10^{10}	ergs
watt-hours	2655	foot-pounds
watt-hours	859.85	gram-calories
watt-hours	1.34×10^{-3}	horsepower-hours
watt-hours	3.6×10^{3}	joule
watt-hours	0.8605	kilogram-calories
watt-hours	367.1	kilogram-meters
watt-hours	10^{-3}	kilowatt-hours
watt (internationl)	1.0002	watt (absolute)
watt/(cm^2)($^{\circ}$C/cm)	693.6	Btu/(hr)(ft^2)($^{\circ}$F/in)
wave length of the red line of cadmium	6.43847×10^{-7}	meters
webers	10^{3}	electromagnetic cgs units
webers	3.336×10^{-3}	electrostatic cgs units
webers	10^{5}	kilolines
webers	10^{8}	lines
webers	10^{8}	maxwells
webers	3.336×10^{-3}	statwebers
webers/sq in	1.550×10^{7}	gausses
webers/sq in	10^{8}	lines/sq in
webers/sq in	0.1550	webers/sq cm
webers/sq in	1,550	webers/sq meter
webers/sq meter	10^{4}	gausses
webers/sq meter	6.452×10^{4}	lines/sq in
webers/sq meter	10^{-4}	webers/sq cm
webers/sq meter	6.452×10^{-4}	webers/sq in
weeks	168	hours
weeks	10,080	minutes
weeks	604,800	seconds

<u>Multiply</u>	<u>by</u>	<u>to obtain</u>
yards	91.44	centimeters
yards	3	feet
yards	36	inches
yards	9.144×10^{-4}	kilometers
yards	0.91440	meters
yards	4.934×10^{-4}	miles (naut.)
yards	5.682×10^{-4}	miles (stat.)
yards	914.4	millimeters
years (sidereal)	365.2564	days (mean solar)
years (sidereal)	366.2564	days (sidereal)
years (tropical, mean solar)	365.2422	days (mean solar)
years (common)	8760	hours
years (tropical, mean solar)	8765.8128	hours (mean solar)
years (leap)	366	days
years (leap)	8784	hours
years (tropical, mean solar)	3.155693×10^{7}	seconds (mean solar)
years (tropical, mean solar)	1.00273780	years (sidereal)

II. BASIC AND SUPPLEMENTARY UNITS

<u>A meter(m)</u> is 1 650 763.73 wavelengths in vacuo of the radiation
corresponding to the transition between the energy levels $2p_{10}$
and $5d_5$ of the krypton 86 atom.

<u>A kilogram (kg)</u> is the mass of the international prototype in the
custody of the Bureau International des Poids et Mesures at Sevres
in France.

<u>A second (sec)</u> is the interval occupied by 9 192 631 770 cycles of
the radiation corresponding to the transition of the caesium-133
atom when unperturbed by exterior fields.

<u>An ampere</u> is the constant current which if maintained in two parallel
recti-linear conductors of infinite length of negligible circular
cross-section and placed at a distance of one meter apart in vacuo
would produce between these conductors a force equal to 2×10^{-7}
newton per meter length.

<u>A kelvin (^{o}K)</u> is the degree interval of the thermodynamic scale on
which the temperature of the triple point of water is 273.16 degrees.

<u>A candle</u> is such that the luminance of a full radiator at the temperature
of solidification of platinum is 60 units of luminous intensity per
square centimeter.

<u>A mole (mol)</u> is the amount of substance which contains as many
elementary units as there are atoms in 0.012 kg of carbon - 12.
The elementary unit must be specified and may be an atom, an ion,
an electron, a photon, etc. or a given group of such entities.

<u>A radian</u> is the angle subtended at the cent of a circle by an arc
of the circle equal in length to the radius of the circle.

<u>A steradian</u> is the solid angle which, having its vertex at the center
of a sphere, cuts off an area of the surface of the sphere equal to
that of a square with sides of length equal to the radius of the sphere.

III. DERIVED UNITS AND QUANTITIES

The liter was defined in 1901 as the volume of 1 kilogram of pure water
at normal atmospheric pressure and maximum density equal therefore
to 1.000 028 dm^3. This 1901 definition applied for the purpose of
the 1963 Weights and Measures Acts.

By a resolution of the twelfth Conference General des Poids et Mesures
(CGPM) in 1964 the word "liter" is now recognised as a special name
for the dm^3, but is not used to express high precision measurements.
It will be used widely in engineering and the retail business, where
the discrepancy of 28 parts in 1 million is of negligible significance.

A newton (N) is that force which, when applied to a body of mass of one
kilogram gives it an acceleration of one meter per second per second.

Stress is defined as the resultant internal force per unit area resisting
change in the shape or size of a body acted on by external forces, and
is therefore measured in newtons per square meter. (N/m^2)

A bar is a pressure equivalent to 100 000 newtons acting on an area of
one square meter.

A joule (J) is the work done when the point of application of a force of
one newton is displaced through a distance of one meter in the direction
of the force.

A watt is equal to one joule per second.

Dynamic Viscosity is the property of a fluid whereby it tends to resist
relative motion within itself. It is the shear stress, i.e. the
tangential force on unit area, between two infinite horizontal planes
at unit distance apart, one of which is fixed while the other moves
with unit velocity. In other words, it is the shear stress divided
by the velocity gradient, i.e. $(N/m^2) \div (m/sec/m) = N \ sec/m^2$

Kinematic Viscosity is the dynamic viscosity of a fluid divided by its density,
i.e. $(N \ sec/m^2)/(kg/m^3) = m^2/sec$

Density of Heat Flow Rate (or Heat Flux) is the heat flow rate (W) per
unit area, i.e. W/m^2.

Coefficient of Heat Transfer is the heat flow rate (W) per unit area per
unit temperature difference, i.e. $W/m^2 {}^oC$.

Thermal Conductivity is the quantity of heat which will be conducted in unit
time through unit area of a slab of material of unit thickness with a unit
difference of temperature between the faces; in other words, the heat flow
rate (W) per unit area per unit temperature gradient, i.e. $W/[m^2({}^oC/m)] = W/m {}^oC$.

The Heat Capacity of a substance is the quantity of heat gained or lost by
the substance per unit temperature change, i.e. $J/{}^oC$.

Specific Heat Capacity is the heat capacity per unit mass of the substance,
i.e., $J/kg {}^oC$.

Internal Energy is the kinetic energy possessed by the molecules of a substance
due to temperature and is measured in joules (J).

Specific Internal Energy (u) is the internal energy per unit mass of the
substance, i.e. J/kg. When a small amount of heat is added at constant
volume the increase in specific internal energy is given by: $du = c_v \, dT$,
where c_v is the specific heat capacity at constant volume, and
dT is the increase in absolute temperature.

Specific Enthalpy (h) is defined by the equation: $h = u + pv$ where p is the
pressure and v is the specific volume. Specific enthalpy is measured
in J/kg. When a small amount of heat is added to a substance at constant
pressure, the increase in specific enthalpy is given by:- $dh = cp \, dT$, where
cp is the specific heat capacity at constant pressure.

The Specific Latent Heat of a substance is the heat gained per unit mass
without an accompanying rise in temperature during a change of state at
constant pressure. It is measured in J/kg.

The Entropy (S) of a substance is such that when a small amount of heat is
added, the increase in entropy is equal to the quantity of heat added
(dQ) divided by the absolute temperature (T) at which the heat is absorbed;
i.e. $dS = dQ/T$, measured in $J/^{\circ}K$.

The Specific Entropy (s) of a substance is the entropy per unit mass, i.e.
$J/kg^{\circ}K$.

A volt is the difference of electric potential between two points of a
conductor carrying a constant current of one ampere when the power dissipated
is one watt.

A weber (Wb) is the magnetic flux through a conductor with a resistance of one
ohm when reversal of the direction of the magnetic flux causes the transfer
of one coulomb in the conductor loop.

The magnetic flux density is the normal magnetic flux per unit area and
is measured in teslas.

A lumen, the unit of luminous flux, is the flux emitted within unit solid angle
of one steradian by a point source having a uniform intensity of one candle.

A lux is an illumination of one lumen per square meter.

Luminance is the luminous intensity per unit area of a source of light or of an
illumination. It is measured in candles per square meter.

IV.   PHYSICAL CONSTANTS

Standard	$= 273.15\ ^oK$ and 1.013×10^5 N/m^2
Temperature and	$= 0\ ^oC$ and 1.013 bar
Pressure (S.T.P.)	$= 0\ ^oC$ and 760 mm Hg
Molecular Volume of ideal gas at S.T.P.	$= 22.41$ liters/mol
Gas Constant (R)	$= 8.314$ J/mol ^oK
$RT_{(273.15\ ^oK)}$	$= 2.271 \times 10^3$ J/mol
Avogadro Constant	$= 6.023 \times 10^{23}$/mol
Boltzmann Constant	$= 1.3805 \times 10^{-23}$ J/K
Faraday Constant	$= 9.6487 \times 10^4\ ^oC$/mol (=A s/mol)
Planck Constant	$= 6.626 \times 10^{-34}$ J sec
Stefan-Boltzman Constant	$= 5.6697 \times 10^{-8}$ W/m^2 K^4
Ice Point of Water	$= 273.15\ ^oK\ (0^oC)$
Triple Point of Water	$= 273.16\ ^oK\ (0.01\ ^oC)$
Speed of light	$= 2.998 \times 10^8$ m/sec
Acceleration of (Standard) Gravity (Greenwich)	$= 9.80665$ m/s^2 $\begin{bmatrix} \text{Take g as} \\ 9.81\ \text{m/s}^2 \end{bmatrix}$ $= 9.81188$ m/s^2
Universal Constant of Gravitation	$= 6.670 \times 10^{-11}$ Newton m^2/kg^2
Mass of hydrogen atom	$= 1.6734 \times 10^{-27}$ kg

V. PROPERTIES OF WATER

Temper-ature (°F)	Specific Weight, γ (lb/ft³)	Mass Density, ρ (lb-sec²/ft⁴)	Dynamic Viscosity, $\mu \times 10^5$ (lb-sec/ft²)	Kinematic Viscosity, $\nu \times 10^5$ (ft²/sec)	Surface Energy,* $\sigma \times 10^3$ (lb/ft)	Vapor Pressure, p_v (lb/in.²)	Bulk Modulus, $E \times 10^{-3}$ (lb/in.²)
32	62.42	1.940	3.746	1.931	5.18	0.09	290
40	62.43	1.938	3.229	1.664	5.14	0.12	295
50	62.41	1.936	2.735	1.410	5.09	0.18	300
60	62.37	1.934	2.359	1.217	5.04	0.26	312
70	62.30	1.931	2.050	1.059	5.00	0.36	320
80	62.22	1.927	1.799	0.930	4.92	0.51	323
90	62.11	1.923	1.595	0.826	4.86	0.70	326
100	62.00	1.918	1.424	0.739	4.80	0.95	329
110	61.86	1.913	1.284	0.667	4.73	1.24	331
120	61.71	1.908	1.168	0.609	4.65	1.69	333
130	61.55	1.902	1.069	0.558	4.60	2.22	332
140	61.38	1.896	0.981	0.514	4.54	2.89	330
150	61.20	1.890	0.905	0.476	4.47	3.72	328
160	61.00	1.896	0.838	0.442	4.41	4.74	326
170	60.80	1.890	0.780	0.413	4.33	5.99	322
180	60.58	1.883	0.726	0.385	4.26	7.51	318
190	60.36	1.876	0.678	0.362	4.19	9.34	313
200	60.12	1.868	0.637	0.341	4.12	11.52	308
212	59.83	1.860	0.593	0.319	4.04	14.7	300

VI. PERIODIC TABLE OF THE ELEMENTS

Complements of

Lenox Institute of Water Technology

Groups → Periods & sub-shells ↓	1 IA	2 IIA	3 IIIB	4 IVB	5 VB	6 VIB	7 VIIB	8 VIII	9 VIII	10	11 IB	12 IIB	13 IIIA	14 VIA	15 VA	16 VIA	17 VIIA	18 O
1 1s	1 H 1.00794 Hydrogen																1 H 1.00794 Hydrogen	2 He 4.00260 Helium
2 2s2p	3 Li 6.941 Lithium	4 Be 9.01218 Beryllium											5 B 10.811 Boron	6 C 12.011 Carbon	7 N 14.0067 Nitrogen	8 O 15.9994 Oxygen	9 F 18.9984 Fluorine	10 Ne 20.179 Neon
3 3s3p	11 Na 22.9897 Sodium	12 Mg 24.305 Magnesium											13 Al 26.9815 Aluminum	14 Si 28.0855 Silicon	15 P 30.9738 Phosphorus	16 S 32.066 Sulfur	17 Cl 35.4527 Chlorine	18 Ar 39.948 Argon
4 4s3d4p	19 K 39.098 Potassium	20 Ca 40.078 Calcium	21 Sc 44.9559 Scandium	22 Ti 47.88 Titanium	23 V 50.9415 Vanadium	24 Cr 51.996 Chromium	25 Mn 54.938 Manganese	26 Fe 55.847 Iron	27 Co 58.933 Cobalt	28 Ni 58.69 Nickel	29 Cu 63.546 Copper	30 Zn 65.39 Zinc	31 Ga 69.723 Gallium	32 Ge 72.561 Germanium	33 As 74.9216 Arsenic	34 Se 78.96 Selenium	35 Br 79.904 Bromine	36 Kr 83.80 Krypton
5 5s4d5p	37 Rb 85.468 Rubidium	38 Sr 87.62 Strontium	39 Y 88.9059 Yttrium	40 Zr 91.224 Zirconium	41 Nb 92.9064 Niobium	42 Mo 95.94 Molybdenum	43 Tc (98) Technetium	44 Ru 101.07 Ruthenium	45 Rh 102.906 Rhodium	46 Pd 106.42 Palladium	47 Ag 107.868 Silver	48 Cd 112.411 Cadmium	49 In 114.82 Indium	50 Sn 118.710 Tin	51 Sb 121.75 Antimony	52 Te 127.60 Tellurium	53 I 126.90 Iodine	54 Xe 131.29 Xenon
6 6s4f5d6p	55 Cs 132.905 Cesium	56 Ba 137.327 Barium	57 La 138.906 Lanthanum	72 Hf 178.49 Hafnium	73 Ta 180.948 Tantalum	74 W 183.85 Tungsten	75 Re 186.207 Rhenium	76 Os 190.2 Osmium	77 Ir 192.22 Iridium	78 Pt 195.08 Platinum	79 Au 196.97 Gold	80 Hg 200.59 Mercury	81 Tl 204.383 Thallium	82 Pb 207.2 Lead	83 Bi 208.98 Bismuth	84 Po (209) Polonium	85 At (210) Astatine	86 Rn (222) Radon
7 7s5f6d	87 Fr (223) Francium	88 Ra (226) Radium	89 Ac (227) Actinium	104 Rf (261) Rutherfordium	105 Ha (262) Hahnium	106 Sg (263) Seaborgium	107 Ns (262) Nielsbohrium	108 Hs (265) Hassium	109 Mt (266) Meitnerium	110	111	112						

	31	32
6 4f	58 Ce 140.115 Cerium	59 Pr 140.91 Praseodymium	60 Nd 144.24 Neodymium	61 Pm (145) Promethium	62 Sm 150.35 Samarium	63 Eu 107.26 Europium	64 Gd 157.25 Gadolinium	65 Tb 158.925 Terbium	66 Dy 162.50 Dysprosium	67 Ho 164.930 Holmium	68 Er 167.26 Erbium	69 Tm 168.934 Thulium	70 Yb 173.04 Ytterbium	71 Lu 174.967 Lutetium
7 5f	90 Th 232.038 Thorium	91 Pa (231) Protactinium	92 U 238.029 Uranium	93 Np (237) Neptunium	94 Pu (244) Plutonium	95 Am (243) Americium	96 Cm (247) Curium	97 Bk (247) Berkelium	98 Cf (251) Californium	99 Es (252) Einsteinium	100 Fm (257) Fermium	101 Md (258) Mendelevium	102 No (259) Nobelium	103 Lr (262) Lawrencium

698

Index